Life-Work *Cuntze* - *a compilation* -

The Failure-Mode-Concept *FMC*

– a physical and theoretical Material Symmetry-driven basis to generate Strength Criteria, that gave a reason to look after a 'more closed' Strength Mechanics Building –

& Very Much on Structural Materials, Techniques and Design

including work-life experiences of the author in many engineering fields.

Material Symmetry seems to tell:

In the case of ideally homogeneous materials a generic number is inherent. This is valid for elastic entities, yield modes and fracture modes, for yield strengths $R_{0.2}$ and fracture strengths R , fracture toughness entities K_c and for the invariants used to generate strength criteria.

This **generic number** is
2 for isotropic and 5 for transversely–isotropic materials,

One might think:

"Mother Nature gives Strength Mechanics a mathematical order?"

STRENGTH is still his Life !

"Anyone who stops learning is old,
whether at twenty or beyond eighty.
Anyone who keeps learning stays young.
The greatest thing in life is to keep your mind young"

[Henry Ford]



The author after the yearly 'pilgrimage'
Kloster Indersdorf (home) ↔ Kloster Scheyern
83/2 km (26 miles): 9 h, 9 min, 9 s ?.
→ Back to Life Work, September 2022.

Application-oriented engineer with a scientific touch for material modelling and with the hope to be some bridge-builder between mechanical and civil engineering (construction).

This document includes results of the author's non-funded, non-supported research work.
The paper basically addresses the author's strength-dedicated work with numerical results found over the past decades.

"As single author - due to my age - I am quite forced to publish this work as quickly as possible. Peers could only be very limited found. I therefore ask the readers to deal generously with the shortcomings they will find".
This wide-spread work contains many invitations for discussion.

Permanent address in January 2023: Carbon Connected | Prof. Ralf Cuntze (carbon-connected.de)

Prof. Dr.-Ing. habil. Ralf Cuntze VDI, Ralf_Cuntze@t-online.de

1964: Dipl.-Ing. Civil Engineering CE (construction, ***TU Hannover***)
1968: Dr.-Ing. in Structural Dynamics (CE)
1978: Dr.-Ing. habil. Venia Legendi in Mechanics of Lightweight Structures (TU-M, CE)
1980-1983: Lecturer at Universität der Bundeswehr München: on 'Fracture Mechanics' in the construction faculty and 1990-2002 on 'Composite Lightweight Design' in the aerospace faculty
1987: Full professorship 'Lightweight Construction', not started in favor of industry
1998: Honorary professorship at Universität der Bundeswehr München
1968-1970: FEA-programming (***DLR***-Essen/Mühlheim)
1970-2004: MAN-Technologie (München and Augsburg). Headed the Main Department 'Structural and Thermal Analysis'. 50 years of life with fibers CF, AF, GF, BF, BsF.
Theoretical fields of work: structural dynamics, finite element analysis, rotor dynamics, structural reliability, partial/deterministic safety concepts, material modeling and model validation, fatigue, fracture mechanics, design development 'philosophy' & design verification
Mechanical Engineering applications at ***MAN****:* ARIANE 1-5 launcher family (design of different parts of the launcher stages inclusively Booster) Cryogenic Tanks, High Pressure Vessels, Heat Exchanger in Solar Towers (GAST Almeria) and Solar Field, Wind Energy Rotors (GROWIAN Ø103 m, WKA 60, AEROMAN. Probably the first world-wide wind energy conference organized in 1979), Space Antennas, Automated Transfer Vehicle (Jules Verne, supplying the space station ISS), Crew Rescue Vehicle (CMC application) for ISS, Carbon and Steel Gas-Ultra-Centrifuges for Uranium enrichment. Material Databank etc.
Civil Engineering applications: Supermarkets, armoring plans, pile foundation, 5th German climbing garden (1980 designed, concreted and natural stone-bricked)
1971-2010*:* Co-author of ***ESA/ESTEC***-Structural Materials Handbook, Co-author and first convener of the ESA-Buckling Handbook and co-author in Working Groups WGs for ESA-Standards 'Structural Analysis', 'High Pressure Vessels' (metal and composites), 'Safety Factors'
1972–2015, ***IASB***: Luftfahrt-Technisches Handbuch HSB 'Fundamentals and Methods for Aeronautical Design and Analyses'. Author/Co-author of numerous HSB sheets, co-transfer with co-translation of the HSB aerospace structural handbook into its present English version.
1980-2011: **Surveyor/Advisor** for German BMFT (MATFO, MATEC), BMBF (LuFo), DFG
1980-2006: **VDI Guideline 2014**, co-author of Parts 1 and 2, Beuth Verlag '*Development of Fiber-reinforced Plastic Components'; Part 3 'Analysis*', editor/convenor/co-author
1986 and 1889: One week lecture on composite design in Pretoria, SA
2019: **GLOSSAR.** "Fachbegriffe für Kompositbauteile - *technical terms for composite parts*". Springerverlag 2019. Edited at the suggestion of carbon concrete colleagues to help to better understand each other in the co-working disciplines
World-Wide-Failure-Exercise WWFE (2000-2013) on UD materials' strength: WWFE-I (2D stress states) non-funded winner against the institutes of the world, WWFE-II (3D states) top-ranked
2009-2021 linked to ***Carbon Composites e.V***. at Augsburg, later ***Composites United CU e.V.*** and to TUDALIT Dresden. Since 2011 working on the light weight material Fiber-reinforced (polymer) Carbon Concrete. **Founded and headed the working groups**: (1) 2009: 'Engineering' linked to the WG Non-Destructive Testing and the WG Connection Technologies, mechanical engineering. (2) 2010: 'Composite Fatigue'. In 2010 the author held an event that was excellently attended by international speakers. (3) 2011: 'Design Dimensioning (Auslegung, Bemessung) and Design Verification (Nachweis)' mainly for carbon concrete. This working group was the foundation stone for the later specialist network ***CU Construction***, aiming at *"Fiber-based lightweight construction*". (4) 2017: 'Automated fabrication in construction including serial production' *(3D-Print)*. (5) 2020, 2021: Forum 'Carbon concrete for practice' at 'Ulm Concrete Days'.

The contents of the compilation stems from the author's papers, presentations, published and non-published design sheets and project works in industry and indicates some work-life experiences.

Keywords:
Structural strength mechanics building, material modelling, failure criteria, multiple failure modes.

Abstract

Novel simulation-driven product development shifts the role of physical testing to virtual testing, to simulation respectively. This requires High Fidelity concerning the material models used. First and usual assumption for the material models is an ideally homogeneous material. Deviations are specifically taken into account.

Material resistance must be generally demonstrated by a positive Margin of Safety *MoS* or a Reserve Factor *RF* = *MoS* - 1 > 1 in order to achieve Structural Integrity for the envisaged Limit State! For the 3D-Demonstration of Strength - *nowadays a must regarding the usual 3D FEA stress output* - principally so-called 3D strength criteria or 3D failure bodies are required to firstly perform Design Dimensioning and to finally achieve Design Verification. In the case of brittle materials it is a fracture (failure) body. The surface of such a failure body is determined by the points of all those stress states that lead to failure. It is mathematically defined by a Failure function *F* which becomes 1 at Onset-of-Failure. Usually these *F*s are written as Strength Failure Conditions (SFC) *F* = 1. SFCs used in this paper are those which have been generated of the author's Failure-Mode-Concept (FMC). The FMC incorporates a rigorous thinking in failure modes and can be briefly described by the features: Failure mode-wise mapping, stress invariant-based formulation, equivalent stress generation, each failure mode is governed by just one strength R^{mode} and all SFC model parameters are measurable entities. This involves a direct use of the friction value μ in the case of compressed brittle materials where the model parameter for friction in the SFC is replaced by the measured μ. Therefore, the very challenging task to transform an SFC in structural stresses into a SFC in Mohr stresses had to be performed.

The difference between a so-called 'global fitting' and a '(failure mode-linked) modal fitting', such as with 'Mises Yielding', of failure test data is pointed out. Further, terms such as mixed failure mode (mode interaction), multiple failure mode action and multi-axial strength are presented and discussed.

During the derivation of the FMC a closer look at material symmetry facts was taken whereby the question arose: "Does a material symmetry–linked Generic Number exist with a number 2 for isotropic and 5 for UD materials? This looks to be proven by the investigation of Normal Yielding NY of plexi-glass and a compressive fracture toughness K_{cr}^{c} for an ideally brittle material.

The SFC approaches consider - following Beltrami and Mohr-Coulomb – that the solid material element may experience, generated from different energy portions, a shape change (HMH), a volume change and friction. The derivation of the SFCs is based on specific FMC ideas and partly builds up on the hypotheses of Beltrami, Hencky-Mises-Huber (HMH) and Mohr-Coulomb.

FMC-based SFCs, nowadays most often termed Strength Criteria are enlisted for a large variety of isotropic brittle structural materials such as porous Concrete Stone, Normal Concrete, UHPC sandstone, monolithic ceramics and for the transversely-isotropic fiber-reinforced polymers Lamina (ply, lamella) and Fabrics. Orthotropic fabrics inclusively fabric ceramics are further included. Available multi-axial fracture test data were mapped to validate the SFCs chosen for the description of the envisaged fracture failure model. For a large variety of materials the course of test data was mapped and the associated fracture bodies displayed with distinct cross–sections of them: Principal stress plane, octahedral stress plane and tensile and meridian planes. Various links or interrelationships between the materials are outlined. Different but similar behaving materials can be basically treated with the same SFC.

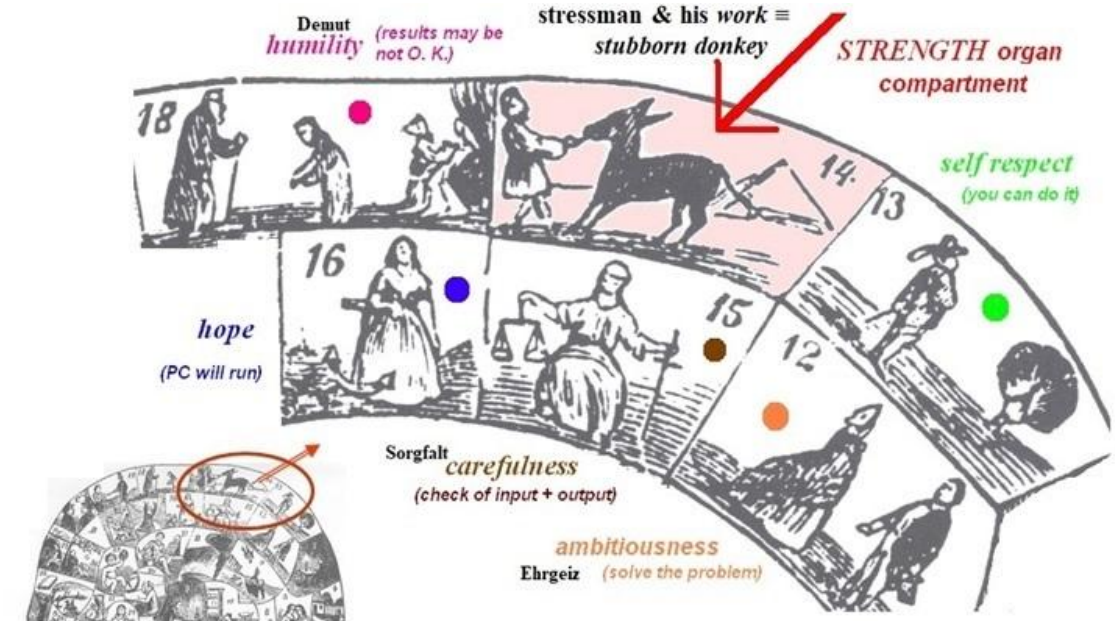
If several failure modes are activated by the stress state then the application of the *material stressing effort Eff* (Werkstoffanstrengung) is very helpful because the full *Eff* consists of the mode portions Eff^{mode}. The contribution of each single Eff^{mode} informs the designing engineer about the importance of the single portions in the SFC and therby about the critical failure driving mode. Whereas the structural engineer is more familiar with the equivalent stress the material engineer prefers above 'material stressing effort' *Eff* . These terms are linked by $\sigma_{\text{eq}}^{\text{mode}} = Eff^{\text{mode}} \cdot R^{\text{mode}}$.

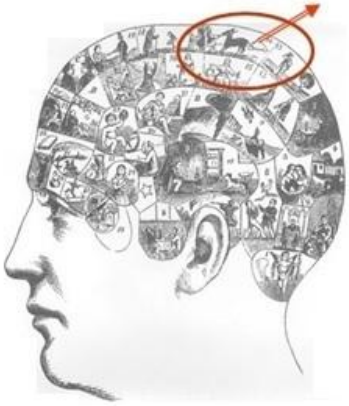
Special attention is paid not only to the porous materials grey cast iron, concrete, foam which possess a *convex* fracture failure surface, but also to the normal yielding experiencing plexiglass PMMA which possesses a *concave* fracture failure surface part in the principal tension stress domain.

Of further intensive concern was to automatically generate Constant Fatigue Life curves on basis of just a few tested Master SN curves together with a physically based model, namely Kawai's 'Modified fatigue strength ratio' Ψ . This procedure is a novelty and applicable for materials like UD plies and isotropic concrete as well.

Two typical Bavarian peculiarities addressing Strength and Composites

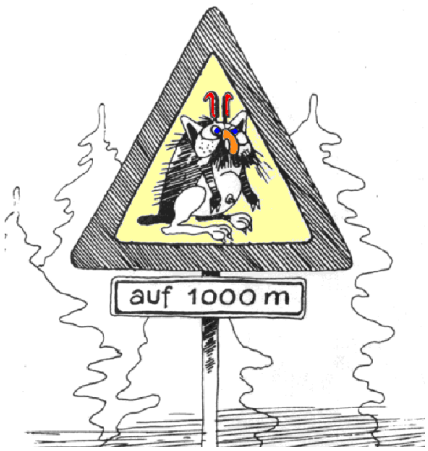
How much do you think this 'organ' is weighing?
***About 15 g → extreme lightweight* !**





- **Strength** is a very **essential** thing.
  Human beings possess strength not just in muscles!
- **This attribute was located by the so-called *Phrenological Society of Munich* as an organ at the top of the head (1860 !)**

The Wolperdinger,
the most famous
Bavarian Composite



Fiber-reinforced Composites in the various technical disciplines are the main topic in this work.
In this context the author tries to more inform about composite applications in construction.
These applications are less known in engineering.

Personal Reminder on Progress in Calculation Tools' Development and 'For Ever Valid Statements'

- 1964 Diploma work, use of a long slide rule (Rechenschiebert), an improvement to the short version
- 1964-1968 Dissertation, programmimg with Algol and use of Zuse Z4 computer
- 1968-1970 Necessity to craft my own FE program from mathematical modules of the University of Hannover. Computer of the DFVLR (name now). Weekly use only possible with punch card transport by car from Essen to Bonn (Research report 70-16 Theoretical determination of the 3D-stress distribution in radial compressors)
- Since 1970 Commercial codes since 1970 at MAN Technologie CDC-Software, NASTRAN, PATRAN, MARC
- Application of HSB design data sheets for structural design dimensioning. Handbook calculation sheets with solutions for relatively simple structural elements are valuable checkers of FE results.

In the context above considering the final quality of results:

1960, Z2 computer time: one must cite a saying of Bronstein & Semendjajew in their) famous book "Paperback of Mathematics (highly valued by me, still now): *"When calculating, you always have to pay attention to the accuracy that you either have to achieve or can achieve. It is quite inadmissible to expect great accuracy if the nature of the task either does not allow it or does not require it. If an approximate value contains superfluous decimal numbers, it must be rounded. In some cases, more realistic but more complicated models can be replaced with simpler ones that give a result with permissible error.*

And 60 years later: Dominique Madier (*Senior FEA/Stress Analyst with long experience*) recommends the stress engineer to answer the 14 following questions before any start of a structure modeling process:
Question 1: Have you clearly identified the model's goals?
Question 2: Which solution do you plan to use, and is it consistent with your problem?
Question 3: Do you trust the geometry you plan to use, and can you change it if necessary?
Question 4: Can you justify your choice of elements?
Question 5: Which boundary conditions will you apply to your model? Why did you select them?
Question 6: Do you understand perfectly the loading you will apply in your model?
Question 7: Have you identified the major load paths in your structure?
Question 8: Are you able to anticipate the response of your structure?
Question 9: At which locations in the model do you plan to extract results?
Question 10: Which accuracy of results do you require?
Question 11: Have you identified all the modeling techniques you will use to build your model?
Question 12: Have you identified discontinuities in the structure you wish to model?
Question 13: Have you identified all the capabilities and limitations of your model?
Question 14: Do you expect any potential sources of nonlinearity?

And now upcoming, Modeling of multi-physics systems using meta-models: Improving product performance is only possible by capturing all system-design relevant parameters of the more or less commonly acting technical disciplines in the system models.

Citing NAFEMS: A '*Model-based system engineering'* MBSE will be performed in future.

Questions posed by the Author during his Work Life and some Findings

In the frame of his material symmetry-driven thoughts the author intended to test-proof some ideas that help to complete the Strength Mechanics Building by finding missing links and by providing engineering-practical strength criteria (SFCs), the parameters of which are directly measurable:

* Beside the standard Shear Yielding SY there should be also Normal Yielding NY analogous to the failure modes Shear Fracture SF and Normal Fracture NF
* Practically, facture mechanics is presently only tensile driven performed using $K_{Ic} = K_{Icr}{}^{t}$ as a clear critical fracture intensity (*the index cr is necessarily to be taken in this document in order to separate tension ^{t} from compression ^{c}*), where the crack plane does not change. K_{IIc} and K_{IIIc} are 'just' very helpful model parameters driving the crack plane in direction of a finally K_{Ic} - failure mode. Why shouldn't there not be a quantity $K_{IIcr}{}^{c}$ that fits to $K_{Icr}{}^{t}$ and where, in an ideal case of no flaws in front of the crack tip, the crack plane grows further along the generated shear fracture angle under a compressive fracture load?
* From experiments is known, that brittle isotropic materials possess a 120°-axially symmetric fracture failure body in the compressive domain. Should ductile materials in the tensile domain not also possess a 120°-axially symmetric yield loci surface instead of the rotationally symmetric 'Mises cylinder'?
* Is a test-validation of 3D-strength criteria models for isotropic concrete, transversely-isotropic UD-material, orthotropic ceramic (fabrics) with visualization of the derived 3D failure surfaces possible?
* Generation possible of a novel porosity-capturing,'Gurson model-linked' ductile metal stress-strain curve $\sigma_{eq}(\varepsilon_{eq})$ from evaluation of the tension bar test specimen by extending the Bridgman-linked hydrostatic stress effect, using Lorrek-Hills model on neck curvature under high plastic strain? Are the used model-parameters are all measurable then! *('Gurson–based formulation growth of voids effect instead of the classical 'Mises-based'*).
* Two neighboring modes are activated: This reduces the strength capacity, the natural frequency and the stability loading, being quantities in these three different fields
* Mode-wise equivalent stresses $\sigma_{eq}^{mode}(\varepsilon_{eq}^{mode})$ are given for transversely-isotropic materials. The combined action of modes is taken over by the material stressing effort *Eff*. For the performance of the non-linear analysis $\sigma_{eq}^{IFF}(\varepsilon_{eq}^{IFF})$ is required for application of the normality rule in the case of the 3 Inter-Fiber-Failure modes IFF (inclusion of FF is not of practical interest)
* The author's WWFE-I and -II contributions had to be based on an intensive assessment of provided test results
* In the case of bending FRPlastic- and FRConcrete-parts, carbon fibers can be only exploited using pretensioning and thereby compressing the tension-sensitive matrices Plastic or Concrete
* Minimum effort fatigue life estimation: A closed procedure was found to generate test data-based Constant Life curves for using Master SN curve + supporting model to determine other required SN-curves (*Kawai Ψ model was the tool*). Applicable for CFRP and concrete
* Indexing is a chaos in the disciplines: It seems to be that the author could find a physically clear indexing system for the 3 material families isotropic, transversely-isotropic UD and orthotropic materials (fabrics etc.). This captures all material properties and allows the switching between.

Purpose of the large glossar part 'Technical Terms': *Hopefully it will be a contribution to a better mutual understanding of 'constructive' engineers from the building industry and engineers from mechanical engineering and further, of engineers from the textile, manufacturing and material discipline as well in order to better manage the more and more interdisciplinary future project tasks*.

The author is not so much concerned with details but with the discipline-links and the procedures.
His motto is: Bridge disciplines and materials by showing up similarities to simplify engineering life!
In this context the author founded his engineering bureau for lightweight **IfL**.

The huge draft at hand is a compilation of the author's work life and not a book.
It requires further checking and still needs filling of some gaps.

It was collected over decades.
Therefore, the structure of the document basically developed automatically.
Covid 19 time was optimally used by performing this work.

Mind. Please, considering

not just Design Dimensioning with its Trade-offs but Design Verification, too.
At the end someone has to sign that the structure will work.

In this context, after a lot of discussions in the last years I'm forced to say:
"Mechanics is one very essential basis when developing light-weight structural components and Artificial Intelligence with its algorithms is a helpful supporting tool.

The novel so-called 'democratization of software use' reminds me of Black Box application.
The results have to be evaluated by people.
These should approximately know the specific result.
In multi-physics applications this evaluation is the work of several experienced engineers.
Otherwise one does not deliver qualified 'Multiple function structural products'.

Only System Engineering with experienced engineers using mechanics and the necessary other disciplines - together with AI - enables to produce qualified products."

Let me add, please: Everything cries out for artificial intelligence, as if it represents the solution to the technical problem. We forget that (*see above*) it can only be one of the tools for this, and that, for example, the solution of the technical problem 'house construction' requires intelligent craftsmen.

Experienced engineers know:
"Check your test together with test data evaluation.
Check your analysis including assumptions."

Warranty
Test data and some theoretical material of this Life Work Compilation come from different sources. Effort was put into checking the accuracy of these input parts. However, the author assumes no liability for damages resulting from the application.

Taking parts from this Compilation requires the permission of the single author.

Using parts of this document, please, see and refer to the ADDRESS:

Carbon Connected | Prof. Ralf Cuntze (carbon-connected.de)

1 Introduction 15
1.1 General on Design 15
1.2 Scheme of Strength Failure Criteria (SFCs) with potential Missing Links 23
1.3 Material properties, Tables, international designations and Invariants 25
1.4 Available knowledge used for the SFC Generation 33
1.5 Beltrami Hypothesis for SFC-generation of isotropic and of UD materials 35
1.6 Stresses and Invariants of Isotropic materials and of UD materials 37
1.7 Material symmetry-based assumptions of the author 40
1.8 Effects to be considered with Isotropic and Transversely-isotropic Materials 41
1.9 Fracture Types and Behavior of the Various Materials 44
1.10 A first Visualization of an Isotropic Failure Body with the Mode Domains SF and NF 50
1.11 Shear Yield failure and Fracture Planes of some Isotropic Materials 52
2 Presentation of FMC-based SFCs and Associated Topics 53
2.1 Introduction with comparison of so-called 'Global' and 'Modal' SFCs 53
2.2 Collected Basic features of the Failure-Mode-Concept FMC (1996) 55
2.3 Modal equivalent stress σ_{eq} and Modal material stressing effort *Eff* 57
2.4 History of FMC with Search of a 'More Closed' Strength Mechanics Building 57
2.5 SFCs for 'dense' and 'porous' Isotropic Material 59
2.6 SFCs for 'dense' and 'porous' transversely-isotropic materials (UD lamina, lamella) 62
2.7 SFCs for differently porous, fabric pattern-dependent orthotropic materials (fabrics) 66
2.8 SFCs for the differently porous Structural Ceramic Materials 70
2.9 Validity limits for SFC applications and Automatic Insertion of 3D Stress States 72
2.10 UD-material, Stress-strain curve parts Strain-hardening and Strain-softening 75
2.11 Note on Polymer Matrix Reinforcement by Fiber Patch work 78
3 Construction Applications, Modelling of 'open' and 'closed' FRP, FRC Components 79
3.1 Some Ssemi-finished Products in Construction 79
3.2 Applications with Fiber-Reinforced Polymer (FRP) matrices 81
3.3 Applications with Fiber-Reinforced Mineral (FRM) matrices 84
3.4 Some Freshly arrived Applications 90
3.5 Some other Fiber-reinforced Bridges in Germany 93
3.6 Influence of Production Process on the Damage of Filaments and Fiber Strands 105
3.7 On Material Modelling of some of the Semi-finished Products in Construction 108

3.8 Structural Modelling and Dimensioning, *in construction usually on cross-section level* . 108
4 Two Missing Links filling the 'Mechanics Building' of Isotropic Materials 113
4.1 Experimental Proof and Description of Normal Yielding NY of Isotropic Materials 113
4.2 ' Some Proof ' of a 2nd Basic Stress Intensity Factor $K_{IIcr}{}^{c}$ beside $K_{Icr}{}^{t}$ 119
4.3 Transversely-isotropic UD lamina materials, 5 fracture toughness properties 124
5 Validation of FMC-SFCs by 3D-Applications with all 3 Material Families 132
5.1 Isotropic Grey Cast Iron 132
5.2 Isotropic Glass C 90 (window pane of ISS) 133
5.3 Isotropic porous Foam Rohacell (SFC is applicable for Concrete Stone material, too) .. 133
5.4 'Isotropic' Normal Concrete (slightly porous) 136
5.5 'Isotropic' UHPC (relatively dense) 139
5.6 Rock Material, example Sandstones 143
5.7 Bi-axial strength of Solid Clay Brick Masonry 153
5.8 Evidence 120°-symmetrical Failure Body of Brittle and Ductile Isotropic Materials 154
6 Transversely-isotropic UD-materials (GFRP, CFRP) 161
6.1 General, UD applications 161
6.2 Transversely-isotropic UD-materials, WWFE-I and WWFE-II applications 165
6.3 2D-Application to (technical) Ceramics isotropic, UD and orthotropic fabrics 190
7 Mohr Stress Transformation to obtain a Friction Parameter-Friction Value Dependence 196
7.1 Dependence of Isotropic Friction Model Parameter on Friction Value μ 196
7.2 Dependence of Transversely-isotr. Friction model parameters on Friction Values $\mu_{\perp\perp}$, $\mu_{\perp\parallel}$ 211
8 Miscellaneous 221
8.1 Bridging Shear Fracture F^{SF} and Yield Failure F^{Mises} with view at Failure 'planes' Θ_{fp} ° 221
8.2 Influence of Compression Stress States on Strength Capacity and Effort 222
8.3 Application of Safety Concepts with Determination of a Reserve Factor 224
8.4 Failure Index $|F|$ versus Material Stressing Effort *Eff* , Example UD 3D-stress state 231
8.5 3D-Print in Mechanical Engineering 232
8.6 Construction-linked Additive Fabrication AF 233
9 Classical Laminate Theory CLT 237
9.1 Theoretical relations of Lamina and Laminate 237
9.2 Some Topics concerning the CLT-analysis of laminates 247
9.3 Collection of CLT Examples 253

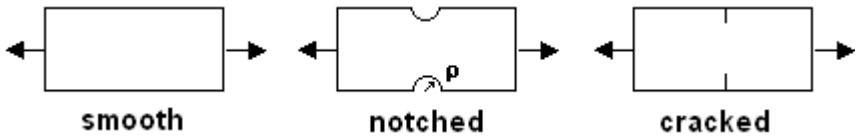
9.4 Coupling Reduction in [*K*] using Tsai's 'Trace-normalized Stiffness' & 'Double-Double'281
9.5 Some further Examples considering distinct Material Effects 303
10 FMC-based Fatigue Life Models, basically displayed for the brittle UD material.....307
10.1 General and Terms.....308
10.2 SN curve (Woehlerkurve) and Haigh-Diagram 313
10.3 Static Residual Strength R_{res} for Proof of Structural Integrity in Projects 317
10.4 Determination of a Load Spectrum-equivalent SN curve 323
10.5 FMC-based Fatigue Life Estimation Model.....324
10.6 Some examples of SN curves 'feeding' Haigh-Diagrams, FF and IFF 331
10.7 Novel Procedure for deriving CFL curve estimates with associated Steps 335
10.8 Check of the FMC-driven Idea to Split the Operational Loading mode-wise.....337
10.9 Estimation of the Haigh Diagram Amplitude and Comparison with the Measured Value 339
10.10 Steps of the FMC-based Fatigue Life Estimation Procedure 340
10.11 Notes on Damage Tolerance and Fracture Mechanics with Cracked Components.....343
11 Procedure on Performing Design Verification in Stability.....346
11.1 General.....346
11.2 Hierarchical approach for stability analysis with application comments 356
11.3 Application cases Isotropic Plate and Orthotropic Plate 361
11.4 Some practical Hints for Applications.....364
12 Structural Reliability, Factors of Safety and Design Values 368
12.1 General on Loads, Risk and Reliability.....368
12.2 RAMS-Achievement, Functional Analysis, FMECA and Critical Points Log.....372
12.3 Failure probability p_f, density functions f(x) and cumulative distribution functions F(x) 373
12.4 Statistical pre-requisites, tests of assumed distributions, and significance level.....378
12.5 Tolerance Interval and Confidence Level C 383
12.6 Factor of Safety (FoS) Concepts ('deterministic format').....385
12.7 Determination of a Design Value.....392
12.8 Determination of Strength Design Allowables.....393
12.9 Probabilistic Safety Concept (Probabilistic Format).....399
12.10 Probabilistic Dimensioning of a full 'Failure System', Example launcher subsystem 401
12.11 Modelling Mode Interaction Equation, Multiple Modes and Interaction Exponent *m* 403
13 Probabilistic Assessment of a Deterministic Margin of Safety MoS 407

13.1 Introduction 407
13.2 Factors of Safety (FoS), Load Cases and Margin of Safety (MoS) 408
13.3 Theoretical Background of the Probabilistic Solution 410
13.4 Numerical Example: Cylindrical part of a pressure vessel 412
13.5 Additional Sensitivity Investigations 418
14 Contributions of the Author to Handbooks, Working Groups, MAN-Projects 426
14.1 Glossary for Civil- and Mechanical Engineering 426
14.2 Contributions to Handbooks, Guidelines 428
14.3 Projects involved: Memories of working life at MAN 434
15 Continuum Mechanics, Continuum (micro-)Damage Mechanics and Multiscale Modeling 456
15.1 Continuum Mechanics (CM) Design Features 456
15.2 Modelling Stress-strain curves including strain-hardening and strain-softening 459
15.3 Continuum (micro-)Damage Mechanics (CDM) of brittle and ductile materials 462
15.4 CDM of Ductile Materials described by a 'Gurson Model' 471
15.5 Multi-scale Materials Modelling MMC 473
15.6 Metallic example for a Multi-scale Material modelling (MMM), Mlikota model 474
16 Structural Tests, Material Tests of Isotropic, UD, and Fabric Materials 486
16.1 Structural Testing 488
16.2 General on Material Testing and some Material Testing Methods 492
16.3 Isotropic Material Testing 501
16.4 Transversely-isotropic UD-materials Testing 522
16.5 Measurement of Friction Values $\mu_{\perp\square}$, $\mu_{\perp\perp}$ 531
16.6 Coefficients of Thermal Expansion and of Moisture Expansion of a UD material 534
17 Material Models from the 'Elastic State' and 'Onset-of-Yielding' via load-controlled 'Onset-of-fracture' until deformation-controlled 'Full Plastic Fracture' (rupture) substantiated by hints on the performance of Linear and Non-linear Stress Analyses 540
17.1 Elasto-plastic Transition Domain ($\overline{\mathrm{R}}_{\mathrm{p}} < \bar{R}_{p0.2} \equiv \bar{R}^{t}_{0.2}$, $\nu_0 < \nu < 0.5$) 542
17.2 Hencky-v.Mises-Huber (yield condition: $\bar{R}^{t}_{0.2} < \sigma < \bar{R}^{t}$, $\nu = 0.5$; $1 < c_\tau < \bar{R}^{t} / \bar{R}^{t}_{0.2}$) 543
17.3 'Extended Mises' Yield Condition ($\overline{\mathrm{R}}^{\mathrm{t}}_{\mathrm{m}} < \sigma_{\mathrm{eq}} < \bar{R}_{\mathrm{ODC}} < \bar{R}_{\mathrm{rupture}}$; $0.5 \geq$ actual ν) 550
17.4 Development of Poisson's Ratio in the "Beltrami" and in the "Gurson" Domain 558
17.5 Mises (HMH) Yield Hypothesis or Tresca Yield Hypothesis? What counts? 566
17.6 Average Properties and Average Stress-strain Curve in Mapping and Design 569

17.7 Linear and Non-linear Analyses of Ductile and Brittle Materials including UD Materials573
18 Structural Vibration and Work Cases 582
18.1 General on Oscillation/Vibration....582
18.2 Damping and Damped Vibrations 586
18.3 The Influence of Dead Mass and Elastic Clamping on the Bending frequency of a slender Tower with linearly reducing Thickness (1969)....590
18.4 Natural Frequencies of Thin Inclined Isotropic Plates (*Cuntze,1969*) 594
18.5 Natural Frequencies (eigenfrequencies) of Orthotropic Deep Beams (Diss.1968,to add) 599
18.6 The influence of Cross-sectional Shear Flexibility and Rotatory Inertia on the Natural Frequencies of Beams with Uniformly Distributed Mass 600
18.7 Analysis of the Natural Frequencies of Laminated Beams of low 'Shear-rigidity' 606
18.8 Influence of low Cross-sectional Shear Rigidity and Rotatory Inertia on the Critical Speeds of Shafts with Uniformly Distributed Mass *(1984)*....609
18.9 Natural Frequencies of a Cracked Beam for Production Quality-testing of Rotor blades 617
18.10 Equivalent Sinusoidal Acceleration corresponding to an Excitation by Random Vibration621
19 Some Flywheels and Rotors....623
19.1 Metallic Energy storage Flywheel for the floating crane ship Swartow (1982)....623
19.2 A New concept of a Composite Flywheel due to novel fiber-reinforced materials (1988)629
19.3 An Axial Energy Storage Rotor, the 'EnWheel' (2015) 633
19.4 Increasing the Limit of Usability of CFRP Tubes by Built-in-Stresses (1993)....644
19.5 The large Windmill GroWiAn GROWIAN (1977-1982), development and build 658
19.6 Design of a Fiber-reinforced Gas-Ultra-Centrifuge Cylinder, GUZ (1971-1986) 676
19.7 Some Winding Theory on Filament Wound Pressure Vessels going to be included 682
19.8 Application of winding technology, re-calculation of above AFRP tank 688
20 Introduction to Beams with Thin-walled Cross-sections going to be included 691
21 Notch Mechanics going to be included....692
22 FMC-Conclusions and FMC-linked Literature....693
22.1 Failure-Mode-Concept, considering the investigated 3 Material Families 693
22.2 Structural Mechanics Building, presumption 'homogeneous material' 694
22.3 Fatigue and Some specific material conclusions....695
22.4 Some remarks considering fidelity in Engineering Design, Analysis, Simulation and Test697
22.5 Lessons Learned LL from the application of the SFCs....698
22.6 Notes on Analyses 699

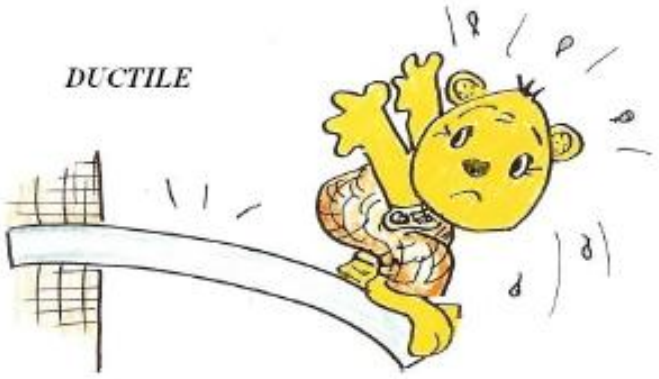
22.7 General FMC-linked Literature 701
23 Basic Terms and Definitions 713
23.1 Introduction 713
23.2 English Technical Terms with Definitions 718
23.3 Deutsche Fachbegriffe in Englisch 761
23.4 Abbreviations/Abkürzungen 768
23.5 Terms and Symbols *considering the guideline VDI 2014 and DIN 1055-100* 778
23.6 Indexing, Laminate Descriptions and Layer Numbering (ply-book) 783

Two basic features are faced by the structures designing engineers, the 3 types of surfaces



and the material behavior whether it is brittle or not.

Depending on stress state and environment a material may behave ductile and brittle.
Here, brittle shall be engineering-like defined as: $R^c > \approx 3 \cdot R^t$ (uni-axial, ambient)



Ductile Fracture = type of failure in a material or a structure generally preceded by a large amount of plastic deformation

One feels good until sudden fracture occurs



[Courtesy: Prof. C. Mattheck]

<u>A Lesson Learned *LL*</u>:

When using brittle materials, more care must therefore be taken than for ductile materials

Considering the fracture-based design verification under Design Ultimate Loading.

In the sense of lightweight construction and sustainability, this deficiency should not lead to the choice of arbitrarily increased design safety factors (FoS j, γ) - as experienced by the author –

in design dimensioning but to a search of an improved knowledge of the material failure behavior.

The delivery of such a better knowledge on failure behavior is one essential intention of this work.

1 Introduction

1.1 General on Design

The variety of new materials in engineering requires the knowledge of the failure state in order to enable verification of the designed structural part. And this much more since lightweight design requires a higher exertion of the material and thereby contributes to sustainable engineering.
Design Verification demands for reliable reserve factors *RF* or Margins of Safety *MoS* and these – beside a reliable structural analysis - demand for reliable Strength Failure **Conditions** (SFCs, usually termed Criteria). Such a condition is the mathematical formulation $F = 1$ of a failure curve or of a failure surface (body). Generally required are a yield strength condition and a fracture strength condition. A load-driven growing yield failure surface is terminated by the fracture failure surface.

A yield SFC usually describes just one mode, namely for isotropic materials the classical 'Mises' shear yielding SY. For PMMA, however, there are two yield modes, SY in the compression domain and normal yielding NY in the tension domain. Fracture SFCs usually describe two independent fracture modes, shear fracture SF and normal fracture NF.

Fig.1-1 displays the structural engineer's tasks he is involved when designing a structural part. It is to demonstrate that the static Dimensioning Load Cases as well as the dynamic and cyclic ones, considering lifetime, and others are fulfilled. Addressed are Design Dimensioning (*Auslegung, Bemessung*) and Design Verification (*Nachweis*), respectively Proof. Of special focus thereby is the strength verification of non-cracked structural components (regime micro-cracking) and the fracture mechanics verification of cracked components (macro-cracking).

Strength verification of non-cracked structural components is demonstrated by SFCs if
"N*o relevant limit failure state is met* considering *all dimensioning load cases".*

The size of the (macro-)damage decides whether it is to apply a Strength Failure Condition SFC, $F = 1$, **(now most often termed strength criterion, which originally means** $F = <=> 1$**)** for the verification of onset-of-fracture of the un-cracked structural part or a fracture mechanics-based Damage Tolerance Condition in case of a technical crack. *Fig.1-2* gives hints where which verification procedure is to apply or in other words: When must be fracture mechanics used and when strength mechanics? The figure refers to: (a) Strength Mechanics versus Linear Elastic Fracture Mechanics (LEFM) analysis; (b) Crack-free and crack-driven fracture through a_0 being an initial flaw size (surface flaw) or a developed crack (for instance an internal delamination). Further, *Fig.1-2* depicts in b where the different technical failure types Normal Fracture NF, Shear Fracture SF and Shear Yielding SY are located.
In order to understand the mechanisms of crack growth itself, it is necessary to consider the phenomena at the tip of a crack on a microscopic level. On the modelling-desired macroscopic structural level, however, such an approach is not practical. Therefore, Fracture Mechanics FM works on a macroscopic scale, and tries to determine parameters from structural response results.

Reliable structural designs are searched in design on various theoretical bases:
Continuum Mechanics ↔ Continuum (micro-)Damage Mechanics ↔ (macro-)Damage Mechanics, the latter with its Fracture Mechanics based Damage Tolerance analysis tools in case of cracks.

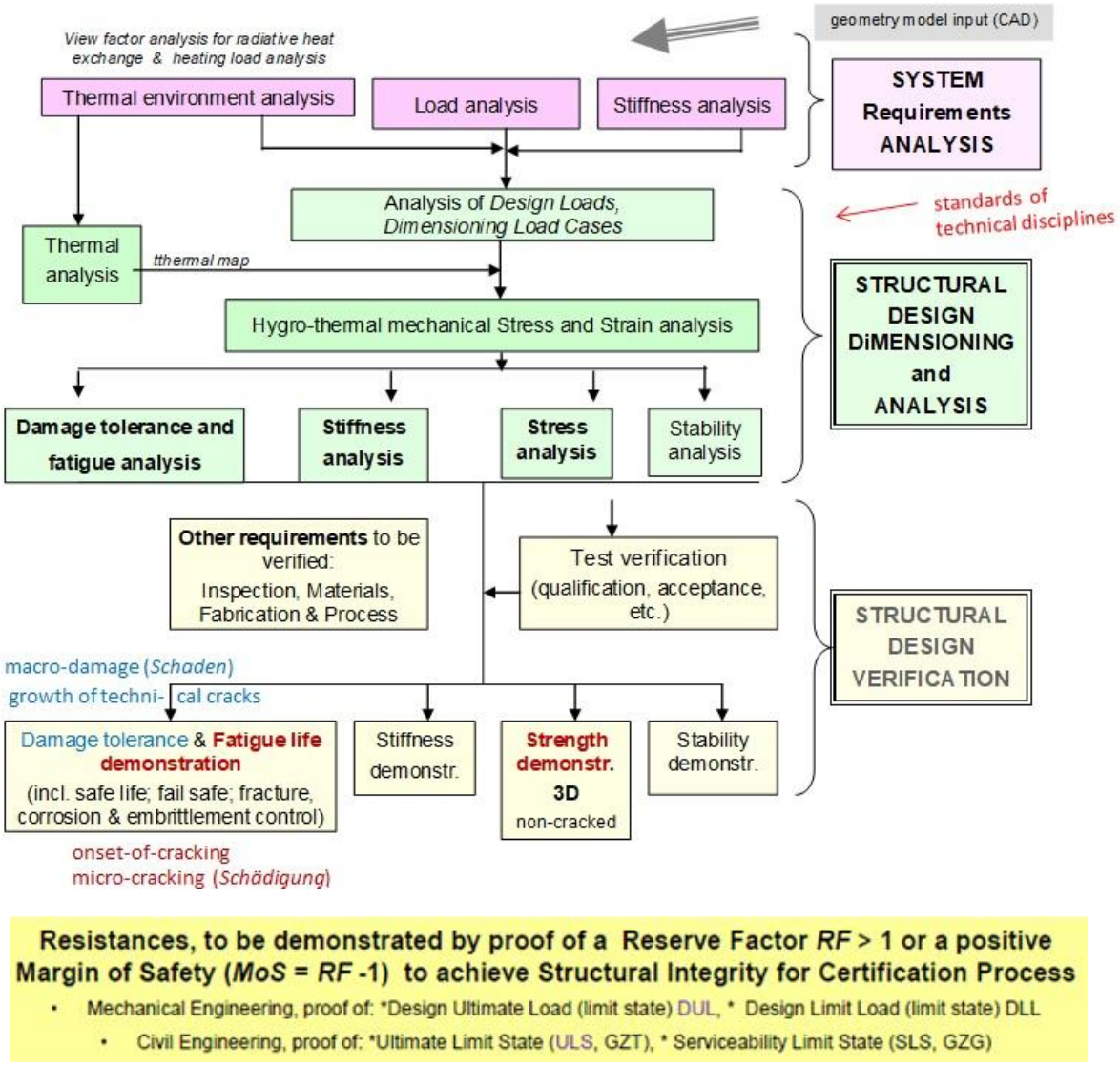


Fig.1-1: Structural engineer's tasks and complete work flow in structural design

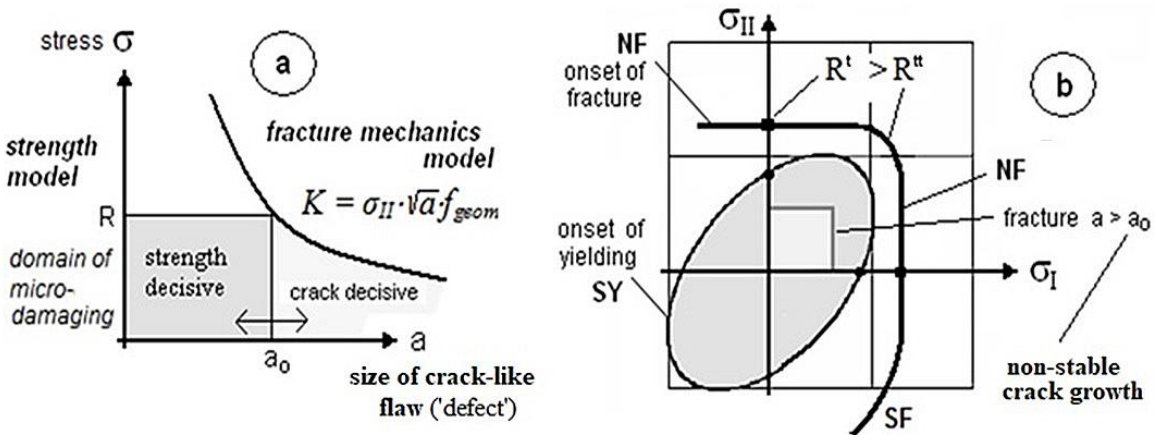


Fig.1-2: (a) Continuum mechanics strength analysis versus fracture mechanics analysis. (b) Crack free fracture onset and crack-driven fracture through f a crack geometry factor, a_0 the initial flaw size (surface flaw, delamination, ..), K is stress intensity factor, a is crack size, NF Normal Fracture, SF Shear Fracture, R is strength value, ^{t} means tensile. σ_{II} is principal stress

‘Unclearness‘or Fuzziness (Unschärfe) is inherent in loadings, strengths, and other design variables such as geometrical parameters, applied engineering models, etc. All these uncertainty sources in design contribute to the overall Structural Risk defined here arbitrarily as Amount of CoSts - *incurred in the case of Later Failure* - times the Probability that the distinct Failure occurs in the structural part. Risk drives the designer to follow *Table 1-1*.

Table 1-1: Design objectives and process

Objective: Reliable Structural Components

Design = compromise of *Design–to-CoSt* and *Design-to-Quality*. Robust design helps to ‘safely’ accept smaller design changes and to ‘survive’ manufacturing flaws, and this saves money and trouble! Optimization-to-production is mandatory considering (as-built, effects-of–flaws and *Design-to-Non-destructive inspection*).

Functional Integration is a basic driver especially with composites when viewing CoSts. Thereby the two essential requirements have to be fulfilled:

- Functional Requirements (tasks to let the developers know what to build, to let the testers know what tests are to run, to let stakeholders know what they are getting [Wikipedia]) and
- Operational Requirements (needed performance capabilities, lifetime etc.)

Aim: Reduction of design uncertainties

Means: Sort out the weakest links in the development process which involve the highest uncertainties. Most often the loadings are the most uncertain design parameters.

Tight schedule constraints often lead to a so-called Success-oriented Development Logic. This however requires excellent specifications, a consistent design philosophy including safety concept with FoS, nonlinear analyses, true and mean (σ,ε)-curves; efficient design methods including strength design allowables and validated failure conditions, mean geometry; a practical risk judging and Simultaneous Engineering..

The next tables present a short survey on loading conditions and Load Cases LC. To consider are effects such as media, temperature, creeping, aging, relaxing.

Table 1-2: Loading types for the design

Static loading: *strength*

Validated 3D strength failure conditions for isotropic (foam, concrete, PMMA,..), transversely-isotropic UD materials, and orthotropic materials (e.g. textiles) to determine ‘Onset-of-fracture‘ and ‘Final fracture‘ in case of benign failure behavior (quasi-ductile).
Standardization of material test procedures, test specimens, test rigs, and test data evaluation for a comparably good structural analysis input.
Consideration of manufacturing imperfections (tolerance width of uncertain design variables) in order to achieve a production CoSt minimum by ”Design-to-Imperfections“, which includes flaws (avoid the term defect) .

Dynamic loading: *hazards, impact, crash loading, blast*

Cyclic loading: *fatigue and crack growth*

Concern is the development of practical, physically-based lifetime-prediction methods and the generation of SN curve test data for the validation of the prediction models, crack growth models, delamination growth models if laminates.

Here, a short note on the Safety Concept might be applied. More details are presented later.

Table 1-3: Design load analysis, loadings, combinations of loadings & Load Cases LC - Mechanical Engineering and Civil Engineering

Design Loadings:

Estimation of all external + internal loadings of the structural component:
- mechanical (static, cyclic, and dynamic) and hygro-thermal,
- acoustical environment as well as of the
- corresponding lifetime requirements (duration, number of cycles)

Loadings are specified by
a Technical Specification from the customer, or an authority or
a common standard (EC codes, DIN, EN, FAA, ESA, automotive, wind energy, ...)

Otherwise a load(ings) analysis is required = Establishment of load events the structure is likely to experience (= load history). Dynamic structural system analysis performed to estimate the loadings. *Examples: launcher in aerospace, 'old' bridge refurbishment in construction*

Combinations of Loadings: → *structural specifications*

Involve usually a Worst Case scenario, w.r.t. combinations of loadings, temperature and moisture, and undetected damage.

→ Set of Combinations of Loadings termed Load Cases (LCs). From this usually vast number of Load Cases - if possible - a minimum

→ Set of (*design driving*) Dimensional Load Cases (DLCs) should be extracted for fast decisions in the case of input changes, to by-pass an FEA output evaluation death and to automatically provide the engineer with a better understanding of the structure's behavior**.**



The caiman mother Maria observes the limit "No trespassing (No pase!)". That was very good for the personal health of my friend Eddi (he unfortunately fell in front of her snout while running away).
We learn: Structural engineers should always observe the limits set by the structural specifications. That is very good for structural health [*Cuntze 2013*]

Design Dimensioning and Design Verification are performed on different structural levels, see *Table 1-4* . The bold letters show the focus viewed here.

Table 1-4: Levels of Design Verification with respect to Static Strength

- Structure level : forces & moments (resistance of a truss element *strut*)
- Cross-section level : section forces (stress resultants) & section moments (resistance of a *shell wall*)
- **Material level : stresses** (strength at a material point, *envisaged most often and here*).

Structural load-carrying capacity is mainly *locally* determined by the stress state in the critical material locations, such as in:

* **undisturbed areas** (uniform material areas, membrane areas etc.),
* disturbed areas (discontinuities such as joints, notches etc.).

Assessment of stress states at critical locations is to be performed for the material families:

* **isotropic material** (concrete, glass, etc.)
* **transversely-isotropic material** (UD := uni-directional material)
* **orthotropic (rhombically-isotropic) material** (textiles etc.).

* The construction (*Bauweise*) of a load-carrying structure must be suitable for the intended task and the materials must then correctly meet the required properties locally
* All designed products should be manufacturable, testable, and maintainable
* Materials used must have known, reliable, and reproducible properties and shall have proven resistance to the environment envisaged
* It has to be shown by:
  - Analyses that the design meets the requirements
  - Manufacturing with Quality Assurance that the structural product meets the requirements
  - Structural Test that the requirements are verified.

Mind: Industry seeks to replace the expensive 'Make and Test' design method by verified and benchmarked predictive tools that engineers could use with confidence. Then, however, the limitations of these predictive tools such as the 'strength failure conditions' should be clearly described.

In *Fig.1-3* the general procedure and a simple static strength verification procedure is visualized for completeness, depicting the levels of possible design verification. The highest level is the load level and the lowest the stress level, where one should better use validated SFCs instead of dbious interaction formulas.

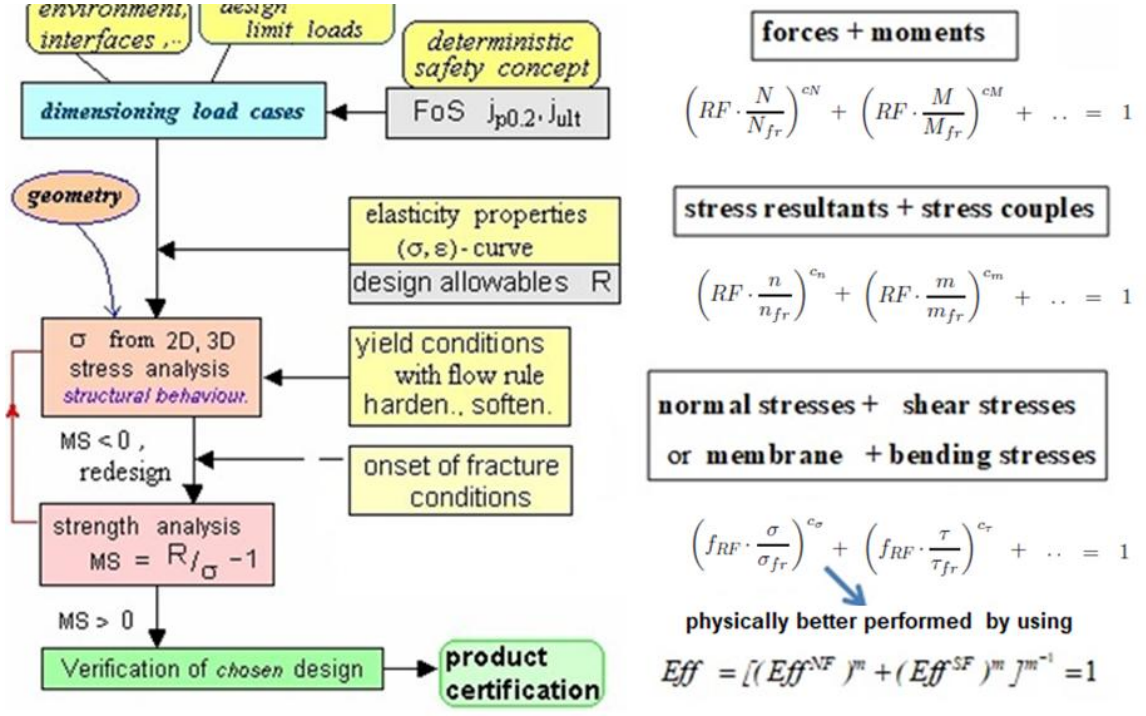


Fig.1-3: Static strength verification procedure. (design) Factor of Safety j, strength R, stress σ. Exponents c from tests, handbooks. λ is a so-called loading multiplier, which corresponds to some extent to RF

Design Dimensioning and Design Verification are to perform considering different stress situations, see *Table 1-5.*

Table 1-5: Analysis Levels of the structural component – static & cyclic

- Stress, locally at a critical material location ('point'): *using strength mechanics.*

Micro-damage domain. Verification by uniaxial ('basic') strengths and multi-axial strength criteria. Applied stresses are local stresses (continuum mechanics, regarding the cyclic growth of initially most often a diffuse and later a localized micro-damage)

- Stress concentration at a notch (often joints): *using notch mechanics.*
  Verification by a notch strength (usually 'Neuber-like', Nuismer, etc.). Applied stress peaks.
  Mind: SN curves of plain material narrow 'notched' SN curves
- Stress 'intensity' (stress intensity factor) at a crack tip: *using fracture mechanics*.
  Macro-damage. Verification by fracture toughness K_{cr} or a critical energy release rate $\mathcal{G}_{cr}$ (energy–related). Applied stresses are 'far'-field stresses (*far from the crack-tip*).
  Task: Cyclic growth of a detected 'technical damage' (i.e. inter-laminar delamination).

Each failure mode contributes to the experienced micro-damage or macro-damage activated by the 3D-stress state:

Strength Mechanics:
If all strength failure modes are activated then the SFC, beyond which onset-of-failure will occur, reads $Eff = f(Eff^{modes}) = 1 = 100\%$ with Eff the so-called material stressing effort (*Werkstoffanstrengung*).

Fracture Mechanics:
If all fracture mechanics failure modes are activated then the failure condition beyond which the crack will begin to propagate reads $\mathcal{G} / \mathcal{G}_{cr} = 1$ with $\mathcal{G} = \mathcal{G}_I + \mathcal{G}_{II} + \mathcal{G}_{III}$ with $\mathcal{G}_{cr}$ the critical energy release rate. For a general stress state the ('tension-related' linear elastic) fracture mechanics situation is fully similar to strength mechanics.

Urgent need to move to 3D failure analysis:

FEA output delivers 3D stress states if required and these are then to assess. Such stress states are encountered in submarine hulls, bolted and screwed joints, in bearings, in the foot of a hoop-reinforced concrete strut, after impact and ballistics, hazards and in applications like inner surface of composite high pressure vessels. In the past, mainly specific and effortful experimental investigations have been performed including 2D and 3D compression (*such as hydrostatic pressure loading p_{hyd}. Thanks for doing it*) and not so much effort was put on analytical investigations. In consequence, there is a strong need to validate failure conditions in the compression domain. 2D models are not sufficient to describe the fracture progress of brittle behaving isotropic materials such as grey cast iron, rock material, concrete, UD-material etc.
For instance an example from tests on Ultra-High-Performance-Concrete proofs that the consideration of a realistic 3D stress state promises advantages: A failure stress state in MPa of (-160, 0, 0) fully corresponds to (-224 -6, -6, -6). In both the cases is $F = 1$ or is 'Onset-of-Fracture' Failure met! → Conclusion: A 3D failure theory with experimental evidence is needed.

Linear and non-linear structural analyses:

Linear and non-linear structural analyses are to perform considering all (D)LCs and design limit states $\mathcal{G}$ which represent all failure modes, Table 1-6. Often the aim of non-linear analysis is just: „Save a structural design or a still produced structure" by making the hidden load carrying reserves visible. Hidden, practically means, that linear analysis was only used in design.

Mind in non-linear analysis, nevertheless:

Standard survival probabilities shall be kept as usually applied in the linear case.

Table 1-6: Linear and nonlinear structural analyses for each LC

Linear Analysis**:** action *S* (stress level) < material resistance *R* (strength)
3D-stress state Design Dimensioning or design dimensioning
with section quantities which depend on the distribution of the structure's stiffness.
Non-linear Analysis**:** action *E* (*Einwirkung*, load level) < structural resistance *W* (*Widerstand*) .

LL:

- *Statically in-determinate structures are redundant and must be treated differently to the statically determinate ones (one load path). Principally, in order to avoid either to be too conservative or too un-conservative, a separation of the always needed analysis of the average structural behavior in Design Dimensioning from the finally following Design Verification is required.*
- *It must be applied: (1) An average σ-ε curve and characteristic (= typical, average) design parameters (Example statically indeterminate continuous beam: Determination for Design Dimensioning of the most realistic section quantities with 50% probability of expectation for the following local cross-section proofs (However, exemplarily, but not only: EuroCode2 reduces the Young's modulus of the compressive stress-strain curve of the concrete. No physical reason given?). (2) Design values: Consideration of minimum values for strength and min, mean or max as project task-required for other properties.*
- *In order to live a consistent design philosophy the higher true stresses as outcome of the material non-linear analysis should be assessed by the higher true strength design allowables.*

Structural Integrity and Design principles in 'Dynamic/Cyclic' Design

The next figure visualizes the design principles in the case of cyclic loading. Depicted are the required A- and B-Design Allowables to be applied aerospace (civil aircraft) and military aircraft with the statistically higher srength B-values.

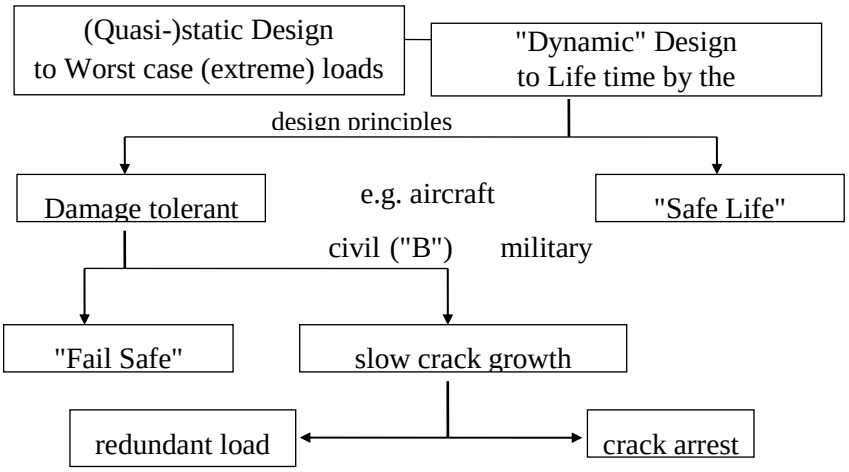


Fig. 1-4: Damage tolerant design principles of a structure

With a design concept in place, all aspects of Structural Integrity need to be assessed in relation to the total life expectancy of the structural part [ESA]. In this context structural integrity control is addressed for the component, the sub-assembly and for the assembled structure or system based on the following issues:

- In what environments is the structural part expected to operate?

- Which are the requirements on structural and material durability?
- Which are the damage tolerance implications for the material of construction? E.g. metal alloys or composites
- What is the fatigue environment in respect of mechanical, acoustic or thermal loading?
- Should Safe-life or Fail-safe principles be applied? This will influence the (design) safety factors?
- Which are the inspection requirements over the life of the structure and does this influence the design?

2 different design principles (philosophies), "Safe Life" and "Damage Tolerance", were depicted in *Fig.1-4*

- Safe Life Design Principle:

  By this principle the structure is thought defect-free over lifetime. The principle is applicable to all types of structures, monolithic as well as redundant elements.

- Damage Tolerance Design Principle:

  A damage tolerant structure can endure the specified design limit load DLL even in case of a pre-damage caused e.g. by fatigue as long as the macro-damage will be discovered by inspection or malfunction and will be repaired. (*This approach differs from the original Fail-Safe philosophy in that it assumes cracks of the smallest allowable size to exist in the structure already at the very first load cycle. Also, a distinction is made between in service-inspectable and non-inspectable structures*). The procedure includes the determination of the macro-damage type and size allowed by the required performance level. Type and size which is not allowed have to be found by inspection. For this reason, the probability of being detected or not detected is important.

In order to achieve structural integrity for composite components, an old but still valid certification procedure for 'Composite Materials' such as for laminates composed of FRP-layers (*smearable when modelling*) shall be depicted and further - similarly applicable - for merely smearable 'Material Composites' such as a bar-grid–reinforced concrete, see *Fig.1-5*.

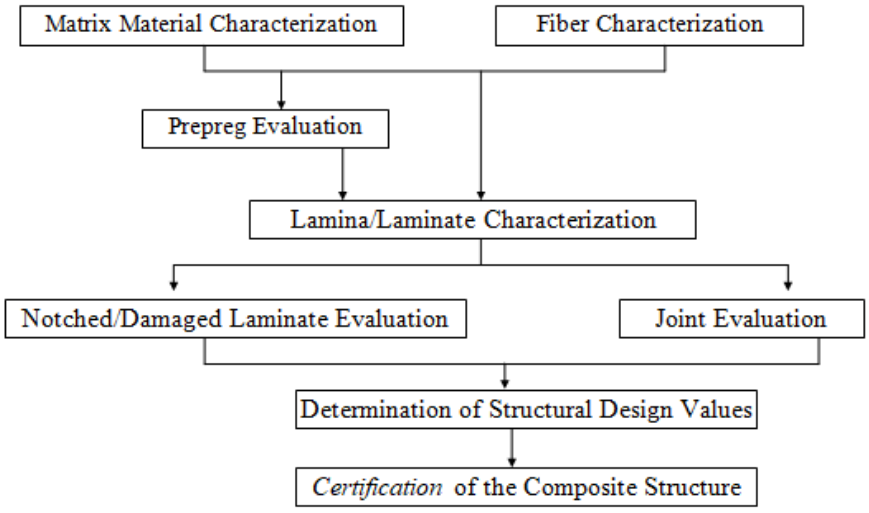


Fig. 1-5: Procedure proposed [MIL-HDBK-17-3C]

Safety Concept Please, see § 8.3 and §13 for details

1.2 Scheme of Strength Failure Criteria (SFCs) with potential Missing Links

In the development of structural components the application of 3D-validated strength failure conditions SFCs *(the function is a condition F = 1 and the design request is whether F < 1, a 'criterion')* is one essential pre-condition for achieving the required fidelity for the user. This includes Yield Failure Conditions (ductile behavior) for the non-linear analysis of the material and the Onset-of-Yield limit verification. It further includes conditions to verify that Onset-of-Fracture does not occur, in the case of brittle and ductile behavior.

Since two decades the author believes in a macroscopically-phenomenological 'complete classification' system, where all strength failure types are included, see *Fig.1-6*. In his assumed system several relationships may be recognized: (1) Shear stress yielding SY, followed by Shear fracture SF addressing 'dense' materials. For porous materials under compression, the SF for dense materials is replaced by crushing fracture CrF. (2) However, to complete a system beside SY also NY should exist. Usual light-weight materials exhibit SY ('Mises'), whereas polymers may further show NY due to crazing! For instance PMMA (plexiglass) with its chain-based texture shows NY. The right side of the scheme shows that a similarity of isotropic materials with UD materials exists. Cuntze developed the 5 'generic' fiber strength failure modes FF1 - IFF3 and further derived a CrF teplacing IFF2 (SY).

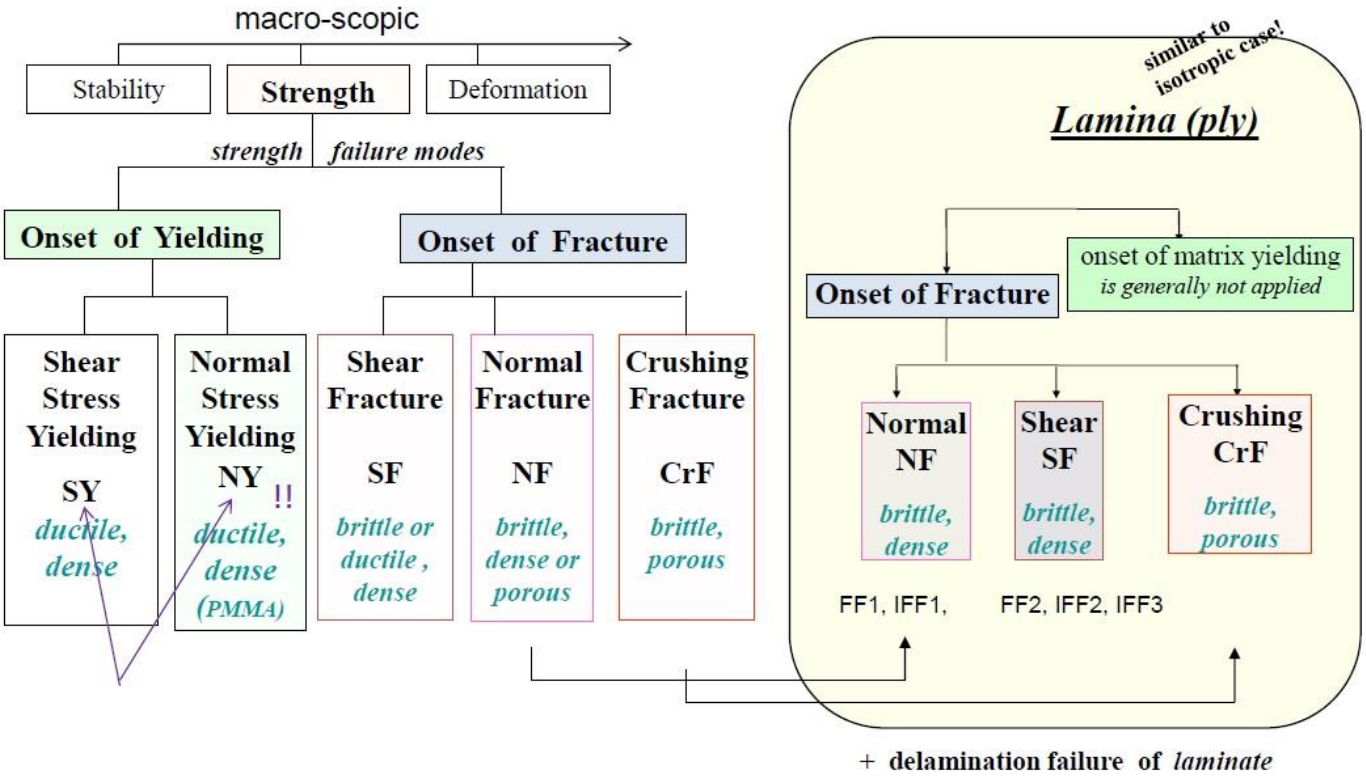


Fig.1-6: Author-proposed scheme to outline interrelations of isotropic and UD materials. Lamina (ply)= lamella in construction.

Capturing all kinds of possible types of failure in a uniform classification scheme is challenging, because the classification can be carried out according to different ways. The author thinks that a material behavior-overarching system delivers a good classification scheme for a macro-mechanics

building including the 3 structural material families. This scheme should be clear and as simple as possible for the dimensioning structural engineer without violating any material-typical facts.
In consequence, the author may conclude:

If one knows from a similar behaving material some material facts,
that can be transferred to the behavior of the 'new' material,
then pre-dimensioning with the new material becomes easier and more trusting!

LL:

- *There are coincidences between brittle UD laminas and brittle isotropic materials*
- *With composites: After an initial matrix yielding of the more or less ductile polymer matrix follows 'Quasi-Yielding' due to diffuse micro-cracking. Increased degradation occurs in the laminate beyond onset of the first Inter-Fiber-Failure IFF*
- *What may be learned from Fig.1-4 and from studying the associated failure conditions? If the shear stress yielding mechanism is still active until fracture its yield failure function remains at least part of the formulation of the fracture failure function F. Or, the same mathematical form of a failure condition (means interaction of stresses within one mode) may be valid from Onset-of-Yielding SY to Onset-of-Fracture SF if the physical mechanism remains, such as with shear yielding in case of ductile steels*
- *Today's FEA gives 3D FE stress results as output. The evaluation of these 3D stress states therefore requires 3D conditions that predict the onset-of-failure. Unfortunately, due to a lack of 3D test results, the known standard 'global' SFCs – even for isotropic materials – are usually not sufficiently well 3D-validated.*
- *A software analysis model is validated by test, whereas a*
- *A hardware/structure is qualified by test*
- *A design is verified by test.*
- *Software Model Verification: „Solve the equations right"*
- *Software Model Validation: „Solve the right equations" (needs testing).*

From above follows an advantage when material symmetry knowledge is applied: Presuming, homogeneity is a valid assessment for the project task-determined model, just a minimum number of properties must be measured, only. This offers significant benefits in CoSt and time.

The author sees two missing links or empty rooms, see *Fig.1-7*, in the assumed Strength Mechanics Building: Why are there not also 2 yield modes (*as still mentioned*) and 2 'basic' critical stress intensity factors (*fracture toughness entities*), only?'

Strength Mechanics		**Fracture Mechanics**
SY	*known*	$K^{t}_{Icr} \equiv K_{Ic}$, K_{IIc}, K_{IIIc} **(tension, shear)**
Normal Yielding NY		K^{c}_{IIcr} **(compression)**

Fig.1-7: Isotropic material, the two searched 'rooms' or missing links ***NY***, $\boldsymbol{K_{IIcr}^{c}}$

(1) ***NY:*** Is there Normal Yielding***?***
NY is known for a long time, but not in structural mechanics design. An explanation for the 'Not known' is that a describing yield failure condition F^{NY} was missing. For establishing this missing link in his 'complete system' the author found applicable test data which he evaluated and mapped with his model and visualized in chapter 5. → Proof is given.
(2) $\boldsymbol{K_{IIcr}^{c}}$**:** Is there a Critical Stress Intensity Factor (SIF) under compression or a fracture toughness under a compression-induced shear, respectively?

Here, the author remembers a two decades old citation of A. Carpinteri that approximately reads: "With homogeneous isotropic brittle materials there are 2 real energy release rates $\mathcal{G}_{Icr}$, $\mathcal{G}_{IIcr}$, one in tension and one in compression. These two $\mathcal{G}s = K^2 \cdot (1-\nu^2) / E$ (*formally, plane strain case*) possess the attribute that the crack plane does not turn and are therefore real (*or 'basic'*) material properties". This forced the author at that time to intensively search K_{IIcr}^{c} as the basic pendant to K_{Icr}^{t}, officially indexed K_{Ic} in fracture mechanics FM, and to postulate in the sense of Carpinteri: "***Only a stable crack growth plane-associated (****self-similar crack growth****) SIF is a 'basic' FM property"***. This is valid in the tension domain for the SIF $K_{Ic} \equiv \boldsymbol{K_{Icr}^{t}}$ above and not for the *model-necessary* K_{IIc} and K_{IIIc}. It should be valid in the compression domain, too, that means failure is shear-linked, which requires to write $\boldsymbol{K_{IIcr}^{c}}$. This missing link will be presented by the author in chapter 6. The author admits at this point that this SIF is not relevant for the treatment of common fracture-mechanical tasks in the compression range because it requires an ideal homogeneous crack-tip situation of a pretty brittle material. However, he believes that the proof of $\mathbf{K_{IIcr}^{c}}$ is an important theoretical task for achieving the desired 'complete system or building'.

1.3 Material properties, Tables, international designations and Invariants

Before treating properties some definitions are presented in order to distiguish all addressed topics accurately. Structural composites can be metallic, non-metallic or a hybrid combination thereof. One distinguishes two structural composite types: Material Composite (*Werkstoffverbund*) and Composite Material (*Verbundwerkstoff*). In this context: Structural Material is usually the model of a homogenized more complex solid *(on the considered scale or level the homogenized model of the envisaged complex solid is modelled as a smeared solid. The objective usually is a macro-model).*

Material Composite is structural-mechanically a composite 'construction of different materials *(a not smearable 'conglomerate' such as i.e. carbon fiber grid-reinforced concrete which is not a 'composite material' despite it is usually termed so.*

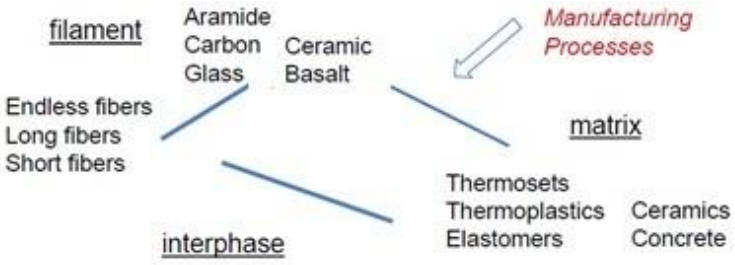
Composite Material is a combination of constituent materials, different in composition (*constituents retain their identities in the composite; that is, they do not dissolve or otherwise merge completely into each other although they act in concert. Normally the constituents can be physically identified, and there is an interface between them to consider regarding its interphase material). This type is hopefully homogenizable to a smeared material such as UD-ply, lamella, short fiber-reinforced concrete, foam etc.*

Very essential for this paper are the fiber-reinforced leightweight materials with its various combinations including polymer matrix and mineral matrix, see *Fig.1-8*. Traditional epoxy resin systems deliver rigid thermoset structures after curing, excellent properties but recycling of the FRP-composite is pretty difficult. Residual stresses from curing are inherent and can merely lowered by a heat treatment process.Thermo-plastics can be deformed after curing and are recycling-friendly and suffer not from residual stresses but have distinct shortcomings in the process. Both, these traditional polymers might be topped by the new VITRIMAX (*US company Mallinda*), that allows bonding across the interface of prepreg-layers even after curing, and this 'endless'. Recycling and residual stresses then would be no problem.

In the context of *Fig.1-8*, various combinations of different constituents building up the final homogenized (*hopefully 'smearing' is possible*) material are possible and to model.

Mind:

Lamina properties used as input for the analysis are test results from *isolated* UD lamina specimens such as a tensile coupon. They are load-controlled derived and the results are of weakest link type whereas the in-situ behavior of an *embedded* UD lamina is deformation-



Filaments: glass, aramide, carbon, ceramics, ..

Fibre preforms from ***roving, tape, weave, braid (2D, 3D)***
knit, stitch, or mixed
as in a ***preform hybrid***
non-crimp fabric laminates



PP/glass/aramidePEEK/
glass –filament-yarn

Matrices : thermosets, thermoplastics, ceramics, concrete, ..

Polymers (crystalline and amorphous)		
Plastics		Elastomers
thermo-plastics	thermo-sets	
Acrylic, polycarbonat, polyimide, polypropylene	epoxy, phenolic, polyurethane, silicon	natural rubber, silicone rubber, polyurethan elastomer

polymers are also bonding materials *(3D understanding)*

Manufacturing: pre-pregging, wet winding, Resin Transfer Molding, casting, SMC, shotcrete

Polymers (crystalline and amorphous)		
Plastics		Elastomers
thermo-plastics	thermo-sets	
Acrylic, polycarbonat, polyimide, polypropylene	epoxy, phenolic, polyurethane, silicon	natural rubber, silicone rubber, polyurethan elastomer

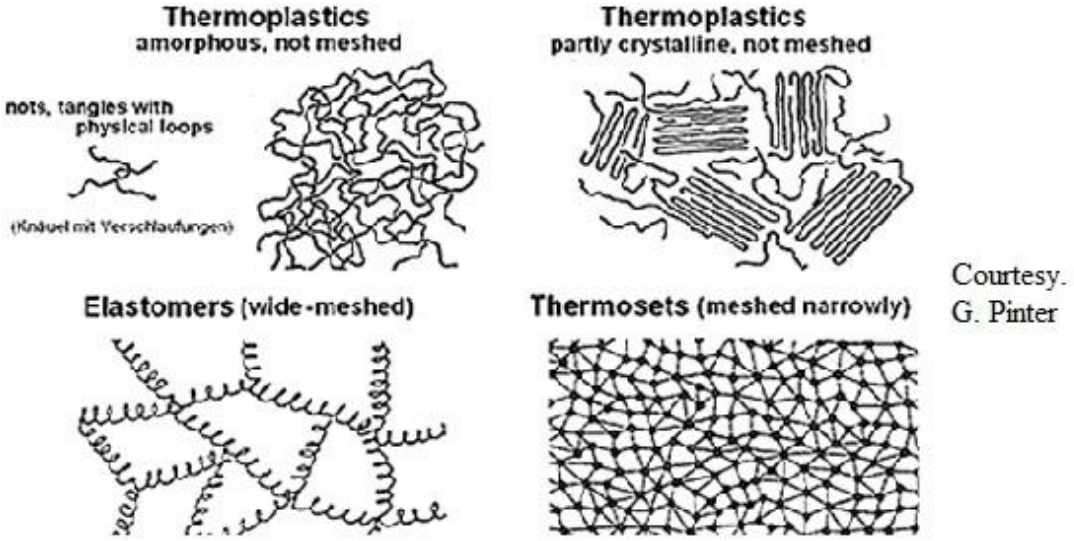


Fig.1-8: Possible combinations of different constituents with various polymers used
Filaments: bor B, glass G, aramide A, carbon C, ceramics, basalt Bs, ..

controlled and therefore of redundant type. This fact shows up that a good mapping of the course (strain-hardening) of 'isolated UD test data' does not involve the full information (strain-softening) necessary for a qualified analysis of laminates which consist of a stack of embedded laminas. Effect of curing-based residual stresses and environment is dependent on hygro-thermal stresses. *Effect of the difference of stress-strain curves of e.g. the usually isolated UD test specimen and the embedded UD lamina (*redundancy, strain-softening part too).*

Notes on some designations:

*As a consequence to isotropic materials (*European standardization*) the letter *R* (≡ f in construction) has to be used for strength. US notations for UD material with letters X (*direction 1*, ∥) and Y (*direction 2*, ⊥) confuse with the structural axes' descriptions X and Y. * R_m := 'resistance maximale' (French) = tensile fracture strength (superscript ^{t} is usually skipped because design runs in tensile domain), *R* is basic strength. Composites are most often brittle and only slightly porous! SF is shear fracture, NF Normal Fracture.

In the following *Tables1-2a* through *1-2c,* on basis of investigations for the VDI-2014 and the formerly planned novel ESA Materials Handbook, Cuntze proposed internationally not confusing designatios for the strength properties and for the physical properties.

Table 1-2a: Self-explaining symbolic designations for strength properties

	Fracture Strength Properties									
	loading	**tension**			**compression**			**shear**			
	direction or **plane**	1	2	3	1	2	3	12	23	13	
9	**general orthotropic**	R_1^t	R_2^t	R_3^t	R_1^c	R_2^c	R_3^c	R_{12}	R_{23}	R_{13}	**friction properties**
5	**UD**	$R_{\parallel}^{\ t}$ NF	$R_{\perp}^{\ t}$ NF	$R_{\perp}^{\ t}$ NF	$R_{\parallel}^{\ c}$ SF	$R_{\perp}^{\ c}$ SF	$R_{\perp}^{\ c}$ SF	$R_{\parallel\perp}$ SF	$R_{\perp\perp}$ NF	$R_{\parallel\perp}$ SF	$\mu_{\perp\perp}$, $\mu_{\perp\parallel}$
6	**fabrics**	R_W^t	R_F^t	R_3^t	R_W^c	R_F^c	R_3^c	R_{WF}	R_{F3}	R_{W3}	$Warp = Fill$
9	**fabrics general**	R_W^t	R_F^t	R_3^t	R_W^c	R_F^c	R_3^c	R_{WF}	R_{F3}	R_{W3}	μ_{W3}, μ_{F3}, μ_{WF}
5	**mat**	R^t	R^t	R_3^t	R^c	R^c	R_3^c	R^τ	R^τ	R^τ	*(≡UD material with turned direction)*
2	**isotropic matrix**	R^t SF	R^t SF	R^t SF	*deformation-limited, cylindrical test specimen bulges: What is then R^c?*			R^τ	R^τ	R^τ	μ
		R^t NF	R^t NF	R^t NF	R^c SF	R^c SF	R^c SF	R^τ NF !	R^τ NF	R^τ NF	μ

number of independent properties due to material symmetry of isotropic materials

Table 1-2b: Self-explaining symbolic designations for elasticity properties

		Elasticity Properties									
	direction or plane	1	2	3	1	2	3	12	23	13	
9	*general orthotropic*	E_1	E_2	E_3	G_{12}	G_{23}	G_{13}	ν_{12}	ν_{23}	ν_{13}	**comments**
5	*UD, ≅ non-crimp fabrics*	$E_{\parallel}$	$E_{\perp}$	$E_{\perp}$	$G_{\parallel\perp}$	$G_{\perp\perp}$	$G_{\parallel\perp}$	$\nu_{\parallel\perp}$	$\nu_{\perp\perp}$	$\nu_{\parallel\perp}$	$G_{\perp\perp} = E_{\perp} /(2+2\nu_{\perp\perp})$ $\nu_{\perp\parallel} = \nu_{\parallel\perp} \cdot E_{\perp} / E_{\parallel}$ *3 is perpendicular to quasi-isotropic 2-3-plane*
6	*fabrics*	E_W	E_F	E_3	G_{WF}	G_{W3}	G_{W3}	ν_{WF}	ν_{W3}	ν_{W3}	*Warp = Fill*
9	*fabrics general*	E_W	E_F	E_3	G_{WF}	G_{W3}	G_{F3}	ν_{WF}	ν_{F3}	ν_{W3}	*Warp ≠ Fill*
5	*mat*	E	E	E_3	G	G_3	G_3	ν	ν_3	ν_3	*G = E /(2+2v) 1 is perpendicular to quasi-isotropic mat plane*
2	*isotropic for comparison*	E	E	E	G	G	G	ν	ν	ν	*G=E /(2+2v)*

Table 1-2c: Self-explaining symbolic designations for hygro-thermal properties

Hygro-thermal properties							
direction, or plane	1	2	3	1	2	3	
general orthotropic	α_{T1}	α_{T2}	α_{T3}	α_{M1}	α_{M2}	α_{M3}	comments
UD, ≅ non-crimp fabrics	$\alpha_{T\parallel}$	$\alpha_{T\perp}$	$\alpha_{T\perp}$	$\alpha_{M\parallel}$	$\alpha_{M\perp}$	$\alpha_{M\perp}$	
fabrics	α_{TW}	α_{TW}	α_{T3}	α_{MW}	α_{MW}	α_{M3}	*Warp = Fill*
fabrics general	α_{TW}	α_{TF}	α_{F3}	α_{MW}	α_{MF}	α_{M3}	*Warp ≠ Fill*
mat	α_T	α_T	α_{T3}	α_M	α_M	α_{M3}	
isotropic	α_T	α_T	α_T	α_M	α_M	α_M	

Comments on properties to be used in analysis:

- Properties are 'agreed' values to achieve a common and comparable design basis
- Properties must be provided with average value and coefficient of variation cov
- Sources of uncertainty should be investigated, because changing a certified material is economically seldom possible

- Model parameters should be measurable, unambiguously properties and physically self-explaining
- Variety of composite properties: Many properties for design and manufacturing are not yet available
- Generally valid for materials: A 3D-stress assessment is not possible on basis of uniaxial strength values alone. Knowledge of material internal friction values, following Mohr-Coulomb, is mandatory in the compression domain (see *Table 1-2a*)
- Suffix of Poisson's ratio: use Maxwell-Betti, check analogously to $\nu_{\perp\square} \cdot E_{\perp} = \nu_{\square\perp} \cdot E_{\square}$
- Shear strains in CLT, α_{Txy} (*elaboration Erik Kappel, DLR, September 2022*): Usually the strains are based on engineering strain formulation $\gamma_{xy,}$ as with the VDI 2014. However, some authors define thermal shear strains *tensorial* and others *engineering-like* which means a factor 2 is to consider, because $\gamma_{eng} = 2 \cdot \gamma_{tens}$. This has an effect on the input of α_{Txy} . ABAQUS follows VDI 2014.

And the strength properties displayed in a vector format:

Isotropic: $\{R\} = (R^t, R^c)^T$ with μ

Transversely-isotropic: $\{R\} = (R^t_{\parallel}, R^c_{\parallel}, R^t_{\perp}, R^c_{\perp}, R_{\perp\parallel})^T$ with $\mu_{\perp\square}, \mu_{\perp\perp}$

Orthotropic: $\{R\} = (R^t_W,\ R^c_W,\ R^t_F,\ R^c_F,\ R_{WF},\ R^t_3,\ R^c_3,\ R_{3F},\ R_{3W})^T$ with $\mu_{WF}, \mu_{3W}, \mu_{3F}$

For a better understanding of the body text the stress-strain relations of the investigated 3 material families are added now:

3D: $\{\varepsilon\} = [S] \cdot \{\sigma\}$ with $[S]$ *C*ompliance matrix, $\{\sigma\} = [C] \cdot \{\varepsilon\}$ with $[C]$ *S*tiffness matrix

Table 1-3: General elasticity matrices, generalized Hooke's law, tensorial format for compliance S and stiffness C

$$\begin{Bmatrix} \varepsilon_{11} \\ \varepsilon_{22} \\ \varepsilon_{33} \\ 2\varepsilon_{23} \\ 2\varepsilon_{13} \\ 2\varepsilon_{12} \end{Bmatrix} = \begin{bmatrix} S_{1111} & S_{1122} & S_{1133} & 2S_{1123} & 2S_{1113} & 2S_{1112} \\ S_{1122} & S_{2222} & S_{2233} & 2S_{2223} & 2S_{2213} & 2S_{2212} \\ S_{1133} & S_{2233} & S_{3333} & 2S_{3323} & 2S_{3313} & 2S_{3312} \\ 2S_{1123} & 2S_{2223} & 2S_{3323} & 4S_{2323} & 4S_{2313} & 4S_{2312} \\ 2S_{1113} & 2S_{2213} & 2S_{3313} & 4S_{2313} & 4S_{1313} & 4S_{1312} \\ 2S_{1112} & 2S_{2212} & 2S_{3312} & 4S_{2312} & 4S_{1312} & 4S_{1212} \end{bmatrix} \begin{Bmatrix} \sigma_{11} \\ \sigma_{22} \\ \sigma_{33} \\ \sigma_{23} \\ \sigma_{13} \\ \sigma_{12} \end{Bmatrix}$$

$$\begin{Bmatrix} \sigma_{11} \\ \sigma_{22} \\ \sigma_{33} \\ \sigma_{23} \\ \sigma_{13} \\ \sigma_{12} \end{Bmatrix} = \begin{bmatrix} C_{1111} & C_{1122} & C_{1133} & C_{1123} & C_{1113} & C_{1112} \\ C_{1122} & C_{2222} & C_{2233} & C_{2223} & C_{2213} & C_{2212} \\ C_{1133} & C_{2233} & C_{3333} & C_{3323} & C_{3313} & C_{3312} \\ C_{1123} & C_{2223} & C_{3323} & C_{2323} & C_{2313} & C_{2312} \\ C_{1113} & C_{2213} & C_{3313} & C_{2313} & C_{1313} & C_{1312} \\ C_{1112} & C_{2212} & C_{3312} & C_{2312} & C_{1312} & C_{1212} \end{bmatrix} \begin{Bmatrix} \varepsilon_{11} \\ \varepsilon_{22} \\ \varepsilon_{33} \\ 2\varepsilon_{23} \\ 2\varepsilon_{13} \\ 2\varepsilon_{12} \end{Bmatrix}$$

Generalized Hooke's law, engineering format, compliance formulations as

$$\begin{Bmatrix}\varepsilon_x\\ \varepsilon_y\\ \varepsilon_z\\ \gamma_{yz}\\ \gamma_{xz}\\ \gamma_{xy}\end{Bmatrix}=\begin{bmatrix}\frac{1}{E} & \frac{-\nu}{E} & \frac{-\nu}{E} & 0 & 0 & 0\\ \frac{-\nu}{E} & \frac{1}{E} & \frac{-\nu}{E} & 0 & 0 & 0\\ \frac{-\nu}{E} & \frac{-\nu}{E} & \frac{1}{E} & 0 & 0 & 0\\ & & & \frac{1}{G} & 0 & 0\\ & (symm.) & & & \frac{1}{G} & 0\\ & & & & & \frac{1}{G}\end{bmatrix}\cdot\begin{Bmatrix}\sigma_x\\ \sigma_y\\ \sigma_z\\ \tau_{yz}\\ \tau_{xz}\\ \tau_{xy}\end{Bmatrix},\qquad \begin{Bmatrix}\varepsilon_I\\ \varepsilon_{II}\\ \varepsilon_{III}\end{Bmatrix}=\begin{bmatrix}\frac{1}{E} & \frac{-\nu}{E} & \frac{-\nu}{E}\\ \frac{-\nu}{E} & \frac{1}{E} & \frac{-\nu}{E}\\ \frac{-\nu}{E} & \frac{-\nu}{E} & \frac{1}{E}\end{bmatrix}\cdot\begin{Bmatrix}\sigma_I\\ \sigma_{II}\\ \sigma_{III}\end{Bmatrix}$$

as fourth-order and a second-order compliances from which follows

$$E\cdot(\varepsilon_x+\varepsilon_y+\varepsilon_z)=-3\cdot\sigma_{hyd}\cdot(1-2\cdot\nu)\quad\text{or}\quad E\cdot\Delta V/V=\sigma_{hyd}\cdot(3-6\cdot\nu),$$

where the bulk modulus $K=E/(3-6\nu)$ is activated.

For UD-lamina-based materials it is valid:

3D: $\{\varepsilon\}=[S]\cdot\{\sigma\}$ with $[S]$ *c*ompliance matrix, $\{\sigma\}=[C]\cdot\{\varepsilon\}$ with $[C]$ *s*tiffness matrix

2D: $\{\varepsilon\}=[S]\cdot\{\sigma\}$ with $[S]$ *c*ompliance matrix, $\{\sigma\}=[Q]\cdot\{\varepsilon\}$ with $[Q]$ *s*tiffness matrix

$$\begin{Bmatrix}\varepsilon_1\\ \varepsilon_2\\ \varepsilon_3\\ \gamma_{23}\\ \gamma_{13}\\ \gamma_{12}\end{Bmatrix}=\begin{bmatrix}\frac{1}{E_\parallel} & \frac{-\nu_{\parallel\perp}}{E_\perp} & \frac{-\nu_{\parallel\perp}}{E_\perp} & 0 & 0 & 0\\ \frac{-\nu_{\perp\parallel}}{E_\parallel} & \frac{1}{E_\perp} & \frac{-\nu_{\perp\perp}}{E_\perp} & 0 & 0 & 0\\ \frac{-\nu_{\perp\parallel}}{E_\parallel} & \frac{-\nu_{\perp\perp}}{E_\perp} & \frac{1}{E_\perp} & 0 & 0 & 0\\ & & & \frac{1}{G_{\perp\perp}} & 0 & 0\\ & (symm.) & & & \frac{1}{G_{\parallel\perp}} & 0\\ & & & & & \frac{1}{G_{\parallel\perp}}\end{bmatrix}\cdot\begin{Bmatrix}\sigma_1\\ \sigma_2\\ \sigma_3\\ \tau_{23}\\ \tau_{13}\\ \tau_{12}\end{Bmatrix}\quad\text{or}\quad \{\varepsilon\}=[S]\,\{\sigma\}\ .$$

In typical engineering applications the stiffness elasticity matrix $\{\sigma\}=[C]\cdot\{\varepsilon\}$ reads

$$\begin{Bmatrix}\sigma_x\\ \sigma_y\\ \sigma_z\\ \tau_{yz}\\ \tau_{zy}\\ \tau_{xy}\end{Bmatrix} = \frac{E}{(1+\nu)\cdot(1-\nu)}\begin{bmatrix}1\text{-}\nu & \nu & \nu & 0 & 0 & 0\\ \nu & 1\text{-}\nu & \nu & 0 & 0 & 0\\ \nu & \nu & 1\text{-}\nu & 0 & 0 & 0\\ 0 & 0 & 0 & 0.5\cdot(1\text{-}2\nu) & 0 & 0\\ 0 & \textit{symm.} & 0 & 0 & 0.5\cdot(1\text{-}2\nu) & 0\\ 0 & 0 & 0 & 0 & 0 & 0.5\cdot(1\text{-}2\nu)\end{bmatrix}\cdot\begin{Bmatrix}\varepsilon_x\\ \varepsilon_y\\ \varepsilon_y\\ \gamma_{yz}\\ \gamma_{zy}\\ \gamma_{xy}\end{Bmatrix}$$

and for invariant investigations $\sigma_{ik} = C_{ijkl}\cdot\varepsilon_{kl}$ in matrix presentation (*C is fourth rank tensor*)

$$\begin{Bmatrix}\sigma_{xx}\\ \sigma_{yy}\\ \sigma_{zz}\\ \sigma_{yz}\\ \sigma_{zy}\\ \sigma_{xy}\end{Bmatrix} = \frac{E}{(1+\nu)\cdot(1-\nu)}\begin{bmatrix}1\text{-}\nu & \nu & \nu & 0 & 0 & 0\\ \nu & 1\text{-}\nu & \nu & 0 & 0 & 0\\ \nu & \nu & 1\text{-}\nu & 0 & 0 & 0\\ 0 & 0 & 0 & 0.5\cdot(1\text{-}2\nu) & 0 & 0\\ 0 & \textit{symm.} & 0 & 0 & 0.5\cdot(1\text{-}2\nu) & 0\\ 0 & 0 & 0 & 0 & 0 & 0.5\cdot(1\text{-}2\nu)\end{bmatrix}\cdot\begin{Bmatrix}\varepsilon_{xx}\\ \varepsilon_{yy}\\ \varepsilon_{zz}\\ 2\varepsilon_{yz}\\ 2\varepsilon_{zy}\\ 2\varepsilon_{xy}\end{Bmatrix}.$$

The spatial UD elasticity matrix [C] in the column-normalized formulation is complicated and therefore seldom documented (*HSB draft, R.Cuntze, 2014*). Therefore, S is used instead of C.

And for completion the full C and S relations of UD-composites:

$$\begin{Bmatrix}\sigma_1\\ \sigma_2\\ \sigma_3\\ \tau_{23}\\ \tau_{13}\\ \tau_{12}\end{Bmatrix} = [C]\cdot\begin{Bmatrix}\varepsilon_1\\ \varepsilon_2\\ \varepsilon_3\\ \gamma_{23}\\ \gamma_{13}\\ \gamma_{12}\end{Bmatrix} = \begin{bmatrix}C_{11} & C_{21} & C_{21} & 0 & 0 & 0\\ C_{12} & C_{22} & C_{32} & 0 & 0 & 0\\ C_{12} & C_{23} & C_{33} & 0 & 0 & 0\\ 0 & 0 & 0 & \dfrac{C_{22}-C_{23}}{2} & 0 & 0\\ 0 & 0 & 0 & 0 & C_{66} & 0\\ 0 & 0 & 0 & 0 & 0 & C_{66}\end{bmatrix}\cdot\begin{Bmatrix}\varepsilon_1\\ \varepsilon_2\\ \varepsilon_3\\ \gamma_{23}\\ \gamma_{13}\\ \gamma_{12}\end{Bmatrix}$$

$$= \begin{bmatrix}S_{22}\cdot S_{33}-S_{32}^2 & S_{12}\cdot(S_{32}-S_{33}) & -S_{12}\cdot(S_{22}-S_{32}) & 0 & 0 & 0\\ S_{12}\cdot(S_{32}-S_{33}) & S_{11}\cdot S_{33}-S_{12}^2 & -S_{11}\cdot S_{32}+S_{12}^2 & 0 & 0 & 0\\ -S_{12}\cdot(S_{22}-S_{32}) & -S_{11}\cdot S_{32}+S_{12}^2 & S_{11}\cdot S_{22}-S_{12}^2 & 0 & 0 & 0\\ 0 & 0 & 0 & G_{23} & 0 & 0\\ \text{(symmetric)} & 0 & 0 & 0 & G_{13} & 0\\ 0 & 0 & 0 & 0 & 0 & G_{12}\end{bmatrix}\cdot\begin{Bmatrix}\varepsilon_1\\ \varepsilon_2\\ \varepsilon_3\\ \gamma_{23}\\ \gamma_{13}\\ \gamma_{12}\end{Bmatrix}$$

with the denominator $N = S_{11}\cdot(S_{22}\cdot S_{33}-S_{32}^2)-S_{12}^2\cdot(S_{33}-2\cdot S_{32}+S_{22})$.

$3D:\ \{\sigma\} = (\sigma_1,\sigma_2,\sigma_3,\tau_{23},\tau_{31},\tau_{21})^T \quad\rightarrow\quad \{\sigma_{eq}^{\text{mode}}\} = \left(\sigma_{eq}^{\parallel\sigma},\ \sigma_{eq}^{\parallel\tau},\ \sigma_{eq}^{\perp\sigma},\ \sigma_{eq}^{\perp\tau},\ \sigma_{eq}^{\parallel\perp}\right)^T$

$2D:\ \{\sigma\} = (\sigma_1,\sigma_2,-,-,-,\tau_{21})^T$ *for* FF and IFF

$2D:\ \{\sigma\} = (-,\sigma_2,-,-,-,\tau_{21})^T$ *for* IFF

$3D:\ \{R\} = (R_{\parallel}^t,R_{\parallel}^c,R_{\perp}^t,R_{\perp}^c,R_{\perp\parallel})^T$ with $\mu_{\perp\square},\mu_{\perp\perp} \Leftarrow \{\bar{R}\} = (\bar{R}_{\parallel}^t,\bar{R}_{\parallel}^c,\bar{R}_{\perp}^t,\bar{R}_{\perp}^c,\bar{R}_{\perp\parallel})^T$ with $\mu_{\perp\square},\mu_{\perp\perp}$

$2D:\ \{R\} = (R_{\parallel}^t,R_{\parallel}^c,R_{\perp}^t,R_{\perp}^c,R_{\perp\parallel})^T$ with $\mu_{\perp\square},\mu_{\perp\perp}$ *for* FF and IFF

$2D:\ \{R\} = (-,-,R_{\perp}^t,R_{\perp}^c,R_{\perp\parallel})^T$ with $\mu_{\perp\square}$ *for* IFF

$$[S] = \begin{bmatrix} \frac{1}{E_\parallel} & \frac{-\nu_{\parallel\perp}}{E_\perp} & \frac{-\nu_{\parallel\perp}}{E_\perp} & 0 & 0 & 0 \\ \frac{-\nu_{\perp\parallel}}{E_\parallel} & \frac{1}{E_\perp} & \frac{-\nu_{\perp\perp}}{E_\perp} & 0 & 0 & 0 \\ \frac{-\nu_{\perp\parallel}}{E_\parallel} & \frac{-\nu_{\perp\perp}}{E_\perp} & \frac{1}{E_\perp} & 0 & 0 & 0 \\ & & & \frac{1}{G_{\perp\perp}} & 0 & 0 \\ & \text{(symm.)} & & & \frac{1}{G_{\perp\parallel}} & 0 \\ & \boxed{\text{transversely isotropic}} & & & & \frac{1}{G_{\perp\parallel}} \end{bmatrix}$$

$$[S] = \begin{bmatrix} \frac{1}{E_W} & \frac{-\nu_{WF}}{E_F} & \frac{-\nu_{W3}}{E_F} & 0 & 0 & 0 \\ & \frac{1}{E_F} & \frac{-\nu_{F3}}{E_F} & 0 & 0 & 0 \\ & & \frac{1}{E_3} & 0 & 0 & 0 \\ & \text{(symm.)} & & \frac{1}{G_{F3}} & 0 & 0 \\ & \boxed{\begin{array}{l}\text{orthotropic (also}\\ \text{called rhombically}\\ \text{anisotropic)}\end{array}} & & & \frac{1}{G_{W3}} & 0 \\ & & & & & \frac{1}{G_{WF}} \end{bmatrix} .$$

It is of interest to present here a short description of invariants used in this document. Especially for UD-composites it is referred to subchapter 9.4.

Use of Ivariants (*after Wikipedia*):

Most often in engineering the invariants of rank two tensors are applied. So-called principal invariants of a second rank tensor $\boldsymbol{T}$ are the coefficients of the characteristic polynomial

$$\text{“ } p(\lambda) = det(\boldsymbol{T} - \lambda\cdot\boldsymbol{I}) = -\lambda^3 + I_1\cdot\lambda^2 - I_2\cdot\lambda + I^3 \text{ “ with } [T] = \begin{bmatrix} T_{11} & T_{12} & T_{13} \\ T_{21} & T_{22} & T_{23} \\ T_{31} & T_{32} & T_{33} \end{bmatrix}$$

(*H. Altenbach: Kontinuumsmechanik, Springer 2012*) and $\boldsymbol{I}$ being the identity tensor and λ the polynomial's eigenvalues as solutions of p(λ) = 0. The derived Principal Invariants (T_{ii} considers Einstein's sum convention) are:

$$I_1 = trace(T) = T_{ii} = T_{11} + T_{22} + T_{33} \ ,$$
$$I_2 = T_{11}\cdot T_{22} + T_{11}\cdot T_{33} + T_{33}\cdot T_{22} - T_{12}\cdot T_{21} - T_{13}\cdot T_{31} - T_{23}\cdot T_{32} \ ,$$
$$I_3 = T_{11}\cdot(T_{22}\cdot T_{33} - T_{23}\cdot T_{32}) + T_{12}\cdot(T_{23}\cdot T_{31} - T_{21}\cdot T_{33}) + T_{13}\cdot(T_{21}\cdot T_{32} - T_{22}\cdot T_{31})$$

Further used are Main and Mixed Invariants in the case of isotropic materials. Main invariants are functions of the principal ones which means coefficients of the characteristic polynomial "$\boldsymbol{T}$ – trace($\boldsymbol{T}$ / 3)". This separation of a principal tensor (coefficients termed *I*) into an isotropic tensor part (sphere tensor) and a deviator tensor part (coefficients termed *J*) is highly welcomed in order to separate, for example, volume effects from shear effects.

In the isotropic material case the usually applied Main Invariants read:

$$I_1 \ , \quad J_2 = I_1^2/3 - I_2 \ , \quad J_3 = 2\cdot I_1^3/27 - I_2\cdot I_1/3 + I_3 \ .$$

Mixed Invariants, such as sums or differences are used for distinct applications.

In structural mechanics invariants of the stress tensor σ_{ik}, the strain tensor ε_{ik} and of the material stiffness tensor C_{ijkl} or its inverse the compliance tensor S_{ijkl} are employed. Invariants of the stress

tensor are used to establish stress-Strength failure criteria (*see the author's FMC for the three material families isotropic, transversely-isotropic and orthotropic*) and invariants of the strain tensor for strain failure criteria. Strength failure criteria use as action the present stress state and as resistance strength properties (*failure stresses*) whereas strain failure criteria use the present strain state and failure strains as resistance properties. Using invariants in the stiffness domain can help to get information for a more reliable estimation of pre-design properties for a novel UD material and thereby saving time and reducing test effort.

A compilation of some Main Invariants shall be presented here (symmetric tensor ***T***):
Isotropic:

$\boldsymbol{\sigma_{ik}}$: $I_1^{\sigma} = I_1 = (\sigma_I + \sigma_{II} + \sigma_{III})$, $I_2^{\sigma} = 0.5 \cdot (\sigma_I \cdot \sigma_{II} + \sigma_{II} \cdot \sigma_{III} + \sigma_I \cdot \sigma_{III})$

$J_2^{\sigma} = (I_1^{\sigma})^2/3 - I_2^{\sigma} = [(\sigma_I - \sigma_{II})^2 + (\sigma_{II} - \sigma_{III})^2 + (\sigma_{III} - \sigma_I)^2] / 6$.

$\boldsymbol{\varepsilon_{ik}}$: $I_1^{\varepsilon} = (\varepsilon_I + \varepsilon_{II} + \varepsilon_{III}) = \varepsilon_{ii} = \varepsilon_{vol}$, $I_2^{\varepsilon} = 0.5 \cdot (\varepsilon_I \cdot \varepsilon_{II} + \varepsilon_{II} \cdot \varepsilon_{III} + \varepsilon_I \cdot \varepsilon_{III})$, ...(like above)

$J_2^{\varepsilon} = (I_1^{\varepsilon})^2/3 - I_2^{\varepsilon}$.

C_{ikjl}: rank four tensor general, C_{ik}: rank two tensor of principal stresses-strains.

Transversely-isotropic UD (see sub-chapter 9.4)

$\boldsymbol{\sigma_{ik}}$:

$$I_1 = I_1^{\sigma} = \sigma_1,\ I_2 = \sigma_2 + \sigma_3,\quad I_3 = \tau_{31}^2 + \tau_{21}^2,\quad I_4 = (\sigma_2 - \sigma_3)^2 + 4 \cdot \tau_{23}^2,$$

$$I_5 = (\sigma_2 - \sigma_3) \cdot (\tau_{31}^2 - \tau_{21}^2) - 4 \cdot \tau_{23} \cdot \tau_{31} \cdot \tau_{21}$$ (from A. Boehler, applied in the FMC) .

The author's motto considering invariants:
I like to use invariants to model material variants.

On the next pages follows the theoretical background of Cuntze's Failure-Mode-Concept (FMC).

The author's consequent FMC thinking in failure modes comes from the discussions about 1985 with my friend Prof. Rüdiger Rackwitz † at the Institute of concrete construction (*head at that time was Prof. Herbert Kupfer*) on SFCs like Drucker-Prager and on the Partial Safety Factor concept. (Thanks Rüdiger).

1.4 Available knowledge used for the SFC Generation

The Hypothesis of Beltrami for isotropic materials states: "At onset-of-failure (*Beltrami said yielding)* the strain energy density W in a solid material element consists of two portions, one describes the strain energy due to a change in volume (= *dilatation or dilation in US*) and the other the strain energy due to a change in shape (*distortion*)". Hence, following Beltrami and Hencky-Mises-Huber HMH (see *Fig.1-9*), each invariant term or a multiple of it in the strength failure function *F* of the SFC, may be dedicated to one physical mechanism in the solid or cubic material element, respectively.
Further, these mechanisms are linked to energies, namely I_1^2 ~ dilatational energy from a volume change, J_2 ~ distortional energy from a shape change caused by shear distortion under volume consistency. Creating SFCs, Beltrami's statement guarantees an advantageous use of the 'physics-based' invariants I_1 and J_2 for very different materials such as grey-cast iron, concrete, plexiglass

PMMA and more structural materials.
Invariants are a combination of stresses – powered or not powered – the value of which does not change when altering the coordinate system CoS. This attribute is used when looking for an optimum formulation of a usually desired scalar SFC.

What is missing in the case of compression-loaded materials is the Mohr-Coulomb-linked friction energy which is mandatory for investigations of so-called pressure-sensitive materials and which is captured by I_1.



Situation of the Poor Designer:
"Is there any Strength Failure Condition SFC ("criterion") I can apply ?"
[originator of the picture not found]

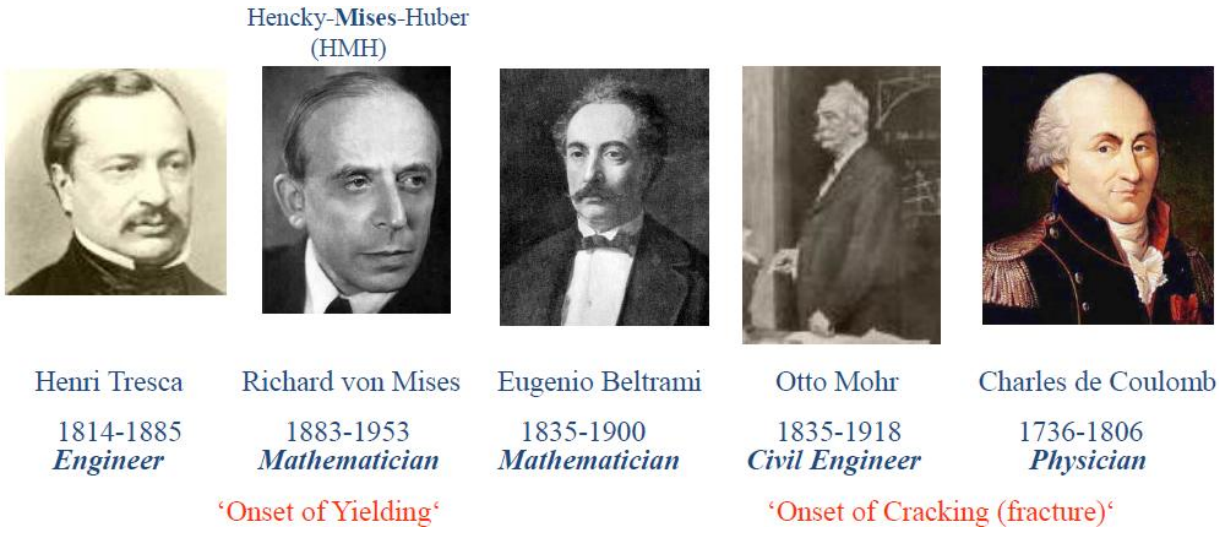


Fig.1-9: Some pioneers which set up strength failure hypotheses (ductile, brittle)

The SFC models of Drucker-Prager and of Ottosen, often used in civil engineering, are shortly treated in *Sub-chapter 9.3.2*.

Material symmetry demands gave reason that the FMC strictly describes just single independent failure modes by its failure mode–wise concept. This will make the derivation of equivalent stresses possible despite of the fact whether the material is isotropic, transversely-isotropic or orthotropic which practically is still a low-level structure and hopefully can be homogenized.

Some Features of the FMC:

1 If a material element can be homogenized to an ideal crystal (= *frictionless*), material symmetry requires for the isotropic and the transversely-isotropic UD material a distinct number of properties (*is witnessed*)
2 A real solid material model is represented by a description of the ideal crystal (*frictionless*) + a description of its friction behavior. Mohr-Coulomb requires for the

real crystal another physical parameter, namely the inherent material friction value μ (*1 value for isotropic and 2 for UD materials)*

3 Fracture morphology finally gives evidence: Each strength corresponds to a distinct *strength failure mode* and to a distinct *strength fracture type,* to Normal Fracture (NF) or Shear Fracture (SF)

4 Exclusive use of experimentally determinable model parameters

5 Note: Densely packed frictional material experiences dilatation when sheared.

In order to only use experimentally derivable material quantities, the author directly introduced in his 3D-SFCs for the compression domain, also the internal friction μ as a parameter. Friction is a well-known physical property in engineering. However, one does not yet find a direct use of μ in the textbooks! Why using Mohr's friction angle φ if $\mu\ (\varphi)$ exists?

For some pre-understanding: How to derive μ will be shown in detail in Chapter 6. Mohr stresses are needed and derived there to determine the friction values μ. The mathematically challenging topic thereby is the derivation of the fracture plane angles $\Theta_{fp}°$, an angle, which is of high interest for understanding the physics behind the desired transformation from structural stress formulations into Mohr stress-based ones. A determination of the Mohr-Coulomb fracture curve is required. This curve captures the tensile-compressive interaction domain or transition zone between the two interacting modes SF and NF. It spans between the uniaxial limit points compressive strength R^c and tensile strength R^t. Its friction-related part ends at the cohesive point R^τ.

It should be noted: The author could not find any investigation wherein the effortful SFC transformation from structural stresses into Mohr stresses has been performed, Chapter 6.

1.5 Beltrami Hypothesis for SFC-generation of isotropic and of UD materials

Beltrami, Schleicher et al. assume at initiation of yield that the strain energy (denoted by W) in a solid cubic element of a material will consist of two portions:

$$W = \int\{\sigma\}\{\varepsilon\}\, d\{\varepsilon\} = W_{Vol} + W_{shape} \quad \text{with} \quad \{\sigma\}=(\sigma_1,\sigma_2,\sigma_3,\tau_{23},\tau_{13},\tau_{12})^T .$$

Including Hooke's law in the case of a ***transversely-isotropic*** (UD solid) the expression will take the form, using s_{ik} := compliance coefficients, E:=elasticity modulus, ν:=Poisson's ratio,

$$W = [s_{11}\cdot\sigma_1^2 + s_{22}\cdot\sigma_2^2 + s_{33}\cdot\sigma_3^2 + s_{44}\cdot\tau_{23}^2 + s_{55}\cdot(\tau_{12}^2 + \tau_{13}^2)] / 2 + s_{12}\cdot(\sigma_1\sigma_2 + \sigma_1\sigma_3) +$$

$$s_{23}\cdot\sigma_2\sigma_3 = \underset{\text{volume}}{\frac{I_1^2}{2\cdot E_{\parallel}}} + \underset{\text{volume}}{\frac{I_2^2\cdot(1-\nu_{\perp\perp})}{4\cdot E_{\perp}}} - \underset{\text{volume}}{\frac{\nu_{\perp\parallel}\cdot I_1\cdot I_2}{E_{\parallel}}} + \underset{\text{shape}}{\frac{I_3}{2\cdot G_{\parallel\perp}}} + \underset{\text{shape}}{\frac{I_4\cdot(1+\nu_{\perp\perp})}{4\cdot E_{\perp}}} .$$

with the invariants $I_1 = \sigma_1,\ I_2 = \sigma_2 + \sigma_3$; $I_3 = \tau_{31}^2 + \tau_{21}^2$; $I_4 = (\sigma_2-\sigma_3)^2 + 4\tau_{23}^2$;

$$I_5 = (\sigma_2 - \sigma_3)(\tau_{31}^2 - \tau_{21}^2) - 4\tau_{23}\tau_{31}\tau_{21}.$$

In the ***isotropic*** case analogously follows, however simpler,

$$W = \left[\frac{1-2\nu}{3} I_1^{iso\,2} + \frac{2+2\nu}{3} 3J_2^{iso}\right] / 2E$$

volume shape

with $I_1^{iso} = \underline{f(\sigma)} = \sigma_I + \sigma_{II} + \sigma_{III}$, $6 \cdot J_2^{iso} = \underline{f(\tau)} = (\sigma_I - \sigma_{II})^2 + (\sigma_{II} - \sigma_{III})^2 + (\sigma_{III} - \sigma_I)^2$,

It is known, both portions in the bracket above are used to formulate a failure function

$$F = c_1 \cdot \frac{(1-2\nu) \cdot I_1^{iso\,2}}{3\bar{R}^2} + c_2 \cdot \frac{(2+2\nu) \cdot 3J_2^{iso}}{3\bar{R}^2} \quad .$$

volume shape

Fig. 1-10 displays for the 2 material families above the physically-based choice of invariants:

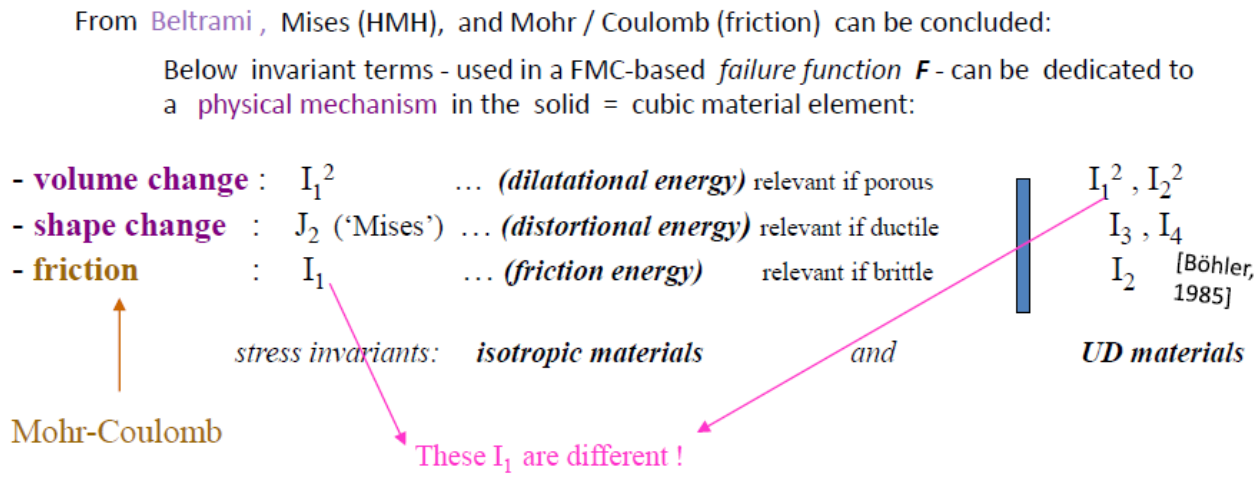


Fig.1-10: Reasons for choosing invariants when creating FMC-based SFCs

Above invariants can be formulated in 3D structural component stresses, in principal stresses and in Mohr stresses. An application is depicted in *Fig.1-11*, representing an isotropic schematic example for the use of the invariants in the case $I_1 < 0$ considering their physical meaning.

shape change friction volume change

$$F^{SF} = c_1^{SF} \cdot \frac{3J_2 \cdot \Theta^{SF}}{(\bar{R}^c)^2} + c_2^{SF}(\mu) \cdot \frac{I_1}{\bar{R}^c} + c_3^{SF} \cdot \left(\frac{I_1}{\bar{R}^c}\right)^2 = 1$$

'Mises Cylinder' formula

Above *general* SFC is normalized by the compressive strength $\bar{R}^c$

Two-fold failure danger can be modelled by using the well known invariant J_3.

The non-circularity function Θ^{SF} includes d^{SF} as non-circularity parameter.

It represents the 120°-rotational symmetry of isotropic materials, caused by the equivalency of the 3 principal stresses and directions (see the fracture bodies, following).

$$\Theta^{SF}(J_3, J_2) = \sqrt[3]{1 + d^{SF} \cdot \sin(3\vartheta)} = \sqrt[3]{1 + d^{SF} \cdot 1.5 \cdot \sqrt{3} \cdot J_3 \cdot J_2^{-1.5}}$$

Compressive Meridian: $\Theta^{SF} = \sqrt[3]{1 - d^{SF}}$, Tensile Meridian: $\Theta^{SF} = \sqrt[3]{1 + d^{SF}}$,

Neutral Meridian: $\Theta^{SF} = 1$.

Fig.1-11: Schematic example for the use of invariants for slightly porous isotropic materials

If in the brittle isotropic case above the same 'strength fracture mode' multiply occurs, then a 120° rotational symmetry of the fracture body is to face. The invariant J_3 can excellently map this.

1.6 Stresses and Invariants of Isotropic materials and of UD materials

At first, in *Fig.1-12* the different stresses applied in structural mechanics are depicted. Secondly for the three material families the associated stresses and invariants are displayed. The suffixes I, II, III denote principal stresses, ||, ⊥ lamina stresses, W (warp), F (fill, weft) fabric stresses. The stresses in the different CoS can be transferred into each other.

Residual stresses are taken into account by adding their values to the Load stresses due to $\{\sigma\} = \{\sigma_L\} + \{\sigma_R\}$. Some relationships follow:

$$I_1 = (\sigma_I + \sigma_{II} + \sigma_{III}) \;=\; f(\sigma)\;, \quad 6J_2 = (\sigma_I - \sigma_{II})^2 + (\sigma_{II} - \sigma_{III})^2 + (\sigma_{III} - \sigma_I)^2 = \; f(\tau) \;\text{'Mises' invariant}$$

$$27J_3 = \; (2\sigma_I - \sigma_{II} - \sigma_{III}) \cdot (2\sigma_{II} - \sigma_I - \sigma_{III}) \cdot (2\sigma_{III} - \sigma_I - \sigma_{II}),$$

$$3 \cdot \sigma_{oct} = \sigma_I + \sigma_{II} + \sigma_{III} = \; \sigma_\ell + \sigma_n + \sigma_t \;\; ; \;\; 9 \cdot \tau_{oct}{}^2 = 6J_2 = 4 \cdot (\tau_{III}{}^2 + \tau_I{}^2 + \tau_{II}{}^2), \;\; \tau_{II} = \max \tau (\textit{mathem.})$$

$\sigma_I, \sigma_{II}, \sigma_{III}$ are principal stresses, $\sigma_I > \sigma_{II} > \sigma_{III}$ are mathematical stresses (> means more positive)

The *Figs.1-12* through *-15* present the invariants and the associated structural component stresses, principal stresses and the Mohr (*fracture plane*) stresses which are necessary to derive the friction value (see *Chapter 6*).

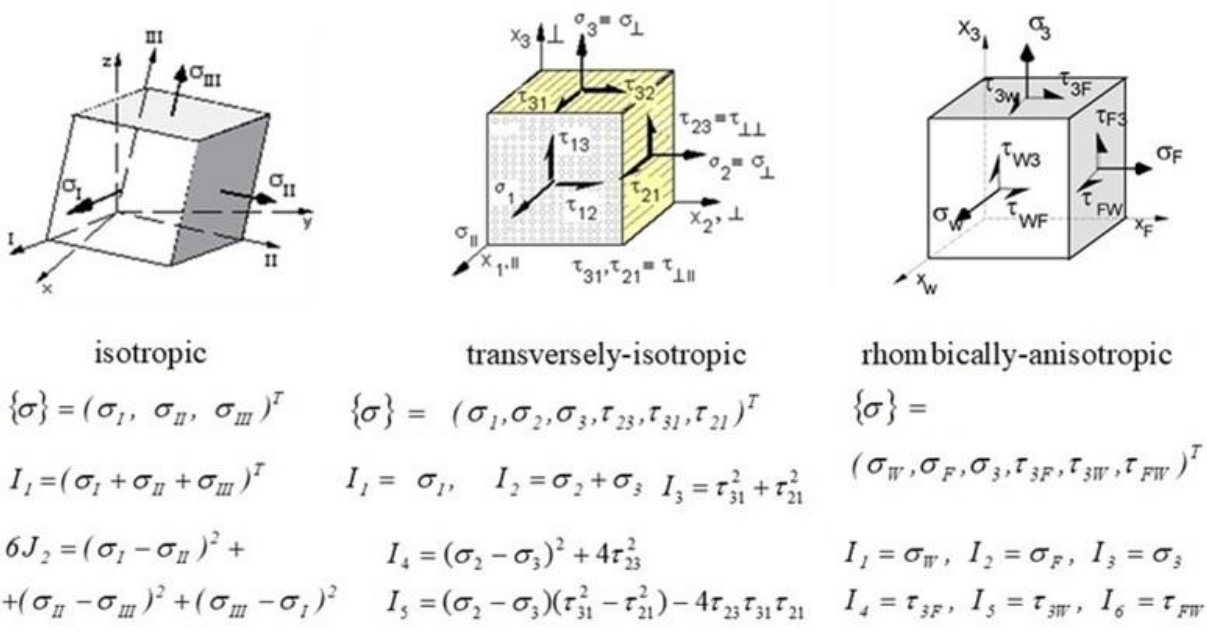
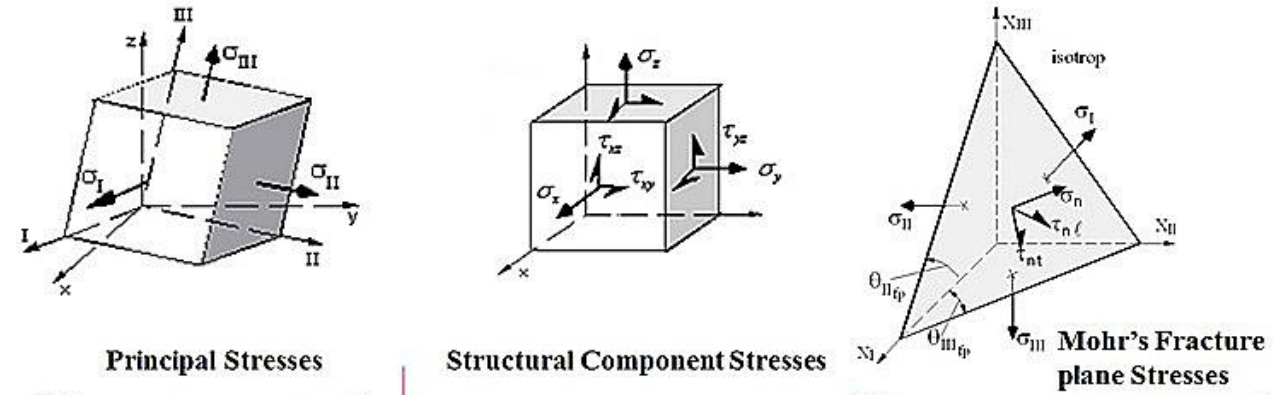


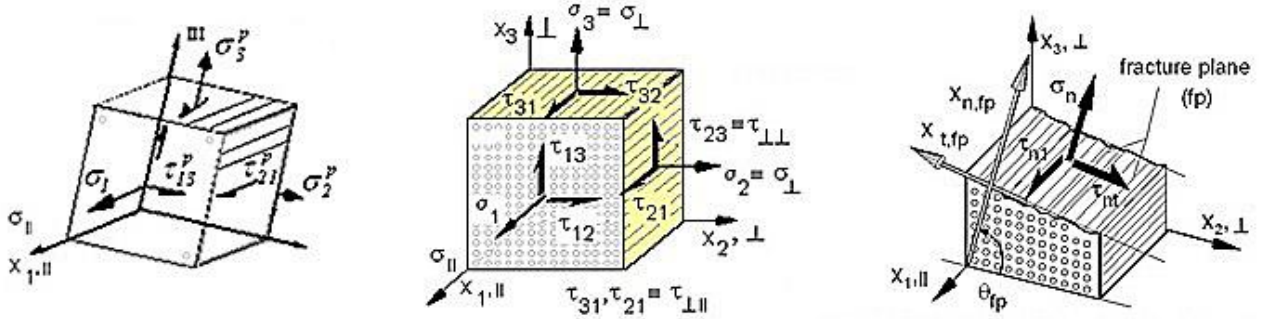
Fig.1-12: Stresses & invariants of isotropic, transversely-isotropic UD and orthotropic materials



Principal Stresses	Structural Component Stresses	Mohr's Fracture plane Stresses
$\{\sigma\}_{principal} = (\sigma_I,\ \sigma_{II},\ \sigma_{III})^T$	$\{\sigma\}_{comp} = (\sigma_x,\ \sigma_y,\ \sigma_z,\ \tau_{yz},\ \tau_{xz},\ \tau_{xy})^T$	$\{\sigma\}_{Mohr} = (\sigma_\ell,\ \sigma_n,\ \sigma_t,\ \tau_{nt},\ \tau_{t\ell},\ \tau_{\ell n})^T$
$I_1 = (\sigma_I + \sigma_{II} + \sigma_{III})^T = 3\sigma_{oct} \equiv f(\sigma),$	**'isotropic' invariants !** $I_1 = (\sigma_x + \sigma_x + \sigma_z)^T$	$I_1 = (\sigma_\ell + \sigma_n + \sigma_t)^T$
$6J_2 = (\sigma_I - \sigma_{II})^2 + (\sigma_{II} - \sigma_{III})^2 + (\sigma_{III} - \sigma_I)^2$ $= 4(\tau_{III}^2 + \tau_{II}^2 + \tau_I^2) = 9\tau_{oct}^2 \equiv f(\tau)$	$6J_2 = (\sigma_y - \sigma_z)^2 + (\sigma_z - \sigma_x)^2 + (\sigma_x - \sigma_y)^2$ $+6(\tau_{yz}^2 + \tau_{zx}^2 + \tau_{xy}^2)$ *(Mises, HMH)*	$6J_2 = (\sigma_n - \sigma_t)^2 + (\sigma_t - \sigma_\ell)^2 + (\sigma_\ell - \sigma_n)^2$ $+6(\tau_{nt}^2 + \tau_{t\ell}^2 + \tau_{n\ell}^2)$

$$27J_3 = (2\sigma_I - \sigma_{II} - \sigma_{III})(2\sigma_{II} - \sigma_I - \sigma_{III})(2\sigma_{III} - \sigma_I - \sigma_{II}),\quad I_e = 4J_2 - I_1^2/3,\quad \sigma_{mean} = I_1/3$$

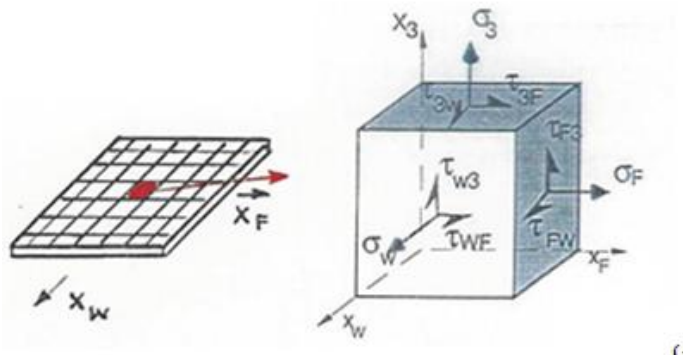
Fig.1-13: Applicable stresses and invariants of <u>isotropic</u> materials. (left) on the material cube's surfaces, (center), structural (component) stresses, and (right) Mohr stresses acting at the associated fracture plane



$\{\sigma\}^{quasi-isotropic\ plane}_{principal} =$ $= (\sigma_1, \sigma_2^p, \sigma_3^p, 0, \tau_{31}^p, \tau_{21}^p)^T$	$\{\sigma\}_{lamina} =$ $= (\sigma_1, \sigma_2, \sigma_3, \tau_{23}, \tau_{31}, \tau_{21})^T$	$\{\sigma\}_{Mohr} =$ $(\sigma_\ell,\ \sigma_n,\ \sigma_t,\ \tau_{nt},\ \tau_{t\ell},\ \tau_{\ell n})^T$
$I_1 = \sigma_1,\quad I_2 = \sigma_2^p + \sigma_3^p$ $I_3 = \tau_{31}^{p\,2} + \tau_{21}^{p\,2}$	$I_1 = \sigma_1,\quad I_2 = \sigma_2 + \sigma_3$ $I_3 = \tau_{31}^2 + \tau_{21}^2$ **'UD invariants'!** *[Boehler]*	$I_1 = \sigma_\ell,\quad I_2 = \sigma_n + \sigma_t$ $I_3 = \tau_{t\ell}^2 + \tau_{n\ell}^2$
$I_4 = (\sigma_2^p - \sigma_3^p)^2 + 0$ $I_5 = (\sigma_2^p - \sigma_3^p)(\tau_{31}^{p\,2} - \tau_{21}^{p\,2}) + 0$	$I_4 = (\sigma_2 - \sigma_3)^2 + 4\tau_{23}^2$ $I_5 = (\sigma_2 - \sigma_3)(\tau_{31}^2 - \tau_{21}^2) - 4\tau_{23}\tau_{31}\tau_{21}$	$I_4 = (\sigma_n - \sigma_t)^2 + 4\tau_{nt}^2$ $I_5 = (\sigma_n - \sigma_t)(\tau_{t\ell}^2 - \tau_{n\ell}^2) - 4\tau_{nt}\tau_{t\ell}\tau_{n\ell}$

Fig.1-14: Applicable stresses and invariants of <u>transversely-isotropic</u> UD materials

In the case of (rhombically-anisotropic) orthotropic materials much more modes and strengths are present, however simple invariants are to apply.



$$\{\sigma\}_{la\ min\ a} = (\sigma_W, \sigma_F, \sigma_3, \tau_{3F}, \tau_{3W}, \tau_{FW})^T$$

$$I_1 = \sigma_W,\ I_2 = \sigma_F,\ I_3 = \sigma_3$$
$$I_4 = \tau_{3F},\ I_5 = \tau_{3W},\ I_6 = \tau_{FW}$$

* rhombically-anisotropic

$$\{\bar{R}\} = (\bar{R}^t_W, \bar{R}^c_W, \bar{R}^t_F, \bar{R}^c_F, \bar{R}_{WF}, \bar{R}^t_3, \bar{R}^c_3, \bar{R}_{3W}, \bar{R}_{3F})^T$$
$$\{\bar{R}\}_{W-F} = (\bar{R}^t_W, \bar{R}^c_W, \bar{R}_{WF}, \bar{R}^t_3, \bar{R}^c_3, \bar{R}_{3W})^T$$

Fig.1-15: Applicable stresses, strengths and invariants of orthotropic materials

The FMC was at first intensively applied to UD materials in the World-Wide-Failure-Exercise.
In this context it makes sense to add here all the hypotheses used for establishing SFCs, describing Inter-Fiber-Failure IFF of the UD- material family. *Table 1-4* shows the basic UD hypotheses.

Table 1-4: Hypotheses used to predict Inter-Fiber-Failure IFF of UD materials

Mohr's Statement for isotropic materials:

" The strengths of a material are determined by the stresses σ_n, τ_{nt} on the fracture plane" (the fracture plane is usually inclined with respect to the action of the external stresses)

Paul's modification of the Mohr-Coulomb Hypothesis:

" Brittle (behaving) material will fracture in either that plane where the shear stress τ_{nt} reaches a critical value which is given by the shear resistance of a fiber-parallel plane increased by a certain amount of friction caused by the simultaneously acting compressive stress σ_n on that plane. Or, it will fracture in that plane, where the maximum principal (tensile) stress reaches the transverse tensile strength $R_\perp^t$ (in the quasi-isotropic plane)"

Hashin [Has80]:

Proposed a modified Mohr-Coulomb IFF approach but did not pursue this idea due to numerical difficulties (Puck succeeded on this way). Also into this paper he included an invariant-based global quadratic approach (Cuntze's invariant way)

Puck's Action Plane IFF Conditions:

Based his IFF conditions on Mohr-Coulomb and Hashin , Puck interacts the 3 Mohr stresses σ_n, τ_{nt}, τ_{n1} on the IFF fracture plane. He uses simple polynomials (*parabolic or elliptic*) to formulate a so-called master fracture body in the $(\sigma_n, \tau_{nt}, \tau_{n1})$ space. A compressive σ_n cannot cause fracture on its action plane

Cuntze Failure-Mode-Concept – based IFF conditions:

Used 3 different invariant IFF conditions, based on his idea that each fracture condition is governed by 1 strength.

1.7 Material symmetry-based assumptions of the author

Under the presumption "homogeneity is an acceptable assessment for the material concerned", and regarding the respective tensors, it follows from material symmetry: *The Number of strengths ≡ number of elasticity properties!* This means, a characteristic number of quantities is fixed: 2 for isotropic material and 5 for the transversely-isotropic UD lamina (≡ lamellas or sheets in civil engineering). Hence, the applicability of material symmetry involves that a *minimum number of properties needs to be measured only* (CoSt + time benefits)! Therefore, material symmetry requirements are helpful when setting up strength criteria and test programs. See the literature of Christensen [Chr98]. Again the experience of the author shows when comparing material behavior: Similarly behaving materials possess the same shape of a fracture body.

Table 1-5 collects the basic conclusions drawn from witnessed material symmetry knowledge. There might be a material 'generic' inherent number (*term was chosen by the author*).

For the theoretical case of homogeneity in *Table 1-6* the author adds additional assumptions of the author assuming that generic numbers really exist, 2 for isotropic and 5 for UD material.
'Basic' fracture toughness properties means, that the crack plane under tension or under compression remains the same after up-loading.

Table 1-5: Assumed Generic Numbers of isotropic and transversely-isotropic materials

Material symmetry demand for the Isotropic Material: generic number 2
- 2 e*lastic 'constants', 2 strengths, 2 strength failure modes fracture* (NF, SF)
- *1 physical parameter (such as coefficient of thermal expansion CTE, coefficient of moisture expansion CME, friction value μ, etc.)*

Material symmetry demand for the Transversely-Isotropic Material: generic number 5

Basic knowledge: *for brittle materials*
- 5 e*lastic 'constants', 5 strengths, 5 strength failure modes fracture* (NF, SF)
- *2 physical parameters (CTE, CME, $\mu_{\perp\perp}$ $\mu_{\perp\parallel}$ etc.)*

Table 1-6: Cuntze's full set of material symmetry-based assumptions.
Extension of Table 2-2 by assumed additional assumptions

Material symmetry demands for the Isotropic Material: assumed as generic number 2

Basic knowledge:
- 2 e*lastic 'constants', 2 strengths, 2 strength failure modes fracture* (NF, SF)
- *1 physical parameter CTE, CME, μ, etc.)*

Author's additional assumptions:

2 'basic' fracture toughness properties, 2 invariants I_1, J_2 , 2 modes yielding* (NY,SY)

(** valid as long as a one-fold acting failure mode is to describe by the distinct SFC and not a multi-fold one. Presumed it is an ideal homogeneous material [Cun17,19a], 2 Master SN curves* (*R =0.1 for 0, tension; 10 for ∞, compression)*

Material symmetry demands for Transversely-Isotropic UD Material: generic number 5

Basic knowledge *from these at most quasi- brittle materials*
- 5 e*lastic 'constants', 5 strengths, 5 strength failure modes fracture* (NF, SF)
- *2 physical parameters (CTE, CME, $\mu_{\perp\perp}$ $\mu_{\perp\parallel}$ etc.)*

Author's additional assumption
- *5 'basic' fracture toughness properties, 5 invariants*, 5 Master SN curves*

Material symmetry shows that the number of strengths is identical to the number of elasticity properties! Using material symmetry in material modelling requires homogeneity as pre-requisite. Then however, the application of material symmetry beneficially fixes the number of material properties that are effortful to measure to a minimum one.

Further should be mentioned: "*The choice of the material model always depends on the efficiency a structural task must be and can be solved and on the required quality of the answer*."

1.8 Effects to be considered with Isotropic and Transversely-isotropic Materials

Pores and crack-like flaws ('defects'):

Fig.1-16 completes the understanding of the effect of crack-like flaws, notches, pores and inclusions. It very well characterizes the different effects of 'round' void flaws and crack-like flaws (*from legal reasons avoid the term defect, please*). Under uniaxial tensile stresses, micro-damage depends on the orientation of the crack-like flaws due to the generated different stress intensity at the crack tips. In the case of round micro-pores the micro-damage effect is pretty similar in both the direction due to similar stress concentrations.

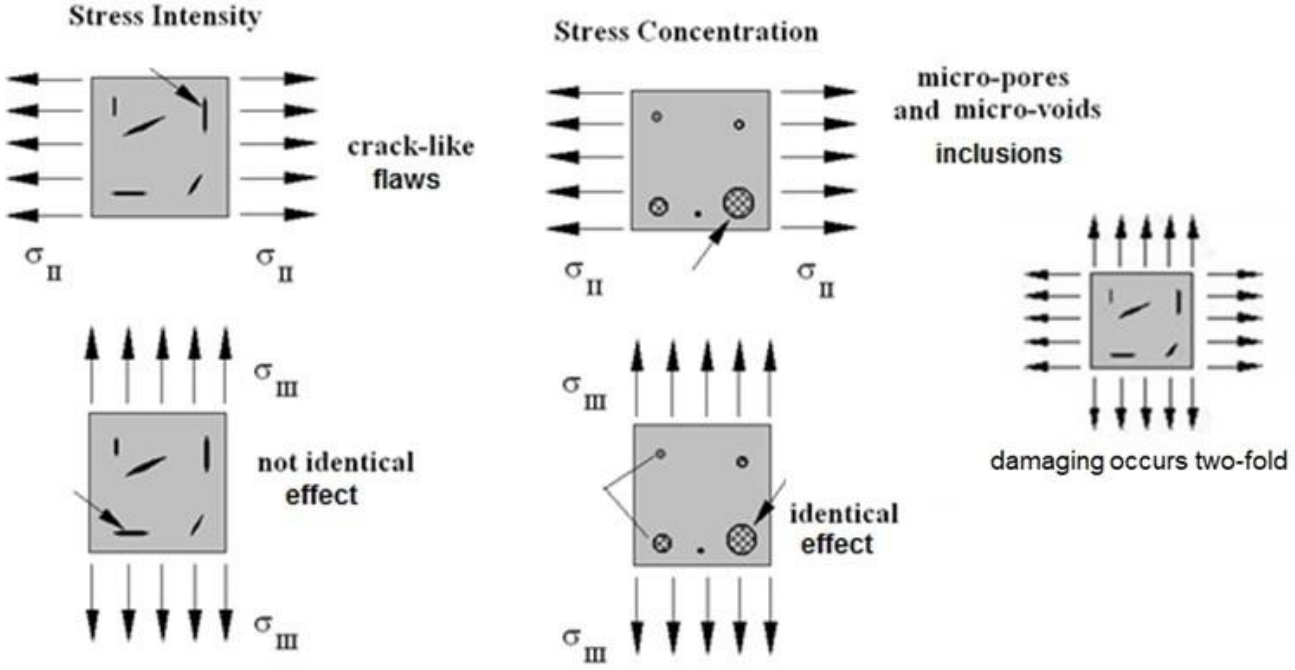


Fig.1-16: Effect of cracks, notches and inclusions as originators of fracture. Influence of flaw type, size and orientation

It is to conclude: Failure causing effects are different for round pores and crack-like flaws. This effect usually increases with the grade of the tri-axiality factor, defined as
$TrF = \sigma_{hyd} / \sigma_{eq}^{Mises} = (I_1/3) / \sqrt{3J_2}$.

Remind:
The decision, whether a *strength design verification* must be performed in a critical material location as strength demonstration or as a *fracture mechanics design verification* in the structural

component, depends on the size of the flaw. If the size becomes a technical crack, then fracture mechanics must demonstrate structural integrity.

Mixed (fracture) Failure and Multi-fold Failure, isotropic and UD:
Fig.1-17 displays the difference between Mixed Failure and Multi-fold Failure which can be recognized in the associated domains indicated in the figure. Due to the small tensile strength R^t of many brittle materials the bi-axial tensile strength R^{tt} of them - for instance of concrete - is not of interest but its bi-axial compressive strength as will be demonstrated later

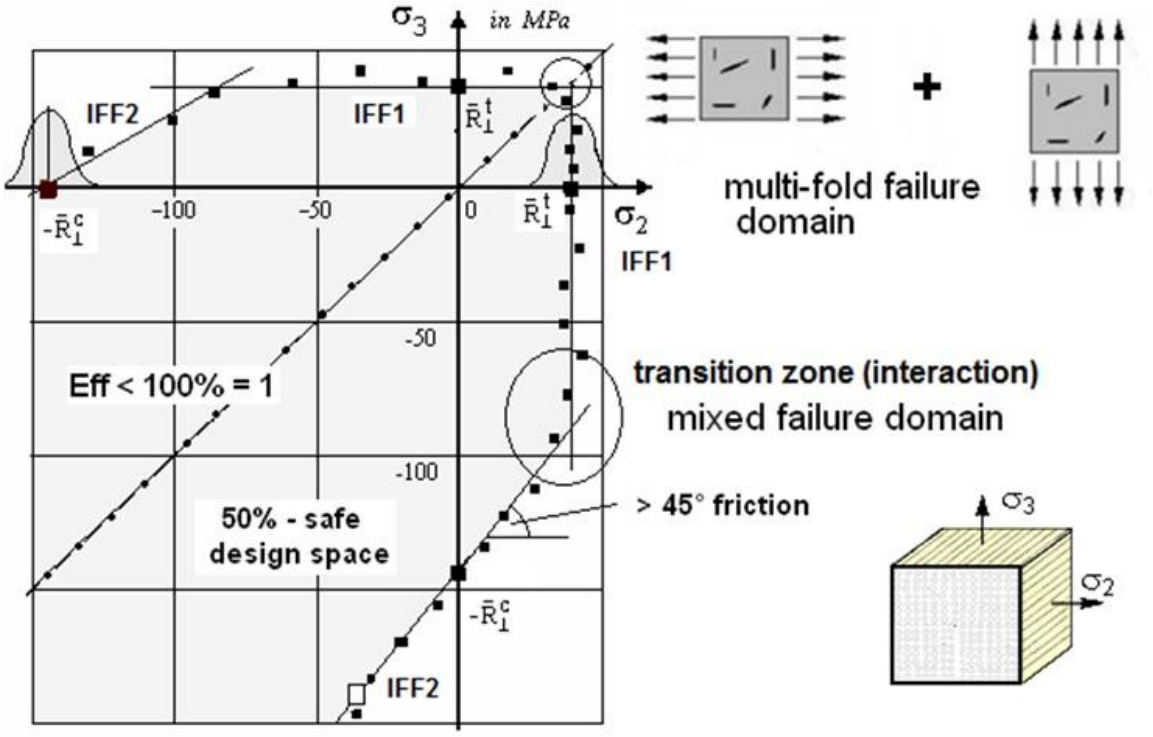


Fig.1-17: Schematic example for a two-fold failure domain and a mixed-failure domain (example UD)

Multi-fold failure effects: *example isotropic*
The existence of twofold and threefold failure effects must be considered:

- A usual SFC just describes a 1-fold occurring failure mode or mechanism
- A multi-fold occurrence of a failure with its joint probabilistic effects must be additionally considered in the formulas: *2-fold* $\sigma_{II} = \sigma_I$ tension or compression is elegantly captured by using the invariant J_3 ; *3-fold* $\sigma_{II} = \sigma_I = \sigma_{III}$ hydrostatic compression, by a closing bottom formula part in the case of porous materials.
  The 120°-located inward tension dents and outward compression bulges of the failure body, as the probabilistic result of the *2-fold* acting of the same failure mode, are described by replacing J_2 by $J_2 \cdot \Theta\,(J_3, J_2)$. It describes the non-circularity of the 120° rotationally-symmetric isotropic fracture body.

Effect of High Failure Probability Domains: *example isotropic*
This effect comes to act where differently large domains of ultimately stressed material parts are given. In the axial load case each material volume is stressed equally high, *Fig.1-18.*

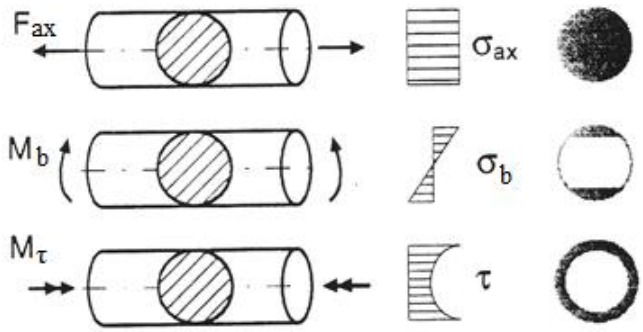


Fig.1-18: Domains of different fracture probabilities for the simple example rod

'Weibull volume effect' and 'Weibull surface effect' are used to estimate the value of a measured strength, especially under tension.

***Redundancy effects** (healing, benign behavior):*

Such effects occur in hydro-static pressure cases. Examples are the materials UltraHighPerformanceConcrete UHPC and UD. In the UD-case the failure curve consists of the most often weakest-link part and a redundant part under p_{hyd}. This requires a different mapping of the course of test data in the p_{hyd}-dominated IFF2 domain and the IFF3 domain (*see WWFE-II, Test Case 2, later*). Such redundancy effects are also given for UHPC, viewing $R^{cc} > R^{c}$. Amount, size and orientation of flaws determine whether the generated crack 'plane' becomes an in-plane or out-of-plane failure.

Hydrostatic pressure seems to 'heal' the adverse effect of flaws (*such as micro-cracks, micro-voids*) and delamination by compressing the flaws and increasing the amount of fracture energy necessary for crack growth. However, when fracture then begins to act this will happen faster and hence more 'catastrophically', which means fracture occurs in this compressed state in a more brittle manner. Thus, hydrostatic compression and in a minor manner through-thickness compression alone improve both static strength capacity and cyclic strength capacity. This issue is of high importance, e.g. at bearings and joints.

In this context mind, please: Opposite to ***redundancy*** (*benign behavior*) the material may experience ***weakest link*** behavior. And in the case of brittle material is valid $R^{tt} < R^{t}$, because flaws are activated by stresses in two orthogonal directions.

Residual stresses (**Eigenspannungen**) and pre-stresses (**Vorspannungen**):

In a lamina of a laminate the curing process generates wall thickness-dependent residual stresses. These stresses are decaying with decreasing stiffness caused by the micro-damage degradation which accompanies an increasing non-linearity. In other words: In parallel to the decay of the stiffness the non-linear analysis releases matrix-dominated stresses.

Pre-stresses are used to lower for instance the stress state in the low tensile strength polymer matrix at the CoSt of the fiber [*Cun93*]. The same is standard in construction with pretension the mineral matrix concrete at the CoSt of the steel or of the carbon fiber reinforcement.

Thickness effect, example UD:

Due to being strain-controlled, the material flaws in a *thin* lamina cannot grow freely up to micro-crack size in the thickness direction (*this is sometimes called 'thin layer effect'*), because the neighboring laminas act as micro-crack-stoppers. Considering fracture mechanics, the strain energy

release rate, responsible for the development of damage in the 90° plies from flaws into micro-cracks and larger, increases with increasing ply thickness. Therefore, the actual absolute thickness of a lamina in a laminate is a driving parameter for initiation or onset of micro-cracks, i.e. [*Fla82*]. Investigations on the more expensive but better performing thin layer laminates are present works.

Viewing the material's behavior:
Based on his experience the author looks at the material's behavior not whether it is a concrete or a grey cast iron for instance. If such a view is permitted, then the mathematical description of a fracture failure body model of a similarly behaving, still multi-axially tested material in the past can be used. This transferability idea was stressed for an isotropic example: Given was a good Foam test data basis which was transferred to a Concrete Stone, due to the lack of multi-axial failure stress test data for the concrete stone.

> ***LL***:
> *Presumption "SHAPE of the fracture failure body of a material is known". Then, just the SIZE of the body needs to be further determined. This can be always performed by the necessarily known (uniaxial) different tensile and compressive strengths. → Helpful, when designing with pretty novel materials.*

1.9 Fracture Types and Behavior of the Various Materials

According to the macroscopic load deformation curve, one can distinguish between deformation-poor and deformation-rich fracture processes. Here, too, the real material plays only a minor role. A mineral material can exhibit the same macroscopic behavior as a carbon fiber material, as a cast material or as a ferritic steel in the low-temperature range. And, a metal and a polymer can show large irreversible deformations up to fracture, although the micro-mechanical deformation mechanisms may be different. The micromechanical failure mechanisms of fracture are material-specific and therefore arbitrarily diverse. This is where (micro-)damage models come in. Some of what appears "similar" at the macro level (e.g. "brittle" behavior) may turn out to be completely different on the micro level. Examples are: A cleavage fracture in ferritic steels is for instance preceded by local *plastic deformations*. A fracture failure of concrete for instance implies small deformations from *damage mechanisms* on different length scales, micro-damage and macro-damage due to the complex microstructure,
Macroscopic fractures can be classified spanning deformation-rich and deformation-poor (grey cast iron, concrete) fractures, respectively. In tension and compression, the deformation-rich material experiences sliding failure under the influence of the failure-driving shear stress. In the deformation-poor case, the material is plastically non-deformable and at first micro-fractures and then macro-fractures under tension perpendicular to the tensile stress as soon as the normal stress reaches the separation (tensile) strength R^t. This is accompanied by cleavage fracture designated here as Normal Fracture NF.

Compression of materials causes shear failure, because the shear stress is decisive. This includes as well sliding failure of ductile materials in the tensile and the compressive range as friction-sliding fracture failure of brittle materials in the compressive range, see *Fig.1-19*.

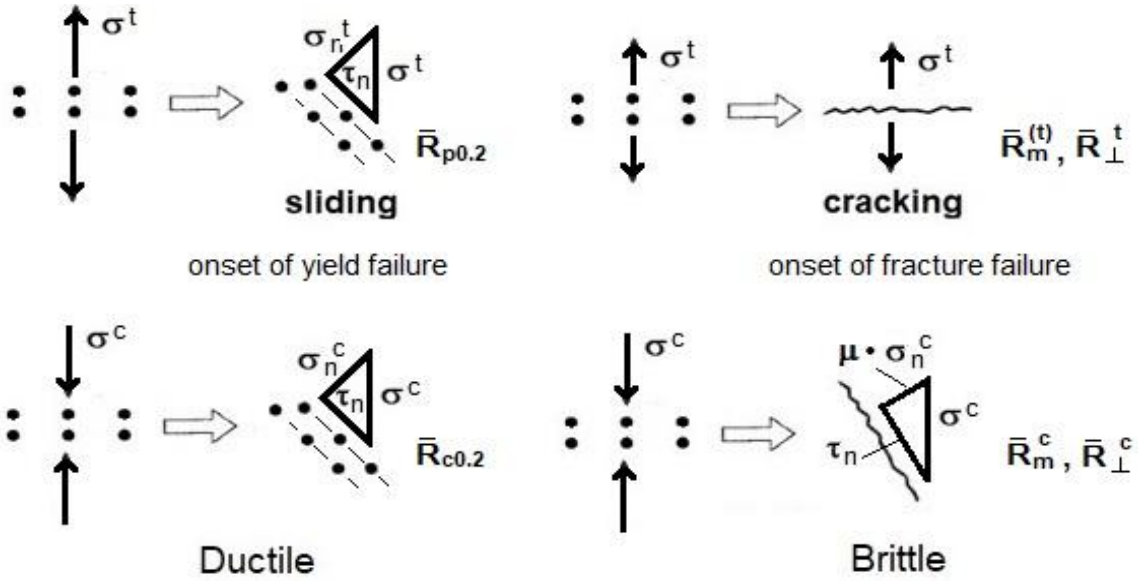


Fig.1-19: Rendering Sliding (micro)Cracking, ductile and brittle and the effect of p_{hyd}

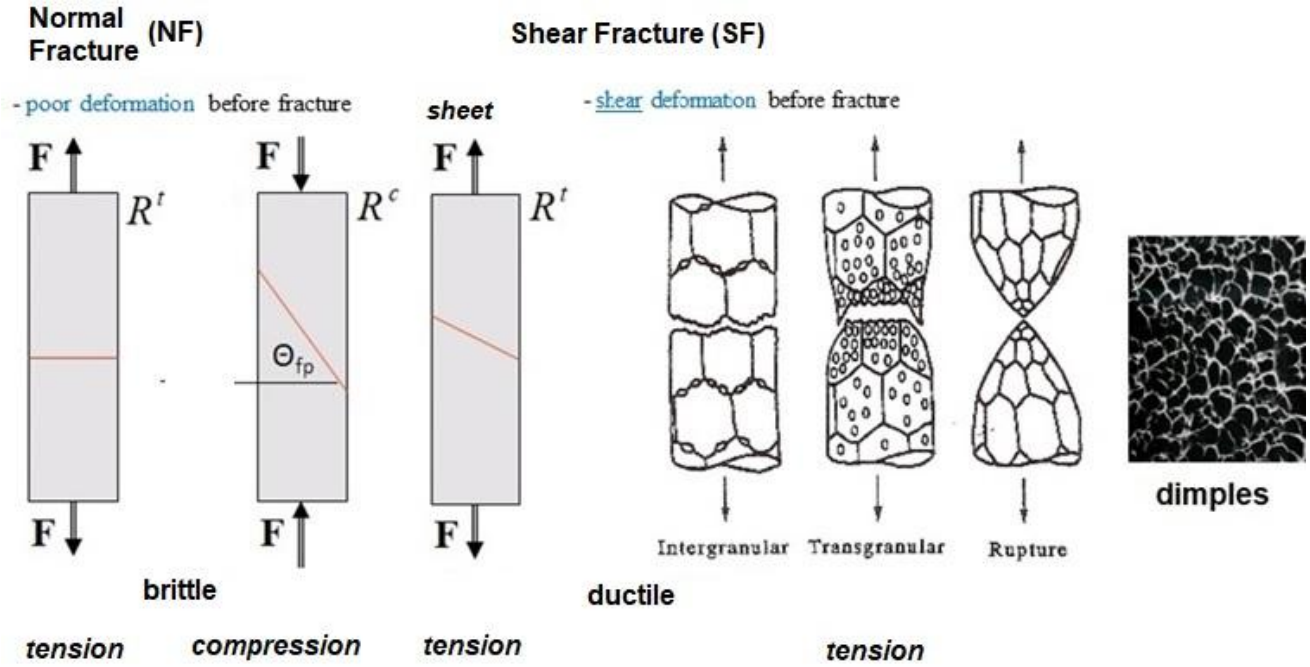


Fig.1-20: Fracture 'plane' sketches of different 'dense'
isotropic tensile test specimens (the angle may complementary defined)

Isotropic dense materials:

If brittle, then failure is fracture failure. The normative suffix $_m$ in $R_{(m)} = R^t$ should and can be dropped in *Fig.1-20* to *-21* in order to achieve a simpler and clearer general designation system.

LL:

** Brittle: failure is fracture failure, 2 failure modes, 2 strengths to be measured.*

** Ductile: failure is yield failure, 1 failure mode, 1 strength $\bar{R}^t$ to be measured (= load-controlled value), $\bar{R}^c$ is neither really existing due to barreling of the cylindrical test specimen nor necessary for design → $R_{0.2}$ is the design driving 'strength'.*

In *Fig.2-12* are depicted (left) Load situations with associated fracture plane sketches and shear fracture pictures, and (right) of tensioned, differently brittle isotropic materials.

Before tensile rupture (end of 'Gurson domain') firstly a diffuse and later a local *necking* with *void growth* occurs associated by a volume change before rupture starts. Dimples are generated under tension.

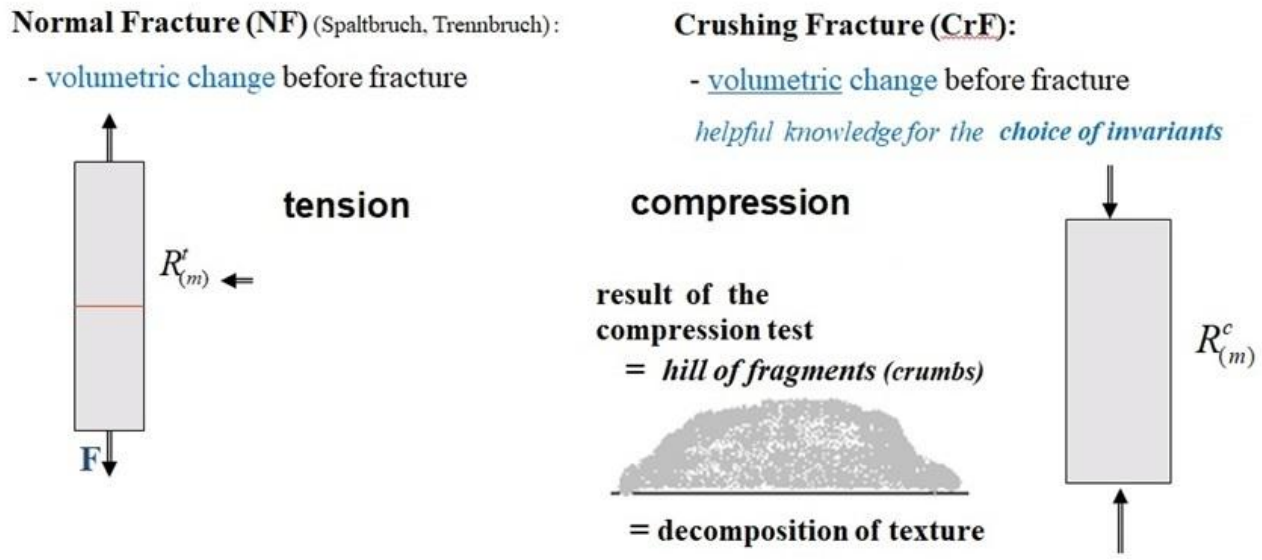


Fig.1-21: Normal Fracture NF and Crushing Fracture CrF of porous isotropic materials

In the case of isotropic brittle porous materials two failure modes are faced above, NF and CrF.

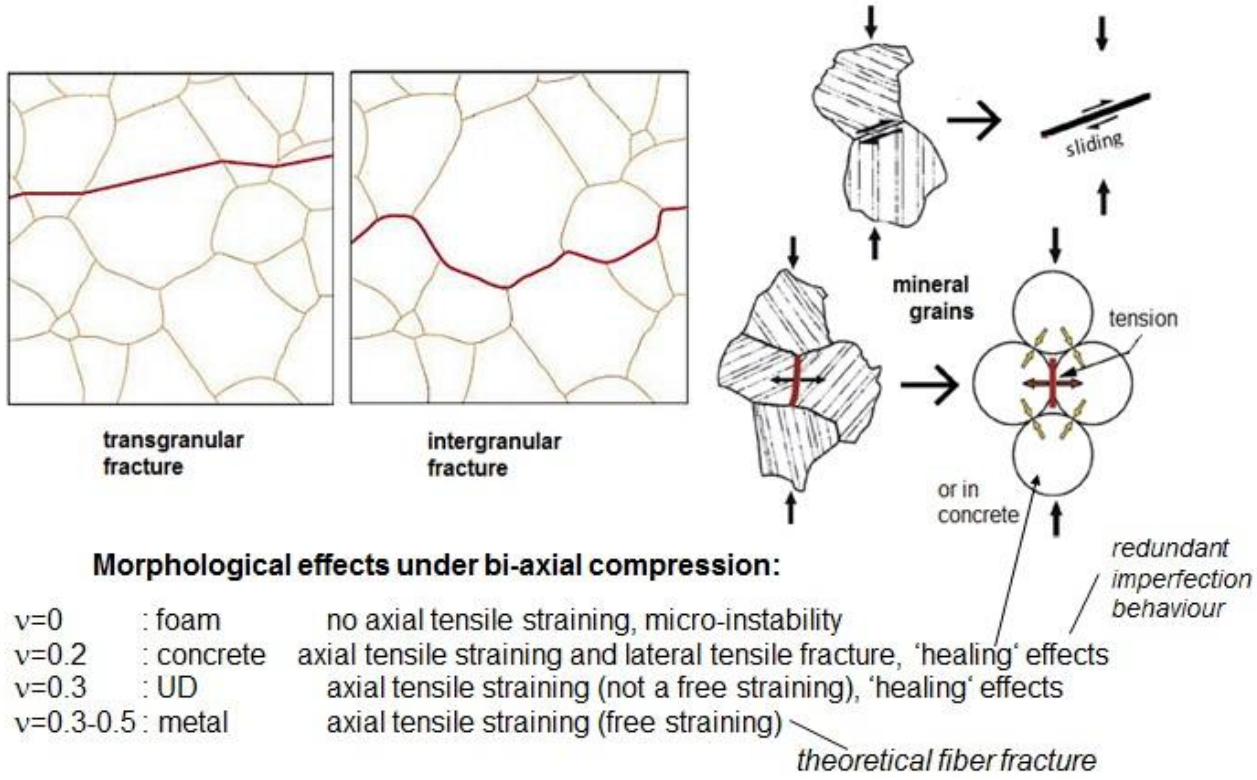


Fig.1-22: (left) Texture influence considering inter-granular and trans-granular fracture under tension; (right) Fracture between the mineral grains under compression due to 3D-tensile stress states

This leads over to **Mineral Grain materials,** see *Fig.1-22 above*. In the case of cracks, in contrast to the strength of intact solid materials, a uniaxial compressive stress causes a tensile stress at the crack tip of an inclined crack. This generates a secondary crack, termed wing (kink) crack, which turns into the direction of the acting compressive stress which may lead to splitting. Principally, this is similar to what happens in the fracture mechanics tension domain to an oblique macro-crack. Under multi-axial stress states the original crack may become instable and kinks with an altering direction of the fracture plane *(strain rate is influencing this behavior*). This problem has attracted much attention and shall be here considered by using a strength failure view,

In the 2D compression case one wing branches off from each end of the initial crack, *Fig.1-23* [*Ger94*]. These wings are generated dynamically. Then the further wing growth proceeds continuously. In the 3D compression case the generation of the wings causes an additional volume (*cavitation*) which is suppressed under multi-axial compression.

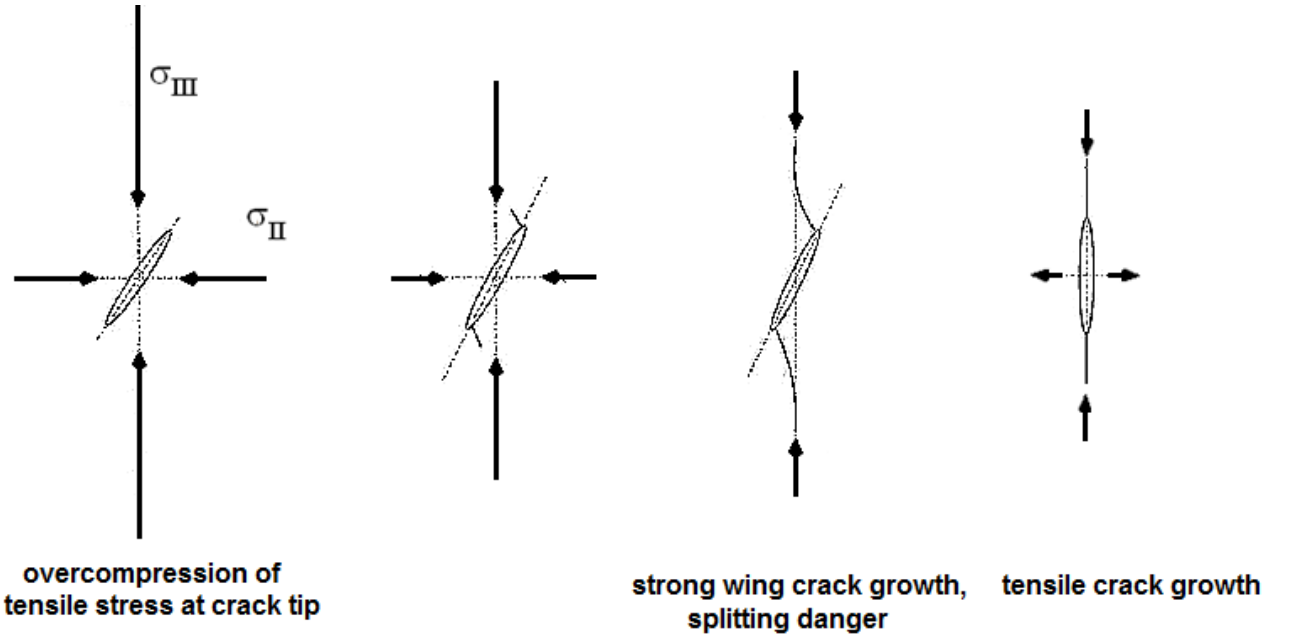


Fig.1-23: Initiation and attennuation of wing cracks (see [Ger94]

***LL**: 2D-models are not sufficient to describe progress of fracture in brittle behaving isotropic [Ger 94] materials such as grey cast iron, rock material, concrete, UD-material etc. 3D-theory and 3D experimental proofs are principally needed.*

For completion, *Fig.1-24* allocates cracks to 2D stress states. Under operational loading open-through crack and closed-through crack situations are to treat.

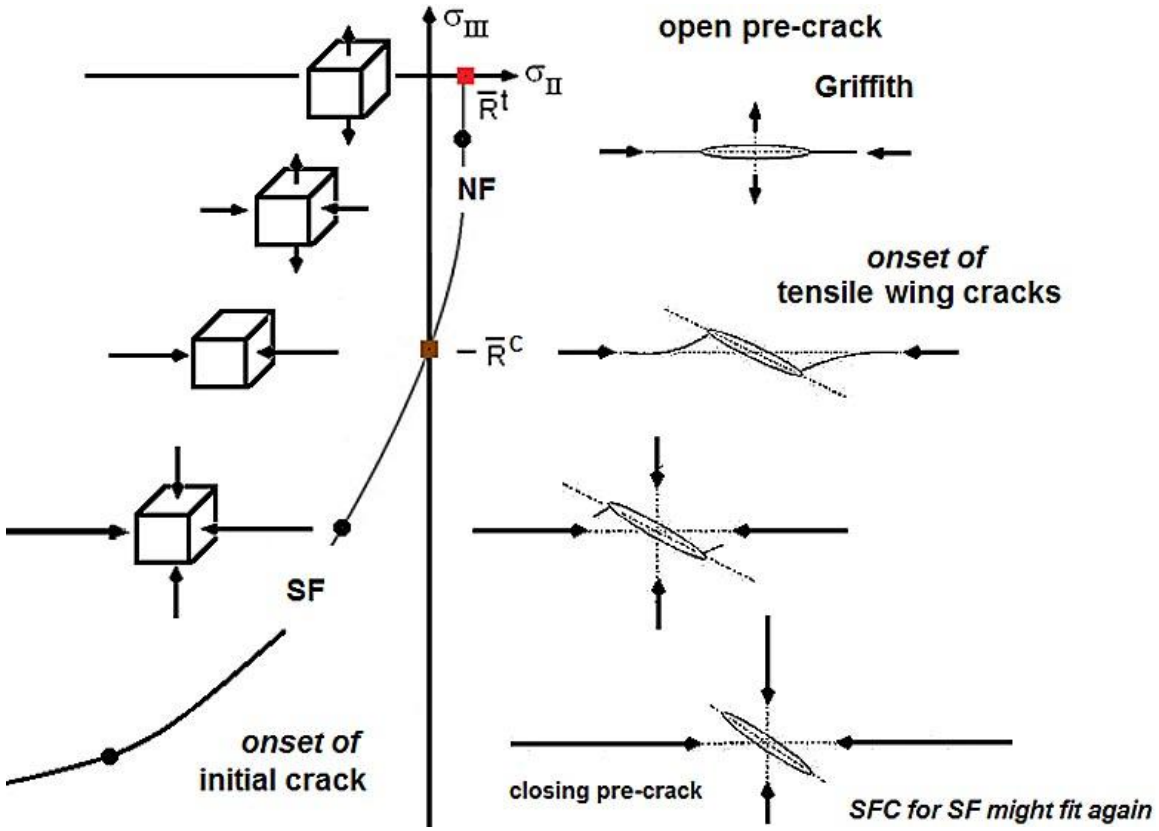


Fig.1-24: Mixed-Mode Compression, isotropic: 2D stress states, Observations w.r.t. failure modes NF and SF and fracture 'planes' in the case of initially crack-free (intact), open-through crack and closed-through crack situations

In the context of this subchapter the influence of porosity shall be shortly addressed.
Porosity is composed of all the cavities that are connected to each other and to the environment (*open porosity*) and the unconnected cavities (*closed*). A highly open-pored material is a honeycomb for instance, closed porosity one finds with foams, see [*Dr. J. Macht, Univ.-Doz., Dr. P. Nischer, Forschungsinstitut der VÖZ, Wien*]. Porous materials, such as foams, porous laminates, porous polymer and concrete matrices, mortar, brick and geo-materials have stress-strain curves, which can be divided into 3 sections: (1) Pressure low: the material behaves elastically, pores are preserved, (2) Pressure increased: pores are compressed, (3) Pressure exceeds a certain limit: finally complete compaction with pulverization of the crushed material. Collapse of the pores during crushing drives the compaction behavior of porous materials.

Transversely-isotropic dense materials:

The *Fig.1-25* presents micro-mechanical fracture of transversely-isotropic UD-material.

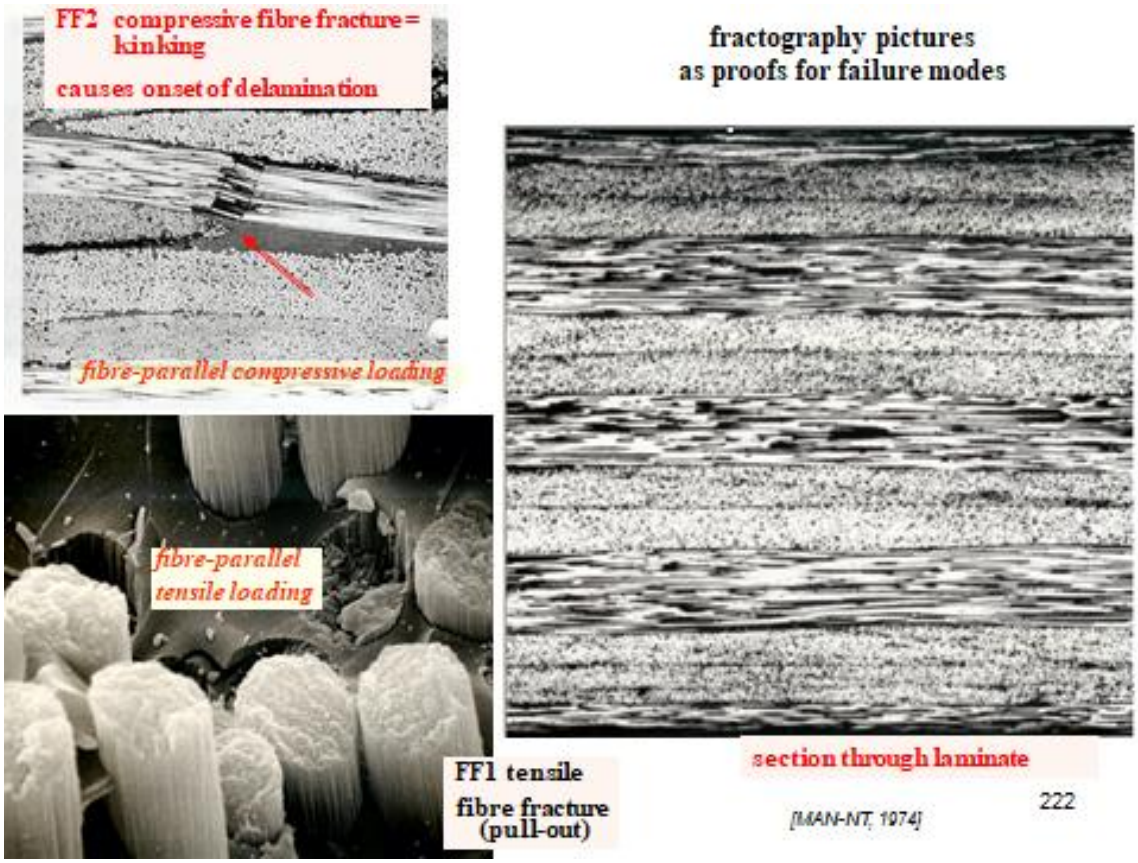


Fig.1-25: Fracture of UD material on micro-level

The observed fracture types of *Fig.1-26* depict failure modes which can be dedicated to the well-known 5 UD fracture failure modes.

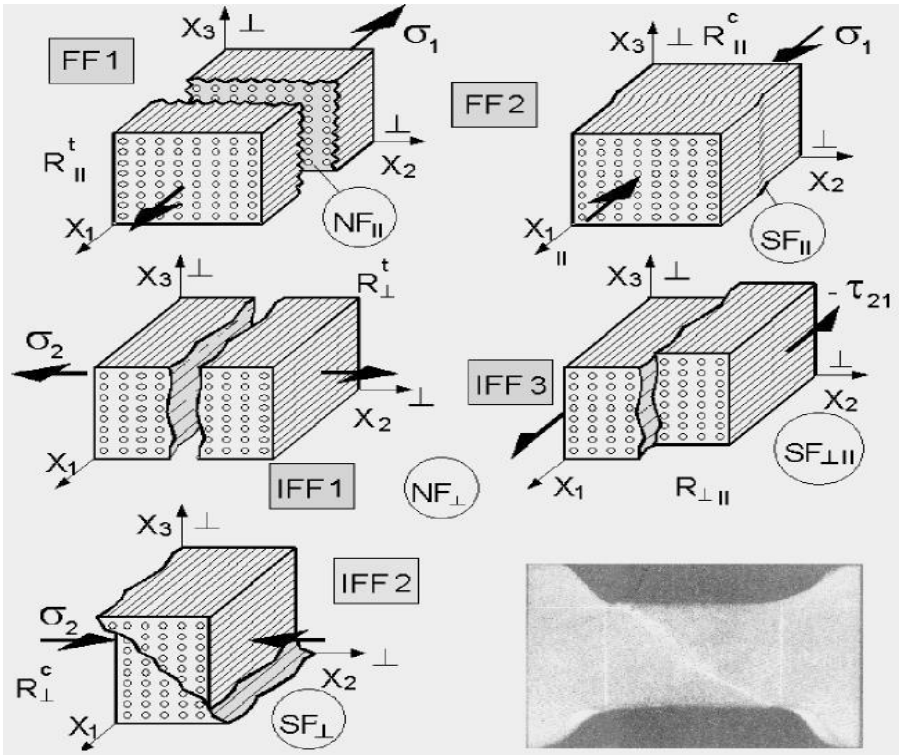


Fig.1-26: Test-observed UD Failure modes

1.10 A first Visualization of an Isotropic Failure Body with the Mode Domains SF and NF

Engineers better learn from meaningful figures than from formulas. Therefore, numerically very effortful visualizations of the generated SFC failure bodies are a strong need, because a failure body shows the designing engineer the 'multiaxial strength capacity' of a material. This task will be exemplarily performed for an isotropic Normal Concrete material where a test data set was available.

A failure body is the location of all 1D-, 2D- and 3D-failure stress states. These are all points on the failure surface. As still mentioned, $F = 1$ or $Eff = 100\%$ mathematically defines the surface of the failure body. Such an isotropic failure body is rendered here using the Haigh-Westergaard-Lode coordinates with $I_1/\sqrt{3}$ as y-coordinate (axial) and $\sqrt{2 \cdot J_2}$ as x-coordinate (hoop), see *Fig.1-27*.

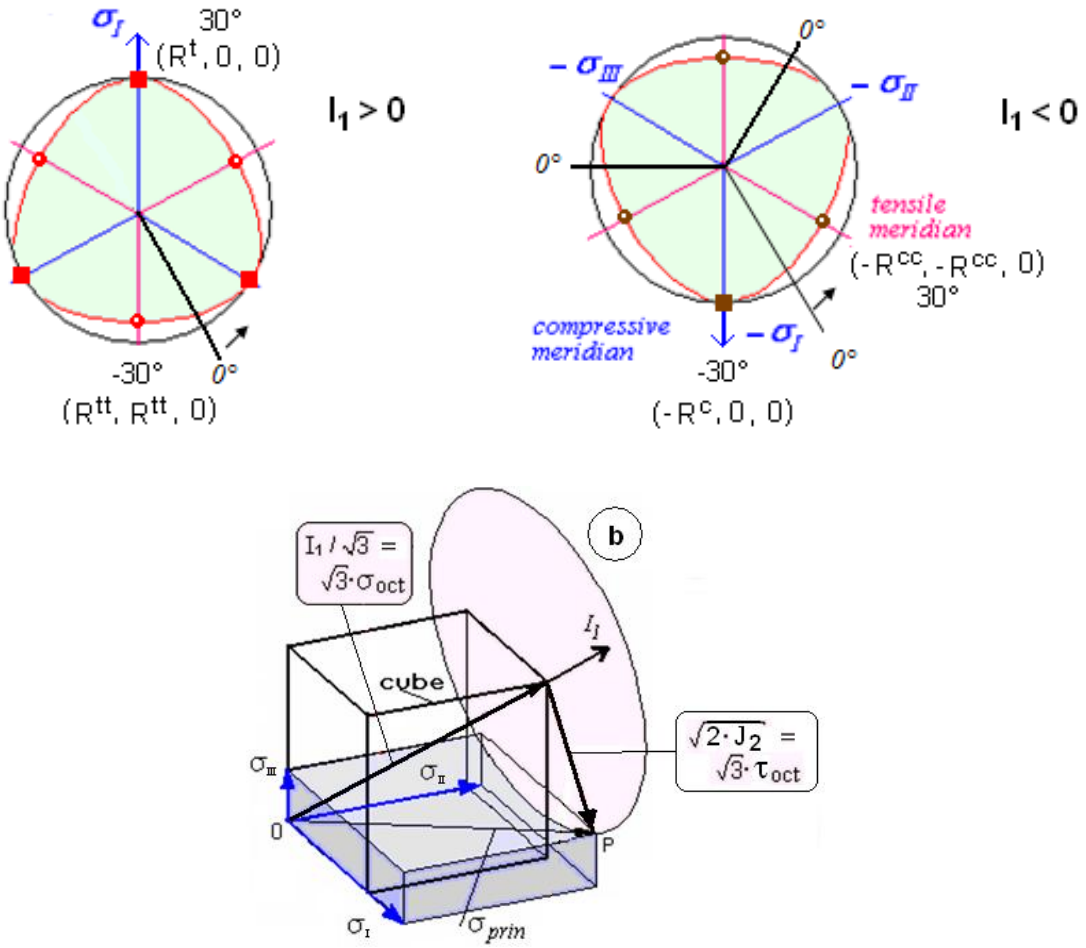


Fig.1-27: Mises cylinder shape, meridians, dents, Lode angle ϑ° around the 120°-hoop. Ansatz: sin(3ϑ) with ϑ°=0° at shear meridian was taken; right figure: visualization of Lode coordinates

In *Fig.1-28* the upper left part figure confirms, that above coordinate choice physically makes sense, because of the equal measurement in all directions. The part figure, left down, depicts the stress states belonging to a tensile meridian and to a compressive meridian. These are those axial cross–sections of the failure body (right) along most of the compression tests are run. On the fracture failure body the 3 main meridians are outlined. For the tensile meridian the Lode angle is $\vartheta = +30°$ and for the compressive meridian -30°. The shear meridian was chosen here as neutral meridian with a Lode angle $\vartheta = 0$. Some 3D-failure stress states are indicated as fracture body

points. Finally, for three essential design quantities the formulas are presented at the right side down.

The 'Mises' cylinder should also show the 120°-symmetry for ductile isotropic metals indicated by $\bar{R}^{tt} > \bar{R}^{t}$! This will be later demonstrated.

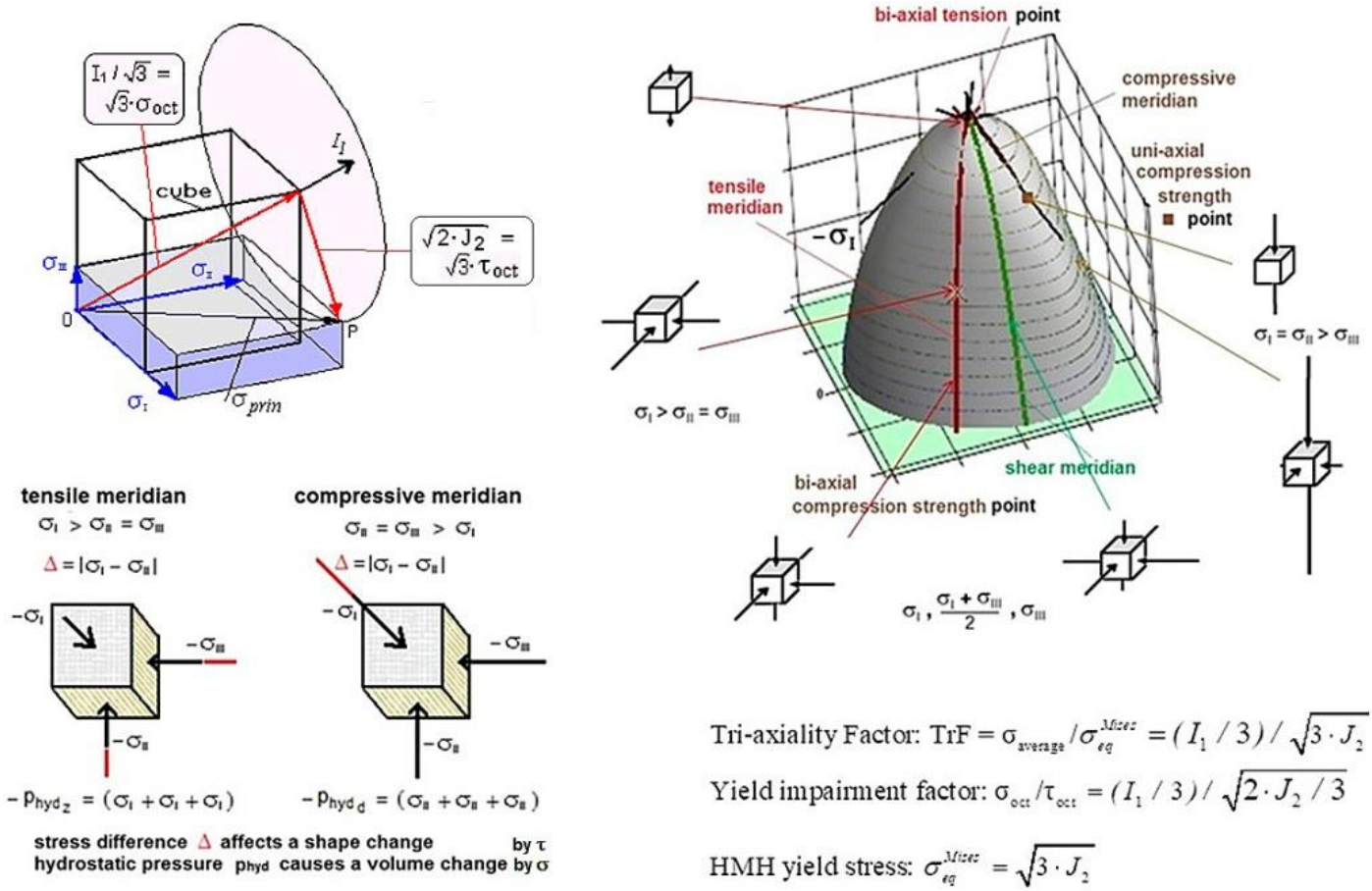


Fig.1-28: Visualization of the main meridians using Haigh-Westergaard Lode-coordinates $I_1/\sqrt{3}$, $\sqrt{2 \cdot J_2}$ and various multi-axial stress states. Squares ■ ■ indicate strength values (strengths are defined as uniaxial failure stresses) and crosses mark bi-axial points (bi-axial failure stresses)

Mind, please:

- Technical strength *R:* 1D-failure stress, defined by standards and cannot be increased considering the same material. Its value for a given material is fixed!
- Test data mapping, using an average strength $\bar{R}$: Results belong to a 50% survival probability expectance value.
- Design verification, using *R*: Result output is with a safety concept-required statistical survival probability
- Material symmetry: fixes the number of measurable properties. A material model that needs more parameters than measurable properties requires the execution of a simulation process with several analysis loops in order to determine these parameters by numerical fitting. This causes a problem in fulfilling the statistical requirements to be considered in the final (single) Design Verification analysis.

1.11 Shear Yield failure and Fracture Planes of some Isotropic Materials

For supporting the idea to think in failure planes four figures shall be displayed below:

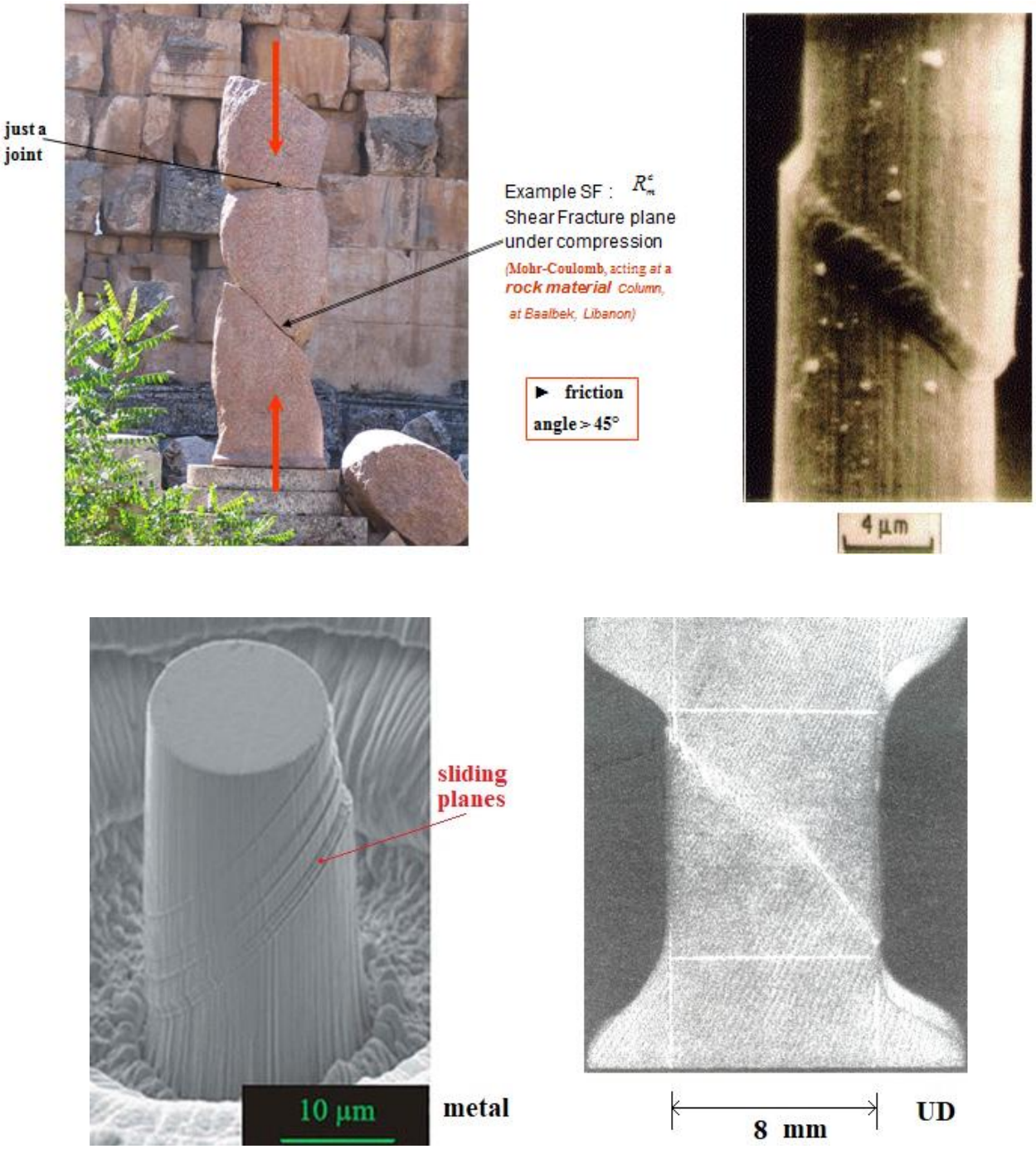


Fig.1-29: Shear failure angles on very different materials and length scales.Three fracture angles of the brittle materials
Rock material, Carbon fiber, ductile metal compression test specimen cut from a single crystal see further § 16.6) and brittle CFRP quasi-isotropic plane

2 Presentation of FMC-based SFCs and Associated Topics

2.1 Introduction with comparison of so-called 'Global' and 'Modal' SFCs

There are a lot of possibilities to generate SFCs. *Fig.2-1* gives a survey about this variety.

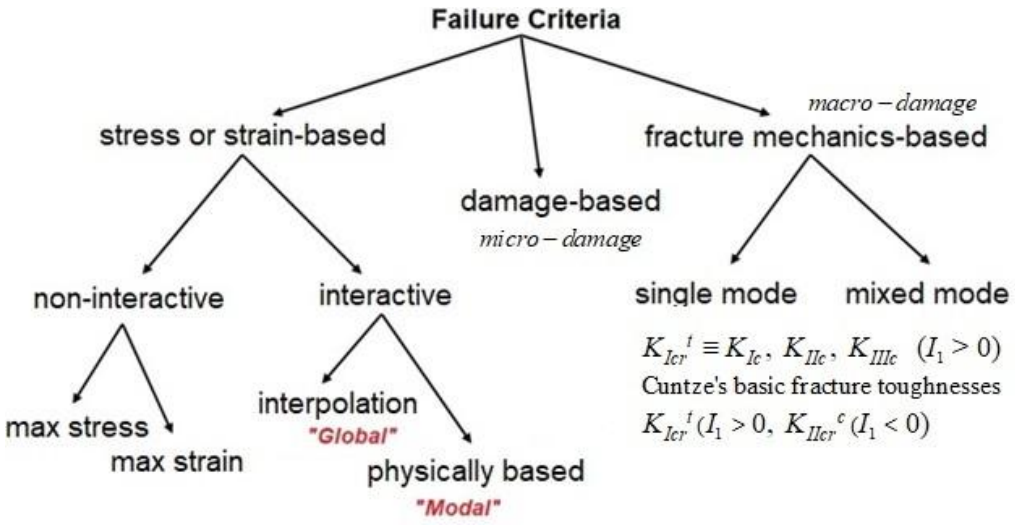


Fig.2-1: Possibilities to generate SFCs when following Klaus Rohwer [Roh14]

Interactive SFCs can be discriminated. To do that the author choose the term "Global" as a 'play on words' to "modal" and both the terms as being self-explaining names. Here, global and modal have a similar level of abstraction, as in the case of stability the terms 'global' and 'local'.

Fig.2-2 presents the main features of global and modal SFCs.

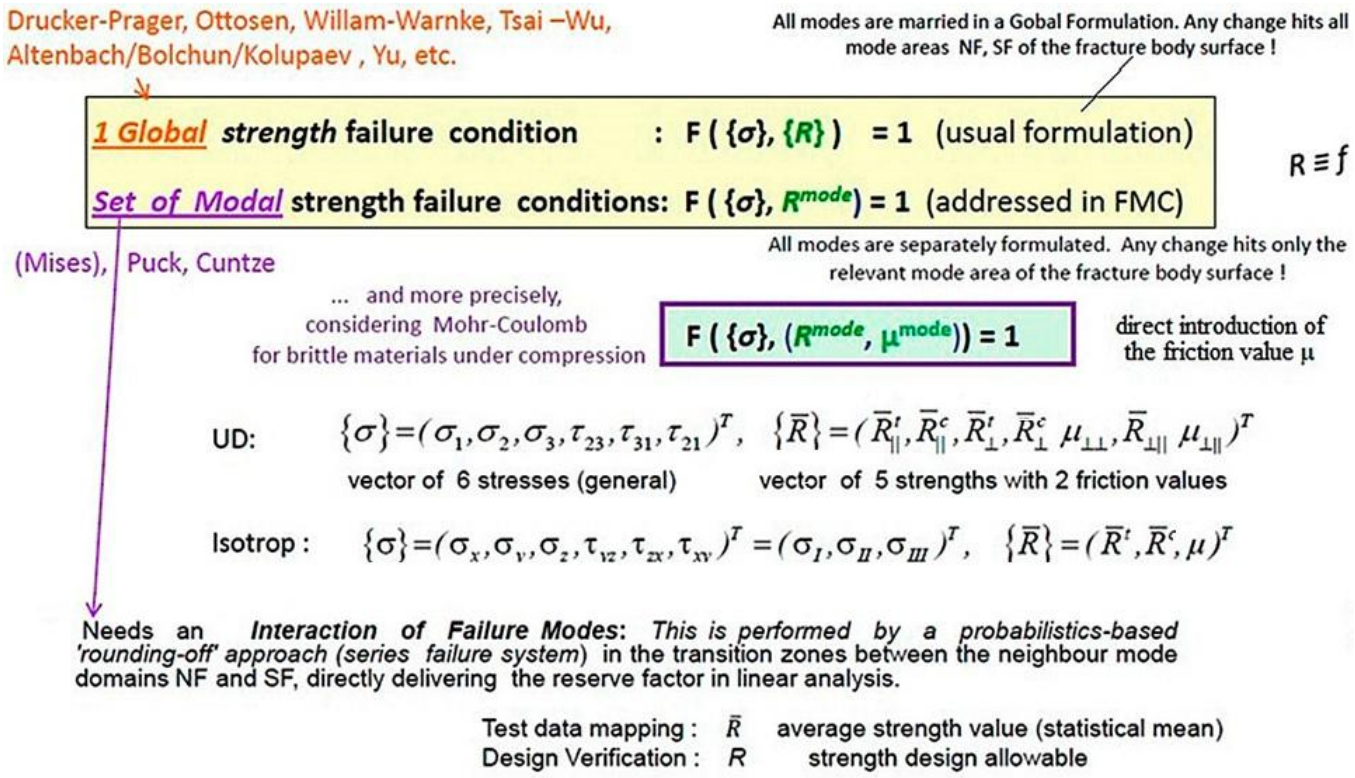


Fig.2-2: 'Global' and 'Modal' SFCs (in construction R → f = Festigkeit

Global SFCs describe the full failure surface by one single equation capturing all existing failure modes such as Normal Fracture (NF, *under tension or shear*) or Shear Fracture (SF, *under compression*). A specific name used for 'global' is 'Single Failure Surface Description'. Modal SFCs describe each failure mode-associated part of the full failure surface by one equation.

Example for the derivation of an isotropic Global SFC: Formulation of shape functions for the failure body describing (1) the hoop cross-section (π-plane $\equiv I_1$ =constant plane regarding the Lode angle ϑ), (2) the axial cross-section = meridian along I_1.

Table 2-1: Pros (+) and Cons (-) of 'global' and 'modal' SFCs

Global SFCs

- (+) Describe the full failure surface by one single mathematical equation
- (-) Usual global SFCs do not capture a multi-fold acting failure mode, i.e. $\sigma_I = \sigma_{II}$ or $\sigma_2 = \sigma_3$ or a 3-fold acting failure mode under σ_{hyd} with tension or compression
- (-) Re-calculation: In the case of a test data change in a distinct mode domain re-calculation of model parameters is mandatory. Any change in one of the 'forcibly married' modes requires a new global mapping which also changes the failure curve in a physically independent failure domain, see *Fig.2-3*. In consequence, the material reserve factor has to be determined again
- (-) The determination of *RF* for multi-axial stress states seems to be questionable for the simple Drucker-Prage model (*conical failure body*) - still often used in civil engineering - see *Sub-chapter 9.3*.

Modal SFCs

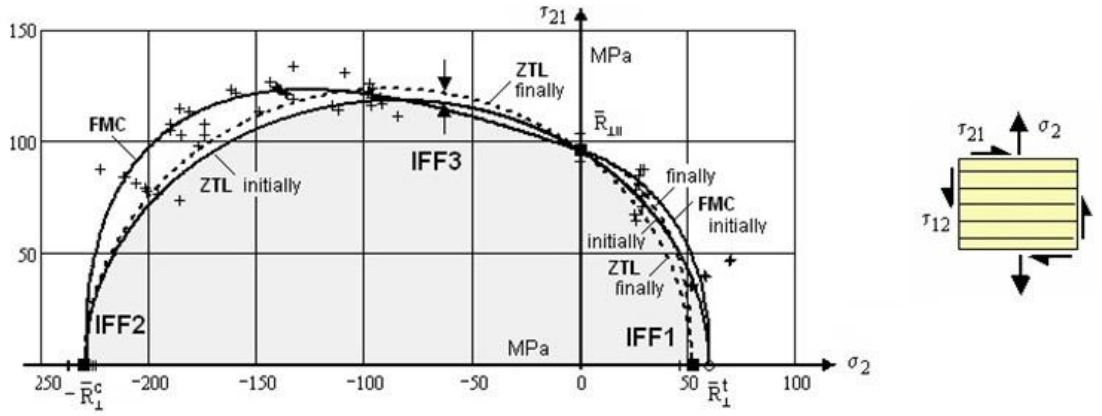
- (+) Describes each failure mode-associated part of the full failure surface by a single equation. Therefore, modal SFCs are more physically-based than global SFCs
- (+) A change within one mode just hits this mode, *see Fig.2-3*. *RF* is just to re-determine in the affected failure mode domain!
- (+) Equivalent stresses σ_{eq} are always determinable for isotropic UD materials
- (+) Cuntze's SFCs capture multi-fold occurring failure modes by an additional term
- (+) Cuntze's SFCs directly use the well to estimate parameter friction value μ
- (-) Affords an interaction of the FMC-based SFCs for the activated failure modes.

Fig.2-3 visualizes for a distinct global SFC, used in a German guideline, how dramatically a change of the tensile strength $\bar{R}_{\perp}^{t}$ affects the failure curve in the compression domain, although no physical impact can be!

In order to only use experimentally derivable material quantities, the author directly introduced in his 3D-SFCs for the compression domain, the internal material friction μ as a SFC model parameter. Friction is a well-known physical property in engineering. However, one does not yet find a direct use of μ in the textbooks! Why using Mohr's friction angle φ if μ (φ) exists? The direct introduction of the measurable friction value is possible for the modal shear fracture SFCs. This possibility was achieved after the performance of an effortful transition of the SFC formulated in structural stresses into a Mohr stresses formulated one (see *Chapter 6*).

Mind, please:

Often, SFCs employ just strengths. This is physically not accurate: Mohr-Coulomb acts in the case of compressed brittle materials! Consequence: The computed *RF* may not be on the safe side.



ZTL: global

$$\frac{\sigma_2^{\,2}}{\bar{R}_\perp^t \cdot \bar{R}_\perp^c} + \sigma_2 \cdot \left(\frac{1}{\bar{R}_\perp^t} - \frac{1}{\bar{R}_\perp^c}\right) + \frac{\tau_{21}^{\,2}}{\bar{R}_{\perp\parallel}} = 1$$

FMC: modal

$$\left(\frac{\sigma_2}{\bar{R}_\perp^t}\right)^m + \left(\frac{-\sigma_2}{\bar{R}_\perp^c}\right)^m + \left(\frac{|\tau_{21}|}{\bar{R}_{\perp\parallel} - \mu_{\perp\parallel} \cdot \sigma_2}\right)^m = 1$$

Fig.2-3: Effect of global modelling, ZTL-SFC

The old ZTL-SFC above is still used in the HSB and intentionally applied in some examples, later).

Considering the shortcomings of Global UD SFCs, my friend John Hart-Smith, cited in [*Har93*]:

"It is scientifically incorrect to employ polynomial interaction failure models (‘global’ ones)***, if the mechanism of failure changes?"***

2.2 Collected Basic features of the Failure-Mode-Concept FMC (1996)

From the investigations and the knowledge above the basic features of the FMC can be derived:

- Each failure mode represents 1 independent failure mechanism and thereby represents 1 piece of the complete (*is global again*) failure surface
- Each failure mechanism is governed by 1 basic strength (this is witnessed)
- Each failure mode can be represented by 1 failure condition SFC [*Cun04,12,15a*]

  Therefore, equivalent stresses can be computed for each mode. This is of advantage when deriving SN curves and Haigh diagrams in fatigue with minimum test effort, see [*Cun17*]
- Consequently, the FMC-approach requires an interaction of all modes!

$$Eff = \sqrt[m]{(Eff^{\text{mode }1})^m + (Eff^{\text{mode }2})^m + ...} = 1 = 100\% \qquad for \quad \text{Onset-of-Failure .}$$

This interaction of adjacent failure modes is modelled by the spring model ‘series failure system’. That permits to formulate the total material stressing effort from all activated failure modes as the ‘accumulation’ of *Eff*s ≡ sum of all the failure danger proportions. *Eff* = 1 represents the mathematical description of the surface of a failure body!

From engineering reasons, Cuntze takes the same interaction exponent *m* for each transition zone between two failure mode domains. The value of *m* depends on the ratio R^c / R^t. For brittle dense materials with about R^c / R^t > 3 the value is about *m* = 2.6, obtained from much mapping experience in the transition zone of the two modes. A smaller *m* is always 'design verification conservative'.

- Failure at the lower microscopic level shall be considered in the applied macroscopic SFC.

The knowledge about the materials - collected above - lead in the FMC to consider: a

- ✓ *Rigorous postulation of a number of failure modes = number of strengths*
- ✓ *Application of a failure mode-wise concept for the generation of SFCs*
- ✓ *Direct use of the friction value μ in the SFC.*

Ideas/desires, formed over the years, became pre-requisites of the author for the 'Creation of the Failure–Mode-Concept FMC' and shall be collected in <u>*Table 2-1:*</u>

Table 2-1: Desires for the generation of effective High Fidelity (Genauigkeit, Verläßlichkeit) SFCs

- applicable for all material families
- rigorous independent treatment of each single failure mode NF, SF, CrF, FF, IFF, ..
- physically convincing mapping method *(then just a minimum test information is needed)*
- numerically robust, unique solutions, simple, as much as physics allows it
- stress invariant-based *(like 'Mises' for the single mode yielding , J_2)*
- application of the hypothesis of Beltrami (isotropic invariants stand for a deformation change J_2 for the shape of the material element and I_1^2 for a volume change. Similarly for UD)
- application of the hypothesis of Mohr-Coulomb, considering internal material friction by use of I_1 in isotropic case
- delivery of equivalent stresses σ_{eq} *(very helpful for a failure mode-based turning of the 'design screw')*
- using a material <u>behavior</u>-linked thinking and not a material-linked one
- an approach, where all model parameters can be measured *(model parameters are to determine separately in each mode domain)*
- viewing the Strength Mechanics 'Building': More physically-based it should become simpler
- shall allow for a simple determination of *RF* or of the so-called *material stressing effort Eff* which is best understood from engineers in stress state assessment of a material. The link is $\sigma_{eq} = Eff \cdot R$,
- use of so-called 'proportional loading' in order to derive *Eff* in case of *mathematically non-homogeneous SFCs*, however, fulfilling the requirement that with a zero failure <u>driving</u> stress σ or τ the *Eff*-value becomes zero, too.

<u>LL:</u>

- ➢ *Failure condition is a condition on which a failure becomes effective*
- ➢ *Criterion is a distinctive feature as a condition for a state F < = >. A SFC means F= 1*
- ➢ *Decisive for a High Fidelity SFC application is: Is the used SFC validated by multi-axial fracture stress states or not? To be not 3D-validated is an essential bottleneck. How sure can the designer be with the 3D validation performed for the used classical strength criterion? Check.*

- *Values of m > 3 could be taken if there is just a very low mutual triggering of the failure effects of the affected modes.*
- *Stress-based SFCs have the advantage that residual stresses can be simply captured in the analysis.*
- *Three energy terms – represented by two invariants, only - are required to establish 'isotropic SFCs'. Hence, the FMC approach is not without any energy basis as some other 'stress-based criteria'*
- *Material symmetry seems to have told the author: In the case of isotropic materials, for the quantities a generic (basic) number of 2 is inherent. This is valid for modes, invariants, yield strengths, fracture strengths, fracture mechanical SIFs [Cun20] and more entities. And this also affects the test effort considering 'What is the minimum test effort to be necessarily measured?*
- *The 120°-rotational symmetry could be mapped by employing J_3 (The occurrence of a double mode is the only reason for the application of a third invariant). A brittle slightly porous concrete in the compression domain (p_{hyd}) can be SFC-described by the same SFC formula as a metal in the ductile rupture or 'Gurson tension domain', respectively due to similarly describable effects of the material element.*

2.3 Modal equivalent stress σ_{eq} and Modal material stressing effort *Eff*

For the failure mode 'yielding' the HMH hypothesis (in short 'Mises') delivers an equivalent stress and this for all stress situations (normal stress, shear stress, torsion stress) when the mode yielding comes to act, *Fig.2-4*. Fully analogously to the (modal) HMH equivalent *yield* stress the equivalent *fracture* stress is related to the material stressing effort

$$Eff^{Mises} = \sigma_{eq}^{Mises} / R_{po.2} \Rightarrow Eff^{fracture\ mode} = \sigma_{eq}^{fracture\ mode} / R_m \ , \ Eff^{mode} = \sigma_{eq}^{mode} / \overline{R}^{mode} \ .$$

Above possibility to formulate equivalent stresses caused Cuntze to differentiate Global from Modal strength criteria types. About more details and the Pros and Cons, see [*Cun16c*].

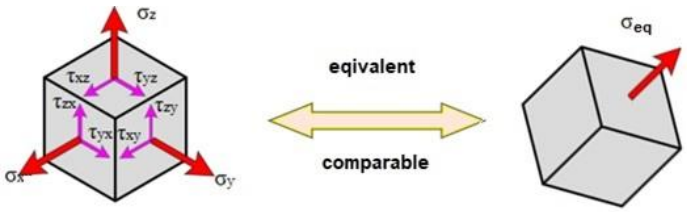


Fig.2-4: multi-axial structural stress state with its representing equivalent stress

Fig.23-5 shows the definition of the material stressing effort. *Eff* is an artificial term, created with the WWFE originators in the UK, because a similar term does not exist in English.

2.4 History of FMC with Search of a 'More Closed' Strength Mechanics Building

After 1985 the author co-worked in several structural reliability groups and projects. Aim in structural reliability is to prove that a distinct limit state is not yet met. In the group of structural limit states the material's strength limit states play a very essential role. The author experienced the advantage to 'Think in strength failure modes', which led him to a rigorous thinking in strength failure mode limit states and that later paved the way for the development of the FMC.

In industry the author headed the department 'Structural and Thermal Analysis'. Therefore, he had to take care of material modelling because he faced a not sufficient 'feeling' in structural engineering considering the strength of non-cracked materials. This experience is valid for the three

material families used isotropic materials, transversely-isotropic (*UD fiber reinforced matrices*) materials and orthotropic (*fabrics etc.)* materials, where design verification for the fabricated structural components had to be performed. Thereby brittle materials were the focus.

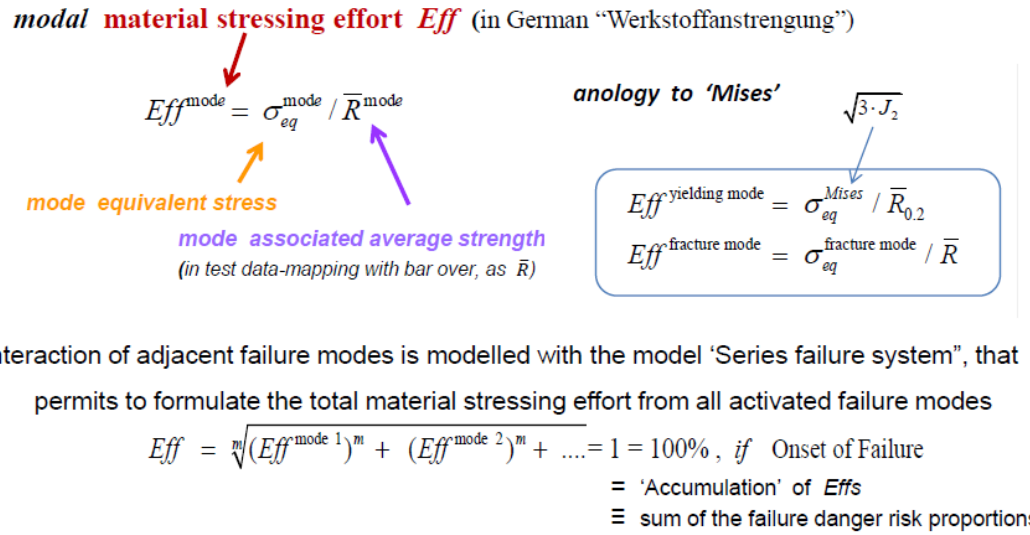
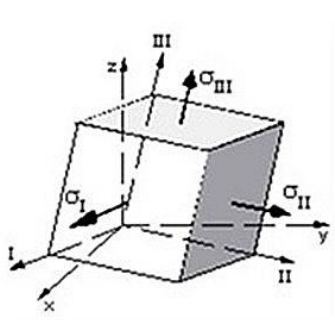


Fig.2-5: Definition of material stressing effort Eff (derivation of the interaction equation in §12.11)

This situation firstly caused the author to think about SFCs for a variety of structural materials and secondly – after being successful with the SFCs – to think about a strength mechanics building that includes the previously assumed missing links as 'rooms'.

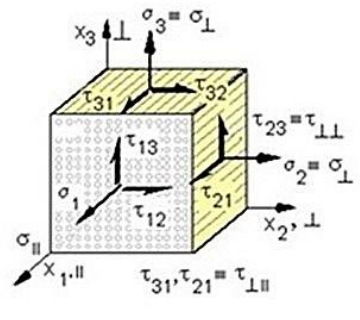
This 'building' includes the assumed full set of strength failure modes for the intact, non-cracked material and also regarded the fracture mechanics modes. The task involved isotropic and transversely-isotropic materials where clear SFCs can be found as long as 'conglomerate materials' can be homogenized ('smeared') to a model material. Orthotropic materials are usually still structures where a separation of fracture failure modes is not difficult.

The FMC-derived SFCs, applied in tensile and in compression domain, are presented in the following Tables. A SFC is a model that should be as simple as possible but should well describe physics macro-mechanically and as far as possible capture the associated micro-mechanically failure events. $F = 1$ or $Eff = 100\%$ mathematically defines the surface of the fracture failure body. For each mode, the SFC model parameters are just to determine in each associated 'pure' failure mode domain. As reminder, before the presentation of the SFCs, all stress state figures of the 3 material families are displayed:



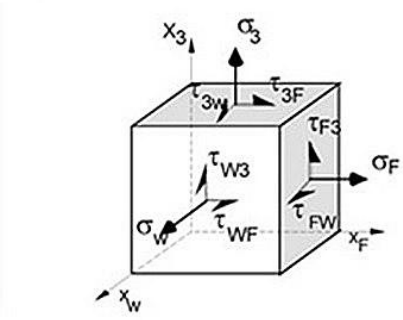
isotropic

$\{\sigma\} = (\sigma_x, \sigma_y, \sigma_z, \tau_{yz}, \tau_{xz}, \tau_{xy})^T$



transversely-isotropic

$\{\sigma\} = (\sigma_1, \sigma_2, \sigma_3, \tau_{23}, \tau_{13}, \tau_{21})^T$



rhombically-anisotropic

$\{\sigma\} = (\sigma_W, \sigma_F, \sigma_3, \tau_{3F}, \tau_{3W}, \tau_{FW})^T$

Addressing mapping it should be noted: 2D test data sets must be mapped by the 3D failure function F broken down to a 2D-one in the 2D principal plane. 3D-test data sets are directly mapped by the 3D-SFC defining the 3D failure body or surface. Meridional shape functions (*cross section of the isotropic failure body*) should be not the result of a separate 2D meridional mapping of the associated isotropic test data, but the result of the desired meridian angle ϑ inserted into the general 3D-SFC.

2.5 SFCs for 'dense' and 'porous' Isotropic Material

Table 2-2 collects all information necessary to design dimension a dense isotropic material.

*Table 2-2 'Dense' materials: SFC formulations for **NF** and **SF**, 120°-rotational symmetry*

Normal Fracture NF for $I_1 > 0$ ↔ Shear Fracture SF for $I_1 < 0$

$$F_\sigma^t = F^{NF} = c^{NF} \cdot \Theta^{NF} \cdot \frac{\sqrt{4J_2 \cdot \Theta^{NF} - I_1^2/3} + I_1}{2 \cdot \bar{R}^t} = 1 \quad \leftrightarrow \quad F_\tau^c = F^{SF} = c_{1\Theta}^{SF} \cdot \frac{3J_2 \cdot \Theta^{SF}}{\bar{R}^{c2}} + c_{2\Theta}^{SF} \cdot \frac{I_1}{\bar{R}^c} = 1$$

$$Eff^{NF} = c^{NF} \cdot \frac{\sqrt{4J_2 \cdot \Theta^{NF} - I_1^2/3} + I_1}{2 \cdot \bar{R}^t} = \frac{\sigma_{eq}^{NF}}{\bar{R}^t} \leftrightarrow Eff^{SF} = \frac{c_{2\Theta}^{SF} \cdot I_1 + \sqrt{(c_{2\Theta}^{SF} \cdot I_1)^2 + 12 \cdot c_{1\Theta}^{SF} \cdot 3J_2 \cdot \Theta^{SF}}}{2 \cdot \bar{R}^c} = \frac{\sigma_{eq}^{SF}}{\bar{R}^c}.$$

If a failure body is rotationally symmetric, then Θ = 1 like for the neutral or shear meridian.

A two-fold acting mode makes the rotationally symmetric fracture body 120°-symmetric and is modelled by $\Theta(J_3)$ using the invariant J_3 and Θ as non-circularity function with d as non-circularity parameter

$$\Theta^{NF} = \sqrt[3]{1 + d^{NF} \cdot \sin(3\vartheta)} = \sqrt[3]{1 + d^{NF} \cdot 1.5 \cdot \sqrt{3} \cdot J_3 \cdot J_2^{-1.5}}, \quad \Theta^{SF} = \sqrt[3]{1 + d^{SF} \cdot 1.5 \cdot \sqrt{3} \cdot J_3 \cdot J_2^{-1.5}}$$

Lode angle ϑ, here set as $\sin(3 \cdot \vartheta)$ with 'neutral' shear meridian angle set $\vartheta = 0°$;

tensile meridian angle 30° $\rightarrow \Theta^{NF} = \sqrt[3]{1 + d^{SF} \cdot (+1)}$; compr. merid. angle -30° $\rightarrow \Theta^{SF} = \sqrt[3]{1 + d^{SF} \cdot (-1)}$.

Equation of the fracture failure body: $Eff = [(Eff^{NF})^m + (Eff^{SF})^m]^{m^{-1}} = 1 = 100\%$ total effort

$$Eff = \sqrt[m]{\left(c^{NF} \cdot \frac{\sqrt{4J_2 \cdot \Theta^{NF} - I_1^2/3} + I_1}{2 \cdot \bar{R}^t}\right)^m + \left(\frac{c_{2\Theta}^{SF} \cdot I_1 + \sqrt{(c_{2\Theta}^{SF} \cdot I_1)^2 + 12 \cdot c_{1\Theta}^{SF} \cdot 3J_2 \cdot \Theta^{SF}}}{2 \cdot \bar{R}^c}\right)^m} = 1.$$

Curve parameter relationships obtained by inserting the compressive strength point (0, -$\bar{R}^c$, 0):

* Rotationally symmetric: $c_1^{SF} = 1 + c_2^{SF}$, $d^{SF} = 0$, friction parameters are equal $c_2^{SF} \equiv c_{2\Theta}^{SF}$

$c_2^{SF} = c_{2\Theta}^{SF} \approx (1 + 3 \cdot \mu)/(1 - 3 \cdot \mu)$ from $\mu = \cos(2 \cdot \theta_{fp}^c° \cdot \pi / 180)$ and for 50° $\rightarrow \mu = 0.174$.

* 120°-rotationally symmetric: $c_{1\Theta}^{SF} = 1 + c_{2\Theta}^{SF} \cdot \sqrt[3]{1 + d^{SF} \cdot (-1)}$ with

c^{NF}, Θ^{NF} from the two points $(\bar{R}^t, 0, 0)$ and $(\bar{R}^{tt}, \bar{R}^{tt}, 0)$ or by a minimum error fit, if data,

c^{SF}, Θ^{SF} from the two points $(-\bar{R}^c, 0, 0)$ and $(-\bar{R}^{cc}, -\bar{R}^{cc}, 0)$ or by minimum error fit.

A paraboloid serves as closing cap $\frac{I_1}{\sqrt{3} \cdot \bar{R}^t} = s^{cap} \cdot \left(\frac{\sqrt{2J_2 \cdot \Theta^{NF}}}{\bar{R}^t}\right)^2 + \frac{\max I_1}{\sqrt{3} \cdot \bar{R}^t}$.

$$I_1 = (\sigma_I + \sigma_{II} + \sigma_{III}) = f(\sigma), \quad 6J_2 = (\sigma_I - \sigma_{II})^2 + (\sigma_{II} - \sigma_{III})^2 + (\sigma_{III} - \sigma_I)^2 = f(\tau)$$

$$27J_3 = (2\sigma_I - \sigma_{II} - \sigma_{III}) \cdot (2\sigma_{II} - \sigma_I - \sigma_{III}) \cdot (2\sigma_{III} - \sigma_I - \sigma_{II}).$$

Considering his investigated materials the athor may conclude: The friction valuel lies in the range $0 < \mu < 0.2$, and from mapping experience the interaction exponent in the range of $2.5 < m < 2.9$.

Failure surface is closed at the top. As closing cap the paraboloid in *Table 3-3* can be applied.

The NF-approach $\sqrt{4J_2 \cdot 1 - I_1^2/3} + I = 2 \cdot \bar{R}^t$ is for the rotationally symmetric failure body. It was constructed by connecting uniaxial strength point and bi-axial strength point by a straight line in the principal stress plane (see *Fig. 5-2)*.

Table 2-3 collects all information necessary to design dimension a porous isotropic material like a foam or a concrete stone. These materials experience *120°-rotational symmetry*.

Table 2-3 'Porous' isotropic material: SFC formulations for NF and CrF, 120°-rotational symmetry

Normal Fracture NF for $I_1 > 0$ $\leftrightarrow$ Crushing Fracture CrF for $I_1 < 0$

$$F^{NF} = c^{NF} \cdot \Theta^{NF} \cdot \frac{\sqrt{4J_2 \cdot \Theta^{NF} - I_1^2/3} + I_1}{2 \cdot \bar{R}^t} = 1 \leftrightarrow F^{CrF} = c^{CrF} \cdot \Theta^{CrF} \cdot \frac{\sqrt{4J_2 \cdot \Theta^{CrF} - I_1^2/3} + I_1}{2 \cdot \bar{R}^c} 1$$

$$Eff^{NF} = c^{NF} \cdot \frac{\sqrt{4J_2 \cdot \Theta^{NF} - I_1^2/3} + I_1}{2 \cdot \bar{R}^t} = \frac{\sigma_{eq}^{NF}}{\bar{R}^t} \leftrightarrow Eff^{CrF} = c^{CrF} \cdot \frac{\sqrt{4J_2 \cdot \Theta^{CrF} - I_1^2/3} + I_1}{2 \cdot \bar{R}^c} = \frac{\sigma_{eq}^{CrF}}{\bar{R}^c}.$$

If a failure body is rotationally symmetric, then $\Theta = 1$ like for the neutral or shear meridian, respectively .
A 2-fold acting mode makes the rotationally symmetric fracture body 120°-symmetric and is modelled by using the invariant J_3 and Θ as non-circularity function with d as non-circularity parameter

$$\Theta^{NF} = \sqrt[3]{1 + d^{NF} \cdot \sin(3\vartheta)} = \sqrt[3]{1 + d^{NF} \cdot 1.5 \cdot \sqrt{3} \cdot J_3 \cdot J_2^{-1.5}} \quad \leftrightarrow \quad \Theta^{CrF} = \sqrt[3]{1 + d^{CrF} \cdot 1.5 \cdot \sqrt{3} \cdot J_3 \cdot J_2^{-1.5}}$$

Lode angle ϑ , here set as $\sin(3 \cdot \vartheta)$ with 'neutral' (shear meridian) angle $\vartheta = 0°$ ($\rightarrow \Theta = 1$) ;
tensile meridian angle 30° $\rightarrow \Theta^{NF} = \sqrt[3]{1 + d^{NF} \cdot (+1)}$; compr. mer. angle -30° $\rightarrow \Theta^{CrF} = \sqrt[3]{1 + d^{CrF} \cdot (-1)}$.

Mode interaction $\rightarrow$ Equation of the fracture body: $Eff = [(Eff^{NF})^m + (Eff^{SF})^m]^{m^{-1}} = 1 = 100\%$

$$Eff = \sqrt[m]{\left(c^{NF} \cdot \frac{\sqrt{4J_2 \cdot \Theta^{NF} - I_1^2/3} + I_1}{2 \cdot \bar{R}^t}\right)^m + \left(c^{CrF} \cdot \frac{\sqrt{4J_2 \cdot \Theta^{CrF} - I_1^2/3} + I_1}{2 \cdot \bar{R}^c}\right)^m} = 1.$$

Curve parameter relationships obtained by inserting the compressive strength point (0, $-\bar{R}^c$, 0):

* Rotationally symmetric $\Theta = 1$: $d^{SF} = 0$, $c_{1\Theta}^{SF} = 1 + c_{2\Theta}^{SF}$
* 120°-rotat. symmetric $\Theta \neq 1$: $c_{1\Theta}^{SF} = 1 + c_{2\Theta}^{SF} \cdot \sqrt[3]{1 + d^{SF} \cdot (-1)}$, with
  c^{NF} , Θ^{NF} from the two points $(\bar{R}^t,\ 0,\ 0)$ and $(\bar{R}^{tt}, \bar{R}^{tt},\ 0)$ or by minimum error fit, if data available,
  c^{CrF} , Θ^{CrF} from the two points $(-\bar{R}^c,\ 0, 0)$ and $(-\bar{R}^{cc}, -\bar{R}^{cc}, 0)$ or by minimum error fit.

The failure surface is closed at both the ends: A paraboloid serves as closing cap and bottom

$$\frac{I_1}{\sqrt{3} \cdot \bar{R}^t} = s^{cap} \cdot \left(\frac{\sqrt{2J_2 \cdot \Theta^{NF}}}{\bar{R}^t}\right)^2 + \frac{\max I_1}{\sqrt{3} \cdot \bar{R}^t} \quad , \quad \frac{I_1}{\sqrt{3} \cdot \bar{R}^t} = s^{bot} \cdot \left(\frac{\sqrt{2J_2 \cdot \Theta^{CrF}}}{\bar{R}^t}\right)^2 + \frac{\min I_1}{\sqrt{3} \cdot \bar{R}^t}$$

Slope parameters s are determined connecting the respective hydrostatic strength point with the associated point on the tensile and compressive meridian, $\max I_1$ must be assessed whereas $\min I_1$ can be measured. $\bar{R}^t$ is normalization strength.

LL:

* *A failure surface is the result of optimally mapping the course of multi-axial test data and, therefore, has the attribute 50% survival probability.*
* *Bi-axial tensile stressing: In [Lem08] the author found for intermediate ratios of tensile stresses σI /σII in Normal Concrete that the combined fracture stress is a little higher than the uniaxial strength! This has been never observed by the author with any brittle material. Might there have been a problem with testing or test data evaluation? From physical interpretation a multi-axial tensile stress state activates more fracture-driving flaws and danger to fracture increases.*
* *A fracture surface confines the 'yield surface (domain)'. A fracture surface may be a strength one (material not cracked) or a damage tolerance one (material cracked).*

For completeness three failure hypotheses, beside 'Mises', of the construction discipline shall be mentioned:

Drucker-Prager fracture hypothesis

Both different uni-axial strengths in tension and compression are involved. Since the Drucker–Prager failure surface is a smooth version of the Mohr–Coulomb failure surface,it is often expressed in terms of the cohesion c and the angle of internal friction φ that are used to describe the Mohr–Coulomb yield surface, expressed in Lode-Haigh–Westergaard coordinates .

N. S. Ottosen fracture hypothesis

A four-parameter SFC, containing all the 3 stress invariants explicitly, is proposed for short-time loading of concrete. It corresponds to a smooth convex failure surface with curved meridians, which open in the negative direction of the hydrostatic axis, and the trace in the deviatoric plane changes from almost triangular to a more circular shape ($\theta \to 1$) with increasing p_{hyd}. The values of the four parameters are determined so that they only depend on the ratio of uniaxial tensile to compressive strength, $\bar{R}^t / \bar{R}^c$.

Tresca yield hypothesis

Known as the maximum shear stress theory or Tresca–Guest criterion.

In terms of the principal stresses the Tresca SFC is expressed as

$$F = 0.5 \cdot max(|\sigma_I - \sigma_{II}|, |\sigma_{II} - \sigma_{III}|, |\sigma_{III} - \sigma_I|) = 0.5 \cdot R^t_{0.2}.$$

2.5.1 Mapping the Decay of the Bi-axial Stress 'Pertubation' of the isotropic failure body

In the hoop direction the bi-axiality-affected zone is automatically mapped and thereby confined by the J_3-120°-symmetry. However, what is the situation in the axial direction of the fracture body. Is it to be handled - along the axis - as a decaying pertubation (Störung) or is the decay practically enough well mapped by the increasing negative I_1, which for large values finally leads to a circle? The author believed that the inward and outward dents of the fracture body should be mapped as a pertubation that can be described by a decay function along the meridian. This affects the non-circularity functions Θ and shall be depicted for

$$\Theta^{NF} = \sqrt[3]{1 + d^{NF} \cdot \sin(3\vartheta)} \Rightarrow \sqrt[3]{1 + D\sigma(y) \cdot \sin(3\vartheta)} \text{ with } D\sigma(y) = \alpha\sigma \cdot \beta\sigma \cdot y^{\beta\sigma - 1} \cdot \exp\left[-\alpha\sigma \cdot y^{\beta\sigma}\right] \cdot D\sigma tt$$

$$\Theta^{SF} = \sqrt[3]{1 + d^{SF} \cdot \sin(3\vartheta)} \Rightarrow \sqrt[3]{1 + D\tau(y) \cdot \sin(3\vartheta)}, D\tau(y) = \alpha\tau \cdot \beta\tau \cdot (-y)^{\beta\tau - 1} \cdot \exp\left[-\alpha\tau \cdot (-y)^{\beta\tau}\right] \cdot D\tau cc$$

.

Below is the Mathcad-derivation of Dσ(y) and Dτ(y) with y, a normalized function across meridian.

abbreviation Lode-coordinate $yt := \frac{Ilt}{\sqrt{3}\cdot Rt}$ $ytt := \frac{Iltt}{\sqrt{3}\cdot Rt}$ $yc := \frac{Ilc}{\sqrt{3}\cdot Rt}$ $ycc := \frac{Ilcc}{\sqrt{3}\cdot Rt}$

Approach NF decay function : $D\sigma(y) = \alpha\sigma\cdot\beta\sigma\cdot(y)^{\beta\sigma-1}\cdot\exp\left[-\alpha\sigma\cdot(y)^{\beta\sigma}\right]\cdot D\sigma tt$

derivation in the bi-axial stress point:

$$\frac{d}{dy}\left[\alpha\sigma\cdot\beta\sigma\cdot(y)^{\beta\sigma-1}\cdot\exp\left[-\alpha\sigma\cdot(y)^{\beta\sigma}\right]\cdot D\sigma tt\right]\rightarrow$$

horizontal tangent required: $\left[\beta\cdot\alpha\cdot D\sigma tt\cdot e^{-\alpha\cdot(y)^{\beta}}\cdot(y)^{\beta-2}\cdot(\beta-1)-\beta^2\cdot\alpha^2\cdot D\sigma tt\cdot e^{-\alpha\cdot(y)^{\beta}}\cdot(y)^{2\cdot\beta-2}\right]\cdot D\sigma tt = 0$

$$\begin{cases}\begin{pmatrix}0\\ \frac{\beta-1}{\beta\cdot y^{\beta}}\end{pmatrix} & \text{if } 0\le \mathrm{Re}(\beta)\vee \mathrm{Re}(\beta)<0\wedge y\neq 0\\ \text{undefined} & \text{otherwise}\end{cases}$$

after insertion of y = ytt : $\alpha\sigma = \frac{\beta\sigma-1}{\beta\sigma\cdot(ytt)^{\beta\sigma}}$

Vorgabe $\beta\sigma := 1.1$

$$\frac{\frac{\beta\sigma-1}{\beta\sigma\cdot(ytt)^{\beta\sigma}}\cdot\beta\sigma\cdot(2ytt)^{\beta\sigma-1}\cdot\exp\left[-\frac{\beta\sigma-1}{\beta\sigma\cdot(ytt)^{\beta\sigma}}\cdot(2ytt)^{\beta\sigma}\right]}{\frac{\beta\sigma-1}{\beta\sigma\cdot(ytt)^{\beta\sigma}}\cdot\beta\sigma\cdot(ytt)^{\beta\sigma-1}\cdot\exp\left[-\frac{\beta\sigma-1}{\beta\sigma\cdot(ytt)^{\beta\sigma}}\cdot(ytt)^{\beta\sigma}\right]} = 0.5$$

Aim: 50% decay at uni-axial strength.

Dstt vanishes!

$A\sigma := \text{Suchen}(\beta\sigma)$ $A\sigma =$ ▮ $\beta\sigma := A\sigma$ $\beta\sigma =$ ▮ $\alpha\sigma := \frac{\beta\sigma-1}{\beta\sigma\cdot(ytt)^{\beta\sigma}}$ $\alpha\sigma =$ ▮

Approach SF decay function : $D\tau(y) = \alpha\tau\cdot\beta\tau\cdot(-y)^{\beta\tau-1}\cdot\exp\left[-\alpha\tau\cdot(-y)^{\beta\tau}\right]\cdot D\tau cc$

analogous $\beta\tau := 1.918$ $\alpha\tau := \frac{\beta\tau-1}{\beta\tau\cdot(-ycc)^{\beta\tau}}$ $\alpha\tau =$ ▮

Resulting function:

$$\Theta\tau(y) = \sqrt[3]{1+D\tau(y)\cdot\sin(3\theta)} = \sqrt[3]{1+\alpha\tau\cdot\beta\tau\cdot(-y)^{\beta\tau-1}\cdot\exp\left[-\alpha\tau\cdot(-y)^{\beta\tau}\right]\cdot D\tau\cdot\sin(3\theta\tau)}$$

Whether the application of above decay function is practically necessary must be cleared by more multi-axial measurements on the tensile and compressive meridians.

Investigating tensile meridian test data from Dr. Scheerer, IfM TU Dresden, on Normal Concrete with and without the pertubation sub-model delivered the result: With the pertubation model mapping was only slightly better. Drawing a conclusion for practice: As it is just one example it is recommended - viewing the scatter of test data – to not presently use the more sophisticated pertubation model. See also the calculation of the Reserve Factor in *Sub-chapter 8.3,* for instance.

2.6 SFCs for 'dense' and 'porous' transversely-isotropic materials (UD lamina, lamella)

2.6.1 Derivation of the SFC Set

A SFC should be numerically-optimally formulated on the usual engineering working level, the macro-mechanical level. Such a SFC formulation should capture micro-mechanical failure that triggers macro-mechanical failure, i.e. UD material will filament-break under a bi-axial stress state $\sigma_2^c = \sigma_3^c$ due to $\varepsilon_{\square} = -\nu_{\perp\square}\cdot(\sigma_2^c+\sigma_3^c)/E_{\square}$.

At the beginning of the WWFE Cuntze's numerically non-optimal set of 5 invariant-based failure functions F was

$$FF1: \quad F_{\parallel}^{\sigma} = \frac{I_1}{\bar{R}_{\parallel}^{t}} \ , \qquad\qquad FF2: \quad F_{\parallel}^{\tau} = \frac{-I_1}{\bar{R}_{\parallel}^{c}} \ ,$$

$$IFF1: F_{\perp}^{\sigma} = \frac{I_2 + \sqrt{I_4}}{2\bar{R}_{\perp}^{t}}, \quad IFF2: F_{\perp}^{\tau} = a_{\perp\perp}\frac{I_2}{\bar{R}_{\perp}^{c}} + \frac{b_{\perp\perp}\sqrt{I_4}}{\bar{R}_{\perp}^{c}}, \quad IFF3: F_{\perp\parallel} = \frac{I_3^{3/2}}{\bar{R}_{\perp\parallel}{}^{3}} + b_{\perp\parallel}\frac{I_2 \cdot I_3 - I_5}{\bar{R}_{\perp\parallel}{}^{3}} \ .$$

$$I_1 = \sigma_1, \ I_2 = \sigma_2 + \sigma_3, \ I_3 = \tau_{31}{}^2 + \tau_{21}{}^2, \ I_4 = (\sigma_2 - \sigma_3)^2 + 4 \cdot \tau_{23}{}^2,$$

$$I_5 = (\sigma_2 - \sigma_3) \cdot (\tau_{31}{}^2 - \tau_{21}{}^2) - 4\tau_{23}\tau_{31}\tau_{21}, \quad I_2 \cdot I_3 \text{ - } I_5 \ \rightarrow I_{23-5} = 2\sigma_2 \cdot \tau_{21}^2 + 2\sigma_3 \cdot \tau_{31}^2 + 4\tau_{23}\tau_{31}\tau_{21}.$$

$$\text{with} \quad a_{\perp\perp}(\mu_{\perp\perp}), \ \mathrm{b}_{\perp\perp}(a_{\perp\perp}), \ \mathrm{b}_{\perp\square}(\mu_{\perp\square})$$

and - regarding IFF3 – had to be improved for numerical reasons.

Above single portions are to interact by an interaction equation, and this requires *Effs*. After inserting $Eff^{\perp\parallel}$ (see below) the solution of a numerically unpleasant third order equation is faced:

$$\frac{I_3^{3/2}}{\bar{R}_{\perp\parallel}{}^{3} \cdot Eff^{\perp\square 3}} + b_{\perp\parallel}\frac{(I_2 \cdot I_3 - I_5)}{\bar{R}_{\perp\parallel}{}^{3} \cdot Eff^{\perp\square 3}} \ .$$

The numerical problem can be bypassed if for $F_{\perp\parallel}$ the usual *principle of proportional stressing* is not applied (all stresses of the actually given state of stress or vector are equally factored). It interprets so-called mode reserve factors as mode stretch factors of the actual stress vector, where the stretching ends when the associated mode failure curve or surface is met. Now, instead of factoring the full state of stress, that means factoring each single stress, just the mode driving shear stresses τ_{21}, τ_{31} are factored and not the transversal normal stresses and shear stress τ_{23} (has a normal stress effect). Unfortunately, with this approach the failure condition includes powers ^{2} and ^{3}

$$\rightarrow \ \frac{I_3^{3/2}}{\bar{R}_{\perp\parallel}{}^{3} \cdot Eff^{\perp\square 3}} + b_{\perp\parallel}\frac{(I_2 \cdot I_3 - I_5)}{\bar{R}_{\perp\parallel}{}^{3} \cdot Eff^{\perp\square 2}} \ .$$

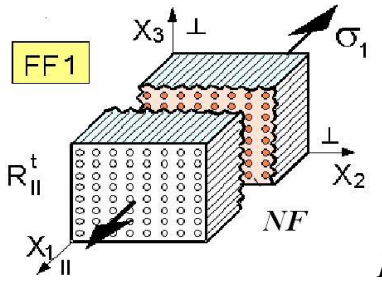
Therefore, the approach for establishing the interaction domain will be modified in order to the numerically advantageous powers 4 and 2

$$\Rightarrow \ \frac{I_3^{2}}{\bar{R}_{\perp\parallel}{}^{4} \cdot Eff^{\perp\square 4}} + b_{\perp\parallel}\frac{(I_2 \cdot I_3 - I_5)}{\bar{R}_{\perp\parallel}{}^{3} \cdot Eff^{\perp\square 2}}$$

allowing, that just a quadratic equation needs to be solved anymore. Of course, the parameter $b_{\perp\parallel}$ is now slightly different to the former one. But this procedure practically has no effect because this condition is used as the new mapping or curve fitting function of the mode IFF3.

There exist limits of the macro-mechanical fiber failure SFCs for FF1 and FF2. In general, the fiber failure mode FF cannot be described by a homogenized (smeared) macro-mechanical stress value σ_1, *Fig.2-6*. Due to Poisson the filaments may fracture under bi-axial compression without any σ_1. Thus, the engineering-like macro-mechanical modelling has to be exchanged by an accurate micro-mechanical failure capturing one. Praiseworthy, this can be approximately well formulated by a macro-mechanical entity which is the FEA-computed output, the macro-mechanical strain ε_1.

Reminding reference [*Cun04*], it follows $\sigma_1 \rightarrow \breve{\sigma}_1 . \sigma_f$ is the filament (fiber) stress which is proportional to the strain and responsible for fracture



$$I_1 = \sigma_1 \cong \nu_f \cdot \sigma_f = \nu_f \cdot \varepsilon_1 \cdot E_f = \varepsilon_1 \cdot E_{\parallel}.$$

Fig.2-6: Capturing micro-mechanical fracture in a macro-mechanical formulation

.

Here it is to mention in order to correct a citation of the WWFE-peers: *Within the FMC, applied to UD material, no fiber properties are required !*

2.6.2 Final set of brittle UD SFCs

Employing the mode *strength* $\bar{R}^{\text{mode}}$ and its *equivalent mode stress* $\sigma_{eq}^{\text{mode}}$, according to the general equation $Eff^{\text{mode}} = \sigma_{eq}^{\text{mode}} / \bar{R}^{\text{mode}}$, the following set of formulas for the material stressing effort of each of the 5 modes can be provided and its relationship to the associated equivalent stress.

An equivalent stress σ_{eq} is always positive such as the strength. It includes all actual load stresses and the residual stresses (from curing etc.) that are acting together in a given mode. The vector of the modes' equivalent stresses reads

$$\left\{\boldsymbol{\sigma}_{\mathbf{eq}}^{\mathbf{mode}}\right\} = \left(\sigma_{eq}^{\parallel\sigma},\ \sigma_{eq}^{\parallel\tau},\ \sigma_{eq}^{\perp\sigma},\ \sigma_{eq}^{\perp\tau},\ \sigma_{eq}^{\parallel\perp}\right)^T .$$

Table 2-4 presents the final set of UD SFCs.

The interaction equation includes all mode material stressing efforts and each of them represents a portion of load-carrying capacity of the material. In practice in thin laminas, at maximum, 3 modes of the 5 modes will physically interact. Considering 3D-loaded thick laminas, there, all 3 IFF modes might interact. Usually, the value of m is obtained by curve fitting of test data in the interaction zone. FRP mapping experience delivered that $2.5 < m < 3$, at least for CFRP. The mode interaction exponent *m* is also termed rounding-off exponent, the size of which is high in case of low scatter and vice versa. A lower value chosen for the interaction exponent is more on the safe side. From engineering reasons the interaction exponent *m* is chosen the same in the transition zones of adjacent domains.

Of interest is not only the interaction of the fracture surface parts in the discussed mixed failure domains or interaction zones of adjacent failure modes, respectively, but further failure in a multi-fold failure domain (superscript $^{\text{MfFD}}$) such as in the (σ_2^t, σ_3^t)-domain. There the associated mode stress effort acts twofold. It activates failure in two directions which may be considered by adding a multi-fold failure term, proposed in [*Awa78*] for isotropic materials. It can be applied to brittle UD material in the transversal (quasi-isotropic) plane as well.

FF1: $Eff^{\|\sigma} = \breve{\sigma}_1 / \bar{R}_{\|}^t = \sigma_{eq}^{\|\sigma} / \bar{R}_{\|}^t$ with $\breve{\sigma}_1 \cong \varepsilon_1^t \cdot E_{\|}$ (matrix neglected)

FF2: $Eff^{\|\tau} = -\breve{\sigma}_1 / \bar{R}_{\|}^c = +\sigma_{eq}^{\|\tau} / \bar{R}_{\|}^c$ with $\breve{\sigma}_1 \cong \varepsilon_1^c \cdot E_{\|}$

IFF1: $Eff^{\perp\sigma} = [(\sigma_2 + \sigma_3) + \sqrt{\sigma_2^2 - 2\sigma_2 \cdot \sigma_3 + \sigma_3^2 + 4\tau_{23}^2}] / 2\bar{R}_{\perp}^t = \sigma_{eq}^{\perp\sigma} / \bar{R}_{\perp}^t$

IFF2: $Eff^{\perp\tau} = [a_{\perp\perp} \cdot (\sigma_2 + \sigma_3) + b_{\perp\perp} \sqrt{\sigma_2^2 - 2\sigma_2\sigma_3 + \sigma_3^2 + 4\tau_{23}^2}] / \bar{R}_{\perp}^c = \sigma_{eq}^{\perp\tau} / \bar{R}_{\perp}^c$

IFF3: $Eff^{\perp\|} = \{[b_{\perp\|} \cdot I_{23-5} + (\sqrt{b_{\perp\|}^2 \cdot I_{23-5}^2 + 4 \cdot \bar{R}_{\perp\|}^2 \cdot (\tau_{31}^2 + \tau_{21}^2)^2}] / (2 \cdot \bar{R}_{\perp\|}^3)\}^{0.5} = \sigma_{eq}^{\perp\square} / \bar{R}_{\perp\square}$

$\left\{\sigma_{eq}^{\text{mode}}\right\} = \left(\sigma_{eq}^{\|\sigma},\ \sigma_{eq}^{\|\tau},\ \sigma_{eq}^{\perp\sigma},\ \sigma_{eq}^{\perp\tau},\ \sigma_{eq}^{\|\perp}\right)^T$, $I_{23-5} = 2\sigma_2 \cdot \tau_{21}^2 + 2\sigma_3 \cdot \tau_{31}^2 + 4\tau_{23}\tau_{31}\tau_{21}$

Inserting the compressive strength point $(0,\ -\bar{R}_{\perp}^c) \rightarrow a_{\perp\perp} \cong \mu_{\perp\perp} / (1 - \mu_{\perp\perp})$, $b_{\perp\perp} = a_{\perp\perp} + 1$

from a measured fracture angle $\rightarrow$ $\mu_{\perp\perp} = \cos(2 \cdot \theta_{fp}^c\,° \cdot \pi / 180)$, for $50° \rightarrow \mu = 0.174$.

$b_{\perp\|} \cong 2 \cdot \mu_{\perp\square}$. Typical friction value ranges: $0 < \mu_{\perp\|} < 0.25$, $0 < \mu_{\perp\perp} < 0.2$.

Interaction Equation:

$$Eff^m = [(\sigma_{eq}^{\|\sigma} / \bar{R}_{\|}^t)^m + (\sigma_{eq}^{\|\tau} / \bar{R}_{\|}^c)^m + (\sigma_{eq}^{\perp\sigma} / \bar{R}_{\perp}^t)^m + (\sigma_{eq}^{\perp\tau} / \bar{R}_{\perp}^c)^m + (\sigma_{eq}^{\perp\square} / \bar{R}_{\perp\square})^m]$$

or $Eff = \sqrt[m]{(Eff^{\text{mode 1}})^m + (Eff^{\text{mode 2}})^m + \ldots.} = 1 = 100\%$ *for* Onset-of-Failure .

As abbreviation, $I_2 \cdot I_3 - I_5 = I_{23-5}$ is used. In the equations above, $\bar{R}$ denotes an average = typical strength value that should be used for the stress-strain curves in stress and deformation analysis. In the design verification the statistically reduced strength values are applied. The superscripts ^{t}, ^{c} stand for tensile, compressive. The superscripts $^\sigma$ and $^\tau$ mark the type of fracture failure whether it is caused by a tensile stress (Normal Fracture, NF, 'cleavage') or a shear stress (Shear Fracture, SF), e.g. due to a compressive normal stress $\sigma_{\|}^c$ or a transverse normal stress $\sigma_{\perp}^c$.

Failure activated in two directions is considered by adding a multi-fold failure term, proposed in [*Awa78*] for isotropic materials. It can be applied to brittle UD material in the transversal (quasi-isotropic) plane as well.

It is to note:

- If formulations in the quasi-isotropic plane of the UD material will be used, then the stresses reduce from 6 lamina (ply) stresses to 5 principal stresses
$$\left\{\sigma^{pr}\right\} = (\sigma_1, \sigma_2^{pr}, \sigma_3^{pr}, 0, \tau_{31}^{pr}, \tau_{21}^{pr})^T$$
- In IFF3 the shear stress τ21 is taken and not τ12 because τ21 causes the failure, which is macroscopically SF however microscopically NF, an NF like for IFF1. This makes 'rounding' in the interaction zone physically-based
- Whether a failure may be called a SF or a NF depends on the envisaged size scale.

<u>Delamination conditions:</u>

Delamination may occur in tensile-shear cases and compression-shear cases (*remember the wedge failure*). Considering delamination a 3D stress state is to be regarded. This is especially the case if bents in the structure are stretched or compressed which generates stresses across the wall thickness. These Delamination SFCs are just a *subset* of the 5 SFCs above. They are intentionally given here in a separate manner because other researchers present special delamination conditions.

With regard to the 3D nature of the IFF conditions, both, IFF1 ($F_{\perp}^{\sigma}$ transverse tensile failure; inter-laminar stresses $\sigma_3^t, \tau_{32}, \tau_{31}$ may cause cracking) and IFF2 ($F_{\perp}^{\tau}$ wedge failure; intra-laminar stresses such as σ_2^c, τ_{21} cause cracking and may initiate a local 3D state of stress, including σ_3) can also serve as conditions for the assessment of *'onset of delamination'* which practically is a *laminate* failure type. One or two modes will be the design driving ones in the critical local material location of a composite lay-up. These are activated by the delamination-critical stress state $\{\sigma\}_{\text{lamina}} = (0, \sigma_2, \sigma_3, \tau_{23}, \tau_{31}, \tau_{21})^T$ which includes all inter-laminar stresses. Introducing the two relevant combinations of the delamination-active stress state above delivers:

Tension/shear stressing

$$(Eff^{\perp\sigma})^m + (Eff^{\perp\parallel})^m = 1 \text{ with } \{\sigma\}_{\text{lamina}} = (0, \sigma_2^t, \sigma_3^t, \tau_{23}, \tau_{31}, \tau_{21})^T$$

Compression-shear stressing

$$(Eff^{\perp\tau})^m + (Eff^{\perp\parallel})^m = 1 \text{ with } \{\sigma\}_{\text{lamina}} = (0, \sigma_2^c, \sigma_3^t, \tau_{23}, \tau_{31}, \tau_{21})^T \ .$$

2.6.2 IFF2-SFC for a 'porous' UD material

UD materials may be pretty porous. This mainly affects IFF2 where a porosity-capturing SFC shall be provided in *Table 2-5*.

Table 2-5 'Porous' UD materials: SFC formulations for IFF2

* IFF2 Failure Function for the dense UD material (for comparison)

$$F^{SF} = [a_{\perp\perp} \cdot I_2 + b_{\perp\perp} \cdot \sqrt{I_4}] \ / \bar{R}_{\perp}^c = 1 \text{ with } a_{\perp\perp} = b_{\perp\perp} - 1 \text{ after inserting } \bar{R}_{\perp}{}^c$$

$$= [a_{\perp\perp} \cdot (\sigma_2 + \sigma_3) + b_{\perp\perp} \cdot \sqrt{(\sigma_2 - \sigma_3)^2 + 4\tau_{23}{}^2}] \ / \bar{R}_{\perp}^c = 1$$

$$= [a_{\perp\perp} \cdot (\sigma_2{}^{pr} + \sigma_3{}^{pr}) + b_{\perp\perp} \cdot \sqrt{(\sigma_2{}^{pr} - \sigma_3{}^{pr})^2 + 0^2}] \ / \bar{R}_{\perp}^c = 1 \ \leftarrow \text{ 2 structural stresses}$$

* IFF2 Failure Function for the porous UD material (index por, *author's simple approach*)

$$F_{porosity}^{SF} = \sqrt{a_{\perp\perp por}{}^2 \cdot I_2{}^2 + b_{\perp\perp por}{}^2 \cdot I_4} - a_{\perp\perp por} \cdot I_2 \ ] \ / 2\bar{R}_{\perp}^c = 1 \ .$$

The two curve parameters are determined - as before performed - from insertion of the compressive strength point and from the bi-axial fracture stress point.

A classification of porous materials according to pore size is presented in [*International Union of Pure and Applied Chemistry*]: 'micro-porous' if pores < 2 nm, 'meso-porous' if pores between 2 nm and 50 nm, 'macro-porous' if pores > 50 nm

2.7 SFCs for differently porous, fabric pattern-dependent orthotropic materials (fabrics)

2.7.1 2D Fabrics

Fig.2-7 depicts the stresses and strengths faced with general orthotropic fabrics.

Orthotropic (rhombically-anisotropic) material is the material family of the highest structural rank, it is already a structural element. *Table 2-6* presents the mode-SFCs directly included in the

interaction equation. According to the existing undulations that cause bending, material homogenization is difficult. In this case of orthotropic material just a formulation in fabric's lamina stresses makes sense. Now, one has to deal with simpler invariants. An UD-FF analogous Poisson-regarding strain-formulation is not necessary. In contrast to the UD lamina a strain formulation of tension FF – due to 2D-compression, in order to capture fiber straining without an acting stress - seems to be not necessary w.r.t. to the undulation effect of the fibers in woven fabrics.

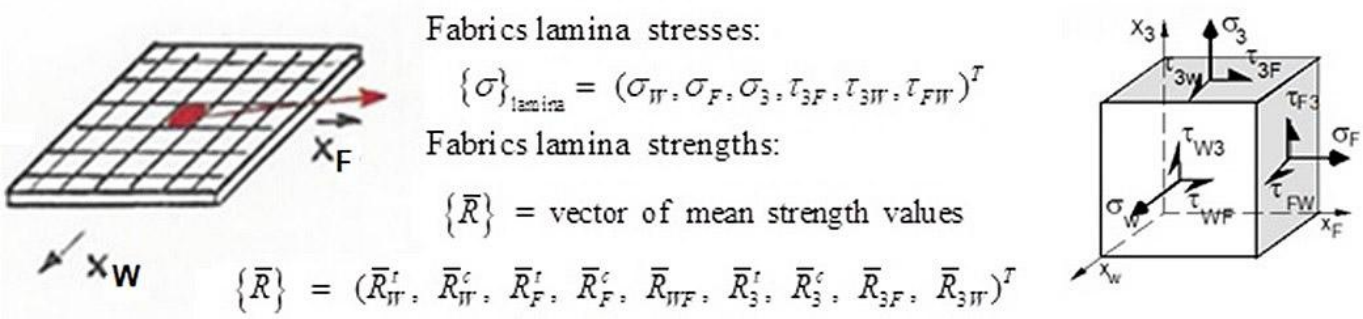


Fig.2-7: Stresses and strength properties of fabrics

Porosity is found within all the textiles where the 2D fabric material type (plain) are most often used in structural engineering.

Table 2-6 'Porous' fabric materials: SFC formulations

Fabrics invariants, privately obtained from J.F. Boehler, 1995

$$I_1 = \sigma_W,\ I_2 = \sigma_F,\ I_3 = \sigma_3,\ I_4 = \tau_{3F}{}^2,\ I_5 = \tau_{3W}{}^2,\ I_6 = \tau_{WF}{}^2,\ I_7 = \tau_{3F} \cdot \tau_{3W} \cdot \tau_{WF}.$$

Invariant SFC formulations

$$F^t_W = I_1 / R^t_W,\ F^t_F = I_1 / R^t_F,\ F^t_3 = I_3 / R^t_3,\ F^c_W = I_1 / R^c_W,\ F^c_F = I_1 / R^c_F,\ F^c_3 = I_3 / R^c_3,$$

$$F_{WF} = I_6 / (R_{WF} - \mu_{WF}(\sigma_W + \sigma_F),\ F^c_{3F} = \sqrt{I_4} / (R_{3F} - \mu_3 \cdot \sigma_3),\ F^c_{3W} = \sqrt{I_4} / (R_{3W} - \mu_3 \cdot \sigma_W)$$

For the insertion into the interaction equation $Eff = 1$ the Eff^{modes} must be provided:

Replacing the invariants by the associated stresses and solving for the Eff^{modes} it reads

The 3D-SFCs are engineering-like simplified to just capture the main physics in the interaction equation :

$$\left(\frac{\sigma_W + |\sigma_W|}{2 \cdot \bar{R}^t_W}\right)^m + \left(-\frac{\sigma_W + |\sigma_W|}{2 \cdot \bar{R}^c_W}\right)^m + \left(\frac{\sigma_F + |\sigma_F|}{2 \cdot \bar{R}^t_F}\right)^m + \left(\frac{-\sigma_F + |\sigma_F|}{2 \cdot \bar{R}^c_F}\right)^m + \left(\frac{|\tau_{WF}|}{\bar{R}_{WF} - \mu_{WF} \cdot \sigma_W}\right)^m$$

$$+ \left(\frac{\sigma_3 + |\sigma_3|}{2 \cdot \bar{R}^t_3}\right)^m + \left(\frac{-\sigma_3 + |\sigma_3|}{2 \cdot \bar{R}^c_3}\right)^m + \left(\frac{|\tau_{3W}|}{\bar{R}_{3W} - \mu_{3W}\sigma^c_3}\right)^m + \left(\frac{|\tau_{3F}|}{\bar{R}_{3F} - \mu_{3F}\sigma^c_3}\right)^m = 1$$

For a cross-ply fabric, Warp = Fill with $\bar{R}^t_W = \bar{R}^t_F$, $\bar{R}^c_W = \bar{R}^c_F$, the inter-laminar *Eff*s go and just the intra-laminar *Eff*s remain.

The range of parameters is $2.5 < m < 2.9$, $0 < \mu_{WF} < 0.15$, $0 < \mu_3 < 0.1$? (no tests).

If σ_F is also active, this double mode contributes via $\left(\frac{|\tau_{WF}|}{\bar{R}_{WF} - \mu_{WF} \cdot (\sigma^c_W + \sigma^c_F)}\right)^m$.

Layers of a laminate show increasing complexity [*Cun19*] *from*

UD-layer → *Non-crimp fabric layer* → *Plain weave layer* → *spatial (3D) textile layer.*

The chosen textile is firstly to model and secondly the associate SFC is to provide for analysis. *Fig.2-7* through *Fig.2-9* point out that the atlas fabric > 1:4 could be modelled by two UD- laminas (*Fig.2-8*).

A SFC choice is directly to link to the possible model choice.

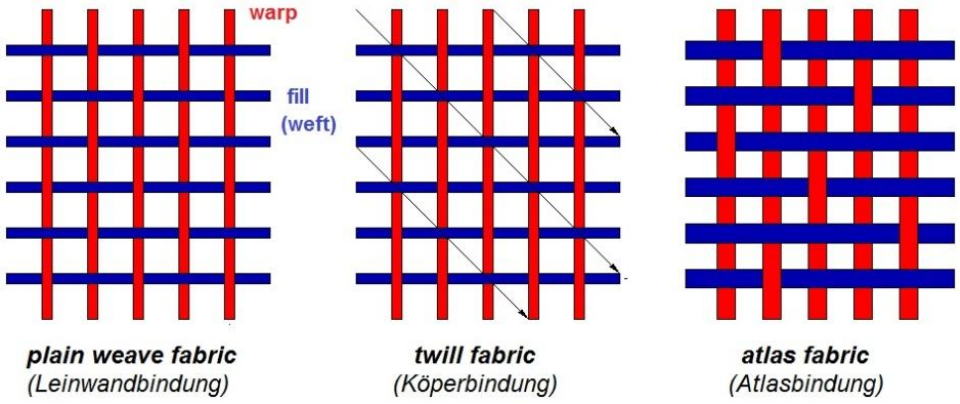


Fig.2-7: Three essential 2D fabrics (Atlas or Satin)

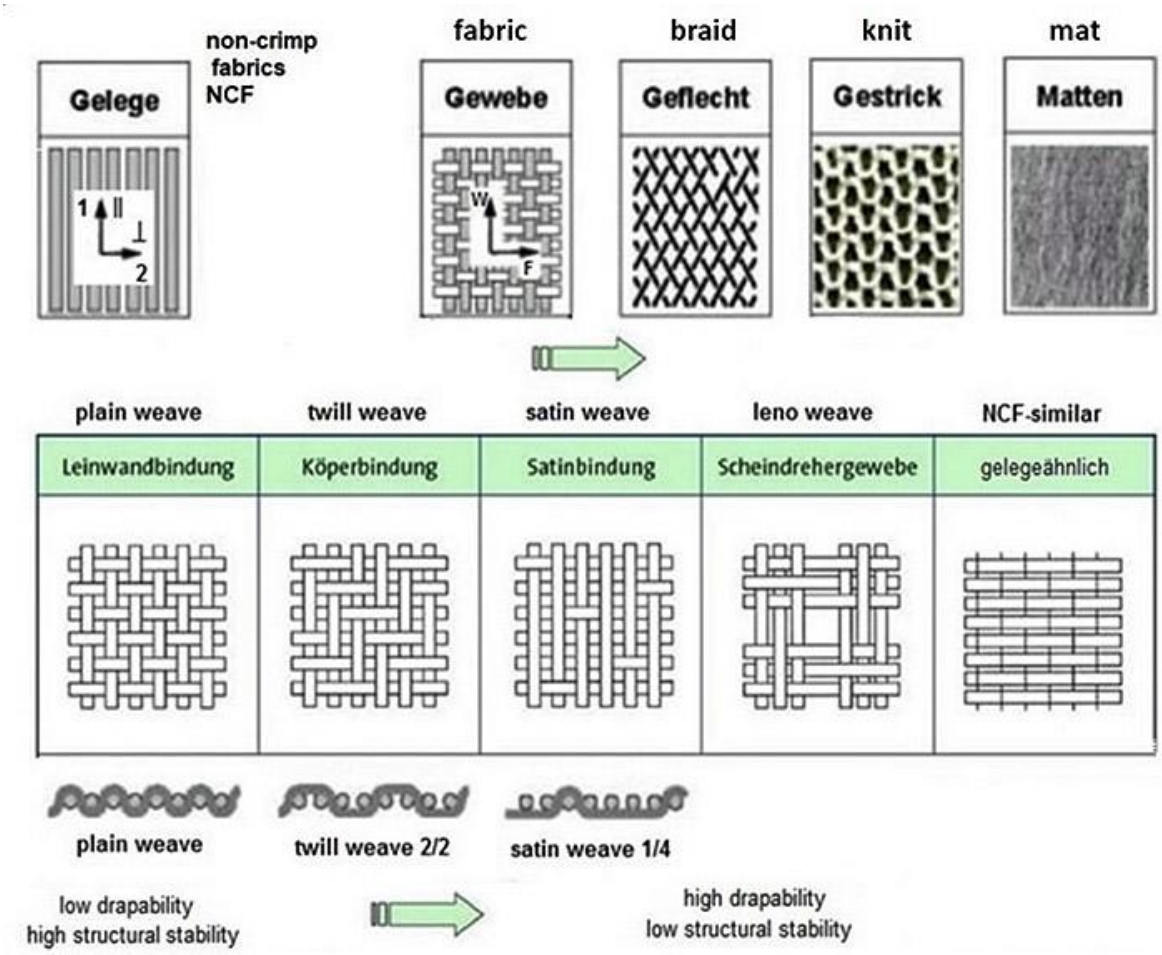


Fig.2-8: Semi-finished plane fabric products

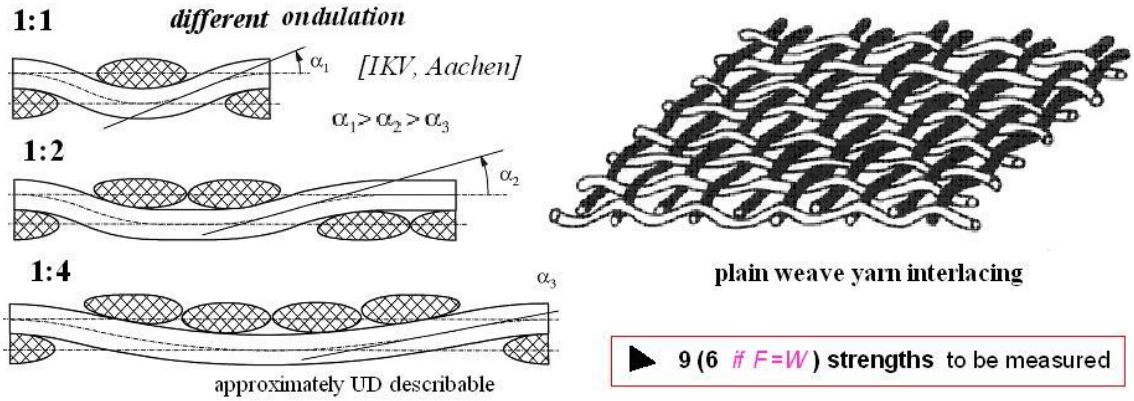


Fig. 2-9: Woven fabric material modelling

LL:

- *Fabrics are still structural elements, it is to check if micro-scopic failure is to consider (see fabric ceramics example in 6.3). 'Maximum stress-SFCs' play an essential role. Friction must be considered in-plane and under lateral pressure in thickness direction, too.*
- *Enough information from acceptable spatial (3D)-tests for a real validation is not yet available!*
- *Interaction has to manage the transition from a micro-mechanical failure of the matrix to the macro-mechanical Warp or Fill fiber failure of the fabric structure. Thereby, the activated strength can be engineering-like applied by increasing the matrix tensile strength $\bar{R}_m^t$ continuously up to the fabric's tensile Warp strength $\bar{R}_W^t > \bar{R}_m^t$ according to - for instance - the stress ratio τ_{WF} / σ_W^t in the tension domain, $\bar{R} = \bar{R}_m^t \cdot (1 - a \cdot e^{-\beta \cdot x})$. Applied later however, for a ceramic fabric in Fig.6.3-7, are physically decay functions for both the modes which become zero at the onset of the adjacent mode domain.*
- *A good exploitation of fibers is only given if they are fully straight built in. Therefore the undulation of fabrics is a big shortcoming especially under cyclic loading.*
- *The use of short recycled fibers in fabrics increase this unpleasant situation*
- *The meaning " 3D- textile" is different*
  - Most often this term is used for a spatial shape of a textile pre-form
  - 3D 'flat' semi-finished product with 3 fiber directions (tri-axial fabric)
  - The material modeller uses it, if the textile is to model like an orthotropic 3D-solid.

2.7.2 3D Fabrics (Textiles)

3D textiles are 3D semi-finished products made with fabrication methods such as weaving, knitting, braiding, or nonwoven. Real 3D textiles are produced with spatial geometry, opposed to 2D textiles that are made in planes. The yarn in 2D textiles is fed along length axis and width axis, while 3D textiles also have an upright weave, using an extra yarn which creates thickness. 3D weaves are orthogonal weave structures, multilayer structures, and possess angle interlocks.

Mechanically 3D textiles are - after curing - orthotropic solids, which have a large number of properties to be provided for dimensioning.

Viewing *Fig. 2-10,* for the modeler at first essential is: What is the meaning of the distinct envisaged 3D. Is it a real 3D fabric or is it a 3D 'flat' semi-finished product with 3 fiber directions (tri-axial fabric) or - in construction - a curved spatial armoring cage, for instance.

3D textiles of continuous fibers add a 3rd direction of reinforcement by the yarns interlacing through the thickness, which improves damage tolerance behavior.

Some characteristics could be derived from literature [*Bil11*]:

- Stacked 2D fabrics: Stapled on top of another and in z-direction stitched together. In-plane properties good, out-of-plane very low
- 3D woven fabrics: In-plane properties good, out-of-plane very low
- 3D braided fabrics: Multiple layers, damage tolerance high, transverse properties low
- 3D knitted fabrics: Fabricated to create near net shape, curved structures such as cone and sphere
- 3D non-woven fabrics: Usually a short fiber-preform, in z-direction reinforced by stitching. Low mechanical properties.

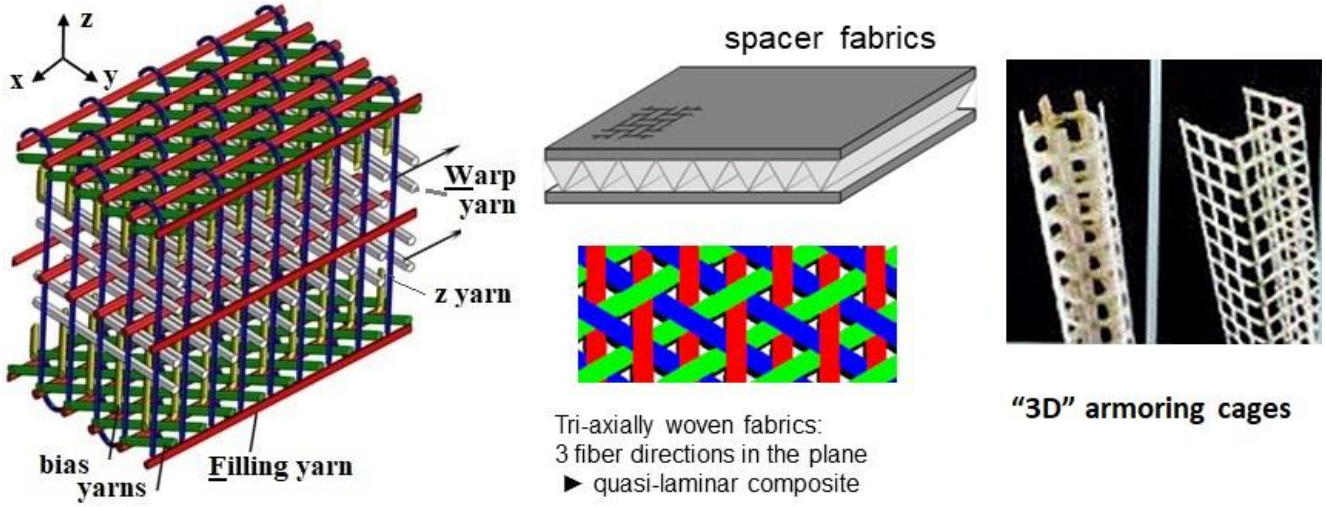


Fig.2-10: Pre-forms termed "3D" ('left' scheme)

www.iccm-central.org/Proceedings/ICCM21proceedings/papers/4198.pdf

However, this opportunity of adding a 3rd dimension to the weave pattern creates stiffness but adds distinct failure and thermo-mechanical behavior. Effective Properties of 3D Woven Composites are to determine for design. This will be usually performed by employing representative volume element (RVE) procedures.

2.8 SFCs for the differently porous Structural Ceramic Materials

2.8.1 Isotropic ceramics

This sub-chapter is dedicated to all the more or less porous structural ceramic materials from an isotropic monotonic, via a transversely-isotropic UD material to an orthotropic fabric ceramic material. In some applications task-associated porosity is intended in order to obtain for instance some quasi-ductile behavior after micro-damage occurred.

SFCs for NF and CrF come from *Table 3-3* 'Porous' isotropic material:

$$Eff^{NF} = c^{NF} \cdot \frac{\sqrt{4J_2 \cdot \Theta^{NF} - I_1^2/3} + I_1}{2 \cdot \bar{R}^t} = \frac{\sigma_{eq}^{NF}}{\bar{R}^t} \quad \leftrightarrow \quad Eff^{CrF} = c^{CrF} \cdot \frac{\sqrt{4J_2 \cdot \Theta^{CrF} - I_1^2/3} + I_1}{2 \cdot \bar{R}^c} = \frac{\sigma_{eq}^{CrF}}{\bar{R}^c}.$$

2.8.2 UD ceramics

Here, just IFF2 has to be replaced by the porous variant.

$$\text{FF1: } Eff^{\|\sigma} = \breve{\sigma}_1 / \bar{R}^t_{\|} = \sigma^{\|\sigma}_{eq} / \bar{R}^t_{\|} \quad \text{with} \quad \breve{\sigma}_1 \cong \varepsilon^t_1 \cdot E_{\|} \text{ (matrix neglected)}$$

$$\text{FF2: } Eff^{\|\tau} = -\breve{\sigma}_1 / \bar{R}^c_{\|} = +\sigma^{\|\tau}_{eq} / \bar{R}^c_{\|} \quad \text{with} \quad \breve{\sigma}_1 \cong \varepsilon^c_1 \cdot E_{\|}$$

$$\text{IFF1: } Eff^{\perp\sigma} = [(\sigma_2 + \sigma_3) + \sqrt{\sigma_2^2 - 2\sigma_2 \cdot \sigma_3 + \sigma_3^2 + 4\tau_{23}^2}\,] / 2\bar{R}^t_{\perp} = \sigma^{\perp\sigma}_{eq} / \bar{R}^t_{\perp}$$

$$\text{IFF2: } F^{SF}_{porosity} = \sqrt{a_{\perp\perp por}^2 \cdot I_2^2 + b_{\perp\perp por}^2 \cdot I_4} - a_{\perp\perp por} \cdot I_2\ ] / 2\bar{R}^c_{\perp} = 1$$

$$\text{FF3: } Eff^{\perp\|} = \{[b_{\perp\|} \cdot I_{23-5} + (\sqrt{b_{\perp\|}^2 \cdot I_{23-5}^2 + 4 \cdot \bar{R}_{\perp\|}^2 \cdot (\tau_{31}^2 + \tau_{21}^2)^2}\,] / (2 \cdot \bar{R}_{\perp\|}^3)\}^{0.5} .$$

2.8.3 Orthotropic fabric ceramics

See SFC formulations in *Table 2-6* are presented within the interaction equation that captures all modes. The combined acting of σ_F and σ_W is considered below.

$$\left(\frac{\sigma_W + |\sigma_W|}{2 \cdot \bar{R}^t_W}\right)^m + \left(-\frac{\sigma_W + |\sigma_W|}{2 \cdot \bar{R}^c_W}\right)^m + \left(\frac{\sigma_F + |\sigma_F|}{2 \cdot \bar{R}^t_F}\right)^m + \left(\frac{-\sigma_F + |\sigma_F|}{2 \cdot \bar{R}^c_F}\right)^m + \left(\frac{|\tau_{WF}|}{\bar{R}_{WF} - \mu_{WF} \cdot (\sigma^c_W + \sigma^c_F)}\right)^m$$

$$\left(\frac{\sigma_3 + |\sigma_3|}{2 \cdot \bar{R}^t_3}\right)^m + \left(\frac{-\sigma_3 + |\sigma_3|}{2 \cdot \bar{R}^c_3}\right)^m + \left(\frac{|\tau_{3W}|}{\bar{R}_{3W} - \mu_{3W}\sigma^c_3}\right)^m + \left(\frac{|\tau_{3F}|}{\bar{R}_{3F} - \mu_{3F}\sigma^c_3}\right)^m = 1 .$$

It seems to be easier to launch a new ARIANE rocket type
than a new idea on strength criteria *[Author, 1996]*





Feeling of the author after generating the various sets of FMC-based SFCs

(left) After so much effort, the pain will be soon over? The top seems to be reached?
(right) No, the view of the SFC-climber widens: Validation by SFC applications will require many long-lasting difficult numerical visualizations → These required most of the time and persistence in the performance of the numerical analyses with graphical visualization

2.9 Validity limits for SFC applications and Automatic Insertion of 3D Stress States

2.9.1 Validity limits for SFC applications

The next table lists comments about and experiences with SFC applicability limits.

Table 2-5: Comments on Validity Limits for the Applicability of a SFC (mainly given for UD)

- As a SFC is a necessary but not a sufficient condition to predict failure *[Leguillon, W. Becker]* a fracture mechanics-based energy condition may be to fulfill, too. Even in plain (smooth) stress regions a SFC can be only a necessary condition which may be not sufficient for the prediction of 'onset of fracture', i.e. the in-situ lateral strength in an embedded lamina. Example: thick layers fail earlier than thin ones under the same 2D stress state see e.g. [*Flaggs-Kural 1982*].
- Attempts to link 'onset-of-fracture' combined with 'onset-of-cracking prediction' methods for structural components are under-gone, see e.g. *[Leg02*]. In his finite fracture mechanics Leguillon assumes a crack as one more unknown but one can solve the equation system by one more equation from fracture mechanics (see later sub-chapter)
- In case of discontinuities such as notches with steep stress decays only a *toughness + characteristic length-based energy balance condition* may form a sufficient set of two fracture conditions
- When applying test data from 'isolated lamina' test specimens (*like tensile coupons*) to an embedded lamina of a laminate one should consider that coupon test deliver tests results of 'weakest link' type. An embedded or even an only one-sided constrained lamina, however, possesses redundant behavior, see *Fig.2-11*
- A SFC usually describes only a one-fold occurrence of a mode or of a failure mechanism, respectively! A multiple occurrence of a mode, such as for $\sigma_I = \sigma_{II}$ or for $\sigma_2 = \sigma_{3,}$ is to map by an additional term in *Eff* = 1 , see for instance in *Table 2-6*
- Each failure stress state belongs to *Eff* = 100% and represents one point on the surface of the failure body. This is valid for 1D- (these are the strength values), for 2D- and for 3D-stress states. In the case of a multiaxial compressive stress state the strength does not increase but the risk to fracture becomes smaller, indicated by *Eff* which then becomes lower than 100 % !
- Each failure mechanism is affected by an associated typical state of stress. The failure mechanism with the highest material stressing effort will dominate the UD failure. The mode effort has to become zero if the mode driving stress is zero
- Not design-driving stresses of a mode might increase or decrease the material stressing effort *Eff* which is basically sized by the design driving one. This influence is considered in the equivalent mode stress $\sigma_{eq}^{\text{mode}}$. Note that the Mises equivalent stress for the mode yielding is not the only equivalent stress
- The 5 strength and 2 friction parameters can be measured and therefore fulfil a basic design verification requirement: Strength properties shall be statistically-based, material friction properties μ are so-called physical quantities which shall be average (typical) values in order to best meet the optimum being the maximum expectation value of 50% probability
- The FFs are special fiber strain failure equations to capture filament fracture under bi-axial compression
- . The NF-function chosen for isotropic and UD materials enables to map a straight line of test data in the principle stress plane
- If the failure body is fully rotational symmetric then c^{NF} ($\Theta^{NF} = 1$ or $d^{NF} = 0$) = 1. Above NF can manage inward and outward dents by c^{NF} (Θ^{NF}) < 1 which renders the 120°-rotational symmetry
- The friction effect decreases with increasing porosity. Ideal dense materials possess no porosity. A fully porous material may be defined by $R^{cc} \cong R^{c}$. This case is modelled like the porous foam material [*Cun16a*]
- When mapping, then $\overline{R}$ must be used, because the average behavior or value is required

- Only Eff = 100% is equal to the SFC F = 1
- If any plane in a 3D stress state is a plane of maximum danger, being possible to become a fracture plane, then that plane with the most unfavorable flaw situation becomes the fracture plane
- Due to IFF the curing stresses decay in parallel to the degradation.

2.9.2 Enabling an Automatic Insertion of 3D stress states into the SFCs, example UD

When automatically inserting the FEA stress output $\{\sigma\}=(\sigma_1,\sigma_2,\sigma_3,\tau_{23},\tau_{13},\tau_{12})^T$ into all 5 effort equations some efforts may become negative which mechanically means zero *Eff*. In order to make an automatic use of the FMC-based fracture SFCs also in a 3D state of stresses possible and to avoid complicate queries in the computer program some specific procedures are to consider:

1) FF, IFF: By the automatic insertion of a 3D state of stress physically incorrect negative efforts and negative equivalent stresses may occur. Then a value of 0 shall replace the negative value. A negative $\sigma_{eq}^{\perp\tau}$ may occur in the case of a combination of a high friction parameter $a_{\perp\perp}$ with a certain state of bi-axial stressing.

These are bypassed by using absolute values

FF: $Eff^{\|\sigma}=(\varepsilon_1+|\varepsilon_1|)\cdot E_{\|}/(2\cdot R_{\|}^{t})$, $Eff^{\|\tau}=(-\varepsilon_1+|\varepsilon_1|)\cdot E_{\|}/(2\cdot R_{\|}^{c})$, and

IFF: $\sigma_{eq}^{\perp\sigma}=(+\sigma_{eq}^{\perp\sigma}+|\sigma_{eq}^{\perp\sigma}|)/2$, $\sigma_{eq}^{\perp\tau}=(-\sigma_{eq}^{\perp\tau}+|\sigma_{eq}^{\perp\tau}|)/2$

or formalistically by taking the Macauly brackets (≡ Föppl symbols {}). They describe a discontinuous function and are defined here by

$$\{Eff^{mode}\}=\begin{cases}0, & Eff^{mode}<0\\ Eff^{mode}, & Eff^{mode}\geq 0\end{cases}.$$

Numerical Use of the Equation of the fracture body:

$$Eff^m=(\{Eff^{\|\sigma}\})^m+(\{Eff^{\|\tau}\})^m+(\{Eff^{\perp\sigma}\})^m+(\{Eff^{\perp\|}\})^m+(\{Eff^{\perp\tau}\})^m$$

Deleting the woven brackets the total efforts reads:

$$Eff=\sqrt[m]{(Eff^{\|\sigma})^m+(Eff^{\|\tau})^m+(Eff^{\perp\sigma})^m+(Eff^{\perp\|})^m+(Eff^{\perp\tau})^m}$$

owever, in Mathcad to be formulated for achieving a solution as

$$Eff=[(Eff^{\|\sigma})^m+(Eff^{\|\tau})^m+(Eff^{\perp\sigma})^m+(Eff^{\perp\|})^m+(Eff^{\perp\tau})^m]^{m^{-1}}.$$

2) (IFF1), IFF2: A problem is originated by the fact that a shear stress τ_{23} can be composed of a normal tensile stress and a normal compressive stress (mind: *only a shear stress can be substituted by (shear) stress components!)* which affects two failure modes but just one is significant in the case of the actual, brittle behaving UD material. Naturally in case of a brittle behaving material a tensile driving effort $Eff^{\perp\sigma}$ is caused together with a compressive effort $Eff^{\perp\tau}$. The compressive effort incorporates a smaller additional failure danger due to $R^t << R^c$. This is simply outlined via the principal stresses in the quasi-isotropic UD domain where a transformation into the two principal stresses is performed

$$\sigma_I=0.5\cdot(\sigma_2+\sigma_3)+\sqrt{(0.5\cdot(\sigma_2-\sigma_3))^2+\tau_{23}{}^2},\quad \sigma_{II}=0.5\cdot(\sigma_2+\sigma_3)-\sqrt{(0.5\cdot(\sigma_2-\sigma_3))^2+\tau_{23}{}^2},$$

setting $\sigma_I: 0,$ if $\sigma_I\geq 0$, σ_I otherwise and $\sigma_{II}: 0,$ if $\sigma_{II}\geq 0$, σ_{II} otherwise.

Then it holds for the more problematic IFF2

$$Eff^{\perp\tau} = [\ b_{\perp\perp} \cdot \sqrt{\sigma_I{}^2 - 2 \cdot \sigma_I \cdot \sigma_{II} + \sigma_{II}{}^2 + 4 \cdot 0^2} + a_{\perp\perp} \cdot (\sigma_I + \sigma_{II})\ ]\ /\ \bar{R}_{\perp}^{c}.$$

$Eff^{\perp\tau} = 1$ delivers for $\sigma_2(\sigma_3)$ two roots and therefore two branches as can be seen in the presented WWFE-II, TC 5, for instance.

Reminder for numerics:

Determination of Eff ≠ 1: $Eff = [\Sigma\ (Eff^{\text{modes}})^m]^{m-1}$

Determination of failure curve Eff = 1: $1 = \Sigma\ (Eff^{\text{modes}})^m$.

2.9.3 A closer Look at Materials addressing Shear Stress and Multi-fold Failure

Principally, shear tests are not uniaxial tests but can be seen to be bi-axial and can be performed bi-axially. In the isotropic and a quasi-isotropic plane τ can be replaced by $\sigma_I^{pr} = \tau$, $\sigma_I^{pr} = -\tau$. Inserting τ or the two principal stresses = τ-stress components does give the same result, *Fig.2-12*.

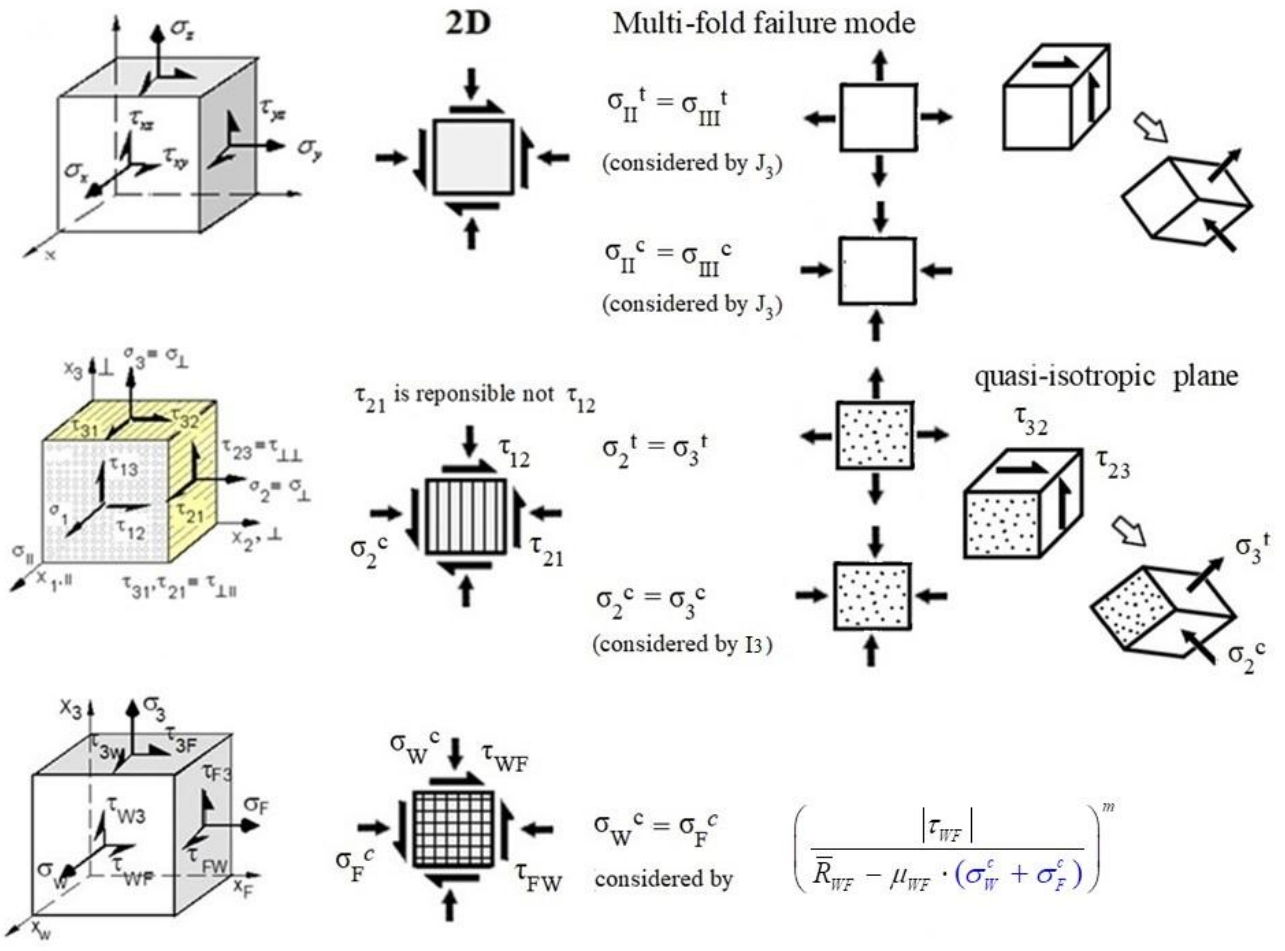


Fig.2-12: Consideration of multi-fold failures

Friction micro-damage is caused by shear stress τ with compression stress σ^c. For instance, for a fabric - experiencing σ_W and σ_F - an additional term must consider this additional failure danger.

For the UD-material the double tensile mode $\sigma_2^t + \sigma_3^t$ or the double compressive mode $\sigma_2^c + \sigma_3^c$ in *Fig.2-12* could be considered by the other form of the invariant I_3, namely $I_3 = \tau_{23}^2 - \sigma_2^t \cdot \sigma_3^t$ or $I_3 = -\sigma_2^{t\,pr} \cdot \sigma_3^{t\,pr}$ from [*Mul67*], by *Eff* = I_3 / $(R^{tt})^2$, similarly to J_3 for the isotropic case.

In this context, keep in mind, please:

"SFCs are principally set up for strength failures which occur only one-fold!"

Table 2-7 depicts how some stresses are related to the equivalent stresses.

Table 2-7: Comparison of shear stress and normal stress acting in SFC applications

* Isotropic, ductile: 1 yield failure mode is failure driving and activated (no friction)

$$I_1 = \sigma_x + \sigma_y + \sigma_z\ ,\quad 6 \cdot J_2 = (\sigma_x - \sigma_y)^2 + (\sigma_y - \sigma_z)^2 + (\sigma_z - \sigma_x)^2 + 6 \cdot (\tau_{xy}^2 + \tau_{yz}^2 + \tau_{xz}^2)$$

$$Eff^{Mises} = \sqrt{\frac{3J_2}{(\bar{R}_{0.2})^2}} = \frac{\sigma_{eq}^{Mises}}{\bar{R}_{0.2}}:\ \text{just}\ \tau_{xy} \neq 0 \rightarrow \sigma_{eq}^{Mises} = \sqrt{3} \cdot \tau_{xy};\ \sigma_x \neq 0 \rightarrow \sigma_{eq}^{Mises} = \sigma_x$$

* Isotropic, brittle, rot. symm. fracture body Θ =1: $\tau_{xy} \rightarrow$ activates 2 fracture failure modes

$$Eff^{fr} = \sigma_{eq}^{fr} / \bar{R}^t:\quad \tau_{xy} \rightarrow I_1 = 0,\ J_2 = \tau_{xy}^2;\ \sigma_x \rightarrow I_1 = \sigma_x,\ J_2 = \sigma_x^2 / 3.\quad c_1^{SF} = 1 + c_2^{SF}$$

$$\sigma_{eq}^{NF} = 1 \cdot (\sqrt{4J_2 \cdot 1 - I_1^2 / 3} + I_1) / 2;\quad \sigma_{eq}^{SF} = (c_2^{SF} \cdot I_1 + \sqrt{(c_2^{SF} \cdot I_1)^2 + 12 \cdot c_1^{SF} \cdot J_2 \cdot 1}\ ) / 2$$

$$\tau_{xy} \rightarrow \sigma_{eq}^{NF} = 1 \cdot \tau_{xy},\ \sigma_{eq}^{SF} = \sqrt{3} \cdot \tau_{xy};\quad \sigma_x \rightarrow \sigma_{eq}^{NF} = 1 \cdot \sigma_x,\ \sigma_{eq}^{SF} = 0.5 \cdot \sigma_x \cdot \sqrt{c_2^{SF\,2} + 4 \cdot (1 + c_2^{SF}) \cdot 1}$$

* Transversely-isotropic UD, brittle: 5 fracture failure modes; τ_{23} acts

out-of-plane shear stress activates 2 modes $\{\sigma\}_L = (0,\ 0,\ 0,\ \tau_{23},\ 0,\ 0)^T = (0,\ \tau_{23}, -\tau_{23},\ 0,\ 0,\ 0)^T$

principal stresses replacement: $\sigma_2^{pr} = 0.5 \cdot (\sigma_2 + \sigma_3) + \sqrt{[0.5 \cdot (\sigma_2 + \sigma_3)]^2 + \tau_{23}^2} = \tau_{23},\ \sigma_3^{pr} = -\tau_{23}$

$$Eff^{\perp\sigma} = [(\sigma_2 + \sigma_3) + \sqrt{(\sigma_2 - \sigma_3)^2 + 4\tau_{23}^2}\,] / 2\bar{R}_\perp^t = \tau_{23} / \bar{R}_\perp^t$$

$$Eff^{\perp\tau} = [(\frac{\mu_{\perp\perp}}{1 - \mu_{\perp\perp}}) \cdot (\sigma_2 + \sigma_3) + \frac{1}{1 - \mu_{\perp\perp}} \sqrt{(\sigma_2 - \sigma_3)^2 + 4\tau_{23}^2}\,] / \bar{R}_\perp^c = \frac{2\tau_{23}}{\bar{R}_\perp^c \cdot (1 - \mu_{\perp\perp})}$$

→ same results for shear stress or replacing principal stresses ≡ shear stress components.

2.10 UD-material, Stress-strain curve parts Strain-hardening and Strain-softening

The behavior of laminas is different for so-called isolated test specimens and embedded test specimens. Isolated test specimens are unconstrained laminas whereas laminas embedded in the laminate are mutually constrained according to the strain-controlled state. This was decisive when mapping WWFE-II, TC3.

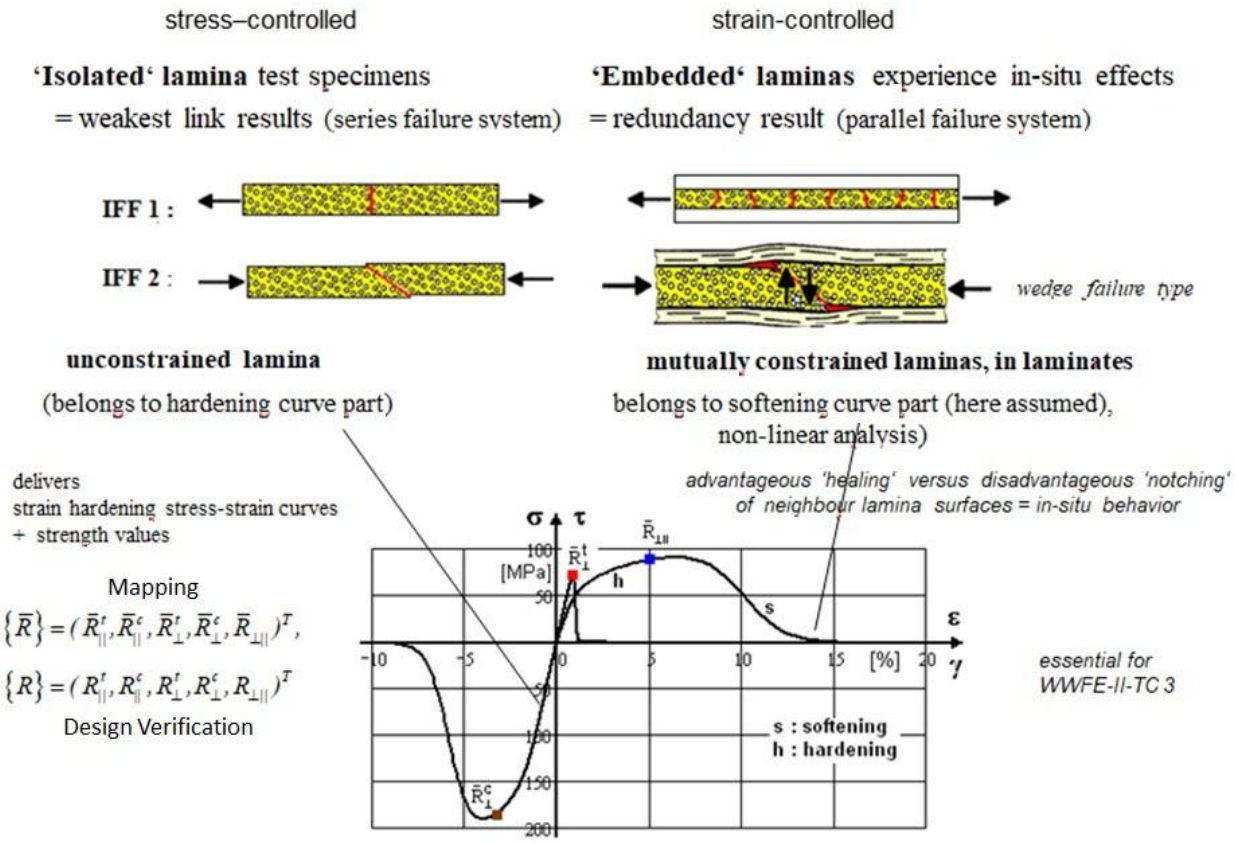


Fig.2-11, CFRP: Strain Hardening and Strain Softening, curve parts of the example UD-material

Isolated test specimens deliver values for the strength = failure stress, which represent the value at the end of the strain-hardening curve. Embedded laminas contribute further to the laminate stiffness and load carrying capacity as long as the microdamage-caused strain-softening curve is active.

Strain-hardening: For strain-hardening materials the classical Ramberg-Osgood (R-O) equation can be applied as mapping function (*in material data sheets like in the HSB R-O parameters for strain-hardening are given)*

$$\varepsilon_{hard} = \sigma / E_0^{mod\,e} + 0.002\,(\sigma / \bar{R}_{0.2}^{mod\,e})^n, \text{ example } \gamma_{21} = \tau_{21} / G_{||\perp} + 0.002 \cdot (\tau_{21} / \bar{R}_{0.2\perp||})^n.$$

Therein the R-O exponent (see Mil Hdbk 5, now MMPDS) reads

$$\bar{n} = \ell n\left(\varepsilon_{pl}(R_m)\right) / \ell n\left(\bar{R}_m^{mod\,e} / \bar{R}_{p0.2}^{mod\,e}\right)$$

and is estimated from the strength point $\left(\bar{R}_{\mathrm{m}}^{\mathrm{mode}},\ \varepsilon_{pl}(\bar{R}_{\mathrm{m}}^{\mathrm{mode}})\right)$ and a 'yield' point information. Of interest for analysis are the secant and the tangent E-modulus

$$\mathrm{E}_{sec} = \sigma / \varepsilon = E_0 / [1 + 0.002 \cdot E_0 / \bar{R}_{0.2} \cdot (\sigma / \bar{R}_{0.2})^{\bar{n}-1}],$$

$$\mathrm{E}_{tan} = d\sigma / d\varepsilon = E_0 / [1 + 0.002 \cdot \bar{n} \cdot E_0 / \bar{R}_{0.2} \cdot (\sigma / \bar{R}_{0.2})^{\bar{n}-1}].$$

For the design dimensioning analysis an average stress-strain curve should be applied in order to obtain the most probable state of the structure. This requires to map the desired average curve of a bunch of measured stress-strain curves. This will lead to a curve that might not run through the points $(\bar{R}_{0.2}^t,\ \varepsilon_{0.2}^t = 0.002)$ and $(\bar{R}^t,\ \bar{\varepsilon}_{fr}^t)$. Hence, the exponent $\bar{n}$ is also the result of the fitting process of the bunch of all measured stress-strain curves. An impressive example was WWFE-II,

TC 2-4.

Strain-softening: The full stress-strain curve consists of a hardening part which can be load-controlled measured and a softening part which is deformation-controlled by the structural vicinity. The associate two separate formulae are linked in the strength point.

The softening formula has to be assumed. This is due to the fact that the designer is generally lacking of experimental information for the degradation of the embedded lamina. An engineering modelling of this softening part or the post initial failure behavior of a laminate requires that assumptions have to be made regarding the decaying properties of the actually degrading lamina or laminas. The author's approach is based on the idea that the softening function is factorizing the Ramberg-Osgood hardening function. A simple function was used to map this softening in order to then derive the secant modulus for the full non-linear analysis. The equations for this effective curve (*smeared over the micro-cracks*) read:

$$\sigma_{soft} = \bar{R}_m / (1+exp[(a_{soft} + \varepsilon) / b_{soft}]) = \bar{R}_m \cdot \eta \qquad \text{using} \quad exp[z] = e^z$$

where η is a degradation function and equals 1 in the hardening domain. The two curve parameters a_{soft}, b_{soft} are determined from two calibration points at least

$$(0.995 \cdot \bar{R}_m,\ \varepsilon(\bar{R}_m)) \qquad \text{and} \qquad (0.1 \cdot \bar{R}_m,\ \varepsilon(0.1 \cdot \bar{R}_m))$$

or from curve fitting if enough test data is available in the softening domain. Applying $1.0 \cdot \bar{R}_m,\ \varepsilon(\bar{R}_m)$ as input is numerically not permitted. The moduli required for the non-linear analysis in the isotropic case read

$$E_{sec}^{hard} = \frac{\sigma}{\varepsilon} = \frac{\sigma}{\frac{\sigma}{E_0} + 0.002 \cdot (\frac{\sigma}{\bar{R}_{0.2}})^{\bar{n}}} = \frac{E_0}{1 + 0.002 \cdot \frac{E_0}{\bar{R}_{0.2}} \cdot (\frac{\sigma}{\bar{R}_{0.2}})^{\bar{n}-1}},$$

$$E_{sec}^{soft} = \frac{\sigma}{\varepsilon} = \frac{E_0}{1 + 0.002 \cdot \frac{E_0}{R_{0.2}} \cdot (\frac{\sigma \cdot \eta}{R_{0.2}})^{\bar{n}-1}} \qquad \text{with} \qquad \eta = \frac{1}{1 + exp(\frac{a_{soft} + \varepsilon}{b_{soft}})}.$$

By employing the equivalent stress reached in each failure mode the associated secant modulus of each mode can be determined for the hardening and the softening regime. For the various modes the same formula is valid, however, the mode parameters are different. Considering a consistent stress concept for all σ_{eq}^{modes} an *explicit* dependency for $E_{sec}(\sigma_{eq}^{modes})$ is provided.

For UD material the *Onset-of-Failure* or *Initial Failure* level, respectively, an appropriate progressive failure analysis method has to be employed, also termed a *Successive Degradation Model* for the description of Post Initial failure, by using a failure mode condition that indicates failure type and micro-damage danger (level of *Eff* <= 100%). Final Failure occurs after the laminate (and thereby the structural part has experienced a stiffness reduction and has degraded to a level where it is no longer capable of carrying additional load.

Note, please: If R-O-material data sets are not provided for the hardening domain then instead of the R-O-approach a more mathematical formulation can be applied which should include both hardening and softening regime.

One formula, that includes both, reads $\sigma = c1 \cdot c2 \cdot \varepsilon^{c1-1} \cdot exp(-c1 \cdot \varepsilon^{c2})$ [*Mathcad manual*].

Another formula from *A. Matzenmiller* reads $\sigma(\varepsilon) = \bar{R} \cdot exp\left[\frac{1}{c1 \cdot e} \cdot \left(\frac{\varepsilon}{\varepsilon_{fracture}}\right)^{c1}\right] \cdot \frac{\varepsilon}{\varepsilon_{fracture}}$.

2.11 Note on Polymer Matrix Reinforcement by Fiber Patch work

Modern automated production methods allow to place the reinforcement there where it is needed thus reducing waste. To mention are the methods AFP (Automated Fiber Placement) and AFPP (Automated Fiber Patch Placement). UD and fabric tapes are cut into a required patch size in order to accurately place the locally required strength and stiffness to build up the multi-stacked laminate wall.

This process is also applied to pressure vessels where the development over the time was: Filament winding → tape winding → patch placing. *See Fig.2-13*.

For design dimensioning essential are the steps of the single patches over the thickness and the interfaces (*with gaps, because of a better draping, or without gaps*) between the patches.

Do these local reinforcements harm the cyclic and the static behavior (less)? This is to consider when modelling and assessing the distinct structural component.



Fig.2-13: AFPP-fabricated dome-reinforcement of a pressure vessel. (CEVETEC, 2021).

www.cevotec.com/verbesserung-der-speichereffizienz-von-verbundtanks/

3 Construction Applications, Modelling of 'open' and 'closed' FRP, FRC Components

Because concrete applications are not well known some shall be presented here.

3.1 Some Ssemi-finished Products in Construction

Before referring to specific SFCs it is helpful to take a look at the variety of upcoming reinforcements in civil engineering especially for concrete reinforcements.

The main semi-finished products are depicted in *Fig.3-1*.

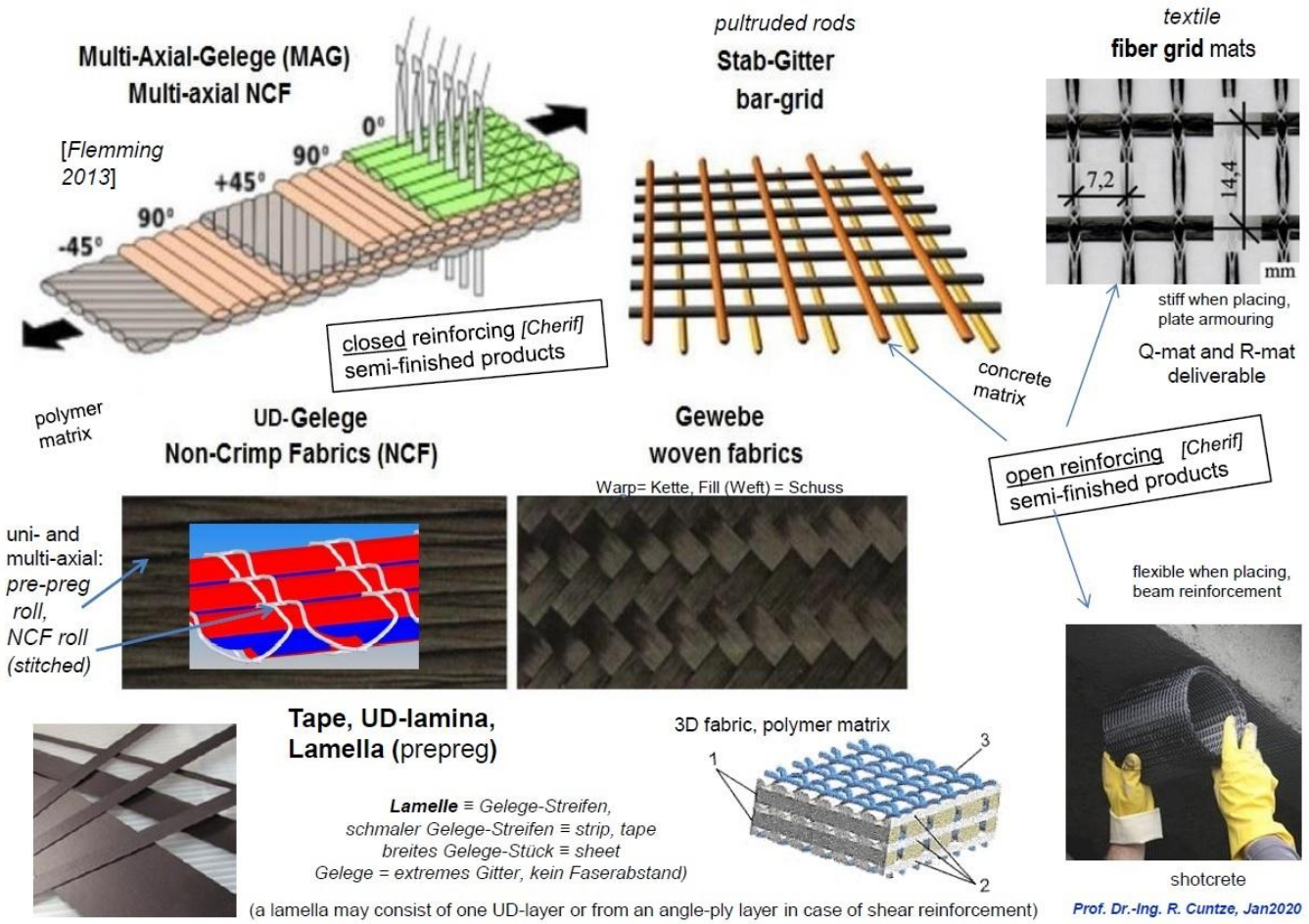


Fig.3-1: Fiber-reinforced semi-finished products in civil engineering [Che11]

There are semi-finished products spanning from pultruded 1D-rods via 2D-non-crimped fabrics up to fiber grids. They are designed as practiced taking the different stress-strain behavior into account. In construction, FRP is used for structural rehabilitation (retrofitting) and new structures. The range is from the huge GFRP tanks and chimneys, profiles and tubes, cables, girders and slabs, bonded stripes, external strengthening by tendons through until reinforcement of beams, slabs and columns. In this chapter some examples of the construction industry are presented. Additional applications can be found in the Springer-published Glossary* of the author.

In construction , so-called 'open reinforcing' such as fiber grids and so-called 'closed reinforcing' semi-finished products are to discriminate, see *Table 2-4* together with *Fig.2-18* and the definitions

in the 'textile book' of Chokri Cherif [*Che11*].

The following table shall comprise the specific terms used in construction. In this context see also the 3 figures below.

Strength designations for fiber-reinforcements of the mineral matrix (concrete) and the polymer matrix

Pultruded rod or bar: transversely-isotropic material, composed of usually heavy tows: cured polymer matrix***:*** $R_{\parallel}^{c}$, $R_{\parallel}^{t}$ (R_f is just fiber strength! [*VDI 2014*]). For the 'fiber strand tensile test specimen' (Faserstrang), cut out of the textile fiber grid, above designations can be used

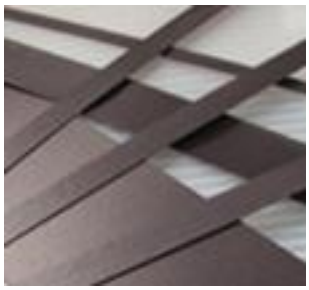
Lamella, UD-lamina: transversely-isotropic material, polymer matrix, 'closed reinforcing': 2D and 3D stress states. Longtime used strength designations $R_{\parallel}^{c}$, $R_{\parallel}^{t}$, $R_{\perp\parallel}$

Fabrics: orthotropic material (if homogenized, smearable), 'closed reinforcing': 2D and 3D materials (not to be confused with 3D*irectional* fabrics = 2D material). Strength designations longtime used for polymer matrix Warp and Fill (weft). F = W → the number of strengths reduces from 9 to 6, in the fabric plane under 2D stress states from 5 to 3

Textile Fiber grids: orthotropic, 2D **'**open reinforcing': 2D semi-finished product: if 'smearable' it is a *composite material* (*Verbundwerkstoff*) other ways a *material composite* ***(****Werkstoffverbund).* According to the textile process the indexing of the fiber grids R-mat and Q-mat (if both directions are equally reinforced then suffix W is equal to F can follow Warp and Fill (weft) of fabrics and according to the usual 2D loadings, basically to be employed in dimensioning. Is the spacing of the tows dense enough to permit 'smearing' in the analysis model then above fabric designations can be used for the composite material. R_{W} is then to be determined on top of the fiber parallel strengths. The number of strengths is like for fabrics. Available are mats of 2m x 6m → 3m x 8m.

Bar-grids of pultruded bars: orthotropic, 2D - **'**open reinforcing':

Strength designations, see bar. Smearable? Load-bearing (effective) width comes in for slabs.







Lamella, fiber grid, pultruded bars (CF, GF, AF, BsF) and bar grid

LL:

** Decisive is a straight orientation of the fibers in the tows. Therefore, of essential influence on the strength are the tow crossings. With the improved production of ideally aligned pultruded bars the possibility is given to mass-optimize the reinforcement of a serial part, if a dominant load case is ruling the design.*

** $R_{\parallel}^{c} < R_{\parallel}^{t}$, because there is usually not enough lateral support in the compression test for the fiber strand to buckle (becomes in-stable). It is usually an instability-linked structural property which we use in design and not a strength material property. H. Schürmann and H. Bansemir proved for CFRP by effortful UD tests that $R_{\parallel}^{c} \cong R_{\parallel}^{t}$ after impeding micro-buckling of the test specimen with a test rig of high lateral support.*

3.2 Applications with Fiber-Reinforced Polymer (FRP) matrices

For *CFRP* with polymer matrix a large variety of applications is *known* such as core wires for the Chinese ultrahigh-voltage power transmission line, constructions in Saudi-Arabia, below.

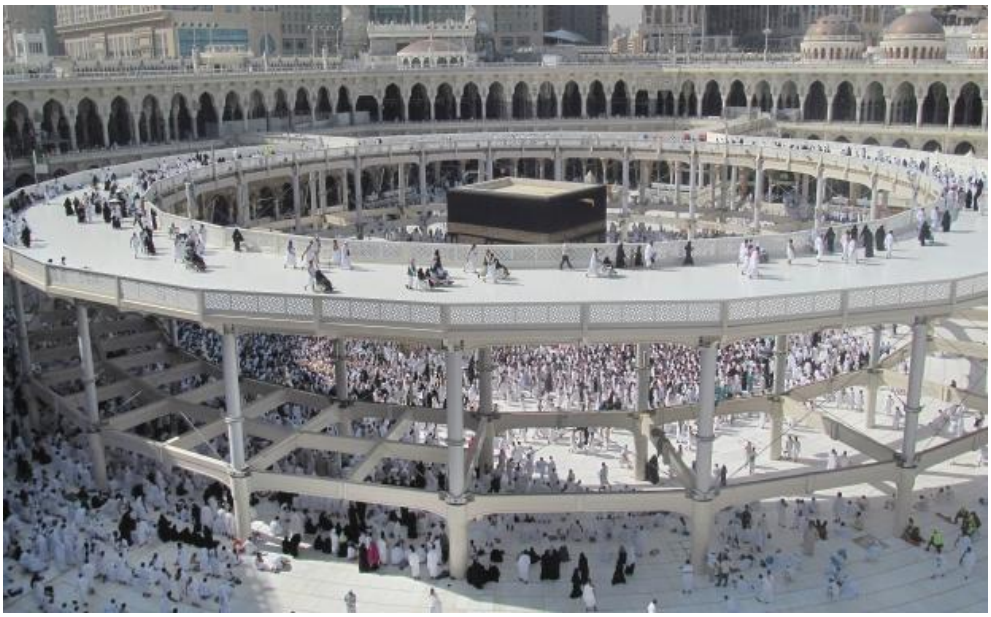


Fig.3-2: Mekkha, CFRP- Pilgrim path construction around the Kaaba. Inner -Φ 80 m, 400 t CFRP [Premier Composite Technology PCT, Dubai, Vancouversun.com]

Much more applications are presented on the next pages.

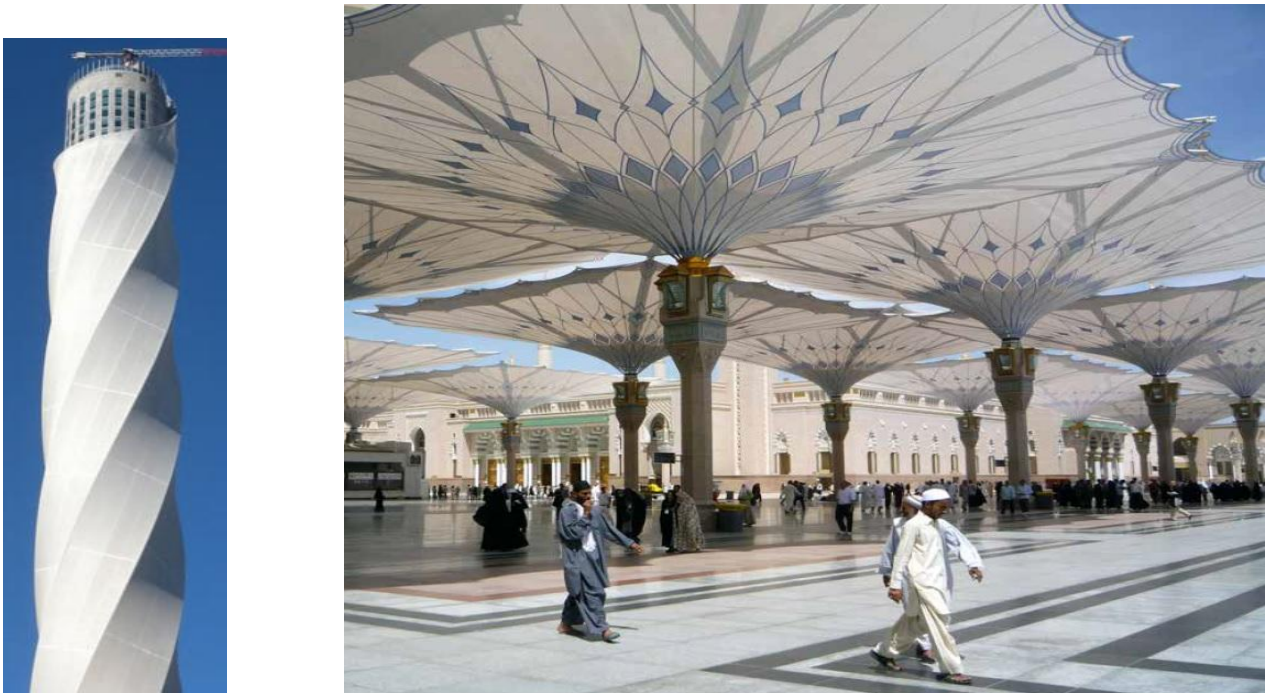


Fig.3-3: (left) Test tower [Jahn/Sobek] transverse vibration-avoiding GF fabric cover of the Thyssen-Krupp test tower for high-speed elevators Rottweil, 245m. (right) Mosque Masjid an Nabawi, Medina, sun protection 'umbrellas', Medina SA, 2010 [ILEK in cooperation with SL-Rasch]



Fig.3-4: Special automated fabrication process with endless fiber strands ‘wound’ over the fixed 'truss' nodes as strand turning points. Lightweight 'fiber pavilion' made of 60 CFRP/GRP components, *BUGA Heilbronn 2020.* Art structure meets load-carrying structure *[Knippers, Koslowski, ITKE Stuttgart; Menges, CD]*.





Fig.3-5: CFRP truss work production using a special strand placement (winding) technique and the fabricated bridge [BaltiCo GmbH, July 2020, Dr. Dirk Büchler]. Thanks Dirk
25 m bicycle and pedestrian bridge made of CFRP in Sassnitz was installed, which was easier than usual due to the weight of just 1.4 tons of a single segment and took place within a single day.
BaliCo Portfolio: Lattice masts, functionalized modular cabin plate elements, bridges, girders, lattice masts, telescopic towers, rotor blades.





Fig.3-6: The Stuttgart Stadtbahn bridge, installed over the A8 motorway on May 3 in Germany, is the world's first network arch railway bridge (127 m) that hangs entirely on tension elements made of carbon fiber-reinforced plastic (CFRP). The 72 hangers are produced by Carbo-Link AG (Fehraltorf, Switzerland) supported by EMPA (Urs Meier. Thanks Urs*), with Teijin carbon fibers (Wuppertal, Germany), Tenax. The bridge meets installation, mass and sustainability goal*



Fig. 3-7: CFRP tension members made of continuous loops for cranes, since 2003 [Liebherr with with the EMPA Spin-Off Company Carbo-Link]



Fig.3-8: Fiber composites in building construction [Sorry. Originator not found in web].
The GFRP profiles of the cooling towers in the combined cycle power plant in Herne received approval on a case-by-case basis (Zustimmung im Einzelfall, ZiE). In addition, the project-related type approval (Bauartgenehmigung) was granted for a cell cooling tower made of these GFRP profiles

3.3 Applications with Fiber-Reinforced Mineral (FRM) matrices

The usual mineral matrix is concrete which leads to the technical term for carbon-fiber reinforced concrete namely CFRC. Additional applications are in the Glossary of the author [*Cun19*].

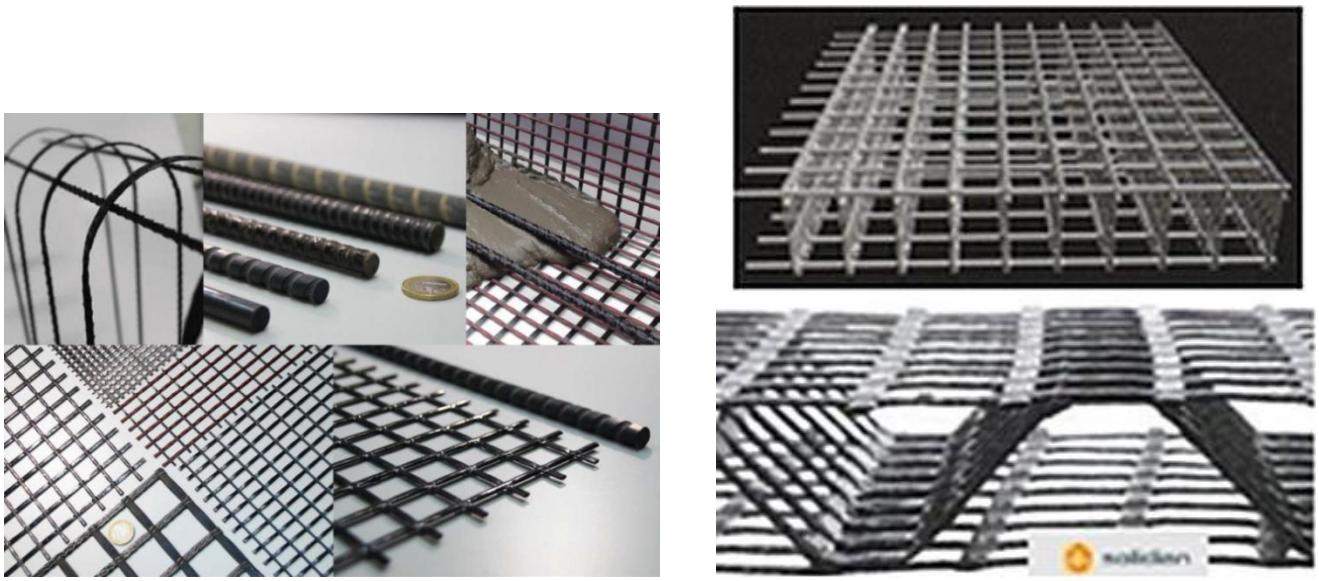


Fig.3-9: (left) Several reinforcements [Frank Jesse],
(right) armoring cages for a sandwich [Fraas, formerly] and an Ω-shaped reinforcement [Solidian].

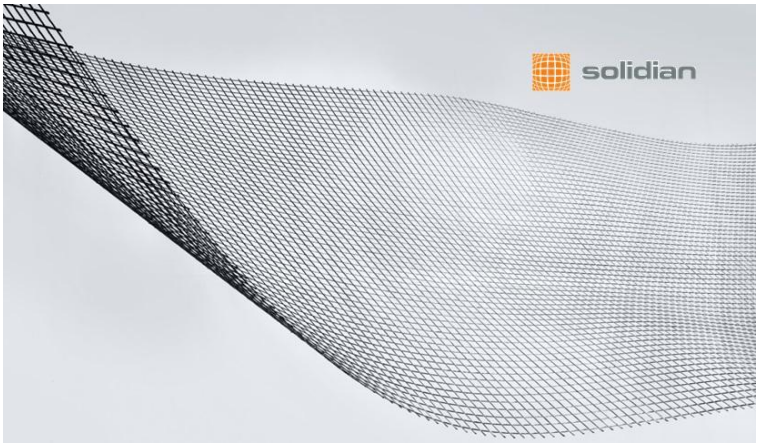


Fig. 3-10: ' solidian GRID_free shape-1' made of carbon fibers with epoxy resin impregnation; characteristic tensile strength > 2.800 N/mm², standard dimension 6,0 x 2,30 m, on request up to 8 x 3 m as well as roll material up to 80 m x 3 m

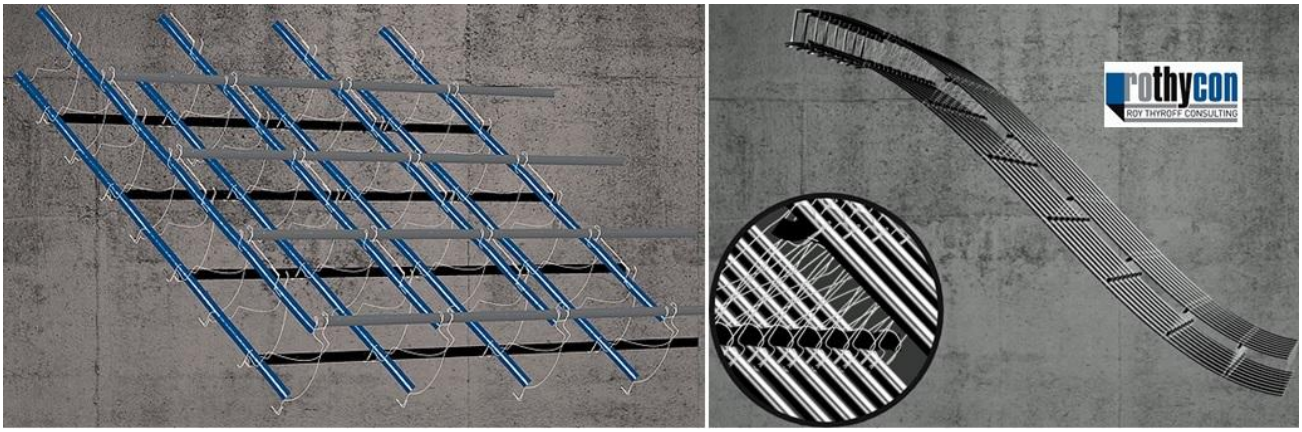




Fig. 3-11: (up) 3D bi-axial spacer fabrics [rothycon], (below) 3D cage

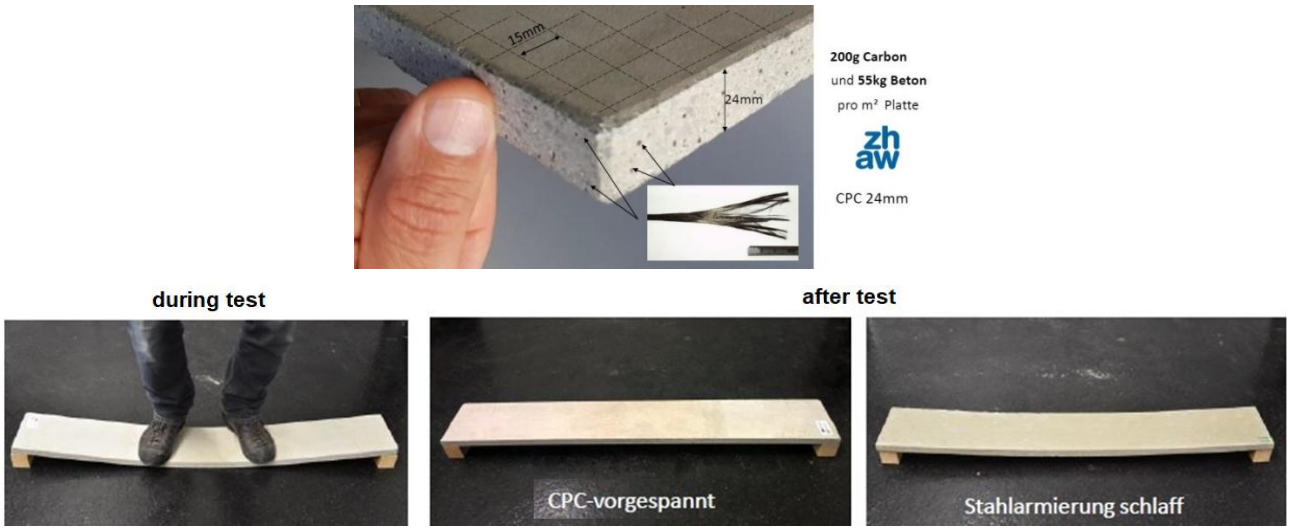


Fig.3-12: Application of pre-tension. The concrete is compression-activated, which massively increases the stiffness of the component, carbon fiber strength can be fully utilized. (center) Stiffness for service loads remains for CPC pre-stressed. (right) Permanent deformation for the slack reinforcement (Stahlarmierung, schlaff) due to the stretched steel reinforcement



Fig.3-13: Hybrid bridge in Turbenthal made of pretensioned CPC slabs and CFRP beam supports. CPC-plate size: 2-7 cm thick, length 3.5 – 17 m [ZHAW, with J. Kurath]. Thanks Sepp



Fig.3-14: Multi-curved textile carbon concrete shell structure. Thanks © Ingelore *Gatzsch*





Fig.3-15: (up) a solidian GRID Q95-CCE-38 fiber grid (mat) [christian.kulas@solidian.com, www.solidian.com] Thanks Christian
(down) First, purely CF-reinforced concrete bridge in the world. Albstadt-Ebingen. 2015.

According to (Construction) Mayor of Albstadt, Udo Hollauer, "The bridge pays off, and is sustainable"

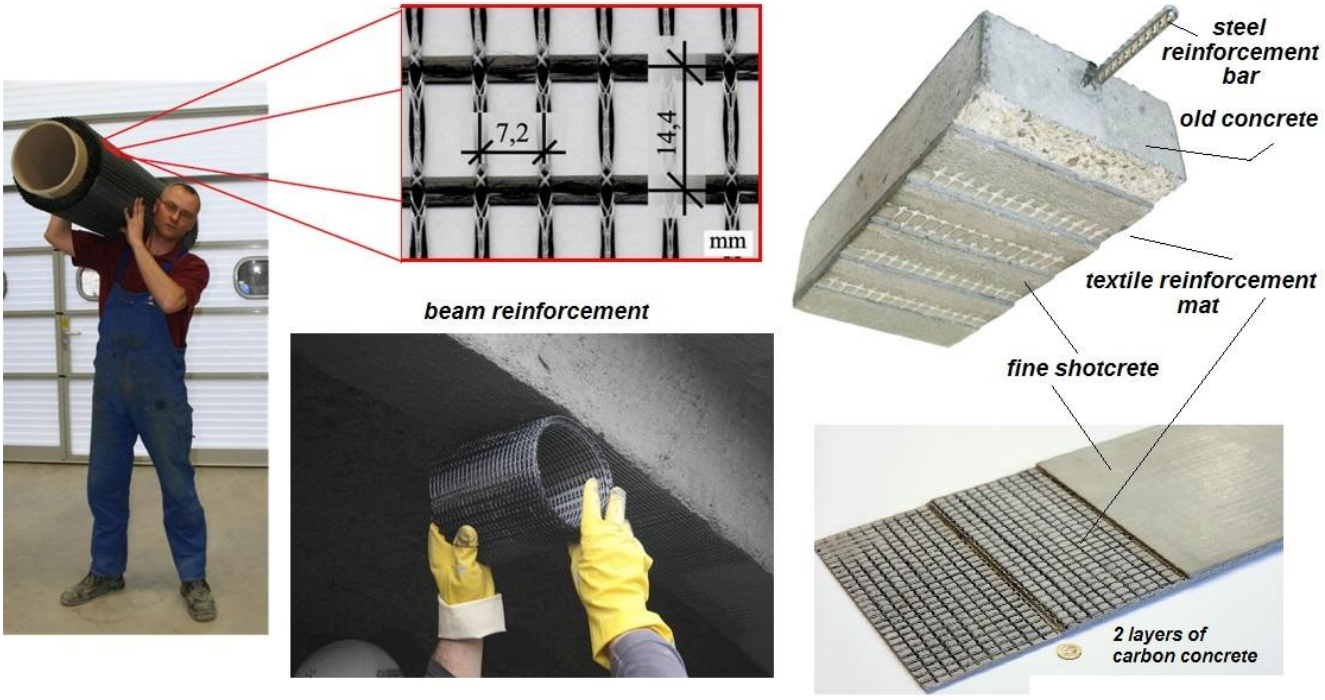


Fig.3-16: for Rehabilitation, retrofitting of a slab. Fiber grid in detail and wrapped on a on roll during application. As an example 2 applied fiber grid lattice layers of CF yarns. [IfM Dresden]



Fig.3-17: light CF-reinforced concrete elements (left) amphibian guidance facility © informbeton GmbH, (right) NTRC – Nonwoven Textile Reinforced Concrete (fleece impregnated with fine mortar, 4.50 m length, 60 cm width, 12 mm thick © Bendl HTS GmbH.

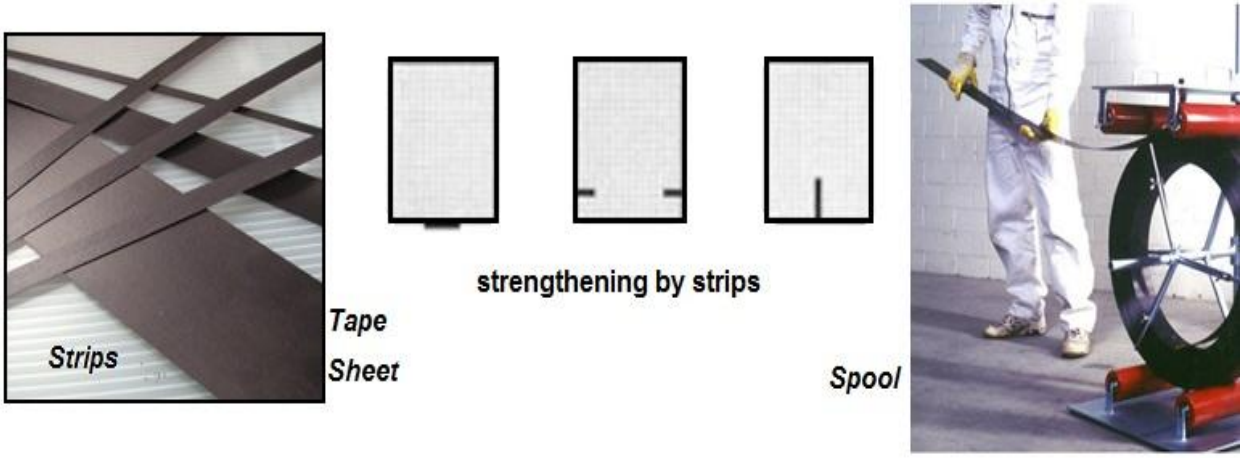




Fig.3-18 Rehabilitation of existing buildings:
(up) Possibilities to strengthen by a pre-tensioned strip or a slack strip.
(down) Reinforcement of slabs due to increased moments by CFRP-lamellas caused by hydrostatic pressure from ground, applying External Reinforced Bonding ERB. Mineralbad "Berg", Stuttgart, 2018, [HPTL].
And for post-reinforcement of 'slab break-throughs' to capture the local stress concentrations
Refurbishment by reinforcement of beams and slabs

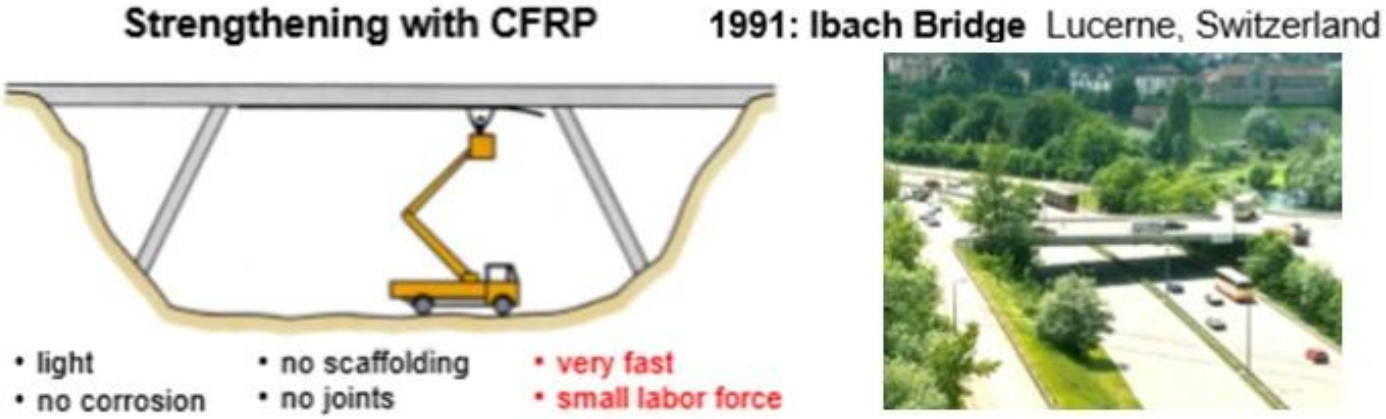


Fig.3-19: Construction Applications of FRM (Urs Meier, EMPA. Thanks Urs)



Fig.3-20: Staircase-Reinforcement with long steel fibers.
[*Faserbeton im Bauwesen, Springer, Bernhard Wietek. Thanks Bernhard*].
What about long C-fibers?

3.4 Some Freshly arrived Applications

From Gabi Boehm, principal architect at PCT, PREMIER COMPOSITE TECHNOLOGIES LLC. Dubai. *Pictures, copyright ENOC. Thanks Gabi*.



Fig.3.4-1 UAE Pavilion: FRP wings (built from a hybrid carbon and glass fiber build-up) and the claddings (built in glass fiber) resulted in an impressive 40% mass saving. The reduced mass was also beneficial during installation and allowed the entire wings to be hoisted in one piece. The wings were produced at PCT facilities to a maximum transportable size. Most wings were transported to the site already assembled – the larger ones arrived in two halves which were bolted together on-site and finished with a seamless joint. The repetitive nature of the FRP panels was critical for the effective use of tooling and CoSt-effective serial production of the wings and claddings. Furthermore, lamination schedule with curing procedure were optimized for each wing and for each zone to meet the structural requirements with a CoSt-effective approach



Fig.3.4-2 E-Trees Sustainability Pavilion: Light and stiff CFRP' steering wheels' keep the load manageable for the mechanical rotation system that allows the E-trees to track the sun as the days progress to ensure that the up to 14 t of PV panels are always ideally positioned to maximize their efficiency.



Fig.3.4-3 ENOC Petrol Station: CFRP was used to construct the entire structure of a service station canopy (roof) . It consists of 133 diamond shaped CFRP frames housing ETFE inflated cushions and photovoltaic panels. The entire structure is supported by an exoskeleton consisting of 9 slender molded CFRP Ghaf trees (the tubes are built using filament winding with molded nodes manufactured from the same carbonfiber fabric).

Awarded the LEED (Energy and Environmental Design) platinum certification. LEED is a classification system for ecological building, the most widely used green building rating system (in Germany: Deutsches Gütesiegel Nachhaltiges Bauen)



Fig.3.4-4: The world's largest composite lock (flood) gates were installed in the Wilhelmina Canal in Tilburg, the Netherlands, at the beginning of 2021. The huge, highly innovative lock gates were manufactured by FiberCore Europe with resins from AOC. Assembly was relatively easy due to the light weight of the parts compared to steel and wood. The composite solution was selected for its extended life expectancy (over 80 years), great durability in prolonged contact with water and minimal maintenance. (Foto: © AOC)

3.5 Some other Fiber-reinforced Bridges in Germany

3.5.1 CU-Bau specialist network (*Managing Director Roy Thyroff*) ***within Composites United e. V.***

Description: The construction industry is an industry in which the topic of high-performance fiber composites is not yet established on the one hand, but on the other hand there is enormous application potential. In order to further prepare, deepen and jointly promote the topic, the CU-Bau network serves as a national and international platform.

Vision: Our vision is that the entire construction industry – builders, architects, planners, approval bodies and construction companies – uses construction products with fiber-reinforced concrete and polymer matrix with confidence and material requirements with appropriate approvals out of knowledge and conviction.

Mission: As a supra-regional specialist network of Composites United e. V. for its members from industry and science, our mission is to promote the acceptance and widespread use of fiber-reinforced materials in the construction industry.

Five working groups are currently active in CU Bau: * Fiber composites for new construction (Neubau) and rehabilitation (Sanierung), * Processes, procedures and digitization, * Design (Entwurf), planning, design dimensioning (Bemessung, Auslegung) and design verification (Nachweis), * Sustainability, health and circular economy and * Education, public relations and cooperation with authorities.

The author, practically, was founder of the CU- Bau specialist network above and would like to present here some innovations about some present fiber-reinforced bridges in Germany. Naturally, not all bridges can be mentioned here.

3.5.2 Introduction to Carbon-Concrete Bridges

80% of all German steel-reinforced concrete bridges are damaged, half should be replaced as soon as possible. The distribution of the causes of damage to concrete surfaces of steel-reinforced concrete bridge structures in the German motorway network states, citing [*Schießl, P.; Mayer, T. F.: Lebensdauermanagement – Teilprojekt A2. DAfStb-Heft 572, Berlin: Beuth, 2007, S. 49-100*], that 2/3 of all causes of damage is chloride-induced corrosion. This most common cause can be avoided by carbon fiber reinforced concrete. They are the hope to improve the situation by acceleration of the full construction time.

Carbon fiber reinforcements have several decisive advantages over conventional reinforcing with a rusting steel: 4 x lighter (ρ = 1.8 compared to 7.8 g/cm^3 of steel), uni-axially about 6 x higher tensile strength (3000 instead of 500 N/mm^2 or MPa) and no rust anymore. This results in a concrete cover of only 15 mm, so that components can remain extremely slim and thus material savings are a further advantage. Hence, the reinforcement made of carbon can be expected to have a service life that is far higher than that of reinforced concrete and thus represents a resource-saving and sustainable alternative in the construction industry. The longer service life is be taken into account especially when building new bridges. The future maintenance costs are significantly reduced by the non-rusting reinforcement. A necessary replacement is also due to the longer service life not expected, where much more than 50 years are the goal. No other material seems to be better suited for road bridge construction than carbon concrete (partly from [*Solidian, Christian Kulas*]).

Two problems faced in steel-reinforced concrete constructions such as bridges: *[partly Wikipedia]*

The alkali-silica reaction, colloquially known as concrete cancer (Betonkrebs oder Betonfrass), is the chemical reaction between alkalis of the cement stone in the concrete and aggregate (Gesteinskörnung) with so-called alkali-soluble silica. It occurs when the concrete is exposed to moisture and has been made with gravel containing too much soluble silica. → The chemical reaction between alkaline and acidic elements leads to the undesired flaking.

Under the action of water and oxygen, steel forms a slightly peeling, porous iron oxide, commonly referred to as rust. If the reinforcement begins to corrode, the associated increase in volume can lead to the concrete spalling over the corrosive steel. The reinforcement in reinforced concrete is protected against corrosion by the high alkalinity of the pore water with pH values between 12.5 and 13.5, since at such pH values a passive layer forms on the steel surface, which practically prevents anodic iron dissolution. This passive corrosion protection can be lost by chloride action such as road salt. → As corrosion progresses, the loss of substance at the reinforcement can endanger the load-bearing capacity of the structure. Statically tension-loaded steel may face under a corrosive environment (sulphide, chloride) a sudden failure due to growing micro-scopic fracture. This failure is termed Stress Corrosion Cracking SCC (Spannungrisskorrosion). Such an effect is the more faced under vibration, termed corrosion fatigue cracking (Schwingungsrisskorrosion), encountered in the dynamically-loaded bridges. Here, a further advantage of carbon-fibers comes in: Its excellent fatigue properties beside the non-corrosion.

Sustainability: Another problem faced is to achieve extremely low-clinker binders, which would result in a CO_2 reduction of two thirds. There is also currently a search for a replacement of the binder cement.

Mind: There is no sustainability without longevity.
Experience promises long-term durability (*Standfestigkeit*) of carbonfiber-reinforced concrete CFRC and fatigue strength (*Ermüdungsfestigkeit*) of the carbon reinforcement.

General requirements for bridges are:

- Environmentally friendly and resource-saving use of building materials (less material, see also above)
- Sustainability (longer life than reinforced concrete bridges, as it is prepared for chloride attack)
- Short construction site phase (minimize street closures to avoid unreasonable costs.
- If a protective layer is omitted, the concrete surface is driven on directly. Thus, it was important that the exposure class XF4 is maintained for an environment of high water saturation with de-icing agent
- Minimal maintenance work (compared to reinforced concrete structures, bituminous coatings on the surface of the bridge can be dispensed with, as the corrosion-resistant reinforcement is not to protect against chlorides. Consequently, rehabilitation work is significantly reduced, since the usual replacement of the bitumen waterproofing is not required)

The above requirements can be met purposefully with pre-fabricated parts, which also comply with the necessary manufacturing tolerance in order to be able to reliably design dimension even in this new case with lower wall thickness and thinner concrete cover. Pre-fabrication not only reduces the construction time, but also has the advantage of being practically independent of the weather conditions.

One problem of the carbon concrete shall be not forgotten: It is the too low operational temperature for some application cases. This is caused by the Polymer in the FRPm (*Fiber-Reinforced Polymer matrix)* reinforcement element. Therefore of high importance is to replace in the next future the polymer matrix by a Mineral matrix one, obtaining a FRMm bar reinforcing element or a bi-axial mat.

3.5.3 Foot Passsenger Bridges in Albstadt, Germany

Albstadt-Lautlingen: In 2010, the longest textile-reinforced concrete bridge was opened. It is still reinforced with glass fibers, in which the breaking stress of 1000 – 1500 N/mm² is significantly lower than with carbon fibers. It is designed as a plate-beam type with a steel pre-tensioning. Two other textile-reinforced concrete bridges of this type are still standing in Oschatz and Kempten. One idea was to get away from additionally pre-tensioning.
While slab-beam bridges are linearly reinforced by bars and often pre-tensioned, here should be reinforced mainly by 2-dimensional 'textile fiber-grid mats' (also possible are 'bar-grids' from pultruded rods). The mat -reinforcements are four layers in the slab and two layers in the cheeks located as close as possible to the surfaces.

The design of such bridges is not yet regulated by the building authorities in Germany, which means formulated in a standard and therefore an 'Approval in single case' (*Zustimmung im Einzelfall, ZiE*) must be obtained. For this purpose, a design method had to be created that is based as analogously as possible on the well-known process of reinforced concrete. This design method in steel-reinforced concrete analogy was then to be validated by static tests. (*Institut für Massivbau an der RWTH Aachen (IMB), Sergej Rempel).* While carbon behaves linearly elastically, steel becomes plastic before failure. This had to be considered in the steel-reinforced concrete analogy.

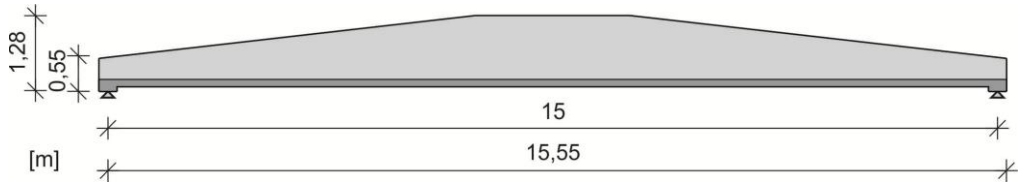
Pedestrian-Bridge Albstadt Ebingen 2018: Completely without steel, the world's first carbon concrete bridge reinforced purely with carbon fibers spans 15 m. The engineering office Knippers-Helbig designed the pedestrian bridge, created the static calculations and accompanied the approval process. The lightweight construction with minimized use of construction materials does not require intensive maintenance, which should reduce maintenance costs and increase service life.



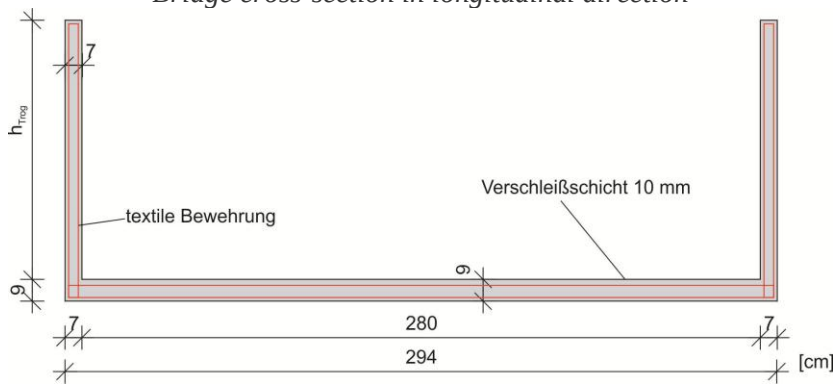
Passenger bridge, Albstadt Ebingen 2015: Length 15 m, width 3 m, mass 14 t.
Erection during one night ! [courtesy Solidian] , soligrid Q-100-CEP-38

The bridge deck is designed as a trough-shaped single-span girder with a fixed and a sliding bearing. The cheeks of the trough are 70 mm thin, their height is affine to the bending line of the beam. The railings are connected directly and flush on the walls via recessed sleeves. For the floor, 90 mm is enough. One can live here without the covering (*Belag*), because the reinforcement does not corrode, and also without the sealing, so that the maintenance will not cause any significant costs in the future. The opening in the applied mat dictates the maximum diameter size of the aggregate in the concrete, and it was chosen here 8 mm. (*Thanks to Sergej and Christian*)

1. Rempel, S.; Will, N.; Hegger, J.: *Zukunftsweisende stahlfreie Fußgängerbrücke aus Carbonbeton*. In: Tudalit Magazin, Tudalit e.V., Nr. 15, 2016, S. 11.
2. Helbig, T.; Rempel, S.; Unterer, K.; Kulas, C.; Hegger, J.: *Fuß- und Radwegbrücke aus Carbonbeton in Albstadt-Ebingen.* Die weltweit erste ausschließlich carbonfaserbewehrte Betonbrücke. In: Beton- und Stahlbetonbau (111), 10/2016, S. 676-685. DOI: 10.1002. ISNN: 0005-9900.
3. Rempel, S.; Kulas, C.: *Fußgängerbrücke in Albstadt. Brückenbau im 21. Jahrhundert*. In: Beton Bauteile Edition 2017. Bauverlag BV GmbH, Gütersloh. 2016, ISBN: 978-3-7625-3676-5



Bridge cross-section in longitudinal direction



Cross-section of the bridge in perpendicular direction. Carbon textile reinforcement, wear layer 10 mm



View of the finished reinforcement cage.
From („Zukunftsweisende stahlfreie Fußgängerbrücke aus Carbonbeton". Dr.-Ing. Sergej Rempel, now Professor at Augsburg)

3.5.4 Bridges in Margrethausem and Pfeffingen

The following figure presents two bridges which had to replace the former ones. This replacement

was a hybrid solution. It consists of steel girders, which secure the load transfer in the longitudinal direction, and the carbon concrete slab as the load-carrying element in the transverse direction. The elements are selectively connected, subsequently, and only in order to be able to transfer the brake forces. A full bond was excluded here.



Some Design data of the carbon grid (mat)
GRID Q95/95-CCE-38, solidian GmbH
Average tensile strength

$\bar{R}^{t}_{\square} = 3200$ MPa, $\bar{e}_{\text{fracture}} = 1.5$ %, E = 205 GPa

mat geometry = 5.0 m □ 1.2 m , fiber strand distance = 38 mm

area fiber strand = 3.62 mm^2, area per m = 95 mm^2/m





(left) Bridge Margrethausen (24 t), Max Bögl, 2016; (right) Bridge Pfeffingen (40 t), 2016. Special concrete C70/85, maximum grain 5 mm, mean compressive strength 90 MPa



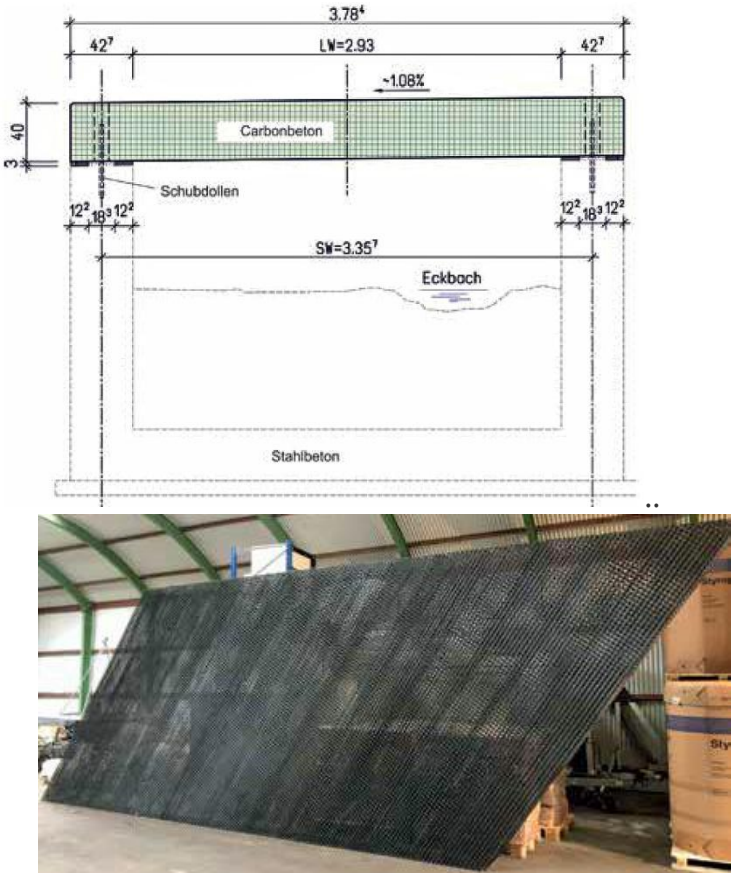
Bridge Pfeffingen Mounting

3.5.5 Road Bridges Gaggenau

These two identical road bridges overpass the Eckbach in Gaggenau. The substructure is a U-profile (*see figure*), which is open at the top and was made of conventional steel-reinforced concrete. The superstructure consists of a pure carbon concrete slab, which is positioned flexibly on the substructure. For the transmission of the brake forces, stainless thrust dolls are used for the connection of the two components. All components were finished parts and were fabricated in the factory of Grötz GmbH. The thickness of the plate is 40 cm, of which one centimeter is used as a wear layer covering.

The bridges were designed according to Eurocode 1 for the traffic load model 1 therein. As a result of the high loads, the shear load bearing capacity could not be proven exclusively with the longitudinal carbon reinforcement. For this reason, a shear force reinforcement was developed in cooperation with the IMB of the RWTH Aachen University. For this purpose, modified double-C profiles were produced from the reinforcement mat Q95/95-CCE-38 and then shaped. Finally they were installed every 40 cm in the complete armoring cage (*see figure*)

The stress-strain curve for the concrete could be taken from Eurocode 2, since the used concrete was a so-called standard concrete. In the case of the carbon reinforcement, the standardized fiberstrand test was used to determine the stress-strain curve, which follows the recommendations in [21]. The determination of the design stress (*Bemessungsspannung*) was determined using a partial safety factor $\gamma_t = 1{,}3$.



(left) Cross-section of substructure and superstructure drawing: R+S Ingenieure
(right) Picture of final bridge 7 m · 3.1 m, ? tons; Grötz construction companyComplete armoring cage with map and transversal double-C profiles to withstand shear

The residual strength test after 10^6 cycles showed no significant impact on the load-carrying capacity.

Reduzierte Bauzeit bei Ersatzneubauten von Straßenbrücken durch Carbonbeton. Dr.-Ing. Sergej Rempel, Dipl.-Ing. (FH) Eugen Kanschin. Tagungsband 30. Dresdner Brückenbausymposium, March 2020, p. 65

[21] Rempel, S.; Ricker, M.: *Ermittlung der Materialkennwerte der Bewehrung für die Bemessung von textilbewehrten Bauteilen.* Bauingenieur 92 (2017), S. 280–288

3.5.6 CarboLight Bridge Demonstrator (see *figure below*)

The *CarboLight Bridge* Demonstrator, an ultra-lightweight construction made of carbon reinforced and Infra-Lightweight Concrete ILC. It is a non-tensioned (slack) bridge for exhibition in the bridge construction department of the Deutsches Museum in Munich. (*Courtesy: Text and figures from Marc Koschemann & Silke Scheerer, Institut für Massivbau, TU Dresden. subprojects Curbach in SPP 1542. Stefan Gröschel, Institut für Massivbau).*



Shape-optimised CarboLight Bridge (Deutsches Museum). [Source: Ansgar Pudenz]

A structure was to be designed where the load path (*flow of force*) is clearly recognizable to any observer from the external shape and whose design follows the principle of form follows force. Raw density $\rho = 800$ kg/m³. An area approximately 9.5 m long and approximately 2.0 m deep between two walls was available to present the demonstrator in the museum as an eye-catcher for construction engineers and public-relation for CarbonFiber-Reinforced Concrete CFRC. Realistic design load cases were applied.

A fully parameterized 3D model of the bridge was created with the software programmes Grasshopper in conjunction with Rhino. By programming an interface to the FEM programme RFEM, it was also possible to transfer the geometry and material data as well as loads from Grasshopper quasi-simultaneously into a FE beam model in the sense of building information modelling BIM. Trade-off studies on variants were performed. Schematic representation of the assembly steps for erecting the CarboLight bridge using the support structure; the temporary supports were height-adjustable and horizontally movable *[Source: Marc Koschemann]*.

Important findings and experience regarding concrete consistencies, processing times and formwork preparation were gathered during the fabrication and the erection of the demonstrator. Even minor deviations in the manufacturing process can influence the quality of the concrete surface. One goal was optimizing the concrete mixtures by testing various curing methods in combination with different impregnation systems. After 28 days, the supporting structure was removed. To minimize cracks due to shrinkage, surface reinforcement was provided for the compression-column acting compression sheets on the bottom and the top sides.

Superstructure (*Brückenüberbau*):

As carbon reinforcement textile SITgrid 040 (*Wilhelm Kneitz Solutions in Textile GmbH*) was chosen. The goal was to achieve compression stresses over the whole cross-section for all load combinations. For the superstructure with a biaxially curved underside, a sandwich three-layer structure consisting of two 20 mm thick carbon reinforced concrete face layers and a core layer of ILC.

The superstructure was mainly calculated for bending and shear force. The uniaxially oriented carbon textile SITgrid 040 was chosen for the underside, mainly because of the dominating curvature in the transverse direction. This textile has a reinforcement cross-section of 141 mm²/m in the longitudinal direction and 28 mm²/m in the transverse direction, which ensures the required fexibility of the reinforcement mesh. The characteristic yarn tensile strength is 2200 N/mm². The upper, flat carbon reinforced concrete layer was reinforced with one sheet of solidian GRID Q95/Q95-CCE-38. This textile has a higher inherent stifness and thus offers advantages for positionally accurate installation in plane sections. The calculated load-bearing capacity could be provided with sufficient certainty for both reinforcement layers.

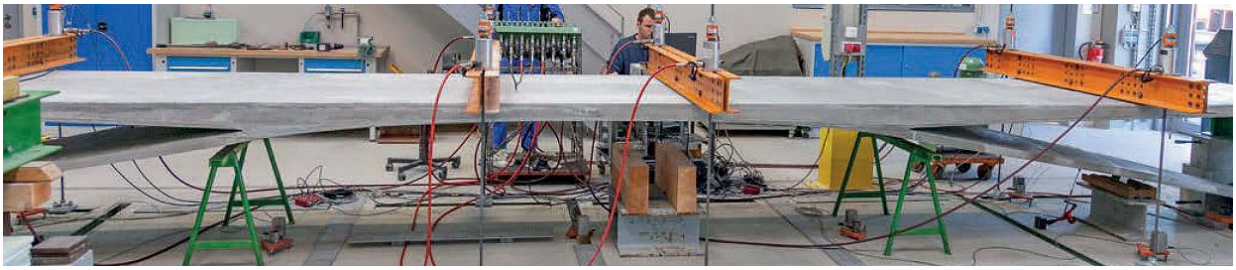
Regarding the sandwich core, the load-bearing capacity of the interface between the layers had to be verified. The formwork planning was based on the 3D model of the demonstrator. The production of individual formwork parts from solid plywood panels using 3D milling technology was carried out by the HICONFORM company.

Fabrication: The mortar mixture had to guarantee a dense and pore-free structure as far as possible, had to be pumpable and flowable and remain workable for at least 30 min Problems similar to SMC fabrication and the path-oriented, extrusion head-placed mortar strand process. The workability of usually pumped concrete has a slump (*Ausbreitmaß*) between 50 mm and 100 mm. A concrete of less than 50 mm slump is impractical for pumping, and in the case of a slump above 125 mm, the aggregate will segregate from the mortar and cement paste. To maintain the concrete cover of about 10 mm, DistTex spacers were used

Compression-loaded inclined plates (sheets) (Druck-Scheiben):

The figure below presents the 5 parts of the CFRC bridge.



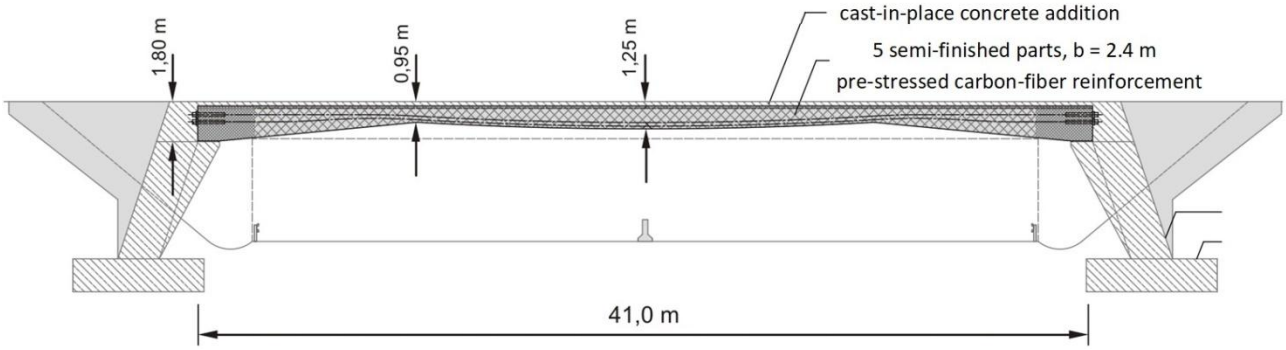


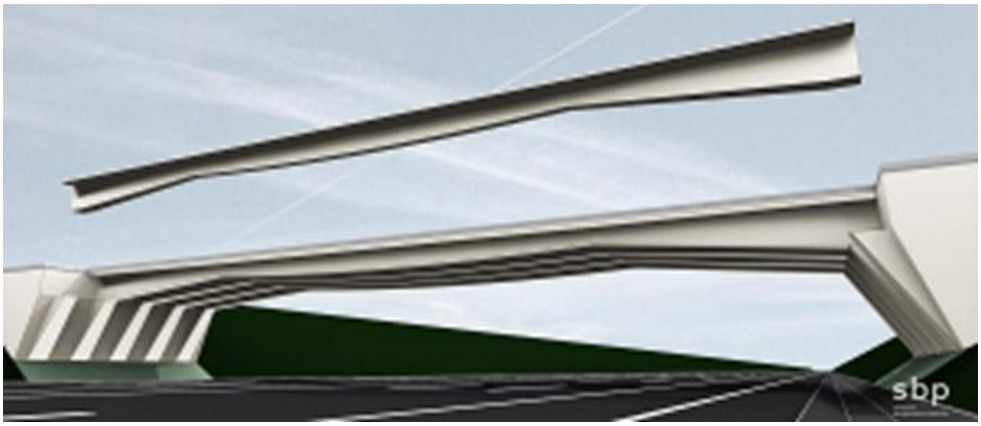
Filigree FRC parts: Bending superstructure width 1.20 m, 3.0 side spans, 3.6 m center span. 2.1 t Buckling endangered compression sheets, inclination 17.5 °. (below) Testing of the bridge at Dresden

3.5.7 First integral pre-tensioned carbonfiber-reinforced concrete bridge

At the TU Berlin (*Mike Schlaich, Professor of design and construction, civil engineering, partner in bureau sbp*), the world's first integral pre-tensioned carbon concrete bridge was built for research purposes. This exhibition bridge is the neighbouring bridge.

To pre-compress the material concrete (*official term is pre-stress*) in order to better exploit the concrete so-called tendons are used. A tendon is basically a cable or a multi-roving fiber strand used for pre-tensioning a structural element such as a beam, column, plate. According to the construction method, there are generally three types to pre-stress concrete: (1) Pre-tensioned Concrete (*tendons are tensioned from the beginning, then concrete is poured),* (2) Un-bonded Post-tensioned Concrete and (3) Bonded Post-tensioned Concrete (*concrete is poured first, tendons are then tensioned*).
Design task was a standard flyover structure.



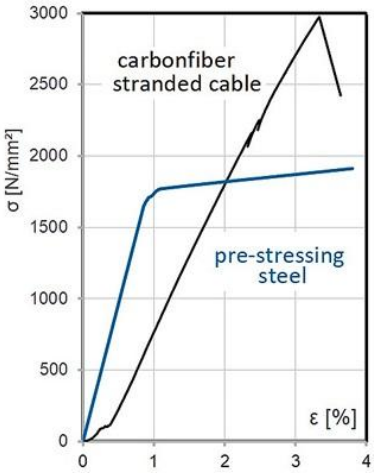


3D-visualization of the integral overpass bridge built of semi-finished pre-tensioned carbon concrete parts. Quelle: C3-Projekt V4.2 Quelle: schlaich bergermann partner © sbp. Demonstrator fabricated for Exhibition Deutsches Museum München)

When fully utilizing CF in a bending beam, the concrete is stretched too much and the SLS is injured. It is advisable to tension the carbon reinforcement for the economic use of the carbon fiber (analogous to my example in § 19.4). The effort for the pre-tensioning process is opposed by the fact that the required amount of carbon fiber can be roughly halved for a bending beam. For ULS (GZT), the pre-tensioned variant can then be optimally exploited.







Carbon Fiber Composite Cable (CFCC) from Tokyo Rope, cable strand diameter 12.5 mm E-Modulus 155000 N/mm², T_{max} = 130 °C. Static tensile tests: fracture load 274 kN per cable or strength 3000 N/mm² per cable strand (Kabellitze) [from presentation F. Jesse]

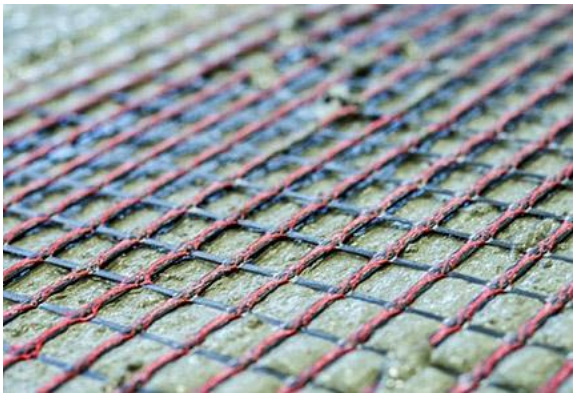
Frank Jesse, Hentschke Bau "Areas of application of C³-Carbon Concrete Composite from the perspective of a medium-sized construction company" and "When does CarbonConcrete pay off and when is its use sustainable?" For your contributions at CU-Bau Forum at 64. Betontage, Ulm, 19.2.2020. Many thanks, Frank.

If a thermo-plastic impregnation resin system is applied, then the reinforcement strand can be formed in contrast to the usually applied epoxy resin system. This is very helpful when caging.

3.5.8 Release Bridge Rplacement (Ersatzneubau) in Wurschen, Landkreis Bautzen, 2022

A replacement of the bridge of the state road S 111 near Wurschen (*district of Bautzen*) was opened to traffic. The former steel-reinforced concrete structure from 1934 was replaced by a carbon-reinforced concrete (CFRC) bridge in the Saxon road network. The bridge is therefore also approved for heavy goods traffic with a vehicle weight of more than 40 tons.





Bridge Wurschen: (left) *Superstructure made exclusively of carbon concrete, shell construction. (right) Textile FRP mats in the super-structure) (Foto: Stefan Gröschel, IMB,TU Dresden)*

The findings gained within the framework of the project, substantiated by continuous measurements, shall be incorporated into future projects. The use of carbon concrete leads to a significant saving of raw materials and thus represents a sustainable alternative in the construction industry. The superstructure of this bridge consists exclusively of carbon concrete

The reinforcement consists of both rods and mats made of carbon fiber reinforced plastic and is non-rusting The reinforcement consists of both rods and mats made of carbon fiber reinforced plastic and is non-rusting. Both rods and mats made of C-fiber strands were used for the bridge.

The C³-Association initiated the project together with the Saxon State Ministry of Economic Affairs, Labour and Transport (SMWA), the State Office for Road Construction and Transport (LASuV) and the LISt Gesellschaft für Verkehrswesen und ingenieurtechnische Dienstleistungen mbH. The planning, execution and supervision was carried out by the members of the C³ association: CARBOCON GMBH, Curbach Bösche Ingenieurpartner, Hentschke Bau GmbH and Technische Universität Dresden. The carbon reinforcement was supplied by Action Composites Hightech GmbH and solidian GmbH.

The very load-bearing, carbon reinforcement can be expected to have a service life that is far above today's reinforced concrete constructions and thus represents a resource-saving and sustainable alternative in the construction industry. Due to the longer service life with considerably lower maintenance costs in the future, there are corresponding cost advantages



Bridge Wurschen: (left) *Shell construction from top.*
(right) Ready bridge. (*Copyright_cbing_Schröder*)

Carbon-textile-concrete pays off if the construction task can only be solved with carbon concrete, if additional functionalities offer added value and, above all, if life cycle costs including maintenance are realistically calculated [*Dr.-Ing. I. Gaitzsch*].

Maintenace cost comparison: CF-reinforcement beats steel-reinforcement from about 10 years on [*HITEXBAU GmbH Augsburg*]. Savings are of course even higher for 100 years of service life.

Finally some orientation values for building material costs are: concrete 80 → 500 €/m^3, steel 750 €/t, CF-rods 24 €/kg, CF-fiber grids 45 €/kg. Load capacity: *Carbon 24 kN entspricht B500S Ø8*





(left) Art structure Mae West [Wikipedia)], München Effnerplatz..Shape of a hyperboloid made of CF-tubes. Height 52 m.Artist: Rita McBride; Production: Franz Weißgerber; Sructural Engineering: Bureau Prof. Werner Sobek. Each tube is 40 meters long, has an outer diameter of 225 to 275 millimeters, with a wall thickness of about 15 millimeters, and weighs only 550 kilograms

(right) Model: *Thanks Franz*)



It is very seldom good to be late!
If we had been half of an hour earlier, after schedule, I would probably lie down in the ravine.
Afterward it was terrible to make a video clip of the falling huge blocks of stone.

In this context my plea is:
"Use the mentioned new fantastic build possibilities, whenever reasonable.
It is not beneficial to wait and to become too late!"

3.6 Influence of Production Process on the Damage of Filaments and Fiber Strands

The structural engineer should keep in mind what production 'makes' with the filament and with the cured stiff roving or thick tow. The author was confronted several times in his life with such a problem, see *Fig.3.5-1* through *3.5-4*.

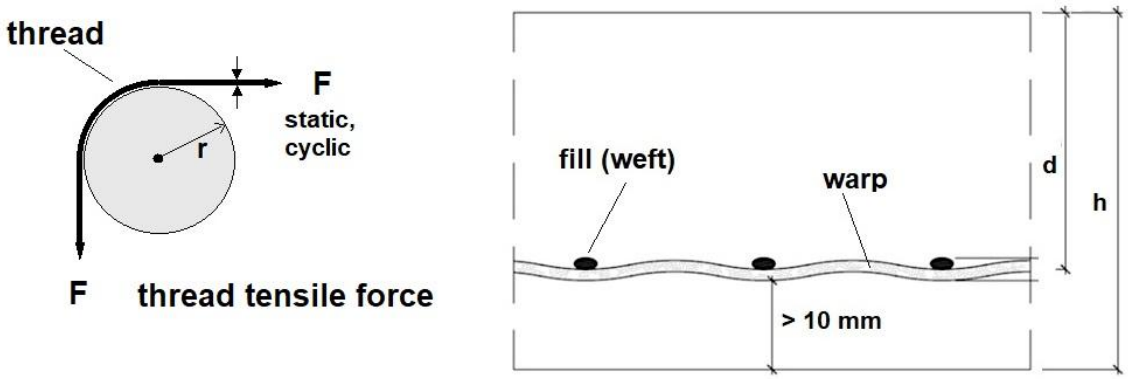


Fig.3.5-1: (left) Sketch of the deflection situation at a thread curvature location. (right) visualization of the waviness of a fiber grid layer within the concrete matrix of a plate. (here, sketch of the determination of the static usable height separated for warp and weft direction)

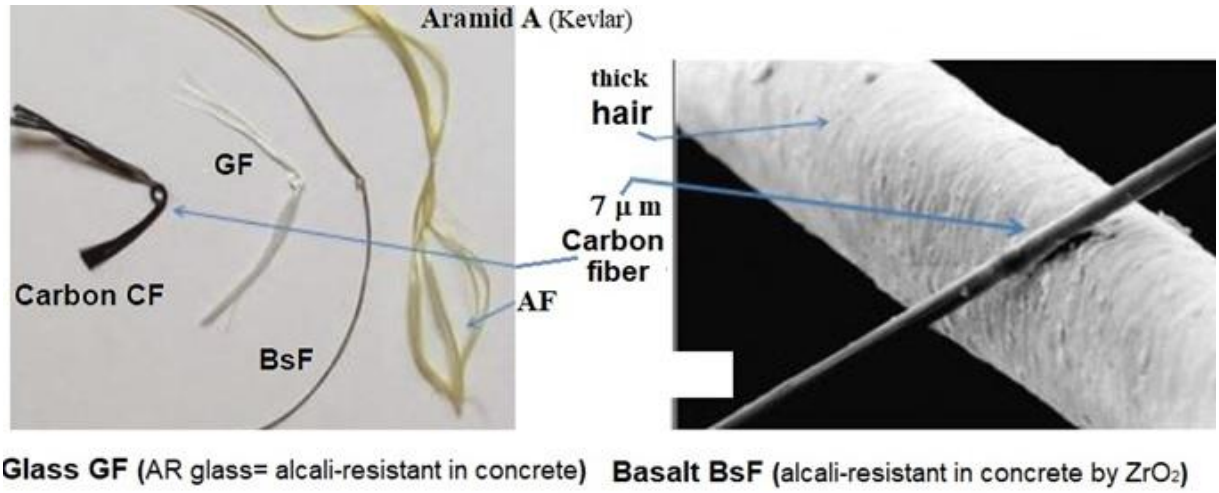


Fig.3.5-2: Different strengthening fibers and comparison CF with human hair

The following information shall improve the knowledge about this problem. It is written for a filament (CF = 7 µm ϕ) but directly transferable to a 4k roving or a thick 49k heavy tow thread, used in order to increase the material feed to speed up production. It is valid for wrapping, tape storage and braiding. For understanding at first some basic terms are presented:

Radius of curvature ρ:
The high stiffness and, above all, brittleness determine the degree of curvature and bending of the

filament during deflection. A simple calculation delivers a thumb value which is of high interest when bending armoring cages:

Single Carbon fiber:

d = 7 µm, fracture strain ε_{fr} =1.5 %, E_f = 240000 N/mm^2, fracture stress $\sigma_{fr} = \varepsilon_{fr} \cdot E_f$.

From this follows $\rho \approx E \cdot I / M = 0.5 \cdot E \cdot d / \sigma_{fr} \rightarrow 0.2$mm. Keep $\rho_{crit} < 1$ mm.

Roving fiber bundle, cured stiff: outer filament of the stiff bundle bent

assumed d = 1 mm, $\rho \approx 0.5 \cdot E \cdot d / \sigma_{fr}$ Keep $\rho_{crit} \approx 20$mm.

Angle of re-direction (*Umlenkwinkel*) $90° > \alpha > 90°$: [*Kun04*]
The contact length of fiber and thread guide roller impacts the stress distribution in the contact area. Thereby, the radius of curvature has much an effect.

Surface structure and roughness of the thread guide roller (Fadenführungsrolle): The friction behavior between filament and thread guide roller influences the damage of the filaments. Glazed porcelain is recommended in [*Kun04*].

Thread tensile force *F*: Due to tensile load of the thread during the production process a stress distribution over the cross-section is caused. This also depends on the shape of the thread guide roller

Thread speed: Determines production rate and is to optimize with *F*

Filament arrangement in the thread: Thread guide roller change the arrangement of the filaments in the cross-section of the roving feed, so that the very important fiber parallelism may be disturbed, especially when braiding.

Winding: The author was several times confronted in his professional life with the strength problems addressed in the two following figures, when winding layers were built up to the required laminate wall thickness.

These production simulation ideas in the Figs.3.5-3 and -4 can be transferred to static and cyclic operational loading.

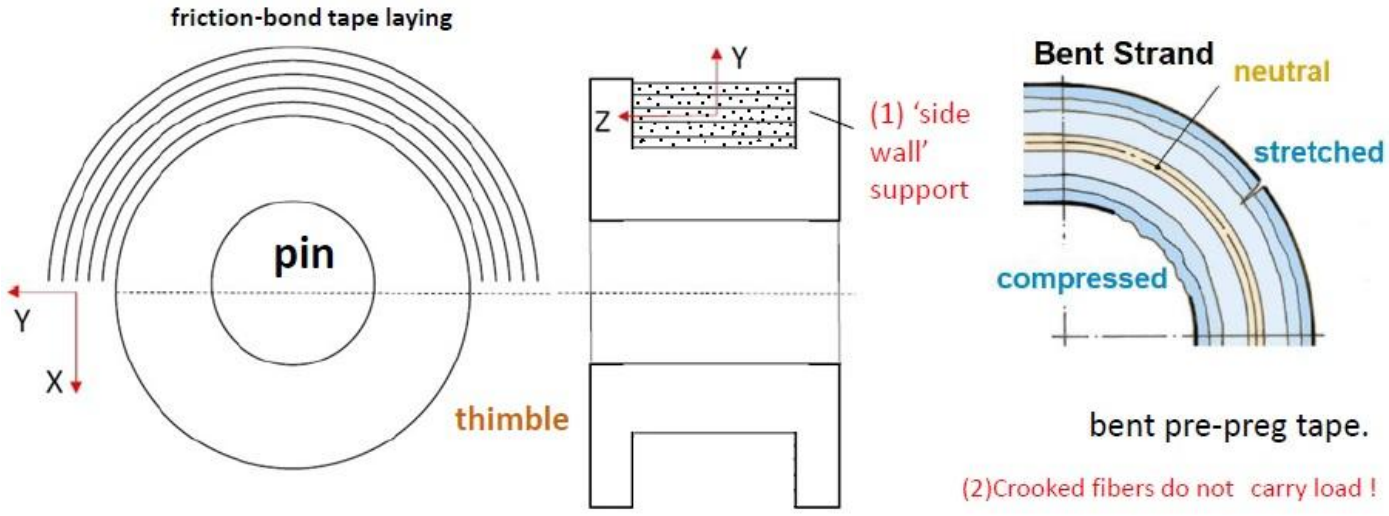


Fig.3.5-3: Benefit of semi-cured layer placing and of a side wall supported layer stack

Some points to consider regarding the design challenge '*Smoothing the Fiber Stress Concentration along the strand loop':*

* Crooked fibers or tapes practically do not carry the desired tensile loading. Fibers or tapes losing some stretch, caused by the winding or tape-laying process, carry much less tensile loading and are not efficiently used (*less exploitation of fiber capacity*).

* Side walls: A 1D-compressive radial stress state in the groove of the thimble would lead to IFF2-caused wedge failure of the laterally compression-loaded UD loop strand. On the other side, in the case of side walls the radial compression generates a positively acting lateral 2D-compressive stress state. Hence, side walls of the groove are mandatory despite of the fact that the fibers experience a little higher tensile stress.

* Thin tapes (layers) help to exploit the capacity of the fibers.

* The contact roving (filament) ↔ thimble principally causes some wear under cyclic loading.

* Critical location is at the 'cheek', where a stress and strain concentration is generated. This causes a changing contact situation with sliding friction and wear. This is important for the fatigue life

* Reducing the bond between the layers increases the strength capacity of the loop, see CarboLink idea → Good Design ideas 'make' structural Strength!

LL: Friction bonding production leads to a fatigue life higher than for full bonding.

High secondary stresses occur in the bolt area when loading laminated strand loops.
The more rigid the fibre and the "thicker" the loop is, the higher the secondary stresses are that will be generated.

Non-laminated strand loops solve this problem. Such a strand loop is made of a very thin UD tape of only 0.12 mm thickness. This tape is continuously laid in the desired number of layers around corresponding deflection bodies (bolts, pins) by an 'endless tape lay-up device'. There is no full bond between the individual layers, just friction bond. The last layer is laminated with the penultimate layer on a length of about 10 cm and anchored with it. *[Winistörfer, A.; Mottram, T.: Finite Element Analysis of Non-Laminated Composite Pin-Loaded Straps for Civil Engineering, Journal of Composite Materials, Vol. 35, 2001. Carbo-Link and EMPA Dübendorf, Prof. Urs Meier*].

When loading the strand loop, a relatively even stress distribution is achieved due to relative shifts possible between the adjacent tape layers. The load transmission between the layers is carried out by friction. This is also more cost-effective because no consolidation of the shifts is required.

Lateral supports increase the load-bearing capacity of strand loops made of carbon fibre. This indicates that in dimensioning of loops it is necessary to apply a 3D-strength analysis (VDI 2014 Part 3, editor: R. Cuntze).

Production experience: full bond
When putting layer upon layer the 'winding tension force' will compress the former layer and reduce the efficiency of the former layer. This situation is improved by an optimal choice of the 'winding tension force' in the process together with intermediate consolidation.

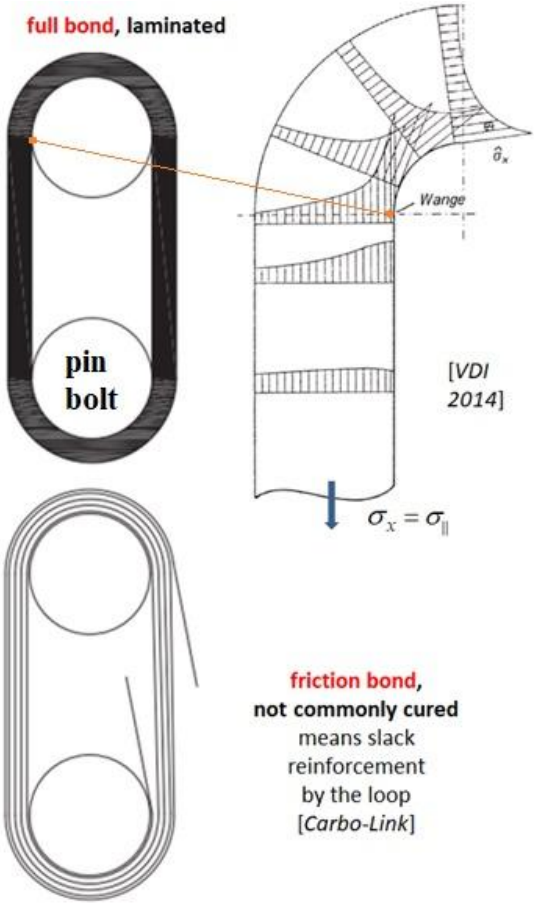


Fig.3.5-4: CarboLink Idea of a flexible construction of the strand loop (Strangschlaufe) to obtain equally stressed layers by friction bonding instead of a full bond solution together with intermediate curing at winding

→ Friction bonding production leads to a higher fatigue life.

3.7 On Material Modelling of some of the Semi-finished Products in Construction

Pultruded Rod: uniaxial loading, usually 1D tensile design dimensioning. Reference cross-section is the fiber cross-sectional area for the strands cut out of the fiber grids and the cross-sectional area resulting from the nominal diameter for pultruded rods. Necessary properties to provide are $E_{\square}$, $R_{\square}^{t} \equiv f_{\square}^{t}$, $R_{\square}^{c} \equiv f_{\square}^{c}$, obtained from test series.

Lamella: ('closed' reinforcing tape for structural habilitation): Uniaxial and bi-axial reinforcement of beams and slabs (*Fig.3-1*): The application is inserting the lamella into cut slits with bonding or external bonding on the surface of the beam or slab. In construction the name lamella is used for the polymer-impregnated (not just surface-coated) lamina layer. If a lamella is multi-axially stressed then the stress state assessment follows the presented lamina procedure.
GFRP-fabrics: ('closed' reinforcing sheet, sun protection 'umbrellas', 2D stress state). If multi-axially plane stressed, the stress state assessment follows Sub-chapter 3.7and the CLT-procedure. Then the lateral properties come in, required for the proof of the limit states ULS and SLS.

Fiber-grids ('open' reinforcing grid, mat): Uniaxial and bi-axial reinforcement of plates and shells: Modelling depends on the grid width and the ratio of the orthogonal reinforcements. The necessary fiber cross-section of the orthogonal directions is separately determined according to the bi-axial loading. In the case of a large grid width the concrete matrix might shear fracture between the reinforcement under compression.

(short) Fiber-Reinforced Concrete (s)FRC: According to the intended (s)FRC production process of a model between oriented and quasi-isotropic short fiber distributions is to set up.

"3D-print" processes: *with / without fiber-reinforcement*

There are basically two types of so-called '3D-print' processes applied in construction.

(1) Powderbed 3D print process (*Pulverbettverfahren*): A real 3D print process unreinforced or reinforced by using short filaments (single endless fibers) from cut rovings which may be intentionally pretty directed up or which shall approach a quasi-isotropic distribution.
(2) Path-oriented, extrusion head-placed mortar strand process incorporating short, or long or endless 'fiber filaments' (*pfad-orientierte Mörtelraupen-Extrusion*). Endless fiber filaments within the tows are inserted in the mortar strand similar to the not fiber-reinforced so-called endless 'polymer filament' (*This looks confusing, however in the process the polymer strand is termed filament for a long time*).

3.8 Structural Modelling and Dimensioning, *in construction usually on cross-section level*

Upcoming standards in Germany are finalized, *Fig.3.7-1*:

- polymer matrix: BÜV 10 update
- mineral matrix: novel DAfStb-Richtlinie "Betonbauteile mit nicht-metallischer Bewehrung".

The DAfStb guideline "Concrete components with non-metallic reinforcement" is intended for fiber-reinforced components with concrete matrix. For engineers it is confusing not to clearly say which material group the guideline is for. Then the suffix $_{nm}$ could be replaced by the indices of the polymer matrix world namely for the pure fiber $_{f}$ and the cured fiber strand $_{||}$. Why sticking further to the letter *f* (strength). Still at the GruSiBau time (*about 1985, development of the excellent partial safety factor concept*) the author used the international letter *R* for the resistance entity strength. Using *R* – internationally and nationally still started - makes life of engineers simpler, internationally at least.

Author's comment: From above follows that these two upcoming standards are not harmonized regarding the designations amongst themselves and w.r.t. terms half a century used internationally in timber construction and with polymer matrices. This is all the sadder for the author, because he edited the VDI 2014 guideline, initiated by civil engineers but not used in construction. The European Codes hopefully will improve this unfortunate situation.

In the context above it seems again to be necessary to cite for the construction discipline two long-time used terms in the composite domain:

Material composite (Werkstoffverbund): structural-mechanically a composed 'construction of different materials.

Note: A not smearable 'conglomerate' is usually the Fiber-grid-Reinforced-Concrete.

Composite material (Verbundwerkstoff): combination of constituent materials, different in composition.

Notes: (1) The constituents retain their identities in the composite; that is, they do not dissolve or otherwise merge completely into each other although they act in concert. Composite materials provide improved characteristics not obtainable by any of the original constituents acting alone. (2) Normally the constituents can be physically identified, and there is an interface between them. (3) Composites include fibrous materials, fabrics, laminated (layers of materials), and combinations of any of them. (4) Composite materials can be metallic, non-metallic or a hybrid combination thereof. Carbon concrete is one example. (5) Probably homogenizable to a smeared material such as FRC, SMC, UD-ply = UD-lamella. The lamella is smearable and therefore it can be modelled as a 'composite material'. (6) Layered materials and foam materials are also forms of composite materials. (7) Cement-based mortar is a 'smearable' composite material (the organization RILEM has a problem here, because they do not discriminate 'material composite' from 'composite material')

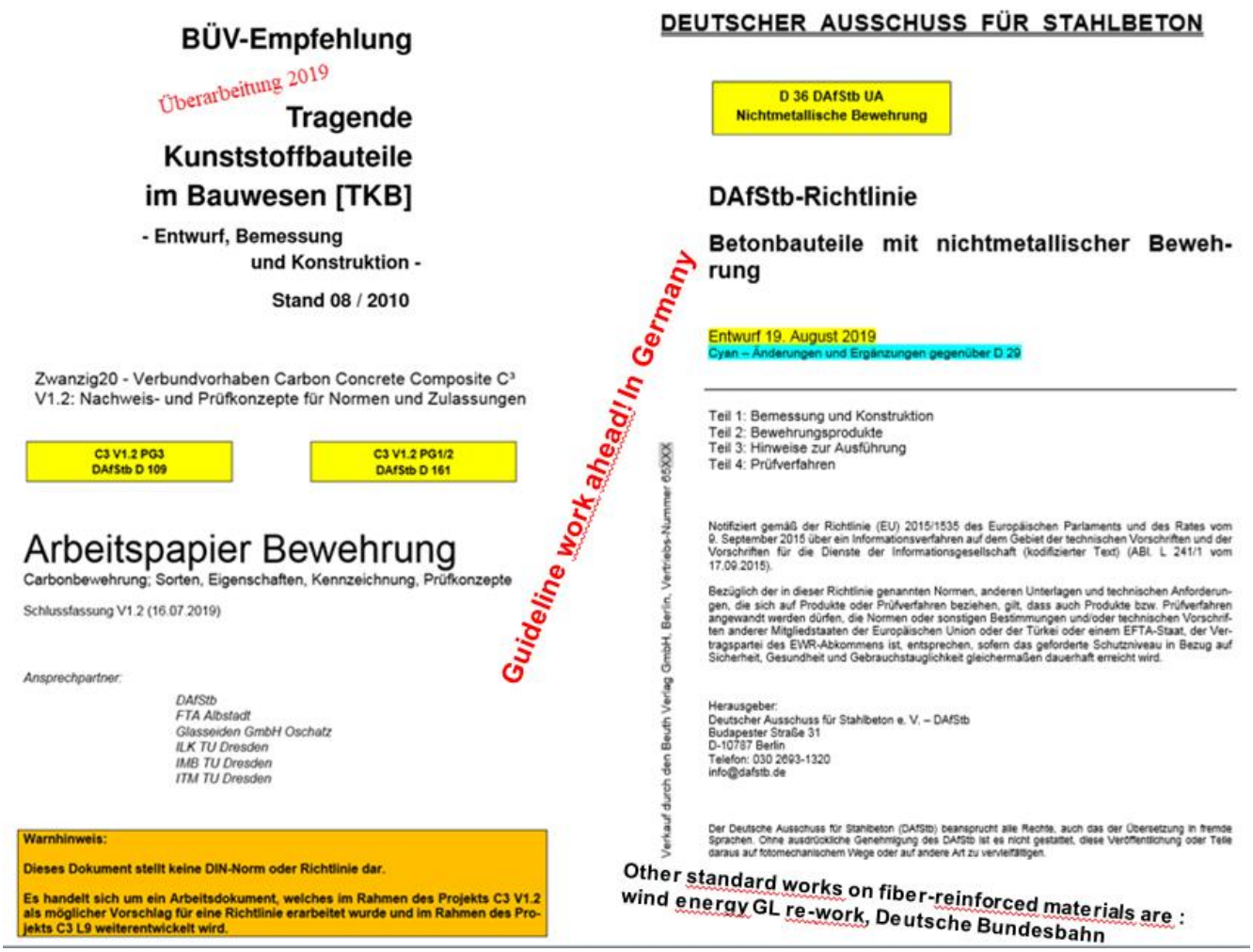


Fig.3.7-1: Guideline work ahead in Germany, BÜV10 update and D 36 novel

In construction, design dimensioning is basically performed at cross-section level:

Beams: N, M, Q, T internal cross-section loading

For fiber-reinforced beams the same models can be applied as with steel reinforcement. This is valid for pre-tensioned beams and for beams with slack reinforcement (*schlaffe Bewehrung*).

Plate and shell elements: n, m. q, t , width-related internal cross-section loading

Smearability depends on the grid width. If smearable then the so-called 'layer-wise failure analysis' can be employed using the Classical-Laminate-Theory CLT (*applied since 1970 by the author to polymer-matrix laminates, see [VDI06]*. The CLT may serve as analysis model for a layered plate or a layered shallow shell. Design dimensioning is to perform in Germany by application of the novel standards above. In the D36, dated August 2019, just the *procedure* of the CLT is addressed.

There are very different grid widths of the available fiber grids to be considered in modelling. S. Rittner shows in *Fig.3.7-2* the intention to replace several small 'k roving layers' by a 48 k Heavy Tow layer fiber grid. This positively increases fabrication speed but unfortunately the anchor length and impacts the shear load transfer problematic in the interface fiber strand-concrete matrix.

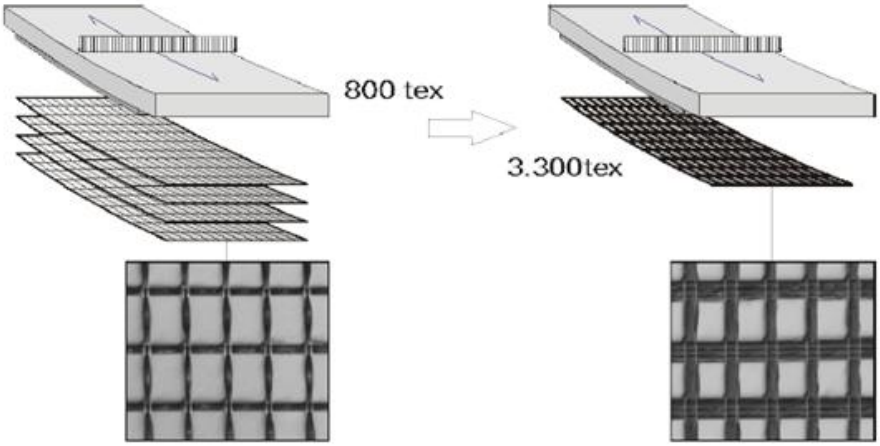


Fig.3.7-2: Difference of 8k-roving and 48k-heavy tow application in fiber grids (armoring mats)
(fineness of a roving, tow: 1 tex = 1 g/km length)

In order to capture stress concentrations at a notch et cetera – instead of manually armoring these spots – at distinct load introduction locations a quasi-isotropic, short fiber–reinforced high performance mortar could help to industrially solve this task. An armoring grade of $V_f < 0.5\%$ C-fiber volume content is then aimed at. The dispersion of the cut rovings into filament pieces (cut to a length < 8 mm) could be performed direction optimal or is quasi-isotropic as required.

Often in discussions the question arises how much base material is needed for the Zirkonoxide added production of the fiber ARglass GF and the alkali-resistant carbon CF.

If basalt fibers BsF will reach a general approval from sustainability reasons they would be much better ecologically and economically due to the fact that enough base material is available. Added ZrO_2 is foreseen to provide alkali resistance.

Fig.3.7-3 shall give a survey about the portions of the structural materials in the market, dated 2016. It shows how insignificant the carbon fiber content presently is in relation to its origin oil and to the material competitor steel.

This is of basic interest and helpful for many discussions. CF is not yet a real market in construction, basically due to the present regulations of the authorities which does not permit a faster gain of knowledge which is always the result of widespread application, only.

Unfortunately, the available property knowledge is not made public.

If the concrete mass saving Carbon Concrete market will become significant, then the CF-production has to be multiplied.

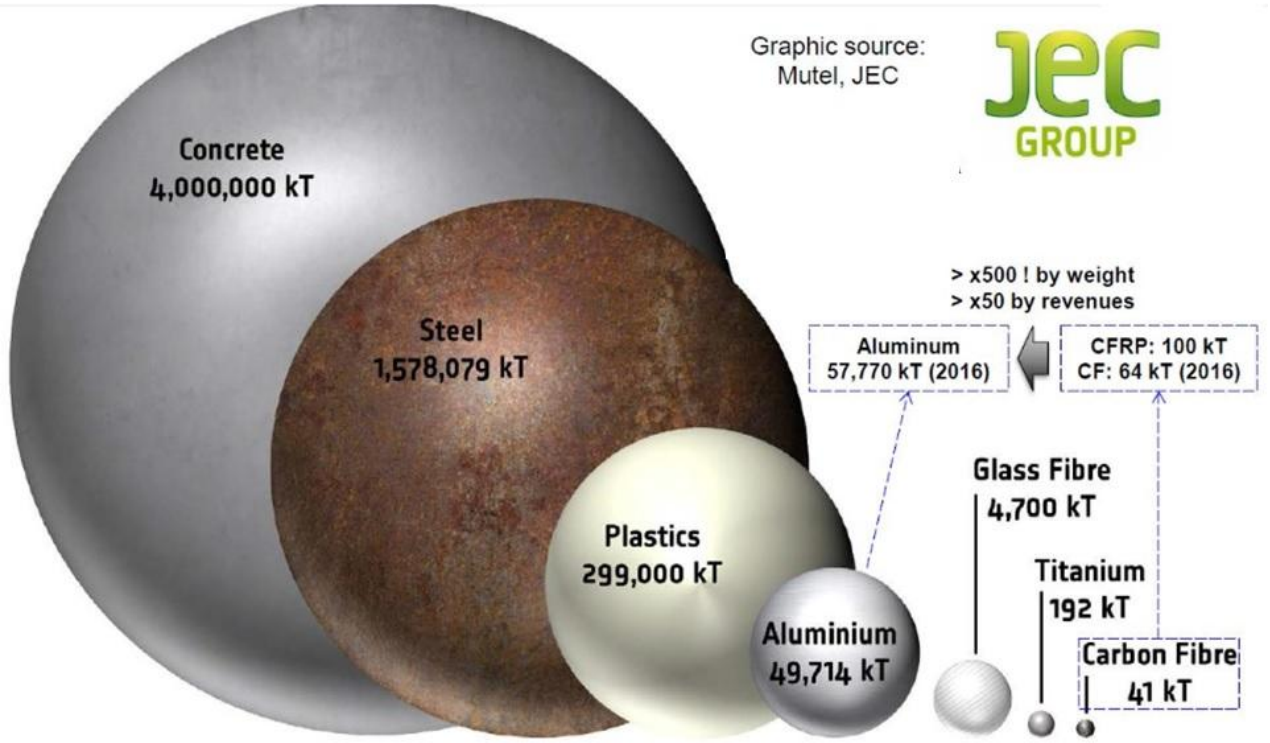


Fig.3.7-3: Weight ratios of structural materials, year 2016

Please keep in mind:
40000 tons carbon fibers would require just about 40,/,4,000,000 = 0.001 % crude oil.
Why is this marginal consumption very often considered to be very harmful to the environment?

CF total / Steel = 1/10000.
In Germany it is CF total / concrete reinforcing steel ≈ 0.1%.
Concrete / crude oil = 1, GF / CF = 100.
Single car consumes about *1 t oil / year.*

Of course, the production of carbon fibers still requires energy. However, this will also be the case if carbon fibers are produced from natural sources in the future.

4 Two Missing Links filling the 'Mechanics Building' of Isotropic Materials

4.1 Experimental Proof and Description of Normal Yielding NY of Isotropic Materials

4.1.1 General

Glassy (amorphous, brittle) polymers like polystyrene (PS), polycarbonate (PC) and PolyMethylMethacrylate (PMMA = plexiglass) are often used structural materials. They experience two different yield failure types, namely crazing under tension and under compression shear stress yielding that is often termed shear-banding. Crazing can be linked to Normal Yielding (NY) which precedes the crazing-following tensile fracture. Crazing occurs with an increase in volume and shear banding does not. Therefore, the dilatational I_1^2 must be employed in the SFC-approach for tension $I_1 > 0$. Under compression, brittle amorphous polymers usually shear-band (SY) and with it they experience friction. Therefore, I_1 must be employed in the approach for $I_1 < 0$ in order to consider material internal friction. For obtaining the complete yield failure body its parts NY and SY are to interact in the transition zone, as performed for concrete before.

Reminder on HMH-linked 'Mises-cylinder' for 'Onset-of-Shear Stress Yielding SY*: There is no friction acting and therefore the yield strengths for compression and tension are the same* $R_{0.2}^c = R_{0.2}^t$ *(≡* $R_{p0.2}$*, in which the superfluous suffix* $_p$ *practically has nothing to do with proportional!). HMH means frictionless yielding and therefore it forms a cylinder.*

Crazing involves the formation of fibrils bridging two neighboring layers of the un-deformed polymer. These subsequently elongate and locally fail which leads to a formation or an elongation of an existing micro-crack, <u>*Fig.4-1*</u>. This micro-crack can be simulated under Fracture Mode-I loading conditions, using K_{Ic} *(later necessarily to be termed* K_{Icr}^t).

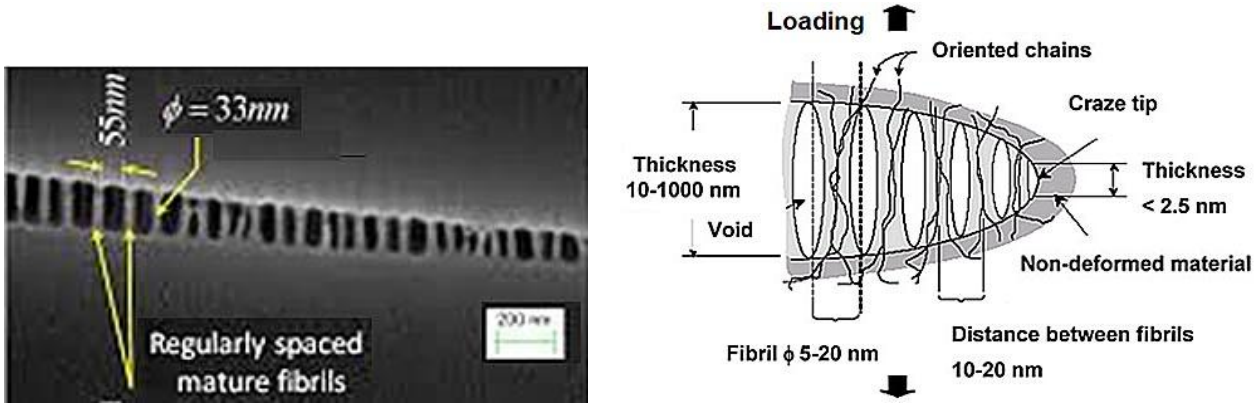


Fig.4-1: PMMA, SEM image of a craze in Polystyrene Image (created by Y. Arunkumar)

The failure type crazing shows a curiosity under tensile stress states: A non-convex shape exists for Onset-of-Crazing ($\bar{R}_{NY}^t$). NY is followed by the crazing-driven fracture NF for which - due to the test-proven similar shape – the NY-SFC can be used too. Under compressive stress states the usual shear band yielding SY occurs and later final shear fracture SF. For both, SY and SF, the same SFC can be applied. Due to the fact, that the Onset-of-Crazing and the Onset-of-Shear yielding associated failure stresses ("strengths") are not yet accurately described, the designations $\overline{R}_{NY}^t$ and $\overline{R}_{0.2}^c$ are used for the average strengths.

Craze and shear band initiation stresses

Two distinct yield mechanisms namely craze formation and shear yielding have to be considered for glassy polymers [*Ste68*]. A craze always propagates transverse to the major principal stress. The phenomenon of craze formation exhibits a region of highly oriented and dilatation-effected material within an essentially glassy matrix of much lower deformation.
In rubber-modified glassy (toughened) polymers toughening results from the localized plastic deformations in the vicinity of the rubbery inclusions. Plastic yielding of glassy polymers at temperatures approaching the glass transition temperature and at slow strain rates is, by contrast, a more homogeneous deformation than it is the craze formation. Craze-driving size and shape of the inhomogeneities in the polymer are practically unknown. Crazing does not occur in uniaxial compression because a positive principal stress has to be met. The level needed cannot be achieved by a pure shear field (or equivalent one principal stress is positive and one of the two is negative). Both, crazing and shear band initiation depend on the full state of stress and not on one particular stress (σ or τ) or tensor component, respectively.

4.1.2 Available test data sets for PMMA

For the validation of the FMC-based SFC for PMMA two data sets were available, one NY-2D-data set from Sternstein-Myers [Ste73] and a SY-3D-data set from Matsushige [Mat73]. These two sets, depicted in *Fig.4-2*, are unfortunately of different origin: (1) Sternstein-Myers performed bi-axial experiments on craze initiation on the surface of thin-walled cylinders (tubes). The loadings were axial tension + internal pressure and tension + torsion. Test temperature was 60° C. Therefore, following literature, to match with Matsushige's ambient test temperature 23°C data, from consistency reasons the value of $\bar{R}_{NY}^{t}$ is to increase to become comparable with Matsushige. (2) Matsushige performed tri-axial experiments on sealed (surface crazing is hindered) solid rods at 23° C, under axial tension + p_{hyd}. The test specimen was pressurized within a chamber. This series along the tensile meridian, characterized by $\sigma_I > \sigma_{II} = \sigma_{III}$, contains the bi-axial point ($-\bar{R}^{cc}_{0.2}$, $-\bar{R}^{cc}_{0.2}$, 0). In comparison to the thin tube the solid rod experiences more bulk crazing than the more dangerous surface crazing. This is essential for test data evaluation.

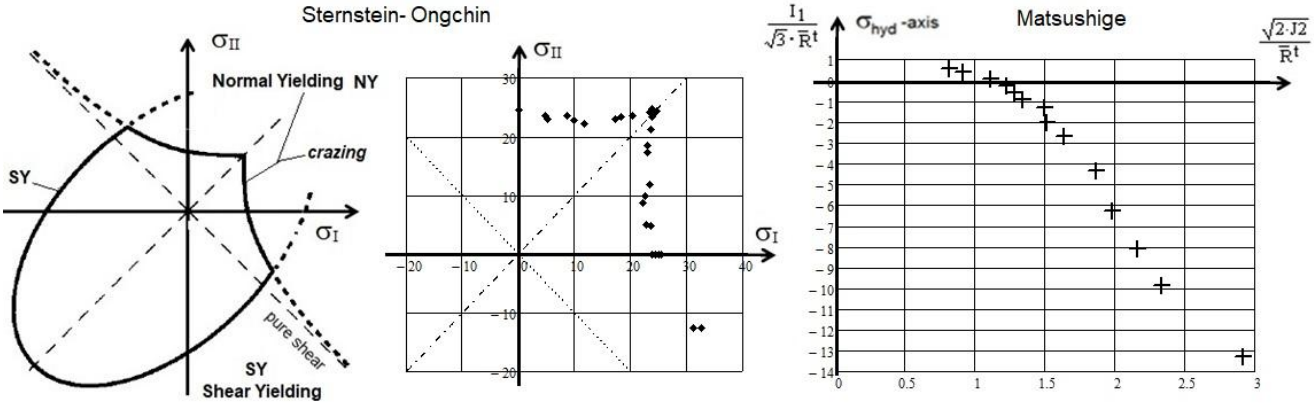


Fig.4-2 PMMA: (left) Sternstein's mapping idea with his 2D test data set (center) in the principal stress plane, (right) Matsushige 3D-PMMA test data set rendered in Haigh-Westergaard-Lode coordinates.

Of special interest for the demonstration of a qualified mapping by SY-SFC and NY-SFC is the mapping of tensile meridian and compressive meridian as the essential cross-sections of the yield

failure body. The definitions of the meridians are given below. Associated test stress states are formulated in principal stresses and in mathematical stresses:

tensile meridian compressive meridian

$$(\sigma^{t}_{ax}-p_{hyd},-p_{hyd},-p_{hyd}) = (\sigma_I,\sigma_{II},\sigma_{III}) \rightarrow \sigma_I>\sigma_{II}=\sigma_{III} \quad \Leftrightarrow \quad (-p_{hyd},-p_{hyd},\sigma^{c}_{ax}-p_{hyd}) = (\sigma_I,\sigma_{II},\sigma_{III}) \rightarrow \sigma_I=\sigma_{II}>\sigma_{III}$$

2D-data set and 3D-data set can be displayed together in the Lode-Haigh-Westergaard diagram. There, the two data sets clearly outline crazing NY (Sternstein) and shear banding SY (Matsushige) and therefore can serve for mapping.

At first a harmonization of above two data sets is necessary: After transferring into MPa, the Matsushige fracture stress values were much higher than the Sternstein ones. Following Sternstein et al the threshold stress value required for crazing (ten minutes hold-time) is about 3900 psi (1000 psi = 6.89 MPa) and for ambient temperature about 5500 psi is guessed. This has the consequence to increase the Sternstein test data by a correction factor of $f_{St} \approx 5500/3900$. The choice finally was $f_{St} = 1.3$.

Fig.4-3 clearly outlines, that the course of test data in the tension domain needs to be differently mapped for the convex-shaped SY and the concave-shaped NY. In the interaction zone from crazing to shearing a brittle-to–ductile transition occurs, p_{hyd} induces the transition from NY to SY by suppressing crazing.

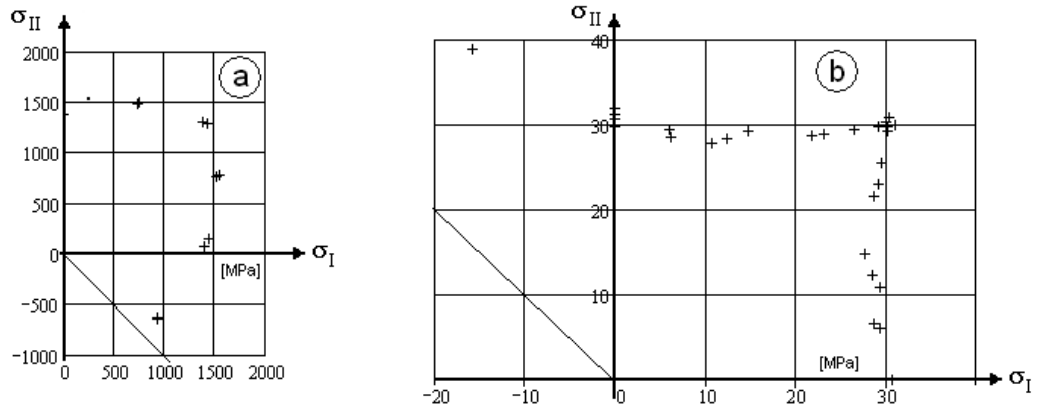


Fig.4-3: Tension domain with (a) Onset-of-Shear Yielding test data for a ductile steel, SY, for comparison; (b) PMMA, Onset-of-Crazing NY. Strength points: $(\bar{R}^{t}_{NY}, 0, 0)$, $(\bar{R}^{tt}_{NY}, -\bar{R}^{tt}_{NY}, 0)$, $(\bar{R}^{c}_{0.2}, 0, 0)$

Table 4-1 collects the SFCs for NY with SY and *Fig.4-4* visualizes the formulas for this isotropic, dense material.

Traditional SFCs describing yielding are related to Hencky-Mises-Huber (HMH hypothesis (*Mises, in short)* or to the 'corner-suffering' Tresca hypothesis. Tresca was preferred in the past due to its less computational effort and is still often mistakenly used as strength fracture failure condition seduced by its failure surface shape in tension in the principal stress plane. HMH delivers an ellipse as the cylinder's cross-section, whereas Tresca leads to a hexagon, see *Fig.4-4*.

Table 4-1 PMMA: SFCs for normal yielding and shear yielding

Normal Yielding NY (hyperboloid) $I_1 > 0$ Shear Yielding SY (paraboloid) $I_1 < 0$

$$F^{NY} = \frac{x^2}{(c_2^{NY})^2} - \frac{(y - c_1^{NY})^2}{c_3^{NY\,2}} = 1 \text{ with } x = \frac{\sqrt{2 \cdot J_2 \cdot \Theta^{NY}}}{\bar{R}^t_{NY}},\ y = \frac{I_1}{\sqrt{3} \cdot \bar{R}^t_{NY}} \Leftrightarrow F^{SY} = c_1^{SY} \cdot \frac{3J_2 \cdot \Theta^{SY}}{\bar{R}^{c\ 2}_{0.2}} + c_2^{SY} \cdot \frac{I_1}{\bar{R}^c_{0.2}} = 1$$

Considering bi-axial strength (failure mode occurs twice, $\Theta \neq 1$). In Effs now, index Θ dropped.

$$Eff^{NY} = \frac{c_3^{NY} \cdot \sqrt{-c_2^{NY\,2} \cdot y^2 + (\Theta^{NY})^2 \cdot (c_3^{NY\,2} + c_1^{NY\,2}) \cdot x^2} + c_2^{NY} \cdot c_1^{NY} \cdot y}{c_2^{NY} \cdot (c_3^{NY\,2} + c_1^{NY\,2})}, \quad Eff^{SY} = \frac{c_2^{SY} \cdot I_1 + \sqrt{(c_2^{SY} \cdot I_1)^2 + 12 \cdot c_1^{SY} \cdot 3J_2 \cdot \Theta^{SY}}}{2 \cdot \bar{R}^c_{0.2}}$$

Onset of Crazing = Normal Yielding NY (for fracture similar)

c^{NY}, d^{NY} from the two points $(\bar{R}^t_{NY}, 0, 0)$ and $(\bar{R}^{tt}_{NY}, \bar{R}^{tt}_{NY}, 0)$ d^{SY} from the point $(-\bar{R}^{cc}_{0.2}, -\bar{R}^{cc}_{0.2}, 0)$

Two-fold failure danger can be modelled by using the well known invariant J_3 including d = non-circularity parameter

$$\Theta^{NY} = \sqrt[3]{1 + d^{NY} \cdot \sin(3\vartheta)} = \sqrt[3]{1 + d^{NY} \cdot 1.5 \cdot \sqrt{3} \cdot J_3 \cdot J_2^{-1.5}} \text{ and } \Theta^{SY} = \sqrt[3]{1 + d^{SY} \cdot \sin(3\vartheta)} = \sqrt[3]{1 + d^{SY} \cdot 1.5 \cdot \sqrt{3} \cdot J_3 \cdot J_2^{-1.5}}$$

Lode angle ϑ, here set as $\sin(3 \cdot \vartheta)$ with 'neutral 'shear meridian angle 0°; compressive meridian angle -30°.

A failure body is rotationally-symmetric if $\Theta = 1$

Equation of the yield failure body: $Eff = [(Eff^{NY})^m + (Eff^{SY})^m]^{m^{-1}} = 1 = 100\%$ total effort, interaction

$0 < d^{NY} < 0.5$, $0 < d^{SY} < 0.5$, meridian angles $\vartheta°$: $\bar{R}^t_{0.2}$, 30° ; $\bar{R}^{tt}_{0.2}$,-30°; $\bar{R}^c_{0.2}$,-30°; $\bar{R}^{cc}_{0.2}$, 30°

4.1.3 Visualization of the Failure Body

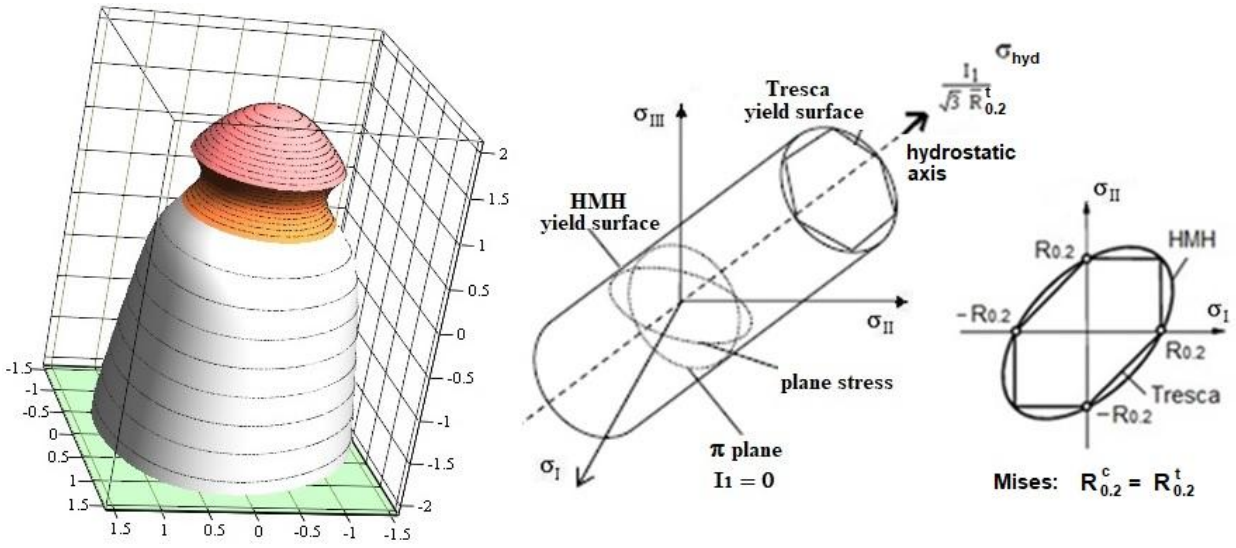


Fig.4-4 PMMA: (left) Onset-of-Yield surface (NY with SY) and for comparison Hencky-Mises-Huber with the Tresca yield surface (engineering yield strengths are used)

$$\bar{R}^t = 37;\ \bar{R}^{tt} = 36;\ \bar{R}^{ttt} = 42;\ \bar{R}^c = 60;\ \bar{R}^{cc} = 69;\ \sigma_{Itm} = 34,\ \sigma_{IItm} = 18,\ \sigma_{It0} = 48,$$
$$\sigma_{IIt0} = -19.\ c_1^{NY} = 0.83,\ c_2^{NY} = 0.66, c_3^{NY} = 0.41, c_1^{SY} = 1.21, c_2^{SY} = 0.24, s^{cap} = -0.81,$$
$$d^{NF} = -0.26;\ d^{SF} = -0.08;\ m = 2.6,\ set \max I_1 = 3 \cdot R^{ttt} = 8.43;\ \min I_1 = -4.58.$$

Check of identical hoop curve at the Cap-NF contact I_1 performed.

The NY yield failure body is a 120°-symmetric one in the deviator plane. This is captured by $\Theta(J_3)$, again. I_1^2 stands for the experienced volume change. Above formula for the failure body is new.

In *Fig.4-5* the two main meridians are presented as the axial-parallel cross-sections of the failure body (upper part) and further the I_1 = constant yield failure curves (lower part).

- In the upper part, the plain failure curves are shown and the magenta coloured curves in the transition zone after interaction. $\bar{R}_{SY}^{c}$ is not clearly defined by Sternstein and Matsushige, but this is not essential, because NY-mapping is the objective. So, instead of the not defined $\bar{R}_{NY}^{t}$ and $\bar{R}_{SY}^{c}$ the usual designations for strengths are kept.
- In the lower part, the 'I_1 = constant yield failure curves' are displayed for the tensile and the uniaxial compressive strength and for the bi-axial strength capacity. In addition the most inner ring of the hyperboloid is included (orange).

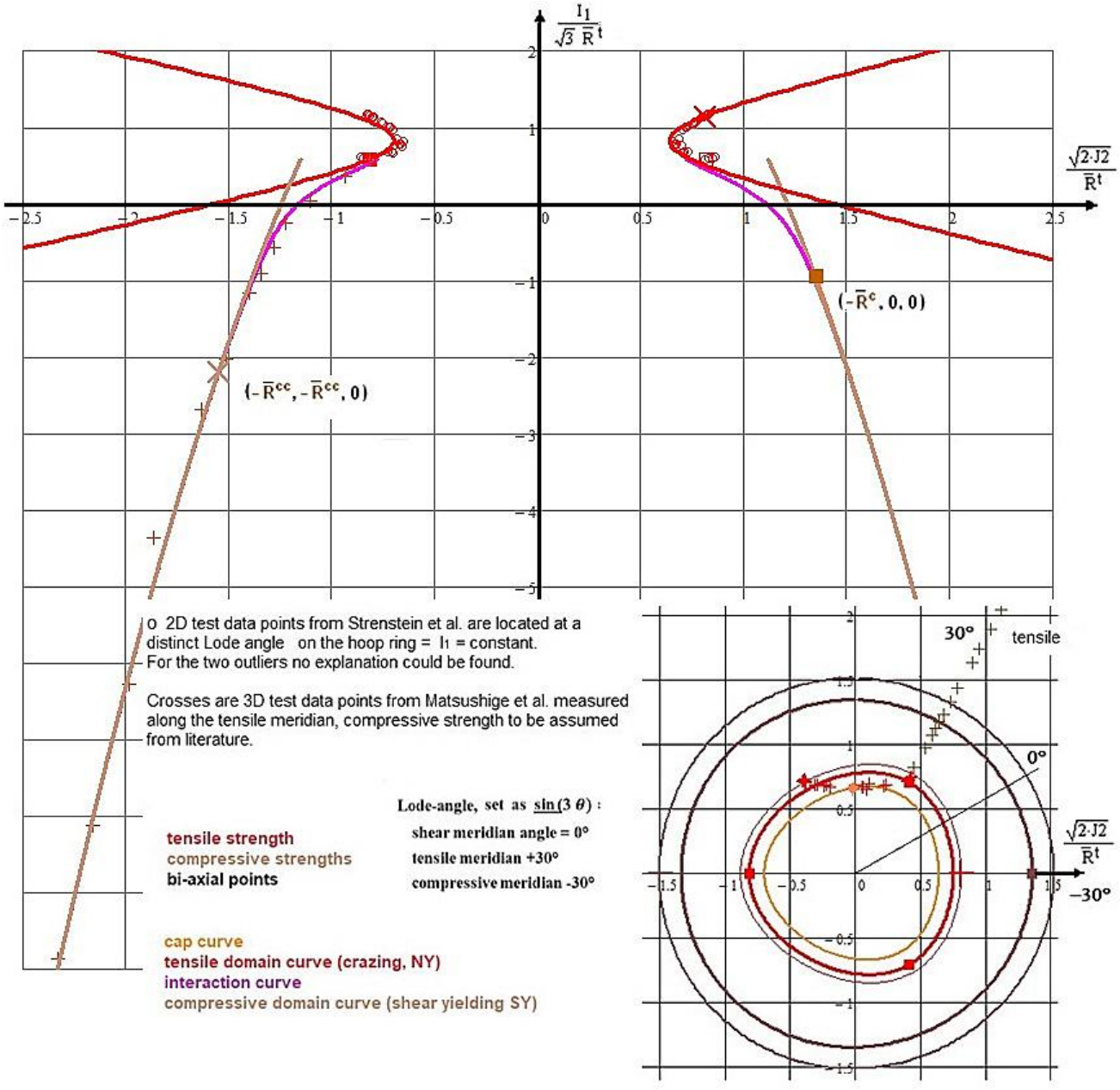


Fig.4-5 PMMA: Tensile (left) and compressive (right) meridians of the fracture body (not optimized, the most negative test points are not shown in the figure); (below) I_1 cross-sections of the NY-SY-body.

Fig.4-5 also shows that the Matsushige tests were run along the tensile meridian. On the hoop plane, due to the 120°-symmetry the inserted test points are three times present. For the derivation

of the tensile *fracture* failure body – due to the similar shape – the NY-SFC→ NF-SFC can be employed too, viewing yield curve and fracture curve presented in [*Bre79*]. For the compression part is similarly valid, SY → SF.

Note: Many years ago the author constructed a hyperboloid function that could map occurring straight test data courses in the principal stress plane for NF-SFC (see the examples before). This NY-SFC enables to manage outward and inward dents in the hoop plane., see Fig.4-5 and 4-6 (principal stress plane).

Fig.4-6 demonstrates, that probably for the first time, 3D mapping of the NY yield surface and the combined NY.SY-surface and its **3D** visualization was successfully performed. A high interaction exponent m = 5.2 was applied due to the fact that the two different yield modes do not occur that mixed in the interaction zone as experienced usual with other materials.

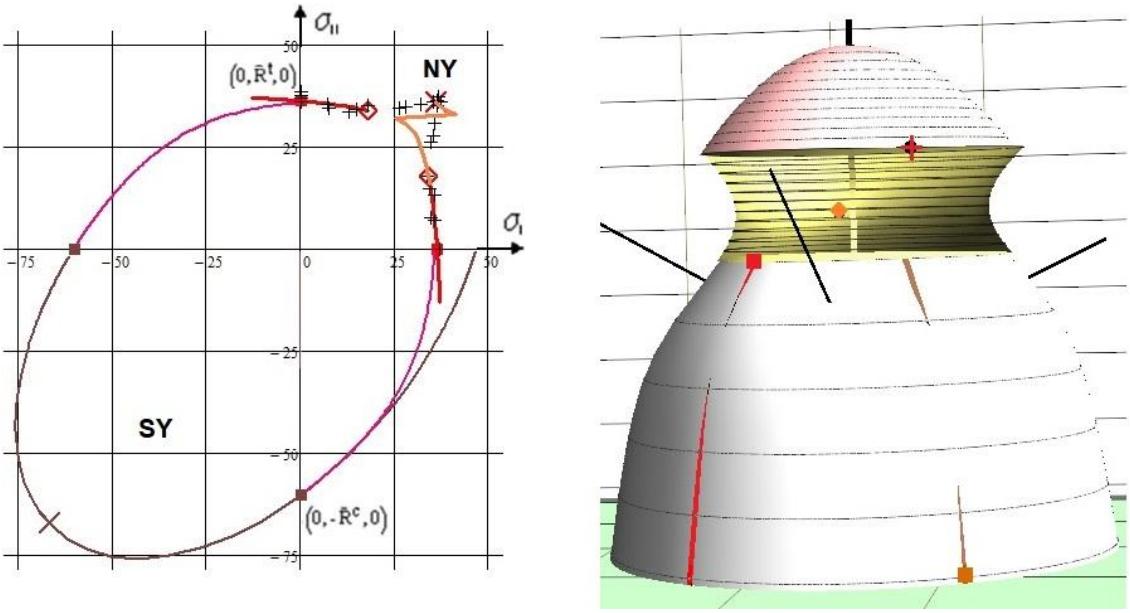


Fig.4-6 PMMA: (left) Mapping test data in tension and compression principal stress domain with and without interaction; (right) depiction of the fracture body shape with some representative points

The **2D**-visualization of the NY failure surface using Mathcad 15 code (*a 35 DIN A4-pages application*) was very challenging considering the solver that has to face a concave 2D principal stress plane situation instead of a usual convex one.

Regarding the successful 3**D** visualization, the success in the principal stress plane was clouded. Also after a huge effort, the author unfortunately could not obtain a mapping of the upper test data in the first quadrant with the used Mathcad 15 code. The computed mapping curve remains a zig-zag even after several different computational approaches as for example from the outer bi-axial point X to the more inner points! Question: Why does the solver in the lower tensile part of the yellow colored failure surface work and captures such a concave situation and in the upper not (zig-zag curve in *Fig. 4-6*)? Therefore, in contrast, the accurately determined points on the 3D body surface of the right figure in *Fig.4-6* were highly appreciated but do not give an explanation for the principal stress plane.

4.2 ' Some Proof ' of a 2nd Basic Stress Intensity Factor $K_{IIcr}{}^{c}$ beside $K_{Icr}{}^{t}$

4.2.1 General about the 2 basic fracture toughness quantities of isotropic materials

Presumption: An ideally homogeneous isotropic material in front of the cracktip. The following investigation is only for the ideal structural mechanics building of importance. In practice, there are usually no ideal homogeneous conditions at the cracktip.

Fracture Mechanics FM is the field of mechanics concerned with the study of the propagation of cracks. These cracks might have been there from the beginning or are formed under loading. Final fracture occurs when cracks propagate up to a limit defined by a critical stress intensity factor SIF or fracture toughness K_{cr}, respectively. The critical SIF K_{Ic} (later necessarily indexed $K_{Icr}{}^{t}$) is found in a plane strain condition, and is accepted as the defining (basic) property in Linear Elastic Fracture Mechanics, considering tension.

Comparing strength mechanics and fracture mechanics a question of the author is: "*Are there any links between them?" :*

* Normal fracture NF acts perpendicular to the mathematically highest stress ('most positive') σ_I. If a centrally cracked test specimen is loaded up to a certain level, the crack theoretically well grows in the given fracture 'plane'. $\bar{R}^{t}$ and $\bar{K}^{t}_{I\,cr}$ correspond, *Fig.4-7*.

*Shear Fracture SF occurs under a compressive stress, that causes a critical combination of the Mohr stresses σ_n, τ_n , leading to a fracture plane angle $\Theta_{fp}{}^{c}$. If a cracked test specimen is loaded up to a certain level the question arises: Does the crack keep its original plane? "Is there a crack plane-linked 'transition' from 'Without crack' (strength mechanics) to 'With crack' (fracture mechanics) also in the compression domain $I_1 < 0$ given?"

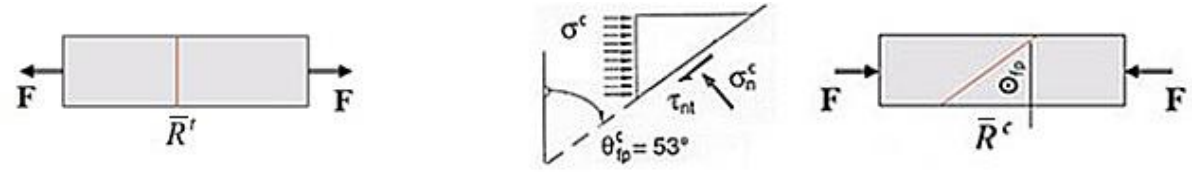


Fig.4-7: Fracture angles of brittle material under tension and compression; (left) NF with tensile strength, (right) SF with compressive strength

Note: In order to cope with the generally in structural engineering used indexing, one has to keep ^{c} for compression and ^{t} for tension and set critical $_{cr}$ for all fracture-mechanical quantities instead of the suffix $_{c}$.

A first response is: From material symmetry information one could conclude that the number of fracture toughness quantities or crack resistances, which are equivalent to the (basic) critical SIFs, is the same as the number of strength fracture resistances, namely R^{t} and R^{c}. The number of the (basic) critical SIFs may be also two, namely $K_{Icr}{}^{t} \equiv K_{Ic}$ and $K_{IIcr}{}^{c}$.

Focusing tension: According to the multi-dimensional stress state present cracks in materials usually do not propagate along their original crack plane but under so-called 'mixed mode loading' they twist on curved paths in which the specific singularity situation at the crack tip is decisive to finally achieve a Fracture Mechanics Mode I state.

The decomposition of a loading state into the three basic deformation modes, the fracture mechanics Modes-I, -II, -III, was introduced by Irwin and the different deformations, not the

loadings, he indicated by arrows, see *Table 4-3*. These 3 deformation states are usually linked in literature, however, to crack driving loadings and then further to stresses: Mode I – Opening mode (*a tensile stress normal to the plane of the crack),* Mode II – Sliding mode (*a shear stress acting parallel to the plane of the crack and perpendicular to the crack front*), and Mode III – Tearing mode (*out-of-plane shear loading*).

Structural engineers, who apply FM tools for predicting lifetime by damage tolerance means, are used to think in stresses. Therefore they claim - considering the usual interpretation that the arrows are loadings - "*The fracture mechanics modes FM II and III are not in local equilibrium*". Bouquet's faces clearly depict this in *Table 4-3*. Of course, the consequence of being not in equilibrium is a turning of the original crack-plane into a direction normal to the principal *tensile* stress σ_I. And this happens to be. The crack runs out of the original ligament plane.

Focusing compression: There is another engineering discipline, namely geo-engineering with rock fracture mechanics, that is pretty decoupled from the tension domain in mechanical engineering, but where FM plays a big role. The cracks to be faced here under compression loads are many meters long and more. Here, a SIF $K_{IIcr}{}^{c}$ is the focus but usually prevented by the secondary wing-cracking accompanied by splitting! Therefore, the situation to detect it and to measure it is complicated.
At the crack tip a local perturbation caused by for instance a stiff or a too large grain can change the local stress singularity situation by not generating a desired 'fine grained, homogeneous micro-structure'. Then the modelling-desired ideal homogenization state is violated and splitting of the brittle test specimen will occur.

Nevertheless, there is the author's postulate, employing crack path stability:

Only an angle-stable, self-similar crack growth plane-associated SIF is a 'basic' FM property.

Note

(1) FM Mode I delivers a real ('basic') fracture resistance property generated under a tensile stress. Both the Modes II K_{IIc}, and III K_{IIIc} do not show a stable crack plane situation but are nevertheless essential FM model parameters to capture 'mixed mode loading' for performing a multi-axial assessment of the far-field stress state.

(2) With the Mode-II compressive fracture toughness $K_{IIcr}{}^{c}$ it is like with strength. One says compressive failure, but actually shear (stress) failure is meant, compressive stress is 'only' the descriptive term. Therefore the (shear) index II is to take.

Literature seems to support the author who assumes that there are two basic critical SIFs, only. His more detailed definition of such a basic SIF is: *The direction of the crack progress remains in the distinct plane if the stress situation remains the same and the ideal singularity situation at the crack tip is not changed by for instance a large grain.* In other words, the crack increases in its original plane, if the stress state remains in the crack case as in the formerly non-cracked strength case. This should be theoretically valid in the compression domain, too.

- Tension domain: One knows from $K_{Icr}{}^{t}$ (tension), that – viewing the transversal angle - it corresponds to R^t.
- Compression domain: The not generally known second basic SIF $K_{IIcr}{}^{c}$ seems to exist under ideal conditions. It corresponds to shear fracture SF happening under compressive stress R^c and leading to the angle $\Theta_{fp}{}^{c}$. The crack surfaces are closed for $K_{IIcr}{}^{c}$, friction sliding occurs.

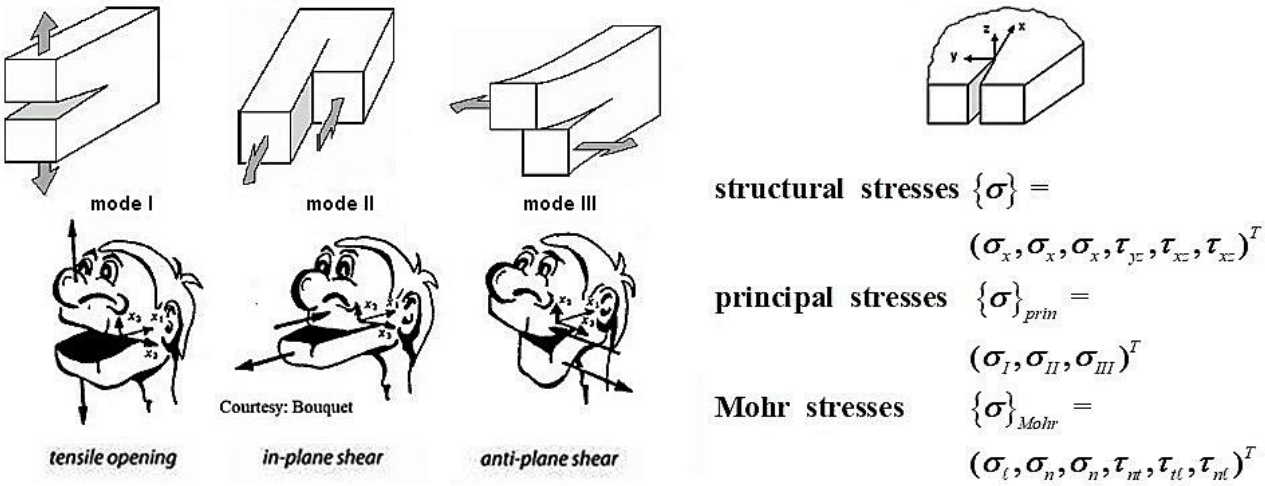
The author's postulate "K_{IIcr}^{c} exists" is firstly supported by an experiment with cracked test specimens under compression and secondly by a still available K_{IIcr}^{c} formula in *[Pha03]* substantiated by the maximum value of the material stressing effort *Eff* for $\alpha = 90 - \Theta_{fp}^{c}$.

4.2.2 Some experimental proofing of K_{IIcr}^{c}

(1) A first proof of the author's postulate could be: There exists a minimum value of the compressive loading at a certain fracture angle. This means that the K_{IIcr}^{c} becomes a minimum, too. Liu et al performed in [*Liu14*] tests using a cement mortar material. They describe the test investigations as

"*The specimens were square plates of 180mm×180mm×50mm, with <u>three</u> collinear artificial and penetrated cracks, which measure 20 mm in length. The ratio of cement, sand, and water was 1 : 1 : 0.35 by weight. The cracks were made by using a 0.1 mm film, placed during casting. Curing period was 28 days. Under controlled temperature 130°C for 2hrs, the films can be easily pulled out. The crack length and their interval distance are the same and equal 1.0 cm. The test specimens were loaded by a tri-axial loading device: The vertical loading is the major principal stress σ_1 and the two horizontal confining stresses are kept as constants during the process of vertical loading*".

Table 4-2: Fracture mechanics modes, stress states



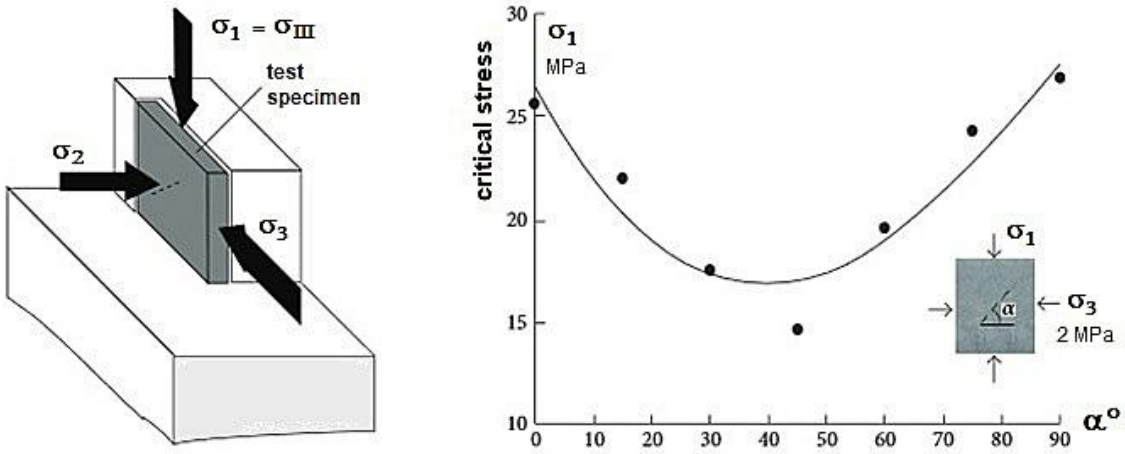


Fig.4-8: Scheme of the test set-up and of the test points obtained for cement mortar [Liu14], σ_1 represents the mathematical stress σ_{III} (largest compressive stress value). Here, literature defines $\Theta_{fp}^{c} = \alpha$

One of the horizontal stresses is denoted σ_3, and the other one σ_2, as shown in *Fig.4-8*. In order to avoid the effect of the friction between the specimen and the loading device, the specimen surfaces were smeared with oil before testing".
→ The significant result of this test series is: A minimum value is located at about $\alpha = \Theta_{fp}^{\,c} \approx 45°$. That fits relatively well. Of course there is some difference between three collinear cracks and a single crack. The validity of the results, to use them as a proof, would have been improved if a single crack angle $\alpha = 50°$ had been tested, too.

Table 4-2 shall build up a feeling about the stress states and the generated fracture angles.

Table 4-2: Considerations about stress state, possible fracture angle plane and fracture toughness
(α = inclination angle, angle $\Theta_{fp}^{\,c}$ is measured in compression test, differently defined)

Tension: 3D-stress state $\{\sigma\} = (\sigma_x, \sigma_y, \sigma_z, \tau_{yz}, \tau_{zx}, \tau_{xy})^T \equiv (\sigma_I, \sigma_{II}, \sigma_{III})^T$

with mathematical stresses $\sigma_I >$ (more positive) $\sigma_{II} > \sigma_{III}$

$\{\sigma\} = (0, \sigma_y, 0, 0, 0, 0)^T \equiv (\sigma_I, 0, 0)^T \Rightarrow K_{Ic} = K_{Icr}^{t}$ (stable crack angle)

$\Theta_{fp} = 0° \leftrightarrow$ strength: $(\sigma_n^t, 0)^T$ with $\Theta_{fp} = 0°$ (fracture angle, NF)

$\{\sigma\} = (0, 0, 0, 0, 0, \tau_{xy})^T \equiv (\sigma_I, 0, \sigma_{III})^T \Rightarrow K_{IIcr} \leftarrow$ (no stable crack angle)

$\{\sigma\} = (0, 0, 0, \tau_{yz}, 0, 0)^T \equiv (\sigma_I, 0, \sigma_{III})^T \Rightarrow K_{IIIcr} \leftarrow$ (no stable crack angle)

if fully ductile, dense: $\rightarrow \Theta_{fp} = 45°$ inclined yield plane

Full farfield stress states: Superposition possible, if linear problem is applicable,

Mixed Fracture Mode condition: altering angle Θ_{fp} turns into the transversal plane of principal tensile stress

$\{\sigma\} = (0, \sigma_y, 0\ \tau_{yz}, 0, \tau_{xy})^T \equiv (\sigma_I, \sigma_{II}, \sigma_{III})^T \leftrightarrow 3D: (\sigma_n^t, \tau_{nt}, \tau_{n\ell})^T, \Theta_{fp}(x,y,z)$

The fracture mechanics modes II and III cause a turning of the original crackplane.

Compression: 3D-stress state $\{\sigma\} = (\sigma_x, \sigma_y, \sigma_z, \tau_{yz}, \tau_{zx}, \tau_{xy})^T \equiv (\sigma_I, \sigma_{II}, \sigma_{III})^T$

with mathematical stresses $\sigma_I > \sigma_{II} > \sigma_{III}$

$\{\sigma\} = (\sigma_x, 0, 0, 0, 0, 0)^T \equiv (0, 0, \sigma_{III})^T \Rightarrow K_{IIcr}^{c}$ (stable crack angle is assumed)

$\Theta_{fp}^{\,c}$ ideal crack tip situation presumed $\leftrightarrow$ strength: $(\sigma_{ncr}^t, \tau_{ntcr})^T$ with $\Theta_{fp}^{\,c}$ (SF fracture angle)

$\alpha \neq \Theta_{fp}^{\,c} \leftrightarrow$ strength: $(\sigma_n^t, \tau_{nt})^T$ (no stable crack angle, wing cracks created)

Full farfield stress states: Superposition possible, if linear problem is given.

Different 3D stress states lead to different Mohr stress states which generate different failure planes Θ_{fp}

$\{\sigma\} = (\sigma_x, 0, 0\ \tau_{yz}, 0, \tau_{xy})^T \equiv (\sigma_I, \sigma_{II}, \sigma_{III})^T \leftrightarrow 3D: (\sigma_n^c, \tau_{nt}, \tau_{n\ell})^T, \Theta_{fp}(x,y,z)$

$\{\sigma\} = (\sigma_x, \sigma_y, 0\ , 0, 0, 0)^T \equiv (\sigma_I, 0, \sigma_{III})^T \leftrightarrow 3D: (\sigma_n^c, 0, \tau_{n\ell})^T, \Theta_{fp}(x,y,z)$

$\{\sigma\} = (\sigma_x, \sigma_y, \sigma_z, \tau_{yz}, \tau_{zx}, \tau_{xy})^T \equiv (\sigma_I, \sigma_{II}, \sigma_{III})^T \leftrightarrow 3D: (\sigma_n^c, \tau_{nt}, \tau_{n\ell})^T, \Theta_{fp}(.x,y,z).$

(2) Formulation and course of the SIF $K_{IIcr}^{\,c}$: The author believes – as a second proof for the existence of the fracture toughness $K_{IIcr}^{\,c}$ - that a formula is still available. P.H. Melville published in [*Mel77*] *(information from [Pha03], in literature for the author not available)*

$$K_{IIcr}^{c} = \sigma \cdot \sqrt{\pi \cdot a} \cdot \sin(\alpha) \cdot [\cos(\alpha) - \tan(\varphi) \cdot \sin(\alpha)] \quad \text{with}$$

σ = far field stress, a = half crack size, α = flaw (crack) angle and $\tan(\varphi) \cong \mu$.

The SIF depends on the size of the friction value μ. It is the highest, if $\Theta_{fp}^{c} = 90 - \alpha$ *(as defined here) Fig.4-9.*

The number on the curves in the right figure marks the maximum value of each 'friction' curve.

Exemplarily assuming the usual linear Mohr-Coulomb $tan(\varphi) = \mu = 0.2$ means that $\Theta_{fp}^{c} = 50°$ A check of the special case "ductile" with $\mu = 0$ works as the angle α then correctly becomes the frictionless shear sliding angle or yield angle 45°.

Finding: → For a brittle material with its associated friction the SIF K_{II}^{c} becomes highest when $\alpha = 90 - \Theta_{fp}^{c}$ and that it will lead to further crack growth in this plane.

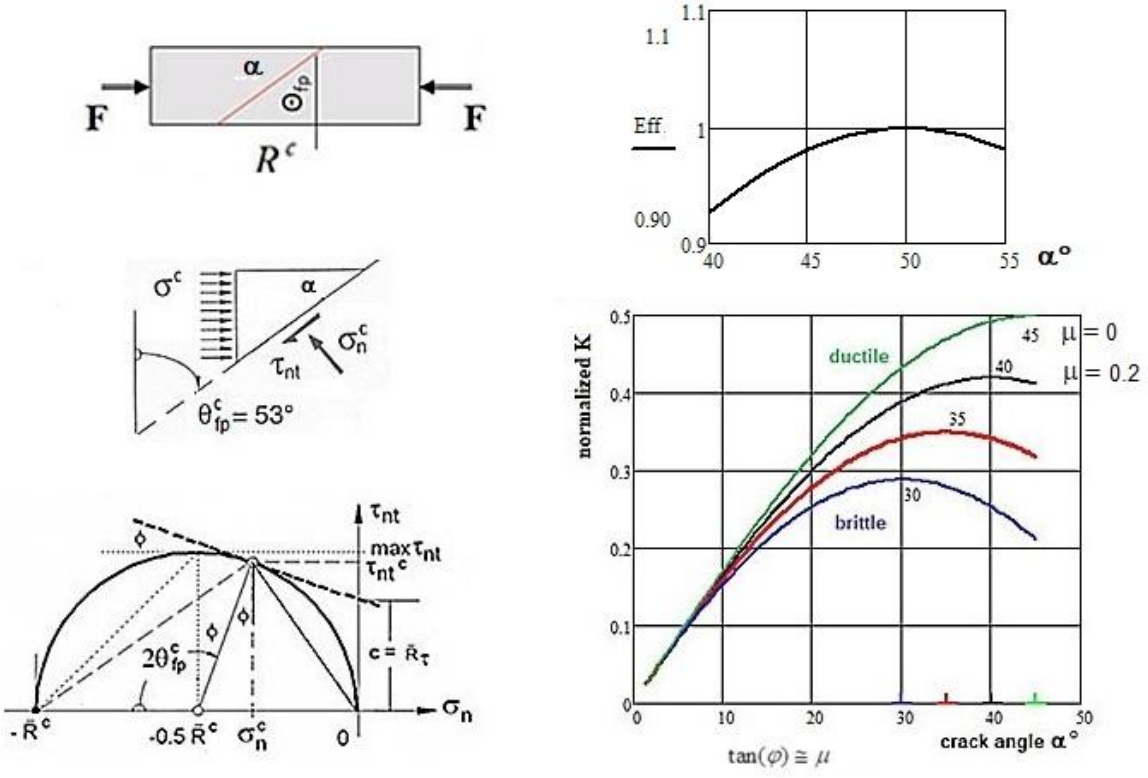


Fig.4-9: (left) the different angles in strength, Mohr-Coulomb; (right up) dependence of the material stressing effort Eff on the inclination angle α, (right down) K_{IIcr}^{c} versus inclination crack α considering the friction value μ (here $\Theta_{fp}^{c} = 90° - \alpha°$ is valid in literature [Mel77])

This means – in the case of isotropic materials - when linking Strength Mechanics and LEFM to investigate the crack growth angle:

* Domain $I_1 > 0$ (tension, classical fracture mechanics in mechanical engineering):
The maximum hoop stress in front of the crack-tip rules - after Erdogan-Sih - the growth direction of the crack. This practically means that a SFC for NF is employed when investigating the turning of the crack in front of the crack-tip under multi-axial far field stress states. K_{Icr}^{t} (= K_{Ic}) rules.

* Domain $I_1 < 0$ (compression, civil engineering, rock mechanics):

Could it not be that under compression also a SFC for SF can be employed? This SFC considers the energy at fracture failure. At which fracture angle becomes the SF-SFC a minimum? This can be performed by using the material stressing effort *Eff* in combination with a minimum necessary energy amount $G = K^2 \cdot (1-\nu^2) / E$.

One can pose the questions:

→ At which angle does *Eff* have a maximum? Applying linear Mohr-Coulomb the material stressing effort follows $Eff = \tau_n / (R^{\tau} - \mu \cdot \sigma_n)$ with R^{τ} the cohesive strength

→ At which angle takes the stress intensity K a maximum?

This was elaborated in the various pictures in *Fig.4-9*, above right side, with the response:

If the inclination angle corresponds to the fracture angle Θ_{fp}^{c} , then a critical state is generated.

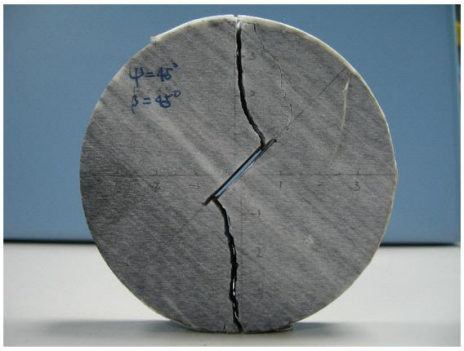


Fig.4-10, Brazilian Disk: Crack growth reality under vertical compression due to large grains ahead of the crack tip. [Sorry, originator of the picture could not be found in a search]

LL:

A crack angle α, inclined the same as a compression-induced fracture shear angle Θ_{fp} of the formerly intact isotropic material is linked to minimum energy and to a maximum SIF. Both these values are critical quantities for further crack growth of the solid material element. This shear fracture angle should be inserted into a flaw-free Brazilian disk above and then compression tested and checked, whether the original crack angle remains stable.

.

4.3 Transversely-isotropic UD lamina materials, 5 fracture toughness properties

4.3.1 Number of Fracture Mechanics (FM) modes

FM is applied here micromechanically to investigate the de-bonding of filament-matrix, macro-mechanically to the UD lamina material (*ply or layer as physical lamina*) and further to investigate the delamination crack of the laminate.

In order to assess the associated stress states the corresponding critical stress intensity factors (*fracture toughness properties*) K_{cr} are to determine. Beside this, it is intended to give another proof that the 'generic' number for the transversely-isotropic UD material is 5.

Before planning a FM test program the probable number of fracture mechanics modes should be checked. After transformation into the quasi-isotropic plane $\sigma_2 - \sigma_3$ from the former 6 lamina stresses 5 stresses remain. Due to the material symmetry and after switching to the unambiguously symbolic indices it is valid for the stress states, (see *Fig.4-11*):

$\{\sigma\} = (\sigma_1,\sigma_2,\sigma_3,\tau_{23},\tau_{31},\tau_{21})^T \rightarrow \{\sigma\} = (\sigma_{\parallel},\sigma_{\perp},\sigma_{\perp},\tau_{\perp\perp},\tau_{\perp\parallel},\tau_{\perp\parallel})^T$

$\{\sigma^{pr}\} = (\sigma_1,\sigma_2{}^{pr},\sigma_3{}^{pr},0,\tau_{31}{}^{pr},\tau_{21}{}^{pr})^T \rightarrow \{\sigma^{pr}\} = (\sigma_{\parallel},\sigma_{\perp}{}^{pr},\sigma_{\perp}{}^{pr},0,\tau_{\perp\parallel}{}^{pr},\tau_{\perp\parallel}{}^{pr})^T$.

$\sigma_{\parallel},\sigma_{\perp}{}^{pr},\tau_{\perp\parallel}{}^{pr}$, neglecting the index ^{pr} leads to $\sigma_{\parallel},\sigma_{\perp},\tau_{\perp\parallel}$ and 5 SFC and 5 FM modes.

In Fracture Mechanics FM of isotropic materials structural stresses are used. The crack plane may be arbitrary which means a reduction to the principal stress treatment is not possible.

$$\{\sigma\} = (\sigma_x,\ \sigma_y,\ \sigma_z,\ \tau_{yz},\ \tau_{zx},\ \tau_{xy})^T \equiv (\sigma_I,\ \sigma_{II},\ \sigma_{III})^T$$

In FM of UD materials the crack plane is practically known in case of relatively thin layers and therefore the isotropic FM shear modes II and III are not to consider. The investigation uses principal lamina stresses and by doing that it reduces to 5 UD FM modes, a reduction to the principal stresses is possible.

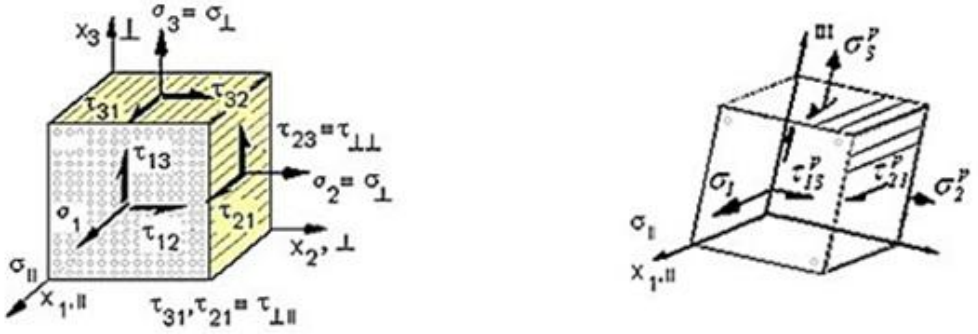


Fig.4-11: Derivation of the number of fracture mechanical modes

<u>*Fig.4-12*</u> visualizes the mode differences between isotropic and UD materials.

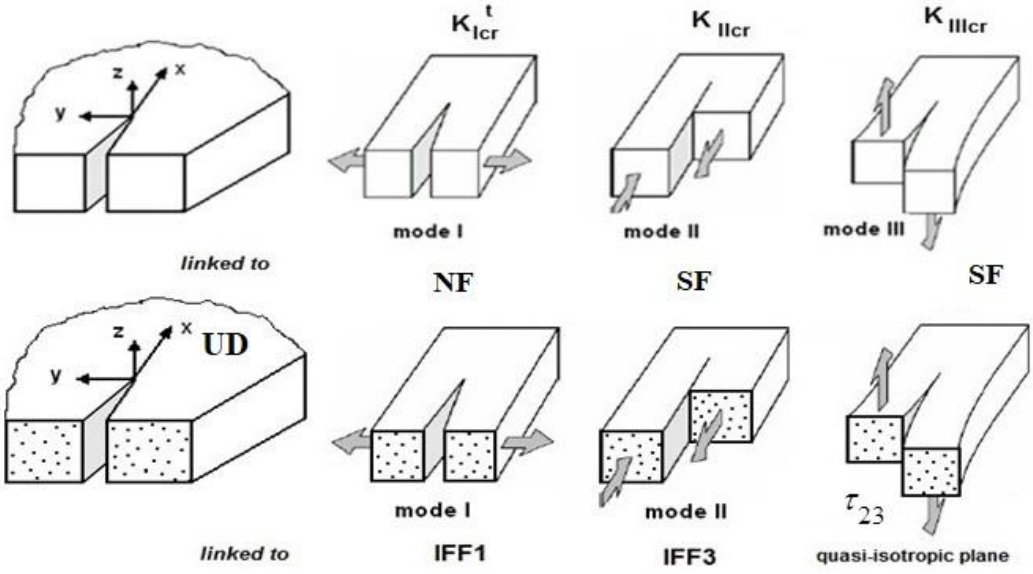


Fig.4-12: Standard fracture mechanics modes for isotropic material and corresponding modes for UD (dots represent the filaments). Mode I opening mode (tension driven), II sliding mode (shear), III tearing mode (scissoring shear), 2D-plate

For UD material, Mode I corresponds to $\sigma_{\parallel}^{t}$ ($\sigma_y \equiv \sigma_n$) or $\sigma_{\perp}{}^{t}$, mode II to τ_{21} (= τ_{12}) and mode III to τ_{23}. In the case of a UD-lamina K_{IIcr} (τ_{21}) can be seen – in contradiction to the isotropic K_{II} (τ_{xy}) – as

a real basic macro-mechanical material property because the fracture plane remains stable under crack growth, due to constraints from the fiber direction. The macro-mechanical stresses are dedicated to single, remote stresses.

The failure condition, beyond which the crack will begin to propagate, reads $K/K_{cr} = 1$. In practical design dimensioning K_{cr} is reduced to a feasible statistically-based value $K_{feasible}$.

Analogous to the SFCs – the following matrix-related and fiber-related stress intensity factors SIFs are to consider. The so-called matrix modes, linked to $\sigma_{\perp}$, $\tau_{\perp\parallel}$ are pretty clear regarding the crack growth, but there is still some un-clearness about the SIFs K of the 2 fiber modes.

* $K_{\parallel}^{t}$: Knowledge about this stress intensity factor is necessary, because an assessment of the crack growth is essential for the final stage of fatigue life. From fatigue investigations at the DTU B. F. Soerensen sorted out for the tensile mode that, see *Fig.4-13*: (1) Fiber failure is not random, (2) All fibers are broken behind the damage front and intact ahead of the damage front, (3) Failure is row-wise step-by-step, (4) Splitting along the fibers is generated [*Soerensen, Comp. Techn. 2019*], (5) There are stress concentrations at the broken fiber end and at the end of the de-bonded zone which moves along the fiber after further cycling. The fiber/matrix debond growth along the broken filament interface is Mode II-related and described by the strain energy release rate $\mathcal{G}$, reading in the very brittle isotropic case $\mathcal{G} = K^2 \cdot (1-\nu^2) / E$. For a long debond length the interface crack growth is self-similar which means remains in its crack 'plane'. For a short de-bonding length the interface crack interacts with the fiber break and its stress concentration.

* $K_{\parallel}^{c}$: From practical reasons this property is not of that interest because critical static kinking must be avoided in design.

* $K_{\perp}^{t}$, $K_{\perp}^{c}$, $K_{\perp\parallel}$: SIFs for cracks within a layer (lamina) or between the layers within a laminate (multilayered tape, sheet). They may be referred to as matrix–linked fracture mechanics modes. UD energy release rates measured, formally follow above $\mathcal{G} = K^2 \cdot (1-\nu^2) / E$.

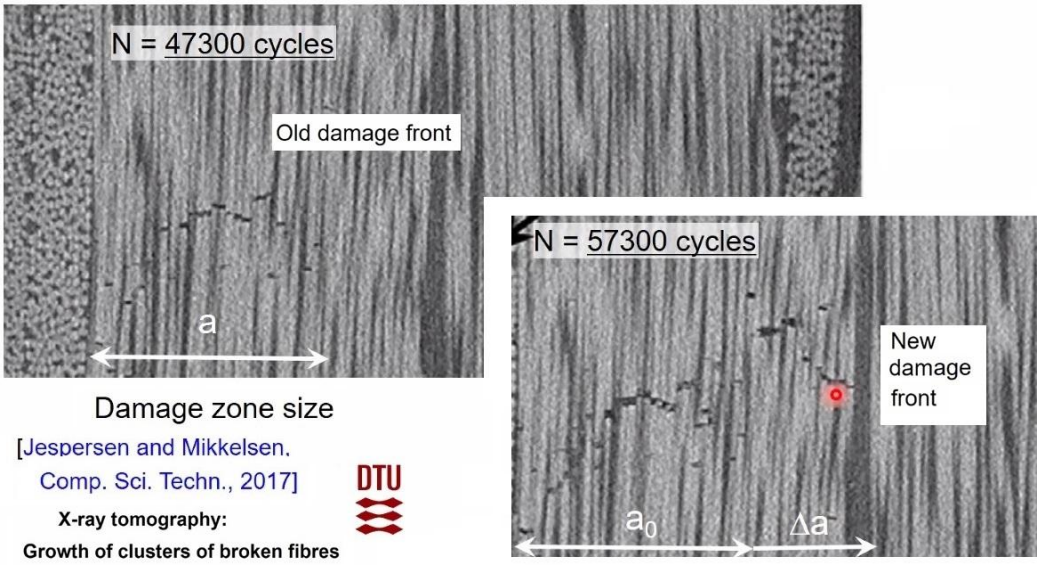


Fig.4-13: Increase of 'crack front'. Presentation B. Soerensen at CU eV, 2010.

Fig.4-14 presents a comparing scheme of FM Modes involving isotropic and UD material. The main difference comes whether the crack plane remains in the case of a self-similar crack growth *('thin' layered laminate*) or not as for the isotropic materials. Considering the SIF $K_{II}{}^{c}$ the reader is referred to the previous chapter.

Fracture toughness quantities $\mathcal{G}_i$ for the 3 modes may be determined by standardized tests helping to assess the danger of failure for an onset-of-static crack growth or delamination growth and to assess the cyclic crack growth. Employing again material symmetry reflections for the transversely-isotropic UD-material 5 fracture mechanics modes should correspond to 5 strength failure modes. *Fig.4-15* indicates how 4 of the 5 test specimens look like.

At the ILK/ZLS at Dresden University, 4 of the 5 principally necessary UD energy release rates $\mathcal{G}$ were measured. Problematic for the quality of the test results is that the test specimens (see literature of [*Pin06*]) may out-of-plane buckle, due to the fact that they are too thin to approximately respect the plane strain condition in order to obtain a real material property.

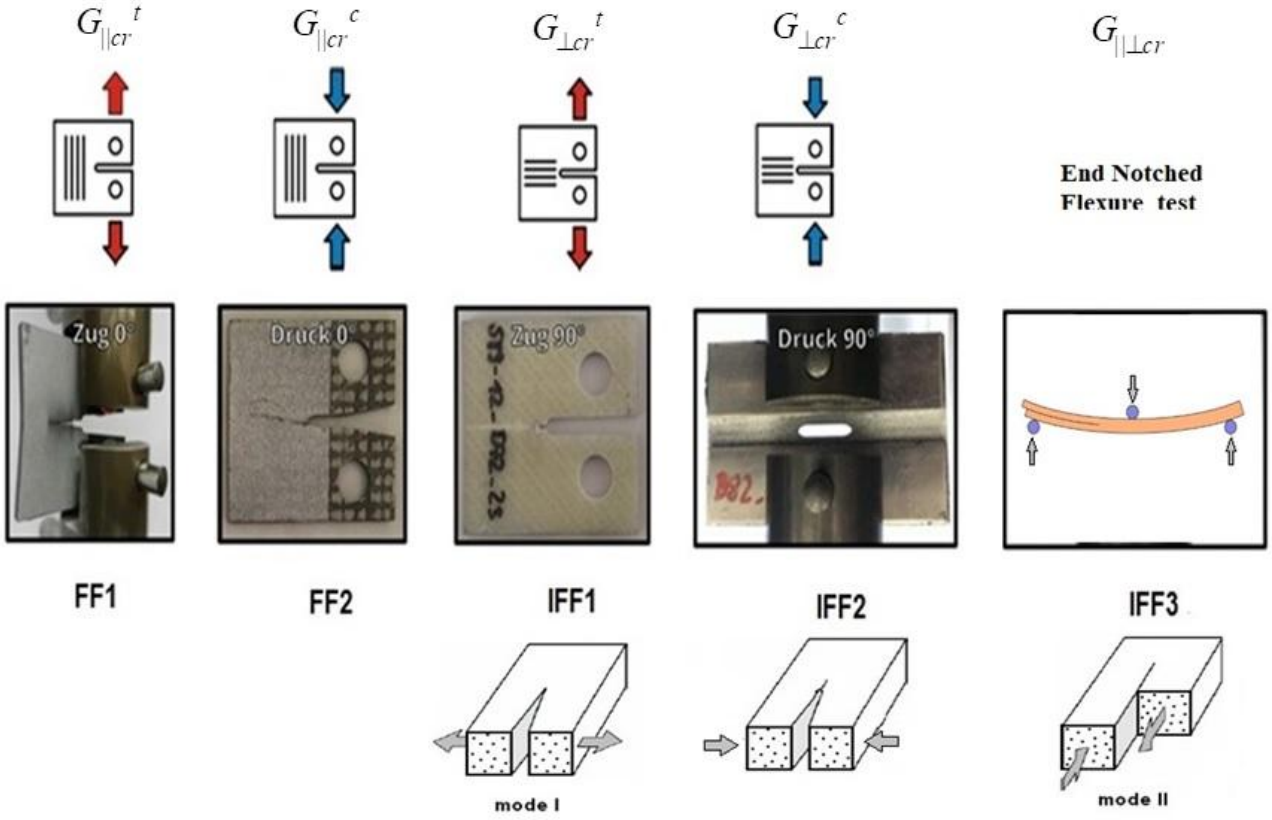
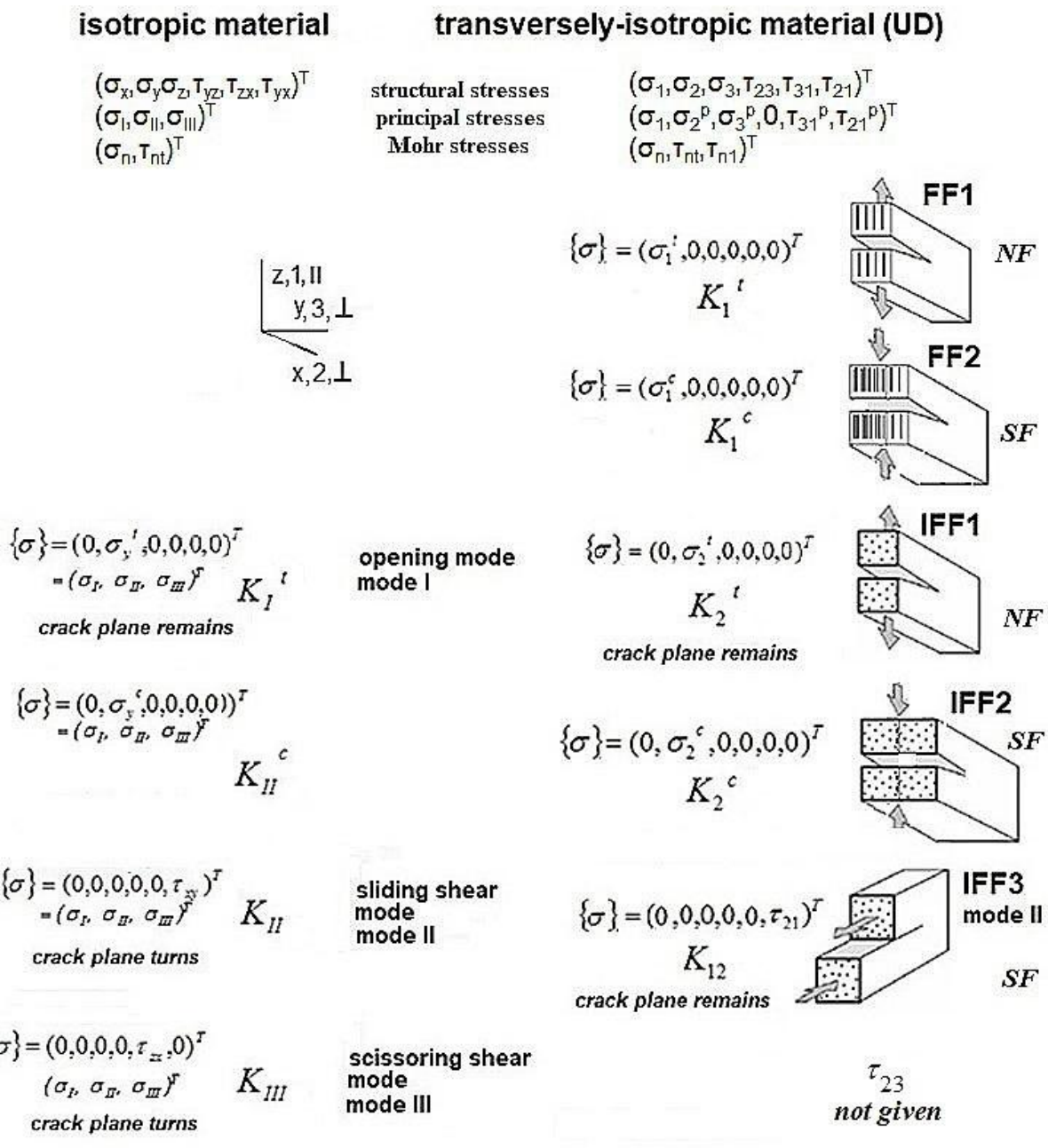


Fig.4-15: Specimens tested under tension in 0°-direction, 90°-direction, and under Compression in 0°-direction, 90°-direction,[ILK, ZLS Dresden]. G = $\mathcal{G}$

LL:

* *Confirmation of the author's assumption, that - according to material symmetry - the number of real strength or FM-related material properties is 2 for isotropic and 5 for transversely-isotropic materials !*
* *The continuum mechanics approach 'captures' the fracture mechanics approach if the fracture plane remains the same (self-similar) after onset-of-cracking at Initial Failure and further loading.*
* *Strain controlled testing requires a very high frame stiffness.*



Interaction Mixed Mode

Strength Failure Modes

Interaction of all micro-damage contributing stresses by the interaction equation

$$Eff = \sqrt[m]{(Eff^{\text{mode 1}})^m + (Eff^{\text{mode 2}})^m + \ldots} = 1$$

Fracture Mechanics Failure Modes

Interaction of three contributing stresses by the Mixed Mode quation

$\{\sigma\} = (0,\sigma_y^t,0,0,\tau_{zx},\tau_{xy})^T$ energy release rate $G = \Sigma\ G_i$ $\{\sigma\} = (0,\sigma_2^t,0,0,\tau_{31},\tau_{12})^T$

to be inserted into $G / G_{feasible} = 1$

Fig.4-14: Scheme of fracture mechanics modes, stress intensity factors K (inherent and model-associated ones) of brittle isotropic and brittle transversely-isotropic UD materials. NF = Normal Fracture, SF = Shear Fracture

4.3.2 Determination of the microcrack-linked softening curve by FM-testing

Fig.4-15 was a guide to the idea of this paragraph, namely the estimation of a softening curve. The shape of this curve is differently described, for instance as a falling straight line. From physical reflections the softening function $\sigma_{soft} = \bar{R} / (1+exp[(a_{soft} + \varepsilon) / b_{soft}]) = \bar{R} \cdot \eta$ (sub-chapter 2-10) was chosen for a lamina embedded in a laminate which is also valid for reinforced concrete. Nature usually behaves smooth in strain-controlled situations. A lamina embedded *(strain-controlled by the material vicinity and deformation-controlled by the test rig)* in a laminate or a reinforced concrete matrix *(strain-controlled)* behave similarly and keep a decaying capacity after onset-of-failure (*after cracking at 'post peak'*). This is very advantageously in limit load cases. After onset-of-cracking embedded lamina and reinforced concrete still contribute to the stiffness and the load carrying capacity of the designed structural element.

Beyond initial failure or cracking one might assume that 'small scale FM' may be approximately used. Therefore, the assumption of setting the work under the softening curve and under the FM crack progress curve $\mathcal{G}_{cr}$ equal, offers a comparison to estimate the area content under the softening curve σ_{soft} .

One curve point is the strength and two others come from the two $\mathcal{G}_{cr}$ values.

In the following formula $\max \delta = \delta_{fracture}$ and $\max \gamma \approx 3 \cdot \gamma(\bar{R}_{\perp\perp})$.

$$\int_{\gamma \text{ at Onset-of-Fracture}}^{\max \gamma} \sigma_{soft} \cdot \gamma_{soft} \cdot d\gamma = \int_{0}^{\max \delta} F(\delta) d\delta = \mathcal{G}_{cr}.$$

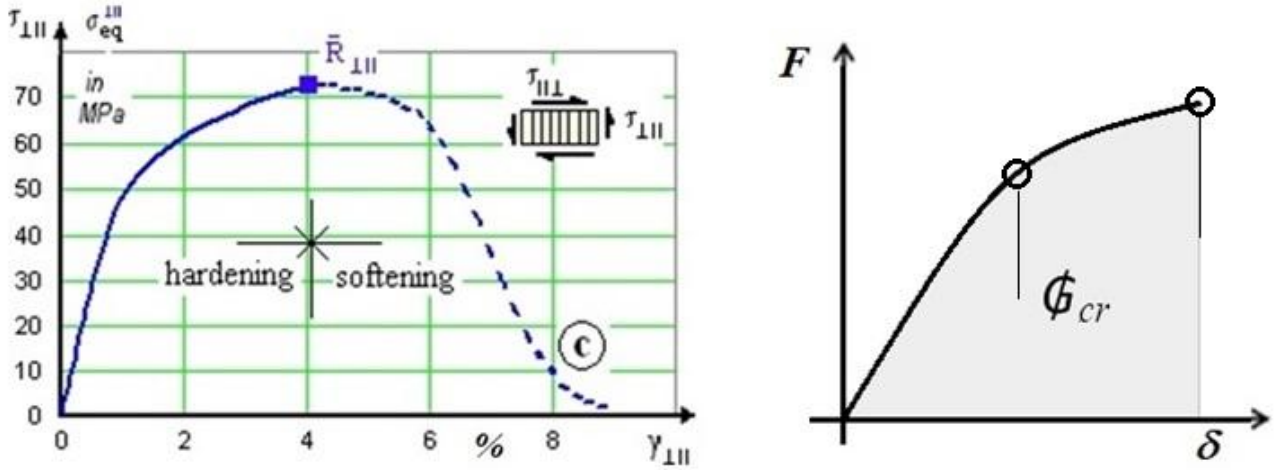


Fig.4-16: Assessment of the area size under the softening curve (example IFF3). F is force and δ deformation or crack opening displacement

Design dimensioning of the laminate deformation-controlled lamina:

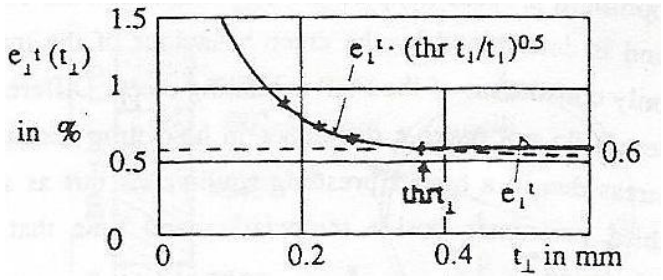
Crack growth is initiated when the energy release rate overcomes a critical value $\mathcal{G}_{cr}$ which is a material property that considers material inherent friction. The associated FM failure condition reads $\mathcal{G} / \mathcal{G}_{cr} = 1$. For an arbitrary combination of all loading modes, the $\mathcal{G}s$ are to superpose.

For the laminate Test Cases, beyond initial failure an appropriate progressive failure analysis method has to be employed (*a successive degradation model for the description of post initial failure*) by using a failure condition that indicates failure mode and a measure for the material

stressing effort *Eff* and accumulated midro-damage. Final failure occurs after the laminate structure has degraded to a level where it is no longer capable of carrying any load.
The altering micro-crack density has to be regarded up to the characteristic damage state (CDS) where the number of micro-cracks reaches its maximum value and beyond where the initiated micro-cracks just increase their size. The softening curve may therefore termed an 'effective' curve.
For the quasi-brittle FRP it can be concluded that so-called cohesive forces still exist at IFF in the fracture process zone at the micro-crack tips in the laminas.

4.3.3 When does flaw size-driven Onset-of-Failure occur in a Lamina?

From fiber-reinforced laminates is known, that a strength failure condition SFC as well as an energy condition must be met at onset-of-failure. For thin layers the strength failure conditions used in Classical Laminate Theory are sufficient, for thicker layers a linear elastic fracture mechanics is to consider. A FM condition (SIF model) is to apply in order to predict failure of the transverse stresses in the '90°- layers'. This is a complicate task. A very old investigation of [*Fla82*] already gives insight how the layer thickness effect acts. The author simply described it by $R_{\perp}^{t}$ ($t_{\perp} < t_{thr}$) = $R_{\perp}^{t}\sqrt{t_{thr} / t_{\perp}}$. → Thin layers are the better choice considering strength capacity.



Thin-layer effect: Corrective means.

M40 with MY750/HY917/DY070.

[*Fla82*], tube test results

It is generally to note:
The application of a SFC must be checked whether it is 'Necessary' and 'Sufficient'. Principally it is to check whether any one energy-based condition is on top to take into account, like a fracture mechanics one. Further to check is: Is the energy a minimum one or is *K* a maximum one?

Above contents leads over to the next paragraph.

4.3.4 Finite Fracture Mechanics linking Continuum Mechanics - Fracture Mechanics

When applying SFCs ideal solids are viewed which are assumed to be free of essential micro-voids or microcrack-like flaws. When applying FM the solid is considered to contain macro-voids or macro-cracks. There are three approaches available to deal with the occurring stress situations: Strength conditions (SFC), Continuum Damage mechanics (CDM) conditions and Conditions of crack fracture mechanics (FM) which employ crack growth models.
As still mentioned before:

> A SFC is a necessary condition but might not be a sufficient condition for the prediction of 'initiation of cracking' (Onset-of-Failure).

A bridge must be built from strength failure conditions to fracture mechanics failure conditions. Neglecting CDM, attempts to link SFC-described 'onset of fracture' prediction methods and FM prediction methods for structural components are actually undergone. Best known is the Hypothesis of Leguillon [*Leg02*]:

> "*A crack is critical when and only when both the released energy and the local stress reach critical values along an assumed finite crack".*

While the application to combined stresses is very common in the instance of SFCs it is not at all common to apply FM conditions to 3D states of stress. Based on physical reasons, a bridge should provide a more unified perspective, because - ahead of the crack tip - both approaches are linked together. Such a bridging approach should respect a 3D-farfield state of stress and a full mixed-mode crack situation.

For the stress concentration examples above an energy-based FM failure condition delivers the second condition to check whether failure occurs or whether failure does not occur. After Leguillon the Linear Elastic Fracture Mechanics (LEFM) delivers the missing failure condition which is an *energetic failure condition* formulated by the above still used

total energy release rate $\mathcal{G} = \Sigma\ \mathcal{G}_i$ to be inserted into $\mathcal{G} / \mathcal{G}_{feasible} = 1$.

with $\mathcal{G}$ being the crack-driving force to create more fracture surface and the crack resistance $\mathcal{G}_{cr}$ *(most often a feasible value)* a fracture energy.

This so-called coupled criterion with *Eff* = 1 together with $\mathcal{G} / \mathcal{G}_{feasible} = 1$ has a pro-termced macroscopic nature. In the case of delamination between plies under normal and/or shear stresses, the determination of the critical energy release rate $\mathcal{G}_{cr}$ is crucial to analyze designs.

Typical methods of determining the critical energy release rate are through experiments, such as the double-cantilever beam (DCB) for mode I, end-notched flexure (ENF) for mode II, and mixed-mode flexure (MMF).

In the case that Linear Fracture Mechanics LEFM is permitted for the given material $\mathcal{G}_{cr}$ is $\mathcal{G}_{cr}(K_{cr})$.

Finite Fracture Mechanics (FFM) fills a gap in FM, since it is an approach to offer a condition to predict the crack initiation in brittle isotropic and UD materials. Within FFM assumed cracks of finite length are considered.

Examples are the locations of stress singularities like the stress concentrations of notched isotropic components or UD layer-composed laminates:

- at notches, where the notch stress causes failure even for relatively low far-field stresses
- the influence of the size of a bore has an effect
- the thickness of the in-situ behavior of an embedded layer in a laminate has an effect.

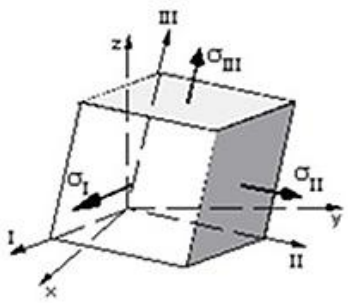
These are typical deformation-controlled stress situations. FFM can be used to predict the open-hole tensile strength of composite laminates. Failure is occurs when both stress-based and energy-based conditions are satisfied. Material properties required by the concept are the elastic properties of the lamina and the laminate unnotched strength and its fracture toughness.

Reminder:

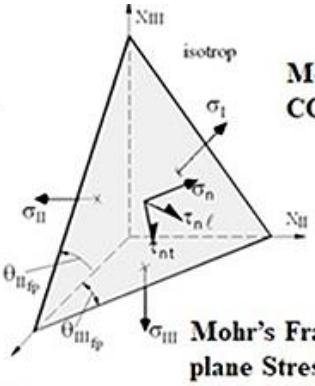
The FMC is originally energy-based, however, the modified forms may not have sufficiently well kept this previously intended characteristic.

5 Validation of FMC-SFCs by 3D-Applications with all 3 Material Families

At first a repetition of the different stress formulations is helpful (s*orry for some old figures*)



The stress states in the various COS can be transferred into each other



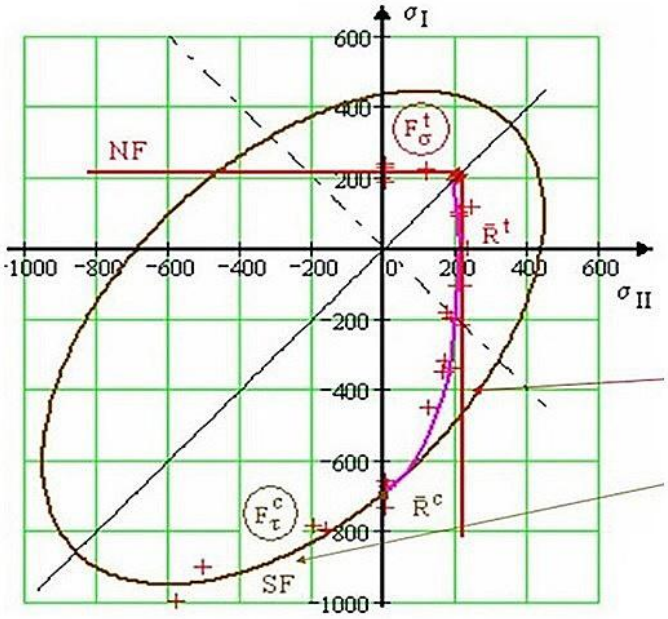
Mohr's COS

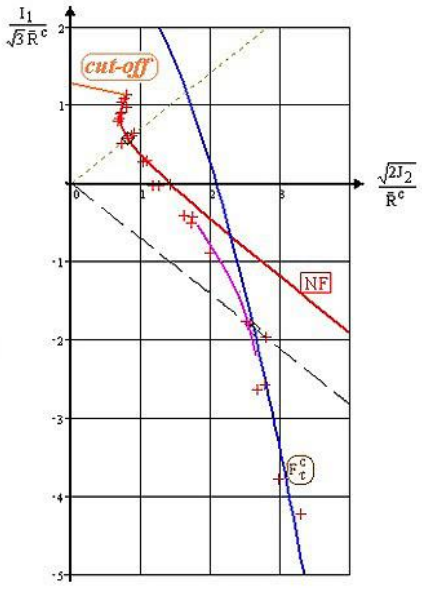
Mohr's Fracture plane Stresses

Principal Stresses	**Structural (component) Stresses**	**Mohr's Fracture plane Stresses**
$\{\sigma\}_{principal} = (\sigma_I,\ \sigma_{II},\ \sigma_{III})^T$	$\{\sigma\}_{comp} = (\sigma_x,\ \sigma_y,\ \sigma_z,\ \tau_{yz},\ \tau_{zx},\ \tau_{xy})^T$	$\{\sigma\}_{Mohr} = (\sigma_\ell,\ \sigma_n,\ \sigma_t,\ \tau_{nt},\ \tau_{n\ell},\ \tau_{\ell n})^T$
$I_1 = (\sigma_I + \sigma_{II} + \sigma_{III})^1 = 3\sigma_{oct} \equiv f(\sigma),$	**'isotropic' invariants !** $I_1 = (\sigma_x + \sigma_x + \sigma_z)^T$	$I_1 = (\sigma_\ell + \sigma_n + \sigma_t)^T$
$J_2 = (\sigma_I - \sigma_{II})^2 + (\sigma_{II} - \sigma_{III})^2 + (\sigma_{III} - \sigma_I)^2$ $= 4(\tau_{III}^2 + \tau_{II}^2 + \tau_I^2) = 9\tau_{oct}^2 \equiv f(\tau)$	$6J_2 = (\sigma_y - \sigma_z)^2 + (\sigma_z - \sigma_x)^2 + (\sigma_x - \sigma_y)^2$ $+6(\tau_{yz}^2 + \tau_{zx}^2 + \tau_{xy}^2)$ *(Mises, HMH)*	$6J_2 = (\sigma_n - \sigma_t)^2 + (\sigma_t - \sigma_\ell)^2 + (\sigma_\ell - \sigma_n)^2$ $+6(\tau_{nt}^2 + \tau_{n\ell}^2 + \tau_{\ell t}^2)$

$$27J_3 = (2\sigma_I - \sigma_{II} - \sigma_{III})(2\sigma_{II} - \sigma_I - \sigma_{III})(2\sigma_{III} - \sigma_I - \sigma_{II}),\quad I_e = 4J_2 - I_1^2/3,\quad \sigma_{mean} = I_1/3$$

5.1 Isotropic Grey Cast Iron





$$Eff^{NF} = 1 \cdot \frac{\sqrt{4J_2 \cdot (1) - I_1^2/3} + I_1}{2 \cdot \bar{R}^t} = \sigma_{eq}^{NF} / \bar{R}^t \qquad \text{deformation-poor mode}$$

$\bar{R}^t = 215$ MPa, $\bar{R}^t = 690$ MPa

$c_1^{SF} = 1.58,\ c_2^{SF} = c_1^{SF} - 1 \quad m = 2.6$

$$Eff^{SF} = \frac{c_2^{SF} \cdot I_1 + \sqrt{(c_2^{SF} \cdot I_1)^2 + 12 \cdot c_1^{SF} \cdot 3J_2 \cdot (1)}}{2 \cdot \bar{R}^c} = \sigma_{eq}^{SF} / \bar{R}^c \qquad \text{considers shear deformation and friction}$$

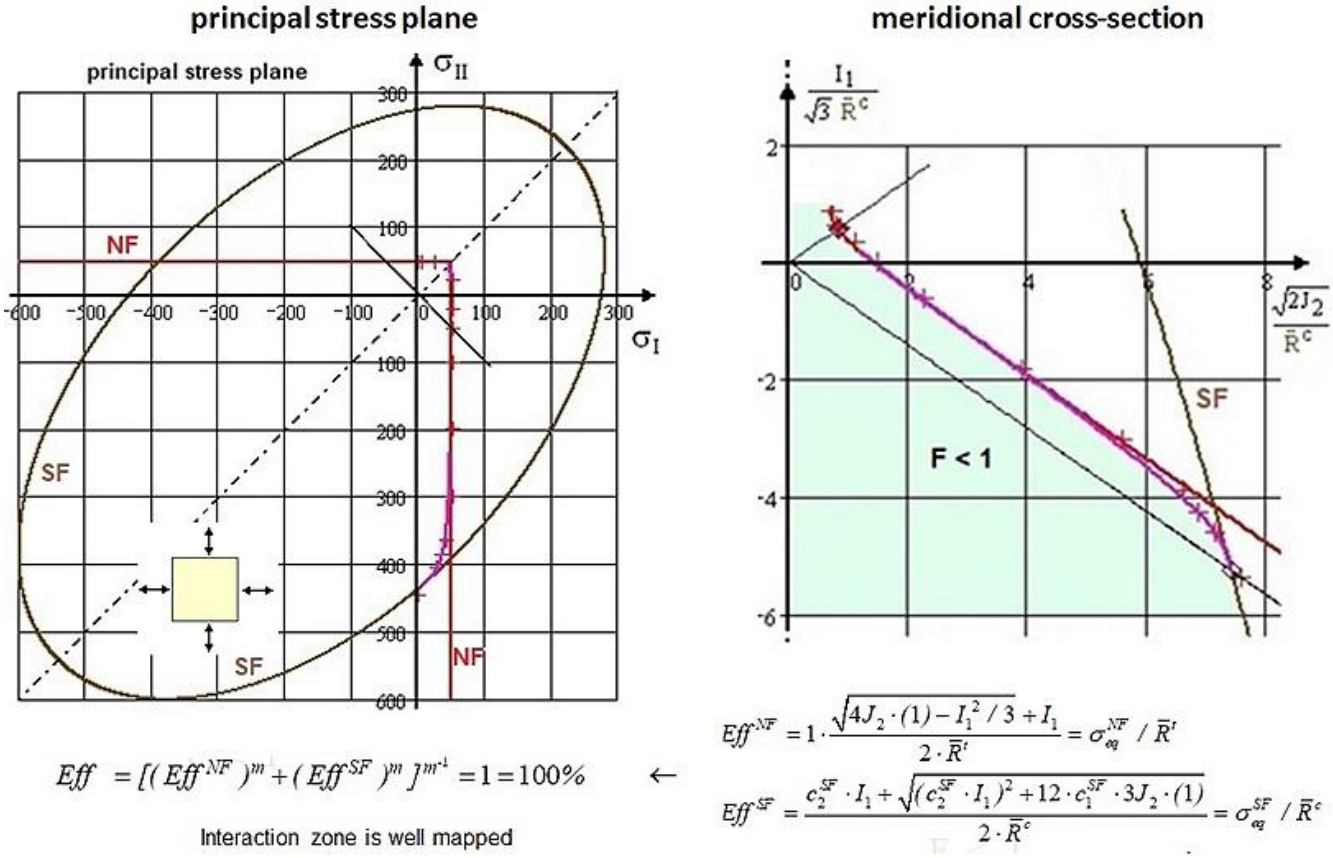
$$\rightarrow\ Eff = [(Eff^{NF})^m + (Eff^{SF})^m]^{m^{-1}} = 1 = 100\%$$

Fig.5-1: 2D-application to Grey-cast Iron [Coffin]. Principal stress plane and meridional cross section

5.2 Isotropic Glass C 90 (window pane of ISS)

A glass fiber SiO_2 (E, S, R, AR) is made by blending raw materials, melting them at 1720°C in a three-stage furnace, extruding the molten glass through a bushing in the bottom of the fore-hearth (Vorherd), cooling the filaments with water (*to prevent the crystallization to quartz and obtain a amorphous, randomly ordered atomic structure we know as glass*) and then applying a chemical sizing. The filaments then are gathered to rovings and wound on spools. Commercial glass fiber can be made from silica alone, other ingredients are added to reduce the working temperature and impart other properties that are useful in specific applications such as making alkali-resistant (by ZrO_2) for use in concrete. [*Source OCV*].

Fig.5-2 presents a 2D-SFC-visualization in the principal stress plane and a 3D-Visualization in the meridional cross-section.



$$Eff = [(Eff^{NF})^m + (Eff^{SF})^m]^{m^{-1}} = 1 = 100\% \quad \leftarrow$$

$$Eff^{NF} = 1 \cdot \frac{\sqrt{4J_2 \cdot (1) - I_1^2/3} + I_1}{2 \cdot \bar{R}^t} = \sigma_{eq}^{NF} / \bar{R}^t$$

$$Eff^{SF} = \frac{c_2^{SF} \cdot I_1 + \sqrt{(c_2^{SF} \cdot I_1)^2 + 12 \cdot c_1^{SF} \cdot 3J_2 \cdot (1)}}{2 \cdot \bar{R}^c} = \sigma_{eq}^{SF} / \bar{R}^c$$

Fig.5-2, Glass C 90: [Kow83], 2D and 3D-visualizations

5.3 Isotropic porous Foam Rohacell (SFC is applicable for Concrete Stone material, too)

Usually, for structural parts of high stiffness, honeycombs are used. With the new Rohacell Hero (Evonik) a PMI (Poly-Methacryl-Imide) structural foam of an increased tensile fracture strain is available which may replace the expensive honeycombs. In order to apply this material in structural parts Structural Integrity must be proven. This requires reliable multi-axial strength test data as well as reliable Strength Failure Conditions SFCs (criteria) for an optimal Design Development process. Given is 'only' a 2D-Test Data Set and therefore just a realistic mapping in the Principal Stress Plane is possible. To apply is the 2D subversion of the 3D SFC. → From this follows: Validation of the 3D SFC is 'just' 2D-based.

The data set used (*thanks to Dr. Kolupaev for the test data set*) reads:

$$\bar{R}^{t} = 1.8;\ \bar{R}^{tt} = 1.25;\ \bar{R}^{ttt} = 1.01;\ \bar{R}^{c} = 1.65;\ \bar{R}^{cc} = 1.4;\ \bar{R}^{ccc} = 1.53,\ \max I_1 = 3.03;$$
$$\min I_1 = -4.58,\ d^{NF} = -0.71;\ d^{CrF} = 0.21;\ c^{CrF} = 1.03, s^{cap} = -0.27;\ s^{bot} = 0.87,$$
$$\vartheta^{NF} = -0.57;\ \vartheta^{CrF} = 0.52; \Theta^{NF} = 1.2;\ \Theta^{CrF} = 1.07, m = 2.5.$$

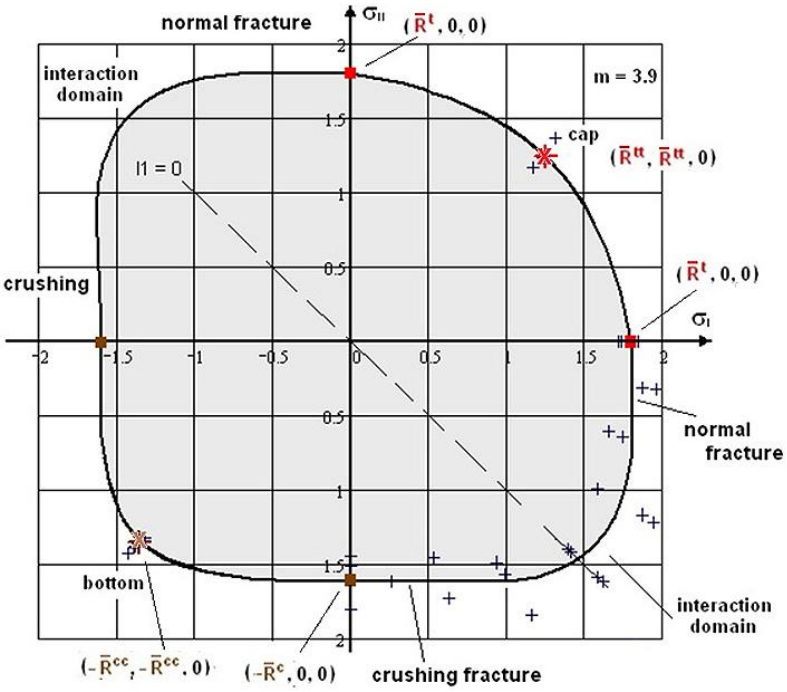


Fig.5-3, Foam Rohacell 71 IG: Mapping of 2D-test data in the Principal Stress Plane. MathCad plot [test data: courtesy V. Kolupaev, LBF Darmstadt]

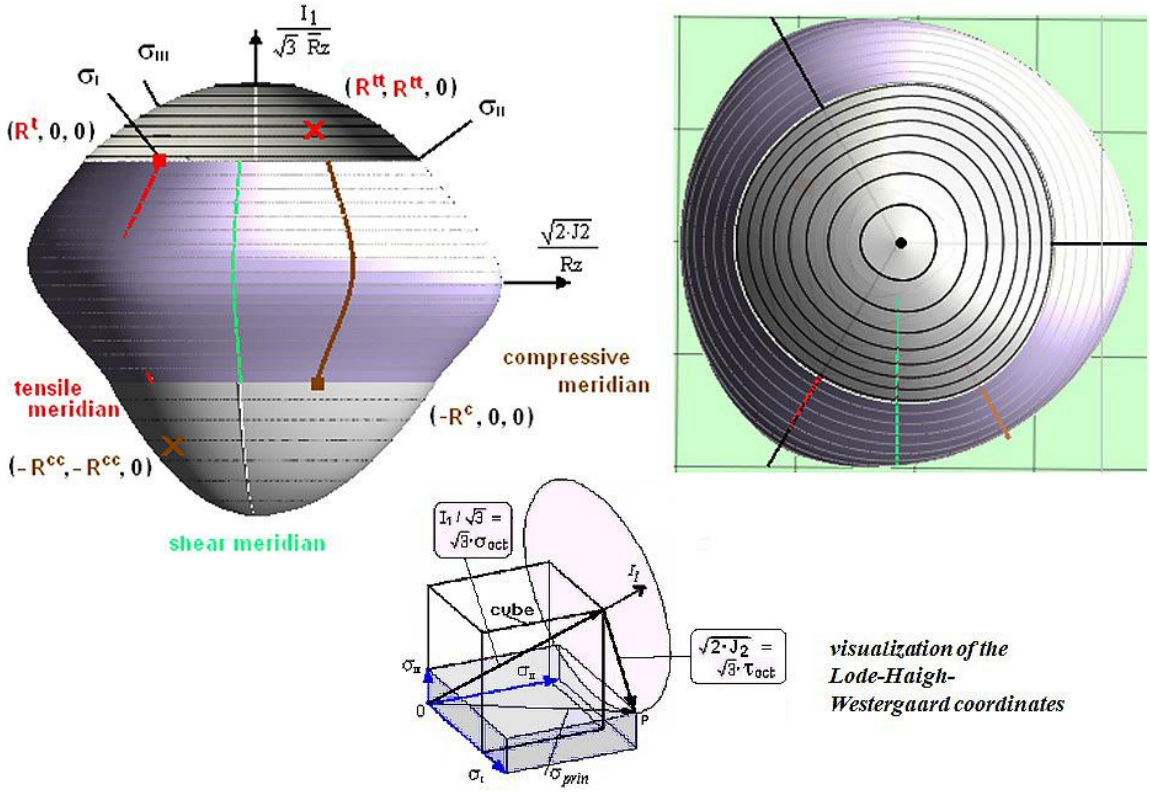


Fig.5-4, Rohacell 71 IG: Fracture body with its different meridians (left) and view from top (right).

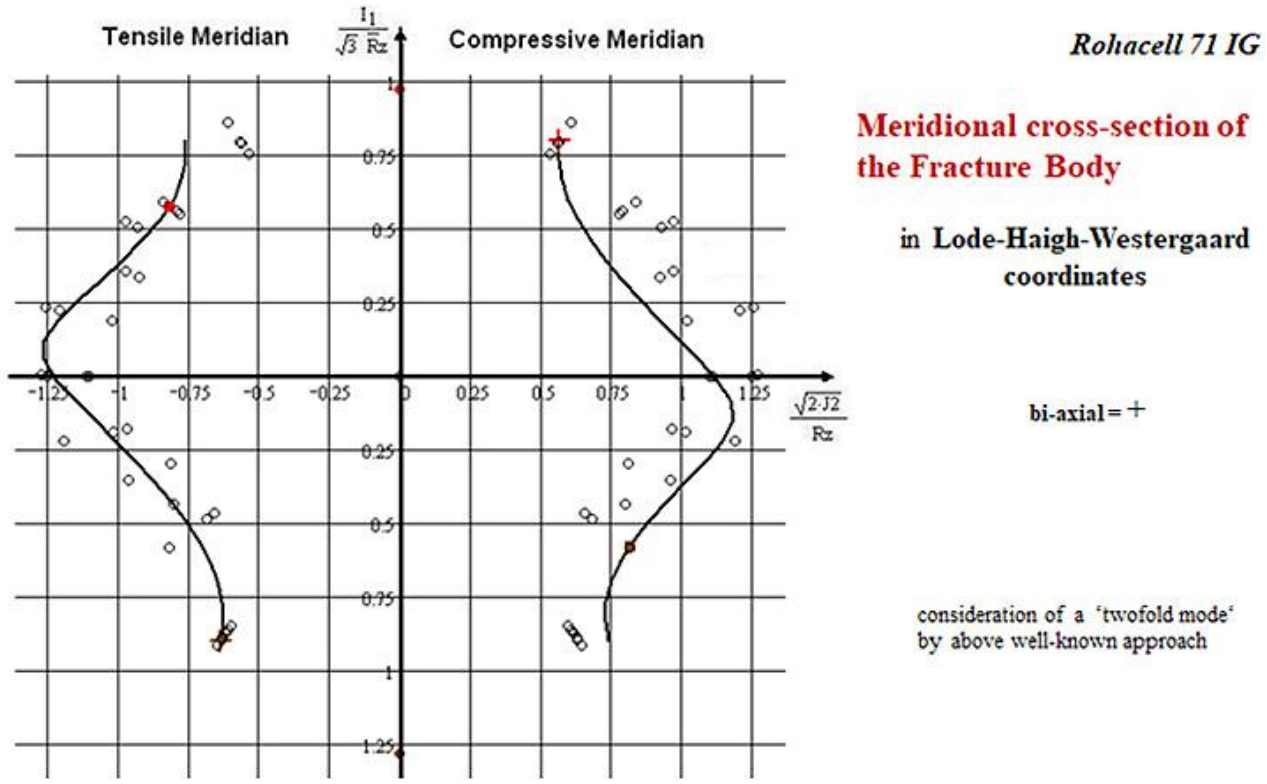


Fig.5-5: The test points are located at a distinct Lode angle of its associated ring o, 120°-symmetry. Cap and bottom are closed by a cone shape, a shape being on the conservative side

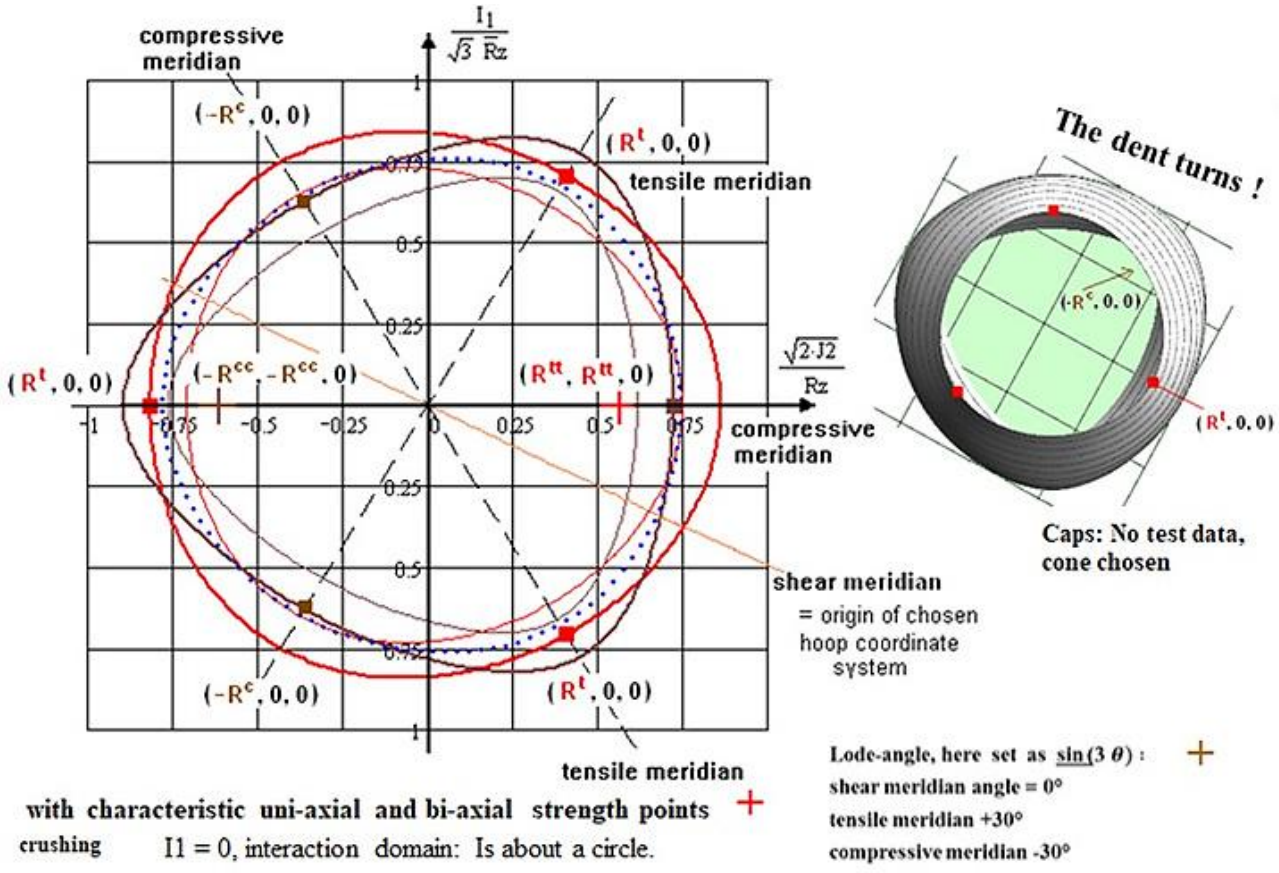


Fig.5-6: 2D Test Data and Mapping in the Orthogonal Stress Plane (brittle, porous)
Caps were taken away to better visualize that the dent turns for this material along the hydrostatic axis. Bar over not set

As still mentioned, $F = 1$ or $Eff = 100\%$ mathematically defines the surface of the fracture failure body. Such a body is rendered here using the Lode-Haigh-Westergaard coordinates with $I_1/\sqrt{3}$ as y-coordinate and $\sqrt{2 \cdot J_2}$ as x-coordinate. *Fig.5-4* depicts the stress states belonging to a tensile meridian and to a compressive meridian. These are those axial cross–sections of the failure body (right) along most of the compression tests are run.

Mechanical strength behavior shows up: Different structural materials

- can possess similar material behavior or
- can belong to the same class of material symmetry.

Welcomed Consequence is: The same strength failure function SFC can be used for different materials. The Foam SFC is exemplarily applicable to Concrete Stone. → For concrete stone more information is available for pre-dimensioning + modelling in the case of a newly applied material from the foam experimental results as a still being tested similarly behaving material.

5.4 'Isotropic' Normal Concrete (slightly porous)

On the fracture failure body figure below the 3 main meridians are outlined. For the tensile meridian a Lode angle $\vartheta = +30°$ is valid and for the compressive meridian -30°. The shear meridian was chosen by the author as neutral meridian with a Lode angle $\vartheta = 0$. For each mode, the SFC model parameters must be determined in each associated 'pure' failure mode domain. To remember is:

bi-axial tension = 'weakest link failure behavior (schwächstes Glied'-Versagen)

bi-axial compression = redundant (benign) failure behavior (Stützwirkung)

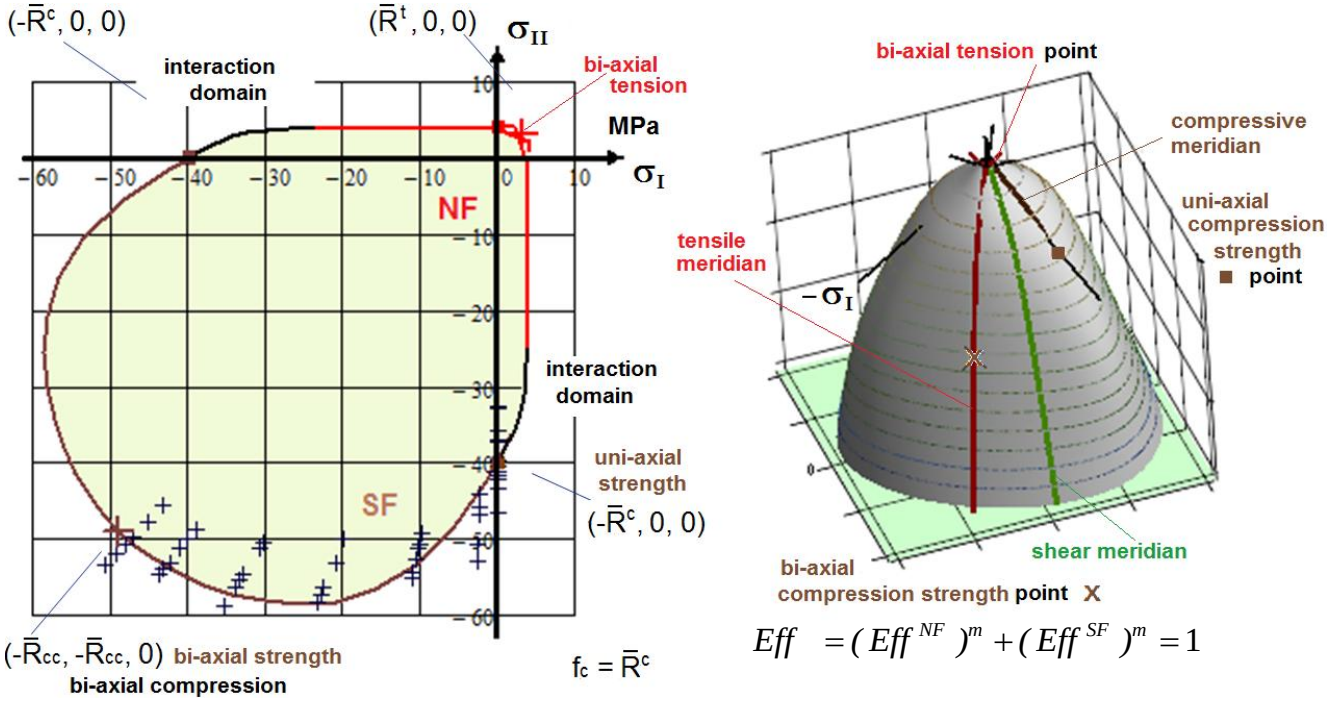


Fig.5-7: Normal Concrete, mapping of 2D-test data in the Principal Stress Plane (bias cross-section of fracture body). R:= strength ≡f;:.t:=tensile, c:=compressive; bar over means mean value. μ = 0.2. (test data, courtesy Dr. S. Scheerer, IfM Dresden).

$\bar{R}^t = 4$ MPa, $\bar{R}^c = 40$ MPa, $\bar{R}^{tt} = 0.8 \cdot \bar{R}^t$ (assumed) = 3.2, $\bar{R}^{ttt} = 2.81$, $\bar{R}^{cc} = 49$ MPa,
$\bar{R}^{ccc} = 1000$ MPa (set, necessary for computation), $\max I_1 = 8.43$; $\min I_1 = -4.58$, $m = 2.5$
120°-rotationally-symmetry parameter: $c_{1\Theta}^{SF} \cdot \Theta^{SF} = 1 + c_{2\Theta}^{SF}$ with $c_{2\Theta}^{SF}$ as friction parameter
$c^{NF} = 0.86$, $d^{NF} = 0.86$, $c_{2\Theta}^{SF} = 0.26$, $c_{1\Theta}^{SF} = 1.04$, $d^{SF} = 0.13$, $\Theta^{SF} = 0.51$, $s^{cap} = -1.31$.

LL:
There is a pretty large scatter of the compressive strength data in Fig.5-7. Mapping of the course of test data with the SFCs worked very well.

Fig.5-8 through 5-*10* present a hoop cross–section (π plane) and two axial cross-sections (meridians) of the failure body. One recognizes that with increasing negative I_1 the hoop shape becomes more and more circular.

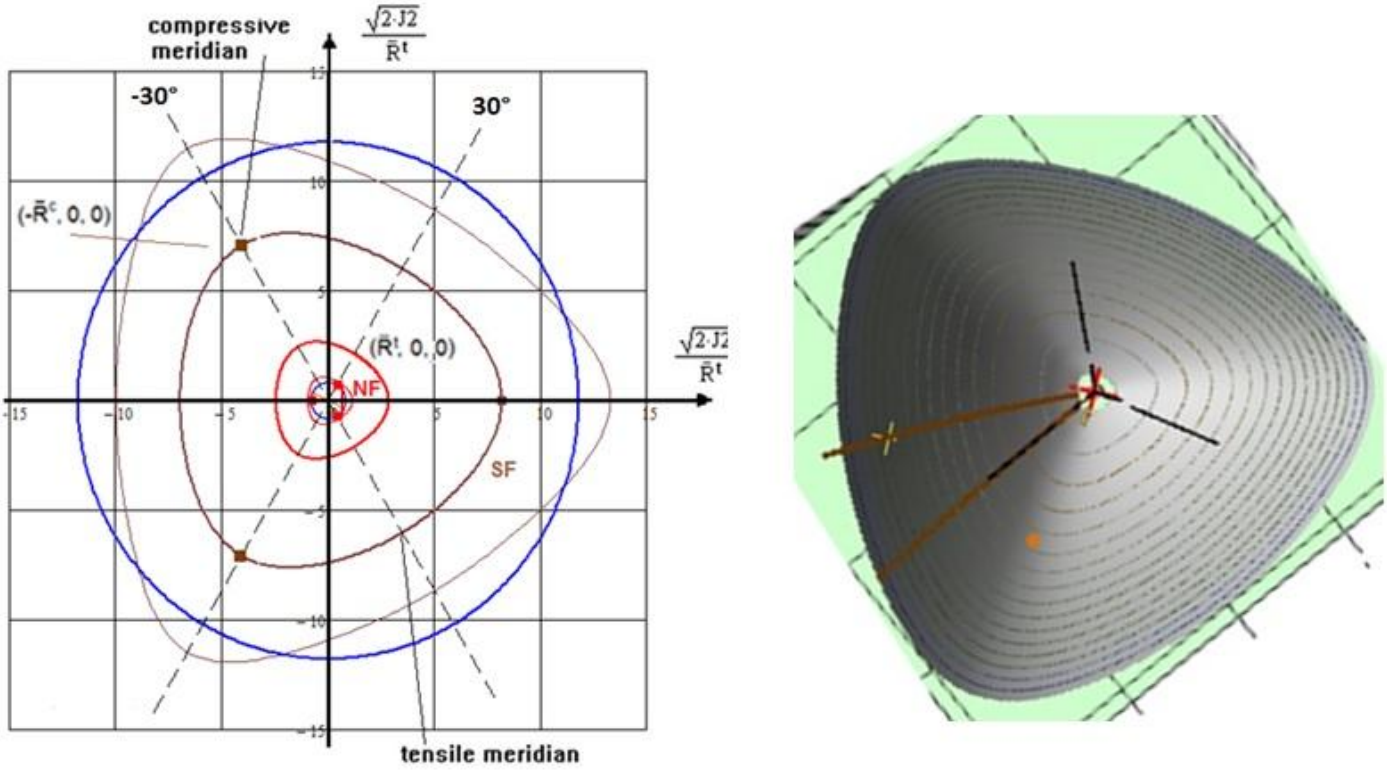


Fig.5-8: Octahedral stress plane or π-plane and view from top
*(**blue** means plane at I_1=0)*

In *Fig.5-9* the modeling of cap, normal and shear fracture domain is depicted.

Modelling of the cap is performed by the function $y_{cap} = \frac{I_1}{\sqrt{3} \cdot \bar{R}^t} = s^{cap} \cdot \left(\frac{\sqrt{2J_2 \cdot \Theta^{NF}}}{\bar{R}^t}\right)^2 + \frac{\max I_1}{\sqrt{3} \cdot \bar{R}^t}$.

Fig.5-10 informs about the test data scatter of the 3D fracture states experienced under hydrostatic pressure when running test on the tensile meridian and on the compressive meridian (-30°).

Test data source and evaluation, Test data from Dr. Scheerer and Dr. Speck, IfM, TU-Dresden. [*Courtesy Prof. Dr.M. Curbach*]: From their general data sets as sub-sets the meridian data sets, the constant Lode angles, have been extracted by the author.

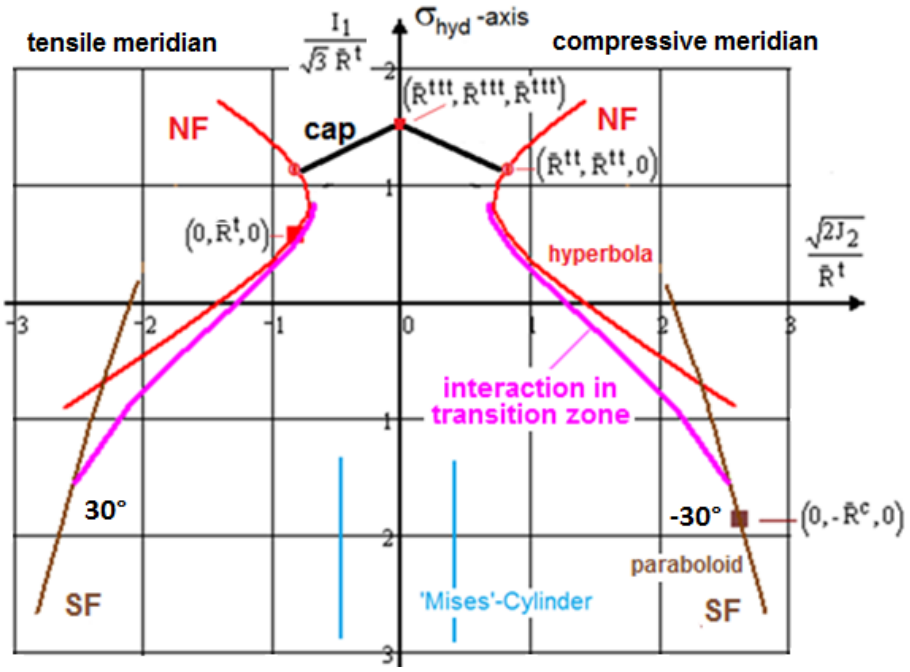


*Fig. 5-9: Visualization of the courses of the 2 mode mapping functions for NF and SF along the meridian cross sections of the fracture body and after **interaction***

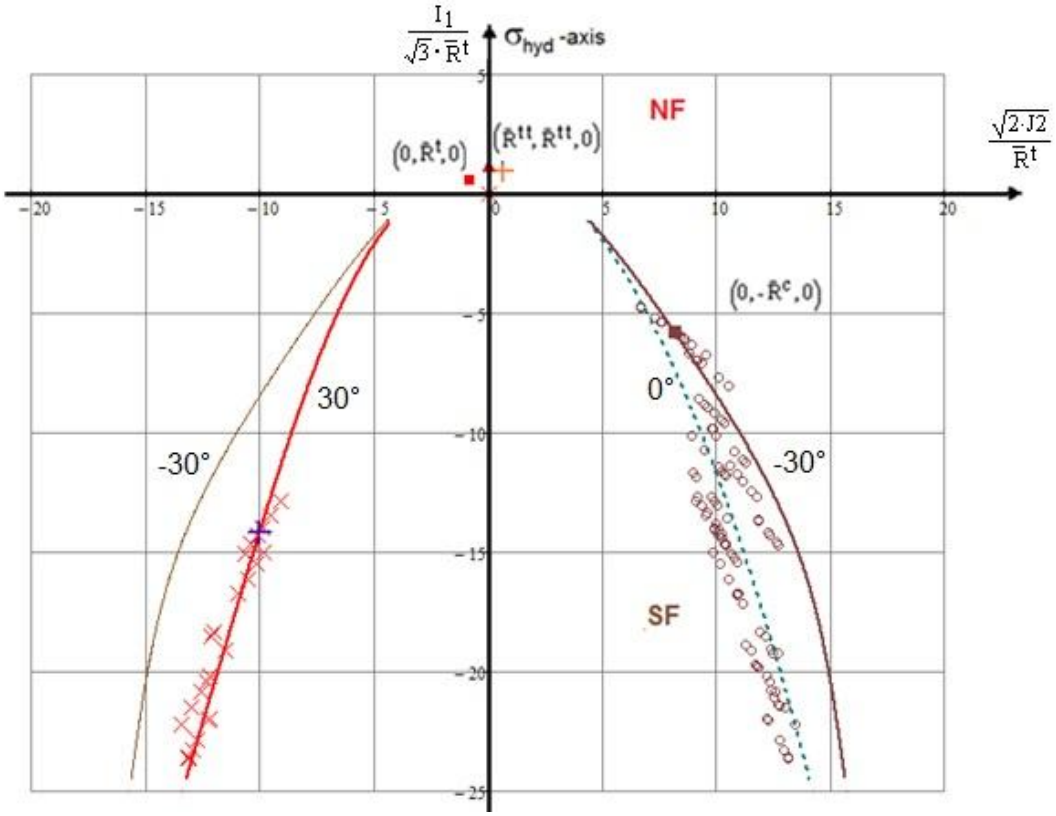


Fig.5-10.: Tensile meridian curve and test data (x, 30°), compressive meridian (-30°) curve and test data on the respective hoop ring o (these circles o are located *at different meridian angles 9), IfM Dresden*

The failure body possesses inward dents for $I_1 > 0$ and outward dents for $I_1 < 0$ in contrast to porous concrete stone, where it is also inward. These dents become smaller with increasing $|I_1|$. Due to the Poisson effect it should be checked whether the material may tensile fracture (NF) under biaxial compression, $\varepsilon_{axial} > \max\varepsilon$.

5.5 'Isotropic' UHPC (relatively dense)

Ultra-High-Performance-Concrete UHPC principally behaves similarly to Normal Concrete unless the normalized hydrostatic compression does not become larger than $|I_1/ R_t \cdot \sqrt{3}| \approx 10$ (> 300 MPa), see *Fig.5-10*. From about this stress state a different failure behavior takes places, which can be substantiated best by the still mentioned test result: Just a slight hydrostatic pressure of 6 MPa or N/mm^2 increases the uniaxial strength capacity from 160 MPa up to 230MPa - 6 MPa = 224 MPa!

$$\sigma_{fracture} = (\sigma_I,\ \sigma_{II},\ \sigma_{III})_{fracture}^{T} \ :\ (-160,\ 0,\ 0)^T \Rightarrow (-224-6,\ -6,\ -6)^T$$

This explains why for the less 'dense' Normal Concrete R^{cc}/R^c is higher than with UHPC.

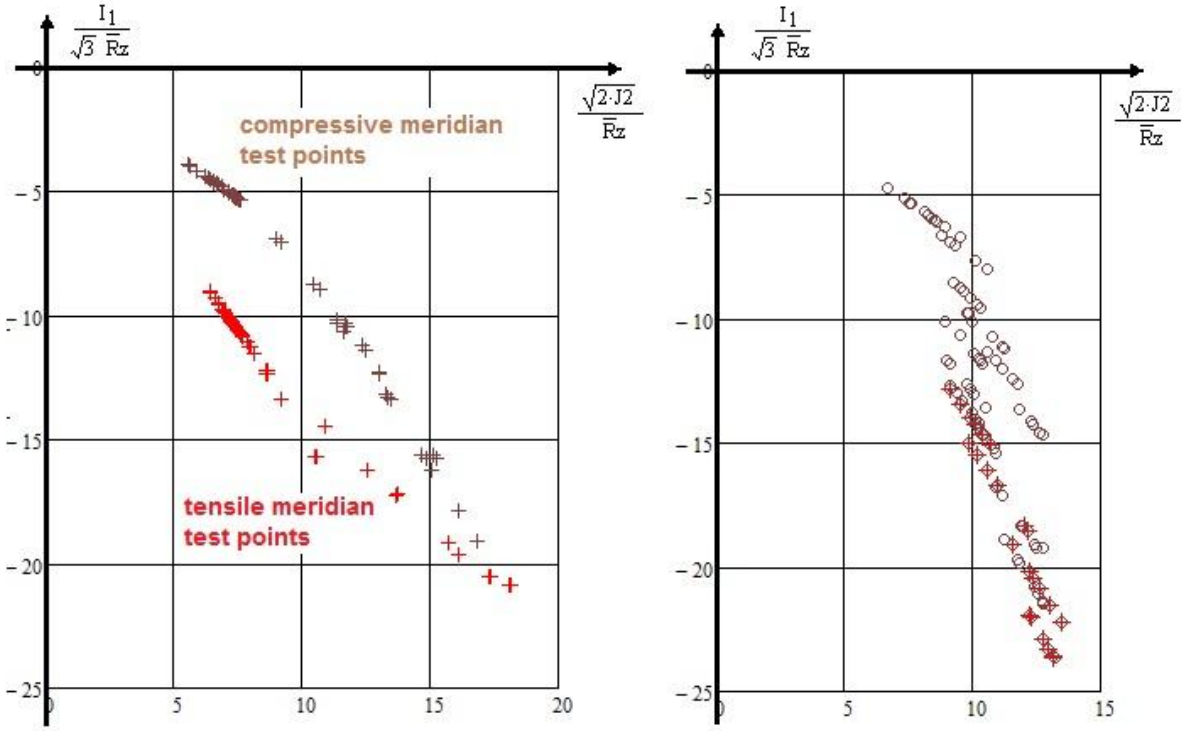
The author dedicates this to the still mentioned 'healing' of the flaw effects. If in addition to shear a volume change happens, then F^{SF} is to replace by F^{SFV} to capture also the dilatation effect, engineering-like, by

$$F^{SF} = c_{1\Theta}^{SFV} \cdot \frac{3J_2 \cdot \Theta^{SF}}{\bar{R}^{c2}} + c_{2\Theta}^{SFV} \cdot \frac{I_1}{\bar{R}^{c}} \ \Rightarrow\ F^{SFV} = c_{1\Theta}^{SFV} \cdot \frac{3J_2 \cdot \Theta^{SF}}{\bar{R}^{c2}} + c_{2\Theta}^{SFV} \cdot \frac{I_1}{\bar{R}^{c}} + c_{3\Theta}^{SFV} \cdot \frac{I_1^2}{\bar{R}^{c2}}.$$

Points for the determination of the SFV-curve are indicated in *Fig.5-12*. By the way, for fiber-reinforced plastics a similar redundant behavior occurs, see [*Cun13, 14*]. Again, mind the Poisson effect. The effortful calculation of the fracture body is in progress.

Fig.5-11 provides a mapping of those test data which are lying on the tensile meridian and on the compressive meridian. In contrast to Normal Concrete with usually relatively low hydrostatic pressure loadings UHPC experiences a hydrostatically activated effect, 'densification with volume shrinkage'. Therefore, the volume change must be considered by I_1^2 in the extended formula, see *Fig.5-12*.

The fracture body of a theoretically dense concrete (matrix) possesses in the high hydrostatic compressive domain ($I1 < 0$) an open fracture surface. Practically however, the fracture body is closed due to impacting flaws, i.e. porosities. Further, the bi-axial compressive strength $R^{cc} \equiv f^{cc}$ may be not only linked to SF but also to NF due to the Poisson's ratio activated tensile strain in the axial direction despite $\sigma_{ax} = 0$.
When searching the data set for the tensile meridian and the compressive meridian out of the full bunch of 3D test data the Lode angle or meridian angle ϑ, respectively, must be computed. It documents by the values which test point belongs more to the tensile meridian $\sin(3\vartheta) = 1$ or to the compressive meridian $\sin(3\vartheta) = -1$. The shear meridian angle reads $\sin(3\vartheta) = \vartheta = 0$.



UHPC test points: (left) tensile meridian + and compressive meridian +;
(right) all 3D test points are marked by **o** *(hoop ring), visualizing to be located at different meridians*

Fig.5-11 UHPC:Compressive and tensile meridian points

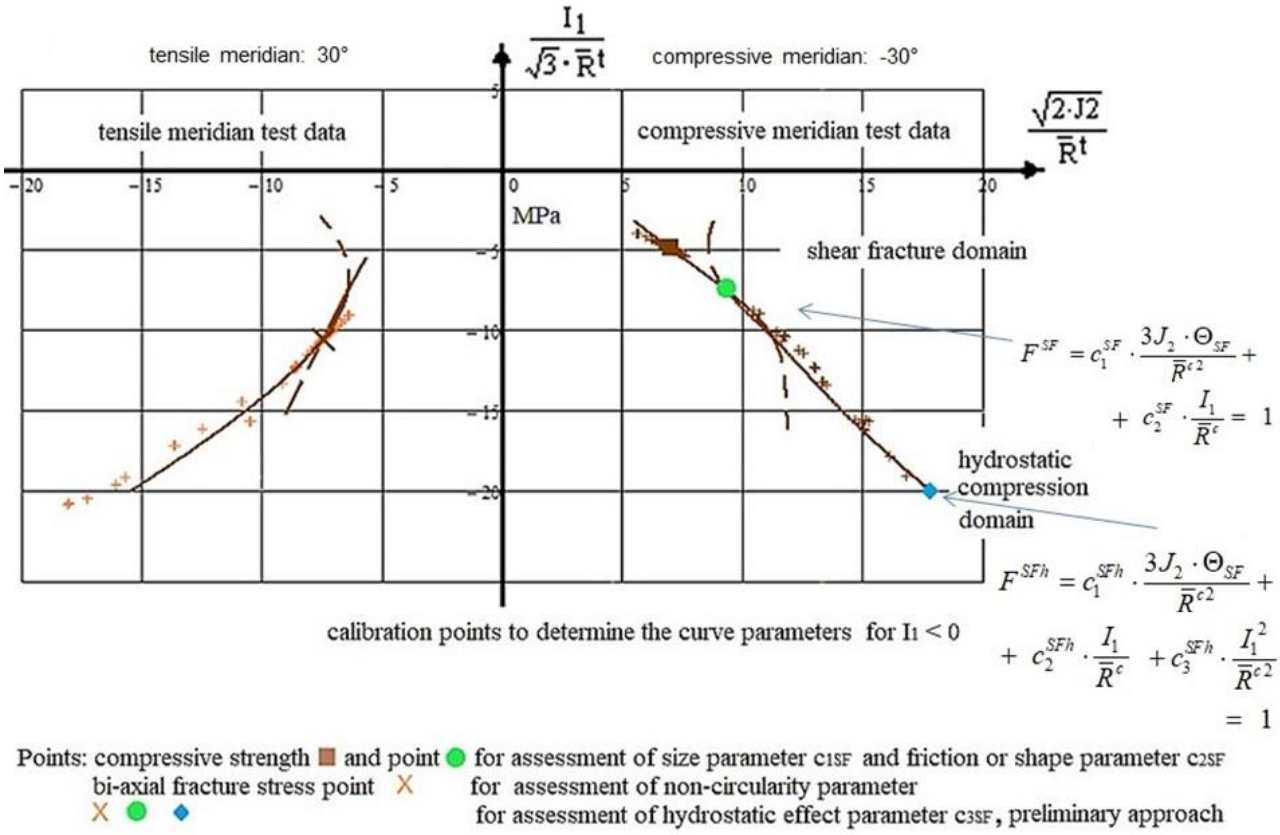


Fig.5-12 Ultra-High-Performance-Concrete (UHPC):
[Test data: Dr. Speck, IfM, TU-Dresden]. From this general data set as sub-sets the meridian data sets (constant Lode angles) have been extracted by the author

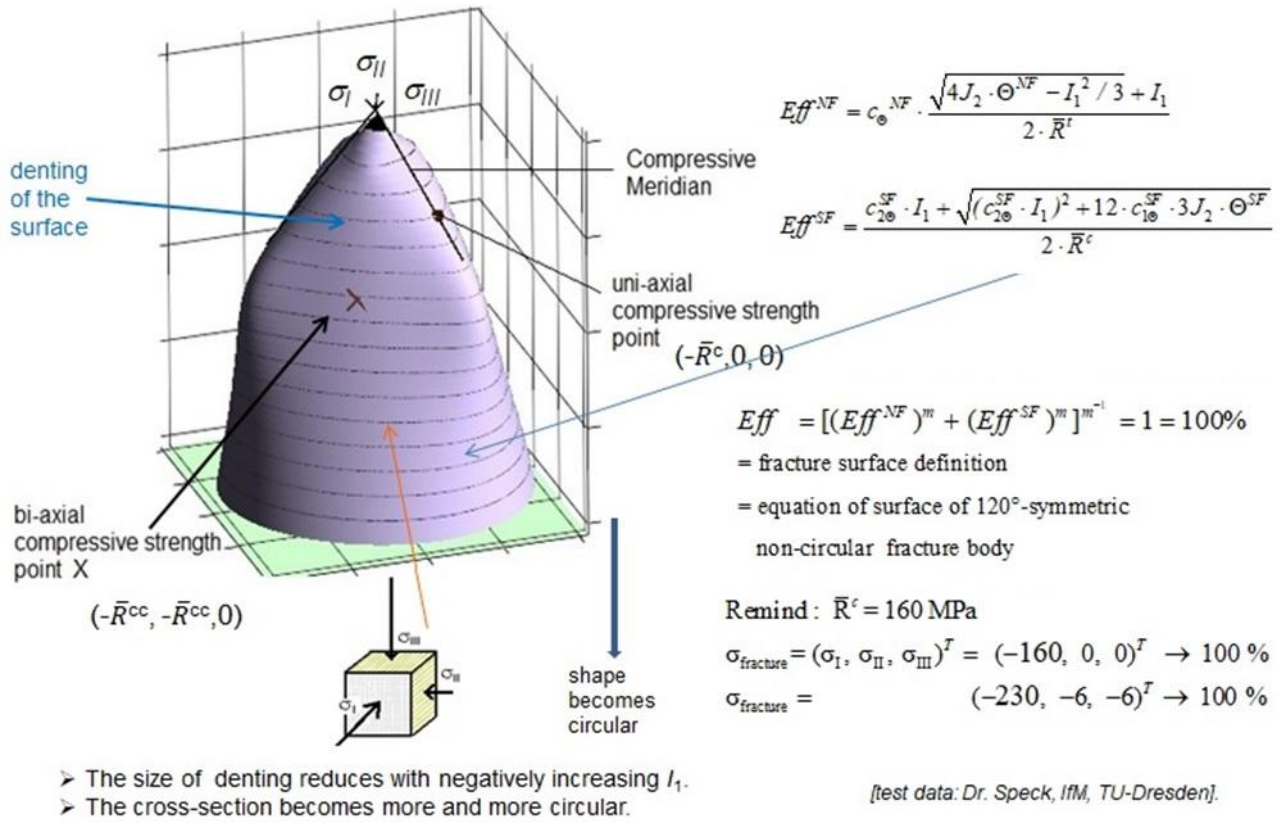


Fig.5-13, UHPC: Fracture body showing decay of denting with a negative I_1

Fig.5-14 shows a graph bi-axial compressive strength over uniaxial compressive strength. It turns out that with increasing uniaxial strength the bi-axial strength approximates the uniaxial strength.
The author tries to explain this:
The effect of redundancy under hydrostatic loading can be interpreted as an out-smoothing of stress concentrations. In the case of Normal Concrete this effect becomes more chances according to being more roughly grained than UHPC. This explains why the bi-axial strength capacity increase of a roughly grained Normal Concrete is higher than for UHPC.

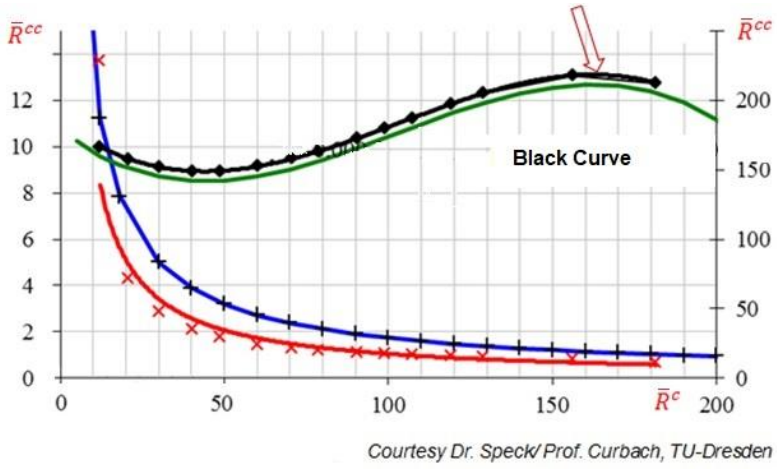


Fig.5-14: compressive strength capacity ratio of concrete $\bar{R}^{cc} / \bar{R}^c$ (R = f),
$\bar{R}^{cc} / \bar{R}^c$ (Normal Concrete) > $\bar{R}^{cc} / \bar{R}^c$ (UHPC)

In *Fig.5-15* are depicted the 2 mode domains and its transition zone obtained with the interaction formula.

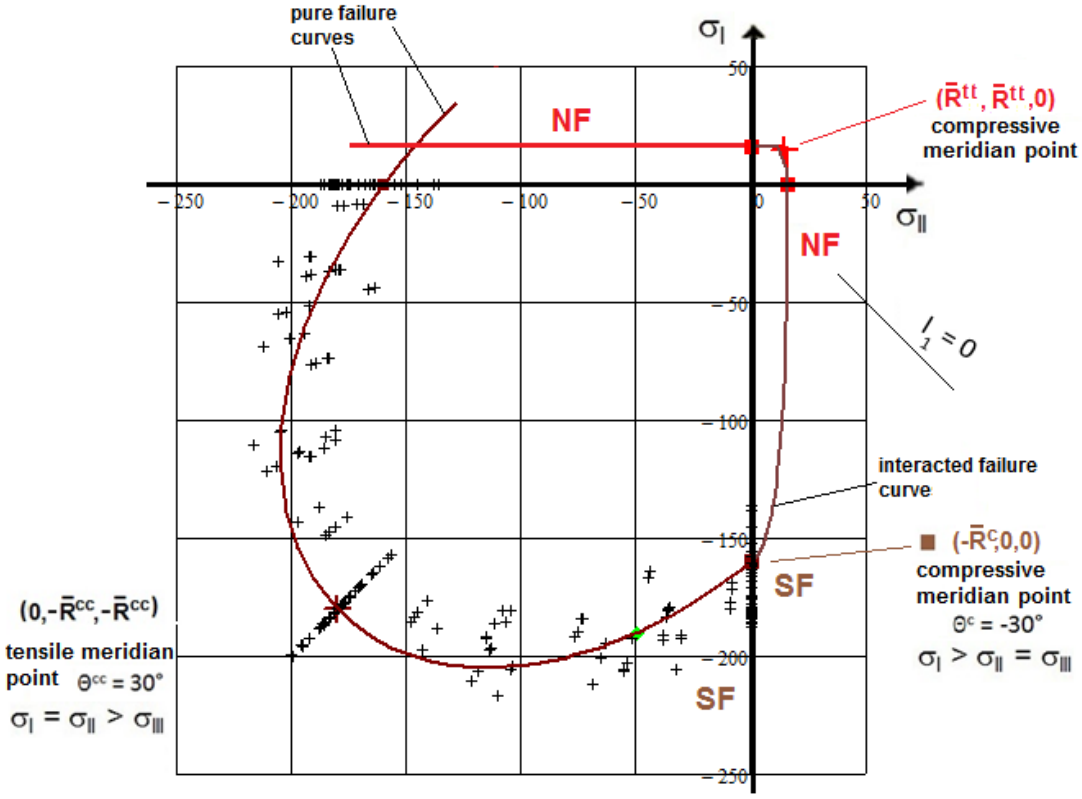


Fig.5-15, UHPC: principal stress plane with measured test data and evaluated strength points

Table 5-2 present some characteristic measured failure stress states. The table shows the Lode angle $\vartheta°$.

Table 5-2: Characteristic material data when evaluating UHPC fracture tests. E = 20000 MPa, ν = 0.2, $\tau_{max} = \sigma_I - \sigma_{III}$). $\sigma_{II} = \sigma_{III}$: $\varepsilon_{ax} = -2 \cdot \nu / E$.

	Stress state *in MPa*	$I_1/\sqrt{3}$ $/R^t$	$\sqrt{2 \cdot J2}$ $/ R^t$	τ_{max} *in MPa*	$(\sigma_{hyd}; \sigma_{ax})$ *in MPa*	$\vartheta°$	$\varepsilon_{ax\ el}$ *in* 10^{-3}	*remarks*
R^{tt}	(14, 14, 0)	1	0.7	-	-	-30	0.6	*two-fold NF*
R^c	(0 , 0, -160)	-5.8	8.2	80	(-0; -160)	-30	-8	Eff_{SF}
	(-6, -6,-230)	-8.7	11.4	111	(-6; -224)	-30	-11	
Compr	(-16,-16,-272)	-11.0	13.1	128	(-16; -256)	-30	-13	
essive	(-35,-35,-350)	-15.2	16.1	157	(-35; -315)	-30	-17	
	(-83,-83, -490)	-23.7	20.8	204	(-83; -407)	-30	-23	
comput.	(**-23,-23,-305**)	-12.6	14.4	141	(-23; -282)	-30	-15	
	(0,-175,-175)	-12.6	8.9	88	(0;-)	+30	3.5	*two-fold SF*
R^{cc}	(-2,-210,-210)	-15.2	10.6	104	(-2; -)	+30	4.1	
Tensile	(-24,-310,-310)	-23.2	14.6	143	(-24; -)	+30	5.0	
R^t	(-54,-388,-388)	-30	17	167	(-54; -)	+30	5.1	
	(16, 0, 0)	0.6	0.8	-	-	+30	0.8	Eff_{NF}
shear	(9, -9, 0)	0	0.8	9	-	0	0.5	$Eff_{NF} > Eff_{SF}$
change	(0,-52,-193)	-8.8	8.8	97	-	-15	-9.1	

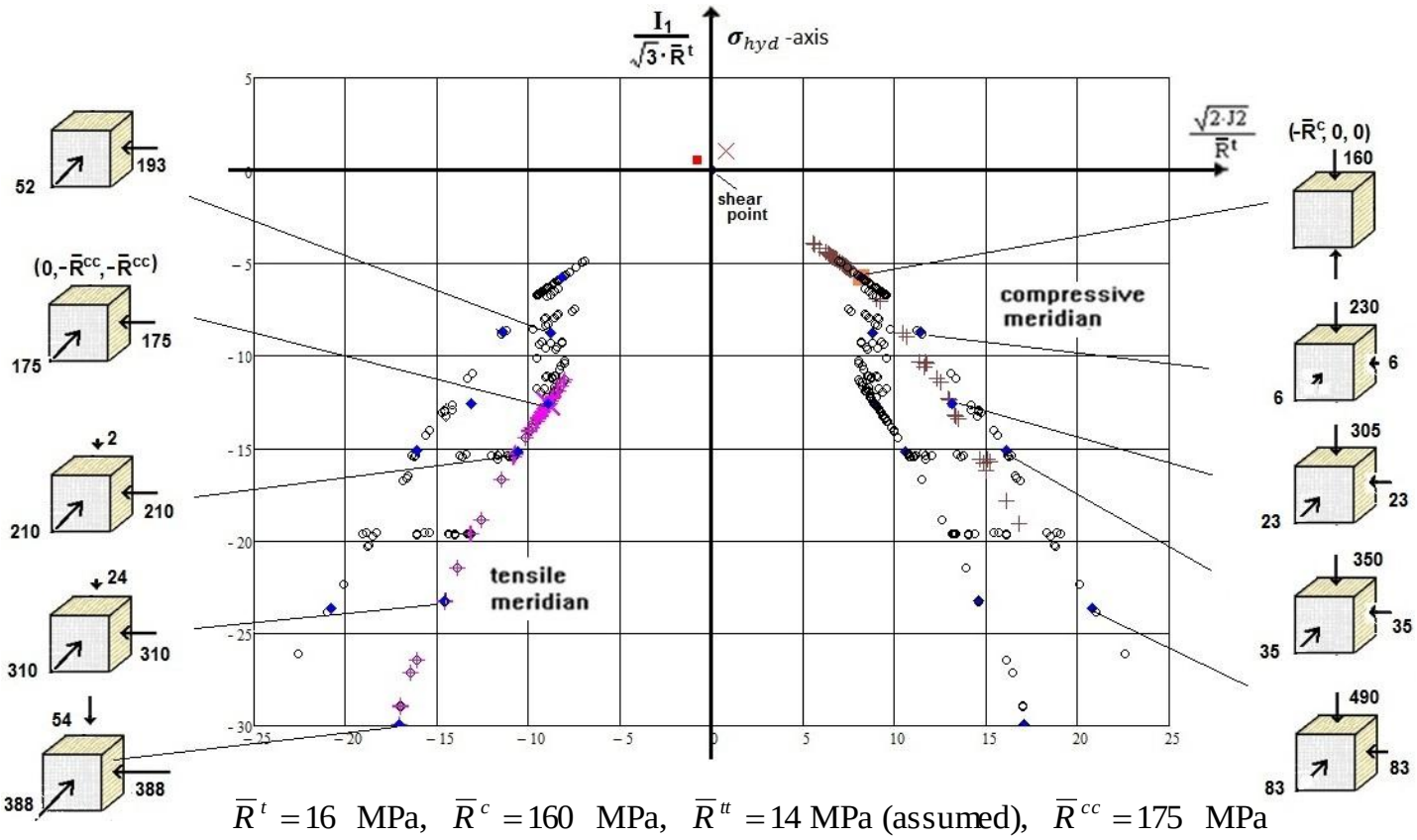


Fig.5-16, UHPC: Compressive and tensile meridian of the fracture body with associated stress states

Fig. 5-16 links multi-axial stress states to the Lode angle. Only stress states on the two meridians can be really depicted in the cross-sections. All other test points lie on the fixed hoop radius but on a Lode angle, different to +30° and -30°.

On basis of redundancy effects it may be concluded that with increasing hydrostatic pressure both the meridians run into a common scatter band → circle shape of the hoop. Then, the effect of flaws generating micro-damaging in this heterogeneous material reduces. Thereby, the fracture body (*has an open bottom fracture surface)* becomes more and more cylindrical.

5.6 Rock Material, example Sandstones

5.6.1 Required Properties for Underground Rock Failure Stress Analysis

Tension domain:

Also in rock materials in the vicinity of excavations and boreholes tensile stresses will occur. Further, an undesirable brittle sudden failure is to prevent when a bore-hole is drilled. Therefore, the tensile strength proof requires a tensile strength $\bar{R}^t$ for the distinct rock material.

An estimation for the tensile strength value delivers the Brazilian splitting test (*indirect* tensile strength test) because a classical tensile test specimen is merely to obtain. A solid cylinder or disk (short cylinder) test specimens is used for the initially crack-free (intact) material, see *Fig.5.6-1*. The evaluation is performed via the formula $f_{sp} = \bar{R}^t = 2\cdot q\ /(\pi\cdot d\cdot \lambda)$ [*The constructor.org*].

This difficulty caused researchers to predict a value by using a Mohr-Coulomb-based SFC but the determined value is doubtful. In this context the author fully supports Mingqing You [*You15*] that a

tensile strength R^t is a separate parameter and cannot be estimated by models working in the tensile-compressive transition zone. Chapter 7.1 investigates the Mohr-Coulomb model (*physically just a friction-related compression domain model which runs into the tensile domain but is not representative for the tensile domain*) and clearly derives that the Mohr-Coulomb model is applied in the transition zone between the Normal Fracture mode under tension and the Shear Fracture mode under compression. The result in sub-chapter 8.1 and in Fig.5.6-1 is: A real value for $\bar{R}^t$ is only to obtain by a uniaxial tensile stress test $\{\sigma\} = (\sigma^t_{ax} = F^t/A,\ 0,\ 0)^T$

Compression domain:

Usual test series for concrete material (*see the concrete applications before)* are performed along the compressive meridian and not so often along the tensile meridian. For the general demonstration of concrete strength capacity, however, the full fracture failure body is required because all mixed 3D-compressive stress states are principally possible.

In rock mechanics the stress situation is linked to stress states along the compressive meridian. This explains why no bi-axial strength $\bar{R}^{cc}$ is provided in rock literature (entity that enables to describe the 120°-symmetry). However, it simplifies the task: Just the functional description of the compressive curve remains of interest.

A stress state in a material, formulated in Mohr's *mathematical* stresses, reads

$\{\sigma\} = (\sigma_I,\ \sigma_{II},\ \sigma_{III})^T$ with σ_I becoming the smallest failure stress (most positive)

$\sigma_I > \sigma_{II} > \sigma_{III}$ mathematically and σ_{III} the largest compressive failure stress (most negative).

Tensile stresses must be signed positive in this context, otherwise confusion becomes extreme!

For the tensile meridian follows $\{\sigma\} = (\sigma_I,\ \sigma_{II},\ \sigma_{III} = \sigma_{II})^T$ with $\sigma_I = \sigma^t_{ax} - p_{hyd}$

and the compressive meridian $\{\sigma\} = (\sigma_I = \sigma_{II},\ \sigma_{II},\ \sigma_{III})^T$ with $\sigma_{III} = \sigma^c_{ax} - p_{hyd}$.

The tensile meridian captures $\bar{R}^{cc}$ (and $\bar{R}^t$, in the domain of the Normal Fracture mode) and the compressive meridian captures $\bar{R}^c$ (and $\bar{R}^{tt}$, in the domain of the Normal Fracture mode).

In rock mechanics the term hydrostatic pressure, used, when testing concrete and UD material, is to replace by the Confining Pressure CP. This makes to introduce some definitions of rock mechanics terms: *Here, tensile stress is still negative, but not always which makes literature interpretations difficult!*

- Multi-axial rock compressive strength capacity [Y*ou15*]
  (the stress-sketch in Figure 1 of [Lan19] must be corrected. It does not fit to the provided failure stress states. In Fig.5.6-1 this is corrected)
  $\sigma_{III} \equiv \sigma_S \equiv \sigma_1$ termed here *minor* principal stress
- 1D uniaxial strengths: UTS = $\bar{R}^t$, UCS = $\bar{R}^c$
  Unfortunately the author found different meanings: In engineering design dimensioning UTS means Ultimate Tensile Strength and not Uniaxial Tensile Strength and UCS ultimate compressive strength *(still also applied in 'geo engineer'! Why is it not generally used in rock mechanics?)* and not for instance Unconfirmed Compressive Strength [*Wikipedia*]. UCS stands for the maximum axial compressive stress that a specimen can bear under zero Confining Pressure CP (*compressive stress*), which means it is nothing else than the usual simple standardized technical compression strength $\bar{R}^c$ in engineering
- ✓ Confining pressure CP: maximum level of hydrostatic compression applied in a tri-axial compression test of a concrete, a rock material or a neat resin test specimen defined by

$\{\sigma\}$ = ($\sigma_{ax}{}^{t}$ - CP , -CP, -CP) or with $\sigma_{ax}{}^{c}$ (tensile meridian)

$\{\sigma\}$ = ($\sigma_{ax}{}^{c}$ - CP , -CP, , -CP) (*induced by test rig brushes in case of concrete*)

✓ Confining lithostatic pressure: CP = p_{hyd} + overlying weight.

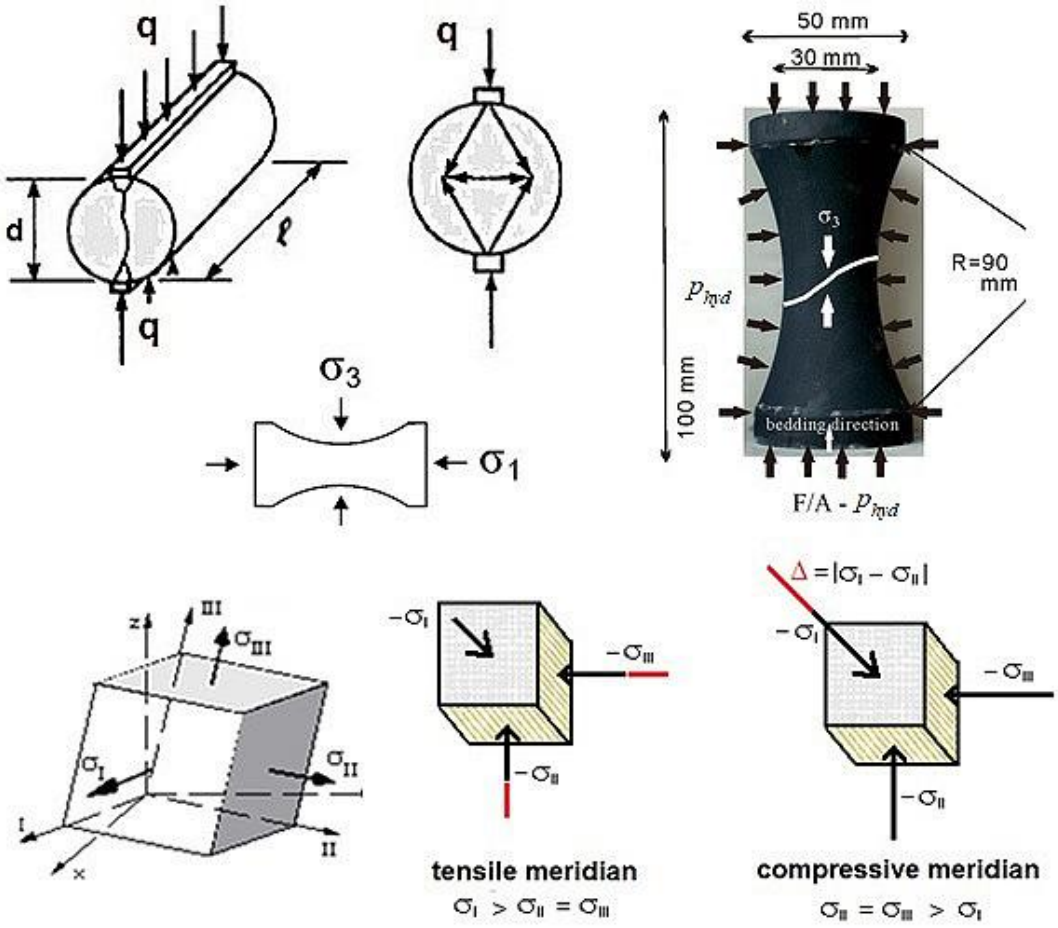


Fig. 5.6-1: Brazilian cylinder or disk (short length) for an indirect estimation of $\bar{R}^t$ *and dog-bone (sealed, highest preparation effort, grinding from solid block with axial bedding layers) test specimen for direct measurement of tri-axial fracture stress states along compressive meridian including the tension-compression domain.*
(Δ *depicts the differential stress entity causing shear stress with shear deformation)*

The author would like to conclude: *using usual mathematical stresses and taking a look at Fig.5-16*

- Sealed, polished dog-bone test specimens deliver the failure stress points ($-\bar{R}^{ccc}$,$-\bar{R}^{ccc}$,$-\bar{R}^{ccc}$) no pore pressure, ($-\bar{R}^{c}$, 0, 0) , ($\bar{R}^{t}$, 0, 0) and further multi-axial compressive failure stresses on the compressive meridian.
- A bi-axial compressive failure stress ($-\bar{R}^{cc}$,-, 0) is obtainable by the dog-bone test specimen for $\sigma_1 = 0$ or $\sigma_{ax}{}^{t} = -CP$. However, the author did not find one single bi-axial strength value $\bar{R}^{cc}$ in the papers he examined!
- A bi-axial tensile failure stress ($\bar{R}^{tt}$, $\bar{R}^{tt}$, 0) can be obtained by cube test specimens prepared by a good gluing in order to load the needed bi-axial tensile stresses.

Test procedure: The confining pressure CP is achieved and then kept constant during the test. The axial stress σ_1 is increased at a certain rate until the test specimen fails at $\max\sigma_1$. It is to consider whether the porosity of the rock or the soil material and the saturation plays a role.
Fig.5.6-2 presents fracture pictures of the investigated Berea sandstone. Essential is that the fracture angle increases with CP.



Fig.5.6-2 Sandstone: Fracture pictures of Berea sandstone from [Lan19].

The author's definition of the center of the transition zone between the tensile domain and the compressive domain is when the first invariant becomes zero:

$$I_1 = \sigma_1 + \sigma_2 + \sigma_3 = 0, \text{ means pure shear. For } \sigma_2^c = \sigma_3^c \rightarrow \sigma_1^t = 2 \cdot \sigma_3^c .$$

The ability for mobilizing friction processes depends on active compression stresses that cause via the friction value μ the necessary shear.

> Keep in mind, please:
> Unfortunately, engineers in other disciplines become pretty stressed because we civil engineers use construction design tools which still call tensile stresses negative stresses, so as depicted in the *Fig.5.6-3*. This completely disturbs the logic of the well-known 'civil engineer' Mohr in context with the definition of his mathematical stresses!

5.6.2 Test data for three sandstone materials

Some data sets from tests, running along the compressive meridian, were available for the foreseen modelling and further investigation. The graphs in *Fig.5.6-3* are formulated in rock mechanics terms. For general purpose, these graphs at first have to be transformed from the usual rock-mechanics depiction into the standard mechanical one in Lode coordinates. For this the usual rock mechanics letters will be used (*unfortunately these letters fully confuse with the standard fiber-reinforced UD composite indices*)

$$\{\sigma\} = (\sigma_1,\ \sigma_2,\ \sigma_3 = \sigma_2)^T \quad with \quad \sigma_1 \equiv \sigma_{III} = \sigma_{ax}^c - CP, \quad \sigma_2 = -CP.$$

As long as $(\sigma_1^t, \sigma_2^c, \sigma_3^c = \sigma_2^c)$ is given, due to the confinement in this so-called "*confined, direct tensile test on intact rock*", friction processes still act which influence the combined failure stress state in this transition zone before tension cut-off. It is not mentioned i.e. in [*Lan15*], how the bi-axial tensile stresses are applied to the test specimen. Test results show in the transition zone: Frictional processes diminish when passing $(\bar{R}^{tt}, \bar{R}^{tt}, 0)$ and failure becomes dominated by tensile strength $\bar{R}^t$ and the bond between the grains. The graphs unfortunately use different scales. Therefore, for a better comparison *Fig.5.6-4* was generated.

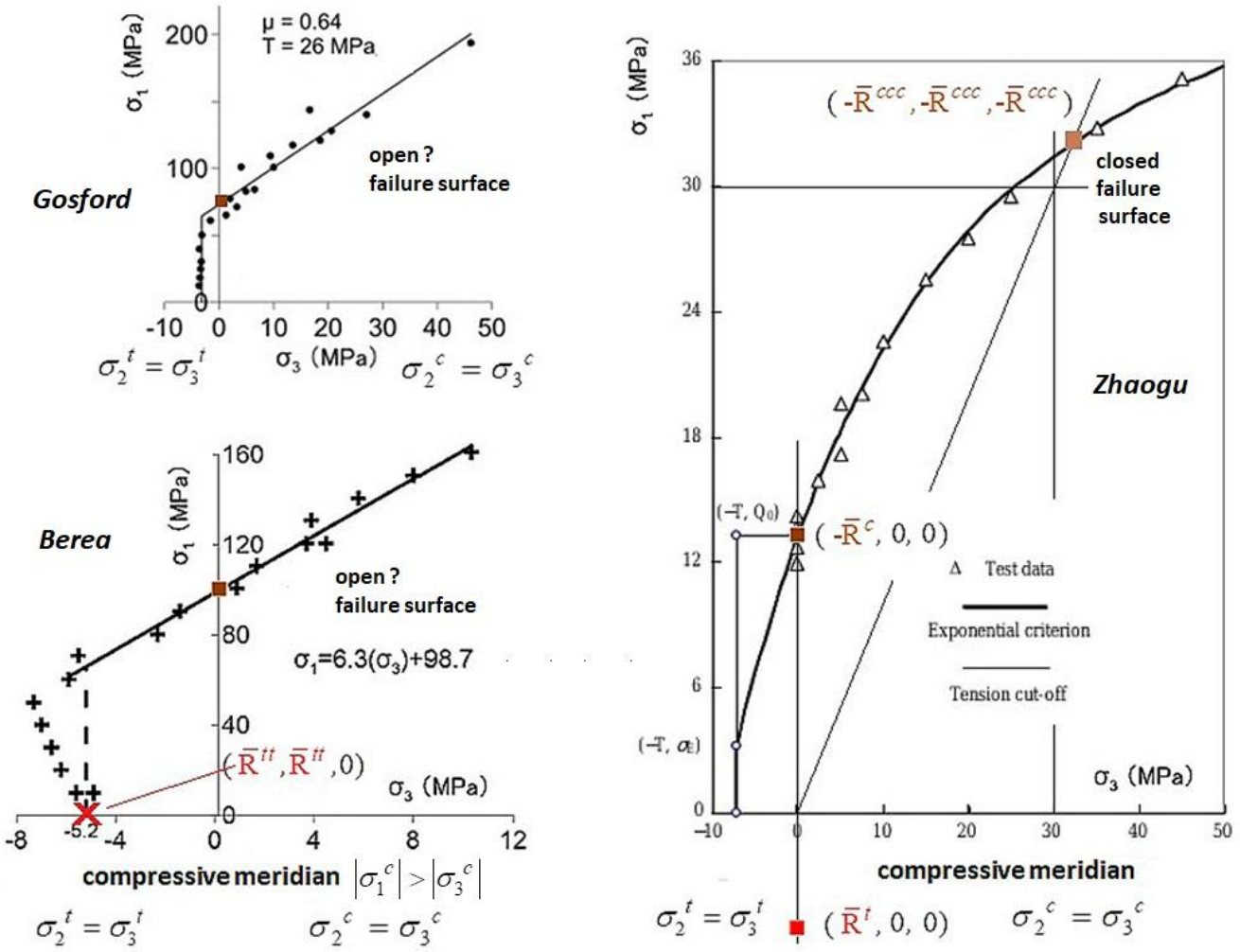


Fig. 5.6-3: Three sandstone materials with depiction of the failure stress points = 'strength'. (left down) Berea sandstone [Lan19}; (left up Gosford sandstone [Lan19]); (right) Zhaogu sandstone [You15].

The courses of test data in *Fig.5.6-3* are presented for the different sandstones and show different scaling. Only a presentation with the same scaling enables to draw comparative conclusions, *Fig.5.6-4*.

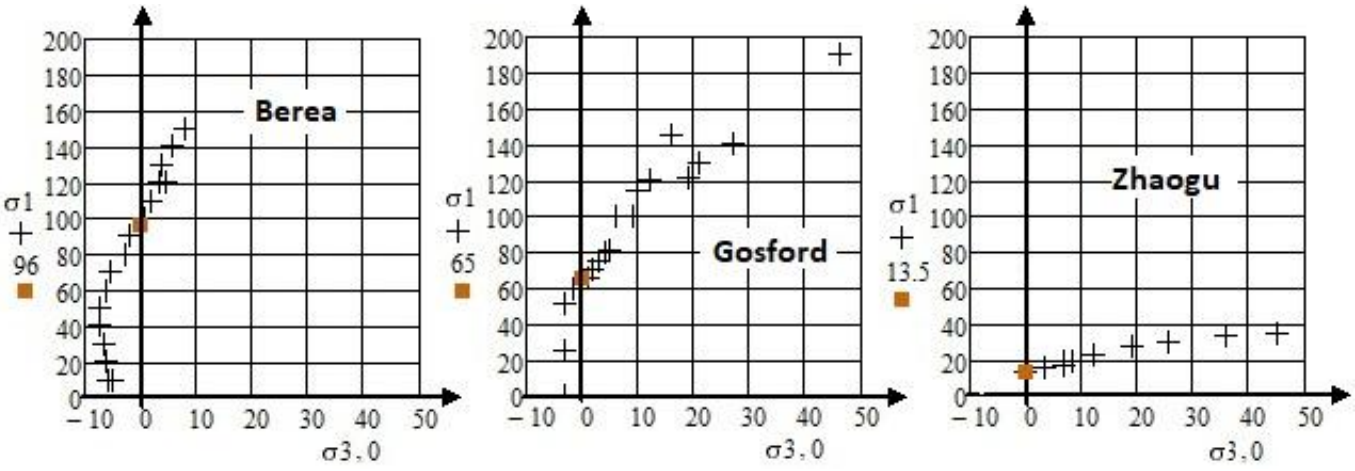


*Fig. 5.6-4: Comparison for Berea, Gosford and Zhaogu sandstones, same scale.(*tensile stress is negative using the convention in civil engineering)

From interpretation of the given test data sets in literature, depicted in the equally scaled *Fig.6.6-5*, the author likes to conclude:

(a) Berea sandstone, Figure 2 in [*Lan19*]: $\mu \approx 0.76$ *(computation),* failure surface seems to be open.

From the course of the test data can be derived $\bar{R}^t \cong 6$ MPa, $\bar{R}^c = 96$ MPa . No bi-axial compressive strength $\bar{R}^{cc}$ is provided for this sandstone material. Missing $\bar{R}^{cc}$ means: The fracture failure body cannot be computed like for the concrete materials. Bi-axial strength is to know to sort out whether a 120°-symmetrical failure body or a fully rotational one is to face. Remind: Tensile meridian and compressive meridian are the opposite axial cross-sections of the failure body (*see concrete material pictures before*).

Discussion Berea sandstone from *[You15]*: Was taken by the author as a challenge for the author's SFC application

- The author could not find how the bi-axial tensile stresses are introduced into the test specimen (*gluing devices*)
- The Berea sandstone shows no typical tension cut-off. Does this come from glueing in context with a suppression of the flaw impact on the failure by the axial compression?
- From experience with brittle materials the author was just one time confronted with such a huge friction value of a structural material, namely within WWFE-I, TC1, UD lamina, GFRP (I*n the WWFE the author could sort out that the responsible test points were not right*). This makes insecure for the Berea sandstone when mapping the course of test data. The friction value of $\mu = 0.76$ is very high compared to a usual concrete value which is a little above 0.2. This needs to be checked.
- The reason for the increase of the fracture angle (see *Chapter 7)* with CP needs to be discussed.
- The axial compression head plate causes friction under the plate and usually disturbs the 3D stress state. How essential was this?

(b) Gosford sandstone, Figure 5 in [*Lan19*]: $\mu \approx 0.39$, *failure surface seems to be open*

From the course of given test data can be derived,

$$\bar{R}^{tt} \cong 3.5 \text{ MPa}, \ \bar{R}^t \cong 4 \text{ MPa (assumed)}, \ \bar{R}^c = 65 \text{ MPa}.$$

Discussion Gosford sandstone from *[Lan15]*:

- The comparison with Berea shows a less steep increase $\sigma_1(\sigma_3)$
- Cuntze computed $\mu = (c2\tau - 1) / (3 \cdot c2\tau + 3) = 0.39$. In [*Lan19*] ahigh value of $\mu \approx 0.64$ is given, which needs to be checked.

(c) Zhaogu sandstone, Fig.4 in [*You15*]: $\mu \approx -0.46$, *failure surface seems to be closed*

From the course of given test data can be derived $\bar{R}^{ccc} \cong 32$ MPa and $\bar{R}^c = 13.5$ MPa. $\bar{R}^t \cong 7.2$ MPa (measured). As usual, no bi-axial compressive strength $\bar{R}^{cc}$ is provided for this sandstone material. Because the failure surface seems to be closed the closing bottom point on the axis is to estimate applying the previously used Awaji-formula.

$I_1 = -3 \cdot \bar{R}^{ccc}$, $J_2 = 0$: $I_1 / (\bar{R}^t \cdot \sqrt{3}) = -20$, $\sqrt{2 \cdot J_2} / \bar{R}^t = 0$

A closed fracture surface can be described by

$$F^{SF} = c_{1\Theta}^{SF} \cdot \frac{3J_2 \cdot \Theta^{SF}}{\bar{R}^{c2}} + c_{2\Theta}^{SF} \cdot \frac{I_1}{\bar{R}^c} = 1 \quad \Rightarrow \quad c_{1\Theta}^{SF} \cdot \frac{3J_2 \cdot \Theta^{SF}}{\bar{R}^{c2}} + c_{2\Theta}^{SF} \cdot \frac{I_1}{\bar{R}^c} + c_{3\Theta}^{SF} \cdot \left(\frac{I_1}{\bar{R}^c} \right)^2 = 1.$$

Discussion of *[You15]*:

- In Fig.1 and 2 (halite) of [*You15*] the increase of the axial compressive stress (termed there σ_s . *Why not σ_1?*) under CP = σ_3 increases as experienced. However in Fig.4 (Zhaogu sandstone) $\sigma_1(\sigma_3)$ is depicted with a never experienced low increase. Is this accurate? Is there a conversion error to be seen in context with the next point?
- Table 1 in [*You15*] should present $\bar{R}^c$ =13.5 MPa ≡ UCS but gives σ_1 = 132 MPa at CP = 45 MPa !?
- The last 2 test points *beyond* the tri-axial compression strength are to investigate. Mind in this context: Confirmed by fracture pictures found in literature the fracture usually shows a wide scatter and different fracture patterns, crushing with shearing acts
- A computed negative friction value underpins the question marks.

In advance of applying the author's FMC-based SFCs (criteria) a view at *Fig.5.6-5* will show the differences of the mapping approaches due to the failure criteria of Mohr-Coulomb (M-C) and Hoek-Brown (H-B). The Hoek-Brown parameters defined as σ_{ci} is the uniaxial compressive strength $\bar{R}^c$, m_i is a steep parameter based on the rock type, σ_1 the maximum absolute compressive stress and σ_3 the minimum compressive stress (Why does it not read 'negative CP'?).

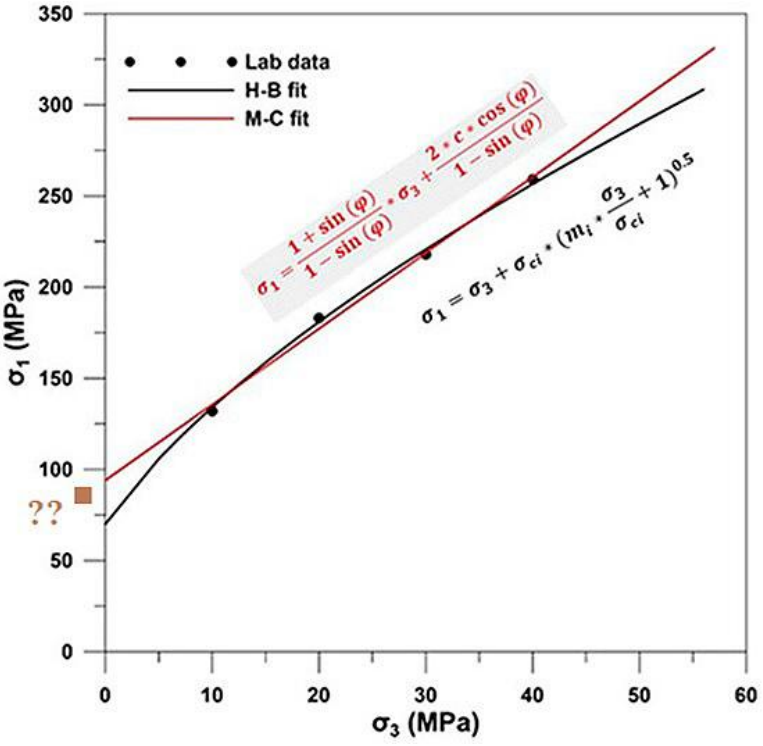


Fig.5.6-5: Geo Engineer, tri-axial compression test, Rock Laboratory, Testing Rock Mechanics. (compression stress here positive). 'Universal confined tensile strength' of intact rock. Available from: https://www.researchgate.net/publication/332447674_Universal_confined_tensile_strength_of_intact_rock

The linear M-C (*Mohr assumed that the mean stress σ_{II} is of no influence*) – due to its logic – just linearly maps by employing the friction angle φ. H-B maps non-linearly. However, why do both the approaches not run through the fix point 'compression strength' at $\sigma_1(\sigma_3 = 0) \rightarrow (-\bar{R}^c, 0, 0)$? No value is provided for $\bar{R}^c$, indicated in *Fig.5.6-5* by two question marks.

Fig.5.6-6 displays the course of data in the classical diagram using the physically-based Lode-Haigh-Westergaard coordinates. Tensile and compressive meridian belong to an axial cross-section of the fracture failure body. The two meridians outline a 120°-symmetric failure body.

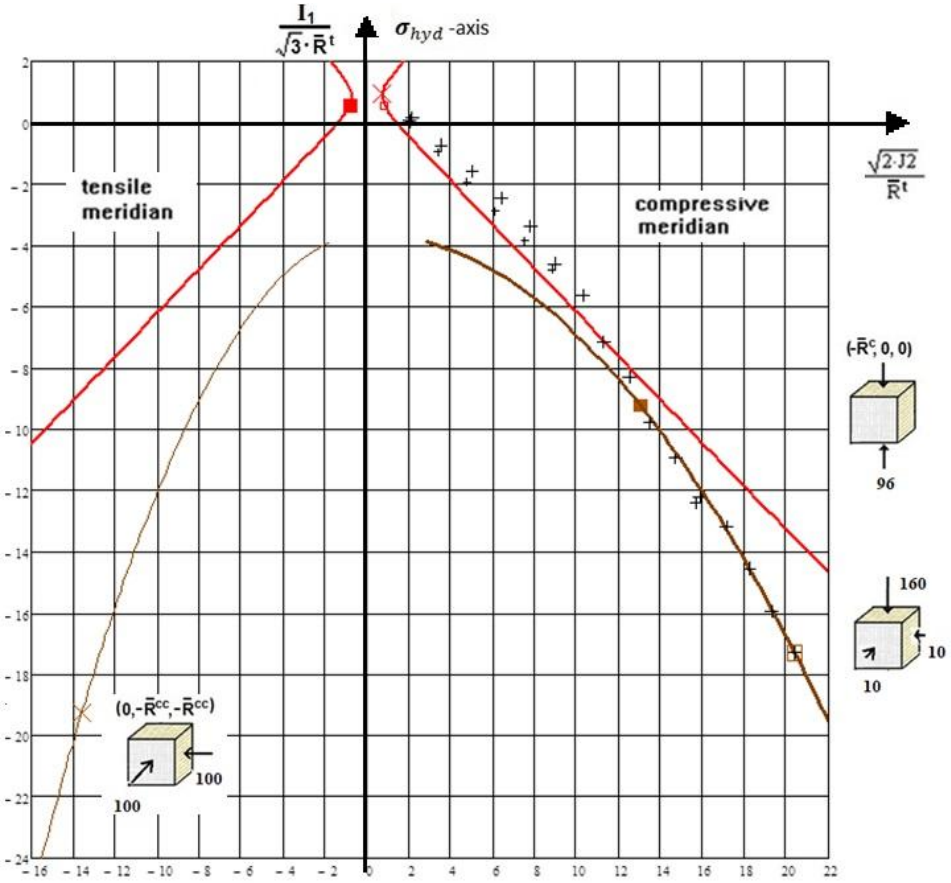


Fig.5.6-6 Berea Sandstone: Compressive meridian test data sets, not delivering $\bar{R}^{cc}$, X. Squares are uni-axial tensile and uniaxial compressive strength.
transition zone on compressive meridian between the modes, mapped by the interaction equation.
(here: tensile stresses are positive stresses due to the general convention in engineering).

$$\bar{R}^t = 6;\ \bar{R}^{tt} = 5.2;\ \bar{R}^c = 96;\ \bar{R}^{cc} = 100;\ d^{SF} = 1.06;\ c_{1\Theta}^{SF} = -3.21,\ c_{2\Theta}^{SF} = -2.54,$$
$$\vartheta^{SF^\circ} = -30°,\ \vartheta^{SF} = 0.5;\ m = 2.5.$$

The brown curve maps the course of test data in the negative domain experiencing Shear Fracture SF whereas the red curve experiences NF. The upper part of the compression meridian runs from the compressive strength test point $(-\bar{R}^c, 0, 0)$ through the transition zone follows with an end at the equi-biaxial tensile strength point $(\bar{R}^{tt}, \bar{R}^{tt}, 0)$. In the transition zone the contributions to failure come from NF together with SF failure events, which is due to the statistical and probabilistic flaw situation behavior. That usually is captured by an adequate interaction equation. The standard FMC-based interaction equation does not numerically work for this material since the SF curve lies

inward. Intentionally, in the transition zone, there was no fitting procedure for a better mapping of the course of test points employed just the two SFCs with the associate parameters were used with the compressive strength as fix point. This might be a further task.

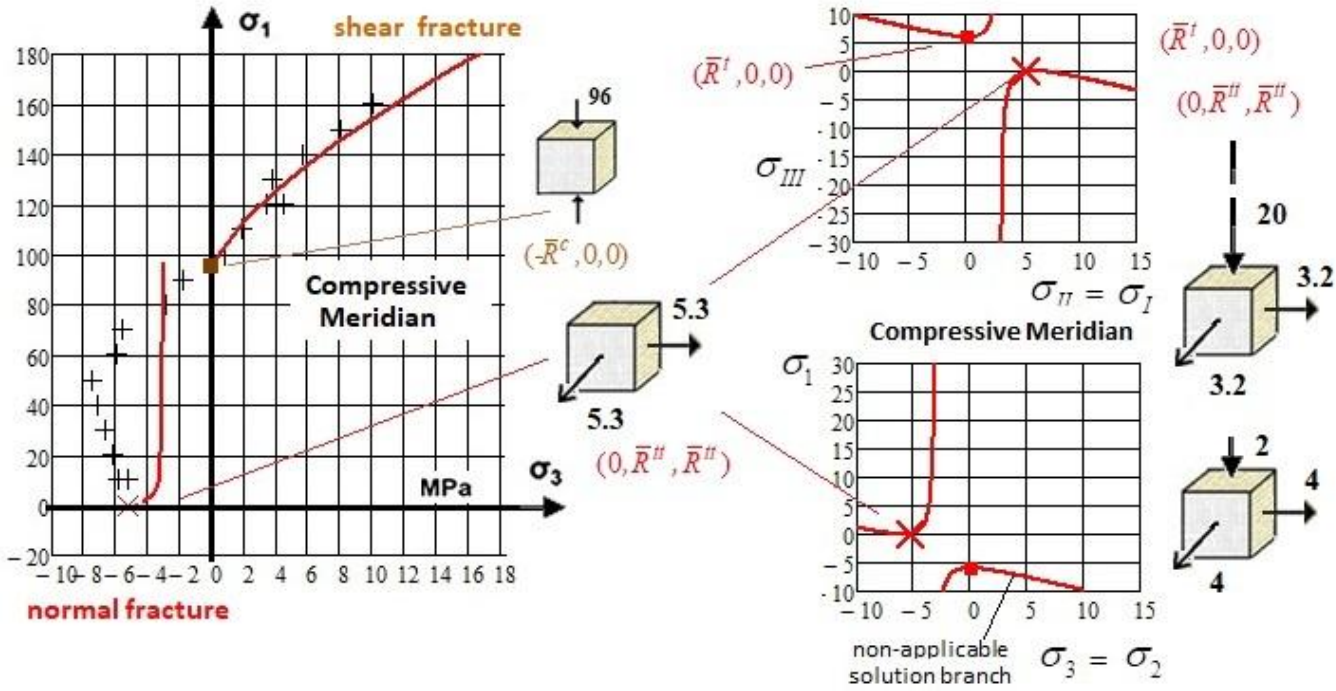


Fig.5.6-7 Berea Sandstone: (left) Simple mapping of the course of test data. X bi-axial tensile strength, square uniaxial tensile strength. (right) details in normal mode domain

General conclusions and specifically on Berea sandstone: *Fig.5.6-7*

Author's experience after mapping the 3D-fracture stress dates of various isotropic and of transversely-isotropic (*faced in layered rock materials, too!*) materials:

- Each domain has to be mapped separately in order to optimally fulfill physical conditions. In this context Mohr-Coulomb M-C is right if it just maps the compression domain with its shear fracture failure mechanism (SF). The cohesive strength $\bar{R}^{\tau}$ belongs to the transition zone and is more reigned by NF than by SF. The tensile domain belongs to normal fracture NF, and therefore needs another SFC
- The transition zone between these domains can be mapped by an adequate interaction condition – if necessary in the special material case - as performed by the author
- In the case of Berea sandstone the 'transition' test points directly follow the test points of the compression domain. Therefore no interaction equation is applicable and is to apply. Un-usually high friction values and (here combined) high ratios $\bar{R}^{c} / \bar{R}^{t}$ require different mapping in the transition zone
- In the full transition zone the test data points lie outside of the NF failure envelope. The author tried to improve the situation by taking a constant value of $\bar{R}^{tt} = 5.3$ MPa , indicated by the small crosses. It did not solve the (physical) problem
- Tension cut-off in the 3D-Lode diagram: Limit is defined by $I_1 / (\sqrt{3} \cdot \bar{R}^{t} = 1/\sqrt{3}$.

Following Mohr and his mathematical stress formulations and regarding the designations of rock mechanics all the relationships are collected in *Table 5.3*:

Table 5.3, isotropic materials: Collection of the respective relations and formulas

Fromulas for the Computation Procedure

$I_1 = (\sigma_I + \sigma_{II} + \sigma_{III}) \;=\; f(\sigma),\; 6J_2 = (\sigma_I - \sigma_{II})^2 + (\sigma_{II} - \sigma_{III})^2 + (\sigma_{III} - \sigma_I)^2 \;=\; f(\tau)$

$$27J_3 = (2\sigma_I - \sigma_{II} - \sigma_{III}) \cdot (2\sigma_{II} - \sigma_I - \sigma_{III}) \cdot (2\sigma_{III} - \sigma_I - \sigma_{II}),$$

$\sigma_I, \sigma_{II}, \sigma_{III}$ principal stresses, $\sigma_I > \sigma_{II} > \sigma_{III}$ mathematical stresses (> means more positive).

With the tradional rock mechanics letters the stresses read: regarding $\sigma_2 = \sigma_3 = CP$

$I_1 = (\sigma_1 + \sigma_2 + \sigma_3)$, $6J_2 = (\sigma_1 - \sigma_2)^2 + (\sigma_2 - \sigma_3)^2 + (\sigma_3 - \sigma_1)^2 = (\sigma_1 - \sigma_2)^2 + (\sigma_3 - \sigma_1)^2$

$27J_3 = (2\sigma_1 - \sigma_2 - \sigma_3) \cdot (2\sigma_2 - \sigma_1 - \sigma_3) \cdot (2\sigma_3 - \sigma_1 - \sigma_2) = 2(\sigma_1 - \sigma_3) \cdot (\sigma_2 - \sigma_1) \cdot (\sigma_3 - \sigma_1).$

For the determination of the failure curve in the transition domain the use of the *Eff*s is mandatory

$$Eff^{NF} = \frac{\sqrt{4J_2 - I_1^2/3} + I_1}{2 \cdot \bar{R}^t} = \frac{\sigma_{eq}^{NF}}{\bar{R}^t} \;\leftrightarrow\; Eff^{SF} = \frac{c_{2\Theta}^{SF} \cdot I_1 + \sqrt{(c_{2\Theta}^{SF} \cdot I_1)^2 + 12 \cdot c_{1\Theta}^{SF} \cdot 3J_2 \cdot \Theta^{SF}}}{2 \cdot \bar{R}^c} = \frac{\sigma_{eq}^{SF}}{\bar{R}^c}.$$

with $\Theta^{SF} = \sqrt[3]{1 + d^{SF} \cdot \sin(3\vartheta)} = \sqrt[3]{1 + d^{SF} \cdot 1.5 \cdot \sqrt{3} \cdot J_3 \cdot J_2^{-1.5}}$

tensile meridian angle 30° $\rightarrow \Theta^{NF} = \sqrt[3]{1 + d^{SF} \cdot (+1)}$; compr. meridian angle -30° $\rightarrow \Theta^{SF} = \sqrt[3]{1 + d^{SF} \cdot (-1)}$.

The tension-compression transition zone between the modes NF and SF - analogous to concrete - is mapped by the interaction equation that determines the surface of the fracture failure body:

$Eff = [(Eff^{NF})^m + (Eff^{SF})^m]^{m^{-1}} = 1 = 100\%$ total material stressing effort,

$$Eff = \sqrt[m]{\left(\frac{\sqrt{4J_2 - I_1^2/3} + I_1}{2 \cdot \bar{R}^t}\right)^m + \left(\frac{c_{2\Theta}^{SF} \cdot I_1 + \sqrt{(c_{2\Theta}^{SF} \cdot I_1)^2 + 12 \cdot c_{1\Theta}^{SF} \cdot 3J_2 \cdot \Theta^{SF}}}{2 \cdot \bar{R}^c}\right)^m} = 1.$$

It also determines the transition from the tension part $I_1 > 0$ of the compressive meridian to its compression part $I_1 < 0$.

Curve parameter relationships obtained by inserting the compressive strength point (0, -$\bar{R}^c$, 0):

* Rotationally symmetric: $c_1^{SF} = 1 + c_2^{SF}$, $d^{SF} = 0$, friction parameters are equal $c_2^{SF} \equiv c_{2\Theta}^{SF}$

* 120°-rotationally symmetric: $c_{1\Theta}^{SF} = 1 + c_{2\Theta}^{SF} \cdot \sqrt[3]{1 + d^{SF} \cdot (-1)}$ with $c_{2\Theta}^{SF}$ friction parameter .

c^{SF} , d^{SF} from the two points $(-\bar{R}^c,\ 0, 0)$ and (-$\bar{R}^{cc}$,-$\bar{R}^{cc}$, 0) or by minimum error fit .

The function for the compressive meridian curve - of interest is the pure compression domain - is derived by implicitely solving for σ_1, $CP = \sigma_3$ (explicitely is not possible here) with the

compressive meridian Lode angle δ = -30° $\rightarrow \Theta^{SF} = \sqrt[3]{1 + d^{SF} \cdot (-1)}$

$$\frac{c_{2\Theta}^{SF} \cdot I_1 + \sqrt{(c_{2\Theta}^{SF} \cdot I_1)^2 + 12 \cdot c_{1\Theta}^{SF} \cdot 3J_2 \cdot \Theta^{SF}}}{2 \cdot \bar{R}^c} = 1.$$

In the case of essential porosity the porosity-considering SFCs are to employ.

On the ‘peak of porosity’: Namibia, 300m high, largest sand dune of the world



5.7 Bi-axial strength of Solid Clay Brick Masonry

Here without any discussion, just three pictures of loadings in the principal stress plane shall be shown. For information see [*Pag81, Pag83, Pap96*]. Papa considers masonry as a composite material. Its mechanical properties are obtained by taking into account the properties of the components brick and mortar through a homogenization technique. To describe the behavior of the material components a unilateral damage model is proposed by him that is based on three micro-damage variables. The model was applied to the simulation of tests on masonry panels and miniaturized walls [*Pap96*]. Numerical results are discussed by Papa and successfully compared with experimental data.

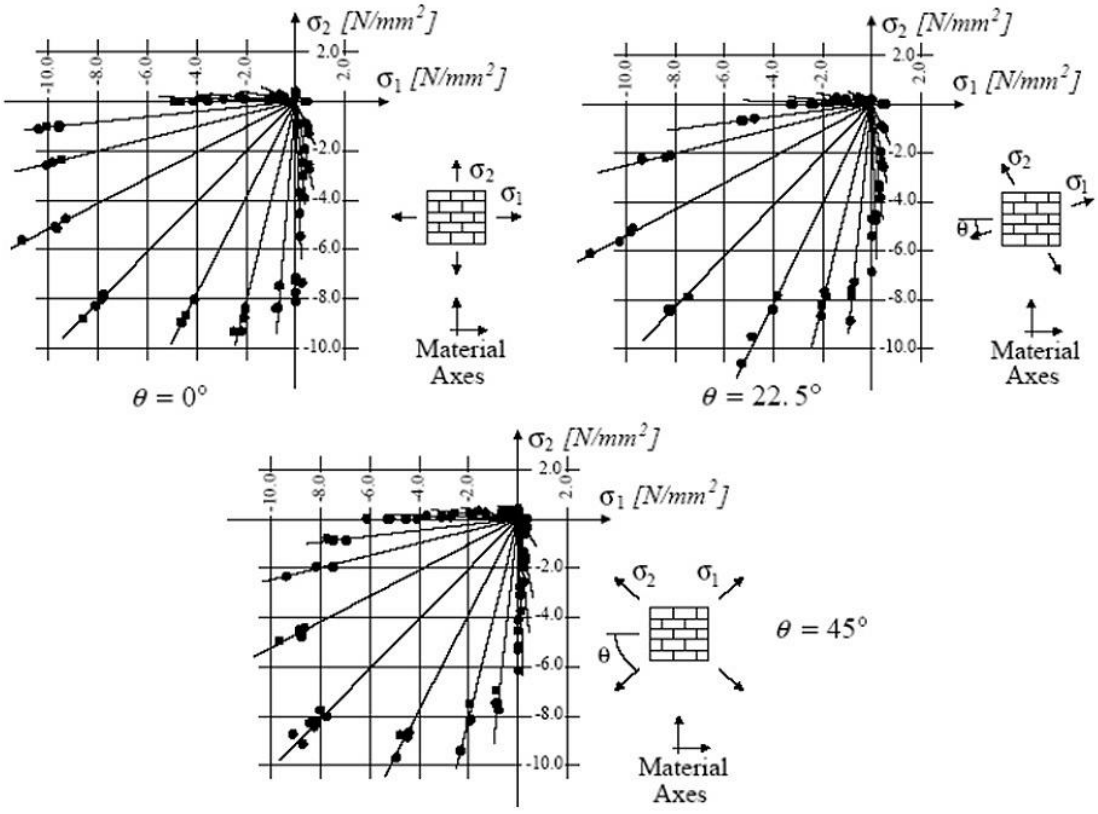


Fig.5.7 -1: Bi-axial strength of solid clay units Masonry, [*Pag81, 83*].
$\sigma_2(\sigma_1)$, numbers in construction $\leftarrow$ $\sigma_{II}(\sigma_I)$, general indexing

5.8 Evidence 120°-symmetrical Failure Body of Brittle and Ductile Isotropic Materials

5.8.1 General

According to the French saying " Les extrêmes se touchent" and based on the FMC-thinking the author assumed that there is a large similarity in the description of the behavior of very ductile and very brittle materials. Also with ductile materials the 120°-rotational symmetry should be found and a vertex must be given, representing the equi-triaxial tensile strength for a load-controlled strength situation.

In order to prove the 120°-rotational symmetry, test results from bi-axially measuring cruciform test specimens are necessary. As the vertex stress state $(\text{true}\bar{R}^{ttt}, \text{true}\bar{R}^{ttt}, \text{true}\bar{R}^{ttt})$ practically cannot be measured a 3D-stress state closest possible to the vertex must be employed, a stress state is to achieve namely $(\text{true}\sigma_{ax} + \sigma_{hyd}, \sigma_{hyd}, \sigma_{hyd})$. by investigating the center of an (un-)notched tension rod test specimen, being the 'hot spot' in the test specimen.

However, with notched rods the original notch radius ρ increases and thereby the critical surface stress concentration reduces a little and the criticality wanders to the center. With un-notched rods a neck radius builds up and increases with further increasing axial tensile stress. Due to the diameter reduction an hydrostatic stress state is generated and can be determined from the zero volume strain condition in a fully plastic regime faced in the minimum neck cross-section. Hereby, difference due to rolling of the sheet material and how the test specimen is cut out are neglected and full isotropicity assumed.

Searched is the description of a complete failure body . This requires that the SFC captures both the positive and the negative I_1-domain. Further, the 120°- rotational symmetry should be mapped by the SFC approach (*use of* J_3), too.

Brittle: In order to show the difference of brittle to ductile materials *Fig. 5.8-1* outlines the brittle material with its features $\bar{R}^{tt} < \bar{R}^{t}$ and $\bar{R}^{cc} > \bar{R}^{c}$, depicted in the figure. See further § 2.5.

Ductile: Deformation measurements prove that for the same strain value of the growing yield surface it holds that equi-biaxial stress $\bar{\sigma}^{tt}(2D) > \bar{\sigma}^{t}(1D)$. This is similar to brittle concrete in the compressive domain where $\bar{R}^{cc} > \bar{R}^{c}$ and it demonstrates the validity of the 120°-axial symmetry here, too. From the test rig loading comes the subsequently effective stress '$\text{true}\sigma_{ax}$', whereas the remaining neck cross-section experiences in the center the multi-axial stress state $(\text{true}\sigma_{ax} + \sigma_{hyd}, \sigma_{hyd}, \sigma_{hyd})$, estimated by the Bridgman model. In order to better understand the stress situation in the rod center the effect of increasing σ_{hyd} is of interest, depicted below.

It is to conclude from the following relations, that a hydrostatic stress does not change Mises's representative invariant J_2 for shape deformation of the solid. However, σ_{hyd} affects the tri-axiality value *TrF* which might be interpreted to cause some quasi-embrittlement of the material.

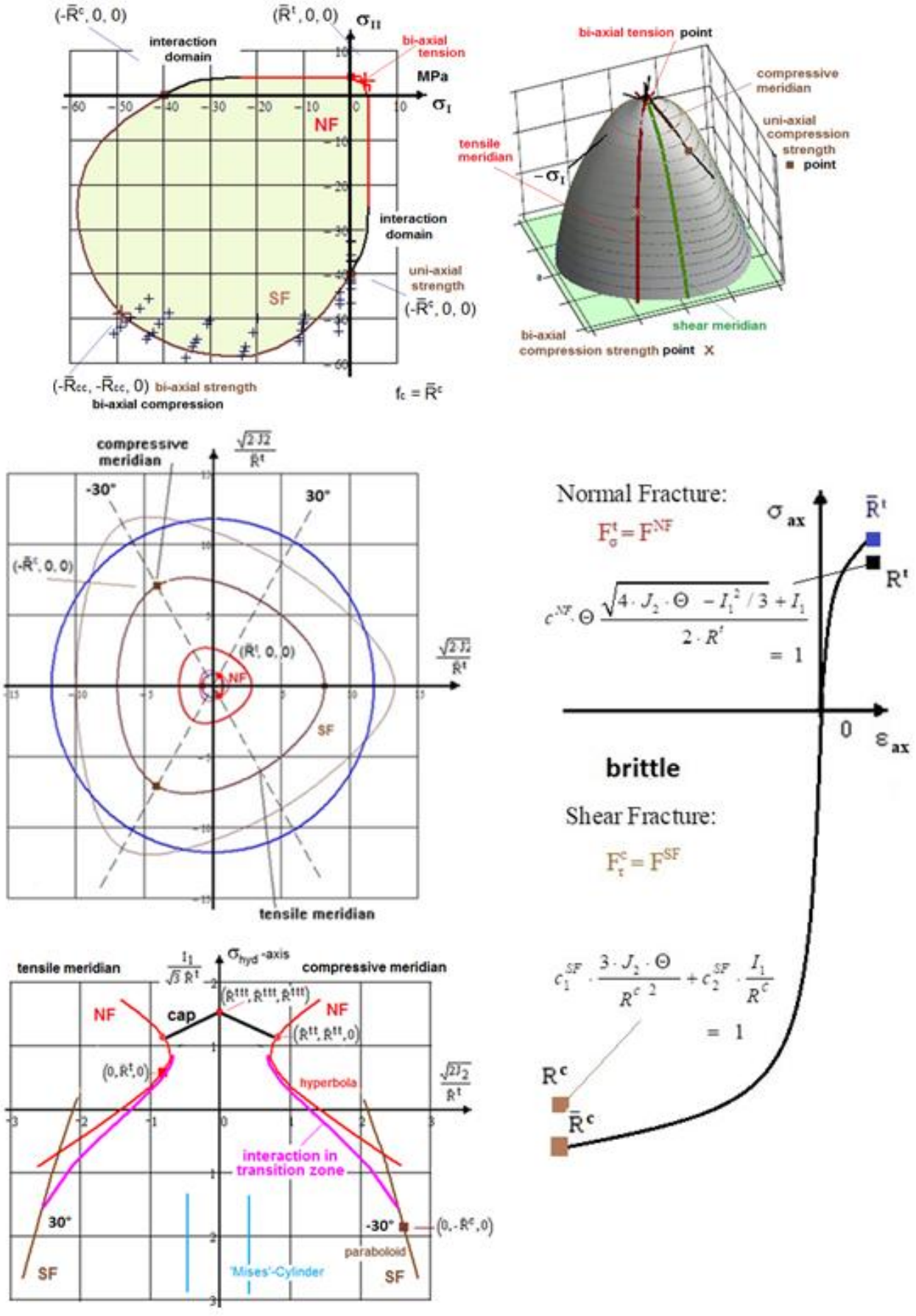


Fig.5.8-1: Visualization of the behavior of a brittle material (Normal Concrete) considering 1D stress-strain curve with 2D- and 3D-fracture failure curves and fracture body (surface). 120°-rotationally-symmetric

$$I_1 = (\sigma_I + \sigma_{II} + \sigma_{III}) \;=\; f(\sigma)\;,\quad 6J_2 = (\sigma_I - \sigma_{II})^2 + (\sigma_{II} - \sigma_{III})^2 + (\sigma_{III} - \sigma_I)^2 \;=\; f(\tau)$$

$$(\text{true}\bar{\sigma}_{ax} + \sigma_{hyd},\ \sigma_{hyd},\ \sigma_{hyd})\,,\quad \sigma_{ax}^{t}(r) = \sigma_F + \sigma_{hyd}$$

$$\sigma_{eq}^{Mises} = \sqrt{3J_2} = \sqrt{3}\cdot\sqrt{(\sigma_F^{M.} - \sigma_{h.} - \sigma_{h.})^2 + 0 + (\sigma_{h.} - \sigma_F^{M.} - \sigma_{h.})^2} \;\rightarrow\; \sigma_{eq}^{Mises} = \sigma_F^{\ Mises}$$

$$TrF = \sigma_{mean} / \sigma_{eq}^{Mises} = (I_1 / 3) / \sqrt{3J_2} = \left[\sqrt{2} / 3\right] \cdot (I_1 / \sqrt{3}) / \sqrt{2J_2}$$

$$I_1 = (\text{true}\sigma_{ax} + 3\sigma_{hyd}) \;=\; f(\sigma)\;,\quad 6J_2 = (\sigma_I - \sigma_{II})^2 + (0)^2 + (\sigma_{III} - \sigma_I)^2 \;=\; f(\tau)$$

uni-axial σ_{ax}, multi-axial $(\sigma_{ax} + \sigma_{hyd}, \sigma_{hyd}, \sigma_{hyd})$ in the rod's minimum neck section $\Rightarrow \sigma_{eq}^{Mises}$.

Considering now ductile isotropic materials one can conclude:

* The original versions of Hill's yield criterion were established for material that did not have pressure-dependent yield surfaces which are needed to model polymers, concrete and foams. 'Quadratic Hill' depends only on the deviatoric stresses and is pressure-independent like Mises. It predicts the same yield stress in tension and in compression°. *Why is it not correctly called 'I_1-independent', becauseboth the tension side and the compression side are to address? The term pressure-dependent is only correct and clear in the compression case.*
* In the 'Gurson domain'($I_1 > 0$) the tensile stress-strain curve is driven from the increase of the void volume (*porosity f*). A 120°-rotational symmetry of isotropic materials is also given in the tensile range with ductile isotropic materials but cannot be described by the multi-parameter Gurson model. It is known, that a material symmetry-related 120°-rotationally symmetrical subsequent flow surface or a fracture body applies more or less protermced to all isotropic materials. Mises can't depict this, nor can Hill and Gurson.
* The two-parameter Extended Mises model captures both domains and the 120°-rotational symmetry.

$$\text{Mises}\quad \frac{3J_2}{\bar{R}_{0.2}^{t\ 2}} = c_\tau^{Mises} \quad\Rightarrow\quad \text{Extended Mises}\ \frac{3J_2 \cdot \Theta}{\bar{R}_{0.2}^{t\ 2}} + c12\frac{I_1^2}{\bar{R}_{0.2}^{t\ 2}} = c_\tau^{ExtMises}$$

with non-circularity parameter d^t, being zero at $R_{0.2}$ and maximum at $\text{true}R^t$. c_{12} is the elliptical shape parameter, that captures via I_1^2 the porosity, with being zero at $R_{0.2}$ (still Mises) and grows with porosity *f*, c_τ is the size parameter growing from 1 at $R_{0.2}$.

(Material anisotropy further would be a completely different point for sheet metal.
The 120°-rotational symmetry can be best displayed in the principal stress plane (*inclined cross-section of the failure body)* and the octahedral stress plane which is a cross-section of the failure body at a distinct I_1.

Fig.5.8-2 left presents curves through the uniaxial tensile strength points and the equi-biaxial strength R^{tt}. The curves are inclined cross-sections of the failure body. *Fig.5.8-2 right,* for completion, displays the Beltrami potential surface (egg shaped) and the principal axes.
The picture shows extreme examples in the positive principal stress range for curves at $\text{true}R^t$ level. The red curve is occupied by the data of Kuwabara given below. The author was able to map the course of all the corresponding test data points with his SFC models.

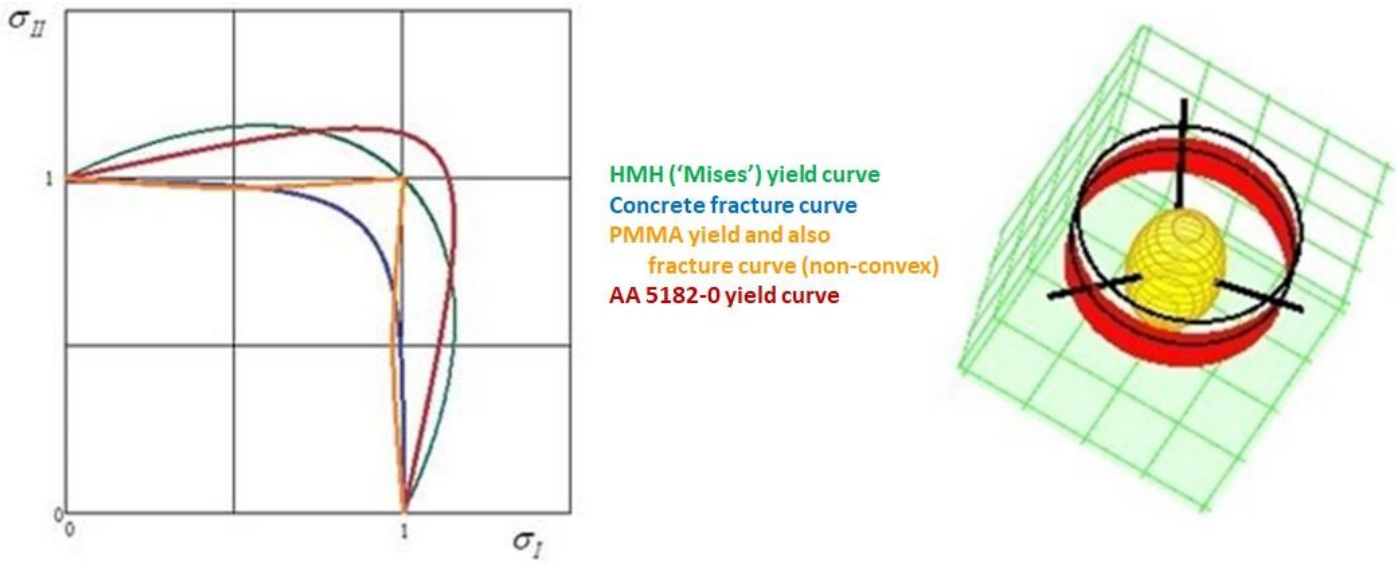


Fig.5.8-2: (left) Plane failure curves of a set of fully different isotropic materials. (right) Failure body surface

Note:

Brittle: bi-axial tension	*= 'weakest link failure behavior*	*(schwächstes Glied'-Versagen)*
Brittle: bi-axial compression	*= redundant (benign) failure behavior*	*(Stützwirkung)*
Ductile: bi-axial compression	*= redundant (benign) failure behavior*	*(Stützwirkung)*

The elaboration with the Mathcad calculation program for AA2219 leads to the picture below: Mises is the green curve. Red square: tensile strength point, cross: equi-biaxial tensile strength point ductile (trueR^{tt}, trueR^{tt}, 0), a cross x. For ductile metals for R^{tt} about 1.1 x Rt can be attached.
The points and curves on the spatial body are projected onto the octahedral plane. Since they depend on I_1, they have different cross-section heights I_1, such as the uniaxial strength point and the equi-biaxial strength point x. The metal test data AA 5182-0 are from Kuwabara [*Kuw98*].

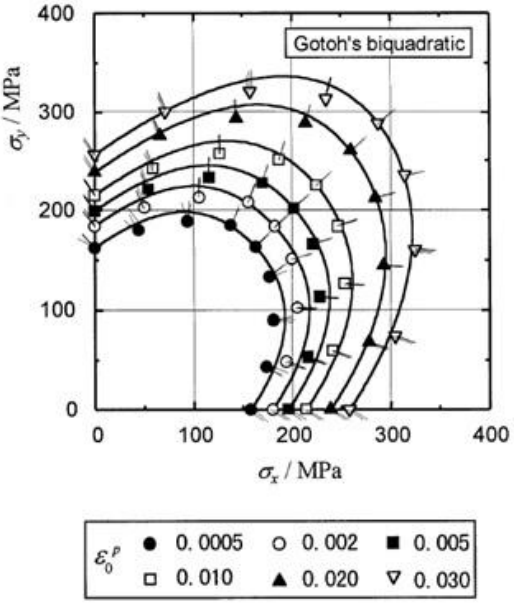
Fig 5.8-3 depicts several failure cross-sections of an isotropic steel that shows the 120°-rotational symmetry like the brittle isotropic materials – like concrete - in the compression and others in the tensile domain.
Biaxial tensile tests of cold-rolled low-carbon steel sheet were carried out using flat cruciform specimens with the biaxial loads maintained in fixed proportion.
Contours of plastic work were determined in stress space under the strain range of o 0 p50.03 and compared with existing yield criteria. The results obtained in this study are summarized as follows.
(1) The successive contours of plastic work measured for the present material changed their shapes progressively in stress space: the degree of expansion was

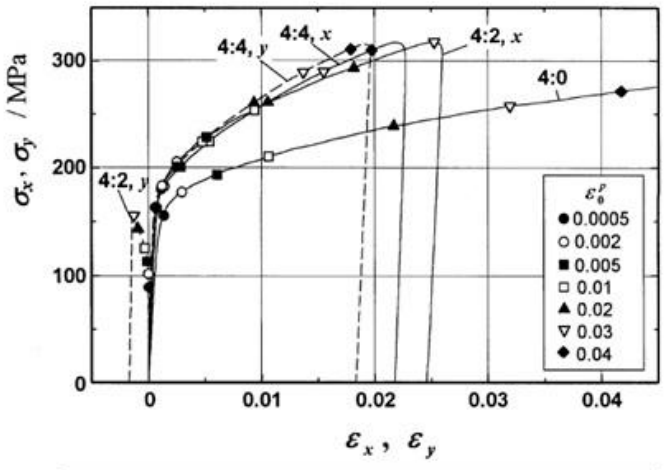
Each symbol corresponds to a plastic work line *W* of a particular plastic strain.

True stress–logarithmic strain curves for different loading levels are fund in Fig.5.5-2. Significance is given in the directions of the equibiaxial tension direction.
In *Fig 5.8-3* furthermore a table of measured significant test quanties is presented.

For general information: The following table presents a complete data set of a ductile material.

$\overline{R}_{p0.2}$	$true\overline{R}_{p0.2}$	$\overline{R}_m$	$true\overline{R}_m$	$\overline{R}_{ock}$	A_{gl}	A_5	Z	$R_{p0.2}$	R_m	R_{ock}
352	354	453	478	535	4.06	7.7	20	297	417	492
averages (mean, typical, characteristic)					minima					





ε_0^p	0.0005	0.002	0.005	0.010	0.020	0.030	0.040
W (MPa)	0.07	0.33	0.89	1.92	4.19	6.68	9.33
σ_0 (MPa)	158	180	196	214	239	258	273
σ_{90} (MPa)	162	184	199	215	238	256	271
σ_{bi} (MPa)	163	184	202	225	260	288	310

Fig.5.8-3: (left) Test points as function of the experienced plastic straining ε_0^{pl}. Mapping by using Gotoh's biquadratic criterion. (right) True stress–logarithmic strain curves for different biaxial loadings. Measured values using r_0, r_{45}, r_{90} . T = 1mm, flat cruciform.(right) Stress-strain curves under different stress ratios T. Kuwabara et al. : Journal of Materials Processing Technology 80–81 (1998) 517–523

Gotoh's biquadratic yield criterion (not given here) was used in [*Kuw98]* to map the test data of the cold-rolled low-carbon steel AA 5182-0 sheets.

In *Fig.5.8-3* at left is presented the failure body. The center figure fully proves the embossed isotropic 120° material symmetry. The Mises ellipse is added.
The right octahedral figure shows the inner green curve with the Mises circle (*cylinder*) at the beginning of the flow and the outer one at tensile strength Rt. Also here the 120°-rotational symmetry is fully demonstraed.

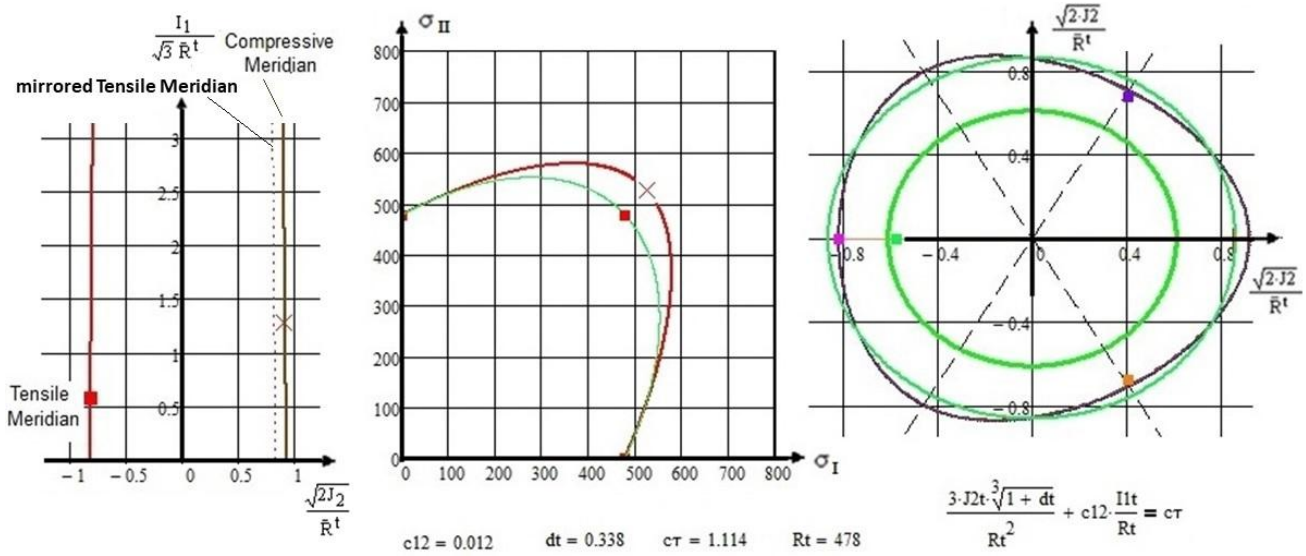


Fig.5.8-4 isotropic steel AA5182-0: Visualization of the behavior of a ductile material. (left) Yield body in Haigh-Lode-Wintergaard coordinates; (center) 120°-symmetry, visualized in the principal stress plane; (right) 120°-symmetry, visualized in the octahedral stress plane

The next Table collects all relevant descriptions for the determination of fracture failure and of yield loci.

LL: Don't give up, when searching novel relationships. It made me waiting a lot of years here.

Table 5.8-4: Collection of all relevant descriptions for the determination of fracture failure of brittle z

Failure Limit States for static **Design Verification** of *'Dense'* Materials (design allowables R)

* Onset-of-Yielding $\Theta = 1$ $\quad F_\tau^{Mises} = \dfrac{3 \cdot J_2 \cdot \Theta}{R_{0.2}^{t\ 2}} = 1$ ductile , $\quad Eff^{Mises} = \sqrt{3J_2 / \bar{R}_{0.2}^{t}}$

* Onset-of-Ductile Fracture max load $\dfrac{3 \cdot J_2 \cdot \Theta(\vartheta)}{R_{0.2}^{t\ 2}} = \dfrac{R^{t2}}{R_{0.2}^{t\ 2}}$ $\quad \Theta \geq 1$, d >1, mild steels; $\Theta = 1$ high strength steels

* Onset-of-Ductile Cracking' before rupture ($_{odc}$) $\quad c_{1\tau}^t \cdot \dfrac{3 \cdot J_2 \cdot \Theta}{R_{0.2}^{t\ 2}} + c_{2\tau}^t (porosity\ f) \cdot \dfrac{I_1^{\ 2}}{R_{0.2}^{t\ 2}} = 1$ ductile

* Normal Fracture: $\quad F_\sigma^t = F^{NF} = c^{NF} \cdot \Theta^{NF} \cdot \dfrac{\sqrt{4 \cdot J_2 \cdot \Theta \ - I_1^{\ 2} / 3} + I_1}{2 \cdot R^t} = 1$, $\Theta \leq 1$, d < 1, brittle, $R^t < R^{tt}$

* Shear Fracture: $\quad F_\tau^c = F^{SF} = c_1^{SF} \cdot \dfrac{3 \cdot J_2 \cdot \Theta}{R^{c\ 2}} + c_2^{SF} (\ friction\ \mu) \cdot \dfrac{I_1}{R^c} = 1$, $\Theta \geq 1$, d >1, brittle, $R^c < R^{cc}$

Mode domain description for mapping and **structural analysis**

(subsequent potential surfaces, mapping 50%-values,$\bar{R}$)

* Potential surfaces in elastic Beltrami domain $\nu_0 \leq \nu \leq 0.5$:

* Yielding in Mises domain $\quad \nu = 0.5,\ \Theta(I_1) \geq 1,\ \sigma^t < \sigma^{tt}$: $\quad \dfrac{3 \cdot J_2 \cdot \Theta}{\bar{R}_{0.2}^{t\ 2}} = c_\tau^{Mises\ 2} \quad Eff^{Mises} = \sqrt{3J_2 / \bar{R}_{0.2}^{t}}$

$\max c_\tau = \bar{R}_m^t / \bar{R}_{0.2}^t,\ \sigma_{eq}^{Mises} = \sqrt{3J_2} = \sqrt{0.5} \cdot \sqrt{\left[(\sigma_I - \sigma_{II})^2 + (\sigma_{II} - \sigma_{III})^2 + (\sigma_{III} - \sigma_I)^2 \right]} = \sqrt{2} \cdot \sqrt{\tau_{III}^2 + \tau_I^2 + \tau_{II}^2}$

$c_\tau = \bar{R}^t / \bar{R}_{0.2}^t$ better $\quad c_\tau = true\bar{R}^t / true\bar{R}_{0.2}^t$ due to $\Theta \neq 1$

* Large Yielding in Gurson domain $\quad 0.5 \geq \nu,\ \Theta \cong 1.\quad F_\tau^{ExtMises} = c_{1\tau}^t \cdot \dfrac{3 \cdot J_2 \cdot \Theta}{\bar{R}_{0.2}^{t\ 2}} + c_{2\tau}^t \cdot \dfrac{I_1^{\ 2}}{\bar{R}_{0.2}^{t\ 2}} = c_\tau^{ExtMises\ 2}$

$\max c_\tau < \bar{R}^t / \bar{R}_{0.2}^t > \bar{R}_{odc} / \ \bar{R}_{0.2}^t \qquad \dfrac{3J_2}{\bar{R}_{0.2}^{t\ 2}} + c_{12\tau}^{\ t} \cdot \dfrac{I_1^{\ 2}}{\bar{R}_{0.2}^{t\ 2}} = c_\tau^{t2} (porosity\ \ f).$

Additional information:

120°-rotationally symmetric: $c_{1\Theta}^{SF} = 1 + c_{2\Theta}^{SF} \cdot \sqrt[3]{1 + d^{SF} \cdot (-1)}$ $\quad$ with

c^{NF} ,Θ^{NF} from the two points $(\bar{R}^t,\ 0,\ 0)$ and $(\bar{R}^{tt}, \bar{R}^{tt},\ 0)$ or by a minimum error fit, if data available,

c^{SF} ,Θ^{SF} from the two points $(-\bar{R}^c,\ 0, 0)$ and $(-\bar{R}^{cc}, -\bar{R}^{cc}, 0)$ or by minimum error fit .

$I_1 = (\sigma_I + \sigma_{II} + \sigma_{III}) = f(\sigma)$, $\quad 6J_2 = (\sigma_I - \sigma_{II})^2 + (\sigma_{II} - \sigma_{III})^2 + (\sigma_{III} - \sigma_I)^2 = f(\tau)$

$27 J_3 = (2\sigma_I - \sigma_{II} - \sigma_{III}) \cdot (2\sigma_{II} - \sigma_I - \sigma_{III}) \cdot (2\sigma_{III} - \sigma_I - \sigma_{II})$,

$\sigma_I, \sigma_{II}, \sigma_{III}$ are principal stresses, $\sigma_I > \sigma_{II} > \sigma_{III}$ are mathematical stresses (> means more positive)

A 2-fold acting mode or an orthogonal stress state makes the rotationally symmetric fracture body 120°-symmetric and is modelled by using the invariant J_3 and Θ as non-circularity function with d as non-circularity parameter $\quad \Theta = \sqrt[3]{1 + d \cdot \sin(3\vartheta)} = \sqrt[3]{1 + d \cdot 1.5 \cdot \sqrt{3} \cdot J_3 \cdot J_2^{-1.5}}$.

with Lode angle ϑ , here set as $\sin(3 \cdot \vartheta)$ setting the 'neutral' shear meridian angle $\vartheta = 0°$

If a failure body is rotationally symmetric, then Θ = 1 like for the neutral or shear meridian, respectively .

$$\varepsilon_{eq}^{Mises} = \sqrt{2} \cdot \sqrt{(\varepsilon_I - \varepsilon_{II})^2 + (\varepsilon_{II} - \varepsilon_{III})^2 + (\varepsilon_{III} - \varepsilon_I)^2} / 3, \qquad \sigma_{eq}^{Mises} = \sqrt{3 \cdot J_2}.$$

Whether Onset-of-Yielding or Onset-of-ductile Fracture is design-driving depends on the ratio with the associated FoS: $\quad R_{0.2}^t / j_{02}$ or R^t / j_{ult}

$true\varepsilon = \ln(1 + eng\varepsilon),\ \ eng\varepsilon = e^{true\ \varepsilon} - 1,\ \ true\sigma = eng\sigma \cdot (1 + eng\varepsilon)$ and $eng\sigma = true\sigma / \exp(true\varepsilon)$

$true\varepsilon_{ax} = \ln(\ell / \ell_0) = \ln(1 + eng\varepsilon_{ax})$.

6 Transversely-isotropic UD-materials (GFRP, CFRP)

6.1 General, UD applications

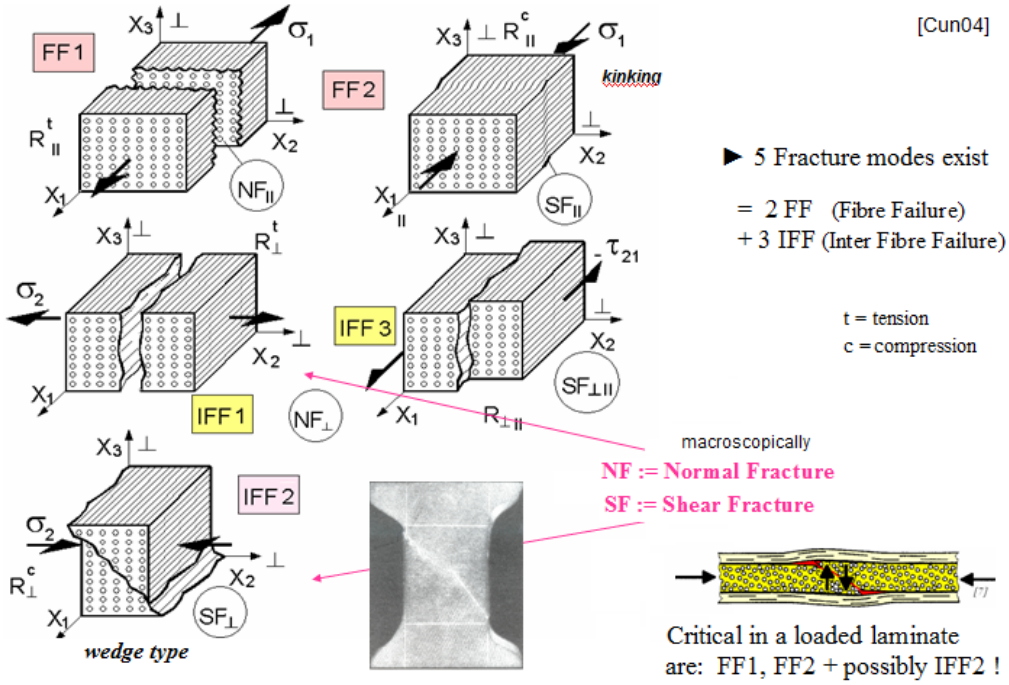


Fig. 6-1: Reminder Fracture failure modes of UD material, NF = Normal fracture, SF = Shear fracture

Mind, please: This is partly a very old figure collection of the author in Chapter 6.

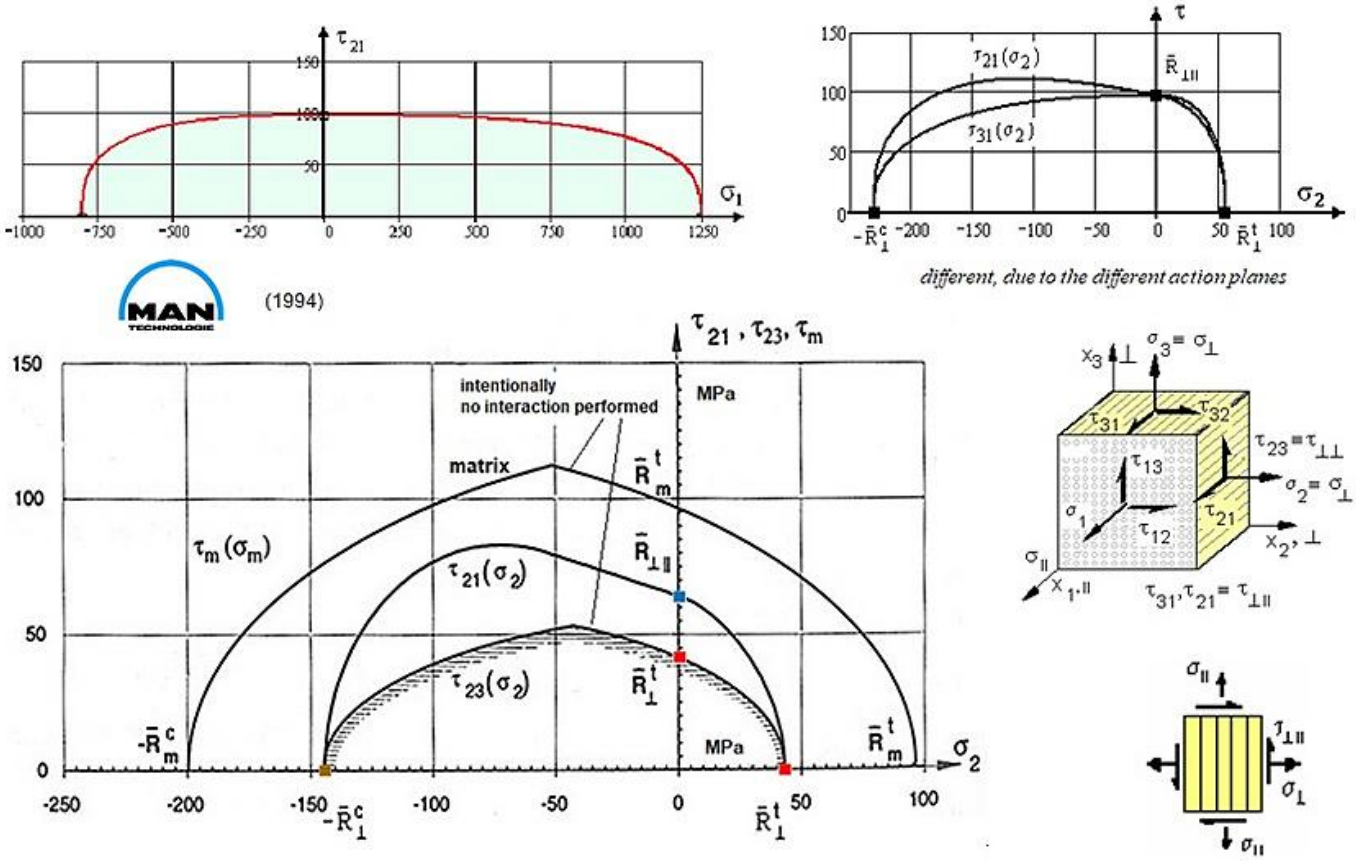


Fig.6-2: Various fracture failure curves linked to UD material

The fracture stress curves exhibit the actions of a shear stress, which is a stress that is composed for τ_{23} of a normal shear stress component and a compression shear stress component. By the way, here, the use of the term 'stress component' is correct. Stresses are tensor components or stress vector components.

I_5 reflects the different action of τ_{21} and τ_{31} in *Fig.6-2*.

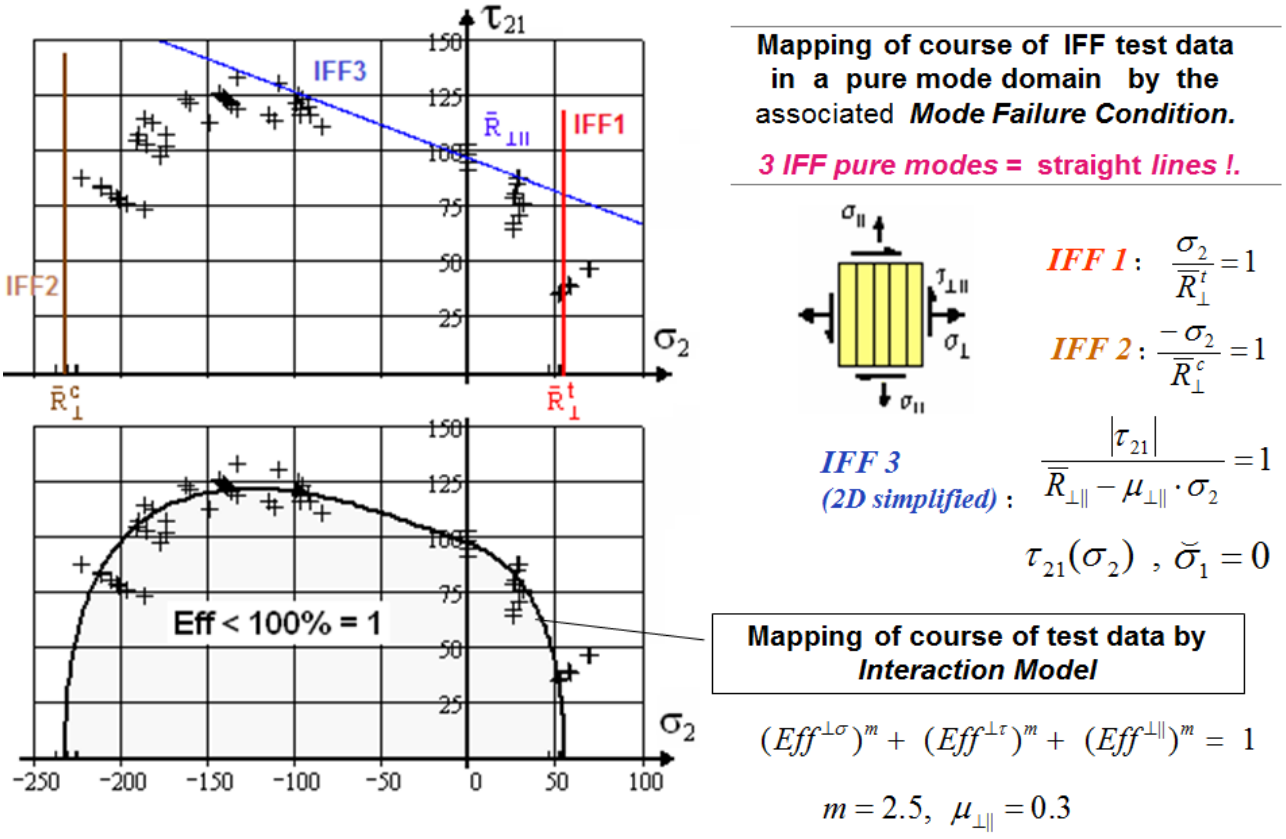


Fig.6-3: Visualsation of the interaction with a UD-material

LL: Only some years ago the author found :

If one replaces the stresses by the associate equivalent mode stresses
then the 2D-failure body becomes a general 3D-failure body.

This became considered in the original old *Fig.6-4* by adding the lower part.

Fig.6-5 left shows the main cross-section of the stress-based failure body, whereas the *right* figure outlines the strength distributions.

The corner depicts the double failure mode $\sigma_2 = \sigma_3$, whereby the straight lines become inward-curved according to the hgher failure danger because flaws are twofold 'activated'.

Fig.6-6 shows the mapping of the transversal cross-section of the failure body in *Fig.6-4*. This cross-section is the basic one for 2D-design dimensioning.

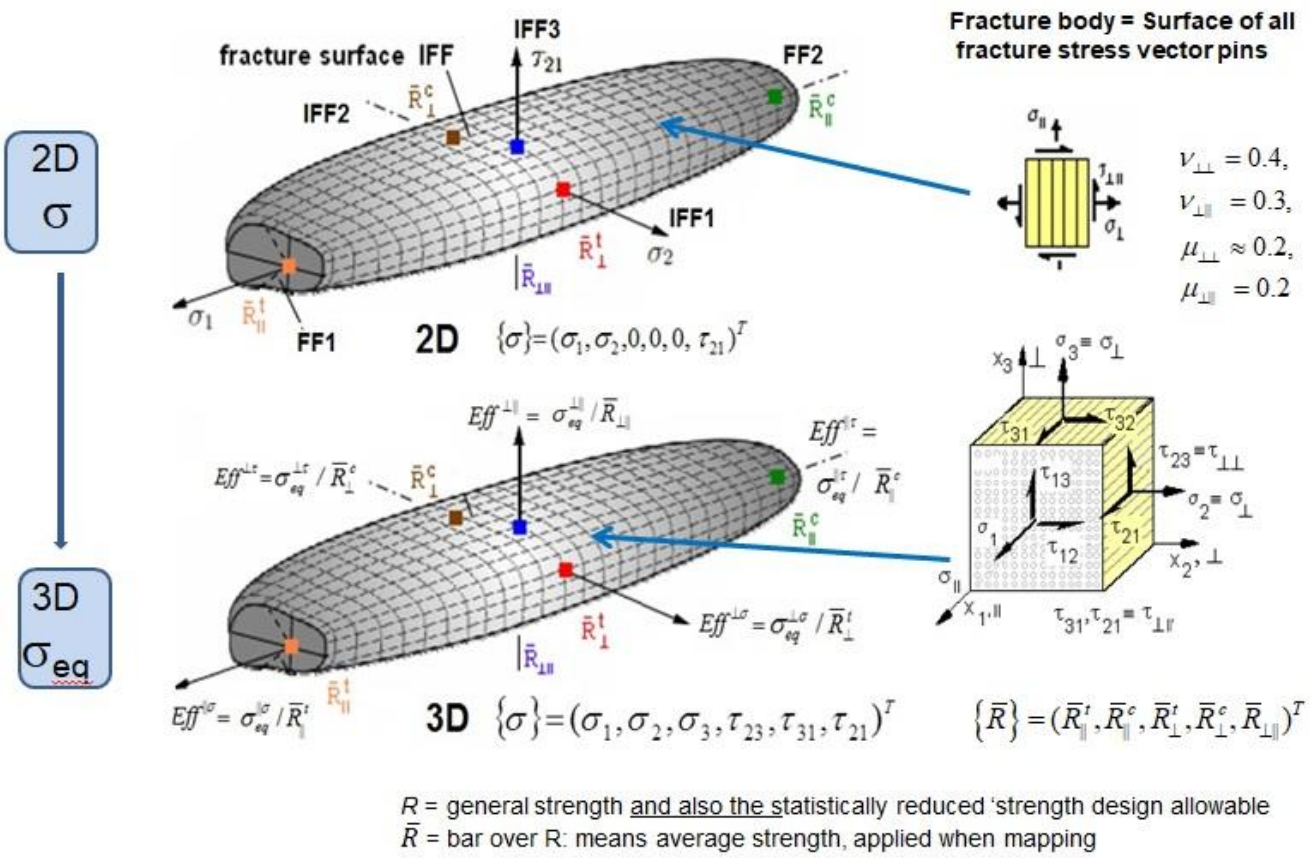
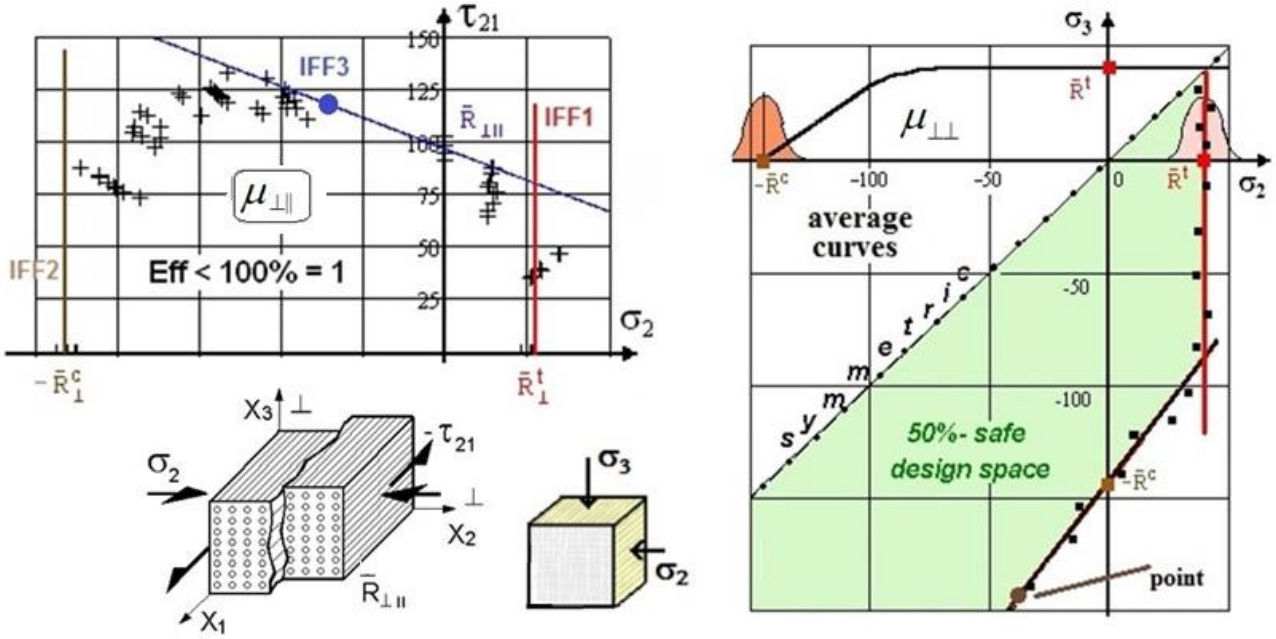


Fig.6-4: From 2D failure body to 3D failure body by replacing stresses by equivalent stresses



$$\mu_{\perp\parallel} = (\tau_{21,fr} - R_{\perp\parallel}) / \sigma_{2,fr}\,,\; b_{\perp\perp} = (\sigma_{2,\perp fr} + \sigma_{3,\perp fr} + R^c_{\perp}) / (\sigma_{2,\perp fr} + \sigma_{3,\perp fr} + \sqrt{(-\sigma_{2,\perp fr} + \sigma_{3,\perp fr})^2})$$

Fig. 6-5: Display of typical fracture test points to estimate the 2 friction parameters b.
When mapping, an average curve is searched, being statistically marked by a bar over: $R \rightarrow \bar{R}$

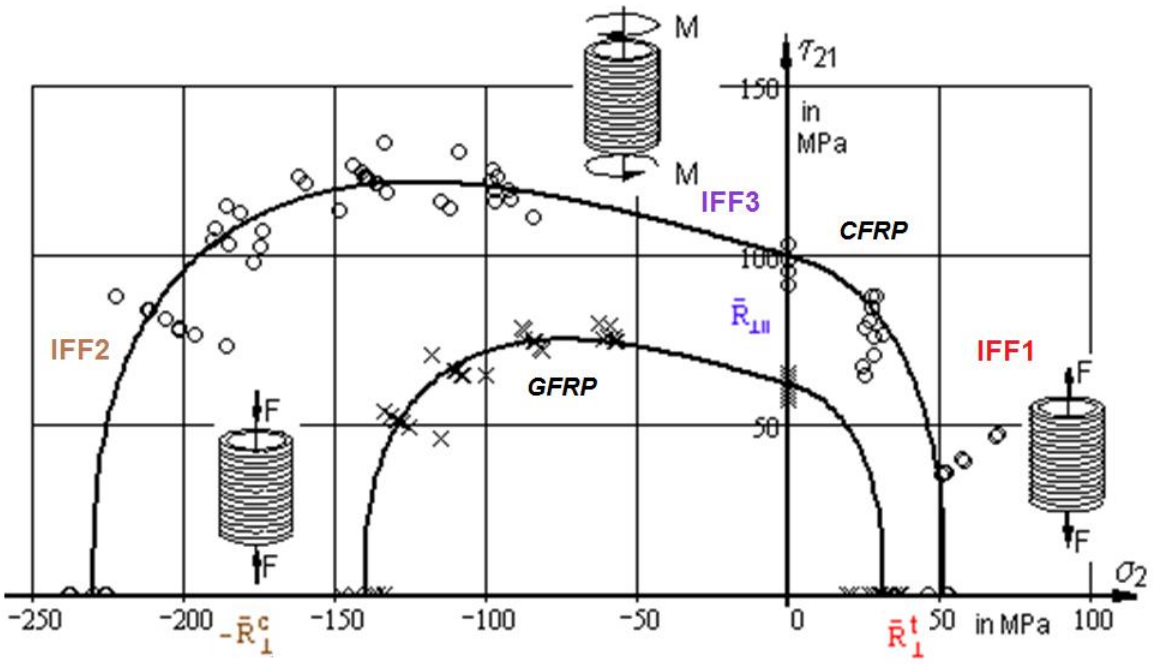
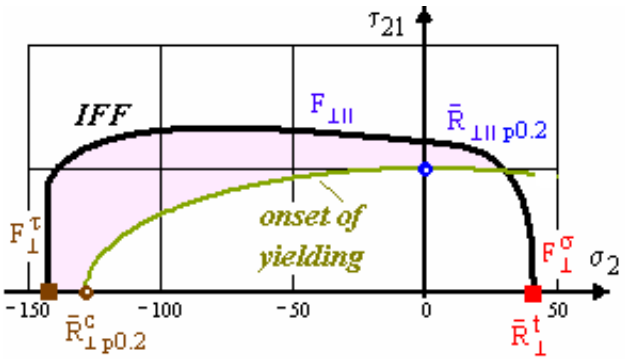


Fig.6-6, own IFF test results: 2 GFRP, 1 CFRP test series

Fig.6-7 gives information about 'Onset-of-(quasi)yielding' and how the failure body shrinks under degradation. This degradation is caused by some matrix yielding and diffuse micro-cracking. *Fig. 6-7* presents a schematic display for the most affected IFF cross-section.



$$\frac{I_3}{(\bar{R}_{\perp\parallel 0.2})^2} + \frac{I_4}{(\bar{R}^c_{\perp 0.2})^2} = c_y{}^2$$

Fig. 6-7: Schematic display of yielding boundaries

The degree of non-linearity in ***strain hardening*** regime essentially depends on the degrading matrix material. Beyond IFF strength and stiffness decay subsequently. This affects the secant IFF moduli. In the post-IFF regime the embedded lamina experiences no sudden death but still has residual strength and stiffness due to the in-situ effect.

Fig.6-8 shows two cross-sections of the 2D failure body: Originally and after shrinking, due to a distinct IFF degradation. Fibers take over load from matrix. Points, marked in figure, are depicted here to highlight effects that are essential for the initial failure load (1, *validity of the assumption of linearity*) and for final failure load (2, *laterally shrinking failure body*).

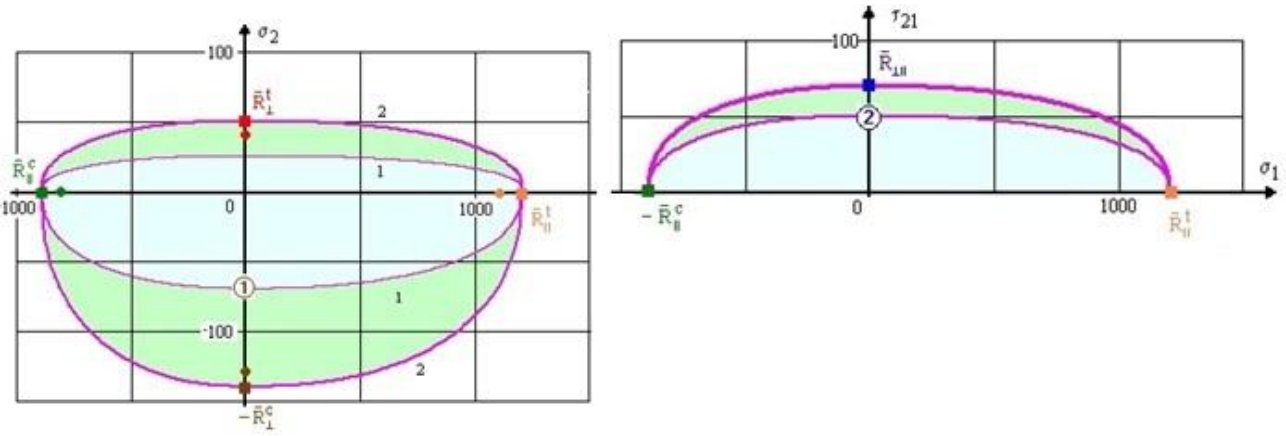


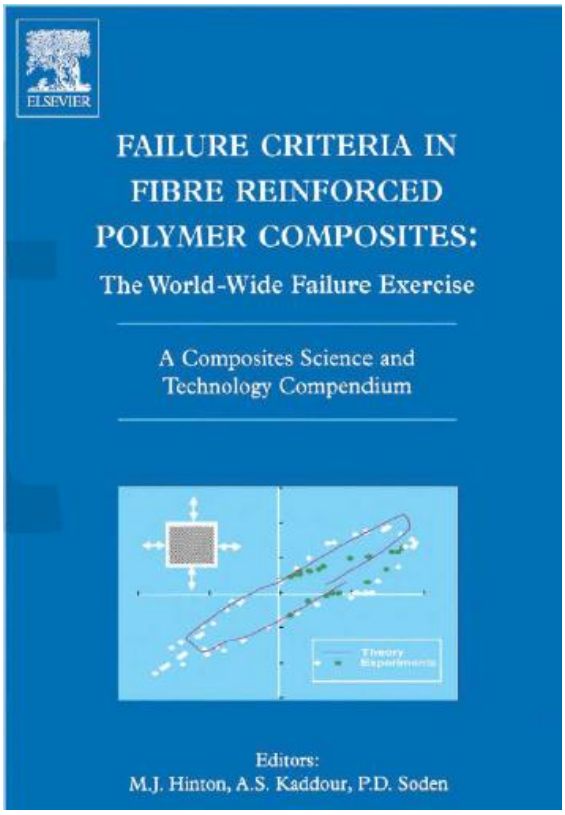
Fig. 6-8: Display of UD material degradation effects under loading

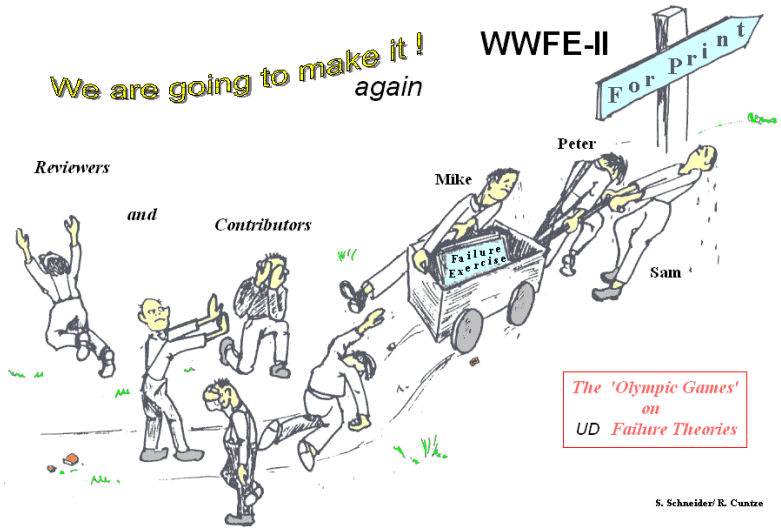
6.2 Transversely-isotropic UD-materials, WWFE-I and WWFE-II applications

6.2.1 WWFE-Introduction

State-of-the-Art: "Static Strength Analysis of the transversely-isotropic UD laminas is best represented by the results of the World-Wide-Failure-Exercises (below) about Static Strength Criteria for high-performance UD composite parts".

This is primarily right, but – after WWFE-I and –II - some uncertainty remains open!





Organizer: ***QinetiQ , UK,*** since 1991

[Hinton, Kaddour, Soden, Smith, Shuguang Li]

Aim: *(was for the UD materials, only)*

'Testing Predictive Failure Theories for Fiber–Reinforced Polymer Composites to the full !'

Many thanks to the QinetiQ-team, UK, the organizers Mike, Sam and Peter for setting up and survive such a long lasting effortful world-wide exercise.

The author did not participate in WWFE-III, the part *Micro-damage Theories*.

Method of the World-Wide-Failure-Exercises I and II :

Part A : *Blind Predictions on basic strength data*

Part B: *Comparison Theory-Test with hopefully reliable Uniaxial 'Failure Stress Test Data' (the technical basic strengths)* and *Multi-axial 'Failure Stress Test Data' from* plain test specimens (not notched) as well.

We contributors know that you could only provide the contributors with test data sets which were available. The quality of them was not known enough well. Hence, the following information shall be given before mapping the courses of test data sets:

- *Part A: Prediction was to made without provision of all needed properties. With strength values alone – in general - a SFC cannot be validated. For compression, however, a friction information must be given.*
- *Part B: Test data sets partly not applicable. Comments on the respective input are given in each Test Case TC.*
- *Validation of lamina SFCs models can be only achieved by lamina 2D- and 3D- test results. 3D-laminate results serve for verification of the laminate design.*

At first, what was the meaning of the term 'Failure' in the WWFEs?

"If the structural part does not fulfil its design requirements FF, IFF, leakage, deformation limit, delamination size limit, …). This was significant in the Test Cases."

Primarily depicted and discussed will be the essential critical lamina-related TCs of WWFE-I and –II because these serve the UD-material Model Validation.
The laminate-examples serve for Design Verification, 'only'.
For the complete Laminate-TCs it is referred to the author's contributions WWFE-IB and WWFE-IIB.

6.2.2 WWFE-provided UD stress-strain curves and properties

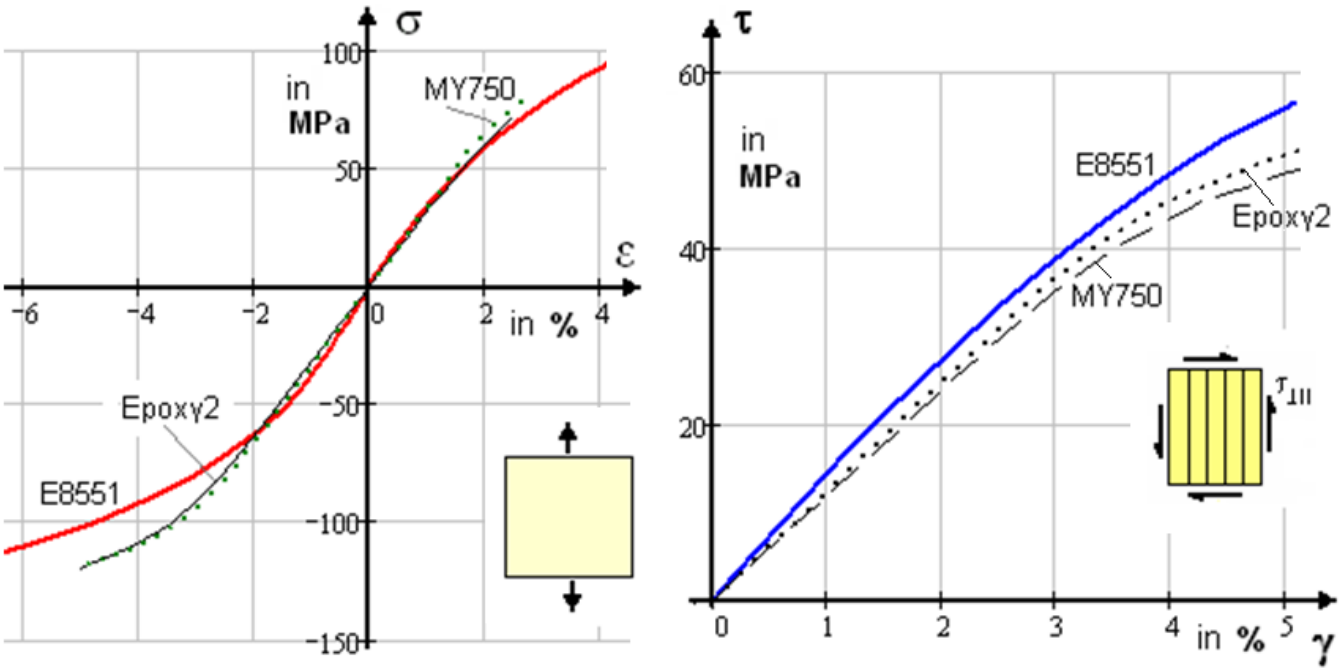


Fig. 6-9: (left) Stress-strain curve of some resin matrices. (right) In-plane shear stress-strain curves of a CFRP lamina

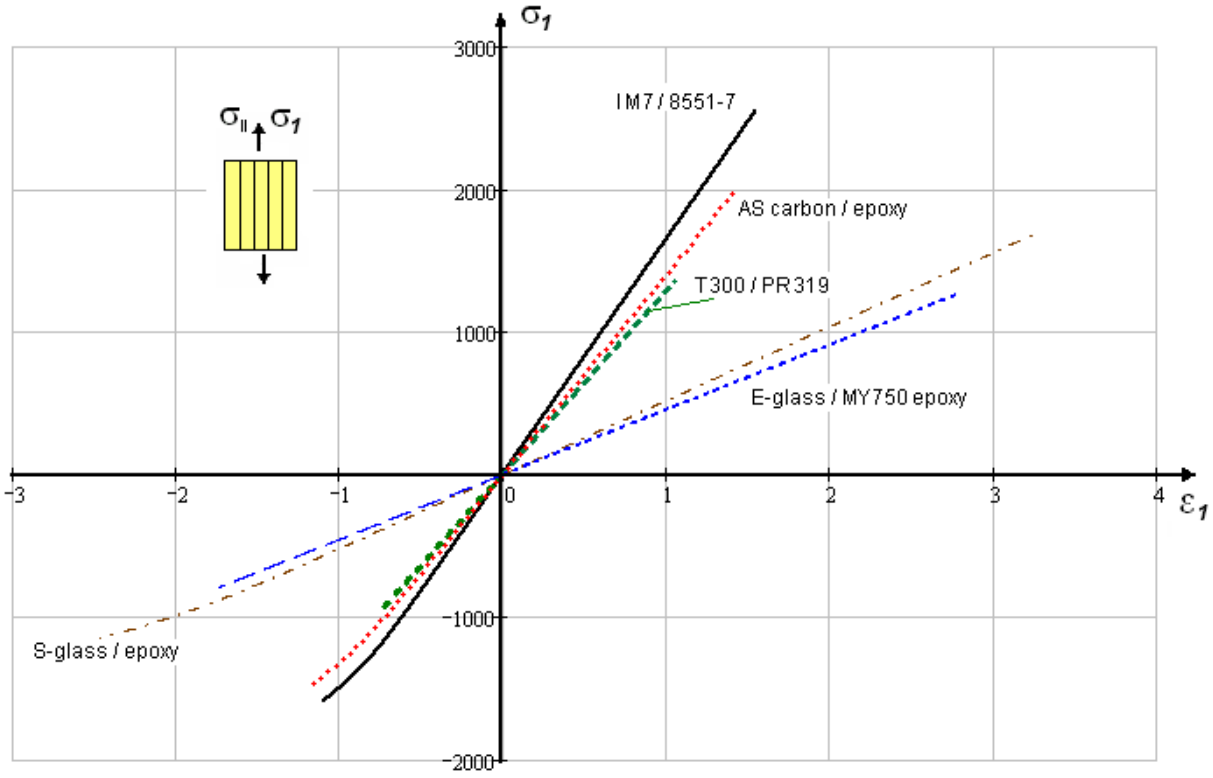


Fig. 6-10: FRP fiber-parallel stress-strain curves of a lamina, $\sigma_{\parallel}(\varepsilon_{\parallel}) \equiv \sigma_1(\varepsilon_1)$

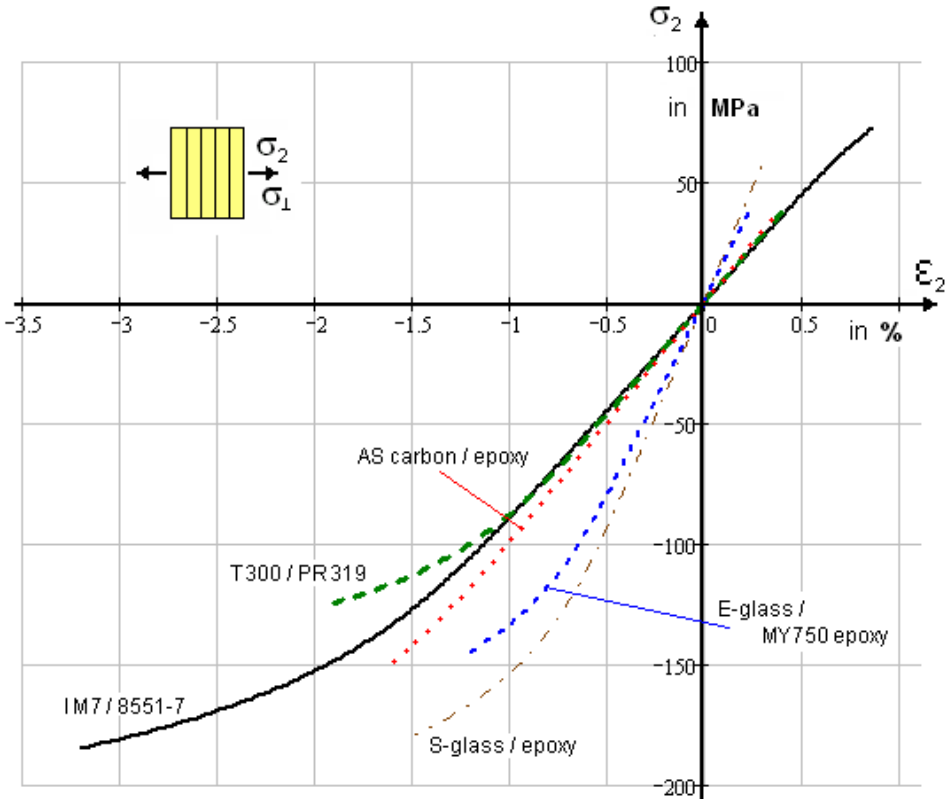


Fig. 6-11: FRP fiber-transversal stress-strain curves of a lamina, $\sigma_{\perp}(\varepsilon_{\perp}) \equiv \sigma_2(\varepsilon_2)$

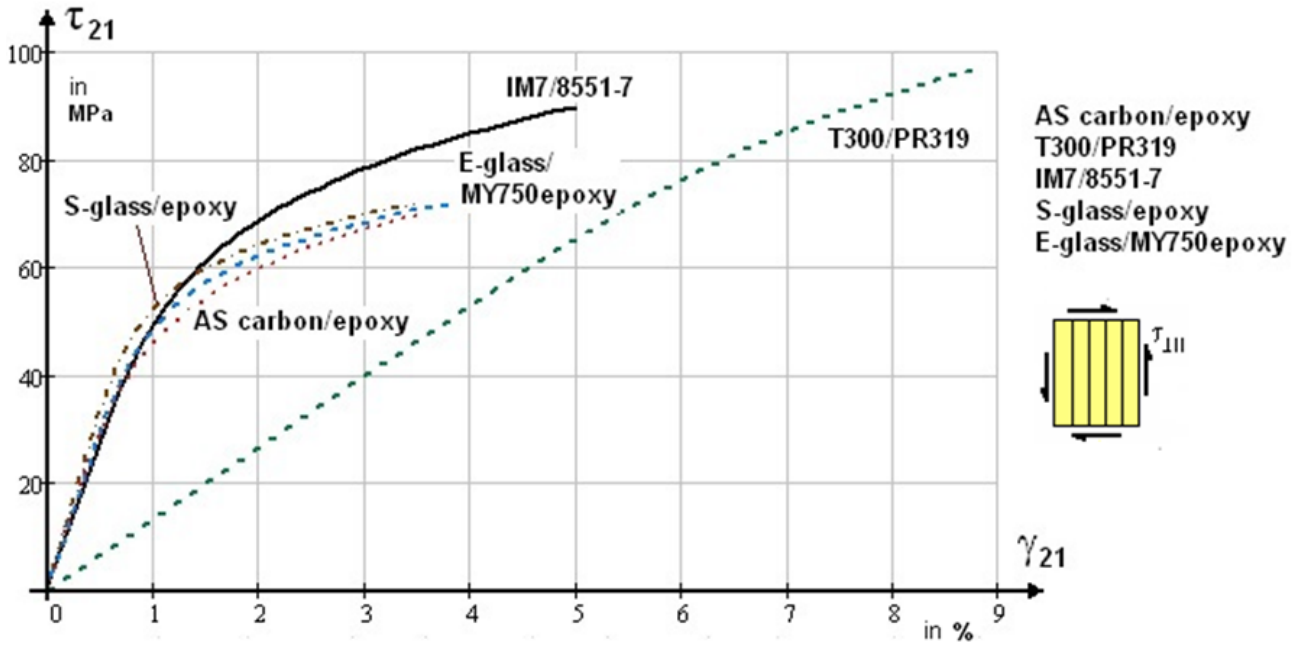
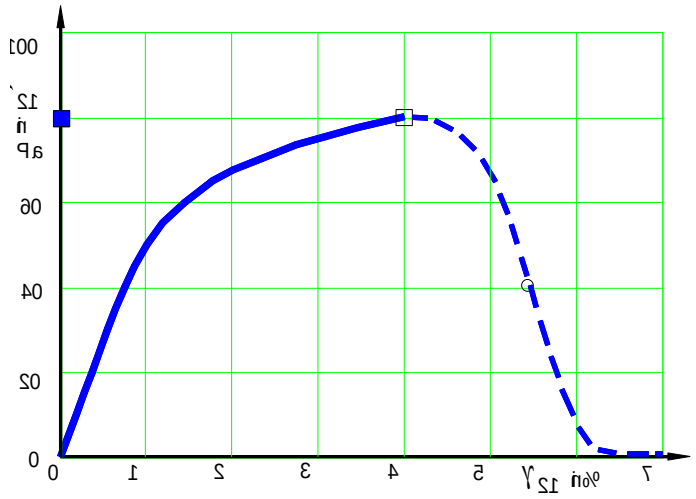
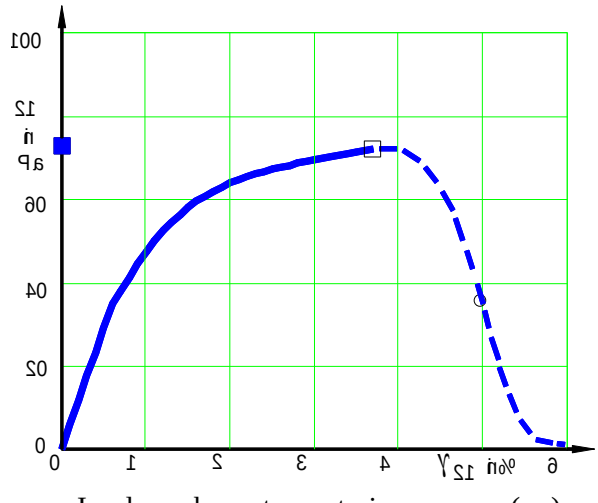


Fig. 6-12: FRP in-plane shear stress-strain curves of a lamina, $\sigma_{\perp\perp}(\gamma_{\perp\perp}) \equiv \tau_{12}(\gamma_{12})$

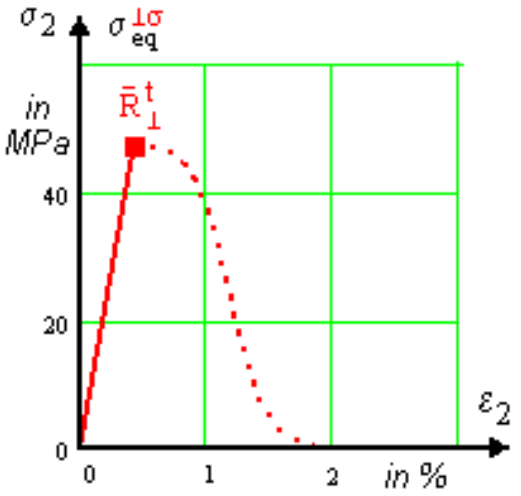


In-plane shear stress-strain curve τ_{21} (γ_{21});
UD-lamina, CFRP (degradation assumed).
T300/BSL914C epoxy.
$\overline{R}_{\perp||}$= 80 MPa, $\overline{G}_{||\perp 0}$ = 5.5 GPa;
$n^{\perp||} = 5; a_s^{\perp||} = -7.0\%, b_s^{\perp||} = 0.53\%$
Degradation in softening curve part assumed.

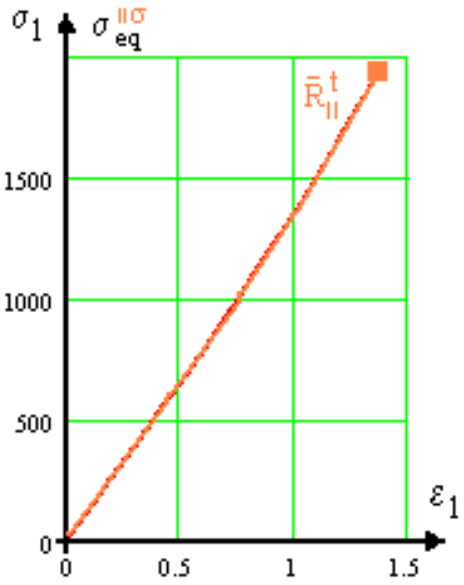


In-plane shear stress-strain curve τ_{21} (γ_{21});
UD-lamina, GFRP (degradation assumed).
E-glass/LY556/HT907/DY063.
$\overline{R}_{\perp||}$= 72 MPa, $\overline{G}_{||\perp 0}$ = 5.83 GPa;
$n^{\perp||} = 5; a_s^{\perp||} = -7.0\%, b_s^{\perp||} = 0.54\%$
$\overline{R}_{\perp||}$= 73 MPa, $\overline{G}_{||\perp 0}$ = 5.83 GPa;
$n^{\perp||} = 6.6; a_s^{\perp||} = -7.0\%, b_s^{\perp||} = 0.53\%$

Figure $\sigma_{\perp\perp}(\gamma_{\perp\perp}) \equiv \tau_{12}(\gamma_{12})$. Degradation in softening curve part assumed

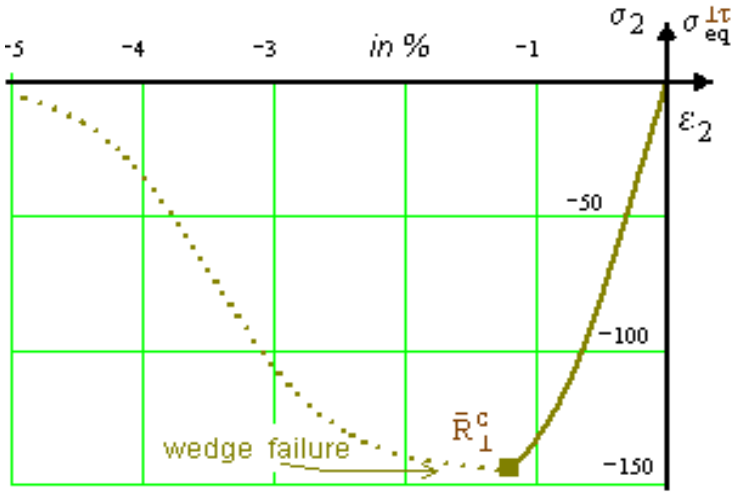


Transverse tensile stress/strain curve $\sigma_2^t(\varepsilon_2^t)$
UD-lamina (softening assumed).
CFRP: AS4/3501-6 epoxy.
$\bar{R}_\perp^t = 48\,\text{MPa}, \bar{E}_{\perp 0}^t = 11\,\text{GPa}$;
$a_S^{\perp t} = -1.2\%,\ b_S^{\perp t} = 0.15\%$

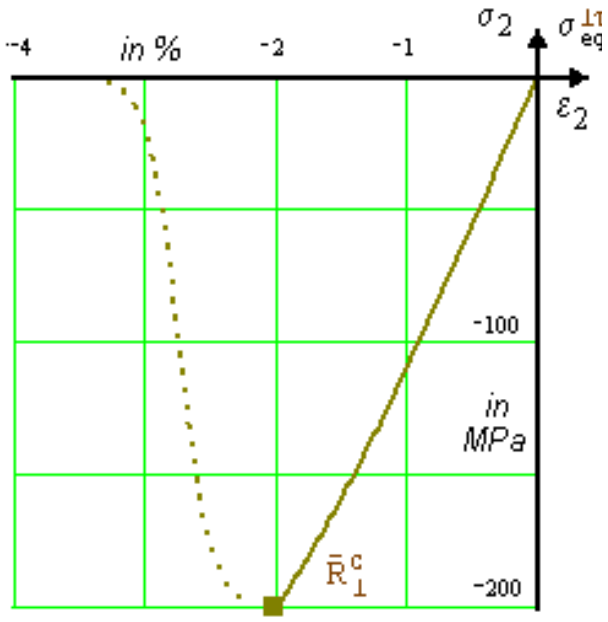


Longitudinal. tensile stress/strain curve $\sigma_1^t(\varepsilon_1)$
UD-lamina. CFRP: AS4/3501-6 epoxy.
$\bar{R}_{||}^t$ = 1950 MPa, $\bar{E}^t{}_{||0}$ = 126 GPa

Figure left: $\sigma_\perp(\varepsilon_\perp) \equiv \sigma_2(\varepsilon_2)$. *Figure right:* $\sigma_{\perp\perp}(\gamma_{\perp\perp}) \equiv \tau_{12}(\gamma_{12})$

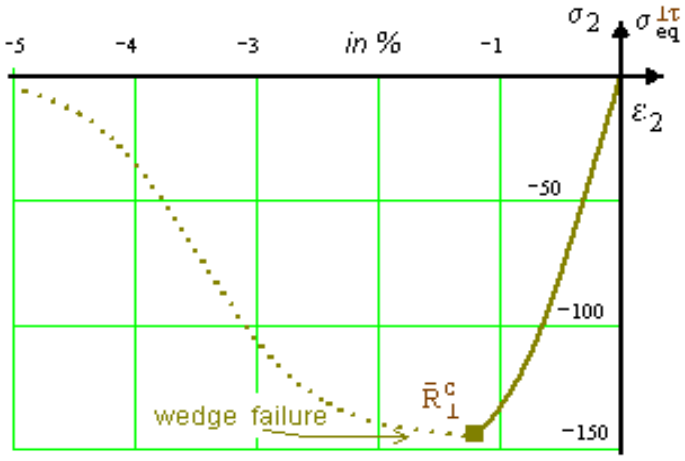


Transv. compr. stress/strain curve $\sigma_2^c(\varepsilon_2)$;
UD-lamina (softening assumed).
GFRP: E-glass/MY750/HY917/DY063.
$\bar{R}_\perp^c$ = 145 MPa, $\bar{E}^c{}_{\perp 0}$ = 16.2 GPa;
$n^{\perp c} = 6.6; a_s^{\perp c} = -3.45\%, b_s^{\perp c} = 0.47\%$

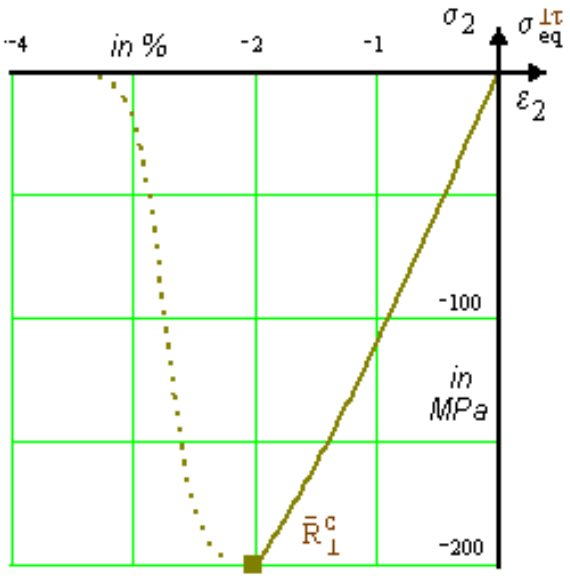


Transv. compr. stress/strain curve $\sigma_2^c(\varepsilon_2)$;
UD-lamina (softening assumed).
CFRP: AS4/3501-6 epoxy.
$\bar{R}_\perp^c$ =200 MPa, $\bar{E}^c{}_{\perp 0}$ = 11 GPa;
$n^{\perp c} = 5; a_d^{\perp c} = -2.7\%, b_d^{\perp c} = 0.12\%$

Figures $\sigma_\perp(\varepsilon_\perp) \equiv \sigma_2(\varepsilon_2)$



Transv. compr. stress/strain curve $\sigma_2^c(\varepsilon_2)$;
UD-lamina (softening assumed).
GFRP: E-glass/MY750/HY917/DY063.
$\bar{R}_\perp^c$ = 145 MPa, $\bar{E}^c{}_{\perp 0}$ = 16.2 GPa;
$n^{\perp c} = 6.6; a_s^{\perp c} = -3.45\%, b_s^{\perp c} = 0.47\%$



Transv. compr. stress/strain curve $\sigma_2^c(\varepsilon_2)$;
UD-lamina (softening assumed).
CFRP: AS4/3501-6 epoxy. Formel
$\bar{R}_\perp^c$ =200 MPa, $\bar{E}^c{}_{\perp 0}$ = 11 GPa;
$n^{\perp c} = 5; a_d^{\perp c} = -2.7\%, b_d^{\perp c} = 0.12\%$

Figures $\sigma_\perp(\varepsilon_\perp) \equiv \sigma_2(\varepsilon_2)$

Citation:
"Below matrix properties are considered to be low compared with typical data in literature. It was not attempted to change them in order to facilitate a comparison with the test data in Part B"!!
This citation is not irrelevant for the comparison Test-Theory.

Matrix type	8551-7 epoxy	PR913 epoxy	Epoxy 1	Epoxy 2	MY750
Elastic Modulus E_m (GPa)	4.08	0.95 *	3.2	3.2	3.35
Elastic Shear modulus G_m (GPa)	1.478	0.35 *	1.2	1.2	1.24
Elastic Poisson's ratio υ_m	0.38	0.35	0.35	0.35	0.35
Tensile strength Y_{mT} (MPa)	99	70	85	73	80
Compressive strength Y_{mC} (MPa)	130	130	120	120	120
Shear strength S_m (MPa)	57	41	50	52	54 $\equiv R_\tau$
Tensile failure strain ε_{mT} (%)	4.4	7.3	2.65	5	5 ?
Compressive failure strain ε_{mC} (%)	9	13.6	3.75	5	5
Shear failure strain γ_m (%)	5.1	11.5	-	-	-
Thermal expansion coefficient α_m (10^{-6}/°C)	46.7	60	58	58	58

The following Table includes the WWFE-provided FRP-test data

Fibre type	IM7	T300	A-S	S2-glass	E-Glass
Matrix	**8551-7**	**PR-319**	**Epoxy1**	**Epoxy2**	**MY750**
Fibre volume fraction V_f (%)	60	60	60	60	60
Longitudinal modulus E_1 (GPa)	*165**	*129*	*140**	*52*	*45.6*
Transverse modulus E_2 (GPa)	*8.4*	*5.6+*	*10*	*19*	*16.2*
Through-thickness modulus E_3 (GPa)	8.4	5.6+	10	19	16.2
In-plane shear modulus G_{12} (GPa)	*5.6**	*1.33+*	*6**	*6.7**	*5.83**
Transverse shear modulus G_{13} (GPa)	5.6*	1.33+	6*	6.7*	5.83*
Through-thickness shear modulus G_{23} (GPa)	2.8	1.86	3.35	6.7	5.7
Major Poisson's ratio υ_{12}	*0.34*	*0.32*	*0.3*	*0.3*	*0.28*
Major transverse Poisson's ratio υ_{13}	0.34	0.32	0.3	0.3	0.28
Through-thickness Poisson's ratio υ_{23}	*0.5*	*0.5*	*0.49*	*0.42*	*0.4*
Longitudinal tensile strength X_T (MPa)	*2560*	*1378*	*1990*	*1700*	*1280*
Longitudinal compressive strength X_C (MPa)	*1590*	*950*	*1500*	*1150*	*800*
Transverse tensile strength Y_T (MPa)	*73*	*40*	*38*	*63*	*40*
Transverse compressive strength Y_C (MPa)	*185***	*125***	*150***	*180***	*145***
Through-thickness tensile strength Z_T (MPa)	63	40	38	50	40
Through-thickness compressive strength Z_C (MPa)	185**	125**	150**	180**	145**
In-plane shear strength S_{12} (MPa)	*90***	*97***	*70***	*72***	*73***
Transverse shear strength S_{13} (MPa)	90**	97**	70**	72**	73**
Through-thickness shear strength S_{23} (MPa)	57	45	50	40	50
Longitudinal tensile failure strain ε_{1T} (%)	*1.55*	*1.07*	*1.42*	*3.27*	*2.81*
Longitudinal compressive failure strain ε_{1C} (%)	*1.1*	*0.74*	*1.2*	*2.21*	*1.75*
Transverse tensile failure strain ε_{2T} (%)	*0.87*	*0.43*	*0.38*	*0.33*	*0.246*
Transverse compressive failure strain ε_{2C} (%)	*3.2*	*2.8*	*1.6*	*1.5*	*1.2*
Transverse tensile failure strain ε_{3T} (%)	0.76	0.43	0.38	0.263	0.25
Through-thickness compressive failure strain ε_{3C} (%)	3.2	2.8	1.6	1.5	1.2
In-plane shear failure strain γ_{12u} (%)	*5*	*8.6*	*3.5*	*4*	*4*
Transverse shear failure strain γ_{13u} (%)	5	8.6	3.5	4	4
Through-thickness shear failure strain γ_{23u} (%)	2.1	1.5	1.5	0.59	0.88
Longitudinal thermal coefficient α_1 (10^{-6}/°C)	-1	-1	-1	8.6	8.6
Transverse thermal coefficient α_2 (10^{-6}/°C)	18	26	26	26.4	26.4
Through-thickness thermal coefficient α_3 (10^{-6}/°C)	18	26	26	26.4	26.4
Energy release rates G_{Ic}, G_{IIc} ($J/m^2 = 1N/m$)	200				240, 1500
mixed (fracture mechanics) mode to be assumed					
Stress free temperature (°C)	177	120	120	120	120
Test Case	TC10,11,12	TC2,3,4	TC7	TC6	TC1,5,8,9

* Initial modulus. ** Nonlinear behaviour and stress strain curves and data points are provided

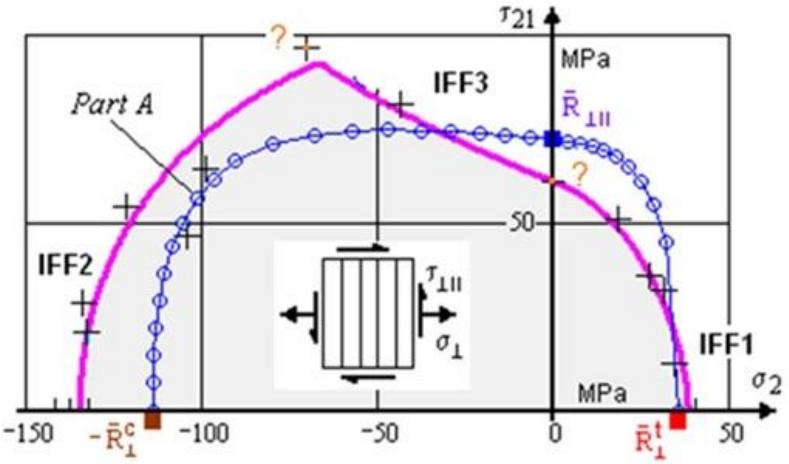
\+ These values are considered to be low, compared with typical data for the same material published somewhere else or quoted by the manufacturers. We have not attempted to change them in order to facilitate a comparison with test data in Part B.

6.2.3 WWFE-I UD Lamina Test Cases

WWFE-I, TC1, UD lamina, GFRP, E-glass/LY556 Ep [*Test data DLR Stuttgart*]

How looks the main cross-section of the IFF body?

Task: Determination of fracture failure curve, capturing IFF3, IFF1 and IFF2 by performing a so-called 'tension-compression-torsion tube test' campaign



Tube, 90°-filament hoop wound

$\sigma_1 = \hat{\sigma}_y = \hat{\sigma}_{hoop} = p \cdot r_{int} / t$

$\sigma_2 = \hat{\sigma}_{ax} = p \cdot r_{int} / (2 \cdot t) + F_{ax} / (2\pi \cdot r_{int} \cdot t)$

$\tau_{21} = M_t$/critical cross section area

*test evaluation based on un-deformed geometry

*monotonic loading performed in test

$\{\bar{R}\} = (1140,\ 570,\ 35,\ 135,\ 72)^T$ PartB-change

$b_\perp^\tau = 1.09$; $b_{\perp\parallel} = 0.13$; $b_{\perp\parallel}^\tau = 0.4$; $m = 3.1$

$\mu_{\perp\parallel} = 0.6$ compared to usual $\mu_{\perp\parallel} = 0.25$

$\Delta T = -68°C$ (after curing)

Part A, prediction: Data of elasticity properties, UD strengths $\bar{R}$ provided, only. No friction value μ for IFF3 slope provided! Lowest value for μ in Part A assumed (safe side)

Part B: the 3 strength points were altered! Two doubtful (?) failure stress points were provided. Nevertheless, QinetiQ asked to map the course of PartB-test data (magenta curve) despite of the fact that a Poissons ratio $\mu_{\parallel\parallel}$ had to be taken which is much too large, compared to values of own and other test campaigns !

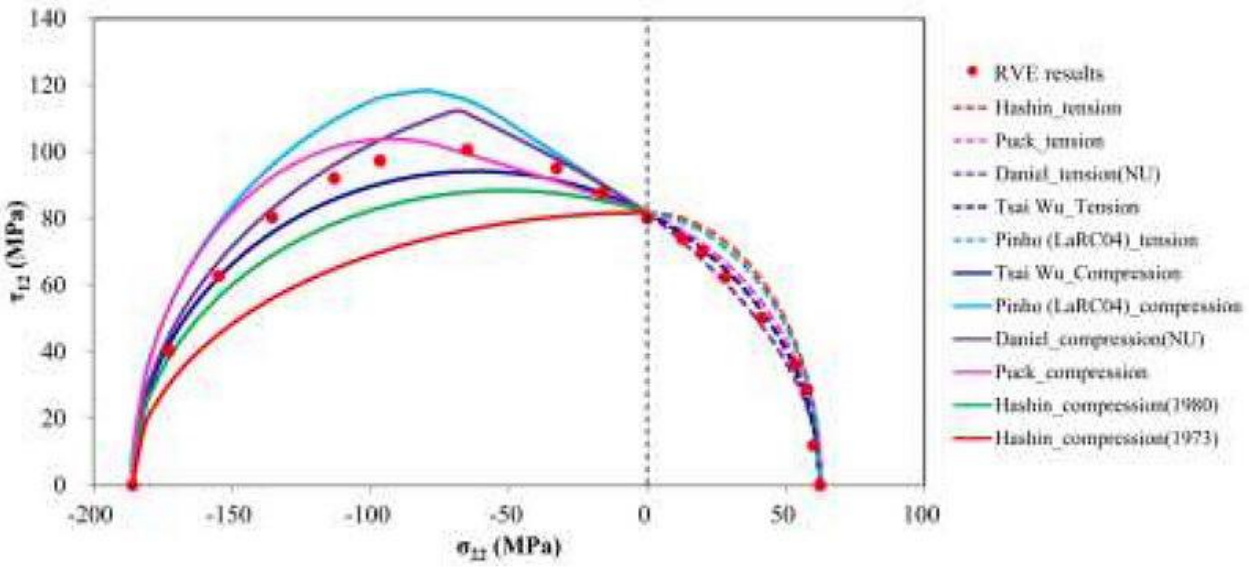
- Before test data evaluation: Check whether a thin tube test specimen (r / t > 10), otherwise ‚thick' formula is tu use.
- No reasonable PartA-mapping possible with the provided PartA-information, see blue curve!
- After later discussion with the former test engineer at DLR: "The upper test point must be false"!
  ► TC1 test data set (Part B) is not acceptable for a model validation!

For the TC1 above, the author knew about the test inaccuracy of the two comparison-decisive test points indicated by the question marks-marked test points above. Nevertheless, over the last decade false test results – like above - are un-intentionally taken for a comparison of theories.

Below figure shows by the red dots a micro-mechanical prediction of points of the in-plane shear stress-strain curve and its comparison to predictions from many fracture criteria. Regarding the theoretical results and comparing them to own test data the prediction is good (see *Fig.6-7*). But, the practicability of the micro-mechanical formula is nevertheless to check and cannot be simpler than the author's macro-mechanical strength criteria set employing just physically-based, measurable 5 strengths and 2 friction values. For certification statistically-based strength design allowables are to apply. How does the present micro-mechanical procedure fulfill this structural integrity requirement?

LL:
Non-accurate test results can barely be mapped by a physically based, test validated SFC.
However test-validated SFCs give a possibility to check the goodness of test data courses.

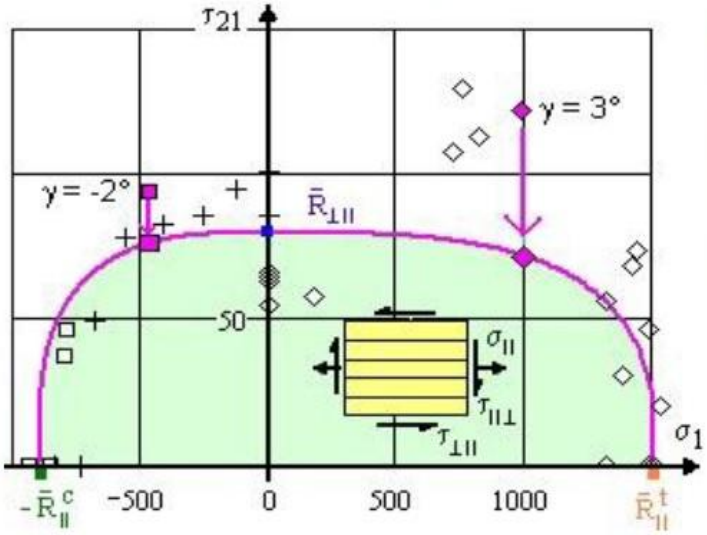
Therefore: Before performing a criteria-comparison on basis of provided test results, one should check the quality of these test results in advance !



Failure Criteria of Unidirectional Carbon Fiber Reinforced Polymer Composites Informed by a Computational Micromechanics Model.[Qingping Suna†, Guowei Zhoub,c†, Zhaoxu Mengd†, Haiding Guoa, Zhangxing Chene, Haolong Liua, Hongtae Kangf, Sinan Ketend, Xuming. ghd@nuaa.edu.cn]*

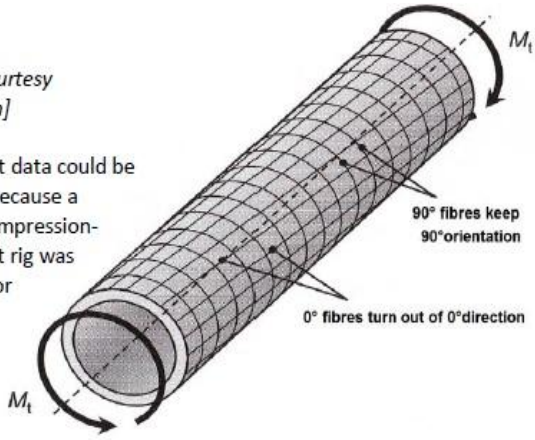
WWFE-I, TC2, UD lamina, CFRP, T300/BSL914C Ep, $\tau_{21}^{fr}(\sigma_1)$

Task: Determination of IFF curve, capturing IFF3, FF1 and FF2



[Figure: courtesy IKV Aachen]

Bi-axial test data could be obtained because a tension-compression-torsion test rig was available for tubes



Tube (90°-hoop wound) $\sigma_1 = \sigma_{hoop}$, $\sigma_2 = \sigma_{axial}$,

$\{\bar{R}\} = (1500,\ 900,\ 27,\ 200,\ 80)^T$,

Part B: $b_{\perp\parallel} = 0.13$; $m = 3$, $\Delta T = -125°C$ (after curing)

Part A, prediction: Strength data only provided, no friction value (slope) μ.

Part B, comparison: Strength data sets were provided, partly from 0°-test specimens (axial fiber direction) and partly from the traditional 90°- tube test specimen! After transformation, the two chosen ■◆, by executing a *non-linearly CLT*-computed shear strain analysis, these two 0°-points exemplarily could be shifted onto the magenta envelope. The shear strength point (blue) had to be adjusted according to new B information.

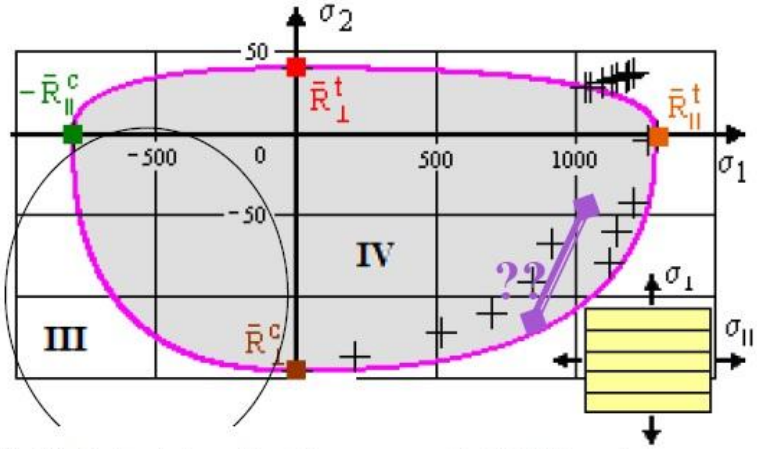
- Data from 0°- tube test specimens ◊ cannot be used like hoop-wound 90°-tube test specimens, physically non-sense.
- The coordinate system of the 0°-test specimen lamina twists under torsion by γ. Hence, 0°-test data must be transferred into the twisted material coordinate system.

► TC2 test data set could serve for material model validation after correction by the author and choosing just 90°- wound tubes.

WWFE-I, TC3, UD lamina, GFRP, E-glass/MY750EP $\sigma_2(\breve{\sigma}_1 \equiv \sigma_1)$

Which is the fracture envelope σ_2 (σ_1) ?

Task: Mapping in all four quadrants without obtaining sufficient test results fracture modes: (FF1, FF2, IFF1, IFF2, –)



Tube (90°-hoop filament wound)

$\sigma_1 = \sigma_{hoop}, \quad \sigma_2 = \sigma_{axial}$

$\{\bar{R}\} = (1280,\ 800,\ 40,\ 145,\ 73)^T$

(Part A, old IFF3 formula:

$b_{\perp\parallel} = 0.13,\ b^r_{\perp\parallel} = 0.4,\ b^r_{\perp} = 1.5,\ m = 3)$,

Part B: $b_{\perp\parallel} = 0.13, b^r_{\perp} \rightarrow b_{\perp\perp} = 1.5;$

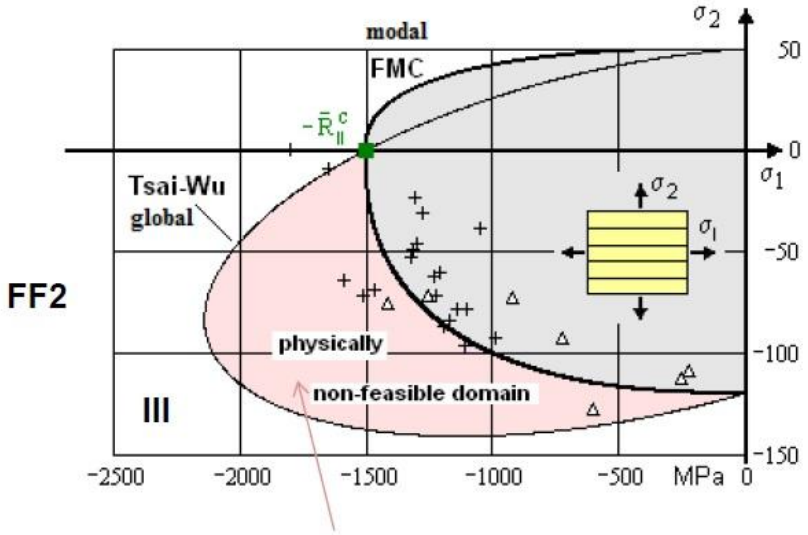
$m = 3$

Part A: Data of strength points were provided $\{\bar{R}\}$. Remaining necessary frictions μ were assumed by the author.

Part B: For the quadrants II and III no multi-axial data sets were provided. Test data in quadrant IV show discrepancy ! Real winding angle was ±85° instead of 90° (effect on strength and stiffness was not regarded w.r.t. other missing information and to scatter). *IKV , Aachen with Puck, filled the gap in the Tsai-Wu non-feasible domain, of quadrant IV.*

- *In quadrant IV it seems that two different 'test procedures' have been used obvious in the domain of 1000 MPa.*
- *In quadrant I the test data set could be better mapped by a higher m-value, however this was not done due to the inside oriented scattering data in quadrant IV and that m = 3 well matched the IKV-data set in quadrant III (next slide).*
  - ► *The provided TC3 test data set cannot really serve for a SFC material model validation. Questions arise w.r.t. quadrant IV: (1) Are different tests used? (2) Was the test data evaluation, regarding the specimen type, performed considering widening of the tube?*

Mapping in the 'Tsai-Wu non-feasible domain' (quadrant III)



[Data, quadrant III: courtesy, Knops, IKV Aachen, 2003]

The modal FMC maps correctly, the **global** *Tsai-Wu formulation predicts a non-feasible domain !*

► *TC3 test data set does serve for validation of the SFC model in quadrant III after obtaining the IKV test results.*

Steve Tsai's F_{12}-parameter problem. Some months ago Steve informed me: "*Prof. Shuguang Li was most helpful to explain the conditions for the interaction term F_{12} in the failure criterion*". And: *We are happy to have Shuguang Li in Chapter 9 to show that -1/2 is in fact the correct value*

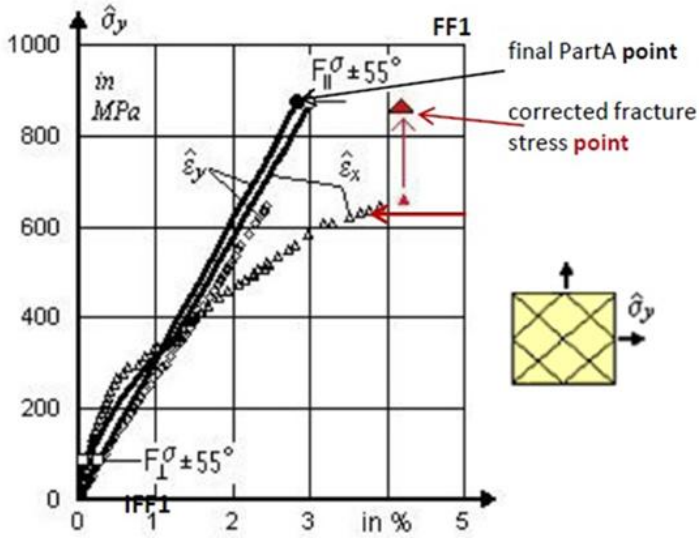
for the interaction term if it is assumed that the failure envelope is a paraboloid (with very large resistance to triaxial compression, the same assumption made for the von Mises criterion for isotropic materials). It is important to have removed one critical uncertainty of the Tsai-Wu criterion".

See CHAPTER 9 *Fully Rationalised Tsai-Wu Failure Criterion for Transversely Isotropic Materials*. Tsai's Book *Double-Double*. 2022

WWFE-I, TC11, UD, GFRP, E-glass/ MY750 [+55/-55/55/-55] , $\hat{\sigma}_y(\hat{\varepsilon}_y)$ and $\hat{\sigma}_y(\hat{\varepsilon}_x)$

Which are the stress-strain curves for $\hat{\sigma}_y : \hat{\sigma}_x = 2 : 1$ (*'pressure vessel, well designed to one single load case 'pressure loading'* p_{int}) ?

Task: Non-linear determination of the tube (*waterhose*) strains



Tube, filament wound, end-reinforced

Coupon Test Specimen, test data TC 8

$\{\bar{R}\} = (1280,\ 800,\ 40,\ 145,\ 73)^T$,

$\varepsilon_f^{fract} = 2.8\%$

$\Delta T = -68°C$ (after curing)

PartB :

$b_{\perp\perp} = 1.09$; $b_{\perp\parallel} = 0.13$; $m = 3$

Part A: Data of strength points were provided $\{R\}$.

Part B: (1) The evaluated, measured (on outer surface) laminate fracture stresses are about 25% lower than the predicted one. However, due to the end-reinforcement the shape of the tube bulges, becomes a barrel. The radius increases. Bulging will degrade the axial direction more than the hoop direction and probably may change the angle to a slightly higher value according to scissoring. (2) The ratio of the fracture strains is 2:1. The design is fibre-oriented and net theory (matrix stiffness put zero) must be approximately usable at fracture. It is then σ ~ ε and the strain in all directions should be almost the same. (3) The measured hoop strain 4.2 % is higher than the fiber fracture strain 2.8%, but this is for a net theory designed tube at fracture ! → What is the meaning of 4.2% ?

Net theory, increasingly valid after full IFF1 damaging, would show after the curves intersection approximately linearly running curves with about the same strain level. This is not to view. Why? At low stress levels continuum theory gives better results then net theory, of course.
The analysis of the bulging of the full barrel requires a FEA, which is not possible for the author. The axial strain at the gauge position is affected by the end constraints more than the hoop strain. The boundaries are too close to the locations of the strain gauges that the readings of the strain gauges are affected by the end conditions. The twofold failure in adjacent 55° layers is subjected to 'joint failure probability' which reduces the IFF load carrying capacity a little. Mind: Such a high straining is usually not permitted in structural applications.

Laminate quantities have the index roof, such as $\hat{\sigma}$.

The fiber direction angle counts from x-axis (0°) to y-axis (90°).

The critical lamina is the outer lamina that experiences stretching from membrane loading together with bending. Bending comes from the end-reinforced boundaries because these are not so far away from the locations of the strain gauges, so, that barreling could be really avoided.

As cylindrical widening cannot explain the difference of the curves, the effect must have come from above barreling. Fracture by 'barreling (bulging) bending' seems to be the main reason for the difference.

The analysis of the TC11 requires a non-linear FE calculation with an excellent solver to capture the anisotropic stiffness degradation from IFF1 till FF1.

Therefore, TC11 is not so much an exercise for failure criteria but for excellent FE codes.

In addition, another nocturnal thought about the discrepancy Prediction ↔ Measurement shall be presented:

* Designed by using Net Theory: $\hat{\sigma}_y = \hat{\sigma}_{hoop} = 2 \cdot \hat{\sigma}_{ax}$

  Fiber direction angle $\alpha = arctan\sqrt{\hat{\sigma}_y / \hat{\sigma}_x} = arctan\sqrt{2} \rightarrow \alpha° = \alpha \cdot 180° / \pi = 54{,}75°.$

* Measured fracture strains of the bulged laminate tube wall are

  On outer surface at fracture $\left\{\hat{\varepsilon}_{outer}^{fracture}\right\} = (+4.2,\ +2.4,\ 0)^T\ \%$.

  Checking the 'scissor effect' = increase of angle $\hat{\alpha} = \alpha° \cdot \pi / 180°$

  $$\hat{\alpha}_{final} = \arctan(\tan\hat{\alpha} \cdot (1 + \hat{\varepsilon}_{hoop}^{fracture}) / (1 + \hat{\varepsilon}_{ax}^{fracture}) = 0.97 \rightarrow \alpha°_{final} = \hat{\alpha}_{final} \frac{180°}{\pi} = 55.5°.$$

  Result: Practically, there is no scissor effect.

* Evaluation of measured strain values

  Because of the negligible scissor effect, the fiber strain can be calculated by

  $$\varepsilon_f^{fr} = \varepsilon_{\square}^{fr} = 1 - \sqrt{1.042^2 + 1.024^2} = 0.046 = 4.6\% = 1.64 \cdot 2.8\% \ \text{!?}$$

  This is 64% highe than the given fiber fracture strain of 2.8 %.!

  It does also not fit to the given (nominal geometry-related?) failure stress $\hat{\sigma}_{hoop} = 645\text{MPa}$.

  Result: Are there open questions with WFE-I TC11 ?

The provision of strains, measured on the outer surface, together with the value of the internal pressure would have been clearer. Based on un-deformed initial geometry the 'vessel formulas' read:

$$\hat{\sigma}_y = \hat{\sigma}_{hoop} = p \cdot (r_{int} + \Delta r)/\ t, \quad \hat{\sigma}_x = \hat{\sigma}_{ax} = 0.5 \cdot \hat{\sigma}_{hoop} + F / (2\pi \cdot r_{int} \cdot t) \ \text{ with } \ F = 0.$$

Each interpretation of test results is helpful if it improves understanding.
Unfortunately this was not the case with QinetiQ in the WWFEs.

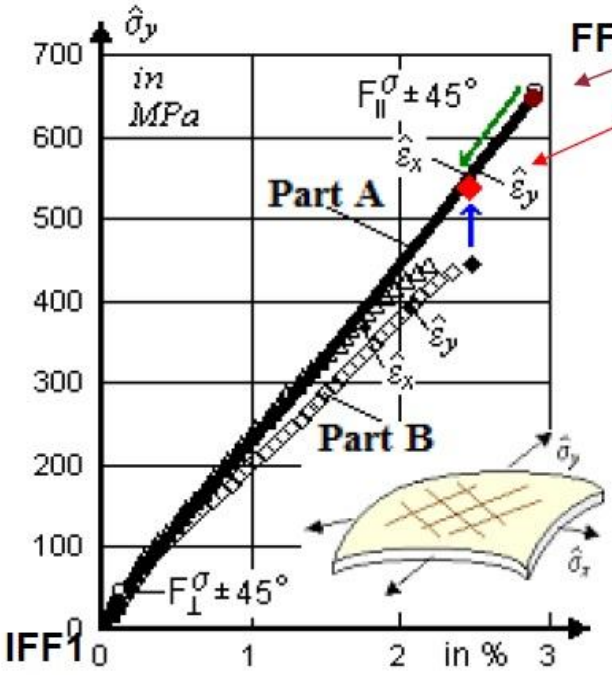
LL:

- WWFEs aim: *Testing Predictive Failure Theories for Fiber–Reinforced Polymer Composites to the full !' This includes UD strength criteria and numerical tools.*
- User: *Thinks only at a comparison of UD strength criteria!*

- *Tube qualification testing by internal pressure requires a test set-up where the membrane stresses cause the failure.*

WWFE-I, TC13, UD, GFRP, E-glass/MY750/Ep, [45/-45/45/-45]s , $\hat{\sigma}_y(\hat{\varepsilon}_y)$, $\hat{\sigma}_y(\hat{\varepsilon}_x)$

Which are the stress-strain curves for $\hat{\sigma}_y : \hat{\sigma}_x = 1:1$ *(p_{int} + axial tension)* ?



Final blind PartA prediction point.

PartB test point *after* the two corrections ◆

Tube, end-constrained

$\hat{\sigma}_y = \hat{\sigma}_{hoop}$

$\{\bar{R}\} = (1280,\ 800,\ 40,\ 145,\ 73)^T$, $\Delta T = -68°C$ (after curing)

$E_{\parallel} = 45600$ MPa, $\varepsilon_f^{fracture} = 2.8\%$.

Using netting theory of this fibre-dominated laminate for a bulging assessment of fracture it follows with the PartB-information on $\hat{\varepsilon}_{hoop}^{fracture} = 0.022$, $\hat{\varepsilon}_{axial}^{fracture} = 0.025$ and setting $\sigma_{\perp} = \tau_{\perp\parallel} = 0$ (zero matrix stiffness) the laminate stresses read $\hat{\sigma}_x = \hat{\sigma}_y = 530$ MPa, delivering lamina stress $\sigma_{\parallel}^f = 1062$ MPa. From this a reduction is derivable

$$\hat{\sigma}_y^{reduced} = 660 \text{ MPa} \cdot (1062/1280) = 547 \text{ MPa}.$$

Part A: Data of elasticity properties, UD strengths $\{\bar{R}\}$ and ε were provided. Remaining data assumed.

Part B: No modification of model ! Obvious in the graph is the high fracture load predicted compared to test. Also, non-linearity comes not out. However, bulging with the axially altering widening of the end-constrained tube is reported in experiment. This additional test data information – supported by simple netting analysis – caused to *reduce the computed fracture strain* and to *increase the failure stress* after assessing bulging !

Fibre-dominated design and laminate behavior

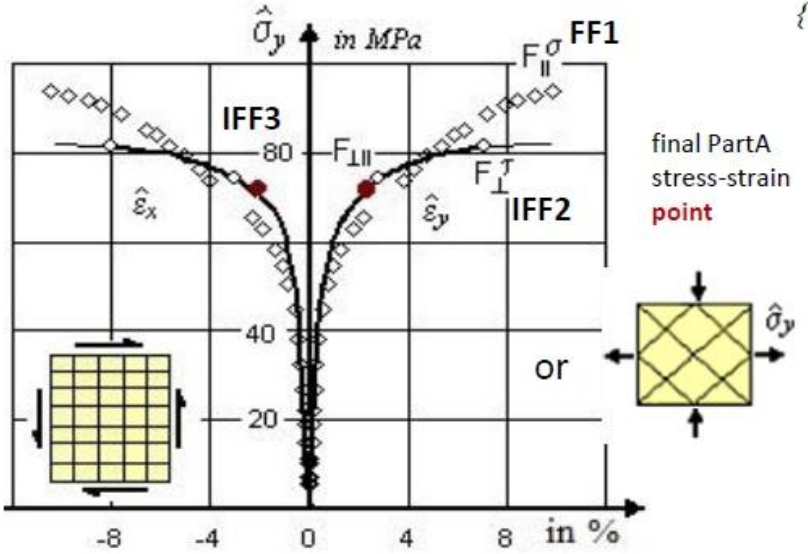
It is to expect that bulging together with the relatively large deformation will mainly cause that the two test curves do not lie upon another and are shorter than the predicted ones. An interpretation of the PartB-provided strains was helpful. The test fracture points could be raised and the predicted fracture points could be lowered. Bulging must be treated by a FEA program.

► *After re-evalation, the TC13 test data set is applicable for the verification of the laminate design. Mapping quality became very good, which proves the used UD material SFC model*

WWFE-I, TC14, UD, GFRP, E glass/ MY750 Ep, [45/-45/45/-45]s, $\sigma_y(\varepsilon_y)$, $\sigma_y(\varepsilon_x)$

Which are the stress-strain curves for $\hat{\sigma}_y : \hat{\sigma}_x = 1 : -1$ *(means shear, realized by* p_{int} *+ axial compression)* ?

Task: Non-linear determination of the tube (using radial stress $\hat{\sigma}_y = \hat{\sigma}_{hoop} \equiv \hat{\sigma}_{tangent}$ induced by internal pressure $p_{internal} \cdot \bar{r} / t$ and an axial over-compressed $\hat{\sigma}_{ax} = \hat{\sigma}_x = F/ 2\pi \cdot r \cdot t$)



$\{\hat{\sigma}\} = (-\hat{\sigma}_y, \hat{\sigma}_y, 0, 0, 0, 0)^T = (0, 0, 0, 0, 0, \hat{\tau}_{xy})^T$

Tube, wound → anti-symmetic lay-up

$\hat{\sigma}_y = \hat{\sigma}_{hoop}$, TC8 data

$\bar{r} / t = (r_{inn} + t) / t = (50 + 5.9) / 5.9 = 9.5 < 10$

$\{\bar{R}\} = (1280,\ 800,\ 40,\ 145,\ 73)^T$

$\Delta T = -68°C$ (after curing), $\varepsilon_f^{fracture} = 2.8\%$.

Part B: Using $\hat{\varepsilon}_{hoop}^{fracture} = 0.10$, $\hat{\varepsilon}_{axial}^{fracture} = -0.11$

$\hat{\alpha} = 45 \cdot \pi / 180$ the real fracture angle

$\alpha_{final} = \arctan(\tan\hat{\alpha} \cdot (1 + \hat{\varepsilon}_{hoop}^{fracture}) / (1 + \hat{\varepsilon}_{ax}^{fracture})$

$\Rightarrow$ 51° after final scissoring.

Part A: Data of elasticity properties, UD strengths $\{\bar{R}\}$ and $\varepsilon_{fracture}$ were provided. Remaining data assumed by author.

Part B: „Thick cylinder theory was used in test evaluation. Strains were measured at the inside surface of the tube and provided. Bulging reported. Formula applied for thick cylinder was not provided."
Stiffness of the test curves of this matrix-dominated laminate are smaller from the beginning.
Bulging → slight modification Part A to Part B for allowing to compute a higher fracture hoop strain by increasing the maximum shear strain in the computation from 4% to 10%.

Matrix-dominated laminate behaviour is faced.
(1) Joint failure behavior of adjacent layers acts and causes in test as well an earlier in-plane shear failure as a stiffness loss.
(2) The large strain/ bulging deformation behavior cannot be captured by the simple secant modulus non-linearity approach of the author. The author did not trigger his non-linear analysis, FEA is needed with its excellent solvers. The utilized softening curve does not allow for efficient stress-redistribution.
(3) The strain-controlled, embedded fibres take over degradation-caused loading, and seem, due to redundancy effects, to still act above the 'weakest link value' level. Mind here my softening curves! Benign IFF2, here.
(4) Mind, please: Typical engineering applications are limited to < 1.5 % operational strain !
► *TC14 test data set is applicable for the verification of the laminate design. It proofs the used UD material SFC model.*

There are numerous SFCs describing fracture failure of the uni-directionally fiber-reinforced material family. In the World-Wide-Failure-Exercises-I and –II, practically running from 1992 to 2012. R. Cuntze and A. Puck could place their theories at the top. Cuntze participated successfully with his 'Invariant-based, mode-distinguishing FMC theory' and Puck with his 'Mohr-Coulomb-based Action Plane Theory'.
Two non-funded German engineers won WWFE-I with their failure criteria: Cuntze with his Failure-Mode-Concept based criteria (*scalar process*) and Puck with his IFF-Action Plane criteria (*vectorial process, fracture plane angle needed*).

Nevertheless, I share Shuguang Li's statement on the originators of the WWFE theories:
"*Scientists are still human beings and it is inevitably to leave blind spots behind a theory, no matter how wishful one would like to be free of such blind spots*".

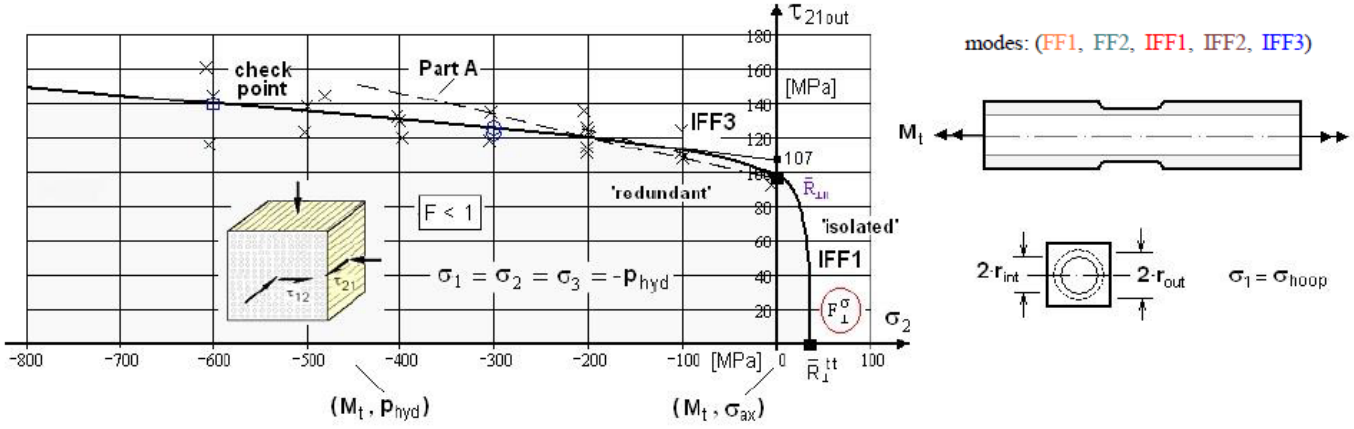
A model is always a compromise. *See for instance Chapter 7, determination cohesive shear strength*.

6.2.4 WWFE-II UD Lamina Test Cases

WWFE-II, TC2, UD lamina, CFRP, T300/PR319Ep, $\tau_{21}(\sigma_2 = -p_{hyd})$

Which is the influence of p_{hyd} on in-plane fracture shear stress or shear stress failure envelope ?

Task: Non-linear determination of the tube shear failure stress curve under hydrostatic pressure $\tau_{21}^{fr}(\sigma_2 = \sigma_1 = \sigma_3 = -p_{hyd})$



Part A: Data of strengths were provided. Remaining necessary data were assumed by author. The prediction of the *average* curves in TC2 and TC3 would have required the provision of an *average* curve however an upper' stress- strain curve was provided. No information on the acting 2nd-Tg effect. It is assumed that τ_{out} is the provided shear stress. From the formula $\tau = 2 \cdot M_T \cdot r / [\pi \cdot r_{out}^4 \cdot (1 - r_{inn}^4 / r_{out}^4)]$ follows $\tau_{out} \cong 1.4 \cdot \tau_{inn}$

Part B: Barrelling of the specimen was reported. The course of the provided test data does not exhibit the existing 2ndTg-effect demonstrated by a slope beyond the epoxide-typical '-200 MPa kinking point (hydrostatic pressure). Why? Open failure surface in p_{hyd}-direction. The data set of the 90° tube is only used but not the 0° tube set, regarding its twisting.

TC2 is fully linked to TC3 and TC4. TC2 and TC3 are average curves. Nevertheless, for Part A an 'upper stress-strain' curve was provided. The use of this curve does not lead to fully linked TCs! With the provided TC4 information of Part B, the author could determine the necessary average curve. Good Mapping was obtained first, after re-evaluation of provided data and the use of the ***average stress-strain curve*** *and by a* ***novel physical interpretation*** *of test data, discriminating in modelling near* $\sigma_2 = 0$*, the two domains of 'isolated' and 'embedded (redundant)' failure stress states, if* $\sigma_2 < 0$ *! Having known the average curve in Part A, the predicted curves would not differ from the Part B ones.*
► *TC2 test data set, - after a new evaluation and interpretation - finally became applicable for SFC model validation.*

In TC2 and TC 3 included is the modelling of the 2nd Tg-effect for the UD material. Both the figures are also examples for a redundant part (IFF3) and a weakest-link part (IFF2) of a failure curve, which were separately mapped to achieve an accurate mapping.

WWFE-II, TC2- TC3- TC4: Short derivation of the average stress-strain curve

Only the derivation of the average curve made it possible to carry out the required mapping. Without this curve, the existing checkpoint in the three graphs would not be hit. This checkpoint $\gamma_{21} = 0.142 = 14.2\%$, $\tau_{21} = 140$ MPa, $p_{hyd} = 600$ MPa was intentionally not optimized.

The required curve is a fitting curve through all the fracture points of the shear strain-shear stress Ramberg-Osgood curves (*R-O was the chosen fitting function. All four R-O parameters vary with* p_{hyd} *or with* σ_3) according to the formula

$$\gamma_{fr,\sigma 2} = \tau_{fr,\sigma 2} / G_{\sigma 2} + 0.002 \cdot (\tau_{fr,\sigma 2} / R_{\perp\parallel 0.2,\sigma 2})^{n_{\sigma 2}}.$$

* The jump in data size at p_{hyd} =0 can be explained again by the redundancy influence of the be almost straight), between the 'check point' and the above failure strain γ_{fr}

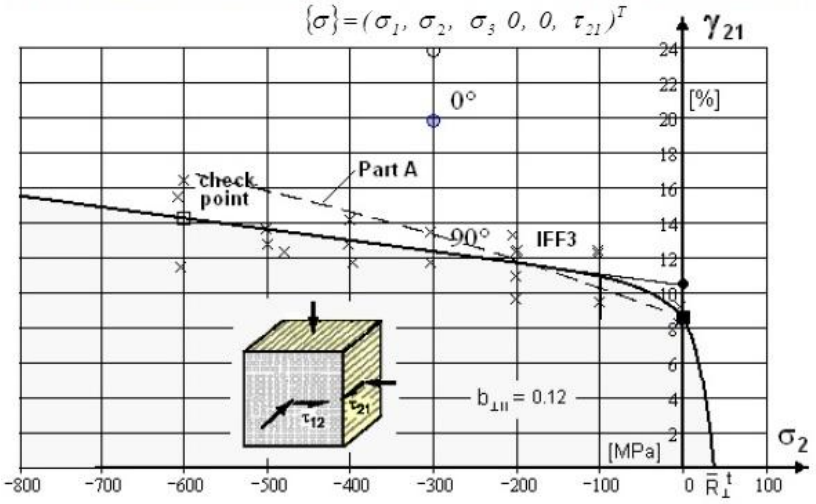
$$\gamma_{fr}(\sigma_2) = c_1 + c_2 \cdot \sigma_2 \quad \text{with} \quad c_1 = 0.104, \; c_2 = -6.33 \cdot 10^{-5}.$$

* The final rounding procedure is performed analogously to TC2 by a correction function, with

$$f_{TC3} = (1 - c_3 / e^{-\sigma_2 / c4}), \text{ with } \quad c_3 = 0.173, \; c_4 = 22 .$$

WWFE-II, TC3, UD lamina, CFRP, T300/PR319Ep

Task: Non-linear determination of one normal stress-shear strain curve of the tube γ_{21} (σ_2^{fr}, τ_{21}^{fr}) **TC3**



Tube hoop wound, data for TC2, TC3, TC4

$\sigma_{hoop} = \sigma_1$, $\sigma_{radial} = \sigma_3$, thick-walled

$\{\bar{R}\} = (1378,\ 950,\ 40,\ 125,\ 97)^T$ MPa,

$\{\varepsilon_{fracture}\} = (1.07,\ 0.74,\ 0.43,\ 2.8,\ 8.6)^T$ %,

$\{E\} = (129000,\ 129000,\ 5600,\ 5600,\ 1330)^T$ MPa

$E_{m0} = 950$ MPa, $\nu_m = 0.35$, $G_{23} = 1860$ MPa,

$\nu_{\perp\perp} = 0.48$, $\nu_{\perp\parallel} = 0.32$, $m = 2.8$,

Check point □ : ($\gamma_{21} = 0.142$, $\tau_{21} = 140$, $p_{hyd} = 600$)

$b_{\perp\perp} = 1.09$; $b_{\perp\parallel} = 0.12$ (in PartA = 0.3),

2^{nd} Tg effect could not be considered in Part B,

$\Delta T = -68$°C (after curing)

Part A: Data of strengths were provided. Remaining necessary data were assumed by author. The prediction of the *average* curve, task in TC3, would have logically required the provision of an *average* curve (see TC4), however an 'upper' stress-strain curve was provided. No information on the really active 2nd-Tg effect. PartA curve with assumed $b_{\perp\parallel} = 0.3$

Part B: Barrelling of the specimen was reported. The course of the provided test data does not exhibit the existing 2ndTg-effect demonstrated by a slope beyond the epoxide-typical kinking point at -200 *MPa* hydrostatic pressure. Why? The slope of the curve covers the hidden 2nd-Tg effect. Open failure surface in p_{hyd}-direction.

Two 0°- test specimen data (circles) are shown just for information. These are not used due to the twisting effect.

TC2 is fully linked to TC3 and TC4. TC2 and TC3 are <u>average</u> curves. The provided 'upper curve' did not lead to fully linked TCs in Part A! Linking successed: (1) With the provided TC4 information of Part B the author could determine the necessary average curve. (2) However good mapping of the pretty scattering test data was obtained first, <u>after</u> a ***novel physical interpretation*** *of the course of test data, by discriminating at $\sigma_2 = 0$ 'isolated failure stress states' for $\sigma_2 > 0$ from the 'embedded (redundant) ones for $\sigma_2 < 0$! This required a separate mapping of the isolated curve part and the embedded curve part with a following interaction work at $\sigma_2 = 0$. Then, the TC2-TC3-TC4-Check points were met and proved the quality of the final approach.*

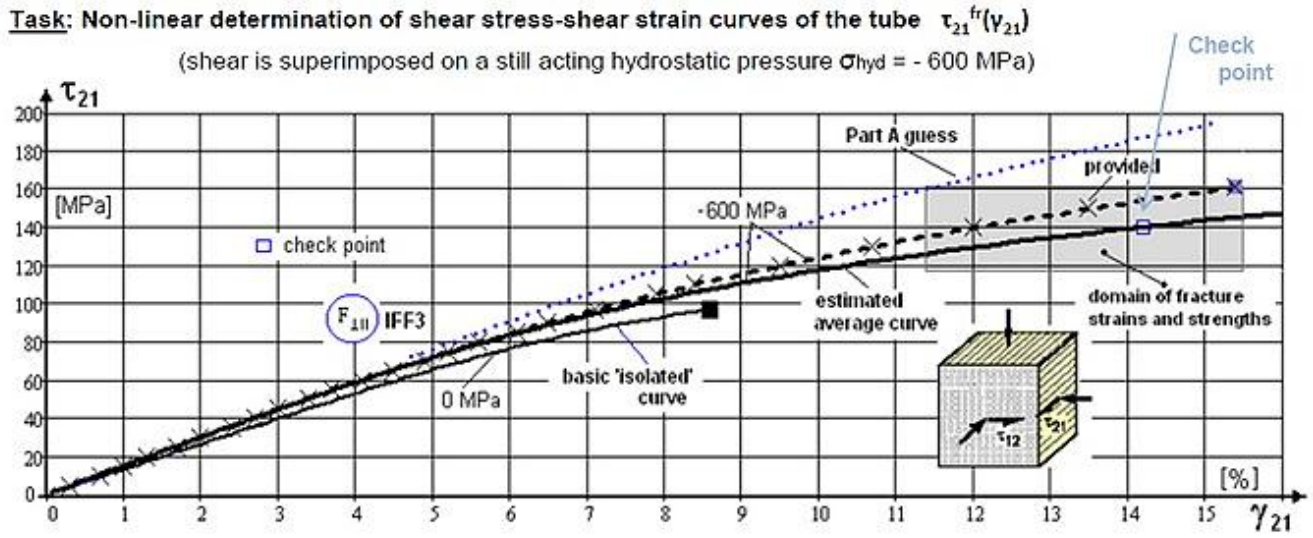
► *TC2 test data set - after a new evaluation and interpretation - finally became applicable for SFC model validation.*

Mind, please:

WWFE-II TC 2, TC3 and TC4 are fully linked!

WWFE-II, TC4, UD lamina, CFRP, T300/PR319Ep

Which is the in-plane transversal stress-shear strain curve for the tri-axial loading σ_{hyd} = - 600 MPa?



Part A: Data of strengths were provided. Remaning necessary data were assumed by the author. For the PartA guess curve (dotted) to be predicted it was assumed. $\mu_{\perp\parallel} = 0.3$, $\tau_{21} \equiv \tau_{out}$

Part B: Shaded is the area of the PartB-provided shear failure stresses and strains. On basis of this information the required average shear stress-shear strain curve could be estimated. From the shaded area can be seen, that the PartA-provided curve is an 'upper' curve (dashed). Effortful tuning gave the average curve. Change, necessary to the new information: $b_{\parallel\parallel} = 0.3 \rightarrow 0.12$.

PartA guess is far from the PartB reality according to the non-sufficient input. (1) Assuming a constant shear strain, it can be recognized that the shear failure stress increases with p_{hyd}. (2) With increasing p_{hyd} the failure strains increase, too.

► *TC4 test data set, after a new evaluation (the provided upper stress-strain curve was not an accurate input for test data mapping. Average properties had to be provided !) and interpretation, finally became applicable for SFC model validation*

WWFE-II, TC3 with WWFE-I, TC2: investigation of 0°-tubes and comparison with 90°-tubes

Just 90°-test specimen data was provided in Part A. For completing the understanding of pressure dependency on the shear behavior of composites, in Part B additionally, 0°-test specimen data was offered. Already since WWFE-I TC2 was clear that the different stress situations between 0°-tubes and 90° tubes under torsion loading have to be investigated in order to sort out whether the 0° tubes are usable or not.

In the case of only hydrostatic loading a 0° tube initially experiences (*good approach*) $\sigma_{hoop} = \sigma_{rad} = \sigma_{ax} = -p_{hyd}$ $\sigma_{hoop} \equiv \sigma_3 = -p_{hyd}$, $\sigma_1 = \sigma_{ax} = -p_{hyd}$ and a 90° tube a varying $\sigma_{hoop} \equiv \sigma_1$ with $\int \sigma_1(r) \cdot dr = -p_{hyd} \cdot \pi(r_{out}^{\ 2} - r_{\text{int}}^{\ 2})$, and $\sigma_{rad} \equiv \sigma_3 = \sigma_2 = -p_{hyd}$.

This outlines a clearer stress situation for the 0° tube. As far as the angle is small the test results are simpler interpretable than those of the 90° tubes. But this is not anymore true when the larger angles at fracture are encountered. Then, the stresses have to be transformed due to the fact that shearing under torsion loading turns the fiber direction and the lamina coordinate system is not anymore identical with the coordinate system of the tube. The state of stress, applied at significant angles, does not represent lamina stresses (in the *material coordinate system*) anymore but structural stresses in the x, y CoS.

$$\{\sigma\} = (\sigma_x, \sigma_y, \sigma_z, \tau_{yz}, \tau_{zx}, \tau_{xy})^T \equiv (\sigma_{ax}, \sigma_{hoop}, \sigma_{radial},\ 0,\ 0, \tau_{xy})^T ,$$

which have to be transformed into a 3D state of lamina stresses

$$\{\sigma\} = (\sigma_1, \sigma_2, \sigma_3, 0, 0, \tau_{21})^T = (\sigma_{||}, \sigma_{\perp}, \sigma_z, 0, 0, \tau_{\perp||})^T$$

to perform strength verification or data mapping. Otherwise, one would compare apples and oranges if using 90° and 0° data in a mixed way.

In TC2 of WWFE-I, such a transformation has been performed, however there, it was just a simple 2D problem.

Now here, for one 0° test point a transformation is performed by non-linear CLT analysis, via the relationship $\gamma \cdot L = R_0 \cdot \hat{\varphi}$, with γ the given shear strain, $L = 14.24\ \text{mm}$ the gauge length, $R_0 = 4.57\ \text{mm}$ the outer radius of the tube, and $\hat{\varphi} = \varphi \cdot (\pi / 180^\circ)$ the twist in radians). The following computation, using the relationship $\{\sigma\} = [T_\sigma]^{-1} \cdot \{\sigma'\} = [T_\varepsilon]^T \cdot \{\sigma'\}$ from [*CLT*], delivers the real lamina stresses

$$\sigma_{||} = \sigma_x (\cos\varphi)^2 + \sigma_y (\sin\varphi)^2 + 2\tau_{xy} \cos\varphi \sin\varphi ,$$

$$\sigma_{\perp} = \sigma_x (\sin\varphi)^2 + \sigma_y (\cos\varphi)^2 - 2\tau_{xy} \cos\varphi \sin\varphi ,$$

$$\tau_{\perp||} = (-\sigma_x + \sigma_y) \cdot \sin\varphi \cdot \cos\varphi + \tau_{xy} \cdot ((\cos\varphi)^2 - (\sin\varphi)^2) .$$

Just to give an impression, it is exemplarily compared one 0°-test point (full circle) with one 90°-test point at -300*MPa*. With above equation and for a simple linear elastic model, taking non-linearity not into account, in contrast to the WWFE-I -TC2, the stresses and stressing efforts

<u>0° tube</u>: from TC3: $(\sigma_x, \sigma_y, \sigma_z, \tau_{xy})^T = (-300, -300, -300,\ 123)^T\ MPa\ ,\ \varphi = 19.8°$

$$\Rightarrow (\sigma_{||}, \sigma_{\perp}, \sigma_z, \tau_{\perp||})^T = (-222, -378, -300,\ 95)^T\ MPa\ ;$$

$Eff_o = 0.78$ from $Eff^{||\tau} = 0.005$, $Eff^{\perp||} = 0.78$

are determined. This is to be compared to a 90° curve point (average) at $-300MPa$

<u>90° tube</u>: $(\sigma_{||}, \sigma_{\perp}, \sigma_z, \tau_{\perp||})^T = (-300, -300, -300,\ 126)^T\ MPa\ ;$

$Eff_{90} = 1.08$ from $Eff^{||\tau} = 0.114$, $Eff^{\perp||} = 1.08$

and characterizes the two very different states of lamina stresses.

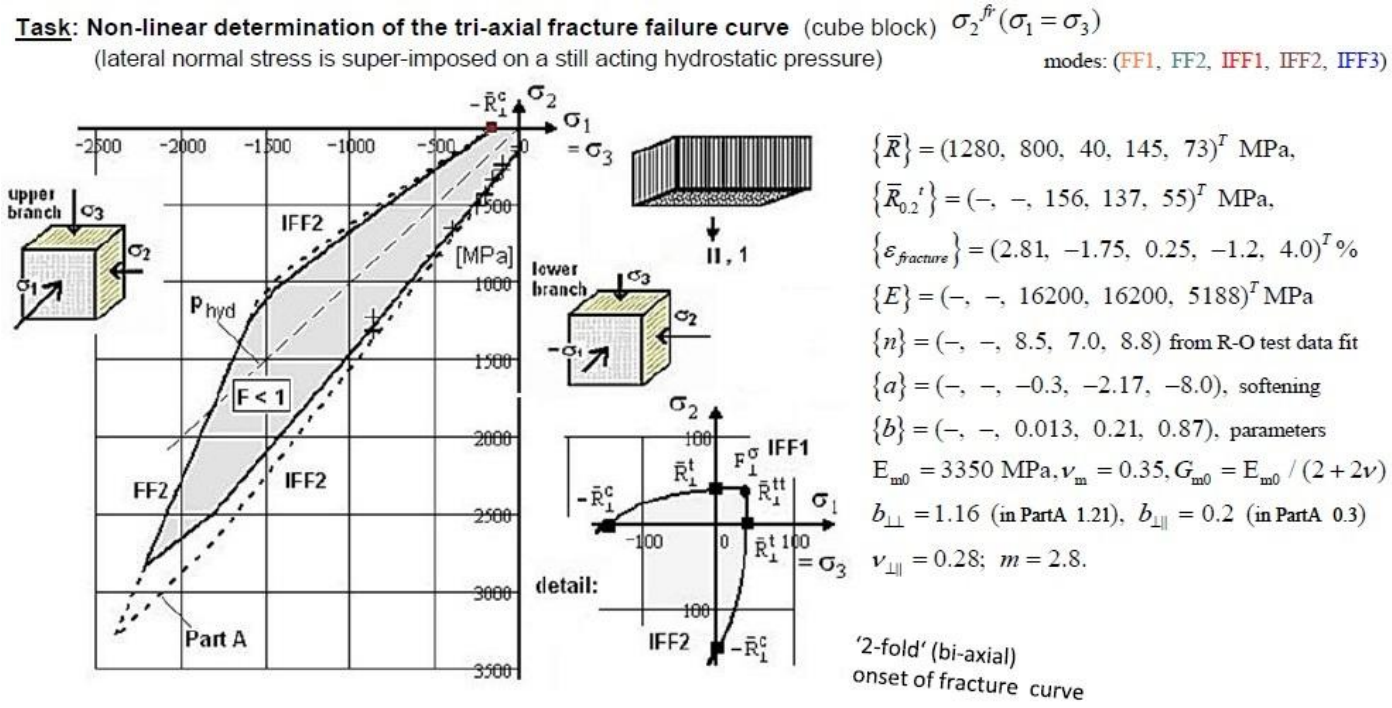
<u>LL:</u>

** A failure stress point of the 0°-data set cannot be put into a diagram together with 90°-data. Therefore, they are <u>not used</u> in Part B. 90° tube test data can be 2D formulated as $\sigma(-p_{hyd}, \tau_{\perp||})$ and thereby visualized by a 2D diagram, whereas for the 0°-tube a 4D stress state (stresses are different, see above) is to be visualized. In the simple 2D-TC2 of WWFE-I this was still possible.*

** Above coarse comparison further shows that the 0°-tube's twisting generates a reduced shear stress; equilibrium is achieved because the longitudinal fibers take over load. Remember that these 0°- tubes were not wound but hot-press molded.*

WWFE-II, TC5, UD, GFRP, E-glass/ MY750 EP

How much lateral stress σ_2 can the UD material sustain if a fiber-parallel stress σ_1 acts which is equal to a through-thickness stress σ_3? Test practice: p_{hyd} is superimposed by a lateral compressive stress σ_2^c at the σ_2-surfaces. The stress σ_1 is the stress acting at the respective coupon surface; the diagonal is the $p_{hyd}-line$. $\{\sigma\}=(\sigma_1=\sigma_3,\ \sigma_2,\ \sigma_3,\ 0,\ 0,\ 0)^T$



Part A: Data of strength points provided, remaining necessary properties were assumed by author

Part B: More information became available and the applicability of the provided test data set could be checked. Due to missing test data information in the transition zone IFF2-IFF1 no interaction was performed. 2nd Tg effect could not considered

PartA-prediction was not satisfying, due to missing and partly false input. Considering the lower branch, the test data set had to be re-evaluated by QinetiQ. Good Mapping, after the organizer "QinetiQ" was asked to re-evaluate the lower branch test data ! Then, the upper branch is fitting test data from DeTeresa [DeTer99], too, after subtracting his data by p_{hyd}. Failure curve is closed. ► After re-evaluation, the TC5 test data set became applicable for the validation of the SFC model

Task: Determination of the fracture failure curve $\sigma_{2,fr}(\sigma_1=\sigma_3)$ in the quadrants III and IV.

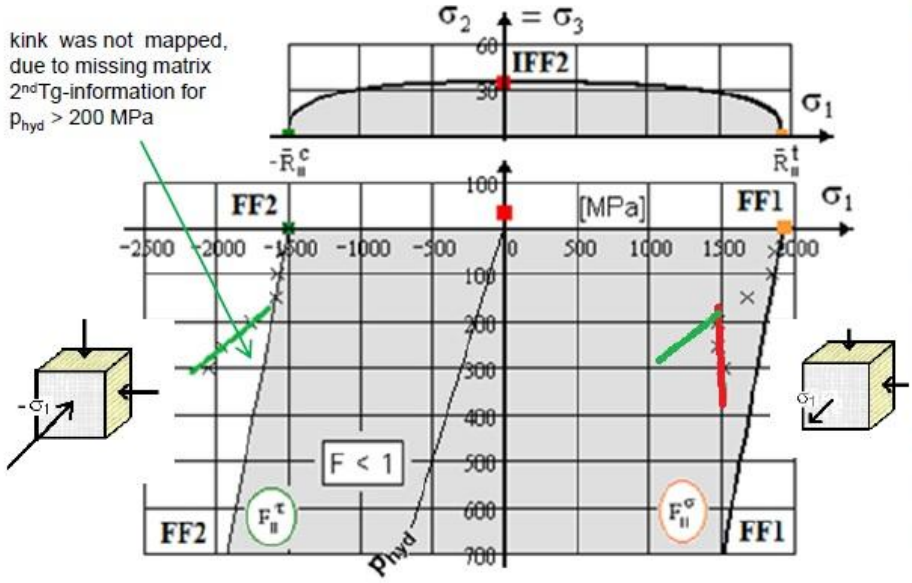
- The course of provided test data could be well mapped. The failure curve is closed.
- Assuming that the model pre-requisites remain valid, final failure by kinking, FF2, is possible under p_{hyd} according to the relationship $E_{\parallel}\cdot\varepsilon_1=-p_{hyd}\cdot(1-2\cdot\nu_{12})$, ν_{12} as larger Poisson's ratio.
- Computation indicates wedge failure IFF2 in quadrant III. Under σ_3^t, IFF1 means final failure.

For information:
Test data from de Teresa [*deTer99*] for the upper branch (2nd solution) of the failure curve in quadrant III are lying on the predicted upper branch after being re-evaluated by subtracting p_{hyd}.

WWFE-II, TC7, UD, CFRP, A-S-carbon/ EP 1

How much compressive fiber-parallel stress can the UD material sustain when a lateral compressive stress acts which is equal to a through-thickness stress (p_{int} + axial tension) ?

Task: Non-linear determination of tri-axial failure curves σ_{1fr} ($\sigma_2 = \sigma_3$)



$\{\sigma\} = (\sigma_1,\ \sigma_2,\ \sigma_3 = \sigma_2,\ 0,\ 0,\ 0)^T$

Dogbone test specimens, [Wronski-Parry] :

$\{\bar{R}\} = (1990,\ 1500,\ 38,\ 150,\ 70)^T$ MPa,

$\{\bar{R}_{0.2}{}^t\} = (-,\ -,\ 156,\ 137,\ 55)^T$ MPa,

$\{\varepsilon_{fracture}\} = (2.81, -1.75, 0.25, -1.2, 4.0)^T$ %

$\{E\} = (140000, 140000, 10000, 10000, 6000)^T$ MPa

$\{n\} = (-,\ -,\ 8.5,\ 7.0,\ 8.8)$ from R-O fit

$\{a\} = (-,\ -,\ -0.3,\ -2.17,\ -8.0)$,

$\{b\} = (-,\ -,\ 0.013,\ 0.21,\ 0.87)$,

$E_{m0} = 3350$ MPa, $\nu_m = 0.35$,

$G_{m0} = E_{m0} / (2 + 2\nu)$

$b_{\perp\perp} = 1.16$ (in PartA 1.21), $b_{\perp\parallel} = 0.12$;

$\nu_{\perp\parallel} = 0.30$; $m = 2.8$

Part A: Strength data and Poisson's ratio *v* provided as necessary input, friction values μ(b) assumed

Part B: No explanation for different slopes !? Equal slopes would proof the strength capacity reducing 2ndTg-effect, which must act equally in the fourth quadrant. If the two green curves – as data mapping curves - were provided, then the author would have simulated them with his 2ndTg-effect capturing program.

From physical reasons, the effect of the 2ndTg-effect must cause a similar orientation for both the branches and slopes
No satisfactory mapping is possible in the quadrants III and IV. The course of data points exhibits probable contradictions that cannot be explained by the author. Mapping is sufficient for p_{hyd} < 150 MPa, only. Idea, concerning a probable error-prone data evaluation: The compressive curve would better match with TC7 data if the p_{hyd} value would have been subtracted from σ_1^c . No mapping possible, due to missing 2ndTg information!
► *TC7 test data set is not acceptable for SFC model validation.*

LL:

**In general, it was pretty hard for the author (as for QinetiQ) – not only within the 2 WWFEs – to retrieve enough information on test specimen, test conditions and the raw test data evaluation. Other ways, accurate mapping is merely possible.*

**Reporting is always of personal nature and therefore differently complete..*

**Without having enough access to reliable composite test data sets, progress in composite design verification will remain very hampered.*

After the WWFE efforts:

"The generation of reliable multi-axis fracture test data
and the associated understanding-learning
of the fracture mechanisms is more complex
than the establishment of an associated theory.

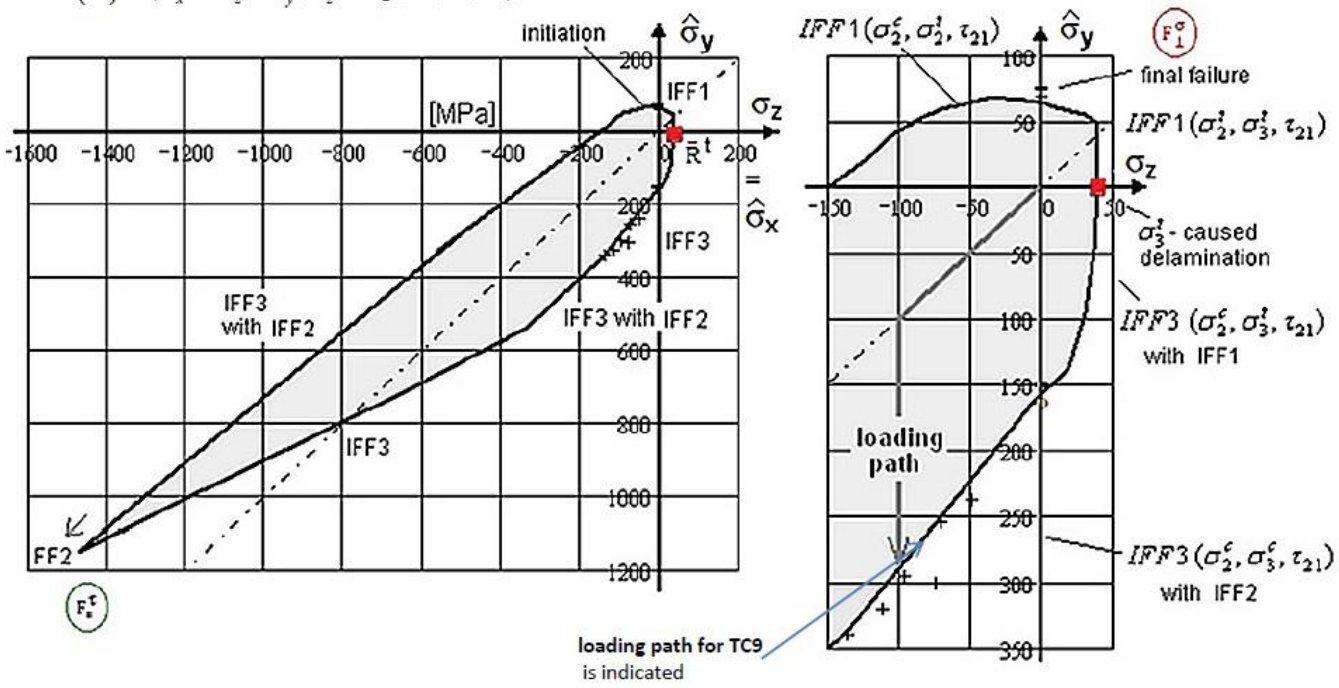
But a reliable theory makes the whole thing practicable." Ralf Cuntze, 2013

WWFE-II, TC8, UD, GFRP, E-glass/ MY750Ep, angle-ply $[35/-35/35/-35]_s$

Which is the effect of the applied surface pressure $\sigma_z = -p$ (*through-thickness stress*) on the size of the normal section force $n_y = \hat{\sigma}_y / t$ at fracture, with $n_x / t = \hat{\sigma}_x = \sigma_z$ and t as laminate thickness of the filament wound tube.

Task: Non-linear determination of the average fracture stress $\hat{\sigma}_y^{fr}(\sigma_z = \hat{\sigma}_x)$

$$\{\hat{\sigma}\} = (\hat{\sigma}_x = \sigma_z,\ \hat{\sigma}_y, \sigma_z = -p,\ 0,\ 0,\ 0)^T$$



Part A: Data of strength points $\{\bar{R}\}$ were provided, only. Remaining necessary data μ were assumed by the author

Part B: No SFC and program modification from Part A to Part B. More information now available. Organizers were asked to re-evaluate the provided test data set. Curing stress from effective temperature 120°-23° = 97° is σ_2^t = 15 MPa

LLs: After the organizer's re-evaluation of the test data set a good mapping with the SFCs could be achieved
► TC8 test data set is applicable for the verification of the laminate design. Proofs the used UD material SFC models

Data for the upper branch is missing. Data for the quadrants I, II, IV could be not provided in order to have a good basis for the validation. The high values of the 3 test data at the positive y-axis can be not explained by *"The test data were taken from [Wronski-Parry] and the test specimens were filament wound tubes"*.

A re-investigation of the friction parameter $b_{\perp\perp}$ by some curve 'data fitting' showed that it had to be reduced to 1.16 as for TC5. This value is substantiated by information from WWFE-I. The other friction parameter $b_{\perp\parallel}$ is obtained by mapping the test data provided for quadrant III.

Note, please: TC5, TC8 and TC9 possess the same material but belong to different test specimens which will naturally cause some difference in strengths values.

An improved non-linear programming is necessary, especially due to the fact that in the linked TC9 both the failure modes IFF2 and IFF3 have a similar risk to fracture, or - in other words - the material stressing effort is almost equal for both modes in the envisaged two-fold failure domain.

Change from Part A to Part B:

The fiber volume contents had to be increased from the initial *60%* up to V_f = 67% (almost "dry" filament situation). This would make a correction necessary so that the TC8 data do not remain the same as for TC5, but, the driving strengths in the *compression* domain might not become better and were kept. An increase of the fiber volume content on the elasticity properties is not considered due to the other uncertainties and that the given stress-strain curve would have to be adapted and hardening parameters to be reworked with all its work consequences.

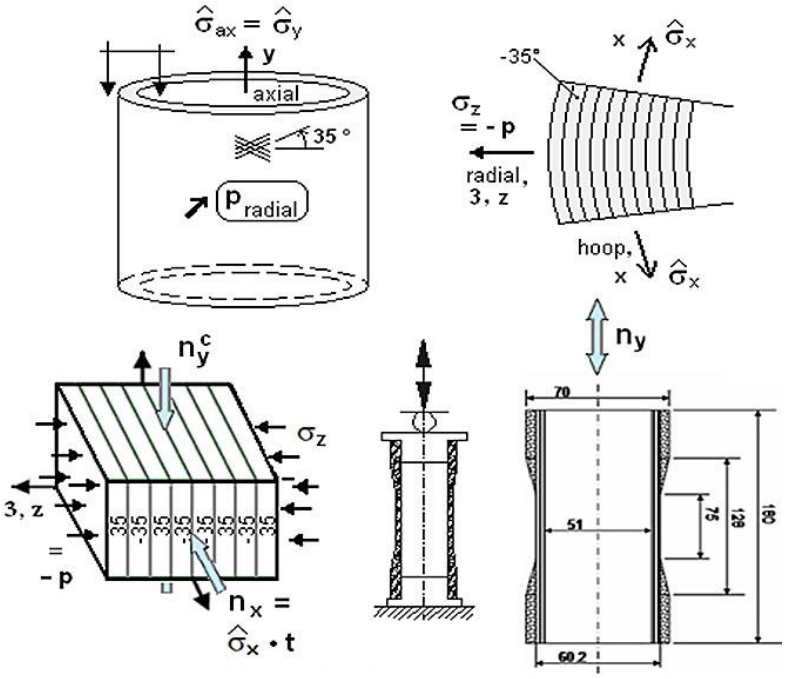
For TC8 and TC9, the analysis followed the mentioned 3D-CLT-MathCad program:

- IFF1 at the positive σ_z-axis belongs to a weakest link value or is an 'isolated' value $\bar{R}_{\perp}^{t}$, initial failure from σ_3^t means final failure. The curing stress has no direct effect, because it acts in the laminate plane.
- At the positive σ_y-axis axis some redundancy governs and the *initial* failure behavior is more benign. The curing stress has a direct effect. The provided 3 test data belong to *final* failure of this specimen at about $\bar{\sigma}_y^{final} = 72\,MPa$. This value can be explained: IFF1 micro-cracks decrease the stiffness and the fiber angle 35° ≡ 90°-55° increases. Under non-linear shear loading, more and more load is put onto the fibers until final failure occurs. Mapping of test data is not fully satisfactorily in domains (*this is valid for TC9, too*) where the complicate non-linear treatment of the commonly acting two modes IFF2 and IFF3 (*of about the same size of* Eff^{mode}) is located. There, the MathCad program faced numerical problems for some stress combinations and did not converge correctly. With respect to the small data basis μ was kept 0.2 and not increased to 0.25 for optimum mapping.

  The Birch matrix effect was considered.

The failure curve is closed. The complete failure surface consists of piecewise smooth regimes (*partial failure surfaces*). Each regime represents one failure mode which is governed by a single basic strength.

For more information: **Modelling of TC8 test situation,** in short



Tube (still thick walled, hoop-wound)

[*Wronski - Parry*, [20]]:

modes: (FF1, FF2, IFF1, IFF2, IFF3)

$\{\bar{R}\} = (1280,\ 800,\ 40,\ 145,\ 73)^T$ MPa,

$\{\varepsilon_{fracture}\} = (2.81,\ 1.75,\ 0.25,\ 1.2,\ 4.0)^T$ %

$\{E\} = (-,\ -,\ 16200,\ 16200,\ 5188)^T$ MPa

$\{n\} = (-,\ -,\ 8.5,\ 7.0,\ 8.8)$ from R-O test data fit

$\{a\} = (-,\ -,\ -0.3,\ -2.17,\ -8.0)$, softening

$\{b\} = (-,\ -,\ 0.013,\ 0.21,\ 0.87)$, parameters

$E_{m0} = 3350$ MPa, $\nu_m = 0.35$, $G_{m0} = E_{m0} / (2 + 2\nu)$

$b_{\perp\perp} = 1.16$ (in PartA 1.21), $b_{\perp\parallel} = 0.2$ (in PartA 0.3);

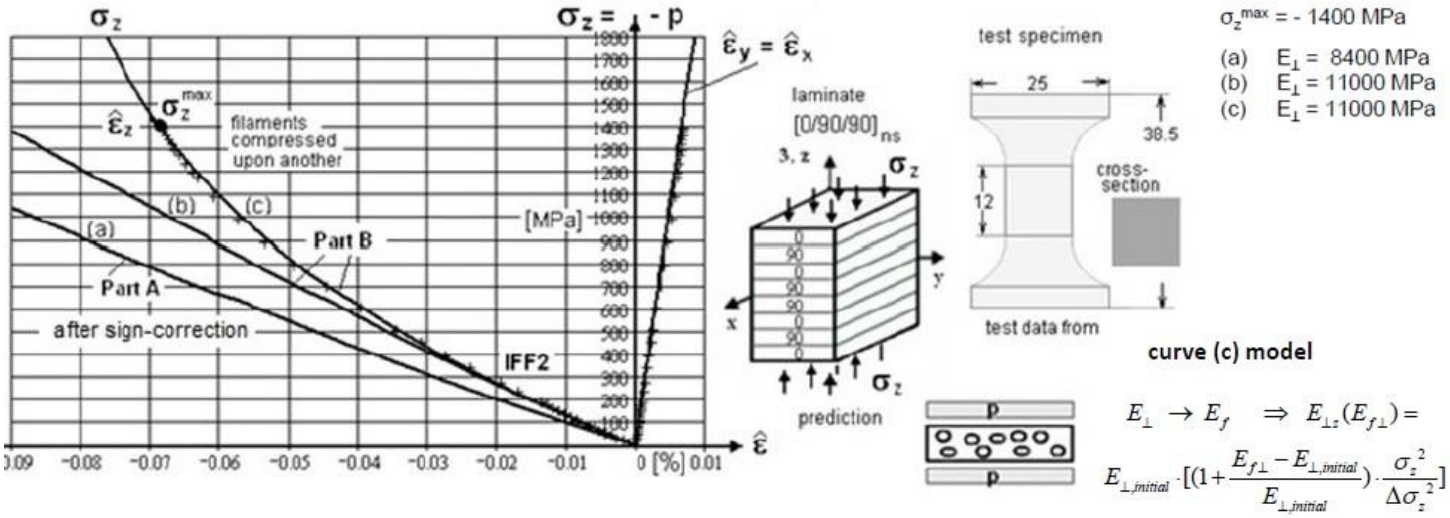
$\nu_{\perp\square} = 0.28$; $m = 2.8$,

2^{nd} Tg effect could not be considered.

WWFE-II, TC12, UD, CFRP, IM7/8551-7, cross-ply $[0/90/0/90]_{ns}$, balanced-symmetric

Which is the effect of the applied surface pressure σ_z = -p (through-thickness compressive stress) on the strains for $\hat{\sigma}_x = \hat{\sigma}_y = 0$?

Task: Non-linear determination of the 3 average strains as function of σ_z . The roof denotes a smeared stress



Part A: Data of strength {R} were provided. Remaining necessary property μ was assumed by the author .

Part B, Modifications from Part A to Part B: (1) Correction of a mistake (*author's curvature of the predicted curve in Part A was wrong, caused by a typing error in the equations coded*), curve (a). (2) Increase of the initial lateral elasticity modulus at origin from of Part A to 11000 MPa in Part B. (3) Consideration of a growing filament contact by a stiffness increase model. Properties TC10. It is not clear why this TC is marked as a cross-ply but the curve stems from a lay-up that is a quasi-isotropic angle-ply! The given test data set (crosses) stems from a quasi-isotropic laminate $[]_{45/0/-45/90]_{ns}}$! More information became available that led to an improved curve (b). Remaining difference was tackled by above assumption and curve (c) model. Then, a good mapping <u>after</u> this necessary physical interpretation of the course of test data could be achieved with curve (c).

The test specimen finally fails <u>structurally,</u> exhibiting a failure mode change. <u>Structural</u> failure cannot be described by a (<u>material</u>) SFC !
► TC12 test data set is not applicable for validation of a SFC model, because a SFC is a material model.

<u>Assumption:</u> "Filaments are finally pressed upon another which stiffens!"

This is tackled by a model that transfers the Part B data-improved curve (b) to (c) as compression-dependent increase generated by the filament lateral stiffness $E_{f\perp}$.

Regarding the Test Cases before, it may be concluded:

Test results can be far away from the reality like a bad theoretical model;
theory creates a model of the reality, whereas an experiment is 'one' realization of the reality.

6.2.5 UD, Novel modelling of Porosity in the quasi-isotropic domain

The effect of friction is reduced by increasing porosity. In order to map this, the author proposes a simple failure function *F* that spans from dense to pretty porous materials. The following formulas for the transversely-isotropic UD material are the basis for the curves in *Fig.6.2-1* below.

* Failure Function for a dense UD material

$$F^{SF} = [a_{\perp\perp} \cdot I_2 \; + \; b_{\perp\perp} \cdot \sqrt{I_4}\,] \;/\; \bar{R}_{\perp}^{c} = 1 \;\text{ with }\; a_{\perp\perp} = b_{\perp\perp} - 1 \;\text{ after inserting }\; \bar{R}_{\perp}^{\,c} = 104 \;\text{ MPa}$$

$$= [a_{\perp\perp} \cdot (\sigma_2 + \sigma_3) \; + \; b_{\perp\perp} \cdot \sqrt{(\sigma_2 - \sigma_3)^2 + 4\tau_{23}^{\,2}}\,] \;/\; \bar{R}_{\perp}^{c} = 1$$

$$= [a_{\perp\perp} \cdot (\sigma_2^{\,p} + \sigma_3^{\,p}) \; + \; b_{\perp\perp} \cdot \sqrt{(\sigma_2^{\,p} - \sigma_3^{\,p})^2 + 0^2}\,] \;/\; \bar{R}_{\perp}^{c} = 1 \quad \leftarrow \text{ 2 structural stresses}$$

* Failure Function for a porous UD material (index por, *author's simple approach*)

$$F_{porosity}^{SF} = \sqrt{a_{\perp\perp po}^{\;2} \cdot I_2^{\,2} + \; b_{\perp\perp por}^{\;2} \cdot I_4} - \; a_{\perp\perp por} \cdot I_2 \;] \;/\; 2\bar{R}_{\perp}^{c} = 1\,.$$

The two curve parameters are determined - as before performed - from insertion of the compressive strength point and from the bi-axial fracture stress point.

In *Fig.6.2-1* the parallel lines mark that a 'dense' UD material does not shear fracture. This is caused by the axial straining under a bi-axial compression stress state which is impeded by the constraining fibers.

When applying $a_{\perp\perp por} = 0$, then parallel lines can be obtained. The parallel lines represent density or zero porosity and exhibit the capability of the simple approach.

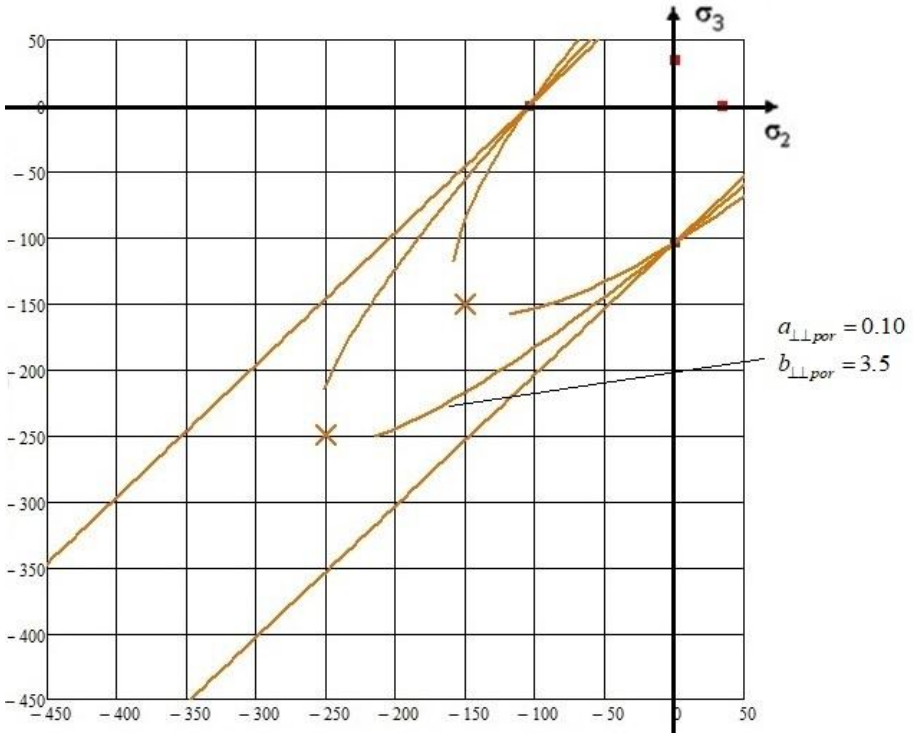


Fig. 6.2-1: Fracture failure curves of UD material regarding two different porosity grades. $a_{\perp\perp por}$ for 0, 0.10, 0.22 and $b_{\perp\perp por}$ for 4.0, 3.5, 2.9

Ideal dense materials possess no porosity. A fully porous material may be defined by $R_{\perp}^{cc} \cong R_{\perp}^{c}$. This case can be modelled like foam materials in the quasi-isotropic domain [*Cun16a*].

Conclusion points on the evaluation of the effortful WWFEs

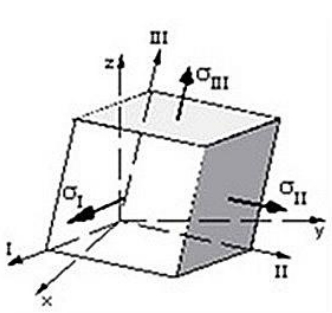
- Cuntze's 3D-failure criteria set for transversely-isotropic laminas is as well invariant-based (transfer between coordinate systems is automatically given) like 'Mises' as physically-based
- An invitation, to speak about the many obviously false test data, found no response at QinetiQ. Users still apply the false test data for model validation! This is a pity. One cannot validate a hopefully good failure criterion using false test data, however one can check the course of test data with an associated validated failure criterion
- The WWFE spoke about failure theories to be tested to the full. The ***WWFE failure theory*** includes 3 elements: ***Failure criterion, numerical procedure (such as FE codes) and non-linear analysis tools.*** However, the user looks just for a reliable macro-mechanical failure criterion that hopefully captures the micro-scopic failures by the proposed equations
- Above discrepancy lead to the WWFE-II-citation: Cuntze needs 75 parameters. The reality is: For his set of 5 failure criteria Cuntze needs 5 strengths, 2 friction values (*other contributors and Qinetiq seem not to know that for a reliable modelling material friction values must be used! Mohr-Coulomb acts and therefore the use of 5 parameters is not accurate*) and a given interaction exponent m. This results in 7 measurable properties. Hence, it is "not the power of 70 parameters" as R. M. Christensen interpreted → For all those contributors which did not perform all required tasks a smaller number of parameters has been counted, of-course
- The single isotropic test case was not sufficient to obtain enough knowledge for the matrix and the necessary micro-mechanical analysis. Here, QinetiQ provided just micromechanical material properties but forgot to provide with the associated micromechanical relationship. This is mandatory and therefore the author found a discrepancy of factor 2 for the data to be predicted! The description of the matrix Test Case did not fully inform whether one should use 'Mises' for a ductile matrix or 'Mohr-Coulomb' for a brittle matrix (*friction of a brittle matrix under compression and shear was dominating in WWFE-II*)
- Does it make sense to require from a physically different failure criterion for transversely-isotropic material that it should capture the isotropic matrix failure behavior, too?
- The author still informed in WWFE-I that in TC 1 apples and oranges (90° with 0° test specimen results) have been put together. One cannot depict in the same diagram 90°-wound tube test specimen data together with 0- wound tube data. However in WWFE-II TC 2 the same mistake happened again
- Stress- or strain-based failure criteria? Stresses are used in Fracture Mechanics and allow to 'add' residual stresses in solid strength mechanics. Strains are used in forming materials like ductile metals
- Closed and open failure envelopes: The cap is always closed whereas the bottom might be closed or not. Porosity leads to closure. In contrast to an isotropic dense material, at ultra-high pressures the fiber fails by tensile fracture caused by the acting Poisson effect
- Delamination is a failure in the 'structure' laminate or at its edges termed edge effect. Between the layers of a laminate it can be predicted by the application of the 3D failure criteria (here intentionally termed SFCs). At the laminate edges it is - due to the stress singularity – a task of fracture mechanics tools using cohesive zone models.

Mind, please: Cuntze's failure criteria for isotropic and transversely isotropic materials have no corners like the onset-of-yield predicting 'Tresca'. Stress concentration around holes is not addressed. Size and rate effects still wait for investigation.

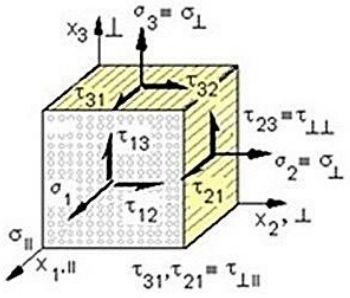
6.3 2D-Application to (technical) Ceramics isotropic, UD and orthotropic fabrics

As reminder, all stress state figures of the 3 material families are depicted again.

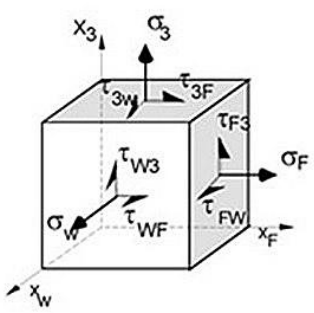
Ceramic (fiber) Matrix Composites CMC represent the applications where ceramic fibers are used for strengthening when facing high temperature



isotropic



transversely-isotropic



rhombically-anisotropic

$\{\sigma\} = (\sigma_x, \sigma_y, \sigma_z, \tau_{yz}, \tau_{xz}, \tau_{xy})^T$ $\{\sigma\} = (\sigma_1, \sigma_2, \sigma_3, \tau_{23}, \tau_{13}, \tau_{21})^T$ $\{\sigma\} = (\sigma_W, \sigma_F, \sigma_3, \tau_{3F}, \tau_{3W}, \tau_{FW})^T$

Isotropic: $\{\bar{R}\} = (\bar{R}^t, \bar{R}^c)^T$ with μ

Transversely-iso.: $\{\bar{R}\} = (\bar{R}^t_{\parallel}, \bar{R}^c_{\parallel}, \bar{R}^t_{\perp}, \bar{R}^c_{\perp}, \bar{R}_{\perp\parallel})^T$ with $\mu_{\perp\square}, \mu_{\perp\perp}$

Orthotropic: $\{\bar{R}\} = (\bar{R}^t_W, \bar{R}^c_W, \bar{R}^t_F, \bar{R}^c_F, \bar{R}_{WF}, \bar{R}^t_3, \bar{R}^c_3, \bar{R}_{3F}, \bar{R}_{3W})^T$ with $\mu_{WF}, \mu_{3W}, \mu_{3F}$

6.3.1 Isotropic (monolithic)

Ceramic material is an inorganic, non-metallic oxide, nitride, or carbide material. Monolithic ceramic materials are brittle, hard, strong in compression (if just slightly porous), and weak in tension and in consequence in shearing too. They are applied if wear and high temperature are faced. The material properties are inseparably linked to the manufacturing process steps, consisting of *preparation of the powder* (base material boron nitride, silicon carbide or aluminum oxide) and *shaping* with targeted influence on the microstructures in the final *sintering* process. Decisive for the material properties in the structural component are type, frequency and distribution of flaws.

A common application example is silicon-enriched silicon carbide SiC, which is manufactured under shielding gas from silicon and carbon powder and which is characterized by chemical resistance and corrosion resistance. An example for the reinforcement of a metal with ceramic particles is the hybrid metal-ceramic composite AO-403 [*CeramTec*] that has material parameters of metal alloy 60 vol.-% AlSi9MgMn, ceramic 40 vol.-% Al2O3 density 3.21 g/cm3, flexural strength 550 to 620 MPa, tensile strength 380 to 460 MPa, fracture strain ≈ 0.5%.

The SFCs applicable for isotropic ceramics must capture the porosity. Dependent on the grade of porosity $\bar{R}^c > \bar{R}^{cc}$ or $\bar{R}^c < \bar{R}^{cc}$ (very porous, similar to foam). In *Fig.6.3-1* as a failure curve example for a differently porous ceramic material is depicted.

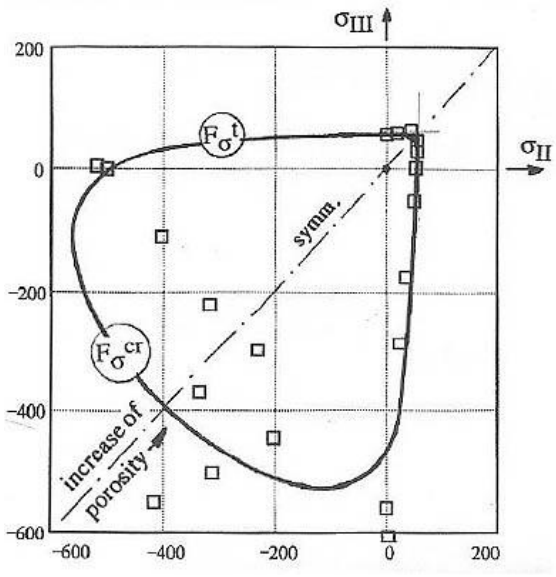
In future Additive ceramic Fabrication will require AF production modelling combined with structural modelling including SFCs to assess stress states in the structures built up by the distinct ceramic materials such as $Zr0_2$, Al_2O_3. Recently a Whitepaper was published of the future guideline VDI 3405, sheet 8.2 (English & German) on test specimens

Fig.6.3-1: Porous monolithic ceramics [Kowaltchuk]

Twofold failure occurrence with UD materials

at $\sigma_{II} = \sigma_{III}$ (tension cut-off)

$$\left\{\bar{R}\right\} = (\bar{R}^t, \bar{R}^c)^T \text{ with } \mu$$



6.3.2 UD

For the uniaxial and bi-axial reinforcement of ceramics filaments are produced and collected in a roving and then embedded into a ceramic matrix. Compared to monolithic ceramics, fiber-reinforced ceramic components such as silicon carbide fiber-reinforced silicon carbide (SiC/SiC) reduce brittleness, which means it improves damage tolerance by hindering the spread of cracks in the matrix through the fibers. The ceramic filaments are produced from various polymers, so-called precursors, by pyrolysis. The ceramic fibers are divided into oxide and non-oxide fibers (derived from [*Wikipedia*]).

Fig.6.3-2 outlines the similarity to FRP material. The same SFCs are to apply as with UD-FRP, regarding the porosity.

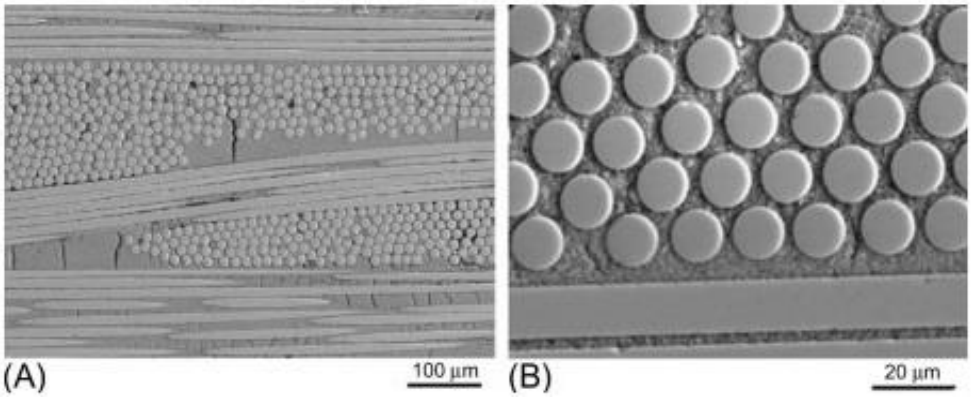


Fig.6.3-2. SEM images of Nextel™ 610/mullite composites with 0/90 fiber orientation, (A) fiber bundles and (B) almost regular and dense packing of fibers within a bundle.
From Simon RA. Progress in processing and performance of porous-matrix oxide/oxide composites. Int J Appl Ceram Technol 2005;2:141–9.

Fig.6.3-3 presents an UD example. The test data set was not provided, unfortunately

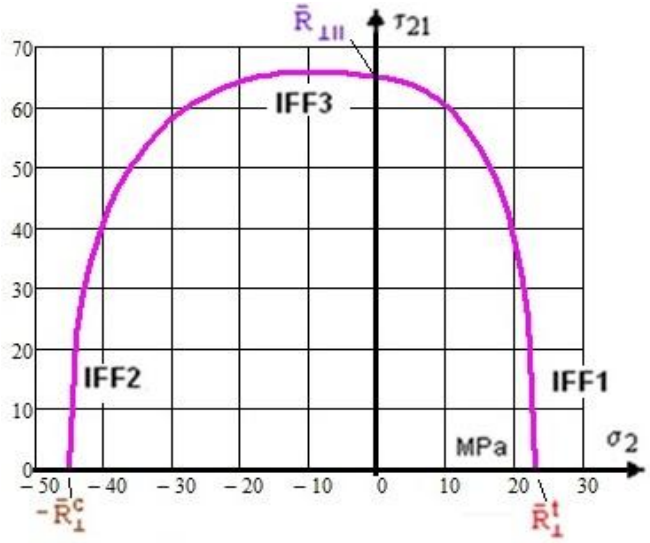


Fig. 6.3-3: UD CMC material, WHIPOX™ C/C-SiC,. Filament wound tube. Strength provided from [WHIPOX™ C/C-SiC, DLR Stuttgart, [Jai20]]. WHIPOX = Wound Highly Porous Oxide Material of the DLR

$$Eff^{\perp\sigma} = [(\sigma_2) + \sqrt{\sigma_2^{\,2}}]/2\bar{R}^t_\perp = \sigma^{\perp\sigma}_{eq} / \bar{R}^t_\perp$$

$$Eff^{\perp\tau} = [a_{\perp\perp}\cdot(\sigma_2) + b_{\perp\perp}\sqrt{\sigma_2^{\,2}}] / \bar{R}^c_\perp = \sigma^{\perp\tau}_{eq} / \bar{R}^c_\perp$$

$$Eff^{\perp\parallel} = \{[b_{\perp\parallel}\cdot I_{23-5} + (\sqrt{b_{\perp\parallel}^{\,2}\cdot I_{23-5}^{\,2} + 4\cdot\bar{R}_{\perp\parallel}^{\,2}\cdot(\tau_{21}^2)^2}]/(2\cdot\bar{R}_{\perp\parallel}^{\,3})\}^{0.5}$$

$$I_{23-5} = 2\sigma_2\cdot\tau_{21}^2,\ b_{\perp\perp} = a_{\perp\perp} + 1 = 1/(1-\mu_{\perp\perp}),\ b_{\perp\parallel} \cong 2\cdot\mu_{\perp\square}$$

$$\{\bar{R}\} = (\bar{R}^t_\parallel, \bar{R}^c_\parallel, \bar{R}^t_\perp, \bar{R}^c_\perp, \bar{R}_{\perp\parallel})^T = (279\ ,243,\ 22.5\ ,45,\ 65)^T$$

with assumed $\mu_{\perp\square} = 0.15$, $\mu_{\perp\perp} = 0.15$

$$\left(\frac{\sigma_2^{\,t}}{\bar{R}_2^t}\right)^m + \left(\frac{-\sigma_2^{\,c}}{\bar{R}_2^c}\right)^m + \left(\frac{|\tau_{12}|}{\bar{R}_{\perp\square} - \mu_{\perp\square}\cdot\sigma_2^c}\right)^m = 1$$

Fig.6.3-4 presents filament-wound tube test results. Mapping was performed by a Mathcad 15 - based computation.

Mapping was not sufficiently possible due to a not logical drop of the shear failure stress points in the low σ_2-domain around -8 MPa. An estimated 'reduced' design curve is added in the figure.

Vorgabe

$\tau := 1$ $\quad Rst := 3 \quad Rsc := 27 \quad Rsp := 22 \quad \mu sp := 0.6 \quad mint := 2.6$

$$\left(\frac{\sigma + |\sigma|}{2\cdot Rst}\right)^{mint} + \left(\frac{\tau}{Rsp - \mu sp\cdot\sigma}\right)^{mint} + \left(\frac{-\sigma + |\sigma|}{2\cdot Rsc}\right)^{mint} = 1$$

$\tau 2(\sigma) := Suchen(\tau)$ $\quad j := 0..Rsc + Rst$

$\sigma_j := j - Rsc$ $\quad \tau_j := \tau 2(\sigma_j)$

$k := 0..2$ $\quad R := \begin{pmatrix} Rst & 0 \\ 0 & Rsp \\ -Rsc & 0 \end{pmatrix}$

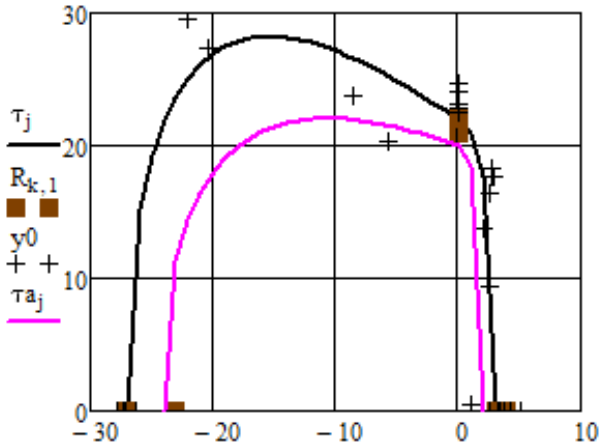
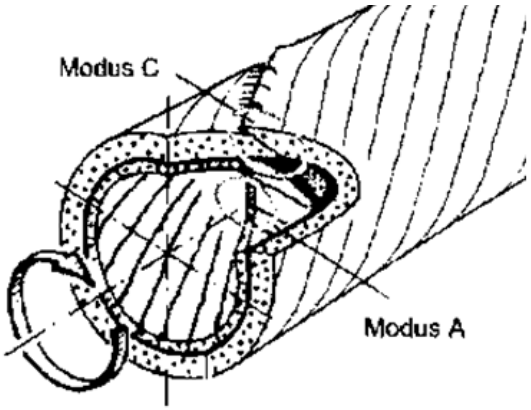


Fig. 6.3-4: 88°-CMC helically-wound tube test specimen, ***lay-up [/-],***
(Courtesy: Schunck and ILK-Dresden)



For understanding of the IFF under torsion:

A.Puck's sketch delivers that in a helically-wound tube under a torsion moment one helix layer is tensioned (IFF1) and one is compressed (IFF2).

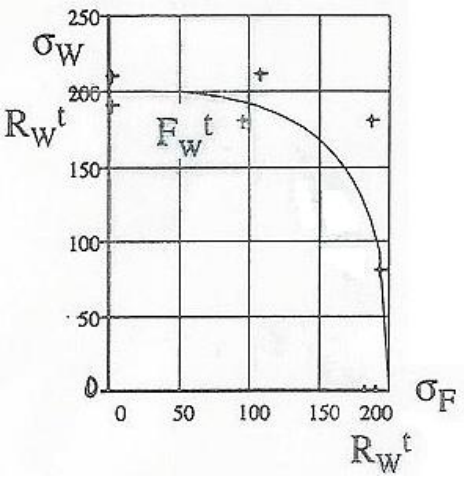
6.3.3 Orthotropic fabric laminas

For a faster understanding the interaction equation, necessary for mapping the course of test data in the transition domains reads:

$$\left(\frac{\sigma_W+|\sigma_W|}{2\cdot\bar{R}_W^t}\right)^m+\left(-\frac{\sigma_W+|\sigma_W|}{2\cdot\bar{R}_W^c}\right)^m+\left(\frac{\sigma_F+|\sigma_F|}{2\cdot\bar{R}_F^t}\right)^m+\left(\frac{-\sigma_F+|\sigma_F|}{2\cdot\bar{R}_F^c}\right)^m+\left(\frac{|\tau_{WF}|}{\bar{R}_{WF}-\mu_{WF}\cdot(\sigma_W+\sigma_F)}\right)^m$$
$$+\left(\frac{\sigma_3+|\sigma_3|}{2\cdot\bar{R}_3^t}\right)^m+\left(\frac{-\sigma_3+|\sigma_3|}{2\cdot\bar{R}_3^c}\right)^m+\left(\frac{|\tau_{3W}|}{\bar{R}_{3W}-\mu_{3W}\sigma_3}\right)^m+\left(\frac{|\tau_{3F}|}{\bar{R}_{3F}-\mu_{3F}\sigma_3}\right)^m=1\ .$$

This equation is valid if the in-plane shear mode occurs two-fold. An friction-active stress σ_F is considered in the fifth bracket.

Some simple stress states are investigated and visualized in *Figs.6.3-5* through -*7*.



$$\{\bar{R}\}=$$
$$(\bar{R}_W^t,\ \bar{R}_W^c,\ \bar{R}_F^t,\ \bar{R}_F^c,\ \bar{R}_{WF},\ \bar{R}_3^t,\ \bar{R}_3^c,\ \bar{R}_{3F},\ \bar{R}_{3W})^T$$
$$=(200,\ -,\ 195,\ -,\ -,\ -,\ -,\ -,\ -)^T$$

$$\left(\frac{\sigma_W+|\sigma_W|}{2\cdot\bar{R}_W^t}\right)^m+\left(-\frac{\sigma_W+|\sigma_W|}{2\cdot\bar{R}_W^c}\right)^m=1$$

Fig.6.3-5: C/SiC tube for X38 Body Flap, $\sigma_W(\sigma_F)$, *RT, MAN, m =3*

Often used as test specimens are coupon test specimen, cut out from a plate under distinct angles.

Here one reminder comes in before one should begin to map, see *Fig. 6.3-7*:

High Fidelity macro-mechanical SFCs must 'consider' micro-mechanical failure effects caused by the distinct tested specimen.

...

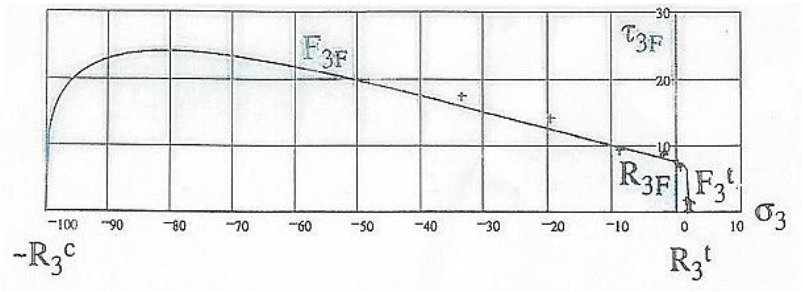
$$\left(\frac{\sigma_3+|\sigma_3|}{2\cdot\bar{R}_3^t}\right)^m+\left(\frac{-\sigma_3+|\sigma_3|}{2\cdot\bar{R}_3^c}\right)^m+\left(\frac{|\tau_{3F}|}{\bar{R}_{3F}-\mu_{3F}\sigma_3^c}\right)^m=1$$

$$\{\bar{R}\}=(\bar{R}_W^t,\ \bar{R}_W^c,\ \bar{R}_F^t,\ \bar{R}_F^c,\ \bar{R}_{WF},\ \bar{R}_3^t,\ \bar{R}_3^c,\ \bar{R}_{3F},\ \bar{R}_{3W})^T$$
$$\bar{R}_W^t,\ \bar{R}_W^c,\ \bar{R}_F^t,\ \bar{R}_F^c,\ \bar{R}_{WF},\ 3,\ 99,\ 7,\ \bar{R}_{3W})^T$$

with $\mu_{WF}, \mu_{3W}, \mu_{3F} = 0.3$

Fig. 6.3-6: C/SiC tube, $\sigma_W(\sigma_F)$, RT, m =3

[test data from dissertation B. Thielicke on tube test specimens,1997



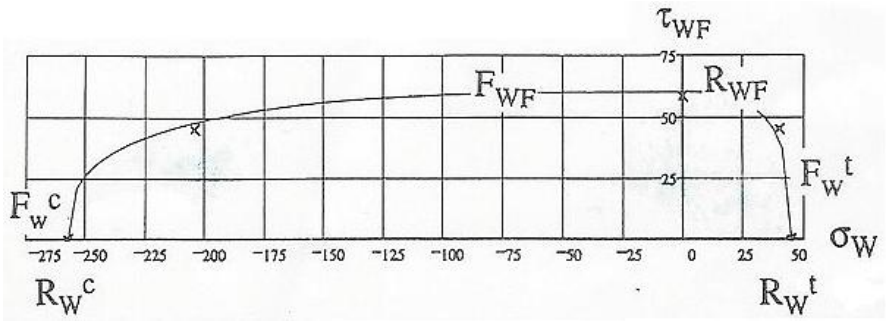


Fig.6.3-7: C/C-SiC tube, $\tau_{WF}(\sigma_W)$ fracture curve, T =1600°C, m=4 [Gei97]

$$\{\bar{R}\}=(\bar{R}_W^t,\ \bar{R}_W^c,\ \bar{R}_F^t,\ \bar{R}_F^c,\ \bar{R}_{WF},\ \bar{R}_3^t,\ \bar{R}_3^c,\ \bar{R}_{3F},\ \bar{R}_{3W})^T=(45,\ 260,\ -,\ -,\ 59,\ -,\ -,\ -,\ -)^T$$

For the uniaxial stress states $\sigma_W{}^c$ (*Stability danger. The same is valid for the Fill direction*) and $\sigma_W{}^t$ clear fiber failure modes are identified. Under τ_{WF}, accompanied by scissoring, matrix failure is faced. This is of marginal importance for $(\sigma_W{}^c, \tau_{WF})$ but essential for $(\sigma_W{}^t, \tau_{WF})$. Namely, physics in the positive domain $\tau_{WF}(\sigma_W{}^t)$ let assume that there is a small domain where tensile matrix fracture may occur. At small tensile warp stresses fracture danger for the matrix due to σ_m^t under shear stresses τ_{WF} is given. This lasts until fiber tensile failure stress $\sigma_W{}^t \equiv \sigma_{\square}{}^t$ dominates the failure state. Matrix tensile fracture leads to an inward dent as logical consequence.

A relatively sudden change from a micro-mechanical matrix failure to a macro-mechanical tensile failure of the fabric warp fiber strand under $\sigma_W{}^t$ occurs. Sudden changes of failure mode domains take the simple series spring system incorporated in the interaction formula to the limit. An increase of *m* cannot work because an inward dent cannot be mapped. As still successfully applied a decay function for each of the interacting modes was employed. These functions are terminated by the onset of the other pure domain.

Fig.6.3-7 considers this fracture failure situation.

> *LL: Application limit of the usually and here applied series spring model is given if abrupt changes of a mode are faced.*

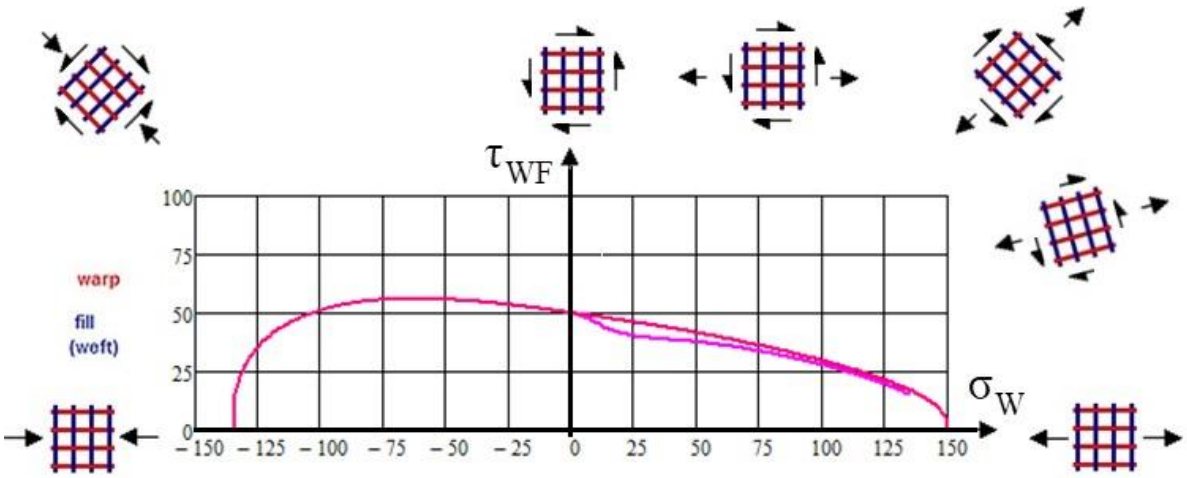


*Fig. 6.3-7: Inplane fracture failure curve with and **without** mapping of the inward dent.*
Plain weave fabric Ceramic Matrix Composite (CMC), defined strength values.
Not yet published test data lie on the magenta curve

Fig.6.3-8 presents the computation of the two curves above.

Vorgabe $\tau := 20$ **without decay function, both domains**

$$\left[\left(\frac{\sigma + |\sigma|}{2Rt}\right)^m + \left(\frac{-\sigma + |\sigma|}{2Rc}\right)^m + \left(\frac{|\tau|}{RWF - \mu\cdot\sigma}\right)^m\right] = 1$$

$f(\sigma) := Suchen(\tau)$

$j := 0..Rc + Rt$ $\quad \sigma_j := j - Rc$ $\quad \tau_j := f(\sigma_j)$

Vorgabe $\tau := 20$ **with decay function, positive domain**

$$\left[\left[\frac{\sigma + |\sigma|}{2\left(Rt\cdot\frac{1}{1 + e^{\frac{c1Wt-\sigma}{c2Wt}}}\right)}\right]^m + \left(\frac{-\sigma + |\sigma|}{2Rc}\right)^m + \left[\frac{|\tau|}{(RWF - \mu\cdot\sigma)\cdot\frac{1}{1 + e^{\frac{c1WF-\sigma}{c2WF}}}}\right]^m\right] = 1$$

$A(\sigma) := Suchen(\tau)$ $\quad j := 0..Rc$ $\quad \sigma_j := j$ $\quad \tau_j := A(\sigma_j)$

Fig. 6.3-8: MathCad computation of the mapping of the inward dent. $\sigma_W = \sigma,\ \tau_{WF} = \tau$

The course in the domain $\sigma_W{}^c, \tau_{WF}$ seems to contradict to *Fig. 6.3-6*, however, the materials are different and the distribution of the provided test points is not comparable. Here the saying fits:

Well-<u>understood</u> experiments have to verify the design assumptions made!

In this context Avula stated in 1987 "Experimental observations and measurements are generally accepted to constitute the backbone of physical sciences and engineering because of the physical insight they offer to the scientist for formulating the theory. Concepts, which are developed from observation, are used as guides for the design of new experiments, which in turn are used for validation of the theory. Thus, experiments and theory have a hand-in-hand relationship.

Thanks to Roman (*Prof. Dr.-Ing. Roman Keppeler, UniBw*) and Thorsten (*Dr.-Ing. Thorsten Steinkopff, Siemens AG*) for the discussions and suggestions on fabric ceramics.

7 Mohr Stress Transformation to obtain a Friction Parameter-Friction Value Dependence

7.1 Dependence of Isotropic Friction Model Parameter on Friction Value μ

7.1.1 General

Fig.7.1-1 informs about the stress terms and angle terms used in the envisaged uniaxial stress state $\sigma^c = F\ /\ Area$. These are φ ($\equiv \rho$) for the slope and c ($\equiv R^{\tau}$) for the cohesive strength. Further, the fracture plane angle Θ_{fp} is displayed on the test specimen together with its complementary angle α.

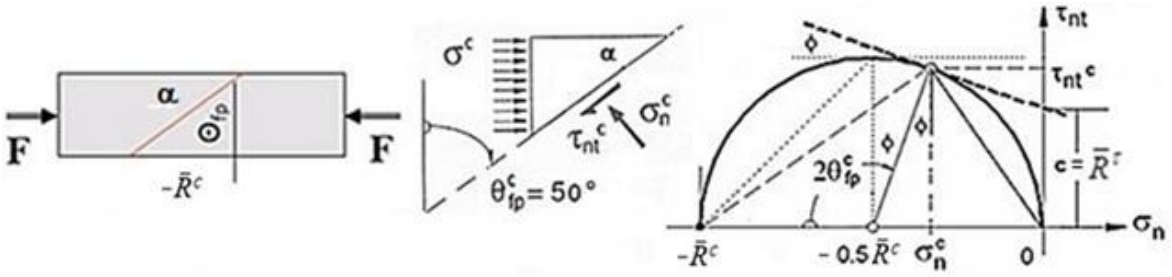


Fig.7.1-1: Shear fracture plane angles in touch point and 'linear' Mohr-Coulomb friction curve. The touch point is $(\sigma_n^c, \tau_{nt}^c)$

Mohr fracture stresses act on the fracture plane. Mohr's failure envelope is generally a curved line which most often is approximated by a straight line described by the cohesive strength $\bar{R}\tau \equiv$ c and the frictional part, often written as $\tau_{nt} = c - \sigma_n \cdot \tan(\phi)$ (in civil engineering: $c + |\sigma_n| \cdot \tan(\phi)$). When dealing with fracture plane angles and Mohr-Coulomb theory some further basic notions should be visualized. In Fig.7.1-2 an arbitrary spatial fracture plane is shown for an isotropic and a transversely-isotropic material, a fiber-reinforced polymer or a fiber-reinforced concrete matrix.

For practical purposes, it is sufficient to reduce the mathematical variety of possible fracture planes problem by defining a distinct plane. Tests are performed on basis of mathematical stresses where σ_{III} is the most negative stress

- Uniaxial stress states: $\{\sigma\} = (0,\ \sigma_{II},\ 0)^T$
- Bi-axial stress states: $\{\sigma\} = (0,\ \sigma_{II},\ \sigma_{III})^T$
- Hydrostatic pressure-linked stress states along Tensile Meridian and Compressive Meridian are $\{\sigma\} = (\sigma_I,\ \sigma_{II},\ \sigma_{III})^T$ for the cube test specimen and $\{\sigma\} = (\sigma_{\varphi},\ \sigma_r,\ \sigma_{ax})^T$ for the cylindrical test specimen

  In mathematical stresses the stress situation under p_{hyd} in the tests reads:

  Tensile Meridian: $(\sigma_{ax}^t - \boldsymbol{p_{hyd}}, -\boldsymbol{p_{hyd}}, -\boldsymbol{p_{hyd}}) = (\sigma_I, \sigma_{II}, \sigma_{III}) \rightarrow \sigma_I > \sigma_{II} = \sigma_{III}$

  Compressive Meridian: $(-\boldsymbol{p_{hyd}}, -\boldsymbol{p_{hyd}}, \sigma_{ax}^c - \boldsymbol{p_{hyd}}) = (\sigma_I, \sigma_{II}, \sigma_{III}) \rightarrow \sigma_I = \sigma_{II} > \sigma_{III}$.

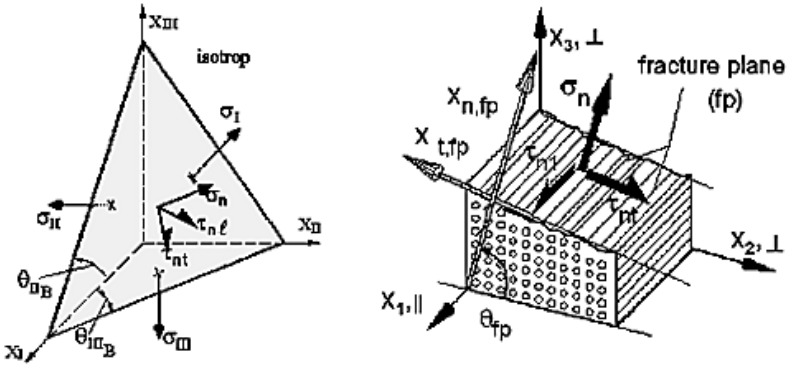


Fig7.1-2: Mohr stresses of isotropic materials and transversely-isotropic UD materials

7.1.2 Pure F^{SF}-based Mohr-Coulomb Fracture Curve and Cohesive Strength Prediction

A Mohr-Coulomb (M-C) curve is fully linked to the second quadrant of the principal structural stress plane $\sigma_y(\sigma_x)$ or $\sigma_{II}(\sigma_{III})$, respectively. In other words, the M-C curve is the result of two commonly acting modes, namely SF and NF. *Fig.7.1-3* demonstrates that for this special brittle material at $\sigma_{III} = > -30$ MPa the F^{NF} begins to dominate the additional fracture danger portions of $F^{NF} + F^{SF}$ in the modes' interacting transition zone or, respectively, NF tops SF. The sketch at the right highlights the stress state in the associated test specimen.

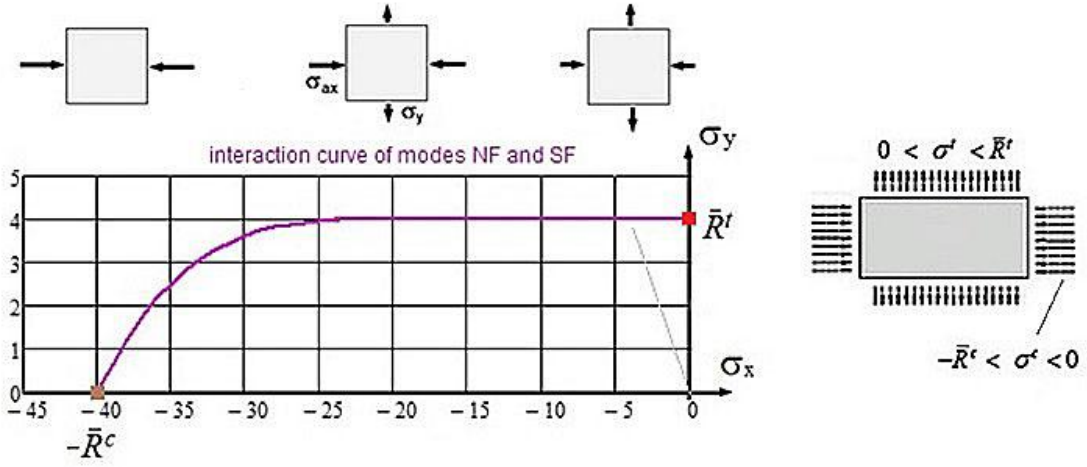
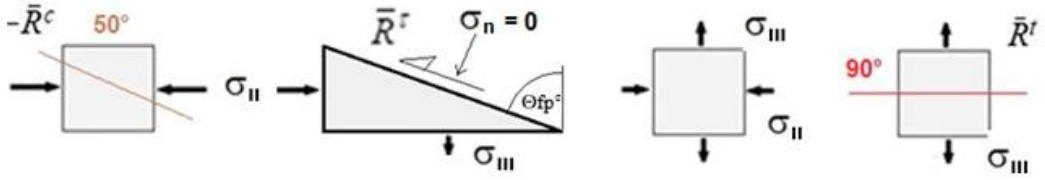


Fig.7.1-3: Visualization of principal structural stress states belonging to the Mohr-Coulomb curve

Physical experience: The fracture plane angle at the compressive strength point (uniaxial, mode SF) is about 50° for brittle materials like Normal Concrete, grey cast iron and is approximately 70° at the cohesive strength point $(\bar{R}^\tau,\ \sigma_n = 0) \equiv (\sigma_{II} = -\bar{R}^\tau \cdot s/c,\ \sigma_{III} = \bar{R}^\tau \cdot c/s)$, *Table 7.1-1*,



Span: $(\tau_{nt}{}^c, \sigma_n{}^c) \rightarrow (\bar{R}^\tau,\ 0) \rightarrow (\tau_{nt}, \sigma_n) \rightarrow (0,\ \sigma_n = \bar{R}^t) \Leftrightarrow (\sigma_{II} = -\bar{R}^c, 0) \rightarrow (\sigma_{II},\ \sigma_{III}) \rightarrow (0,\ \sigma_{III} = \bar{R}^t)$

Table 7.1-1: Transformation of Cartesian principal stresses into Mohr stresses, addition theorem relations

* Cartesian coordinate system, isotropic

$$\{\sigma\}=\begin{Bmatrix}\sigma_\ell\\ \sigma_n\\ \sigma_t\\ \tau_{nt}\\ \tau_{t\lambda}\\ \tau_{t\lambda}\end{Bmatrix}=\begin{bmatrix}1&0&0&0&0&0\\ 0&c^2&s^2&2sc&0&0\\ 0&s^2&c^2&-2sc&0&0\\ 0&-sc&sc&(c^2-s^2)&0&0\\ 0&0&0&0&c&-s\\ 0&0&0&0&s&c\end{bmatrix}=\begin{Bmatrix}\sigma_I\\ \sigma_{II}\\ \sigma_{III}\\ 0\\ 0\\ 0\end{Bmatrix},$$

$$\varphi=\varphi^\circ\cdot\frac{\pi}{180^\circ}$$

Transformed struct. stresses and addition theorems used: $\tau=0$

$s=\sin(\varphi),\quad c=\cos(\varphi),\quad s^2+c^2=1,\quad S^2+C^2=1,\quad C=c^2-s^2=2c^2-1,$

$\sigma_n=c^2\sigma_{II}+s^2\sigma_{III}=0.5\cdot[(C+1)\cdot\sigma_{II}+(1-C)\cdot\sigma_{III}],\quad \sigma_t=s^2\sigma_{II}+c^2\sigma_{III}$

$\tau_{nt}=-s\cdot c\cdot\sigma_{II}+s\cdot c\cdot\sigma_{III},\ S=2sc,\ \ c^2=(C+1)\cdot 0.5,\ \ s^2=(1-C)\cdot 0.5\ .$

$\sigma_n-\sigma_t=C\cdot(\sigma_{II}-\sigma_{III}),\quad \tau_{nt}=-s\cdot c\cdot(\sigma_{II}-\sigma_{III})=-0.5\cdot S\cdot(\sigma_{II}-\sigma_{III})$

$\sigma_n-\sigma_t=c^2\cdot(\sigma_{II}-\sigma_{III})-s^2\cdot(\sigma_{II}-\sigma_{III})=C\cdot(\sigma_{II}-\sigma_{III}),\quad C=\cos(2\varphi)$

$\sigma_n+\sigma_t=\sigma_{II}+\sigma_{III}\ ,\quad \tau_{nt}=-0.5\cdot S\cdot(\sigma_{II}-\sigma_{III}).\ S=\sqrt{1-C^2}$

The derivation yields the slope in the touch point ($\sigma_{III}=0$), index ^{c} :

$$d\sigma_n/d\Theta_{fp}=d(c^2\cdot\sigma_{II}+s^2\cdot\sigma_{III})/d\Theta_{fp}=-2\cdot s\cdot c\cdot\sigma_{II}=$$
$$=-S^c\cdot\sigma_{II}$$
$$d\tau_{nt}/d\Theta_{fp}=d(-s\cdot c\cdot\sigma_{II}+s\cdot c\cdot\sigma_{III})/d\Theta_{fp}=(-c^2+s^2)\cdot\sigma_{II}=$$
$$=-C^c\cdot\sigma_{II}$$

$$\Rightarrow\quad \frac{d\tau_{nt}}{d\sigma_n}=-\frac{C^c}{S^c}=\operatorname{cotan}(2\Theta_{fp}),\ C^c=\cos(2\cdot\Theta_{fp}{}^\circ\cdot\pi/180^\circ)$$

* Cartesian coordinate system, transversely-isotropic UD

(1 is fiber direction)

$$\{\sigma\}=\begin{Bmatrix}\sigma_\ell\\ \sigma_n\\ \sigma_t\\ \tau_{nt}\\ \tau_{t1}\\ \tau_{t1}\end{Bmatrix}=\begin{bmatrix}1&0&0&0&0&0\\ 0&c^2&s^2&2sc&0&0\\ 0&s^2&c^2&-2sc&0&0\\ 0&-sc&sc&(c^2-s^2)&0&0\\ 0&0&0&0&c&-s\\ 0&0&0&0&s&c\end{bmatrix}=\begin{Bmatrix}\sigma_1\\ \sigma_2\\ \sigma_3\\ 0\\ 0\\ 0\end{Bmatrix},$$

$\sigma_n-\sigma_t=c^2\cdot(\sigma_2-\sigma_3)-s^2\cdot(\sigma_2-\sigma_3)=C\cdot(\sigma_2-\sigma_3)$

$\sigma_n+\sigma_t=\sigma_2+\sigma_3\ ,\quad \tau_{nt}=-0.5\cdot S\cdot(\sigma_2-\sigma_3).\ S=\sqrt{1-C^2}$

Structural stresses:

$I_1=\sigma_x+\sigma_y+\sigma_z\ ,$

$I_2=\sigma_x\cdot\sigma_y+\sigma_y\cdot\sigma_z+\sigma_x\cdot\sigma_z-\tau_{xy}^2-\tau_{yz}^2-\tau_{xz}^2$

$I_3=\sigma_x\cdot\sigma_y\cdot\sigma_z+2\tau_{xy}\cdot\tau_{yz}\cdot\tau_{xz}-\sigma_x\cdot\tau_{yz}^2-\sigma_z\cdot\tau_{xy}^2-\sigma_y\cdot\tau_{xz}^2$

$6J_2=(\sigma_y-\sigma_z)^2+(\sigma_z-\sigma_x)^2+(\sigma_x-\sigma_y)^2+6\cdot(\tau_{xy}^2+\tau_{yz}^2+\tau_{xz}^2)$

$27J_3=2I_1^3-9I_1\cdot I_2+27I_3$

$2D:\ I_1=\sigma_x+\sigma_y$

$6J_2=(\sigma_y)^2+(-\sigma_x)^2+(\sigma_x-\sigma_y)^2+6\cdot\tau_{xy}^2$

Principal stresses:

$I_1=\sigma_I+\sigma_{II}+\sigma_{III}=\ f(\sigma)$

$6J_2=(\sigma_I-\sigma_{II})^2+(\sigma_{II}-\sigma_{III})^2+(\sigma_{III}-\sigma_I)^2=\ f(\tau)$ ('Mises')

$27J_3=\ (2\sigma_I-\sigma_{II}-\sigma_{III})\cdot(2\sigma_{II}-\sigma_I-\sigma_{III})\cdot(2\sigma_{III}-\sigma_I-\sigma_{II})$

$3\cdot\sigma_{oct}=\sigma_I+\sigma_{II}+\sigma_{III}=\ \sigma_\ell+\sigma_n+\sigma_t;$

$9\cdot\tau_{oct}{}^2=6J_2=4\cdot(\tau_{III}{}^2+\tau_I{}^2+\tau_{II}{}^2)$

$\tau_{II}=\max\tau(mathematically)\ ,\ \sigma_I,\sigma_{II},\sigma_{III}$ are principal stresses,

$\sigma_I>\sigma_{II}>\sigma_{III}$ are mathem. stresses (sign > means more positive)

$2D:\ I_1=\sigma_{II}+\sigma_{III}$

$6J_2=\ 2\cdot(\sigma_{II}{}^2+\sigma_{II}\cdot\sigma_{III}+\sigma_{III}{}^2)$

$27J_3=\ (-\sigma_{II}-\sigma_{III})\cdot(2\sigma_{II}-\sigma_{III})\cdot(2\sigma_{III}-\sigma_{II}).$

Mohr stresses: fracture angle measure C

$I_1=\sigma_n+\sigma_\lambda+\sigma_t\ ,\quad I_2=\sigma_n\cdot\sigma_t+\sigma_t\cdot\sigma_\lambda+\sigma_n\cdot\sigma_\lambda-\tau_{nt}^2-\tau_{t\lambda}^2-\tau_{n\lambda}^2$

$I_3=\sigma_n\cdot\sigma_t\cdot\sigma_\lambda+2\tau_{nt}\cdot\tau_{t\lambda}\cdot\tau_{n\lambda}-\sigma_n\cdot\tau_{t\lambda}^2-\sigma_\lambda\cdot\tau_{nt}^2-\sigma_t\cdot\tau_{n\lambda}^2$

$6J_2=(\sigma_n-\sigma_t)^2+(\sigma_t-\sigma_\lambda)^2+(\sigma_\lambda-\sigma_n)^2+6\cdot(\tau_{nt}^2+\tau_{t\lambda}^2+\tau_{n\lambda}^2)$

$27J_3=2I_1^3-9I_1\cdot I_2+27I_3$

$2D:\quad I_1=\sigma_n\ +\sigma_t,\quad I_2=-\tau_{nt}^2+\sigma_n\cdot\sigma_t,\quad I_3=0$

$6J_2=(\sigma_n-\sigma_t)^2+(\sigma_t)^2+(-\sigma_n)^2+6\cdot\tau_{nt}^2$

$27J_3=2(\sigma_n+\sigma_t)^3-9\cdot(\sigma_n+\sigma_t)\cdot(\sigma_n\cdot\sigma_t-\tau_{nt}^2).$

According to Mohr's theory the stress σ_t is not effective.

It can be eliminated in 2D case using addition theorems, thus linking structural to Mohr stresses

$\sigma_n-\sigma_t=C\cdot(\sigma_x-\sigma_y),\quad \sigma_t=\sigma_n-C\cdot(\sigma_x-\sigma_y),\quad C=\cos(2\cdot\Theta_{fp}{}^\circ\cdot\pi/180^\circ)$

Interpreting struct. stresses as mathem. stresses means $\sigma_x\equiv\sigma_{III},\sigma_y\equiv\sigma_{II}$.

7.1.3 Finding the relationship friction parameter c2 ↔ friction value μ

In the next two tables, *Table 7.1-1* and the following table, *Table 7.1-2* , all the necessary relations are presented which are necessary for the not simple transformation task.

In *Table 7.1-3* the traditional way of predicting $\tau_{nt}(\sigma_n)$ and cohesive strength $\bar{R}^\tau$ is presented.

Table 7.1-2: Derivation of the Mohr stresses-transformed FMC-based strength failure conditions

$$F^{SF} = c_{1\Theta}{}^{SF} \cdot \frac{3J_2 \cdot \Theta^{SF}}{\bar{R}^{c2}} + c_2{}^{SF} \cdot \frac{I_1}{\bar{R}^c} = 1 \quad \text{or} \quad Eff^{SF} = \frac{c_{2\Theta}^{SF} \cdot I_1 + \sqrt{(c_{2\Theta}^{SF} \cdot I_1)^2 + 12 \cdot c_{1\Theta}^{SF} \cdot 3J_2 \cdot \Theta^{SF}}}{2 \cdot \bar{R}^c}$$

Inserting compressive strength $\bar{R}^c$ delivers $1 + c_{2\Theta}{}^{SF} = c_{1\Theta}{}^{SF} \cdot \Theta^{SF}$ with the

non-circularity function $\Theta^{SF} = \sqrt[3]{1 + d^{SF} \cdot \sin(3\vartheta)} = \sqrt[3]{1 + d^{SF} \cdot 1.5 \cdot \sqrt{3} \cdot J_3 \cdot J_2{}^{-1.5}}$

which reads $\Theta = 1$ if $\bar{R}^{cc} = \bar{R}^c \Leftrightarrow$ rotationally-symmetric

$$\frac{c_{1\Theta}^{SF}}{2\bar{R}^{c2}} \cdot [(\sigma_n - \sigma_t)^2 + (\sigma_t - \sigma_\lambda)^2 + (\sigma_\lambda - \sigma_n)^2 + 6 \cdot (\tau_{nt}{}^2 + \tau_{n1}{}^2 + \tau_{t1}{}^2)] + c_{2\Theta}{}^{SF} \cdot \frac{\sigma_n + \sigma_\lambda + \sigma_t}{\bar{R}^c} = 1$$

Derivation of the slope equation in Mohr stresses, $\sigma_\lambda,\ \tau_{t\lambda},\ \tau_{n\lambda} = 0$

$$\frac{dF^{SF}}{d\sigma_n} = \frac{c_{1\Theta}{}^{SF}}{2\bar{R}^{c2}} \cdot [4\sigma_n - 2\sigma_t - 2\sigma_\lambda] + \frac{c_{2\Theta}{}^{SF}}{\bar{R}^c}; \qquad \frac{dF^{SF}}{d\tau_{nt}} = 12\frac{c_{1\Theta}{}^{SF} \cdot \tau_{nt}}{2 \cdot \bar{R}^{c2}}$$

$$\frac{d\tau_{nt}}{d\sigma_n} = -\frac{dF}{d\sigma_n} / \frac{dF}{d\tau_{nt}} \text{ (implicit diff.)} = -\left[\frac{c_{1\Theta}{}^{SF}}{\bar{R}^{c2}} \cdot [2\sigma_n - \sigma_t - \sigma_\lambda] + \frac{c_{2\Theta}{}^{SF}}{\bar{R}^c}\right] / \left[6\frac{c_{1\Theta}{}^{SF} \cdot \tau_{nt}}{\bar{R}^{c2}}\right]$$

Transformed structural stresses and addition theorems used: $\sigma\lambda = 0$ set

$$S^2 + C^2 = 1,\ C = c^2 - s^2 = 2c^2 - 1,\ S = 2sc,\ c^2 = (C+1) \cdot 0.5,\ s^2 = (1-C) \cdot 0.5$$

$$\sigma_n - \sigma_t = C \cdot (\sigma_{II} - \sigma_{III}),\ \tau_{nt} = -s \cdot c \cdot (\sigma_{II} - \sigma_{III}) = -0.5 \cdot S \cdot (\sigma_{II} - \sigma_{III})$$

Transformation relations for equalizing the angle in the touch point , $\sigma_{II} - \sigma_{III} = \eta$

$$\frac{d\tau_{nt}}{d\sigma_n} = -\left[\frac{c_{2\Theta}{}^{SF} \cdot \eta + c_{1\Theta}{}^{SF} \cdot (2 \cdot c^2 - s^2) \cdot \eta}{6 \cdot c_{1\Theta}{}^{SF} \cdot (-s \cdot c \cdot \eta)}\right] = -\left[\frac{c_{2\Theta}{}^{SF} - c_{1\Theta}{}^{SF}\left(2\frac{C+1}{2} - \frac{1-C}{2}\right)}{6 \cdot c_{1\Theta}{}^{SF} \cdot (-0.5 \cdot S)}\right].$$

Equal slope of curves in touch point: η is multi-axial and cut out

$$\frac{d\tau_{nt}}{d\sigma_n} = \frac{C}{S} = -\left[\frac{c_{2\Theta}{}^{SF} - c_{1\Theta}{}^{SF}\left(C + 1 - \frac{1-C}{2}\right)}{6 \cdot c_{1\Theta}{}^{SF} \cdot (-0.5 \cdot S)}\right] \quad \text{with} \quad C \Rightarrow C^c = \frac{c_{2\Theta}{}^{SF} - c_{1\Theta}{}^{SF}}{-3 \cdot c_{1\Theta}{}^{SF}}$$

Determination of $c_{2\Theta}{}^{SF}$ after inserting $1 + c_{2\Theta}{}^{SF} = c_{1\Theta}{}^{SF}$ for neutral meridian $\Theta^{SF} = 1$:

$$C^c = \frac{c_{2\Theta}{}^{SF} - (1 + c_{2\Theta}{}^{SF})}{-3 \cdot (1 + c_{2\Theta}{}^{SF})} = \frac{-1}{-3 \cdot (1 + c_{2\Theta}{}^{SF})} \Rightarrow \quad c_{2\Theta}{}^{SF} = \frac{-3 \cdot C^c + 1}{3 \cdot C^c + 1}$$

Mohr, linear fracture condition: $\tau_{nt} = \mathrm{R}^\tau - \mu \cdot \sigma_n$ *or* $F = \frac{\tau_{nt}}{\mathrm{R}^\tau - \mu \cdot \sigma_n} = 1$

$$\frac{d\tau_{nt}}{d\sigma_n} = -\frac{dF}{d\sigma_n} / \frac{dF}{d\tau_{nt}} = -\frac{\tau_{nt} \cdot \mu}{(\mathrm{R}^\tau - \mu \cdot \sigma_n)^2} / \frac{1}{\mathrm{R}^\tau - \mu \cdot \sigma_n} = -\frac{\tau_{nt} \cdot \mu}{(\mathrm{R}^\tau - \mu \cdot \sigma_n)} = -\mu \equiv \frac{C^c}{S^c}$$

Now, it is possible to sort out the relations between all friction-linked parameters

$$\mu = -\tan\rho = \frac{d\tau_{nt}}{d\sigma_n} = \frac{-C^c}{S^c}, \text{ small friction angles} \cong -C^c, \quad \tan\phi \equiv \tan\rho$$

$$c_{2\Theta}{}^{SF} = \frac{3\mu + 1}{-3\mu + 1} \quad \text{and} \quad \text{if an angle is measured, then} \quad C^c = \cos\left(\frac{2 \cdot \Theta_{fp}{}^\circ}{180^\circ} \cdot \pi\right).$$

From *Fig.*7.1-1, relationships can be derived and from them follows for $\Theta_{fp}^c{}^\circ = 50^\circ$

brittle $\Theta_{fp}^c{}^\circ = 50^\circ \rightarrow C^c = -0.174,\ c_{2\Theta}{}^{SF} = c_2{}^{SF} = 3.7\ ,\ \mu = 0.18,$

F^{SF}bound $\Theta_{fp}^c{}^\circ = 45^\circ \rightarrow C^c = 0;\ \mu = 0,\ \rho = -\mathrm{atan}(\mu) = 0.$

Table 7.1-3: Derivation of Mohr shear curve $\tau_{nt}(\sigma_n)$ and cohesive strengths from different models

Rotationally symmetric	SFCs	120°-Rotationally symmetric
$F^{SF} = c_1^{SF} \cdot \frac{3J_2 \cdot 1}{\bar{R}^{c2}} + c_2^{SF} \cdot \frac{I_1}{\bar{R}^c} = 1$	$\Leftrightarrow$	$F^{SF} = c_{1\Theta}^{SF} \cdot \frac{3J_2 \cdot \Theta^{SF}}{\bar{R}^{c2}} + c_{2\Theta}^{SF} \cdot \frac{I_1}{\bar{R}^c} = 1$
$Eff^{SF} = \frac{c_1^{SF} \cdot I_1 + \sqrt{(c_2^{SF} \cdot I_1)^2 + 12 \cdot c_1^{SF} \cdot 3J_2}}{2 \cdot \bar{R}^c}$	$\Leftrightarrow$	$Eff^{SF} = \frac{c_{1\Theta}^{SF} \cdot I_1 + \sqrt{(c_{2\Theta}^{SF} \cdot I_1)^2 + 12 \cdot c_{1\Theta}^{SF} \cdot 3J_2 \cdot (\Theta^{SF})}}{2 \cdot \bar{R}^c}$

$\Theta^{NF} = \sqrt[3]{1 + d^{SF} \cdot (+1)} \equiv \Theta^{TM}$, $\Theta^{SF} = \sqrt[3]{1 + d^{SF} \cdot (-1)} \equiv \Theta^{CM}$, $\Theta^{NM} = \sqrt[3]{1 + d^{SF} \cdot (0)} = 1$

$\Leftrightarrow$ Determination of friction-related parameters using

* Information $c_2(C_{fp}^c)$ assumption $c_2^{SF} \approx (1 + 3 \cdot \mu)/(1 - 3 \cdot \mu)$ here friction parameter

$c_1^{SF} = 1 + c_2^{SF}$, $d^{SF} = 0$ $\leftarrow$ inserting $(-\bar{R}^c,\ 0) \rightarrow c_{1\Theta}^{SF} = 1 + c_{2\Theta}^{SF} \cdot \sqrt[3]{1 + d^{SF} \cdot (-1)}$

* Mapping of the course of available test data by a minimum error fit

Simulation process necessary: Numerical tuning to optimally map the course of test data

* Approximated, by using information on $\theta_{fp}^c\,°$ or μ: $C^c = \cos(2 \cdot \theta_{fp}^c\,° \cdot \pi / 180) \cong -\mu$,

point $(-\bar{R}^c,\ 0)$ from compr. meridian test *plus* $(-\bar{R}^{cc}, -\bar{R}^{cc},\ 0)$ trom tensile meridian test.

* The Mohr-Coulomb curve $\tau_{nt}(\sigma_n)$ depends on the non-circularity function Θ^{SF}

* Introducing σ_λ, τ_{nt}, $\tau_{nt} = 0$, $1 + c_{2\Theta}{}^{SF} = c_{1\Theta}{}^{SF} \cdot \Theta^{SF}$.

$$\frac{c_{1\Theta}{}^{SF}\Theta^{SF}}{2\bar{R}^{c2}} \cdot [(\sigma_n - \sigma_t)^2 + (\sigma_t - 0)^2 + (0 - \sigma_n)^2 + 6 \cdot (\tau_{nt}{}^2)] + c_{2\Theta}{}^{SF} \cdot \frac{\sigma_n + 0 + \sigma_t}{\bar{R}^c} = 1.$$

$\Leftrightarrow$ Determination of the $\tau_{nt}(\sigma_n)-$curve using addition theorems and inserting $(-\bar{R}^c,\ 0)$

$(\sigma_{II} - \sigma_{III}) = \eta = -\bar{R}^c$, $\sigma_n - \sigma_t = C \cdot \eta$, $\tau_{nt} = -s \cdot c \cdot \eta = -0.5 \cdot S \cdot \eta$, $\sigma_n - C \cdot \eta = \sigma_t$

$$\frac{c_{1\Theta}^{SF} \cdot \Theta^{SF}}{2\bar{R}^{c2}} \cdot [(C \cdot \eta)^2 + (\sigma_n - C \cdot \eta)^2 + (-\sigma_n)^2 + 6 \cdot (\tau_{nt}{}^2)] + c_{2\Theta}^{SF} \cdot \frac{\sigma_n + \sigma_n - C \cdot \eta}{\bar{R}^c} = 1$$

$$\tau_{nt}(\sigma_n) = \frac{\sqrt{3 \cdot \sqrt{-c_{1\Theta}^{SF} \cdot \Theta^{SF} \cdot (c_{1\Theta}^{SF} \cdot \Theta^{SF} \cdot [C^2 \cdot \bar{R}^{c2} + C \cdot \bar{R}^c \cdot \sigma_n + \sigma_n{}^2] - \bar{R}^{c2} + c_{2\Theta}^{SF} \cdot [C \cdot \bar{R}^{c2} + 2 \cdot \bar{R}^c \cdot \sigma_n])}}{3c_{1\Theta}^{SF} \cdot \Theta^{SF}}$$

$c_{2\Theta}{}^{SF} = (3\mu + 1)/(1 - 3\mu)$, $\mu = -\tan\rho \cong -C^c = -\cos(2 \cdot \Theta_{fp}^c\,° \cdot \pi / 180°)$

Example: $\Theta_{fp}^c\,° = 50° \rightarrow C^c = -0.174$, $\mu = 0.176 \cong -C^c$, $d^{SF} = 0.49$, $\Theta^{SF} = 0.80$

Rotationally-symmetric $c_2{}^{SF} = 3.7$, $c_1{}^{SF} = 1 + c_2{}^{SF} = 4.7$, $C = C^c$

120°-rot.-sym:metric $c_{2\Theta}{}^{SF} = c_2{}^{SF}$, $c_{1\Theta}{}^{SF} = 1 + c_{2\Theta}{}^{SF} \cdot \Theta^{SF} = 5.88$, C alters with ϑ

$\Leftrightarrow$ Determination of cohesive shear strengths:

Linear Mohr-Coulomb: $\bar{R}^\tau = \tau_{nt}{}^c + \mu \cdot \sigma_n{}^c$, $\mu = -(1 - c_2{}^{SF})/(-3c_2{}^{SF} + 3)$, $\bar{R}^\tau = 17$ MPa

Rotationally-symmetric: point $(\tau_{nt} = \bar{R}^\tau,\ \sigma_n = 0)$, $\bar{R}^\tau = 13.5$ MPa or N/mm^2

120°-Rotat.-symm.: point $(\tau_{nt} = \bar{R}^\tau,\ \sigma_n = 0)$, $\bar{R}^\tau = 12.5$ MPa, δ = -25.1°,

$(\bar{R}^\tau,\ \sigma_n = 0) \equiv (\sigma_{II} = -\bar{R}^\tau \cdot s/c,\ \sigma_{III} = \bar{R}^\tau \cdot c/s) = (\sigma_{II} = -32$ MPa $, \sigma_{III} = 3.33$ MPa$)$

Geometry: $d\tau_{nt} / d\sigma_n = \tan\rho = (0.5 \cdot \bar{R}^c - |\sigma_n{}^c|) / \tau_{nt}{}^c \rightarrow \tau_{nt}{}^c = (0.5 \cdot \bar{R}^c - |\sigma_n{}^c|)/\tan\rho$

$$\tau_{nt}{}^c = \sqrt{|\sigma_n{}^c| \cdot (\bar{R}^c - |\sigma_n{}^c|)} = \left(\frac{(0.5 \cdot \bar{R}^c - |\sigma_n{}^c|)}{\tan\rho}\right)^2, \quad |\sigma_n{}^c| = \frac{(\bar{R}^c + \bar{R}^c \cdot \tan\rho^2) - \bar{R}^c \cdot \tan\rho \cdot \sqrt{1 + \tan\rho^2}}{2 + 2 \cdot \tan\rho^2}$$

Touch point coordinates: $\tau_{nt}{}^c = 19.7$ MPa, $\sigma_n{}^c = -16.5$ MPa.

Input: $\bar{R}^t = 4$ MPa, $\bar{R}^c = 40$ MPa (on CM), $\bar{R}^{cc} = 49$ MPa (on TM), further point on the CM (or TM) is required, CM test curve point, $(I_1/(\bar{R}^t \cdot \sqrt{3}) = -20,\ \sqrt{2 \cdot J_2}/\bar{R}^t = 14)$, usual normalisation by $\bar{R}^t$.

As a numerical example a material has been chosen above a fracture angle $\Theta^{c}_{fp}\,°$ from which follow the friction entities $\Theta^{c}_{fp}\,° = 50° \rightarrow C^{c} = -0.174,\ \ \mu = 0.176$.

Mohr-Coulomb relation:

In order to be able to derive the friction value μ, the slope of the linear Mohr envelope at the compressive strength associated point, termed touch point, must be provided. $\Theta_{fp}{}^{c}$ denotes the fracture angle in the touch point which is linked to the compressive strength, indexed ^{c}. Viewing *Fig.7-1* the relation exists ($\rho \equiv \phi$): $\mu = -\tan\rho \cong -\ C^{c} = -\ \cos(2\cdot\Theta^{c}_{fp}\,°\cdot\pi/180°)$.

Table 7.1-4 summarizes the derivation and all relations.

Table 7.1-4: Derivation of relations $\mu(\Theta_{fp}{}^{c})$ applying the Linear Mohr-Coulomb approach

$$F^{SF}_{Mohr} = \frac{\tau_{nt}}{\bar{R}^{\tau} - \mu\cdot\sigma_n} = 1 \qquad \text{- compressive SFC, angle } \Theta_{fp}{}^{c} \text{ unknown}$$

$$\frac{dF^{SF}_{Mohr}}{d\sigma_n} = \frac{\mu\cdot\tau_{nt}}{(\bar{R}^{\tau} - \mu\cdot\sigma_n)^2} \qquad \text{and} \qquad \frac{dF^{SF}_{Mohr}}{d\tau_{nt}} = \frac{1}{\bar{R}^{\tau} - \mu\cdot\sigma_n}$$

$$\rightarrow \frac{d\tau_{nt}}{d\sigma_n} = \frac{-\mu\cdot\tau_{nt}}{(\bar{R}^{\tau} - \mu\cdot\sigma_n)^2} \Big/ \left(\frac{1}{\bar{R}^{\tau} - \mu\cdot\sigma_n}\right) = \frac{-\mu\cdot\tau_{nt}}{(\bar{R}^{\tau} - \mu\cdot\sigma_n)^1} = \frac{-\mu\cdot(\bar{R}^{\tau} - \mu\cdot\sigma_n)}{(\bar{R}^{\tau} - \mu\cdot\sigma_n)}$$

$$= -\mu \quad \text{(negative sign due to implicite differentiation).}$$

$$F^{NF}_{Mohr} = \sigma_n / \bar{R}^{t} = 1 \qquad \text{- tensile SFC,} \qquad \text{angle } \Theta_{fp}{}^{t} = 90°$$

The following chapters show applications where 2D- and 3D-test data sets could be obtained.

Fig.7.1-4 at first verifies that the in reality bi-axial Mohr-Coulomb shear curve practically captures the transition zone between the uniaxial border points compressive strength and – if extended – the tensile strength which means it has to capture the interaction between the two modes F^{SF} and F^{NF}.

The upper left sketch in *Fig.7.1-4* depicts the decomposition of cohesive strength into its normal failure stress components still indicating that the tensile stress will dominate the failure behavior.

The upper right sketch in *Fig.7.1-4* depicts three stress states generated between the compressive strength and the cohesive strength point.

The lower curves in *Fig.7.1-4* present $\tau_{nt}(\sigma_n)$-curves including the models Linear Mohr-Coulomb, rotationally-symmetric F^{SF} and 120°-rotationally-symmetric F^{SF}.

The differences between the classical rotationally-symmetric cylinder model and the 120°-rotationally symmetric model is caused since the 120°-rotationally symmetric model does not stay with the compressive meridian CM which runs through the uniaxial compressive strength point. It reflects that under bi-axial stressing the meridian-marking Lode angle ϑ varies from CM via NM (ϑ *= 0°, due to J_3 = 0! This corresponds to the rotationally symmetric model*) at the cohesive strength point into the direction of the tensile meridian TM with $\vartheta = 90°$.

The results obtained by the three shear stress mode-linked approaches *Linear Mohr-Coulomb*, *Rotationally Symmetric* and the more realistic *120°-Rotationally Symmetric* model reveal for the

cohesive strength $\bar{R}^{\tau}$ that the 'extrapolated' value decreases with the better description but nevertheless stays a little too high as will be proven.

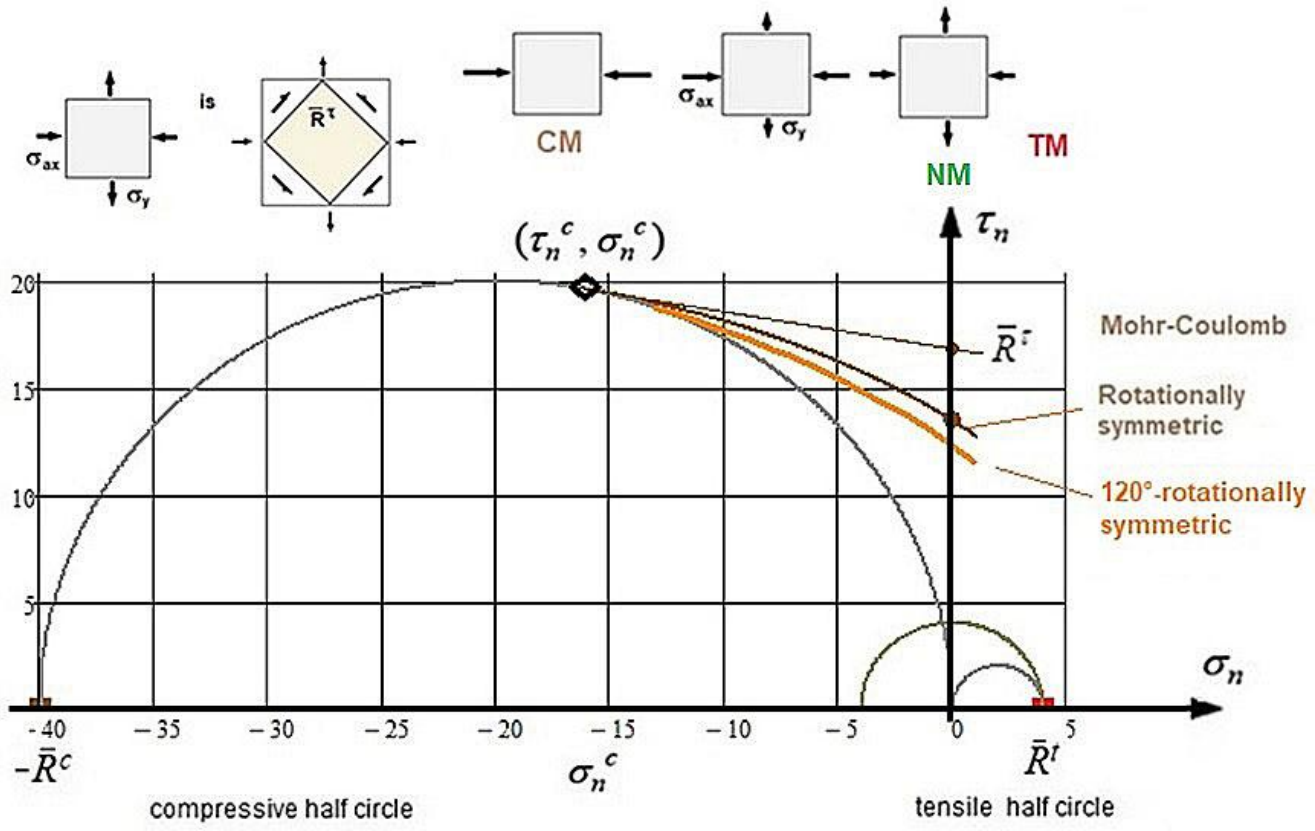


Fig.7.1-4: (upper left) Decomposition of cohesive strength into its normal failure stress components; (upper right) Stress states along the Mohr-Coulomb failure curve; /lower) Mohr stresses- dedicated failure curves $\tau_{nt}(\sigma_n)$ and cohesive strengths $\bar{R}^{\tau}$. Example $\Theta_{fp}{}^c = 50°$ or $\mu = 0.176$, CM means compressive meridian, TM tensile meridian, NM neutral meridian

LL:

(1) The M-C curve is an interaction curve describing the associated transition zone. For small compressive Mohr stresses σ_n the curve is ruled by NF and not by SF anymore

(2) The cohesive (shear) strength $\bar{R}^{\tau}$ is defined by ($\tau_{nt} = \bar{R}^{\tau}$, $\sigma_n = 0$), which means in principal stresses ($\sigma_I = -\sigma_{II}$) or ($\sigma_I = -\sigma_{III}$) or another combination and in Mohr's mathematical stresses ($\sigma_I = +\sigma_{III}$)

(3) The cohesive shear fracture stress is a stress that is composed of a normal stress component and a compression stress component. Here, the use of the term 'stress component' is to accept ! This indicates the relationship to tension

(4) Reminder on Mohr: Mohr did not define his limit curve as envelope of all fracture cycles, respectively.

(5) Real isotropic materials have deficiencies to the ideal isotropic material. Hence, fracture will occur according to the actual flaw situation. In the case of crack-like flaws so-called wing-cracks (rock mechanics) occur where the wing crack finally grows into the direction of the acting compression force [Cun20b]

(6) A physically realistic investigation, performed in structural stresses and including both the modes, tells that the fracture angle at the cohesive strength point, where $\sigma_n = 0$, must approach 90° for really brittle materials like normal concrete

(7) The friction value μ is a so-called 'physical' property. This practically means: A good average value is sufficient for analysis in design dimensioning where always average values should be used

(8) The rotationally-symmetric model corresponds to the Neutral Meridian Θ^{NM} *($\vartheta = 0°$)*

(9) *The failure plane angle Θ_{fp} reduces with increasing hydrostatic pressure, which means that the behavior becomes more ductile. This increase of 'ductility', documented by Θ_{fp} from about 50° → 45°, is witnessed, even for marble*

(10) *Mohr stresses τ_{nt}, σ_n grow with p_{hyd}, like the driving principal shear stress $\tau_I = (\sigma_{II} - \sigma_{III}) / 2$.*

Some Pre-notes on Testing, Test Specimens and Standards:

- Most of the tri-axial tests of the used materials are performed on tensile and compressive meridians. These meridians are the opposite lines of an axial cross-section of the fracture failure body, see *Fig.7.1-5*.
- Looking at the Mohr-Coulomb curve, the angle alters with Θ from (ϑ = -30°) via Θ^{NM} (ϑ = 0°, *it represents the rotationally-symmetric model*) → Θ^{TM} (ϑ = +30°). In other words, an essential change is faced with C from $C^c \approx$ - 0.2 at ($\sigma_{II} = -R^c$, 0) along the bi-axial stress states (σ_{II}, σ_{III}).
- Measurement results are 'only' the result of a test agreement defined in a standard, a guideline etc. which serves the comparability of different test investigations and the credibility of the process. The test agreement consists of test facility, test certificate, test specimen and evaluation procedure. This means that we can only speak of 'exact' test results within the frame of the test agreement.
- It must be noted that environment and loading rate affect the results.
- The compressive strength of concrete is determined by a pressure test with specially manufactured test specimens. These are concrete cubes with usually 15 cm edge length (sample cubes) or 30 cm long concrete cylinders with 15 cm diameter (DIN EN 12390-1)
- For the production and storage of test cubes for strength tests, DIN EN 12390-2 applies in addition. The compressed surfaces should be flat and parallel. Otherwise, they must be sanded wet or provided with a thin matching layer.

7.1.4 Fracture Body, Friction Quantities and Mohr-Coulomb Curve of Normal Concrete Invariants, Strength Failure Conditions SFCs and Material data set of Concrete

For preparing the solution of this task, in the previous chapters still associated sub-tasks have been solved. Nevertheless, at first the full input for the isotropic example Normal Concrete shall be collected in order to pave the way for a shorter performance of the main numerical task presented in *Table 7.1-5*. The material input data set for the computation reads:

$\bar{R}^t = 4$ MPa, $\bar{R}^c = 40$ MPa, $\bar{R}^{tt} = 0.8 \cdot \bar{R}^t$ (assumed), $\bar{R}^{cc} = 51$ MPa, $\bar{R}^{ccc} = 1000$ MPa (set)

120°-rotationally-symmetry parameter: $c_{1\Theta}^{SF} \cdot \Theta^{SF} = 1 + c_{2\Theta}^{SF}$ with $c_{2\Theta}^{SF}$ as friction parameter

$\mu = 0.17$, $\Theta_{fp}{}^c = 50°$, $c_{2\Theta}^{SF} = 3.70$, $c_{1\Theta}^{SF} = 5.88$, $d^{SF} = 0.49$, $\Theta^{SF} = \Theta^c = \Theta^{CM} = 0.51$.

For the interaction exponent $m = 2.6$ and $\mu = 0.17$ is set. *A smaller μ value is more conservative.*

As still mentioned the usual tests are run along the tensile meridian and the compressive meridian. This means, that the fracture angle Θ_{fp} is meridian-dependent or dependent on the Lode angle ϑ, respectively. This situation causes to apply the realistic 120°-rotationally-symmetric model.

The tests are performed by adding an axial load generating σ_{ax} upon a hydrostatic loading p_{hyd}. In *Fig.7.1-5* the meridian failure curves are depicted and some test points are inserted indicating where the determination of the Mohr quantities τ_{nt} , σ_n , Θ_{fp} has been performed. As coordinates, the Lode-Haigh-Westergaard coordinates are used which equally count in all directions of the 3D stress space.

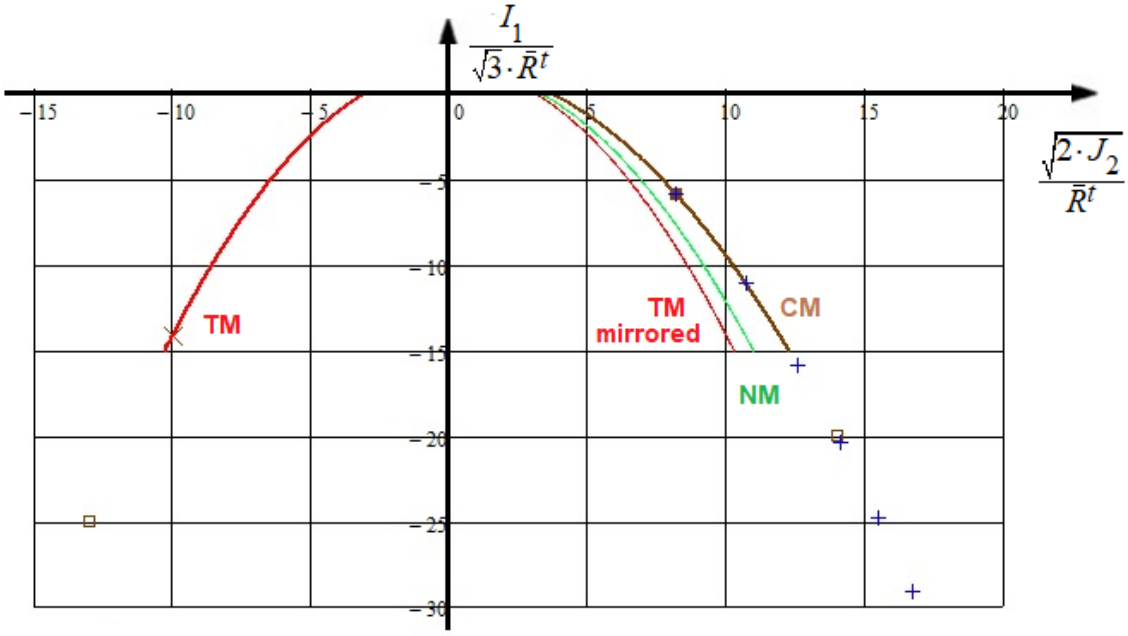


Fig.7.1-5: Display of all basic meridians of Normal Concrete. The + are the points where the evaluation of τ_{nt}, σ_n, Θ_{fp} was performed. $p = p_{hyd}$.

(Mathcad unfortunately did not draw below -15 !?. An often faced problem)

The basic three meridians, depicted in *Fig.7.1-5*, are Tensile Meridian TM (ϑ = +30°) inside, Neutral Meridian NM (0°) and Compressive Meridian CM (ϑ = -30°), outside. Test points lie on the respective meridian, determined by ϑ, which means on different distances from the axis for a specific $I_1 / \sqrt{3 \cdot \bar{R}^t}$. The tensile strength is used for normalization in the case of brittle materials

7.1.5 Fracture Failure Body and Principal stress plane Cross-section

Fig.7.1-6 shows the fracture body of the Normal Concrete, see [*Cun15*].

The three basic meridians and the two strength points, compressive strength (dot) and bi-axial compressive strength (cross), are indicated.

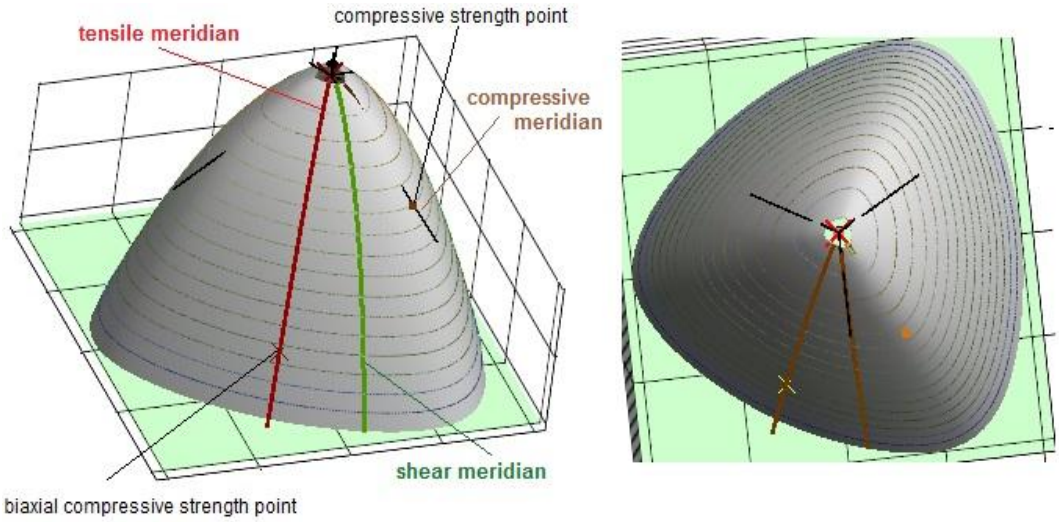


Fig.7.1-6: Two views of the 120°-rotationally-symmetric fracture body (hoop cross-section) of the Normal Concrete with the basic three meridians and the two strength points [Cun17]

Table 7.1-5: Input formulas for main task. TM tensile meridian, CM compressive meridian

* Transfomation of Efforts in Mohr stresses-based ones

$$Eff^{NF} = c^{NF} \cdot \frac{\sqrt{4J_2 \cdot \Theta^{NF} - I_1^2/3} + I_1}{2 \cdot \bar{R}^t}, \qquad \Theta^{NF} \rightarrow \Theta^{TM} = \sqrt[3]{1 + d^{NF} \cdot (+1)},$$

in this application can be set: $c^{NF} = \Theta^{NF} = 1,$

$$Eff^{NF} = 1 \cdot \frac{\sqrt{4 \cdot [(\sigma_n - \sigma_t)^2 + \sigma_t^2 + (-\sigma_n)^2 + 6 \cdot \tau_{nt}^2] \cdot 1/6 - (\sigma_n + \sigma_t)/3} + (\sigma_n + \sigma_t)}{2 \cdot \bar{R}^t}.$$

$$Eff^{SF} = \frac{c_{2\Theta}^{SF} \cdot I_1 + \sqrt{(c_{2\Theta}^{SF} \cdot I_1)^2 + 12 \cdot c_{1\Theta}^{SF} \cdot J_2 \cdot \Theta^{SF}}}{2 \cdot \bar{R}^c}, \quad \Theta^{SF} \rightarrow \Theta^{CM} = \sqrt[3]{1 + d^{SF} \cdot (-1)},$$

$$Eff^{SF} = \frac{\sqrt{c_{2\Theta}^{SF\,2} \cdot (\sigma_n + \sigma_t)^2 + c_{1\Theta}^{SF} \cdot \Theta^{SF} \cdot 2 \cdot [(\sigma_n - \sigma_t)^2 + \sigma_t^2 + (-\sigma_n)^2 + 6 \cdot \tau_{nt}^2]}}{2\bar{R}^c} + c_{2\Theta}^{SF} \cdot \frac{\sigma_n + \sigma_t}{2\bar{R}^c}.$$

In contrast to the friction quantities, which are determined in the compressive strength point, where Θ^{SF} is the constant above, Θ now changes with the Lode angle ϑ. This requires J_3 in Mohr stresses) which can be performed when employing the basic form $27 \cdot J_3 = 2 \cdot I_1^3 - 9 \cdot I_1 \cdot I_2 + 27 \cdot I_3 \cdot I_1^2 \cdot 2/27 - I_1$ because the I_1, I_2, I_3 can be displayed in Mohr stresses (Table 3-1). For the present 2D case it reads :

$I_1 = \sigma_n + \sigma_t$, $6J_2 = (\sigma_n - \sigma_t)^2 + \sigma_t^2 + (-\sigma_n)^2 + 6 \cdot \tau_{nt}^2$, $27J_3 = 2(\sigma_n + \sigma_t)^3 - 9 \cdot (\sigma_n + \sigma_t) \cdot (\sigma_n \cdot \sigma_t - \tau_{nt}^2)$

* Addition theorems considering $\eta = \sigma_{II} - \sigma_{III}$, σ_λ, $\tau_{t\lambda}$, $\tau_{n\lambda} = 0$

$$\sigma_n - \sigma_t = c^2 \cdot \eta - s^2 \cdot \eta = C \cdot \eta \;,\; S = \sqrt{1 - C^2},\; C = c^2 - s^2 = 2c^2 - 1 = 1 - 2s^2,$$

$$\sigma_n + \sigma_t = \sigma_{II} + \sigma_{III} = I_1,\; \tau_{nt} = -0.5 \cdot S \cdot \eta = -0.5 \cdot \sqrt{1 - C^2} \cdot \eta,\; \sigma_t = \sigma_n - C \cdot \eta \;.$$

* Fracture interaction equation ≡ mathematical equation of the fracture body surface

$$Eff = [(Eff^{NF})^m + (Eff^{SF})^m]^{m^{-1}} \Rightarrow \text{numerically simpler } (Eff^{NF})^m + (Eff^{SF})^m = 1 = 100\% \;.$$

Fig.7.1-7 displays the course of the measured 2D test data of Normal Concrete, provided by Dr. Silke Scheerer at IfM TU-Dresden (Head: *Prof. M. Curbach*). It depicts the large scatter of the multi-axial compression tests, which influences the statistically reduced design strength *R* significantly. *Fig 7.1-7 left* is a bias cross-section of the Normal Concrete fracture body which is the shape of the principal stress plane. As coordinates the still mentioned Lode-Haigh-Westergaard coordinates are used which equally count in all directions of the 3D stress space.

The measurement of a realistic fracture angle – based on the usually small-scale test level - is practically not possible. The determination of the curve parameters *c* by mapping the course of test data points is the better and practical procedure. Then, the relationship of the curve parameter c to the friction value μ and to the fracture angle Θ_{fp} can be derived. These relations are obtained in the *touch point,* pointed out in *Fig.7.1-1*.

The generation of a realistic Mohr-Coulomb curve requires the determination of the slope *along* the full curve, not a single specific value in the touch *point* only. This slope $d\tau_{nt}/d\sigma_n$ is linked to the unknown *fracture plane measure,* described by $C(\Theta_{fp})$. An equation to determine C comes from the differentiation of the Mohr stress-transformed interaction equation because both the two modes are

activated. This means, instead of the single SF-formulation the SF-NF-coupling *Eff*-formulation is to apply when moving from the structural stress formulation to a Mohr stress one. *Table 6-2* will show the full procedure, later.

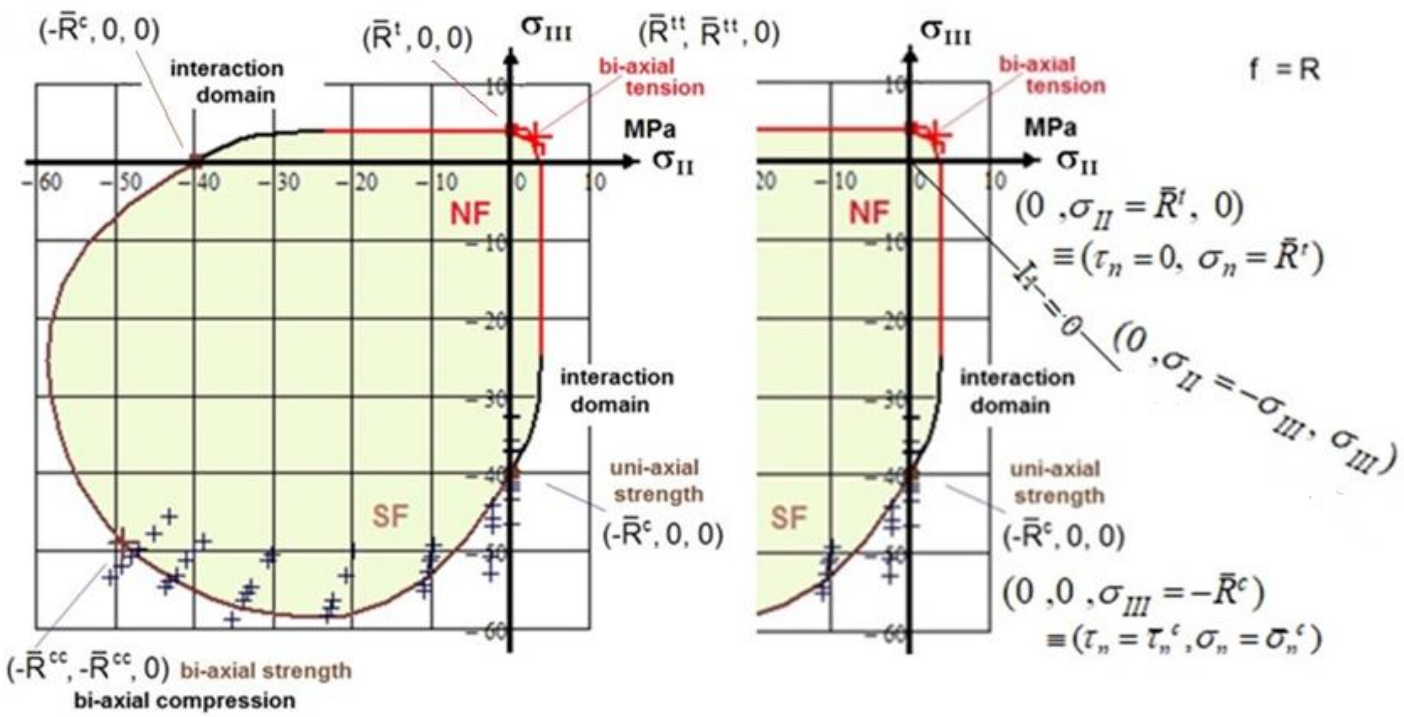


Fig.7.1-7: Bi-axial failure curve of Normal Concrete, 2D-test data set

Reminder:

The basic assumption of O. Mohr was: *"The strength of a material is determined by the (Mohr) stresses on the fracture plane".* This means for the here applied linear Mohr-Coulomb (M-C) formulation $\tau_{nt} = \bar{R}^{\tau} - \mu \cdot \sigma_n$. Herein, the value μ is an intrinsic friction property of the material and $\bar{R}^{\tau}$ the so-called cohesion strength. The shear stresses $\tau_{t\lambda}$, $\tau_{n\lambda}$ are zero together with the normal stress σ_{λ}. The normal stress σ_t must be accounted for in the investigation but will finally have no influence, which has to be proven when following Mohr and this must be shown.

Fig.7.1-8 displays the 2nd quadrant of the bi-axial failure curve formulated in structural stresses. This fully represents the Mohr-Coulomb curve domain. The joint mode situation of the Mohr-Coulomb curve - capturing the transition zone between the pure mode domains NF and SF - requires the application of the interaction equation $(Eff^{NF})^m + (Eff^{SF})^m = 1$. It spans over the regime $0 < \sigma_{III} < \bar{R}^t$ and the Lode angles $(-30° < \delta < +30°)$.

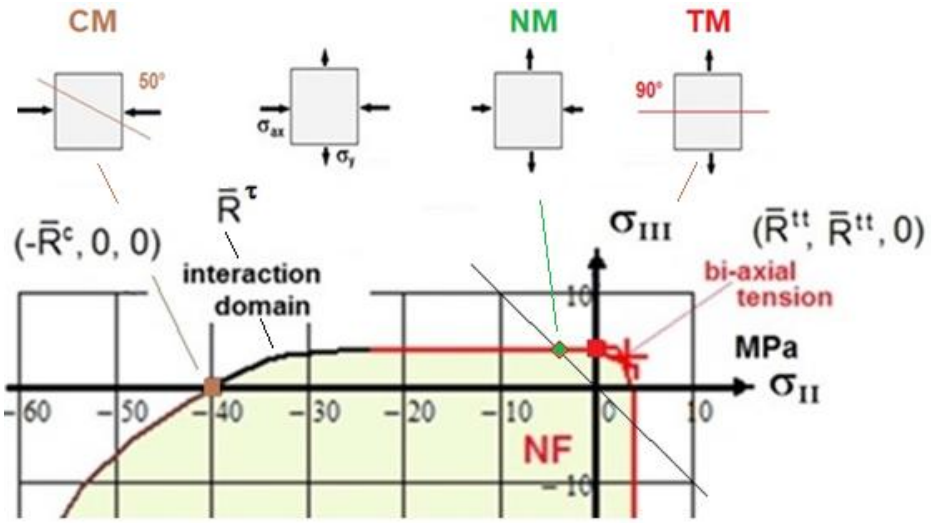


Fig.7.1-8 Second quadrant and associated stress states, transition zone between the 2 mode domains SF, NF

7.1.5 Improved Mapping of Failure Stress data with Derivation of a more realistic $\Theta_{fp}°(\vartheta)$

The F^{SF}-curve outlines a local shortcoming of the FMC-based choice of the SF-formula. Negative values of Eff^{SF} are sorted out by a McCauley-procedure, but positive values have to be made inactive in the domain about $\sigma_{II} = -\sigma_{III}$, see Fig.7.1-9 . In design-verification the Eff^{SF} contribution to *Eff* is not a problem because the interaction is a conservative procedure. However, when searching a local fracture angle $\Theta_{fp}°$ a correction should be material-dependently applied to numerically determine a better value for $\Theta_{fp}°$.

Searching a procedure it is helpful to know how the pure mode efforts of the activated modes NF and SF share its influence with σ_{II}. *Fig.7.1-9* shows the courses of the efforts Eff^{NF} (= Eff^{σ}) and Eff^{SF} (= Eff^{τ}) representing the components of the *measured* fracture stress curve.

According to the fact that the compression strength point is located on the compressive meridian and the tensile strength point on the tensile meridian the different Lode angle ϑ is to consider in order to achieve an accurate approach when investigating the Mohr-Coulomb curve. This requires to consider the 120°-rotationally-symmetric $Eff^{SF\Theta}$.

Mathematically-caused, the Eff^{SF}-curve and the $Eff^{SF\Theta}$–curve become positive in the pale colored curve part and numerically contribute its effort portion to the total effort (again, no problem for designing). This is physically not accurate and could be by-passed by a query in the numerical process not permitting - after a previous decay – the newly increase. Also one could apply a decay function that – physically logically - keeps Eff^{SF} zero, like for the UD material in chapter 7.

The shear material stressing effort $Eff^{\tau} = Eff^{SF}$ must physically become zero at the tensile strength point (0, R^{t}). This specific shortcoming cannot be by-passed by an increased interaction exponent *m*. This is brought about by a correction function that defines the decay of Eff^{τ} and is practically performed by setting $Eff^{\tau} = 0$ at $\sigma_{II} = 0$. As function was taken an exponential one, namely

$$f_d = 1/(1+\exp(\frac{c_{1d}+\sigma_{II}}{c_{2d}}), \quad \text{with} \quad c_{1d}, c_{2d} \text{ fixed at } (-\bar{R}^{c}, 0.995) , (-0.01,+0.01).$$

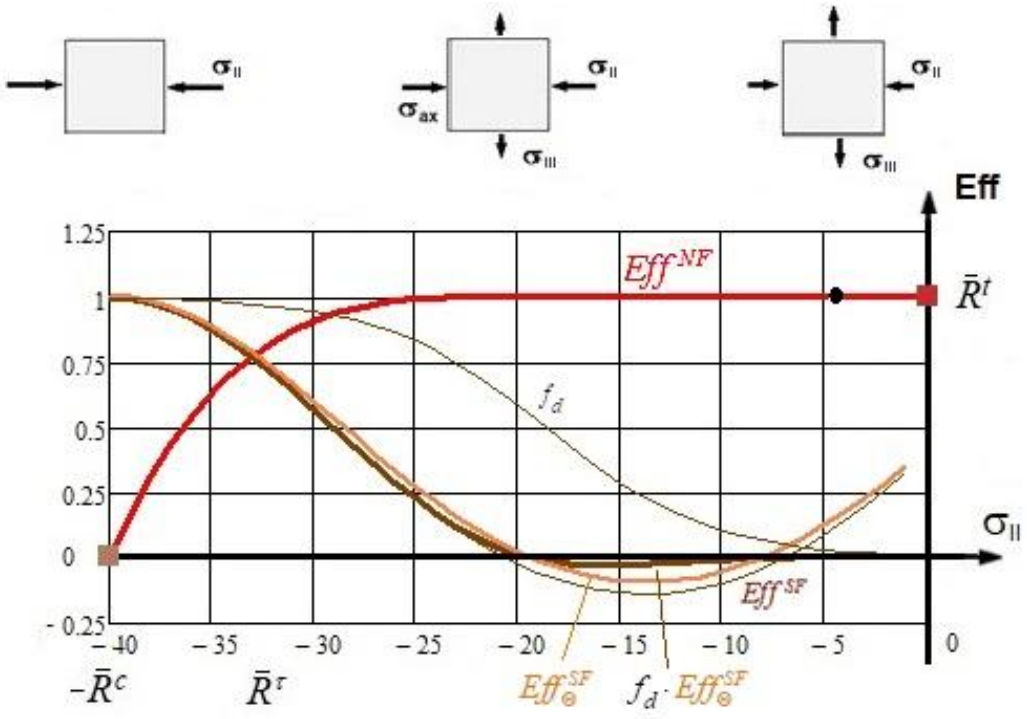


Fig.7.1-9: Visualisation of the course of the pure mode efforts Eff^{mode} *supporting the need to interact them in the case of bi-axial stress states to not exceed Eff = 100 %.* $c_{1d} = 18.6$, $c_{2d} = 4.04$.

Eff^{NF} , Eff^{SF}, $Eff^{SF\Theta}$, $f_d \cdot Eff^{SF\Theta}$

The corrected Eff^{SF}–curve delivers the desired improvement of $\Theta_{fp}°$ and lowers $\bar{R}^{\tau}$ from 12.5 → 11.0 MPa. With this correction, then the envisaged transformation was performed.

Note, please:
Applying - instead of the present Modal SFC - a so-called Global SFC, which globally maps in a single mathematical equation all test data and modes, a similar difficulty would be found too.

7.1.6 Derivation of a realistic Modes-Interaction Considering Mohr-Coulomb Curve $\tau_n(\sigma_n)$

Table 7.1-6 summarizes the relations for the derivation of $\tau_{nt}(\sigma_n)$ and $\Theta_{fp}°$ from a given fracture curve $\sigma_{II}(\sigma_{III})$. It is to consider the change of the fracture plane angle $\Theta_{fp}°$ with the Lode angle ϑ from $\Theta_{fp}{}^{c}°$ at $\vartheta = -30°$ on. The biggest challenge is the necessary differentiation of the interaction equation $Eff = 1$ within Mathcad. This further produces a giant formula output, that 'generously' can be cut down by using addition theorems and by inserting the given structural stresses input via its invariants I_1, J_2, J_3.

In the transformation of structural stresses into the Mohr stresses the advantage of invariants fully comes out: *They do not depend on the coordinate system, one can simply switch between the systems!*

Fig.7.1-10 displays several failure curves and the course of the altering fracture plane angle $\Theta_{fp}°$. Its left part presents the entities in a structural stresses diagram and the right part in a Mohr stresses diagram. This involves the Linear Mohr-Coulomb fracture curve and the real SF-NF interaction curve $\tau_{nt}(\sigma_n)$. The 3 Mohr circles are incorporated.

Table 7.1-6: Transformation of a 2D structural stresses-based failure curve into Mohr-Coulomb one

* Task: Known $\sigma_{II}, \sigma_{III}; \bar{R}^t, \bar{R}^c$. To determine: σ_n, τ_{nt}, $\Theta_{fp}°(C)$, $C = \cos(2 \cdot \Theta_{fp}° \cdot \pi / 180°))$

σ_λ, $\tau_{t\lambda}$, $\tau_{n\lambda} = 0$. $\eta = \sigma_{II} - \sigma_{III}$, $\sigma_{II} + \sigma_{III} = \sigma_n + \sigma_t = I_1$, $\sigma_n - \sigma_t = C \cdot \eta$,

$\sigma_t = \sigma_n - C \cdot \eta$, $\sigma_n = 0.5 \cdot [(C+1) \cdot \sigma_{II} + (-C+1) \cdot \sigma_{III}]$, $\tau_{nt} = -0.5 \cdot \sqrt{1-C^2} \cdot \eta$.

* Interaction equation because 2 modes are activated: $(Eff^{NF})^m + (Eff^{SF})^m = 100\%$

$$Eff^{NF} = \frac{\sqrt{4 \cdot [(\sigma_n - \sigma_t)^2 + \sigma_t^2 + \sigma_n^2 + 6 \cdot \tau_{nt}^2] / 6 - (\sigma_n + \sigma_t)^2 / 3} + (\sigma_n + \sigma_t)}{2 \cdot \bar{R}^t},$$

$$\frac{Eff^{SF}}{f_d} = \frac{c_{2\Theta}^{SF} \cdot (\sigma_n + \sigma_t)}{2 \cdot \bar{R}^c} + \frac{\sqrt{(c_{2\Theta}^{SF} \cdot (\sigma_n + \sigma_t))^2 + 2 \cdot c_{1\Theta}^{SF} \cdot \Theta^{SF} [(\sigma_n - \sigma_t)^2 + \sigma_t^2 + \sigma_n^2 + 6 \cdot \tau_{nt}^2]}}{2 \cdot \bar{R}^c}$$

* Solution of the task: equalizing the slopes at each stress state $\sigma_{II}(\sigma_{III})$

Slope 1: from differentiation of structural stresses-linked Mohr stresses delivers

$$\frac{d\tau_{nt}}{d\sigma_n} = \frac{(s^2 - c^2) \cdot \eta}{-2 \cdot s \cdot c \cdot \eta} = \frac{C}{S} = \frac{C}{\sqrt{1-C^2}} \text{ , valid uni-axially and bi-axially}$$

Slope 2: from differentiation of the interaction equation, abbreviation $\eta_m = 2\sigma_n - C \cdot \eta$

$$Eff^{NF} = \left\{ \sqrt{4 \cdot [(C \cdot \eta)^2 + (\sigma_n - C \cdot \eta)^2 + \sigma_n^2 + 6 \cdot \tau_{nt}^2] / 6 - \eta_m^2 / 3} + \eta_m \right\} / 2 \cdot \bar{R}^t, \quad \Theta^{NF} = 1$$

$$Eff^{SF} = \left\{ c_{1\Theta}^{SF} \cdot \eta_m + \sqrt{(c_{2\Theta}^{SF2} \cdot \eta_m^2 + 2 \cdot c_{1\Theta}^{SF} \cdot \Theta^{SF} \cdot [(C \cdot \eta)^2 + (\sigma_n - C \cdot \eta)^2 + \sigma_n^2 + 6 \cdot \tau_{nt}^2]} \right\} / 2 \cdot \bar{R}^c$$

$F = (Eff^{NF})^m + (Eff^{SF})^m$ with $dF / d\sigma_n$ and $dF / d\tau_{nt}$

Equating the 2 equations and replacing Mohr stresses by structural stresses

$$\frac{C}{\sqrt{1-C^2}} = -\frac{dF / d\sigma_n}{dF / d\tau_{nt}}$$ a huge formula for the determination of the fracture angle measure C

$$\Theta^{SF}(\vartheta) = \sqrt[3]{1 + d^{SF} \cdot \sin(3\vartheta)} = \sqrt[3]{1 + d^{SF} \cdot 1.5 \cdot \sqrt{3} \cdot J_3 \cdot J_2^{-1.5}}$$ inserting

$6J_2 = 2 \cdot (\sigma_{II}^2 - \sigma_{II} \cdot \sigma_{III} + \sigma_{III}^2)$, $27J_3 = (-\sigma_{II} - \sigma_{III}) \cdot (2\sigma_{II} - \sigma_{III}) \cdot (2\sigma_{III} - \sigma_{II})$

Implicite solution when determining C for the bi-axial stress states $(\sigma_{II}, \sigma_{III})$

$\sigma_n = (C+1) \cdot 0.5 \cdot \sigma_{II} + (1-C) \cdot 0.5 \cdot \sigma_{III}$, $\tau_{nt} = -0.5 \cdot \sqrt{1-C^2} \cdot (\sigma_{II} - \sigma_{III})$

a = $(12J_2 - I_1^2) / 3$, b = $\left((c_{2\Theta}^{SF} \cdot I_1 + \sqrt{d}) / 2\bar{R}^c \right)^{m-1}$,

c = $4I_1 \cdot (c_{2\Theta}^{SF2} + c_{1\Theta}^{SF} \cdot \Theta^{SF})$, d = $c_{2\Theta}^{SF2} \cdot I_1^2 + 2c_{1\Theta}^{SF} \cdot \Theta^{SF} \cdot 6J_2$.

Vorgabe C:= - 0.1 and inserting points $(\sigma_{II}, \sigma_{III})$

$$\frac{C}{\sqrt{1-C^2}} = -\frac{0.5 \cdot \sqrt{a} \cdot [(\bar{R}^t \cdot b \cdot c) / 4] + \bar{R}^c \cdot \sqrt{d} \cdot (\frac{2\sigma_n + \sqrt{a} - C \cdot \eta}{2\bar{R}^t})^{m-1} + \bar{R}^t \cdot c_{2\Theta}^{SF} \cdot b \cdot \sqrt{d}}{\tau_{nt} \cdot [\bar{R}^c \cdot \sqrt{d} \cdot (\frac{2\sigma_n + \sqrt{a} - C \cdot \eta}{2\bar{R}^t})^{m-1} + 3\sqrt{a} \cdot \bar{R}^t \cdot c_{1\Theta}^{SF} \cdot \Theta^{SF} \cdot b]}$$

Search(C) $\rightarrow$ equation for the fracture angle measure $C(\Theta_{fp}°)$ and for σ_n, τ_{nt}

$C = C(\sigma_{II}, \sigma_{III}) = \cos(2 \cdot \Theta_{fp})$, $\Theta_{fp} = 0.5 \cdot \arccos C$, $\Theta_{fp}° = \Theta_{fp} \cdot 180° / \pi$,

$\sigma_n = (C+1) \cdot 0.5 \cdot \sigma_{II} + (1-C) \cdot 0.5 \cdot \sigma_{III}$, $\tau_{nt} = -0.5 \cdot \sqrt{1-C^2} \cdot (\sigma_{II} - \sigma_{III})$.

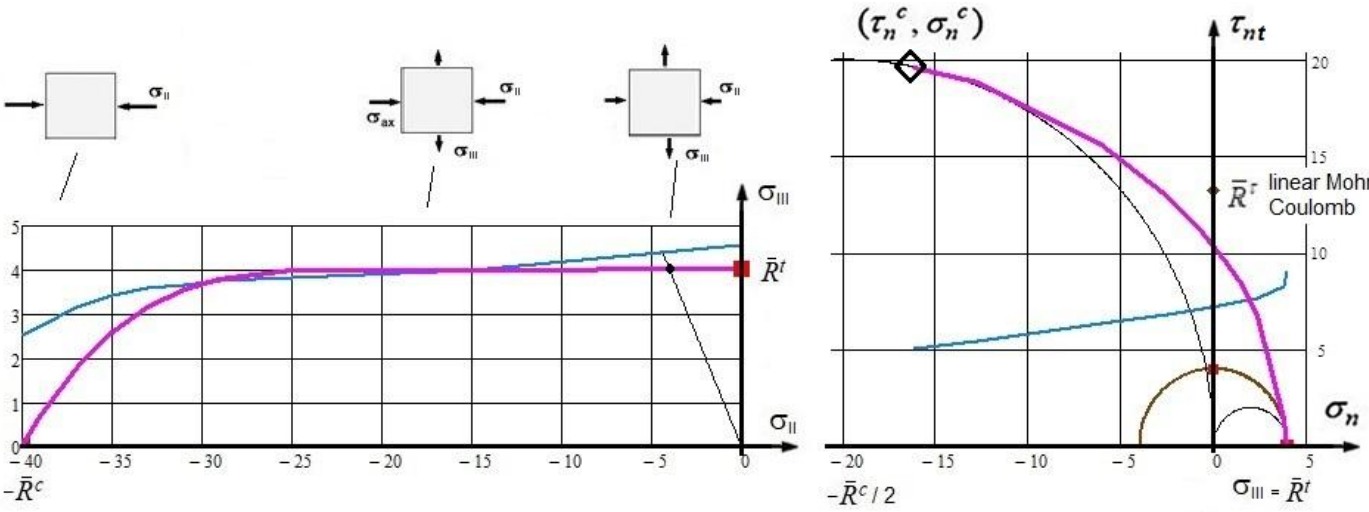


Fig.7.1-10: Joint display of the magenta failure curve in principal stresses (left) and in Mohr stresses (right). Fracture angle increase $\Theta_{fp}°$, , scaled by twenty (left) and ten (right), is incorporated . 120°-rotational-symmetric model and improved mapping of the measured failure curve due to f_d

$c_{1\Theta}^{SF} \cdot \Theta^{SF} = 1 + c_{2\Theta}^{SF}$ with $c_{2\Theta}^{SF}$ the friction parameter, $c_{2\Theta}^{SF} = 3.70$, $c_{1\Theta}^{SF} = 5.88$, $d^{SF} = 0.49$,

$\bar{R}^t = 4$ MPa, $\bar{R}^c = 40$ MPa, $\Theta_{fp}^{c\,\circ} = 50.5°$, $C^c = -0.192$, friction value $\mu = 0.195$,

$\bar{R}^\tau = 11$ MPa, $\Theta_{fp}^{\circ} = 72°$, $\sigma_{II} = -32$ MPa, $\sigma_{III} = 3.3$ MPa, $\delta = -25°$.

$\tau_{nt}^c = 19.6$ MPa, $\sigma_n^c = -16.2$ MPa, $c_{1d} = 18.6$, $c_{2d} = 4.04$, $\Theta^{SF} = \Theta^c = \Theta^{CM} = 0.51$.

The interpretation of the two diagrams in *Fig. 7.1-10* leads to the following results:

- ✓ The interaction equation *Eff* - representing the surface of the fracture body - in structural stresses can be transferred into Mohr stresses
- ✓ The alteration of the fracture plane angle $\Theta_{fp}°$ can be computed
- ✓ Complete failure danger is composed of portions Eff^{NF} and Eff^{SF}, following the idea of the FMC that NF and SF commonly add its *Eff* portions. This leads to the conclusion that the $\Theta_{fp}°$ is approximately 70° at the cohesive strength point
- ✓ The SF approach (*for this sub-task too simple*) could not offer a full accuracy of the fracture plane angle $\Theta_{fp}°$ and the Mohr-Coulomb curve to be predicted. Eff^{SF} had to be physically adjusted by a decay function f_d.



Venezuela
Me and the guide

Experience
after solving the very
challenging task
of this chapter:

"Challenging tasks strengthen!"

7.2 Dependence of Transversely-isotr. Friction model parameters on Friction Values $\mu_{\perp\perp}$, $\mu_{\perp\parallel}$

7.2.1 Invariants, strength fracture conditions SFCs and fracture body

As with the isotropic materials at first the derivation of the UD-SFCs shall be shortly presented. Therefore invariants and associated stresses used for the transversely-isotropic UD material are collected in *Fig.7.2 -1.*

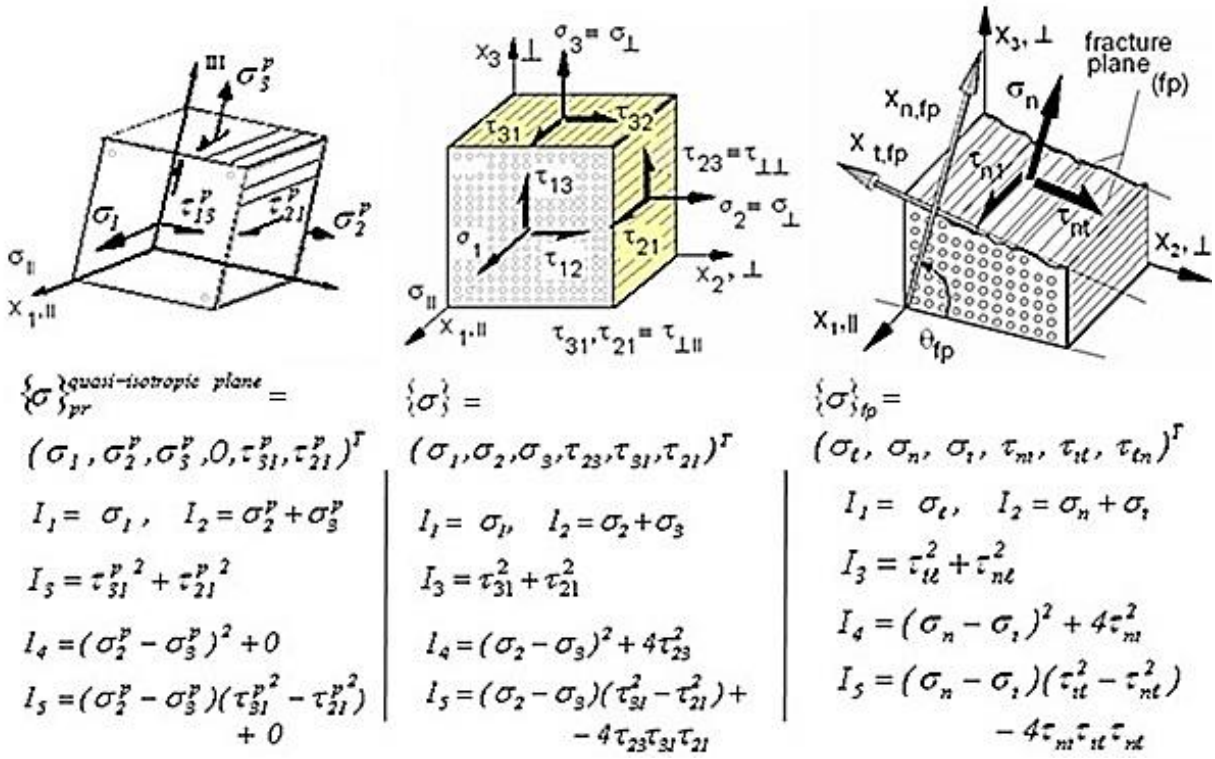


Fig.7.2-1: UD-Invariants and associated stresses (indices $\ell \equiv 1$, $p \equiv pr$)

Repeating the author's invariant-based Failure Mode Concept (FMC) 5 SFCs are to be derived in total. Replacing the UD-invariants by the stresses they are composed of and after simplifications with practical numerical modifications to by-pass probable 3D-solution problems the set of UD-SFCs for fiber-reinforced material, embedded in a matrix (plastic or mortar), is given in *Fig.7.2-2*.

The interaction of the separate five modes, 2 FFs (*Fiber-Failure*) + 3 IFFs (*Inter-Fiber-Failure*), is performed as with the isotropic material, by applying the interaction equation

$$Eff^m = (Eff^{\parallel\tau})^m + (Eff^{\parallel\sigma})^m + (Eff^{\perp\sigma})^m + (Eff^{\perp\tau})^m + (Eff^{\perp\parallel})^m = 1\,.$$

Due to mapping experience in the transition zones the interaction exponent is $2.5 < m < 3$. This is as for isotropic materials. For reasons of simplicity the same value is applied for all transition zones. The smaller the value is the more the design verification is conservative!
The Poisson effect is to consider in the macro-mechanical SFCs because bi-axial compression strains the filament without any external σ_1. In *Fig.7.2-2* this failure of the fiber constituent is considered in the equation FF1.

The transformation task takes place in the $\sigma_2(\sigma_3)$ quasi-isotropic plane. This requires the equations IFF1 and IFF2 from the following list.

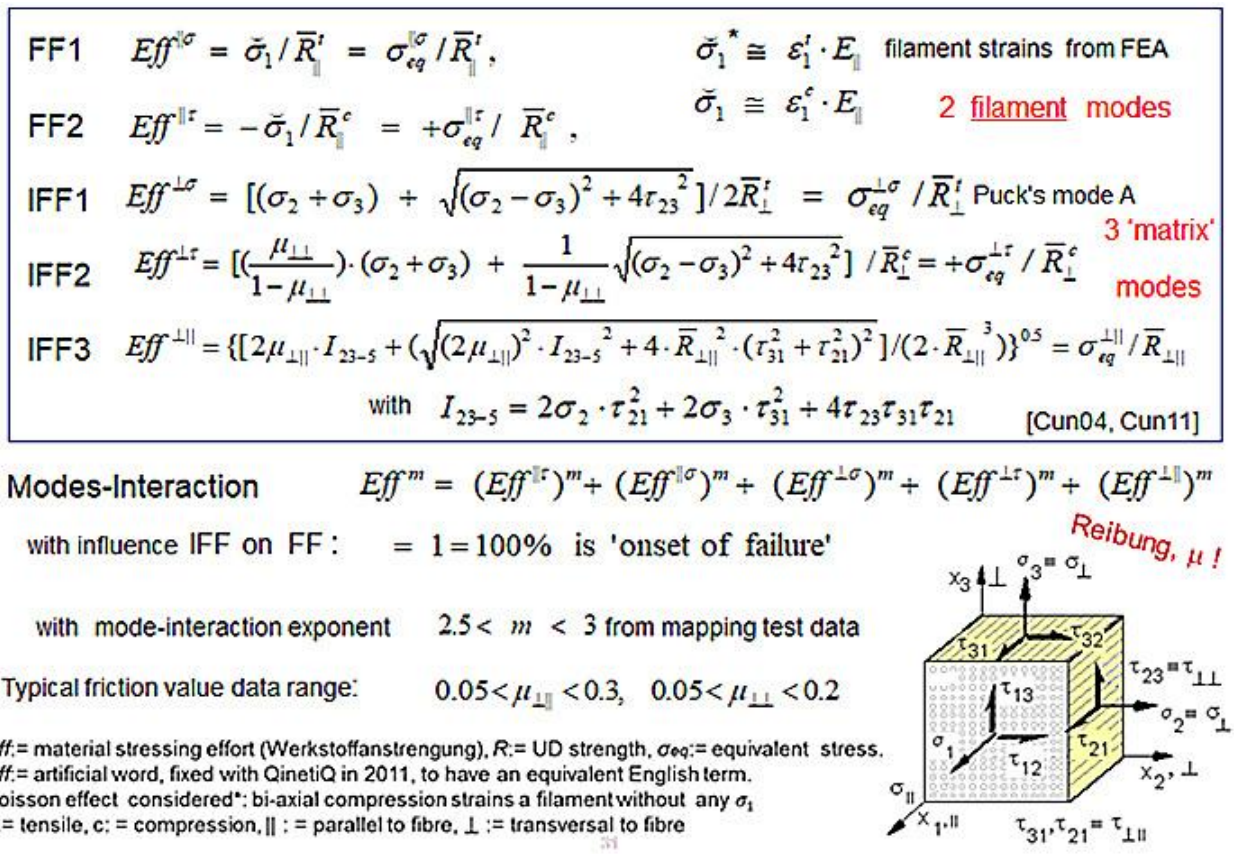


Fig.7.2-2: UD-SFCs for 'Onset of fracture failure', mode's interaction, and value ranges [Cun04, 12]

Fig.7.2-3 presents a visualization of the associated fracture body surface. The composite designations follow the guideline *VDI 2014, sheet 3 [VDI 06]*.

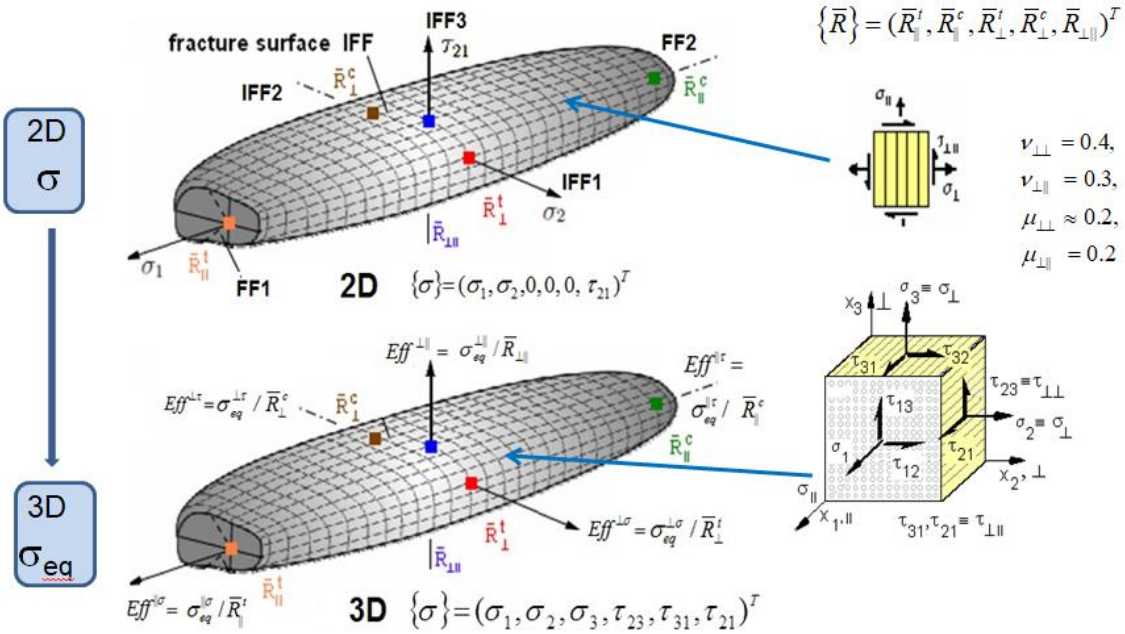


Fig.7.2-3: Fracture body of UD material (lamina, lamella, sheet, tape) for 2D and 3D stress states

NOTES:

(1) The invariant-based formulation for IFF2 is a pretty simple approach. It is mathematically homogeneous, which means that $F = Eff$. A functional approach is always a compromise

(2) Here, it is - *like for the isotropic concrete material* - a compromise 'on the safe reserve factor side', however, the approach is not accurate enough, if a fracture angle is to determine in cases of not highly brittle materials such as with values below $R_{\perp}^{c'} / R_{\perp}^{t'} < 5$. This is valid for the present UD material.

7.2.2 Main fracture curves

The M-C-curve runs in the transition zone between IFF2 and IFF1. Hence, focus here is the M-C-associated quasi-isotropic plane $\sigma_2(\sigma_3)$, displayed in *Fig.7.2-4*. Applying the shear fracture SFC IFF2 (*brown*) and computing the interaction curve (*magenta*) IFF1-IFF2 the failure curves in three quadrants are obtained. The curves are symmetric to the diagonal. For further information in *Fig.7.5* a sketch of the classical tension/compression-torsion UD test specimen is included.

One can assume that the interaction curve does not optimally map the usual course of test data (*like for isotropic mapping*) or – respectively - the mapping quality of IFF2 is not fully sufficient if the alteration of the fracture angle Θ_{fp} in the transition zone is to determine. This transition zone between a normal fracture mode domain NF and a shear fracture mode domain SF is ruled by interaction and corresponds to the bi-axially stressed M-C curve. This requires both the Eff-modes for the insertion into the interaction-linked M-C curve. The span of the investigated domain is:

Span: $(\tau_{nt}^{c}, \sigma_{n}^{c}) \rightarrow (\bar{R}_{\perp\perp}^{\tau},\ 0) \rightarrow (0,\ \sigma_n = \bar{R}_{\perp}^{t})$ or

$(\sigma_2 = -\bar{R}_{\perp}^{c},\ 0) \rightarrow (\sigma_2,\ \sigma_3 = -\sigma_2) \rightarrow (0,\ \sigma_3 = \bar{R}_{\perp}^{t})$

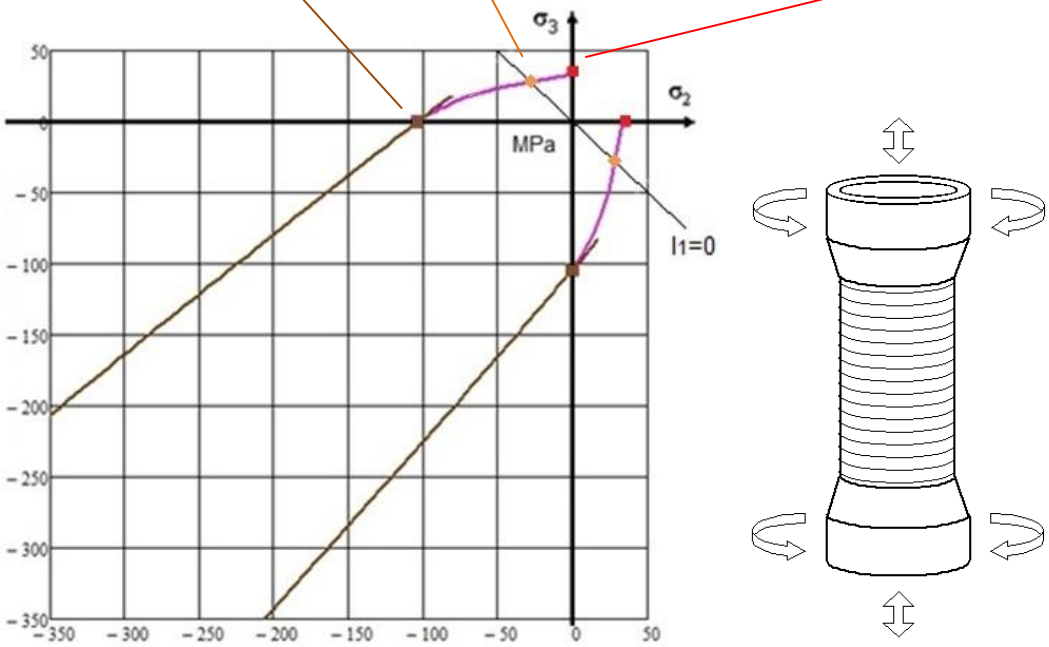


Fig. 7.2-4: The UD fracture stress curves in the quasi-isotropic plane.(right) Scheme of the 90°-wound tension/compression-torsion test specimen

Also a 3D fracture failure body $\tau_{21}(\sigma_2, \sigma_3)$ is shown in *Fig.7.2-5* for teaching the spatial understanding of the SFC.

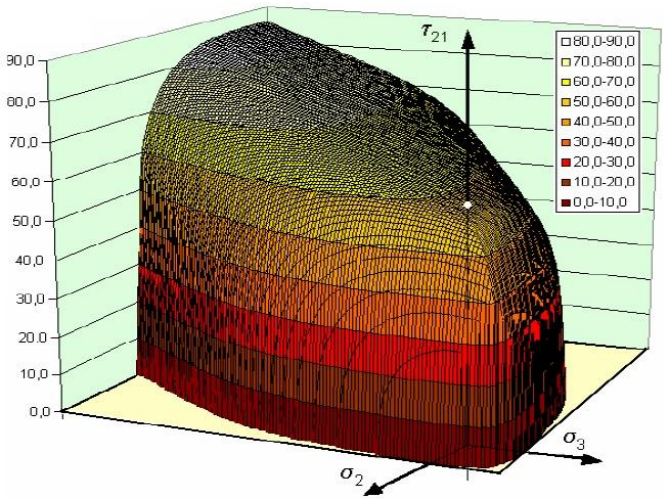


*Fig. 7.2-5: 3D fracture body [figure Cuntze-Sukarie, still in **19**97]*

As before with isotropic materials: The M-C curve is a bi-axial fracture stress curve and its course in the 2nd quadrant of $\sigma_3(\sigma_2)$ is identical to the so-called Mohr envelope or Mohr-Coulomb curve $\tau_{nt}(\sigma_n)$, respectively. The interaction curve (magenta) can be dedicated to the basic Mohr-Coulomb curve namely from the compression strength point till the tensile strength point, see *Fig.7.2-4*.

Similar to the isotropic case the bi-axial stress-ruled M-C curve is oppositely dominated by two modes, IFF2 (SF) with IFF1 (NF). Therefore, attention must be paid again to the interaction of both these modes in the transition zone in order to finally obtain an 'accurate' fracture angle Θ_{fp}, being the pre-condition to determine the two Mohr stresses τ_{nt} , σ_n with high fidelity.

In *Fig.7.2-6* the **failure curve** in the second quadrant of Fig.7.2-4 is enlarged. For additional information $\tau_{23}(\sigma_2)$ is included. The cohesive (shear) strength point (square) is at the crossing $\sigma_2 = -\sigma_3$!

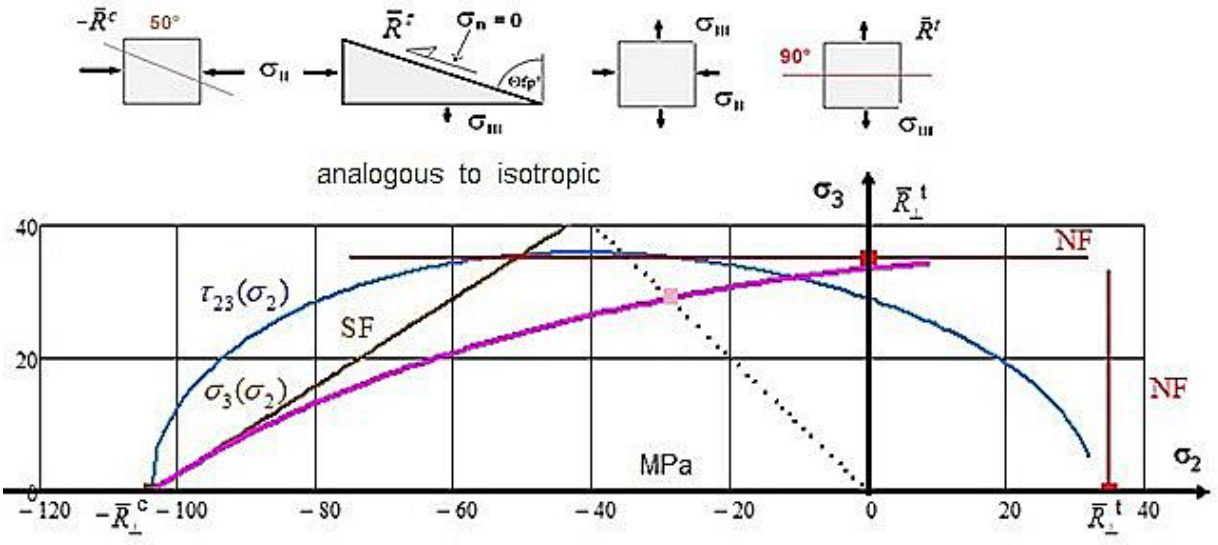


Fig. 7.2-6, zoom of Fig.7.2-4, 2nd quadrant: Alteration of fracture angle Θ_{fp}° allocated to the associated altering failure stress state $\sigma_2(\sigma_3)$, faced in the transition zone.

$\bar{R}^c_\perp = 104MPa$, $\bar{R}^t_\perp$ =35 MPa, $C^c_{fp} = -0.174$, $\Theta_{fp}° = 51°$, $a_{\perp\perp} = 0.26$, $\mu_{\perp\perp} = 0.18 \cong -C^c_{fp}$

As with the isotropic material the magenta curve cannot accurately map the course of test data. Fig.7.1-6 shows that with the IFF2-function the shear effort $Eff^{\perp\tau}$ cannot become zero in the M-C domain being a transition zone. This numerical behavior is a shortcoming in the transition zone of the IFF2 approach between the two modes SF and NF. An accurate alteration of the fracture angle $\Theta_{fp}°$ and of the associated Mohr stresses $\tau_{nt,}$ σ_n is not to achieve with the mathematical course of the IFF2 function or of $Eff^{\perp\tau}$, respectively. In order to find an improvement it is essential to know how the pure mode efforts of the activated modes IFF1 and IFF2 ($Eff^{\perp\tau}$) share its influence along the σ_2-axis, *Fig.7.2-7*.

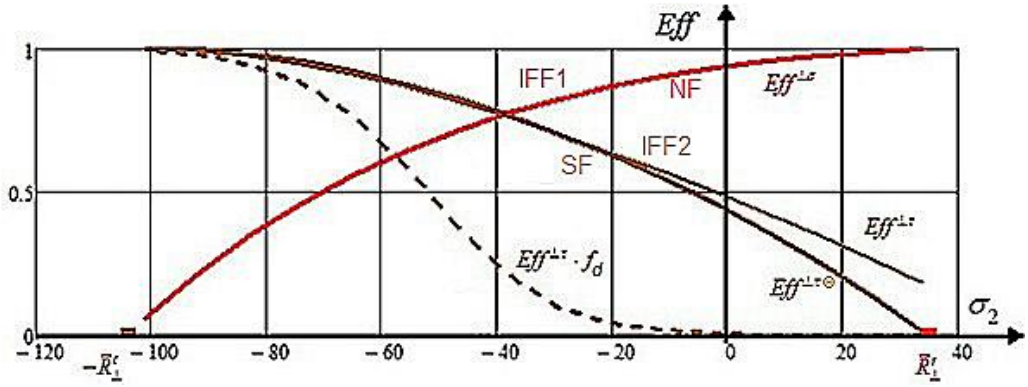


Fig.7.2-7: Course of the two efforts Eff^{NF}, Eff^{SF} *composing the fracture stress curve Eff =1. c_1 = 48.3, c_2 = 10.5. (d is index for decay)*

$Eff^{\perp\tau}$ firstly become zero at $\sigma_2 = \sigma_3 = R^{tt} < R^t$, termed equi-biaxial tensile 'strength'. This zero point is physically 'too late' for a revised local mode description. For a realistic transformation of the test curve formulated in principal stresses into a Mohr stress formulation it must be solved that $Eff^{\perp\tau}$ (SF) becomes physically zero when reaching the pure NF domain. This is brought about by a correction function $f_{d,}$ that defines the decay of $Eff^{\perp\tau}$ and is practically performed by setting $Eff^{\perp\tau} = 0$ at $\sigma_2 = 0$. As function for the decay the still applied exponential one is taken again

$$f_d = 1/(1+\exp(\frac{c_{1d}+\sigma_2}{c_{2d}}), \quad \text{with} \quad c_{1d}, c_{2d} \text{ fixed at } (-\bar{R}_\perp^c, 0.995), (-0.01, +0.01).$$

The interactive use of above $Eff^{\perp\tau}$ (SF) and $Eff^{\perp\sigma}$ (NF) is not problematic for design verification.

7.2.3 Relation of Friction parameter $a_{\perp\perp}$ to Fracture angle Θ_{fp}^c and to Friction value $\mu_{\perp\perp}$

The measurement of a realistic fracture angle is practically not possible. The determination of the curve parameters $a_{\perp\perp}$ and $b_{\perp\perp}$ by mapping the course of test data points is the practical procedure. Then, the relationship of the curve parameter to the friction value and to the fracture angle can be derived according to *Table 7.2-1*.

Analogous to the isotropic case the required IFF2-relationships are to derive: The basic assumption, lying behind all action-plane SFCs (e.g. UD Puck/Hashin) is the *brittle-fracture hypothesis* which goes back to O. Mohr's "*The strength of a material is determined by the Mohr stresses on the fracture plane".* This means for the here again applied Linear Mohr-Coulomb (M-C) formulation $\tau_{nt} = \bar{R}_{\perp\perp}^{\tau} - \mu_{\perp\perp}\cdot\sigma_n$. The friction value μ is an intrinsic property of the UD material and

If IFF occurs in a parallel-to-fiber plane of the UD lamina, the components of the failure stress vector are the normal Mohr stress σ_n and the two Mohr shear stresses τ_{nt} and τ_{n1}. The shear stress τ_{tl} and the normal stress σ_t will have no influence and is to be proven in the derivation. τ_{n1} belongs to IFF3 and therefore is not of interest in the following investigations.

The transformation of the SFC IFF2 in lamina stresses into a Mohr stresses one works via the addition theorems in *Table 7.2-1.* In the equations the bar over is dropped.

LL:

- *The Linear Mohr-Coulomb model can be employed to obtain a sufficiently good relationship for the determination of the friction value μ in the compressive stress point* $\sigma_2 = -\bar{R}_\perp^c$.
- *Establishing the relationship it is assumed that the tangent of the FMC-curve has the same value as that of the straight Linear Mohr envelope curve* $\tau_{nt}(\sigma_n)$ *in the touch point with Mohr's circle, see respective figure*
- σ_1 *is not relevant. The shear stress* τ_{23} *can be assumed zero because it would anyway vanish after a principal stress transformation. No reduction of generality is caused*
- *The stress* σ_t *has no influence! It is not representative such as Mohr supposes. Failure responsible are* τ_{nt} *and* σ_n, *only. But mind: For the differentiation* σ_t *cannot be simply set zero at the beginning of the derivations but must be considered due to its relation to* σ_n,
- *Above derivation further proves that, if really desired, the fracture plane angle* $\Theta_{fp}{}^c$ *of an UD-material could be determined from the FMC-based SFC formulated in structural stresses*
- *Viewing Fig.7.2-6 and -7 (indicator* $Eff^{\perp\sigma}$*) the cohesive strength* $\bar{R}_{\perp\perp}^{\tau}$ *belongs to the transition zone of the normal fracture mode domain IFF1 and therefore not alone to the shear fracture mode domain IFF2. One cannot extrapolate from a compressive strength point.*

7.2.4 Determination of Mohr shear curve, Touch point coordinates and Cohesive strength

Touch point coordinates $\tau_{nt}{}^c, \sigma_n{}^c$ *:*

From transformation equations: $c = \cos(\Theta_{fp}^c) = \cos(\Theta_{fp}^{c\,\circ} \cdot \pi / 180^\circ)$

$\sigma_n = c^2 \cdot \sigma_2$, $\tau_{nt} = -s \cdot c \cdot \sigma_2$ and $\Theta_{fp}^{c\,\circ} = 51.$, $\bar{R}_\perp^c = 104$ MPa

$\sigma_n{}^c = \cos(\Theta_{fp}^c)^2 \cdot (-\bar{R}_\perp^c) = -41.3$ MPa, $\tau_{nt}{}^c = -\sin(\Theta_{fp}^c) \cdot \cos(\Theta_{fp}^c) \cdot (-\bar{R}_\perp^c) = 50.9$ MPa or

$\sigma_n{}^c = 0.5 \cdot (C+1) \cdot (-\bar{R}_\perp^c) = -41.3$ MPa, $\tau_{nt}{}^c = -0.5 \cdot \sqrt{1-C} \cdot (-\bar{R}_\perp^c) = 50.9$ MPa .

From Mohr circle geometry:

$\tan\rho = (0.5 \cdot \bar{R}_\perp{}^c - |\sigma_n{}^c|) / \tau_{nt}{}^c$ and $\tan\rho = \tau_{nt}{}^c / (\bar{R}_\perp{}^c - |\sigma_n{}^c|) = |\sigma_n{}^c| / \tau_{nt}{}^c$

$\rightarrow \tau_{nt}{}^c := \sqrt{|\sigma_n{}^c| \cdot (\bar{R}_\perp{}^c - |\sigma_n{}^c|)} = \left((0.5 \cdot \bar{R}_\perp{}^c - |\sigma_n{}^c|) / \tan\rho\right)^2$

$\rightarrow |\sigma_n{}^c| = (\bar{R}_\perp{}^c + \bar{R}_\perp{}^c \cdot \tan\rho^2) - \bar{R}_\perp{}^c \cdot \tan\rho \cdot \sqrt{1+\tan\rho^2} / (2 + 2 \cdot \tan\rho^2)$.

Table 7.2-1 compiles all the necessary relations for the transformation of lamina stresses into Mohr stresses. (index p means principal).

Table 7.2-1: Relationships during derivation of $\tau_{nt}(\sigma_n)$, Θ_{fp}° *from a measured fracture curve* $\sigma_3(\sigma_2)$

$$Eff^{\perp\tau} = Eff^{SF} = [a_{\perp\perp}\cdot(\sigma_2{}^p + \sigma_3{}^p) + b_{\perp\perp}\cdot\sqrt{(\sigma_2{}^p - \sigma_3{}^p)^2 + 0^2}\,] / \bar{R}_\perp^c = 1$$

$$\equiv [a_{\perp\perp}\cdot(\sigma_n + \sigma_t) + b_{\perp\perp}\cdot\sqrt{(\sigma_n - \sigma_t)^2 + 4\tau_{nt}{}^2}\,] / \bar{R}_\perp^c = 1$$

$$Eff^{\perp\sigma} = Eff^{NF} = (\sigma_2{}^p + \sigma_3{}^p) + \sqrt{(\sigma_2{}^p - \sigma_3{}^p)^2 + 0^2}\,] / 2\cdot\bar{R}_\perp^t = 1$$

$$\equiv [(\sigma_n + \sigma_t) + \sqrt{(\sigma_n - \sigma_t)^2 + 4\tau_{nt}{}^2}\,] / 2\cdot\bar{R}_\perp^t = 1\,.$$

Known: $\sigma_2{}^p$, $\sigma_3{}^p$. Searched: σ_n, τ_{nt}, $\Theta_{fp}\,(C = \cos(2\cdot\Theta_{fp}{}^\circ\cdot\pi/180°))$

Two quantities are known and three are to be determined

Use of addition theorems, $\sigma_\lambda = 0$, index ^{p} now dropped

$$\sigma_n - \sigma_t = c^2\cdot(\sigma_2 - \sigma_3) - s^2\cdot(\sigma_2 - \sigma_3) = C\cdot(\sigma_2 - \sigma_3),\ \ S = \sqrt{1 - C^2}$$

$$\sigma_t = \sigma_n - C\cdot(\sigma_2 - \sigma_3),\ C = c^2 - s^2 = 2c^2 - 1 = 1 - 2s^2,$$

$$\sigma_n + \sigma_t = \sigma_2 + \sigma_3,\ \ \tau_{nt} = -0.5\cdot S\cdot(\sigma_2 - \sigma_3) = -0.5\cdot\sqrt{1 - C^2}\cdot(\sigma_2 - \sigma_3)$$

Fracture (interaction) equation ≡ mathematical equation of the fracture body

$$Eff = [(Eff^{NF})^m + (Eff^{SF})^m]^{m^{-1}} \quad or \quad \text{computationally simpler}$$

$$(Eff^{NF})^m + (Eff^{SF})^m = 1 = 100\% \quad \text{total effort.}$$

Differentiation of structural stresses-linked Mohr stresses delivers

$$\frac{d\tau_{nt}}{d\sigma_n} = \frac{(s^2 - c^2)\cdot(\sigma_2 - \sigma_3)}{-2\cdot s\cdot c\cdot(\sigma_2 - \sigma_3)} = \frac{C}{S},\ \ \text{valid } \textit{uni}\text{- and } \textit{bi}\text{-}\textit{axial} \text{ (like isotropic!)}$$

Missing equation from differentiation of the interaction equation, σ_t to insert before,

$$\{[(\sigma_n + \sigma_n - C\cdot(\sigma_2 - \sigma_3)) + \sqrt{(\sigma_n - \sigma_n - C\cdot(\sigma_2 - \sigma_3))^2 + 4\tau_{nt}{}^2}\,] / 2\cdot\bar{R}_\perp^t\}^m +$$

$$+\{[a_{\perp\perp}\cdot(\sigma_n + \sigma_n - C\cdot(\sigma_2 - \sigma_3)) +$$

$$+ b_{\perp\perp}\cdot\sqrt{(\sigma_n - \sigma_n - C\cdot(\sigma_2 - \sigma_3))^2 + 4\tau_{nt}{}^2}\,] / \bar{R}_\perp^c\}^m = 1.$$

$$d[(Eff^{NF})^m + (Eff^{SF})^m]/d\sigma_n =$$

$$m\cdot\{2\sigma_n - C\cdot(\sigma_2 - \sigma_3) + \sqrt{(C\cdot(\sigma_2 - \sigma_3))^2 + 4\tau_{nt}{}^2}\,]/2\bar{R}_\perp{}^t\}^{m-1}/\bar{R}_\perp{}^t +$$

$$+2a_{\perp\perp}\mathrm{m}\cdot\{a_{\perp\perp}(2\sigma_n - C\cdot(\sigma_2 - \sigma_3)) + b_{\perp\perp}\sqrt{(C\cdot(\sigma_2 - \sigma_3))^2 + 4\tau_{nt}{}^2}\,] / \bar{R}_\perp{}^c\}^{m-1}/\bar{R}_\perp{}^c,$$

$$[d(Eff^{NF})^m + (Eff^{SF})^m]/d\tau_{nt} =$$

$$\frac{2m\cdot\tau_{nt}\cdot\{2\sigma_n - C\cdot(\sigma_2 - \sigma_3) + \sqrt{(C\cdot(\sigma_2 - \sigma_3))^2 + 4\tau_{nt}{}^2}\,]/2\bar{R}_\perp{}^t\}^{m-1}}{\bar{R}_\perp{}^t\cdot\sqrt{(C\cdot(\sigma_2 - \sigma_3))^2 + 4\tau_{nt}{}^2}} +$$

$$+4b_{\perp\perp}\mathrm{m}\cdot\{a_{\perp\perp}(2\sigma_n - C\cdot(\sigma_2 - \sigma_3)) + b_{\perp\perp}\sqrt{(C\cdot(\sigma_2 - \sigma_3))^2 + 4\tau_{nt}{}^2}\,] / \bar{R}_\perp{}^c\}^{m-1}/\bar{R}_\perp{}^c.$$

Equating the two equations and replacing Mohr stresses by structural stresses

via $\sigma_n = (C+1)\cdot 0.5\cdot\sigma_2 + (1-C)\cdot 0.5\cdot\sigma_3,\ \ \tau_{nt} = -0.5\cdot\sqrt{1-C^2}\cdot(\sigma_2 - \sigma_3)$

yields an equation for the fracture angle measure C; m vanishes

$$\frac{C(\sigma_2,\sigma_3)}{\sqrt{1-C^2}} = -\left[\frac{m\cdot A}{\bar{R}_\perp{}^t} + \frac{2\cdot a_{\perp\perp}\cdot m\cdot B}{\bar{R}_\perp{}^c}\right] / \left[\frac{2\cdot m\cdot A}{\bar{R}_\perp{}^t\sqrt{(\cdot\sigma_2 - \sigma_3)^2}} + \frac{4\cdot b_{\perp\perp}\cdot m\cdot B\cdot\tau_{nt}}{\bar{R}_\perp{}^c\sqrt{(\cdot\sigma_2 - \sigma_3)^2}}\right]$$

$$\mathrm{A} = \left[\frac{\sigma_2 + \sigma_3 + \sqrt{(\sigma_2 - \sigma_3)^2}}{2\cdot\bar{R}_\perp^t}\right]^{m-1},\ \ \mathrm{B} = \left[\frac{a_{\perp\perp}\cdot(\sigma_2 + \sigma_3) + b_{\perp\perp}\cdot\sqrt{(\sigma_2 - \sigma_3)^2}}{\bar{R}_\perp^c}\right]^{m-1}$$

and finally $\Theta_{fp}{}^\circ$ and the Mohr stresses σ_n, τ_{nt}

$$C = \cos(2\cdot\Theta_{fp}),\ \ \Theta_{fp} = 0.5\cdot\arccos\mathrm{C}\,,\ \ \Theta_{fp}{}^\circ = \Theta_{fp}\cdot 180°/\pi,\ \ c^2 = (C+1)\cdot 0.5$$

$$\sigma_n = (C+1)\cdot 0.5\cdot\sigma_2 + (1-C)\cdot 0.5\cdot\sigma_3,\ \ \tau_{nt} = -0.5\cdot\sqrt{1-C^2}\cdot(\sigma_2 - \sigma_3).$$

Mohr shear curve $\tau_{nt}(\sigma_n)$**:** *based on IFF2, only, is an extrapolation from compressive strength*

In the case of brittle materials the Mohr-Coulomb curve is the result of two commonly acting failure modes. Now, neglecting IFF1 (the normal fracture part) and considering just the shear fracture IFF2 leads to the curve in Fig.7.2-8 according to the relations

$$Eff^{\perp\tau} \equiv F^{IFF2} = [a_{\perp\perp}\cdot(I_2) + b_{\perp\perp}\cdot\sqrt{I_4}] \;/\; \bar{R}_{\perp}^{c} = 1 \text{ with } a_{\perp\perp} = b_{\perp\perp} - 1 \text{ after inserting } \bar{R}_{\perp}^{c}$$

$$= [a_{\perp\perp}\cdot(\sigma_n + \sigma_t) + b_{\perp\perp}\cdot\sqrt{(\sigma_n - \sigma_t)^2 + 4\tau_{nt}^{\,2}}] \;/\; \bar{R}_{\perp}^{c} = 1$$

$$I_2 = \sigma_n + \sigma_t = \sigma_2 + \sigma_3\;,\quad \sigma_n - \sigma_t = C\cdot(\sigma_2 - \sigma_3) = C\cdot\eta,\quad \tau_{nt} = -0.5\cdot\sqrt{1-C}\cdot\eta$$

In the compression strength point $(\sigma_2 = -\bar{R}_{\perp}^{c},\ \sigma_3 = 0),\ \eta = -\bar{R}_{\perp}^{c}$ is obtained $C \to C^c$,

$$a_{\perp\perp}\cdot(2\sigma_n + C^c\cdot\eta) + b_{\perp\perp}\cdot\sqrt{(C^c\cdot\eta)^2 + 4\tau_{nt}^{\,2}}] \;/\; \bar{R}_{\perp}^{c} = 1 \quad \Rightarrow \quad \tau_{nt}(\sigma_n,\ C^c).$$

For a better orientation the four Mohr half-circles are included in *Fig.7.2-8*. Both the shear curves 'Linear Mohr-Coulomb' and the 'FMC-based equation' above – due to the definition of the friction value – are linear and equal, because $C = C^c(\mu_{\perp\perp})$ is constant along σ_2.

The touch point and the cohesive shear strength point are depicted in the figure.

Cohesive strength $\bar{R}_{\perp\perp}^{\tau}$: *extrapolation from compressive strength point*

* From the Linear Mohr approach: $\bar{R}_{\perp\perp}^{\tau} = \tau_{nt}^{\,c} + \mu\cdot\sigma_n^{\,c} \;\Rightarrow \bar{R}_{\perp\perp}^{\tau} = 42$ MPa.

* From the IFF2 equation : $\tau_{nt}(\sigma_n,\ C^c)$: $\bar{R}_{\perp\perp}^{\tau} = \tau_{nt}(\sigma_n = 0) = 42$ MPa.

* General note on prediction of $\bar{R}_{\perp\perp}^{\tau}$ and of Puck's $\bar{R}_{\perp\perp}^{A}$: $R_{\perp}^{t} = 35$ MPa

  For the cohesive strength, denoted $\bar{R}_{\perp\perp}^{A}$ by Puck, he gave the formula $R_{\perp\perp}^{A} = R_{\perp}^{c} / (2 + 2\cdot p_{\perp\perp}^{c})$ with $0.25 < p_{\perp\perp}^{c} > 0.30$ for CFRP. Inserting above set of strength properties $R_{\perp}^{c} = 104$ MPa into Puck's formula $R_{\perp\perp}^{A}$ becomes 41 MPa as extrapolation of the transition zone point $\bar{R}_{\perp\perp}^{A}$ from the compressive domain.

* Fig.7.2-9 will outline as the more realistic mode interaction result $\bar{R}_{\perp\perp}^{\tau} = 39$ MPa.

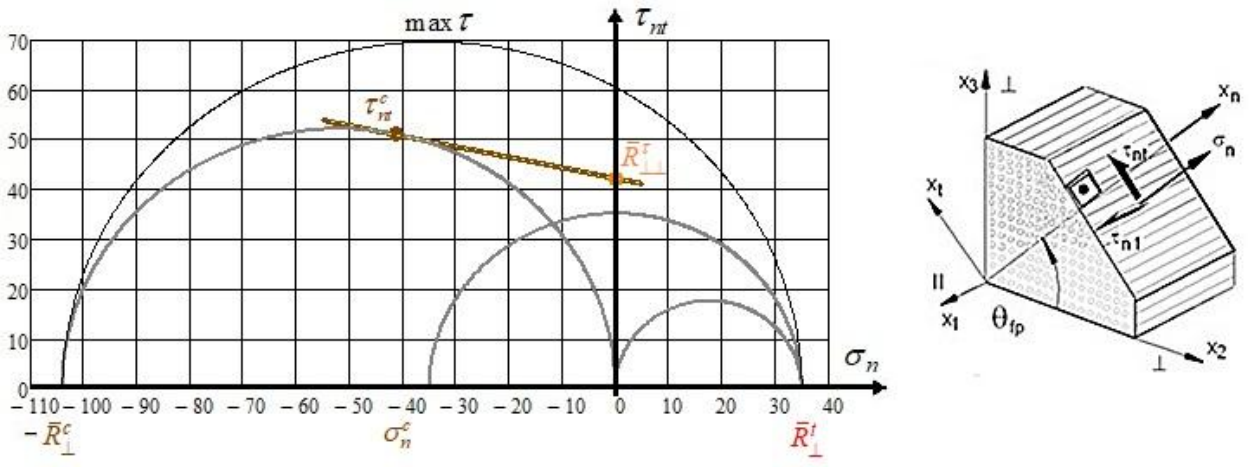


Fig. 7.2-8: Mohr shear curves τnt (σn) with its special end points and the four Mohr half-circles.

$\bar{R}_{\perp}^{t} = 35\text{MPa},\ \bar{R}_{\perp}^{c} = 104\ \text{MPa},\ \Theta_{fp}^{c\,\circ} = 51°,\ \bar{R}_{\perp\perp}^{\tau} = 42\ \text{MPa},\ \sigma_n^{\,c} = -41.3\ \text{MPa},\ \tau_{nt}^{\,c} = 50.9\ \text{MPa}$

$C_{fp}^{c} = \cos(2 \cdot \Theta_{fp}^{c}\,° \cdot \pi / 180°):\ \mu = -\tan\rho = -C_{fp}^{c} / S_{fp}^{c} = -C_{fp}^{c} / \sqrt{1 - C_{fp}^{c\,2}} \cong -C_{fp}^{c}.$

7.2.5 Derivation of the real $\tau_{nt}(\sigma_n)$ and of course of Θ_{fp} from a measured fracture curve $\sigma_3(\sigma_2)$

In the previous chapters, for isotropic materials the author proved that a transformation from structural stresses to the desired formulations in Mohr stresses is possible. The same is analogously possible for a UD material, where the quasi-isotropic plane has to be investigated in order to determine the lateral cohesive strength.

In *Table 7.2-1* all relations necessary for the transformation of a measured fracture curve $\sigma_3(\sigma_2)$ into a Mohr-Coulomb curve $\tau_{nt}(\sigma_n)$ were listed. The formulas for the searched entities τ_{nt}, σ_n, $\Theta_{fp}°$ are presented. These entities are only accurate if the physically necessary correction of the design-practical 'simple' IFF2 (or $Eff^{\perp\tau} \equiv Eff^{SF}$) is considered by the decay function f_d. In order to implement f_d one just has to replace $a_{\perp\perp}$ by $f_d \cdot a_{\perp\perp}$ and $b_{\perp\perp}$ by $f_d \cdot b_{\perp\perp}$.

Fig.7.2-9 presents the full range of the MathCad-computed Mohr entities:

Upper diagram: Mohr stresses

- straight Linear Mohr Coulomb curve (*extrapolation*)
- IFF2-determined Mohr-Coulomb fracture curve (*IFF2 extrapolation is like Mohr*)
- course of the fracture plane angle $\Theta_{fp}°$ *(bold, decay function corrected)*
- IFF2-IFF1-interacted Mohr-Coulomb fracture curve *(bold, decay function-corrected)*

Lower diagram: lamina stresses

- course of the fracture plane angle $\Theta_{fp}°/2$
- IFF2-IFF1- interacted fracture curve (*thin, original IFF2. From the simple approach, that does not consider* $\bar{R}_{\perp}^{tt}$ *, the curve cannot run through* $\bar{R}_{\perp}^{t}$)
- IFF2-IFF1- interacted fracture curve *(upper, bold, IFF2 decay function corrected, which better maps the course of measured fracture stress data).*
-

In order to find all relationships in one diagram the Mohr stresses are inserted as functions of the lamina stresses and not of σ_n, which is the usual diagram form and was used for the isotropic materials before.

The figure further includes the development of the fracture plane angle as function of the structural stress σ_2 and the various predicted values for the cohesive strength R^{τ}. The numerical example stems from a measurement of the fracture plane angle $\Theta_{fp}°$ in [*Cun97*].

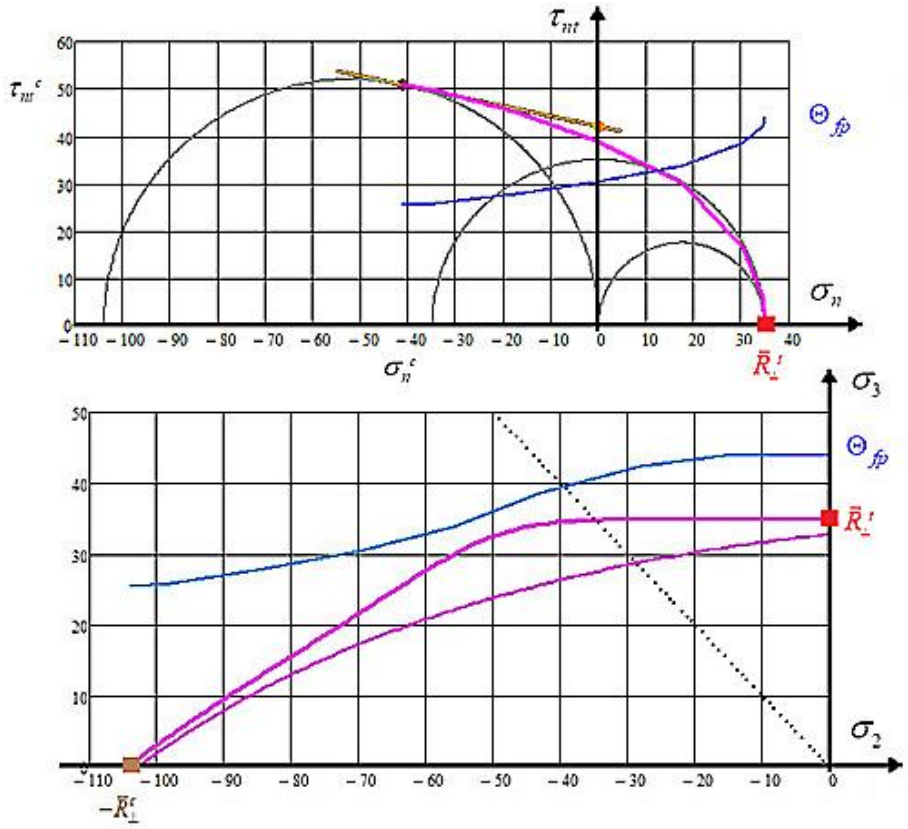


Fig.7.2-9: Joint display of the UD failure curve in Mohr stresses (above) with ***fracture angle increase*** $\Theta_{fp}°$ *when approaching* $\bar{R}_\perp^t$ *and in lamina stresses (below).*

Linear: $\bar{R}_{\perp\perp}{}^{\tau} = 42$ MPa, $\Theta_{fp}^{c\,\circ} = 51°$, Improved by f_d: $\bar{R}_{\perp\perp}{}^{\tau} = 39$ MPa, $\Theta_{fp}{}^{\circ} = 61°$, $\sigma_2 = -70$ MPa, $\sigma_3 = 22$ MPa.

$\bar{R}_\perp^t = 35$ MPa, $\bar{R}_\perp^c = 104$ MPa, $\Theta_{fp}^{c\,\circ} = 51.0°$, $C^c = -0.206$, $\mu_{\perp\perp} = 0.211$, $\tau_{nt}^c = 50.9$ MPa, $\sigma_n^c = -41.3$ MPa

The interpretation of *Fig.7.2-9* leads to the following conclusions:

- *A SFC* in structural stresses can be transferred into a Mohr-Coulomb type
- The alteration of the fracture plane angle $\Theta_{fp}°$ can be determined, too
- The idea of the FMC that IFF1 and IFF2 commonly add its *Eff* portions lead to the result that the $\Theta_{fp}°$ is about 70° at the cohesive strength point $\bar{R}_{\perp\perp}^{\tau}$
- The general macro-mechanical IFF2 approach cannot offer a full accuracy of the realistically predicted Mohr-Coulomb curve. Just the *physically-based* decay function correction delivers the desired fidelity
- The definition of the cohesive (shear) strength is $(\tau_{nt} = \bar{R}_{\perp\perp}^{\tau},\ \sigma_n = 0)$, which means in lamina stresses $(\sigma_2 = -\sigma_3)$. It's value was determined as $\bar{R}_{\perp\perp}{}^{\tau} = 39$ MPa.

8 Miscellaneous

8.1 Bridging Shear Fracture F^{SF} and Yield Failure F^{Mises} with view at Failure 'planes' $\Theta_{fp}°$

The Failure-Mode-Concept is dedicated to brittle materials ($R^c/R^t > 3$) whereas 'Mises' (Hencky-v. Mises-Huber, a modal SFC) describes the yield behavior of ductile materials.
Both the failure conditions shall be used to enlighten the difference between the failure function *F* and an effort *Eff* of both the SFCs. The difference is essential in the elastic domain, where – caused by the design safety factor – most of the structural parts with its critical locations are to be strength-assessed. Basis is the application of the so-called proportional loading, where all stress states alter proportionally. Difference comes up if *F* is not a so-called homogeneous function where the function parts possess the same power.
The following table displays all relations: ($\bar{R}$ is the average strength, used in test data mapping)

FMC-based Strength Failure Condition F^{SF} for brittle materials (non-homogeneous equation)

Brittle: $\bar{R}^c > \cong 3\,\bar{R}^t$, rotational symmetry of the failure body is assumed, $\Theta_\tau = 1$

$$F^{SF} = c_1^{SF} \cdot \frac{3J_2 \cdot \Theta_\tau}{\bar{R}^{c2}} + c_2^{SF} \cdot \frac{I_1}{\bar{R}^c} = 1 \qquad \text{..... Onset-of-Shear Fracture}$$

or in *Eff* after applying 'proportional loading'

$$c_1^{SF} \cdot \frac{3J_2 \cdot 1}{\bar{R}^{c2} \cdot Eff^2} + c_2^{SF} \cdot \frac{I_1}{\bar{R}^c \cdot Eff} = 1 \;\Rightarrow\; Eff^{SF} = \frac{c_2^{SF} \cdot I_1 + \sqrt{(c_2^{SF} \cdot I_1)^2 + 12 \cdot c_1^{SF} \cdot J_2}}{2 \cdot \bar{R}^c} = 100\% \;.$$

Inserting $(\bar{R}^c, 0)$ delivers $1 + c_2^{SF} = c_1^{SF} \cdot \Theta_\tau$ with c_2^{SF} the friction parameter

For a single failure mode like Onset-of-Shear Fracture F^{SF} or Onset-of-Yielding F^{Mises} equivalent stresses can be easily formulated σ_{eq}^{SF} or σ_{eq}^{Mises}

$$Eff^{SF} = \frac{c_2^{SF} \cdot I_1 + \sqrt{(c_2^{SF} \cdot I_1)^2 + 12 \cdot c_1^{SF} \cdot J_2 \cdot \Theta_\tau}}{2 \cdot \bar{R}^c} = \frac{\sigma_{eq}^{SF}}{\bar{R}^c} \;.$$

Basic relations (derivation see *Table* 7.1-2): $C_{fp} = \cos\left(\frac{2 \cdot \Theta_{fp}°}{180°} \cdot \pi\right), \quad \mu \cong -C_{fp}$, $c_2^{SF} = \frac{3\mu + 1}{-3\mu + 1}$

Numerical example: $\mu = 0.18$, $c_2^{SF} = 3.7$, $C_{fp} = -0.174$, $\Theta_{fp}^c° = 50°$,

Bound of F^{SF} for $\mu = 0$, $c_2^{SF} = \frac{3\mu + 1}{-3\mu + 1} = 1$, $\mu \cong -C_{fp} = 0$, $\Theta_{fp}° = 45°$, ductile.

$$F^{SF} = 2 \cdot \frac{3J_2 \cdot 1}{\bar{R}^{c2}} + 1 \cdot \frac{I_1}{\bar{R}^c} = 1$$ (as limit of zero friction with $\Theta_\tau = 1$, $c_2^{SF} = 1$, $c_1^{SF} = c_2^{SF} + 1$).

$-2 \cdot R^{cc}(TM) < I_1 < -R^c(CM) < 0 \;\leftarrow$ main mode domains $\rightarrow\; I_1 > 0 < R^t$ (TM) $< 2 \cdot R^{tt}$ (CM)

Mathematical stresses. TM = Tensile Meridian and CM = Compressive Meridian of the failure body.

Θ_{fp} of very brittle materials with R^c much larger than $3 \cdot R^t$ is caused by

$\sigma^c \rightarrow (\tau_{nt}, \sigma_n{}^c)$ | $\sigma^t \rightarrow (\tau_{nt}, \sigma_n{}^t)$

$> 45° < \Theta_{fp°} < 90°$, *μ-dependent* | $\Theta_{fp°} = 90°$ to σ^t at critical plane

cohesive strength R^τ at $(\tau_{nt}, \sigma_n = 0)$ is NF-dominated $\rightarrow R^\tau >= R^t$.

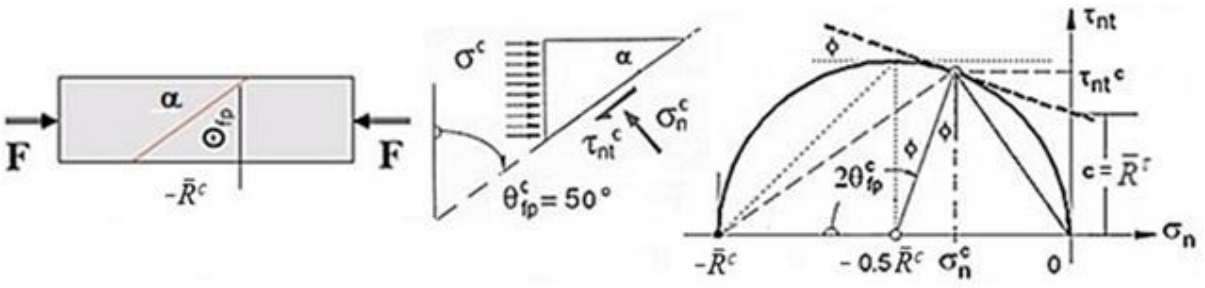


Fig. 8.1-1: Definitions

For providing some more information on the differences of F^{SF}, F^{Mises} some features are presented:

Ductile, Mises: $I_1 < 0$, $R_{02}{}^c$ | $I_1 > 0$, $R_{02}{}^t$

In the case of very ductile materials ($R_{02}{}^t = R_{02}{}^c$, see sketch below) the yield plane angle is caused by the shear stress τ_n on the sliding plane (of course σ_n exists from equilibrium condition, too, but is not of influence for sliding in case of very ductile materials: $\tau_{nt} = |\sigma_n| = 0.5\ \sigma$, see figure below). The sliding angle under maxτ_n is derived from the figure to be 45°.

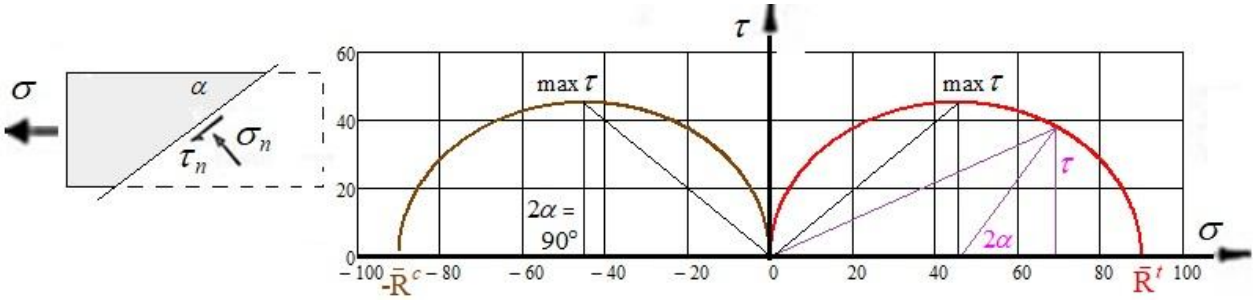


Fig. 8.1-2:Mohr circles in the ductile case

F versus Eff

'Mises' Yield Condition for ductile materials (homogeneous equation)

$$\bar{R}_{0.2}{}^t \cong \bar{R}_{0.2}{}^c = \bar{R}_{0.2}$$

$$F^{Mises} = \sqrt{\frac{3J_2}{\bar{R}_{0.2}}} = \sqrt{\frac{3\cdot(\sigma_n-\sigma_t)^2+(\sigma_t-\sigma_\lambda)^2+(\sigma_\lambda-\sigma_n)^2+6\cdot(\tau_{nt}{}^2+\tau_{n1}{}^2+\tau_{t1}{}^2)}{2\cdot\bar{R}_{0.2}{}^2}} = 1$$

$$F^{Mises} = \frac{\sqrt{3J_2}}{\bar{R}_{0.2}} = 1 \quad \rightarrow \quad \frac{\sqrt{3J_2}}{\bar{R}_{0.2}\cdot Eff} = 1 \quad \rightarrow \quad Eff^{Mises} = \frac{\sqrt{3J_2}}{\bar{R}_{0.2}} = \frac{\sigma_{eq}^{Mises}}{\bar{R}_{0.2}} .$$

$$\Rightarrow F = Eff \quad \text{in case of a homogeneous equation.}$$

8.2 Influence of Compression Stress States on Strength Capacity and Effort

On the surface of the fracture failure body the material stressing effort *Eff* is 100%. Located on the surface are the uniaxial failure stress points, termed technical strengths, equi-biaxial 'strengths' and all other 2D and 3D failure stress points.

Keep in mind:

* *'Higher' multi-axial failure stresses have nothing to do with an increase of strength. In the case of multi-axial compression stress states of dense brittle materials the strength is not increased but the risk of shear fracture becomes smaller indicated by a smaller Eff value!*
* *Also in the strain softening domain the material stressing effort Eff keeps 100%.*

8.2.1 Isotropic materials, SF (example concrete, UHPC test data, courtesy IfM Dresden)

Test paths: Tensile meridian $\sigma_I = \sigma_{II} > \sigma_{III}$ and compressive meridian $\sigma_I > \sigma_{II} = \sigma_{III}$ with σ_{III} the mathematically lowest stress. The test is performed by superimposing an axial stress σ_{ax} to a hydrostatic pressure p_{hyd}. The results display the difference of the rotationally-symmetric and the 120°-rotationally-symmetric model.

	Rotational Symmetry Stress States			Eff in %	120° Symmetry Stress States			Eff in %
	- p	- p	- p + σ_{ax}	100	- p	- p	- p + σ_{ax}	100
	σ_I	σ_{II}	σ_{III}		σ_I	σ_{II}	σ_{III}	
1D	0	0	- R^c	100	0	0	- R^c	100
2D	0	0.25 R^c	- R^c	72	0	0.25 R^c	- R^c	34
	0	- R^c	- R^c	60	0	- R^c	- R^c	35
3D	- 0.5 R^c	- 0.5 R^c	- R^c	16	- 0.5 R^c	- 0.5 R^c	- R^c	6
1D	UHPC test result [*Cun17*] in MPa				0	0	-160	100
3D	UHPC test result in MPa				-6	-6	-6 - 224	100

Conclusions:

(1) *Multiaxial compression lowers Eff. (2) 2D compression generates a tensile strain in axial direction, which is to be considered in design. (3) The physically accurate 120°-rotationally–symmetric model delivers a lower Eff-value for the stress states above.*

8.2.2 Transversely-isotropic UD materials, IFF2 (example CFRP)

Here, the difference between a proportionally-stressing derived *Eff* and a driving stress-derived *Eff* is intentionally outlined. The two concepts invite for discussion. ⊥ = s

$$Eff2 := \frac{(\sigma 2 + \sigma 3)\cdot ass + \sqrt{(\sigma 2 - \sigma 3)^2}\cdot bss}{Rsc} \quad \rightarrow \quad Eff2 := \frac{bs \cdot \sqrt{0.25(\sigma 2 - \sigma 3)^2}}{Rsc - as\cdot(\sigma 2 + \sigma 3)}$$

Stress States			Eff in %	Eff in %
	σ_2	σ_3		
1D	0	$-R_\perp^c$	100	100
2D	- 0.5 $R_\perp^c$	- $R_\perp^c$	24	45
	- $R_\perp^c$	- $R_\perp^c$	-52	0
			$a_{\perp\perp} = 0.26,\ b_{\perp\perp} = a_{\perp\perp} + 1$	as = 0.26, bs = 2.52
			proportional	driving stress

Conclusions:

(1) *Again, multiaxial compression lowers Eff. (2) In the case of 'dense' UD materials bi-axial compression causes no fracture failure, Eff < 0. (3) 2D compression generates a tensile stress because the fibers withstand axial straining. This stress from the constraint situation is usually easily captured by the fiber, on top of the loading stress* $\sigma_1 = \sigma_{\square}$.

The 'driving stress concept' leads to higher *Effs*. About the pros & cons, discussion is desired.

In the context of the investigated *Eff*s it makes sense to continue with the Safety Concept including Design Safety Factor and Reserve Factor. The former content gives a better background to assess a computed value of a distinct Reserve Factor.

8.3 Application of Safety Concepts with Determination of a Reserve Factor

8.3.1 General

A Safety Concept implements the necessary reliability into the structural component, to robustly endure uncertain design parameters (variables). Different formats are available to capture the uncertainties of the design parameters:

* Lumped, Deterministic Safety Factor Concept: for more insight see examples

Concept, that deterministically accounts for design uncertainties in a lumped manner through enlarging the 'design limit loads' by multiplication with a design Factor of Safety FoS j. This provides an unknown not really deterministically quantifiable 'safety distance' between load and load resistance ('strength') represented by the required positive Margin of Safety ($MoS = RF-1$).

* Partial Safety Factor Concept:

Concept, that semi-probabilistically bridges the deterministic format and the more complicated probabilistic format. A probabilistic format can model each single design parameter's uncertainty into a stochastic uncertainty described by a probability density function. Accounting for uncertainties informs about the robustness of the design and considers the correlations of the design variables.

In the deterministic formats the worst case scenario is usually applied for loadings considering temperature, moisture, undetected damage. Further, a load is to increase by a 'Design FoS' and the resistances are to decrease. For strength, statistical distributions are used. If the loading is also based on a statistical distribution, then one speaks about a semi-probabilistic format.

FoS capture uncertainties, small inaccuracies, and simplifications in analyses w.r.t. manufacturing process, tolerances, loadings, material properties (strength, elasticity, ..), geometry, strength failure conditions etc. FoS j or FoS γ (*in civil engineering*) do not capture missing accuracies in modeling, analysis, test data generation and test data evaluation! FoS are used to counteract the risk of a structural failure or to decrease the chance of failure by capturing the uncertainties of all the given variables outside the control of the designer. Presently, in mechanical engineering the loading is increased by one lumped FoS j , and in civil engineering the procedure is improved by using several partial Design FoS γ for the uncertain stochastic design variables.

Engineers in mechanical and in civil engineering practically want to know "How much can one further increase the loading"? In this context, for the example *ultimate load case* (DUL ≈ ULS ≈ GZT) it is to demonstrate in *strength design verification* by moving from $\bar{R}$ (mapping)$\rightarrow R$. The difference Linear Analysis to Non-inear Analysis is depicted below:

Linear analysis is sufficient solution (presumption): σ ∝ load $\rightarrow RF \equiv f_{\text{RF}} = 1 / \text{Eff}$

material reserve factor $$f_{\text{RF},\,ult} = \frac{\text{Strength Design Allowable } R}{\text{Stress at } j_{ult} \cdot \text{Design Limit Load}} > 1,$$

Non-linear analysis required: σ not proportional to load

reserve factor (load-defined) $$RF_{ult} = \frac{\text{Predicted Failure Load at } Eff = 100\%}{j_{ult} \cdot \text{Design Limit Load}} > 1.$$

In other words and terms the question in the engineering disciplines below is.

* In mechanical engineering: *Is there a sufficient reserve of load-bearing capacity?*
* In construction: *Is there a sufficient reserve of reinforcement?*

Load combinations: These combinations become the design load cases. Since not all loads occur simultaneously at full height and in the worst possible combination, variable loads may be reduced in construction by a combination coefficient Ψ . Its value depends on the observed limit state.

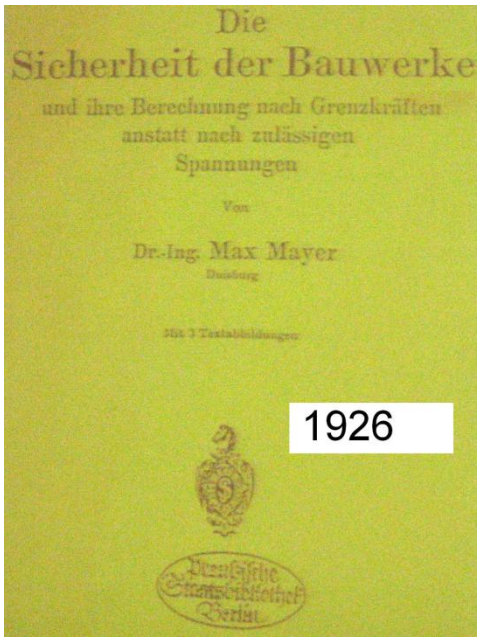
Save the Design! In order to use hidden load carrying reserves, structural non-linear analysis is to perform until material failure is reached in the critical location which is indicated for the exhausted material by *Eff* = 100%.

In construction, the material reserve factor f_{RF} is defined, fully analogous to mechanical engineering and to aerospace by a formulation $f_{RF} = (f_k / \gamma_m) / (\sigma (G_k) \cdot \gamma_G)$ with the stress level design values (Bemessungswerte) $f_k \rightarrow f_{ck}$ for instance for concrete (*index c normative* !) as the characteristic strength (*index k normative*) and the partial safety factors $\gamma_{G,static}$ for loading and for material scatter $\gamma_m \rightarrow \gamma_{c,static}$ (example concrete)

On the loading side - in the ultimate load design case - the usual FoS read:

- Spacecraft DUL [*Cun12*] : load model factor 1.2 x load factor 1.25 = 1.5, too!
- Aircraft DUL : lumped load factor $j_{ult} = 1.5$
- Construction ULS (GZT) ≡ DUL : partial load factor, weight $\gamma_{G,\,static} = 1.35$
  partial material factor concrete $\gamma_{c,\,static} = 1.5$.

In aerospace, on the resistance side, for *R* so-called *strength design allowables* are applied (see definitions) → A-values and B-values (these higher B strength-values are also allowed for the redundant multi-directional laminates).



Unfortunately, viewing
Max Mayer's publication in 1926,

still nowadays,
instead of the accurate term
strength design allowable

the not anymore allowed old term

'allowable stress'

is used, despite of the fact that for
F = 100%

Allowable stress · j ≡
Strength design allowable *R !!*

In this context: I'm sorry, but unfortunately I must say that again and again

A FoS is given for a safe Design Dimensioning and it is not to calculate like a MoS that demonstrates Design Verification!

For the determination of MoS and RF= MoS +1 statistic. reduced strength values are to use.

8.3.2 Two simple Examples for the Determination of a Reserve Factor RF

From personal experience:

Comodo Waran, 80 kg

It was worthwhile,
to put some distance to the
Waran
by using a 'Safety Stick'



In the simplest Partial Safety Factor Concept the strength is statistically reduced and all the other uncertainties are included just in a single loading increasing 'Design Factor of Safety' [*Cun12*].

The material is exhausted if the material stressing effort *Eff* reaches 100%, which means *RF* = 1.

Objective of the material strength analysis in the Design Verification is the determination of the reserve factor *RF* in the single critical locations of the structure. $\bar{R} \to R$.

I: Isotropic Material: example Normal Concrete

The *3D stress state FEA output* is automatically to insert into the distinct SFCs. In order to check the accurate working of this a not so practical, however, challenging 3D stress state will be used in the following *RF* calculation beside the checks in the uniaxial and bi-axial strength points. If all of this works, the *RF*s will be accurate in the sense of the applied model (hypothesis). Negative Effs are a physical nonsense and are to be by-passed in the calculation procedure.
General stress states activate 2 modes NF and SF. Hence, interaction is required to consider both the failure danger portions.

Cuntze's modal SFCs:

Assumptions: (1) Linear elastic analysis is good enough for this brittle behaving material → $f_{RF} \equiv RF$, (2) Residual stresses from manufacturing are zero. (3) Non-symmetric failure body, $\Theta \neq 1$ (only Θ^{SF} considered, because for the NF domain due to the small tensile strength, is not necessary to consider Θ^{NF} for this example)

Loading: Stress state $\{\sigma\} = (\sigma_x,\ \sigma_y,\ \sigma_z,\ \tau_{yz},\ \tau_{zx},\ \tau_{xy})^T \equiv (\sigma_I,\ \sigma_{II},\ \sigma_{III})^T = (2,\ -15,\ -40)^T$

Strength design allowables:

$R^t = 4,\ R^c = 40,$ assumed $R^{tt} = 0.8 \cdot R^t$, $R^{cc} = 49,\ R^{ttt} = 2.81$ for cap [MPa]

After Awaji-Sato → Weibull-based estimation $R^{ttt} = R^t / 3^{-M}$ with $M = \ln(2) / \ln(R^t / R^{tt})$

SFC Model with model parameters and Efforts:

$$Eff^{NF} = c^{NF} \cdot \frac{\sqrt{4J_2 \cdot \Theta^{NF} - I_1^2/3} + I_1}{2 \cdot R^t} = \frac{\sigma_{eq}^{NF}}{R^t} \leftrightarrow Eff^{SF} = \frac{c_{2\Theta}^{SF} \cdot I_1 + \sqrt{(c_{2\Theta}^{SF} \cdot I_1)^2 + 12 \cdot c_{1\Theta}^{SF} \cdot 3J_2 \cdot \Theta^{SF}}}{2 \cdot R^c} = \frac{\sigma_{eq}^{SF}}{R^c}$$

$$\Theta^{NF} = \sqrt[3]{1 + d^{NF} \cdot \sin(3\vartheta)} = \sqrt[3]{1 + d^{NF} \cdot 1.5 \cdot \sqrt{3} \cdot J_3 \cdot J_2^{-1.5}},\ \Theta^{SF} = \sqrt[3]{1 + d^{SF} \cdot 1.5 \cdot \sqrt{3} \cdot J_3 \cdot J_2^{-1.5}}$$

Lode angles of failure points given on the meridians:

tensile meridian 30° → $\Theta^{NF} = \sqrt[3]{1 + d^{SF} \cdot (+1)}$; compr. meridian -30° → $\Theta^{SF} = \sqrt[3]{1 + d^{SF} \cdot (-1)}$.

From estimation via fracture angle μ = - Cc/Sc, Cc = $\cos(2\Theta_{fp}^{c}\,° \cdot \pi/180°)$, Sc = $\sqrt{1 - Cc^2}$,

the friction parameter $c_{2\Theta}^{SF} = (1+3\mu)/(1-3\mu)$, $c_{1\Theta}^{SF} = (1 + c_{2\Theta}^{SF}) / \sqrt[3]{1 - d^{SF}}$

for $\Theta_{fp}^{c}\,° = 49° \rightarrow c_{2\Theta}^{SF} = 2.46,\ \mu = 0.14;\ \Theta_{fp}^{c}\,° = 51° \rightarrow c_{2\Theta}^{SF} = 4.52,\ \mu = 0.21.$

$$Eff = [(Eff^{NF})^m + (Eff^{SF})^m]^{m^{-1}} \quad \rightarrow \quad f_{RF} \equiv RF = 1/Eff$$

$$Eff = \sqrt[m]{\left(\frac{\sqrt{4J_2 \cdot 1 - I_1^2/3} + I_1}{2 \cdot \bar{R}^t}\right)^m + \left(\frac{c_{2\Theta}^{SF} \cdot I_1 + \sqrt{(c_{2\Theta}^{SF} \cdot I_1)^2 + 12 \cdot c_{1\Theta}^{SF} \cdot 3J_2 \cdot \Theta^{SF}}}{2 \cdot \bar{R}^c}\right)^m}$$

Reserve Factors, 120°-rotationally symmetric body: Calculation using the Mathcad 15 code ⇒1.13.

Shape parameters: $c2\Theta SF = 3.86$ $c1\Theta SF = 6.1$ $dSF = 0.493$ $mint := 2.7$

Statistically reduced Strengths:

Stress state: $\sigma I := 2$ $\sigma II := -15$ $\sigma III := -40$

$Rt := 4$ $Rc := 40$ $Rttt := 2.81$

$Rtt := 0.8 \cdot Rt$ $Rcc := 49$

$$I1 := \sigma I + \sigma II + \sigma III$$

$$J2 := \frac{(\sigma I - \sigma II)^2 + (\sigma II - \sigma III)^2 + (\sigma III - \sigma I)^2}{6} \qquad J3 := \frac{(2\cdot\sigma I - \sigma II - \sigma III)\cdot(2\cdot\sigma II - \sigma I - \sigma III)\cdot(2\cdot\sigma III - \sigma II - \sigma I)}{27}$$

$$\sqrt{4\cdot J2 - \frac{1}{3}\cdot I1^2} = -I1$$ Limit negativ

$$J2NF = \frac{I1NF^2}{3}$$

$$\Theta SF := \sqrt[3]{1 + dSF\cdot 1.5\cdot 3^{0.5}\cdot J3\cdot J2^{-1.5}}$$

$$\sigma I := \begin{cases} \sigma I & \text{if } \sigma I > 0 \\ 0 & \text{otherwise} \end{cases} \quad \sigma II := \begin{cases} \sigma II & \text{if } \sigma II > 0 \\ 0 & \text{otherwise} \end{cases}$$

$$\sigma III := \begin{cases} \sigma III & \text{if } \sigma III > 0 \\ 0 & \text{otherwise} \end{cases}$$

$$EffSF := \left| \frac{\frac{1}{2}\cdot c2\Theta SF\cdot I1 + \frac{1}{2}\cdot\left(c2\Theta SF^2\cdot I1^2 + 12\cdot c1\Theta SF\cdot J2\cdot\Theta SF\right)^{0.5}}{Rc} \right|$$

$EffSF = 0.81$

$I1NF := \sigma I + \sigma II + \sigma III$ $J2NF := \frac{(\sigma I - \sigma II)^2 + (\sigma II - \sigma III)^2 + (\sigma III - \sigma I)^2}{6}$

$$EffNF := \frac{\sqrt{4\cdot J2NF - \frac{1}{3}\cdot I1NF^2} + I1NF}{2Rt}$$

$EffNF = 0.5$

$$Eff := \left(EffNF^{mint} + EffSF^{mint}\right)^{\frac{1}{mint}}$$

$Eff = 0.89$ $RF := \frac{1}{Eff}$ $RF = 1.13$

Estimation of fracture parameter via guess of fracture angle

$\Theta fpc^\circ := 50.5$ $Cc := \cos\left(2\cdot\Theta fpc^\circ\cdot\frac{\pi}{180}\right)$ $Cc = -0.191$ $Sc := \left(\sqrt{1 - Cc^2}\right)$ $Sc = 0.98$ $\mu := -\frac{Cc}{Sc}$ $\mu = 0.194$ $c2\Theta SF := \frac{1 + 3\cdot\mu}{1 - 3\cdot\mu}$ $c2\Theta SF = 3.8$

Effect of uniaxial and multi-axial stress states on the Reserve Factor *RF*:

$(\sigma_I, \sigma_{II}, \sigma_{III})^T = (4, 0, 0)^T \Rightarrow Eff^{NF} = 1.0, \quad RF = 1/Eff = 1$

$(\sigma_I, \sigma_{II}, \sigma_{III})^T = (2, 2, 0)^T \Rightarrow Eff^{NF} = 1.0, \quad RF = 1/Eff = 1$

$(\sigma_I, \sigma_{II}, \sigma_{III})^T = (0, 0, -40)^T \Rightarrow Eff^{SF} = 1.0, \quad RF = 1/Eff = 1$

$(\sigma_I, \sigma_{II}, \sigma_{III})^T = (0, -49, -49)^T \Rightarrow Eff^{SF} = 1, \quad RF = 1/Eff = 1$

$(\sigma_I, \sigma_{II}, \sigma_{III})^T = (0, -15, -40)^T \Rightarrow Eff^{SF} = 0.72, RF = 1/Eff = 1.39$

$(\sigma_I, \sigma_{II}, \sigma_{III})^T = (2, -15, -40)^T \Rightarrow Eff^{SF} = 0.89, RF = 1/Eff = 1.13$.

- *Loading could be further monotonically increased by the factor $RF = f_{RF}$ to reach fracture.*

For comparison, ***Drucker-Prager's global SFC, rotationally-symmetric body (cone)****:*

This SFC is often used in civil engineering. It was originally introduced to deal with the 'plastic' (in-elastic) deformation of soils. Its many variants have been applied to brittle construction materials like rock, concrete, polymers, foams, and other pressure-dependent (*this practically just means that I_1 is to use*).

$$\frac{\sqrt{J2}-B\cdot I1}{A}=1\rightarrow Eff=\frac{\sqrt{J2}-B\cdot I1}{A}\quad \text{with B}=\frac{\sqrt{J2c}-\sqrt{J2t}}{I1c-I1t}\text{ , A}=\sqrt{J2t}-B\cdot I1\text{t}$$

$$I1t=Rt,\ \ I1c=-Rc,\ \sqrt{J2t}=Rt^3/3,\ \ \sqrt{J2c}=Rc^3/3.$$

For the civil engineers basically the SF domain is of interest.

$$(\sigma_I,\ \sigma_{II},\ \sigma_{III})^T=(4,\ 0,\ 0)^T \quad\Rightarrow\quad Eff=1.0,\quad RF=1/Eff=1$$
$$(\sigma_I,\ \sigma_{II},\ \sigma_{III})^T=(2,\ 2,\ 0)^T \quad\Rightarrow\quad Eff=1.0,\quad RF=1/Eff=1$$
$$(\sigma_I,\ \sigma_{II},\ \sigma_{III})^T=(0,\ 0,\ -40)^T \quad\Rightarrow\quad Eff=1.0,\quad RF=1/Eff=1$$
$$(\sigma_I,\ \sigma_{II},\ \sigma_{III})^T=(0,\ -49,\ -49)^T \quad\Rightarrow\quad Eff=-4.3,\quad RF=1/Eff=-0.23$$
$$(\sigma_I,\ \sigma_{II},\ \sigma_{III})^T=(0,\ -15,\ -40)^T \quad\Rightarrow\quad Eff=-1.4,\quad RF=1/Eff=-0.73$$
$$(\sigma_I,\ \sigma_{II},\ \sigma_{III})^T=(2,\ -15,\ -40)^T \quad\Rightarrow\quad Eff=-0.93,\ RF=1/Eff=-1.07\ .$$

Comparing the FMC-based results with the Drucker-Prager results it is to conclude: (1) The Reserve Factor values are different. (2) An automatic application of Drucker-Prager's model above without any queries is not possible and can be not recommended. Just the uniaxial strength points are captured, the equi-biaxial compressive strength not.

Ottosen's global SFC,

N.S. Ottosen improved above situation by applying $\vartheta(J_3)$, thereby capturing the 120° symmetry with the bi-axial strength point. As with Cuntze's SFC models he includes 4 model parameters A,B,K_1,K_2. Required test points are: $\bar{R}^t$, $\bar{R}^c$,$\bar{R}^{cc}$ + one point on the compressive meridian.

Ottosen's 4-parameter failure criterion for concrete has the form, but was not investigated here

$$A\cdot\frac{J_2}{(\bar{R}^c)^2}+\Lambda(K_1,K_2(\vartheta,J_3))\cdot\frac{\sqrt{J_2}}{\bar{R}^c}+B\cdot\frac{I_1}{\bar{R}^c}=1\ .$$

II: Transversely-Isotropic UD (sheet) Material

Assumption: Linear elastic problem is valid for the envisaged brittle behaving CFRP.
Residual stresses: 0 (effect vanishes with increasing micro-cracking)
Mode interaction exponent: m = 2.7 and friction:

Stress state:and Strength state: in MPa or N/mm^2

$$3D:\ \{\sigma\}=(\sigma_1,\sigma_2,\sigma_3,\tau_{23},\tau_{31},\tau_{21})^T \quad\rightarrow\quad \left\{\sigma_{eq}^{\text{mode}}\right\}=\left(\sigma_{eq}^{\parallel\sigma},\ \sigma_{eq}^{\parallel\tau},\ \sigma_{eq}^{\perp\sigma},\ \sigma_{eq}^{\perp\tau},\ \sigma_{eq}^{\parallel\perp}\right)^T$$
$$2D:\ \{\sigma\}=(\sigma_1,\sigma_2,-,-,-,\tau_{21})^T \quad \text{for FF and IFF}$$
$$2D:\ \{\sigma\}=(-,\sigma_2,-,-,-,\tau_{21})^T \quad \text{for IFF}$$

$$3D:\ \{R\}=(R_\parallel^t,R_\parallel^c,R_\perp^t,R_\perp^c,R_{\perp\parallel})^T \text{ with } \mu_{\perp\square},\mu_{\perp\perp} \Leftarrow \{\bar{R}\}=(\bar{R}_\parallel^t,\bar{R}_\parallel^c,\bar{R}_\perp^t,\bar{R}_\perp^c,\bar{R}_{\perp\parallel})^T \text{ with } \mu_{\perp\square},\mu_{\perp\perp}$$
$$2D:\ \{R\}=(R_\parallel^t,R_\parallel^c,R_\perp^t,R_\perp^c,R_{\perp\parallel})^T \text{ with } \mu_{\perp\square},\mu_{\perp\perp} \text{ for FF and IFF}$$
$$2D:\ \{R\}=(-,-,R_\perp^t,R_\perp^c,R_{\perp\parallel})^T \quad \text{with } \mu_{\perp\square} \quad \text{for IFF}$$

Design Verification requires a Reserve Factor RF ≥ 1.00.

A short example depicts the calculation procedure:

Asssumption: Linear analysis permitted, design FoS $j = 1.25$

* 2D-stress state: $\{\sigma\} = (\sigma_1, \sigma_2, \sigma_3, \tau_{23}, \tau_{31}, \tau_{21})^T \cdot j = (0,\ -60,\ 0,\ 0,\ 0,\ 50)^T$

* Residual stresses: 0 $\left(\textit{effect vanishes with increasing micro-cracking}\right)$

* Strengths: $\{R\} = (R_{\parallel}^t, R_{\parallel}^c, R_{\perp}^t, R_{\perp}^c, R_{\perp\parallel})^T = (1050,\ 725,\ 32,\ 112,\ 79)^T$ MPa

$\{\bar{R}\} = (1378,\ 950,\ 40,\ 125,\ 97)^T$ estimated from average values

* Friction values : $\mu_{\perp\parallel} = 0.3,\ (\mu_{\perp\perp} = 0.35)$, Mode interaction exponent: $m = 2.7$

* $Eff^{\perp\sigma} = \dfrac{\sigma_2 - |\sigma_2|^*}{2 \cdot \bar{R}_{\perp}^t} = 0,\ Eff^{\perp\tau} = \dfrac{-\sigma_2 + |\sigma_2|}{2 \cdot \bar{R}_{\perp}^c} = 0.60,\ Eff^{\perp\parallel} = \dfrac{|\tau_{21}|}{\bar{R}_{\perp\parallel} - \mu_{\perp\parallel} \cdot \sigma_2} = 0.51$

$$Eff^m = (Eff^{\perp\sigma})^m + (Eff^{\perp\tau})^m + (Eff^{\perp\parallel})^m$$

$$\Rightarrow Eff = 0.72,\ RF = 1/Eff = 1.39,\ \text{MoS} = RF - 1 = 0.39 \text{ (must be positive!).}$$

The certification–relevant load-defined Reserve Factor *RF* corresponds in the linear case to the material reserve factor f_{RF}. It's value here is 1.39 > required limit 1.00 → Laminate design is verified!

Inserting the compressive strength point $(0,\ -\bar{R}_{\perp}^c) \rightarrow a_{\perp\perp} \cong \mu_{\perp\perp} / (1 - \mu_{\perp\perp})$, $b_{\perp\perp} = a_{\perp\perp} + 1$

from a measured fracture angle → $\mu_{\perp\perp} = \cos\ (2 \cdot \theta_{fp}^c\,° \cdot \pi / 180)$, for $50° \rightarrow \mu = 0.174$.

$b_{\perp\parallel} \cong 2 \cdot \mu_{\perp\square}$. Typical friction value ranges: $0 < \mu_{\perp\parallel} < 0.25,\ 0 < \mu_{\perp\perp} < 0.2$.

Interaction Equation:

$$Eff^m = [(\sigma_{eq}^{\parallel\sigma} / \bar{R}_{\parallel}^t)^m + (\sigma_{eq}^{\parallel\tau} / \bar{R}_{\parallel}^c)^m + (\sigma_{eq}^{\perp\sigma} / \bar{R}_{\perp}^t)^m + (\sigma_{eq}^{\perp\tau} / \bar{R}_{\perp}^c)^m + (\sigma_{eq}^{\perp\square} / \bar{R}_{\perp\square})^m]$$

or $Eff = \sqrt[m]{(Eff^{\text{mode 1}})^m + (Eff^{\text{mode 2}})^m + \ldots} = 1 = 100\%$ *for* Onset-of-Failure .

$$Eff^{\perp\sigma} = \frac{\sigma_2 - |\sigma_2|}{2 \cdot \bar{R}_{\perp}^t} = 0,\ Eff^{\perp\tau} = \frac{-\sigma_2 + |\sigma_2|}{2 \cdot \bar{R}_{\perp}^c} = 0.60,\ Eff^{\perp\parallel} = \frac{|\tau_{21}|}{\bar{R}_{\perp\parallel} - \mu_{\perp\parallel} \cdot \sigma_2} = 0.51$$

$$Eff^m = (Eff^{\perp\sigma})^m + (Eff^{\perp\tau})^m + (Eff^{\perp\parallel})^m \Rightarrow Eff = 0.72,$$

$$\text{RF} = f_{RF} = 1/Eff = 1.39,\ \text{MoS} = \text{RF} - 1 = 0.39.$$

8.3.3 Concept of Proportional Loading

As still mentioned, there exists a conflicct when applying the concept of Proportional Loading to failure criteria, which mathematically may be of a so-called homogeneous or a non-homogeneous formulation.This conflict has an impact on the Reserve Factor.

The author requires from a strength criterion to become zero, if the driving stress of a distinct acting mode becomes zero. To underline this, *Table 8-1* collects some investigated examples which ask for discussion.

Table 8-1: Derivation of Effs for the chosen failure function F, $^{p = pr}$

Homogeneous and non-homogeneous mathematical function F. Concept of proportional loading

* Homogeneous mathematical Function F: index ^{p} for principal stresses

$$F^{IFF1} = [I_2 + \sqrt{I_4}] / 2\bar{R}_{\perp}^{c} = [(\sigma_2{}^{p} + \sigma_3{}^{p}) + \sqrt{(\sigma_2{}^{p} - \sigma_3{}^{p})^2 + 0^2}] / 2\bar{R}_{\perp}^{c}$$

$$\rightarrow [(\sigma_2{}^{p} + \sigma_3{}^{p}) + \sqrt{(\sigma_2{}^{p} - \sigma_3{}^{p})^2}] / (2\bar{R}_{\perp}^{c} \cdot Eff^{\perp\sigma}) = 1$$

$$Eff^{\perp\sigma} \equiv [(\sigma_2{}^{p} + \sigma_3{}^{p}) + \sqrt{(\sigma_2{}^{p} - \sigma_3{}^{p})^2}] / 2\bar{R}_{\perp}^{c} \quad \Rightarrow \text{ no difference } |F| \leftrightarrow Eff$$

$$F^{IFF2} = [a_{\perp\perp} \cdot I_2 + b_{\perp\perp} \cdot \sqrt{I_4}] / \bar{R}_{\perp}^{c} = [a_{\perp\perp} \cdot (\sigma_2{}^{p} + \sigma_3{}^{p}) + b_{\perp\perp} \cdot \sqrt{(\sigma_2{}^{p} - \sigma_3{}^{p})^2}] / \bar{R}_{\perp}^{c}$$

$$\rightarrow [a_{\perp\perp} \cdot (\sigma_2{}^{p} + \sigma_3{}^{p}) + b_{\perp\perp} \cdot \sqrt{(\sigma_2{}^{p} - \sigma_3{}^{p})^2}] / (\bar{R}_{\perp}^{c} \cdot Eff^{\perp\tau})$$

$$Eff^{\perp\tau} \equiv a_{\perp\perp} \cdot (\sigma_2{}^{p} + \sigma_3{}^{p}) + b_{\perp\perp} \cdot \sqrt{(\sigma_2{}^{p} - \sigma_3{}^{p})^2}] / \bar{R}_{\perp}^{c} \Rightarrow \text{ no difference } |F| \leftrightarrow Eff$$

$$F^{IFF3,\ 2D} = \tau_{21} / (\bar{R}_{21} - \mu_{\perp\square} \cdot \sigma_2) \quad \text{simple 2D formulation, } \mu_{\perp\square} = 0.3$$

$$\frac{\tau_{21}}{Eff^{IFF3,\ 2D}} / (\bar{R}_{21} - \mu_{\perp\square} \cdot \frac{\sigma_2}{Eff^{IFF3,\ 2D}}) = 1 \rightarrow Eff^{IFF3,\ 2D} = \frac{\tau_{21} + \mu_{\perp\square} \cdot \sigma_2}{\bar{R}_{21}} \quad \text{not permitted}$$

$\Rightarrow$ Eff does not become zero if the driving stress becomes zero

$$\frac{\tau_{21}}{Eff^{IFF3,\ 2D}} / (\bar{R}_{21} - \mu_{\perp\square} \cdot \sigma_2) = 1 \quad \rightarrow \quad Eff^{IFF3,\ 2D} = \frac{\tau_{21}}{\bar{R}_{21} - \mu_{\perp\square} \cdot \sigma_2} \quad \text{permitted .}$$

* Non-homogeneous mathematical function F

$$F^{IFF2} = [a_{\perp\perp} \cdot I_2 + b_{\perp\perp} \cdot I_4 / \bar{R}_{\perp}^{c}] / \bar{R}_{\perp}^{c}$$

$$\rightarrow [a_{\perp\perp} \cdot (\sigma_2{}^{p} + \sigma_3{}^{p}) + b_{\perp\perp} \cdot (\sigma_2{}^{p} - \sigma_3{}^{p})^2 / (\bar{R}_{\perp}^{c} \cdot Eff^{\perp\tau})] / (\bar{R}_{\perp}^{c} \cdot Eff^{\perp\tau}) = 1$$

$$Eff^{\perp\tau} \equiv a_{\perp\perp} \cdot (\sigma_2{}^{p} + \sigma_3{}^{p}) + b_{\perp\perp} \cdot \sqrt{(\sigma_2{}^{p} - \sigma_3{}^{p})^2}] / \bar{R}_{\perp}^{c}, \text{ difference } |F| \leftrightarrow Eff \ .$$

LL *on obtained 3D--Reserve Factors:*

(1) The RF depends on the chosen model.

(2) Fidelity: Are the generally used Standard SFCs really 3D-validated like Cuntze's SFCs?

(3) What about the numerical treatment in the determination of the RFs

(4) Use of the absolute sign (or of McCauley) avoids the computation of senseless negative Effs.

(5) Loading may be increased by the factor RF until obtaining the fracture failure Limit State at Eff = 100% ≡ RF = 1

(6) The concept of proportional loading can be only applied, if the strength criterion or the Eff^{mode} becomes zero when the failure driving stress or the failure driving equivalent stress is zero.

8.4 Failure Index |*F*| versus Material Stressing Effort *Eff* , Example UD 3D-stress state

The use of |F| alone is only possible if a 'global' SFC is applied. In the case of the physically better mapping 'modal' SFCs an interaction of the modes is faced and modal *Effs* are required to 'feed' the interaction equation.

In design, from cyclic loading comes the designation 'Proportional Loading' for the increase of the stress state under a loading. As 'loading' in general is not proportional to 'stressing' the concept as it is applied in the elastic static cases should read 'proportional stressing'.

Some differences shall be pointed out in the following, discriminating the standard “Proportional Loading concept” from a “Failure stress-driven loading” concept. The latter is mandatory if *F* or *Eff* do not become zero with a vanishing failure driving stress, see the Mohr example below.

***LL**: In the case of a mathematically homogeneous failure function Eff = F.*

To bring material modeling with structural modelling back into focus in Sub-chapter 8.5 the 3D-printing is shortly presented. (*The author founded in 2017 the first German 3D-printing working group in civil engineering or construction*).

8.5 3D-Print in Mechanical Engineering

There are different material categories used in 3D-printing. Powder,‘filaments‘ on bobbins, and fluids. (Filament is here to understand in the original sense of a single endless fiber or thread). This ‘feed material’ is decisive for the field of application. For example, laser-fused powder materials are suitable for precise components that have to withstand high stress states and to deliver net shapes. Filament material feed is used for less accurate shapes of prototypes and depends on the diameter of the extruded strand. Liquid materials, such as resin systems, can be used to produce precise components of not high strength capacity.

Of interest for the achievement of high-performance structural parts the insertion of endless fibers is an upcoming process performed by a second extrusion nozzle. The result of such a ‘filament print’ process is depicted in *Fig.8.5-1*. During 3D *filament printing of the matrix constituent* in parallel through the second nozzle an *endless* CFRP-*fiber* tow *as reinforcing constituent*, consisting of one or more rovings, is laid layer-by-layer along the contour of the envisaged CFRP part. At the end of each layer, the nozzle cuts off the fiber tow.

And on another scale: A special printing system shall be mentioned that is used to produce nano-scale load-carrying structures and material test specimens used in nano metal micro-damage models and tests. This additive nano-printing process is based on the comparatively simple process of electroplating. For this purpose, positively charged copper ions from a copper salt solution are used here. When this solution comes into contact with a negatively charged electrode, the metal ions combine with the electrons present there, forming a neutral metal atom that settles on the electrode and forms a solid metal layer, *Fig.8.5-2*.



Fig.8.5-1
Filament print process [Markforged]

https://www.msn.com/de-de/feed

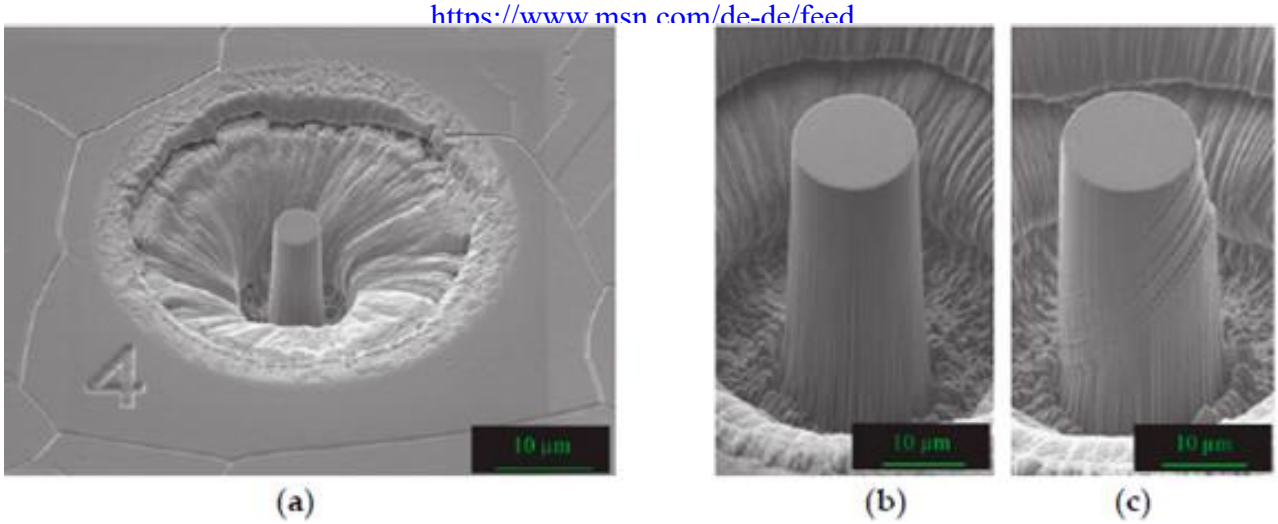


Fig.8.5-2: Example of (a) 5µm and (b) 15µm pillars, cut within large grains, and (c) deformed pillar after compression. (right) shear planes after compression.

from Materials Letters,'Determination of the critical resolved shear stress and the friction stress in austenitic stainless steels by compression of pillars extracted from single grains'. GhiathMonnetaManuel A.Pouchonb, Volume 98, 1 May 2013, Pages 128-130 with permission from Elsevier

J. Bauer and O. Kraft created a truss structure (*Fig.8.5-3*) with laser lithography. Pyrolysis at 900°C then created an 80% shrunk nano-framework made of glass-like carbon, which can be compressed (*Incomprehensible: Compressive strength meant? But it is a stability loading and not a strength loading*! *How was the test performed*?) of up to three GPa should withstand, a scale above the usual MPa.

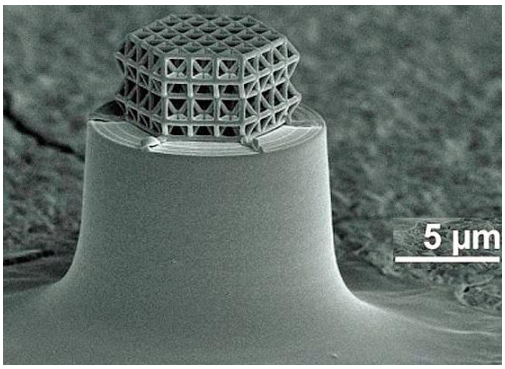


Fig.8.5-3:
The world's smallest truss in an electron microscope.
The glassy carbon struts are 200 nanometers thick and one micrometer µm long.
© J. Bauer/ KIT, 2016

Advanced Materials, Progress Report, 'Nanolattices: An Emerging Class of Mechanical Metamaterials'.JensBauer,Lucas R. Meza, Tobias A. Schaedler, Ruth Schwaiger, Xiaoyu Zheng, Lorenzo Valdevit.September 2017,Wiley Online Library

Any material that can be glued, welded or melted can be used in AF. For industrial purposes, metals, plastics, sand and ceramics are common materials, but the process is to adapt.

8.6 Construction-linked Additive Fabrication AF

Classification of fabrication processes: Subtractive processes (waste), Formative processes and Additive processes (automatically digitized fabrication now) [*VDI 2403*]. *The term manufacture is not accurate: Manus* and *facere → means made by hand.*

1. In subtractive processes, the geometry to be created is created by defining the removal of individual volume regions. Typical representatives of this group of manufacturing processes are machining processes such as turning, drilling or milling. (timber construction etc.)
2. Formative processes refer to the production of geometries by forming in compliance with volume constancy. Formative manufacturing processes are deep drawing, forging or primary forming.
3. Additive fabrication processes create a geometry by joining together volume elements (so-called "voxels"), such as the standard processes concreting, bracketing, plastering a wall etc.

The engineer's desire is to obtain accurate process names such as above, however, the term 3D print does not give a clear process information. Therefore some basic definitions are provided:

The two basic digitized additive fabrication processes in construction are:

(3.a) P**owder bed process:** True 3D printing in construction: Total cross-section including the 'openings' is produced in a powder bed layering process. Layer thickness is usually << 1 mm. For formwork production, usually).

(3.b) **Extruded mortar-strand deposit method (**'3D printing'): Total cross-section including 'openings' is produced in a 'path tracking operation'. Layer thickness is several mm, depending on the strand thickness. (*Extrusion process for walls and other compressed load-bearing structures!. That's why there is no fully '3D-printed house' exsisting).*

The engineer's desire is to obtain accurate process names however the term ***3D print*** does not give a clear process information. Therefore some basic definitions are provided:

Printing definition: *Procedure, to apply something by pressure like printing a book*

(3.a) ISO/ASTM 52900: Automatic digitized fabrication AF is a process of joining materials to make parts from 3D-model CAD data, usually layer upon layer

(3.b) VDI-Ri-3405, Blatt 3.4, Fused *(geschmolzen)* Deposition Modelling or Fused Layer Modelling: Cold extrusion process, whereby the building material is deposited continuously via a nozzle. Transferred to construction "Extruded deposit of a mortar strand (Mörtel-Strang, Mörtel-Raupe). Is analogous to the so-called polymer-filament strand depositing → Extruded mortar strand deposit is clear for the designing engineer.

Following RILEM Technical Committee 276 the descriptions below are given:

(3.a) **Powder-bed binding** (3D-printing. AF process in which particles are selectively joined using a bonding agent, includes binder jetting as sub-class and includes the technique Selective Laser Sintering. *Does pretty well correspond with the printing definition*

(3.b) Material extrusion with cementitious and polymer agents ('3D-printing' → Extruded mortar strand deposit). *Does not correspond to the printing definition but nevertheless is also used here as meaningless catchphrase "3D-print" confusing by not delivering the necessary knowledge about the actual fabrication process. One should not take the same term 3D-print" for fully different fabrication processes.*



Fig.8.6-1: Particle-bed technique (up left), Mortar strand depositing (up, right); (below) Peri GmbH 2021, two-story house in Beckum

In construction, above two main additive processes above can be also described as follows:

(3.a) Total cross-section, including the 'openings', is produced in a 'layering process'. The layer thickness is usually much smaller than 1mm. Powder bed technique for formwork production with the steps (see *Fig.8.6-1, up left):* * 3D geometry model or a 3D-scan info for the robot, * application of a layer of powdered material < 1mm, * solidification of the material, repetition by building platform lowering for the next layer, * loose powder removed, * complete part.

(3.b) Mortar strand depositing: The total cross-section, including the 'openings', is produced in a 'path tracking operation'. The layer thickness is several mm, strand thickness-dependent (Extrusion process for walls). *Here, also the path is to define digitally. See Fig.8.6-1 down.*

In both processes, the layer thickness is determined digitally for each structural application.

Of interest for civil engineering are the similarly working techniques in mechanical engineering:

- Sheet Molding Compound SMC := compound, containing short fibers (CF-SMC, GF-SMC, flächige Pressmasse, Spritzguss)
- Bulk Molding Compound BMC := compound containing short fibers (3D-SMC Pressmasse, Spritzguss)

- Shotcrete (Mörtel-Spritzguss):= process is somehow related to SMC, could be performed with and without short fibers
- (short) Fiber-Reinforced Concrete FRC:= process is somehow related to BMC.

AF-design requires knowledge about the process of the *Fresh Printable Cement-based Materials* (RILEM TC PFC) and the actual local material characteristics, valid for 3a and even more for 3b. Specific topics for mortar strand depositing are:

1) Gravitational flow of the deposited strand. The figure excellently depicts the primary problem. Rheology-based production process simulation is required – using computational fluid dynamics CFD - in order to finally achieve Buildability and Shape Stability of the freshly manufactured part.
2) Appropriate recipes for the mortar in order to achieve the desired time- and path dependent consolidation
3) No dispersion of admixture in print head
4) Bypassing the 2 failure modes: (1) material failure (material flows away, because the current yield strength is too low for the mass upon). (2) Structural failure (the erected wall loses its stability).
5) Material characterization, time-dependent properties of the fresh mortar after being deposited and further in the build-up process with consolidation
6) Introduction of armoring to withstand usual bending of the structural part by short, long and endless fibers (coming up)
7) Post-processing (rough surface)
8) Quality assurance of mortar, fibers, concrete and fabrication process
9) Fabrication process with 'real' reinforcement of components that can be tension-stressed and not only compression-stressed. Possibilities: (1) mortar, (2) concrete and vice versa. Slack armoring and pre-tensioning of structural elements
10) Static & cyclic fatigue due to notched layers and surface
11) Normative-linked Dimensioning. Special load-bearing capability certificate necessary termed the still mentioned approval procedure (ZiE).

Combined simulation using process analysis with structural analysis is the challenging task, here. Extrusion-based processes require a knowledge about speed, time and cross-section of the strand-depending material flow with a good knowledge about the following solidification of the mortar strand (see i.e. [*Mec21*]).

For the engineer, facing, '*Mortar Strand Depositing'*, there are many variants to model:

- Fully isotropic mortar without any steel- and fiber-reinforcement,
- Reinforcement with polymer filament strands or strands stochastically mixed with short fibers
- Production-directed short fiber reinforcements are anisotropically to model
- Design verification of classical armoring by endless reinforcements remains as before.

9 Classical Laminate Theory CLT

9.1 Theoretical relations of Lamina and Laminate

There are two basic theories used to statically design composites: The *Netting Theory* neglecting the matrix loading capability completely and the *Classical Laminate Theory* (CLT) continuum-mechanically considering both the constituents of the composite the fiber and the matrix.

The ***2D continuum theory***, applied to laminates, is referred to as Classical Laminate Theory (CLT, *here not Cross-Laminated timber as in construction*). It includes the so-called Kirchhoffian plate theory and is used to determine the in-plane stresses and in-plane strains in each individual lamina of the laminate. Principally, the procedure is not only valid for UD laminas but for ply, lamella, mat, fiber-grid, too. Also cross-ply textiles may be treated regarding the stiffness analysis. Decisive is the 'smear ability'. A layer is a physical sub-unit of the laminate, whereas a lamina (ply) is a computational building block in the laminate analysis which might be half of a layer, a double layer or also a single layer of a non-crimped fabric NCF.

A CLT procedure can be used in linear and non-linear analyses. For design verification the CLT-obtained (2D) intra-laminar stresses are inserted into the SFCs to judge whether a FF or an IFF limit state is met or not yet met. In this context four specifics are regarded:

- The coordinate system with the reference plane (*in literature, unfortunately the direction of the CoS is often arbitrarily chosen, however, here the right hand system is applied*)
- The fiber orientation angle α
- The lay-up with the laminate stacking sequence and
- The layer numbering or counting sequence.

In the following sub-chapters all these specifics are pointed out.

9.1.1 Lamina

Modeling the single ply as a solid homogenized material, then *fig1* in *Fig.9-1* displays the UD material cube with the stresses in the UD lamina Coordinate System CoS, also termed material CoS.

The following assumptions are made for the UD lamina material:

- The UD lamina is macroscopically homogeneous. It can be treated as a homogenized ('smeared') material
- The stress-strain relationship is linear
- The UD lamina is transversely-isotropic. On planes, parallel with the fiber direction $x_1 \equiv x_{||}$, it behaves orthotropic and on planes transverse to the fiber direction it behaves quasi-isotropic.

Different notations are used in the FEA programs and manuals.

- Matrix notation: ε_i, σ_i , indexed $i = 1, 2...6$,
- Engineering notation: using so-called engineering strains and stresses σ, τ , indexed 1, 2, 3.

***LL**:*
** A symbolic, self-explaining indexing, especially of properties, helps to avoid misinterpretations.*
** In many FEA manuals the normal technical (engineering) stresses and normal strains are doubly indexed. Forgive the 'upper pedantic' author: What for? Stress and strain are not tensor-linked anymore and therefore not accurate. Still in 1970 NASA did the differences exactly display in a fiber-reinforced composite 'Glossary'.*

In *Table 9-1* the 3D compliance matrices [S] = $[C]^{-1}$ of the three material families were presented. Elasticity matrices [C] were not fully displayed because of their complexity. The compliance matrix is simpler and better to use in test data evaluation for the determination of the elasticity 'constants'. The 3D subsets = 2D-Elasticity Stress-Strain Relationships are depicted for the fiber-reinforced materials UD, fabric, mat, necessary for the application of the CLT. After setting the 3 inter-laminar stresses zero, stress vector and strain vector read (engineering notation) with the in-plane compliance matrix [S[and [Q] denoted 'reduced 3D stiffness matrix' [C].

$$\{\varepsilon\} = (\varepsilon_1, \varepsilon_2, \gamma_{12})^T, \quad \{\sigma\} = (\sigma_1, \sigma_2, \tau_{12})^T \text{ and for the k}^{th} \text{ lamina in the laminate}$$

$$\{\varepsilon\}_k = [S]_k \cdot \{\sigma\}_k \;, \quad \{\sigma\}_k = [Q]_k \cdot \{\varepsilon\}_k \text{ with } [Q]_k = [S]_k^{-1}$$

Table 9-1: 2D elasticity matrix [Q] and compliance matrix [S]. 1 ≡ ∥, 2 ≡ ⊥

UD lamina

$$\{\varepsilon\}_k = (\varepsilon_1, \varepsilon_2, \gamma_{21})_k^T = [S]_k \{\sigma\}_k \qquad \{\sigma\}_k = (\sigma_1, \sigma_2, \tau_{21})_k^T = [Q]_k \{\varepsilon\}_k$$

$$\varepsilon_i = S_{ij}\,\sigma_j \qquad \sigma_i = Q_{ij}\,\varepsilon_j \qquad (i,j = 1, 2, 6) \qquad \text{i.e. } (\varepsilon_6 \equiv \gamma_{21},\ \sigma_6 \equiv \tau_{21})$$

$$\begin{Bmatrix} \varepsilon_1 \\ \varepsilon_2 \\ \gamma_{21} \end{Bmatrix} = \begin{bmatrix} S_{11} & S_{12} & 0 \\ S_{21} & S_{22} & 0 \\ 0 & 0 & S_{66} \end{bmatrix} \begin{Bmatrix} \sigma_1 \\ \sigma_2 \\ \tau_{21} \end{Bmatrix} \qquad \begin{Bmatrix} \sigma_1 \\ \sigma_2 \\ \tau_{21} \end{Bmatrix} = \begin{bmatrix} Q_{11} & Q_{12} & 0 \\ Q_{21} & Q_{22} & 0 \\ 0 & 0 & Q_{66} \end{bmatrix} \begin{Bmatrix} \varepsilon_1 \\ \varepsilon_2 \\ \gamma_{21} \end{Bmatrix}$$

Maxwell-Betti $\nu_{\perp\parallel} E_\perp = \nu_{\parallel\perp} E_\parallel$ (material) stiffness matrix

$$[S] = \begin{bmatrix} \frac{1}{E_\parallel} & \frac{-\nu_{\parallel\perp}}{E_\perp} & 0 \\ \frac{-\nu_{\perp\parallel}}{E_\parallel} & \frac{1}{E_\perp} & 0 \\ 0 & 0 & \frac{1}{G_{\perp\parallel}} \end{bmatrix} \qquad [Q] = \begin{bmatrix} \frac{E_\parallel}{1-\nu_{\parallel\perp}\nu_{\perp\parallel}} & \frac{\nu_{\perp\parallel}E_\perp}{1-\nu_{\parallel\perp}\nu_{\perp\parallel}} & 0 \\ \frac{\nu_{\parallel\perp}E_\parallel}{1-\nu_{\parallel\perp}\nu_{\perp\parallel}} & \frac{E_\perp}{1-\nu_{\parallel\perp}\nu_{\perp\parallel}} & 0 \\ 0 & 0 & G_{\perp\parallel} \end{bmatrix}$$

$$[Q] = [S]^{-1}$$

$$\{\alpha_T\}_k = (\alpha_{T\parallel}, \alpha_{T\perp}, 0)_k^T \qquad \{\alpha_M\}_k = (\alpha_{M\parallel}, \alpha_{M\perp}, 0)_k^T$$

$$\{\varepsilon\}_k = [S]_k \{\sigma\}_k + \{\varepsilon_H\}_k \qquad \{\sigma\}_k = [Q]_k \cdot (\{\varepsilon\}_k - \{\varepsilon_H\}_k)$$

$$\{\varepsilon_H\}_k = \Delta T_k \{\alpha_T\}_k + \Delta M_k \{\alpha_M\}_k$$

Fabric lamina

$$\begin{Bmatrix} \varepsilon_W \\ \varepsilon_F \\ \varepsilon_{FW} \end{Bmatrix} = \begin{bmatrix} \frac{1}{E_W} & \frac{-\nu_{WF}}{E_F} & 0 \\ & \frac{1}{E_F} & 0 \\ (\text{symm.}) & & \frac{1}{G_{FW}} \end{bmatrix} \begin{Bmatrix} \sigma_W \\ \sigma_F \\ \tau_{FW} \end{Bmatrix}$$

$$\nu_{FW} E_F = \nu_{WF} E_W$$

Which Poisson's ratio will be the larger depends on the fibre volume contents ratio for warp and fill.

Mat lamina

$$\begin{Bmatrix} \varepsilon_x \\ \varepsilon_y \\ \varepsilon_{xy} \end{Bmatrix} = \begin{bmatrix} \frac{1}{E} & \frac{-\nu}{E} & 0 \\ & \frac{1}{E} & 0 \\ (\text{symm.}) & & \frac{1}{G} \end{bmatrix} \begin{Bmatrix} \sigma_x \\ \sigma_y \\ \tau_{xy} \end{Bmatrix}$$

$$G = \frac{E}{2 \cdot (1+\nu)}$$

Rotation of the UD lamina into the laminate

$$\{\varepsilon'\} = (\varepsilon_x, \varepsilon_y, \gamma_{xy})^T = [T_\varepsilon] \cdot \{\varepsilon\} = [S'] \{\sigma'\} + \{\varepsilon_H\}$$

$$\{\sigma'\} = (\sigma_x, \sigma_y, \tau_{xy})^T = [T_\sigma] \cdot \{\sigma\} = [Q'] \{\varepsilon'\}$$

$$\{\sigma\}_k = [Q]_k \cdot (\{\varepsilon\}_k - \{\varepsilon_H\}_k)$$

$$s = \sin\alpha, \quad c = \cos\alpha, \quad [T_\varepsilon]^{-1} = [T_\sigma]^T$$

$$[T_\sigma] = \begin{bmatrix} c^2 & s^2 & -2sc \\ s^2 & c^2 & 2sc \\ sc & -sc & (c^2 - s^2) \end{bmatrix} \qquad [T_\varepsilon] = \begin{bmatrix} c^2 & s^2 & -sc \\ s^2 & c^2 & sc \\ 2sc & -2sc & (c^2 - s^2) \end{bmatrix}$$

$$\{\alpha_T'\} = (\alpha_{Tx}', \alpha_{Ty}', \alpha_{Txy}')^T$$

$$\{\alpha_M'\} = (\alpha_{Mx}', \alpha_{My}', \alpha_{Mxy}')^T$$

$$[Q'] = \begin{bmatrix} Q'_{11} & Q'_{12} & Q'_{16} \\ & Q'_{22} & Q'_{26} \\ (\text{symm.}) & & Q'_{66} \end{bmatrix} \begin{Bmatrix} \varepsilon_x \\ \varepsilon_y \\ \gamma_{xy} \end{Bmatrix} \qquad Q'_{16} \text{ and } Q'_{26} \neq 0!$$

$$Q'_{11} = Q_{11}\,c^4 + 2\,(Q_{12} + 2\,Q_{66})\,s^2c^2 + Q_{22}s^4$$

Hygrothermal loading

$$\{\varepsilon_H'\} = [T_\varepsilon] \cdot \{\varepsilon_H\} = [T_\varepsilon]\,(\Delta T \{\alpha_T\} + \Delta M \{\alpha_M\}) = \Delta T \{\alpha_T'\} + \Delta M \{\alpha_M'\}$$

$$\{\sigma'\} = [T_\sigma] \cdot \{\sigma\} = [T_\sigma] \cdot [Q] \cdot (\{\varepsilon\} - \{\varepsilon_H\}) = [Q'] \cdot (\{\varepsilon'\} - \{\varepsilon_H'\})$$

The main axes of the laminate do not generally coincide with those of the lamina. For this reason transformation relationships are required for the rotation from the laminate CoS x to the lamina (ply) CoS $x_1 = x_{||}$ with a positively measured α_k from x to x_1. This freely chosen rotation means "*What does the off-axis lamina contribute to the laminate*?". This is also oppositely defined.

The laminate CoS is used as reference system. Each single lamina quantity is rotated by a positive angle α_k from laminate CoS to the lamina CoS. Row-normalized indexing is preferred and not the column-normalized one. The relationships above are used for an in-plane stress-strain analysis.

9.1.2 Laminate

The laminate considered in *Fig.9-2* is a plane plate with an in-plane (intra-laminar) stress state. It consists of n UD laminas each having a constant thickness t_k.

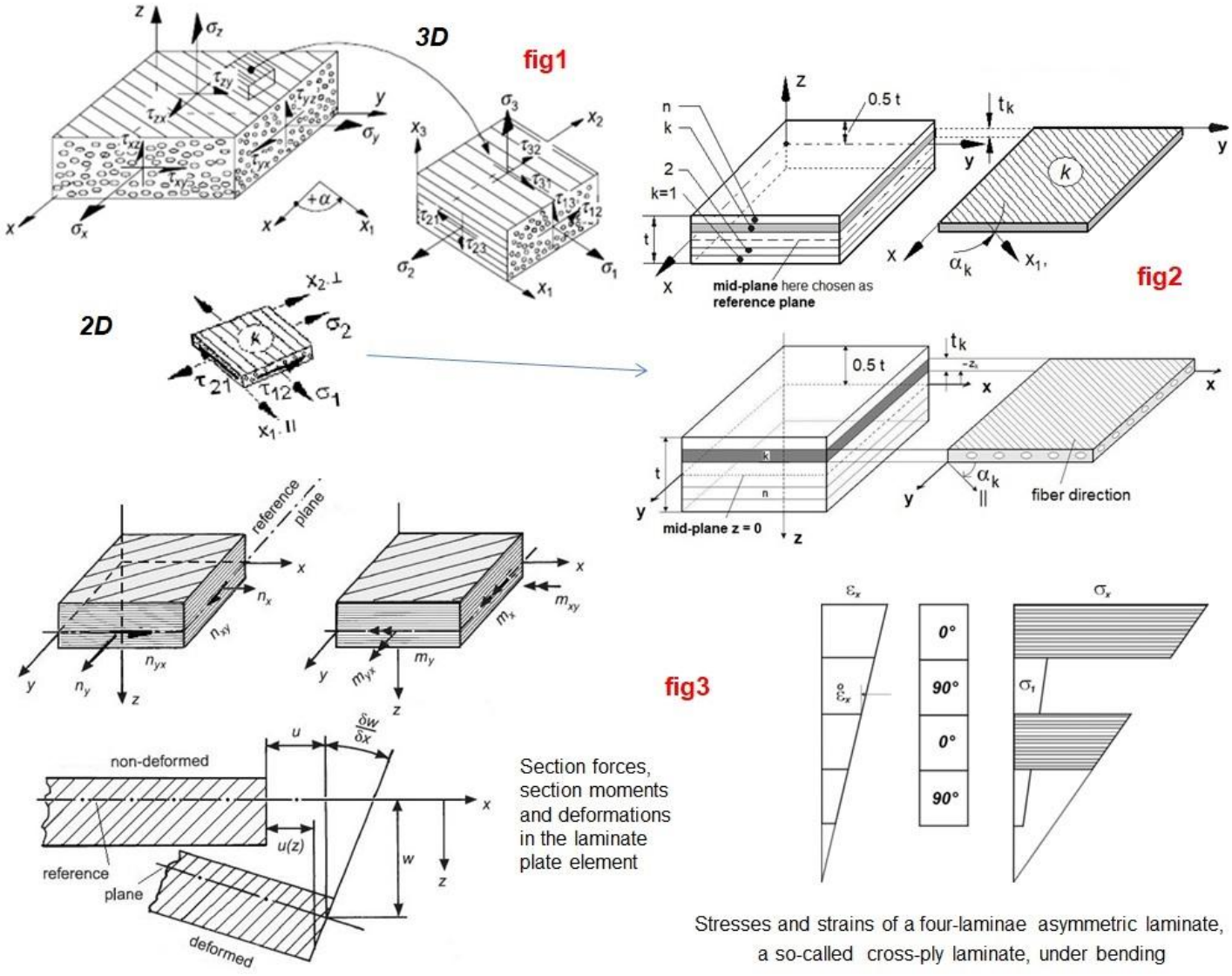


Fig.9-2: Basic entities within CLT

According to the classical thin plate theory [Kirchhoff-Love] the following pre-requisites must be observed:

- The plate thickness *t* is small with respect to other dimensions and the transverse deflection of the mid-plane is small compared to *t* ,

- Cross-sections remain planar (Bernoulli hypothesis). This means that the thickness of the plate does not change during a deformation and that the plate is assumed to be rigid to shear stresses ,
- Straight lines, normal to the reference plane, remain normal.

The CLT-assumptions pre-suppose that all *n* laminas fully adhere to each other. Hence, the strain vector $\{\varepsilon'\}_k$ at any point of the plate wall at a distance of z_k from the reference plane can be expressed as $\{\varepsilon'\}_k = \{\varepsilon^0\} + z_k \cdot \{\kappa\}$, where the superscript ^{0} denotes the reference plane, and where $\{\kappa\}$ represents the curvatures.

$$\{\varepsilon^0\} = \left(\frac{\partial u^0}{\partial x}, \frac{\partial v^0}{\partial y}, \frac{\partial u^0}{\partial y} + \frac{\partial v^0}{\partial x} \right)^T , \quad \{\kappa\} = \left(-\frac{\partial^2 w^0}{\partial x^2}, \frac{\partial v^0}{\partial y}, -2\frac{\partial^2 w^0}{\partial x \cdot \partial y} \right)^T .$$

If advantageous, the geometric mid-plane is selected as reference plane. Above equation may also be used for curved shallow shells.

Strains and curvatures of the reference plane, expressed by the displacements (u^0, v^0, w^0) or the slopes φ of the reference plane, respectively, are displayed in fig.3 of *Fig.9-2*.

Counting in z-direction, z_k denotes the distance of the more far surface of the kth layer from the reference plane z = 0 and z_{k-1} denotes the difference of the surface of the kth layer less far from the reference plane, $z_k > z_{k-1}$. In fig2 intentionally two different z-choices were displayed.

LL: *For avoiding misinterpretations*

- ✓ *Check always, by applying the Maxwell-Betti formula, that "The smaller ν times the larger Young's modulus $E_1 = E_{||}$ is equal to the product of the larger ν times the smaller Young's modulus $E_2 = E_3 = E_\perp$". Maxwell-Betti works in the non-linear case, too. One should always take the larger Poisson's ratio in [S] or [C] because the larger one is the better measurable one.*
- ✓ *Using symbolic suffixes reduces the danger to use a wrong property as input and to mark a stress or a strain in a distinct task*
- ✓ *Using numbers is standard in the computations*
- ✓ *In common literature different sets of indices are used. Hence, in order to avoid a wrong input of a FEM code's material card the actual utilization of the suffixes is to be checked. See VDI 2014, sheet 3, and later a note on indexing of Poisson's ratios.*

The 3 section forces in $\{n^0\}$ and the 3 section moments in $\{m\}$ are obtained by summing up all lamina contributions over the laminate thickness *t,* see *Table 9-2*. The vectors of the so-called section quantities, the section forces (tractions) and section moments (stress resultants per unit width), are depicted below. If 'section quantities' do not act in the chosen reference plane they must be transferred to it. Values for each of the three section forces and section moments in $\{n^0\}$ and $\{m\}$ are derived from structural component analysis. [K] is the symmetric stiffness matrix of the laminate. It is indexed i, j = 1, 2, 6 (*the 6 considers that τ_{12} is placed at the sixth position of the contracted 3D stress-strain relation*). The symmetric sub-matrices of [K] are termed extensional (membrane) stiffness matrix [A], coupling stiffness matrix [B] and bending (flexural) stiffness matrix [D], which are yielded by summing up the lamina portions.

Table 9-2: Section quantities-strain relations

$$\{n^0\} = (n_x^0, n_y^0, n_{xy}^0)^T = \int \{\sigma'\} dz = \sum_{k=1}^{n} \int_{z_{k-1}}^{z_k} \{\sigma'\}_k \, dz = \Sigma \int [Q']_k \{\varepsilon'\}_k dz \qquad \begin{Bmatrix} n^0 \\ m \end{Bmatrix} = \begin{bmatrix} A & B \\ B & D \end{bmatrix} \cdot \begin{Bmatrix} \varepsilon^0 \\ \kappa \end{Bmatrix} = [K] \begin{Bmatrix} \varepsilon^0 \\ \kappa \end{Bmatrix}$$

$$\{m\} = (m_x, m_y, m_{xy})^T = \int \{\sigma'\} z dz = \Sigma \int \{\sigma'\}_k z dz = \Sigma \int [Q']_k \{\varepsilon'\}_k z dz \qquad t_k = z_k - z_{k-1}, \; z_{km} = 1/2 \, (z_k + z_{k-1})$$

$$[A] = \Sigma [Q']_k (z_k - z_{k-1}) = \Sigma [Q']_k t_k$$

(matrix of in-plane stretching or extensional stiffnesses)

$$[B] = 1/2 \, \Sigma [Q']_k (z_k^2 - z_{k-1}^2) = \Sigma [Q']_k t_k z_{km}$$

(matrix of (bending-stretching) coupling stiffnesses)

$$[D] = 1/3 \, \Sigma [Q']_k (z_k^3 - z_{k-1}^3) = \Sigma [Q']_k (t_k^3/12 + t_k z_{km}^2)$$

(matrix of the plate or bending stiffnesses)

After integration the laminate stiffness matrix [K] is known.
Considering – beside mechanical loading – hygro-thermal loading (index $_H$) delivers

$$\begin{Bmatrix} n^0 \\ m \end{Bmatrix} = [K] \cdot \begin{Bmatrix} \varepsilon^0 \\ \kappa \end{Bmatrix} - \begin{Bmatrix} n_H^0 \\ m_H \end{Bmatrix}, \quad \{n_H^0\} = \Sigma \, (\Delta T_k \, [Q']_k \, t_k \, \{\alpha_T'\}_k + \Delta M_k \, [Q']_k \, t_k \, \{\alpha_M'\}_k) \qquad \{m_H\} = \Sigma \, (\Delta T_k \, [Q']_k (z_k^2 - z_{k-1}^2) \, \{\alpha_T'\}_k + \Delta M_k \, [Q']_k (z_k^2 - z_{k-1}^2) \, \{\alpha_M'\}_k$$

After calculation of $\{\varepsilon^0\}$ and $\{\kappa\}$ of the laminate the stresses and strains in the individual laminas can be calculated with $z = z_k$ or z_{k-1}, depending on whether the upper or lower lamina boundary is meant. If just membrane forces act, then the section forces can be formulated by smeared laminate stresses $\hat{\sigma}$. Dependent on the lay-up, coupling between the sub-matrices is possible which may cause undesired deformations and especially twisting, <u>*Fig.9-2*</u>.

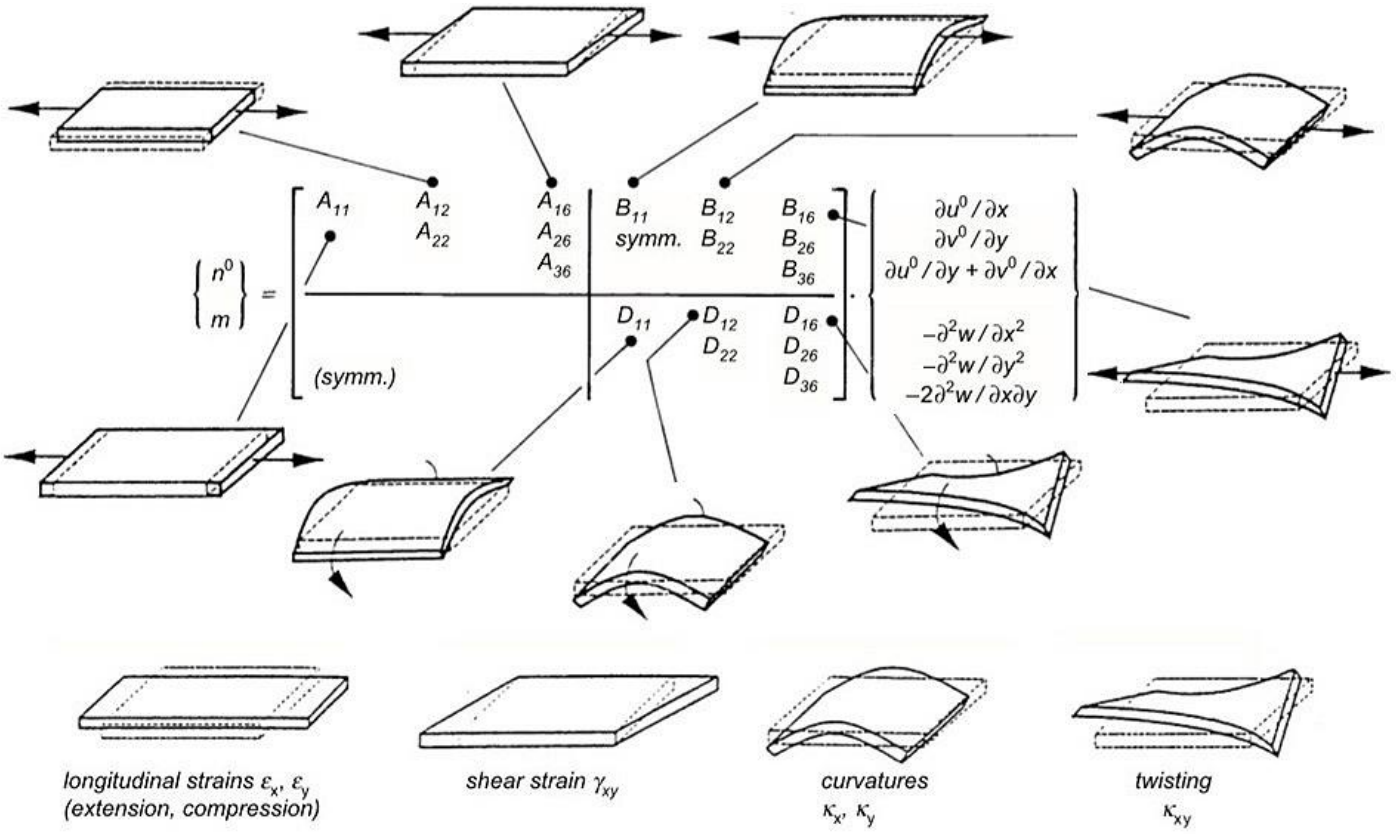


Fig.9-2: Effects of the stiffness components in [K].

Units: *MPa·mm* for A_{ij}, *MPa·mm²* for B_{ij}, *MPa·mm³* for D_{ij}.

Finally *Fig.9-3* displays the CLT procedure to achieve design verification for the finally chosen laminate design.

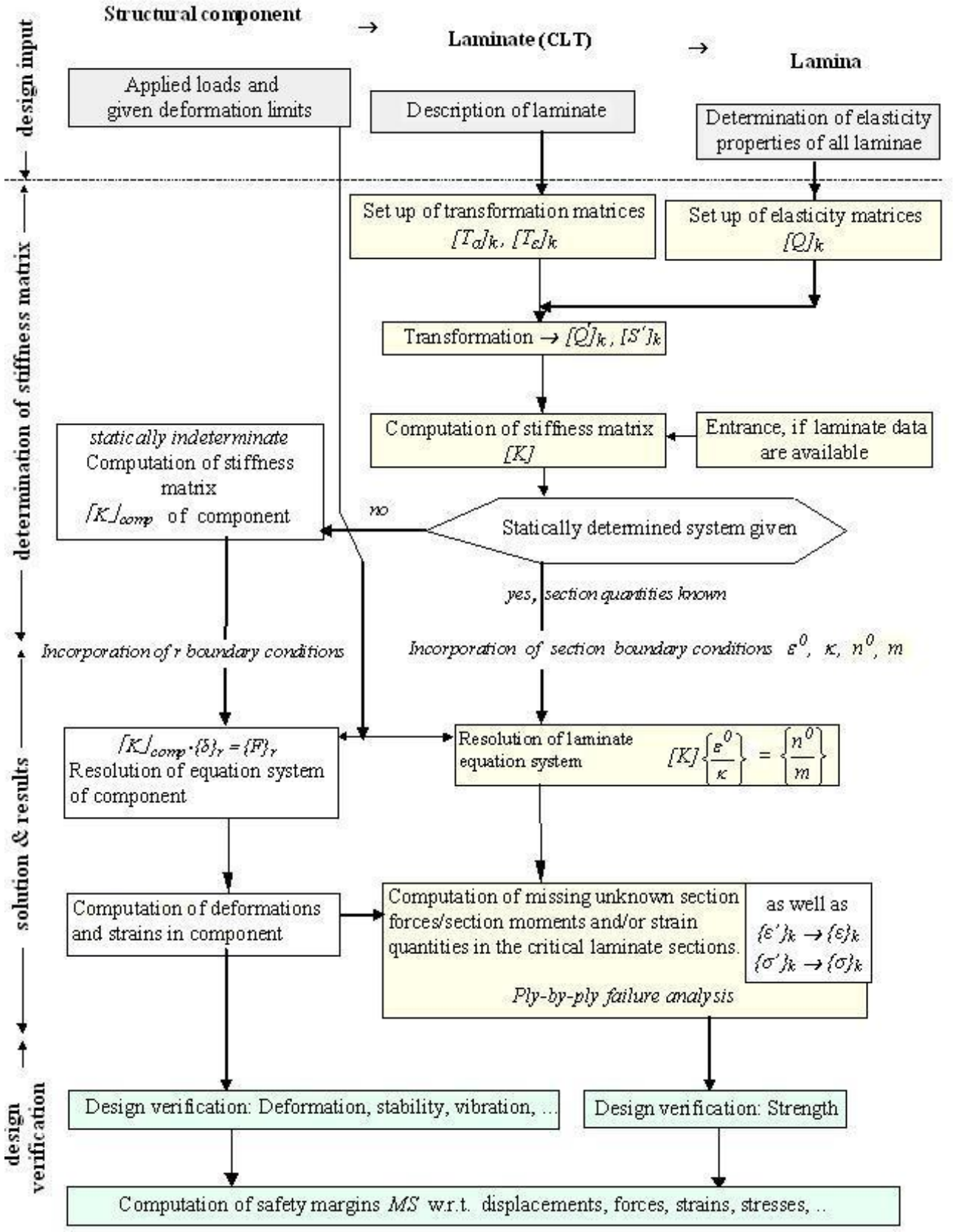


Fig.9-3: CLT procedure considering laminate design verification

Above flow chart of the CLT design analysis shows that a stiffness matrix can be obtained on three different ways. The chosen way depends on the input and which accuracy is required. Carefully determined and evaluated experimental data are necessary as input properties. The calculation procedure is performed according to the posed task. The often mixed boundary conditions, considering force & moment, strain & curvature, must be known.

Some application remarks

- All the relationships above are practically the same as for the isotropic plate. They mathematically describe the behavior of the "thin" laminated plate, elastic theory is used.
- In a general lay-up (stack) case, an elastic plate-parallel symmetry plane does not exist which would enable to solve the membrane plate problem and the bending plate problem independently. This is only possible in case of a symmetrical lay-up where [B] = 0
- The transversal shear moduli $\hat{G}_{xz}$, $\hat{G}_{yz}$ of most of the laminates are relatively small compared with isotropic plate materials. Therefore, it is only permitted to neglect the influence of the interlaminar shear stresses τ_{xz}, τ_{yz} or of the corresponding strains on the deformation behavior of the laminate if the slenderness ratio (length ℓ / thickness *t*) is larger than a certain limit, a limit which depends on the grade of anisotropy. For instance, for the example: ℓ/t = 20 and $\hat{E}_x / \hat{G}_{xz}$ = 50, the deformation w_0 derived with the 'simple' relationships above is 20% too low
- The elasticity properties for the computation input are obtained from so-called "isolated" test specimens (*weakest link failure behavior*) whereas an embedded lamina underlies a redundant in-situ behavior. The embedded lamina will not lose its full stiffness after the first inter-fiber-crack IFF. This is to consider when applying inelastic theory.
- For the reduction of micro-cracking from the edge effect the change of the orientation angle should be minimal, i.e. 45°. This will be possible if multi-directional tapes are optimally stacked
- Benefit of applying thin plies: Using thin plies, early micro-cracking with onset of micro-delaminations is reduced. The conflict of the designer (desires thin layers) with manufacture (desires to cluster if the same direction of neighboring layers is given, thick layers) will be smoothed due to the presently available multi-angle tapes. This makes it possible to improve stack optimization in order to minimize the non-symmetry. Also the ply-drop problem is reduced. An optimal permutation of thin layers can even lead to a compressive interlaminar normal stress σ_3
- The reduction of bending-torsion coupling (A_{16} = A_{26} = 0) by the right stacking is mandatory for a well designed and optimally behaving laminate. The lower part of the flow chart describes the laminate structural analysis. Thereby it is distinguished whether the structural analysis problem is a statically indeterminate one or a statically determined one. In the latter case, after including the boundary conditions of the structural laminate element, all interesting structural variables can be directly determined.

On a HSB-sheet the 2D-CLT is extended to a 2.5 ELT (Extended LT) in order to approximate the more difficult 3D-computations resultsof laminates.

9.1.3 Effective Elasticity Constants and Effective Stiffnesses of the Laminate

Sometimes the effort in laminate analysis can be reduced by applying a simpler, homogenized model which is elasticity-equal. For instance, if a direct input is necessary for the use of an analytical formula or for a finite-element laminate shell analysis, then elasticity 'constants' are

required or equivalent laminate stiffnesses. This may be the case for a plate (unit width "1") or for a strip (b >> t). These specific properties shall be computed now by using the CLT plate theory.
A plate has the unit width "1" and for a strip is valid w >> t.

Effective elasticity constants and effective stiffness quantities are derived by comparing the stiffness of the 'homogenized' laminate cross-section with the non-homogeneous cross-section via the relations Effective elasticity constants and effective stiffness are derived by comparing the stiffness of the 'homogenized' laminate cross-section with the non-homogeneous cross-section via the relations

$$n = \widehat{Et}\cdot\varepsilon,\ m = (EI)_{ef}\cdot\kappa = \widehat{EI}\cdot\kappa\ ,\quad m_{xy} = D_{66}\cdot\kappa_{xy}\ \text{ to relate to }\ m_t = \widehat{GI_t}\cdot\vartheta'.$$

for the laminate's section forces and section moments with ϑ the specific angle of twist. The hat marks that the derived stiffness property is a 'smeared' laminate quantity. The provision of effective elasticity (engineering) constants makes only sense for [B] = 0, otherwise irritation will be faced by the user. The full laminate stiffness matrix and its inverse read:

$$[K] = \begin{bmatrix} A_{11} & A_{12} & A_{16} & B_{11} & B_{12} & B_{16} \\ A_{12} & A_{22} & A_{26} & B_{12} & B_{22} & B_{26} \\ A_{16} & A_{26} & A_{66} & B_{16} & B_{26} & B_{66} \\ & & & D_{11} & D_{12} & D_{16} \\ & (sym) & & D_{12} & D_{22} & D_{26} \\ & & & D_{16} & D_{26} & D_{66} \end{bmatrix},\ [K]^{-1} = \begin{bmatrix} a_{11} & a_{12} & a_{16} & b_{11} & b_{12} & b_{16} \\ a_{12} & a_{22} & a_{26} & b_{12} & b_{22} & b_{26} \\ a_{16} & a_{26} & a_{66} & b_{16} & b_{26} & b_{66} \\ & & & d_{11} & d_{12} & d_{16} \\ & (b^T) & & d_{12} & d_{22} & d_{26} \\ & & & d_{16} & d_{26} & d_{66} \end{bmatrix}$$

For the components of the inverse, $[K]^{-1}$, the letters a, b, d or A*, B*, D* are internationally used.

(a) Effective elasticity constants ('engineering constants') of the membrane, [B] = 0

Elasticity constants are effective (*index ef*) values if the cross-section is not homogeneous. They are also termed 'engineering constants' but they are constants, only, as far as their initial values are addressed. The provision of engineering constants makes sense for orthotropic symmetric laminates, only, where $B_{ik} = 0$ and $A_{16} = A_{26} = 0$.

Procedure via stiffness:

The used section forces-strain relationship reads

$$\begin{Bmatrix} n_x^0 \\ n_y^0 \\ n_{xy}^0 \end{Bmatrix} = \begin{bmatrix} A_{11} & A_{12} & 0 \\ A_{12} & A_{22} & 0 \\ 0 & 0 & A_{66} \end{bmatrix} \cdot \begin{Bmatrix} \varepsilon_x^0 \\ \varepsilon_y^0 \\ \gamma_{xy}^0 \end{Bmatrix}.$$

For the plate, subjected to "membrane" loading, the following effective elasticity constants of the laminate are derived. At first the E-modulus $\{n^0\} = (n_x^0,\ 0,\ 0)^T$ with $n_x^0 = \hat{E}_x \cdot t \cdot \varepsilon_x^0$

$$\widehat{E_x}: \quad n_x^0 = A_{11}\cdot\varepsilon_x^0 + A_{12}\cdot\varepsilon_y^0 \quad \text{and} \quad 0 = A_{12}\cdot\varepsilon_x^0 + A_{22}\cdot\varepsilon_y^0$$

$$n_x^0 = \hat{E}_x\cdot t\cdot\varepsilon_x^0 \equiv \varepsilon_x^0\cdot(A_{11} - A_{12}^2/A_{22})\ ,$$

$$\widehat{\nu_{xy}}: \quad 0 = A_{12}\cdot\varepsilon_x^0 + A_{22}\cdot\varepsilon_y^0 \quad \Rightarrow \widehat{\nu_{xy}} = -\varepsilon_y^0/\varepsilon_x^0 = A_{12}/A_{22}$$

$$n_x^0 = n_y^0 = 0,\ n_{xy}^0 = \widehat{G_{xy}}\cdot t\cdot\text{"1"}\cdot\gamma_{xy}^0$$

$$\widehat{G_{xy}}: \quad n_{xy}^0 = \widehat{G_{xy}}\cdot t\cdot\gamma_{xy}^0 \quad \Rightarrow \widehat{G_{xy}}\cdot t\cdot\gamma_{xy}^0 = \gamma_{xy}^0\cdot A_{66}.$$

Eventually all effective elasticity constants of the transversely-isotropic laminate read

$$\widehat{E_x} := \frac{A_{11} - A_{12}^2/A_{22}}{t} = \frac{1}{t \cdot A_{11}^*},\ \widehat{E_y} = \frac{A_{22} - A_{12}^2/A_{11}}{t},\ \widehat{G_{xy}} = \frac{A_{66}}{t},\ \widehat{\nu_{xy}} = +\frac{A_{12}}{A_{22}}.$$

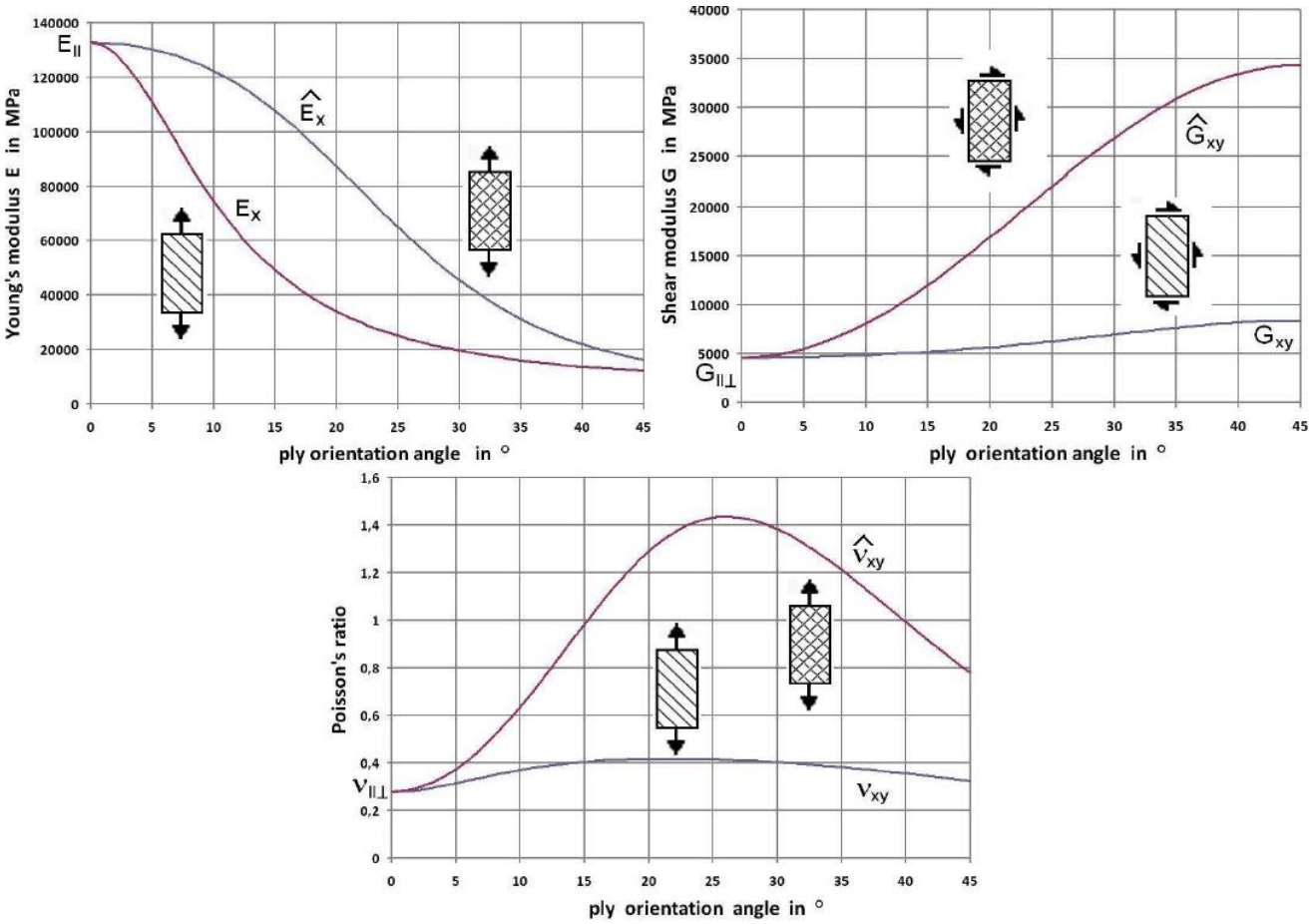
They simplify for the isotropic case to

$$\widehat{E_x} = E_x = \frac{A_{11} - A_{12}^2/A_{22}}{t} = \frac{Q_{11} - Q_{12}^2/Q_{22}}{t} \cdot t = \frac{E}{1-\nu^2} - \frac{E \cdot \nu^2}{1-\nu^2} = E \cdot \frac{1-\nu^2}{1-\nu^2} = E.$$

Procedure via compliances: *advantageous way via inverse*

$$\widehat{E_x} := \frac{1}{A_{11}^* \cdot t} = \frac{A_{11} - A_{12}^2/A_{22}}{t},\ \widehat{E_y} = \frac{1}{A_{22}^* \cdot t},\ \widehat{G_{xy}} = \frac{1}{A_{66}^* \cdot t},\ \widehat{\nu_{xy}} = -\frac{A_{12}^*}{A_{11}^*} = \frac{A_{12}}{A_{22}}.$$

Below an example for the difference of a one-layer and a balanced two-layer lay-up.



Dependence of the properties of the off-axis lamina and the balanced angle-ply on varying ply angle α and half-crossing angle ω!

LL: The so-called 'engineering constants' (= homogenized laminate properties) above can be determined for pure membrane stress and pure bending stress states. This is possible with and without obstruction of the contraction of the cross-section.

(b) Effective bending and torsion stiffness (rigidity) of the symmetric laminate

The use of specific effective elastic constants for bending and twisting makes no sense, in general, however the use of effective stiffness quantities. These are determined for s*ymmetric laminates*, only,

where $[B] = 0$, $D_{16} = D_{26} = 0$. Then the bending equations reduce to

$$\begin{Bmatrix} m_x \\ m_y \\ m_{xy} \end{Bmatrix} = \begin{bmatrix} D_{11} & D_{12} & D_{16} \\ D_{12} & D_{22} & D_{26} \\ (sym) & D_{12} & D_{66} \end{bmatrix} \cdot \begin{Bmatrix} \kappa_x \\ \kappa_y \\ \kappa_{xy} \end{Bmatrix} \Rightarrow \text{ isotropic } \quad \{m\} = \frac{t^2 \cdot E}{12 \cdot (1-\nu^2)} \cdot \begin{bmatrix} 1 & \nu & 0 \\ \nu & 1 & 0 \\ 0 & 0 & (1-\nu)/2 \end{bmatrix} \cdot \{\kappa\}$$

The size of the D_{ik} elements is linked to the chosen reference plane.

(I) Curvature-constrained wide plate, using stiffness

Considering, that due to the large width the plate is curvature-constrained in y-direction ($\kappa_y = 0$), and that it is subjected to $m = EI_{ef} \cdot \kappa = \widehat{EI} \cdot \kappa$, exemplarily is derived

$$\widehat{EI_x}: \quad m_x = D_{11} \cdot \kappa_x + D_{12} \cdot 0 = \widehat{EI_x} \cdot \kappa_x \quad .$$

The torsional moment (torque), required for twisting, is termed (effective) torsional stiffness or rigidity $\widehat{GI}t$. In contrast to two, themselves balancing bending moments, four balancing twisting moments must be considered for a plate. They collectively build up the *internal twisting.*
All effective laminate stiffness then read*:*

$$\widehat{EI_x} = D_{11}, \; \widehat{EI_y} = D_{22}, \quad \widehat{GI_t} = 4 \cdot D_{66}.$$

For the isotropic is simply obtained:

$$D_{ik} = Q_{ik} \cdot \frac{(0.5 \cdot t)^3 - (-0.5 \cdot t)^3}{3} = Q_{ik} \cdot \frac{t^3}{12}, \; D_{11} = \frac{E}{1-\nu^2} \cdot \frac{t^3}{12}, \; D_{22} = D_{11}, \quad D_{12} = \nu \cdot D_{11}$$

$$D_{66} = 0.5 \cdot D_{11} \cdot (1-\nu) = 0.5 \cdot \frac{E}{1-\nu^2} \cdot \frac{t^3}{12} \cdot (1-\nu) = G \cdot t^3/12 \quad ,$$

$$\widehat{EI_x} = D_{11} = Q_{11} \cdot \frac{t^3}{12} \cdot (1-\nu^2) = E \cdot t^3/[12 \cdot (1-\nu^2)]; \widehat{GI_t} = 4 \cdot D_{66} = G \cdot t^3/3.$$

(II) Free wide plate, using compliances

In the general non-symmetric case the application of the curvature constraints ($\kappa_y = 0$) to determine $\widehat{EI}_x$ and of ($\kappa_x = 0$) to determine $\widehat{EI}_y$ would lead to an over-determination. Curvature constraints cannot be regarded anymore. Therefore, the inverse $1/d_{11}$ is used accepting lower stiffness values.

$$\begin{Bmatrix} \varepsilon_x^0 \\ \varepsilon_y^0 \\ \gamma_{xy}^0 \\ \kappa_x \\ \kappa_y \\ \kappa_{xy} \end{Bmatrix} = \begin{bmatrix} a_{11} & a_{12} & a_{16} & b_{11} & b_{12} & b_{16} \\ a_{12} & a_{22} & a_{26} & b_{12} & b_{22} & b_{26} \\ a_{16} & a_{26} & a_{66} & b_{16} & b_{26} & b_{66} \\ & & & d_{11} & d_{12} & d_{16} \\ & (b^T) & & d_{12} & d_{22} & d_{26} \\ & & & d_{16} & d_{26} & d_{66} \end{bmatrix} \cdot \begin{Bmatrix} n_x^0 \\ n_y^0 \\ n_{xy}^0 \\ m_x \\ m_y \\ m_{xy} \end{Bmatrix}$$

Notes :

(a) Way *(I)* above, using stiffness, is intentionally gone with respect that the engineers primarily use stiffnesses. Way *(II)* is applying compliances (= elements of the inverted stiffness matrix K^{-1}) . and thereby is to use simpler relationships, for instance as approximation $\widehat{EI}_x = 1 / d_{11;}$ value on safe side

(b) $[B] \neq 0$: In this case, membrane loading cannot be separated from bending. Therefore, the derivation of effective elasticity constants principally makes no sense for i.e. a 3-D lamina-composed symmetric laminate [45/-45$_2$/45]

(c) Poisson's ratio ν: In comparison to metals the larger Poisson ratio may be larger than 0.3 (for [45/-45/-45/45] i.e. $\nu_{xy} = \nu_{yx} = 0.8$) and also smaller than 0.3. Of course, this is moduli-dependent. Further, the product of the associated Poisson ratios $\nu_{xy} \cdot \nu_{yx}$ may be smaller than 0.3^2.

(c) Stiffness of the non-symmetrical laminate $\{n^0\} = 0$

For the often utilized balanced laminates extension--shear coupling is zero ($A_{16} = A_{26} = 0$), if for instance 45°-layers are used such as in the non-symmetric stack [0/90/45/-45/], however the bending stiffnesses do not vanish, i.e. D_{16} and $D_{26} \neq 0$, This means, that bending-torsion coupling occurs and care must be taken to this effect.

In special cases a global information on the laminate stiffness may be desired despite of $[B] \neq 0$ for an analytical approximate calculation. Then, the 'effective' stiffness matrix D_{ik} of a non-symmetric laminate is calculated and the obtained bending stiffness quantities serve as comparison "numbers", only.

If $\{n^0\} = 0$ and if the coupling stiffnesses do not vanish, then the bending moments are just linked to the curvatures $\{\kappa\}$. Thereby the associated stiffness becomes the so-called modified bending stiffness matrix $[\tilde{D}] = [D] - [B]^T \cdot [A]^{-1} \cdot [B]$.

This $[\tilde{D}]$−matrix is independent of the choice of the reference plane. For symmetric orthotropic laminates $[\tilde{D}] = [D]$ is valid, due to $B_{ij} = 0$.

Note: Bending and torsion of plates can be well described by $[\tilde{D}]$. Is there a need to tackle the stability problem by a geometrically non-linear analysis then the full K-matrix should be used.

9.2 Some Topics concerning the CLT-analysis of laminates

9.2.1 Free Edge Effect and CLT

The CLT is based on the assumption of a plane state of stress. However, in the vicinity of laminate joints, at ply drop-offs and at free laminate edges of curved notches, straight strips, plates or coupons, a 3D state of stress is faced (next figure). These peak stress states occur strongly localized with the possible consequence of an undesired premature failure associated by delamination.

Due to its underlying assumptions the CLT cannot capture such a 3D stress situation. However, the LT is a good approximation in regions remote from the edge because the 3D stress fields at the free edges decay very fast, and in the inner unperturbed laminate regions CLT prevails. This causes that sizing of composite structures is often performed using CLT exclusively. Sizing of composite structures can be only reliably performed if the engineer has some knowledge about the nature of the free-edge effect and its implication, still knowing, that the free-edge stress fields are usually confined to an area of the size of about one laminate thickness *t*.

Free-edge effects are mainly caused by the (theoretically) abruptly changing elastic properties in the interphase of adjacent laminate layers which results in a mismatch of the stress-strain-

relationship and thus in an incompatible deformation behavior. Due to this incompatibility, a singular 3D stress field is encountered at free edges of composite laminates at the interfaces between dissimilar layers which may be of substantial influence concerning the failure behavior of such structures. This stress concentration singularity, denoted by the size of the tensile notch factor K^t) is the result of the 'simple' linear analysis modelling and not modelling a non-linear analysis before 'onset of macro-cracking' will occur. Under a critical edge notch or/and a distinct free edge stress state edge-delamination can occur which cause an even higher stress singularity (crack-linked stress intensity factor K, not to confuse with the stiffness matrix [K] of the laminate) to be treated by means of fracture mechanics. The delamination effect is important in the assessment of test data from laminate coupons. Generally, the generated inter-laminar stresses, building the full 3D stress state, decrease if the difference between the orientations of two adjacent layers decreases.

The analysis of free-edge effects is rather difficult. Exact closed-form solutions do not exist, even for the simplest thinkable cases like plane symmetrically laminated specimens under uniaxial extension as depicted in *Fig.9-4.* The analysis of free-edge effects is usually performed by using adequate finite element models that require a distinct mesh refinement in the vicinity of the free edges due to the stress singularities that are encountered at the free edges. However due to the linear treatment the following result is faced: The finer the mesh the higher the singularity or the stress peak, respectively. However, the analyses give an engineering 'feeling' for the design variant and for comparisons of design variants, despite of the fact that one cannot really quantify it.

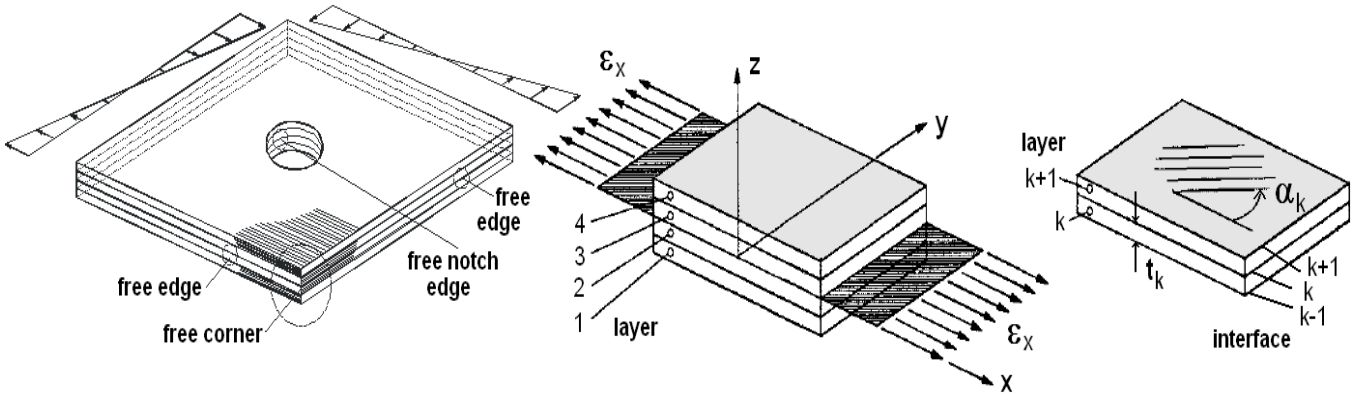


Fig.9-4: Sketch of a general plate strip under axial torsion. Edge problems and definitions (courtesy Mittelstedt/Becker]

Finally, the *Fig.9.5* and *9.6* illustrate the free-edge effect in a qualitative sense, indicating the significant interlaminar stresses, see. [*Mit07*]. For the laminate example [0/90/90/0], *Fig.9.5* gives an idea about the distribution of the interlaminar shear stress _yz and of the tensile stress in thickness direction $\sigma_z \equiv \sigma_3$. Both these stresses act together and are responsible for micro-delaminations at the free edge. *Fig.9.6* depicts the stress situation for the symmetric laminate example [45/-45/-45/45]. In both the cases y / *t* = 1 marks the end of the affected domain

The free edge singularity cannot be assessed by strength criteria. However, it is nevertheless advantageous to alleviate the free edge effect of a laminated structural part qualitatively by comparing designs as far as possible despite of the fact that one cannot really quantify the effect.

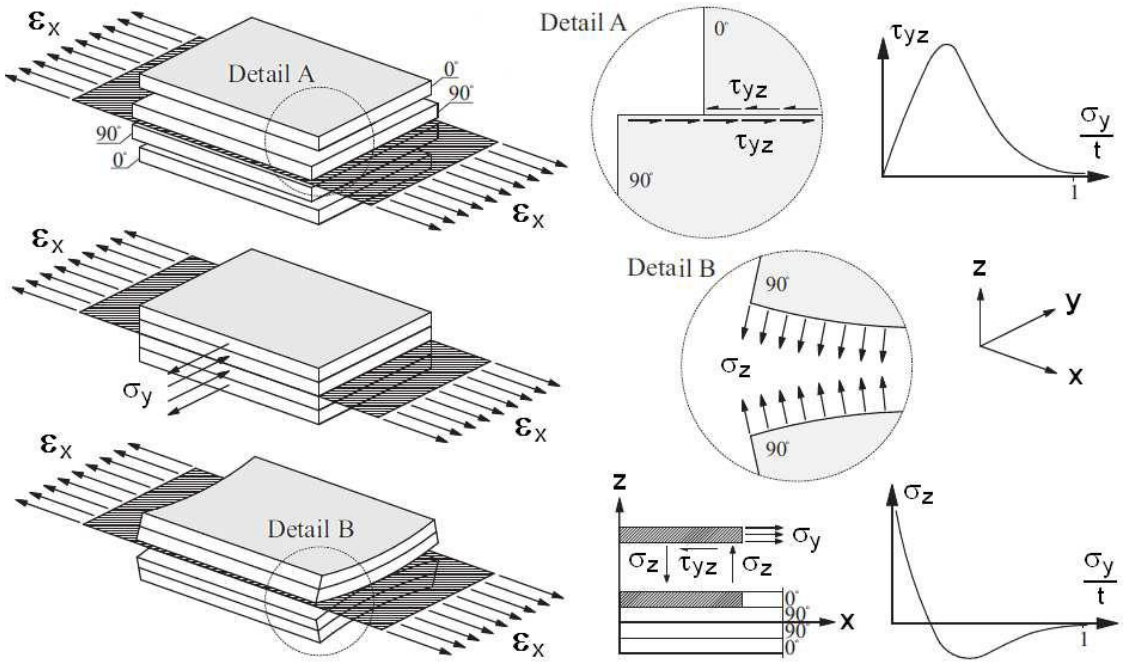


Fig.9-5: Plate strip showing the stresses under axial tension of a [0/90/90/0] laminate (courtesy Mittelstedt). Layer indices of σy are not indicated at the single ones

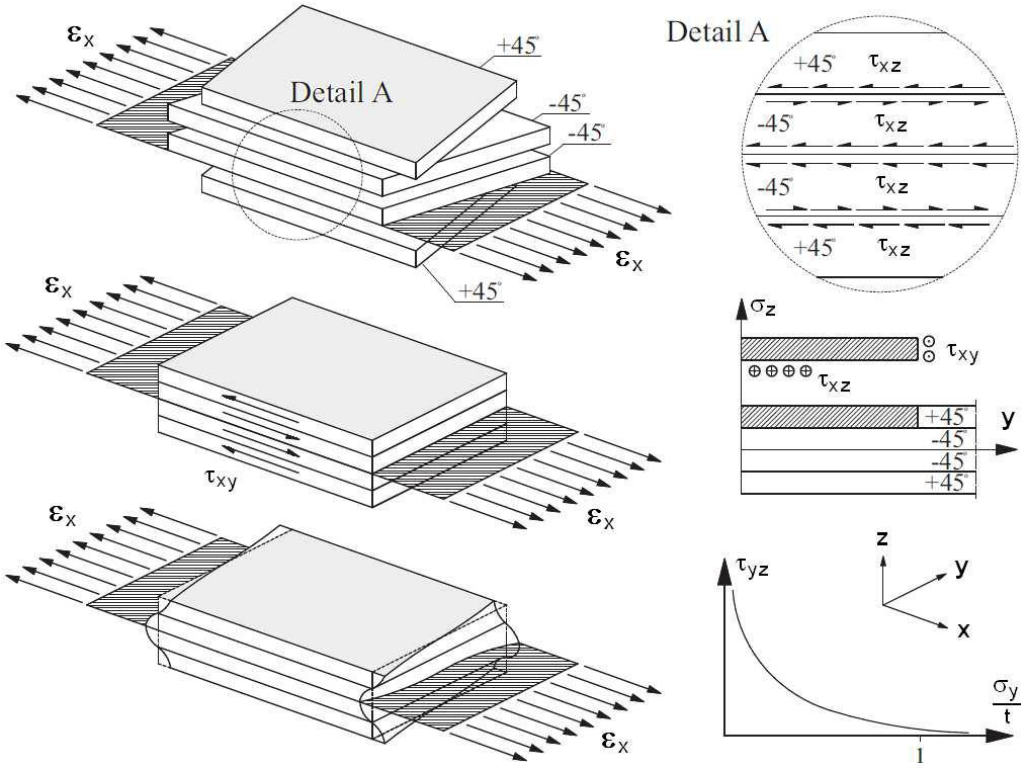


Fig.9-6: Plate strip showing the stresses under axial tension of a [45/-45/-45/45] laminate (courtesy Mittelstedt)

9.2.2 Layer numbering and reference system choice

Non-compatible layer numbering and reference system is an essential problem for the modeler. Also a stress engineer is usually required to follow the manufacturer drawing (a) when building up his FE model. In order to avoid any mistake, the following procedure is suggested for the laminate brick (a):

- Check of ply numbering and of orientation in the manufacturing document/drawing and comparison with the CLT definition
- Check of the loading direction and comparison with the CLT definition
- If different, transformation of layer angles necessary (i.e. complementary angle with a different positive α counting), layer numbering and loading into the CLT reference system is required by the analysis.

The following figures shall visualize this.

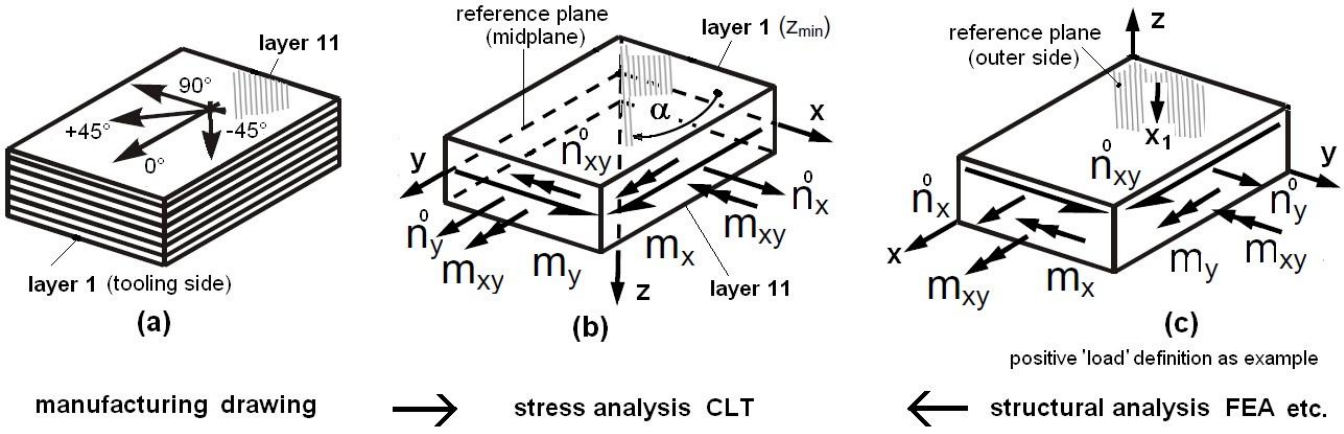


Fig.9-7: Layer numbering and reference system

The different worlds, which must be brought together, will be now more detailed:

1. Manufacturing world, sketch (a): Given in the manufacturing drawing (a) is a lay-up [45/0/-45/90/0/0/90/-45/0/45/-45] with t_k = 0.125mm, t = 1.375mm with the outer surface (top layer) counting 11 with an orientation angle of -45°
2. CLT world, sketch (b): Reference plane = mid-plane = action plane. $\{n_0\}= (20, 40, 60)^T$ N/mm, $\{m\} = (40, 15, 35)^T$ N·mm/mm. According to the CoS (b), which is applied in the stress analysis, the numbering and the positively angle-counted (x → x1) lay-up is to be transformed into the chosen CoS of (b) obtaining [45/-45/90/45/0/90/90/0/45/90/-45]. The top layer with an orientation angle of +45° counts 1, because the agreed sequence in writing the layers begins from left [45/0/..] beginning with 1 in positive direction of z
3. Analysis world, FEA, sketch (c): Reference plane is bottom surface (layer 1). Further, the loading is transformed from (b) into (c). Due to the change in direction the forces and moments to be inserted in the analysis read $\{n^0\}= (40, 20, 60)^T$ N/mm, $\{m\} = (15 - 40 \cdot t/2, 40 - 20 \cdot t/2, 35 - 60 \cdot t/2)^T = (-12.5, 26.25, 6.25)^T$ with {m} in N·mm/mm, z_n = t/2. The lay-up will be denoted in (c) as [-45/90/45/0/90/90/0/45/90/-45/45]. The top layer counts 11 with an orientation angle of +45° (x→ x1)
4. Re-transformation of the FEA-result into the stress analysis documentation convention, if applicable.

9.2.3 Note on indexing Poisson's ratios of UD materials in CLT

The definition of Poisson's ratios is not standardized, see e.g. *Tsai, Composites Design* with ν_{12} *(formerly).* Of course, there is no objective reason for the sequence of indices or to index ν_{21} or ν_{12}. This might have been the cause for the different use. In the international Aerospace Handbook HSB for instance ν_{12} is used for the larger Poisson's ratio to be conform with most of the FE manuals!

In the very early days, however, indexing of Poisson's ratio followed 'location' before 'cause'. This makes more sense and - in addition - follows the convention for the load quantities. This was the reason why, after many discussions and extensive literature work of the VDI-2014 working group in the nineties, to remain with the 'old' sequencing $\nu_{21} = - \varepsilon_2/\varepsilon_1$ as the larger Poisson's ratio. This corresponds to a so-called 'column normalization' which allows for a simple interpretation of uniaxial tests.

By the way: Tsai uses now again the 'old' suffix sequencing 'location' before 'cause' for the major Poisson's ratio as we have sticked to in the VDI 2014 Guideline, opposite to the HSB sheets. How can a provided Poisson's ratio be checked? In order to avoid misuse, each user of a program is asked to perform the Maxwell-Betti check (larger ν · smaller E-modulus = smaller ν · larger E-modulus) to become sure with the input. This check works for the lamina and the laminate as well.

> ***LL**: It should be mentioned that the letter C is used for the spatial or 3D stiffness elasticity matrix and the letter S for the compliance matrix as the inverted formulation of the stiffness matrix. This is just the other way round as the letters say and is unfortunately sometimes mixed- up.*

9.2.4 Conventions, Coordinate System of Plate and Beam

In structure-mechanical analyses, the definition of the coordinate system (CoS) is very differently performed. The same is valid for the path coordinate *s* in torsion and shear analysis. It is desirable to have a consistent use of the coordinate system *x, y, z* (deformations *u, v, w*) and of the path coordinate *s* as well.

- Right-handed (right-turning screw) coordinate system (CoS), *Fig.9-8*
- Positive section forces show at the positive section side (normal on the cross section shows in positive direction) in the positive coordinate direction
- Positive moments are mathematically defined for a beam by a right hand rule
- Path coordinates in case of thin-walled beams basically take a continuous course. They should always start at a free profile edge where the shear flow is zero. Sub-path coordinates of profile off-branches should start at free edges as well.

For a beam, no problem arises defining positive moments that are oriented in positive coordinate direction. From mathematics is known, that the curvature ρ of the beam is related to the function $w(x)$ by the relationship $\kappa = 1/\rho = w''/(1+w'^2)^{3/2}$, where ρ is the radius of the curvature. In geometrically linear elastic analysis the slope w' can be neglected in comparison to 1, leading to $\kappa \approx w''$. It is known from mechanics that the local curvature $\kappa(x)$ is proportional to the respective local bending moment $M_y(x)$. The three moments M_x, M_y, M_z are defined to be positive in positive coordinate directions. Hence, in beam theory a positive curvature causes a negative moment M_y =

$-EI_y \cdot w''$ but a positive $M_z = +EI_z \cdot v''$, *see Fig.9-9.* For a plate, no general definition is possible without violating any of the several procedures used: Mathematically positive moments pointing in the direction of the positive coordinates, or the positive moment-curvature relation, or the following convention. Therein a general agreement is accepted: the double arrows of bending and twisting moments are defined in a way that in a reference zone (e.g. many civil engineers are accustomed to using a dashed line for the beam and zone for the plate) normal stress and shear stress. In beam theory, the right hand rule applies for moments and M_y is a moment about the y-axis computed from σ_x-stresses, whereas in plate theory m_y is a moment that is computed from σ_y-stresses and acts about the x-axis.

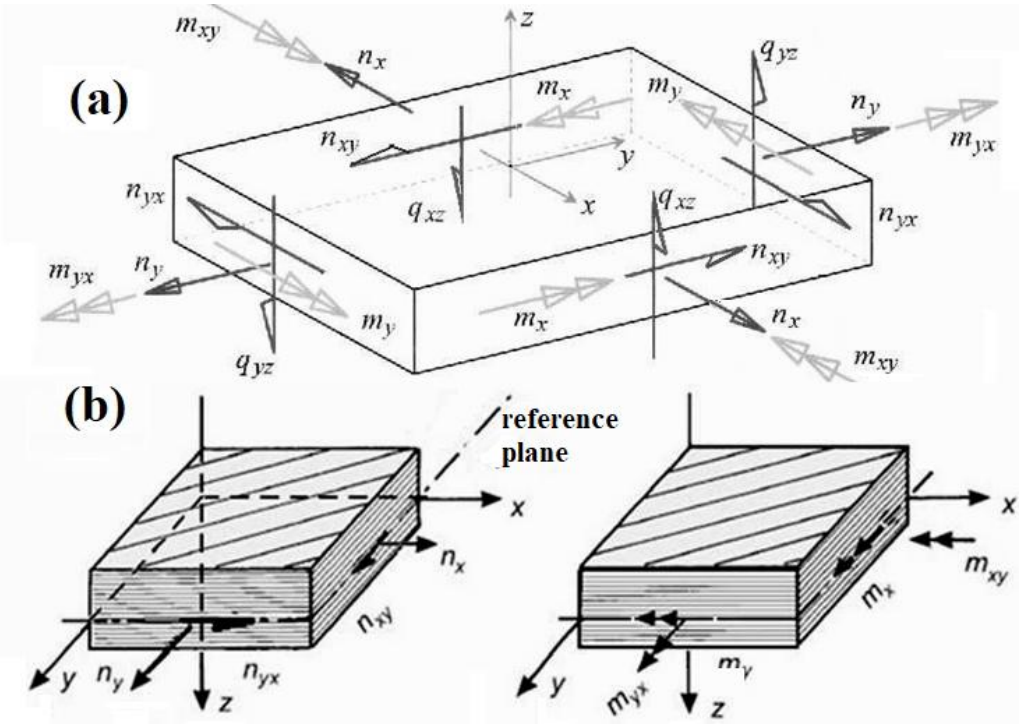


Fig.9-8: Plate designations, coordinates, section forces an section moments

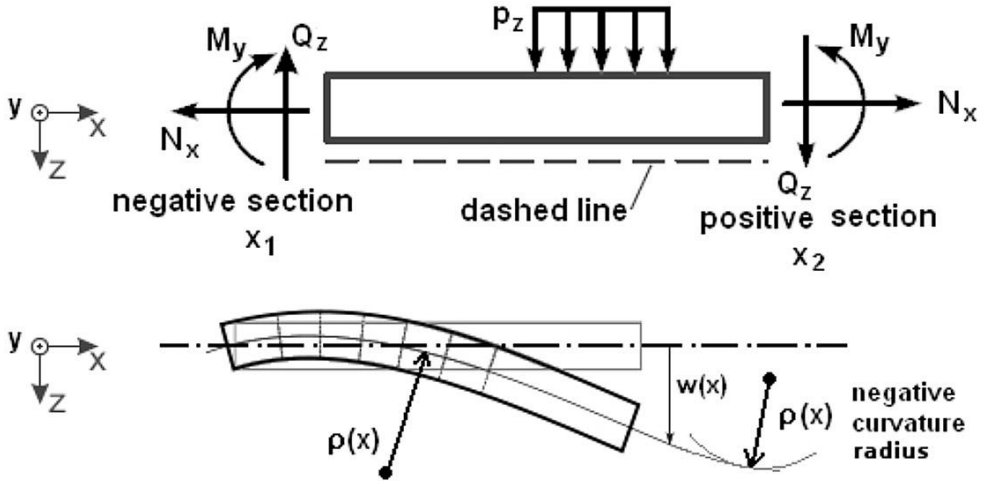


Fig.9-9: Coordinates, section forces and moment, deformation and curvature of a beam

Curvature relation of a Beam

9.2.5 Note on CLT-modelling of textile composites

When the CLT for laminates composed of UD laminas should be applied to textile-reinforced composites, the following steps need to be undertaken: (1) Theoretical decomposition of the textile composites into idealized UD laminas ((i)-UD layers). (2) Evaluation of experimentally determined stress-strain curves in different directions of the textile-reinforced composite.(3) Identification of the engineering constants of the i-UD layer by inverse identification or by numerical analysis.

- *Composites reinforced with non-crimp fabrics*

Composites reinforced with non-crimp fabrics (NCF) can usually be modelled without any major difficulties by the CLT for laminates composed of UD laminas as long as the fiber volume content in thickness direction is low enough. Most of the NCF composites have a polymeric stitch thread which melts during manufacturing. In this case, the CLT can be recommended. The correctness of CLT-based predictions for NCF composites with a reinforcing not melting stitch thread decreases with increased stitch thread volume content density.

- *Composites reinforced with woven fabrics*

It has to be stated that the reverse identification of engineering constants for i-UD layers of woven composites is not always possible especially when the warp/fill(weft) fiber content is not 1:1 such as a plain weave (e.g. for Atlas 1:4 reinforcement). Furthermore, research has shown that the reverse identification could lead to too high engineering constants so that the theoretically obtained stress-strain response of the woven composite is usually overestimated. To overcome this drawback, several researchers proposed so-called textile-specific correction factors. All engineering constants are multiplied with these factors in order to consider the influence of fiber waviness or of fiber misalignment on the engineering constants.

9.3 Collection of CLT Examples

Basis: The non-edited VDI 2014, sheet 3 Examples (Draft, about 2000) and an also non-edited HSB Draft 37103-01 (about 2015). The author retired later from this Working Group, IASB, he belonged to since 1972.

> *From these two Drafts the following CLT examples are 'copied' . For the shadows my Sorry.* The author could not bypass them. From legal reasons, a draft of an upcoming standard must be marked diagonally by the word DRAFT. Even the originator has then no further access.

In order to illustrate how the stack affects laminate stiffness matrix K and lamina stresses σ two types of use cases are presented. The first set refers to plates and the second to tubes. According to their rotational symmetry a tube cannot experience curvatures κ. This simplifies the computational work. Residual stresses and strength analysis are not addressed. As different units (*percent and micro-strain*) are used for the strains this is applied too in the tables of results.

***Given Materials*:** Two typical FRP/Epoxy UD material data sets, taken from HSB 37106-01 (moisture, [13]) and HSB 37110-01, [9].

* Lamina data: $V_f = 60\%$, the units for the α_M are written in a manner, similar to α_T. The 2D analysis requires 4 UD elasticity properties

* For the single layer or single ply (physical lamina) of the stack the following properties are given with the symbolic subscripts being related as 1= ||, 2 = ⊥ (*experience proved that the use of symbolic indices helps to avoid input mistakes with the properties*):

	$E_{\parallel}$	$E_{\perp}$	$G_{\parallel\perp}$	$\nu_{\parallel\perp}$	$\alpha_{T\parallel}$	$\alpha_{T\perp}$	$\alpha_{M\parallel}$	$\alpha_{M\perp}$
	MPa	MPa	MPa	–	$10^{-6}\cdot$ mm/(mm·K)		$10^{-4}\cdot$ mm/(mm·%)	
GFRP	45200	11600	4500	0.27	6	22	0	55
CFRP	132700	9300	4600	0.28	0.23	29	1	42

Configuration: z-coordinate and numbering of layers 'downward'

$$\{\varepsilon\}_k = [S]_k \cdot \{\sigma\}_k\,, \quad \{\sigma\}_k = [Q]_k \cdot \{\varepsilon\}_k \quad \text{with} \quad [Q]_k = [S]_k^{-1}$$

$$\{\varepsilon\}_k = [S]_k \cdot \{\sigma\}_k\,, \quad \{\sigma'\}_k = [Q]'_k \cdot \{\varepsilon'\}_k \quad \text{with} \quad [Q']_k = [T_\sigma]_k \cdot [Q]_k \cdot [T_\sigma]_k^{T}$$

$$\{\varepsilon\}_k = [T_\varepsilon]_k^{-1} \cdot \{\varepsilon'\}_k = [T_\sigma]_k^{-1} \cdot \left(\{\varepsilon^0\} + z_k \cdot \{\kappa\}\right)\,.$$

$$\begin{Bmatrix} n^0 \\ \hline m \end{Bmatrix} = [K] \begin{Bmatrix} \varepsilon^0 \\ \hline \chi \end{Bmatrix} \quad \text{mit} \quad [K] = \left\{\begin{array}{c|c} A & B \\ \hline B & D \end{array}\right\} \cdot \begin{bmatrix} \square & \square & & & & \\ \square & \square & & & & \\ & & \square & & & \\ & & & \square & \square & 0 \\ & & & \square & \square & 0 \\ & & & 0 & 0 & \square \end{bmatrix}$$

$$[S] = \begin{bmatrix} \frac{1}{E_{\parallel}} & \frac{-\nu_{\parallel\perp}}{E_{\perp}} & 0 \\ \frac{-\nu_{\perp\parallel}}{E_{\parallel}} & \frac{1}{E_{\perp}} & 0 \\ 0 & 0 & \frac{1}{G_{\perp\parallel}} \end{bmatrix} \qquad [Q] = \begin{bmatrix} \frac{E_{\parallel}}{1-\nu_{\parallel\perp}\nu_{\perp\parallel}} & \frac{\nu_{\perp\parallel}E_{\perp}}{1-\nu_{\parallel\perp}\nu_{\perp\parallel}} & 0 \\ \frac{\nu_{\parallel\perp}E_{\parallel}}{1-\nu_{\parallel\perp}\nu_{\perp\parallel}} & \frac{E_{\perp}}{1-\nu_{\parallel\perp}\nu_{\perp\parallel}} & 0 \\ 0 & 0 & G_{\perp\parallel} \end{bmatrix}$$

9.3.1 CFRP: Symmetric Stack [0/90/90/0] = [0/90]s, t =1.0 mm, t_k = 0.25 mm

Task:

"*Determination of stiffness matrix, lamina strains and stresses considering 3 reference planes".*

Calculation: Material data see above

The computation is linear. Two variants of reference planes (a), (b) are to investigate. At first, the stiffness (elasticity) matrix of the UD material in the (local) lamina CoS is computed

$$[Q] = \begin{bmatrix} 133433 & 2618 & 0 \\ 2618 & 9351 & 0 \\ 0 & 0 & 4600 \end{bmatrix} \text{MPa}\,.$$

In order to achieve the contribution of each lamina to the laminate stiffness the associated stiffness matrix of each lamina has to be transformed into the laminate COS by the transformation matrices

$$[T_\sigma]_2 = [T_\sigma]_3 = \begin{bmatrix} 0 & 1 & 0 \\ 1 & 0 & 0 \\ 0 & 0 & -1 \end{bmatrix}\,, \quad [T_\sigma]_1 = [T_\sigma]_4 = \begin{bmatrix} 1 & 0 & 0 \\ 0 & 1 & 0 \\ 0 & 0 & 1 \end{bmatrix}$$

which delivers in the (global) laminate CoS

$$[Q']_1 = [Q']_4 = \begin{bmatrix} 133433 & 2618 & 0 \\ 2618 & 9351 & 0 \\ 0 & 0 & 4600 \end{bmatrix} \text{MPa}, [Q']_2 = [Q']_3 = \begin{bmatrix} 9351 & 2618 & 0 \\ 2618 & 133433 & 0 \\ 0 & 0 & 4600 \end{bmatrix} \text{MPa}.$$

<u>Variant (a)</u> : Loading acts in mid-plane, midplane is chosen as reference plane

Given: Loading $\{n^0\} = (300, 0, 0)^T$ N/mm, $\{m\} = (50, 0, 0)^T$ N·mm/mm

The superscript ^{0} denotes the reference plane, which might be the mid-plane!

The laminate stiffness matrix reads

$$[K] = \begin{bmatrix} A & B \\ B & D \end{bmatrix} = \begin{bmatrix} 71392 & 2618 & 0 & 0 & 0 & 0 \\ 2618 & 71392 & 0 & 0 & 0 & 0 \\ 0 & 0 & 4600 & 0 & 0 & 0 \\ 0 & 0 & 0 & 9827 & 218.2 & 0 \\ 0 & 0 & 0 & 218.2 & 2072 & 0 \\ 0 & 0 & 0 & 0 & 0 & 383.3 \end{bmatrix}$$

with $[A]$ in MPa ·mm =N/mm, $[B]$ in MPa ·mm^2= N, $[D]$ in MPa ·mm^3 and its inverse

$$[K]^{-1} = \begin{bmatrix} 1.40 & -0.05 & 0 & 0 & 0 & 0 \\ -0.05 & 1.40 & 0 & 0 & 0 & 0 \\ 0 & 0 & 21.7 & 0 & 0 & 0 \\ 0 & 0 & 0 & 10.2 & -1.07 & 0 \\ 0 & 0 & 0 & -1.07 & 48.4 & 0 \\ 0 & 0 & 0 & 0 & 0 & 260.9 \end{bmatrix} \cdot 10^{-5}$$

.

The effective elasticity constants of the laminate (*membrane loading*) are computed via stiffness or via compliances as

$$\widehat{E_x} = \frac{A_{11} - A_{12}^2/A_{22}}{t} = (71392 - 2613^2/71392)/1.00\,\text{MPa} = 71296\,\text{MPa}$$

$$\widehat{E_x} = \frac{1}{A_{11}^* \cdot t} = 1/(1.40 \cdot 10^{-5} \cdot 1.00)\,\text{MPa} = 71296\,\text{MPa}.$$

$$\widehat{E_x} = 71296\,\text{MPa} = \widehat{E_y}, \quad \widehat{G_{xy}} = 4600\,\text{MPa}, \quad \widehat{\nu_{xy}} = -\frac{-0.05}{1.40} = 0.037 = \widehat{\nu_{yx}}.$$

Effective laminate stiffness per width for bending and torsion follows as

$$\widehat{EI_x} = D_{11} = 9827\,\text{MPa}\cdot\text{mm}^3 > D_{11}^{*-1}, \widehat{EI_y} = 2072\,\text{MPa}\cdot\text{mm}^3, \widehat{GI_t} = 4 \cdot 383.3\,\text{MPa}\cdot\text{mm}^3.$$

Finally, the 'rotated' strains of the midplane, regarding the laminate CoS, are calculated as

$$\{\varepsilon^0\} = \begin{Bmatrix} 4.2 \\ -0.2 \\ 0 \end{Bmatrix} \cdot 10^{-3}, \qquad \{\kappa\} = \begin{Bmatrix} 5.1 \\ -0.5 \\ 0 \end{Bmatrix} \cdot 10^{-3} \cdot 1/\text{mm}\,.$$

Herewith, the vector of strains at the boundary surfaces of the laminas can be determined

layer number	1	1	2	2	3	3	4	4
fiber angle	0°	0°	90°	90°	90°	90°	0°	0°
z in mm	−0.5	−0.25	−0.25	0	0	0.25	0.25	0.5
ε_x in 10^{-3} ·mm/mm	1.7	2.9	2.9	4.2	4.2	5.5	5.5	6.8
ε_y in 10^{-3} ·mm/mm	0.1	0	0	-0.2	−0.2	−0.3	-0.3	−0.4
γ_{yx} in 10^{-3} ·mm/mm	0	0	0	0	0	0	0	0

and the lamina strains and stresses in the four laminas

z in mm	−0.5	−0.25	−0.25	0	0	0.25	0.25	0.5
$\varepsilon_{\|\|}$ in $10^{-3}\cdot$mm/mm	1.7	2.9	0	−0.2	−0.2	−0.3	5.5	6.8
$\varepsilon_{\perp}$ in $10^{-3}\cdot$mm/mm	0.1	0	2.9	4.2	4.2	5.5	-0.3	−0.4
$\gamma_{\perp\|\|}$ in $10^{-3}\cdot$mm/mm	0	0	0	0	0	0	0	0
$\sigma_{\|\|}$ in MPa	221.5	391.3	5.0	-9.6	-9.6	-24.2	730.8	900.6
$\sigma_{\perp}$ in MPa	5.4	7.5	27.4	38.9	38.9	50.5	11.7	13.7
$\tau_{\perp\|\|}$ in MPa	0	0	0	0	0	0	0	0

Consideration of the Off-set of Section forces: For variant (b)

Section forces which do not act in the reference plane can be considered by

$$\{m\} = (m_x, m_y, m_{xy})^T = \int_{z_{bot}}^{z_{top}} \{\sigma'\}\cdot z\cdot dz - [z_{off}]\cdot\{n^0\} \quad \text{with} \quad [z_{off}] = \begin{bmatrix} z_{off_x} & 0 & 0 \\ 0 & z_{off_y} & 0 \\ 0 & 0 & z_{off_{xy}} \end{bmatrix}$$

defining the offset of the action plane of each section force. Values for each of the three section forces $\{n^0\}$ and three section moments $\{m\}$ are derived from component analysis. Of course, one could geometrically link those section forces and moments which act in the same plane.

Assuming a linear law of elasticity the following relations are obtained for the laminate

$$\begin{Bmatrix} n^0 \\ m \end{Bmatrix} = \begin{bmatrix} \boldsymbol{A} & \boldsymbol{B} - |z_{off}|\cdot\boldsymbol{A} \\ \boldsymbol{B} - |z_{off}|\cdot\boldsymbol{A} & \boldsymbol{D} - |z_{off}|\cdot\boldsymbol{B} \end{bmatrix} \cdot \begin{Bmatrix} \varepsilon^0 \\ \kappa \end{Bmatrix} = [K]\cdot\begin{Bmatrix} \varepsilon^0 \\ \kappa \end{Bmatrix}.$$

Usually, the loadings are delivered from the structural analysis such that just one z_{off} is to consider.

<u>Variant (b):</u> Loading acts in mid-plane, top surface is chosen as reference plane

Given:

The given midplane force is acting at a distance of z= +0.25 mm to the reference plane. This is considered in the reference plane by an additional moment.

$$\{n^0\} = (300,\ 0,\ 0)^T \text{ Nmm}, \quad \{m\} = (50 + z_{off,nx}\cdot 300,\ 0,\ 0)^T \text{ Nmm/mm}, \quad z_{off,nx} = 0.25\text{mm}$$

The laminate stiffness matrix and its inverse read

$$[K] = \begin{bmatrix} \boldsymbol{A} & \boldsymbol{B} \\ \boldsymbol{B} & \boldsymbol{D} \end{bmatrix} = \begin{bmatrix} 71392 & 2618 & 0 & 17848 & 655 & 0 \\ 2618 & 71392 & 0 & 655 & 17848 & 0 \\ 0 & 0 & 4600 & 0 & 0 & 1150 \\ 17848 & 655 & 0 & 14289 & 382 & 0 \\ 655 & 17848 & 0 & 382 & 6534 & 0 \\ 0 & 0 & 1150 & 0 & 0 & 671 \end{bmatrix},$$

$$[K]^{-1} = \begin{bmatrix} 2.04 & -0.12 & 0 & -2.55 & 0.27 & 0 \\ -0.12 & 4.43 & 0 & 0.27 & -12.1 & 0 \\ 0 & 0 & 38.0 & 0 & 0 & -65.2 \\ -2.55 & 0.27 & 0 & 10.2 & -1.07 & 0 \\ 0.27 & -12.1 & 0 & -1.07 & 48.4 & 0 \\ 0 & 0 & -65.2 & 0 & 0 & 260.9 \end{bmatrix} \cdot 10^{-5}.$$

The effective elasticity constants are as in Variant (a) but the effective laminate stiffness read

$$\widehat{EI_x} = 14289\,\text{MPa}\cdot\text{mm}^3,\ \widehat{EI_y} = 6534\,\text{MPa}\cdot\text{mm}^3,\ \widehat{GI_t} = 4\cdot 671\,\text{MPa}\cdot\text{mm}^3.$$

The strains of the reference plane are calculated as

$$\{\varepsilon^0\} = \begin{Bmatrix} 2.9 \\ 0 \\ 0 \end{Bmatrix} \cdot 10^{-3}, \qquad \{\kappa\} = \begin{Bmatrix} 5.1 \\ -0.5 \\ 0 \end{Bmatrix} \cdot 10^{-3} \cdot 1/\text{mm}\,.$$

Herewith, the vector of strains $\{\varepsilon'\}$ at the boundary surfaces of the laminas can be determined

layer number	1	1	2	2	3	3	4	4
fiber angle	0°	0°	90°	90°	90°	90°	0°	0°
z in mm	−0.25	0	0	0.25	0.25	0.5	0.5	0.75
ε_x in 10^{-3} · mm/mm	1.7	2.9	0	-0.2	−0.2	−0.3	5.5	6.8
ε_y in 10^{-3} · mm/mm	0.1	0	2.9	4.2	4.2	5.5	- 0.3	−0.4
γ_{yx} in 10^{-3} · mm/mm	0	0	0	0	0	0	0	0

and the lamina stresses and strains at the boundary surfaces

z in mm	−0.25	0	0	0.25	0.25	0.5	0.5	0.75
$\varepsilon_{\parallel}$ in 10^{-3} · mm/mm	1.7	2.9	0	−0.2	−0.2	−0.3	5.5	6.8
$\varepsilon_{\perp}$ in 10^{-3} · mm/mm	0.1	0	2.9	4.2	4.2	5.5	-0.3	−0.4
$\gamma_{\perp\parallel}$ in 10^{-3} · mm/mm	0	0	0	0	0	0	0	0
$\sigma_{\parallel}$ in MPa	221.5	391.3	5.0	-9.6	-9.6	-24.2	730.8	900.6
$\sigma_{\perp}$ in MPa	5.4	7.5	27.4	38.9	38.9	50.5	11.7	13.7
$\tau_{\perp\parallel}$ in MPa	0	0	0	0	0	0	0	0

.

Notes on the effect of differently chosen reference planes in both the variants:

Variant (a)

$$\kappa_x = m_x/D_{11} = (50\,\text{N}\cdot\text{mm/mm})/9827\,\text{N}\cdot\text{mm} = 5.1\cdot10^{-3}\,\text{mm}^{-1} \equiv 50\cdot10.2\cdot10^{-5}\,\text{mm}^{-1}$$

$$\begin{Bmatrix} \varepsilon_x^0 \\ \varepsilon_y^0 \\ \gamma_{xy}^0 \\ \kappa_x \\ \kappa_y \\ \kappa_{xy} \end{Bmatrix} = \begin{bmatrix} 1.40 & -0.05 & 0 & 0 & 0 & 0 \\ -0.05 & 1.40 & 0 & 0 & 0 & 0 \\ 0 & 0 & 21.7 & 0 & 0 & 0 \\ 0 & 0 & 0 & 10.2 & -1.07 & 0 \\ 0 & 0 & 0 & -1.07 & 48.4 & 0 \\ 0 & 0 & 0 & 0 & 0 & 260.9 \end{bmatrix} 10^{-5} \cdot \begin{Bmatrix} 300 \\ 0 \\ 0 \\ 50 \\ 0 \\ 0 \end{Bmatrix},$$

Variant (b)

$$\kappa_x = B_{11}\cdot n_x^0 + D_{11}\cdot(m_x + z_{offx}\cdot n_x^0) =$$

$$(-2.55\cdot10^{-5}/\text{N})\cdot300\,\text{N/mm} + (10.2\cdot10^{-5}/\text{N}\cdot\text{mm})\cdot125\,\text{N} = 5.1\cdot10^{-3}\,\text{mm}^{-1}\ \text{using}$$

$$\begin{Bmatrix} \varepsilon_x^0 \\ \varepsilon_y^0 \\ \gamma_{xy}^0 \\ \kappa_x \\ \kappa_y \\ \kappa_{xy} \end{Bmatrix} = \begin{bmatrix} 2.04 & -0.12 & 0 & -2.55 & 0.27 & 0 \\ -0.12 & 4.43 & 0 & 0.27 & -12.1 & 0 \\ 0 & 0 & 38.0 & 0 & 0 & -65.2 \\ -2.55 & 0.27 & 0 & 10.2 & -1.07 & 0 \\ 0.27 & -12.1 & 0 & -1.07 & 48.4 & 0 \\ 0 & 0 & -65.2 & 0 & 0 & 260.9 \end{bmatrix} \cdot 10^{-5} \cdot \begin{Bmatrix} 300 \\ 0 \\ 0 \\ 125 \\ 0 \\ 0 \end{Bmatrix}.$$

The increase in laminate bending stiffness has no effect on κ_x due to the transferred moment, similar to strains and stresses.

<u>Variant (c):</u> loading acts at the top surface, that is further taken as reference plane

Given: Loading $\{n^0\} = (300,\ 0,\ 0)^T\ \mathrm{N\cdot mm},\quad \{m\} = (200,\ 0,\ 0)^T\ \mathrm{N\cdot mm/mm}.$

The laminate stiffness matrix (in MPa, mm) reads

$$[K] = \begin{bmatrix} A & B \\ B & D \end{bmatrix} = \begin{bmatrix} 71392 & 2618 & 0 & 35696 & 1309 & 0 \\ 2618 & 71392 & 0 & 1309 & 35696 & 0 \\ 0 & 0 & 4600 & 0 & 0 & 2300 \\ 35696 & 1309 & 0 & 27675 & 873 & 0 \\ 1309 & 35696 & 0 & 873 & 19920 & 0 \\ 0 & 0 & 2300 & 0 & 0 & 1533 \end{bmatrix},$$

Effective elastic constants are as in Variant (a). Effective laminate stiffness reads

$$\widehat{EI_x} = 27675\ \mathrm{MPa\cdot mm^3},\ \widehat{EI_y} = 19920\ \mathrm{MPa\cdot mm^3},\ \widehat{GI_t} = 4\cdot 1533\ \mathrm{MPa\cdot mm^3}$$

As strains of the reference plane are calculated

$$\{\varepsilon^0\} = \begin{Bmatrix} 1.7 \\ 0.1 \\ 0 \end{Bmatrix} \qquad \{\kappa\} = \begin{Bmatrix} 5.1 \\ -0.5 \\ 0 \end{Bmatrix} \cdot 10^{-3}\cdot 1/\mathrm{mm}.$$

The strains (laminate CoS) at the boundary surfaces of the 4 layers read

layer number	1	1	2	2	3	3	4	4
fiber angle	0°	0°	90°	90°	90°	90°	0°	0°
z in mm	0	0.25	0.25	0.5	0.5	0.75	0.75	1.0
ε_x in $10^{-3}\cdot$mm/mm	1.7	2.9	2.9	4.2	4.5	5.5	5.5	6.8
ε_y in $10^{-3}\cdot$mm/mm	0.1	0.0	0.0	-0.2	-0.2	-0.3	-0.3	-0.4
γ_{yx} in $10^{-3}\cdot$mm/mm	0	0	0	0	0	0	0	0

In order to sort out those laminas which might be critical, both the lamina surfaces, marked by z_{k-1} and z_k, in the laminate are to check. Often, the worse side is still known from mechanical considerations.

And the lamina strains and stresses

z in mm	0	0.25	0.25	0.5	0.5	0.75	0.75	1.0
$\varepsilon_{\parallel}$ in $10^{-3}\cdot$mm/mm	1.7	2.9	0	−0.2	−0.2	−0.3	5.5	6.8
$\varepsilon_{\perp}$ in $10^{-3}\cdot$mm/mm	0.1	0	2.9	4.2	4.2	5.5	-0.3	−0.4
$\gamma_{\perp\parallel}$ in $10^{-3}\cdot$mm/mm	0	0	0	0	0	0	0	0
$\sigma_{\parallel}$ in MPa	221.5	391.3	5.0	-9.6	-9.6	-24.2	730.8	900.6
$\sigma_{\perp}$ in MPa	5.4	7.5	27.4	38.9	38.9	50.5	11.7	13.7
$\tau_{\perp\parallel}$ in MPa	0	0	0	0	0	0	0	0

9.3.2 CFRP: Anti-symmetric Stack [0/90/0/90], t = 1.00 mm, t_k = 0.25 mm

Just the main results of this "cross-ply"-laminate are summed up in this paragraph.

Task: Determination of stiffness matrix, lamina strains and stresses (computation is linear).

Given: Loading $\{n^0\} = (140,\ 0,\ 0)^T\ \mathrm{Nmm},\quad \{m\} = (0,\ 10,\ 0)^T\ \mathrm{Nmm/mm}$

Action plane = mid-plane = reference plane

Computation:

According to the asymmetric stack the sub-matrix [B] is not zero anymore.
The laminate stiffness matrix [K] , inverse $[K]^{-1}\cdot 10^{-5}$ read

$$\begin{bmatrix} 71392 & 2618 & 0 & -7755 & 0 & 0 \\ 2618 & 71392 & 0 & 0 & 7755 & 0 \\ 0 & 0 & 4600 & 0 & 0 & 0 \\ -7755 & 0 & 0 & 5949 & 218 & 0 \\ 0 & 7755 & 0 & 218 & 5949 & 0 \\ 0 & 0 & 0 & 0 & 0 & 383 \end{bmatrix}, \quad \begin{bmatrix} 1.63 & -0.06 & 0 & 2.13 & 0 & 0 \\ -0.06 & 1.63 & 0 & 0 & -2.13 & 0 \\ 0 & 0 & 21.7 & 0 & 0 & 0 \\ 2.13 & 0 & 0 & 19.6 & -0.72 & 0 \\ 0 & -2.13 & 0 & -0.72 & 19.6 & 0 \\ 0 & 0 & 0 & 0 & 0 & 261 \end{bmatrix} \cdot 10^{-5}$$

As elastic constants are yielded

$$\widehat{E_x} = 71296\,\text{MPa} = \widehat{E_y},\ \widehat{G_{xy}} = 4600\,\text{MPa},\ \widehat{\nu_{xy}} = 0.037 = \widehat{\nu_{yx}}.$$

The strains in the reference plane and the layer surfaces are

$$\{\varepsilon^0\} = \begin{Bmatrix} 2.3 \\ -0.3 \\ 0 \end{Bmatrix} \cdot 10^{-3}, \qquad \{\kappa\} = \begin{Bmatrix} 2.9 \\ 2.0 \\ 0 \end{Bmatrix} \cdot 10^{-3} \cdot 1/\text{mm}$$

layer number	1	1	2	2	3	3	4	4
fiber angle	0°	0°	90°	90°	0°	0°	90°	90°
z in mm	−0.5	−0.25	−0.25	0	0	0.25	0.25	0.5
ε_x in 10^{-3} · mm/mm	0.8	1.6	1.6	2.3	2.3	3.0	3.0	3.7
ε_y in 10^{-3} · mm/mm	−1.3	-0.8	−0.8	- 0.3	−0.3	0.2	0.2	0.7
γ_{yx} in 10^{-3} · mm/mm	0	0	0	0	0	0	0	0

z in mm	−0.5	−0.25	−0.25	0	0	0.25	0.25	0.5
$\varepsilon_{\parallel}$ in 10^{-3} · mm/mm	0.8	1.6	−0.8	−0.3	2.3	3.0	0.2	0.7
$\varepsilon_{\perp}$ in 10^{-3} · mm/mm	−1.3	-0.8	1.6	2.3	−0.3	0.2	3.0	3.7
$\gamma_{\perp\parallel}$ in 10^{-3} · mm/mm	0	0	0	0	0	0	0	0
$\sigma_{\parallel}$ in MPa	108	206	-101	-33.6	304.5	403	33.7	101
$\sigma_{\perp}$ in MPa	-9.8	-3.3	12.5	20.6	3.2	9.7	28.7	36.8
$\tau_{\perp\parallel}$ in MPa	0	0	0	0	0	0	0	0

9.3.3 CFRP: Non-symmetric Stack [0/10/90/70]**,** t = 0.5 mm, t_k = 0.125 mm

Just the main results are summed up in this paragraph.

Task: Determination of stiffness matrix, lamina strains and stresses (computation is linear).

Given: Loading $\{n^0\} = (100,\ 0,\ 0)^T$ Nmm, $\{m\} = (15,\ 10,\ 0)^T$ Nmm/mm

Action plane = mid-plane = reference plane

Computation:

$$[Q']_1 = \begin{bmatrix} 133433 & 2618 & 0 \\ 2618 & 9351 & 0 \\ 0 & 0 & 4600 \end{bmatrix} \text{MPa}, \quad [Q']_2 = \begin{bmatrix} 126207 & 6103 & 20183 \\ 6103 & 9608 & 1036 \\ 20183 & 1036 & 8084 \end{bmatrix},$$

$$[Q']_3 = \begin{bmatrix} 9351 & 2618 & 0 \\ 2618 & 133433 & 0 \\ 0 & 0 & 4600 \end{bmatrix} \text{MPa}, \quad [Q']_4 = \begin{bmatrix} 11559 & 14926 & 5272 \\ 14926 & 106611 & 34607 \\ 5272 & 34607 & 16907 \end{bmatrix},$$

The laminate stiffness matrix [K] , inverse $[K]^{-1}\cdot 10^{-5}$ read

$$\begin{bmatrix} 35069 & 3283 & 3182 & -3769 & 261 & -34 \\ 3283 & 32376 & 4455 & 261 & 3247 & 803 \\ 3182 & 4455 & 4274 & -34 & 803 & 261 \\ -3769 & 261 & -34 & 749 & 86 & 37 \\ 261 & 3247 & 803 & 86 & 622 & 158 \\ -34 & 803 & 261 & 37 & 158 & 106 \end{bmatrix}, \begin{bmatrix} 7.22 & -0.37 & -4.82 & 36.1 & -1.53 & 6.74 \\ -0.37 & 6.54 & -0.256 & -0.32 & -34.0 & 1.90 \\ -4.82 & -0.256 & 34.96 & -17.4 & -30.9 & -33.7 \\ 36.1 & -0.32 & -17.4 & 318.6 & -34.2 & -3.41 \\ -1.59 & -34.0 & -30.89 & -34.2 & 476 & -365 \\ 6.74 & 1.90 & -33.7 & -3.41 & -365 & 1559 \end{bmatrix} \cdot 10^{-5}$$

Users may want elasticity constant values, although the presumptions are violated!

$$\widehat{E_x} = 65400\,\text{MPa},\ \widehat{E_y} = 55462\,\text{MPa},\ \widehat{G_{xy}} = 6893\,\text{MPa},\ \widehat{\nu_{xy}} = 0.001,\ \widehat{\nu_{yx}} = 0.001.$$

Also, despite of the fact, that accurate effective laminate stiffness quantities of a laminate (membrane loading) can be just computed for 'symmetric lay-up', they may be further interested in a stiffness information:

$$\widehat{EI_x} = 749\,\text{MPa}\cdot\text{mm}^3,\ \widehat{EI_y} = 622\,\text{MPa}\cdot\text{mm}^3,\ \widehat{GI_t} = 4\cdot 106\,\text{MPa}\cdot\text{mm}^3.$$

Strains and curvatures in the laminate CoS read

$$\{\varepsilon^0\} = \begin{Bmatrix} 12.6 \\ -0.4 \\ -7.4 \end{Bmatrix} \cdot 10^{-3}, \qquad \{\kappa\} = \begin{Bmatrix} 83.9 \\ -6.7 \\ 6.2 \end{Bmatrix} \cdot 10^{-3} \cdot 1/\text{mm}\,.$$

and at the surfaces

layer number	1	1	2	2	3	3	4	4
fiber angle	0°	0°	10°	10°	90°	90°	70°	70°
z in mm	−0.25	−0.125	−0.125	0	0	0.125	0.125	0.25
ε_x in $10^{-3}\cdot$mm/mm	-8.3	2.1	2.1	12.6	12.6	23.1	23.1	33.6
ε_y in $10^{-3}\cdot$mm/mm	1.3	0.4	0.4	-0.4	-0.4	-1.3	-1.3	-2.1
γ_{yx} in $10^{-3}\cdot$mm/mm	-9.0	-8.2	-8.2	-7.4	-7.4	-6.6	-6.6	-5.9

z in mm	−0.25	−0.125	−0.125	0	0	0.125	0.125	0.25
$\varepsilon_{\|\|}$ in $10^{-3}\cdot$mm/mm	-8.3	2.15	0.7	11.0	-0.4	-1.3	-0.5	0.2
$\varepsilon_{\perp}$ in $10^{-3}\cdot$mm/mm	1.3	0.4	1.9	1.25	12.6	23.1	22.4	31.3
$\gamma_{\perp\|\|}$ in $10^{-3}\cdot$mm/mm	-8.98	-8.2	-8.3	-11.4	7.4	6.6	-10.6	-18.5
$\sigma_{\|\|}$ in MPa	-1109	288	97.7	1467	-22.4	-107	-13.5	107.8
$\sigma_{\perp}$ in MPa	-9.98	9.61	19.4	40.43	117	213	208	293.3
$\tau_{\perp\|\|}$ in MPa	-41.3	-37.7	-38.2	-52.6	34.1	117	-48.7	-84.9

.

9.3.4 Inclined test specimen application, UD CFR Epoxide and Nylon-reinforced Elastomer

1. Tasks *"Important for 'inclined tensile test specimen' (not recommended) and for tire industry)"*

- Searched: Elasticity matrices and stress vector, strain vector
- Given: Loading and Geometry: $\{\sigma'\} = (400, 60, 15)^T$ in laminate CoS, t = 1 mm,

  rotation angle α = +45° to lamina CoS

  Lay-up: [45°]

  test data set for $V_f = \varphi = 0.6$

	CFRP	Nylon-reinforced elastomer	
$E_{\|\|}$	135000	910	N/mm^2
$E_{\perp}$	9470	7.24	
$G_{\|\|\perp}$	5270	1.81	
$\nu_{\perp\|\|}$	0.28	0.36	

2. CFRP inclined test specimen, Calculations

2.1 Determination of the transformation matrices $[T_\sigma]$ und $[T_\varepsilon]$, $s^2 = \sin(45°)^2 = \left(\sqrt{2}/2\right)^2 \equiv c^2$

$$[T_\sigma] = \begin{bmatrix} c^2 & s^2 & 2sc \\ s^2 & c^2 & -2sc \\ -sc & sc & c^2-s^2 \end{bmatrix} = \begin{bmatrix} 0.5 & 0.5 & 1.0 \\ 0.5 & 0.5 & -1.0 \\ -0.5 & 0.5 & 0 \end{bmatrix}, \quad [T_\varepsilon] = \begin{bmatrix} c^2 & s^2 & sc \\ s^2 & c^2 & -sc \\ -2sc & 2sc & c^2-s^2 \end{bmatrix} = \begin{bmatrix} 0.5 & 0.5 & 0.5 \\ 0.5 & 0.5 & -0.5 \\ -1 & 1 & 0 \end{bmatrix},$$

2.2 Determination of elasticity matrices, stiffness matrix [Q], compliance matrix [S]

$$[Q] = \begin{bmatrix} 135747 & 2666 & 0 \\ 2666 & 4522 & 0 \\ 0 & 0 & 5270 \end{bmatrix} \frac{N}{mm^2}, \quad [S] = \begin{bmatrix} 0.74 & -20.74 & 0 \\ -20.74 & 10.56 & 0 \\ 0 & 0 & 18.98 \end{bmatrix} \cdot 10^{-5} \frac{mm^2}{N} \quad \text{orthotropic}$$

2.3 Determination of the rotated matrices [Q'], [S'] with the 'matrix multiplication procedure'

$$[Q'] = [T_\sigma]\,[Q]\,[T_\sigma]^T \qquad [S'] = [T_\varepsilon]\,[S]\,[T_\varepsilon]^T = [Q']^{-1}$$

$$\begin{bmatrix} 0{,}5 & 0{,}5 & -0{,}5 \\ 0{,}5 & 0{,}5 & +0{,}5 \\ +1 & -1 & 0 \end{bmatrix} \qquad \begin{bmatrix} 0{,}5 & 0{,}5 & -1 \\ 0{,}5 & 0{,}5 & 1 \\ 0{,}5 & -0{,}5 & 0 \end{bmatrix}$$

$$\begin{bmatrix} 1357{,}47 & 26{,}66 & 0 \\ 26{,}66 & 45{,}22 & 0 \\ 0 & 0 & 52{,}70 \end{bmatrix} \begin{bmatrix} & & \\ +52{,}70 & -52{,}70 & 0 \end{bmatrix} \begin{bmatrix} 0{,}741 & -20{,}74 & 0 \\ -20{,}74 & 10{,}56 & 0 \\ 0 & 0 & 18{,}98 \end{bmatrix} \begin{bmatrix} \\ \\ 0 \end{bmatrix}$$

$$\begin{bmatrix} 0{,}5 & 0{,}5 & 1{,}0 \\ 0{,}5 & 0{,}5 & -1{,}0 \\ -0{,}5 & 0{,}5 & 0 \end{bmatrix} = \begin{bmatrix} 42{,}92 & 32{,}38 & -31{,}56 \\ & 42{,}92 & -31{,}56 \\ (\text{symm}) & & 34{,}98 \end{bmatrix} \begin{bmatrix} 0{,}5 & 0{,}5 & 0{,}5 \\ 0{,}5 & 0{,}5 & -0{,}5 \\ -1 & 1 & 0 \end{bmatrix} = \begin{bmatrix} 7{,}47 & -2{,}02 & 4{,}91 \\ & 7{,}47 & 4{,}91 \\ (\text{symm}) & & 11{,}72 \end{bmatrix}$$

$[Q']$ in 10^3 N/mm^2 $\qquad$ $[S']$ in 10^{-5} mm^2/N

2.4 Determination of the lamina stress vector $\{\sigma\}$ from transformation $\{\sigma\} = [T_\sigma]^{-1} \cdot \{\sigma'\}$

$$\{\sigma'\} = (400, 60, 15)^T \quad \rightarrow \quad \{\sigma\} = (215, 245, 170)^T \text{ N/mm}^2$$

$$\begin{bmatrix} 0{,}5 & 0{,}5 & -1 \\ 0{,}5 & 0{,}5 & 1 \\ 0{,}5 & -0{,}5 & 0 \end{bmatrix} \cdot \begin{bmatrix} 400 \\ 60 \\ 15 \end{bmatrix} \text{ N/mm}^2 = \begin{bmatrix} 215 \\ 245 \\ 170 \end{bmatrix} \text{ N/mm}^2$$

2.5 Some 'rotated' lamina strain vectors $\{\varepsilon'\} = [S']\,\{\sigma'\}$

$$\{\sigma'\} = (400, 0, 0)^T \rightarrow \{\varepsilon'\} = [S']\,\{\sigma'\} = [29.9, -8.1, +19.6)^T \cdot 10^{-3}$$

$$10^{-5} \frac{mm^2}{N} \begin{bmatrix} 7{,}47 & -2{,}02 & 4{,}91 \\ -2{,}02 & 7{,}47 & 4{,}91 \\ 4{,}91 & 4{,}91 & 11{,}72 \end{bmatrix} \cdot \begin{bmatrix} 400 \\ 0 \\ 0 \end{bmatrix} N/mm^2 = \begin{bmatrix} 29{,}9 \\ -8{,}1 \\ 19{,}6 \end{bmatrix} \cdot 10^{-3} \cdot$$

And in lamina CoS $\{\sigma\} = (200, 200, 200)^T$ N/mm^2, $\{\varepsilon\} = (1.07, 20.7, 38.0)^T \cdot 10^{-3}$

All 3 strains are caused. This is a warning for the use of the " Inclined tensile test specimen "!

$\alpha = +45°$, $\{\sigma'\} = (0, 0, 15)^T \quad \rightarrow \quad \{\varepsilon'\} = [S']\,\{\sigma'\} = (0.736, +0.736, +1.76)^T \cdot 10^{-3}$

$\alpha = -45°$, $\{\sigma'\} = (0, 0, 15)^T \quad \rightarrow \quad \{\varepsilon'\} = (-0.736, -0.736,, +1.76)^T \cdot 10^{-3}$

$\{\sigma\} = (15, -15, 0)^T$ N/mm^2, $\{\varepsilon\} = (0.142, +1.62, 0)^T \cdot 10^{-3}$

3. Nylon reinforced elastomer and CFRP: Comparison

3.1 Compliance elasticity matrix of Nylon reinforced elastomer ($\alpha = +45°$)

$$[S] = \begin{bmatrix} 1.1 & -39.6 & 0 \\ -39.6 & 138.0 & 0 \\ 0 & 0 & 552.5 \end{bmatrix} \cdot 10^{-3}\, mm^2 / N$$

3.2 Dependence of shear angle γ_{12} from lamina fiber angle α

For the stress state $\{\sigma'\} = (+400, 0, 0)^T$ N/mm^2 its behavior can essentially be studied in regarding

$S'_{61} = -2\, S_{11}\, c^3 s + 2\, S_{22}\, cs^3 - 2\, S_{12}\, (cs^3 - c^3 s) + S_{66}\, (c^3 s - cs^3)$ with c = CoS(α), s = sin (α)

It results for different positive angles α, whereby /α/ = ω, the following table

	α	-45°	-15°	0°	15°	30°	45°	60°	75°	90°
Nylon	S'_{61}	-0.069		0	0.124	0.149	0.069	-0.03	-0.055	0
	γ_{yx}	-27.4		0	> 0	> 0	> 0	-12.0	< 0!	0
CFRP	S'_{61}	0.491		0	0.402	0.60	0.491	+0.25	0.07	0
	γ_{xy}	-0.020		0	> 0	> 0	+0.020	> 0	> 0	0

***LL**:*
Tire industry material thus responds in an angular range +45° < α < +75° with a desired negative shear angle γ_{xy} !

9.3.5 Stresses in CFRP test specimens under mechanical, temperature and humidity loading

1 Task *"Comparison of 2D Stress states caused by three unity load cases"*

- Calculation of laminate distortions and lamina stresses
- Evaluation of lamina stresses with specified uniaxial strength values.

2 Input

- Tensile test specimen with 8 Prepreg layers, width 16 mm and laminate lay-up $[0/90/45/-45]_s$
- Given: Properties CFRP , see Table.

a) Temperature decay by $\Delta T_k = \Delta T = -100$ K (curing level → room temperature)

b) Change of moisture concentration by a take-up of $\Delta M_k = \Delta M = 1$ % (*after saturation, when the relative humidity changes by approximately 55% at room (ambient) temperature*).

c) Uniaxial normal load F / b = n_x = 100 N/mm ($\hat{\sigma}_x = n_x/t$, laminate average stress).

t_k	α
$t_1 = 0.125$	$\alpha_1 = 0°$
•	$\alpha_2 = 90°$
•	$\alpha_3 = +45°$
•	$\alpha_4 = -45°$
•	$\alpha_5 = -45°$
•	$\alpha_6 = +45°$
•	$\alpha_7 = 90°$
$t_8 = 0.125$	$\alpha_8 = 0°$

$E^t_{\|\|}$	181000 N/mm^2		$E^t_{\perp}$	10300 N/mm^2
$G_{\|\|\perp}$	7170 N/mm^2		$\nu_{\perp\|\|}$	0.28
$R^t_{\|\|}$	1500 N/mm^2		$R^t_{\perp}$	40 N/mm^2
$R^c_{\|\|}$	1500 N/mm^2		$R^c_{\perp}$	246 N/mm^2
$R_{\perp\|\|}$	68 N/mm^2		ILSS	N/mm^2
$\alpha_{T\|\|}$	$0.02 \cdot 10^{-6}$/K		$\alpha_{T\perp}$	$22.5 \cdot 10^{-6}$/K
$\alpha_{M\|\|}$	0.0		$\alpha_{M\perp}$	0.6

3 Solution

The internal force-strain relationships to be considered are $\{n\} = [A] \cdot \{\varepsilon\} - \{n_T\} - \{n_M\}$.

3.1 Determination of the stiffness matrix [A] of the specimen

Determination of the stiffness matrix [Q]:

$$[Q] = \begin{bmatrix} 181811 & 2897 & 0 \\ 2897 & 10346 & 0 \\ 0 & 0 & 7170 \end{bmatrix}$$ with exemplarily $Q_{\|\perp} = 2897\ N/mm^2 = \nu_{\|\perp} \cdot E_{\|} / (1 - \nu_{\|\perp} \cdot \nu_{\perp\|})$.

Calculation of all transformed stiffness elasticity matrices [Q']:

e.g. $Q'_{11,3} = 56658\ N/mm^2 = Q_{\|} \cdot (CoS\alpha_3)^4 + Q_{\perp} \cdot (\sin\alpha_3)^4 + 1/2 \cdot (Q_{\|\perp} + 2G_{\|\perp}) \cdot (\sin\alpha_3)^2$

$$[Q']_2 = \begin{bmatrix} 10346 & 2897 & 0 \\ 2897 & 181811 & 0 \\ 0 & 0 & 7170 \end{bmatrix}, \quad [Q']_1 = [Q] \ , \quad [Q']_2 = \begin{bmatrix} \overset{+}{\underset{(+)}{}}56658 & \overset{+}{\underset{(+)}{}}42318 & \overset{-}{\underset{(+)}{}}42866 \\ & \overset{+}{\underset{(+)}{}}56658 & \overset{-}{\underset{(+)}{}}42866 \\ sym. & & \overset{+}{\underset{(+)}{}}46591 \end{bmatrix}$$

Calculation of the plate stiffness matrix [A] by summing up the lamina proportions

$[A] = \sum_{k=1}^{8} [Q']_k (z_k - z_{k-1}) = \sum_{k=1}^{8} [Q']_k t_k$ with for instance

$A_{13} = \sum_{k=1}^{8} Q'_{13,k} \cdot t_k = 0\ N/mm = (0 + 0 - 42866 + 42866 + 42866 - 42866 + 0 + 0) \cdot 0.125$.

After completion it becomes $$[A] = \begin{bmatrix} 7.63682 & 2.26074 & 0 \\ 2.26074 & 7.63682 & 0 \\ 0 & 0 & 2.68804 \end{bmatrix} \cdot 10^4\ N/mm^2 \cdot$$

Calculation of the plate compliance matrix by inversion of [A]: $$[A]^{-1} = \begin{bmatrix} 1.4352 & -0.4249 & 0 \\ 0.4249 & 1.4352 & 0 \\ 0 & 0 & 3.7202 \end{bmatrix} \cdot 10^{-5} \frac{mm}{N}.$$

3.2 Determination of lamina coefficients of thermal expansion (rotated CoS) $\{\alpha'_T\}_k = [T_\varepsilon]_k \cdot \{\alpha_T\}_k$

For the 8th lamina $\alpha = 0°$ it becomes

For $\{\alpha'_M\}$ analogous

$$\begin{bmatrix} 1 & 0 & 0 \\ 0 & 1 & 0 \\ 0 & 0 & 1 \end{bmatrix}_8 \cdot \begin{bmatrix} 0.02 \\ 22.4 \\ 0 \end{bmatrix} 10^{-6} / K = \begin{bmatrix} 0.02 \\ 22.4 \\ 0 \end{bmatrix}_8 10^{-6} / K = \{\alpha'_T\}_8$$

Determination of fluxes $\{n\}$, $\{n_T\}$, $\{n_M\}$

Fluxes (cross-section forces) from external loads: $$\{n\} = \begin{bmatrix} n_x \\ n_y \\ n_{xy} \end{bmatrix} = \begin{bmatrix} 100 \\ 0 \\ 0 \end{bmatrix} N / mm.$$

Calculation of the "fictitious thermal forces": $\{n_T\} = \Delta_T \cdot \frac{t}{8} \sum_{k=1}^{8} [Q']_k \{\alpha'_T\}_k = \begin{bmatrix} -15{,}1 \\ -15{,}1 \\ 0 \end{bmatrix}$ N/mm.

Calculation of the "fictitious forces from moisture swelling": $\{n_M\} = \Delta M \cdot \frac{t}{8} \sum_{k=1}^{8} [Q']_k \{\alpha'_M\} = \begin{bmatrix} 39{,}7 \\ 39{,}7 \\ 0 \end{bmatrix}$ N/mm.

3.4 Calculation of the strains of the laminate from total loading

Boundary conditions: Freely movable in x- and y-directions.

By resolving the equilibrium conditions after the strains

$$\{\varepsilon\} = [A]^{-1} \cdot \{n\} + [A]^{-1} \cdot \{n_T\} + [A]^{-1} \cdot \{n_M\} = \begin{bmatrix} \varepsilon_x \\ \varepsilon_y \\ \gamma_{xy} \end{bmatrix} = \{\varepsilon_{mech}\} + \{\varepsilon_T\} + \{\varepsilon_M\}$$

$$= \left(\begin{bmatrix} 14.352 \\ -4.249 \\ 0 \end{bmatrix} + \begin{bmatrix} -1.524 \\ -1.524 \\ 0 \end{bmatrix} + \begin{bmatrix} 4.014 \\ 4.014 \\ 0 \end{bmatrix} \right) \cdot 10^{-4} = \begin{bmatrix} 16.842 \\ 1.759 \\ 0 \end{bmatrix} 10^{-4}.$$

with the example (matrix-multiplication shown)

$$\{\varepsilon_T\} = [A]^{-1} \cdot \{n_T\} = 10^{-5} \frac{\text{mm}}{\text{N}} \cdot \begin{bmatrix} 1.4352 & -0.4249 & 0 \\ -0.4249 & 1.4352 & 0 \\ 0 & 0 & 3.7202 \end{bmatrix} \cdot \begin{bmatrix} \text{-15.1 N/mm} \\ \text{-15.1 N/mm} \\ 0 \end{bmatrix} = \begin{bmatrix} -1.524 \cdot 10^{-4} \\ -1.524 \cdot 10^{-4} \\ 0 \end{bmatrix}.$$

3.5 Calculation of lamina strains and stresses from total loading

Strain compatibility of laminate and single laminas: $\{\varepsilon'\}_k = \{\varepsilon\}$

Transformation of $\{\varepsilon'\}_k$ into the lamina CoS: $\{\varepsilon\}_k = [T_\varepsilon]_k^{-1} \cdot \{\varepsilon'\}_k$,

For instance for the 4th lamina, α = -45°, $\{\varepsilon\}_4 = \begin{bmatrix} 0.5 & 0.5 & -0.5 \\ 0.5 & 0.5 & +0.5 \\ +1 & -1 & 0 \end{bmatrix}_4 \cdot \begin{bmatrix} 16.842 \cdot 10^{-4} \\ 1.759 \cdot 10^{-4} \\ 0 \end{bmatrix}_4 = \begin{bmatrix} 9.30 \cdot 10^{-4} \\ 9.30 \cdot 10^{-4} \\ 15.08 \cdot 10^{-4} \end{bmatrix}_4$

and analogously reads $\{\varepsilon_T\}_k = [T_\varepsilon]_k^{-1} \cdot \{\varepsilon'_T\}_k$, $\{\varepsilon_M\}_k = [T_\varepsilon]_k^{-1} \cdot \{\varepsilon'_M\}_k$.

Calculation of lamina stresses "natural stresses):

$$\{\sigma\}_k = [Q]_k \cdot (\{\varepsilon\}_k - \{\varepsilon_T\}_k - \{\varepsilon_M\}_k) .$$

→ Table of stress state results:

Lamina	1 u. 8	2 u. 7	3 u. 6	4 u. 5
loading a	from temperature difference ΔT = -100°C			
σ_1	-21.3	-21.3	-21.3	-21.3
σ_2	+21.3	+21.3	+21.3	+21.3
τ_{12}	0	0	0	0
loading b	from moisture concentration change ΔM = 1%			
σ_1	+56.8	+56.8	+56.8	+56.8
σ_2	-56.8	-56.8	-56.8	-56.8
τ_{12}	0	0	0	0
loading c	from mechanical loading n_x = 100 N/mm			

σ_1	+259.7	-73.1	+93.3	+93.3
σ_2	-0.2	13.6	+6.7	+6.7
τ_{12}	0	0	+13.3	-13.3
loading a + b + c	Sum of the combined loading			
σ_1	+295.2	-37.6	+128.8	+128.
σ_2	-35.7	-219	-28.8	-28.8
τ_{12}	0	0	+13.3	-13.3

4 Results with above simple Evaluation

Assumption was: No curing or mounting–caused residual stresses are in the laminate.

Residual stress from moisture uptake reduce curing stresses and mechanical stresses. This is different due to the different elastic and physical properties of GFRP and CFRP.

But mind:

The results presume that micro-cracking has not lead to a substantial change of the CTEs and CMEs! Because strength fracture criteria are not applied here a simple judgement of the lamina stresses is performed using the fracture strengths.

- Generated stress states of the 3 unity loadings are at the same scale
- No lamina has reached its fracture point
- Stresses from moisture concentration changes have a beneficial effect on curing stresses.

9.3.6 Influence of the CoS reference choice on a CFRP laminate stiffness matrix [K[

1 Task and Input

- Geometry, loading: t = 2 mm, F = 10 N/mm at the upper edge of the laminate plate strip
- Lay-up:
- Properties of the material lamina: T800/Epoxide

$E^t_{\parallel}$	$E^t_{\perp}$	$G_{\parallel\perp}$	$\nu_{\perp\parallel}$
N/mm^2	N/mm^2	N/mm^2	-
160000	9300	5400	0.34

- Searched:
  - [K] matrices for a section force *F* that attacks at different 'heights' over the cross-section
  - Strains upper surface and lower surface.

2. Calculation

- Modellbildung:

  System: strip of a plate

  {n}:= vector of membrane stress resultants per unit length or vector of section forces (fluxes of the plate)

  {m}:= vector of bending stress resultants per unit length or vector of section moments

The section quantities-deformation relationships read:

$$\begin{Bmatrix} n^0 \\ \hline m \end{Bmatrix} = [K] \begin{Bmatrix} \varepsilon^0 \\ \hline \chi \end{Bmatrix} \; mit \; [K] = \begin{Bmatrix} A & B \\ \hline B & D \end{Bmatrix}$$

Technical elasticity quantities ('constants') of the laminate are for information:

E_x	E_y	G_{xy}	ν_{yx}
N/mm^2	N/mm^2	N/mm^2	-
85100	85100	5400	0.374

3. Results from five chosen reference planes

Fall	1	2	3	4	5
z in mm	+1.0	0.0	-1.0	0.4451	-0.4451
e_o. in ‰	0.968	0.968	0.968	0.968	0.589
e_u. in ‰	-0.290	-0.290	-0.290	-0.290	0.589

- The [A] matrix remains the same. [B] and [D] "regulate" the CoS choice-dependent coupling
- The surface strains remain the same.

9.3.7 Cross-sectional Design Verification, GFRP plate strip under Mechanical Loading

1 Task Design Verification of a laminate (Schichtenverbund)

- Lay-up (stack): $[90_2/0_2/90_2/0_2]$, 0.25 mm = 2 layers = 1 lamina, L =
- Loading:

  Bending moment flux $m_x = q \cdot L = 50$ N · mm

  Normal force flux $n_x = n = 300$ N/mm.

  With regard to the geometric center surface, the laninate is unbalanced.

k	t_k in mm	α_k in °
1	0.25	0
2	0.25	90
3	0.25	0
4	0.25	90
	t = 1.0	

- Searched:
  - Stresses and reserve factors of this asymmetrically constructed laminate
  - Cross-section design verification by CLT directly in front of the clamping cross-section
- Properties:

  $E^c_{||} = E^t_{||}$ and $E^c_{\perp} = E^t_{\perp} = E_{\perp}$ applied in the low compressive stress range

$E_{||}$	46000 N/mm^2		$E_{\perp}$	13000 N/mm^2
$G_{||\perp}$	4400 N/mm^2		$\nu_{\perp||}$	0.30
$R^t_{||}$	700 N/mm^2		$R^t_{\perp}$	40 N/mm^2
$R^c_{||}$	500 N/mm^2		$R^c_{\perp}$	110 N/mm^2
$R_{\#}$	45 N/mm^2			

2 Solution

2.1 Modelling

- The geometric center surface (mid-surface) is selected as reference plane.
- Boundary conditions: No strain obstruction before the clamping cross-section

The system of equations to be worked on is: $\begin{Bmatrix} n^0 \\ m \end{Bmatrix} = \begin{bmatrix} A & B \\ B & D \end{bmatrix} \cdot \begin{Bmatrix} \varepsilon^0 \\ \chi \end{Bmatrix} = [K] \cdot \begin{Bmatrix} \varepsilon^0 \\ \chi \end{Bmatrix}.$

Determination of [K] and $[K]^{-1}$ of the plate strip:

Stiffness matrix of the UD layer $[Q] = \begin{bmatrix} 47200 & 4002 & 0 \\ & 13340 & 0 \\ (\text{symm}) & & 4400 \end{bmatrix} \text{N/mm}^2 \cdot$

Calculation of the rotated $[Q']_k$: (*analogous to before*)

Calculation of the total stiffness matrix [K]:

According to the already shown determination of the strain stiffness matrix [A], the two remaining submatrices, the coupling matrix [B] and the bending stiffness matrix [D], are still to be determined

$$[K] = \left[\begin{array}{ccc:ccc} 302070 & 4000 & 0 & 2120 & 0 & 0 \\ 4000 & 302070 & 0 & 0 & -2120 & 0 \\ 0 & 0 & 4400 & 0 & 0 & 0 \\ \hdashline 2120 & 0 & 0 & 2520 & 330 & 0 \\ 0 & -2120 & 0 & 330 & 2520 & 0 \\ 0 & 0 & 0 & 0 & 0 & 370 \end{array}\right]$$ with A_{ij} in N/mm, B_{ij} in N, and D_{ij} in N·mm

and compliance matrix (K-inversion): $$[K]^{-1} = \left[\begin{array}{ccc:ccc} 3.58 & -0.47 & 0 & -3.0 & 0 & 0 \\ -0.47 & 3.58 & 0 & 0 & 3.0 & 0 \\ 0 & 0 & 22.7 & 0 & 0 & 0 \\ \hdashline -3.0 & 0 & 0 & 42.9 & -5.67 & 0 \\ 0 & 3.0 & 0 & -5.67 & 42.9 & 0 \\ 0 & 0 & 0 & 0 & 0 & 237.0 \end{array}\right] \cdot 10^{-5}$$

2.2 Determination of section forces and moments

$$\{n\} = \begin{bmatrix} n_x \\ n_y \\ n_{xy} \end{bmatrix} = \begin{bmatrix} 300 \\ 0 \\ 0 \end{bmatrix} \text{N/mm} \ , \qquad \{m^0\} = \begin{bmatrix} m_x \\ m_y \\ m_{xy} \end{bmatrix} = \begin{bmatrix} 50 \\ 0 \\ 0 \end{bmatrix} \text{N/mm.}$$

2.3 Calculation of the distortions of the plate strip just before the clamping cross-section

With known section quantities {n}, $\{m^0\}$, the strains of the mid-plane can be determined

$$\begin{Bmatrix} \varepsilon^0 \\ \chi \end{Bmatrix} = [K]^{-1} \begin{Bmatrix} n \\ m^0 \end{Bmatrix}, \quad \text{e.g. is } \varepsilon_x = 3.58 \cdot 10^{-5} \cdot 300 - 3. \cdot 10^{-5} \cdot 50 = 9.24 \cdot 10^{-3}.$$

	z = -0.5	z = -0.25	z = 0	z = 0.25	z = 0.5
ε_x	$3.0 \cdot 10^{-3}$	$6.1 \cdot 10^{-3}$	$9.2 \cdot 10^{-3}$	$12. \cdot 10^{-3}$	$15.4 \cdot 10^{-3}$
ε_y	0	$-0.7 \cdot 10^{-3}$	$-1.4 \cdot 10^{-3}$	$-2.1 \cdot 10^{-3}$	$-2.8 \cdot 10^{-3}$
ε_{xy}	0	0	0	0	0

3 Results with Reserve Factors

The strains $\{\varepsilon\}_k$ are then transformed into the CoS of the layer $\{\varepsilon\}_k = [T_\varepsilon]_k^{-1}\ \{\varepsilon'\}_k$

With the relationship $\{\sigma\}_k = [Q]_k \cdot \{\varepsilon\}_k$ the following stress states result at the top and bottom of each layer

Schicht	1u	1o	2u	2o	3u	3o	4u	4o
σ_1	12.0	-9.0	285.7	429.9	-30.0	-51.0	574.0	718.1
σ_2	40.0	78.7	15.0	18.0	117.4	156.1	21.0	24.0
τ_{12}	0	0	0	0	0	0	0	0

- IFF: Top of layer 3 is relevant

Layer 3 is most stressed at its top (z = +0.25) due to the high stress.

The IFF failure limit (intentionally the old ZTL-hypothesis of the HSB is used)

$RF_{IFF} = 2 / [R_1 + (R_1^2 + 4\ R_2)^{0,5}]$ with $R_1 = \sigma_2 \cdot (1/ R^t_\perp - 1/R^c_\perp) = 156.1\ (1/40 - 1/110) = 2.48$

$R_2 = \sigma_2^2 / (R^t_\perp \cdot R^c_\perp) + (\tau_{12}/R_{21})^2 = 156.12 / (40 \cdot 110) = 5.54$,

$RF_{IFF} = 2 / [2.48 + (2.482 + 4 \cdot 5.54)0,5] = 0.26$ ($\approx \sigma_2 / R^t_\perp$) $\rightarrow$ $MoS_{IFF} = - 0.74$ surpassed.

- FF: Layer 4 is relevant

$$RF_{FF} = \frac{R^z_{||}}{\sigma_1^2} = \frac{1700}{718.1} = 2.37 \qquad \rightarrow \qquad MoS_{FF} = 1.37\ .$$

Due to the stress rearrangements from the cracked 90°- layers into the 0° layers, the limit load capacity is somewhat smaller and therefore it is assumed and set *MoS* = 1. Design is acceptable if the IFF carcks can be tolerated.

9.3.8 Analysis of a Plate strip composed of Different Materials

1. Task *"Assessment of the strains for the four materials"*

- Searched:
  2D stiffness elasticity matrix [Q] and **C**ompliance elasticity matrix [**S**] for GFRP and CFRP

- Given: Loading and Geometry: $\{\sigma'\} = (400, 60, 15)^T$, t = 1 mm

Material data : Property set for a standard fiber volume fraction $V_f = 0.6$

	Stahl	Alu	CFK	GFK	
$E_{\|\|}$	210000	73500	135000	47000	N/mm^2
$E_\perp$	(210000)	(73500)	9470	11000	
$G_{\|\|\perp}$	(81000)	(28000)	5270	5300	
$\nu_{\perp\|\|}$	0.30	0.31	0.28	0.30	

2. Calculation

2.1 Determination of the Q_{ik} and S_{ik} for CFRP- and GFRP-UD-lamina ($\equiv$ 1 $\equiv$ x)

CFRP:

$\nu_{\perp||}$ = $0.28 \rightarrow \nu_{||\perp} = 0.28 \cdot 9470 / 135000 = 0.0196$, $1 - \nu_{\perp||} \cdot \nu_{||\perp} = 1 - 0.28 \cdot 0.0196 = 0.9945$

Q_{11} = $E_{||} / (1-\nu_{\perp||} \cdot \nu_{||\perp}) = 135000 / 0.9945 = 135747$ N/mm^2, $Q_{22} = 9470 / 0.9945 = 9522$ N/mm^2

Q_{66} = 5270 N/mm^2, $Q_{12} = (9470 / 0.9945)\ 0.28 = Q_{21} = 2666$ N/mm^2

S_{11} = $1 / 135000 = 0.407 \cdot 10^{-5}$ mm^2/ N, $S_{22} = 1 / 9470 = 10.56 \cdot 10^{-5}$ mm^2/ N

S_{66} = $1 / 5270 = 18.98 \cdot 10^{-5}$ mm^2/ N , $S_{12} = - 0.28 / 135000 = - 20.74 \cdot 10^{-5}$ mm^2/ N

$$[Q]=\begin{bmatrix}135747 & 2666 & 0\\ 2666 & 4522 & 0\\ 0 & 0 & 5270\end{bmatrix},\quad [S]=\begin{bmatrix}0.741 & 20.74 & 0\\ -20.74 & 10.56 & 0\\ 0 & 0 & 18.98\end{bmatrix}10^{-5}\cdot$$

GFRP: analogous

$\nu_{\|\perp}$ = $0.30 \cdot 4700 / 11000 = 0.070$, $1 - \nu_{\perp\|} \cdot \nu_{\|\perp} = 1 - 0.30 \cdot 0.070 = 0.979$

Q_{11} = $47000 / 0.979 = 48008$ N /mm^2 , $Q_{22} = 11000 / 0.979 = 11236$ N/mm^2 ,

Q_{66} = 5300, Q_{12} $= 0.30 \cdot 11000 / 0.979 = Q_{21} = 3371$ N/mm^2

S_{11} = $1 / 47000 = 2.128 \cdot 10^{-5}$ mm^2/N, $S_{22} = 1 / 9470 = 10.56 \cdot 10^{-5}$ mm^2/ N

S_{66} $= 1 / 5300 = 18.87 \cdot 10^{-5}$ mm^2/ N, $S_{12} = - 0.30 / 47000 = -0.638 \cdot 10^{-5}$ mm^2/ N.

2.2 Strains of the different plates including a comparison with two metals $\{\varepsilon\}=[S]\cdot\{\sigma\}$

	Steel	Alu	CFK	CFK	
ε_1	1.82	5.19	2.84	8.13	in 10^{-3} or ‰
ε_2	-0.29	-0.88	+5.51	+2.90	
γ_{12}	0.19	0.54	2.85	2.83	

3. Assessment

- In the case of the metals the strain ratio corresponds to the ratio of the elasticity moduli
- In the case of CFRP, GFRP just for ε_1 the ratio of the $E_{\square}$-moduli applies *and for* the perpendicular strain $\varepsilon_2 \equiv \varepsilon_\perp$ leads for metals to negative values and for FRP to positive values (anisotropy effect).

9.3.9 UD CFRP lamina in the rotated CoS, plane stress state 2D

1. Task *(essential for the 'oblique tension test specimen')*

- Searched: Elasticity matrices and stress vector, strain vector
- Given: Loading and Geometry: $\{\sigma'\}= (400, 60, 15)^T$, t = 1 mm,

rotation angle α = +45° test data set for $\varphi = V_f = 0.6$

Intentionally opposite positive α-direction →[Tσ]

	CFRP	Nylon-reinforced elastomer	
$E_{\|}$	135000	910	N/mm^2
$E_\perp$	9470	7.24	
$G_{\|\perp}$	5270	1.81	
$\nu_{\perp\|}$	0.28	0.36	

2. Calculations

2.1 Determination of the transformation matrices $[T_\sigma]$ und $[T_\varepsilon]$, $s^2 = \sin(45°)^2 = \left(\sqrt{2}/2\right)^2 \equiv c^2$

$$[T_\sigma]=\begin{bmatrix}c^2 & s^2 & 2sc\\ s^2 & c^2 & -2sc\\ -sc & sc & c^2-s^2\end{bmatrix}=\begin{bmatrix}0.5 & 0.5 & 1.0\\ 0.5 & 0.5 & -1.0\\ -0.5 & 0.5 & 0\end{bmatrix},\quad [T_\varepsilon]=\begin{bmatrix}c^2 & s^2 & sc\\ s^2 & c^2 & -sc\\ -2sc & 2sc & c^2-s^2\end{bmatrix}=\begin{bmatrix}0.5 & 0.5 & 0.5\\ 0.5 & 0.5 & -0.5\\ -1 & 1 & 0\end{bmatrix},$$

2.2 Determination of elasticity matrices, stiffness matrix [Q], compliance matrix [S]

$$[Q]=\begin{bmatrix}135747 & 2666 & 0\\ 2666 & 4522 & 0\\ 0 & 0 & 5270\end{bmatrix}\frac{N}{mm^2},\quad [S]=\begin{bmatrix}0.74 & -20.74 & 0\\ -20.74 & 10.56 & 0\\ 0 & 0 & 18.98\end{bmatrix}\cdot 10^{-5}\,\frac{mm^2}{N}$$ orthotropic

2.3 Determination of the rotated matrices [Q'], [S'] with the '*matrix multiplication procedure'*

$$[Q'] = [T_\sigma]\,[Q]\,[T_\sigma]^T \qquad [S'] = [T_\varepsilon]\,[S]\,[T_\varepsilon]^T = [Q']^{-1}$$

$$\begin{bmatrix} 0{,}5 & 0{,}5 & -0{,}5 \\ 0{,}5 & 0{,}5 & +0{,}5 \\ +1 & -1 & 0 \end{bmatrix} \qquad \begin{bmatrix} 0{,}5 & 0{,}5 & -1 \\ 0{,}5 & 0{,}5 & 1 \\ 0{,}5 & -0{,}5 & 0 \end{bmatrix}$$

$$\begin{bmatrix} 1357{,}47 & 26{,}66 & 0 \\ 26{,}66 & 45{,}22 & 0 \\ 0 & 0 & 52{,}70 \end{bmatrix} \begin{bmatrix} & & \\ & & \\ +52{,}70 & -52{,}70 & 0 \end{bmatrix} \begin{bmatrix} 0{,}741 & -20{,}74 & 0 \\ -20{,}74 & 10{,}56 & 0 \\ 0 & 0 & 18{,}98 \end{bmatrix} \begin{bmatrix} & & \\ & & \\ & & 0 \end{bmatrix}$$

$$\begin{bmatrix} 0{,}5 & 0{,}5 & 1{,}0 \\ 0{,}5 & 0{,}5 & -1{,}0 \\ -0{,}5 & 0{,}5 & 0 \end{bmatrix} = \begin{bmatrix} 42{,}92 & 32{,}38 & -31{,}56 \\ & 42{,}92 & -31{,}56 \\ (\text{symm}) & & 34{,}98 \end{bmatrix} \begin{bmatrix} 0{,}5 & 0{,}5 & 0{,}5 \\ 0{,}5 & 0{,}5 & -0{,}5 \\ -1 & 1 & 0 \end{bmatrix} = \begin{bmatrix} 7{,}47 & -2{,}02 & 4{,}91 \\ & 7{,}47 & 4{,}91 \\ (\text{symm}) & & 11{,}72 \end{bmatrix}$$

$$[Q'] \text{ in } 10^3 \text{ N/mm}^2 \qquad [S'] \text{ in } 10^{-5} \text{ mm}^2/\text{N}$$

2.4 Determination of the rotated stress vector {σ'}

$$\{\sigma'\} = (400, 60, 15)^T \rightarrow \quad \{\sigma\} = [T_\sigma]^{-1}\,\{\sigma'\} = (215, 245, 170)^T \text{ N/mm}^2$$

$$\begin{bmatrix} 0{,}5 & 0{,}5 & -1 \\ 0{,}5 & 0{,}5 & 1 \\ 0{,}5 & -0{,}5 & 0 \end{bmatrix} \cdot \begin{bmatrix} 400 \\ 60 \\ 15 \end{bmatrix} \text{ N/mm}^2 = \begin{bmatrix} 215 \\ 245 \\ 170 \end{bmatrix} \text{ N/mm}^2$$

2.5 Rotated strain vector {σ'} due to σ_x and τ_{xy} solely

$$\{\sigma'\} = (400, 0, 0)^T \rightarrow \quad \{\varepsilon'\} = [S']\,\{\sigma'\} = [29.9, -8.1, +19.6)^T \cdot 10^{-3}$$

$$10^{-5}\,\frac{mm^2}{N} \begin{bmatrix} 7{,}47 & -2{,}02 & 4{,}91 \\ -2{,}02 & 7{,}47 & 4{,}91 \\ 4{,}91 & 4{,}91 & 11{,}72 \end{bmatrix} \cdot \begin{bmatrix} 400 \\ 0 \\ 0 \end{bmatrix} N/mm^2 = \begin{bmatrix} 29{,}9 \\ -8{,}1 \\ 19{,}6 \end{bmatrix} \cdot 10^{-3}$$

$$\{\sigma\} = (200, 200, 200)^T \text{ N/mm}^2, \; \{\varepsilon\} = (1.07, 20.7, 38.0)^T \cdot 10^{-3}$$

All 3 strains are caused. This is warning for the " Inclined tensile test specimen "!

$$\{\sigma'\} = (0,\ 0,\ 15)^T \quad \rightarrow \quad \{\varepsilon'\} = [S']\,\{\sigma'\} = (0.736, +0.736, +1.76)^T \cdot 10^{-3}$$

$$\{\sigma\} = (-15, 15, 0)^T \text{ N/mm}^2, \quad \{\varepsilon\} = (-0.142, 1.62, 0) \cdot 10^{-3}.$$

For comparison for α = - 45°

$$\{\sigma'\} = (0, 0, 15)^T; \qquad \{\varepsilon'\} = (-0.736, -0.736,, +1.76)^T \cdot 10^{-3}$$

$$\{\sigma\} = (15, -15, 0)^T \text{ N/mm}^2, \quad \{\varepsilon\} = (0.142, +1.62, 0)^T \cdot 10^{-3}$$

3. Comparison calculations Nylon reinforced elastomer with CFRP

3.1 Compliance elasticity matrix of Nylon reinforced elastomer (α = +45°)

$$[S] = \begin{bmatrix} 1.1 & -39.6 & 0 \\ -39.6 & 138.0 & 0 \\ 0 & 0 & 552.5 \end{bmatrix} \cdot 10^{-3}\, mm^2 / N$$

3.2 Dependence of shear angle τ_{12} from lamina fiber angle α

For the stress state $\{\sigma'\} = (+400, 0, 0)^T$ N/mm^2 its behavior can essentially be studied in regarding

$$S'_{61} = -2\,S_{11}\,c^3 s + 2\,S_{22}\,cs^3 - 2\,S_{12}\,(cs^3 - c^3 s) + S_{66}\,(c^3 s - cs^3) \text{ with } c = \text{CoS}(\alpha),\ s = \sin(\alpha)$$

It results for different positive angles α, whereby /α/ = ω, the following table

	α	-45°	-15°	0°	15°	30°	45°	60°	75°	90°
Nylon	S'_{61}	-0.069		0	0.124	0.149	0.069	-0.03	-0.055	0
	γ_{yx}	-27.4		0	> 0	> 0	> 0	-12.0	< 0!	0
CFRP	S'_{61}	0.491		0	0.402	0.60	0.491	+0.25	0.07	0
	γ_{xy}	-0.020		0	> 0	> 0	+0.020	> 0	> 0	0

LL: Above tire industry material thus responds in an angular range +45° < α < +75° with a negative shear angle γ_{xy} !

3.3 For comparison: stiffness elasticity matrix of the material UD lamina with the stiffness matrix of the structure laminate (CFRP: t = t_1 = 1 mm. [K] in $10^{-3}\,N/mm^2$, $[K]^{-1}$ in $10^{-5}\,mm^2/N$

$$[K] = \begin{bmatrix} 42.92 & 32.38 & \mp 31.56 & 0 & 0 & 0 \\ 32.38 & 42.92 & -31.56 & 0 & 0 & 0 \\ \mp 31.56 & \mp 31.56 & 34.98 & 0 & 0 & 0 \\ 0 & 0 & 0 & 3.577 & 2.698 & \mp 2.630 \\ 0 & 0 & 0 & 2.698 & 3.577 & \mp 2.630 \\ 0 & 0 & 0 & \mp 2.630 & \mp 2.630 & 2.915 \end{bmatrix}, \quad [K]^{-1} = \begin{bmatrix} 7.47 & -2.02 & \pm 4.91 & 0 & 0 & 0 \\ -2.02 & \mp 7.47 & \pm 4.91 & 0 & 0 & 0 \\ \pm 4.91 & \pm 4.91 & 11.72 & 0 & 0 & 0 \\ 0 & 0 & 0 & 89.58 & -24.27 & \pm 58.91 \\ 0 & 0 & 0 & -24.27 & 89.58 & \pm 58.91 \\ 0 & 0 & 0 & \pm 58.91 & \pm 58.91 & 140.6 \end{bmatrix}$$

with $E_x = 13400\ N/mm^2$, $E_y = 13400\ N/mm^2$, $G_{xy} = 8536\ N/mm^2$, $\nu_{yx} = +0.2709$ $(= \nu_{xy})$.

9.3.10 Influence of the CoS choice on a CFRP laminate stiffness matrix [K[

1 Task

- Geometry, loading: t = 2 mm, F = 10 N/mm at the upper edge of the laminate plate
- Properties of the material lamina: T800/Epoxide

$E^t_{\parallel}$	$E^t_{\perp}$	$G_{\parallel\perp}$	$\nu_{\perp\parallel}$
N/mm^2	N/mm^2	N/mm^2	-
160000	9300	5400	0.34

- Searched:
  - [K] matrices for a section force F that acts at different locations over the cross-section height
  - Strains upper surface and lower surface.

2. Calculation

- Modeling:

  System: strip of a plate

  {n}:= vector of membrane stress resultants per unit length or vector of section forces (fluxes of the plate)

  {m}:= vector of bending stress resultants per unit length or vector of section moments

  The section quantities-deformation relationships read:

$$\begin{Bmatrix} \underline{n} \\ \underline{\underline{m}} \end{Bmatrix} = [K] \begin{Bmatrix} \overset{\circ}{\varepsilon} \\ \underline{\chi} \end{Bmatrix} \text{ mit } [K] = \left\{ \begin{array}{c|c} A & B \\ \hline B & D \end{array} \right\}$$

Technical elasticity quantities ('constants') of the laminate are for information:

E_x	E_y	E_{xy}	ν_{yx}
N/mm^2	N/mm^2	N/mm^2	-
85100	85100	5400	0.374

3. Results

Fall	1	2	3	4	5
z in mm	+1.0	0.0	-1.0	0.4451	-0.4451
e_o. in ‰	0.9679	0.9679	0.9679	0.9679	0.5888
e_u. in ‰	-0.2902	-0.2902	-0.2902	-0.2902	0.5888

- The [A] matrix remains the same. [B] and [D] "regulate" the CoS choice-dependent coupling shares
- Case 5 addresses the "neutral fiber" in the z-x plane
- The surface strains remain the same.

9.3.11 Cross-sectional Design Verification, GFRP plate strip under Mechanical Loading

1 Task Design Verification of a laminate (Schichtverbund)

- Lay-up (stack): $[90_2/0_2/90_2/0_2]$, 0.25 mm = 2 layers = 1 lamina, L =
- Loading:

  Bending moment $m_x = q \cdot L = 50$ N · mm

  Normal force $n_x = n = 300$ N/mm.

  With regard to the geometric center surface, the laninate is unbalanced.

k	t_k in mm	α_k in °
1	0.25	0
2	0.25	90
3	0.25	0
4	0.25	90
	t = 1.0	

- Searched:
  - Stresses and reserve factors of this asymmetrically constructed laminate
  - 'Cross-section Verification' of the laminate with CLT.before the clamping cross-section
- Properties:

  $E^c_{||} = E^t_{||}$ and $E^c_{\perp} = E^t_{\perp} = E_{\perp}$ applied for low compressive stress range

$E_{\|}$	46000 N/mm^2	$E_{\perp}$	13000 N/mm^2
$G_{\|\perp}$	4400 N/mm^2	$\nu_{\perp\|}$	0.30
$R^t_{\|}$	700 N/mm^2	$R^t_{\perp}$	40 N/mm^2
$R^c_{\|}$	500 N/mm^2	$R^c_{\perp}$	110 N/mm^2
$R_{\#}$	45 N/mm^2		

2 Solution

2.1 Modelling

- The geometric center surface (mid-surface) is selected as reference plane.
- Boundary conditions: No strain obstruction before the clamping cross-section

The system of equations to be worked on is: $\begin{Bmatrix} n \\ \overset{\circ}{m} \end{Bmatrix} = \begin{bmatrix} A & B \\ B & D \end{bmatrix} \begin{Bmatrix} \overset{\circ}{\varepsilon} \\ \chi \end{Bmatrix} = [K] \begin{Bmatrix} \overset{\circ}{\varepsilon} \\ \chi \end{Bmatrix}$.

Determination of [K] and $[K]^{-1}$ of the plate strip:

Stiffness matrix of the UD layer $[Q] = \begin{bmatrix} 47200 & 4002 & 0 \\ & 13340 & 0 \\ (\text{symm}) & & 4400 \end{bmatrix} \text{N / mm}^2 \cdot$

Calculation of the $[Q']_k$, rotated $[Q]_k$:(*analogous to before*)

Calculation of the total stiffness matrix [K]:

According to the already shown determination of the strain stiffness matrix [A], the two remaining submatrics, the coupling matrix [B] and the bending stiffness matrix [D], are still to be determined

$$[K] = \left[\begin{array}{ccc:ccc} 302070 & 4000 & 0 & 2120 & 0 & 0 \\ 4000 & 302070 & 0 & 0 & -2120 & 0 \\ 0 & 0 & 4400 & 0 & 0 & 0 \\ \hdashline 2120 & 0 & 0 & 2520 & 330 & 0 \\ 0 & -2120 & 0 & 330 & 2520 & 0 \\ 0 & 0 & 0 & 0 & 0 & 370 \end{array}\right]$$ with A_{ij} in N/mm, B_{ij} in N and D_{ij} in N·mm

and compliance matrix (K-inversion): $[K]^{-1} = \left[\begin{array}{ccc:ccc} 3.58 & -0.47 & 0 & -3.0 & 0 & 0 \\ -0.47 & 3.58 & 0 & 0 & 3.0 & 0 \\ 0 & 0 & 22.7 & 0 & 0 & 0 \\ \hdashline -3.0 & 0 & 0 & 42.9 & -5.67 & 0 \\ 0 & 3.0 & 0 & -5.67 & 42.9 & 0 \\ 0 & 0 & 0 & 0 & 0 & 237.0 \end{array}\right] \cdot 10^{-5}$

2.2 Determination of loads $\{n\} = \begin{bmatrix} n_x \\ n_y \\ n_{xy} \end{bmatrix} = \begin{bmatrix} 300 \\ 0 \\ 0 \end{bmatrix} \text{N/mm}$, $\left\{\overset{\circ}{m}\right\} = \begin{bmatrix} m_x \\ m_y \\ m_{xy} \end{bmatrix} = \begin{bmatrix} 50 \\ 0 \\ 0 \end{bmatrix} \text{N/mm.}$

2.3 Calculation of the distortions of the plate before the clamping cross-section

With known section quantities {n} , { $\overset{\circ}{m}$ }, the strains of the mid-plane can be determined

$\begin{Bmatrix} \overset{\circ}{\varepsilon} \\ \chi \end{Bmatrix} = [K]^{-1} \begin{Bmatrix} n \\ \overset{\circ}{m} \end{Bmatrix}$, e.g. is $\varepsilon_x = 3.58 \cdot 10^{-5} \cdot 300 - 3. \cdot 10^{-5} \cdot 50 = 9.24 \cdot 10^{-3}$.

	z = -0.5	z = -0.25	z = 0	z = 0.25	z = 0.5
ε_x	$3.0 \cdot 10^{-3}$	$6.1 \cdot 10^{-3}$	$9.2 \cdot 10^{-3}$	$12. \cdot 10^{-3}$	$15.4 \cdot 10^{-3}$
ε_y	0	$-0.7 \cdot 10^{-3}$	$-1.4 \cdot 10^{-3}$	$-2.1 \cdot 10^{-3}$	$-2.8 \cdot 10^{-3}$
ε_{xy}	0	0	0	0	0

3 Results with Reserve Factors

The strains $\{\varepsilon\}_k$ are then transformed into the CoS of the layer. With the relationship .....
the following stress states result at the top and bottom of each layer

Schicht	1u	1o	2u	2o	3u	3o	4u	4o
σ_1	12.0	-9.0	285.7	429.9	-30.0	-51.0	574.0	718.1
σ_2	40.0	78.7	15.0	18.0	117.4	156.1	21.0	24.0

τ_{12}	0	0	0	0	0	0	0	0

IFF: Top of layer 3 is relevant

Layer 3 is most stressed at its top (z = +0.25) due to the high stress.

The IFF failure limit (intentionally the old German ZTL-hypothesis of the HSB is used)

$RF_{IFF} = 2 / [R_1 + (R_1^2 + 4\, R_2)^{0,5}]$ with $R_1 = \sigma_2 \cdot (1/ R^t_\perp - 1/R^c_\perp) = 156.1\ (1/40 - 1/110) = 2.48$

$R_2 = \sigma_2^2 / (R^t_\perp \cdot R^c_\perp) + (\tau_{12}/R_{21})^2 = 156.12 / (40 \cdot 110) = 5.54$,

$RF_{IFF} = 2 / [2.48 + (2.482 + 4 \cdot 5.54)0,5] = 0.26$ ($\approx \sigma_2 / R^t_\perp$) $\rightarrow$ $MoS_{IFF} = - 0.74$ surpassed.

FF: Layer 4 is relevant $$RF_{FF} = \frac{R^z_{||}}{\sigma_1^2} = \frac{1700}{718.1} = 2.37 \qquad \rightarrow \qquad MoS_{FF} = 1.37\ .$$

Due to the stress rearrangements from the cracked 90°- layers into the 0° layers, the limit load capacity is somewhat smaller and therefore it is assumed and set *MoS* = 1. Design is acceptable if the IFF carcks can be tolerated.

9.3.12 Issues with Symmetric and Non-symmetric Laminates, CFRP

$[0/90/45/-45]_S$, $t_{k,s}$ $\Leftrightarrow$ $[0/90/45/-45]$, *balanced laminate*, $t_{k,ns} = 2 \cdot t_{k,s}$; t = 1.0 mm

Task: *"Investigation of the associated bending stiffness matrices"*

Computation: *Mid-plane is reference plan*

(1) Determination of stiffness matrices **[K] $\rightarrow$ [K] $\cdot 10^5$ and effective properties**

* For the *symmetric laminate was computed*

$$\begin{bmatrix} 56499 & 17512 & 0 & 0 & 0 & 0 \\ 17512 & 56499 & 0 & 0 & 0 & 0 \\ 0 & 0 & 19493 & 0 & 0 & 0 \\ 0 & 0 & 0 & 7093 & 528 & 242 \\ 0 & 0 & 0 & 528 & 4185 & 242 \\ 0 & 0 & 0 & 242 & 242 & 694 \end{bmatrix} \Rightarrow \begin{bmatrix} 1.96 & -0.61 & 0 & 0 & 0 & 0 \\ -0.61 & 1.96 & 0 & 0 & 0 & 0 \\ 0 & 0 & 5.13 & 0 & 0 & 0 \\ 0 & 0 & 0 & 14.4 & -1.56 & -4.48 \\ 0 & 0 & 0 & -1.56 & 24.6 & -8.04 \\ 0 & 0 & 0 & -4.48 & -8.04 & 148.4 \end{bmatrix}$$

$$\widehat{E_x} := 1/(1.96 \cdot 10^{-5} \cdot 1.00)\ \text{MPa} = 51071\ \text{MPa},$$

$$\widehat{E_x} = 51071\ \text{MPa} = \widehat{E_y},\ \widehat{G_{xy}} = 19493\ \text{MPa},\ \widehat{\nu_{xy}} = 0.31 = \widehat{\nu_{yx}}$$

And as a laminate stiffness per width under bending and torsion (*formulas see § 9.1.3*)

$$\widehat{EI_x} = 7093\ \text{MPa} \cdot \text{mm}^3,\ \widehat{EI_y} = 4185\ \text{MPa} \cdot \text{mm}^3,\quad \widehat{GI_t} = 4 \cdot 694\ \text{MPa} \cdot \text{mm}^3.$$

Notes:

(1) The Aij are independent of the stack. (2) For a balanced laminate lay-up is $A_{16} = A_{26} = 0$ and $D_{16} = D_{26} = 0$. (3) Non-zero values A_{16}, A_{26} mean: coupling of extension and shear; non-zero D_{16}, D_{26} mean: coupled bending and twisting.

* For the *non-symmetric* laminate [0/90/45/−45] follows if mid-plane is ref. plane (off-set to consider)

[K] $\rightarrow$ [K] $\cdot 10^5$ and effective properties

$$\begin{bmatrix} 56499 & 17512 & 0 & 7601 & -3723 & -1939 \\ 17512 & 56499 & 0 & -3723 & -154 & -1939 \\ 0 & 0 & 19493 & -1939 & -1939 & -3723 \\ 7601 & -3723 & -1939 & 6647 & 1459 & 969 \\ -3723 & -154 & -1939 & 1459 & 2769 & 969 \\ -1939 & -1939 & -3723 & 969 & 969 & 1624 \end{bmatrix} \Rightarrow \begin{bmatrix} 4.01 & -1.56 & 0.97 & -7.7 & 8.38 & 4.74 \\ -1.56 & 2.6 & 0.44 & 4.02 & -4.69 & 2.64 \\ 0.97 & 0.44 & 9.73 & -1.73 & 0.38 & 24.8 \\ -7.7 & 4.02 & -1.73 & 32.8 & -23.8 & -13.7 \\ 8.38 & -4.69 & 0.38 & -23.8 & 67.1 & -20.6 \\ 4.74 & 2.64 & 24.8 & -13.7 & -20.6 & 147.7 \end{bmatrix}$$

$$\widehat{E_x} = 51071\,\text{MPa} = \widehat{E_y},\ \widehat{G_{xy}} = 19493\,\text{MPa},\ \widehat{\nu_{xy}} = 0.31 = \widehat{\nu_{yx}}$$

Notes:

(1)The Aij depend on the stack, only. (2) The B_{ij} are zero for symmetric laminates. (3) Optimizing the stack is a means to reduce the B_{ij}-influence in the couplings which have an impact on buckling and warping, and on mounting of parts and joining. (4) The generation of material properties with test specimens - possessing non-zero B_{ij} - is not reliable, especially the generation of strength design allowables is questionable. (5) The bending-twisting affecting D_{ij} significantly depend on the stack. The D_{16}, D_{26} must be included in the structural analysis of non-symmetric stacks. (6) Following the US Handbook CMH-17: As laminate stiffness per width under bending and torsion, also 'permitted' for the non-symmetrc case, are to be taken from [D*]

$$\widehat{EI_x} = 1/D_{11}^* = 10^5/32.8\,\text{MPa}\cdot\text{mm}^3 = 3049\,\text{MPa}\cdot\text{mm}^3,$$
$$\widehat{EI_y} = 1/D_{22}^* = 10^5/67.1\,\text{MPa}\cdot\text{mm}^3 = 1490\,\text{MPa}\cdot\text{mm}^3.$$

(2) Investigation of a reference plane choice-independing bending stiffness matrix

Orthogonalization of the problem by $\left[\tilde{D}\right] = [D] - [B]^T \cdot [A]^{-1} \cdot [B]$ leads to a bending stiffness matrix which is independent of the choice of the reference system. A comparison of the bending stiffness matrices

$$[D] = \begin{bmatrix} 6647 & 1459 & 969 \\ 1459 & 2769 & 969 \\ 969 & 969 & 1624 \end{bmatrix}, \text{and } \left[\tilde{D}\right] = \begin{bmatrix} 4708 & 1866 & 700 \\ 1886 & 2311 & 497 \\ 700 & 497 & 811 \end{bmatrix}$$

gives an information about the different stiffness element values of the laminate [0/90/45/−45].

The D_{ii} are smaller than the $\tilde{D}_{ii}$. For a balanced symmetric laminate is obtained

- Mid-plane is reference plane: [K] $\rightarrow$ [K] $\cdot 10^5$ and effective properties

$$\begin{bmatrix} 71392 & 2618 & 0 & 0 & 0 & 0 \\ 2618 & 71392 & 0 & 0 & 0 & 0 \\ 0 & 0 & 4600 & 0 & 0 & 0 \\ 0 & 0 & 0 & 9827 & 218.2 & 0 \\ 0 & 0 & 0 & 218.2 & 2072 & 0 \\ 0 & 0 & 0 & 0 & 0 & 383.3 \end{bmatrix} \Rightarrow \begin{bmatrix} 1.40 & -0.05 & 0 & 0 & 0 & 0 \\ -0.05 & 1.40 & 0 & 0 & 0 & 0 \\ 0 & 0 & 21.7 & 0 & 0 & 0 \\ 0 & 0 & 0 & 10.2 & -1.07 & 0 \\ 0 & 0 & 0 & -1.07 & 48.4 & 0 \\ 0 & 0 & 0 & 0 & 0 & 260.9 \end{bmatrix}$$

$$D = \begin{bmatrix} 9827 & 218.2 & 0 \\ 218.2 & 2072 & 0 \\ 0 & 0 & 383.3 \end{bmatrix} = D_{sym} \quad \text{and} \quad \tilde{D} = \begin{bmatrix} 9827 & 218 & 0 \\ 218 & 2072 & 0 \\ 0 & 0 & 383 \end{bmatrix}$$

- Top surface is reference plane:[K] $\rightarrow$ [K] $\cdot 10^5$ and effective properties

$$\begin{bmatrix} 71392 & 2618 & 0 & 17848 & 655 & 0 \\ 2618 & 71392 & 0 & 655 & 17848 & 0 \\ 0 & 0 & 4600 & 0 & 0 & 1150 \\ 17848 & 655 & 0 & 14289 & 382 & 0 \\ 655 & 17848 & 0 & 382 & 6534 & 0 \\ 0 & 0 & 1150 & 0 & 0 & 671 \end{bmatrix} \Rightarrow \begin{bmatrix} 2.04 & -0.12 & 0 & -2.55 & 0.27 & 0 \\ -0.12 & 4.43 & 0 & 0.27 & -12.1 & 0 \\ 0 & 0 & 38.0 & 0 & 0 & -65.2 \\ -2.55 & 0.27 & 0 & 10.2 & -1.07 & 0 \\ 0.27 & -12.1 & 0 & -1.07 & 48.4 & 0 \\ 0 & 0 & -65.2 & 0 & 0 & 260.9 \end{bmatrix}$$

$$D = \begin{bmatrix} 14289 & 382 & 0 \\ 382 & 6534 & 0 \\ 0 & 0 & 671 \end{bmatrix} \text{ and } \tilde{D} = \begin{bmatrix} 9827 & 218 & 0 \\ 218 & 2072 & 0 \\ 0 & 0 & 383 \end{bmatrix} = D_{sym}.$$

Note:

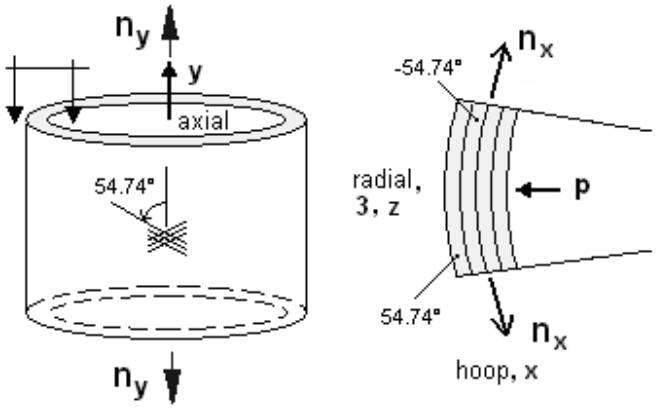
The so-called modified bending stiffness matrix $\left[\tilde{D}\right]$ is independent of the choice of the reference plane. It is used in buckling analysis.

9.3.13 Thin axial-loaded CFRP tube, Water Hose

In the case of sufficiently thin (*approximately t / R < 1/10*) rotationally symmetrical FRP tubes (shells) CLT can be used, too. For the tube, the coupling effect disappears for reasons of symmetry and in-plane and laterally loaded plate problems can be considered separately.

Task: *"Determination of wall strains and stresses in the layers"*

Hoop winding of tubes (see sketch below) usually makes, that the angle alters due to +-+- . Otherwise an effortful change of the winding direction would be necessary in order to reduce crossings in the winding pattern. Further, the actual width of the applied roving strand reduces the 90° angle a little.



Above fiber angle stems from application of the net-theory to an internally pressure-loaded waterhose where the "vessel formula" delivers $\tan(\pi \cdot 54.74° / 180°) = \sqrt{2} = \sqrt{n_{hoop} / n_{axial}}$.

y = axial, x = hoop (*see Test Case 11 of WWFE-I, CoS differently chosen there*), p = internal pressure

Given:

- Geometry:[- 54.7/54.7/-54.7/54.7]**,** t= 0.5 mm, t_k = 0.125 mm
- Applied loading: Internal pressure causing

$$n_{axial} = n_y = (p \cdot \pi \cdot r^2) / 2 \cdot \pi \cdot r \cdot t = p \cdot r / 2 \cdot t, \;\; n_x = p \cdot r / t$$

resulting in $\{n^0\} = (100, 50, 0)^T$ N/mm, $\{m\} = (0, 0, 0)^T$ N·mm/mm;

- Loading acts in mid-plane = reference plane

Computation: Determination of stiffness matrices [K] $\Rightarrow$ $[K]^{-1}$ (*to be multiplied by* 10^5)

From reasons of rotational symmetry the curvature $\{\kappa\}$ is zero.

$$\begin{bmatrix} 12114 & 14546 & 0 & 0 & 0 & 621 \\ 14546 & 32804 & 0 & 0 & 0 & 1207 \\ 0 & 0 & 15537 & 621 & 1207 & 0 \\ 0 & 0 & 621 & 252 & 303 & 0 \\ 0 & 0 & 1207 & 303 & 683 & 0 \\ 621 & 1207 & 0 & 0 & 0 & 324 \end{bmatrix} \Rightarrow \begin{bmatrix} 17.7 & -7.66 & 0 & 0 & 0 & -5.48 \\ -7.66 & 6.84 & 0 & 0 & 0 & -10.8 \\ 0 & 0 & 7.49 & -5.48 & -10.8 & 0 \\ 0 & 0 & -5.48 & 851 & -368 & 0 \\ 0 & 0 & -10.8 & -368 & 329 & 0 \\ -5.48 & -10.8 & 0 & 0 & 0 & 360 \end{bmatrix}$$

Effective elasticity constants, lamina strains and lamina stresses are

$$\widehat{E_x} = \frac{A_{11} - A_{12}^2/A_{22}}{t} = \frac{11328}{0.5}\,\text{MPa}, \;\; \widehat{E_y} = \frac{30674}{0.5}\,\text{MPa}, \;\; \widehat{G_{xy}} = \frac{A_{66}}{t} = 31074\,\text{MPa},$$

$$\widehat{\nu_{xy}} = +\frac{A_{12}}{A_{22}} = \frac{14546}{32804} = 0.44 = -\frac{A_{12}^*}{A_{11}^*} - \frac{-7.66}{17.7}, \;\; \widehat{\nu_{yx}} = (\widehat{E_y}/\widehat{E_x}) \cdot \widehat{\nu_{xy}} = 1.2,$$

$$\{\varepsilon^0\} = \begin{Bmatrix} 1.0 \\ 2.61 \\ 0 \end{Bmatrix} \cdot 10^{-3}, \qquad \{\kappa\} = \begin{Bmatrix} 0 \\ 0 \\ 0 \end{Bmatrix}.$$

layer number	1	1	2	2	3	3	4	4
z in mm	−0.25	−0.125	−0.125	−0	0	0.125	0.125	0.25
fiber angle	-54.7°	-54.7°	54.7°	54.7°	-54.7°	-54.7°	54.7°	54.7°
$\sigma_{\|\|}$ in MPa	260	260	260	260	260	260	260	260
$\sigma_{\perp}$ in MPa	19.8	19.8	19.8	19.8	19.8	19.8	19.8	19.8
$\tau_{\perp\|\|}$ in MPa	-7.0	-7.0	7.0	7.0	-7.0	-7.0	7.0	7.0

Note:
The CLT-stresses in the laminas of this balanced 'water hose stack' are equal. According to linear CLT (continuum theory) the axial strain is less than half of that in hoop direction. With increasing micro-crack damaging under higher loading both the strains approach the ratio 1:2 according to net-theory.

9.3.14 Laminate lay-up comparison: GFRP internally pressurized tube

1 Task *"Investigation of the stress-strain states of 3 different laminate lay-ups or stacks"*

2 Input

- Loading: Internal pressure causes the forces $n_{ax} = 50$ N/mm $= n_y$, $n_x = n_{ax} \cdot 2 = 100$ N/mm .
- Geometry: t = 1.00 mm laminate wall thickness
- Lay-ups,
  a) [+54.74 / -54.74] 2 layers, winding angle from $\tan \alpha = n_y/n_x$ following net theory
  b) [+45 /90/ -45] 3 layers, optimized in order to achieve zero τ_{12} : $m = \sigma_2/\sigma_1 = E_{\perp} \cdot (1 + n_{\perp||})/E_{||} \cdot (1 + n_{||\perp})$
  c) [-60 /+18] 2 layers with intentionally set angles (*accidental angle choice of A. Puck's secretary*).

- Properties:

$E^t_{\|\|}$	N/mm^2	38600
$E^t_{\perp}$	N/mm^2	8270
$G_{\|\|\perp}$	N/mm^2	4140
$\nu_{\perp\|\|}$	-	0.26

The fracture values are not required and are therefore omitted

3 Solution From 'vessel formula'.

$\hat{\sigma}_y = n_{ax}/t = 50 / 1 = 50$ N/mm^2, $\sigma_{hoop} = \hat{\sigma}_x = 100$ N/mm^2.

Although in all three cases it is an asymmetrically constructed laminate, the examples can be calculated solely with the membrane stiffness matrix [A] of the laminated plate, because the cylindrical tube prevents curvature of the wall.

4 Results and evaluation stresses in N/mm^2 and strains in %

layer	1	2	3		
a	+54.74°	-54.74°			
σ_1	124.3	124.3		$\overset{\circ}{\varepsilon}_x$	0.149
σ_2	25.7	25.7		$\overset{\circ}{\varepsilon}_y$	0.382
τ_{12}	-9.1	9,1		$\overset{\circ}{\gamma}_{xy}$	0
b	-45°	90°	+45°		

σ_1	119.5	119.5	119,5	$\overset{\circ}{\varepsilon}_x$	0.289
σ_2	30.5	30.5	30,5	$\overset{\circ}{\varepsilon}_y$	0.289
τ_{12}	0	0	0	$\overset{\circ}{\gamma}$ xy	0
c	-60°	18°			
σ_1	101.6	132.7		$\overset{\circ}{\varepsilon}_x$	0.130
σ_2	43.2	38.0		$\overset{\circ}{\varepsilon}_y$	0.558
τ_{12}	25.7	-27.2		$\overset{\circ}{\gamma}$ xy	**-0.5**

In the first two cases, the layer stresses are the same in each case. This is a step towards an optimal laminate. However, the strains are very different in case (a) with $\varepsilon_y/\varepsilon_x$ = 382/149 and in case (b) of the same size. Which laminate is chosen depends on other aspects such as production, strength, etc.

An effect, which is present in case (c) is, that the tube turns under internal pressure! This twisting could be used for instance for a pressure gauge. The twisting of the tube can be made visible by a pointer and a scale.

9.3.15 Pre-dimensioning of a GFRP watertank wall (for Airbus 320), cylinder area

1. Task *"Wall thickness of the cylindrical part* $t_{90} + t_{\omega}$ *"*

- Design requirements from the requirement specifications:
  - V: 216 l; M ≤ 9.5 kg; $l_{ges} \leq$ 1190 mm, d ≤ 535 mm
  - MEOP := safe pressure loading (≡ DLL = Design Limit Load) = 2.1 bar = 0.21 N/mm^2
    p_{proof} = 3.1 bar, $p_{ultimate}$ = 5,18 bar (design burst pressure ≡ Design Ultimate Load = DUL),
    This means j_{proof} = 1,48, j_{ult} = 2.47 as design safety factors *j*
  - n = 60000 cycles between 0 and MEOP (stress ratio R=0) during design life of 48000 flight hours;
    j_{Life} = 4
  - Temperature domain - 55°C < T < + 85°C, • Vibration, shock, constant acceleration
    Standards such as FAR/JAR 25.853 with regard to flammability, as well as flue gas emission (*gas exciting to the atmosphere)* and toxicity are to consider and determine the matrix choice

2. Dimensioning

- Choice of material: The glass fiber fabric WLB 8.4515.6 (Interglas 92105) is considered for the cylinder, alone. The epoxy resin system LY564/HY2954 serves as matrix. The Table below summarizes some basic design parameters. In order to take into account the effect of ageing and fatigue damage (*see [VDI-2014 sheet 3*], $N = 10^6$ *as fracture cycle number, where simplified* $R = \min\sigma / \max\sigma = \text{const} = 0$ *was applied*), the average tensile strength value $\bar{R}^t_{\parallel}$ is reduced to a lower tolerance limit of $R^t_{\parallel}$ = 100 N/mm^2.

In this context mind, please: Presenting a procedure is the aim.

ρ	g/cm^3	2,1
E	N/mm^2	22500
ν	-	0.11
$\bar{R}^t_{\parallel}$	N/mm^2	320
$\bar{R}^c_{\parallel}$	"	275
$\bar{R}^t_{\perp}$	"	80
p_{int}	"	0.21
α_T	10^{-6}/K	14

Table:
design parameter

(The strength values are fracture values, fiber volume content V_f = 55 %.

t = tension, c = compression

- Modelling: for internal pressure p_{int} (considered here alone)

  System: Thin-walled tube using membrane shell theory

Equilibrium: $n_{hoop} = p_{internal} \cdot d / 2 \rightarrow$ required t_{90} ("vessel formula"), $n_{ax} = n_{hoop} / 2 \rightarrow$ required t_{ω}

Failure modes: 1) Burst due to FF, 2) Micro-damage accumulation during fatigue life.

a) Geometry:

Being here practically free in length, the maximum allowed outer diameter is set at 534 mm, i.e. the average cylinder diameter is 533 mm. The angle of the helix angle is $\omega = 16°$.

b) Cylinder wall thickness (net theory viewing the ultimate limit state ULS for fracture)

erf $t_{90} \approx$ (MEOP $\cdot$ j_{ult} $\cdot$ d/2) / $R_{||}^{t}$ = (0.21 $\cdot$ 2.47 $\cdot$ 533/2)/100 = 1.38 mm,

erf t_{ω} = (MEOP $\cdot$ j_{ult} . d/2) / (2$\cdot$ $R_{||}^{t}$ $\cdot$ $CoS^2\omega$) = 0.75 mm.

For reasons of manageability (stiffness) and tightness t_{90} = 1.7 mm is proposed.

3. Pre- Design Verification for the critical hoop layer

- Results: Chosen was t_{90} = 1.6 mm (*thickness according to production requirements*)
- Lifetime: RF_{Life} = N / (n$\cdot$ j_{Life}) = 1000000 / (60000$\cdot$4) = 4.1
- Maximum static loading during life: *RF* = chosen $t_{90}\cdot$ $R_{||}^{t}$ / (MEOP$\cdot$ j_{ult} $\cdot$ d/2) = 1.16.

$\rightarrow$ Static *RF* and cyclic RF_{Life} are accepted.

9.3.16 Optimization of a Laminate Tube

1 Task *"Determination of an optimized laminate lay-up under certain restrictions"*

- Design requirements:

Two fiber directions α

Elongation stiffness in axial direction: $\min A_{11}$ = 200000 N/mm,

Fiber Failure: j_{ult} = 1.60, IFF: j_{pr} = 1,0.

Strength values are lower tolerance limits ($\pm 2\sigma$ tolerance width concept). The elasticity quantities are average secant moduli in order to best describe the component w.r.t. obtain an average stress and deformation state.

Load case: Internal pressure MEOP p_{int} = 204 bar (DLL)

- Searched: t_{90}, ω.

2 Pre-dimensioning (initial design)

- Mechanical model:

System: Thin-walled short tube $\rightarrow$ lay-up $[90/+\omega/-\omega]_S$

Theory: Membrane theory is sufficient. This means CLT is a solution method for the wall calculation

Limit states:
1. Limit of serviceability: tightness, linked to IFF
2. Ultimate limit state : fracture FF

Equilibrium:
$n_{hoop} = p_{int} \cdot d/2$, $n_{ax} = n_{hoop}/2$

Flux-strain relations: $\{n\} = [A]\cdot\{\overset{\circ}{\varepsilon}\}$

For simplification the properties of the cracked layers are set zero.

Limit state functions: intentionally the old ZTL of the HSB is applied

1. $g_1 = 1 - \sigma_2^2/(R^t_{\perp} R^c_{\perp}) - (\sigma_2/R^t_{\perp} - \sigma_2/R^c_{\perp}) - (\tau_{12}/R_{\perp||})^2$

2. $g_2 = 1 - (\sigma^t_1 / R^t_{||})^2$

with (σ_1, σ_2, τ_{12}) from CLT results

X_j	μ_j	
$E^t_{\|\|}$	170000	N/mm^2
$E^t_{\perp}$	6500	"
$G_{\|\|\perp}$	5000	"
$\nu_{\perp\|\|}$	0.26	-
$E^c_{\|\|}$	170000	N/mm^2
$E^c_{\perp}$	7500	"
$R^t_{\|\|}$	1816	"
$R^c_{\|\|}$	1142	"
$R^t_{\perp}$	30.8	"
$R^c_{\perp}$	111	"
$R_{\perp\|\|}$	81.7	"
p_{int}	20.4	"
d_m	150	mm
ρ	1.6	g/cm^3

- Pre-dimensioning (initial design)

  Choice of material: fiber T800, matrix LY556/HT976

  Manufacturing and assembly specifications:

  $\omega_1 = \omega_6 = 90°$, $t = \sum_{k=1}^{6} t_k$

  $t_2 = t_3 = t_4 = t_5 = t_\omega/4$; $t_1 = t_6 = t_{90}/2$

  Design proposal:

  Symmetric lay-up [90/+ω/-ω/-ω/+ω/90]

  Results:

  t_{90} ≈ 1.8 mm, ω ≈ 25°; t_ω ≈ 1.8 mm

- Optimization model:

  Objective function:

  OF ($\underline{X}$) = minimum mass

Design variables:

t_{90}, t_ω, ω

Restrictions:

g_1; g_2; $g_3 = \min A_{11} - A_{11}(\underline{X})$

Start parameters:

t_1, t_6 = 1,0 mm; Rest 0,5 mm.

3 Solution of the optimization task

Formulation of the problem:

min {OF($\underline{X}$) | h($\underline{X}$) = 0; g($\underline{X}$) > 0}

with h($\underline{X}$) = Vector of the structure mechanical equations to determine stresses and deformations. Here computed by the NASTRAN code)

Calculation:

Search algorithm of the minimum with "optimization module" in NASTRAN (version 66).

4. Design verification

Results :

Input requirement : $t_\omega \cong$ 1.80 mm

t_{90} = 1.7 mm, ω = 28°.

Realization as final design:

t_{90} = 1.76 mm, ω = 26° (*according to production*), t = 3.56.

Design verification calculation of the final design stack:

The CLT computation delivers

- $A_{11} = 2.1 \cdot 10^5$ > requiredA_{11}
- MoS (IFF) = 0.1 ; MoS (FF) ≈ 1.0.

Assessment:

The required safety margins could be achieved. The stiffness is sufficient.

9.4 Coupling Reduction in [*K*] using Tsai's 'Trace-normalized Stiffness' & 'Double-Double'

9.4.1 Introduction

In the following two subchapters invariants are used by to estimate a normalized Master-ply stiffness matrix [Q] for the estimation of laminate stiffness quantities in the case of a novel UD material and by Kappel for the estimation of laminate-CTE values.

Invariants and their Applications (*see sub-chapter 1.3, too*

Before coming to the details of the next sub-chapters it seems to be helpful to shortly present the manifold Use of Invariants. Most often in engineering the invariants of rank two tensors are applied. So-called principal invariants of a second rank tensor ***T*** are the coefficients of the characteristic polynomial

$$\text{“ } p(\lambda) = det(\boldsymbol{T} - \lambda\cdot\boldsymbol{I}) = -\lambda^3 + I_1\cdot\lambda^2 - I_2\cdot\lambda + I^3 \text{ “ with } [T] = \begin{bmatrix} T_{11} & T_{12} & T_{13} \\ T_{21} & T_{22} & T_{23} \\ T_{31} & T_{32} & T_{33} \end{bmatrix}$$

and ***I*** being the identity tensor and λ the polynomial's eigenvalues as solutions of p(λ) = 0. The derived Principal Invariants are (T_{ii} considers Einstein's sum convention)

$$I_1 = trace(T) = T_{ii} = T_{11} + T_{22} + T_{33} \ , \ (\text{index } ^{tr})$$
$$I_2 = T_{11}\cdot T_{22} + T_{11}\cdot T_{33} + T_{33}\cdot T_{22} - T_{12}\cdot T_{21} - T_{13}\cdot T_{31} - T_{23}\cdot T_{32} \ ,$$
$$I_3 = T_{11}\cdot(T_{22}\cdot T_{33} - T_{23}\cdot T_{32}) + T_{12}\cdot(T_{23}\cdot T_{31} - T_{21}\cdot T_{33}) + T_{13}\cdot(T_{21}\cdot T_{32} - T_{22}\cdot T_{31})$$

Main invariants are functions of the principal ones which means coefficients of the characteristic polynomial "***T*** – trace(***T*** / 3)". In the isotropic material case the Main Invariants used read:

Main Invariants: I_1 , $J_2 = I_1^2/3 - I_2$, $J_3 = 2\cdot I_1^3/27 - I_2\cdot I_1/3 + I_3$.

Mixed Invariants, such as sums or differences are used for distinct applications.

In structural mechanics transversely-isotropic invariants UD material of the stress tensor σ_{ik}, the strain tensor ε_{ik} and of the material stiffness tensor Q_{ik} or its inverse the compliance tensor S_{ik} are employed. These invariants base on tensorial formulations. Invariants of the stress tensor are used to establish stress-strength failure criteria and invariants of the strain tensor for strain failure criteria. Using invariants in the stiffness domain helps to get information for a more reliable estimation of pre-design properties for a novel material in pre-design and thus saving time and reducing test effort.

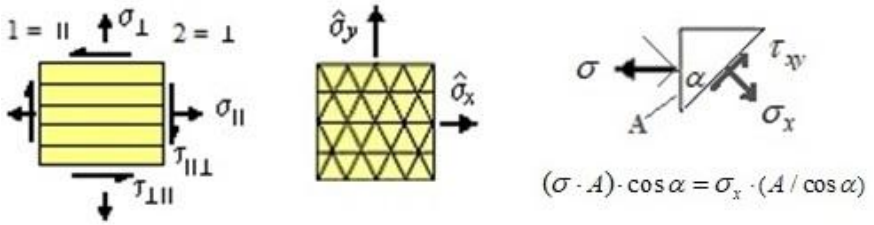
$$I_1 = I_1^{\sigma} = \sigma_1,\ I_2 = \sigma_2 + \sigma_3,\quad I_3 = \tau_{31}^{\ 2} + \tau_{21}^{\ 2},\quad I_4 = (\sigma_2 - \sigma_3)^2 + 4\cdot\tau_{23}^{\ 2},$$
$$I_5 = (\sigma_2 - \sigma_3)\cdot(\tau_{31}^{\ 2} - \tau_{21}^{\ 2}) - 4\cdot\tau_{23}\cdot\tau_{31}\cdot\tau_{21} \quad \text{(from A. Boehler, applied in the FMC)}$$

The focus now is on the rank two tensor Q_{ik} being the *2D-reduced rank four tensor* C_{ikjl} .

Engineering and tensorial stress-strain formulations (*mandatory for invariant determination*) read:

$$\begin{Bmatrix}\sigma_1\\ \sigma_2\\ \tau_{12}\end{Bmatrix}=[Q]\cdot\begin{Bmatrix}\varepsilon_1\\ \varepsilon_2\\ \gamma_{12}\end{Bmatrix}=\begin{bmatrix}Q_{11} & Q_{12} & 0\\ Q_{21} & Q_{22} & 0\\ 0 & 0 & 1\cdot Q_{66}\end{bmatrix}\cdot\begin{Bmatrix}\varepsilon_1\\ \varepsilon_2\\ \gamma_{12}\end{Bmatrix}\Rightarrow\begin{Bmatrix}\sigma_{11}\\ \sigma_{22}\\ \sigma_{12}\end{Bmatrix}=\begin{bmatrix}Q_{11} & Q_{12} & 0\\ Q_{21} & Q_{22} & 0\\ 0 & 0 & 2\cdot Q_{66}\end{bmatrix}\cdot\begin{Bmatrix}\varepsilon_{11}\\ \varepsilon_{22}\\ \varepsilon_{12}\end{Bmatrix}=[Q^{Tr}]\cdot\begin{Bmatrix}\varepsilon_{11}\\ \varepsilon_{22}\\ \varepsilon_{12}\end{Bmatrix}$$

$[Q^{Tr}]$ is necessary for later use. The scalar invariants do not change if the CoS is changed. Therefore in order to derive them the rotation into another CoS must be executed. The following figure presents the various stresses faced with laminas and laminates and a stress transformation for the normal stress into the inclined CoS, exemplarily. These relations are used in the following text.



From equilibrium at the inclined section plane of a tensioned test specimen, balancing the forces in normal and tangential direction, follow the equations below compiled in the standard matrix shape and adapted to UD material, with $[T_\sigma]$ as defined in VDI 2014.

$$\{\sigma'\}=\begin{Bmatrix}\sigma_x\\ \sigma_y\\ \tau_{xy}\end{Bmatrix}=\begin{Bmatrix}\sigma_1\cdot c^2+\sigma_2\cdot s^2-2\tau_{12}\cdot sc\\ \sigma_1\cdot s^2+\sigma_2\cdot c^2+2\tau_{12}\cdot sc\\ \sigma_1\cdot sc-\sigma_2\cdot sc+\tau_{12}\cdot(c^2-s^2)\end{Bmatrix}=\begin{bmatrix}c^2 & s^2 & -2sc\\ s^2 & c^2 & 2sc\\ sc & -sc & c^2-s^2\end{bmatrix}\cdot\begin{Bmatrix}\sigma_1\\ \sigma_2\\ \tau_{12}\end{Bmatrix}=[T_\sigma]\cdot\begin{Bmatrix}\sigma_1\\ \sigma_2\\ \tau_{12}\end{Bmatrix}$$

The tensorial formulations of the stress-strain relations are derived as follows

$$\{\sigma'\}=[Q']\cdot\{\varepsilon'\}=[T_\sigma]\cdot[Q]\cdot[T_\sigma]^T\cdot\{\varepsilon'\}=[T_\sigma]\cdot[Q^{Tr}]\cdot[R]^{-1}\cdot\{\varepsilon'\}\qquad\text{with the}$$

$$\text{Reuter Matrix }[R]=\begin{bmatrix}1 & 0 & 0\\ 0 & 1 & 0\\ 0 & 0 & 2\end{bmatrix},\ [R]^{-1}=\begin{bmatrix}1 & 0 & 0\\ 0 & 1 & 0\\ 0 & 0 & 1/2\end{bmatrix};\ \varepsilon_{xy}=\frac{\gamma_{xy}}{2},\ \varepsilon_{12}=\frac{\gamma_{12}}{2},\ \sigma_{12}\equiv\tau_{12}$$

'Trace'- Invariant Idea of Tsai *(of interest for aerospace community)*

After pre-information in 2014 Steve sent me in 2015 the book *[Tsa15]. Tsai S W and Melo J D*: "*Composite Materials Design and Testing - unlocking mystery with invariants on the Trace idea".* I thought: This is an excellent idea to improve laminate optimization in cases where the UD-material remains the same in the laminate. Hence, in order to make it edible in our notation, I transferred it - still in 2014 - into the designations described in the guideline VDI 2014 which I issued in 2006 and which are also used in the German Aerospace Handbook HSB (*Fundamentals and Methods for Aeronautical Design and Analyses*). Unfortunately, the response in the associated HSB-editorial board IASB (*I was member since 1972*) was disappointing. The IASB did not pick up the Trace idea, but later Prof. Rother at HS Munich did.

For the author, the UD Trace invariant $I_1^Q=Q_{11}+Q_{22}+2\cdot Q_{66}$, numerically *Tr*, is successfully to use as a 'generic laminate quantity', presuming the same UD material is used building a monolithic laminate. This reminds him of his FMC, where he found that isotropic materials have a 'generic' number of 2 *(elastic constants, strengths, strength failure modes, decisive invariants, fracture-angle stable fracture toughness properties*) and the transversely-isotropic UD material a generic number

of 5. Such knowledge effortful guides engineering work, reduces the test amount and makes engineering life simpler and more practical like Steve's Trace idea in laminate design dimensioning or sizing, respectively.

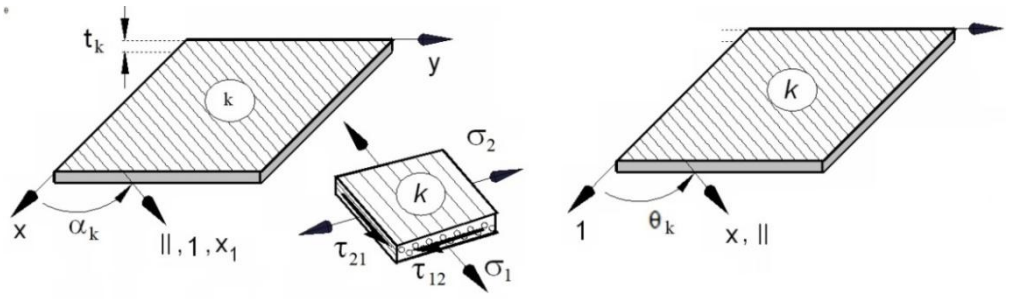
Double-Double (DD) Laminates Idea = coupling reduction concept

In 2022 for the author a customization and industrialization of Trace followed enhanced by the DD working group, generating an easily applicable tool and giving the community "Double-Double - A New Perspective in the Manufacture and Design of Composites", [*Tsa22*], ISBN 978-0-98192-43-2-9 e-book.

In the following paragraphs the author intends to shortly give his thoughts on above ideas and application. This will be performed with the support of Dr. Erik Kappel, who is preparing his Habilitation Work in this composite field. However before, some confusion-causing inconsistencies must be addressed considering notions and terms the author faced during his investigation.

The bottleneck, Notations:

Please, mind the differences in [Tsa22, Sha20, VDI 2014] at first. Figure and text below show the basic differences of VDI 2014 and Tsai in UD notation.



VDI 2014 **Tsai-Melo [Tsa15]**

(1) Please, take a look at the figure above regarding the differently applied suffix 1 for the coordinates and the different positive angle direction

(2) Trace invariant: In [Sha20] it reads $Tr = trace([Q^{Tr}]) = Q_{11} + Q_{22} + 2 \cdot Q_{66} = trace(\boldsymbol{Q}^{Tr})$ *and in [Tsa22]* $trace([Q^{Tr}]) = Q_{xx} + Q_{yy} + 2 \cdot Q_{SS}$. *This is confusing for the user, because in the younger publication [Tsa22] x and y were used according to* $x = 1 = \parallel$, $y = \perp$. *Sha20-contributors also contributed to [Tsa22]. Above formulation still uses tensor notation, indicated by the factor 2, and not matrix notation as it is normal practice and applied in the VDI 2014*

(3) Contributions of a lamina (ply) to the laminate stiffness is performed by firstly rotating [Q] into [Q'], which means from the material CoS into the CoS of the laminate and then summed up by the CLT. The laminate CoS is a structural CoS and in mechanics the axes are required to be indexed by x, y

(4) For the components in the sub-matrices of the inverse, $[K]^{-1}$, *the letters a, b, d or A*, B*, D* are internationally used, since decades! This leads to a conflict in the latter case considering Tsai's star * to mark the thickness-normalized sub-matrices of [K]*

(5) The definition of the larger Poisson's ratio v changed within the last 4 decades twice. Therefore apply Maxwell-Betti. Also the notation of the UD natural axes changed. This would not have been a problem if one outlines the symbols $\parallel, \perp$ as well

(6) A UD-layer may consist of several UD-laminas, also a C-ply-layer may contain several differently oriented UD-laminas

(7) In Tsa15, page 53, the prime is used as a classical rotation index(as applied in the VDI 2014), and on page 14 to indicate compressive or negative!?

[Tsa15, page 53] right $\left[Q'\right]_k = \left[T_\sigma\right]_k \cdot [Q]_k \cdot \left[T_\sigma\right]_k^T$, *however* [Tsa15, page 94 reads $\left[A\right] = \sum_1^n [Q_k] \cdot (z_k - z_{k-1})$

and also in [Sha22], page 27 considering [D], instead of the accurate $\left[A\right] = \sum_1^n [Q'_k] \cdot (z_k - z_{k-1})$

(8) Bar over $\bar{Q}$ *is used in some literature as abbreviation for* Q' *(it should be not used, because statistics claims the bar over).. Please, forgive: The author's creation of his* Life Work Compilation *made an upper senior teacher of him*

(9) [Tsa15]: Index 0 belongs to a general reference plane. This might be the mid-plane

(10) UD-invariants I_1, I_2 *are fixed for decades in UD mechanics as* $I_1 = \sigma_1$, $I_2 = \sigma_2 + \sigma_3$. *On top the choice of J2= trace[S] confuses with the Mises invariant for isotropic materials.*

In order to bypass above conflicts, the author uses in the following Subchapter 9.4 text the notations of the VDI 2014 guideline. These had been carefully checked in the eighties w.r.t. international publications.

Moving from the tensorial to the contracted engineering notation under the presumption 'Symmetry of stress, strain and stiffness elasticity matrix' for the transfer to the stiffness matrix no correction factor is necessary but for the compliance matrix, due to:

Shear strain $\varepsilon_{12} = 0.5 \cdot (\partial u / \partial y + \partial v / \partial x)$ *tensorial* $\rightarrow$ $\varepsilon_6 \equiv \gamma_{12} = 2 \cdot \varepsilon_{12}$ *engineering*.

This is important, because the derivation of the Trace idea requires tensor formulations.

9.4.2 Trace Idea

In general a trace sums up the elements on the main diagonal of a square matrix such as [Q].
If the matrix is tensorial, then trace becomes an invariant, termed Trace by Tsai.

Lamina (ply) and Laminate stiffness quantities:

[Q] is the 2D stiffness elasticity matrix or stiffness matrix of the elastic UD material, respectively.
[K] is the stiffness matrix of the elastic structural element the laminate.

Table 9.4-1 presents the elements of the stiffness elasticity matrix [Q] and of its inverse the elasticity compliance matrix [S]. Into [Q] the five engineering 'constants' are to insert.

Table 9.4-1: Transfer of the UD elasticity properties. After VDI 2014.
Stiffness quantities in matrix spelling and intentionally also in symbolic spelling,
$x_1 \equiv 1 \equiv \parallel$, $2 \equiv \perp$, *the prime' indicates the rotated lamina*. Mind Maxwell-Betti: $\nu_{21} \cdot E_2 = \nu_{12} \cdot E_1$.

The stress and strain relations for the UD lamina in lamina CoS and rotated CoS read

$$\{\sigma\} = (\sigma_1, \sigma_2, \tau_{12})^T \quad , \quad \{\sigma'\} = (\sigma_x, \sigma_y, \tau_{xy})^T = [T_\sigma] \cdot \{\sigma\}$$

$$\{\sigma'\} = [T_\sigma] \cdot \{\sigma\} = [T_\sigma]\,[Q]\,\{\varepsilon\} = [T_\sigma] \cdot [Q] \cdot [T_\varepsilon]^{-1}\,\{\varepsilon'\} = [T_\sigma]\,[Q]\,[T_\sigma]^T\,\{\varepsilon'\} = [Q']\,\{\varepsilon'\}.$$

$$\left\{\varepsilon\right\}_k = \left[S\right]_k \cdot \left\{\sigma\right\}_k, \qquad \left\{\sigma\right\}_k = \left[Q\right]_k \cdot \left\{\varepsilon\right\}_k \quad \text{with} \quad \left[Q\right]_k = \left[S\right]_k^{-1}, \; \left[T_\varepsilon\right]^{-1} = \left[T_\sigma\right]^T$$

$$\left\{\varepsilon'\right\}_k = \left[S'\right]_k \cdot \left\{\sigma'\right\}_k, \; \left\{\sigma'\right\}_k = \left[Q'\right]_k \cdot \left\{\varepsilon'\right\}_k \quad \text{with} \quad \left[Q'\right]_k = \left[T_\sigma\right]_k \cdot \left[Q\right]_k \cdot \left[T_\sigma\right]_k^T$$

$$[Q] = \begin{bmatrix} \frac{E_1}{1-\nu_{21}\cdot\nu_{12}} & \frac{\nu_{21}\cdot E_2}{1-\nu_{21}\cdot\nu_{12}} & 0 \\ \frac{\nu_{12}\cdot E_1}{1-\nu_{21}\cdot\nu_{12}} & \frac{E_2}{1-\nu_{21}\cdot\nu_{12}} & 0 \\ 0 & 0 & G_{12} \end{bmatrix} = \begin{bmatrix} Q_{11} & Q_{12} & 0 \\ Q_{21} & Q_{22} & 0 \\ 0 & 0 & 1\cdot Q_{66} \end{bmatrix} \quad \text{and} \quad [Q]^{-1} = [S] = \begin{bmatrix} \frac{1}{E_{\square}} & \frac{-\nu_{\square\perp}}{E_{\perp}} & 0 \\ \frac{-\nu_{\perp\square}}{E_{\square}} & \frac{1}{E_{\perp}} & 0 \\ 0 & 0 & \frac{1}{G_{\square\perp}} \end{bmatrix}$$

Table 9.4-2: Derivation of the Proof 'Trace is an invariant'

Engineering formulations, VDI2014: Rotation from UD-lamina CoS ∥, ⊥ to Laminate CoS x, y

$$\{\sigma'\}=\begin{Bmatrix}\sigma_x\\ \sigma_y\\ \tau_{xy}\end{Bmatrix}=[T_\sigma]\cdot\begin{Bmatrix}\sigma_1\\ \sigma_2\\ \tau_{12}\end{Bmatrix},\ \{\sigma\}=\begin{Bmatrix}\sigma_1\\ \sigma_2\\ \tau_{12}\end{Bmatrix}=[Q]\cdot\begin{Bmatrix}\varepsilon_1\\ \varepsilon_2\\ \gamma_{12}\end{Bmatrix}=\begin{bmatrix}Q_{11} & Q_{12} & 0\\ Q_{21} & Q_{22} & 0\\ 0 & 0 & 1\cdot Q_{66}\end{bmatrix}\cdot\begin{Bmatrix}\varepsilon_1\\ \varepsilon_2\\ \gamma_{12}\end{Bmatrix},\{\varepsilon'\}=\begin{Bmatrix}\varepsilon_x\\ \varepsilon_y\\ \gamma_{xy}\end{Bmatrix}=[T_\varepsilon]\cdot\begin{Bmatrix}\varepsilon_1\\ \varepsilon_2\\ \gamma_{12}\end{Bmatrix}.$$

To apply the Trace idea one uses a tensorial formulation σ, ε and also within engineering quantities σ, τ, γ.

engineering: $\{\sigma'\}=[T_\sigma]\cdot\{\sigma\},\ [Q']=[T_\sigma]\cdot[Q]\cdot[T_\sigma]^T,\ \{\varepsilon\}=[T_\varepsilon]^{-1}\cdot\{\varepsilon'\},\ [T_\varepsilon]^{-1}=[T_\sigma]^T,\ [Q^{Tr}]=[Q]\cdot[R]$

tensorial: $\{\sigma'\}_{tens}=[T_\sigma]\cdot[Q^{Tr}]\cdot[T_\sigma]^T\cdot\{\varepsilon'\}_{tens}=[T_\sigma]\cdot[Q]\cdot[R]\cdot[T_\sigma]^T\cdot[T_\varepsilon]^{-1}\cdot\{\varepsilon'\}_{tens}$,

with the abbreviation $[Q^{Tr}']=([T_\sigma]\cdot[Q]\cdot[R])\cdot[T_\sigma]^T$, $\varepsilon_{xy}=\gamma_{xy}/2$

At first $([T_\sigma]\cdot[Q]\cdot[R])$ is derived as follows

$$\square\begin{bmatrix}Q_{11} & Q_{12} & 0\\ Q_{12} & Q_{22} & 0\\ 0 & 0 & Q_{66}\end{bmatrix}\ \text{matrix multiplication}\ \square\begin{bmatrix}1 & 0 & 0\\ 0 & 1 & 0\\ 0 & 0 & 2\end{bmatrix}$$

$$\begin{bmatrix}c^2 & s^2 & -2sc\\ s^2 & c^2 & 2sc\\ sc & -sc & c^2-s^2\end{bmatrix}=\begin{bmatrix}c^2Q_{11}+s^2Q_{12} & c^2Q_{12}+s^2Q_{22} & -2sc\cdot Q_{66}\\ c^2Q_{12}+s^2Q_{11} & s^2Q_{12}+c^2Q_{22} & 2sc\cdot Q_{66}\\ sc(Q_{11}-Q_{21}) & sc(Q_{12}-Q_{22}) & (c^2-s^2)\cdot Q_{66}\end{bmatrix}=\begin{bmatrix}c^2Q_{11}+s^2Q_{12} & c^2Q_{12}+s^2Q_{22} & -2sc\cdot Q_{66}\cdot 2\\ c^2Q_{12}+s^2Q_{11} & s^2Q_{12}+c^2Q_{22} & 2sc\cdot Q_{66}\cdot 2\\ sc(Q_{11}-Q_{21}) & sc(Q_{12}-Q_{22}) & (c^2-s^2)\cdot Q_{66}\cdot 2\end{bmatrix}$$

and then $[Q^{Tr}']=([T_\sigma]\cdot[Q]\cdot[R])\ \cdot\ [T_\sigma]^T$ as the final multiplication

$$\square\begin{bmatrix}c^2 & s^2 & sc\\ s^2 & c^2 & -sc\\ -2sc & 2sc & c^2-s^2\end{bmatrix}$$

$$\begin{bmatrix}c^2Q_{11}+s^2Q_{12} & c^2Q_{12}+s^2Q_{22} & -2sc\cdot Q_{66}\cdot 2\\ c^2Q_{12}+s^2Q_{11} & s^2Q_{12}+c^2Q_{22} & 2sc\cdot Q_{66}\cdot 2\\ sc(Q_{11}-Q_{21}) & sc(Q_{12}-Q_{22}) & (c^2-s^2)\cdot Q_{66}\cdot 2\end{bmatrix}=\begin{bmatrix}c^2\left[c^2Q_{11}+s^2Q_{12}\right]+s^2\left[c^2Q_{12}+s^2Q_{22}\right]-2sc\cdot[-2scQ_{66}]\cdot 2 & . & .\\ . & . & .\\ . & . & .\end{bmatrix}$$

resulting in the matrix

$$[Q^{Tr}']=\begin{bmatrix}c^2\left[c^2Q_{11}+s^2Q_{12}\right]+s^2\left[c^2Q_{12}+s^2Q_{22}\right]-2sc\cdot[-2scQ_{66}]\cdot 2 & . & .\\ . & Q_{22}^{Tr}' & .\\ . & . & Q_{66}^{Tr}'\end{bmatrix}.$$

$Q_{11}^{Tr}'=c^2[c^2Q_{11}+s^2Q_{12}]+s^2[c^2Q_{12}+s^2Q_{22}]-2sc[-2sc\cdot Q_{66}\cdot 2]$, $Q_{22}^{Tr}'=s^2[c^2Q_{12}+s^2Q_{11}]+c^2[s^2Q_{12}+c^2Q_{22}]+$

$+\ 2sc[2sc\cdot Q_{66}\cdot 2]$, $Q_{66}^{Tr}'=sc[sc(Q_{11}-Q_{21})]-sc[sc(Q_{12}-Q_{22})]+(c^2-s^2)^2\cdot[Q_{66}\cdot 2]$ which delivers

Trace = $trace([Q^{Tr}'])=\ \Sigma\ c^2[c^2Q_{11}+s^2Q_{12}]+s^2[c^2Q_{12}+s^2Q_{22}]+8s^2c^2[Q_{66}]+$

$+\ s^2[c^2Q_{12}+s^2Q_{11}]+c^2[s^2Q_{12}+c^2Q_{22}]+8s^2c^2[Q_{66}]+\ 2\cdot(s^2c^2[Q_{11}-2Q_{21}+Q_{22}]+(c^2-s^2)^2[2Q_{66}])$

$=\ (c^4+s^4+2s^2c^2)[Q_{11}]+(c^4+s^4+2s^2c^2)[Q_{22}]+s^2c^2(+0\cdot Q_{12})+(8s^2c^2+2(c^2-s^2)^2)[Q_{66}]$

$=\ \Sigma(Q_{11}+Q_{22}+2Q_{66})\ =\ \Sigma(\ Q_{11}^{Tr}'+\ Q_{22}^{Tr}'+2Q_{66}^{Tr}')$, tensorial q.e.d.

Addition theorems: $C=c^2-s^2=\cos 2\alpha$, $c^2=C+s^2=C+(1-c^2)$, $4s^2c^2=(1+C)\cdot(1-C)=1-C^2$

$8s^2c^2+2(c^2-s^2)^2=2(1-C^2)+2C^2=2$, $c^4+s^4+2s^2c^2=(c^2-s^2)^2+4s^2c^2=C^2+(1-C^2)=1$.

$$[T_\sigma]=\begin{bmatrix} c^2 & s^2 & -2sc \\ s^2 & c^2 & 2sc \\ sc & -sc & c^2-s^2 \end{bmatrix},\ [T_\sigma]^T=\begin{bmatrix} c^2 & s^2 & sc \\ s^2 & c^2 & -sc \\ -2sc & 2sc & c^2-s^2 \end{bmatrix},\ [T_\sigma]^{-1}=\begin{bmatrix} c^2 & s^2 & 2sc \\ s^2 & c^2 & -2sc \\ -sc & sc & c^2-s^2 \end{bmatrix},[T_\varepsilon]=\begin{bmatrix} c^2 & s^2 & -sc \\ s^2 & c^2 & sc \\ 2sc & -2sc & c^2-s^2 \end{bmatrix}$$

Idea behind Trace-invariant and Proof $Tr = I_1^Q = Q_{11} + Q_{22} + 2\cdot Q_{66}$, [*Tsa15, p.63 and Net94*].

Invariants and their linear combinations are helpful quantities in mechanics because they are independent of the CoS used in analysis. Hence, moving to tensor quantities the stress-strain relation takes the shape (i, j = 1,2,6).
Unifying stiffness analyses by an invariant–based theory makes design analysis and testing simpler. A trace - being the sum of the diagonal elements of the stiffness matrix $[Q^{\mathrm{Tr}}]$- is an invariant but this is not the case with the trace of the [Q] matrix. The trace$[Q^{\mathrm{Tr}}]$, termed Trace by the authors, was welcomed to hopefully more systematically estimate the stiffness quantities of novel laminates lacking of sufficient data in pre-design. The desired novel stiffness quantities are assumed to be fractions of the invariant Trace. *Table 9.4-2* above describes the derivation that Trace is an invariant.

The factor on the shear stress arises from the classical definition of shear strain, which is twice the tensorial shear strain. Being editor of the VDI 2014, sheet 3, the author had to use the more generally applied VDI notation. This caused some problems because literature does not show full consistency. For the sake of survey some relevant formulas shall be provided:

$$\begin{Bmatrix}\sigma_x\\ \sigma_y\\ \tau_{xy}\end{Bmatrix}=\begin{bmatrix} Q_{11}' & Q_{12}' & Q_{16}' \\ Q_{12}' & Q_{22}' & Q_{26}' \\ Q_{16}' & Q_{26}' & Q_{66}' \end{bmatrix}\cdot\begin{Bmatrix}\varepsilon_x\\ \varepsilon_y\\ \gamma_{xy}\end{Bmatrix}=\begin{bmatrix} Q_{11}^{Tr}' & Q_{12}^{Tr}' & 2Q_{16}^{Tr}' \\ Q_{12}^{Tr}' & Q_{22}^{Tr}' & 2Q_{26}^{Tr}' \\ Q_{16}^{Tr}' & Q_{26}^{Tr}' & 2Q_{66}^{Tr}' \end{bmatrix}\cdot\begin{Bmatrix}\varepsilon_x\\ \varepsilon_y\\ \varepsilon_{xy}\end{Bmatrix}=\left[Q^{Tr}'\right]\cdot\begin{Bmatrix}\varepsilon_x\\ \varepsilon_y\\ \varepsilon_{xy}\end{Bmatrix}=\left[Q^{Tr}'\right]\cdot[R]^{-1}\begin{Bmatrix}\varepsilon_x\\ \varepsilon_y\\ \gamma_{xy}\end{Bmatrix}$$

$$\begin{Bmatrix}\varepsilon_1\\ \varepsilon_2\\ \gamma_{12}\end{Bmatrix}=[R]\cdot\begin{Bmatrix}\varepsilon_1\\ \varepsilon_2\\ \varepsilon_{12}\end{Bmatrix}=[R]\cdot[T_\varepsilon]^{-1}\begin{Bmatrix}\varepsilon_x\\ \varepsilon_y\\ \varepsilon_{xy}\end{Bmatrix}=[R]\cdot[T_\sigma]^T\cdot\begin{Bmatrix}\varepsilon_x\\ \varepsilon_y\\ \varepsilon_{xy}\end{Bmatrix}=[R]\cdot[T_\sigma]^T\cdot[R]^{-1}\cdot\begin{Bmatrix}\varepsilon_x\\ \varepsilon_y\\ \gamma_{xy}\end{Bmatrix}.$$

LL:

(1) Trace = trace$([Q^{Tr}]) = (Q_{11}^{Tr}' + Q_{22}^{Tr}' + 2Q_{66}^{Tr}') = (Q_{11} + Q_{22} + 2\cdot Q_{66}) \neq Q_{11}' + Q_{22}' + 1\cdot Q_{66}'$, *abbreviated Tr, is UD lamina (ply) material-related and not dependent on the rotation angle α or θ.*

(2) Lay-up (stacking sequence) and thickness are geometric quantities.

(3) Trace could be seen as an independent stiffness property. Hence, it seems that one can advantageously use Trace as a factor Tr of the stiffness quantities in the matrices A, B, D of the laminate stiffness matrix

To the honor of Steve, in [Sha20] the authors termed
- as analogous quantity to the Young's modulus E in isotropic case –
the transversely-isotropic UD invariant Trace the 'Tsai modulus' .

Laminate Relationships

Based on test data, Tsai and Melo investigated, that CFRP laminates have common 'generic' stiffness properties after normalization with above Trace invariant of the 2D-stiffness elasticity matrix [Q]. They found that Trace offers a basic measure to capture the behavior of the UD ply material independently of the CoS and of any lay-up. Replacing [Q] by the invariant-dedicated [Q^{Tr}] leads to benefits in laminate design, especially the optimization of the stack.

For stiff fibers, like carbon-fibers, Q_{11} dominates above Trace, whereas the matrix-dominated stiffness terms contribute just a little. This is an essential benefit that can be exploited when designing laminates. The Trace can be used to show that a wide range of materials have almost identical entries if one looks 'Trace-normalized' at the elasticity coefficients.
Meanwhile studies have demonstrated the beneficial use of trace in design dimensioning and optimization, fast notched strength prediction and in fracture mechanics [*Sha20*].

Thickness-Normalization:

Under mechanical loading the general equilibrium conditions of the plate read (^{0} is reference plane)

$$\begin{Bmatrix} n^0 \\ m \end{Bmatrix} = \begin{bmatrix} A & B \\ B^T & D \end{bmatrix} \cdot \begin{Bmatrix} \varepsilon^0 \\ \kappa \end{Bmatrix} \quad \text{with} \quad \{n^0\} = t \cdot \{\hat{\sigma}\} = \Sigma \{\sigma'\}_k \cdot t_k = [A] \cdot \{\varepsilon^\circ\}, \; [Q']_k = [T_\sigma]_k \cdot [Q]_k \cdot [T_\sigma]_k^T$$

$$[A] = 1 \cdot \sum_{n=1}^{n} [Q'_k] \cdot (z_k - z_{k-1}) \; , \; [B] = \frac{1}{2} \cdot \sum_{n=1}^{n} [Q'_k] \cdot (z_k^{\,2} - z_{k-1}^{\,2}) \; , \; [D] = \frac{1}{3} \cdot \sum_{n=1}^{n} [Q'_k] \cdot (z_k^{\,3} - z_{k-1}^{\,3})$$

Thickness-Normalization of the [*K*]-sub-matrices shall be now generated in order to achieve the same units, in GPa or MPa, in all sub-matrices and also to numerically achieve homogenized laminates. The resulting submatrices are marked by a roof sign analogous to the roof sign used to indicate homogenized (smeared) laminate stresses $\hat{\sigma}$ or strains $\hat{\varepsilon}$ used in the VDI 2014. In *Table 9.4-2* the sub-matrices after the thickness-normalization are depicted for the classical and for the invariant case.

Table 9.4-2: Thickness-normalization of laminate sub-matrices, $[Q]$-based. t = laminate thickness

$$[A] = \begin{bmatrix} A_{11} & A_{12} & A_{16} \\ A_{12} & A_{22} & A_{26} \\ A_{16} & A_{26} & A_{66} \end{bmatrix} \quad \text{and} \quad [a] = [A]^{-1}, \; [\hat{a}] = \left[\hat{A}\right]^{-1},$$

$$\text{defining} \qquad \left[\hat{A}\right] = [A]/t, \quad \left[\hat{B}\right] = [B] \cdot 2/t^2 \; , \quad \left[\hat{D}\right] = [D] \cdot 12/t^3.$$

Secondly the prosperous Trace shall be induced. This procedure is termed Trace-normalization.

Trace-normalization:

For the UD-material IM7-977 Erik Kappel, by *Table 9.4-3*, provided the author with the following material input data set (*originally from Tsai-Melo*) and further with the computed elements of the sub-laminates as an example of trace-normalization.
The example is a so-called 'quad laminate' from aerospace industry with the classical 4 fiber directions. (*Many thanks Erik*).

Table 9.4-3: Trace-normalized lamina quantities $\left[Q^{Tr}\right]$ *-based, [courtesy E. Kappel]*

Lay-up $[0_2/\,45/\text{-}45/90]_{4S}$, t_k = 0.125 mm, 40 layers or UD-laminas, t =5 mm

$\left\{\bar{R}\right\} = (3250,\ 1600,\ 62,\ 98,\ 75)^T$ MPa, $\left\{E\right\} = (191000,\ 191000,\ 9940,\ 9940,\ 7790)^T$ MPa, $\nu_{21} = 0.35$

$$\left[Q^{Tr}\right] = \begin{bmatrix} Q_{11} & Q_{12} & 0 \\ Q_{21} & Q_{22} & 0 \\ 0 & 0 & 2\cdot Q_{66} \end{bmatrix} = \begin{bmatrix} 192.2 & 3.501 & 0 \\ 3.502 & 10.008 & 0 \\ 0 & 0 & 2\cdot 7.790 \end{bmatrix} \text{ GPa}$$

$$\rightarrow \text{Trace} = Tr = 192.2 + 10.008 + 2\cdot 7.790 = 217.81 \text{ GPa}$$

$$\text{or} \qquad [Q]\cdot[R] \;=\; \left[Q^{Tr}\right] = Tr\cdot\begin{bmatrix} 0.883 & 0.016 & 0 \\ 0.016 & 0.046 & 0 \\ 0 & 0 & 2\cdot 0.036 \end{bmatrix} \text{ GPa.}$$

$$\rightarrow \text{Trace} = Tr\cdot(0.883 + 0.046 \;+\; 2\cdot 0.036)\ \text{GPa} = Tr\cdot 1\ \text{GPa}\,.$$

The classical elements of the A-B-D-submatrices *(A in N/mm, B in N, D in N·mm)* read

$$[A] = \begin{bmatrix} 514651 & 99540 & 0 \\ 99540 & 332429 & 0 \\ 0 & 0 & 120983 \end{bmatrix},\ [B] = \begin{bmatrix} 0 & 0 & 0 \\ 0 & 0 & 0 \\ 0 & 0 & 0 \end{bmatrix},\ [D] = \begin{bmatrix} 1227866 & 192634 & 0 \\ 192634 & 566364 & 0 \\ 0 & 0 & 237308 \end{bmatrix}$$

And after Trace-normalization with Thickness-Normalization *(in MPa)* with $t = n\cdot t_k$.

$$\left[\hat{A}^{Tr}\right] = Tr\cdot\begin{bmatrix} 0.473 & 0.091 & 0 \\ 0.091 & 0.305 & 0 \\ 0 & 0 & 0.111 \end{bmatrix},\ \left[\hat{B}^{Tr}\right] = Tr\cdot\begin{bmatrix} 0 & 0 & 0 \\ 0 & 0 & 0 \\ 0 & 0 & 0 \end{bmatrix},\ \left[\hat{D}^{Tr}\right] = Tr\cdot\begin{bmatrix} 0.541 & 0.085 & 0.006 \\ 0.085 & 0.250 & 0.006 \\ 0.006 & .0006 & 0.105 \end{bmatrix}.$$

where the last expressions assume identical thickness for all plies → laminate thickness $t = n\cdot t_k$.
The check of the traces proofs that the sum of the diagonal terms

$$\text{trace}\,[\hat{A}^{Tr}] \;=\text{trace}\,[\hat{D}^{Tr}] \equiv \text{Trace} \quad \text{or} \quad \text{is} \;\; 1 \quad \text{if Trace-normalized.}$$

Above relations require that any performed transformation from engineering to tensorial must be considered in order to use standard CLT-programs.

Tsai and Melo gave in [*Tsa15, pages 62 and 65*] rotation relations when rotating from the UD-material CoS to a CoS, rotated by an angle α (c = cosα, s = sinα):

$$\begin{aligned} Q_{11}' &= c^2(c^2Q_{11} + s^2Q_{12}) + s^2(c^2Q_{12} + s^2Q_{22}) + 4\cdot c^2s^2Q_{66} \\ Q_{22}' &= s^2(s^2Q_{11} + c^2Q_{12}) + c^2(s^2Q_{12} + c^2Q_{22}) + 4\cdot c^2s^2Q_{66} \\ Q_{66}' &= c^2s^2(Q_{11} + Q_{22}) - 2\cdot c^2s^2Q_{12} + (c^4 - 2c^2s^2 + s^4)Q_{66} \\ Q_{12}' &= c^2s^2(Q_{11} + Q_{22}) + (c^4 + s^4)Q_{12} - 4\cdot c^2s^2Q_{66} \qquad . \end{aligned}$$

$$I_1 = trace(T) = T_{ii} = T_{11} + T_{22} + T_{33} \ ,$$

From $$I_2 = T_{11} \cdot T_{22} + T_{11} \cdot T_{33} + T_{33} \cdot T_{22} - T_{12} \cdot T_{21} - T_{13} \cdot T_{31} - T_{23} \cdot T_{32} \ ,$$

$$I_3 = T_{11} \cdot (T_{22} \cdot T_{33} - T_{23} \cdot T_{32}) + T_{12} \cdot (T_{23} \cdot T_{31} - T_{21} \cdot T_{33}) + T_{13} \cdot (T_{21} \cdot T_{32} - T_{22} \cdot T_{31})$$

follows for the stiffness elasticity invariants using the tensorial UD matrix $[Q^{tr}]$:

$$I_1{}^Q = Trace = trace([Q^{tr}]) = Tr = Q_{11} + Q_{22} + 2 \cdot Q_{66} \ , \text{ see [Tsa15, p. 65]}$$

$$I_2{}^Q = 0.5 \cdot \left((trace[Q^{tr}])^2 - trace[Q^{tr}]^2 \right) = 2 \cdot Q_{66} \cdot (Q_{11} + Q_{22}) + Q_{11} \cdot Q_{22} - Q_{12}{}^2)$$

$$I_3{}^Q = \text{determinant}[Q^{tr}] = 2 \cdot Q_{66} \cdot (Q_{11} \cdot Q_{22} - Q_{12}{}^2) \ .$$

Kappel extended the Trace idea and observed $2 \cdot I_{1-2}^Q = Q_{11} + Q_{22} + Q_{66} + Q_{12}$ to be an invariant.

This invariant takes the full Q-set into account in contrast to Trace. However, this is still not a complete set of invariants. Hence, E. Kappel tried to generalize the determination of UD elasticity stiffness invariants by applying an optimization procedure. As approach he set up a four-parameter objective function

$$\left| p_1 \cdot (Q_{11}\,' - Q_{11}) + p_i \cdot (Q_{22}\,' - Q_{22}) + p_i \cdot (Q_{12}\,' - Q_{12}) + p_i \cdot (Q_{66}\,' - Q_{66}) \right|$$

with the constraints $p_i > 0$. The parametric solution reads:

$$b \cdot Q_{11}\,' + (b-a) \cdot Q_{12}\,' + b \cdot Q_{22}\,' + (b+a) \cdot Q_{66}\,' = b \cdot Q_{11} + (b-a) \cdot Q_{12} + b \cdot Q_{22} + (b+a) \cdot Q_{66}$$

with the parameter set (b, a) .

Special cases of the parametric solution equation capture all invariants below (*courtesy Kappel*).

$8 \cdot U_1 = \quad 3Q_{11} + 3Q_{22} + 2Q_{12} + 4Q_{66}$ .....Case b =3, a = 1

$8 \cdot U_4 = \quad 2Q_{11} + 2Q_{22} + 6Q_{12} - 4Q_{66}$ .....Case b =1, a = -5

$\text{Trace} = trace[Q^{tr}] = \ Q_{11} + Q_{22} + 2Q_{66}$ .....Case b =1, a = 1

$I_{12} = \quad = Q_{11} + Q_{22} + 2Q_{12}$ ..... .Case b =1, a = -1

$2 \cdot I_{1-2}^Q = \ \text{Trace} + I_{12} \ = Q_{11} + Q_{22} + Q_{12} + Q_{66}$ ..... .Case b =1, a = 0 .

Kappel's idea to avoid the difficulty in 'jumping' between tensorial and engineering quantities. Of course, to think in tensorial quantities is theoretically convincing however to remain with engineering quantities makes an investigation more understandable for engimeers.

9.4.3 Masterply Concept - application to Estimate the Stiffness Matrix [Q] of a Novel UD Lamina

Table 9.4-4 presents material data sets for very different UD CFRP (epoxy) materials. The columns represent the elasticity properties, the Trace (*Tr*) *scalar* values and the Trace-normalized elements Q_{ij} / Tr of the UD laminas. Invariant elastic properties give comprehensive information about the in-plane stiffness potential of a laminate consisting of a distinct composite material. All elastic stiffness quantities are fractions of the Trace invariant.

Taking all data sets into account the main finding of Kappel (*analogous to Tsai, Melo*) is, that the fiber-dominated CoV is pretty small and counts just 2.25 %. The higher matrix-dominated CoVs do not contribute to *Tr* that much. Since the originators use the Median and not the Average the resulting plane stiffness matrix for setting-up the desired 'Master ply' reads in line:

$$[Q]_{\text{ply}}^{\text{Master}} = Tr \cdot ([Q]_{\text{ply}}^{\text{Master}} / Tr) = 167.7 \cdot \begin{bmatrix} 0.888 & 0.017 & 0 \\ 0.017 & 0.052 & 0 \\ 0 & 0 & 0.028 \end{bmatrix} \text{GPa} \rightarrow (0.888 + 0.052 + 2 \cdot 0.028) = 1.$$

Kappel took all stiffness matrix elements into account in his invariant I^Q and also proved the invariance of I^Q. The result is

$$[Q]_{\text{ply}}^{\text{Master}} = I^Q \cdot ([Q]_{\text{ply}}^{\text{Master}} / I^Q) = 167.7 \cdot \begin{bmatrix} 0.899 & 0.017 & 0 \\ 0.017 & 0.053 & 0 \\ 0 & 0 & 0.029 \end{bmatrix} \text{GPa} \rightarrow (0.899 + 0.053 + 0.029 + 0.017) = 1 .$$

With this extension of Tsai's Trace idea he could reduce the fiber-dominated CoV from 2.25% to 1.51%, such improving the Trace-based results.

Table 9.4-4: Prepreg specific elasticity moduli, normalized stiffness coefficients,

$I_1^Q = Tr$ *and* $I_{1-2}^Q \equiv I^Q$ *,.* $2\,I^Q = Q_{11} + Q_{22} + Q_{66} + Q_{12}$, $I_1^Q = Tr = Q_{11} + Q_{22} + 2 \cdot Q_{66}$, .

Courtesy Tsai-Melo [Tsa15, black entries] and Kappel (red entries).

To find in the upcoming *Habilitation scriptum* of Erik Kappel

Material	E_1	E_2	ν_{12}	G_{12}	Tr	Q_{11}/Tr	Q_{22}/Tr	Q_{12}/Tr	Q_{66}/Tr
IM7/977-3	191.0	9.9	0.35	7.79	217.8	0.883	0.046	0.016	0.036
T800/Cytec	162.0	9.0	0.40	5.00	182.5	0.895	0.050	0.020	0.027
T700 C-Ply 55	121.0	8.0	0.30	4.70	139.2	0.875	0.058	0.017	0.034
T700 C-Ply 64	141.0	9.3	0.30	5.80	162.8	0.871	0.057	0.017	0.036
AS4/3501	138.0	9.0	0.30	7.10	162.0	0.857	0.056	0.017	0.044
IM6/epoxy	203.0	11.2	0.32	7.10	229.6	0.889	0.049	0.016	0.031
AS4/F937	148.0	9.7	0.30	4.55	167.7	0.888	0.058	0.017	0.027
T300/N5208	181.0	10.3	0.28	7.17	206.5	0.880	0.050	0.014	0.035
IM7/8552	171.0	9.1	0.32	5.29	191.6	0.897	0.048	0.015	0.028
IM7/MTM45	175.0	8.2	0.33	5.50	195.1	0.901	0.042	0.014	0.028
IMA/M21E	154.0	8.5	0.32	4.20	171.8	0.901	0.050	0.016	0.024
AS4/8552	141.0	9.8	0.27	5.20	161.9	0.875	0.061	0.016	0.032
700GC/M21	110.0	8.0	0.31	8.20	135.2	0.819	0.060	0.018	0.061
T700/M21	135.0	8.5	0.33	4.20	152.9	0.889	0.056	0.018	0.027
T700/M21 m	117.0	7.8	0.33	3.50	132.7	0.888	0.059	0.020	0.026
T800H/3900-2	129.1	7.5	0.33	3.52	144.5	0.899	0.052	0.017	0.024
IM7/977-2	159.0	9.2	0.25	4.37	177.6	0.899	0.052	0.013	0.025
CoV I_1^Q	16.95	10.62	10.3	26.2	16.1	2.25	9.83	11.1	27.3
Average $= Tr$	151.5	8.99	0.314	5.48	172.4	0.883	0.053	0.017	0.032
Median	148.0	9.0	0.32	5.2	167.7	0.888	0.052	0.017	0.028
CoV I_{1-2}^Q	16.95	10.62	10.3	26.2	16.1	1.51	10.09	11.07	28.55
Average *replaces*	151.5	8.99	0.314	5.48	169.79	0.897	0.054	0.017	0.033
Median Tr	148.0	9.0	0.32	5.2	166.04	0.899	0.053	0.017	0.029

Master-Ply Concept:

For design development with a new UD material one can work with the computed value *Tr* (or I_Q) from the measured [Q] of the new UD material and the derived Master Ply coefficients applying

$$Tr^{\text{new}}_{\text{material}} = \text{trace}\left[Q^{\text{measured}}_{\text{new material}}\right] \quad \Rightarrow \text{ approach } \quad \left[Q^{\text{pre-design}}_{\text{new material}}\right] = Tr^{\text{new}}_{\text{material}} \cdot \left[Q\right]^{\text{Master}}_{\text{ply}} \quad .$$

This procedure is similar to the author's experience with strength criteria models when designing new materials. Analogous to the determination of the elasticity stiffness coefficients in $\left[Q^{\text{measured}}_{\text{new material}}\right]$ *only the strength values in* $\{R^{\text{measured}}_{\text{new material}}\}$ *are to determine. Strength failure behavior and criterion SFC are still known for the full family analogous to* $\left[Q\right]^{\text{Master}}_{\text{ply}}$ *which also represents the full CFRP family.*

Before presenting the Double-Double idea it is to remind regarding the scatter of the numerically obtained Trace-based stiffness quantities:

- If the average behavior of a laminate shall be modelled and a prediction for a new laminate is to provide - as best basis - average properties are to use in CLT analysis, which alone guarantees the optimally achievable estimation, namely 50% reliability.
- Considering the production-based scatter, Automated Fabrication (AF) of the semi-finished carbon- plies will keep scatter lower. (*By the way: It is not AM Automated Manufacture anymore, but Automated Fabrication AF, due to the fully digitized process).*
- One can further conclude that laminates usually have smaller CoVs. This is due to the favorable compensation of the effect of the flaws across the laminate thickness. The linearly design value impacting average value is even though slightly lower, but the CoV-influence is more than 2.3 times in the calculation of the design value. Secondly, normalization leads to insensitivity among many laminas which justifies the creation of a 'Master-ply', helpful when predesigning with novel UD laminas of the same family. Hence, certification may permit lesser tests, at least of the smooth coupon test specimen campaigns.
- This reminds the author of an analogy to his FMC: In the case a novel material is to apply. Then, if the material behavior of the novel material is similar to that of a tested known material set, the same strength criterion can be used and certification requires lesser tests because former test results can be applied, too.

LL: The Master ply idea fully corresponds to statistics, where the best prediction is achieved with maximum information about the parent distribution, preferably the CoV.

Citation Steve Tsai:

"*Off-axis ply angles other than 45° may open up great opportunities for design. Instead of the standard discrete plies angles, we propose the use of ply angles with angles much shallower than the 45° ".*

9.4.4 Double-Double Sub-laminate Family Idea

(0°, 45°,-45°, 90°) laminate family in aerospace $\longrightarrow$ ($\pm\,\varphi°,\ \pm\,\psi°$) a Tsai-proposed novel family type

Two angle-plies of different fiber angles form a four-ply sub-laminate,

a multi-ply semi-fished product identified by {..} to discriminate it from [..] for the UD-layer stacks,

as building block of a monolithic laminate wall.

Double-Double means two angle-plies or it means two doubles.

Reduction of Coupling:

The ABD-matrix of the laminate determines whether a laminate experiences undesired twisting and warping for in-service loads and also due to manufacturing. This encourages the optimization of the ABD or K-matrix and above all to reduce the coupling responsible B_{ij}. The sub-matrix A in *Fig. 9.4-1* is not dependent on the stack in contrast to the D matrix. A symmetric stack makes the B matrix zero (blue dots), however, this is a bottleneck for classical design and production, because it cannot be realized economically. Appropriate stacking of a non-symmetric laminate to reduce the size of the [B] matrix is possible by using many thin layers compared to fewer thick layers. Thereby coupling will be reduced and mass saving can be obtained.

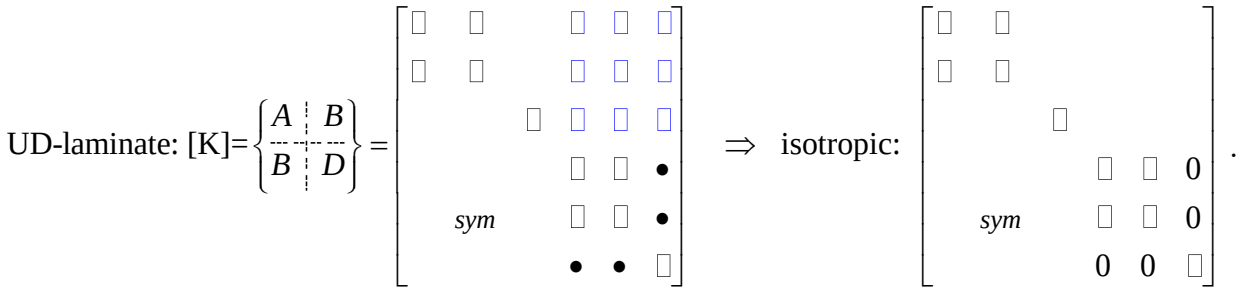


Fig.9.4-1: Occupancy (filling) of laminate stiffness matrix [K] in the transversely-isotropic UD case and in the isotropic case

Modern tapes composed of non-crimp fabrics, still representing sub-laminates, allow now the use of thin single layer stacks, whereby coupling effects and CoSts can be reduced. The conflict, between the designer (*desires many thin layers in order to reduce the fracture-mechanics-based low lateral micro-cracking level in transversal ply direction*) and the production engineer who prefers fewer 'thick' layers for production CoSt reasons, is not that a big issue anymore. To reduce above bottleneck problem, the target is the 'homogenization of the laminates'. This means to generate a laminate-stiffness matrix ABD that is approximately filled like the isotropic one but nevertheless provides different stiffness and strength capacities for plates and shells in the different directions. Warping and twisting of a laminate can be suppressed by a sufficient number of repeats and the ABD-laminate stiffness matrix will approximately look like the simple isotropic one. However laminate stiffness and strength resistance will not become quasi-isotropic but remain oriented.

Homogenization goal of Double-Double DD:
A minimally-filled ABD matrix, enabled by repeated 4-ply building blocks,
where full mid-plane symmetry is no longer needed.

The DD-tool to realize this is a novel lay-up strategy that incorporates a 4-ply semi-finished product NCF-sub-laminate $\{\pm\varphi / \pm\psi\}$ and uses building blocks stacked upon each other.

Traditional Laminates versus DD Laminates

Traditional UD-ply composed laminate families, for decades used in aerospace, have the layer angles (0°,45°,-45°,90°), which means 4 fixed fiber directions α. They are designed according to rules, built up from experience. Basic rules are to get D_{16} and D_{26} approximately zero in order to avoid coupling between bending and twisting and to achieve symmetric laminates obtaining $[B] = 0$. Further, balanced stacks decouple extension and shear $A_{16} = A_{26} = 0$.

The novel C-PLY™ (™ *is Trade Mark*) is a dry, multi-axial, gap-free, stitched (*by stitching chain polyester, which harms the stack a little*) CF semi-finished Non-Crimp Fabric product with an Ep-powder binder fully cured later later in the final resin-system infusion process, see *Fig.9.4-2*. Its definition is $\{\varphi / -\varphi / \psi / -\psi\}$ or $\{\varphi / -\psi / -\varphi / \psi\}$, which means a double balanced angle ply, with the angles counted relative to the length orientation of the C-PLY™ = 4 plies = 1 physical layer ≡ 1 numerical lamina = sub-laminate = building block of the full laminate. See sub-chapter 23.6. In the laminate stack the given angles are referred to the difference of the C-PLY™-orientation angle and the laminate CoS x,y. The angular difference of successive layers in the C-PLY™ and the laminate should be as small as possible in order to keep the shear stresses in the interface low. The special feature of the balanced angle ply C-Ply™-NCF out of the bunch of usually applied 'quad-NCFs' is that it fits directly to the production of the '[B]=0 DD-laminates'.

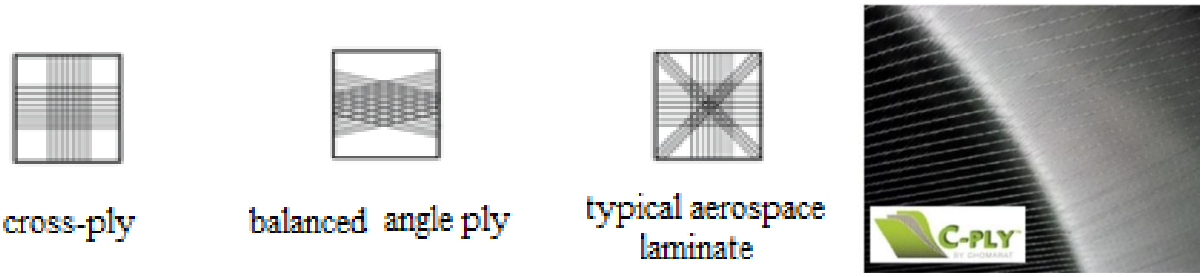
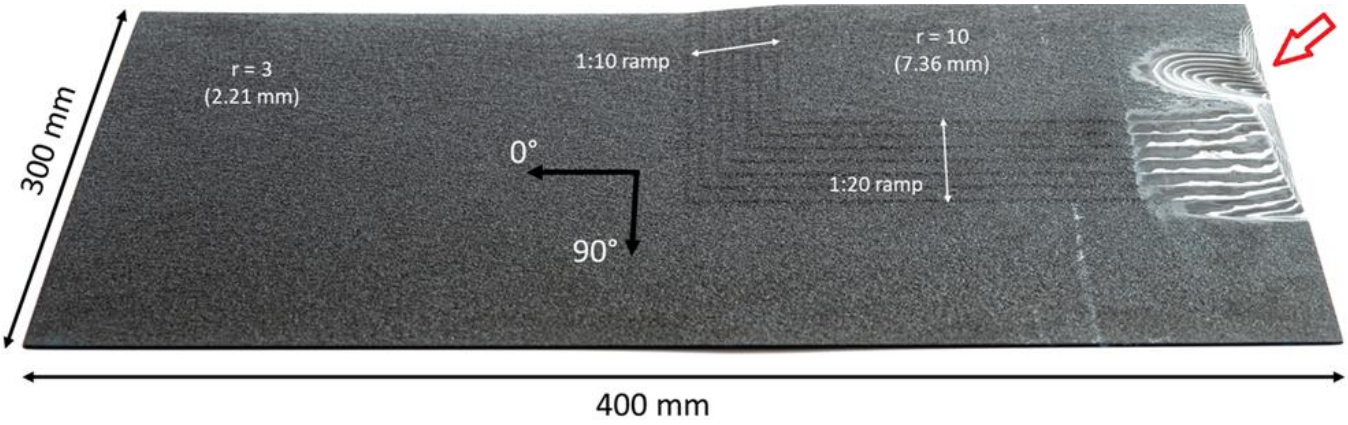


Fig. 9.4-2: (left) Lay-uptypes; (right) C-PLY™ example (from DD-book)

Fig.9.4-3 presents a plate composed according to the DD concept and thereby replacing a *C-PLY*™ 'building block' by a similarly built four UD-layer 'building block'. The material is UD M21E/IMA (*from Hexcel, A 350 aircraft material*) medium-grade prepreg of 0.184 mm, $t_{building\ block}$ = 0.736 mm.



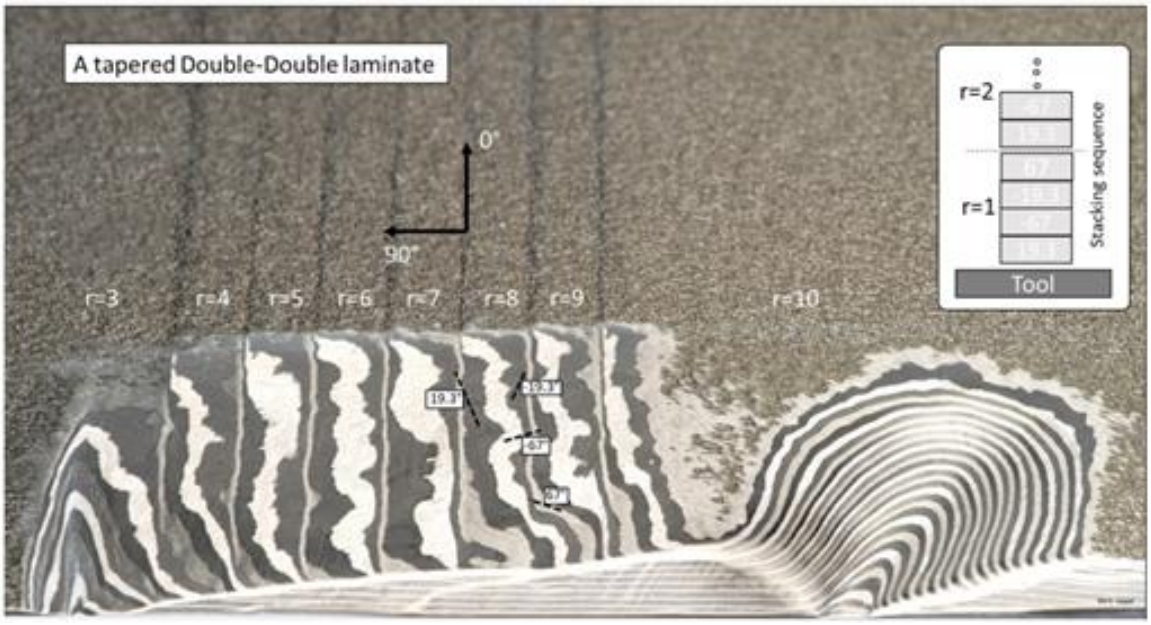


*Fig.9.4-3, tapered 'Double-Double laminate': (up) Test specimen, lay-up: {19.3/ -67/ -19.3/ 67}$_{3\text{-}10}$; (down) inclined cross-section cut (r ≡ classical running index k). [*Courtesy Erik Kappel, DLR]

In the figure above fine polishing of the surface was performed to identify the individual plies of the building block-stack. The inclined cut through the cross-section of the laminate, see upper picture, shows the individiual plies in one building block which is here a UD-ply-representation of a building block C-PLY™-layer. The optical folding is the result of a flatter cut. From the first displayed building block, indicated k = 3, the thickness is unfortunately not visible on the image. Indexing runs via 1 < k < n with k the running C-PLY™-layer and n the total number of C-PLY™ -layer repetitions. In classical UD-CLT it reads 1 < k < n with n the total number of UD layers.

A DD laminate consists of four-ply laminate building blocks, which are repeated as indicated by the repetition parameter *r* . In order to approximately achieve UD-strength high performance quality (*no crossings which cause micro-crack damage*), angle-ply Non-Crimp Fabric (NCF) layers are applied in production. An angle-ply set of two angle-plies builds up a sub-laminate $[\pm\varphi / \pm\psi]$ as a building block, counting $r = 1$. This means that two angle-ply layers are laid upon another and then stitched for a good handling. The angle values are determined by solving an optimization task.
The C-PLY™ represents such a deliverable angle-ply set. This specific 'ply' is developed using the most advanced technology and tow spreading process [*Composites World*]. The C-PLY, *produced at Chomarat,* is comprised of unidirectional or multidirectional stitched plies from 50 g/m^2 to 600 g/m^2 per ply. The used carbon tows possess 12, 24, 48 k filaments and are provided in the domains HS (*High Strength*), IM (*Intermediate Modulus*) or HM (*High Modulus*). There are only two DD stacking sequences to be selected and not the classical hundreds or more.

As an example a sub-laminate lay-up, stacked [15/-15/50/-50], may serve. It belongs to the family (15°,-15°, 50°,-50°). (*For a fixed lay-up the [...] bracket is used, different to that for a family (...)).*

The concept provides a novel stacking method of a new family of laminates for optimal sizing. Trace idea and Double-Double concept intend to fulfill the traditional design requirements by a novel procedure. The aim is an approximated decoupling by achieving $[B] \cong 0$ and finally optimally targeting the relatively "simple" isotropic K-matrix. The quality of the procedure depends

on the repeats *r*. The coefficients B_{ij} depend on 1/r, whereas the D_{16} and D_{26} (*bold black-dotted in above Fig.9.4-1)* depend on $1/r^2$ and thus the decaying effect by r^2 is stronger! For more details, especially on the applied Thickness-/Trace-normalized sub-matrices, see [*Kap22*]. Therein, it is found for an Omega stringer profile that a B matrix-minimal lay-up is $\{\varphi / -\psi / -\varphi / \psi\}$.

Final challenge is the application in optimization considering Minimum Mass, several Load Cases and production Side Constraints. Of course, to obtain an optimal stack in the sizing phase of the design usually requires the consideration of numerous permutations. This number of permutations can be reduced by applying in the optimization the Trace-normalized stiffness quantities. After optimization, several sub-laminate stacks may be optimal and one has to decide which one should be taken. The quadratic distribution of the inter-laminar shear stress across the thickness of an isotropic cross-section under shear delivers some measure for the achieved homogenization of the laminate stack.

In *Table 9.4-5* a classical laminate stack is compared to two DD-stacks, representing a repeat number $r = 1$ and $r = 8$. The material input is the CFRP above, namely IM7-977. Computation of [A] is driven here from the pre-condition 'Equal membrane stiffness in all three examples'.

Optimum stack determination

Principally there are two different tasks (1) DD-substitution of a conventional quad-stack laminate and (2) Fully free DD-optimization, performed analogously to the sizing of sheets.
According to the fact that each DD-sublaminate is balanced the normal strains in the plane are decoupled from the shear strains. This simplifies extremely the optimization procedure.

Table 9.4-5: Examples classical aerospace laminate versus two BB-stacks [courtesy E. Kappel]

$\{E\}$ = (191000, 191000, 9940, 9940, 7790)^T MPa, ν_{21} = 0.35. Elasticity stiffness matrix in 'Trace format':

$$[Q^{Tr}] = \begin{bmatrix} Q_{11} & Q_{12} & 0 \\ Q_{21} & Q_{22} & 0 \\ 0 & 0 & 2\cdot Q_{66} \end{bmatrix} = \begin{bmatrix} 192.2 & 3.501 & 0 \\ 3.502 & 10.008 & 0 \\ 0 & 0 & 2\cdot 7.790 \end{bmatrix} \text{ GPa}$$

Lay-up $[0/\ 45/-45/90]_{4s}$, t_k = 0.125 mm, 32 layers or UD-laminas, t = 4 mm

The elements of the classical A-B-D-submatrices read (A in N/mm, B in N, D in N·mm)

$$[A] = \begin{bmatrix} 322425 & 96089 & 0 \\ 96089 & 322425 & 0 \\ 0 & 0 & 113193 \end{bmatrix},\ [B] = \begin{bmatrix} 0 & 0 & 0 \\ 0 & 0 & 0 \\ 0 & 0 & 0 \end{bmatrix},\ [D] = \begin{bmatrix} 499515 & 126770 & 11389 \\ 126770 & 362849 & 11389 \\ 11389 & 11389 & 149643 \end{bmatrix}$$

Invariant, after Trace-normalization with Thickness-normalization (in MPa)

$$[\hat{A}^{Tr}] = Tr\cdot \begin{bmatrix} 0.370 & 0.110 & 0 \\ 0.110 & 0.370 & 0 \\ 0 & 0 & 0.130 \end{bmatrix},\ [\hat{B}^{Tr}] = Tr\cdot \begin{bmatrix} 0 & 0 & 0 \\ 0 & 0 & 0 \\ 0 & 0 & 0 \end{bmatrix},\ [\hat{D}^{Tr}] = Tr\cdot \begin{bmatrix} 0.430 & 0.109 & 0.010 \\ 0.109 & 0.312 & 0.010 \\ 0.010 & 0.010 & 0.129 \end{bmatrix}.$$

Check of traces proved, that the 'Trace sum' of the diagonal terms, meaning factor 2 for the third, becomes 1.

1 = 0.430 + 0.312 + 2 · 0.129 or trace $[\hat{A}^{Tr}]$ = trace $[\hat{D}^{Tr}]$ = 217810 MPa.

Lay-up $\{22.5/\ -22.5/67.5/-67.5\}_r$, r = 1, t_k = 1.0 mm, 4 layers → t = 4 mm

The elements of the A-B-D-submatrices read (A in N/mm, B in N, D in N·mm)

$$[A] = \begin{bmatrix} 322425 & 96089 & 0 \\ 96089 & 322425 & 0 \\ 0 & 0 & 113193 \end{bmatrix},\ [B] = \begin{bmatrix} -257700 & 0 & -64425 \\ 0 & 257700 & -64425 \\ -64425 & -64425 & 0 \end{bmatrix},\ [D] = \begin{bmatrix} 429900 & 128051 & 82033 \\ 128051 & 429900 & -82033 \\ 82033 & -82033 & 150924 \end{bmatrix}$$

After Trace-normalization with Thickness-normalization (in MPa = N/mm^2)

$$[\hat{A}^{Tr}] = Tr\cdot \begin{bmatrix} 0.370 & 0.110 & 0 \\ 0.110 & 0.370 & 0 \\ 0 & 0 & 0.130 \end{bmatrix},\ [\hat{B}^{Tr}] = Tr\cdot \begin{bmatrix} -0.148 & 0 & -0.037 \\ 0 & 0.148 & -0.037 \\ -0.037 & -0.037 & 0 \end{bmatrix},\ [\hat{D}^{Tr}] = Tr\cdot \begin{bmatrix} 0.370 & 0.110 & 0.071 \\ 0.110 & 0.370 & -0.071 \\ 0.071 & -0.071 & 0.130 \end{bmatrix}$$

The check of the 'Trace sum' of the normalized terms delivers 1.

Lay-up $\{22.5/\ -22.5/67.5/-67.5\}_r$, r = 8, t_k = 0.125 mm, 32 layers or UD-laminas → t = 4 mm

The elements of the A-B-D-submatrices read (A in N/mm, B in N, D in N·mm)

$$[A] = \begin{bmatrix} 322425 & 96089 & 0 \\ 96089 & 322425 & 0 \\ 0 & 0 & 113193 \end{bmatrix},\ [B] = \begin{bmatrix} -32213 & 0 & -8053 \\ 0 & 32213 & -8053 \\ -8053 & -8053 & 0 \end{bmatrix},\ [D] = \begin{bmatrix} 429900 & 128051 & 1282 \\ 128051 & 429900 & -1282 \\ 1282 & -1282 & 150924 \end{bmatrix}$$

After Trace-normalization with Thickness-normalization (in MPa)

$$[\hat{A}^{Tr}] = Tr\cdot \begin{bmatrix} 0.370 & 0.110 & 0 \\ 0.110 & 0.370 & 0 \\ 0 & 0 & 0.130 \end{bmatrix},\ [\hat{B}^{Tr}] = Tr\cdot \begin{bmatrix} -0.018 & -0.005 & -0.005 \\ -0.005 & 0.018 & -0.005 \\ -0.005 & -0.005 & 0.000 \end{bmatrix},\ [\hat{D}^{Tr}] = Tr\cdot \begin{bmatrix} 0.370 & 0.110 & 0.001 \\ 0.110 & 0.370 & -0.001 \\ 0.001 & -0.001 & 0.130 \end{bmatrix}$$

The check of the 'Trace sum' of the normalized terms delivers 1.

(1) In the Substitution case – from the various possibilities – in the general case one could apply

Two objective functions based on $\left[\hat{A}\right]$, $\left[\hat{D}\right]$ for i = 1, 2, 6 it is to search

$$\rightarrow \quad \min\left(\left|\hat{A}_{ii} - \hat{A}_{ii,ref}\right|\right) \quad \text{and} \quad \min\left(\left|\hat{D}_{ii} - \hat{D}_{ii,ref}\right|\right) .$$

If the structural task is an in-plane problem then one can apply $\min\left(\left|\hat{A}_{ii} - \hat{A}_{ii,ref}\right|\right)$ and for a bending problem $\min\left(\left|\hat{D}_{ii} - \hat{D}_{ii,ref}\right|\right)$.

(2) Fully free DD-optimization case with, due to the design task, differently combined side constraints.

For the design requirements Loading and Stiffness are to consider and is to provide

* Side constraint “Stability”: Buckling condition,
* Side constraint “Stress limit (= strength)”: Strength failure condition (criterion)
* Side constraint “Strain limit”: Strain failure condition
* Side constraint “Deformation limit”: Deformation limit.

It is to discriminate structural limit steas of material-linked design limit states.

LL:

- *Trace-based Master-ply stiffness and strength makes optimization possible and practical.*
- *The influence of the repeat factor r with 1/r and 1/r² is clearly shown by the decreasing off-diagonal elements of the two laminates with r =1 and r = 8 in see Table 9.4-5.. [$\hat{A}^{Tr}$] and [$\hat{D}^{Tr}$] become narrower for increasing repeats r which is a desired homogenization effect.*

Optimum Patching

Repair requires local thickening of the existing laminate. For design reasons, the stiffness matrix must not be changed.

The BB procedure with building-blocks (4-plies at once) is of interest for the upcoming production methods Automated Fiber Placement AFP, Automated Tape Laying ATL and AFPP (Automated Fiber Patch Placement). These AF methods permit to reduce the stress concentration problems at ply-drops, resin pockets and other flaw locations. *Fig.9.4-4.*

The figure below presents a procedure when using Automated Fiber Patch Placement. Why not moving here from the varying quad-stack family (0°, 45°, 90°) to BB-stacks?

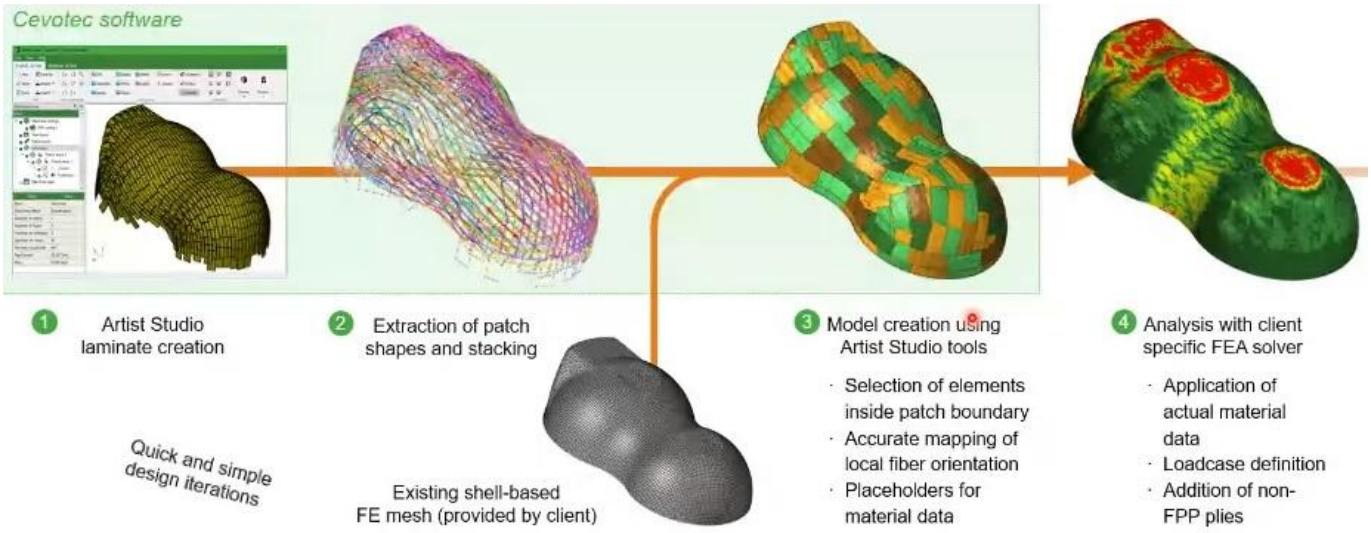


Fig.9.4-4: Automated Fiber Patch Placement [courtesy Cevotec Software].

DD-modelling, analysis and design verification: same UD-material in the laminate as precondition

In strength analysis the repeated double angle-ply sub-laminate and the full laminate can be modelled ply-wise as $\{\varphi / -\varphi / \psi / -\psi\}$ in each sub-laminate stack.

By the way: $\pm\varphi,\ \pm\psi$ *corresponds to the* ω*-angle in net-theory* $\pm\omega_1, \pm\omega_2$*, where*

$$\alpha_1 = \omega_1,\ \alpha_2 = -\omega_1,\ \alpha_3 = \omega_2\ ,\ \alpha_4 = -\omega_2\ .$$

Of-course, stitching of the C-ply harms the UD material, however this is captured in the material tests determining the material design values in test data evaluation.

For designing mind again, please:

* Whereas the modelling is performed with average properties and average stress-strain curves, in the verification of the final laminate design - task-required - upper or lower or average properties are to insert in the analysis.
* The present stress-based design verification in Aerospace requires stress criteria and A- or B-strength design allowables. A strain-based design verification as precondition for certification, would need permission of the FAA including strain criteria coupled to strain design allowables.

9.5 Master-ply Concept - application to estimate Laminate CTEs

Before, the impact of Trace was on the reduction of warping. Now, reduction of Process-induced Distortion (PiD) shall be the objective. This means, to check whether the Master-ply concept may help to obtain sufficiently good CTE estimations and further help to reduce the test effort necessary for pre-design (transferred from *[E. Kappel: On invariant combinations of Q_{ij} coefficients and a novel invariant I_Q), Composites Part C: Open Access 10 (2023) 100335], 4 pages*).

Table 9.5-1 shows the CoVs of the A-coefficients are found to be very small , and using Trace are found between 0.76% and 6.52%. It can be seen that the master-ply data is very close to the determined median values. Choosing $I^Q = (Q_{11} + Q_{22} + Q_{66} + Q_{12}) \equiv I^Q_{1-2}$ the results still become better.

When laminate stiffness is focused, the chosen stiffness-normalizing invariant has a strong effect, however, the CTE determination process is variant-independent. This will be shown in the following paragraph. *Table 9.4-6* indicates that the exact ply data is not essential for adequate CTE-predictions, as the scatter of the different materials in terms of the thickness-normalized coefficients is very small.

Table 9.5-1: $[0_2/45/-45/90]_{4S}$ CFRP laminate

Material	$\tilde{A}_{11}^{\Pi+2}$	$\tilde{A}_{22}^{\Pi+2}$	$\tilde{A}_{66}^{\Pi+2}$	$\tilde{A}_{12}^{\Pi+2}$	I_{1-2}^{Q}
IM7/977-3	0.47	0.31	0.11	0.09	217.8
T800/Cytec	0.48	0.31	0.11	0.10	182.5
T700 C-Ply 55	0.47	0.31	0.11	0.09	139.2
T700 C-Ply 64	0.47	0.31	0.11	0.09	162.8
AS4/3501	0.47	0.31	0.11	0.09	162.0
T300/N5208	0.47	0.31	0.11	0.09	206.5
IM6/epoxy	0.47	0.31	0.11	0.09	229.6
AS4/F937	0.48	0.31	0.11	0.10	167.7
IM7/8552	0.48	0.31	0.11	0.10	191.6
IM7/MTM45	0.48	0.31	0.11	0.09	195.1
IMA/M21E	0.48	0.31	0.11	0.10	171.8
AS4/8552	0.47	0.31	0.11	0.09	161.9
T700GC/M21	0.46	0.30	0.12	0.08	135.2
T700/M21	0.48	0.31	0.11	0.10	152.9
T700/M21-measured	0.48	0.31	0.11	0.10	132.7
T800H/3900-2	0.48	0.31	0.11	0.10	144.5
IM7/977-2	0.48	0.31	0.11	0.10	177.6
CoV	1.30	0.76	2.13	6.52	16.11
Average	0.47	0.31	0.11	0.09	172.21
Median	0.48	0.31	0.11	0.10	168.05
Master ply	0.47	0.31	0.11	0.10	168.4

For deriving the laminate-CTEs the thermal relations are of interest:

$$\{\varepsilon'\} = (\varepsilon_x, \varepsilon_y, \gamma_{xy})^T = [T_\varepsilon] \cdot \{\varepsilon\} = [T_\varepsilon] \cdot ([S] \cdot \{\sigma\} + \{\varepsilon_T\}), \; [T_\sigma]^{-1} = [T_\varepsilon]^T, \; [T_\varepsilon]^{-1} = [T_\sigma]^T$$

$$\{\sigma'\} = (\sigma_x, \sigma_y, \tau_{xy})^T = [T_\sigma] \cdot \{\sigma\} = [T_\sigma] \cdot [Q] \cdot (\{\varepsilon\} - \{\varepsilon_T\}) = [Q'] \cdot (\{\varepsilon'\} - \{\varepsilon_T'\}) \quad \text{with}$$

$$\{\varepsilon_T'\} = \{\alpha_T'\} \cdot \Delta T = [T_\varepsilon] \cdot \{\varepsilon_T\} = [T_\varepsilon] \cdot \{\alpha_T\} \cdot \Delta T; \; \{\alpha_T'\} = (\alpha_{Tx}, \alpha_{Ty}, \alpha_{Txy})^T, \; \{\alpha_T\}_k = (\alpha_{T\parallel}, \alpha_{T\perp}, 0)_k^T$$

$$\begin{Bmatrix} \sigma_x \\ \sigma_y \\ \tau_{xy} \end{Bmatrix} = \begin{bmatrix} Q_{11}' & Q_{12}' & Q_{16}' \\ & Q_{22}' & Q_{26}' \\ (symm) & & Q_{66}' \end{bmatrix} \begin{Bmatrix} \varepsilon_x \\ \varepsilon_y \\ \gamma_{xy} \end{Bmatrix}, \; [T_\sigma] = \begin{bmatrix} c^2 & s^2 & -2sc \\ s^2 & c^2 & 2sc \\ sc & -sc & c^2 - s^2 \end{bmatrix}, \; [T_\varepsilon] = \begin{bmatrix} c^2 & s^2 & -sc \\ s^2 & c^2 & sc \\ 2sc & -2sc & c^2 - s^2 \end{bmatrix}.$$

Focusing Process-induced Distortion PiD, from general equilibrium of the plate the membrane loading relation is of interest. From this equation the laminate CTEs can be determined for zero

mechanical loading under the presumption that the temperature change is constant over the laminate thickness:

$$\{n^0\} = [A]\cdot\{\varepsilon^0\} - \{n_T{}^0\} \;\Rightarrow\; \{n^0\} = [A]\cdot\{\varepsilon^0\} - \{n_T{}^0\} = 0 \;\rightarrow\; \{\varepsilon^0\} = [A]^{-1}\cdot\{n_T{}^0\}$$

The laminate rotated expressions are $\{\varepsilon^0\} = \{\alpha_T{}'\}^{\text{laminate}}\cdot\Delta T = [T_\varepsilon]\cdot\{\alpha_T\}\cdot\Delta T$

For the laminate: Same ply material is used!

$$\{\varepsilon^0\} = \{\alpha_T{}'\}^{\text{laminate}}\cdot\Delta T = [T_\varepsilon]\cdot\{\alpha_T\}\cdot\Delta T \text{ and also } \{\varepsilon^0\} = [A]^{-1}\cdot\{n_T{}^0\}\ .$$

$$\{n_T{}^0\} = \sum[Q']_k\,[T_\varepsilon]_k\cdot\{\alpha_T\}\cdot\Delta T\cdot t_k,\quad [Q']_k = [T_\sigma]_k\cdot[Q]_k\cdot[T_\sigma]_k{}^T,\ [T_\sigma]^T = [T_\varepsilon]^{-1}$$

$$\Rightarrow\ \{\alpha_T{}'\}^{\text{laminate}}\cdot\Delta T = [A]^{-1}\cdot\{n_T{}^0\} = [A]^{-1}\cdot\sum_{k=1}^{n}[Q']_k\cdot[T_\varepsilon]_k\cdot\{\alpha_T\}\cdot\Delta T\cdot t_k$$

$$\{\alpha_T{}'\}^{\text{laminate}}\cdot\Delta T = [A]^{-1}\cdot\sum_{k=1}^{n}[T_\sigma]_k\cdot[Q]_k\cdot[T_\sigma]_k{}^T\cdot[T_\varepsilon]_k\cdot\{\alpha_T\}\cdot\Delta T\cdot t_k$$

$$\{\alpha_T{}'\}^{\text{laminate}} = [A]^{-1}\cdot\sum_{k=1}^{n}[T_\sigma]_k\cdot[Q]_k\cdot 1\cdot\{\alpha_T\}\cdot t_k$$

$$(\alpha_{Tx},\alpha_{Ty},\alpha_{Txy})^T = \left(\sum_{n=1}^{n}[Q'_k]\cdot t_k\right)^{-1}\cdot\{\alpha_T\}\cdot t_k = \left(\sum_{n=1}^{n}[T_\sigma]_k\cdot[Q]_k\cdot[T_\sigma]_k{}^T\cdot t_k\right)^{-1}\cdot\{\alpha_T\}\cdot t_k.$$

Introduction of all elements involves I_Q with $[Q] = I_Q\cdot[Q_Q^{Master}]$

$$(\alpha_{Tx},\alpha_{Ty},2\alpha_{Txy})^T = \left(\sum_{n=1}^{n}[T_\sigma]_k\cdot I_{1+2}{}^Q\cdot[Q_Q^{Master}]\cdot[T_\sigma]_k{}^T\cdot t_k\right)^{-1}\cdot\sum_{n=1}^{n}[T_\sigma]_k\cdot I_{1+2}{}^Q\cdot[Q_Q^{Master}]\cdot\{\alpha_T\}\cdot t_k$$

$$(\alpha_{Tx},\alpha_{Ty},2\alpha_{Txy})^T = \left(\sum_{n=1}^{n}[T_\sigma]_k\cdot I_{1+2}{}^Q\cdot[Q_Q^{Master}]\cdot[T_\sigma]_k{}^T\right)^{-1}\cdot\sum_{n=1}^{n}[T_\sigma]_k\cdot I_{1+2}{}^Q\cdot[Q_Q^{Master}]\cdot\{\alpha_T\}$$

$$(\alpha_{Tx},\alpha_{Ty},2\alpha_{Txy})^T = \left(\sum_{n=1}^{n}[T_\sigma]_k\cdot[Q_Q^{Master}]\cdot[T_\sigma]_k{}^T\right)^{-1}\cdot\sum_{n=1}^{n}[T_\sigma]_k\cdot[Q_Q^{Master}]\cdot\{\alpha_T\}\ .$$

The shear portion α_{Txy} only becomes zero if symmetrical stacking with a balanced angle ply of the angle ω is given. The rotated CTEs are just dependent on the material choice and not dependent on the invariant I_Q.

Laminate CTEs are found independent of *Tr or* I_Q, which explains the observation, that laminates with a certain stacking, made from different prepregs show usually very similar laminate CTEs, even though ply engineering constants (properties) differ strongly.

Above equations are a basis for determining high-quality CTE-estimates of laminates without knowing the exact UD-ply properties.

LL:
The Master-ply concept can be extended to the application for CTE determination but needs further investigation.

[*Kap22*] Kappel E: *Double–Double laminates for aerospace applications - Finding best laminates for given load sets*. Composites Part C: Open Access 8 (2022) 100244

[*Kap23*] Kappel E: Habilitation Work at DLR Braunschweig
[*Net94*] Nettles A T: *Basic Mechanics of Laminated Composite Plates*. NASA-RP-1351, 1994
[*Sha20]* Sharma N et al: *A case for Tsai's Modulus, an invariant-based approach to stiffness*. Composite Structures 252 (2020), 112683

Many thanks to Erik for peering above two sub-chapters and
for helping me to better understand Trace- Procedure and DD-optimization Process
in favor of laminate-optimizing structural engineers working after VDI 2014 and the HSB.

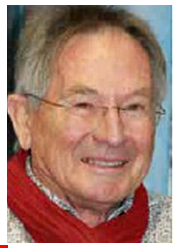
Long ago at a conference at San Diego
Steve said to me:

"I will switch the lights on and off.
Ralf, please, share the session".

Now - many decades later- I say to him:

Dear Steve,
being still practical in your age
and editor of the book DD
takes me to say
"Now, you are a 'role model' for me to also
remain fully active in future,
as long as it is possible!"





I'm very grateful for being able to follow you with unbroken motivation.

And, above *all* of course, ***for being still able to set up my huge Life-Work Compilation.***

9.5 Some further Examples considering distinct Material Effects

9.5.1 Mechanically and hygro-thermally stressed UD Strip

uniaxial stress state $x \equiv \|$, strip, laminate, layer k

Task 1 *"Determination of strains and stresses of the plate strip"*

- Geometry and loading $\{n^0\} = (F / b, 0, 0)^T$, $\{n_T\} = 0$, $\{n_M\} = 0$
- Boundary condition: free
- $\{\sigma\}_k$, necessary for later cross-sectional stress verification.
- Computation

$$\{n\} = (n_x, n_y, n_{xy})^T = [A]\{\varepsilon\} - \{n_T\} - \{n_M\} = \quad (1)$$

$$\rightarrow \quad \{\varepsilon\} = [A]^{-1}(\{n\} + \{n_T\} + \{n_M\})$$

$$= \{\varepsilon_{mech}\} + \{\varepsilon_T\} + \{\varepsilon_M\} \quad (2)$$

$$\{\varepsilon'\}_k = \{\varepsilon\} \quad \text{.....compatibility} \quad (3)$$

- Results

$$\{\varepsilon\}_k = [T_\varepsilon]_k^{-1}\{\varepsilon'\}_k \quad \text{.....transformation} \quad (4)$$

$$\{\sigma\}_k = [Q]_k(\{\varepsilon\}_k - \{\varepsilon_T\}_k - \{\varepsilon_M\}_k) \quad (5)$$

with $\{\varepsilon_T\}_k = [T_\varepsilon]_k^{-1}\{\varepsilon_T\}_k$, $\{\varepsilon_M\}_k = [T_\varepsilon]_k^{-1}\{\varepsilon_M\}_k$.

Task 2 *"Consideration of different cross-sectional boundary conditions"*

- Computation a

Boundary conditions: On both sides hinged (fixed) UD lamina

$$\varepsilon = \varepsilon_{mech} + \varepsilon_T + \varepsilon_M = 0 \text{ , fixed} \quad \text{.....strain boundary condition} \quad (1)$$

$$\varepsilon' = \varepsilon \quad \text{.....compatibility} \quad (2)$$

$$\varepsilon_{\|} = \varepsilon_1 = [T_\varepsilon]^{-1} \cdot \varepsilon' \quad \text{with } [T_\varepsilon]^{-1} = 1 \quad (3)$$

$$\sigma_{\|} = \sigma_1 = [Q](0 - \varepsilon_T - \varepsilon_M) \quad \text{with } [Q] = E_{\|} \text{ .} \quad (4)$$

Note: Stability is to consider under generated compression.

- Computation b

Boundary conditions: On both sides free UD lamina beam

$$\varepsilon = \varepsilon_{mech} + \varepsilon_T + \varepsilon_M, \quad \text{free} \quad (1)$$

$$\varepsilon' = \varepsilon \quad \text{.....compatibility} \quad (2)$$

$$\varepsilon_{\|} = \varepsilon_1 = \varepsilon' \quad (3)$$

$$\sigma_{\|} = \sigma_1 = E_{\|}(\varepsilon_1 - \varepsilon_T - \varepsilon_M) = 0 \quad \text{.....stress boundary condition} \quad (4)$$

$$\varepsilon_{\|} = \varepsilon_1 = \varepsilon_T + \varepsilon_M \text{ .}$$

Note: Temperature with moisture change determines together the strain.

9.5.3 Micro-mechanical Estimation of the Strain Magnification Factor around filaments

Task

- Given:

Glass $E_{f\perp} = E_{f\|} = E_f$ (isotropic); $E_m / E_f = 0.05$; $\varphi = 0.60$

- Assumption:

"Series spring model" meaning irealized a quadratic package of filament arrangement (*Packungsart*)

- Geometric relations

  $\ell_m = \ell_0 - d \quad \rightarrow \quad \ell_m/\ell_0 = 1 - d / \ell_0$,

  $\varphi = \pi \cdot d^2 / 4 \cdot \ell_0^2 \quad \rightarrow \quad d/\ell_0 = 2\,\varphi^{0.5} / \pi^{0.5}$ and $\ell_m/\ell_0 = 1 - \varphi^{0.5}/\pi^{0.5}$

- Mechanical equilibrium: due to use of the series spring model

  On an average $\sigma_\perp$ acts as well at the matrix portion as at the filament portion $\rightarrow$ $\sigma_\perp = \sigma_{f\perp} = \sigma_{m\perp}$

- Hookean law:

  $\sigma_\perp = E_\perp \cdot \varepsilon_\perp$; $\sigma_{f\perp} = E_{f\perp} \cdot \varepsilon_{f\perp}$; $\sigma_{m\perp} = E_m \cdot \varepsilon_{m\perp}$

- Strain relations:

  $\varepsilon_\perp = \Delta\ell/\ell_0$ mit $\Delta\ell = \Delta\ell_f + \Delta\ell_m \rightarrow \varepsilon_\perp \cdot \ell_0 = \varepsilon_f \cdot \ell_f + \varepsilon_m \cdot \ell_m$

Strain magnification factor [*after A. Puck*] $f_\varepsilon = \varepsilon_m / \varepsilon_\perp$

$\varepsilon_m/\varepsilon_\perp = 1 / [\ell_m/\ell_0 + (1 - \ell_m/\ell_0)\, E_m / E_f]$ (> 1)

$= 1 / [1 - 2\cdot\varphi^{0.5}\,(1 - E_m/E_f) / \pi^{0.5}] = 6$ for the values above.

Conclusion:
Above value causes - for practical design reasons - the use of matrix-systems possessing a fracture strain of > 6 % !

9.5.4 Material data prediction and moisture strain determination for a CFRP (T300/914C)

1. Task

- Searched:
  - Backcalulation, because test data is missing
  - Prediction of $\alpha_{M\parallel}, \alpha_{M\perp}$ for another V_f
  - Magnitude of the moisture strain in a matrix.

- Given: Set of material properties

given micro-mechanical values							composite measurement			
Fasern	E_f	$\nu_{\perp\parallel f}$	Matrix	E_m	ν_m	α_{Mm}	$\alpha_{M\parallel}$	$\alpha_{M\perp}$	V_f	ψ
	N/mm^2			N/mm^2						
T300	218800	0.23	914C	3500	0.35	0.242	0.008	0.420	0.60	0.69
E-Glas	74500	0.25	CY209	3500	0.35	0.255	0.003	0.552	0.60	0.76

by back-calculation determined

2. Solutions

a) Prediction of properties for UD material (P-ES in VDI 2014)

Using the micro-mechanics formula, as recalculated matrix value for T300/914C is obtained

$\alpha_{Mm} = \{\alpha_{M\parallel}\,[\nu_m(1-\varphi)+\nu_{\perp\parallel f}\cdot\varphi]+\alpha_{M\perp}\}(1-\psi)/[(1-\varphi)(1+\nu_m)]$

$= \{0.008\cdot[0.35\cdot0.40 + 0.23\cdot0.60]+0.420\}\cdot0.1/[0.4\cdot1.35]$

$= \{0.002+0.20\}\cdot0.31 / 0.54 = 0.242$.

(For checking the obtained α_{Mm} is inserted into

$\alpha_{M||} = \alpha_{Mm}\,(1-\varphi)\,(1-\psi)\,/[(\varphi\,(E_f / E_m - 1) +1)] = 0.0081$).

b) For $\varphi = 55\ \%$ with $\rho_m / \rho_f = 1.30 / 1.74 = 0.75$ is obtained via

$\psi = 1/[1 + \rho_m / \rho_f(1/\varphi-1)] = 1/[1+0.75(1/0.55-1)] = 0.62$,

$\alpha_{M||} = (0.242\ (0.45)/[(0.55\ (62-1) +1) \cdot 0.38] = 0.0083$,

$\alpha_{M\perp} = \alpha_{Mm}.(1-\varphi)\cdot(1+\nu_m)/(1-\psi) - \alpha_{M||}\,[\nu_m(1-\varphi) + \nu_{\perp||f} \cdot \varphi] = 0.387$

$= 0.242\cdot(0.45)\cdot(1.35)/(0.38) - 0.0083\cdot[0.35\cdot(0.45) + 0.23\cdot 0.55]$.

c) Magnitude of the moisture elongation of the matrix

In a matrix, with the characteristic values

$\alpha_{Tm} = 40 \cdot 10^{-6}/\,K$ und $\alpha_{Mm} = 0{,}242$

for a change of moisture of $\Delta M_{eff} = 1.65\ \%$ strains of the same size, namely

$\varepsilon_{Mm} = \Delta M_{eff} \cdot \alpha_{Mm} = 0.0165 \cdot 0.242 = 0.4\ \%$ as for $\Delta T = 100$ K

$\varepsilon_{Tm} = \Delta T \cdot \alpha_{Tm} = 100\ K \cdot 40 \cdot 10^{-6}/K = 0.4\ \%$ are achieved.

→ Moisture strains can balance temperature strains.

In HSB i.e. is used $\varphi \equiv V_f$ = fiber volume ratio , $\psi \equiv$ fiber mass ratio .

9.5.5 Use of the Micro-mechanical Formulas: Back-calculation and prediction

1. Task

- Searched
  - Elasticity quantities from UD test data employing micro-mechanical formulas for the non-measurable fiber properties
  - Property prediction for $V_f = \varphi = 0{,}55$, $\rho_m / \rho_f = 0{,}75$
- Given: Property data sets a) and b)

		Measurement matrix		Measurement composite $V_f = \varphi = 0{,}6$; $\psi = 0{,}67$				
Back-calculation	a)	E_m N/mm² 3500	ν_m - 0.35	$E_{||}$ N/mm² 160000	$E_\perp$ N/mm² 9300	$G_{||\perp}$ N/mm² 5400	$\nu_{\perp||}$ - 0.32	$\gamma_{\perp\perp}$ - 0.40
Prediction	b)	5000	0.32					

2. Solution with micro-mechanical formulas [VDI2014]

$$E_{||} = E_{||f} \cdot V_f + E_m \cdot (1-V_f) \cong E_f \cdot V_f, \quad \text{within regime } 0.3 \le V_f \le 0.65;$$

$$\nu_{\perp||} = \nu_{\perp||f} \cdot V_f + \nu_m \cdot (1-V_f), \quad G_m = E_m / (2 + 2 \cdot \nu_m).$$

$$E_\perp = \frac{E_m}{1-\nu_m^{\,2}} \cdot \frac{1 + 0.85 \cdot V_f^{\,2}}{(1-V_f)^{1.25} + V_f \cdot E_m / (E_{\perp f} \cdot (1-\nu_m^{\,2}))}; \quad G_{\perp||} = \frac{G_m \cdot (1 + 0.4 \cdot V_f^{\,0.5})}{(1-V_f)^{1.5} + V_f \cdot G_m / G_{\perp||f}}.$$

a) Back-calculation

$E_{f\|} = [E_\| - E_m \cdot(1 - \varphi)] / \varphi = 264333 \text{ N/mm}^2 \approx E_\| / \varphi$

$\nu_{f\perp\|} = [\nu_{\perp\|} - \nu_m \cdot(1 - \varphi)] / \varphi = [0.32 - 0.35 \cdot (0.40)] / 0.60 = 0.30$

$E_{f\perp} = \varphi \cdot E_m \cdot E_\perp / [E_m \cdot(1 + 0.85\, \varphi^2) - E_\perp \cdot(1 - \varphi)^{1,25} \cdot (1 - \nu_m^2)] = 9890 \text{ N/mm}^2$

$G_{f\|\perp} = \varphi\, G_m\, G_\# / [G_m\, (1 + 0.60\, \varphi^{0,5}) - G_\# (1 - \varphi)^2] = 4060 \text{ N/mm}^2$

$\nu_{f\perp\perp} = [\nu_{\perp\perp} - \nu_m \cdot(1 - \varphi) \cdot (1 + \nu_m - \nu_{\perp\|} \cdot E_m / E_\|) / (1 - \nu_m^2 + \nu_m \cdot \nu_{\perp\|} \cdot E_m / E_\|)] / \varphi = 0.31$.

Control check is to perform!

b) Prediction

The values of matrix and fiber volume fraction change:

$\psi = 1/[1 + 0.75\, (1/0.55\text{-}1)] = 0.62$ fiber mass volume

$2 \cdot G_m = 5000 \cdot (1 + 0.32) = 6600 \text{ N/mm}^2$

$E_\| = 264333 \cdot 0.55 + 5000\, (0.45) = 147600$

$E_\perp = (5000/(1\text{-}0.32^2)) \cdot [1+0.85 \cdot 0.55^2) / (0.45^{1.25} + 0.55 \cdot 5000/9889 = (1 - 0.32^2))] = 10800 \text{ N/mm}^2$

$G_{\|\perp} = 3300 \cdot (1 + 0.6 \cdot 0.55^{0.5}) / [(1\text{-}0.55)^{2.\,0} + 0.55 \cdot 3300 / 4059] = 7340 \text{ N/mm}^2$

$\nu_{\perp\|} = 0.300 \cdot 0.55 + 0.2\, (0.45) = 0.31$

$\nu_{\perp\perp} = 0.38.$

10 FMC-based Fatigue Life Models, basically displayed for the brittle UD material

Before going into details of fatigue (initially crack free) and (macro-)damage tolerance (cracked) the two different design principles (philosophies) used, "Safe Life" and "Damage Tolerance", shall be shortly outlined, see *Fig.10-0:*

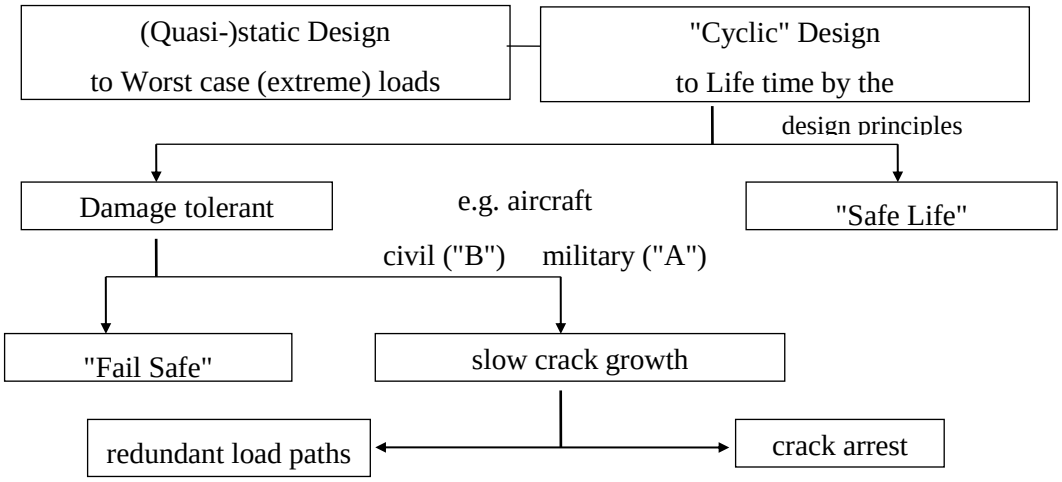


Fig. 10-0: Principles when designing a structure (example aircraft)

- Safe Life Design Principle:

  By this principle the structure is thought defect-free over lifetime. The principle is applicable to all types of structures, monolithic as well as redundant elements.

- Damage Tolerance Design Principle:

  A damage tolerant structure can endure the specified design limit load even in case of a pre-damage caused e.g. by fatigue or an impact as long as the damage will be discovered by inspection or malfunction and will be repaired. This approach differs from the original Fail-Safe philosophy in that it assumes cracks/damage of the smallest allowable size to exist in the structure already at the very first load cycle. Also, a distinction is made between in service-inspectable or non-inspectable structures.

  The procedure includes determination of damage type and size allowed by the required performance level. Type and size not allowed have to be found by inspection. For this reason, the probability of being detected or not detected is important.

Cyclic fatigue Life consists of three phases. This means for the focus example *laminate*:

Phase I: Increasing micro-damage in embedded laminas up to discrete micro-damage onset. Determination of accumulating micro-damage portions (Schädigungen) initiated at the end of elastic domain and dominated by diffuse micro-cracking + matrix yielding inclusively cavitation under 3D-tensile stressing, and finally little cracks such as micro-delaminations. Degradation begins with onset of diffuse micro-damage in the strain hardening domain until IFF1 or IFF3 occurs.

Phase II: Stable local discrete micro-damage growth within the laminate up to the growth of the dominating discrete micro-cracks' widths incl. micro-delaminations, after onset of discrete micro-damage. In cyclic loading, degradation is more diffuse than in static loading. Phase is usually associated to fatigue, linked to micro-damage)

Phase III: Final in-stable fracture of laminate initiated by FFs and IFF2 of any lamina and possible criticality of the loaded laminate due to the macro-damage delamination.
This phase is usually associated to fracture mechanics, to macro-damage and cracking.

10.1 General and Terms

Methods for the prediction of durability (Dauerhaftigkeit) regarding the lifespan of the structural material and thereby of the component, involves long time static loading which is linked to 'static Fatigue'(→Dauer-Standfestigkeit) and cyclic fatigue (→Dauer-Schwingfestigkeit ≡ Dauer-festigkeit). The latter is treated here. Fatigue failure occurs if the structural material is cyclically loaded. This provokes design questions and requires a Procedure for Fatigue Life Estimation necessary for design verification:

❖ **Design questions**

- When does micro-damage start? How can one consider a micro-damage portion?
- How can the single portions be accumulated essential for *fatigue verification*?
- When do the accumulated micro-damage portions build up macro-damage (Schaden)?
- When does such a damage (delamination in case of FRP) become so big to be of a technically critical size?
- How is then the critical damage growth (task for a *damage tolerance verification*) in this second phase of fatigue life in order to determine the part replacement time or the inspection intervals?

❖ **Domains of Fatigue Scenarios and Analyses**

LCF: high stressing and straining
HCF: intermediate stressing 10.000 < n < 2.000.000 (*rotor tubes, bridges, towers, off-shore structures, planes, etc.)*
VHCF: low stress and low strain amplitudes (see SPP1466 Very High Cycle Fatigue) > 10^7 cycles (*centrifuges, wind energy rotor blades, etc.)*

❖ **Design requirements**

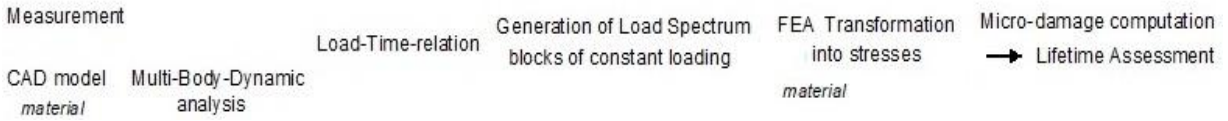
- To consider - beside the prediction procedure itself - environment, material, possible failure modes, statistical basis and accelerated testing for the full design verification.
- To ensure, that the structure can perform its primary function during its life.
- To think maintenance CoSt throughout life. Avoid premature failures and their CoSts. Consider in the case of multi-axial stress states whether amplitude and mean stress can be simplified considered as proportional and synchronous.

❖ **Input**

- Operational (Service) Loading: Load time curves with a counting model like *rain flow*
  Time domain: cycle-by-cycle or block-by-block (less computation effort) fatigue analysis
  Frequency domain: operational loading spectra (loss of loading sequence effects) fatigue analysis
- Safety Concept: Design safety factor Life j_{Life} = 3 – 10 or a project task-fixed inspection interval or a replacement time
- Procedure for the determination of the cyclic-caused micro-damage portions
- Accumulation model like the Linear Palmgren-Miner 'rule' or a more sophisticated non-linear one
- Haigh Diagram $\sigma_a(\sigma_m)$, that 'represents all available necessary SN curve information by its 'Constant Fatigue Life (CFL) curves

❖ **Transfer of operational loadings into stresses** σ_a, σ_m by using structural analysis like FEA.

Fig.10-1 presents in the upper part "How to come to the fatigue–driving stresses?" and in the lower part the domains of multi-axial cyclic loading.



Scheme: Way to Life-time Assessment for a Load Case. How to come to the fatigue-causing stresses?

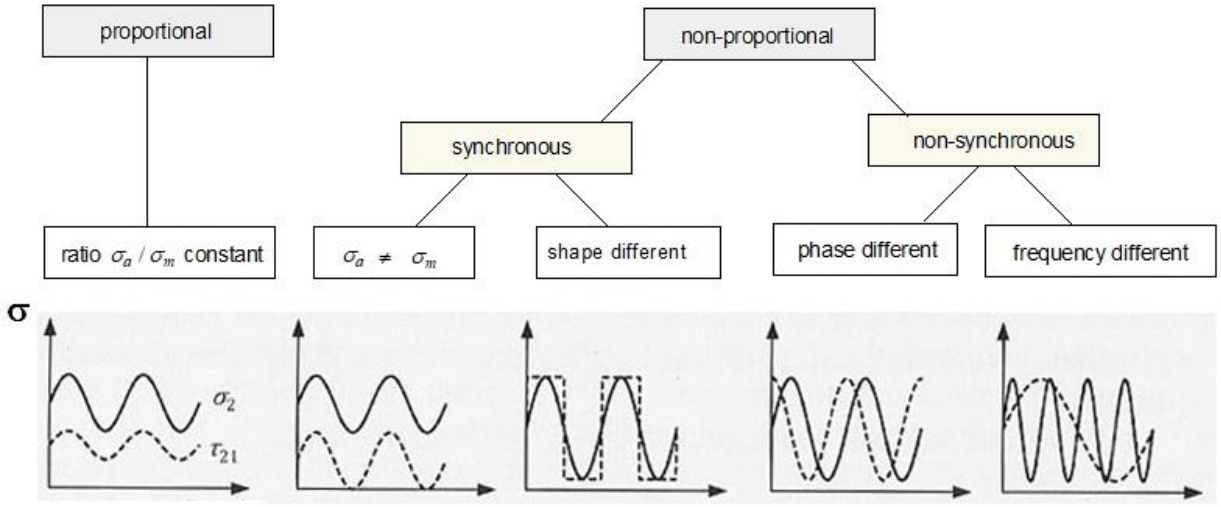


Fig.10-1: (upper) Fatigue –driving stresses.
(lower) Domains of multi-axial cyclic loading (courtesy Hah14, after [Rad07]
[Radaj D and Vormwald M: Ermüdungsfestigkeit-Grundlagen für Ingenieure. Springer-Verlag, 2007]

***LL**:*

- *The Palmgren-Miner rule cannot account for loading sequence effects, residual stresses, and for stresses below the fatigue limit (life → ∞ ?).*
- *Designing light-weight structures means a reduction of dead mass. Therefore, the ratio 'variable load / dead load' reduces, fatigue becomes more decisive and fatigue prediction procedures become also more mandatory in construction industry, for instance!*
- *In the LCF regime non-linearity causing effects such as creeping, relaxation are to regard.*
- *Whether the material's micro-damage driver remains the same from LCF until VHCF must be verified in each given design case.*
- *Whether a material has an endurance fatigue limit is usually open still regarding its 'old' level of N = 2·10^6 and further the lack of VHCF tests. However, e.g. CFRP has a high fatigue limit.*
- *A fatigue failure of brittle reinforcements is not antermced by plastic deformations.*
- *A fatigue-related failure of compressed concrete is antermced due to some cracking that is linked to some progressive deformation.*

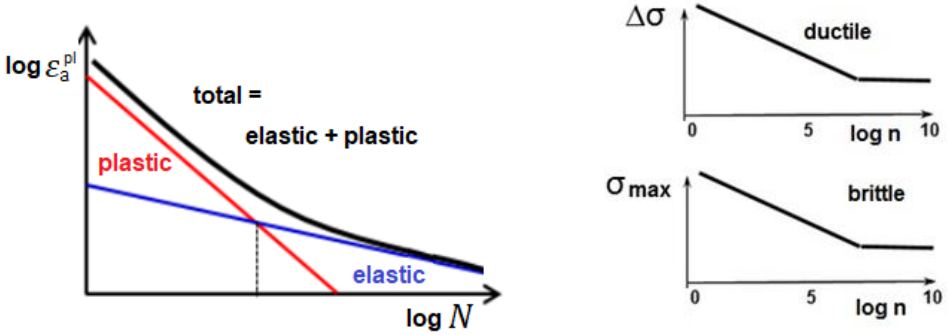


Fig.10-2: Difference of ductile and brittle materials. Plastic strain amplitude ε_a^{pl}

Models and Diagrams used

There are *strain-life* (plastic deformation decisive) and *stress-life* models used. *Fig.10-2* displays when the elastic strain amplitude becomes dominant and this is valid for brittle materials.

Above two models can be depicted in the Goodman diagram and in a Haigh diagram. The Goodman diagram shows the maximum tolerable stresses of the material σ_{max}. It is commonly used in construction specifically for concrete. The Haigh diagram will be applied here because in general just to use σ_a or $\Delta\sigma = 2 \cdot \sigma_a$ is not sufficient, however, (σ_a, σ_m) or (σ_a, R).

For ductile materials *strain-life* (strain-based) models are applied because single yield mechanism dominate. With brittle materials micro-damage mechanisms drive fatigue failure and several fracture mechanisms may come to act. This asks for a modal approach that captures all failure modes which are here fracture failure modes. In this context shall is stated below.

Fatigue Micro-Damage Drivers of Ductile and Brittle behaving Materials

There are basic differences between ductile and brittle materials:

- Ductile Material Behavior, isotropic materials: mild steel
  1 *micro-damage* mechanism *acts* ≡ *"slip band shear yielding"* drives micro-damage under tensile, compressive, shear and torsional cyclic stresses: *This single mechanism is the damaging driver. It is primarily described by 1 SFC, a yield failure condition (HMH, 'Mises')!*
- Brittle Behaving Material Behavior, isotropic materials: concrete, grey cast iron, etc
  2 *micro-damage* driving mechanisms act ≡ *2 fracture failure modes Normal Fracture failure (NF) and Shear Fracture failure (SF) under compression described by 2 fracture conditions, the SFCs for NF and SF (porosity is to consider)*
- Brittle Behaving Material Behavior, transversely-isotropic materials: UD Materials,
  5 *micro-damage* driving fracture failure mechanisms act ≡ 5 fracture failure modes *described by 5 SFCs or strength fracture failure conditions*.

State-of-the-art considering Cyclic strength analysis of UD ply-composed Laminates

- Experience with to-date composites of fiber-reinforced plastics FRP (*fiber-dominated laminates are used in high performance stress applications whereby fiber-dominated means that there are 0°-plies in all significant loading directions → > 3 fiber direction angles α*) behave brittle, experience early fatigue damage, but show benign fatigue failure behavior in case of 'well-designed' laminates until finally a pretty 'Sudden Death' occurs.
- No Lifetime Prediction Method is available, applicable to any lamina (lamella) and UD ply-composed laminate. The procedures base on specific laminate lay-ups and therefore test results cannot be generally applied. Embedded ply-degradation must be non-linearly considered
- Endurance strength procedures often base – as with metals – on σ_a, σ_m
- Present Engineering Approach in Mechanical Engineering:
  Up to now as Engineering Approach: Applying a *Static Design Limit Strain* of $\varepsilon < 0.3\%$ in multi-axial laminate design practically means negligible matrix-micro-cracking in the cases of many (>3) fiber-directions. Design experience proved: No IFF-caused fatigue danger of a laminate is given
  Future: *Design Limit Strain* shall be increased beyond $\varepsilon \approx 0.5\%$ (EU-project: MAAXIMUS to better exploit UD-materials). Then, dependent on the matrix, *first filament breaks may*

change the early diffuse matrix micro-cracking to a discrete and more critical localized one.

- Present Engineering Approach in Civil Engineering for FRP materials and its semi-finished products such as a pultruded rod, a strand cut-out of a fiber-grid, lamella (tape) etc. In the case of a 'not predominantly static loading' (nicht vorwiegend ruhende Belastung) the required fatigue life must be demonstrated by measured SN curves, operational loading spectrum and a hypothesis for the accumulation of the micro-damages are required. Bounds are set by the required minimum micro-crack width of the Serviceability Limit State SLS (GZG) and deformation restrictions for instance for bridge bending.

Considering the high-performance UD lamina-composed laminates the classical fatigue tests are performed on laminates. The idea of the author-founded Germany-wide group BeNa (in 2010) with his colleagues however was to base fatigue life prediction 'embedded lamina-wise' in order to be more general in fatigue life design in the future and to save test CoSts and time. Associated test specimens shall capture the interface effect of the lamina embedded in the laminate.

Constant amplitude loading and variable amplitude loading:

Cyclic loadings are most often given by an operational loading spectrum with its automatic loss of the stress-time relationship.
In *Fig.10-3* variable amplitude loading of the structure in operation or service is displayed ending with the 'operational fatigue life curve' after Gaßner. Further given is the harsher 'constant amplitude loading'. A loading spectrum-representing block-loading instead of mapping the loading spectrum by a single constant amplitude loading stands for more realistic fatigue life estimation. Good information about the loading spectrum pays off.

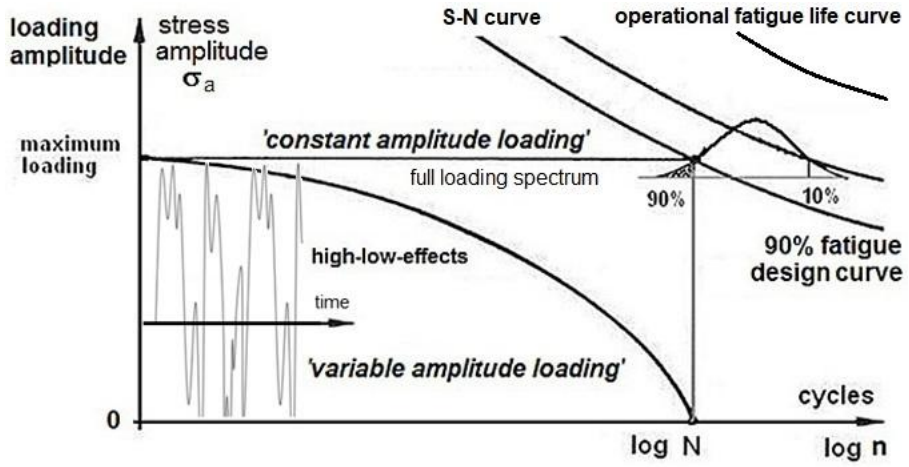


Fig.10-3: Display of constant amplitude loading and load history-linked variable amplitude loading

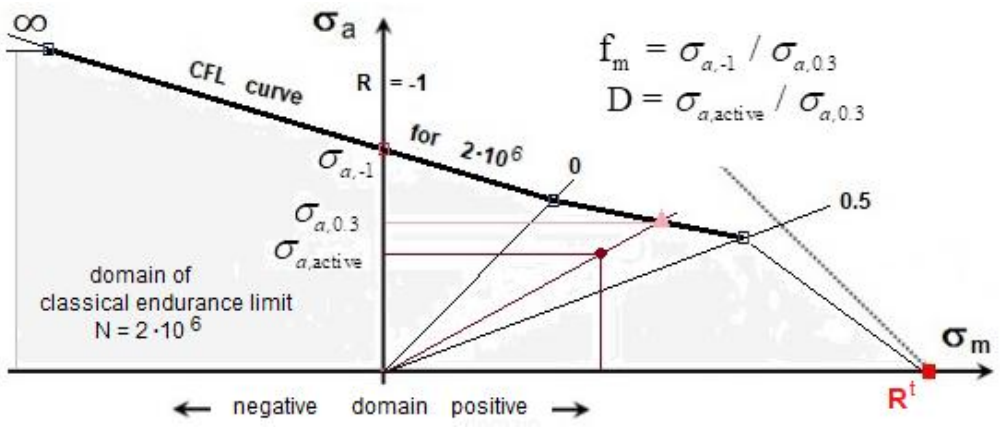
Brittle behavior: σ_{max} (Oberspannung) or σ_{min} or its mixture is responsible for micro-damage.

Proportional and non-proportional stressing (loading)

Compared to proportional stressing a non-proportional stressing (e.g. 90° out-of-phase) may lead to a significant life reduction. Due to the time-dependent, differently oriented stress states the growing flaws may have a better chance for coalescence viewing slip bands in ductile materials under strain-controlled fatigue testing or viewing micro-cracks in brittle materials.

Mean stress sensitivity

Not fully ductile isotropic materials show an influence of the mean stress on the fatigue strength depending on the (static) tensile strength and the material. Mean stresses in the tensile range ($\sigma_m > 0$ MPa) lead to a lower permanently sustainable amplitude, whereas compressive mean stresses ($\sigma_m < 0$ MPa) increase the permanently sustainable amplitude or in other words: A tensile mean stress lowers the fatigue strength and a compressive mean stress increases the fatigue strength. How strongly the material reacts to mean stresses is described by the so-called mean stress sensitivity, the relationship between the mean stress and the permanently sustainable amplitude. Mean stress sensitivity *M* is captured by a correction function f_m (*not topic here because brittle materials are basically addressed).* The following sketch informs about the relationships, *Fig.10-4*.



Ductile behavior : $M \rightarrow 0$, amplitude stress σ_a is responsible for yielding (slipping)
Brittle behavior : σ_{max} (Oberspannung) or σ_{min} or its mixture is responsible for micro-damage.

Fig.10-4: Mean stress sensitivity

The more brittle the material the more mean stress influence acts. This is why micro-damage is not anymore caused by yielding (1 strength failure mode, quantified by σ_{eq}^{Mises}) alone but by micro-cracking which is caused by many fracture strength failure modes. Brittle materials like the transversely-isotropic UD material with its five fracture failure modes possess a strong mean stress sensitivity. That requires a failure mode-linked treatment which cannot be captured by a mean stress correction as usually performed with not fully ductile materials. See later the example CFRP lamina in the Haigh diagram in *Fig.10-5* (here as test example used is UD material with 2 fiber failure modes) where the huge effect of the mean stress sensitivity of brittle materials is demonstrated very impressively.

Determination of Micro-Damage Portions, *FF1-linked example*

In service, an outstanding number of ups and downs is given as varying stress input (*Fig.10-3*). Counting methods help to reduce the number of turning points in this time-domain provided course of the stress in order to achieve a set of simple stress reversals. This allows the application of Miner's rule in order to estimate the fatigue life under complex loading. The rain-flow counting method from Endo-Matsuishi, 1968, is the most often used method. Stress amplitude and mean stress may be collected in a Markov matrix, see *Fig.10-5*. A distinct stress state with the largest stresses σ_{max} and σ_{min} possesses the stress ratio $R = \sigma_{min} / \sigma_{max}$ and defines a SN curve. Analogous to

the ductile material case where a complex stress state is captured by an equivalent stress σ_{eq}^{Mises} it may be assumed that for anisotropic materials the same is valid for each single strength failure mode, if equivalent stresses are available such as with the FMC-based SFCs of the author. A change from σ_{max} to $\sigma_{eq,max}$ will simplify the analysis.

10.2 SN curve (Woehlerkurve) and Haigh-Diagram

10.2.1 Modelling of SN curves and choice of an appropriate SN curve

SN curves can be modelled linearly and non-linearly in semi-log and log-log diagrams. Possible mapping formulations are non-linear curves such as from the Weibull-model and the Wearout-model *[VDI 2014]* or linear models in the log-log diagram. Below, five SN curve mapping models are investigated and displayed.

As still mentioned, for brittle behaving materials it is physically reasonable to use the strength (*the average value, that is marked by a bar over*) as maximum stress σ_{max} at n = N = 1. This advantageously reduces the number of free parameters by one. (*Mind: In literature, like the HSB, the strength at origin is not taken in order to get more freedom for a better mapping in the domain of highest interest, most often LCF in aircraft*). The choice of the SN model mainly depends on the fact whether an endurance limit for VHCF is given, that should be mapped or not. Such a limit should exist for the example FF1 of CFRP (*thermoset polymer at least*), the course of test data from *M. Kawai* is mapped. The following conclusions can be drawn considering the desire "minimum number of free parameters", just as many as physically required in the given work case.

1) 3 free parameter-Weibull + strength

$$\sigma_{max}(N) = c1 + \frac{\bar{R} - c1}{e^{\left(\frac{\log(N)}{c3}\right)^{c2}}}$$

2) 2 free parameter-Weibull + strength

$$\sigma_{max}(N) = \frac{\bar{R}}{e^{\left(\frac{\log(N)}{c3}\right)^{c2}}}$$

3) 2 free parameter + strength point, Sendecky, Wear-out Model

$$\sigma_{max}(N) = \bar{R} \cdot \left(\frac{1 - c1}{N - c1}\right)^{c2}$$

4) 2 free parameter + strength point

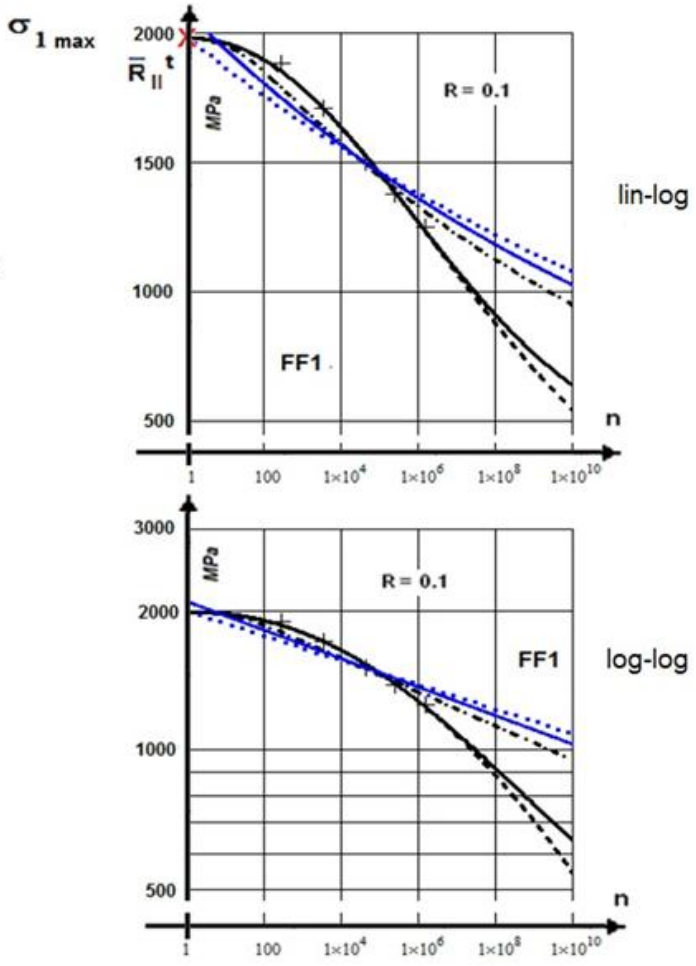
$$\sigma_{max}(N) = c1 \cdot \bar{R} \cdot N^{c2}$$

5) 1 free parameter + strength point

$$\sigma_{max}(N) = \bar{R} \cdot N^{c1}$$

is straight line in log-log diagram

$$\log \sigma_{max}(N) = \log \bar{R} + c1 \cdot \log N$$



In the HCF-regime (10^3 through $2 \cdot 10^6$, the course of test data is mapped with the following results: Lin-log curves with model 1 (bold black) and model 2 (dashed black) work very well. Model 2 approximately may consider an endurance limit in the VHCF regime and Log-log curves. The models 1 and 2 show highest mapping capability due to the higher number of free parameters. The simple model 5 (blue dotted) may work sufficiently well in appropriate courses of test data. Strength point should be fix point. Considering the stochastic nature of the problem, it seems to be sufficient for many engineering applications to apply model 5 in the HCF regime. In this work the models 1 and 5 are applied.

Lack of data? Then, a 'Haibach-correction' at the end of the HCF domain is often performed by halving the HCF-determining decay angle for $n > 2 \cdot 10^6$ or another estimation method is used.

In the VHCF domain, similar to da/dN (ΔK_0) in fracture mechanics, micro-mechanically different damage may occur in comparison to the macro-mechanical technical crack domain. Such a change of the destructive mechanism may require the mapping of two distributions.

LL:

**In the case of extrapolation of the HCF regime, $n > 2 \cdot 10^6$ cycles, the choice of the mapping function determines the obtained lifetime value! In this context it is to consider for metals: It is known that the failure origin for VHCF changes from surface flaws, notches to internal flaws such as different inclusions.*

**Because a physical average curve - from probabilistic reasons - will not show a kink a more complicated two-regime SN-modelling should be not applied but for instance the 4-parameter Weibull model 1.*

10.2.2 General information on Markov Matrix, SN curve and Haigh diagram

Fig.10-5 collects a Markov matrix, a Haigh diagram with 3 CFL curve examples, a SN curve and the computation of a SN curve, with curve parameter determination example performed by Mathcad. The so-called SN (Stress-failure cycle N) curve is a constant amplitude curve, see bottom picture. Unfortunately in practice, the SN curve is linked also to the letter R. The reason for this is that R is now the Ratio of $\sigma_{min}/\sigma_{max}$. The average strengths are kept bias letters *R*.

For the design, SN curves are to formulate. There are practically two possibilities to present them: (1) using in the case of ductile materials the stress amplitude $\sigma_a(R,N)$, also termed alternating stress, and (2) using in the case of brittle materials the maximum or upper stress $\sigma_{max}(R,N)$, usually termed *fatigue strength*. The latter is physically simpler to understand by the stress man than the amplitude. Namely, a decaying SN curve is interpretable like a decaying 'static' strength after a micro-damage process with *n* cycles. Thereby, the static material stressing effort *Eff* (Werkstoffanstrengung, $N_f = 1$) is replaced by the accumulated cyclic micro-damage sum $D(N)$. Applied here is the classical 3-parameter Weibull curve. Hence, in the case of brittle behaving materials the strength value $\bar{R}^t = \sigma_{max}$ (n = N = 1) is preferably used as origin in the tension domain and anchor point of the SN curve and in the compression domain $-\bar{R}^c = \sigma_{min}$ (n = N = 1).

* The following part-figures present a FF–linked example to visualize the next step of the process the determination of micro-damage portions: There are two stress states indicated in the Markov matrix and the Haigh diagram. Exemplarily, just for n_1 the necessary associated SN curve is provided. For the first of the two marked loading cycles $n(\sigma_{1a},\sigma_{1m})$ the calculation

delivers $D_{\|1} = n_1/N_1$ for the FF1 mode and for the second $D_{\|2} = n_2/N_2$ for the FF2 mode-linked stress state.

* The Haigh diagram in *Fig.10-5* shows the maximum tolerable stress (loading) amplitudes of the material $\sigma_a(\sigma_m)$. Again, one can see the huge effect of the mean stress sensitivity very clearly.

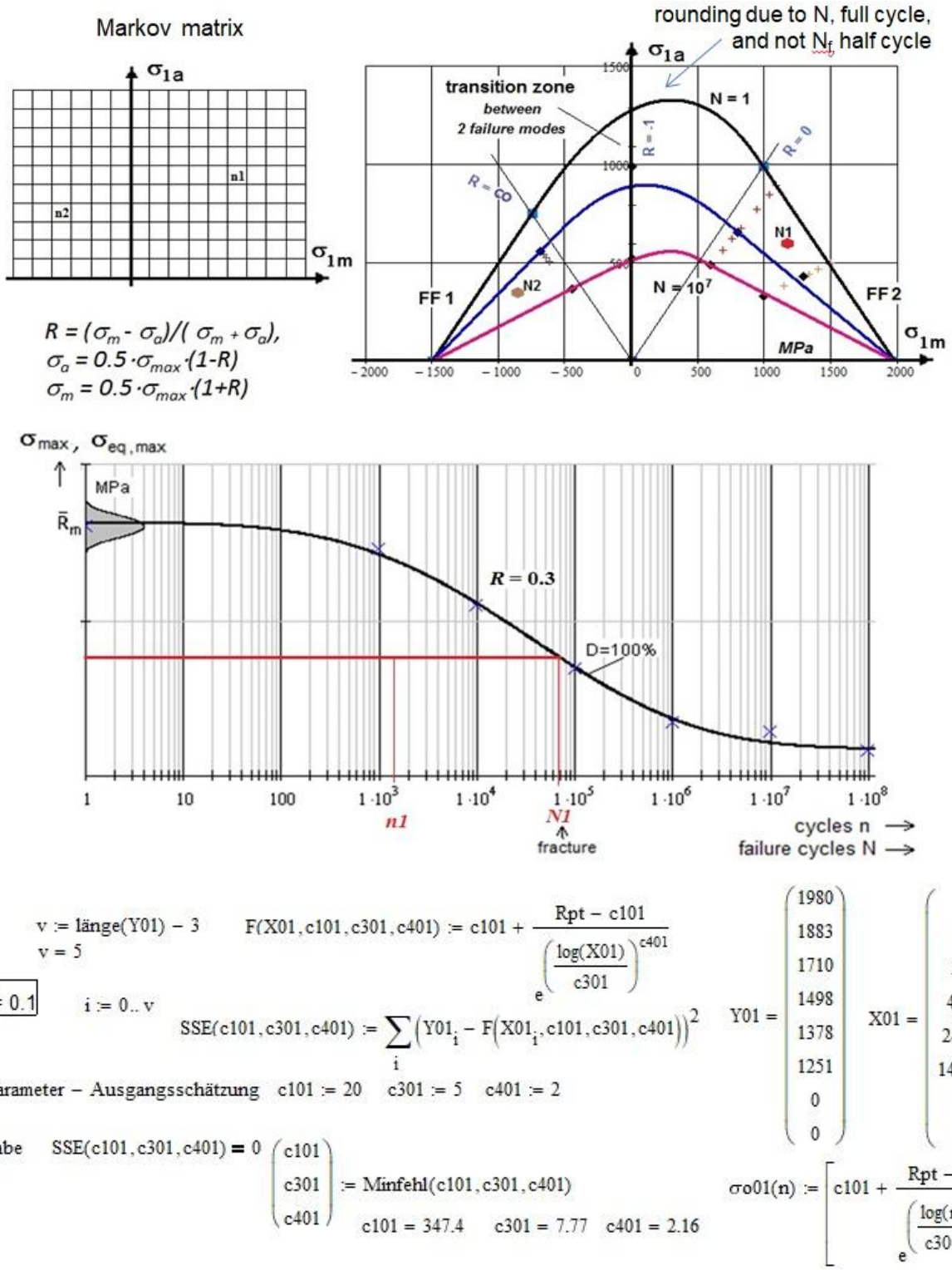


Fig.10-5:Markov matrix, Haigh diagram, SN curve with computation example.
Application of 'Miner rule'. D = 100% means that these 100% meet a survival probability of 50%

Fig 10-6 visualizes the transfer from the static load-driven increase of the material stressing effort *Eff* = 100% (or F =1) at the strength point to the cycle-driven cyclic micro-damage sum D = 0.5 = 50% of the SN curve. The evolution of *Eff* is linked to the accumulation of the static micro-damage $0 < D < 1$ after reaching onset-of-micro-cracking, where *Eff* is still > 0.

Mapping: Static failure $\rightarrow \max\sigma = \bar{R}_{static}$, $F = 1$ and cyclic failure $\max\sigma = \bar{R}_{cyclic}$, $D = 0.5$.

Verification: Static failure $\rightarrow \max\sigma = R_{static}$, $Eff = 1$ and cyclic failure $\max\sigma = R_{cyclic}$, $D = 1$.

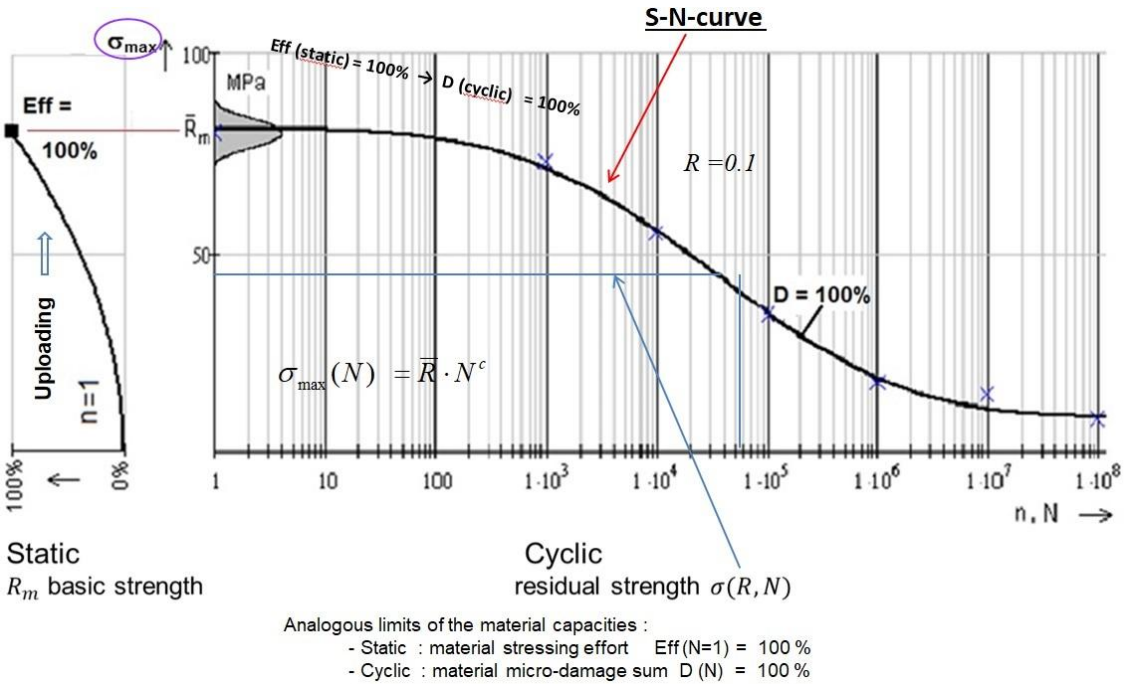


Fig.10-6: Eff versus D regarding a 50% survival probability P

As within static strength design the average SN curve cannot be applied in fatigue life design verification, a statistically reduced curve is to determine as design curve.

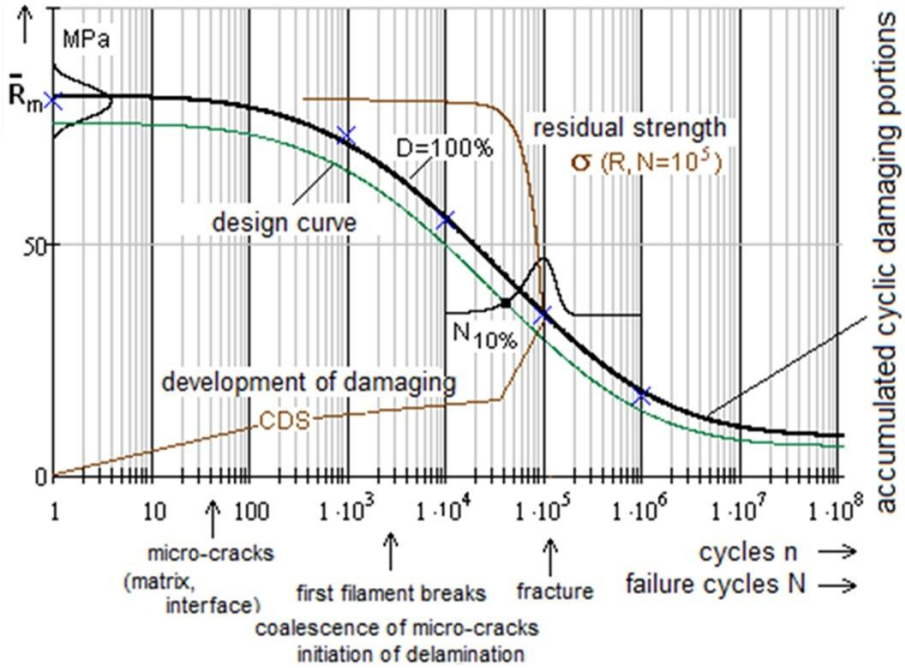


*Fig.10-7: **Fatigue average curve** and **design curve.** CDS is 'characteristic damage state' of a lamina*

Note:

VHCF > 10^7 cycles > an apparent fatigue strength *(scheinbare 'Dauerfestigkeit)* at $2 \cdot 10^6$ cycles.

Certain materials have an endurance limit which represents a stress level below which the material does not fail and can be cycled infinitely. If the applied stress level is below the endurance limit of the material is said to have an infinite life. This might have been acceptable in some cases for the old HCF-level of 10^6 cycles, however needs to be checked for VHCF because the failure mechanism might be not fully the same as for HCF and above endurance limit is an apparent fatigue strength. *[Pyt11] Pyttel B, Schwerdt D and Berger C: Very high cycle fatigue – Is there a fatigue limit? In: Intern. J. Fatigue (33), 2011, 1, pp. 49–58*

Cyclic failure always depends on the amount and distribution of flaws at the surface (*formerly often termed Weibull surface effect*) of the structural component and on those within the critical material domain (*formerly often termed Weibull volume effect)*. This is especially valid for the novel 3D-printed parts. For metals it is further valid that in the case of cubic surface-centered and of hexagonal crystals often a further drop of the SN curve is faced. Hence, a dedication to surface-generated failure at HCF and to volume-generated failure at VHCF looks possible supported by novel VHCF experiments. This forced the material scientists to think about two different SN curves to apply in the micro-damage accumulation range, one associated to the surface flaws and one to the volume flaws. However the author believes: As this problem is a probabilistically-driven strength problem and not an instability problem the course of the cyclic failure test data cannot show some sort of a downward jump. A continuous four parameter Weibull mapping approach will capture the course.

10.3 Static Residual Strength R_{res} for Proof of Structural Integrity in Projects

11.3.1 General

Residual strength *Rres* is the fracture stress after pre-damage and re-loading. Not only in mechanical engineering but also in civil engineering residual strength values are required such as in soil mechanics or for hangers of the network arch railway bridge at Stuttgart or for tension rods of cranes. This involves micro-damaged structural components (*phase 2 fatigue life, using strength tools*) and macro-damaged ones (*phase 3 of fatigue life, fracture mechanics problem, using damage tolerance mechanics tools*), see *Fig.10-8*. The loading may range from constant amplitude-loading up to spectrum-loading and has to capture proportional and non-proportional loading scenarios.

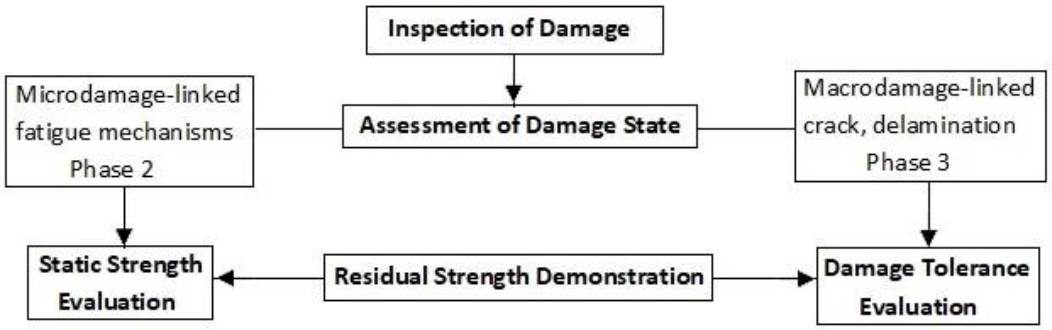


Fig.10-8: Elements of Damage Tolerance procedure

Beside uniaxial loading tasks the residual strength task is a further task in the demonstration of structural integrity, which shall be only shortly mentioned here. Such a task exemplarily comes up

in cases: A multiple site damage phenomenon is faced with aerospace components such as fabrication-induced flaw clouds (*fatigue strength problem*) or real short-crack 'clouds' from e.g. multiple rivet holes in stringer-stiffened panels of aging aircraft components (*fracture mechanics problem*). In some projects a number for the residual strength at a certain operation cycle value is required. This is well known in an impact case of laminated panels. There, a compression-after-impact (CAI) test is to execute after the impact event because the impact may result in a non-(barely) visible external damage and it may generate a dramatic reduction of compressive strength due to separation of layers which results in large bending stiffness loss. Regarding the crack-linked residual strength problems the reader is referred to the literature and to a short fracture mechanics sub-chapter, later.

Residual strength tests are long-lasting and expensive. Therefore, procedures are searched that help to reduce the test effort. Regarding the different micro- and macro-damage-linked residual strength situations also different procedures are applied when estimating *Rres.*

Basic task of the micro-mechanically fatigue-linked *Rres* is the mapping of the fracture cycle N(R)-dedicated curve, performed here by taking the 4-parameter Weibull function

$$\mathrm{R = constant:} \quad \sigma_{\max}(\mathrm{R},N) = c1 + (c2 - c1)/\exp(\log N / c3)^{c4}.$$

SN-curve mapping describes the relation between cyclic loading and the number of cycles to failure *N*. On the horizontal axis the number of cycles to failure is given on logarithmic scale. On the vertical axis (*either linear or logarithmic*) the stress amplitude $\sigma_{amplitude}$ (*sometimes the maximum stress* σ_{max}) of the cycle is given. SN-curves, R = constant, base on the fatigue test measurement types pearl-chain testing or horizontal load level testing. Considering residual strength, measurements on the vertical axis at *n* = constant are required.

Fatigue curves are given for unnotched test specimens (Kt = 1) and for notched ones. The loading can be uniaxial and multi-axial stress states. A suitable 'permitted' stress criterion is to apply.

In design verification very often as fractile (quantile), representing the survival probability p_f, 5% or 10% are taken in order to capture some uncertainty compared to the average of 50%. For the loading side the design FoS j, in construction γ, capture the uncertainty of the loading. The residual strength design verification has to meet DUL.

Moving to the required statistical properties some notions are to depict. Capturing the uncertainty of the resistance quantities, the following is performed: Denoting P the survival probability and C the confidence level applied, when estimating a basic population value from test samples, partly enriched by some knowledge of the basic population. Regarding C a one-sided tolerance level it reads:

Static → Statistical reduction of average strength from (P= 50%, C= 50%) to e.g. (P = 90%, C = **95**%).

Cyclic→ Statistical reduction of average SN curve from (P=50%, C= 50%) to e.g. (P= 90%, C= **50**%). In order to improve this situation the maximum accumulated micro-damage is firstly reduced in design verification from the fictitious theoretical 'Miner value' D = 1= N_{50} / N_{50} (P= 50%, C= 50% with N based on the average curve) to a feasible value $D_{feasible}$ (P= 90%, C= **50**%) and further imposed by a FoS $j_{Life} > 5$. This feasible D, linked to the lower

design SN curve, is determined by (P = 90%, C = 50% → $D_{feasible} = N_{90} / N_{50}$ for a distinct N_{50} value and associated stress.

All this is executed to keep a generally accepted survival reliability of about $\Re = 1 - p_f > 1 - 10^{-7}$.

Residual strength R_{res} may be determined by different procedures in the fatigue phases 2 and 3. It depends on the stress ratio $R = \min\sigma/\max\sigma$ and the fracture cycle N. R_{res} should not be confused with *residual stress* or *eigenstress* σ_{res}.

11.3.2 Residual Strength, Fatigue Phase 2, HCF regime, constant stress ratio R

*** *Rres, classical way,*** *deterministic → semi-probabilistic*

Determination via the interpretation "*The course of the residual strength is the difference of the static strength and the maximum strength* $\sigma_{max}(N)$ *of an SN curve* R", see Fig.11.7. This leads to the formulation $R_{res} = \sigma_{max}(N) + [R^t - \sigma_{max}(N)] \cdot \rho(n)$ with $\rho(n) = 1-(n/N)^p \equiv 1-D^p$,

where the exponent p describes the decay of the residual strength capacity [*Hah14*] and D the micro-damage quantity. Fig.11-7 depicts for R = 0.1 the average 50% and the 90% SN-curve. The residual strength curve *Rres* is given for the point (10^5 cycles, σ = 34 MPa). The stress σ belongs to a so-called 'one stage test' or constant amplitude test.

Regarding residual strength and 90% SN-curve the question arises: Where does the necessary statistical basis for a reduced SN-curve come from if not sufficient test series on vertical and horizontal levels were run? Due to missing test data a realistic work case cannot be presented.

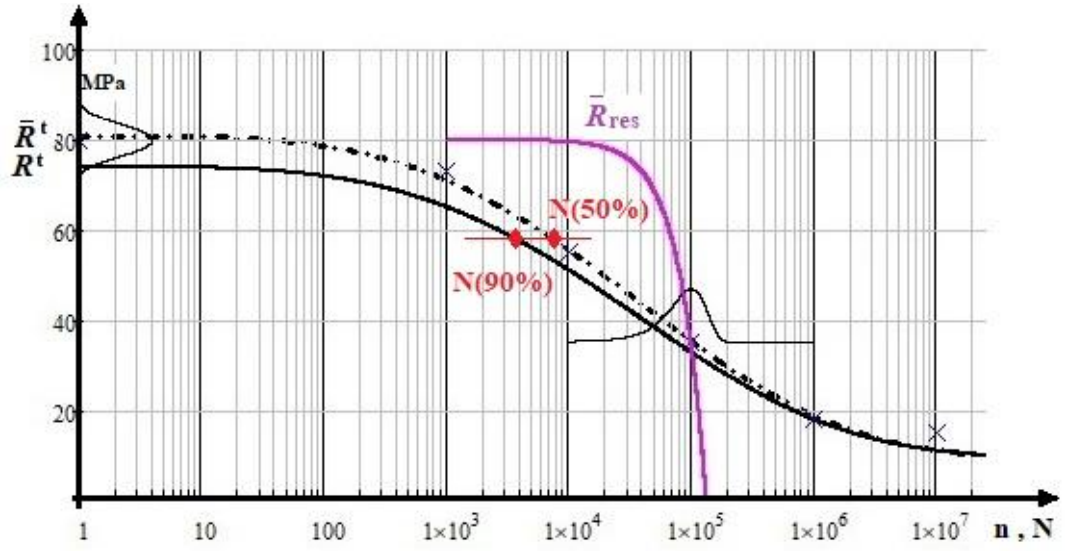


Fig.10-7: Schematic example, uniaxial loading, R=0. $\bar{R}_{res}$ *is average tensile residual strength*

In [*Hah14*] an assessment of the residual strength of a stress collective on basis of a linear (Miner) micro-damage accumulation has been performed, see *subchapter 11.4.*

***** IDEA Cuntze, ***Convolution integral,*** *probabilistic way to determine a 90% value*

A possibility to determine a 90%-value is given by the so-called convolution integral, using density distributions of R_{res} and of N with the hope to find them measured, *Fig.10-8*. The numerical analysis is based here on the assumption: 'The density distributions on x- (f_N) and y-axis (f_R) are approximately basic populations and of ND-type'. For the density distributions also a logarithmic, a Weibull density function or a truncated function could be employed. However, this requires further studies.

The convolution integral, solved by Mathcad 15 within a second, reads

$$p_f = \int_{-\infty}^{\infty} \left(\int_{Rres}^{\infty} f_R(R) \cdot dR \cdot f_N(N)\, dN \right) = 90\% \text{ fractile} \quad \text{for ND density distributions}$$

with $f_{ND}(x) = \frac{1}{\sigma \cdot \sqrt{2 \cdot \pi}} \cdot exp\ [-\frac{1}{2}(\frac{x-\mu}{\sigma})^2]$ for abscissa N and ordinate R^t .

Data base of the numerical example is:

* Static strength distribution μ = 80 MPa, σ = 3.2 MPa
* R_{res} distribution in computation point, y-axis, μ = 43.5 MPa, σ = 2.8 MPa
* Cycle distribution in computation point, x-axis, μ = 3430 cycles, σ = 858 cycles and the Coordinates of the chosen computation point * (38 MPa, n = 2000 cycles in *Fig.10-8*).

The presented application outlines a limit of the Mathcad 15 code application. Mathcad has no computation problem with the computation of the convolution integral. However, when visualizing the probability hill in Fig.10-9, it is not able to manage the 'big data' problem and runs into endless loops. Therefore the author had to sort out a work case with reduced stress and cycle regimes. The original SN data set was for fiber fracture (FF) of CFRP with $\mu_n = 100000$ *cycles,* $\sigma_n = 13000$ *cycles,* $\mu_{res} = 1500$ *MPa,* $\sigma_n = 150$ *MPa .*

This reduction to just a relatively simple numerical example does not matter because the procedure is of interest. The constructed work case can be handled by Mathcad although the 'big data handling', when producing the figures took 30 times the usual CPU-time due to always running into endless loops.

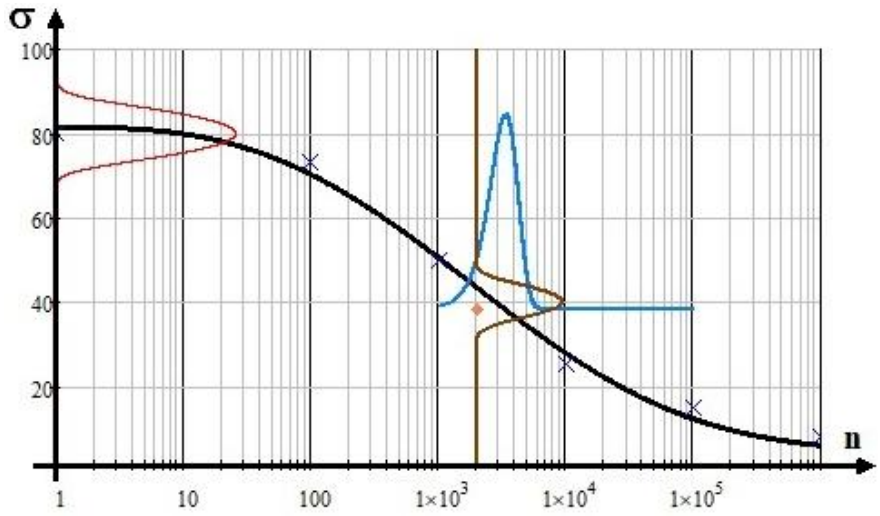


Fig.10-8: Assumed distributions of residual strength curve with cycles curve linked to R_{res} *(38 MPa, 2000 cycles). SN-curve,* R = *0: c1= 20 MPa, c2= 80 MPa , c3= 3.77, c4= 2.92*

Fig.10-8 depicts the SN-curve, the chosen computation point, static strength distribution with assumed residual strength distribution and cycle distribution through the computation point*. It is a semi-logarithmic graph.

As it is a brittle example material, the use of σ_{max} (involves R^t as origin!) is of advantage for the 'strength-oriented' design engineer compared to the stress amplitude σ_a .

The probabilistic treatment delivers the 'joint' probability hill of both the distribution functions in *Fig.11-9,* right figure. The hill's average center coordinates are 43.5 MPa, 3430 cycles. The figure further depicts the density distributions of the residual strength $R_{res}(\sigma)$ curve and of the fracture cycle N (n) curve. In this right figure, the residual strength distribution is not clearly visible due to additional Mathcad-drawn beams running out from the origin. The task seems to be an overloading of the Mathcad code which could not anymore handle the numerically effortful task for too large cycle numbers. The left figure shows the projection of the probability hill with lines of equal probability belonging to the chosen computation point *.

Below, the computation parameter input set is depicted above the figure.

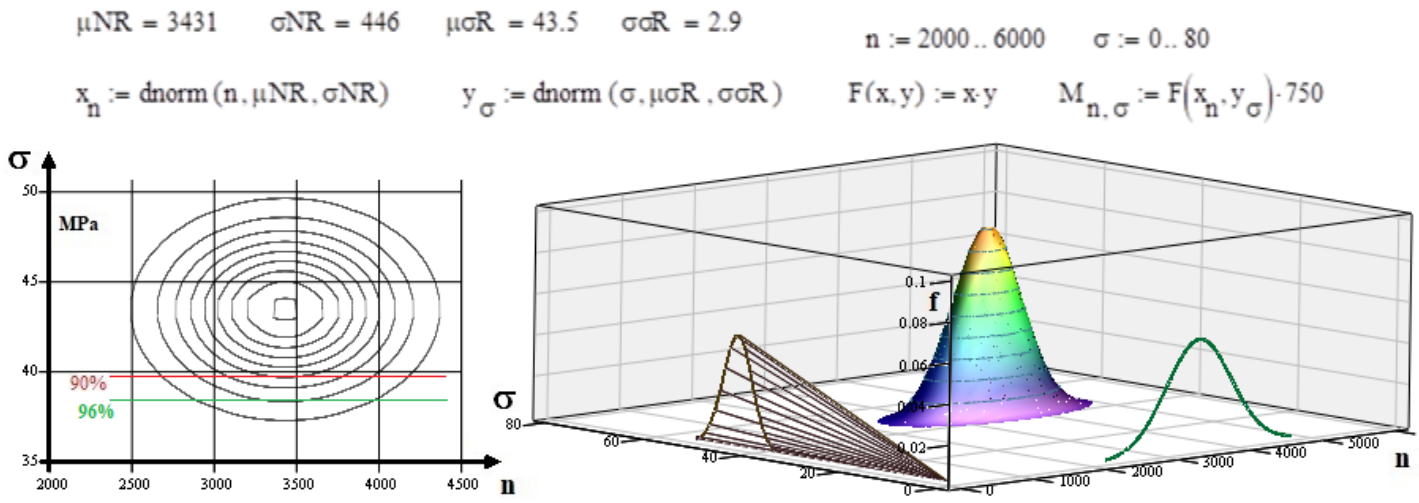


Fig.10-9: Assumed distributions.
(left) Projection of rings of equal survival probability with the residual strength line, (right) Distributions with with the survival probability hill applying the convolution integral, M_n is the hill designation

Design Safety considering the scatter of the design parameters is tackled as follows:

The scatter of loading is considered in the residual strength design verification because DUL with its design safety factor j_{ult} has to be verified. The scatter of the residual strength R_{res} and of the fracture cycle N is captured by a joint probability calculation indicated below. This procedure is effortful, but of high fidelity if test data is available.

Under above assumptions an estimation of a required 90%- residual (tensile) strength value can be determined according to the Mathcad formula

$$pü := \int_{\sigma res}^{Rt+\sigma Rt} \int_{2500}^{5500} \frac{1}{\sigma\sigma R\cdot\sqrt{2\pi}}\cdot e^{\left[\frac{-1}{2}\cdot\left(\frac{y-\mu\sigma R}{\sigma\sigma R}\right)^2\right]}\cdot\left[\frac{1}{\sigma NR\cdot\sqrt{2\pi}}\cdot e^{\left[\frac{-1}{2}\cdot\left(\frac{x-\mu NR}{\sigma NR}\right)^2\right]}\right] dx\,dy$$

and delivers for the running variable σ_{res} = 39.5 MPa the required survival probability pü = 90% = (1- p_f)→ σ_{res} becomes R_{res}. For the chosen point (38.0 MPa, 2000 cycles) the value is pü = 95%.

11.3.3 Fatigue phase 3, HCF regime, Fracture Mechanics

The certification of cracked components in aircraft structures requires a damage tolerance assessment. The associated results of the performed crack growth and residual strength analyses are the basis for the design verification and the definition of the inspection intervals.
For this Fracture Mechanics-linked part, here, just some basic information shall be given in order to complement the fatigue phase 2 process, and to stick to the author's objective to approximately provide a holistic content of a subject.

Now in phase 3, R_{res} ($\equiv \sigma_{cr}$) is the gross-sectional tensile failure stress of a component that contains a crack (*failure stress is the general synonym for the strength resistance R*). The crack length at the beginning of the static loading a_o will increase to its critical value a_{cr}.
In general, the prediction techniques are based on the critical value of the stress-intensity factor for a given geometry and loading. Using fracture toughness failure criteria, the decay in critical stress can be obtained in terms of crack size.

Many lines of this paragraph are taken from the HSB 61121 etc and the author's fracture mechanics lecture (*Many thanks to my former colleagues of the IASB, editor of the excellent HSB, that collects more than 4000 sheets for structural design*).
The concept of the stress intensity factor leads to the statement that a component will fail if the stress intensity factor *K* reaches its critical value K_c, termed fracture toughness $K_I / K_{Ic} < 1$ (mode I). This depends on the material behavior, i.e. brittle or ductile. Conditions for the usage of above concept for isotropic materials are: • The plastic zone at the crack tip is small compared to crack length and structural dimensions. • The remote stress is related to the gross-sectional area and thus does not depend on the crack length
The estimation of the residual strength capacity depends on the operational time of the distinct component and its crack size, which requires a crack growth relationship $a_{cr}(t)$ and a critical stress $\sigma_{fr}(a)$. The critical crack length a_{cr} can be predicted knowing the fracture toughness K_{Ic} ($\equiv K^t_{Icr}$, in order to distinguish tension from compression cases logically indexed by $_{cr}$ instead of $_c$ (compression) in this document) of the material, linked to the case of plane strain, for mode I crack opening. Given data K_{Ic} are most often valid for room temperature and plane strain conditions. A minimum plate thickness *t* for which the plane strain condition is applicable is to respect. For a thickness below the minimum thickness the stress state is mixed plane stress / plane strain. The fracture toughness in that case is higher than the plain strain fracture toughness.
The residual strength of a plate strip is computed by using the formula

$$\sigma_{cr} = K_{c0} / (\sqrt{\pi \cdot a_0} \cdot f)$$

with the so-called apparent fracture toughness K_{c0} and the crack geometry-linked correction function *f* of the crack situation in the distinct application case. Above equation is only valid if the following requirements are met: •The crack considered is a through-the-thickness-crack. •The remote tensile stress is perpendicular to the crack (mode I). See a later sub-chapter.

Crack Resistance curve (unfortunately often shortly termed R-Curve, too): Just for completeness: see literature, HSB 62232-05 and sub-chapter10.11.

10.4 Determination of a Load Spectrum-equivalent SN curve

In Standards 'recommended' operating load-spectra (collectives) for aircraft, wind energy, automotive etc are given as input for the lifetime estimation. These spectra no longer include a sequence of the loading or its stress history, respectively. If they do model finely mixed processes the prediction quality using the linear Miner micro-damage accumulation formula with $D_{maximum} = 1 = 100$ % is best. Such operating load spectra are filled differently, whereby the area under a SN curve is marked as 100%. For practical use, the spectrum is sensibly divided into a few individual reasonable blocks, which then means to perform one-level tests with its constant amplitude loading.

The derivation of a spectrum-loading replacing one-level test would be very practical for the design engineer. It would further help to essentially reduce test CoSts.
This task is executed on basis of an equivalent micro-damage sum D_{total} of the spectrum and of the one-level test. The same micro-damage has been accumulated in both situations at the end of $\sum n_i = N$. Thus the solution leads to the equivalent substitute stress level $\sigma_{substitute} = 45$ MPa

$$\sigma_{substitute} \cdot \sum n_i / N = \sigma_{substitute} \cdot 1 = \sum_{i=1}^{number\ of\ classes} \sigma_i \cdot D_i / D_{total} \quad \text{in } \underline{Fig.10\text{-}3}$$

of the one-level test.
Herein, the micro-damage portions of the individual classified loading-blocks are weighted with the corresponding stress horizon analogous to $\sigma_i \cdot n_i / N_i$. In other words: The 'i-class micro-damage effective area' $\sigma_i \cdot n_i$ is divided by the associate fracture cycle value N_i in order to get the right proportion of the loading class i. Hence, the residual strength equation becomes

$$R_{res}^{collective} = \sigma_{substitute}(N) + [R^t - \sigma_{substitute}(N)] \cdot (1 - D^p)\ .\ (\text{see } [Hah14]).$$

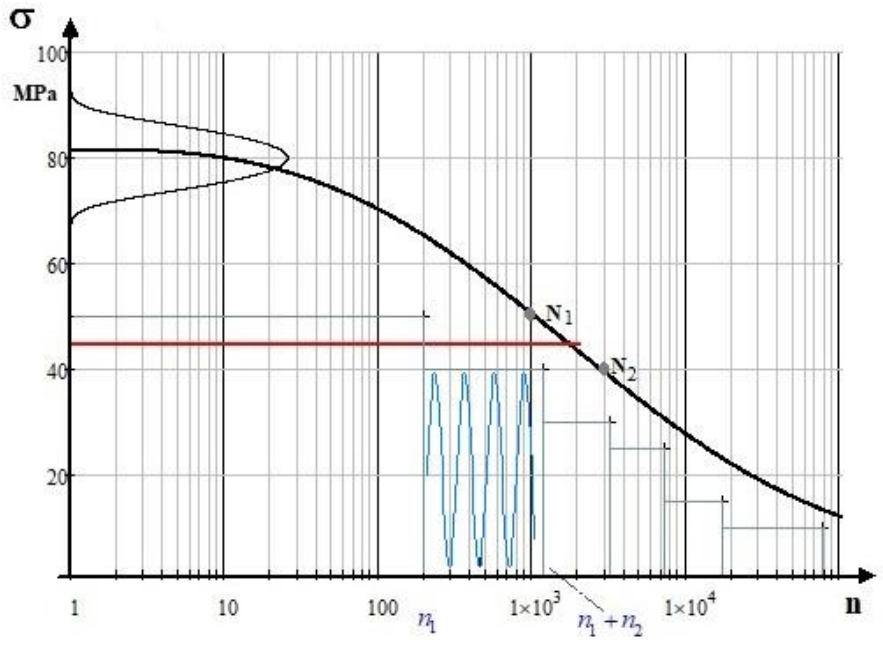


Fig.10-3: Loading blocks, relevant SN-curve R *and equivalent substitute stress level*

For not finely mixed processes the question arises whether the statistical quality is good enough for design verification and to establish a sufficient value for $D_{eff} < 1$.

10.5 FMC-based Fatigue Life Estimation Model

10.5.1 Idea of an Automatic Establishment of Constant Fatigue Life Curves $\sigma_a(\sigma_m, N = \text{constant})$

In aircraft industry, for a design-necessary interpolation to achieve constant fatigue life (CFL) curves much effort is spent to map them piece-by-piece by straight lines, see for instance the respecting sheets on metals in the HSB (Hickethier H.: *Interpolation and Extrapolation of SN data*). Regarding curved CFLs, the dissertation of Clemens Hahne [*Hah15*] is highly recommended. Therefore, an automatic possibility to generate CLFs is highly desired in order to avoid difficult interpolations between the constant life curves. A reliable procedure helps to save test CoSts and development time.

Here, for the multiple failure mode 'suffering' brittle materials an automatic establishment of the non-piecewise straight CFLs in Haigh Diagrams is searched – generally applicable to brittle isotropic (including compressed concrete) and UD-materials.

Detailed ideas of the author for achieving these CFL curves

- Measurement of only a minimum number of SN curves (*Einstufenversuch R = const*)
- Finding a physically-based model to predict other SN curves, required for fatigue analysis, on basis of a Master SN curve of each mode
- Presumption: An appropriate Master SN curve for each failure mode domain compression (SF) and tension (NF) is available
- In order to map the test data in the transition domain, where the modes interact (*most problematic region in the Haigh diagram*) a practicable mode domain decay function is looked for to regard the opposite decay of the modes.

In order to achieve this, a reliable Assumption is needed:

"If the failure mechanism of a mode cyclically remains the same as in the static case, then the fatigue micro-damage-driving failure parameters are the same and the applicability of static SFCs is allowed for quantifying micro-damage portions".

11.5.2 Modal Dedication of Kawai's Modified Fatigue Strength Ratio Ψ, applied for example UD

Ideas of Kawai

- Kawai's Fatigue Strength Ratio Ψ: *Normalization of the fatigue strength* $\sigma_{max}(N)$ *by a static strength* $\psi = \sigma_{static} / \bar{R} = 1 \ (\equiv Eff)$ *such referring to Eff (see also Fig.10-6,* $Eff \rightarrow D$*)*
- Kawai's Modified Fatigue Strength Ratio Ψ: *Reformulation in order to get the stress ratio* R *into the static concept* $\psi = (\sigma_a + \sigma_m) / \bar{R} = 1$

  $\Rightarrow \quad 1 = (\sigma_a + \sigma_m) / \bar{R} \quad \Rightarrow \quad \sigma_a / (\bar{R} - \sigma_m) = \Psi \equiv \text{cyclic part / 'static' part}.$

  *Each measured SN-curve is normalized by its static strength and the 'bulk' of SN curves (*hopefully is more than one SN curve measured within the *domains and in the transition zone) then fitted to obtain the Master curve. Masamichi Kawai used all R-curves to obtain* Ψ (R_{fit})*, independent of the inherent failure mode). Whether it practically makes sense to determine a Master curve by fitting all curves is to check: tension (*R*=0.1, 0.5, compression (*R*=10) and of the transition zone* R*= -1,* R_{trans}.

For visualization of Ψ see the following pictures

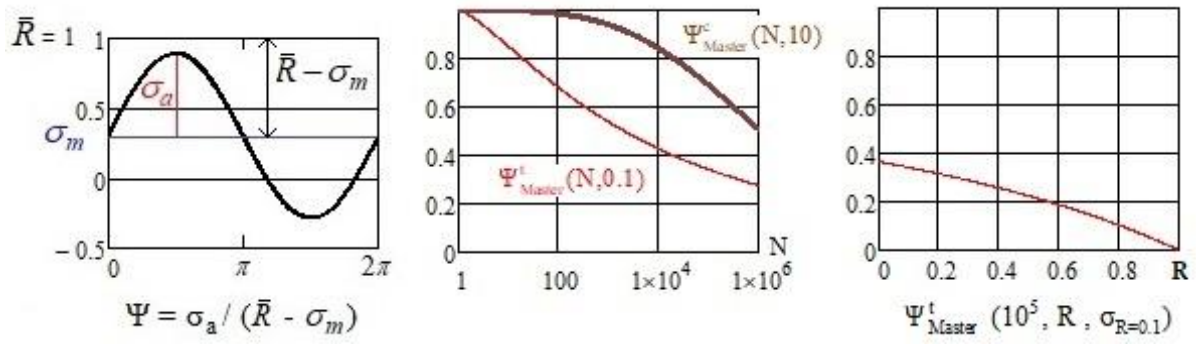


Table 10-1: Determination of SN curves on basis of Kawai's Ψ model with Master SN curve. Full procedure of the automatic determination of a Constant Fatigue Life curve

* Relationships

$\sigma_{max} = \Delta\sigma / (1-\mathrm{R}) \equiv 2 \cdot \sigma_a / (1-\mathrm{R})$ with $\Delta\sigma$ = stress range, σ_a is positive

$\mathrm{R} = (\sigma_m - \sigma_a) / (\sigma_m + \sigma_a)$, $\sigma_a = \sigma_m \cdot (1-\mathrm{R}) / (1+\mathrm{R})$

R = – 1 , fully reversed alternating stress. R = 0, R = 100 (∞), extreme swelling stresses.

$\bar{R}^t = \sigma_{max}(n = N = 1)$, $\bar{R}^c = \sigma_{min}(n = N = 1)$

$\sigma_a = 0.5 \cdot \sigma_{max} \cdot (1-\mathrm{R})$, $\sigma_m = 0.5 \cdot \sigma_{max} \cdot (1+\mathrm{R})$; $\sigma_a = -0.5 \cdot \sigma_{min} \cdot (1-\mathrm{R}^{-1})$, $\sigma_m = \sigma_{min}(1\text{-}0.5 \cdot (1-\mathrm{R}^{-1}))$

* Choice of problem-adequate mapping function and individual mapping of course of test data

$$\sigma_{max}(\mathrm{N}) = c1 + (\bar{R} - c1) / \exp\left(\frac{log(N)}{c3}\right) \;,\; \sigma_{min}(\mathrm{N}) = c1 + (-\bar{R} - c1) / \exp\left(\frac{log(N)}{c3}\right)^{c2}$$

* Test input and mapping of available Master curves (usually just available for R=0.1 and 10)

$$\sigma_{R=0.1} = c_1^{NF} + (\bar{R}^t - c_1^{NF}) / \exp\left(\frac{log(N)}{c_3^{NF}}\right)^{c_2^{NF}} \;,\; \sigma_{R=10} = c_1^{SF} + (-\bar{R}^c - c_1^{SF}) / \exp\left(\frac{log(N)}{c_3^{SF}}\right)^{c_2^{SF}}$$

* Mode dedicated Application of Kawai's model $\psi = \sigma / \bar{\mathrm{R}}$; ψ, Ψ positive

Static failure occurs at $\sigma_{max} = \bar{R}^t = \sigma_a + \sigma_m$ and $\sigma_{min} = -\bar{R}^c = -\sigma_a + \sigma_m$.

$\sigma_{max} = \bar{R}^t = \sigma_a + \sigma_m \rightarrow \sigma_a = \bar{R}^t - \sigma_m \rightarrow 1 = \sigma_a / (\bar{R}^t - \sigma_m) \equiv$ cyclic / 'static'

Kawai 's *cyclic* danger intensity to fail ($N > 1$) is given for tension and compression

$\Psi^t_{Master} = \sigma_a / (\bar{R}^t - \sigma_m)$ and $\Psi^c_{Master} = \sigma_a / (\bar{R}^t + \sigma_m)$.

* Relationship of available Master curves with Ψ

Inserting σ_a , σ_m brings the stress ratio R into the model

$\Psi^t_{Master} = 0.5 \cdot \sigma^{Master}_{max} \cdot (1-\mathrm{R}) / [\bar{R}^t - 0.5 \cdot \cdot \sigma^{Master}_{max} (1+\mathrm{R})]$

$\Psi^c_{Master} = \sigma^{Master}_{min} \cdot (1-\mathrm{R}) / [2 \cdot \mathrm{R} \cdot \bar{R}^c + \sigma^{Master}_{min} \cdot (1+\mathrm{R})]$.

* Resolution of above equations for a novel S-N curve or of a CFL curve (inserting σ_a ,σ_m)

$\sigma_{\mathrm{NFdomain}} = 2 \cdot \bar{R}^t \cdot \Psi^t_{Master} / (\Psi^t_{Master} - \mathrm{R} + \mathrm{R} \cdot \Psi^t_{Master} + 1)$, $0 < \mathrm{R} < 1$

$\sigma_{\mathrm{SFdomain}} = -2 \cdot \bar{R}^c \cdot \mathrm{R} \cdot \Psi^c_{Master} / (\Psi^c_{Master} + \mathrm{R} + \mathrm{R} \cdot \Psi^c_{Master} - 1)$

$\sigma_{R=0} = 2 \cdot \bar{R}^t \cdot \Psi^t_{Master} / (\Psi^t_{Master} - 0 + 0 \cdot \Psi^t_{Master} + 1)$ for R = 0

$\sigma_{R=100} = -2 \cdot \bar{R}^c \cdot 100 \cdot \Psi^c_{Master} / (\Psi^c_{Master} + 100 + 100 \cdot \Psi^c_{Master} - 1)$ for R = 100 (≈ ∞)

* For information: Decay function $f_{\mathrm{decay}} = 1 / (1 + exp(c1 + \sigma_m / c2)$.

All formulations, necessary for the author's mode-dedicated variant, are put together in *Table 10-1*. As material example a UD material with the modes FF1 and FF2 is stressed.

LL:
**The author remains with the FMC and sticks to mode domain separation in the following. He tracks a mode-dedication of Kawai's Modified Fatigue Strength Ratio Ψ. This requires - as usual in FMC application - to tackle the transition zone between the modes separately.*
**Due to missing test data the author could not investigate whether Kawai's global fitting Ψ (R_{fit}) of all SN curves enables to predict a desired more or less reliable SN curve in the transition zone.*

Thank you, Masamichi, for informing me about your paper [Kaw04]
because my former work was performed using physically not such good ideas.

In the context of the UD material choice:
Fatigue pre-dimensioning of 'well-designed' (*optimal fiber directions and minimum amount of fiber reinforcement for all load cases*), high-performance UD lamina (ply)-composed laminates just by single lamina-dedicated, mode-representative Master ('basic') SN curves, derived from sub-laminate test specimens, which capture the embedding (in-situ) effects, and on SN data from automatically derivable Constant-Fatigue–Life curves or from numerically constructed Haigh Diagrams, respectively.

Justification check: To prove the general applicability of the 'mode-dedicated Kawai model-predicted SN curves', the curves in *Fig.10-6* have been numerically derived. *Fig.10-6* shows the Master SN curves and the predicted SN curves. With respect to the FMC mode domain view R= -1 is not depicted in *Fig.10-6*.

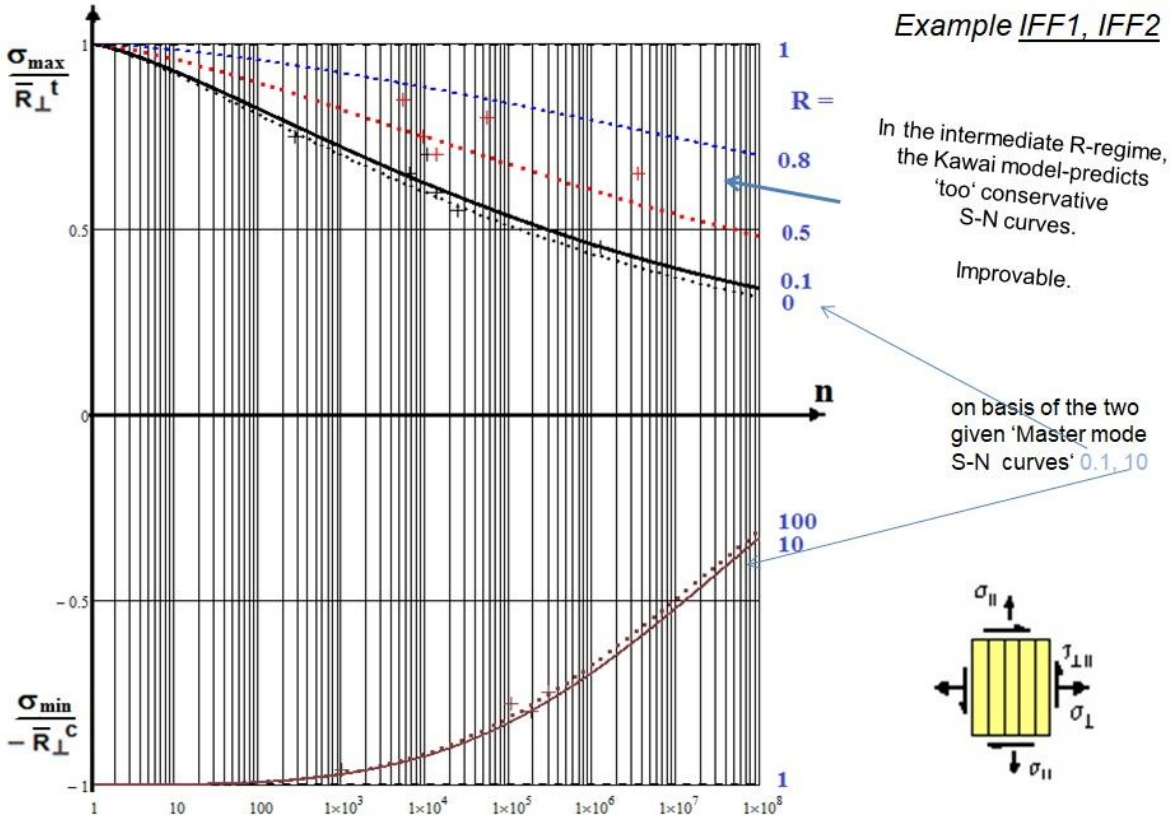


Fig.10-6: Mode-dedicated Kawai model-derived SN curves. + R=0.5 *test data,* +R=0.1 *test data.*

→ Kawai's model looks very promising.

The application results for IFF demonstrate:

- Limit Curves R = 1, 0 and 100 (∞), 1 could be generated
- The question, whether the intermediate Kawai-curves in the range between the limit curves and R = 1 are good enough, can be only responded by further test results and associated modelling research work
- The question, whether Kawai's global fit of all available SN curves is satisfactory could be not supported due to lack of test data. Kawai's model would make it possible to also predict the SN curves in the transition zone $\infty > R > 0$.

To become practical a work case of fatigue life estimation shall be presented. It represents the Design Verification of a critically cycled UD lamina within a chosen laminate.

Example UD material, IFF1-IFF2: Test data, courtesy C. Hahne, Fig.9

* Given: $\sigma_2 = \sigma_{2a} + \sigma_{2m}$, $\bar{R}^t_\perp = 51$ MPa

  $n_1 = 50000$ cycles, R = 0.5, $\sigma_2 = 32$ MPa; $n_2 = 100000$ cycles, R = 0, $\sigma_2 = 30$ MPa

  $$\sigma^{\text{Master}}_{\max} = c1 + (\bar{R}^t_\perp - c1) / \exp\left(\frac{log\,(N)}{c3}\right)^{c2}$$ with c1 = 7.1, c2 = 1.34 , c3 = 6.05

  $$\Psi^t_{Master} = \frac{\sigma_{2a}}{\bar{R}^t_\perp - \sigma_{2m}} = 0.5 \cdot \sigma^{\text{Master}}_{\max} \cdot (1 - R) / (\bar{R}^t_\perp - 0.5 \cdot \cdot \sigma^{\text{Master}}_{\max} (1 + R))$$

  and after resolution an equation for the determination of a desired S-N curve, inserting R

  $$\sigma_{\max} = 2 \cdot \bar{R}^t_\perp \cdot \Psi^t_{Master} / (\Psi^t_{Master} - R + R \cdot \Psi^t_{Master} + 1), \quad 0 < R < 1$$

* Estimation of fracture cyles N at $D_i = n_i / N_i = 100\%$

  $$\sigma_{R=0.5} = 2 \cdot \bar{R}^t_\perp \cdot \Psi^t_{Master} / (\Psi^t_{Master} - 0.5 + 0.5 \cdot \Psi^t_{Master} + 1) = \sigma_2 \rightarrow N_1 = 4.6 \cdot 10^5$$

  $$\sigma_{R=0} = 2 \cdot \bar{R}^t_\perp \cdot \Psi^t_{Master} / (\Psi^t_{Master} - 0 + 0 \cdot \Psi^t_{Master} + 1) = \sigma_2 \rightarrow N_2 = 1.7 \cdot 10^6 .$$

* Summing up the micro-damage portions → $\text{total}D_i = \Sigma\, n_i / N_i = 0.17 < 1 = 100\%$

* From experience with the SN-scatter → RF_{Life} should be > 5 (termed 'Relative Miner').

  RF_{Life} = 100% / total D = 1 / 0.17 = 6 > 5 !

10.3.3 Constant Fatigue Life CFL curves in the Transition Domain

There is no problem to establish Haigh diagrams for FF and IFF3 due to the fact 'The strength values are of similar size in each case'. The static interaction formula was almost sufficient. However for a Haigh Diagram for really brittle materials, indicated by a R_{trans} that is very different to R = -1, a solution procedure has to be looked for. Chosen was a mode-linked exponentially decaying function f_d, that practically ends where the other pure mode begins to reign.
As the employment of the decay function is too lengthy in the work case above just two SN curves in the pure tension domain were stressed.

Table 10-2 informs about the steps for an example IFF1-IFF2 where mode interaction has to be taken into account. Mode decay functions f_d for tension and compression domain are displayed.

Table 10-2: Mode decay function f_d for tension and compression domain in the Haigh diagram

$$Eff = [(Eff^{NF})^m + (Eff^{SF})^m]^{m^{-1}} = 100\%$$

formulated in amplitude and mean stresses reads

$$\left(\frac{-(\sigma_{2m}-\sigma_{2a})+|\sigma_{2m}-\sigma_{2a}|)}{2\cdot \bar{R}_{\perp}^{\,c}\cdot f_d}\right)^m + \left(\frac{\sigma_{2m}+\sigma_{2a}+|\sigma_{2m}+\sigma_{2a}|)}{2\cdot \bar{R}_{\perp}^{\,t}\cdot f_d}\right)^m = 1$$

delivering the CFL curve for N = 1 cycle, f_d = 1, activating both NF with SF.

To obtain a CFL curve for higher N and larger ratios such as $R_{trans} = -\bar{R}^c / \bar{R}^t$ above interaction formula, working in the transition zone, is engineering-like to adjust because the action of a mode ends where the other mode begins. Chosen is an exponential decay function f_d that decays from the end of the pure SF mode at R = ∞ (R=10 possible) down to zero at the beginning of the pure NF mode at R = 0 (R=0.1 possible) and vice versa

$$\rightarrow \quad f_d = 1/[1 + \exp(\frac{c_1+\sigma_m}{c_2})] .$$

Fig.10-7 visualizes the effect of the formulas above. Bounds are given by the straight SN lines for R = ∞ : $\sigma_a = -\sigma_m$ and R = 0: $\sigma_a = \sigma_m$.

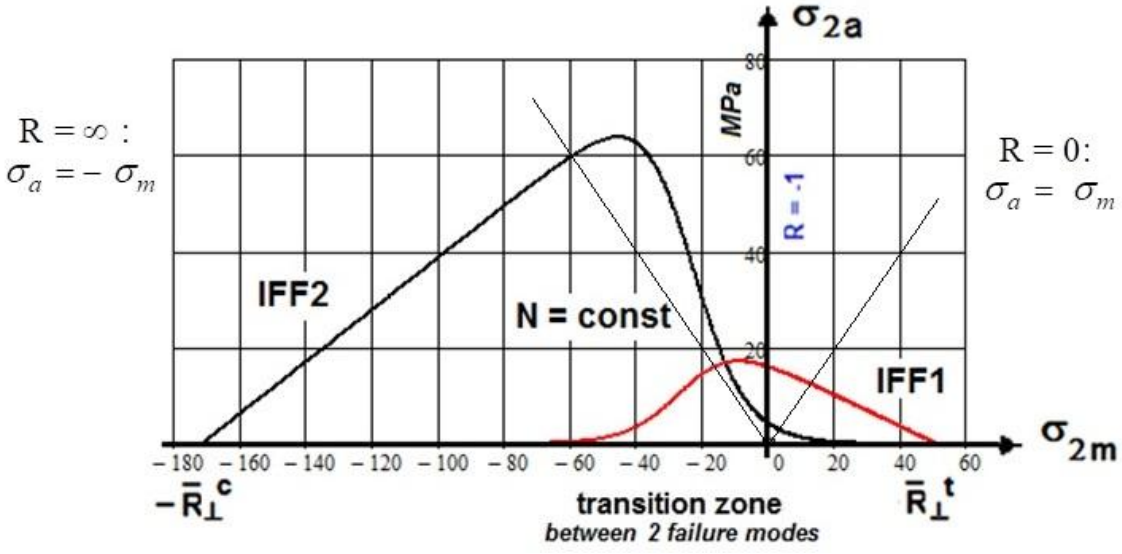


Fig.10-7: Effect of the decay function in the transition zone $-\infty < R < 0$

For fully ductile materials no transition zone between 2 modes exists, because just one single mode reigns, namely 'shear yielding'. There, it is no mean stress effect to correct.

Table 10-3 presents the parameter determination of the decay function in the SF and the NF domain. In the added figure the resulting curves are displayed.

The quality of the approach for the transition zone is practically checked by “How good is the test data course along the stress ratio R_{trans}-line mapped?”

Table 10--3: *Numerical derivation of the parameters of the decay function* $f_d = 1/[1+\exp(\frac{c_1+\sigma_m}{c_2})]$

Vorgabe $c1sSF := -20$ $c2sSF := -5$

$$0.998 = \frac{1}{1+e^{\frac{c1sSF-\sigma m105}{c2sSF}}} \qquad 0.01 = \frac{1}{1+e^{\frac{c1sSF+\sigma m015}{c2sSF}}}$$

$AsSF := Suchen(c1sSF, c2sSF)$ $\quad AsSF = \begin{pmatrix} -40.55 \\ -5.553 \end{pmatrix}$ $\quad c1sSF := AsSF_0$ $\quad c2sSF := AsSF_1$

$c1sSF = -40.55$ $\quad c2sSF = -5.553$

Vorgabe $c1sNF := -20$ $c2sNF := 5$

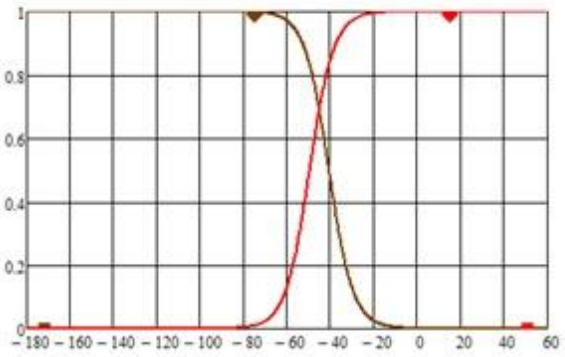
$$0.01 = \frac{1}{1+e^{\frac{c1sNF-\sigma m105}{c2sNF}}} \qquad 0.998 = \frac{1}{1+e^{\frac{c1sNF+\sigma m015}{c2sNF}}}$$

$AsNF := Suchen(c1sNF, c2sNF)$ $\quad AsNF = \begin{pmatrix} -49.532 \\ 5.553 \end{pmatrix}$ $\quad c1sNF := AsNF_0$ $\quad c2sNF := AsNF_1$

$c1sNF = -49.532$ $\quad c2sNF = 5.553$

$$fsNFa(\sigma m) := \frac{1}{1+e^{\frac{c1sNF-\sigma m}{c2sNF}}}$$

$$fsSFa(\sigma m) := \frac{1}{1+e^{\frac{c1sSF-\sigma m}{c2sSF}}}$$



10.3.4 CFL curve application using the decay functions f_d in the Haigh-Diagram

At first *Fig.10-8* shall schematically show the pure domains and the transition zone.

The figure is also applicable for brittle isotropic material like concrete.

For N = 1 the static procedure is applicable using the strength failure envelope represented by the interaction formula. In the negative domain lie the SF-determined SN-curves, in the positive domain the NF determined ones. In the transition zone 2 modes are principally activated which shows either a more SF- or a more NF-determined interaction visualized by the two pale colors.

In *Fig.10-9* two CFL-curves are displayed, the static envelope N=1 and a curve for N= 10^7. The pure mode domains are colored and the transition zone is separated by R_{trans} into two influence parts. The course of the R-value is depicted by the bold dark blue lines.

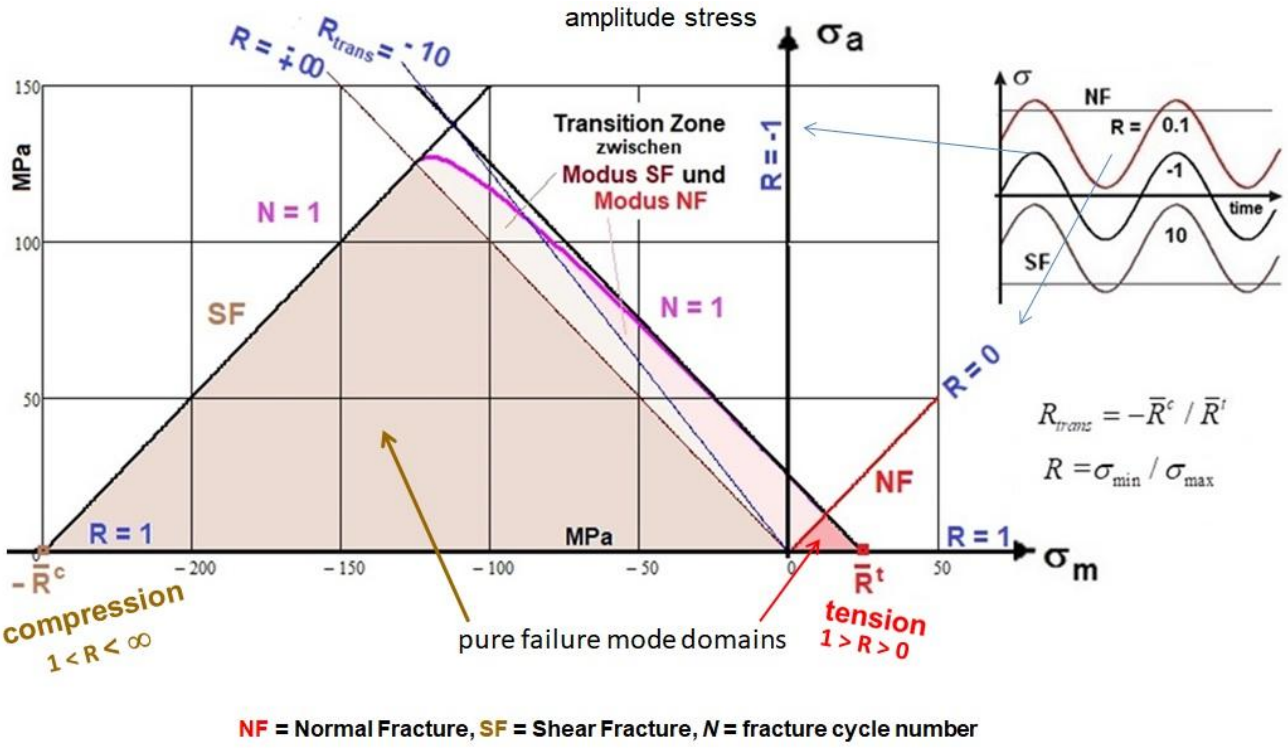


Fig.10-8: Scheme for understanding a Haigh-Diagram of a Brittle Isotropic Material
Up right: alternating stress states of 3 R *curves*

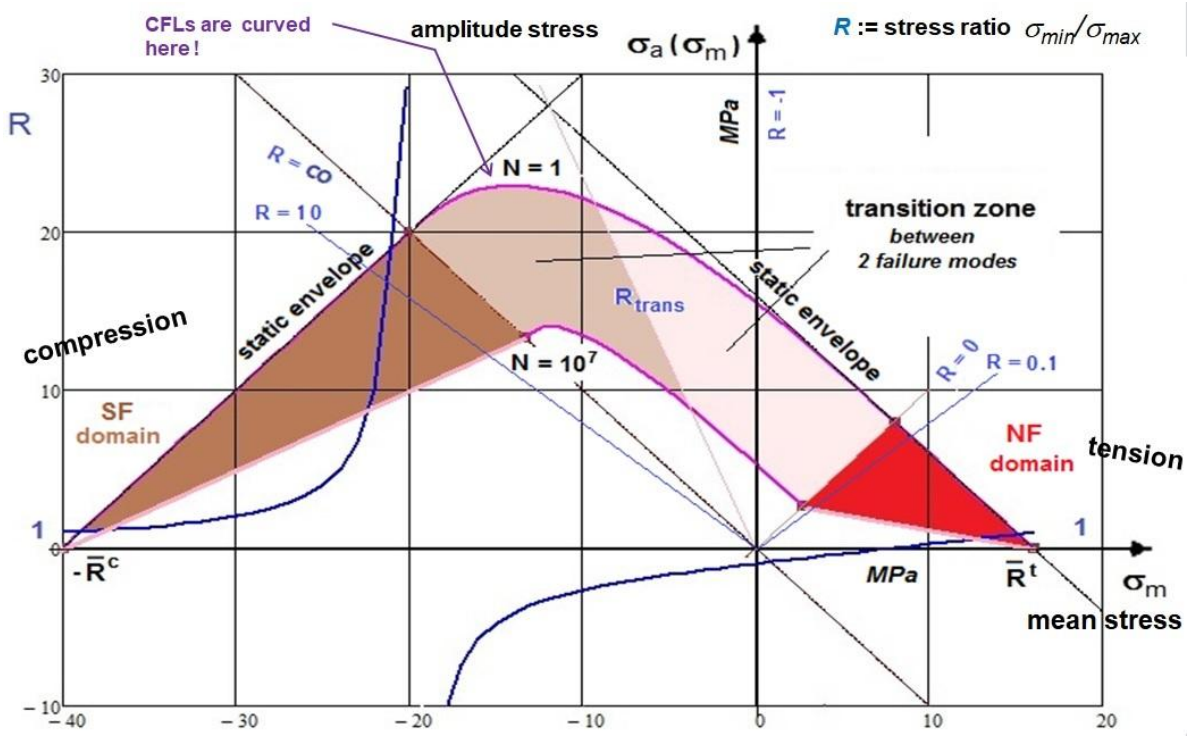


Fig.10-9: Scheme of pure mode domains, course of R *and transition zone parts*

Mind: *The CFL curve N=1 is curved at top because 2 modes act in the case of brittle materials. This is in contrast to uniaxial static loading, depicted by the straight static envelopes.* $N \neq N_f$. *One cycle micro-damage is the sum of 2 micro-damage portions!*

Fig.10-10 gives a feeling how the 'rich bulk' of tested SN curves usually looks.
It further shows how the mapped curve is running in the higher VHCF regime. There is no fidelity given when using extrapolated values far off the tested range.

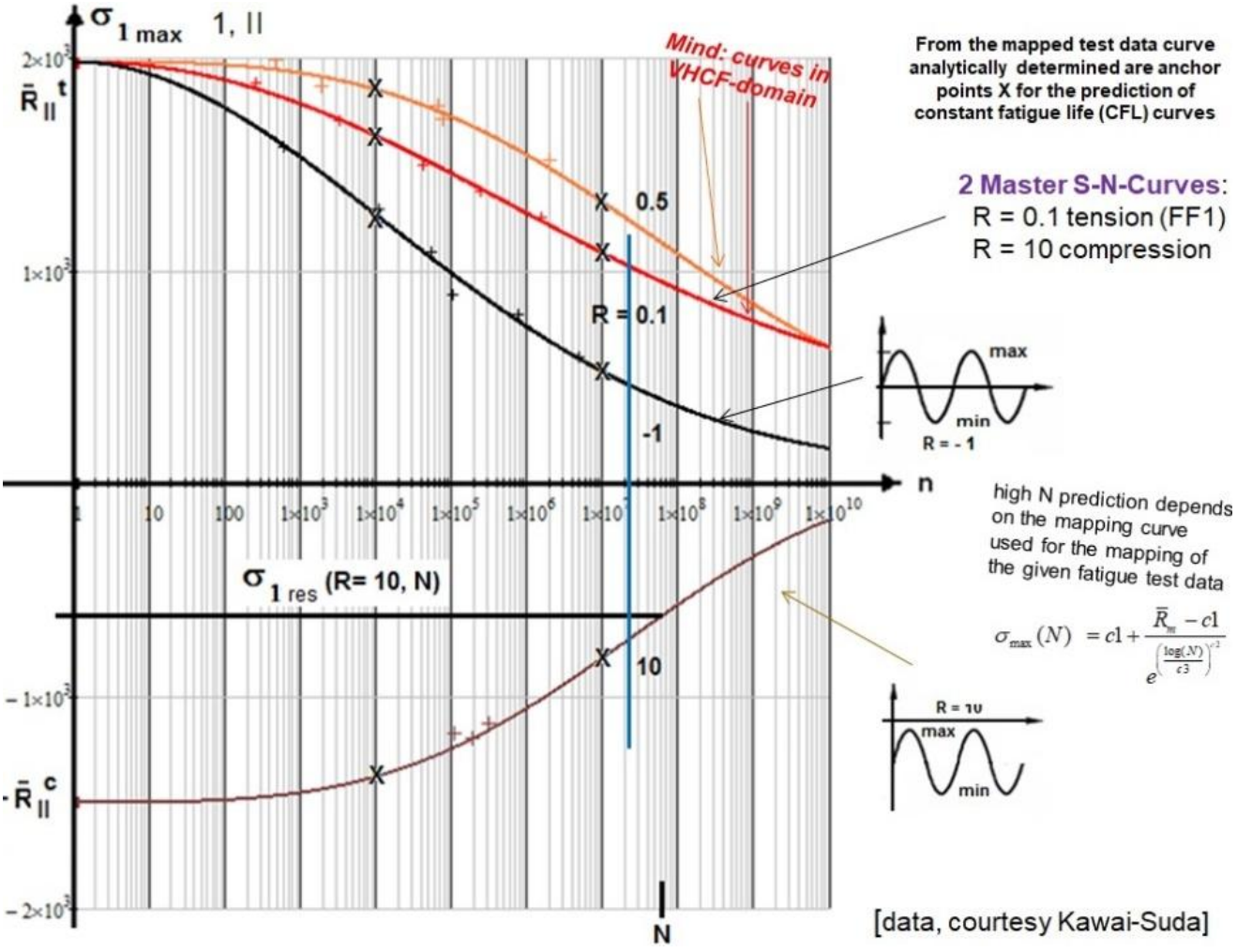


Fig.10-10, Test example UD: Individually lin-log mapped FF1-FF2-linked SN curves

The bold blue vertical fatigue strengths $\sigma^5_{max}(R, 10^5)$, $\sigma^5_{min}(R, 10^5)$ replace the static strengths.

10.6 Some examples of SN curves 'feeding' Haigh-Diagrams, FF and IFF

At first the author likes to thank Dr.-Ing. Clemens Hahne, AUDI, for his valuable UD test results making the generation of the following figures possible and thereby the application of the author's CFL model. The reader is invited to read the content-rich and imaginative dissertation [*Hah14*] and this not only for comparing the different CFL modeling ideas of Hahne and Cuntze.

Fig.10-11 presents failure mode-linked CFL curves σ_a (σ_m , N = constant). The computed 'SN curve X-points' are fixed points (*anchors*) for mapping the CFL curves to be predicted. The blue curve is for $N = 10^5$.

The used SN test curve data is still given in the previous figure, *Fig.10-10*.

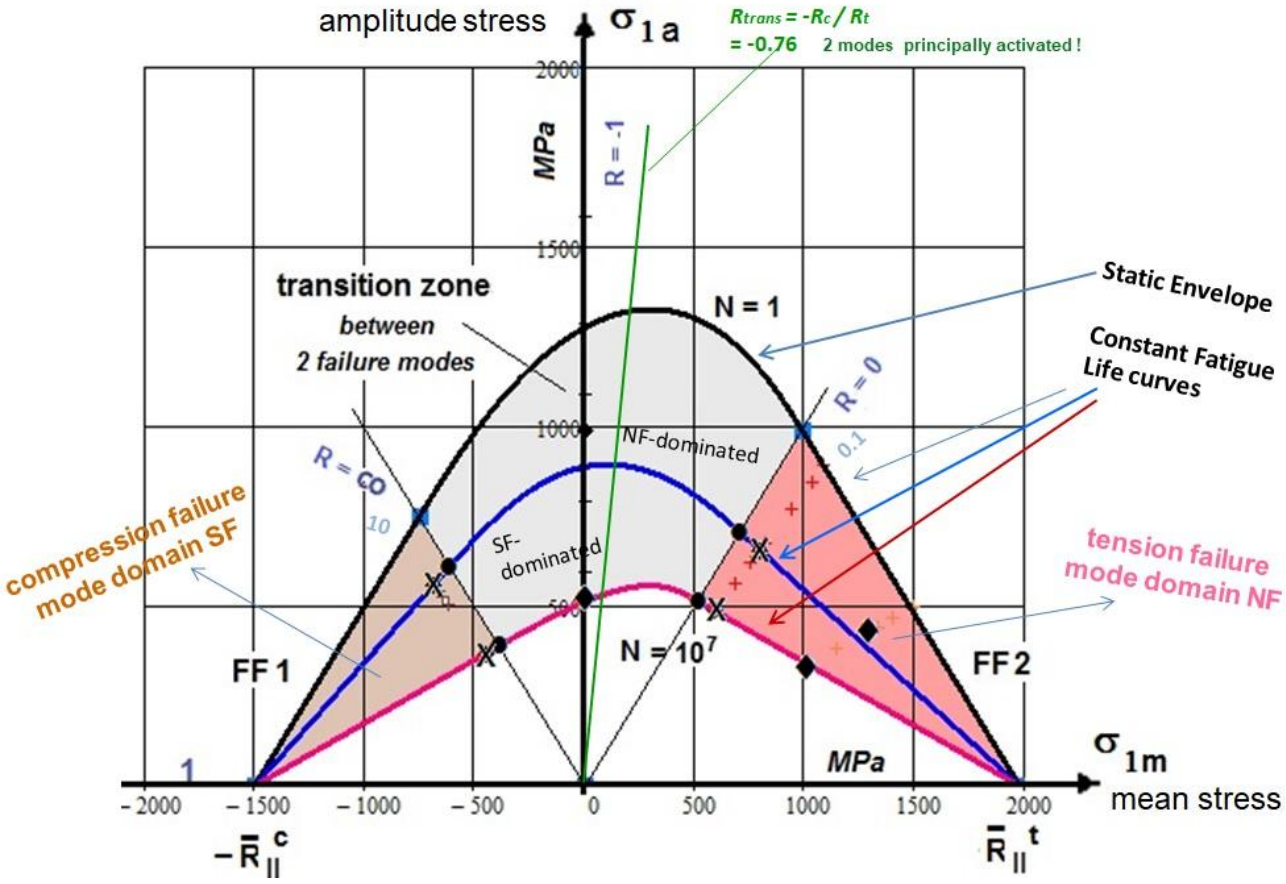


Fig.10-11: Rigorous Interpretation of the Haigh diagram for the UD example FF1-FF2 displaying failure mode domains and transition zone. Test data [Hah14].
CFRP/EP, $\bar{R}^t_{\parallel} = 1980,\ \bar{R}^c_{\parallel} = 1500,\ \bar{R}^t_{\perp} = 51,\ \bar{R}^c_{\perp} = 172,\ \bar{R}_{\perp\parallel} = 71$ [MPa].

Fig.10-12 presents two mapped IFF3 SN curves.

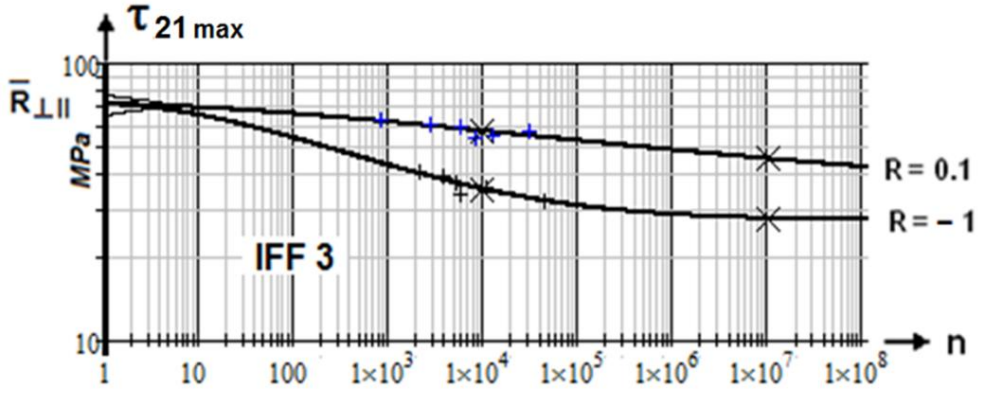


Fig.10-12: Log-log IFF3-linked SN curves [data, courtesy C. Hahne]

Fig.10-13 depicts the CFL curves derived. Obvious is the symmetry and that the two-fold mode micro-damage effect flattens the curve at $\sigma_m = 0$.

In *Fig.10-14* mapped IFF SN-curves are presented.

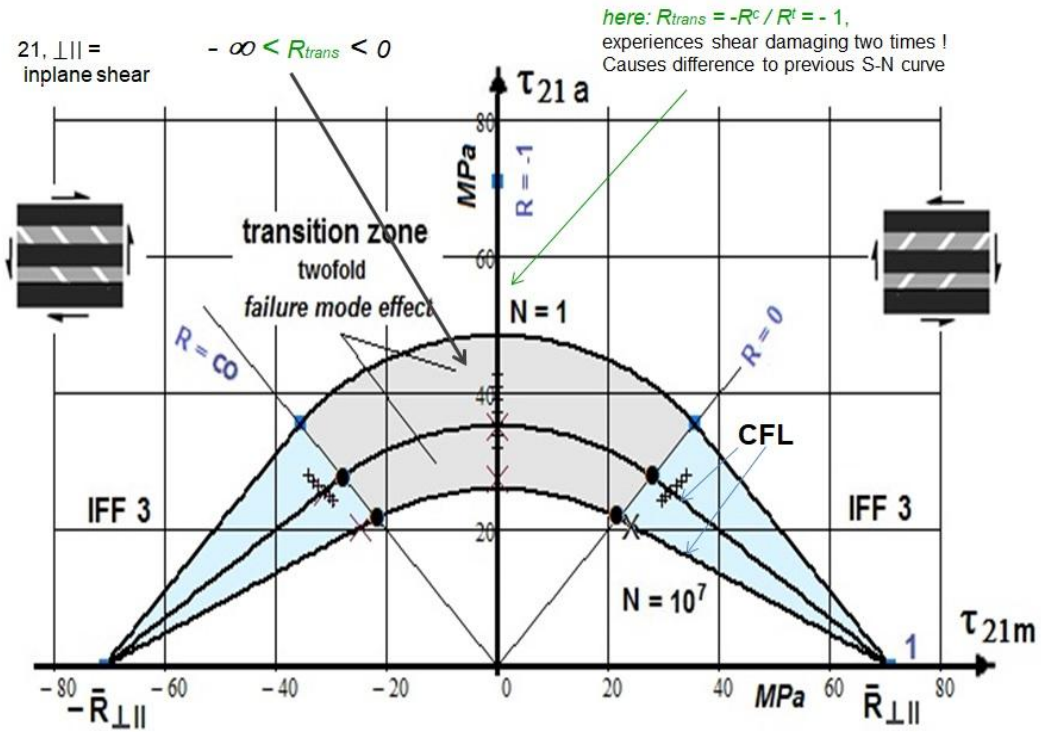


Fig.10-13: IFF3 UD Haigh diagram, Display of a two-fold mode effect (a:= amplitude, m:= mean, N := number of fracture cycles, $\bar{R}$:= strength and R := $\sigma_{min}/\sigma_{max}$*). Test data CF/EP, courtesy [Hah15]*

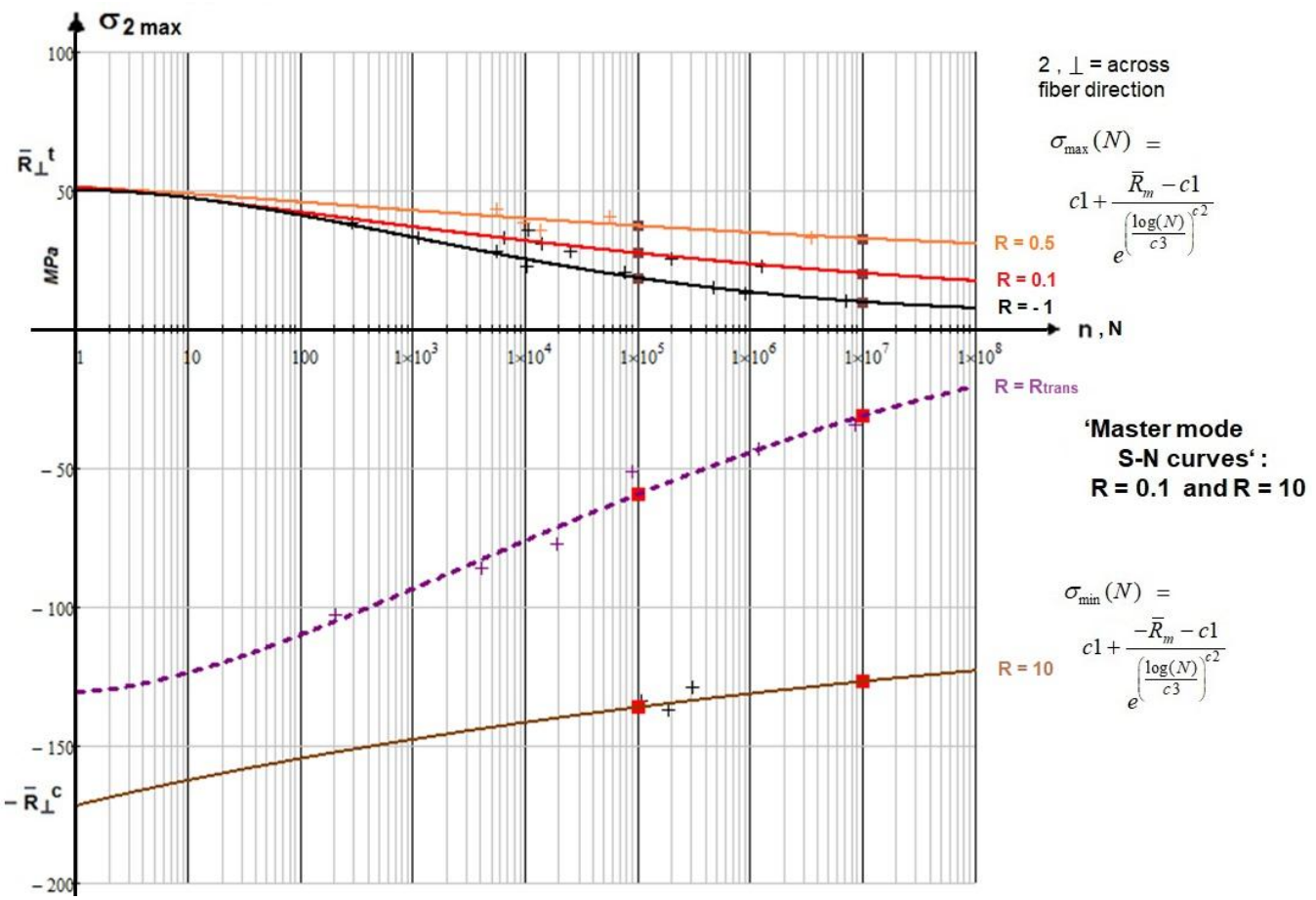


Fig.10-14: Mapped lin-log IFF1-IFF2-linked SN curves [test data, courtesy C. Hahne]

LL: UD-SN curve determination:

Testing conventionally requires 5 different stress amplitude levels for a distinct SN curve with three repetitions at each level considered as the minimum, with scatter around the averaged curve

Of highest interest are the SN curves in the transition zone around R_{trans} and R= -1 which have other origin values then the strengths of the modes. The R_{trans} curve is not standard and needs some explanation. Its origin is not given and has to be determined before mapping. Applied was the static interaction curve, N = 1, because points on the boundary must fulfill the static equilibrium:

$$R_{trans} = -\bar{R}_{\perp}^{c} / \bar{R}_{\perp}^{t} = -3.4 : \quad \left(\frac{\sigma_{2\,fr}}{\bar{R}_{\perp}^{t}}\right)^{m} + \left(\frac{\sigma_{2\,fr} \cdot R_{trans}}{\bar{R}_{\perp}^{c}}\right)^{m} = 1 \rightarrow \sigma_{2\,fr} = -131\ \text{MPa},$$

$$R = -1 \quad : \quad \left(\frac{\sigma_{2\,fr}}{\bar{R}_{\perp}^{t}}\right)^{m} + \left(\frac{\sigma_{2\,fr} \cdot R}{\bar{R}_{\perp}^{c}}\right)^{m} = 1 \rightarrow \sigma_{2\,fr} = 50.1\ \text{MPa}.$$

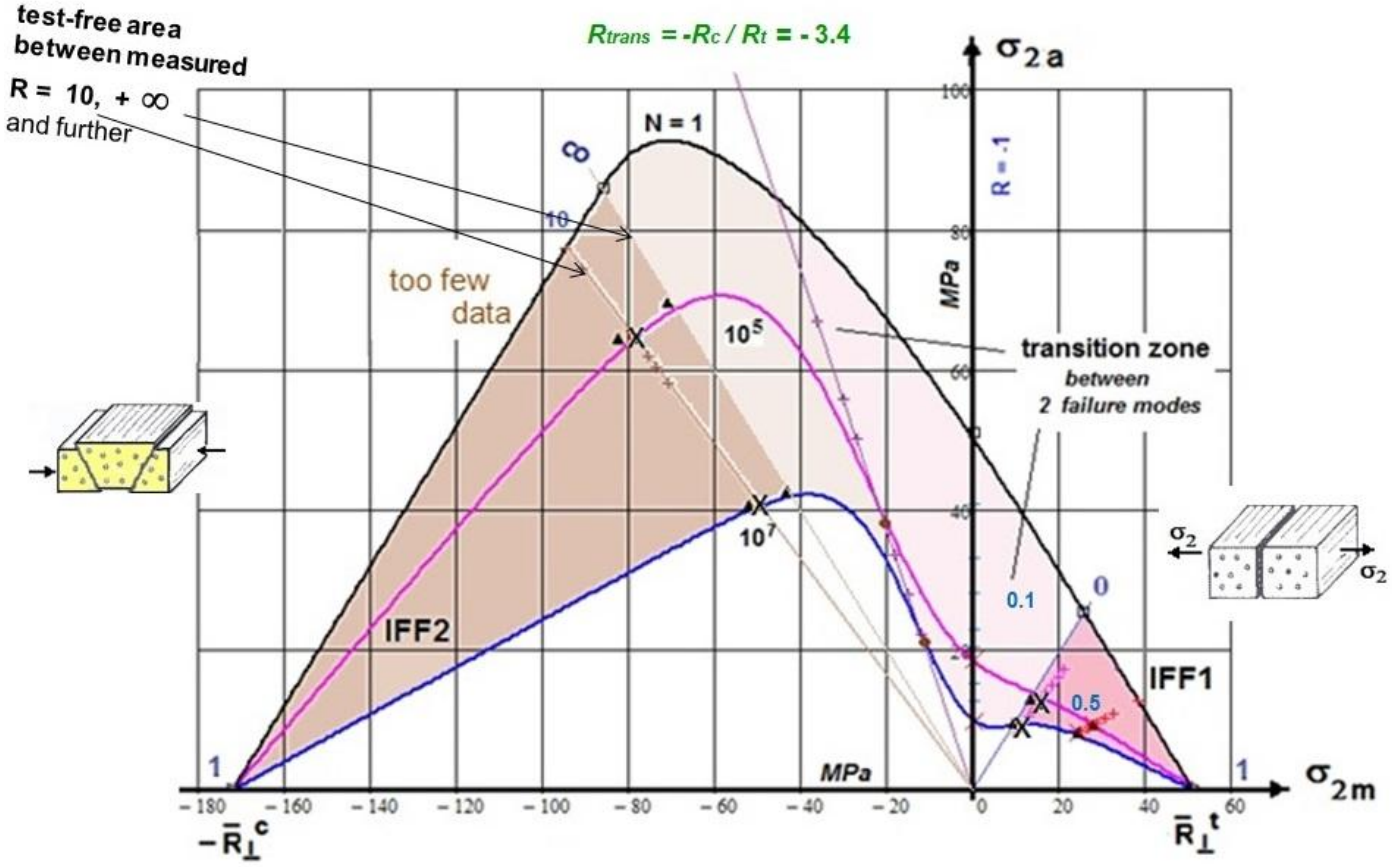


Fig.10-15: IFF1- IFF2 UD Haigh diagram (similar for UD, lamella and concrete) displaying the failure mode domains, transition zone [data courtesy C. Hahne]

10.7 Novel Procedure for deriving CFL curve estimates with associated Steps

The author proposes his procedure in *Table 10-4* for deriving CFL curve estimates on basis of one Master SN curve of each mode. As example serves UD-material stressed in the modes IFF1 and IFF2.

If static failure $\rightarrow$ $\max\sigma = \bar{R}_{static}$, $Eff = 1$ and if cyclic failure $\max\sigma = \bar{R}_{cyclic}$, $D = 1$.

Table 10-5 then presents the associated steps to generate the CFL curve.

Table 10-4: Estimation of a CFL curve $\sigma_{2a}(\sigma_m \equiv \sigma_{2m}, \mathrm{N} = \mathrm{const})$ *for IFF, N = 10^5 cycles*

S-N curves in the two Mode Domains IFF1, IFF2

* From FMC reasons - in contradiction to Kawai - a strict mode separation is to apply.
* S-N curves are generally given for domains IFF1, IFF2 and sometimes R = -1, R_{trans}. Available Master curves are usually just the standard ones R = 0.1 (IFF1), R = 10 (IFF2)
* Computation of the CFL curve parameters for the 2 domains (example N = 10^5, indexed 5)

$$\sigma^{Master}_{max,5}(10^5, \mathrm{R}{=}0.1) = \sigma_{R=0.1}(10^5, \mathrm{R}{=}0.1) = c_1^{NF} + (\bar{R}^t - c_1^{NF}) / \exp\left(\frac{log\,(10^5)}{c_1^{NF}}\right)^{c_2^{NF}} = \bar{R}^t \cdot \Psi^{t,5}_{Master}$$

$$\sigma^{Master}_{min,5}(10^5, \mathrm{R}{=}10) = \sigma_{R=10}(10^5, \mathrm{R}{=}0.1) = c_1^{SF} + (\bar{R}^c - c_1^{SF}) / \exp\left(\frac{log\,(10^5)}{c_1^{SF}}\right)^{c_2^{SF}} = -\bar{R}^c \cdot \Psi^{c,5}_{Master}.$$

* The fatigue strengths $\sigma^5_{max}(\mathrm{R}, 10^5)$, $\sigma^5_{min}(\mathrm{R}, 10^5)$ replace static strengths

$$\sigma^5_{max}(\mathrm{R}) = 2 \cdot \bar{R}^t \cdot \Psi^{t,5}_{Master} / (\Psi^{t,5}_{Master} - \mathrm{R} + \mathrm{R} \cdot \Psi^{t,5}_{Master} + 1), \quad 0 < \mathrm{R} < 1$$

$$\sigma^5_{min}(\mathrm{R}) = -2 \cdot \bar{R}^c \cdot \Psi^{c,5}_{Master} / (\Psi^{c,5}_{Master} + \mathrm{R} + \mathrm{R} \cdot \Psi^{c,5}_{Master} - 1), \quad 1 < \mathrm{R} < 100\ (\infty).$$

with $\mathrm{R} = (\sigma_m - \sigma_{2a,5}) / (\sigma_m + \sigma_{2a,5})$.

CFL curves $\sigma^5_{max}(\mathrm{R}, 10^5)$ within the 2 IFF domains $\bar{R} \rightarrow \sigma^5(\mathrm{R})$

$$\frac{-(\sigma_{2m} - \sigma_{2a}) + |\sigma_{2m} - \sigma_{2a}|}{2 \cdot \bar{R}_\perp^{\,c}} = 1 \quad \text{and} \quad \frac{\sigma_{2m} + \sigma_{2a} + |\sigma_{2m} + \sigma_{2a}|}{2 \cdot \bar{R}_\perp^{\,t}} = 1 \ \text{static}$$

$$\frac{-(\sigma_{2m} - \sigma_{2a}) + |\sigma_{2m} - \sigma_{2a}|}{2 \cdot \sigma^5_{min}(\mathrm{R})} = 1 \quad \text{and} \quad \frac{\sigma_{2m} + \sigma_{2a} + |\sigma_{2m} + \sigma_{2a}|}{2 \cdot \sigma^5_{max}(\mathrm{R})} = 1 \ \text{cyclic.}$$

Modelling in the Transition Zone between the mode domains

* The transition zone where both the modes interact requires the interaction equation

$$Eff = [(Eff^{NF})^m + (Eff^{SF})^m]^{m^{-1}} = 100\% = 1.$$

Formulated in CFL coordinates σ_a and σ_m the static interaction equation reads

$$\left(\frac{-(\sigma_{2m} - \sigma_{2a}) + |\sigma_{2m} - \sigma_{2a}|}{2 \cdot \bar{R}_\perp^{\,c}}\right)^m + \left(\frac{\sigma_{2m} + \sigma_{2a} + |\sigma_{2m} + \sigma_{2a}|}{2 \cdot \bar{R}_\perp^{\,t}}\right)^m = 1 \ \text{static curve, n} = 2\mathrm{N}_f.$$

* For the N = n = 1 cycle with $n = 2 \cdot N_f$: Static interaction equation delivers a curve which still runs through the full Haigh diagram.

CFL curves in the full Haigh diagram

* To obtain a CFL curve for higher N and larger ratios $R_{trans} = -\bar{R}^c / \bar{R}^t$ the two opposite mode decays in the transition zone are to adjust by $f_d = 1/[1+\exp((c_1+\sigma_m)/c_2)]$.
* Inserting $\mathrm{R} = (\sigma_m - \sigma_{2a,5}) / (\sigma_m + \sigma_{2a,5})$ for $\sigma_m \rightarrow \sigma_{2m}$ as running variable the CFL curve $\sigma_{2a}(\sigma_{2m}, \mathrm{N} = \mathrm{const})$ is to determine by solving the complicate implicit equation for σ_{2a} below

$$\left(\frac{-(\sigma_{2m} - \sigma_{2a,5}) + |\sigma_{2m} - \sigma_{2a,5}|}{2 \cdot \sigma^5_{max}(\mathrm{R}) / (1 + e^{\frac{c_{1SF} + \sigma_{2m}}{c_{2SF}}})}\right)^m + \left(\frac{(\sigma_{2m} + \sigma_{2a,5}) + |\sigma_{2m} + \sigma_{2a,5}|}{2 \cdot \sigma^5_{max}(\mathrm{R}) \cdot / (1 + e^{\frac{c_{1NF} + \sigma_{2m}}{c_{2NF}}})}\right)^m = 1.$$

Table 10-5: Steps to generate a CFL curve. IFF, N=10^5 cycles, via 'side lines' of the Haigh diagram

1 Choice of the distinct CFL (example N =10^5)

2 Determination of the 2 Master curves

Assumption: usual test curves R=0.1 (NF), R=10 (SF) are sufficient instead of R=0, R=1000 ≅ ∞

$$\sigma_{max}^{Master}(N,\mathrm{R}=0.1) \rightarrow = \sigma_{R=0.1} = c_1^{NF} + (\bar{R}^t - c_1^{NF}) / \exp\left(\frac{log(N)}{c_1^{NF}}\right)^{c_2^{NF}}$$

$$\sigma_{min}^{Master}(N,\mathrm{R}=10) \rightarrow = \sigma_{R=10} = c_1^{SF} + (-\bar{R}^c - c_1^{SF}) / \exp\left(\frac{log(N)}{c_1^{SF}}\right)^{c_2^{SF}} .$$

3 Assumption: Straight asymptotic side lines in the 2 mode domains $\sigma_a(\sigma_m) = c_1 + c_2 \cdot \sigma_m$

2 strength points are given and 2 mean $\sigma_a(\sigma_m, N)$ of R=0.1 and R=10 are to compute as a fixed point of each side line

4 Computation of the fixed points in the domains NF, SF (n MPa)

$$\sigma_{R=0.1}^{100000} = 27.3 \rightarrow \sigma_{a\,R=0.1}^{100000} = 0.5 \cdot \sigma_{R=0.1}^{100000} \cdot (1\text{-}0.1) = 12.3, \quad \sigma_{m\,R=0.1}^{100000} = \sigma_{R=0.1}^{100000} - \sigma_{a\,R=0.1}^{100000} = 15.0,$$

$$\sigma_{R=10}^{100000} = -136.5 \rightarrow \sigma_{a\,R=10}^{100000} = -0.5 \cdot \sigma_{R=10}^{100000} \cdot (1\text{-}1/10) = 61.4, \quad \sigma_{m\,R=10}^{100000} = \sigma_{R=10}^{100000} + \sigma_{a\,R=10}^{100000} = -75.$$

5 Function for the decay of mode influences $\sigma_a(\sigma_m)$ over the transition zone

Parameters sets from the strength point and a fixed point $f_d = 1/[1+\exp((c_1+\sigma_m)/c_2)]$.

f_d(SF): $(\sigma_a, \sigma_m, N, R=10) \rightarrow 0.99$ with $(\sigma_a, \sigma_m, N, R=0.1) \rightarrow 0.01$;

f_d(NF): $(\sigma_a, \sigma_m, N, R=10) \rightarrow 0.01$ with $(\sigma_a, \sigma_m, N, R=0.1) \rightarrow 0.99$.

6 'Static' envelope curve: Solving the interaction equation for $\sigma_a(\sigma_m, N = 1)$

$$\left(\frac{-(\sigma_{2m}-\sigma_{2a}) + |\sigma_{2m}-\sigma_{2a}|}{2 \cdot \bar{R}_\perp^{\,c}}\right)^m + \left(\frac{\sigma_{2m}+\sigma_{2a} + |\sigma_{2m}+\sigma_{2a}|}{2 \cdot \bar{R}_\perp^{\,t}}\right)^m = 1 \rightarrow \sigma_{2a}(\sigma_{2m}, \bar{R}_\perp^{\,c}, \bar{R}_\perp^{\,t}).$$

7 Assymptotic side line approach for the decaying curves $\sigma_a(\sigma_m, N > 1)$

$$[\sigma_{2a}(\sigma_{2m},N)]^m = (c_{1SF} + c_{2SF} \cdot \sigma_{2m})^m + (c_{1NF} + c_{2NF} \cdot \sigma_{2m})^m$$

Work case N = 10^5 cycles, m = 2.5

$c_{1SF} = 0.63 = c_{2SF}$, $c_{1NF} = 0.34 = -c_{2NF}$; $c_{1SF5} = -40.6$, $c_{2SF5} = -5.56$, $c_{1NF5} = -49.5$, $c_{2NF5} = 5.55$

$$\sigma_{2a}(\sigma_{2m},N=10^5, c_i) = \left[\left(\frac{c_{1SF} + c_{2SF} \cdot \sigma_{2m}}{1+\exp(\frac{c_{1SF5}+\sigma_{2m}}{c_{2SF5}})}\right)^m + \left(\frac{c_{1NF} + c_{2NF} \cdot \sigma_{2m}}{1+\exp(\frac{c_{1NF5}+\sigma_{2m}}{c_{2NF5}})}\right)^m\right]^{-1/m} .$$

10.8 Check of the FMC-driven Idea to Split the Operational Loading mode-wise

The failure mode-based FMC forces to think about the idea "*The loading* o = - *1 can be split into 2 swelling loadings*", see <u>*Fig.10-16*</u>. A separation is performed due to the activated inherent

different failure modes. For a UD-material the fully reversed alternating SN curve R = -1 is split into its mode portions associated to the tensile IFF1 and compressive domain IFF2.

The FMC principally permits predictions in the transition zone from the pure domains information $\sigma_{R=0}$,$\sigma_{R=\infty}$. Hence, in *Table 10-6* an attempt was made to estimate the fatigue life of the fully (mode) reversed R = -1 from the 'Master' (Basic) SN curves of the 2 modes.

Question was: "Is the sum of micro-damage D on basis of 2 strengths and 2 Master SN curves the same as for R = -1?"

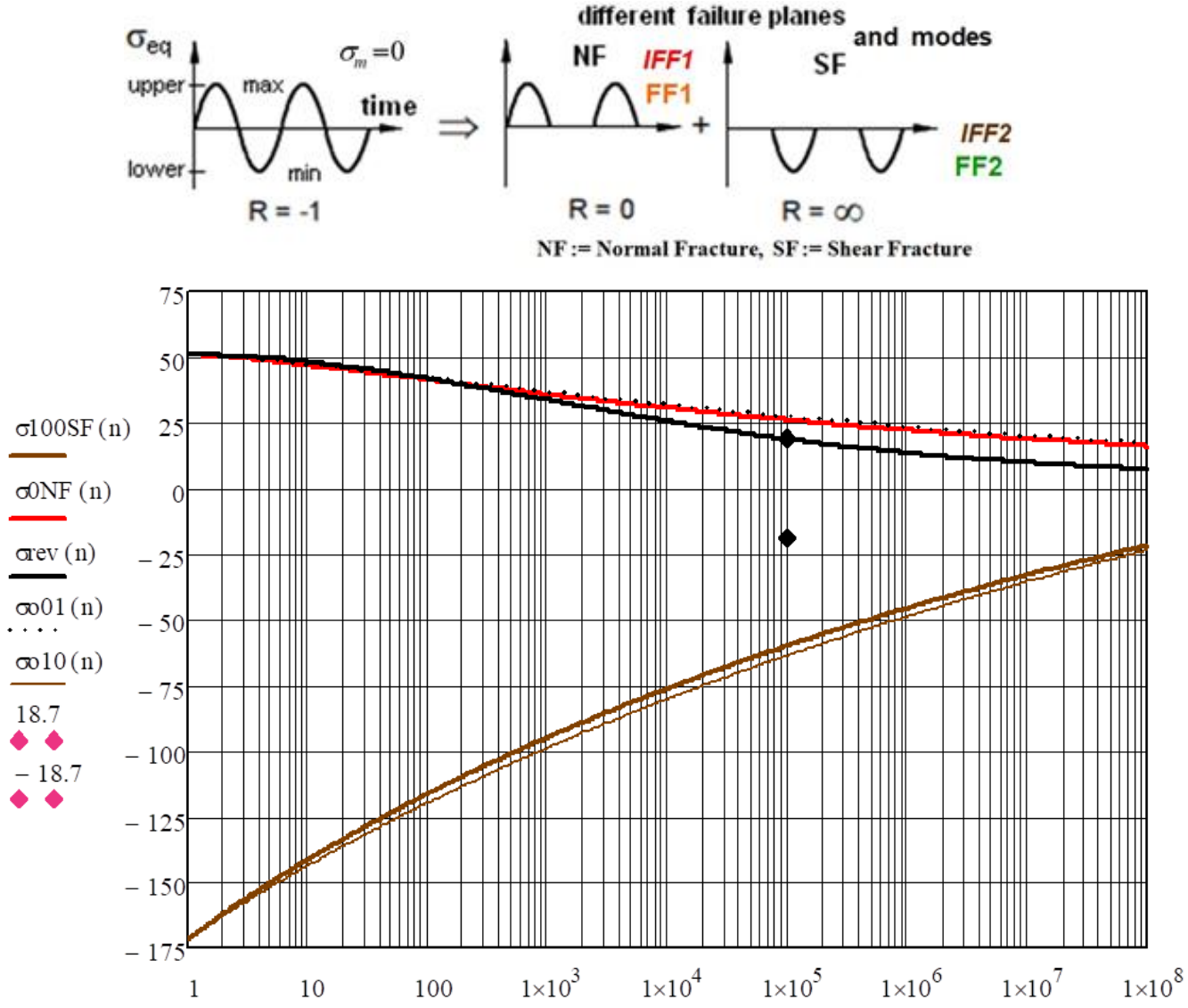


Fig.10-16: (up) IFF mode-wise modeling of loading cycles (example R = -1) for high-performance 'fiber-dominated designed' UD laminas-composed laminates. (down) SN curves used, $\sigma_{rev} \equiv \sigma_{R=-1}$

Table 10-6: Numerical example and idea check. $\bar{R}^t_{\parallel} = 1980$, $\bar{R}^c_{\parallel} = 1500$, $\bar{R}^t_{\perp} = 51$, $\bar{R}^c_{\perp} = 172$, $\bar{R}_{\perp\parallel} = 71$ [MPa].
From mapping of SN test curves: $c_1^{SF}=87$, $c_1^{SF}=9.47$, $c_3^{SF}=0.96$; $c_1^{NF}=7.1$, $c_2^{NF}= 6.05$, $c_3^{NF}=1.34$ *and for reversed alternating stress* $c_1^{rev}=5.0$, $c_2^{rev} = 4.5$, $c_3^{rev} =1.84$

Check of Idea 'Mode Separation of Loading R = - 1' ($\sigma_m = 0$) is possible

R = – 1 reversed alternating stress → split into the 2 swelling parts R = 0 and 100 (∞).

Fatigue Life prediction: Estimation for R= -1 on basis of $\sigma_{R=0}$, $\sigma_{R=\infty}$

The FMC *should* permit predictions in the transition zone from pure domain information, only

* From testing as Master S-N curves are available

$$\sigma_{max}^{Master}(N, R = 0.1) = \sigma_{R=0.1} = c_1^{NF} + (\bar{R}^t - c_1^{NF}) / \exp\left(\frac{log(N)}{c_1^{NF}}\right)^{c_2^{NF}}$$

$$\sigma_{min}^{Master}(N, R = 10) = \sigma_{R=10} = c_1^{SF} + (-\bar{R}^c - c_1^{SF}) / \exp\left(\frac{log(N)}{c_1^{SF}}\right)^{c_2^{SF}} .$$

* Determination of Ψ (defined positiv)

$$\Psi^t_{Master} = \frac{0.5 \cdot (1-R) \cdot \sigma^{Master}_{max}}{\bar{R}^t - 0.5 \cdot (1+R) \cdot \sigma^{Master}_{max}} \quad \text{and} \quad \Psi^c_{Master} = \frac{(1-R) \cdot \sigma^{Master}_{min}}{(1+R) \cdot \sigma^{Master}_{min} + 2 \cdot R \cdot \bar{R}^c} .$$

* Transfer to boundary SNs as the mode-Basic SN-curves R = 0 and R = 100 (≅ ∞) using

$$\sigma_{R=0}(N^{NF} = 0, R) = 2 \cdot c_1^{NF} + (\bar{R}^t - c_1^{NF}) / \exp\left(\frac{log(N^{NF})}{c_1^{NF}}\right)^{c_2^{NF}} / (\Psi^t_{Master} - R + R \cdot \Psi^t_{Master} + 1)$$

$$\sigma_{R=100}(N^{SF} = 100, R) = 2 \cdot c_1^{SF} + (-\bar{R}^c - c_1^{SF}) / \exp\left(\frac{log(N^{SF})}{c_1^{SF}}\right)^{c_2^{SF}} \sqrt{\ } (\Psi^c_{Master} + R + R \cdot \Psi^c_{Master} - 1)$$

Application: Work case 10^5cycles (indexed by^5, stresses in MPa, N and n in cycles)

IFF1-IFF2: Test data Hahne, *Fig*.10-15, $\sigma_{2a} = 18.7$ MPa ≡100% computed from mapping $SN_{R=-1}$

* Given: R = -1, n = N = 10^5, $\sigma_{2a} = 18.7$, $\sigma_{2m} = 0$, D = 100 %.

$\sigma_{R=0}(N^{NF*}, R = 0) = 18.7 \rightarrow N^{NF*} = 2 \cdot 10^9$; $\sigma_{R=100}(N^{SF*}, R = 100) = -18.7 \rightarrow N^{SF*} = 2 \cdot 10^{11}$

* Estimation of micro-damage portions and of $D = n / N^{NF*} + n / N^{SF*}$

⇒ R = -1, n = N = 10^5cycles, $\sigma_{2a} = 18.7$, *D* =100 %, failure.

⇒ Split into 2 modes: *D* < 1 % → FMC-Idea: not applicable.

The results in *Table 10.3* demonstrate that the FMC-fed hope "In the case of brittle materials fatigue treatment may become simpler by mode-wise load splitting" was not fulfilled. The micro-damage process depends on the alteration effects and in the transition zone the scatter of test data is larger than in the pure domains.

This reminds the author of his former (1968-1970) colleague Wolf Elber †, when Wolf worked on his crack-closure concept for metallic materials. Here, one must also think about the closure effect with its micro-damage causing opening/closing of flaws in brittle materials.

LL: Compute a realistic example before trusting a hope. A close view at Fig.10-16 would have revealed the reality to the author. However, also a 'bad' idea should be published. Test data from R = - 1 are necessary to record the crack closure/opening micro-damage impact.

10.9 Estimation of the Haigh Diagram Amplitude and Comparison with the Measured Value

The data set of the example before is further used for a prediction example that compares it with the measurement.

Estimation of maximum σ_{2a} using Constant Fatigue Life curve: R = -1, m = 2.5

$$c_{1SF} = 0.63 = c_{2SF},\ c_{1NF} = 0.34 = -c_{2NF};\ c_{1SF5} = -40.6,$$
$$c_{2SF5} = -5.56,\ c_{1NF5} = -49.5,\ c_{2NF5} = 5.55$$

$$\sigma_{2a}(\sigma_{2m}, N=10^5, c_i) = \left[\left(\frac{c_{1SF} + c_{2SF} \cdot \sigma_{2m}}{1+\exp\left(\frac{c_{1SF5}+\sigma_{2m}}{c_{2SF5}}\right)} \right)^m + \left(\frac{c_{1NF} + c_{2NF} \cdot \sigma_{2m}}{1+\exp\left(\frac{c_{1NF5}+\sigma_{2m}}{c_{2NF5}}\right)} \right)^m \right]^{1/m}$$

$$\rightarrow \sigma_{2a} = 17.4 \text{ MPa} < 18.7 \text{ MPa} \quad \text{from measurement.}$$

Result:

Micro-damage portion D = 100% is still reached at a lower amplitude stress $\Rightarrow$ conservative.

10.10 Steps of the FMC-based Fatigue Life Estimation Procedure

The steps of the fatigue life estimation procedure are depicted in the following figures. ***Step 1*** is searching measured SN curves. *Fig.10-17* presents a measured SN-curve that serves as master SN curve. This SN curve can be mapped by a straight line in a log-log diagram.

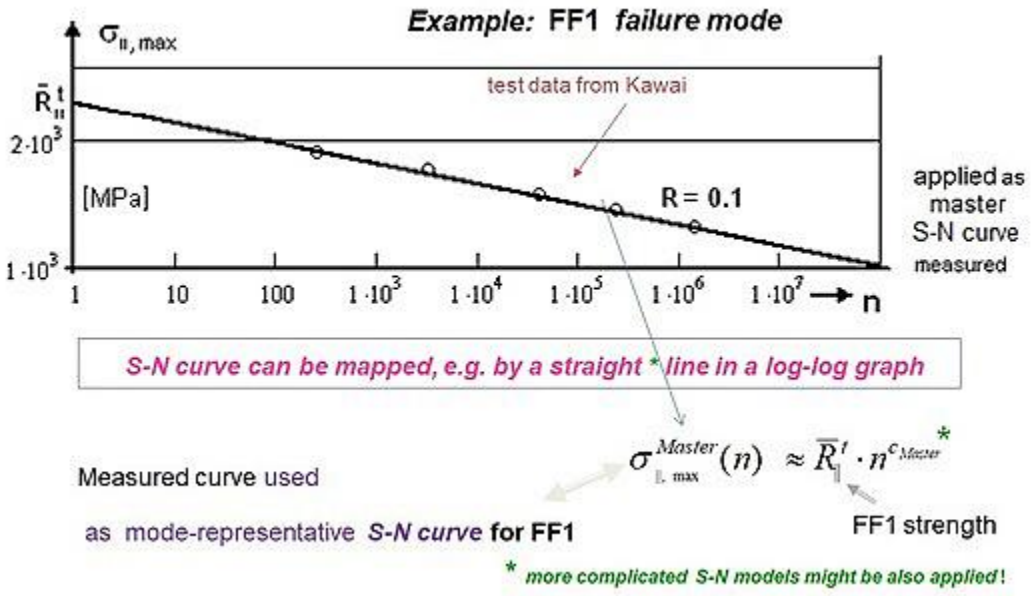


Fig.10-17: Mapping of UD SN data and mode-representative Master SN curve, FF1 here

In the case of variable amplitude loading several SN curves are needed. This will be performed for the tension domain in *Fig.10-18* by application of Kawai's model however here by a mode-wise application.

Statistical analyses have shown that the fatigue life estimation using the linear accumulation method of Palmgren-Miner tends to be too optimistic, *Fig.10-19*. However a satisfactory reason could not yet found. One explanation is the right use of the right SFC. A more severe explanation is the loss of the loading sequence which is different for ductile and brittle materials. This is to consider in the design by the application of Relative Miner with a $D_{feasible} < 100\%$.

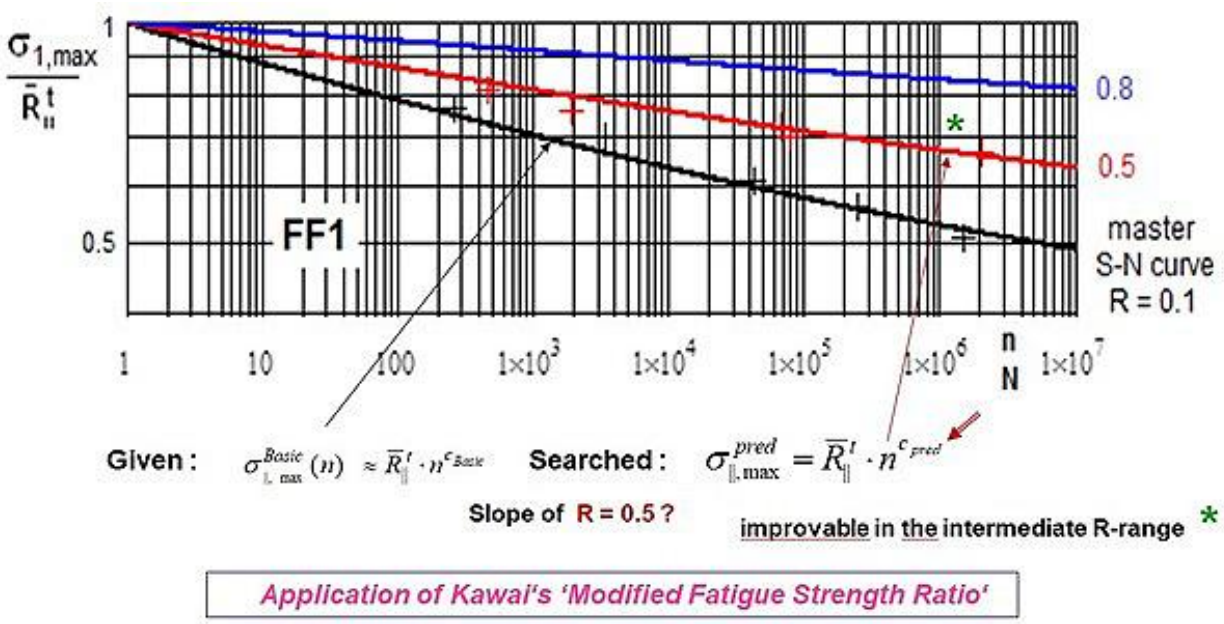


Fig.10-18: Prediction of other needed FF1 SN curves from Master mode SN curve and Cuntze's mode-dedicated Kawai model (Ψ curve)

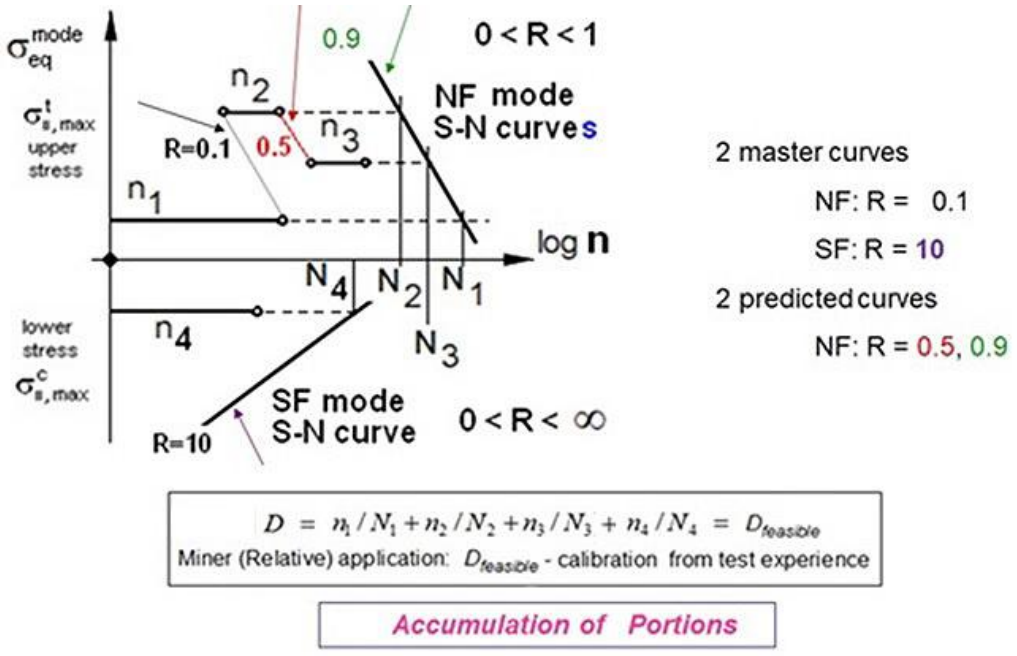


Fig.10-19: Lifetime Prediction (estimation) Method.
Schematic application of a simple example, 4 blocks. $D_{feasible}$ from test experience

Fig.10-20 finally shall briefly give the fatigue life estimation procedure for the example laminate. Due to the lack of test data regarding ductile and slightly brittle metals the author could not generally apply the CFL generation method above.

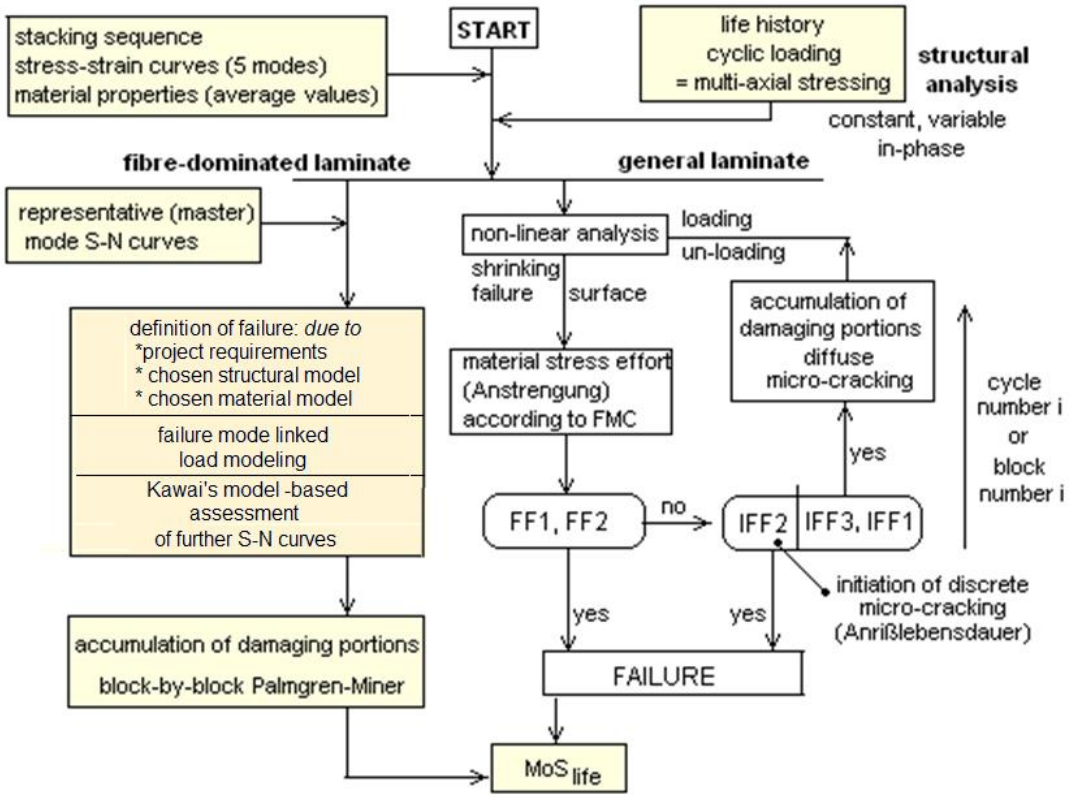


Fig.10-20: Non-linear estimation of a laminate's fatigue life

After having had some pushing new ideas one should not think to be at the top, but just an intermediate High Fidelity level is reached. The next figure enables to get a feeling how the author feels regarding the High Fidelity level reached with his 3D-fatigue modelling to be always linked to applicable 3D-SFCs and available 2D and 3D-test data sets.



After a tough ascent, considering the fatigue life estimation idea, comes the arrival at the 'top'.
"But , is it really the top? No. It goes even higher".

A High Fidelity level is not fully reached with the given models according to missing test data.

Information on Access to composite fatigue data: K. Vallon gave 2015, in *Fatigue of Textile Composites. http://dx.doi.org/10.1016/B978-1-78242-281-5.00004-3, Copyright © 2015 Elsevier Ltd. All rights reserved his view on Databases for fatigue analysis in composite materials. Basic source was the wind-energy where the rotor blades have to be fatigue verified. A collection of data sets is available in the OptiDat database. It can be downloaded as an Excel document from http://www.wmc.eu/optimatblades_optidat.php. The database was updated in 2011 with the results of the more recent UpWind project. It can also be used for the development and validation of models to predict fatigue life under various conditions, or material behavior in complex stress states, extreme conditions, variable amplitude fatigue, etc.*

"*Everything in the world is terminated by chance and fatigue*". *Heinrich Heine*

10.11 Notes on Damage Tolerance and Fracture Mechanics with Cracked Components

In order to complete the before treated residual strength topic this paragraph shall be added since for the design of load-carrying components, knowledge of the damage tolerance behavior is required. This includes crack growth under oscillating stress and addresses the residual strength under static stress.

10.11.1 Static Crack Fracture

Fig.10-8 presents the elements of the Damage Tolerance procedure of cracked (macro-damaged) structural components. In this context, due to HSB 62201-01, two questions are posed in analysis:

- What is the static strength if a crack is present (residual strength problem)? These questions can be answered using the analytical methods of fracture mechanics. For practical application the concept of linear-elastic stress intensity factor K is usually applied
- What is the crack propagation behavior (crack growth problem)?

The crack-linked residual strength R is the gross-sectional tensile stress σ at failure of a structural component containing a crack. R of the last fatigue phase is to discriminate from R_{res} in the previous fatigue phase. Thereby, the crack length a_0 at the beginning of the static loading will increase to its critical value a_{cr} in general.

A structural component will fail in the case of static loading if the stress intensity factor (SIF) K of a brittle material reaches its critical value at $K = K_{cr}$, termed fracture toughness, which depends on the material behavior. The determination of the K_{cr} values requires in the so-called K-concept above the fulfilment of a geometric bound in order to achieve a real minimum value by a minimum test specimen thickness of $t > 2.5 \cdot (K_{Icr} / R^t_{0.2})^2 \rightarrow \sigma_{cr} = K_{Icr} / (\sqrt{\pi \cdot a_0} \cdot f(a_0))$.

In the ductile material case the limit reads $\mathcal{G} = \mathcal{G}_{cr.}$

The R-Curve or Crack Growth Resistance Curve

The depiction of crack growth resistance $\mathcal{G}_{cr}$ over crack extension Δa is termed crack growth resistance curve or R-curve in fatigue phase 3, not to be confused with R_{res} as residual strength of

the previous, still non-cracked fatigue phase. See (*Wang, C. H. "Introduction to Fracture Mechanics," DSTO Aeronautical and Maritime Research Laboratory, DSTO-GD-0103, 1996*).

R-Curves are used for the prediction of the

- residual strength of the structure for a given crack position and crack length and
- critical length of an initial crack under given loads.

A plot of energy release rate $\mathcal{G}$ versus crack extension Δa for a particular loading situation is termed driving force curve. This 'action' curve relative to the 'resisting' *R*-curve of the material determines the static stability of a crack.

Crack extension occurs when the stress intensity factor (SIF) *K* or the strain energy release rate $\mathcal{G}$ attains a critical value. A plot of *R* versus crack extension is a resistance curve, termed *R*-curve, whereas the plot of $\mathcal{G}$ versus crack extension is termed driving force curve, see *Fig.10.21*. It is important to note that the driving force $\mathcal{G}$-curve is entirely dependent on the structure geometry and loading condition, whilst the R-curve is a material property dependent on temperature, environment, and loading rate etc. Most brittle materials exhibit a distinct constant resistance level.

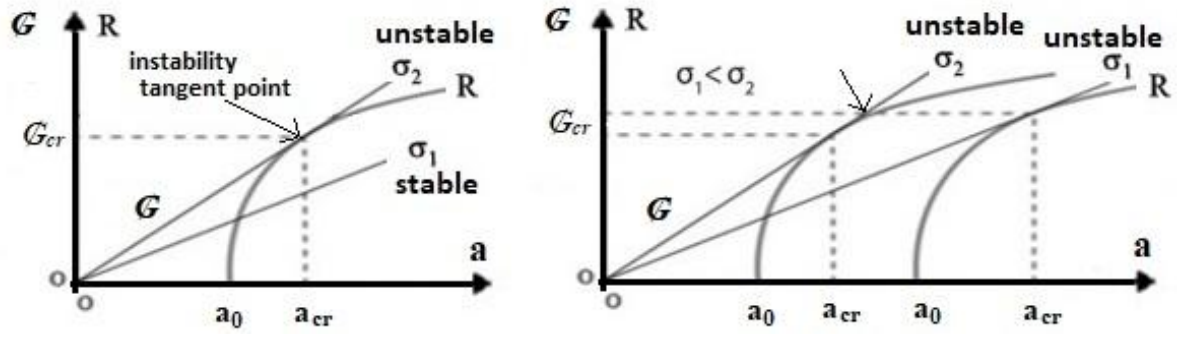


Fig.10-21: Rising crack-growth resistance curves = R-curves. (left) stable and unstable stress states, (right) two unstable stress states in case of two different materials.

(On the Fracture Toughness of Advanced Materials by Maximilien E. Launey, and Robert O. Ritchie. Crack-resistance curves. Schematic illustrations of flat and rising crack-growth resistance curves (R-curves).

For instance for a plate with a through-crack of initial length $2a_{0,}$ loaded by a remote stress σ, the energy release rate $\mathcal{G}$ varies linearly with the present crack size a. The crack will grow if the applied $\mathcal{G}$ reaches the limit value $\mathcal{G}_{cr.}$

* For brittle materials with its flat *R*-curves, there is no stable crack extension and the initial crack size a_0 is the same as the critical crack size a_{cr}. Then, a single value of toughness characterizes the material.

* For the ductile materials (*such as low strength steels*) with a rising *R*-curve there is no single value of toughness that characterizes the material as the driving force for unstable crack propagation depends on the extent of crack growth. Reason is that the plastic zone at the crack tip increases with crack growth and length, hence the energy dissipated to overcome plastic deformation will increase. In materials with a rising *R*-curve, stable crack growth occurs and the critical crack size will be larger than the initial crack size. Measurements are needed to determine how the resistance to fracture evolves with crack extension. For instance, still for a cracked metal plate - rehabilitated with a composite patch - one cannot uniquely give a single toughness value $\mathcal{G}_{cr}$. In this case, one defines 'Crack growth will occur when $d\mathcal{G}/da > dR/da$ and $\mathcal{G} \geq R$'. This corresponds to 'The driving

force curve is tangent with the *R*-curve' as depicted in *Fig.10.21*. It can be interpreted as the critical condition when the energy available in the component for crack growth exceeds the maximum amount that the material can dissipate.

Crack-growth resistance curves are conveniently plotted with crack extension Δa instead of crack size *a*, because the shape of the R-curve does not vary with the crack size, as shown in *Fig.10.21 right*. Therefore, the two given curves could be shifted to the origin. The driving force for crack propagation can be quantified by the characterizing parameters K, $\mathcal{G}$, or J.

Following HSB 62200-01 the determination of the static residual strength for single load paths must be made with statistically significant A-values; for multiple load paths, B-values may be used. For composite components it is hardly possible to demonstrate the service life and damage growth by predictions. Consequently, damage tolerance can then only be proven by representative structural tests in the presence of artificially introduced macro-damage from production flaws, accidental damage, stone impact, a bird strike or a lightning strike in areas with the lowest static reserves. In such instances, the no-growth concept is frequently applied, requiring that the expected macro-damage is not increasing under operating loads.

10.11.2 Cyclic Crack Fracture

Just as short information the basic relation shall be mentioned.

Operational loading causes crack-growth. This is usually teated by the Paris-Erdogan 'law' defining the crack-growth rate for a load cycle *n* according to

$$da / dn = C \cdot (\Delta K)^m \quad \text{with} \quad \Delta K = \max K - \min K ,$$

and the Paris parameters *C* and *m* are experimentally to obtain [*ASTM, E647*].
In the case of metallic materials the crack-growth behavior is determined by constant amplitude tests using appropriate cracked test specimens. The actual crack length *a* due to constant amplitude loading is measured depending on the applied load cycles *n* in consideration of $\sigma_{\max}$ and $\sigma_{\max}$.

Remind, please: Above equation gives the growth portion for a single cycle of constant-amplitude loading. The realistic variable-amplitude loading sequence is often tried to be replaced by an equivalent constant-amplitude test.

11 Procedure on Performing Design Verification in Stability

11.1 General

This chapter provides introductory information about buckling of columns (beams), plates, panels and shells. It addresses essential features in stability analysis. Special aspects of composite structures are illustrated and the use of the knock-down factor (KDF) in shell stability analysis is indicated. This chapter is dealing with static stability problems. It covers a very basic background in order to guide the practicing designer to better understand the manuals of commercial analysis software.

The following contents basically stems from the creation of the ESA Buckling Handbook, ECSS-E-HB-32-24A (Cuntze was first convener and founder of the team as well as a co-author of the later prepared HSB 40100-04] from R. Cuntze and J. Broede.

Different levels of analysis complexity will be treated. Going in steps from the lower level of complexity to the higher level of complexity (which will be denoted as a "hierarchical approach") the structural analyst is able to carry out and to successfully interpret analyses at the highest level of complexity, typically finite element computations.

Using such an engineering procedure the engineer is able to analyze the stability of (large) structures composed of structural elements (also referred to in literature as structural components or structural items) such as indicated in *Fig.11-1.* The term structural element includes typical elements such as columns and beams, plates, panels, and shells. In practice these structural elements often contain structural details, e.g. shells containing openings or reinforcements. The associated "basic" structural elements, the elements without structural details are denoted in the ECSS as "Typical Structural Elements".

Detailed information on stability analyses is not intended here. Therefore, reference is made to appropriate documents and handbooks. Non-axial symmetric shells and truss systems are not addressed. Generally, formulas will be not given

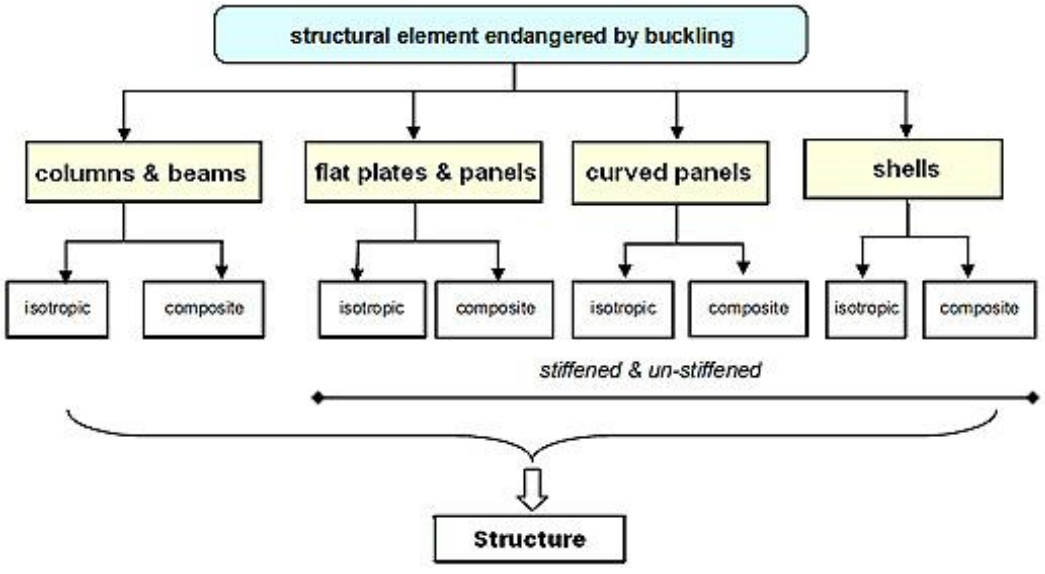


Fig.11-1: Breakdown of buckling of endangered structural elements

In structural design it must be demonstrated both: *Material* Strength, applying SFCs, strength criteria, and *Structural* Strength, applying buckling resistance conditions. Thereby, uncertainties of

the design parameters such as material properties, geometry, support conditions and imperfections are to consider.

Under certain loading conditions, a structural system can assume more than one equilibrium state. This phenomenon, known as buckling, is a property of the system as a whole. The condition, where the system equilibrium changes, is characterized by the buckling resistance. Corresponding values depend on arbitrarily chosen models, e.g. the location at which the so-called buckling stress is determined. For this reason, the buckling stress is not a system property but just a vehicle for its description, which may be useful to predict the system response under operational loading, e.g. to predict *RF*. In case of pure elastic stressing, the system returns into its original equilibrium state during unloading. Then, as the elasticity limits have not been exceeded at any location of the system, the structure remains completely intact. In case of inelastic buckling, the locations of highest stresses are to be checked for inelastic deformation behavior.

> *LL: In stability, similarly to the failure mode-linked FMC, the buckling modes may interact and trigger commonly the instability behavior. Therefore, a separation of potentially 'commonly' occurring buckling modes is a standard design objective. Whereas strength is a material attribute, stability is a structural attribute. Therefore, strength may confine the stability load carrying capacity.*

Buckling Terms: *buckling terms are unfortunately differently used*

- Bifurcation point: point in a load-displacement space where two equilibrium paths intersect. *Note: Bifurcation buckling is a type of instability which is accompanied with a sudden change of shape of the structure*
- Buckling: response of a structural system where more than one state of system equilibrium is possible under the present static or dynamic loading and where the structural system tends to change into the stable equilibrium state. *Note: Buckling (global as well as local buckling) does not necessarily lead to structural failure. Which type of phenomenon is considered as failure depends on the project-defined purpose and intent of a structural design. In some application cases, it is expected that a structure in a local buckling mode is still able to carry operational loads. Global buckling includes phenomena such as column buckling, plate buckling, shell buckling, lateral buckling of deep beams, snap through buckling. Local buckling includes skin buckling.*
- Buckling factor *k*: factor to obtain the critical buckling resistance of the investigated structural system from a generic problem characterizing quantity. *Note: The buckling factor includes the effects of different support conditions, different cross section properties and non-uniformly distributed applied stresses. It is also applicable for prediction of the critical buckling stress. Examples are Beams, the critical force* $F_{cr} = k \cdot \pi^2 \cdot EI/l^2$ *and Plates, the critical buckling stress with* $\sigma cr = k \cdot \frac{\pi^2 \cdot E}{12-12\nu^2} \cdot (\frac{t}{b})^2$
- According to the definition of the strength design FoS a buckling design FoS does not cover the effect of dimensional tolerances, load misalignment, worse specified boundary conditions and imperfections
- Buckling load: load level at which buckling occurs (*an action term is - unfortunately - used as a resistance property. This is confusing from general logic however become a standard designation)*
- Buckling resistance: resistance of the structure equal to the smallest load under which the structure can respond in more than one system equilibrium state
- Buckling stress: key value of a stress field associated with the buckling resistance in the non-buckled equilibrium state. *Note: The buckling stress is utilized to characterize a strength property of a structural system. Again, the action term buckling stress is used as synonym for buckling strength*

- Characteristic buckling resistance: buckling resistance determined under the pre-requisite of possible inelastic material response, geometrical and structural imperfections, follower load effects and residual stresses.
- Critical buckling resistance: buckling resistance determined with a model under the prerequisite of idealized conditions: critical buckling resistance > characteristic buckling resistance > design buckling resistance (*statistically reduced*)
- Design buckling resistance: design value of the buckling resistance taking into account the uncertainties of the model-based prediction
- Design load: factorized Design Limit Load (*not the result of a buckling load simulation as sometimes is written !)*
- Imperfection: state or an instance of being imperfect, or a shortcoming (e.g. generated 'manufacturing signatures').
  Note: Traditional imperfections are of geometric type, only.
- Knock-down factor (KDF): reduction factor used to predict the characteristic buckling resistance from the value gained with a model treated under a classic theory.

Note: Rarely, KDFs may be obtained from statistical evaluation of test results

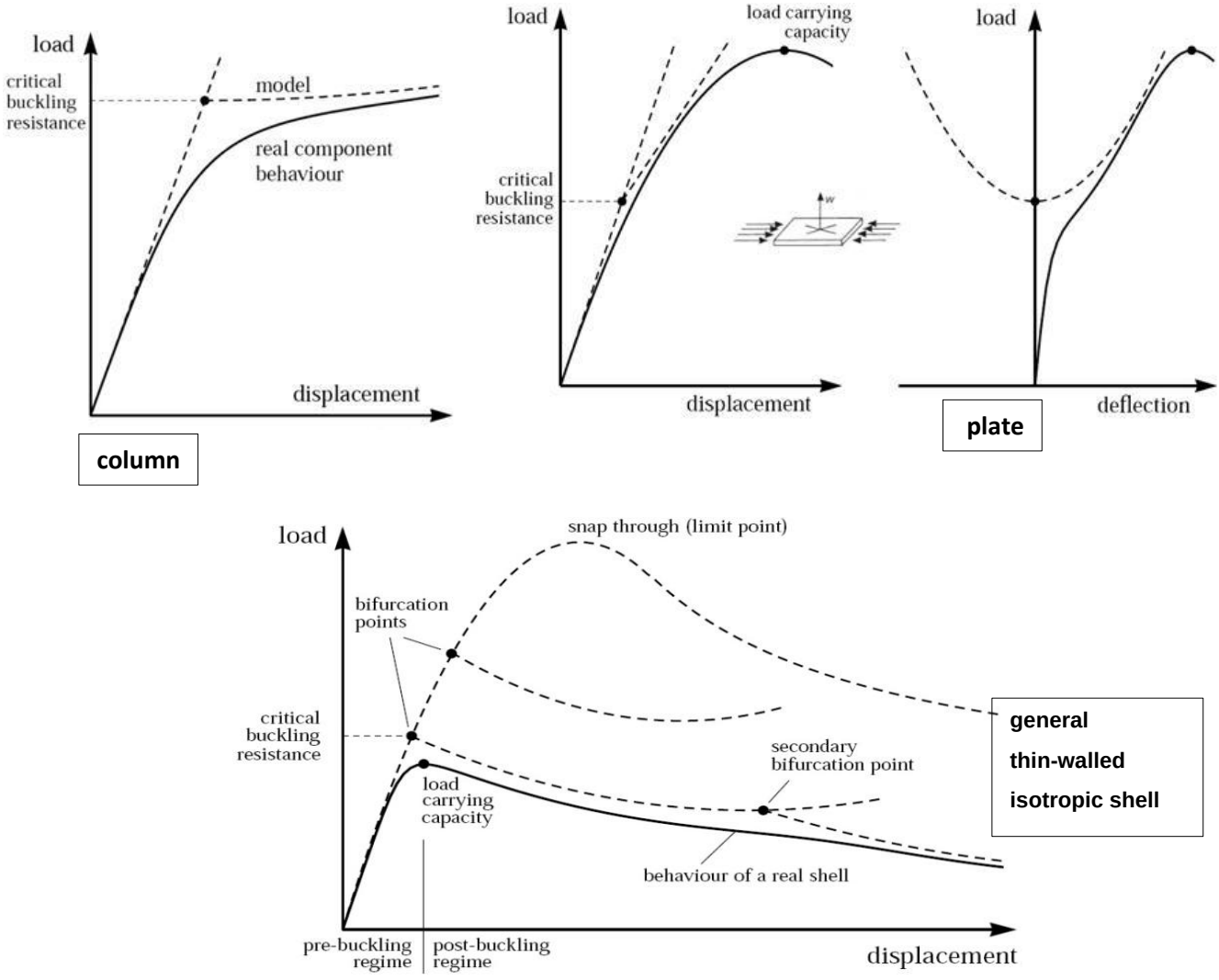


Fig.11-2: Buckling Behavior of Typical Structural Elements (components) [HSB]

- Knock-down factor (KDF): reduction factor used to predict the characteristic buckling resistance from the value gained with a model treated under a classic theory
  Note: Rarely, KDFs may be obtained from statistical evaluation of test results
- Limit points: point along the equilibrium path where the 'stiffness is zero*' (see following figure)*
- Panel: flat or curved thin-walled structural element that is usually reinforced.
  Note: May be a stiffener-reinforced part (barrel) of a fuselage section. Is not used fully compatibly the term plate
- Plate: flat, thin-walled, smooth structural element (sheet) of almost uniform thickness.
- Post-buckling: designation, if the structural element operates in a regime where the applied load is beyond the critical buckling load.
  - Stability design allowable: usually not available due to missing test series
  - Stability design value : approximation of a stability design allowable.

Buckling Behavior of Typical Structural Elements Columns, Plates and Shells

Here, buckling includes snapping of slender beams, buckling of flat plates, buckling of cylindrically curved panels, three-dimensionally curved shells, rib crippling and skin buckling of a sandwich. The general buckling behavior of columns, plates and shells was shown in *Fig.11-2*. Solid lines give an impression of the real structural element (component) behavior whereas dashed lines represent predictions based on suitable models.

Columns, beams: *Fig.11-2* presents the relation between compressive load and corresponding displacement in the axis of the column. Characteristic for column buckling (*Knicken*) is that the predicted critical buckling resistance is a fairly good estimate for the system's load carrying capacity. Cross-sections with an open profile Z, L, C or I twist and torsional buckling (*Drillknicken*) is possible together with parts of the stiffened skin the profile is attached to. Data about a possible exceedance of critical buckling stress is not available. Therefore one should design in order to avoid this buckling mode. Two important further modes are lateral torsional-flexural buckling (*Biegedrillknicken*), where bending under compression leads to undesired torsional deformations and further lateral buckling of deep beams (*Kippen hoher Balken*).

Plates*:* The figure also shows the general buckling behavior of flat and slightly curved plates. In the left hand part, the relation between compressive in-plane load and corresponding in-plane displacement is depicted. The right hand part explains the deflection (deformation perpendicular to the plane) under the same load. For plate buckling, it is to be observed that the system's load carrying capacity exceeds the predicted critical buckling resistance.

Thin-walled isotropic shells: The bottom figure illustrates in principle the buckling response of a thin-walled isotropic shell. Usual models are able to predict several bifurcation points. Characteristic is that the load carrying capacity can be lower than the critical buckling resistance, and that it decreases further in the post-buckling regime.

Thin-walled, orthotropically-stiffened shells: The following figure depicts the buckling response of an orthotropically stiffened cylindrical shell. The behavior depends strongly on the stiffness relations of the longitudinal and the circumferential stiffeners. The figure is representative for strong circumferential stiffeners and weaker longerons. Typical models are able to predict initial local buckling (usually of the skin), subsequent load re-distribution and overall load carrying capacity. Similar to plates, the load carrying capacity can significantly exceed the initial local buckling resistance.

Thin-walled cylinders under axial compression load: A thin-walled cylinder under axial compression loading is very sensitive to geometrical and other imperfections, *Fig.11-3*. This becomes obvious, as even the 'perfect' cylinder shows a sudden drop of the sustainable load in the post buckling regime. This cylinder behavior is illustrated in the right sub-figure. In contrast, the buckling behavior of a stiffened cylindrical shell, left, is pretty benign.

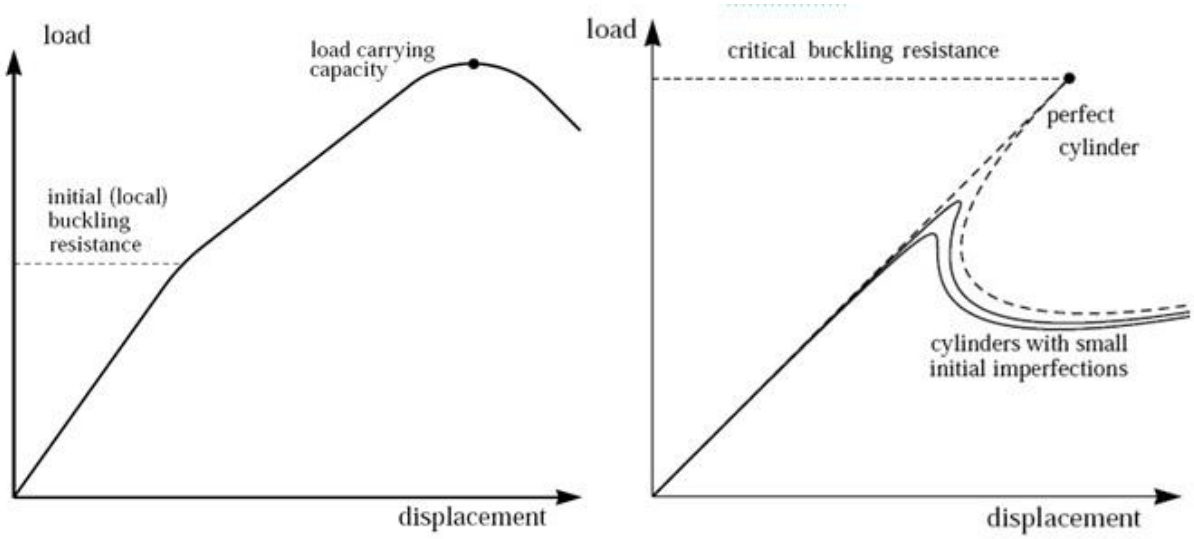


Fig.11-3, axial compression: (left) Thin-walled orthotropically stiffened cylindrical shell; (right) thin-walled cylinder [courtesy Dr. J. Broede]

LL:
(1) The designer should avoid torsional-flexural buckling, because this type is critical and test data are seldom available.
(2) Local buckling is permitted if the structure is designed in a way that local buckling (i.e. skin buckling) does not trigger global buckling as proven by stiffened panels and shells with their inherent redundancy.

Imperfections and failure behavior of typical structural elements

If there are compressive stresses or shear stresses in a structure or a structural element thereof, the initial state or so-called fundamental stress state may become instable, when the load is statically increased [*VDI 2014*] or is dynamically applied. The load displacement curves branches off from that of the fundamental state branch, see *Fig.11-3*. Thereby, the structural element experiences transversal (lateral) deflection. This deflection, which may occur suddenly, is transverse to the direction of the compressive stresses, and the phenomenon is known as buckling. The form of the deflection that occurs in addition to the fundamental state deflection is termed shape of the buckling mode. The loads at which buckling occurs are termed buckling loads. The obtained pattern of deflection which superimposes itself on the fundamental state is termed buckling mode, but might be more exactly termed shape of the buckling mode.

In reality, structures exhibit differences from the ideal shape, which is known as initial geometric imperfection. Further, loads may be not transferred precisely as it has been assumed for the analysis, or – and this applies in particular to FRP structures – the stiffness differs locally from the desired values as a consequence of delaminations, for example. All these irregularities are covered by the expression imperfection. Such an imperfection, depending on type and magnitude, usually reduces the buckling resistance.

Structural stability depends on the applied load and geometric parameters like slenderness, boundary conditions and imperfections. Furthermore, it is influenced by material parameters.
Often, the load intensity level is sufficiently small to keep the material behavior within the elastic range. The material parameters, however, can be affected by environmental conditions like temperature and moisture changes and by the loading velocity (*rate dependency*) as well. Beyond the elastic limits the material can show a nonlinear load deflection behavior which should be considered in the stability analysis. Also the material strength is of importance. Surpassing the yield strength limit, even if it is only locally, may result in a change of the structural shape and lead to a worse stability behavior.

The grade of importance of a specific buckling type depends on the actual situation faced. Because of their significance, buckling analysis of plates and shells has received considerable attention in the literature. In the case of plates and shells several formulas are provided for the buckling resistances and the buckling modes, and these cover a number of relevant loading cases and support/boundary conditions. It should however be noted that formulas of this kind can only be given for special structural elements with specific boundary conditions and simplified fundamental state conditions, such as flat rectangular plates or circular cylinders which are simply supported (*free to rotate and free to warp*) and assuming a membrane fundamental state (*assuming that the pre-buckling stress state is uniform in the structure*).

An excellent collection of plates (*anisotropic, stiffened, parallelogram-shaped etc*) are developed and presented as HSB design sheets (author: J. Broede, basically). These design sheets involve (a) columns, (b) flat and slightly curved panels, (c) thin-walled isotropic shells, and (d) stiffened shells.

A more precise description of the actual shape of the structure and its structural elements, of the boundary conditions and of the stress state may be obtained by numerical analysis using finite element analysis (FEA). However, analyses of this type may require a great effort of time combined with a significant numerical effort since very fine element meshes may be necessary. In order to obtain suitable structural element subdivisions and boundary conditions, convergence studies should be carried out using meshes of different resolutions.

Geometrical input, imperfections, and boundary conditions

One basic input is the geometry of the structure and its local thicknesses and stiffness properties. This includes the tolerance band for determining the minimum thicknesses being influenced from manufacturing and the so-called 'manufacturing signatures'. Manufacture naturally produces physical and geometrical imperfections which dominate the stability design as very important design parameters of the dimensioning process. Manufacturing signatures from the chosen manufacturing process, including ovalization of a cross-section, delaminations and flaws must be reliably controlled. Which design parameter, such as an elasticity modulus or an imperfection might be sensitive to the buckling failure mode in mind, depends not only on the manufacturing process but also on the type of the structural element being a smooth shell, stiffened shell etc. and the applied material.

The *'geometrical imperfections'* are the most important parameters for light weight structures when investigating instability phenomena. Depending on the type of the structure the geometrical imperfections differently influence the load carrying capacity. To be considered are for instance:

wall thickness and ovalization, waviness of fibers and eccentric load introduction; misalignments; etc.
The *'physical imperfections'* are related to the material properties and to certain state variables. These are caused by manufacturing processes like forging or welding, machining or forming, manufacturing of the lay-up and molding etc. All these processes influence the value, the scatter and the distribution of a material property (e.*g. of strength, elasticity modulus, ..*).
Unstiffened shells show the highest sensitivity to imperfections. Slightly curved panels fall between the flat plates and the uniaxially curved cylindrical shells when regarding their post-buckling behavior and imperfection sensitivity. With curvature, the buckling resistance becomes higher.

Boundary conditions inclusively support conditions, assumed in the design analysis, are chosen in such a way as to ensure that they achieve a realistic or at least a conservative model of the construction as the realized 'as–built' design. The boundary condition is a very sensitive parameter i.e. an uneven support line of a cylinder may cause a severe reduction of the buckling resistance.

Levels of analysis

It is convenient to distinguish three types of analyses, corresponding to three levels of increasing analysis complexity related to the discretization: (1) Level-1, Analytical solution; (2) Level-2, Semi-analytical solution; (3) Level-3, FEA solution.
Characteristics of these three types of analysis are:

- Level-1 Analytical solution:
  Methods based on series expansions (trial function methods) are used. The two most commonly used methods are the Galerkin method, which starts from the governing differential equations, and the Rayleigh-Ritz method, which starts from an energy expression. Sets of algebraic equations are obtained and an eigenvalue problem needs to be solved. Often simple support boundary conditions and a simplified pre-buckling state solution can be considered, only.
- Level-2 Semi-analytical solution:
  A one-dimensional discretization is obtained in a characteristic direction of the structure after a Fourier decomposition of the solution in the second main direction of the structure has been carried out.
- Level-3 FEA solution:
  Level-3 solutions correspond to a non-linear FEA. If one uses an appropriate model, one can obtain pretty accurate solutions in which all nonlinear effects are properly accounted for.

A linear buckling analysis (= eigenvalue analysis) is in general the starting point for a buckling analysis. The effect of imperfections is subsequently to investigate through a nonlinear response analysis or nonlinear buckling analysis, respectively.

Imperfection sensitivity analysis of plates and shells

As still shown by Koiter, for light-weight structures the level of instability failure is sensitive to imperfections. There are various methods of estimating the reduction of buckling load level due to these imperfections. The normal procedure is to carry out analyses with different assumed deviations from the ideal shape of the plate or shell. In many cases, imperfections are assumed which correspond to the theoretical buckling modes or to linear combinations of these. Analyses of this kind must be based on a non-linear shell theory and are therefore very time-consuming to compute. Sensitivity to imperfections is particularly high in cylindrical shells under axial loading,

and is all the more remarkable, the greater the ratio between radius and wall thickness or the thinner the shell wall is.

The particular sensitivity to imperfections lies in the fact that so-called strain-less post-buckling patterns exist whose deformation energy differs from the deformation energy of the unbuckled shell by only a relatively low amount of bending energy. These post-buckling types can be determined via introduced imperfections which reduce the buckling load level. In comparison with the flat plate, the theoretical buckling load level of the curved panel is increased by a curvature transverse to the direction of loading, along the y-axis. The method is linked to geometrically non-linear and if applicable to material non-linear analysis, too.

To investigate the important effects of the two main imperfections, the geometrical and the physical one, their influences can be investigated in a non-linear analysis.

* *Geometrical imperfections* are obtained from the measurement of the hardware by quality assurance with statistical background and its implementation into the model. The analysis involves: Searching for zero eigenvalue states and application of these modes or linear combinations of them in the model
* *Physical imperfections* encountered are as (1) Residual stresses from the manufacturing process and as (2) effects of manufacture on material data and on structural behavior. A detailed imperfection sensitivity analysis is usually performed by a non-linear FEA. This FEA looks for limit points and/or bifurcation points and is accompanied by an appropriate eigenvalue extraction at certain loading states. It follows the essential topics from above plus: a
  - Careful modelling of the structure, idealization of geometry and loading including boundary conditions
  - Similarity checks with literature, experience, handbooks
  - Consideration of literature, experience w.r.t. meshing (*elements, mesh density, and so forth*)
  - Mesh convergence study with different refinements
  - Parameter studies with respect to boundary conditions and variation of the amplitude of imperfection.

The choice of the calculation method is always an important point when beginning to design a structure. Depending on loading, type of structure and the material used, the engineer has to decide the analysis method. For that reason the engineer always keeps to weigh the possibilities given by tests, analytical solutions, and numerical methods.

In order to finally achieve the necessary ‘High Fidelity ‘design, available data sheets are very useful in the early design phase. Formulas provided for instance in the various 40000 HSB sheets make it possible to make comparisons in a simple manner between different columns on the one hand or between different plates, panels and shells on the other hand. They should be, moreover, also be used as benchmarks for checking numerical analysis models.

Special aspects with Composites

Bending-twisting coupling generally has a major impact on the stability behavior of laminated plates. Usually, this coupling effect in laminates has the highest practical relevance. Bending-twisting coupling can lead to a significant drop of the buckling resistance. Furthermore, bending-twisting coupling (*see the CLT chapter before)* causes a dependence of the results on the direction of the applied load, e.g. under in-plane shear loading, because shear can be replaced by a

compressive part with a tensile loading part. A shortcoming is the fact that bending-twisting coupling makes the development of closed-form analytical approximate solutions a rather challenging and sophisticated task.

Due to the manufacturing process, in the case of laminated walls special aspects are to consider:

Composite structures have skins (*face sheets of a sandwich panel, skin of a stringer or a ring stiffened shell, skin of a corrugated shell*) which are built up by fiber reinforced layers with different fiber orientation of the various layers. After the curing process in an autoclave oven under heat and pressure there can occur a significant deformation, depending on the laminate characteristic layer orientation and laminate wall thickness.

This undesired deformation generates residual stresses and can be reduced if (a) the layers lay-up with the different fiber orientation is symmetrical to the mid-plane and balanced to one axis in the plane (symmetric laminates), (b) the fiber volume ratio V_f of the layers is equal, (c) the fiber orientation is realized by manufacturing 'as designed'.

If the stack of the layers is not symmetric a spring-back of the panels may be obtained after curing which leads to a final geometric deformation (imperfection) and probably to additional constraints caused by a constrained mounting which leads to residual stresses.

Knock-down factor in shell analysis

Unavoidable imperfections of the shell shape, of the boundary conditions, and of the distribution of stresses or of the stiffness (including delaminations) will lead to resistance values below the theoretical value, which is termed *critical buckling resistance*. For this reason it is necessary to introduce reductions. Such a reduction factor should not be confused with a design safety factor *j*, γ on the loading. The knock-down factor KDF has nothing to do with a margin policy.

A KDF is a reduction factor in shell analysis. It is used to analytically derive a *characteristic buckling resistance* from a predicted theoretical buckling resistance (load) value according to $P_{ch} = KDF \cdot P_{cr}$.

KDFs consider the influence of geometrical imperfections, of residual stresses and of simplifications in the analysis method (boundary conditions, pre-buckling deformations). A KDF should at least correct the difference between values of a calculation model and of a test on average level (50% expectance). The KDF is differently defined. In the case of NASA SP-8007 the slenderness ratio dependent KDF is based on a lower bound design curve of the cylindrical shell test data. Here one might say that the KDF is directly applied to a *characteristic buckling resistance*, however the given test series are unfortunately differently based.

A KDF shall cover the effects that cannot be considered in the applied structural model. The application of the KDF takes primarily place in the classical eigenvalue extraction (linear or non-linear), where the *critical buckling resistance* value is decreased by the KDF.

The engineering KDF method usually bases on the analysis of the ideal, perfect structure. It is the most simple and historically the first approach to correct stability analysis results achieved for general instability or global buckling. Test-based KDF data (usually not available, sufficient test data are rarely made available) are referenced to a known imperfection level, to a certain geometry and to a specific type of load.

To obtain a realistic buckling resistance the results of detailed initial imperfection measurements on full scale structures can be used effectively to develop improved design criteria for mass critical, low margin of safety, axially compressed cylindrical shells, because it is known such shell

structures are usually buckling critical.
A typical design procedure used for the layout of such structures can be summarized as follows: a) Lay-out (sizing) of the preliminary dimensions applying the given FoS; b) Selection of a wall construction and a stiffening concept; c) Usage of one of the many shell of revolution codes to calculate the buckling resistance of the 'perfect' structure taking into account the appropriate boundary conditions and the pre-buckling deformations; d) Selection of a KDF to account for the imperfections present in the finished structural product.

A similar investigation for composite shells by Hilburger and Starnes has shown that the nonlinear analysis procedure, which includes traditional and non-traditional initial imperfections can be used successfully to determine accurate high-fidelity design knockdown factors that can be used for predicting composite shell buckling and collapse loads in the design process. The non-traditional imperfections consisted of boundary (shell-end) geometric imperfections, shell-wall thickness variations, material property variations, local shell-wall ply-gaps associated with the fabrication process, variations in loads applied to the end of the shell, and elastic boundary support conditions., Above authors further have convincingly shown that investing time and effort in carefully measuring the initial imperfections of a set of shells fabricated by a given manufacturing process can be used to establish the manufacturing imperfection signature needed for deriving a knowledge-based KDF representative of the said process.
The value of the KDF approaches the more 1.00 the more accurate the applied stability analysis is when following the strategy for a hierarchical high fidelity analysis, shown below.

A sufficient number of relevant tests are the only basis to determine a statistically-based stability design allowable. The computation of a buckling resistance can never deliver more than an approximation of a stability design allowable. So, as a stability design allowable obtained from test series is usually not available, one only can achieve a value which can be termed 'stability design value' representing a stability failure load.

In the case of pure linear-elastic stressing, the system returns into its original equilibrium state after the loads have been reduced. As the elasticity limits have not been exceeded at any location of the system, the structure remains completely intact. In case of inelastic buckling, the locations of highest stresses are to be checked for plastification. These locations are not necessarily those for which the buckling stress has been determined what may particularly happen if the stress is not uniformly distributed.
For shells, solutions which neglect the effects caused by the edge restraints, can still be used to great advantage to establish the approximate behavior of a shell subjected to the specified external loading condition.
If there is no information available about the expected 'manufacturing signature' (t*he initial imperfections that a certain manufacturing process will produce*), one can only use the traditional lower bound design philosophy. However, it has been shown conclusively that tools for a reliable and accurate simulation of the buckling behavior of axially compressed thin walled shells are available. They can be used if there is at least some information available about the expected manufacturing signature of the shell. It is also clear, the more information one has the more accurate and reliable the theoretical buckling resistance predictions become. Thus, for a more specific prediction of the final collapse load, the final goal of a "High Fidelity Buckling Resistance Analysis," one should conduct a refined analysis including measured values of the traditional shell-wall imperfections and variations in the shell-end or loading surface geometry.

When judging the analytical results one has to keep in mind that many influences may lower the buckling resistance level: *Loadings (static, conservative/non-conservative, strain-rate, impact); *Scattering design variables and uncertainties; *Temperature and moisture; *Manufacturing and assembling processes; Mismatch, misalignment, tolerances and joining. It has been shown in literature that it is possible for isotropic shells to achieve excellent correlation between the analytical predictions and the experimental results if realistic boundary imperfections are included in the numerical analysis.

Whenever necessary, in order to be able to arrive at a reliable prediction of the critical buckling resistance and to make an estimate of its imperfection sensitivity that can be used with confidence, one should proceed in a step by step manner from simple to more complex models and solution procedures in order to understand the response characteristics of the structural element of interest. In particular, to make a reliable estimate of its imperfection sensitivity, the nonlinear effects caused by the edge restraint conditions should be included in the analysis.

The steps listed below are an example for an engineering approach, based on the use of KDFs, to evaluate buckling of imperfection sensitive shell structures:

- Pre-dimensioning by data sheets e.g. for some representative skin + ribs,
- Linear Bifurcation Analyses + KDF = 0.65 applied, e.g. (*'coarse', Quad4 element w.r.t. design modifications, time, numerical stability)*
- Non-linear Analyses, (implies KDF < 1) of chosen design with different imperfection patterns similar to buckling modes
- Refined Non-linear Analyses (KDF ≈ 1) on the selected worst imperfection pattern chosen, delivers global + local modes
- Analysis of Actual Test Article.

11.2 Hierarchical approach for stability analysis with application comments

Usually, a real 'large' structure is composed of several structural elements, such as beams, plates or shells. For the analysis of individual structural elements in general several possibilities are available. Good designs are obtained by proceeding step by step from simple analytical solutions, called here Level-1 solutions, to increasingly more complex models up to Level-3. Such a hierarchical approach leads to the high fidelity required in stability analysis. After satisfactory results have been obtained at a certain level, one can proceed with the next level, *Fig.11-4*.

Level-1 analysis and Level-2 analysis (analytical solutions and semi-analytical solutions) have a prominent position in the buckling analysis of structures. Often, for instance, for the buckling analysis of panel-type structures, the accuracy that can be obtained is satisfactory.

Moreover, in view of the high number of load cases that is to be considered in the design process, the time required to carry out Level-3 (Finite Element Analysis) calculations would be prohibitive. The methods that are available to carry out Level-1 analysis are relatively well documented and are also described in the still mentioned HSB 40000 sheets. Level-3 FE analysis plays an important role in the case of structures with a complicated geometry, or in the case of structures that are imperfection sensitive, such as unstiffened shell structures. In the latter case a nonlinear FEA can be essential for a robust and economical design. When one carries out a nonlinear Level-3 FEA for buckling calculations, it is essential that one can have confidence in the results that are obtained. In the context of cylindrical shells, a systematic approach has been proposed by Arbocz et al. in order to obtain a reliable prediction of the buckling resistance and imperfection sensitivity of the shell. In

this “hierarchical approach” one proceeds step by step from simple analytical (Level-1) and semi-analytical solutions (Level-2) to more complex models and solution procedures (Level-3).

When the geometry of the structure is relatively simple, as for instance it is the case for a structural element without structural details such as cut-outs, reinforcements, or discrete stiffeners, then the Level-1 and Level-2 methods are often available in handbooks or in special purpose codes. These structural parts are denoted here as “Typical Structural Elements” such as beams, rectangular plates, cylindrical shells, and shells of revolution.

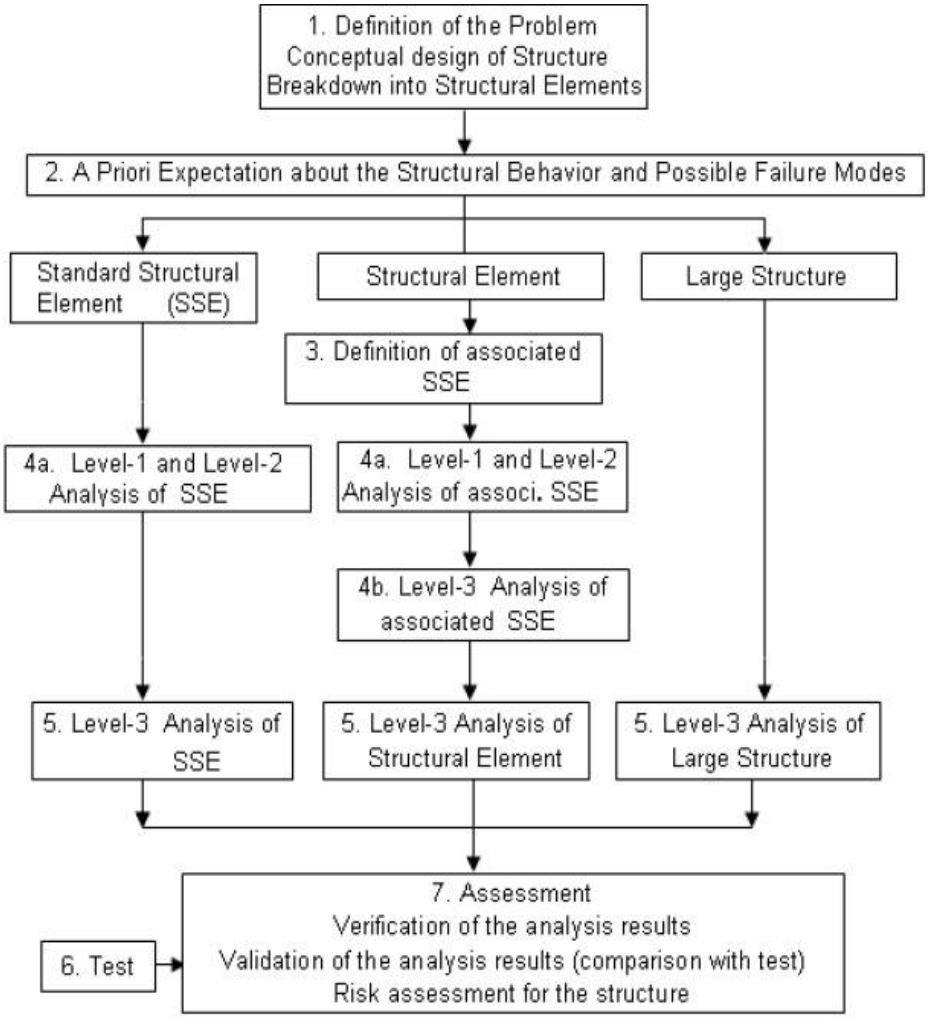


Fig.11-4: Flow chart of stability design verification. SSE is Standard Structural Element

Often the actual structural element (including structural details) to be analyzed bears sufficient similarity to a corresponding Typical Structural Element (the actual structural element without its structural details), for which analytical or semi-analytical methods have been developed. In such a case one can make use of this similarity and carry out an engineering, systematic approach in order to arrive at reliable results for the analysis of the actual structural element. An example is a cylindrical shell with cut-outs, reinforcements, or discrete stiffeners.

Central in this engineering “hierarchical approach” is the possibility of identification of an idealized, simplified structure without structural details. The associated Typical Structural Element corresponds to the real, actual structural element under consideration. The idealized “Standard

Structural Element" then represents a reference model, which is a simplification of the real structural element under consideration, but reflects important characteristics of the geometry and behavior of the real, actual structural element.

There are structural analysis problems in which the geometry of the structure is very complicated and where the structure might consist of several structural elements. In such a case an idealized, simplified structure cannot be directly identified. These structures will be denoted here as "Large Structures". For its structural elements, however, this reference Typical Structural Element modelling is often applicable in a natural way. Among the idealized Typical Structural Elements (beam, plate, panel, and shell-type structures) shells of revolution are the most "advanced" ones and they form the idealization of many important structural components in various branches of engineering.

The buckling analysis of shells of revolution is therefore the most relevant application of the hierarchical approach. It corresponds to the steps 3, 4, and 5 in the schedule for nonlinear Finite Element buckling analysis in *Fig.11-4*.

The Level-1 and Level-2 solutions form reference solutions for the Finite Element model of the idealized, simplified structure (the Typical Structural Element). When the Finite Element results of the idealized structure are in satisfactory agreement with the results of the Level-2 analysis, the Finite Element model of the real structure (the actual Structural Element) can be developed on the basis of the Finite Element model of the idealized structure. This can be seen as an essential first step in the development of the Finite Element model of the actual Structural Element.

In case of pure linear-elastic stressing, the system returns into its original equilibrium state after the loads have been reduced. As the elasticity limits have not been exceeded at any location of the system, the structure remains completely intact. In case of inelastic buckling, the locations of highest stresses are to be checked for plastification. These locations are not necessarily those for which the buckling stress has been determined what may particularly happen if the stress is not uniformly distributed.

For shells, the Level-1 solutions which neglect the effects caused by the edge restraints, can still be used to great advantage to establish the approximate behavior of a shell subjected to the specified external loading condition.

If there is no information available about the expected 'manufacturing signature' (*the initial imperfections that a certain manufacturing process will produce),* one can only use the traditional lower bound design philosophy. However, it has been shown conclusively that the tools for a reliable and accurate simulation of the buckling behavior of axially compressed thin walled shells are available. They can be used if there is at least some information available about the expected manufacturing signature of the shell. It is also clear, the more information one has the more accurate and reliable the theoretical buckling resistance predictions become. Thus, for a more specific prediction of the final collapse load, the final goal of a "High Fidelity Buckling Resistance Analysis," one should conduct a refined Level-3 analysis including measured values of the traditional shell-wall imperfections and variations in the shell-end or loading surface geometry and other imperfections.

When judging the analytical results one has to keep in mind that many influences may lower the buckling resistance level: Loadings (static, conservative/non-conservative, strain-rate, impact); Scattering design variables and uncertainties; Temperature and moisture; Manufacturing and assembling processes; Mismatch, misalignment, tolerances and joining.

Besides *general buckling* modes of for instance a ring-stiffened cylindrical shell, there are local buckling modes such as local skin or local web buckling. *Local buckling* is often not considered to be a failure mode when it may believed that the structure can properly operate during and after loading. This has to be fixed in the design.
However, because of the interaction of local and general instability modes and the interaction of various local instability modes, critical buckling loads calculated for an assembled perfect structure are usually lower than those calculated separately for parts of this structure modelled with simplified geometric boundary conditions, e.g. hinged. Therefore, fully optimized structures are more buckling sensitive.
A *stabilizing load* which increases buckling margins of safety of the structure if applied in conjunction with destabilizing loads usually is not considered. The interaction of two narrow located stability modes leads to a lower combined mode! This is as with the strength modes and vibrational frequency modes.

LL:
(1) It has been shown in literature for isotropic shells that it is possible to achieve excellent correlation between the analytical predictions and the experimental results if the boundary imperfections are included in the numerical analysis. Whenever necessary, in order to be able to arrive at a reliable prediction of the critical buckling resistance and to make an estimate of its imperfection sensitivity which can be used with confidence, one should proceed in a step-by-step manner from simple to more complex models and solution procedures in order to understand the response characteristics of the structural element of interest. In particular, to make a reliable estimate of its imperfection sensitivity, the nonlinear effects caused by the edge restraint conditions should be included in the analysis.
(2) In the non-linear regime, buckling may be termed an imperfection-induced strength failure problem.

Eventually, the reader is provided with some guidance in stability design verification by the procedure depicted in the following flow chart, *Fig.11-5*. The establishment of the required mechanical and physical properties has to include the effects of the environmental conditions, the material selection, procurement, production and verification. This verification includes destructive and non-destructive test methods, see [Standard ECSS-E-30 Part 8A].

Main aspect is to gather the demands for the provision of those material data and associated information which are required for the buckling analysis. *Fig.11-6* shall give the basis for the analyses from sizing until design verification with calculation of the stress effort in the buckling critical location. It shall clarify the material properties, which have to be inserted into the "buckling formulae" or filled into the "material cards" of FEA codes for detailed numerical simulation (metallic, non-metallic).

Building block in the laminate case is the lamina which is relatively brittle if using fiber reinforced plastics (FRP). Nevertheless, the laminate may behave quasi-ductile according to the redundancy built in by the stacking sequence. UD-composed laminates exhibit high sensitivity to stress concentration but low sensitivity to fatigue

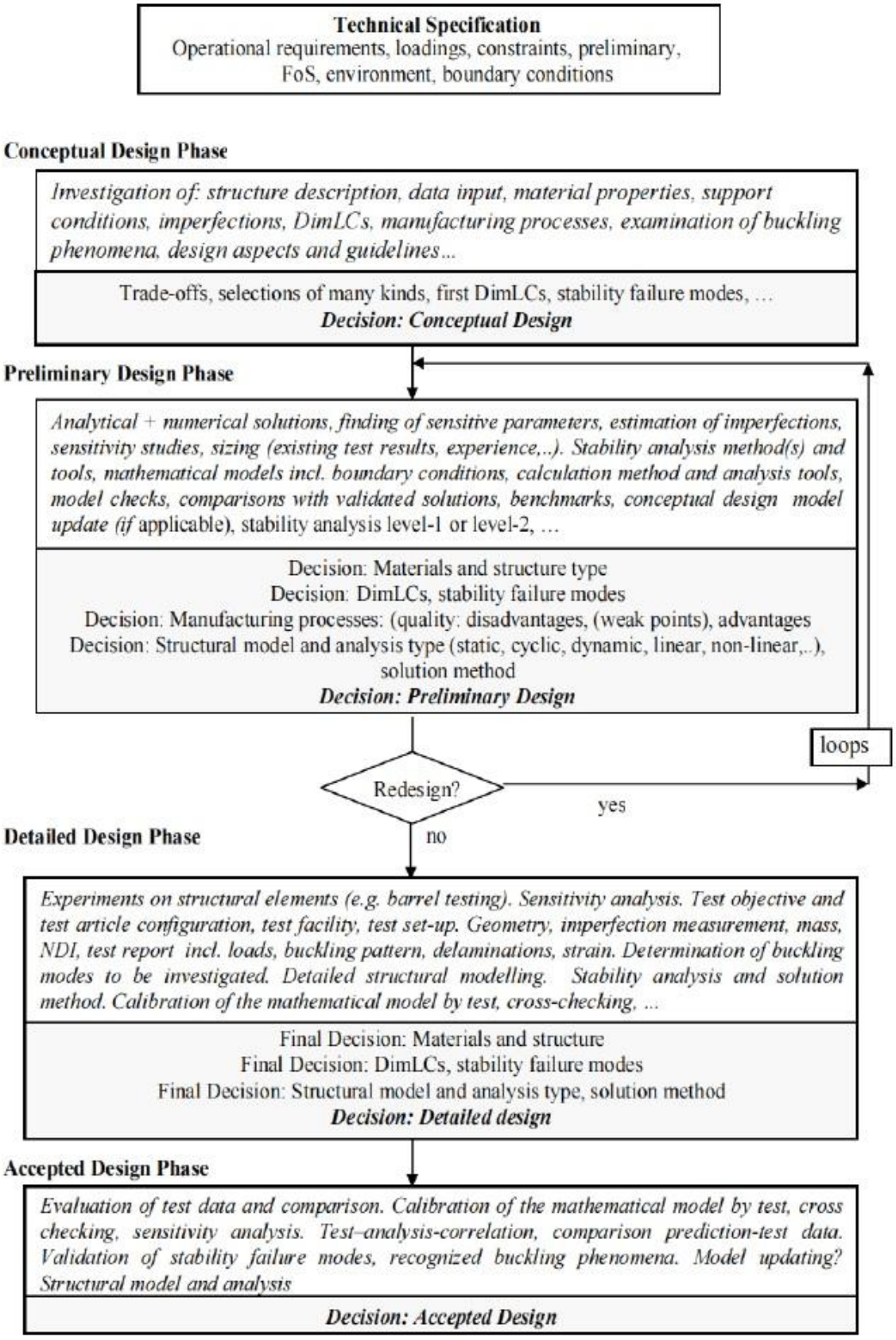


Fig.11-5: Exemplary procedure for a stability design verification process [R. Cuntze]

Layered materials such as GLARE, which is applied in the AIRBUS 380 are behaving ductile and are designed as a ductile metal with hybrid properties.

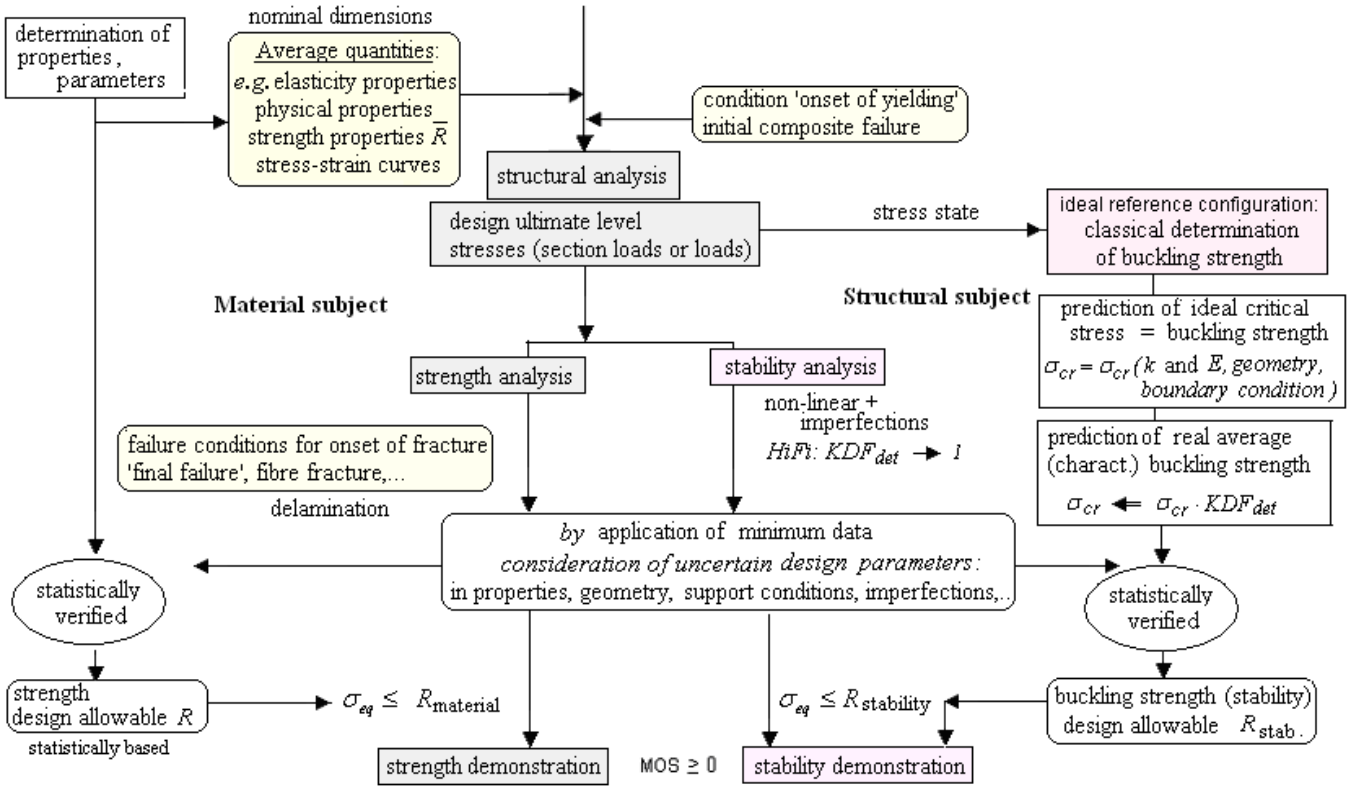


Fig. 11-6: Visualization of the (actually) required deterministic input demands.

KDF usually corrects difference of calculation model to experiment (50% expectance value), k:=buckling factor (from handbook tables), MoS:=Margin of Safety

Noteworthy:

In the HSB, section 40000, for a wide spectrum of columns, rods, rings and deep beams design sheets are found. The same is given in the chapter plates where the available design sheets on anisotropic plates provided by J. Broede and colleagues are outstanding sheets.

11.3 Application cases Isotropic Plate and Orthotropic Plate

The procedure to obtain a buckling factor *k* shall be demonstrated for a rectangular isotropic plate under uniformly distributed uniaxial compressive load and with simple boundary conditions. Since composites are a topic of this work, just the results of the isotropic plate shall be transferred to the composite plate. (after VDI + HSB 45111-08)

Uniaxial loading:

The differential equation for buckling of a simply supported **isotropic plate** reads

$$D\left[\frac{\partial^4 w}{\partial x^4} + 2\cdot\frac{\partial^4 w}{\partial x^2\cdot\partial y^2} + \frac{\partial^4 w}{\partial y^4}\right] + n_x\cdot\frac{\partial^2 w}{\partial x^2} = 0$$

A solution of this linear partial differential equation is found when using the harmonic functions

$$w(x,y) = \sin\frac{m\cdot\pi\cdot x}{a}\cdot\sin\frac{m\cdot\pi\cdot y}{b},$$

which satisfy the simply supported boundary condition (M = 0, w = 0) or hinged supports at all four edges. The substitution of w(x, y) into the differential equation delivers

$$\left\{D\cdot\left[\left(\frac{m\cdot\pi}{a}\right)^4+2\cdot\left(\frac{m\cdot\pi}{a}\right)^2\cdot\left(\frac{n\cdot\pi}{b}\right)^2+\left(\frac{n\cdot\pi}{b}\right)^4\right]+n_x\cdot\left(\frac{m\cdot\pi}{a}\right)^2\right\}\cdot\sin\frac{m\cdot\pi\cdot x}{a}\cdot\sin\frac{m\cdot\pi\cdot y}{b}=0$$

Above equation is satisfied for all values of (x, y) if

$$n_x=-D\cdot\left(\frac{\pi\cdot a}{m}\right)^2\cdot\left[\left(\frac{m}{a}\right)^2+\left(\frac{n}{b}\right)^2\right]^2.$$

with m and n being the number of half waves in the x and y-direction. It is to recognize that the smallest value of n_x for all values of a, b and m is obtained if n = 1. This means that only one half wave will be formed in the direction perpendicular to the load application. Then, the simple form

$$n_{xcr}=-\left[\frac{mb}{a}+\frac{a}{mb}\right]^2\cdot\left(\frac{\pi}{b}\right)^2\cdot D=-k_x\cdot\left(\frac{\pi}{b}\right)^2\cdot D\,.$$

for the critical buckling resistance n_{xcr} is obtained. The parameter m is integer and determines how many half waves will fit into the length of the plate. While the aspect ratio a/b is known, m is still unknown. Its value must be found by plotting the buckling factor *k* as a function of a/b for subsequent values of m, see *Fig.11-7.* In the case of an isotropic beam D = E·I / b.

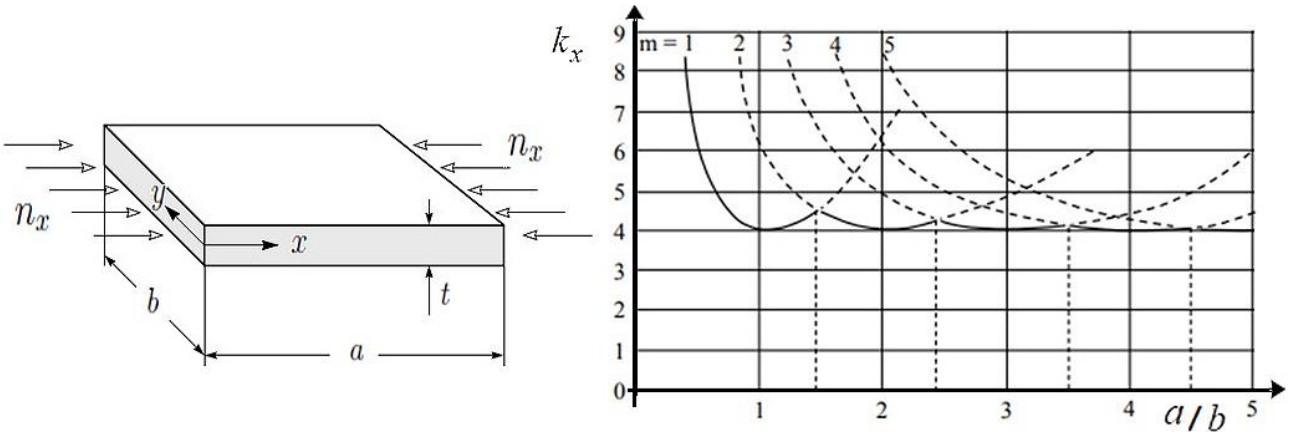


Fig.11-7: 'Garland curve' of buckling factor kx

Transfer to composite plates or FRP plates, respectively.

The majority of theoretical investigations and associated tests have been carried out for symmetrical laminates. If a non-symmetrical layered composite is concerned, then the first thing to calculate is the modified bending stiffness matrix

$$\left[\tilde{D}\right]=[D]-[B]^T\cdot[A]^{-1}\cdot[B]\ \text{for symmetric laminates}\left[\tilde{D}\right]=[D].$$

which is independent of the choice of the reference plane. For orthotropic laminates, the components of the laminate stiffness matrix [K] with the subscript 3 vanish. Again, with regard to the in-plane or membrane stiffness [A], laminates with a balanced lay-up are orthotropic ($A_{13} = A_{23} = 0$) but 'simple' orthotropicity does not necessarily exist with regard to bending stiffness [D] and

laminate bending-stretching coupling stiffness [B] as well, see *CLT chapter*. In comparison with orthotropic analysis, the theoretical buckling loads and buckling modes are reduced. The associated analysis requires for considerable effort and is not worthwhile, at least in the design study stage, since the influence of anisotropy on "rationally" designed composites remains minor.

In the case of an **orthotropic plate** it is to apply $D = D_{11} - D_{12}^{\,2} \cdot D_{22}$

Prerequisites are given from CLT:

- Flexural response of the plate is decoupled from extensional response. [B]-matrix is zero; this is always the case if the lay-up is symmetric.
- The plate material behaves orthotropic (i.e. main orthotropic axes are parallel to the plate edges meaning that bending and twisting response are decoupled; the elements D_{16} and D_{26} of the flexural stiffness matrix are zero).
- The plate is thin compared to the plate area dimensions (t/a < 0.05, t/b < 0.05). This means that transverse shear deformation has no significant influence on the buckling behavior.

The stiffness of the plate is described with three matrices (extensional stiffness [A], coupling stiffness [B] and flexural (or bending) stiffness [D]). Under the pre-requisites above, only the elements D_{11}, D_{22}, D_{12} and D_{66} of the flexural stiffness matrix are involved in the present procedure for buckling resistance prediction. For this case, the plate stiffness matrix [K], also known as ABD-matrix, has the configuration as depicted in *Fig.9.2,* CLT chapter.

Helpful is the introduction of three non-dimensional stiffness parameters, defined as

• Effective aspect ratio , • Seydel's orthotropicity parameter , • Transverse contraction

$$\bar{\alpha} = \frac{a}{b} \cdot \sqrt[4]{\frac{\tilde{D}_{22}}{\tilde{D}_{11}}} \quad , \qquad \beta = \frac{\tilde{D}_{12} + 2 \cdot \tilde{D}_{66}}{\sqrt{\tilde{D}_{11} \cdot \tilde{D}_{22}}} \quad , \qquad \nu_D = \frac{\tilde{D}_{12}}{\sqrt{\tilde{D}_{11} \cdot \tilde{D}_{22}}} \quad .$$

For many materials, β is found in the range $0 < \beta < 3$. For isotropic materials is $\beta = 1$. The parameter ν_D depends on β and lies in the range $0.33 \cdot \beta - 0.04 < \nu_D < 0.33 \cdot \beta + 0.04$. ν_D has not been found outside the range $0 < \nu_D < 1$. For isotropic materials, ν_D is equal to ν.

Then the critical buckling resistance can be calculated from

$$\bar{\alpha} < 1: \ \mathrm{n}_{cr} = -k_x \cdot \left(\frac{\pi}{a}\right)^2 \cdot \tilde{D}_{11} \ , \qquad \bar{\alpha} \geq 1: \ \mathrm{n}_{cr} = -k_x \cdot \left(\frac{\pi}{b}\right)^2 \cdot \sqrt{\tilde{D}_{11} \cdot \tilde{D}_{22}} \quad .$$

The buckling factor k_x depends mainly on the effective aspect ratio $\bar{\alpha}$, the orthotropicity parameter β and the support conditions. If at least one of the plate edges is free, the buckling factor additionally depends on ν_D.

The buckling factor of an orthotropic plate can be described or at least approximated as the buckling factor of a corresponding isotropic plate plus an orthotropic function (+ part). For the special case that all plate edges are simply supported an exact analytical equation for the buckling factor is known:

$$\bar{\alpha} < 1: \ k_x = (1 + \bar{\alpha}^2)^2 \ + \ 2 \cdot \bar{\alpha}^2 \cdot (\beta - 1) \ , \qquad \bar{\alpha} \geq 1: \ k_x = \left(\frac{m}{\bar{\alpha}} + \frac{\bar{\alpha}}{m}\right)^2 + \ 2 \cdot (\beta - 1)$$

with m being an integer such that $m - 1 \leq \bar{\alpha}^2 / m < \mathrm{m} + 1$.

Combined loading

If all membrane section forces n_x, n_y, n_{xy} are active, the critical membrane tension state will then be fixed by (n_{nx}, n_{ny}, n_{nxy}). After the calculation of the critical membrane forces for compression along the *x* axis, compression along the *y* axis and for shear, the common buckling factor λ can then be estimated on the safe side by means of the interaction equation

$$\lambda = n_x / n_{xcr} + n_y / n_{ycr} + n_{xy} / n_{xy\,cr} = 1 .$$

11.4 Some practical Hints for Applications

11.6.1 Design Process and Modelling

Structure design is a balance between mass and safety (*structural reliability*) with an essential goal to be as light as possible (*required not in aerospace only*). The designer must develop a structure which has to meet stiffness, loads, environments, mass requirements and CoSts. Thus, Dimensioning is a complex process: It shall combine the different external and internal loadings acting on the structure of the sources: static, dynamic (impact), cyclic, thermal, environmental, residual stresses. Special concern is on the effect of local loadings due to attachments, joints and so on. This is particularly true in buckling design, when different kinds of loadings act on the same structure and it is to correctly combine mechanical, thermal and local loading. Once the first design is obtained, the resistance against local and global buckling of the structure can be assessed according to the procedures presented above.

Always a series of calculation with different sets of loadings is to perform in order to:

- understand the behavior of the structure with respect to buckling,
- define a reference configuration with a set of imperfections.

In the case of a large structure like a launcher the full structure had to be sectioned in the past, considering the computer power, into sub-structures and all the analyses are carried out at the level of these sub-structures, see *Subchapter 17.1*. In addition, various contractors Design Dimension specific sections of the launcher and provide finite element sub-structures for the complete mathematical model. This model is dedicated to dynamic analysis. As a result of the sectioning, the first buckling mode can appear on an adjacent structure and not on the envisaged one due to unrealistic boundary conditions in stiffness. In this case, the challenge for the designer is to locally modify the structural stiffness of the adjacent parts in order to make the buckling mode appear first in the studied structure. In any case, the load path should not be changed by these modifications

11.6.2 Loading processing

The loading to which each structure is submitted can be classified in two categories:

- the destabilizing loads, which create a stress field decreasing the apparent stiffness of the structure leading to its buckling. For instance, for a launcher tank, destabilizing loads are external pressure or compression loads.
- the stabilizing loads, which in the case of the buckling create a field of constraints increasing the apparent stiffness of the structure. In the case of a cylindrical shell, they can be the internal pressure or the tension loads.

A loading combination which does not take into account the distinction between these two types of loads leads to apply the same FoS to both loading types *destabilizing* and *stabilizing* and therefore leads to increase these loads simultaneously until the structure breaks down. This way to consider the loads is correct if it is assumed that the stabilizing loads are statistically dependent on the destabilizing loads, which is a priori not always the case. In this last case, the method is optimistic with regard to the critical buckling load and overestimates it. If the two types of loads are statistically independent, the approach to be followed is to apply the FoS to the destabilizing loads and to increase them until collapse whereas stabilizing loads are maintained at their specified level (*design limit loads DLL*).

Exemplarily for a shell it is to be accounted for: (1) Geometric specifica of the structural elements tubes, frames, stiffeners, (2) Geometrical deviations (w*eld joints*), (3) Ovalization effects. Radial buckling and axial buckling may occur.

11.6.3 Validation of the mathematical model (see also Subchapter 17.1)

Essential step of the qualification process is the correlation of the numerical models, see *Fig.11-8,* a task where the time devoted to it is often underestimated. The part of the logic discussed is the one surrounded by the blue oval in *Fig. 11-8*.

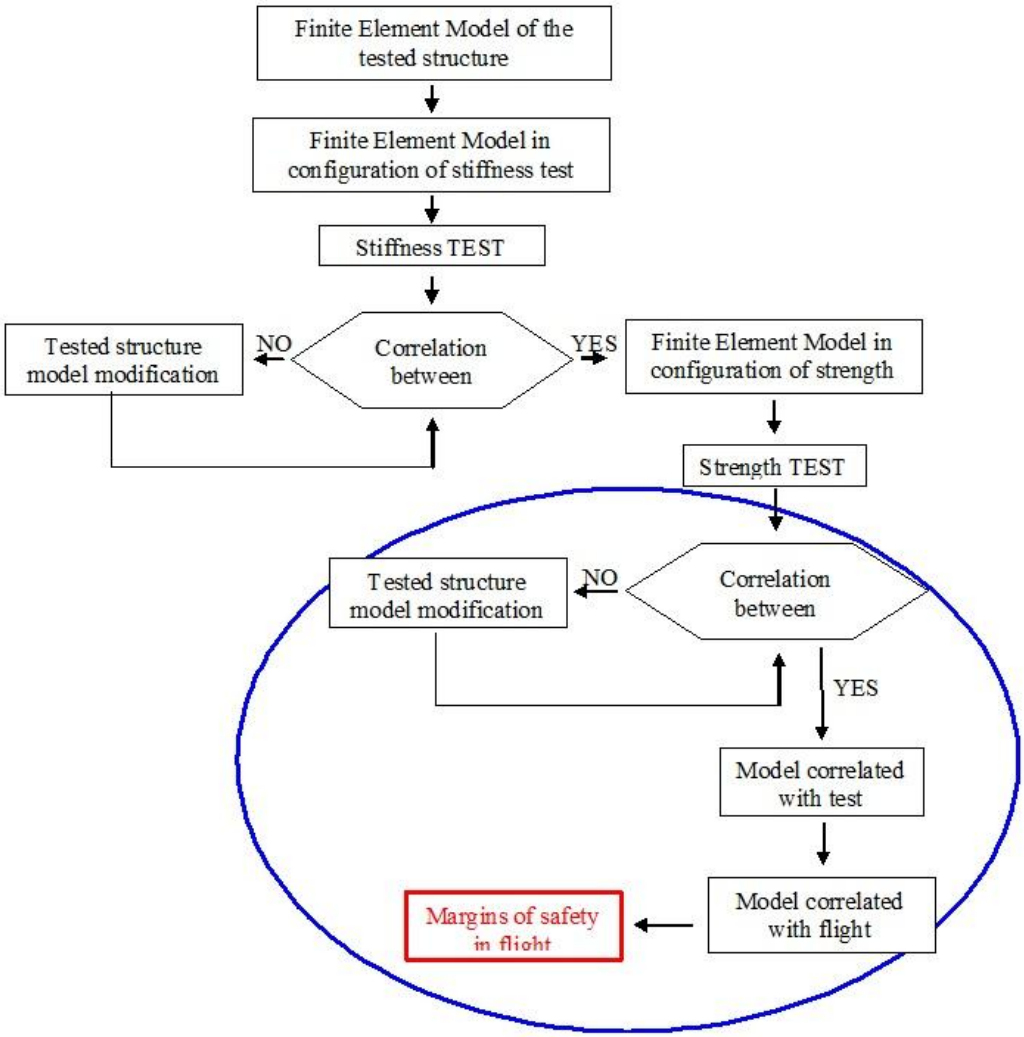


Fig.11-8: Logic of model correlation

The correlation task consists in, first comparing the test predictions to the measured data and checking the mismatches, and second, if the mismatches are considered as not acceptable, to adapt the model according to several means. Among others, the main ones are:

- refining meshes - globally or locally, by using volume finite elements
- being fully representative of the fine geometry (all discontinuities like stiffeners, connections, holes…).

Criteria of acceptation of a 'good enough coherency' between predictions and test results are commonly agreed by the design responsible and the customer. One example of the Ariane community asked for less than 15% of mismatch on displacements and 20% on stresses.

Once the correlation is considered as acceptable (*correlation by comparison with the test or by cross-checking*), the numerical model is considered to be validated. However, it is not to forget that the full reality of loadings and boundary conditions cannot be implemented because of the complexity to perform tests on large structures and its components and because of the consequent CoSt and time which is usually not affordable.

Eventually *Table 11-1* shall collect all the features which are to consider in an Instability Design Verification of a 'Large structure' such as the Ariane 5 ECA launcher configuration.

Chapter-dedicated references:

[1] VDI 2014 Guideline: Part 3, Development of Fiber-Reinforced Plastic Components – Analysis *[Cuntze: editor, contributor]*

[2] HSB 40100-01: *Buckling - General remarks and terms*. Issue A, 2010. *[Broede, Cuntze]*

[3] ECSS Handbook Space Engineering: *Buckling of Structures*. ECSS-E-HB-32-24A. March 2010. *[Cuntze: organizer, contributor]*

[4] Arbocz J and Hilburger M W: *Toward a Probabilistic Design Criterion for Buckling Critical Composite Shells*. AIAA Journal, Vol. 43, No. 8, August 2008, pp. 1823-1827

[5] Arbocz J: *About the State of the Art of Shell Design*: Memorandum M-629, Delft University of Technology, 1990

[6] Arbocz J, Starnes H S Jr. and Nemeth M P: *A Hierarchial Approach to Buckling Load Calculations*. AIAA Paper No. 99-1232, Proceedings of the 40th AIAA/ASME/ASCE/Structures, Structural Dynamics and Materials Conference, St. Louis, 1999

[7] Bushnell D: *Computerized Buckling Analysis of Shells*. Kluwer Academic Press, The Netherlands, 1985

[8] Brush D O and Almroth B O: *Buckling of Bars, Plates and Shells*. McGraw HillBook Company, New York, 1975

[9] Elishakoff I, Li Y and Starnes J H: *Non-classical problems in the theory of elastic stability*. Cambridge University Press. 2001

[10] Falzon B G and Hitchings D: *An Introduction to Modelling Buckling and Collapse*. NAFEMS publication, ISBN 1 874 376 18 2, 2006

[11] Hertel H: Leichtbau. Springer-Verlag Berlin, 1980

[12] Hilburger M W, Nemeth M P and Starnes J H: *Shell Buckling Design Criteria Based on Manufacturing Imperfection Signatures*. AIAA Journal, Vol. 44, No. 3, March 2006, pp. 654-663

[13] Hühne C, Rolfes R and Tessmer J: *A new approach for robust design of composite cylindrical shells under axial compression*. Proceedings European Conference on Spacecraft Structures, Materials and Mechanical Testing, 9-13 May 2005, Noordwijk, ESA SP-581 (2005).

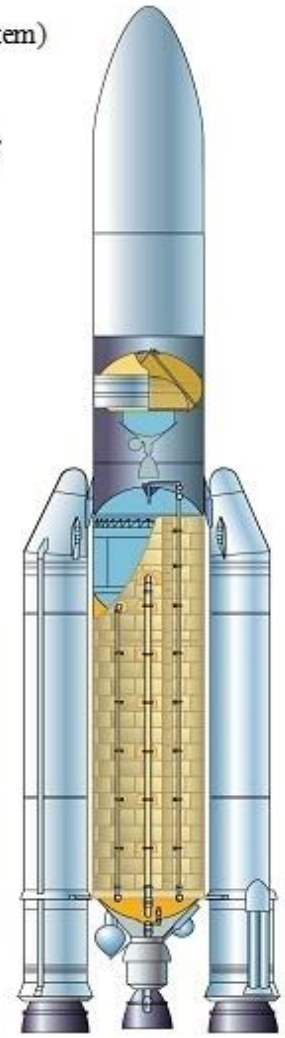
[14] Nemeth M P and Starnes H S Jr: *The NASA Monographs on Shell Stability Design Recommendations - A Review and Suggested Improvements*. NASA/TP- 1998-206290, ASA, Hampton, Virginia, 1998

[15] Reddy J N: *Mechanics of Laminated Composite Plates and Shells*. CRC Press, Boca Raton et al., 2004

[16] Van der Neut A: *The interaction of local and overall buckling of thin-walled structures*. 9th Congr. Internat. Counc. Aeron. Sci., Haifa, 1974. ICAS Paper No.74-07
[17] Koiter W T: *On the Stability of the Elastic Equilibrium*. NASA-TT-F-10833, 1967
[18] Sarafin T P (editor): *Spacecraft Structures and Mechanics - from concept to launch*. Kluwer Academic Publischers, Dordrecht, 2nd printing 1997
[19] Singer J, Arbocz J and Weller T: *Buckling Experiments, Volume 1: Basic Concepts, Columns, Beams and Plates*. John Wiley & Sons, Chichester, UK, 1998.
[20] Singer J, Arbocz J, Weller T: *Buckling Experiments, Volume 2: Built-Up Structures, Composites and Additional Topics*. John Wiley & Sons, Chichester, UK, 2002
[21] Timoshenko S, Gere J M: Theory of Elastic Stability.McGraw-Hill, New York and London, 1961
[22] Thompson J M T, Tulk J D und Walker A C: *An experimental study of imperfection sensitivity in the interactive buckling of stiffened plates*. Buckling of Structures, 149-159, 1976

Table 11-1: Content of Buckling analysis & Test report for a 'Large structure'

1. *Introduction, task*
2. *References* (applicable references, informative references)
3. *Terms, definitions, abbreviations and symbols*
4. *Structure description* (drawings, unit system of measures, coordinate system)
5. *Structural analysis input*
   - *5.1 Requirements, dimensioning load cases, and model assumptions*
   - *5.2 Design factors of safety (FoS) and other design factors or margins*
   - *5.3 Examined buckling phenomena and failure modes*
   - *5.4 Material properties and strength design allowables*
6. *Design*
   - *6.1 Design aspects and guidelines*
   - *6.2 Estimation of imperfections*
   - *6.3 Sizing*
   - *6.4 Miscellaneous* (residual stresses, etc)
7. *Buckling analysis method(s) and tools*
   - *7.1 Mathematical models incl. boundary conditions*
   - *7.2 Calculation method and analysis tools*
   - *7.3 Model checks, comparisons with validated solutions*
   - *7.4 Mathematical model update* (if applicable)
8. *Buckling analysis*
   - *8. k Buckling analysis of "item k"*
   - *8. k Test prediction of „item k"*
   - *8. k Test correction factor of "item k"*
9. *Experiments on structural elements* (e.g. barrel testing)
   - *9. k Test objectives, test article configuration, test facility, test set-up*
   - *9. k Geometry, imperfection measurement, mass, NDI*
   - *9. k Test report* incl. loads, buckling pattern, delaminations, strains
10. *Test–Analysis correlation*
11. *Conclusions*
    - *11.1 Buckling analysis summary table*
    - *11.2 Minimum margins of safety summary*
    - *11.3 Final recommendations*
12. *Analysis annexes* (as far as reasonable)



12 Structural Reliability, Factors of Safety and Design Values

12.1 General on Loads, Risk and Reliability

Conservatism in the traditional design is governed by accounting for a worst case scenario of actions (Einwirkungen) such as temperature with moisture, and of undetected micro-damage and macro-damage, practically cracks. Furthermore, design parameters are mostly not constants but variables which are of different influence (sensitivity) on the actual failure mode investigated, [*Cru94, Cun88, Guo97, Gri89, Rac86, Ver92]*. Effects of the actions are internal forces, deformations, crack widths vibrations etc.

Probabilistic design may be used as an assessment of the deterministic design or as design method required if a *reliability* target $\Re$ or its complement, the probability of failure p_f, is assigned instead of a FoS. However, alone the possibility to disclose the risk characteristics should interest a designer to apply structural probabilistic tools whenever possible and reasonable to achieve structural reliability. Namely, the goal of the design engineer should be a robust design. For instance, distinct stochastic design parameters Xj can be searched to 'economically' improve the robustness of the design by reducing its sensitivity to changes of Xj and keeping p_f at the prescribed level. This is a very interesting optimization problem.

A structural reliability analysis in a Hot Spot reveals the influence of each stochastic design parameter on the distinct failure mode by means of sensitivity measures like the later defined sensitivity measures α_j. If the variability of the structural response, e.g. a stress field, can be reduced then more confidence in the analytical results is provided. Both, an increasing mean strength value and a decreasing standard deviation of load and resistance quantities like strength will lower p_f. Further, reducing the scatter of important geometrical tolerances will improve the design and an improved stochastic load model almost always will create a more economic design. Truncated distributions, to be achieved by some more effort in measurement and controlling within the Non-Destructive Inspection, will lead to an improved reliability, too.

Engineers, especially those working in the aerospace industry, tend to start to shiver once they notice minor negative *MoS* in strength analysis when demonstrating the strength of a structural component necessary for achieving 'design verification'. This has often led in the past and still leads today to an over-reaction attempting to get rid of the negative value, and this is not necessarily a rational engineering response. Engineers should always bear in mind that a *MoS* value is the result of *modelling a structural problem*, and modelling as such is always affected by uncertainties. Here, the term 'uncertainties' should be understood to include inaccuracies as well as any simplifications in the modelling.

MoS-values should not be strictly taken as absolute safety measures. Structural reliability 'thinking', this means thinking in uncertainties of the driving design parameters, will improve the deterministic design procedure. One should concentrate at a reduction of the uncertainty of the stochastic design parameters Xj. A MoS-value cannot provide a substantial 'feeling' about the failure risk. In contrast, already a simple probabilistic example could give such a feeling.

In engineering, a probability of failure of about $p_f < 1 \cdot 10^{-6}$ is very often accepted for design verification (proof), i.e. 1 element of 1 million similar and equally loaded elements fails.

Taking the aerospace industry as an example, the first task is load analysis. In any load analysis to establish are all load events the structure is likely to experience in later application. This includes as

well the estimation of loadings induced by the hygro-thermal, mechanical *(static, cyclic and impact)* and acoustical environment of the structure as further the corresponding lifetime requirements (*duration, number of cycles*), specified by an authority or a standard.
Then, the so-called Limit Load (*LL*) values are determined, usually derived from mission simulations utilizing the so-called mathematical models of the full structure (*dynamical analyses, at first on basis of the preliminary design*). In above context *Table 12-1* shall outline the difference of designations in aerospace. The term 'basic design load' is used in order to obtain a common logic for aircraft and spacecraft.

Table 12-1: Loading designations in aerospace engineering (from HSB 02000-01 Essential topics in the determination of a reliable reserve factor, [Cun12])

Design & Analysis	**Aircraft** (generally used terms)	**Spacecraft** (ECCS-E-30 Standard)
loads from system load scenario analyses of full aerospace structures (generated by load engineer based on pre-design structural models)	balanced global aircraft loadings (from certification and operational requirements)	Limit Load (LL)
basic design load	limit load (ll) (in German: sichere Last)	Design Limit Load $DLL = LL \cdot K_{PM}$ (K_{PM} consideres the uncertainty of the system analysis model and project goal uncertainties, usually $K_{PM} \approx 1.2$)
load assumed for design to a detrimental permanent deformation failure	design load equal to limit load ($ll \cdot j_{0.2}$ with $j_{0.2} = 1$, for civil aircraft and partially for military aircraft)	Design Yield Load $DYL = DLL \cdot j_{0.2}$ (usually $j_{0.2} \approx 1.1$)
load assumed for design to a fracture failure	ultimate load ($ll \cdot j_{ult}$) (often $j_{ult} = 1.5$, j_{ult} may be seen composed of a load uncertainty factor 1.25 and of a design uncertainty factor 1.2,	Design Ultimate Load $DUL = DLL \cdot j_{ult}$ (usually $j_{ult} \approx 1.25$)
Prepared: Dr. R. Cuntze	Checked: Dr. J. Broede	Date: 02.07.2012 IASB

Fig.12-1 shall visualize some essential topics: (1) Difference between spacecraft and aircraft, (2) From load-level down to stress-level in order to be able to assess the stresses by strengths, (3) Allowable Stress safety concept (*not to apply in case of non-linear behavior*) versus Strength Design Allowable safety concept.

The ARIANE5 General Specification A5-SG-1-10, e.g., defines the *LL* as follows: (a) if a statistic dispersion of the single load is known, the *LL* is at least equal to the load having a 99 % probability of not being exceeded in service with a confidence level of 90 % ; (b) if a statistic dispersion of the load is unknown, the *LL* is determined on the basis of a rational conservative estimate. Then the *LL*

values may have to be multiplied by an assumed factor K_{PM} (*is of the magnitude of the FoS j*), which shall compensate the uncertainty of the estimate obtained from the mathematical model. Additional project factors, due to uncertainties in the project targets, have to be included here. The Load Model uncertainty factor $K_{PM} \equiv j_{PM}$ should decrease with the maturity of the design of the structure.

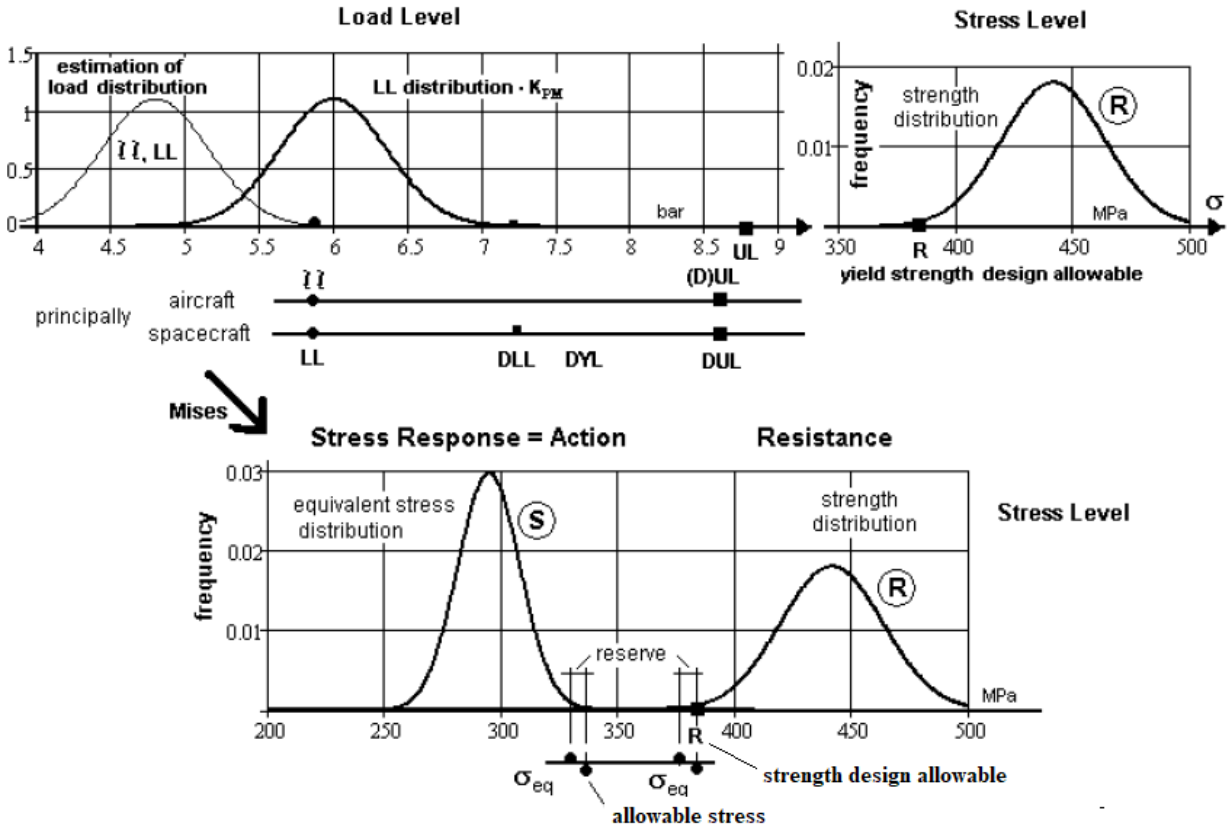


Fig. 12-1: Visualization of the difference of the aerospace load terms used in the Strength Design Allowable Safety Concept and of the 'hopefully forgotten' Allowable Stress Safety Concept

The product $LL \bullet j_{LM}$ becomes the so-called Design Limit Load (*DLL*). The *DLLs* of the various load cases are the input for the design engineer and they are the largest anticipated loads, which a structure may have to sustain during its service life in association with the applicable operating conditions.

In the case of load combinations the statistic definition above is applicable for the resulting load combination too, however it is not used in the usual deterministic design due to the higher complexity compared to single loads. In the probabilistic design this statistic definition can be considered and it has a mass saving effect.

In the next stage, from all potentially design-relevant load combinations all those have to be extracted which are finally really design decisive. They are derived from the probably hundreds or thousands of load combinations by engineering judgment or by (linear) Finite Element Analysis achieved by computing all combinations. In case of linear behavior the treatment of all combinations would be possible however the critical ones of them must be searched for fast management decisions. Namely, in practice often fast decisions have to be made during the design development phases and for these only a reduced number of really essential design driving load cases are required. These load cases are referred to as *Dimensioning Load Cases*.

Table 12-2 collects the basic features of a Safety Concept.

Table 12-2: Safety-Concept

Uncertainties in the Design:

- physical nature (scatter of design parameters strength, load, E-modulus, geometrical tolerances, ...)
- statistical nature (lack of information like a too small sample)
- calculation model
- Measurement.

Consideration of the Uncertainties:

Deterministic Safety Concept (e.g. German Aerospace):

→ (Design Limit Load (DLL)) or "Safe Life"
increasing Design-Factors of Safety (DFoS) j_B; $j_{p0,2}$; j_L such as

j_{ult} = 1,5 (fracture) for (Design Ultimate Load)
$j_{p0,2}$ = 1,1 (initiation of yield) for Acceptance (Proof Test)
j_L = 4 (lifetime)
j_{inst} = (instability).

Semi-probabilistic Safety Concept:

→ Utilization of partial FoS distinguishing uncertainties affecting stress and strength.

The higher the uncertainty is the more likely errors will be made and errors will result in additional CoSts. *Fig.12-2* depicts a CoSt pyramid, which illustrates the individual tasks in structural analysis, their impact, shares in CoSts, and which crucial affects potential errors can have. The obvious conclusion with respect to the load parameter is that reducing the load uncertainty pays off and it also improves the accuracy of the *MoS* values.

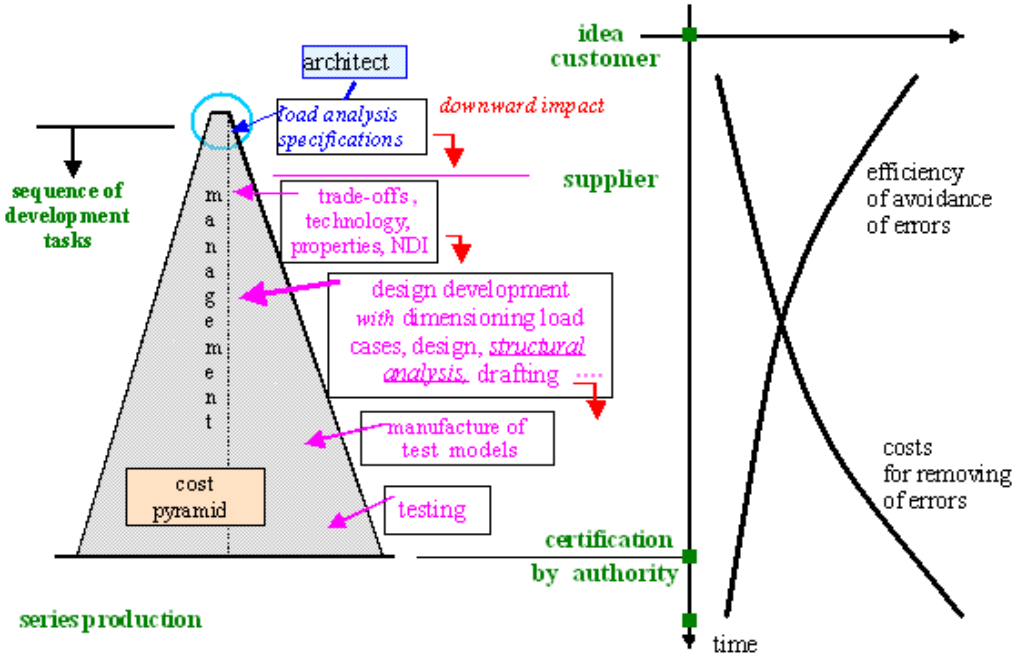


Fig. 12-2: 'CoSt pyramid' in structural analysis respecting the effect of re-design

Note: Very often the estimate of DLL is that design parameter which carries the highest uncertainty of all parameters. Improving the accuracy of load estimation might eliminate slightly negative safety margins.

In aerospace industry RAMS (Reliability, Availability, Maintainability, Safety *of men.* See *Table 12.3*) activities support engineering and management decisions to identify and evaluate technical risks. In the last two decades a major trend in structural design has been the promotion of structural reliability principles to account for the uncertain nature of the design parameters. However, a number of practical difficulties, including lack of suitable design data and the inability to undertake design optimization in a rational and efficient way, preclude their widespread application.

Table 12-3: Definition within RAMS

Reliability is the aptitude of a product to perform the required functions at certain performance levels under specific conditions and for given period of time, expressed in terms of the probability to do so.
Availability is the aptitude of a product to be - at a certain time or during a certain time - in a position to provide the functions, expressed in terms of probability.
Maintainability is the probability that the product can be kept in or returned to a state in which it can provide its functions, when maintenance is applied. Maintenance comprises adequate storage, controls, preventive actions, e.g. repair of surface protection.
Safety is defined as "absence of circumstances liable to cause death, or degradation or loss of equipment within limits of probability of occurrence" of these events.

Reliability comprises "Reliability in Operation" and "Integrity". “Reliability in Operation” itself covers the characteristic, which refers to the functional behavior of the structure over a given time of operation. “Integrity” covers the capability of the structure to withstand the functional, operational, and environmental loadings during a given duration of use. In order to achieve structural integrity, adequate non-destructive inspection and control procedures need to be applied during production of the hardware. This is essential to ensure that deviations or imperfections in excess of those be

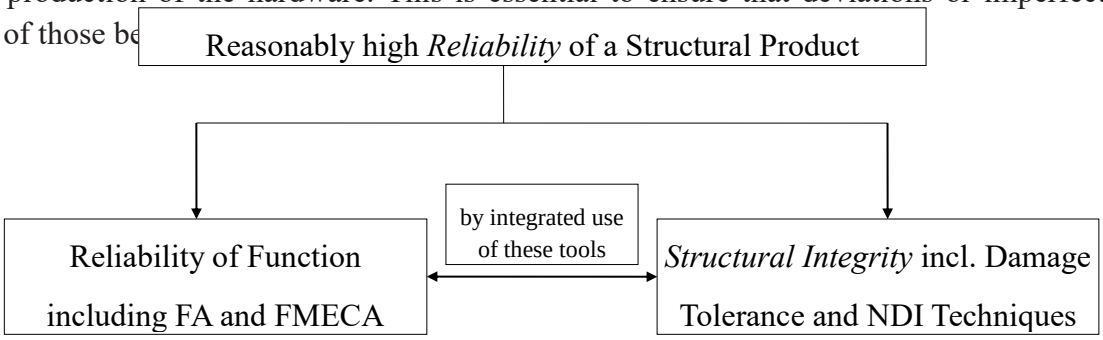


Fig. 12-3: RAMS objectives

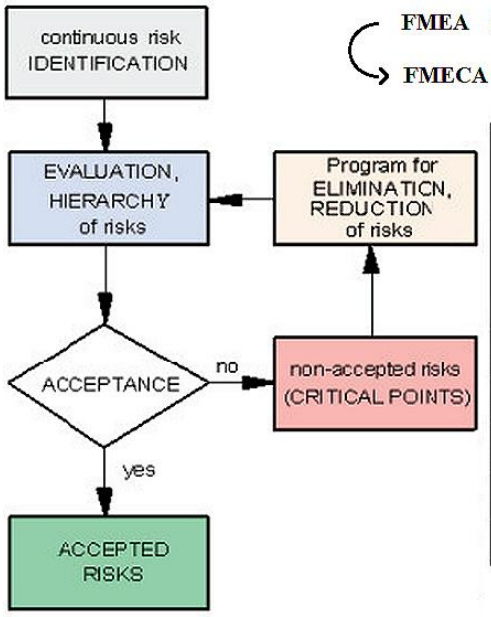
The RAMS-objectives are to ensure that the Integrity of Structures, *Fig. 12-3.* This must take due account of operational conditions and design loads in conjunction with defined damage tolerance and general safety requirements. It should be emphasized that integrity control relates to *structures* irrespective of their materials.

12.2 RAMS-Achievement, Functional Analysis, FMECA and Critical Points Log

One supporting tool to produce reliably working structures is to follow a so-called RAMS Achievement Process including Risk Control. *Table 12-3* shows for a structural product the

relations between the RAMS tools Functional Analysis (FA), Failure Mode Effect and Criticality Analysis (FMECA), Critical Points Lists (CPL) and Probabilistic Predictions for the validation of the results. Concern of this activity is at first a failure mode effect analysis FMEA which mounts in a failure mode effect critical analysis FMECA. The terms FMEA (failure mode effect analysis) and FMECA (*failure mode effect and criticality analysis*) in the risk treatment process are common standard names used. Above tools guide "What is to be done?"

As far as safety is concerned, major efforts have to focus on risk identification, risk assessment and management with the understanding that risk is linked to the probability of loss of human life, loss of equipment and of damage. Risk management is ensured through a so-called critical points list, which categorizes items with respect to the consequences of their worst-case effects. *Fig.12-4* depicts the main elements of a risk control process. These are the elements identification, evaluation / hierarchy, reduction / elimination, and acceptance [*Gri03]*. Finally, *the* figure also illustrates the interdependence of the risk (criticality) level on the severity of the failure and its probability of occurrence. Design must take care of the risk. As can be seen in the risk assessment *Fig.12-4*, it is important to define hazard classes. The classification into probability classes should follow the product exposition severity times the occurrence frequency. This is done in all technical disciplines. The figure impressively demonstrates that one should always consider the real risk entities and not view just the *MoS*-value.



Probability P =	effect on: / Severity S =	safety: catastrophic 0_A (16)	safety: fatal 0_B (8)	mission objective: major 1 (4)	performance availability: minor 2 (2)	no effects: negligible 3 (1)
very probable	16	256	128	64	32	16
probable	8	128	64	32	16	8
less probable	4	64	32	16	8	4
improbable	2	32	16	8	4	2
very improbable	1	16	8	4	2	1

Fig.12-4: Process of risk control and risk assessment in structural development. Risk = P x S [Gri04]

Note: Essential question with respect to all uncertainties is whether these increase the risk to an un-acceptable level or not. This has to be evaluated and may result in avoiding additional CoSts [see Sar97]

12.3 Failure probability p_f, density functions f(x) and cumulative distribution functions F(x)

Probabilistic concepts require stochastic modeling which means statistics and an assumption of the density function type (*such as the distributions Normal, Log-Normal, Weibull, Extreme Value etc*.) of each essential uncertain design variable. This is basically the same as with the classical procedure where both mechanical modeling and stochastic modeling are required in principle.
Applying a probabilistic concept, in addition a so-called logical modeling of the failure system is to choose (*as a series failure system or a parallel failure system or a combination there of)* considering

the effect on the probability of commonly acting failure modes and obtaining a so-called 'joint failure probability'. Advantage: Even, if only the type of distribution can be assessed and used in analysis and not the tails of the distribution, more reliable information is generated with a probabilistic concept.

A structural component is subjected to an action S (*influence, loading, stress*) and has a resistance *R*, the size of which is distributed with a probability density function PDF or just density function *f*. The f_S, f_R in *Fig.12-5left* have an average or another characteristic value and they scatter around it with a standard deviation. The associated cumulative distribution function CDF (*sum* function) or just distribution function are written F_S and F_R. In the context of above definitions some terms shall be presented here: (1) Random (*zufällig*), by chance, (2) Stochastic quantity (variable = scattering design parameter which is uncertain before realization and random after realization) being well described by a random probability distribution), (3) Uncertain variable (*variable without a certain knowledge*). The x_j are realizations of the stochastic design parameters X_j.

Both density functions overlap with a small intersection. In the domain of the intersection of the action stress and of the resistance strength, the part would fail. The integration of $f_S(x)$ with $f_{R2}(x)$ means solving a multi-dimensional, so-called convolution integral obtaining the failure probability, see *Fig.12-5 left,*

$$p_{f2} = P(R_2 < S) = P(R_2 - S < 0) = P[g(X_1, X_2, X_3, ..)] < 0 = \int f_S(x)\, f_{R2}(x)\, dx = \int_{g(X)\le 0} f_{\underline{X}}(\mathbf{x})\, dx$$

with f_{S2} the function addressed in *Fig.12-5 left* below. The value of p_{f2} is the integrated area under the blue curve, not the fillet under f_S-f_{R2} as unfortunately too often said and sketched!
The p_{fSR2}-distribution function spans between plus infinite and minus infinite. For the simple R-S case intermediate net points in the overlap region of the curve $F(p_{f2})$ can be pointwise computed with the convolution integral above by the MathCad code and then from the continuous F-points the distribution function $F(p_{f2})$ can be derived by mapping.

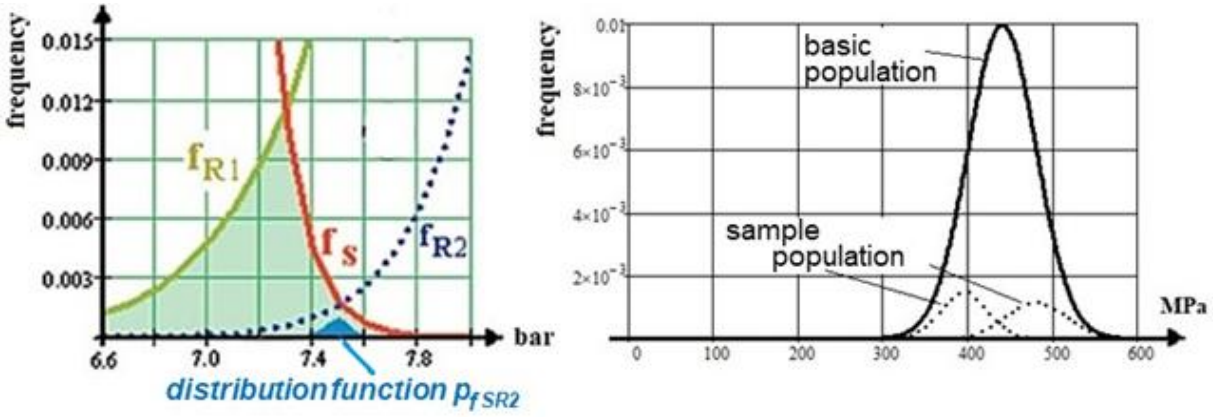


Fig.12-5: (left) Visualization of stress f_S and strength density functions f_R with probability of failure p_f . (right) The area under each distribution is 1. The sample distributions are factorized to mark the smaller sample size n versus a basic population with n = infinite

Fig.12-5right shows a basic distribution of a strength characteristic and within the density distributions of two 'samples by chance', normalized by a factor of ten. For the basic population ND the standard deviation is termed σ and the mean μ . Two thirds (68.26 %) of the measurements are lying in the distance ± σ to the mean value μ; for ± 2σ it is 95.46 % and for ± 3σ it is 99.73 %. The latter corresponds to the so-called "6σ-method" as a method of quality management.

Table 12-4: Density functions f(x) and cumulative distributions F(x) with statistical parameters

* Normal Distribution (Gauß distribution) : $-\infty < x < \infty$, bell-shaped

$$f_{ND}(x) = \frac{1}{\sigma \cdot \sqrt{2 \cdot \pi}} \cdot exp\ [-\frac{1}{2}(\frac{x - \mu}{\sigma})^2],\ F_{ND}(x) = \frac{1}{\sigma \cdot \sqrt{2 \cdot \pi}} \int_{-\infty}^{x} exp\ [-\frac{1}{2}(\frac{t - \mu}{\sigma})^2 \cdot dt$$

μ = mean of basic population, σ= standard deviation of basic population

Area under curve: $\int_{-\infty}^{\infty} \frac{1}{\sigma \cdot \sqrt{2 \cdot \pi}} \cdot exp\ [-\frac{1}{2}(\frac{x - \mu}{\sigma})^2 dx = \frac{1}{\sqrt{2 \cdot \pi}} \cdot \int_{-\infty}^{\infty} exp[-\frac{1}{2} \cdot z^2]\ dz = 1$

with $\Phi(z) = \frac{1}{\sqrt{2 \cdot \pi}} \cdot \int_{-\infty}^{z} exp[-\frac{1}{2} \cdot t^2]$ the Gaussian error integral, t = new integration variable, $z = \frac{t - \mu}{\sigma}$

* Logarithmic Normal Distributions: often used as strength distribution, (single tailed, bias distribution)

y = ln(x), x= exp(y): $f_{lnND}(x) = \frac{1}{y_{ln} \cdot \sqrt{2 \times \pi}} \cdot \frac{1}{x} \exp[-\frac{1}{2}(\frac{\ln(x) - \ln(\beta_{ln})}{y_{ln}})^2],\ F_{lngND}(x) = \int_0^x f(t) \cdot dt$ (natural)

y = lg(x), $x=10^y$: $f_{lgND}(y) = \frac{\lg(e)}{y_{lg} \cdot \sqrt{2 \times \pi}} \cdot \frac{1}{10^y} \cdot \exp[-\frac{1}{2}(\frac{y - \lg(\beta_{lg})}{y_{lg}})^2],\ F_{lgND}(x) = \int_0^x f(t) \cdot dt$ (decadic)

* 2-parameter Weibull Distribution: often preferred to LogND as strength distribution

$f_{WD}(x) = \Lambda \cdot k \cdot (\Lambda \cdot x)^{k-1}\ exp[-(\Lambda \cdot x)^k]$ non-negative, $F_{WD}(x) = 1 - exp[-(\Lambda \cdot x)^k]$

with inverse! scale parameter , $1/\Lambda > 0$ ($\Lambda \approx 1$), and shape parameter k (>1). $0 < x < \infty$, $\lambda \equiv 1/\Lambda$

This distribution maps failure rates of different technical systems. (k is also termed Weibull modulus)

* Exponential Distribution as special case of the WD

$f_{ED}(x) = \Lambda \cdot exp[-\Lambda \cdot x]$ non-negative, $F_{ED}(x) = 1 - exp[-\Lambda \cdot x)]$

* Rayleigh Distribution with scale parameter σ, median $\sigma \cdot \sqrt{2 \cdot ln(2)}$, mean $\sigma \cdot \sqrt{\pi / 2}$

$f_{RD}(x) = (x / \sigma^2) \cdot exp[-x^2 / 2 \cdot \sigma^2]$ non-negative, x > 0 , $F_{RD}(x) = 1 - exp[-x^2 / 2 \cdot \sigma^2]$.

* General formulas for sample population and basic population

Scaled F(x) : $F = \int_{-\infty}^{\infty} f(x) \cdot dx = 1$; Median x_M if : $F = \int_{-\infty}^{xM} f(x) \cdot dx = 1/2$,

Arithmetic mean (or expectation value E(x)) , $\bar{x}$ or $\mu = \int_{-\infty}^{\infty} x \cdot f(x) \cdot dx$;

Second moment $E(x^2) = \int_{-\infty}^{\infty} x^2 \cdot f(x) \cdot dx$; Variance $V(x) = E(x^2) - (E(x))^2$

Coefficient of variation cov = $\sqrt{V(x) / |E(x)|^2}$ with

s^2 = variance, $\bar{z} = \bar{x}r - \bar{x}s$, $s_z = \sqrt{sr^2 + ss^2}$, n = number of tests within the sample

sample mean $\bar{x} = \sum_{i=1}^{n} x_i / n$, sample standard deviation $s = \sqrt{\sum_{i=1}^{n} (x_i - \bar{x}) / (n-1)}$

cov = coefficient of variation: for sample $cov_x = s / \bar{x}$, and basic population $cov_\mu = \mu/\sigma$.

* Transformed Parameters of basic population and sample for ND and LogND:

$$\beta_{ln} = \frac{\mu^2}{\sqrt{\mu^2 + \sigma^2}},\ \gamma_{ln} = \sqrt{\ln\left(\left(\frac{\sigma}{\mu}\right)^2 + 1\right)} \quad \text{and} \quad \bar{y}_{ln} = \ln\left(\frac{\bar{x}^2}{\sqrt{\bar{x}^2 + s^2}}\right),\ s_{ln} = \sqrt{\ln\left(\left(\frac{s}{\bar{x}}\right)^2 + 1\right)}$$

$$\beta_{lg} = \frac{\mu^2}{\sqrt{\mu^2 + \sigma^2}},\ \gamma_{lg} = \sqrt{\lg(e) \cdot \lg\left(\left(\frac{\sigma}{\mu}\right)^2 + 1\right)} \quad \text{and} \quad \bar{y}_{lg} = \lg\left(\frac{\bar{x}^2}{\sqrt{\bar{x}^2 + s^2}}\right),\ s_{lg} = \sqrt{\lg(e) \cdot \lg\left(\left(\frac{s}{\bar{x}}\right)^2 + 1\right)}.$$

LL:
**The integral over any f(x) → F = 1 = 100%. This obviously is the same value as for the failure function (also termed F) namely at failure it is F = 1 !*
**Stress density distribution and resistance density distribution must be so far apart that the intersection is so small to fulfill above desired low probability of failure of $p_f < 10^{-6}$, [Cun12].*

Three of the mainly applied (probability) density functions *f* are presented in *Fig.12-6*.

- Gauß Normal Distribution **ND** (negative values faced) μ, σ
  Application: elasticity entities, physical observations, ...
- Logarithmic Normal Distribution **logND** (no negative values), $\mu_{logND} = ln(\mu)$
  Application: strength, ...
- 2-parameter Weibull Distribution **WD**
  Application: failure state case strength, failure rate case (bathtub).

When generally using the ND for phenomena where the random variable can be only positive (*dimensions, strengths*) the coefficient of variation $cov = \sigma / \mu$ should be < 0.25.
Whereas ND is pretty known just logND and WD shall be shortly described. In practice, l**ogND** is used when only positive values are possible for the running variable, the characteristic x, and if the frequencies in the left area of the distribution are greater than in the right area of the distribution, i.e. if there is a bias (skew) such as with strength and salary. Far from zero there is no difference.

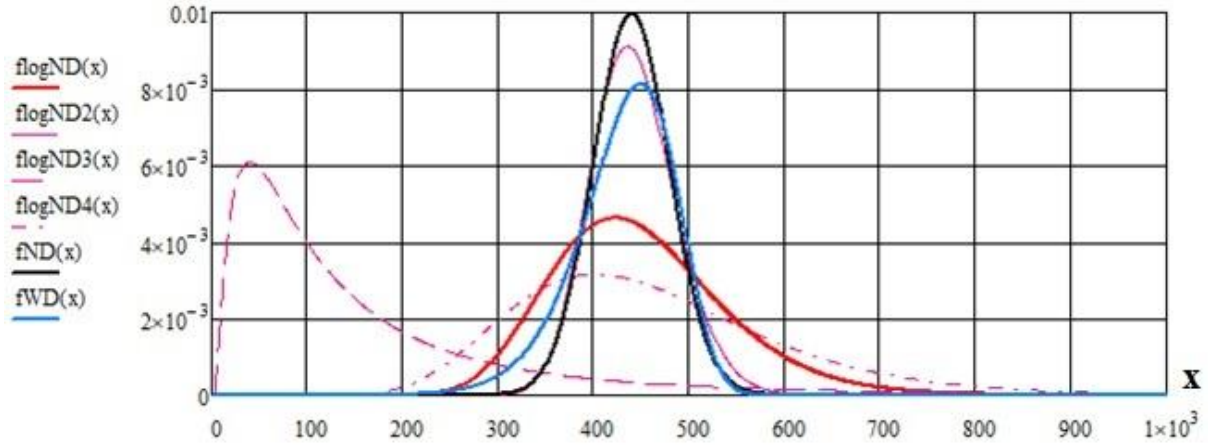


Fig.12-6: Comparative visualization of the 3 standard distribution functions above.
Parameters ND: μ = 40MPa, σ =40 MPa. LogND: μlogND = ln(μ), σlogND = 0.1(flogND2); μlogND = ln(μ), σlogND = 0.2(flogND) ; μlogND = ln(μ)/1.3, σlogND =1 (flogND3; μlogND = ln(μ), σlogND = 0.3(flogND4). WD: Λ=0.0022, k =10

Failure Rate mapping

There are not only *failure states* such as with the strengths failure modes to be investigated but failure rates, too. A typical **failure rate** curve has the shape of a "bathtub". With the widely used bathtub curve, the failure behavior can be described in three phases: The first part is a decreasing failure rate, known as early failures or 'infant mortality' such as for above electronic box. The second part is a constant failure rate, known as random failures during its "useful life". The third part is an increasing failure rate, known as aging of electronic and also of structural elements. This is the rate of "wear out" failures as the product exceeds its design lifetime.
The **WD** can map both the distributions *with increasing failure rate* and distributions *with falling failure rate* by applying an appropriate WD-parameter set. The scale parameter can be used to

model whether early or late failures occur more frequently. Shape parameter k typical values are in the range 0.25. < k < 5. With special k-values, other probability distributions can be realized: For k =1 the exponential distribution (also of interest for extreme value distributions of winds etc) with constant failure rate results, for k=2 the Rayleigh distribution. For k ≈ 3.6 there is already a distribution with vanishing skew obtained, similar to ND. The exponential distribution plays a central role in reliability theory, comparable to the ND in other applications.

Of interest in maintenance is: Mean Time Between Failures (MTBF) which is the English term for the average operating time between failures for repairable units. "Operating time" means the time between two consecutive failures of such a unit. For units that cannot be repaired, the 50% expected value of the distribution of lifetimes is the mean lifetime MTTF probability until an object fails at time t (*after Wikipedia)*.

Fig.12-7 and *-8* show some parameter investigations. *Fig.12-7* proves that for high characteristic values σ the distribution functions F for ND and LogND practically become the same.

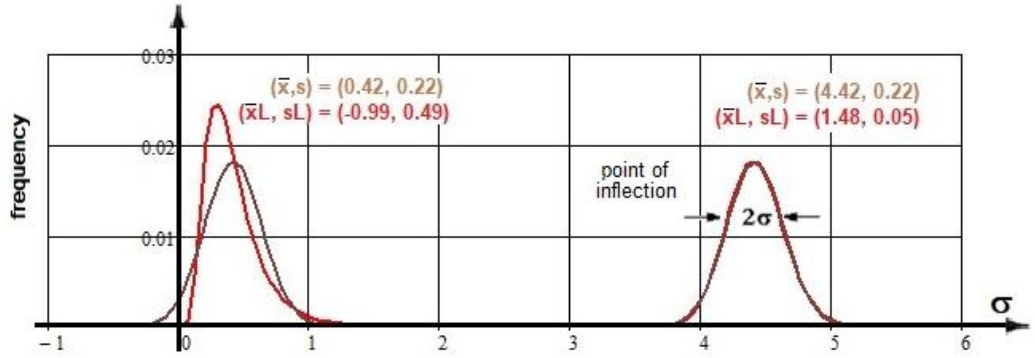


Fig.12-7: Effect of parameters on the shape of the distribution function; x = σ = stress. LogND is indexed by L

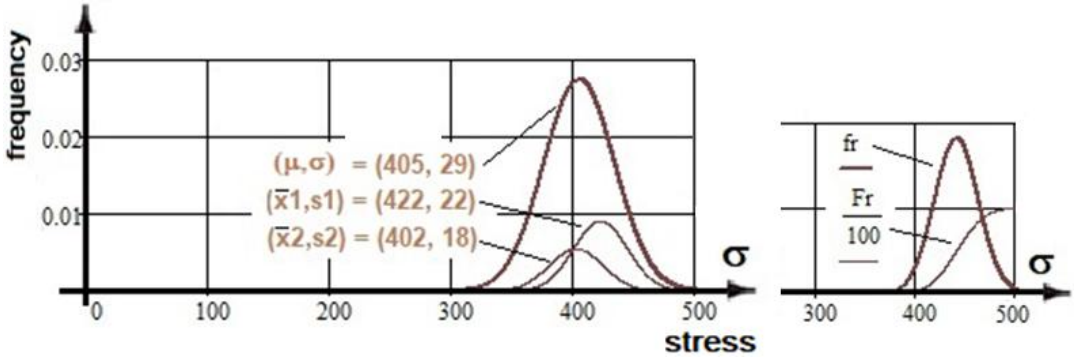


Fig.12-8: Locations of two ND sample distributions within a basic ND population. f(r) density function and F(r) distribution function (cumulative or sum function)

ND-strength density function $f_r(x)$, stress density function fs(x) and difference function $f_{d(if)}$ (x) are visualized in *Fig.12-9*. Setting $\bar{d} = \bar{x}r - \bar{x}s$, $s_d = \sqrt{sr^2 + ss^2}$ enables to calculate for a simple S-R problem the failure probability p_f from $\int_{-\infty}^{\infty} \frac{1}{s_d \cdot \sqrt{2 \cdot \pi}} \cdot \exp\left[-\frac{1}{2}\left(\frac{x-\bar{d}}{s_d}\right)^2\right] \cdot dx$.

The standardized normal distribution is a special normal distribution where the μ = 0 and the standard deviation σ = 1. It allows to compare different data sets and to calculate the probability of certain values occurring. It follows the transformation Z = (X-μ) / σ.

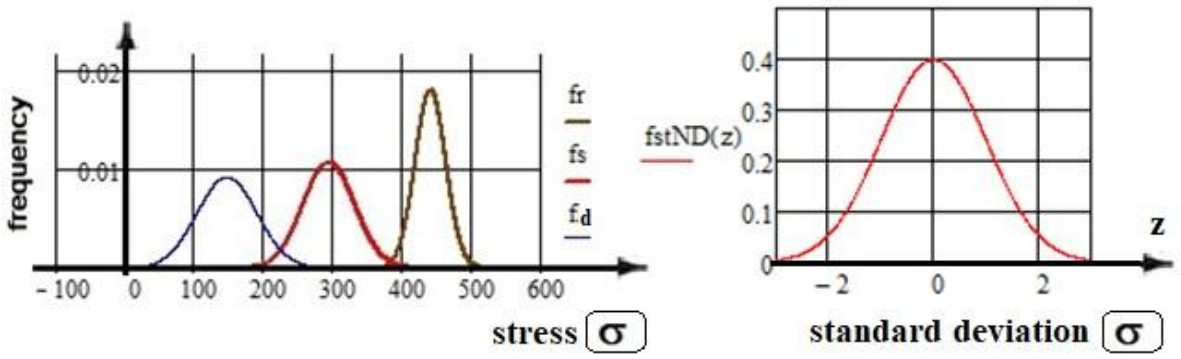


Fig.12-9: Difference distribution (R-S) and the standardized ND (mind the different sigmas)

Estimate for basic population in the case of m samples: These can be united due to $\mu \approx \sum_{j=1}^{m} \overline{x}_j \; / \; m.$

12.4 Statistical pre-requisites, tests of assumed distributions, and significance level

In statistical analyses mapping of a course of test data requires an appropriate choice of the distribution function that underlies the envisaged characteristic (*Merkmal*) x. As statistical prerequisite of statistical models such an assumed distribution must be statistically checked for its applicability. The significance of the assumption is to determine by a statistical test.

Objective is a procedure such that the probability of making a wrong decision is as small as possible. Particularly, in hypothesis testing, the objective is to select sample data from the population and, based on analysis of this sample data set, to decide whether a hypothesis is true or false with a given level of significance (from sheet *[HSB 04200-03]).* A statistical test is a procedure to decide whether a H0-hypothesis on the distribution of a stochastic variable has to be discarded or not. To be included in the statistical test is an alternative hypothesis H1 which - in general - represents the complementary part of H0. This means H1 embraces all possibilities which are not covered by H0.

In these statistical tests the quantile of the one of the following auxiliary distributions is applied: Chi-square distribution (*here used in an example*) or Student's t-distribution (if n > 30).

The decision depends on the value of a suitable stochastic quantity, which is computed on the basis of observations. Due to the randomness it is possible that the decision might be not correct. The significance level α, which has to be chosen a priori, is the maximum of the allowed probability to reject the H0-hypothesis although it is correct in reality. Such a false decision is termed error of the first kind. Often chosen values for α are 1%, 5% and 10%. Because the probability of an error has the chosen small value α the rejection of the H0-hypothesis means acceptance of the alternative hypothesis. Therefore, not rejecting the H0-hypothesis does not necessarily mean acceptance of the H0-hypothesis.

Example 1: Workflow of a statistical test in order to check randomness of a sample (*Probe*).

Example 2: Statistical test to check whether an additional novel similar data set can be united with the present one in order to improve design data.

Example 3: Statistical check whether similar samples can be united in order to efficiently improve design data by this combination and thereby enlarge the reliability of the results.

Example 1: Tests for randomness of a sample

Aim: The performance of this test makes sense, only, if the observations will have a natural sequence.

Usually, such a sequence exists if the data are un-sorted or sorted in chronological order. A natural sequence may also result if data are sorted according to the physical position of the test objects (e.g. strength data according to the original test specimen (*Probekörper*) position cut from raw material) [Table *HSB 04200-03*].

Input:

- Recommended significance level: $\alpha = 5\%$, Sample size: n, requirement $n \geq 10$ observations
- observations:

$n = 15$

1.707	1.113	1.847	2.713	0.676	2.167	3.445	1.284
2.944	3.654	0.821	2.135	2.483	0.715	4.638	

sorted:

0.676	0.715	0.821	1.113	1.284	1.707	1.847	*2.135*
2.167	2.483	2.713	2.944	3.445	3.654	4.638	

Hypotheses: • H_0: Sample is random, H_1: Sample is not random

Test:

1. Position of the observed value sorted in ascending order: $x_{(i)}$
2. Median: $x_M = x_{((n+1)/2)}$, if n is odd; $x_M = \left(x_{(n/2)} + x_{(n/2+1)}\right)/2$, if n is even
3. $(1-\alpha/2)$-quantile of the standardized normal distribution: $u_{1-\alpha/2}$.

- Procedure:
  1. Determination of the median. Remove median from the sample if n is odd
  2. Determination of the number of observations n' above and below the median
  3. Indicate the observations *above* the median with the attribute "A" and *below* with "B"
  4. Determination of the number a of observation series having the same attribute (these series are termed "iterations")
  5. Determination of quantile u:

for $a < n'+1$: $u = (n' + 0.5 - a) \cdot \sqrt{\dfrac{2 \cdot n' - 1}{n' \cdot (n'-1)}}$ for $a = n'+1$: $u = 0$

for $a > n'+1$: $u = (a - n' - 0.5) \cdot \sqrt{\dfrac{2 \cdot n' - 1}{n' \cdot (n'-1)}}$

Table : Quantile u_P of the standardized normal distribution

P	0.5 %	1.0 %	5.0 %	10.0 %	90.0 %	95.0 %	97.5 %	99.0 %	99.5 %
u_P	-2.576	-2.326	-1.645	-1.282	1.282	1.645	1.960	2.326	2.576

Calculation: $n = 15 > 10$

- Median: n is odd, median $x_M = x_{((n+1)/2)} = x_{(8)} = 2.135$
- Because n is odd, the median is to be removed.
- Number of observations above median: $n' = 7$
- Observation-series after removing the median: B, B, B; A; B; A,A; B; A,A; B; A; B; A
- Number of observation-series: $a = 10$
- Quantile u for $a > n'+1 = 8$: $u = (10 - 7 - 0.5) \cdot \sqrt{\dfrac{2 \cdot 7 - 1}{7 \cdot (7-1)}} = 1.391$

Result:

$u = 1.391 \leq u_{1-\alpha/2} = u_{0.975} = 1.960$ "Sample is random" needs not to be rejected.

Example 2: Applicability of a Normal Distribution ND to map a distinct course of test data

Aim: The applicability of a ND provides many benefits due to the available manifold tools and data tables.

An improved standard deviation σ_0 of the basic population from experience with formerly measured similar material data gives a higher reliability to the design data to be determined. In order to sort out whether a new sample may be united with a known ND its standard deviation s is to be checked whether it is compatible with the σ_0-value of the envisaged ND. Then, the former value σ_0 can be improved. [*HSB 04200-03*]

Task:

Check, whether the sample's standard deviation s is compatible with the former basic σ_0

Input:

- Significance level α • Specified σ_0 • Sample size n • Observations $x_1, \ldots, x_n$
- Observations:

$n = 15$:

96.1	96.5	95.4	94.7	105.3	110.1	92.6	107.3
120.7	94.8	101.2	123.3	82.3	114.2	105.6	

$$s = \sqrt{\left[\sum_{i=1}^{n}(x_i - \bar{x})^2\right] / (n-1)}, \quad \text{with} \quad \bar{x} = \left(\sum_{i=1}^{n} x_i\right) / n \qquad \bar{x} = \\ s = 11.19$$

Hypotheses:

- H_0: Sample belongs to known basic population, • H_1: Sample does not belong to

Statistical prerequisites to be checked:

- Sample is random : recommended $\alpha = 5\%$ (small value taken)
- Basic population belongs to a ND: $\alpha = 10\%$

Given:

- Recommended significance level: $\alpha = 10\%$ - Standard deviation: $\sigma_0 = 9.0$

Calculation:

- Check of model prerequisite "Samples are random":

  In the frame of the recommended significance level the hypotheses "Sample is random" and "Basic population belongs to a ND" need not to be rejected.

  $$\sigma\chi = \sqrt{\frac{\sigma_0^2}{n-1} \cdot \chi^2_{1-\alpha}(n-1)} \quad \text{with } \chi^2_{1-\alpha}(f) \text{ and } f = n-1 \text{ degrees of freedom}$$

- Decision data: $s = 11.19$, $\sigma\chi = 11.04$ with $\chi^2_{0.90}(15-1) = 21.06$ (from following Table)

Result:

⇒ As $s = 11.19 > \sigma\chi = 11.04$, the hypothesis "Sample belongs to known basic population" has to be rejected.

The next *Table* enlists the necessary check quantity when using the Quantile $\chi^2_P(f)$ of the chi-square distribution.

Table: Quantile $\chi^2_P(f)$ of the chi-square distribution (from [HSB 04200-03])

f \ P	0.5 %	1.0 %	2.5 %	5.0 %	10.0 %	90.0 %	95.0 %	97.5 %	99.0 %	99.5 %
1	0.000	0.000	0.001	0.004	0.016	2.706	3.841	5.024	6.635	7.879
2	0.010	0.020	0.051	0.103	0.211	4.605	5.991	7.378	9.210	10.597
3	0.072	0.115	0.216	0.352	0.584	6.251	7.815	9.348	11.345	12.838
4	0.207	0.297	0.484	0.711	1.064	7.779	9.488	11.143	13.277	14.860
5	0.412	0.554	0.831	1.145	1.610	9.236	11.070	12.833	15.086	16.750
6	0.676	0.872	1.237	1.635	2.204	10.645	12.592	14.449	16.812	18.548
7	0.989	1.239	1.690	2.167	2.833	12.017	14.067	16.013	18.475	20.278
8	1.344	1.646	2.180	2.733	3.490	13.362	15.507	17.535	20.090	21.955
9	1.735	2.088	2.700	3.325	4.168	14.684	16.919	19.023	21.666	23.589
10	2.156	2.558	3.247	3.940	4.865	15.987	18.307	20.483	23.209	25.188
11	2.603	3.053	3.816	4.575	5.578	17.275	19.675	21.920	24.725	26.757
12	3.074	3.571	4.404	5.226	6.304	18.549	21.026	23.337	26.217	28.300
13	3.565	4.107	5.009	5.892	7.042	19.812	22.362	24.736	27.688	29.819
14	4.075	4.660	5.629	6.571	7.790	21.064	23.685	26.119	29.141	31.319
15	4.601	5.229	6.262	7.261	8.547	22.307	24.996	27.488	30.578	32.801
16	5.142	5.812	6.908	7.962	9.312	23.542	26.296	28.845	32.000	34.267
17	5.697	6.408	7.564	8.672	10.085	24.769	27.587	30.191	33.409	35.718
18	6.265	7.015	8.231	9.390	10.865	25.989	28.869	31.526	34.805	37.156
19	6.844	7.633	8.907	10.117	11.651	27.204	30.144	32.852	36.191	38.582
20	7.434	8.260	9.591	10.851	12.443	28.412	31.410	34.170	37.566	39.997
21	8.034	8.897	10.283	11.591	13.240	29.615	32.671	35.479	38.932	41.401
22	8.643	9.542	10.982	12.338	14.041	30.813	33.924	36.781	40.289	42.796
23	9.260	10.196	11.689	13.091	14.848	32.007	35.172	38.076	41.638	44.181
24	9.886	10.856	12.401	13.848	15.659	33.196	36.415	39.364	42.980	45.559
25	10.520	11.524	13.120	14.611	16.473	34.382	37.652	40.646	44.314	46.928
26	11.160	12.198	13.844	15.379	17.292	35.563	38.885	41.923	45.642	48.290
27	11.808	12.879	14.573	16.151	18.114	36.741	40.113	43.195	46.963	49.645
28	12.461	13.565	15.308	16.928	18.939	37.916	41.337	44.461	48.278	50.993
29	13.121	14.256	16.047	17.708	19.768	39.087	42.557	45.722	49.588	52.336
30	13.787	14.953	16.791	18.493	20.599	40.256	43.773	46.979	50.892	53.672
40	20.707	22.164	24.433	26.509	29.051	51.805	55.758	59.342	63.691	66.766
60	35.534	37.485	40.482	43.188	46.459	74.397	79.082	83.298	88.379	91.952
120	83.852	86.923	91.573	95.705	100.624	140.233	146.567	152.211	158.950	163.648
260	205.020	209.908	217.229	223.663	231.238	289.619	298.611	306.557	315.970	322.487

Example 3: Uniting two Samples

Aim: Improvement of the reliability of a result if similar samples can be united in a combined sample.

For two samples the "Kolmogorov-Smirnov test" procedure is applied.

Input:

- Recommended statistical significance level: $\alpha = 10\%$
- Sample size : $m = 2$
- Observations:

$n_1 = 12$:

19730	24210	19680	20140	22340	20490	20570	25970
19960	19550	20350	20990				

$n_2 = 8$:

18720	19170	19330	18790	23190	18170	18370	20990

- Check of model prerequisite "Samples are random"

The smaller sample is to small and cannot be checked. In the frame of the significance level $\alpha = 10\%$, for sample 1 the hypothesis "Sample is random" needs not to be rejected.

Hypotheses:

- H_0: Samples belong to the same basic population and therefore can be united
- H_1: Samples do not belong to the same basic population and therefore cannot be united.

Calculations:

- Assumption: the samples represent the basic population.
- Procedure (for $m = 2,\ n_1 \geq n_2$)

1. Sort the $(n_1 + n_2)$ observations in ascending order: $y_{(1)} < y_{(2)} < \cdots < y_{(n_1+n_2)}$
2. Mark the observations of the first sample by "1" and the second sample by "2"
3. Determine for each value y_i the empirical cumulative distribution functions

$$F_1(y_i) \text{ and } F_2(y_i) \text{ by } F_j(y_i) = \frac{\text{number of observations of } j^{th} \text{ sample } \leq y_i}{n_j}$$

4. Determine the maximum difference D of the two empirical cumulative distribution functions $D = \max(D_i) = \max_i |F_1(y_i) - F_2(y_i)|$
5. Determine decision values from ***Tab.***, according to chosen value of α for $n_1 \leq 25$: read $n_1 \cdot n_2 \cdot D_{1-\alpha}$ from *Tab.* and compute $D_{1-\alpha}$ for $n_1 > 25$ and $n_1 < 10 \cdot n_2$:

compute $D_{1-\alpha} = \left(S_{1-\alpha} - \frac{0.4 - \alpha}{n_1 + n_2}\right) \cdot \sqrt{\frac{n_1 + n_2}{n_1 \cdot n_2}}$ with $S_{0.95} = 1.3581$, $S_{0.90} = 1.2239$

$\Rightarrow$ Rejection of H_0 if $D > D_{1-\alpha}$

y_i	18170	18370	18720	18790	19170	19330	19550	19680	19730	19960
attribute	2	2	2	2	2	2	1	1	1	1
$F_1(y_i)$	0	0	0	0	0	0	1/12	- 2/12	3/12	4/12
$F_2(y_i)$	1/8	2/8	3/8	4/8	5/8	6/8	6/8	6/8	6/8	6/8
D_i	1/8	1/4	3/8	1/2	5/8	***3/4***	2/3	7/12	1/2	5/12

	20140	20350	20490	20570	20990	20990	22340	23190	24210	25970
	1	1	1	1	1, 2	1, 2	1	2	1	1
	5/12	6/12	7/12	8/12	9/12	9/12	10/12	10/12	11/12	1
	6/8	6/8	6/8	6/8	7/8	7/8	7/8	1	1	1
	1/3	1/4	1/6	1/12	1/8	1/8	1/24	1/6	1/12	0

$D = \max(D_i) = \max_i |F_1(y_i) - F_2(y_i)| = |0 - 6/8| = 0.75$

From *Tab.* follows for $\alpha = 0.10$: $n_1 \cdot n_2 \cdot D_{0.90} = 52$ and finally $D_{0.90} = 52/(12 \cdot 8) = 0.54$

Result: $\Rightarrow$ according to $D > D_{0.90}$ the hypothesis "Samples can be united" has to be rejected.

12.5 Tolerance Interval and Confidence Level C

12.5.1 Tolerance Interval

Interval within which, with a confidence level C, a specified proportion of a sampled population falls.

In practice, technical quantities such as design parameters are stochastic quantities but not constants. For example, the thickness of nominally identical plates will vary, and also, the fatigue lives of nominally identical components under the same load spectrum will be different. Even, if a technical quantity is virtually a constant, it must be considered a random variable due to the variability of its observed values, caused by the not fully accurately working measuring device or by error-prone readings of the observer. For this reason, in technical science the so-called tolerance interval is used (text basically *from HSB 04200-02).*

There are two kinds of tolerance intervals: *Statistical tolerance intervals* and *engineering tolerance intervals:* The statistical tolerance interval is a bound on an estimate of the proportion of data in a population. The engineering tolerance interval specifies the interval of technical acceptability considering characteristic attributes, e.g. from production tolerances. It is usually defined by the design engineer. For example, because of safety aspects the fatigue life of a component should exceed a specified design life value as minimum, or to avoid fitting problems the thickness of a plate should be 2.5 ± 0.2mm. These tolerance intervals are confined by tolerance limits as the engineering tolerance bounds mentioned before and by corresponding statistical tolerance limits.

Intervals consist of two types, the one-sided and the two-sided interval. For example, for above thickness of plates usually a two-sided engineering tolerance interval is used, whereas a one-sided engineering tolerance interval will be used for strength and fatigue life, because there is no infinity.

Statistical methods are used to check whether the value of the characteristic quantity x, such as a property or an observation test data, is within the engineering tolerance interval or not. If shape and parameters of the distribution of the characteristic are known, the interval can be determined, within which a specified portion p (see *Table 12-5*) of the values lies. For example, assuming that the thickness of a plate has a normal-distributed basic population with mean μ and standard deviation σ, a portion of p = 90% of these plates will have a thickness between μ ± 1.645σ. Hereby, μ − 1.645·σ matches with the so-termed p = 5%−quantile or 5%–fractile, respectively, and μ +1.645·σ with the 95%-quantile of the characteristic design parameter thickness. This two-sided engineering tolerance interval spans between both the quantile-defined limits (bounds), namely 5% and 95%.

Table 12-5: Quantile u_P of the standardized ND
P is probability, u_P is a 'distance factor' from the mean

P	0.5 %	1.0 %	5.0 %	10.0 %	90.0 %	95.0 %	97.5 %	99.0 %	99.5 %
u_P	-2.576	-2.326	-1.645	-1.282	1.282	1.645	1.960	2.326	2.576

12.5.2 Confidence level C

Range of estimates for an unknown design parameter. The level of C describes the likeliness, that the sample size can represent the basic population. Confidence interval is used for a parameter which 'pretty safely' contains the unknown value of the parameter.

From samples one obtains estimations for a statistical parameter. For instance, in the case of a ND the sample mean $\bar{x} = \Sigma x_i / n$ is an estimation of the parameter μ of the basic population. In many

cases it is desired to provide not only an estimated value but to indicate the accurateness of the estimated value. The measure of the confidence is expressed by the confidence level C.

The basic notion 'confidence level' is applied when determining confidence intervals and quantiles, see *Table 12-6.* Considering for instance a ND basic population with unknown mean value μ and unknown standard deviation σ, presuming *n* observations, then statistical theory can prove with a distinct probability that the unknown value of μ will be included in the stochastic interval $(-c \cdot S \leq \bar{X} \leq +c \cdot S)$. Here, $\bar{X} = \Sigma X_i / \mathrm{n}$ and $\mathrm{S} = \sqrt{\Sigma (X_i - \bar{X})^2 / (\mathrm{n}\text{-}1)}$ are the estimation functions for μ, σ and $\mathrm{c} = t_{0.95}(\mathrm{n}-1) / \sqrt{n}$ with $t_{0.95}(\mathrm{n}-1)$ represents the here desired 0.95-quantile of the Student t-distribution for $\mathrm{n} - 1 = \mathrm{f}$ degrees of freedom, which is applicable for n > 30. The value $t_{0.95}$ is given in tables, such as in *HSB 04200-03*.

For clarification in *Fig.12-6*, fifty of these sample-based confidence intervals (horizontal lines) for μ are generated by using a random generator and are then depicted in *Fig. 12-6*. At the bottom of the figure the (probability) density function *f* of the basic population is plotted, where the samples have been taken from. This makes it possible to compare the width of the sample-based intervals with the width of the standard deviation σ of the basic population. For the example, n = 10 with C = 90%, follows from a Student table c = 0.580, and the information that in six of the 50 tolerance intervals the mean μ is not contained.

The choice of the confidence level C is determined by considerations on 'safety' (risk) and usability or practicable use. A confidence level of 100% gives a fully reliable confidence interval but does not give user-practicable design information. A confidence level of 50%, in general, results in a narrow interval for μ, however, it will include the real value of μ in 50% of all cases, hence, only low reliability is given. The most often chosen confidence level in engineering is 95%, but more seldom the values 90% and 99% are also used. For comparison, for the mentioned three confidence levels (90%: c = 0.580, 95%: c = 0.715, 99%: c = 1.028), the associated intervals are given for the 36th sample at the bottom of the figure. In *Fig.12-6* it is clearly outlined that for the envisaged 'sample 36' with $\bar{x}$, s as statistical parameters of the sample, the desired μ will be only captured if C = 99%.

The figure also shows how the probability increases with increasing confidence level and that the confidence interval contains the real mean of the basic population, μ.

Also, for the quantile p the notion confidence level is applied despite of the fact that it is not a parameter but a minimum portion (0 < p < 1) of the basic population which shall contain the interval. So, the confidence level C is a measure of the 'safety' that the interval contains at least the desired portion p of the basic population, here of μ.

In the context above:

> *The physicist Marian von Smoluchowski (1872-1917) wrote shortly before his death the article: "On the notion of chance and the origin of the laws of probability in physics.*
> *" How is it possible that the effect of chance can be calculated, i.e. that random causes have lawful effects?"*
> *By 'lawful effect' he meant the law of the empirical mean or, equivalently, the law of large numbers. The 'calculable chance' is revealed in the predictable relative frequencies or generally in the empirical means formed with the random test outcomes of an experiment.*

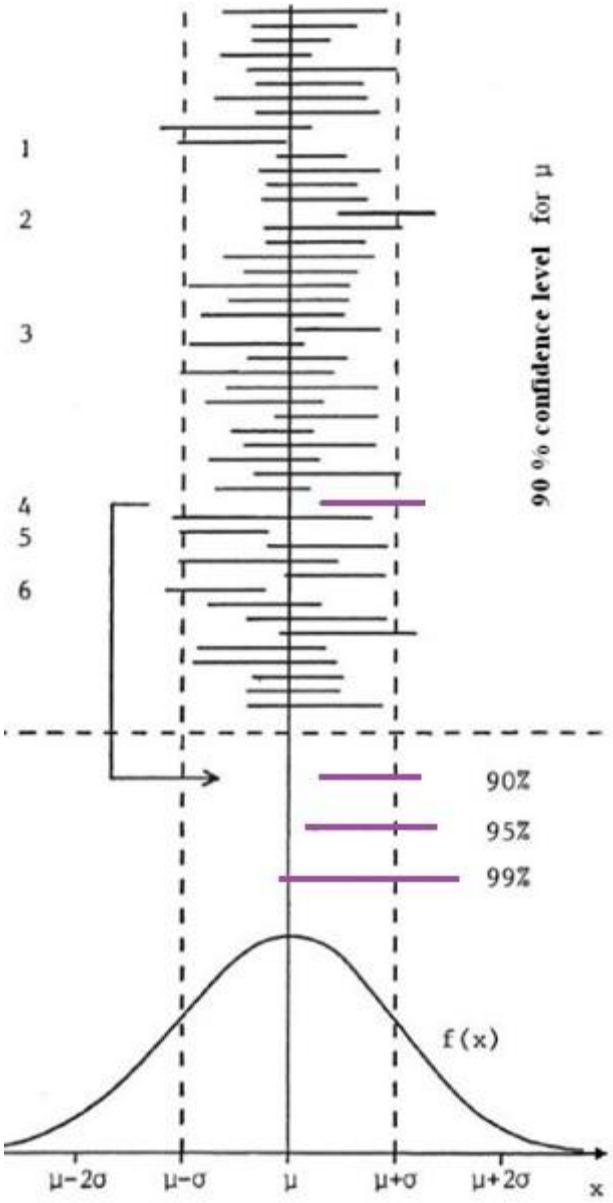


Fig.12-6: Plot of the (probability) density function f of a ND basic population and confidence intervals of 50 random generator-determined samples including 6 outlying ones, with C = 90% for μ. Sensitivity of the 36th tolerance interval to various confidence levels (*HSB 04200-03)*

12.6 Factor of Safety (FoS) Concepts (‘deterministic format’)

FoS are applied to decrease the chance of failure by capturing the uncertainties of all the given variables outside the control of the designer. FoS-values are based on long minimum risk experience.

In the design process the scatter of individual values and parameters is usually treated by using fixed deterministic *Factors of Safety*, which act as load increasing multiplying factors *FoS* and should be called, more correctly, *Design FoS*. A *Safety Concept* means to implement reliability into the structural component by ‘capturing’ the uncertainty of the design parameters! It can just provide an unknown safety distance between load (i.e. ‘stress’ S) and load resistance (‘strength’ R). FoS capture uncertainties, small inaccuracies, and simplifications in analyses w.r.t. manufacturing process, tolerances, loadings, material properties (strength, elasticity, ..), structural analysis,

geometry, strength failure conditions. FoS do not capture missing accuracies in modeling, analysis, test data generation and test data evaluation!

FoS are used to counteract the risk of a structural failure by capturing the uncertainties of all the given variables outside the control of the designer. Presently, in mechanical engineering the loading is increased by one lumped FoS *j*, and in civil engineering the procedure is improved by using several partial Design FoS γ for the uncertain stochastic design variables. These chosen *FoS* are based on long term experience with structural testing. Depending on the risk consequences different classes of *FoS* are applied, e.g. for manned space-crafts higher *FoS* are used than for unmanned space-crafts.

In the deterministic concepts or formats the worst case scenario is usually applied for loadings considering temperature, moisture, undetected damage. Further, a load is to increase by a 'Design FoS' and the resistances are to decrease. For strength, statistical distributions are used. If the loading is also based on a statistical distribution, then one speaks about a semi-probabilistic format.

Basic question of engineers in mechanical and in civil engineering is: "How much could one further increase the loading". What is the reserve?

12.6.1 Deterministic Global Safety Factor Concept, Mechanical Engineering (aerospace)

Concept, that deterministically accounts for design uncertainties in a lumped (global) manner by enlarging the 'design limit loads' through multiplication with a design Factor of Safety FoS j.

- **Present safety concept in space engineering = an *improved global deterministic format*** *(intention: semi-probabilistic)* = 'Simplest' Partial Safety Factor concept: It discriminates load model uncertainties considering factors (K_{Model} , $\boldsymbol{K_{Project}}$, see *Table 1*) from design uncertainties which are considered by j ! Example: $DUL = j_{ult} \cdot$ design limit load DLL

  (*UL represents the real test fracture load, therefore the virtual design value must be discriminated by writing DUL).* It is based on one global FoS and a statistically reduced resistance.

  The to be applied values j for the FoS are risk or task driven. Facts to consider are:

  - Different application in cases of manned, un-manned spacecraft
  - Design verification by Analysis only' (*by the way the usual case in construction*)
  - Different risk acceptance attitude of the various industries.
  -

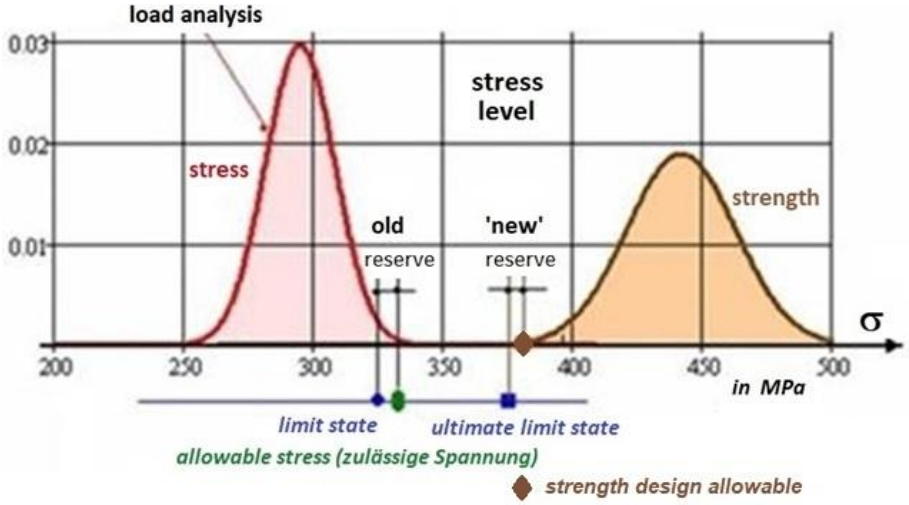


Fig.12-10: Visualization of the present ('new') and the obsolete (old) safety concept

For information, an urgent look back on the

"Old Safety Concept of Allowable Stresses, applied in mechanical and civil engineering".

At least, since 1926 the civil engineer M. Mayer questioned above safety concept, where the *resistance was reduced* by a safety factor. This gives no accurate results in the case of non-linear behavior. In construction this was replaced in DIN 1054 by the Partial Safety Factor concept, which applies safety factors and combination factors for general service loads, live loads, snow, ice loads, and wind loads. Temperature effects are specified in DIN 1055-100.

LL: The citation of the term 'allowable stress' is restricted to the former 'Concept of Allowable Stresses' and shall be not applied within present concepts anymore. Why? The usual application of the abbreviating term 'allowable' instead of 'strength design allowable may not confuse, but 'allowable stress' does confuse because it is valid

j · allowable stress = strength design allowable *! (see figure above)*

Table 12- 7 provides FoS values *j* now applied in aerospace.

Table 12-7: Some global (lumped) FoS j in aerospace.

Structure type / sizing case	FoSy $j_{p0.2}$	FoSu j_{ult}	FoSy *for verification 'by analysis only'*	FoSu *for verification 'by analysis only'*	*Design Factor*	FoSy $j_{p0.2}$	FoSu j_{ult}	j_{proof}	j_{burst}
	external loadings incl. extern pressure					internal pressure			
Metallic structures	1.1	1.25	1.25	1.5		1.0	1.0	1.2	1.5
FRP structures (uniform)	?	1.25	-	1.5		1.0	1.0		1.5
FRP structures (discontinuities)	-	1.25	-	1.5	1.2				
Sandwich struct.: - Face wrinkling - Intracell buckling - Honeycomb shear	-	1.25 1.25 1.25	-	1.5 1.5 1.5					
Glass/Ceramic structures	-	2.5	-	5.0					
Buckling	-	1.5	-	?		(ECSS-E-30-10, spacecraft)			

Note on the given FoS values in *Table 12-7*:
A material with a high coefficient of variation cov disqualifies itself, when computing the statistically derived values. Therefore, one must not penalize it further like performed for glass and ceramics in *Table 12-7*. Besides, the term $j_{p0.2}$ = 1.0 could be deleted for brittle composites with thermoset matrices, however should be kept for some future composites with thermoplastic matrices.

FoS air-craft versus space-craft:

When preparing the HSB sheet [*Cun12*] the author sorted out that there practically is no different risk view between air-craft and space-craft:

Spacecraft: using a dynamic load model obtaining a load prediction LL with a load model uncertainty considering factor j_{LM} =1.2 delivers a Design Limit Load DLL= 1.2 ·LL and it follows DUL = L· j_{LM} j_{ult} =1.2 ·1.25 = **1.5 , also** !

This is the practically the same as for aircraft below !

The DLL level is applied in spacecraft in fatigue life demonstration.

Aircraft: Defining a Limit Load LL (Sichere Last) delivers DUL = LL·**1.5.**

Further, the author found a conflict of terms within aerospace:

There is a conflict because the spacecraft Design Yield Load DYL is termed in aircraft just Limit Load. Recommendation: Use DUL in aircraft, too, as AIRBUS Toulouse still began within the EU-MAAXIMUS project. *The author participated as reviewer*. Then it is clear and no discrepancy with spacecraft will exist anymore.



Personal Experience:
"A safety distance pays off ".
Comodo waran ≈ 80 kg

LL:
**A FoS is given and not to calculate as a Margin of Safety MoS or the Reserve Factor RF = MoS + 1.*
**A MoS is usually the result of worst cases assumptions that does not take care of the common actions of the stochastic design parameters and thereby cannot take care of their common failure action and probability*
**A failure probability here is a 'joint failure probability' because it considers the probability of joint acting.*

12.6.2 Partial Safety Factor (PFoS) Concept in Civil Engineering (construction)

Concept, that replaced the also in civil engineering formerly used global safety factor concept by setting partial safety factors γ according to the necessity to separately capture the different uncertainties of the stochastic design parameters or variables on action side (loadings) and the resistance side (material, geometry, modelling).

The governing variables consist of:

(1) Loading variables acting on the structure or load effects in the structure such as residual stresses, and of

(2) Resistance variables of the structure or of the strength of the materials in the structure. The characteristic values of loads and resistance, or of load effects and material strengths, are chosen as specific quantiles in their respective (probability) density distributions f(x).

The requirements for the loading, not just loads, and the resistance quantities are set such that possible un-favorable realizations of loads (e.g. misalignment) and resistances, as well as their possible simultaneous occurrences, are accounted for to an extent that achieves a satisfactory safety class. Load combinations, Combination Rules for the individual scattering actions (such as permanent actions G, variable actions $Q \cdot \psi$, with $\psi < 1$ a coefficient, considering the frequency of occurrence, are chosen which again aims at unfavorable realizations of a small failure probability.
As with the simple deterministic safety concept, one requires again the accepted safety levels that can be achieved by multiplying action and resistances by partial safety values γ via increasing loads and reducing resistances. Each loading and each resistance has its own Partial FoS (PFoS) value γ which must be fixed for each influence according to the associated uncertainty. It is necessary to check which influence is favorable and which is unfavorable.

The PFoS concept is formulated in DIN EN 1990. It is based on the partial safety factors for the single (design) limit states:

* Limit State of load-carrying capacity (Grenzzustand der Tragfähigkeit GZT ≡ Ultimate limit state ULS or DUL)
* Limit State of serviceability (Grenzzustand. der Gebrauchstauglichkeit GZG ≡ serviceability limit state SLS)
* Requirements to ensure durability (Anforderungen zur Gewährleistung der Dauerhaftigkeit → C_d). The actions to be taken into account in the structural design (load assumptions) are regulated in DIN EN 1991

  Permanent actions: Characteristic value is usually the mean value if the cov < 0.10. For higher values the 95% upper or 5% lower quantile is to consider, *[Hol13]*.

  Varying actions: Characteristic value is usually the 98% quantile, representing a value that is met once in 50 years. In order to capture the frequency of occurrence an associated correction factor ψ for combinations is applied.

For the proof of ULS (load-carrying capacity ≡ DUL), the fixation of the characteristic value (indexed $_k$) of each essential characteristic is important. In general, the characteristic value should be a cautious estimate of the mean. This means that, in cases of no much knowledge about the basic population considering μ, σ or cov_μ and due to a small sample size n, an unfavorable transition from uncertain knowledge and some sample tests to the basic population is to perform (*see a following example*).
This is described in construction, fully analogous to the mechanical engineering formula that reads on the stress level in linear case $RF = R /(\sigma \cdot j)$ by the formulation (see the example later)

$$RF = (f_k / \gamma_{Resistance}) / (\sigma \cdot \gamma_{Stress}) .$$

Often, newer design methods allow more complex approaches that allow a higher utilization of the build materials and thus a higher loading, but in most cases the safety standards have also been increased due to experienced damage cases and increasing safety requirements resulting in higher loads, whereby a proof of existing buildings being load-bearing structures according to current standardization will rarely be possible. For rehabilitation of bridges actual present loading scenarios are monitored and presently evaluated.

Table 12-8: Some partial FoS γ in construction.
(cross-section load level is usually addressed)
Indices: M = Material, m = material scatter, R_d =Resistance design)

	γ_M	γ_m	γ_{Rd}	γ_{Rd1}	γ_{Rd2}
Concrete, c	1.5	1.39	1.1	1.05	1.05
Steel, s	1.15	1.08	1.08	1.025	1.05
non-metallic, nm fiber-grid rebar		1.3 (1.5 DIBt) 1.3			

Action S (Einwirkung E): Estimation of load events, determination of combinations of loadings, fixation of Load Cases and preferably also of a minor number of design driving Dimensioning Load Cases (loads should be statistically based). For reasons of comparison some PFoS are given:
Permanent loads: favorable $\gamma_G = 1.0$, unfavorable $\gamma_G = 1.35$.
Variable loads: favorable $\gamma_Q = 0$, unfavorable $\gamma_Q = 1.5$.
Permanent loads are defined as mean + 3 x standard deviation σ.

Resistance R (Widerstand W): Running test series to evaluate average strength $f_k \cong \bar{R}$ and coefficient of variation cov. Values are defined for γ_M Material, γ_m material scatter , $\gamma_M = \gamma_m \cdot \gamma_{Rd1} \cdot \gamma_{Rd2}$ with γ_{Rd} (design) model uncertainty, γ_{Rd1} analytical/numerical model and γ_{Rd2} geometry uncertainty.

At present for non-metallic materials (suffix$_{nm}$) PFoS γ are defined that capture the different behavior of the various novel fiber reinforcements in construction. To consider are GF (reinforcements of polymer matrices GFRP) and CF (reinforcement of concrete matrix CFRC). Basalt fiber reinforcement is going to become a qualified material, presumably BsFRP and BsFRC. Aramid F and natural fibers are under investigation. Addressing this bunch of fibers the general index $_{nm}$ should be replaced by a clear suffix because different FRPs will be used in future which might behave different to the present CFRP. Further, thermoplastic matrices will behave different to thermoset matrices. This is to consider.

Reduction by environmental factor C_E: textile grid 0.6, rods 0.5 (now required in the standard draft to be < than for the fiber strand in the grid !?)

EN 1992-1-1 enables a nonlinear section quantities determination in the limit states of load-bearing capacity and suitability for use. The section quantities and deformations are determined taking into account the non-linear section quantity-deformation behavior (physical). For SLS the PFoS γ may be set 1.

<u>Mind</u>: Construction industry does not perform design verification (proof) by a reserve factor RF > 1 but usually with the fact that the amount of reinforcement inserted in a beam or plate is greater than the statically required one.

Table 12- 9: Zu den Sicherheitskonzepten (= Nachweisformat) in Maschinenbau und Bauwesen
(intentionally in German)

*** Konzept der 'Zulässigen Spannungen' mit abgeminderten Widerständen: W / j, zulσ = R / j**
(Zur Erinnerung, ist ungültig)

Einwirkung (action S) $E < W / j$ (= statistisch abgeminderter Widerstand / globalen Sicherheitsbeiwert *j)*
Ungültig bedeutet, dass der Begriff 'zulässige Spannungen' nicht mehr zu verwenden ist!
linear elastisch, Spannungsniveau: hier gilt E *(≡ S)* = Spannung σ ; R = Festigkeit ≡ f
→ ***RF*** (spannungsbezogen) = $(R / j) / \sigma(E) > 1$ (ungeeignet für nichtlineare Probleme, Th. 2. Ordnung)

***Deterministisches Konzept der Erhöhten Einwirkungen: $E \cdot j$ Maschinenbau**
Einwirkung E / pauschalen Sicherheitsbeiwert $j < R$ (statistisch abgeminderter Widerstand R)
linear elastisch, Spannungsniveau: → ***RF*** (spannungsbezogen) = $R / \sigma(E \cdot j) > 1$
nicht-linear elastisch, Traglastniveau → ***RF*** (lastbezogen) = $W / (E \cdot j) > 1$

Semiprobabilistisches Konzept der Partiellen Sicherheitsbeiwerte: γ , Bauwesen,** *DIN EN 1990* **
Erhöhung der Einwirkungen E und Abminderung der Widerstände W → $E_d \leq W_d$, $E_d \leq C_d$
linear elastisch, Spannungsniveau : → $RF = (R_{charakt\ Material} / \gamma_{Tragwiderstand}) / (\sigma \cdot \gamma_{Einwirkung}) > 1$
nicht-linear elastisch, Traglastniveau : → $RF = (W_{charakt} / \gamma_{Tragwiderstand}) / (E \cdot \gamma_{Einwirkung}) > 1.$

Da Sicherheitsbeiwerte *j*, γ und damit auch *RF* keinen Hinweis zu einer Versagens-wahrscheinlichkeit p_f geben können, wird der sog. Zuverlässigkeitsindex β (Annahme: GausSNV!) herangezogen. Er ist risikobezogen geknüpft an die sogenannten Zuverlässigkeitsklassen (Reliability Classes) RC1 – RC3, die direkt mit den sogenannten Schadensfolgeklassen („Consequence Classes" gemäß EN 1990:2002 Anhang) CC1 bis CC3 verbunden sind, was analog zu Aerospace ist.

p_f	10^{-1}	10^{-2}	10^{-3}	10^{-4}	10^{-5}	10^{-6}	10^{-7}
β (1 a)	1,28	2,32	3,09	3,72	4,27	4,75	5,20
β (50 a)	–	0,21	1,67	2,55	3,21	3,83	4,41

(Failure probability relations $p_f = \Phi(-\beta)$ for 1 year (a) and 50 years (ageing), given in Eurocode 7)

Werte für 50 Jahre sind: RC1-CC1 (β = 4.3) oder RC3-CC3 (β = 3.3 → p_f = 1-0.99903 aus Gauss-Wahrscheinlichkeitsintegral $\Phi(-\beta)=1-\Phi(\beta)= p_f$. (Zu empfehlen: *Holschemacher K. : Entwurfs- und Berechnungstafeln für Bauingenieure, 6. Auflage, Bauwerk Beuth, 2013. [Hol13).*

Die Kombinationen der einzelnen streuenden Einwirkungen (actions) wie *Ständige Einwirkungen G, Veränderliche Einwirkungen Q·ψ* kommen durch *ψ <1 als die Auftretenshäufigkeit berücksichtigender Kombinationsbeiwert* zur Wirkung. Oder anders ausgedrückt, *ψ* berücksichtigt, dass es unwahrscheinlich ist, dass die ungünstigsten Kombinationen gleichzeitig auftreten.
Aus den Bemessungswerten der Einwirkungen werden die Bemessungswerte der Beanspruchungen ermittelt (Schnittgrößen, Dehnungen, Verschiebungen etc. [*Hol13*]). Im Fall einer linear-elastischen Berechnung des Tragwerks darf der Bemessungswert der Beanspruchungen aus der Überlagerung der Bemessungswerte der voneinander unabhängigen Einwirkungen ermittelt werden.
RF = 0.97 < 1 bedeutet nicht Bruch, sondern nur, dass die angestrebte Bruchversagens-wahrscheinlichkeit von < 10^{-6} für 50 Jahre Lebensdauer *variationsgrößen-abhängig* um Zehnerpotenzen abnimmt. Ein Wert *RF* = 1.03 kann aufgrund der Nichterfassung der Wahrscheinlichkeit von Kombinationen der unsicheren Bemessungsvariablen ein größeres Risiko enthalten als *RF* = 0.97 in einem anderen Fall !
Der Bemessungswert des Tragwiderstands wird nach den einzelnen bauartspezifischen Bemessungsnormen bestimmt. Destabilisierende und stabilisierende Einwirkungen sind zu berücksichtigen.

Table 12-10: Reliability index β , reliability classes RC linked to the consequence classes CC [Hol13]

Tafel 1.5b: Zielwerte des Zuverlässigkeitsindex β

Zuverlässigkeitsklasse	Zielwert für β	
	Bezugszeitraum 1 Jahr	Bezugszeitraum 50 Jahre
RC 3 verknüpft mit CC 3	5,2	4,3
RC 2 verknüpft mit CC 2	4,7	3,8
RC 1 verknüpft mit CC 1	4,2	3,3

Tafel 1.5c: Schadensfolgeklassen

Schadens-folgeklasse[1)]	Merkmale	Beispiele
CC 3	Hohe Folgen für Menschenleben oder sehr große wirtschaftliche, soziale oder umweltbeeinträchtigende Folgen	Öffentliche Gebäude mit hohen Versagensfolgen (z. B. Konzerthallen, Tribünen)
CC 2	Mittlere Folgen für Menschenleben, beträchtliche wirtschaftliche, soziale oder umweltbeeinträchtigende Folgen	Öffentliche Gebäude mit mittleren Versagensfolgen (z. B. Wohn- und Bürogebäude)
CC 1	Niedrige Folgen für Menschenleben und kleine oder vernachlässigbare wirtschaftliche, soziale oder umweltbeeinträchtigende Folgen	Landwirtschaftliche Gebäude ohne regelmäßigen Personenverkehr (z. B. Scheunen, Gewächshäuser)

[1)] Abhängig von Tragwerksart und Bemessungsstrategie können die Teile eines Gesamtragwerks unterschiedlichen Schadensfolgeklasse zugeordnet werden.

12.7 Determination of a Design Value

Value of a property used in design that is assumed to capture its uncertainty.

If one or more of the statistical parameters or even the shape of the distribution are unknown, the still described statistical tolerance interval has to be used. In order to be able to determine such an interval, statistical data (observations) must be available. A statistical tolerance interval is the interval within which - with a confidence level C - at least a specified or a desired probability portion p (generally termed reliability probability P) of the values of the characteristic will lie. If these tolerance intervals are accurately determined, then with a confidence level C the hatched area in *Fig.12-11* is at minimum the probability portion *p*. Due to the required confidence level *C*, a statistical tolerance interval will usually contain a larger portion than the specified portion *p* of the characteristic.

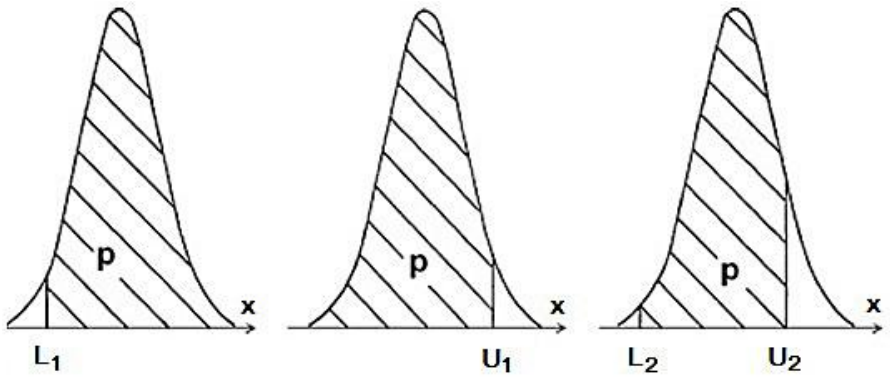


Fig.11: L_1 = lower one-sided statistical tolerance limit, U_1 is upper one-sided tolerance limit, L_2 is lower two-sided tolerance limit, U2 is the upper two-sided tolerance *limits. p is a given portion of the basic population*

L_1 represents an A-design allowable (P = 99%, C = 95%) if n = 298 observations,
L_1 represents a B-design allowable (P = 90%, C = 95%) if n = 29 observations.

To reduce the difference between the expected and the specified portion, all available information should be used. *Fig.12-12* displays the statistically caused loss of uncertainty with a gain of knowledge on the basic population. *The best prediction is to expect if the $cov_\mu = \sigma / \mu$ is known, and the mean μ of the basic population can be estimated from mean $\bar{x}$ and standard deviation s of the sample. Naturally, this procedure requires that the cov_μ of the basic population is a priory known (given, e.g. cov_μ = 5% for R_m of a distinct steel) or the cov_μ needs not to be estimated via the sample parameters $\bar{x}, s$. *See the following examples, please*. *The maximum difference is to expect if both statistical parameters μ, σ have to be estimated from $\bar{x}$, s.
In any case, the difference between the statistical parameters of sample population and basic population decrease with increasing sample size n. Therefore, in a case that several samples are available, it should be tried to combine (to pair) them, but considering thereby the respective statistical checks. A possible unification of several samples is always helpful.

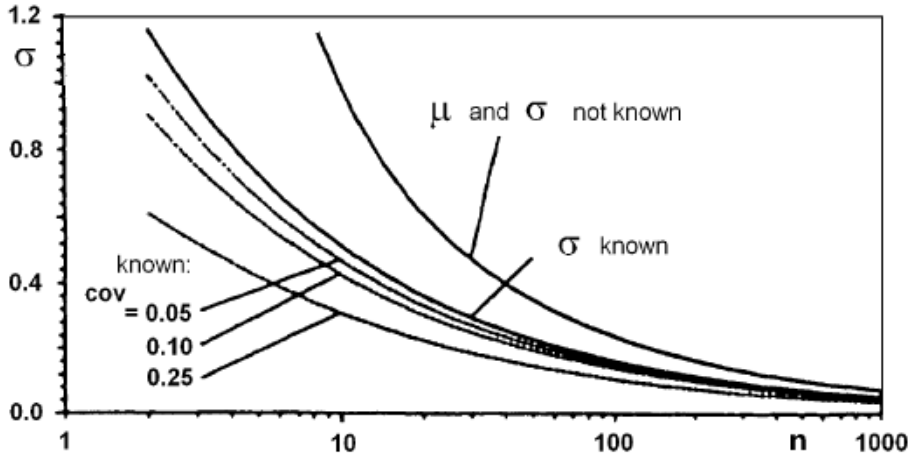


Fig.12: Expected additional width in standard deviations σ in dependence of sample size n for different knowledge of the statistical parameters μ , σ , cov_μ of the normal-distributed basic population (valid for a specified reliability probability P = 90% and confidence level C = 95%)

***LL**: In order to get p_f small, the designer does not use mean values μ for the strength in design verification but statistically reduced ones. High mean values are not exploitable if the scatter is very wide. In this respect, it is always cheaper if a material or structure can be produced in a tightly tolerated manner*

12.8 Determination of Strength Design Allowables

12.8.1 General

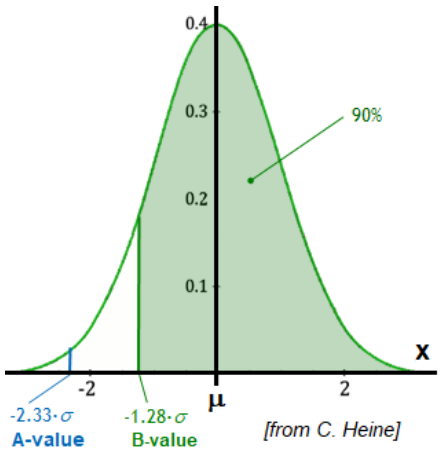
Airworthiness Requirement CS 25.603 "Materials" demands, that for all safety-relevant parts materials must be used, who's durable suitability is proven by tests or based on experience, by use of approved specifications with respect to environmental influences such as temperature, humidity. Industrial specifications, like e.g. Airbus material specifications (AIMS) are accepted in the according AMC 25.603.

CS 25.613 "Material Strength Properties and Material Design Values" deals more detailed with the strength properties themselves. It is required that the design values must be determined on a

statistical basis and based on a sufficient number of tests, [*C. Heine, Airbus, IASB*]. It is distinguished between 2 probability classes, depending on the structural design concept being used:

* Is the load carried only by a single part, who's failure would lead to the failure of the whole component, the strength design allowable (= design value) must be determined with a probability of 99% → value is defined as A-Value (T99-value)
* In case of so called redundant structure, where in case of the failure of a part the loads might be distributed to other parts, the design value must be determined with a probability of 90% → value is defined as B-Value (T90-values), at least 90% data exceed the design value)
* In any case, a confidence level of 95% is required.

For strength the one-sided lower interval is needed. Whether a distribution is suitable is checked by statistical tests, e.g. Student's t test. If no adequate distribution can be found, an analysis can be performed, provided the sample size is sufficiently large. For that purpose all individual test results are sorted in descending order. The A- and B-values are determined by "counting".



Boeing uses for 29 test results:
B ← the lowest value
A not determinable.
for 299 test results:
A ← the lowest value
B ← 22nd lowest value.

$$A-value = \mu - k_{99} \cdot \sigma$$
$$B-value = \mu - k_{90} \cdot \sigma$$

Fig.13: Determination of A- and B-values in case of ' No Distribution *suitable' [Mil Hdbk]. The factors k are given in handbooks, see also Table12-9.*

Aiming to gain fidelity requires a pooling of data which means combining data from different test data sets together under the pre-condition "Only permissible if there are no significant differences between the groups". Thereby the data sets are to check by tests for goodness of mapping a Normal Distribution ND, a Weibull Distribution WD, or a Lognormal Distribution LogND. If non-normality is observed, then the data can be checked to determine if it fits a distinct distribution and then compute the basis values according if this distributions is a reasonably maps the data.

If ND is a reasonable distribution: The data sets to be pooled are standardized by dividing each value x by the mean $\bar{x}$ for that environment. This creates datasets which all have a mean of 1.0 and with a standard deviation of the samples s equal to the coefficient of variation ($cov_x = s / \bar{x}$) of the untransformed data set.

For fiber dominated properties it can be usually assumed: fiber-dominated strength and stiffness properties vary linearly with fiber volume fraction V_f. Then, the results can be normalized and statistics are computed for the normalized results.

Finally *Table 12- 4* displays the procedure when mapping a course of test data.

Table 12-4: Mapping Procedure of test data courses

Given:	*Course of a test data set of a sample*
Choice:	*Mapping function*
Mapping:	*Mapping with the chosen mapping function of the course can be performed by a statistical fitting tool like 'Minfehl' in the code Mathcad (example Fig.10-3)*
Check:	*Statistical check whether the chosen mapping function is acceptable or not (Table 12-4).*

To note:
The applicability of a ND provides many benefits due to the available manifold tools and data tables. Knowledge about the standard deviation of the basic population from experience with formerly measured similar material data (i.e. a similar basic population) gives reliability to the design data to be determined.

12.8.2 Reducing risk in the development process in order to minimize re-design

Often a sample data set with its cov_x captures just a small portion of the material used in the fabrication of the structural component, and might be not representative of the actual production material. The basic population is not clear, because the designer is confronted with the batch-to-batch variability. In order to remain conservative, this specific uncertainty is practically by-passed by an increase of cov_x before calculating the design values A, B of the basic population: For cov_x < 4% → 6% ; For cov_x > 8% an increase is not necessary because statistical reduction will do that, the material disqualifies itself. Above increased values account for sources of material variability, that may not present in the qualification material.

12.8.3 Calculations of A-value Strength Design Allowables and of Characteristic Strengths f_k

The determination and quality of design values essentially depends on the available statistical knowledge. Presented are two examples from [*HSB 04200-02*]:

* ***Example 4***: ND, no pre-information, σ , μ of basic population are unknown. Just sample data $\bar{x}, s$ is available
* ***Example 5***: ND, $cov_\mu = \sigma / \mu$ of basic population is known in addition to the sample data set $\bar{x}, s$.

This result is more reliable than with $\bar{x}$, s only.

Example 4: [*HSB 04200-02*], **ND, no pre-information, just sample data set $\bar{x}$, s**

Task: Determination of Design Values one-sided tolerance limit L_1

Input:

Significance level α;

desired confidence level C , reliability probability P

Often used probabilities and associated quantiles
The u-quantiles are numerically derived by integrating the Gauß probability integral

$$C,\ P = \Phi(x) = \frac{1}{\sqrt{2\cdot\pi}} \cdot \int_{-\infty}^{u} \exp\left(-\frac{x^2}{2}\right) \cdot dx$$

n = 15, $\bar{x}$ =102.7, s = 11.2, cov_x = 8.8 %
(in MPa)

96.1	96.5	95.4	94.7	105.3	110.1	92.6	107.3
120.7	94.8	101.2	123.2	82.3	114.2	105.6	

Statistical prerequisites to be checked:
recommended values

Sample is random (significance level 5%);

Sample population belongs to a ND
(significance level 10%)

$C,\ P$	$u = u_C$ or u_P (one-sided)	$u = u_C$ or u_P (two-sided)
50%	0.000	0.675
90%	1.282	1.645
95%	1.645	1.960
99%	2.326	2.576
99.9%	3.090	3.291

In the frame of the recommended significance level the hypotheses
Sample is random,
Sample population is ND need not to be rejected.

Calculation:

Given:

A-value (Mil HDBK) in aerospace with C = 95%, P = 99%,.

Chacteristic strength f_k in civil engineering with C = 75%, P = 95%.

Determination of a quantile p; determination of sample mean $\bar{x}$; calculation of

Lower one-sided tolerance limit $L_1 = \bar{x} - k_2(P, n) \cdot s$ from following figure or calculated from

Φ (u=1.282) = 90%,
Φ (u=0.674) = 75%,

$$k_2 = \frac{2\cdot n - 2}{2\cdot n - 2 - u_C^2} \cdot \left(u_P + u_C \cdot \sqrt{\frac{2\cdot n - 2 + n\cdot u_P^2 - u_C^2}{2\cdot n^2 - 2\cdot n}} \right)$$

* **Calculation of an A-value strength design allowable:**

From the figure follows for → k_2 = 3.49 and the lower limit → $L_1 = \bar{x} - k_2 \cdot s$ = 102.7 - 3.49 · 11.2 = 63 .

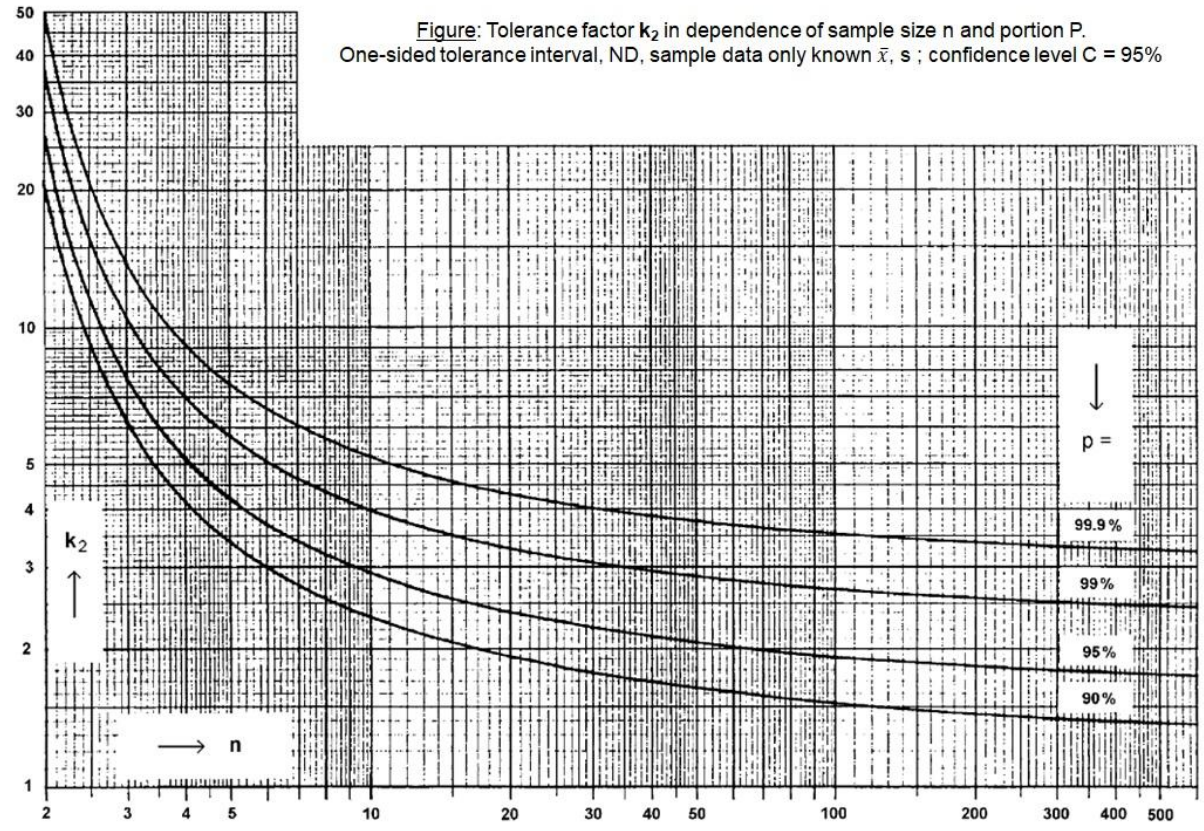
* **Calculation of a characteristic value f_k:**

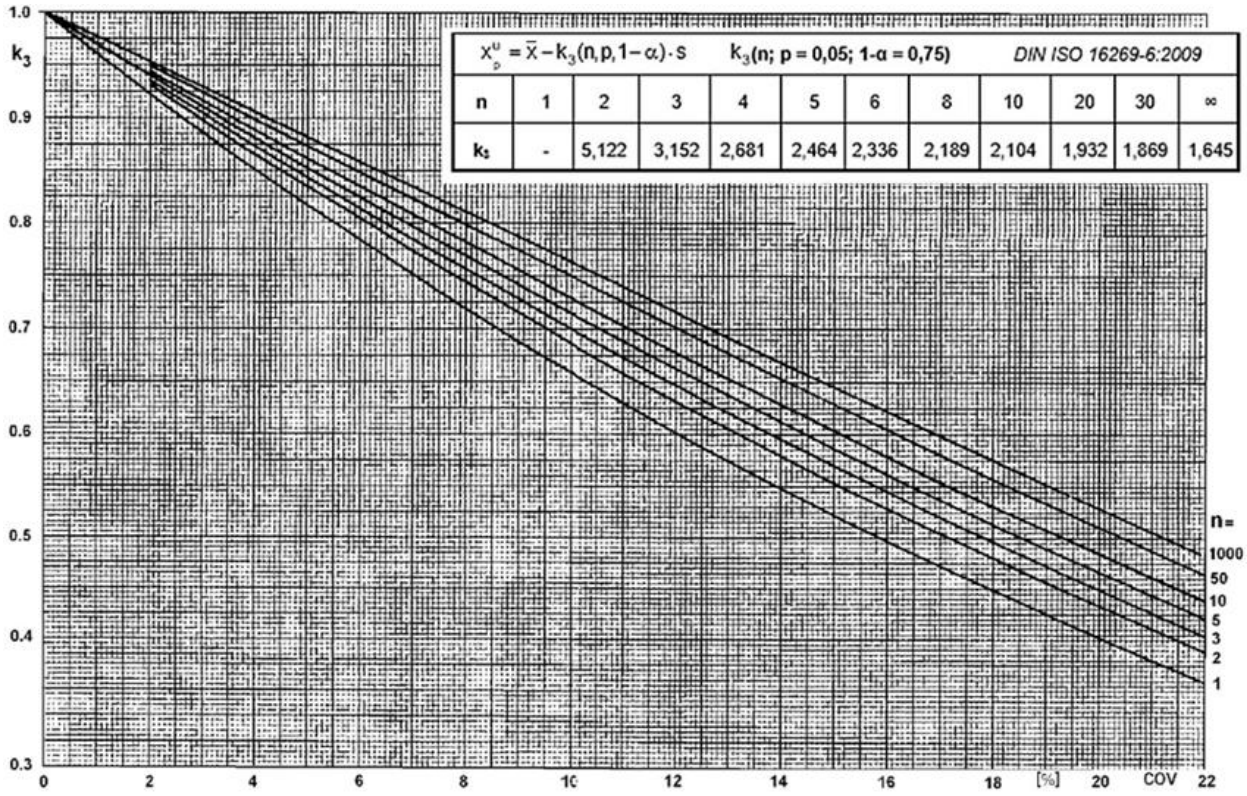
The k_2-condidering value is not given by an available figure, it must be computed
from above formula, yielding k_2 = 1.95, → $L_1 = \bar{x} - k_2 \cdot s$ = 81.

Notes:

Reducing f_k = 81 by a respective material partial FoS γ_M =1.3 leads to the design value f_d the size of which practically corresponds to the aerospace A-value 63, q.e.d. ! It can be concluded that f_k (termed characteristic in construction) is generally a slightly reduced mean value. A pure mean value is usually called typical or characteristic value! This made, that presently in construction a required mean value is to recalculate from f_k.

Table 12-9: k_2- and k_3-factor graphs [HSB04200-02], one-sided tolerance limits





$x_p^u = \bar{x} - k_3(n,p,1-\alpha)\cdot s$ $k_3(n; p = 0{,}05; 1\text{-}\alpha = 0{,}75)$ *DIN ISO 16269-6:2009*

n	1	2	3	4	5	6	8	10	20	30	∞
k_3	-	5,122	3,152	2,681	2,464	2,336	2,189	2,104	1,932	1,869	1,645

Figure: One-sided tolerance interval, ND, confidence level C = 95% , P = 99% → Lower tolerance factor k_3 in dependence of n, cov_μ.
Table: Compilation of the k3-factors for the lower limit of a 5% quantile with a one-sided confidence level of (1-α) = 0.75 with consideration of n construction

:

Example 5: [*HSB 04200-02*], **ND, $cov_\mu = \sigma / \mu$ of basic population is known**

Task: Determination of improved Design Values one-sided tolerance limit

Input:

Sample is random (significance level 5%); desired confidence level C; desired reliability probability P ; basic population belongs to a ND (significance level 10%),

$cov_\mu = cov_0 = 9\%$

Observations with evaluation: (in MPa)

n = 15, $\bar{x}$ =102.7, s = 11.2, cov_x = 8.8 %

96.1	96.5	95.4	94.7	105.3	110.1	92.6	107.3
120.7	94.8	101.2	123.2	82.3	114.2	105.6	

Statistical prerequisites to be checked:

In the frame of the recommended significance level the hypotheses

Sample is random, basic population is ND, $cov_\mu \leq cov_0$ needs not to be rejected.

A-value (Mil HDBK) in aerospace: with C = 95%, P = 99%, cov_0 = 0.10, n = 15

Chracteristic strength f_k in civil engineering : with C = 75%, P = 95%, cov_0 = 0.10, n = 15

Note: L_1 = represents an A-design allowable ($P = 99\%$, $C = 95\%$) if $n = 298$ observations,
L_1 = represents a B-design allowable ($P = 90\%$, $C = 95\%$) if $n = 29$ observations.

Calculation

calculation of the one-sided tolerance limit $L_1 = k_3 (P, n) \cdot \bar{x}$ from the figure above

* Calculation of an A-value strength design allowable: the lower limit

From the figure follows for $cov_0 = 0.09$, $n = 15 \rightarrow k_3 = 0.735 \rightarrow L_1 = 0.77 \cdot 102.7 = 79$

* Calculation of a characteristic value f_k:

A compilation of the k_3 factors for the lower limit of a 5% quantile with a one-sided confidence level of C = 0.75 taking into account the sample size n (normally distributed) can be found in DIN ISO 16269-6:2009.

Result: $L_1 = 79 > 63$. cov_μ could be improved with the sample results

Note considering Construction:

For the ND population, the k-factor of the 5 % quantile shall approximate the value of 1.645 for an infinite number of specimens. For ND populations with C=95%, the k-factor of the 5% quantiles or 95% survivability approximates the value of 1.645 for an infinite number of specimens. It turned out that classical statistics (DIN ISO 16269-6:2009) provide lower values than DIN EN 1990:2010 with a confidence level of C = 75 % and a sample size $n \geq 4$.

References

[1] Broekhof, H. and Hermens, C.A.: *Statistical Tolerance Intervals*. Fokker Report S-130, 1980

[2] DIN 55303, Teil 5: *Statistische Auswertung von Daten - Bestimmung eines statistischen Anteilsbereichs*. Beuth-Verlag GmbH, 1978

[3] Int. Standard ISO 3207-1975 (E): *Statistical Interpretation of Data - determination of a statistical tolerance interval*. ISO Standards Handbook 3 "Statistical Methods", First edition, 1979

[4] HSB 04200-01: *Introduction into statistical distributions, and notions*. Issue B, 2009

[5] HSB 04200-03: *Checking of the statistical prerequisites for various distribution functions*. Issue B, 2009

[6] HSB 04201-01: *Determination of lower tolerance limits in fatigue*. Issue C, 2009

[7] HSB 04205-01: *Fatigue life estimation in case of few test results with associated risk assessment*. .Issue B, 2009

LL: Safety Concepts can be interpreted as different models to obtain a response on the reliability of the design.

12.9 Probabilistic Safety Concept (Probabilistic Format)

Concept, that maps each single design parameter's uncertainty into a stochastic uncertainty, each described by a probability density function f.

Thereby, the so-called 'joint probability of failure' can be considered, which is caused by capturing the combined actions of the stochastic design parameters in the activated failure modes or it respects the combination of all scatter-affected design parameters. Goal of the more effortful probabilistic design is a *robust nominal set of the variable design parameters)*, linked to the multi-dimensional design parameter set captured in the so-called Design Point (*see a later example*).

In structural analysis *Design Verification (Proof of Design)* always has to respect structural reliability directly by a target value or indirectly by a FoS.

This occurs on different levels of structural reliability analysis with level 3 being the highest (reminder of a former common European research work with MAN*)*

Level III - Method [*Thoft-Christensen, Baker*]: calculations are made to determine the "exact" probability of failure for a structure, making use of a full probabilistic description of the joint occurrence of the variables which affect the response of the structure and taking into account the true nature of the failure domain

Level II –Method: certain approximate calculation procedure to obtain an approximation of the failure probability of a structure or structural system, generally requiring an idealization of failure domains and often associated with a simplified representation of the so-called joint probability distribution of the basic uncertain variables, the stochastic design parameters

Level I – Method: method of lowest reliability level in which appropriate degrees of structural reliability are provided on a structural element basis by the use of a number of partial safety factors, related to pre-defined characteristic or nominal values of the major structural and loading design parameters. It is widely applied in civil engineering. It is an improved method for a more reliable proof of design due to the replacement of a global single FoS by sets of Partial Factors of Safety PFoS γ

Level 0 – Method: usually applied method in aerospace, presented before as the global safety factor concept together with the use of increased loads and statistically reduced resistances.

In the fifties it was recognized that the classical handling of structural reliability by design FoS *j* and conservatively chosen characteristic values for material strength and other properties as well as loads and geometrical imperfections may be inadequate. Neither do constant FoS values reflect different uncertainties in these quantities nor can they properly take account of different target reliabilities. The application of statistical methods in the design and quality assurance was proposed but due to mathematical and numerical difficulties was only pursued qualitatively.

However in the seventies more powerful methods arose such as the 1st-Order and 2nd-Order reliability methods (FORM & SORM). The latter yields improved failure probability estimates p_f, respectively a reliability estimate $\Re = 1 - p_f$ or $\rightarrow 1 - \Re_i = p_{f,i} = P\,(g_i\,(Xj) \leq 0)$ for the *i* failure mode-related limit state function g_i. The method can handle arbitrarily distributed random vectors, can compute design sensitivities α_{ij} of the safety measures for stochastic and constant design parameters, can operate with structural systems, and have been extended to time variant reliability problems. With these developments the gap has been closed between classical reliability concepts for operational systems (failure rate) and structural reliability (failure state). Structural systems can

be designed together with the other operational systems in a unified manner based on probabilistic concepts.

It is necessary that the reliability methods are capable to handle statistical and model uncertainties. In practice several competitive failure modes might be active even in a single structural component and to be considered. Probabilistic design methods may be used as an assessment of the deterministic design or the design method needed if a *reliability* target $\Re$ or its complement p_f is assigned instead of a FoS. Alone the possibility to disclose the risk characteristics should interest a designer to apply structural probabilistic tools, whenever possible and reasonable.

The task here is to compute p_f or a good bound of it employing

$$p_f = P(R \le S) = P(R - S \le 0) = P(g(\underline{x}) \le 0) = \int_{Vol} f_{\underline{X}}(\underline{x})(dx) \ .$$

This leads to an ~~convolution~~n integral over the multidimensional density function $f_{\underline{X}}$, which is to be integrated in the failure domain $g \le 0$, i.e. when the stress *S* exceeds the strength *R*. The function $g(X_j) = g(\underline{X}) = 0$ is called limit state function. The vector $\underline{X}$ includes all stochastic design parameters, frequently also denoted as basic random variables, i.e. those which can be described statistically.

For this computational task an effective numerical method is necessary. Best known amongst the analytical methods is the above mentioned 1st-Order reliability method (FORM, see [*Com87*]), which uses a linear approximation of the limit state surface g = 0 and computes the *most likely failure point,* the so called *x**-point or *β*-point, [*Tho82*]. This is the point of the limit state that marks the minimum distance from the origin in the so-called standard normal space, see [*Sch81*]. This minimum distance, as defined by Hasofer and Lind [*Has74*], is termed β the so-called *reliability index,* being the percentile of the standard normal distribution Φ of Gauß

$$p_f = \Phi(-\beta) = 1 - \Phi(\beta) \quad \rightarrow \quad 1 - p_f = \Phi(\beta) = \Re$$

with $\Re$ the survival probability. For any resulting β the corresponding value for Φ can be taken from a statistical handbook such as [*Gra66*] or can be determined by a commercial mathematical code like MATHCAD. The reliability index β is deeply visualized in the connected *Chapter 13*.

The influence of the stochastic design parameters, also called uncertain *basic variables*, on the failure event within a distinct failure mode is best shown in terms of the co-called *α-values*. An α-value is a normalized measure $\sum \alpha_i^2 = 1$ showing the influence of the individual basic variable on the failure event. The α_i are derived from the gradient of the so-called state function with respect to the uncertain basic variables at the β-point and may be interpreted like a percent influence measure. A positive sign indicates an increase of $\Re$ if the mean value of the variable is increased and a negative sign (*typically found for load variables*) indicates a negative influence on $\Re$ for an increasing mean value.

For the most simple limit state, $g = R - S$, one has to treat just two basic random variables, one R and one S-variable. An example is a tensile rod. Assuming the variables to be normal distributed, β as well as p_f can be calculated from the standardized ND, even by hand,

$$\beta = \frac{\mu_R - \mu_S}{\sqrt{\sigma_R^2 + \sigma_S^2}} = \frac{\mu_Z}{\sigma_Z} \quad , \quad \Re = \Phi(\beta) \quad with \quad \Phi(-\beta) = \frac{1}{\sqrt{2\pi}} \int_{-\infty}^{x} e^{-t^2/2} dt \ .$$

Structural reliability analysis methods for direct target probability-based designs are mainly applied to special case design problems, to calibrate the load and a material FoS to be used in the

partial safety factor method, and to design to conditions where limited experience exists. Regarding the Combination Rules for Actions, the higher level probabilistic format captures, that it is unlikely that the most unfavorable combinations will occur simultaneously.

A comparison of deterministic *MoS* values with probabilistic results is pointed out on the simple '*R - S* problem' and described and executed in *Chapter 13*.

$$\sum \alpha_i^2 = 1\,, \quad MoS = \frac{\mu_R - k_R \cdot \sigma_R}{j \cdot (\mu_S + k_S \cdot \sigma_S)} \quad \text{with } k_R, k_S \text{ in subchapter 12.8 Tables .}$$

The chosen factors k_R, k_S depend on the applied stochastic model.

***LL**:*

(1) One basic goal of probabilistic design is to identify that set of design parameters that will experience minimum impact from the scattering.

(2) In deterministic design it is to show for each load case and each failure mode by computation through RF ≥ 1 , that the resistance of a structure is higher than the loading R > S (valid for loads, or cross section loads or stress combinations.).

(3) In probabilistic design, the work is more complex. It's objective is the evaluation of a probability of occurrence of a given failure state demonstrating p_f < target p_f (admissible) or of a survival probability ≡ reliability $\Re = 1 - p_f$ > required $\Re$

(4) With a probabilistic concept the individual failure probabilities p_{fi} are determined and from them a failure probability p_{fsys} for the full system can be computed. This system information can be not obtained by the deterministic concept.

12.10 Probabilistic Dimensioning of a full 'Failure System', Example launcher subsystem

The probabilistic design shall identify a design that will exhibit the smallest sensitivity to scatter. This design is referred to as robust design. Searched is the optimum combination of design variables. This procedure advantageously considers the combined action of the scattering, uncertain design variables. If several failure modes, for instance UD-strength failure modes, are activated the so-called Joint failure probability will be determined.

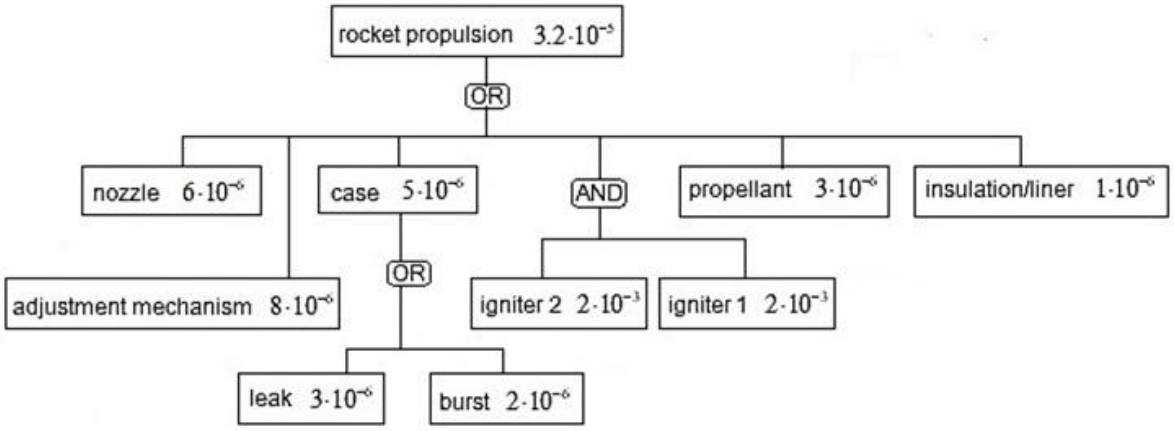
In a general failure system two different types of failure probabilities contribute to failure. These probabilities are provided by the so-called 'Failure-rate (Ausfallrate) responsible engineers' for electronic boxes or similar modules and by 'Failure-state responsible engineers (stress-men)' for the structural parts. The "failure-rate" of (electronic) parts can be captured by decreasing properties in the 'Failure-state' analyses. Its value depends on the aging time and is traditionally estimated from the still mentioned bathtub-curve, set up from experience. If one views in detail the lifetime of a structural part its rate of deterioration (≡ *micro-damage*) may also follow a bathtub-curve.

As early as 1985 for the pre-design of the Ariane 5 launcher target survival probabilities $\Re = 1 - p_f$ were fixed for the several structural parts! The following *Fig.12-14* presents an example of the Ariane launcher for a distinct mixed scenario:

The full system is divided into subsystems and these in turn are divided into elements. The individual elements are then assigned a required probability of failure so that the full system can meet the target value of the survival reliability $\Re = 1 - p_f$ of the launcher subsystem.

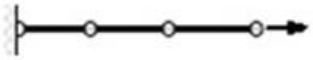
Fig.12-14: Procedure to estimate the reliability of a sub-system of the Ariane launcher

composed of failure rate-driven and failure state-driven parts (AND means redundancy)



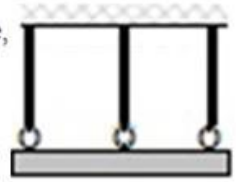
Series failure system:

The reliability of the series system is always smaller than that of the sub-system. The so-called ***or***-link rule applies. The greater the number of sub-systems, the more unreliable the overall system is (breaking of a tension rod and tearing out a bolt at a joint) $\Re_{sys} = \Re_1 \cdot \Re_2 \cdot \Re_3 = 1 - p_f$ with $p_f \leq \sum p_{f,i}$



Parallel failure system:

In the parallel system, there is only one combination that describes a system failure, namely that all components fail at the same time. The ***and***-link rule applies. (rivet rows in a connection). $\Re = 1 - [(1-\Re_1)\cdot(1-\Re_2)\cdot(1-\Re_3)] = 1 - p_f$



Combination:

The reality more often corresponds to a combination of both the failure systems.

In *Fig.12-15* two advantageous applications of the probabilistic tool will be demonstrated and where probabilistic modelling and computation were successfully applied.

*A reduced production tolerance width leads to a reduced mass which sequentially reduced further fuel mass savings

*For the pin connection an optimum number of pins for better assembly process and for reduced mounting stresses.

The author is grateful for the comments on this chapter from Dr. M. Grimmelt (Thanks Martin).



(1) Booster Wall Thickness tolerance:

Former : t = 8.2 +- 0.20 mm

Improved manufacturing : t = 8.2 +- 0.05 mm !

Reduction in scatter permits, when

keeping the same theoretical reliability value $\Re = 1 - p_f = 1 - 5 \cdot 10^{-6}$

a thinner nominal thickness is permitted: ***t = 8.1 +- 0.05***

Less mass!

And much fuel mass savings, in addition

(2) Optimum number of connecting pins of the Booster sections,

Probabilistic modelling of the geometrical tolerances of:

bore hole, pin, position (pitch), strength

in order to support a design decision on

asssembly + fixation of tolerance values.

The pitch was the driving design parameter.

For 180 pins:

Minimum restraints with minimum residual stresses could be achieved

Fig.12-15: Two examples for an essential design advantage after using a probabilistic tool. Booster, Ariane 5

12.11 Modelling Mode Interaction Equation, Multiple Modes and Interaction Exponent *m*

Generally faced are Failure Mode Interaction and Multiple Failure Domains. These are marked by a jointly generated increase of failure danger. Hence, an interaction procedure is to provide. Intentionally as an example the transversally-isotropic UD-material is taken here with the specific task: Derivation of a model to capture the influence of commonly acting Inter-Fiber-Failure *IFF-mode failures* by their *joint probability of failure* p_f , which practically is the failure probability $p_{f,sys}$ of a system. Such an equation will connect adjacent failure modes and shall be as simple as physically still reasonable.

12.11.1 Modelling of Failure Mode Interaction Domains

Derivation of the Interaction Equation:

Probability theory enables to interact modes by deriving an equation for the probability of failure p_f. First step thereby is to set up a reasonable *logical model of the failure system.* This will be here the still mentioned Series Failure System or union U of 3 IFF modes. This IFF-failure system delivers a failure probability

$$p_f\ (p_{f,\ell}) = 1 - (1-F_\perp^t)\cdot(1-F_\perp^c)\cdot(1-F_\perp^\tau) \qquad \text{or} \qquad (1-F_\perp^t)\cdot(1-F_\perp^c)\cdot(1-F_\perp^\tau) = 1 - p_f$$

since small $p_{f,\ell}$ are expected. Correlation among the $\ell = 3$ *component* failures would lead to a

smaller *system failure probability* p_f. Therefore above expression is conservative.

In the case of adequately chosen Weibull-distributed IFF-mode strengths $R_{\perp}^{t}$, $R_{\perp}^{c}$, $R_{\perp||}$ as density function WD is valid (*this function represents the distribution of extreme flaws).* It reads

$F_{WD} = 1 - exp[-(x/\lambda)^k]$ where the x-variable corresponds here to a fracture stress and where λ is the scale parameter, k ≡ 'Weibull modulus' as shape parameter (represents *m*).

F_{WD} describes the probability of failure by $exp[-(x/\lambda)^k] = 1 - p_f$.

This procedure is recommended for very brittle materials such as monolithic ceramics, concrete, brittle laminas. Taking the three failure danger portions and inserting them into above equation delivers

$$exp[-(x/\lambda_1)^{k1} \cdot exp[-(x/\lambda_2)^{k2} \cdot exp[-(x/\lambda_3)^{k3} = 1 - p_f \quad \text{or}$$
$$(x/\lambda_1)^{k1} + (x/\lambda_2)^{k2} + (x/\lambda_3)^{k3} = -ln(1 - p_f)\,.$$

After exchange of *k* by the still introduced letter *m* for the interaction exponent the following equation can be a model for the IFF body

$$(x/\lambda_1)^{m1} + (x/\lambda_2)^{m2} + (x/\lambda_3)^{m3} = -ln(1 - p_f)\,.$$

In the frame of the FMC instead of several stresses for the characteristic x the associate *equivalent stress* as representation of the multiaxial state of stress will be used for the envisaged IFF example. From the general UD equivalent stress set the 3 IFF ones are inserted

$$\left\{\boldsymbol{\sigma}_{\mathbf{eq}}^{\mathbf{mode}}\right\} = \left(\sigma_{eq}^{\parallel\sigma},\ \sigma_{eq}^{\parallel\tau},\ \sigma_{eq}^{\perp\sigma},\ \sigma_{eq}^{\perp\tau},\ \sigma_{eq}^{\parallel\perp}\right)^T \quad \rightarrow \quad x_1 = \sigma_{eq}^{\perp\sigma},\quad x_2 = \sigma_{eq}^{\perp\tau},\quad x_3 = \sigma_{eq}^{\parallel\perp}\ ,$$

which after inserting the average strength of each mode leads to the IFF interaction equation

$$(\sigma_{eq}^{\perp\sigma} / \bar{R}_{\perp}^{\sigma})^{m1} + (\sigma_{eq}^{\perp\tau} / \bar{R}_{\perp}^{\tau})^{m2} + (\sigma_{eq}^{\parallel\perp} / \bar{R}_{\perp\square})^{m3} = -ln(1 - p_f)\,.$$

Replacing the right side by 1= 100% failure danger delivers the IFF interaction equation

$$(\sigma_{eq}^{\perp\sigma} / \bar{R}_{\perp}^{\sigma})^{m} + (\sigma_{eq}^{\perp\tau} / \bar{R}_{\perp}^{\tau})^{m} + (\sigma_{eq}^{\parallel\perp} / \bar{R}_{\perp\square})^{m} = 1.$$

Full UD-interaction equation:

The influence of the FF-modes on IFF and vice versa can be taken into account similarly, representing the full joint failure probability. In other words: The joint failure effect of the interacting modes is captured for the example UD-material by the interaction equation

$$(\sigma_{eq}^{\square\sigma} / \bar{R}_{\square}^{\sigma})^{m} + (\sigma_{eq}^{\square\tau} / \bar{R}_{\square}^{\tau})^{m} + (\sigma_{eq}^{\perp\sigma} / \bar{R}_{\perp}^{\sigma})^{m} + (\sigma_{eq}^{\perp\tau} / \bar{R}_{\perp}^{\tau})^{m} + (\sigma_{eq}^{\parallel\perp} / \bar{R}_{\perp\square})^{m} = 1$$

(modelling means bar over = average).

From practical experience for each mode interaction the same value for *m* was applied.

12.11.2 Estimation of Weibull's Modulus

An estimation of Weibull's modulus *k* (*sometimes also the letter m is used instead of k which was the reason for the author to take the letter m*) is possible [*Pli95*] on basis of a mean value μ and the coefficient of variation of the parent distribution of each envisaged measured strength *R*. The limiting bound for the application is $cov_\mu < 25\ \% = 0.25$).

The scale parameter λ is slightly larger than the average fracture strength $\bar{R}$ and they are related $\bar{R} = \lambda \cdot \Gamma(1+1/k)$ with the Gamma function available from a mathematical Table .

Approximation of Γ function term $\Gamma(1+0.276\cdot/k^{0.776})$, [*Ono*19] $\rightarrow \cong \Gamma(1+CoV/1.2)$.

Example: $\Gamma(1+\text{cov}_\mu/1.2) = \Gamma(1+0.25/1.2) = \Gamma(1.21) = 0.91$ and $k = 1.2/cov_\mu = 4.8 \cong m$.

As estimations for mean $\bar{R}$ and cov_μ the values of a well sized sample are taken *without* considering the confidence interval C.

[Ono19] Kanji Ono: *A Simple Estimation Method of Weibull Modulus and Verification with Strength*. ono@ucla.edu. Appl. Sci. 2019, 9, 1575; doi:10.3390/app9081575

12.11.3 Modelling of Multiple Failure (example UD)

Equi-**biaxial** fracture stress *2D failure points, principal stress curves and failure bodies are addressed*

Trials to estimate the equi-biaxial transversal tensile fracture stress $\bar{R}_\perp^{\,tt}$ in an appropriate test had no success [*VDI97*]. Hence, if a $\sigma_2^t = \sigma_3^t$ *-multifold failure* will occur an analytical estimation is to provide. Using the information "$R_\perp^t$ *is Weibull-distributed*" a good estimation for the practically not sufficiently well measurable equi-biaxial failure stress $\sigma_\perp^{tt} \equiv \text{strength}\, R_\perp^{tt}$ will be possible and the fracture point $(\bar{R}_\perp^{\,tt}, \bar{R}_\perp^{\,tt})$ can be determined by cov_μ of the basic population using following the theoretical model of Awaji [*Awa78*] (*see also Ono*)

$$\bar{R}_\perp^{tt} = \bar{R}_\perp^t / \sqrt[M]{2} \quad with \quad M = 1.2/\text{cov}_\mu \ (\cong m \text{ or } \cong \text{k}) \quad \Rightarrow \quad \sigma_2^t + \sigma_3^t = I_2 < 2\cdot \bar{R}_\perp^{tt} \ .$$

Instead of Awaji's *M* the FMC exponent letter *m* with an experienced value shall be used in an example $m = 2.7 \rightarrow \ \bar{R}_\perp^t / \bar{R}_\perp^{tt} = \sqrt[m]{2} = 1.3$.

Equi-**triaxial** fracture stress *3D failure points, meridian curves and failure bodies*

For brittle isotropic materials the not measurable 3D- *tensile cut-off* point $(\bar{R}^{ttt}, \bar{R}^{ttt}, \bar{R}^{ttt})$, being the cap point of a failure body, can be estimated and also the failure body closing bottom point of porous materials $(-\bar{R}^{ccc}, -\bar{R}^{ccc}, -\bar{R}^{ccc})$.

The calculation delivers an estimation on the safe side following [*Awa78*]

Cap point , $I_1 > 0 : (\bar{R}^{ttt}, \bar{R}^{ttt}, \bar{R}^{ttt}) \rightarrow maxI_1 = 3\cdot\bar{R}^{ttt}$ (measured value $\bar{R}^t$, *estimated* $\bar{R}^{ttt}$)

$$\bar{R}^{ttt} \approx \bar{R}^t / \sqrt[Mt]{3} = \bar{R}^t / (3^{1/Mt}) \quad \text{with} \ \ Mt = \ln(2)/\ln(\bar{R}^t/\bar{R}^{tt})$$

Bottom point , $I_1 < 0 : (-\bar{R}^{ccc}, -\bar{R}^{ccc}, -\bar{R}^{ccc}) \rightarrow minI_1 = -3\cdot\bar{R}^{ccc}$ (closed fracture body)

$$\bar{R}^{ccc} \approx \bar{R}^c / \sqrt[Mc]{3} \quad \text{with} \ \ Mc = \ln(2)/\ln(\bar{R}^c/\bar{R}^{cc}) \ .$$

Examples tension and compression:

$\bar{R}^t = 4$ MPa, $\bar{R}^{tt} = 0.8\cdot\bar{R}^t$ MPa (assumed); ; $\bar{R}^c = 40$ MPa, $\bar{R}^{cc} = 51$ MPa:

$M^t = \ln(2)/\ln(\bar{R}^t/\bar{R}^{tt}) = 3.11$, $\bar{R}^{ttt} = \bar{R}^t / 3^{1/Mt} = 2.8$ MPa, $\max I_1 = 3\cdot\bar{R}^{ttt} = 8.4$ MPa

$M^c = \ln(2)/\ln(\bar{R}^c/\bar{R}^{cc}) = -2.85$, $\bar{R}^{ccc} = \bar{R}^c / 3^{1/Mc} = 59$ MPa, $\min I_1 = 3\cdot\bar{R}^{ccc} = 176$ MPa .

Fracture test data obtainable for *porous* solids (mode *crushing fracture CrF*) such as foam, nesting UD-material, grey cast iron and concrete are found in the previous chapters together with their failure bodies.

LL from the WWFE etc not to forget in probabilistic analyses:

- *Experimental results can be far away from the reality like an in-accurate theoretical model*
- *Theory 'only' creates a model of the reality. However, one experiment is also 'just' one realization of the reality.*

13 Probabilistic Assessment of a Deterministic Margin of Safety MoS

"*Is a CoStly Re-Design really justified if slightly negative MoS are encountered?* "

was a very essential issue for the author in design verification during his working life and due to this it shall be reported in this chapter. The following chapter captures the contents of the split paper [*Cun05*] nd shall contribute to a discussion about above very important question:

(1) How safe is a positive Margin of Safety (MoS)?
(2) What is the real meaning of a slightly negative MoS value because a MoS value itself does neither outline the size of risk nor specify the probability of failure?
(3) Is there a possibility to improve the 'holy MoS > 0 standard situation thinking'?

13.1 Introduction

A value of *MoS* = + 4% in the one case may incorporate a higher risk to fail than a *MoS* = –2% in another case. The author's intention is to make those engineers, who are responsible for 'approving and releasing' structural designs, aware of the real sources of risk. There is no compulsory need to reject a design if a *MoS* becomes slightly negative, e.g. –0.5%. No part of the structure will necessarily loose its functionality or will fracture, but an outright rejection could result in high additional CoSts as well as in a delay of the whole project due to the re-designing efforts required. A numerical example from the aerospace industry – experienced by the author - is used here to illustrate this topic.

Uncertainties can be found in the area of data input and in the analysis of the whole modelling process, a flow diagram of which is depicted in *Fig.13-1*. Stages with uncertainties comprise load analysis, testing and test data evaluation, choice of non-linear stress-strain curve, fabrication process, modelling, material properties and safety concept, choice of yield condition and fracture conditions, structural analysis procedure, and finally the determination of the *MoS* value itself. All these sources contribute to the overall structural **risk**, which let us define here arbitrarily as ***amount of CoSts*** *(direct and consequential)* ***incurred in the case of later failure*** ***the probability that the distinct failure occurs.***

In the *stress* analysis itself as well as in the failure criteria used in the *strength* analysis there are design parameters, which can exhibit relative large uncertainties. The nature of uncertainty of these parameters loads, strength properties, geometry, elasticity properties, etc. is either of *mechanical* one or of *statistical* one (*e.g. the way measurements are performed, lack of accurate information due to insufficient sample size in measurements of a specific design parameter*). Beside this, there is always some uncertainty in the *calculation model* (*e.g. solution procedure, FE mesh, etc.*) as well as in the *results* provided by *testing* and *evaluation* of 'raw test data'. Usually loads are those design parameters with highest uncertainty. Therefore, the design parameter *load* will be looked into more details in this paper in order to emphasize the real structural risks.

For obtaining 'Product Certification' in the aerospace industry, three (quasi-static) '*Design Verifications'* have to be performed in order to demonstrate that the final design possesses sufficient strength. This is achieved if *analytical* and/or *test* methods reveal both MoS_{yield}, and MoS_{ult} to be positive and if damage tolerance is proven (see *Fig.13-2)*. Therefore, a design engineer should not make the mistake to just look at the two *MoS*, where one might get a slightly negative *MoS* value, and forget damage tolerance which addresses static and cyclic failure. If a damage tolerance *demonstration* is to be performed, then MoS_{yield} (*linear analysis, low 'material*

stressing effort' Eff) together with damage tolerance could well compensate the MoS_{ult} (non-linear analysis, high *Eff*) design verification.

In some standards, for example the pressure vessel code ISO 14623, MoS_{ult} is considered to be the *design driver*, even in the case of *ductile* materials. However, past experience with ductile materials is in contradiction with such consideration as here MoS_{yield} should be the design driver with few exceptions depending on the size of the required *Factor of Safety FoS*. Until now, there is no general agreement on a unique procedure how to determine MoS_{ult} accurately. The various procedures applied tend to *under*estimate the real value by many percent.

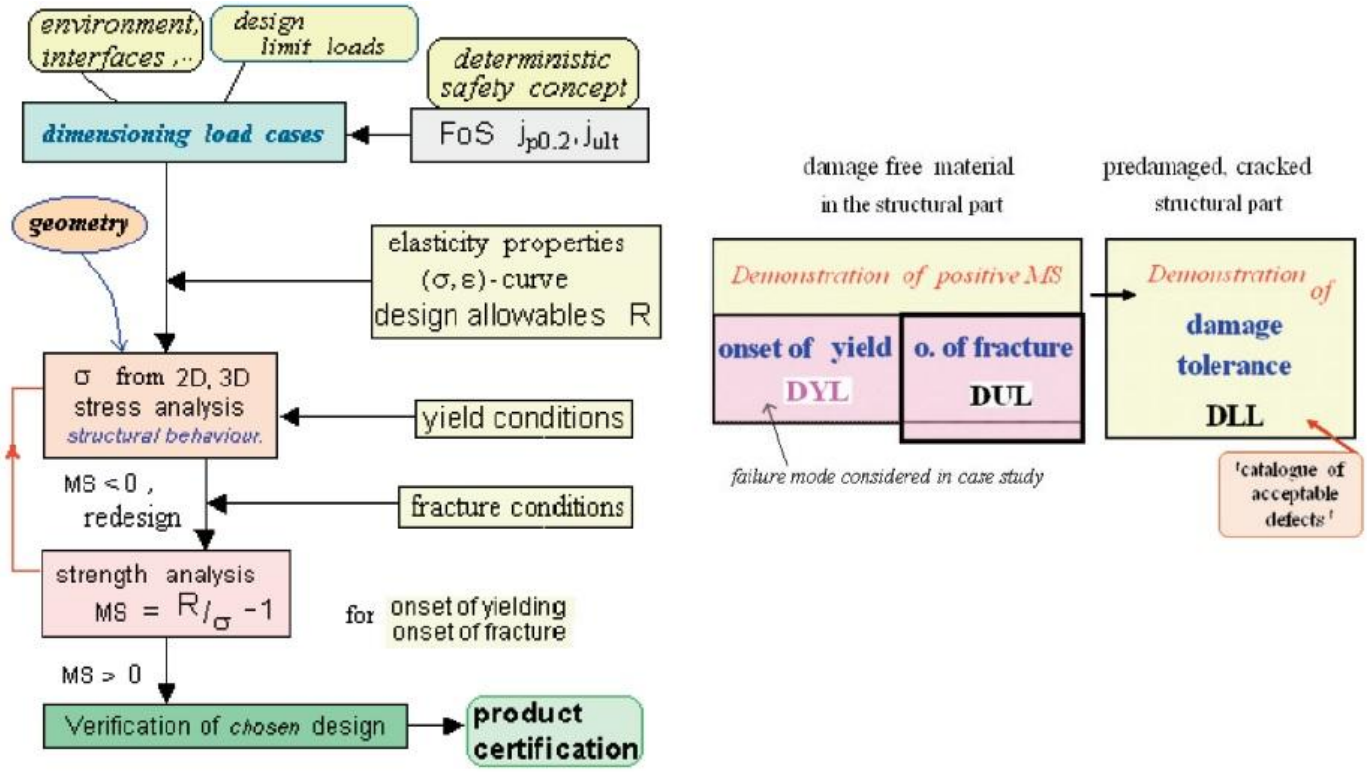


Fig. 13-1 (left): Flow diagram of structural analysis and its input.. FoS:= (design) factor of safety, MS =MoS:= margin of safety, R:= strength design allowable, σ:= stress.

Fig. 13-2 (right): Action quantities in static Design Verification. DLL: = maximum anticipated load or combination of loads the structure is expected to experience.

DYL: = Design Yield Load = DLL · $j_{p0.2}$, DUL: Design Ultimate Load = DLL · j_{ult}

Special aim here is '*Increasing the sensitiveness of the engineer for the actual risk'*. This will be hopefully achieved by presenting quantitative *MoS* values under some assumptions within a case study which compares results of the usual deterministic and the refined probabilistic procedure.

13.2 Factors of Safety (FoS), Load Cases and Margin of Safety (MoS)

13.2.1 Factors of Safety and Load cases

In the design process the scatter of individual values and parameters is usually dealt with by using fixed deterministic *Factors of Safety*, which act as load increasing multiplying factors and should be called, more correctly, *design FoS*. Suitable *FoS 'j'* are taken in the design input to ensure reliability of the structural part. These *FoS* are chosen based on long term experience with structural testing.

Depending on the failure consequences different classes of *FoS* are applied, e.g. for manned spacecrafts higher *FoS* are used than for unmanned spacecrafts.

The previously mentioned *DLLs* have to be multiplied by the *FoS* in order to obtain the Design Ultimate Load (*DUL*) or the Design Yield Load (*DYL*). All three loads are differently allocated *design loads*: *DLL* for fatigue analyses, *DYL* for onset of yielding (= deformation limit), and *DUL* for ultimate fracture analyses. Dimensioning aspects require that the structure has to withstand

- Design Yield Load $= DYL = j_{p0.2} \cdot DLL$ without detrimental deformation and
- Design Ultimate Load $= DUL = j_{ult} \cdot DLL$ without collapse.

The *FoS* $j_{p0.2}$ and j_{ult} determine the design yield limit and the design ultimate limit. E.g. in aerospace, a relatively low value of $j_{ult} = 1.25$ is taken if a static qualification test is foreseen. In case of untested hardware or 'design by analysis' a higher value is required, e.g. a value of *1.5*.

In the case of high pressure vessels the so-called Maximum Design Pressure (*MDP*) is to apply. It should be better termed Design Limit Pressure (*DLP*) [*ECSS documents at ESA*].

13.2.2 Margin of Safety (MoS) in Relation to Structural Reliability

In the design process any structure is first being dimensioned and then checked for each *single* failure mode, thereby distinguishing various strength cases, e.g. *onset of yielding* and *ultimate fracture*. Each of the required two *MoS* computations has to demonstrate a positive margin, $MoS \geq 0$, otherwise the structure is not considered to have met the strength design requirement.

In the following, a probabilistic analysis is used to evaluate the deterministic value *MoS*. Onset of is the driving failure mode because the usually applied materials are ductile behaving materials and yielding can be considered as the only failure mode in this example.
The various computations necessary to evaluate $MoS = MoS_{det}$ and compare it to a MoS_{prob} and a failure probability p_f are delineated in Table 13-1.

Table 13-1: Scheme for a deterministic and a probabilistic MoS determination, example pressure vessel. The prefix da *characterizes a resistance design allowable (load level) being not. a classical strength design allowable (stress level). The star * indicates design point x*-related.*

Deterministic	**Probabilistic**	
det R-S problem	**prob R-S problem**	**general probabilistic problem**
$\sigma_{eq}(p_{int}, d, t)$, $daR_{p0.2}$	COMREL-reduced problem $2X_j: \sigma_{eq}, R_{p0.2}$ distributions	$4X_j: p_{int}, R_{p0.2}, d, t$ distributions
worst case scenario *values for* determination of σ_{det}	probability of the stochastic design parameters to act together is considered by utilizing the *distributions for* determ. of σ^*_{prob}, σ_{prob}	
comparison of σ_{det} with $daR_{p0.2}$	comparison of σ^*_{prob}, σ_{prob} with $da\,R_{p0.2}$	--
MoS_{det}	p_f, $2\alpha_j$; MoS^*_{prob}, MoS_{prob}, from handbook, MATHCAD, or	p_f, $4\alpha_j$ COMREL-computed

Note: *FoS* are based on long engineering experience. The reliability assessment of the *FoS*, applied e.g. in aerospace, outlined that the structures are located in the failure probability regime of 10^{-7} through 10^{-9}. Different industry, however, has different risk acceptance attitudes [*Rac04*]. The *MoS* method exists in

parallel failure systems and do not capture the system. Probabilistic methods permit to regard the joint failure of a system.

13.3 Theoretical Background of the Probabilistic Solution

13.3.1 The Multi-stochastic parameter Problem (see previous chapter for details)

The function $g(X_j) = g(\underline{X}) = 0$ is called limit state function. The vector $\underline{X}$ includes all stochastic design parameters, frequently also denoted as basic random variables. Searched is the *most likely failure point*, the so called x^*-point or β-point, see *Annex I*. This is that point of the limit state that marks the minimum distance from the origin in the so-called standard normal space. This minimum distance, is termed β, the so-called *reliability index.* It allows to compute probabilities due to

$$p_f = \Phi(-\beta) = 1-\Phi(\beta) \quad \text{and} \quad \Re = 1-p_f = \Phi(\beta) \qquad (1, 2)$$

with $\Re$ the survival probability and the Gauss integral Φ.

The influence of the stochastic design parameters, also termed uncertain basic variables, on the failure mode is best shown in terms of the co-called sensitivity measures, the *α-values*. The α_i are derived from the gradient of the limit state function g with respect to the uncertain basic variables at the most likely failure point x^*, and may be interpreted as an effective percentage. A positive sign indicates an increase of $\Re$ if the mean value μ of the basic variable is increased and a negative sign (*typically found for load variables*) indicates a negative influence on the risk $\Re$ for an increasing mean load value.

13.3.2 The Two-stochastic-parameter Problem or the 'so-called' Strength-Stress Problem

In case of the most simple limit state, $g(X_j) = 0 = R - S \equiv$ *resistance R – action S* or, if linear analysis is permitted due to *strength R – stress S*, one has to treat just two basic variables, one *R* and one *S* variable. Assuming a normal distribution for both of these basic variables *R* and *S*, the probabilistic measures β and p_f can be derived by utilizing the formulation

$$\beta = \frac{\mu_R - \mu_S}{\sqrt{\sigma_R{}^2 + \sigma_S{}^2}} = \frac{\mu_Z}{\sigma_Z} \quad , \quad \text{and} \quad \Phi(-\beta) = \frac{1}{\sqrt{2\pi}} \int_{-\infty}^{\beta} e^{-t^2/2} dt \quad , \qquad (3)$$

with μ := mean value, σ := standard deviation of the parent distribution. For this simple '(*R – S)* problem' an approximate comparison of deterministic *MoS* values with probabilistic values of β or p_f is 'per hand' possible.

A MoS can be formulated on load level (defined *level*) and on stress level (*k in subchapter 12.8)*

$$MoS + 1 = \frac{\mu_R - k_R \cdot \sigma_R}{j \cdot (\mu_S + k_S \cdot \sigma_S)} = \frac{load\ resistance\ \ 'design\ allowable'}{design\ load} = \frac{daLR}{design\ load}. \qquad (4a)$$

According to the high measurement CoSt, the load resistance design allowable *daLR* (prefix *da to discriminate for instance da$R_{p0.2}$ on load level from the strength design allowable* $R_{p0.2} \equiv R_{02}^{\ t}$ *on stress level*) for the load resistance of a structure is barely determined. A test series on pressure vessels may be an exception. Therefore, the 'load resistance design allowable' is defined here to be that load when the associated equivalent stress σ_{eq} in the structure achieves the level of the design allowable $R_{p0.2}$ or R_m, respectively.

A stress level formulation may be utilized if a linear structural analysis is permitted:

$$MoS + 1 = \frac{\mu_R - k_R \cdot \sigma_R}{j \cdot (\mu_S + k_S \cdot \sigma_S)} = \frac{strength \quad 'design\ allowable\ '}{stress\ \ at\ \ design\ load\ \ \mathrm{DLL}}. \quad R, S \text{ now on stress level.} \qquad (4b)$$

This simple computation is sufficient, when high *FoS* are required such as for pressure vessels in nuclear industry.

To achieve a reliable design the statistically based design allowable has to be applied. This is a value, above which at least 99% *("A" value, application of military Safe Life Concept*) or 90% *("B" value, application in case of multiple load paths, redundancy, laminates*) of the population of values is expected to fall, with e.g. a 95% confidence level. The factors k_R and k_S respect this.

Above factors k_R and k_S are to be chosen according to reliability goals set for the individual project, and extracted from statistical tables (see e.g. [*HSB*]). They further depend on the stochastic model (*normal distribution, Weibull distribution, etc.),* the statistical basis (*sample size n, one- or two-sided tolerated),* and the desired confidence level for the transfer of the sample population to the basic population. Specifics may be extracted from the following numerical example.

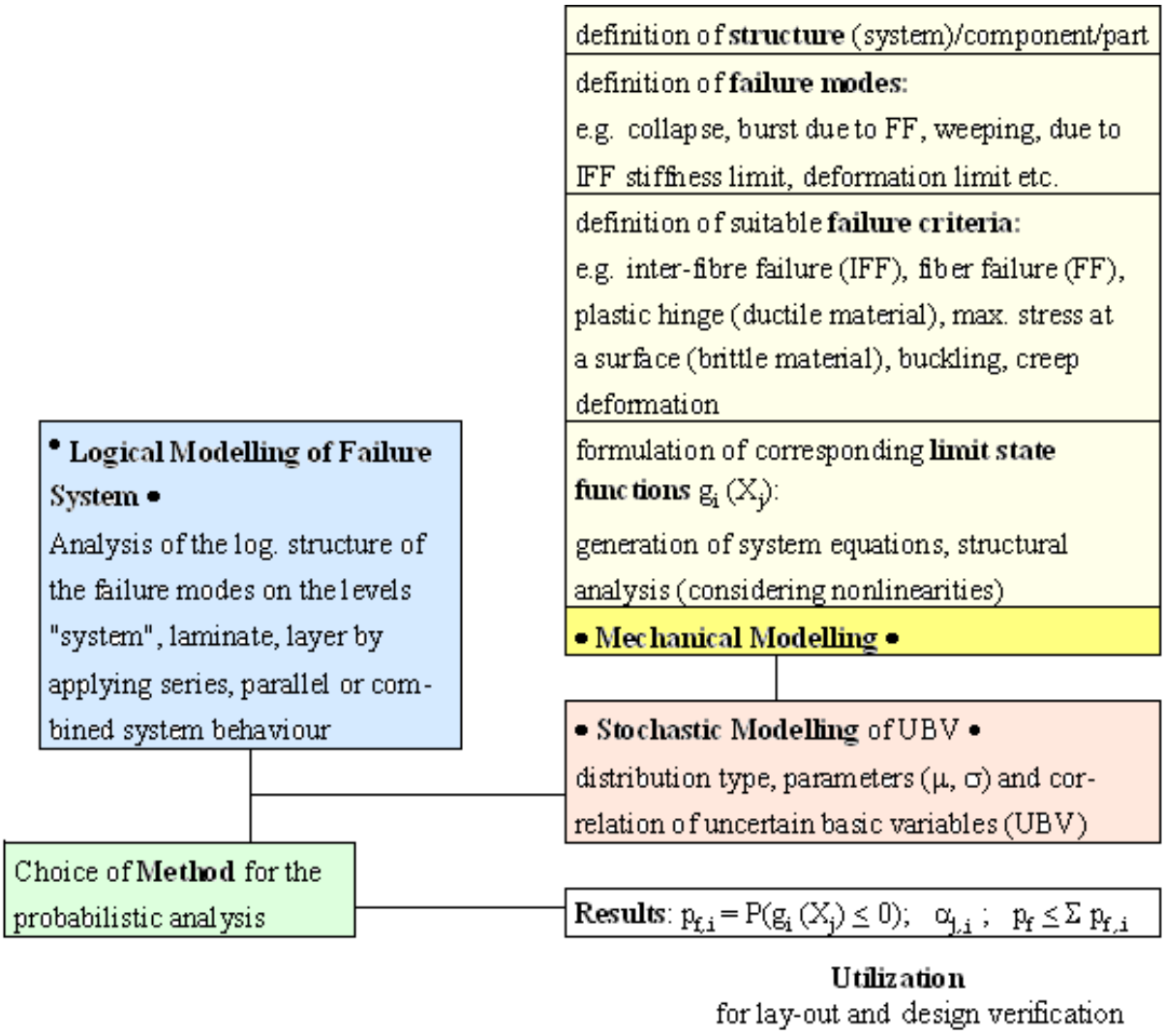


Fig.13-3: Example UD laminate

A system failure is a problem that causes a system to end its intended function (malfunction). The term 'failure system', used in Fig.13-3, shall describe the joint failure action of failure modes which finally might result in a 'system failure'.

13.4 Numerical Example: Cylindrical part of a pressure vessel

13.4.1 Modelling

In the above risk-disclosing context a simple case study shall be employed: the cylindrical part of a safety-critical pressure vessel. In order to demonstrate the effect of the scatter of the stochastic design parameters X_j (*the associated vector reads* $\underline{X}$) on the MoS value a probabilistic computation is performed by computing the previously mentioned convolution integral applying the code COMREL [Com87], see *Table 13-1*.

The input consists of the data for the *mechanical* model, the *stochastic* model, and of the associated modelling equations:

• ***Mechanical Model:*** from load level to stress level using structural mechanics

- The cylindrical part represents a thin-walled tube. It is, due to its membrane state of stress, a non-redundant element. For the derivation of the stress the so-called 'vessel formula' is applied (*linear analysis shall be permitted for reasons of simplification)*

$$\sigma_{hoop} = p_{int} \cdot d \ / 2t \ , \ \ \sigma_{ax} = \sigma_{hoop} / 2 , \tag{5}$$

with the internal pressure p_{int}, the diameter d, and the thickness t as input quantities.

- 'Onset of Mises Yielding' was considered as single failure mode. This delivers

$$\sigma_{eq}^{Mises} = \sqrt{\sigma_{ax}^{\,2} + \sigma_{hoop}^{\,2} - \sigma_{ax}\sigma_{hoop}} \ = \ \sigma_{hoop} \cdot\sqrt{3/4} \ = \ (\frac{p_{int} \cdot d}{2t}) \cdot \frac{\sqrt{3}}{2} \ , \tag{6}$$

- Limit state function $\quad g(\underline{X}) = R_{p0.2} - \sigma_{eq}^{\ Mises} = R_{p0.2} - \frac{p_{int} \cdot d}{4t}\sqrt{3} = 0 \ . \tag{7}$

Table 13-2: Input and still linked here the ComRel-output for the 4- parameter multi-stochastic problem obtaining $p_f = 1.8 \cdot 10^{-7}$. *cov = coefficient of variation, ND := Normal Distribution.*

Input for the later determination of MoS_{prob} *and output of the coordinates* x_j *of the most likely failure point x*, with sensitivity measures* α_j

j	X_j	μ_j	σ_j	f_j	Cov_j	α_j	x_j of x^*	p_f
1	p_{int}	6.00 bar	0.36 bar	ND	6 %	-0.620	7.1 bar	$1.8 \cdot 10^{-7}$
2	$R_{p0.2}$	442 MPa	22.1 MPa	ND	5 %	0.762	356 MPa	
3	d	5000 mm	50 mm	ND	1 %	-0.122	5031 mm	
4	t	4.40 mm	0.05 mm	ND	0.1 %	0.141	4.36 mm	
		assumed basic populations						
		input				output COMREL		

• ***Stochastic Model:***

- The four $X_j = R_{p0.2}, p_{int}, d, t$ are assumed to be statistically independent. For these stochastic

design parameters their means μ_j , standard deviations σ_j , and density functions f_j are to be provided (see *Table 13-2*). For simplicity, all these uncertain basic variables are assumed to follow a normal distribution ND.

- The statistically based *k*-factors shall be specified as $k_R = 3$ and $k_S = 2.3$. The numbers for k correspond to a so-called one-sided percentile for R and S and a probability of survival of *99.86 %* in case of k_R and of *98.9 %* in case of k_S (*C=95 %*).
- Geometrical tolerances are distributions, often truncated by the applied non-destructive inspection method. For reasons of simplicity they are taken here as an infinite ND. This means that the tails are accounted for in the probabilistic calculation.
  It is common practice to assume that a tolerance band width equals 4 standard deviations $\pm 2\sigma$.

• ***Safety Requirements:***

Usually assigned values of failure probability - for such a structural element that may fail - are on the level $p_f = 10^{-7}$. Assuming that the technical specification requires a failure probability of $p_f < 2 \cdot 10^{-7} \equiv p_f^{admissible}$, a probabilistic analysis of the cylinder tube can be conducted for a target value of the reliability $\mathfrak{R} = 1 - p_f$.

• Probabilistic: $\mathfrak{R} = 1 - 2 \cdot 10^{-7}$ (8)

The probabilistic approach above is to be compared with the conventional deterministic one. The latter one is defined by

• Deterministic: $j_{p0.2} = 1.1$ *(assumed to be required by a standard).*

$$DLL = \mu_S + k_S . \sigma_S , \quad daR_{p0.2} = \mu_R - k_R . \sigma_R = \mu_R (1 - k_R \cdot cov_R) \qquad (9)$$

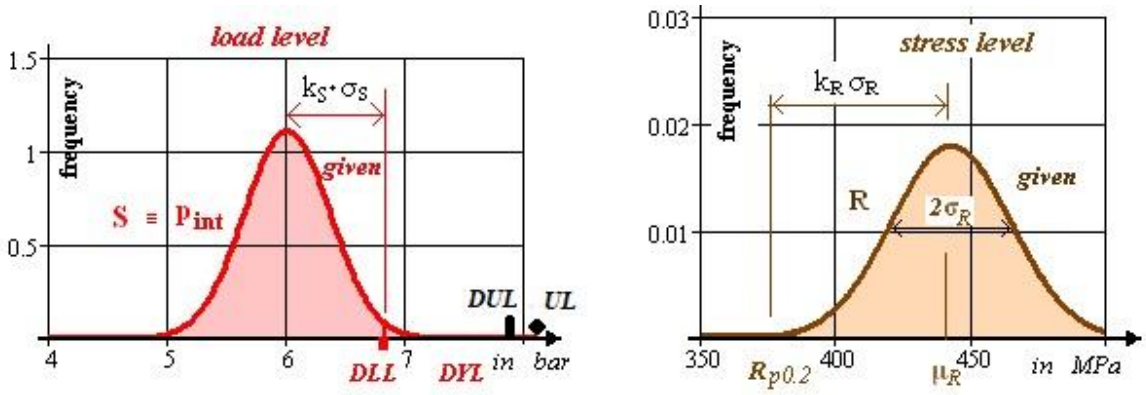


Fig.13-4: Density functions of the load 'internal pressure' (load level) and strength (stress level)
DLL = Design Limit Load, DYL = Design Yield Load = DLL·1.1, σ = standard deviation.
Measured density functions of load S = 'internal pressure' and of strength R.
Here, for the sake of simplicity the scattering load is modelled and rendered by a normal distribution

Notes:

* There is no *100%* safety existing. However, can we imagine what the difference is to an assigned reliability value of for instance $\mathfrak{R} = 99.99$ % ?

* The larger the distance between the stress f_S and the strength density function f_R the larger becomes MoS and the survival probability $\mathfrak{R}$, at least assuming constant cov values.

One cannot perform design verification if the included quantities belong to different levels. Hence, the load action is to transfer into a stress action in order to be able to compare a stress-levelled action with the resistance strength.

13.4.2 Solution and Results

As the objective here is to compare the results of a deterministic determination of the MoS with those of a probabilistic one, it is necessary to point out the essential differences between the two procedures. While the deterministic procedure chooses the worst combination of design parameters (e.g. minimum strengths and maximum loadings), the probabilistic procedure considers all combinations of the stochastic design parameters and taking into account their respective probability. One has to bear in mind, that not all design parameters are necessarily stochastic.

Aim was an approximate assessment of the standard deterministic MoS. Therefore, author intended to compare this deterministic MoS_{det} with a probabilistically determined MoS_{prob} . This can be performed just approximately. For an acceptable comparison the computation of both the *MoS* shall fulfil the same probabilistic requirement $p_f = 1.8 \cdot 10^{-7}$ and some minor other stochastic simplifications.

Deterministic Solution: $\Re = 1 - p_f = \Phi(\beta)$.

Fig.13-5 showed the density distributions of the loading 'internal pressure' p_{int} and of the strength *R*. Input data for the computations (*1 bar = 0.1 MPa)* are the

k-factors, chosen: $k_S = 2.3,\ k_R = 3.$

design loads: $DLL = \mu_L + 2.3 \cdot \sigma_L = 6.0 + 2.3 \cdot 0.36 = 6.83\ bar$,

$DYL = j_{p0.2} \cdot DLL = 1.1 \cdot 6.83 = 7.51\ bar = 0.751\ MPa \equiv p_{int}$

yield level resistance design allowable: $daR_{p0.2} = \mu_R - 3\sigma_R = 442 - 3 \cdot 22.1 = 376\ MPa,$

geometry, see *Table 13-2* : $\max d = 5000 + 2\sigma = 5000 + 2 \cdot 50 = 5100\ mm,$

$\min t = 4{,}40 - 2\sigma = 4.40 - 2 \cdot 0.05 = 4.30\ mm$

This yields the deterministic worst case-based 'Mises equivalent stress'

$$\text{worst case } \sigma_{eq}^{Mises} \equiv \sigma_{det} = \left(\frac{p_{int} \cdot d}{4 \cdot t}\right) \cdot \sqrt{3} = \left(\frac{DLL \cdot j_{p0.2} \cdot \max d}{4 \cdot \min t}\right) \cdot \sqrt{3} = 386\ \text{MPa}, \qquad (10)$$

and a margin of safety of

$$MoS_{det} = \frac{strength\ 'design\ allowable'}{stress\ at\ design\ yield\ load} - 1 = \frac{daR_{p0.2}}{\sigma_{det}} - 1 = \frac{376}{386} - 1 \equiv -2.6\%. \qquad (11)$$

Mind: Results are $\Rightarrow \sigma_{det} = 386\ MPa$ and the standard $MoS = -2.6\%$.

Probabilistic Solution:

a) Solution with 4 stochastic parameters

With the code COMREL [*Com87*] the four-dimensional task with the stochastic design parameters $X_j = R_{p0.2}, p_{int}, d, t = (X_1, X_2, X_3, X_4)$ can be solved according to

$$p_f = P(R \le S) = P(R - S \le 0) = P(g(X_1, X_2, X_3, X_4) \le 0) = \int_{g(\underline{X}) \le 0} f_{\underline{X}}(\underline{x})\, dx\,. \qquad (12)$$

Mind: Results are $\Rightarrow$ in *Table 13-2*.

These results x_j, α_j and p_f are the coordinates x_j of the most likely failure point x* and the sensitivity measures α_j of the X_j. These entities are depicted in *Table 13-2*. All other combinations of x_j in the failure domain have lower failure probability densities than x* .

To make the author's intension to assess a deterministic *MoS* more understandable and convincing the 4-parameter-solution shall be broken down to a 2-parameter one in order to become able to compute a result 'by hand'.

b) Solution with 2 stochastic parameters

If the probabilistic task with four stochastic design parameters $X_j = R_{p0.2}, p_{\text{int}}, d_m, t$ could be reduced to a two-parameter '*R-S* problem', the difference in *MoS* between the deterministic and the probabilistic procedure can be simply estimated and graphically illustrated by two distributions, one stands for *R* and one for *S*. This is done by splitting the problem into a load resistance part, which is identical to the strength part *R, represented by* $R_{p0.2}$, and a stress part *S*, represented by

$$\sigma_{eq} = p_{\text{int}} \cdot \frac{d}{4t} \cdot \sqrt{3} \text{ a Mises equivalent stress}, \qquad (13)$$

which depends on three of the four parameters, thus obtaining a simple two parameter problem.

To be comparable, both the numbers MoS_{prob} and MoS_{det} are to be based on the same failure probability $p_{f\,!}$

With the code COMREL [*Com87*] the density function $f_{\sigma eq}$ can be obtained via computing points on the $F\sigma_{eq}$ –curve followed by NF-mapping the course of the obtained single *F*-point estimates.

Using the limit state function (*failure criterion*) $g(X_1, X_2) = R_{p0.2} - \sigma_{eq} = 0$, (14)

the integral in its various versions (see [*Tho82*, p.73]) (15a)

$$p_f = P(g(R_{p0.2} - \sigma_{eq})) = \int_{-\infty}^{\infty} \left(\int_{-\infty}^{r=s} f_R(r) \cdot dr \right) \cdot f_S(s)\, ds = \int_{-\infty}^{+\infty} \int_{-\infty}^{g=0} f_{R,S}(r,s) \cdot dr \cdot ds = \int_{-\infty}^{+\infty} F_R(x) \cdot f_S(x) \cdot dx$$

can be solved inserting the distribution function $F_R = F_{p0.2}$ and the density function $f_S = f_{\sigma eq}$ (data, see <u>*Table 13-3*</u>).

Now, just a simple 'R-S problem' remains to be tackled, assuming that $f_{\sigma eq}$ is ND-distributed,

$$p_f = \Phi(-\beta) \text{ with } \beta = (\mu_R - \mu_S) / \sqrt{\sigma_R^2 + \sigma_S^2} \ . \qquad (15b)$$

The task needs the determination of the p_f -associated design stress value σ_{prob}, which belongs to the chosen common target value $p_f = 1.8 \cdot 10^{-7}$. As this is a distinct value on the probability distribution function curve $F_S(\sigma_{eq})$ one has to generate this function. The problem again consists in the determination of single **point estimates**. As limit state function serves, analogous to Eq.14,

$$g(X_1, X_3, X_4) = \sigma_{eq} - p_{int} \cdot \frac{d}{4t} \cdot \sqrt{3} \; = 0 \; . \qquad (16)$$

The procedure to determine the σ_{eq} function reads:

1) Increase continuously $\sigma_{eq,k}$
2) Compute an increasing $p_{f,k} = P\,(\,g(\sigma_{eq} - p_{int} \cdot \frac{d}{4t} \cdot \sqrt{3}))$, (*COMREL was utilized*), each representing a **single point** on $F_S(\sigma_{eq})$
3) From the fully derived F_S (normal distribution assumed) estimate its statistical parameters $\mu_{\sigma_{eq}}$, $\sigma_{\sigma_{eq}}$, and an approximate density distribution $f_{\sigma eq} = f_{\sigma eq}^{Mises}$ will be achieved. The accuracy depends on the number *k* of the chosen computation points.

Fig.13-5 (left) renders the procedure, how the density function $f_S\,(\sigma_{eq})$ can be linked to the distribution function $F_S\,(\sigma_{eq})$ via determination of the point estimates.

Now, with the knowledge of $\mu_{\sigma_{eq}}$, $\sigma_{\sigma_{eq}}$, the final *R*-S convolution integral reduces to the desired manually determinable Gauss type integral, if it can be assumed that all stochastic design parameters are normally distributed.
Applying above COMREL results allows the simplified *Eqs.(3)* and *(4)* to be applied in the (R-S)-analysis. As margin of safety, meeting $p_f = 1.8 \cdot 10^{-7}$,

$$MoS^*_{prob} = \frac{strength\ design\ allowable}{stress\ at\ design\ load,\ chosen\ p_f} - 1 = \frac{R_{p0.2}}{\sigma^*_{prob}} - 1 = \frac{376}{356} - 1 \equiv +5.9\ \%$$

is yielded, obviously a very satisfying positive value. The results are collected in *Table 13-3*.
It is of interest that the sensitivity measures practically have not changed by the intermediate probabilistic ComRel-computation step.

Table 13-3: Input and solution (right) of the 2-parameter problem (COMREL-reduced). Assumption: normally distributed equivalent stress

j	X_j	μ_j	σ_j	f_j	Cov_j
1	σ_{eq}^{Mises}	295 MPa	18.6 MPa	ND	6.3 %
2	$R_{p0.2}$	442 MPa	22.1 MPa	ND	5 %

input

α_j	x_j of x^*	p_f
-0.66 +0.76	**356** MPa	$1.8 \cdot 10^{-7}$

results from Annex 1

Results at $p_f = 1.8 \cdot 10^{-7}$: α_j, x_j in *Table 13-3* and σ^*_{prob} = 356 MPa, MoS^*_{prob} = 5.9%.

Mind again: A *MoS* can never be a real probabilistic quantity. Above MoS remains always deterministic and its computation was 'fed' here by a probabilistic input, only.

> *Note*: Much practise in the past - with a distinct type of structures - helped and helps to produce such types of structural parts which are 'safe enough'. The similar results from FoS-based or Reliability-based treatment underline this [*Rac04*].

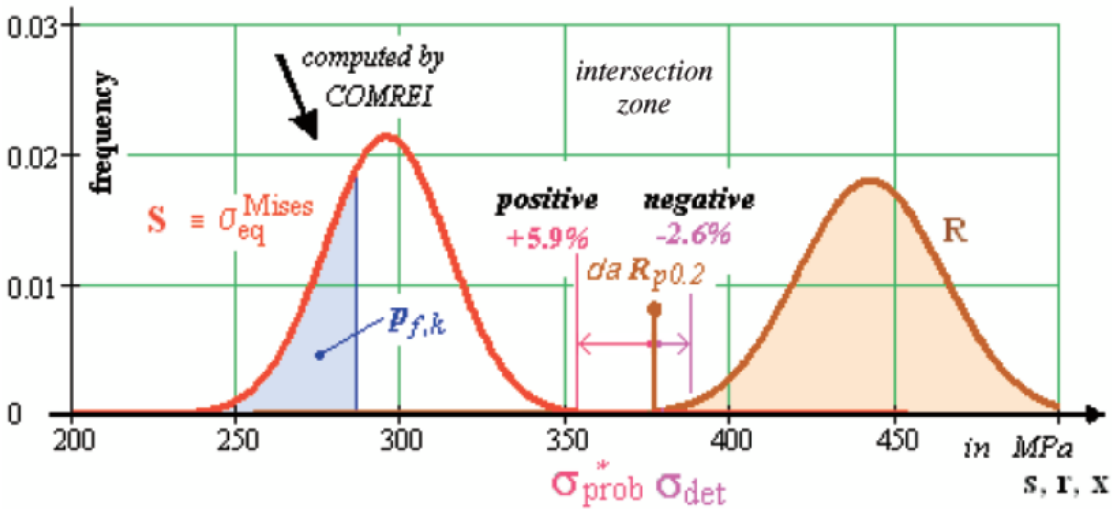


Fig.13-5: Probabilistic and deterministic strength Design Verification on stress level.

σ^*_{prob} *corresponds to the failure situation* $p_f = 1.8 \cdot 10^{-7}$.

$\sigma^*_{prob} = 355$ MPa, $\sigma_{det} = 386$ MPa, $daR_{p0.2} = 376$ MPa

Discussion of results of the case study:

- The most likely failure point is obtained for the combination of x_j values shown in the output section of *Table 13-2* and linked to the failure probability $p_f = 1.8 \cdot 10^{-7}$ that corresponds to a reliability index $\beta = 5.1$.
- The probabilistic calculation leads to $MoS_{p0.2}$ (at *DYL* level) =*+5.9%* (Table 13-4) while the conventional method results in *-2.6%,* thus, a remarkable *8%*-difference between the deterministic-based and the probabilistic-based $MoS_{p0.2}$ is given for above p_f which is marginally smaller than the assigned value $p_f^{admissible} = 2 \cdot 10^{-7}$.
- Structural reliability analysis reveals the influence of each stochastic design parameter on the distinct failure mode through the values of the design sensitivity measures α_j . The code COMREL provides such values that denote the relative importance in the actual failure mode which is here yielding. The uncertain yield strength $R_{p0.2}$ has the dominating influence (α = *+0.76*) on the reliability $\mathfrak{R}$, followed by internal pressure p_{int} (α = *-0.62*), (Table 13-2).

Fig.13-7 illustrates the different results obtained in the deterministic and the probabilistic strength analysis. Given is a load pressure *distribution* not only a fixed *number*. The conventional procedure is to compute *'worst* σ' and compare it with the design allowable $daR_{p0.2}$, which in the case study considered here results in a negative *MS*. In order to understand these values, and to get a comparative feeling about the failure risk, Table 13-4 demonstrates the effect of a consequent probabilistic thinking and its advantages.

Structural reliability thinking, this means 'thinking in uncertainties of the driving design parameters', helps to judge the deterministic design procedure. Understanding how the various design parameters influence the *MS* value, provides a feeling about the failure risk, which an *MS* value alone cannot do. This is best illustrated by the given simple probabilistic example.

An improved data base for the stochastic load model almost always will result in a more economic design. Further, reducing the scatter of important (see sensitivity measures) geometrical tolerances will improve the design. Truncated distributions, to be achieved by some more effort in measurement and in controlling, will lead to an improved reliability, too. Reducing the fluctuation of the structural response (stress field) provides increased confidence in the analytical results.

13.5 Additional Sensitivity Investigations

13.5.1 Sensitivity of MoS and p_f to varying Distribution Parameters (μ, σ)

Fig.13-6a presents the interrelation of a fixed load pressure density function f_S and four hypothetical strength distributions f_R with the associated *MoS* values and the failure probability $p_f = 1 - \mathcal{R}$. *Fig.13-8a* depicts how far – to gain safety distance - the strength

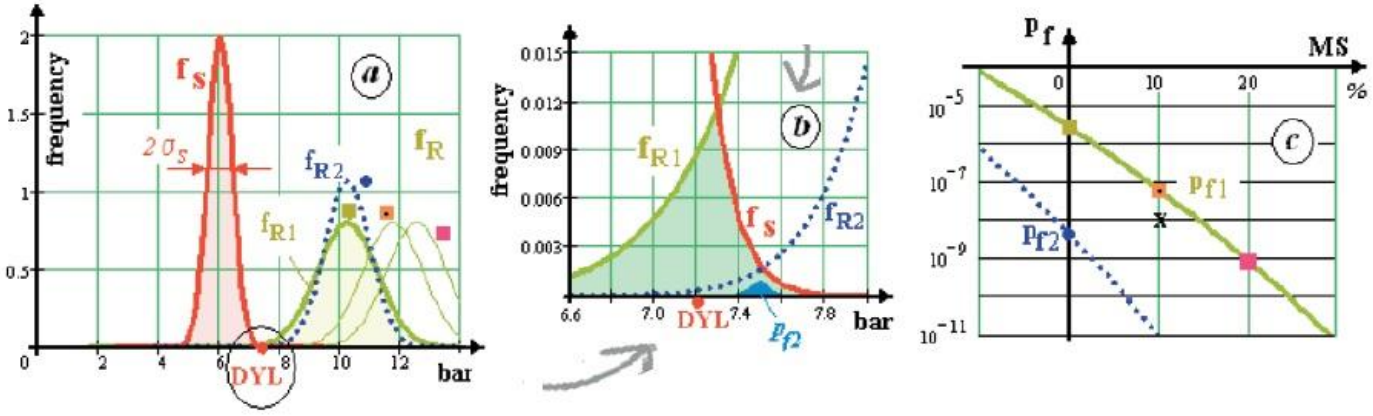


Fig.13-6: Sensitivity of MoS and p_f to density functions (populations) of load S and load resistance R; and 'interrelation of MoS with p_f' for k_R = 3, k_S = 2.3

density function f_{R1} has to be shifted (i.e. μ_R) to reach a *MoS* ($\equiv MoS_{prob}$) = *+10 %* and *+20 %*, keeping cov. Further, keeping the the mean, the effect of lowering the scatter by utilizing f_{R2} instead of f_{R1} is outlined. Thereby it is not to forget: *A MoS is principally not interrelated to β* !

Fig.13-6b zooms the 'intersection zone' of the fixed load distribution with two different load resistance distributions the difference of which is just caused by a different cov, whereas μ remains the same. As the intersection zone is much bigger in case of f_{R1} it becomes $p_{f1} > p_{f2}$. Depicted in the intersection zone is the density function of the failure probability fp_{f2}. The area below this curve corresponds to the value of p_{f2}, see further *Annex 2*.

Whereas the zoom b indicates the different size of the intersection area the curves in c indicate the resulting effect of the different size. The density function f_{R1} leads to a higher failure probability than f_{R2}.

Fig.13-5c depicts how the resistance curve f_{R1} (*Cov* remains constant) has to be shifted to achieve higher *MoS* or p_f -values: *1.) MoS = 0 %, $p_f = 5\ 10^{-5}$; 2.) MoS = 10 %, $p_f = 2 \cdot 10^{-7}$; 3.) MoS = 20 %, $p_f = 1 \cdot 10^{-9}$*. The squares on the p_{f1} curve indicate which reduced failure probability or increased structural reliability is reached in the example for *MoS* is *0 %, 10 %, 20 %*. Reducing the scatter, when taking f_{R2} instead of f_{R1} increases reliability (*reduces failure probability)* and *MoS*. For

the given conditions (f_S, f_R), according to *Fig.8* the following values are computed: $p_f = 1.8 \cdot 10^{-7}$ and *MoS = +10 %.* Probabilistically, this theoretically means failure if as target value e.g. 10^{-8} *is* assigned.

Both, an increasing resistance mean value and a decreasing standard deviation will lower p_f.

13.5.2 Effect of Variation of Strength Density Distribution on MoS and p_f

A variation of the strength density distribution shall highlight the impact on the reliability and on the margin of safety. Due to the achievement of a qualified production process and some more experimental data the mean value decreased a little, from $\mu_{Rp0.2} = 442$ MPa → 440 MPa, but the standard deviation of $\sigma_{Rp0.2}$ was reduced from 22.1 MPa → 19.5 MPa. Thereby the design allowable changes to $daR_{p0.2} = 440 - 3 \cdot 19.5 = 381.5$ MPa. Improved production causes the better values for p_f and *MoS in* <u>*Table 13-4*</u>.

The difference between the deterministic and the probabilistic *MoS* becomes about *6% for* $p_f = 3.2 \cdot 10^{-8}$.

If the design situation allows for the previously taken $p_f = 1.8 \cdot 10^{-7}$, then, the stress situation may be sharpened by shifting f_S from $\mu_S = 295$ MPa to $\mu_S = 302.9$ MPa and σ^*_{prob} = 363 MPa can be even replaced by a value σ_{prob} = *368MPa*. Of course, this leads to a lower MoS, however the p_f requirement $p_f = 1.8 \cdot 10^{-7}$ is still met.

Table 13-4: Effect of variation of strength density distribution. Input, solution and display of deterministic and probabilistic results

j	X_j	μ_j	σ_j	f_j	CoV_j
1	σ_{eq}^{Mises}	295 MPa	18.6 MPa	ND	6.3 %
2	$R_{p0.2}$	**440** MPa	**19.5** MPa	ND	4.4 %

input

α_j	x^*_j	p_f
-0.69	**363** MPa	$3.2 \cdot 10^{-8}$
0.73	**363** MPa	

results from Annex 1

$daR_{p0.2}$ = **381.5**	μ_S = 295	$\sigma_{prob}(p_f)$ = ***363MPa***	$\sigma_{det}(DYL)$ =386 MPa	P_f = **$3.2 \cdot 10^{-8}$**	β = 5.4	MS_{prob} = **+5.1%**	MS_{det} = **- 1.1%**
	μ_S = 302.9	$\sigma_{prob}(p_f)$ > ***368MPa***	$\sigma_{det}(DYL)$ =396MPa	P_f = $1.8 \cdot 10^{-7}$	β = 5.1	MS_{prob} =+ **3.7%**	MS_{det} = **- 3.7%**
stress level *in MPa*				**probabilistically**			**determin.**

Table 13-5: Comparison of deterministically derived MoS-values and failure probabilities p_f due to different resistance distributions. MS =MoS
DLL = $\mu_S + k_S \cdot \sigma_S$, DYL = DLL • jp0.2, chosen: $k_R = 3$, $k_S = 2.3$;
da LR = daLR($R_{p0.2}$) = $\mu_R - k_R \cdot \sigma_R$, MoS_{det} = daLR / DYL

load *in bar*		**load resistance** at yield initiation *in bar*					
μ_j	σ_j	μ_j	σ_j	*da LR*	P_f	β	MS_{det}
6	0.36	10	1.0	7.00	$8.4 \cdot 10^{-5}$	3.76	-6.8%
		10	0.75	7.75	$7.6 \cdot 10^{-7}$	4.81	+3.2%
		11	1.0	8.00	$1.3 \cdot 10^{-6}$	4.70	+6.5%
		12	1.0	9.00	$8.2 \cdot 10^{-9}$	5.65	19.8%
		'evaluated' test results					

Notes:
- *Probabilistic thinking highly pays off*
- *The larger the distance between the stress and the strength distribution the larger become MoS and survival probability = reliability $\mathfrak{R} = 1 - p_f$*
- *Goal of the design is the achievement of a reliable structure. One might reach this goal by the achievement of a positive MoS*
- *A MoS is not linked to β !*

13.4.4 Chapter conclusions

The conclusions drawn from the case study primarily aimed at aerospace engineering, but may also be applicable to other engineering disciplines where risk analysis and safety margins are of importance and where loads get close to the point of failure.

Risk comes in two varieties: a) a Technical Risk, associated with the complex failure potentials and hazardous characteristics of the actual structural system, and b) a Programmatic Risk, associated with the failures to meet the project goals CoSt and schedule.

Of course, the essential findings, presented now, cannot be taken as fully generally valid conclusions. However, they will make us sensitive to think about how one can lower risk and improve risk management. This is delineated by the following bullets:

- A slightly negative *MoS* value must not necessarily be seen critical as demonstrated in the previous case study
- MoS-values should not be interpreted as absolute and final safety measures. They can provide just a 'limited eeling' for the risk of failure. Above simple example has demonstrated for an assigned common p_f a remarkable difference between the deterministic and the probabilistic results
- An appropriate *'Think (about) uncertainties' attitude* has to be developed in order to identify the main sources of uncertainty and to reduce the scatter of the *driving design parameters.* This could result in shorter product development and in CoSt reductions. Such attitude should be

adopted by all parties involved in the design verification and certification process, i.e. design office at the supplier, customers and licensing authorities. The important message is that concentrating efforts on reducing the uncertainties can be far more productive than lengthy discussions over slightly negative margins

- Of all uncertain design parameters it is in many cases the *load* uncertainty, which has the highest scatter and affects analyses and tests most. Therefore, reducing the uncertainties of the stochastic design parameters, especially of the loads, as the project progresses along will be most effective and economic. One has to eliminate all so-called 'pocket factors' (i.e. the load engineer's reserve in the uncertainty considering K-value or, when the design engineer utilizes a too low strength design allowable) along with the maturity of the design and reserve the *MoS* for the still remaining unknown effects that should not be hidden by not officially known pocket factors. A distinct uncertainty has to be covered by clearly dedicated, risk-dependent *FoS*. One should improve the quality of the design input and increase the sample size or improve test information for establishing better strength design allowables and design loads
- In the late phase of development, supplier and customer (*and licensing authorities, if applicable*) should jointly decide whether the risk is acceptable, whether more structural testing is necessary, or whether really a re-design is needed, [*Sar97*]. In this context, slightly negative *MoS* values have to be interpreted with care applying best engineering judgement
- Engineering disciplines where large *FoS* are a prerequisite, e.g. nuclear engineering, are less likely to benefit as any variation in the *MoS*-value between the two concepts will be marginal compared to the *MoS* generated in the case of required very high *FoS*
- The goal of any design engineer should be to end up with a robust design. To achieve this, the main stochastic design parameters have to be used to outline the robustness of the design against the envisaged actual failure mode by firstly computing the sensitivity measures α_j and then investigating the reduction of the design's sensitivity to changes of X_j *while* keeping p_f at the prescribed level. This is important for the production tolerances.

LL:

1. *Robust designs are required (robust to later changes of the design parameters) with identification of the most sensitive design parameters*
2. *Failure probability p_f does not dramatically increase if MoS turns slightly negative*
3. *Both, an increasing mean value and a decreasing standard deviation will lower p_f*
4. *A local safety measure of MoS = -1 % is no problem in design development if a 'Think (about) Uncertainties ' attitude is developed in order to recognize the main driving design parameters and to reduce the scatter (uncertainty) of them. The MoS value does not outline a failure probability!*

Table 13-6: Input and solution of the 2-parameter problem. MS = MoS (reduced by COMREL from the 4-parameter problem) ***355***

j	X_j	μ_j	σ_j	f_j	CoV_j
1	σ_{eq}^{Mises}	295 MPa	18.6 MPa	ND	6.3 %
2	$R_{p0.2}$	442 MPa	22.1 MPa	ND	5 %

input

α_j	x_j of x^*	p_f
-0.66	**356** MPa	$1.8 \cdot 10^{-7}$
+0.76	**356** MPa	

results from Annex 1

stress level *in MPa*	$daR_{p0.2}$ = **376**	$\sigma_{prob^*}(p_f)$ = **355**	$\sigma_{det}(j_{po2})$ = **386**	P_f = 1.8 10^{-7}	β = 5.1	MS_{prob^*} = **+5.9% !**	MS_{det} = **-2.6% !!**
				probabilistically			deterministic.

***Annex 1* : S-R problem visualization -**

Interpretation as example *Tension Rod or the 2-parameter simplified Pressure Vessel*

In this *Annex* some data are provided for *Table 13-7.* Due to Hasofer/Lind 1974 a simple solution is possible:

Input data *in MPa*: $\mu_R = 442,\ \sigma_R = 22.1,\ \mu_S = 295,\ \sigma_S = 18.6.$

1) Vector of stochastic variables:
$\underline{Y} = (X_1, X_2)^T = (R, S)^T$

2) Hasofer-Lind Transformation:

$$\underline{Y} = \begin{Bmatrix} R \\ S \end{Bmatrix} = \begin{bmatrix} \sigma_R & 0 \\ 0 & \sigma_S \end{bmatrix} \begin{Bmatrix} U_R \\ U_S \end{Bmatrix} + \begin{Bmatrix} \mu_R \\ \mu_S \end{Bmatrix} = \left[\underline{T}\{\underline{U}\}\right]$$

3) Limit state function:
$g(\underline{Y}) = g(R, S) = (R - S)$
$= (\sigma_R U_R + \mu_R) - (\sigma_S U_S + \mu_S)$

4) Standardization: $\sigma_Z = (\sigma_R^2 + \sigma_S^2)^{0.5}$

5) Insertion of 2) into Limit state:
$g(\underline{Y})/\sigma_Z = (\sigma_R/\sigma_Z)U_R - (\sigma_S/\sigma_Z)U_S +$
$+(\mu_R - \mu_S)/\sigma_Z = 0$

$= \alpha_R U_R - \alpha_S U_S + \beta = \alpha^T \underline{U} - \alpha^T \underline{u}^* = 0;$
$x_j^* = u_j^* \sigma_j + \mu_j.$

6) Equations for failure probability and reliability index β
$p_f = \Phi(-\beta)$ and
$\beta = (\mu_R - \mu_S)/(\sigma_R^2 + \sigma_S^2)^{0.5} = (\mu_R - \mu_S)/\sigma_Z$

7) Numerical example :
$\sigma_Z = (\sigma_R^2 + \sigma_S^2)^{0.5} = (22.1^2 + 18.6^2)^{0.5} =$
$28.9\ MPa$
$\mu_Z = \mu_R - \mu_S = 442 - 295 = 147\ MPa,$
$\beta = \mu_Z/\sigma_Z = 147/28.9 = 5.1$
$\alpha_R = \sigma_R/\sigma_Z = 22.1/\ 28.9 = 0.765,$
$\alpha_S = -\sigma_S/\sigma_Z = -18.6/28.9 = -0.644$
$\sum \alpha_j^2 = (0.765^2 + 0.644^2) = 1.00$
$u_R^* = -\beta \cdot \alpha_R = -5.1 \cdot 0.765 = -3.88,$
$u_S^* = -\beta \cdot \alpha_S = -5.1 \cdot (-0.644) = +3.28$
$x_R^* = -3.88\ 22.1 + 442 = 356\ MPa \cong x_S^*,$
$x_S^* = +3.28\ 18.6 + 295 = 356\ MPa$
$p_f = \Phi(-\beta) = 1.8 \cdot 10^{-7},\ \Re = 1 - p_f.$

***Annex 2*: Visualization of Characteristic Quantities of the Probabilistic Solution Procedure**

For a specific design case the following fictitious data set with very high standard deviations is chosen for achieving a good visualization of all characteristic quantities (for sensitivity measures α_j not possible) ([*Tho82, Sch81*]).

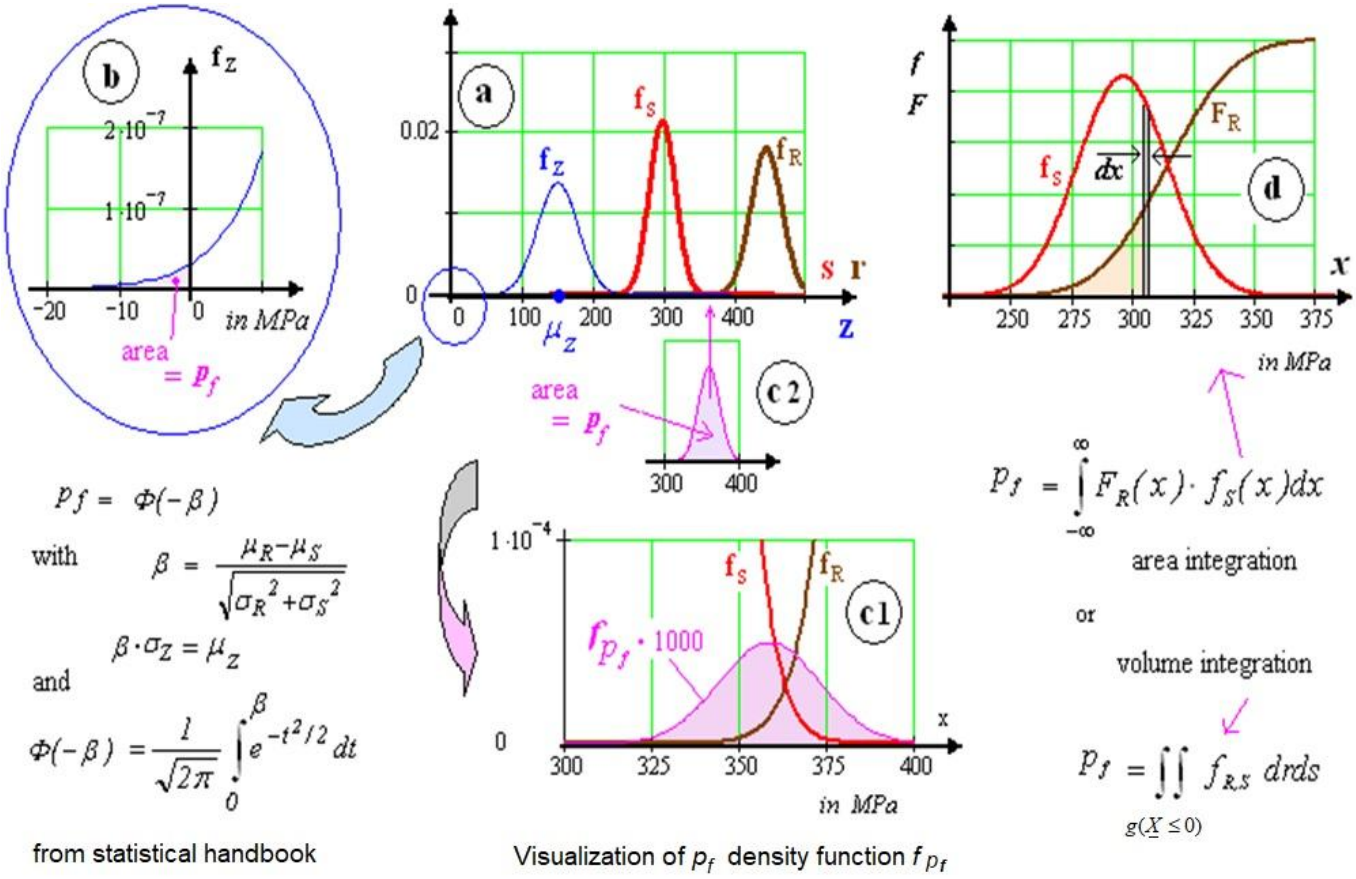
Part figure (a) displays the two density functions f_S and f_R with the difference distribution f_Z. Part figure (b) shows the negative tail of f_Z, the area of which represents p_f (*one way possible in this simple case to achieve and visualize the solution* p_f*).* Part figure (d) depicts the usual calculation procedure. Finally, (c1) and (c2) visualize the distribution of p_f in the intersection zone. Due to the simple 2-parameter problem, the density function of the failure probability p_f could be simply calculated by the author solving the integration problem with the MathCad code. This is a single point estimation procedure again with afterward mapping of the course of points.

Input data (*in MPa*) $\mu_R = 440,\ \sigma_R = 70,\ \mu_S = 300,\ \sigma_S = 50.$

Characteristic quantities

$\sigma_Z = 86.0$ *MPa*, $\mu_Z = 140.0$ *MPa*,
$\alpha_R = 0.814,\ \alpha_S = -0.581,\ \sum \alpha_j^2 = 1.00,$
$\beta = 1.627,\ p_f = 5.2 \cdot 10^{-2},$
$x_R^* \cong x_S^* = 347$ *MPa*, $S = R.$

Attributed to the design case above is a failure probability of $p_f = 5.2 \cdot 10^{-2}$. This corresponds to 5.2 % of the volume of the probability hill $f_{R,S}(r,s)$ vertically cut off by $r = s$ or $g(X) = 0$.



$$p_f = \Phi(-\beta)$$

with $\beta = \dfrac{\mu_R - \mu_S}{\sqrt{\sigma_R^2 + \sigma_S^2}}$

$$\beta \cdot \sigma_Z = \mu_Z$$

and

$$\Phi(-\beta) = \frac{1}{\sqrt{2\pi}} \int_0^{\beta} e^{-t^2/2}\, dt$$

from statistical handbook

Visualization of p_f density function f_{p_f}

$$p_f = \int_{-\infty}^{\infty} F_R(x) \cdot f_S(x)\, dx$$

area integration

or

volume integration

$$p_f = \iint_{g(\underline{X} \le 0)} f_{R,S}\, dr\, ds$$

Figure: Determination of p_f and determination of the density function of the failure probability p_f. Assumption ND, 2 parameters

The following figure displays the most probable failure point x*. A 2-parameter problem can be interpreted as tensionally loaded rod.

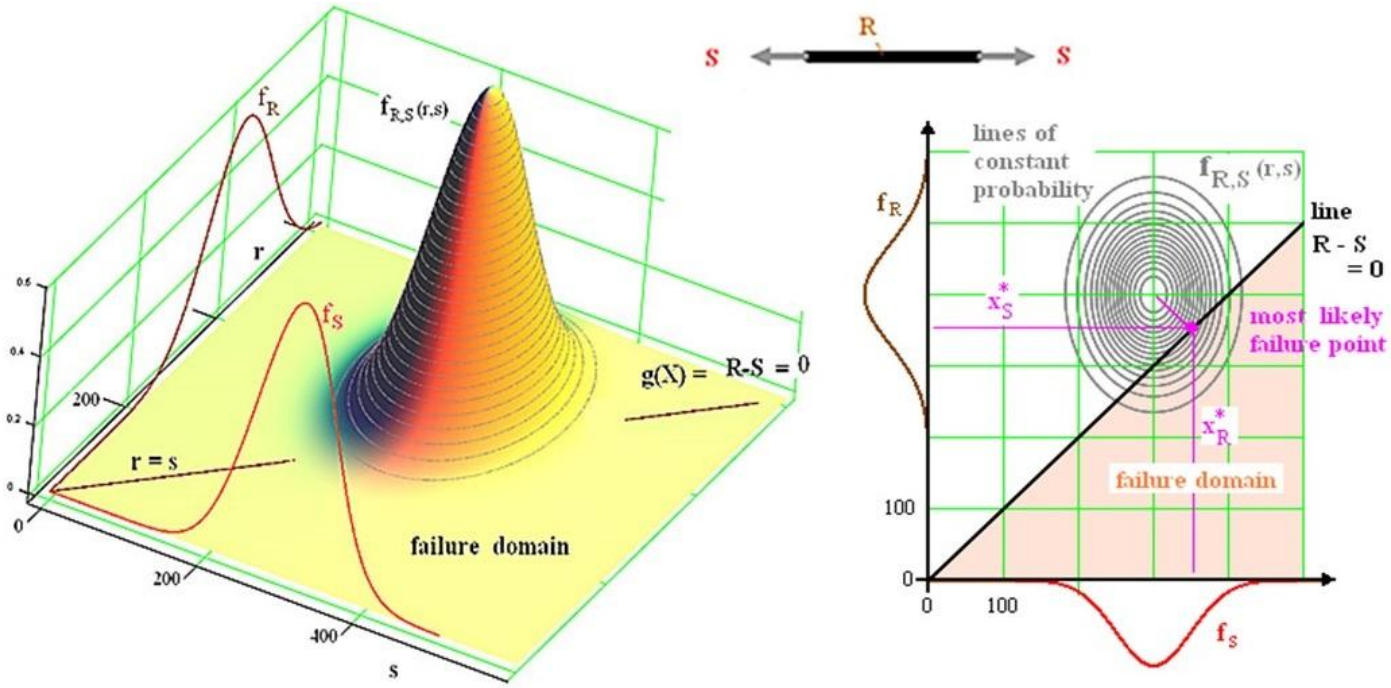


Figure: Visualization of the most likely failure point. (left) Probability hill (joint density function $f_{R,S}(r,s)$) with lines of constant probability density. Data: $\mu_R = 440$, $\sigma_R = 70$, $\mu_S = 300$, $\sigma_S = 50$; $p_f = 5.2 \cdot 10^{-2}$. (right) horizontally projected lines of constant probability density on the 'probability hill'

Acknowledgement concerning parts of this chapter:

The author is grateful to Dr.-Ing. Stefan Gollwitzer (Reliability Consulting and Programs GmbH, München) for executing the structural reliability computations with the COMREL code and for valuable discussions. Further, he is extremely obliged to Dr. Josef Friedl (MAN-Technologie AG, Augsburg) for carefully checking the text. For partly peering the present bodytext the author could find Dr.-Ing. Martin Grimmelt. (*Thanks Martin).*

Chapter References

[Com87] Componential Reliability Analysis, RCP Consult GmbH, Munich 1987-2004, www.strurel.de. Code COMREL.

[Cru94] Cruse TA, Mahadevan S, Huang Q and Mehta S: *Mechanical System Reliability and Risk Assessment*. AIAA Journal 32, no. 11, 1994, 2249-2259

[Cun88] Cuntze R: *Influence of the stochastic Behavior of Design Parameters on the First Ply Failure (FPF) in Pressurized CFRP Tubes*. ESA/ESTEC, European Conference on Spacecraft Structures, Materials and Mechanical Testing, March 1988

[Cun93] Cuntze R.: *Deterministic and Probabilistic Prediction of the Distribution of Inter-Fiber-Failure Test Data of Pre-strained CFRP Tubes composed of Thin Layers and loaded by Radial Pressure*. Wollongong, Advanced Composites '93. The Minerals, Metals & Materials Society, 1993

[ECSS] ECSS-E-30-02: *Mechanical Design, Verification, Qualification and Certification of Pressurised Hardware. European Cooperation for Space Standardization*, ESA/ESTEC, Noordwijk, 2004. Final draft (co-author)

[Gra66] Graf U, Henning HJ and Stange K.: *Formeln und Tabellen der mathematischen Statistik*. Springer, Berlin/Heidelberg/New York, 1966, 2.Auflage

[Gri89] Grimmelt M. and Cuntze R: *Probabilistic Prediction of Structural Test Results as a Tool for the Performance Estimation in Composite Structures Design*. VDI-Bericht 771 (1989), 191-200

[Gri03] Grimmelt M: Private communication on Risk and RAMS. April 2003

[Has74] Hasofer A M and Lind N .: *Exact and Invariant Second Moment Code* Format. ASCE Proc., Vol.100, no. EM1, 1974

[HSF92] Cuntze R., Rackwitz R., Gollwitzer S., Plica S. and Stoeffler G.: *Handbook for the German Ministry of Defence on "Safety Concept for Fiber Reinforced Plastic Structures*". Koblenz, 1992 (in German)

[MIL-Hdbk 17B] *Plastics for Aerospace Vehicles. Vol. III "Utilization of Data*" . Dep. of Defence (DOD), USA

[Rac86] Rackwitz R. and Cuntze R: *Formulations of Reliability oriented Optimization with Application*. NATO Advanced Study Institute. Conference on Computer Aided Optimal Design, Troia, Portugal. June 29 - July 11, 1986

[Rac00] Rackwitz R.: *Optimization, Basis of Code Making and Reliability Verification*. Structural Safety 22, no. 1, 2000, pp. 27 - 60

[Rac04] Rackwitz R: *How Safe is Safe Enough? An Approach by Optimization and the Life Quality* Index. Proc. 1.ASRANet, Int. Colloquium. Glasgow, July 8-10, 2002, 29 pages

[Sar97] Sarafin, T.P. and Larson, W.L.: *Space Craft Structures and Mechanisms - from concept to launch-. Space Technology Series*. Kluwer Academic Published 1997 (2nd print)

[Sch81] Schuëller G .: *Einführung in die Sicherheit und Zuverlässigkeit von Tragwerken*. W. Ernst & Sohn, Berlin-München, 1982

[Tho82] Thoft-Christensen P and Baker M.J: *Structural Reliability Theory and its Applications*. Springer-Verlag, 1982

[Ver92] Verderaime V: *Structural Deterministic Safety Factors Selection Criteria and Verification*. NASA techn. paper 3203, 1992

[Wan98] Wang W Wu. and Lust RV: *Deterministic Design, Reliability-based Design and Robust Design*. NASTRAN Conference 1998

14 Contributions of the Author to Handbooks, Working Groups, MAN-Projects

14.1 Glossary for Civil- and Mechanical Engineering



Fachbegriffe für Kompositbauteile –
Technical terms for composite parts

Glossar für Bauwesen und Maschinenbau –

Glossary for civil- and mechanical engineering
Author: Cuntze, Ralf

Introduction with classification scheme addressed to the beginner who wants to find his product classified in the associated entire technical area

This textbook is a Glossary designed to provide a broad overview of terms used in several disciplines. The focus is on highly stressed components made of fiber composites, i.e. fibers – primarily carbon fibers – with polymer matrix (epoxy, thermoplastic) and concrete matrix (carbon concrete with the technical textile reinforcement grid or with the rod). The wide range of applications includes pipes and containers, rotor blades, pedestrian bridges, textile building envelopes, prefabricated garages, pre-stressed panels, spatial supporting structures made of all possible combinations of a fiber with a matrix, up to a carbon reinforcement of rusty reinforced concrete bridges and waterproof foundations. Several engineering groups are therefore to be connected conceptually with each other.

The author critically deals with some terms and comments on and visualizes them for a better understanding where it seems necessary to him. It is a work to stimulate constructive discussion, which should connect specialist disciplines and help to avoid mistakes and misunderstandings in the development process by “speaking the same language”. This project is made more difficult because some terms have evolved away from the original definition. Thus, terms and their definitions are the central subject of the Glossary. This includes abbreviations and indexing as well as an overview of the classification scheme for component-reinforcing fiber composites. Above all, the dimensioning engineer is addressed.

The Glossary includes a scheme that collects notions and abbreviations in fiber-reinforced composites.

In the notation, self-explaining symbols are used if a property is addressed. A lamina, defined to be the calculation unit, may consist of several physical layers or plies (pre-pregs). Green means applied abbreviations.

Note:

Establishing a Glossary becomes more difficult by the fact that some terms have evolved away from the original definition and further by the fact that, for example, the letter C has long been used for composite and carbon, concrete, ceramics and compressive as well.

Such a problem is not new, as the quotations below show:

"*Unfortunately, we have used these words in so different ways that we no longer clearly understand each other when we say them*" [*A. Donabedian, 1982*] or even much older *"A general system of signs and symbols is of high importance for a logically consistent universal language for scientific use!"* attributed to Gottfried Wilhelm Leibniz, 1700.

Often, the term concrete is used instead of mortar when the component is structurally reinforced.

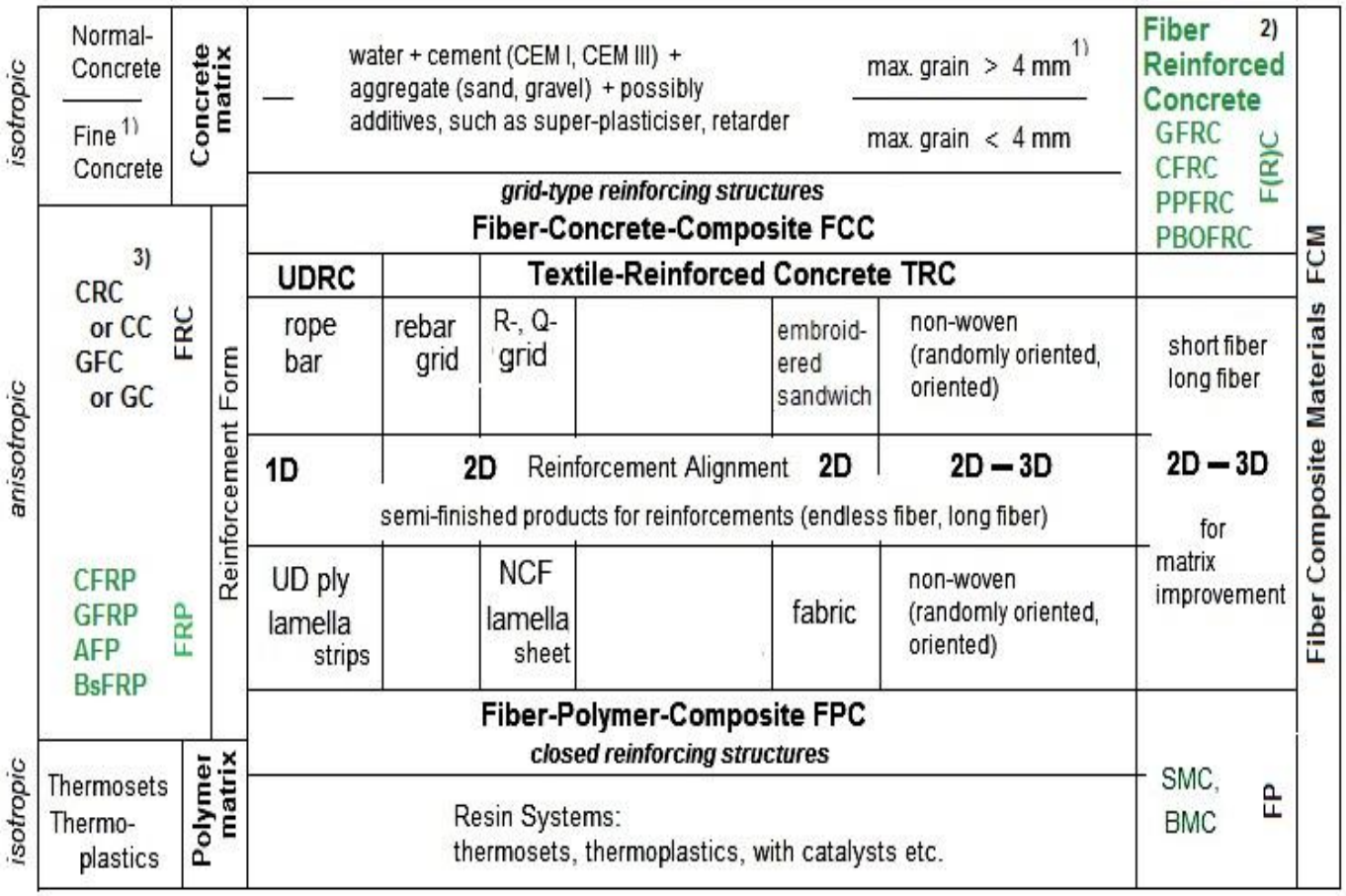


Figure: First Attempt to structure the various composites in Civil Engineering (Cuntze, 2019)

FRP =Fiber-Reinforced Plastic, FRC = longFiber-Reinforced Concrete, sFRC = shortFiber-Reinforced Concrete, CFRC = CarbonFiber-Reinforced Concrete, CFRCp = CarbonFiber-Reinforced Concrete with polymer matrix as impreegnatio of the fiber strand reinforcement, CFRCm = CarbonFiber-Reinforced Concrete with mineral matrix in the reinforcement

14.2 Contributions to Handbooks, Guidelines



HSB HANDBUCH STRUKTUR BERECHNUNG	General description	Issue E Year 2018 Page 1 of 21

Luftfahrt-Technisches Handbuch (**LTH**)

HSB

HANDBUCH STRUKTUR BERECHNUNG

Fundamentals and Methods
for
Aeronautical Design and Analyses

issued by

INDUSTRIE-
AUSSCHUSS-
STRUKTUR-
BERECHNUNGSUNTERLAGEN

Prepared:	Checked:	Date:	
Dr. M. Schagerl	Dr. M. Magin	22.11.2018	IASB / IVW

Digitally signed by Michael Magin
Date: 2020.10.20 00:13:05 CEST

- ***Co- reworker and Co-translator of the 'Airbus' structural handbook into English (2004) , design sheet contributor 1972-2015***

- ***Editor of the VDI 2014 (2006) and contributor since 1980!*** *See →*

ICS 59.100, 83.140.20 VDI-RICHTLINIEN September 2006

VEREIN DEUTSCHER INGENIEURE

Entwicklung von Bauteilen aus Faser-Kunststoff-Verbund Berechnungen

Development of FRP components (fibre reinforced plastics) Analysis

VDI 2014

Blatt 3 / Part 3

Ausg. deutsch/englisch
Issue German/English

Frühere Ausgabe: 04.97 Entwurf, deutsch
Former edition: 04.97 Draft, in German only

Zu beziehen durch / Available at Beuth Verlag GmbH, 10772 Berlin – Alle Rechte vorbehalten / All rights reserved © Verein Deutscher Ingenieure e.V., Düsseldorf 2006

Die deutsche Version dieser Richtlinie ist verbindlich.

No guarantee can be given with respect to the English translation. The German version of this guideline shall be taken as authoritative.

Inhalt Seite

Vorbemerkung . . . 3
1 Anwendungsbereich . . . 3
2 Abkürzungen, Begriffe, Symbole, Indizierung . . . 4
3 Berechnungsablauf . . . 12
3.1 Allgemeines . . . 12
3.2 Auslegungsphilosophie . . . 14
3.3 Berechnungsprogramme . . . 15
4 Modellierung der Schicht . . . 16
4.1 Allgemeines . . . 16
4.2 Eben beanspruchte Schicht . . . 18
4.2.1 UD-Schicht (faserparalleles KOS) 18
4.2.2 G-Schicht und M-Schicht . . . 20
4.2.3 Drehung der UD-Schicht in das Laminat-KOS . . . 21
4.2.4 Berücksichtigung der Schubspannungen aus Querkraft bei UD-Schichten . . . 22
4.3 Räumlich beanspruchte Schichten . . . 23
4.3.1 Mechanische Beanspruchung (faserparalleles KOS) . . . 23
4.3.2 Mechanische Beanspruchung einer UD-Schicht (gedrehtes KOS) . . . 25
4.4 Einfluss von Beanspruchungsarten/-dauer 26
4.4.1 Kurzzeitbeanspruchung . . . 26
4.4.2 Ruhende Langzeitbeanspruchung . 26
4.4.3 Schwingbeanspruchung . . . 30
4.4.4 Stoßbeanspruchung . . . 31
4.5 Festigkeitskriterien . . . 31
4.5.1 Allgemeines . . . 32
4.5.2 Bruchbedingungen für UD-Schichten . . . 36
4.5.3 G-Schicht . . . 44
4.5.4 M-Schicht . . . 45
4.5.5 Einzusetzende Festigkeitswerte . . 46
4.6 Anwendung von Berechnungsprogrammen . . . 46
4.6.1 UD-Schicht . . . 46
4.6.2 G-Schicht . . . 48

Contents Page

Preliminary note . . . 3
1 Scope . . . 3
2 Abbreviations, terminology, symbols, superscripts and subscripts . . . 4
3 Analytical procedure . . . 12
3.1 General comments . . . 12
3.2 Design philosophy . . . 14
3.3 Computer programs . . . 15
4 Modelling the lamina . . . 16
4.1 General comments . . . 16
4.2 Two-dimensionally loaded lamina . . . 18
4.2.1 UD lamina (parallel-to-fibre COS) . 18
4.2.2 WF lamina and M lamina . . . 20
4.2.3 Rotation of the UD lamina into the laminate . . . 21
4.2.4 Inclusion of shear stresses from transverse forces in case of UD laminae . . . 22
4.3 Laminae subject to three-dimensional loading . . . 23
4.3.1 Mechanical loading (parallel-to-fibre COS) . . . 23
4.3.2 Mechanical loading of a UD lamina (rotated COS) . . . 25
4.4 Influence of loading type and duration . . 26
4.4.1 Short-term load . . . 26
4.4.2 Long-term static load . . . 26
4.4.3 Cyclic load . . . 30
4.4.4 Impact load . . . 31
4.5 Strength criteria . . . 31
4.5.1 General comments . . . 32
4.5.2 Fracture conditions for UD lamina . . . 36
4.5.3 WF lamina . . . 44
4.5.4 M lamina . . . 45
4.5.5 Strength values to be used . . . 46
4.6 Application of calculation programs . . . 46
4.6.1 UD lamina . . . 46
4.6.2 WF lamina . . . 48

VDI-Gesellschaft Kunststofftechnik

VDI-Handbuch Kunststofftechnik
VDI-Handbuch Konstruktion

Vervielfältigung – auch für innerbetriebliche Zwecke – nicht gestattet / Reproduction – even for internal use – not permitted

All rights reserved © Verein Deutscher Ingenieure e.V., Düsseldorf 2006

Seite

5 Modellierung des Laminates 48
5.1 Ermittlung von Spannungen und Verzerrungen 49
5.1.1 Netztheorie 49
5.1.2 Klassische Laminattheorie (CLT) . . 55
5.1.3 Interlaminare Spannungen (ILS) . . 61
5.1.4 Berücksichtigung der Verzerrung aus Schubspannungen durch Querkraft 68
5.1.5 Behandlung von Kerben 69
5.2 Schichtenweise Bruchanalyse 72
5.2.1 Grundsätzliche Betrachtungen . . . 72
5.2.2 Nichtlineare Spannungsanalyse vor dem ZFB 73
5.2.3 Kontinuierliche Modulabminderung (Degradation) nach dem ZFB 77
5.2.4 Auswirkung von FB 81
5.2.5 Vereinfachungen und selektive Nachprüfung 81
5.2.6 Maßnahmen zur zielgerichteten Verbesserung von Laminaten 82
5.3 Anwendung der schichtenweisen Bruchanalyse für verschiedene Beanspruchungsarten 83
5.3.1 Kurzzeitbeanspruchung 83
5.3.2 Langzeitbeanspruchung 83
5.4 Schwingbeanspruchte Laminate 89
5.4.1 Schädigungsvorgänge 89
5.4.2 Darstellung von Schwingfestigkeitsergebnissen 92
5.4.3 Bauteilbelastungsgeschichte 96
5.4.4 Methoden der Schwingfestigkeitsanalyse 97
5.4.5 Auslegungshinweise 99
5.5 Anwendung von Berechnungsprogrammen 100
5.5.1 Laminat-Analyseprogramme 100
5.5.2 FEM 101
5.5.3 Berechnung von Anstrengung und „Streckungsfaktor der lastbedingten Spannungen“ bei gleichzeitig wirkenden Eigenspannungen 102

6 Bauteilberechnung 105
6.1 Allgemeines 105
6.2 Stabilitätsberechnungen 107
6.2.1 Knicken von Stäben 109
6.2.2 Beulung ebener Platten 110
6.2.3 Beulung zylindrisch gekrümmter Flächenträger 113
6.2.4 Anmerkungen 120
6.2.5 Berechnungen mit FEM 122
6.3 Verbindungen und Krafteinleitungen 122
6.3.1 Klebverbindungen 123
6.3.2 Bolzenverbindungen 128
6.3.3 Schlaufenanschlüsse 129

Schrifttum 131

Anhang 134

Page

5 Modelling the laminate 48
5.1 Determining stresses and strains 49
5.1.1 Netting theory 49
5.1.2 Classical laminate theory (CLT) . . 55
5.1.3 Interlaminar stresses (ILS) 61
5.1.4 Taking into account the strains arising from shear stresses due to transverse forces 68
5.1.5 Treatment of notches 69
5.2 Lamina-by-lamina fracture analysis 72
5.2.1 Fundamental aspects 72
5.2.2 Non-linear stress analysis before IFF 73
5.2.3 Continuous modulus reduction (degradation) after IFF 77
5.2.4 Effect of FF 81
5.2.5 Simplification and selective reviews 81
5.2.6 Making specific improvements of laminates 82
5.3 Application of lamina-by-lamina fracture analysis for different types of loading . . . 83
5.3.1 Short term loading 83
5.3.2 Long term loading 83
5.4 Cyclically loaded laminates 89
5.4.1 Fracture processes 89
5.4.2 Presentation of fatigue strength results 92
5.4.3 Component loading history 96
5.4.4 Methods of fatigue strength analysis 97
5.4.5 Advices for design 99
5.5 Application of calculation programs . . . 100
5.5.1 Laminate analysis programs 100
5.5.2 FEM 101
5.5.3 Calculating of stress exposure and “stretch factor of the load-determined stresses” with simultaneous by acting residual stresses 102

6 Analysis of FRP components 105
6.1 General comments 105
6.2 Stability analyses 107
6.2.1 Buckling of struts 109
6.2.2 Buckling of flat plates 110
6.2.3 Buckling of cylindrically curved plates and shells 113
6.2.4 Comments 120
6.2.5 Finite element analyses 122
6.3 Joints 122
6.3.1 Bonded joints 123
6.3.2 Mechanically fastened joints 128
6.3.3 Loop joints 129

Bibliography 131

Annex 134

VEREIN DEUTSCHER INGENIEURE

Entwicklung von Bauteilen aus Faser-Kunststoff-Verbund
Zuverlässigkeit und Sicherheit

VDI 2014
Blatt 4 (4. Entwurf)
Zusammengestellt
R. Cuntze, MAN

Development of FRP components
(fibre reinforced plastics)
Reliability and Safety

Einsprüche bis ??.??.1995 an
Verein Deutscher Ingenieure
VDI-Gesellschaft Kunststofftechnik
Postfach 10 11 39
40002 Düsseldorf

Inhalt Seite

Vorbemerkung .....

1. **Anwendungsbereich, Nutzen** .....
2. **Abkürzungen, Begriffe, Symbole** .....
3. **Nachweis** .....
   - 3.1 Allgemeines zu Rechnerischem und Experimentellem Nachweis .....
   - 3.2 Mechanische Modellierung (Grenzzustände)
   - 3.3 Experimenteller Nachweis .....
4. **Traditionelles Sicherheitskonzept (TSK)** .....
   - 4.1 Allgemeines, charakteristische Werte .....
   - 4.2 Unsichere Eingangsgrößen beim Rechnerischen Nachweis .....
   - 4.3 Sicherheitsfaktoren (Auslegung) und Sicherheitsmargen (rechn. und experim. Nachweis)
   - 4.4 Kritik am TSK .....
5. **Probabilistisches Sicherheitskonzept (PSK)** .....
   - 5.1 Allgemeines .....
   - 5.2 Einwirkungsgrößen, Widerstandsgrößen und stochastische Konstruktionsparameter .....
   - 5.3 Teilsicherheitsfaktoren (semiprobabilistische Vorgehensweise) .....
   - 5.4 Stochastische Modellierung und Logische Modellierung des Versagenssystems .....
   - 5.5 Berechnung von Versagenswahrscheinlichkeit oder Zuverlässigkeit .....
6. **Bestimmung von Kennwerten** .....
   - 6.1 Definition und Verwendung von Dimensionierungskennwerten .....
   - 6.2 Ermittlung der statistischen Parameter aus Meßdaten .....
   - 6.3 Ermittlung Charakteristischer Werte .....
7. **Produktsicherung** .....
   - 7.1 RAMS-orientierte Entwicklung .....
   - 7.2 Qualitätssicherungskonzept und Integritätskontrolle mit Prüfmethoden .....
   - 7.3 Versuche zur Erzielung der Strukturzuverlässigkeit des FKV-Bauteils .....

Literatur .....

Anhang 1 Schätzverfahren, Statistische Tests, Updating Verfahren, Bayes .....

Vorbemerkung

Die Richtlinie enthält Empfehlungen für das Entwikkeln von Bauteilen aus Faser-Kunststoff-Verbunden (FKV), die aus einzelnen faserverstärkten Schichten bestehen, bei denen Fasern in einer Kunststoff-Matrix eingebettet sind. Die Bauteilentwicklung wird dargestellt, wobei die Berechnungen eingehender behandelt werden. Die Richtlinie will durch Systematisieren und Vereinheitlichen der Bauteildimensionierung auch die Zulassungsverfahren und die Qualitätssicherung erleichtern. Sie ist in vier Teile gegliedert:

- Blatt 1 Grundlagen
- Blatt 2 Konzeption und Gestaltung .....
- Blatt 3 Berechnung .....
- Blatt 4 Zuverlässigkeit und Sicherheit.

Beispielsammlung: s. VDI Report??

Unfortunately not issued.

ECSS-E-HB-32-24A
24 March 2010

EUROPEAN COOPERATION
ECSS
FOR SPACE STANDARDIZATION

Space engineering

Buckling of structures

ECSS Secretariat
ESA-ESTEC
Requirements & Standards Division
Noordwijk, The Netherlands

This Handbook has been authored and agreed upon by:

J. Arbocz, TU Delft
C. Bisagni, Politecnico di Milano
A. Calvi, ESA-ESTEC (Convenor)
E. Carrera, Politecnico di Torino
R. Cuntze, formerly MAN-Technologie
R. Degenhardt, DLR Braunschweig and PFH Göttingen
N. Gualtieri, Thales Alenia Space
H. Haller, Intales
N. Impollonia, Università di Catania
M. Jacquesson, CNES
E. Jansen, TU Delft
H.R. Meyer-Piening, ETH Zuerich
H. Oery, RWTH Aachen
A. Rittweger, Astrium EADS
R. Rolfes, Leibniz Universitaet Hannover
G. Schullerer, MT Aerospace
G. Turzo, CNES
T. Weller, Technion, Haifa
J. Wijker, Dutch Space

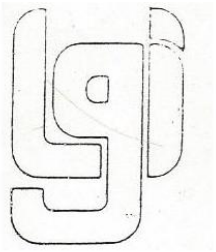
The valuable contributions of the following persons are acknowledged:
C. Huehne, DLR Braunschweig; D. Petry, Astrium EADS;
H. G. Reimerdes, RWTH Aachen; K. Rohwer, DLR Braunschweig;
R. Zimmermann, DLR Braunschweig.

The ECSS-E-HB-32-24 has been prepared by merging the volunteer contributions of the authors. Comments concerning the technical content of this handbook will be welcomed by the European Cooperation for Space Standardization, Noordwijk, the Netherlands, www.ecss.nl.

- **Author was organizer of above Working Group (WG), convener and contributor**

- **Member of DVM-WG "Characteristic Value Determination and Application of Fracture Mechanics".** ***Headed by K.-H. Schwalbe***

- **Founder and organizer of 4 Working Groups at Composites United e.V.**
  - **Engineering**, *aerospace, mechanical engineering*
  - **Composites Fatigue,** *aerospace, mechanical engineering*
  - **Design Dimensioning and Design Verification,** *civil engineering*
  - **Automated fabrication in construction including serial production including *'3D-Printing'*, *civil enineering.)***



SHORT COURSE
DEVELOPMENT OF FIBRE REINFORCED PLASTIC COMPONENTS

Pretoria

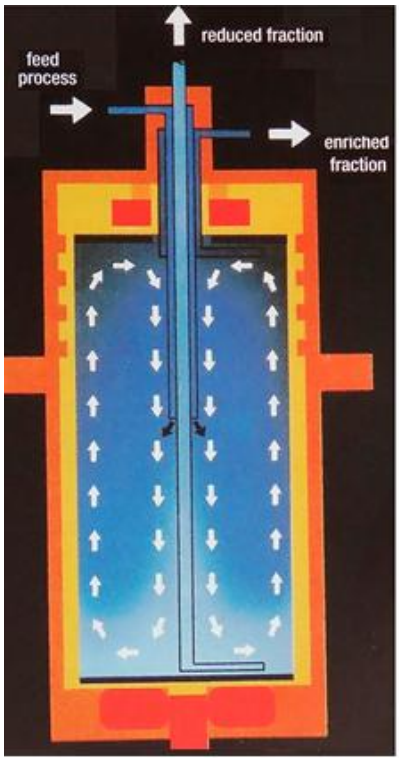
16th to 18th April 1986

Presented by : Dr R G Cuntze

Course Organizer : P A Coetzer

And again 1989

14.3 Projects involved: Memories of working life at MAN

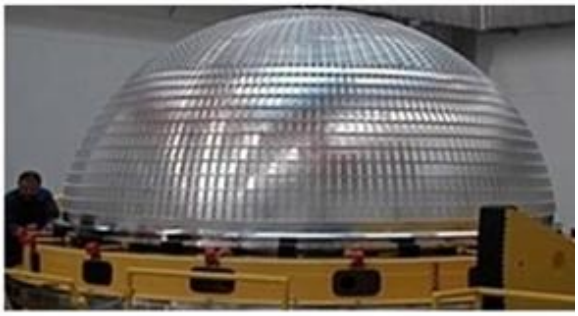




Uranium enrichment in Gas-Ultra-Centrifuges (metal, CFRP). Separation of U235 from U238



CFRP Booster section



Liquid H2-tank dome for Ariane 5



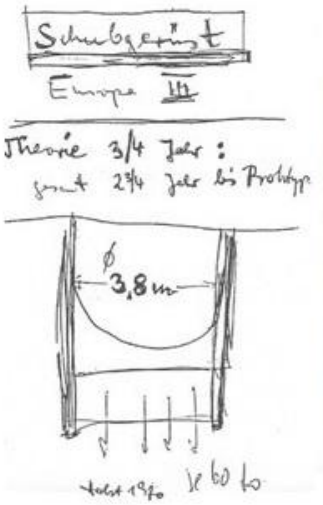
Apogee motor



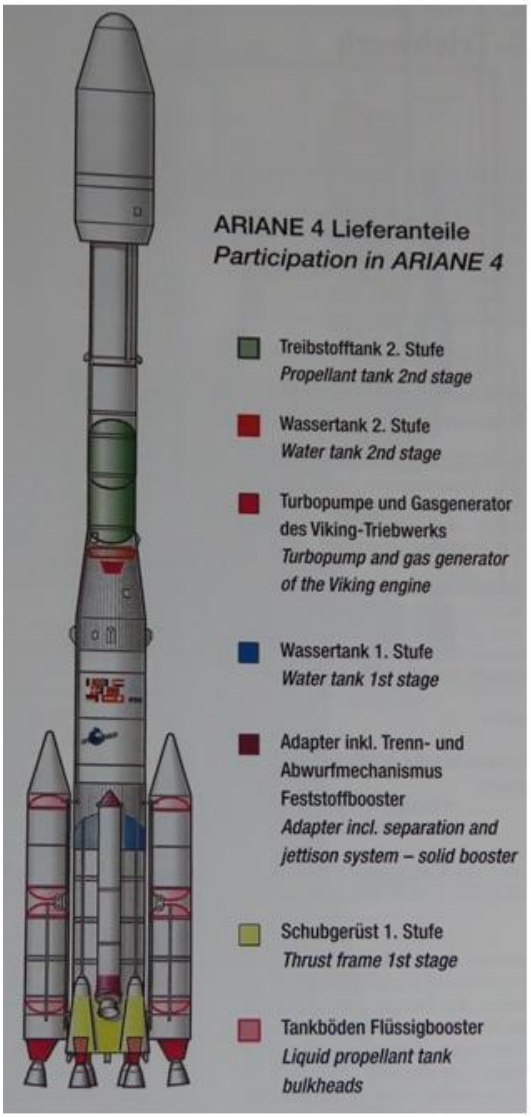
Filament winding of a pressure vessel

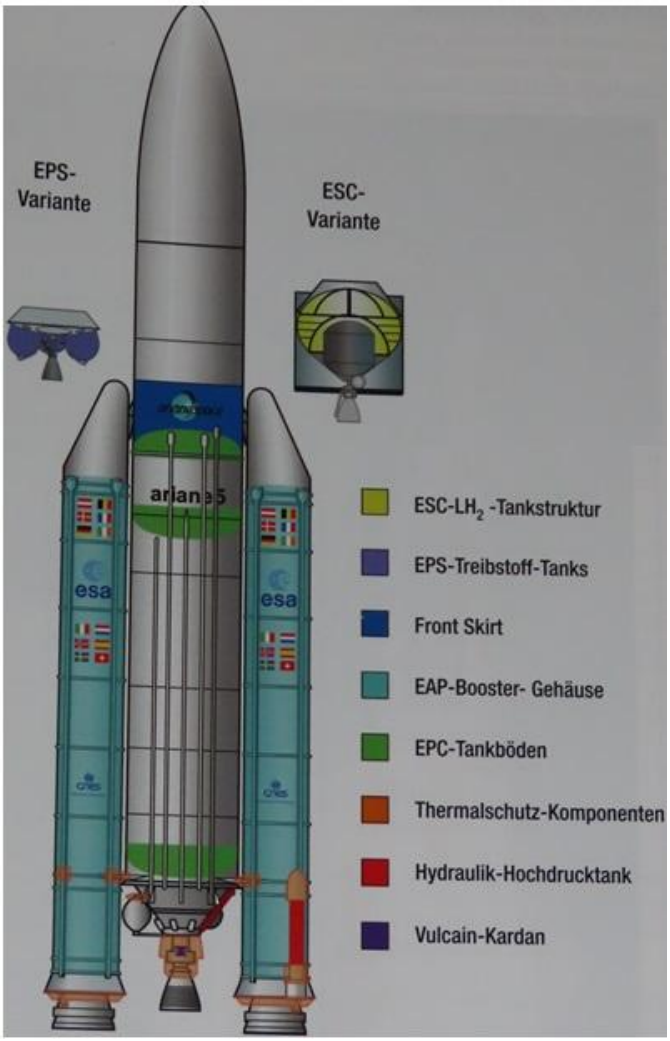
The slip of paper below was the start of my work at MAN-Neue Technologie in 1970 regarding the development of the **Ariane launcher family**:
"Make a design proposal for an offer, please " (Thrust structure).











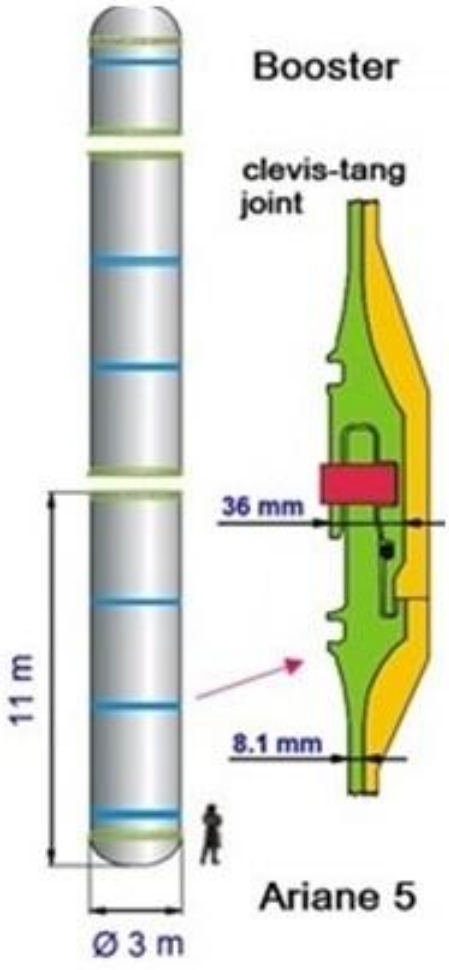


Front Skirt Ariane 5





Tank-in-tank system unconventional 'nested' tank



A502 no structural failure











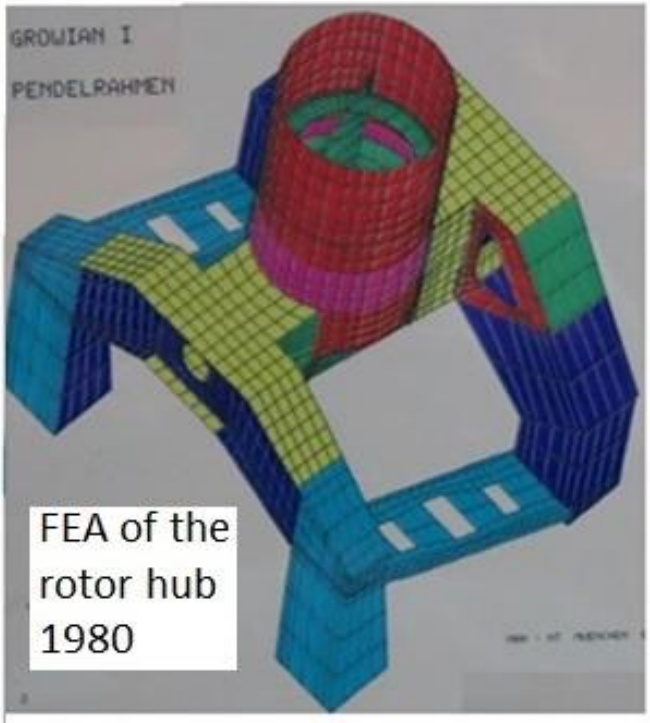
Apogee motors and pressure vessels

Tanktyp	GAM-Hochdruck-tank (Bild 1)	GAT-Hochdruck-tank (Bild 2)
Volumen	183 l	520 l
Operationsdruck	230 bar	450 bar
Mindest-Berstdruck	460 bar	900 bar
Durchmesser	400 mm	400 mm
Länge	1700 mm	4400 mm
Masse	59 kg	200 kg





GROWIAN tested at IABG, 1980, GFRP shell **L = 50 m**





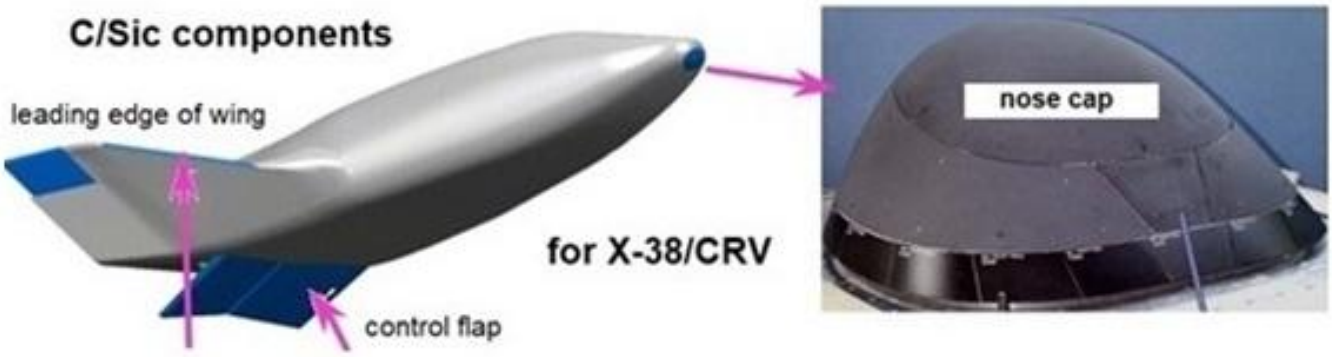
Test specimen
Development of a
Braided CFRP hip shaft

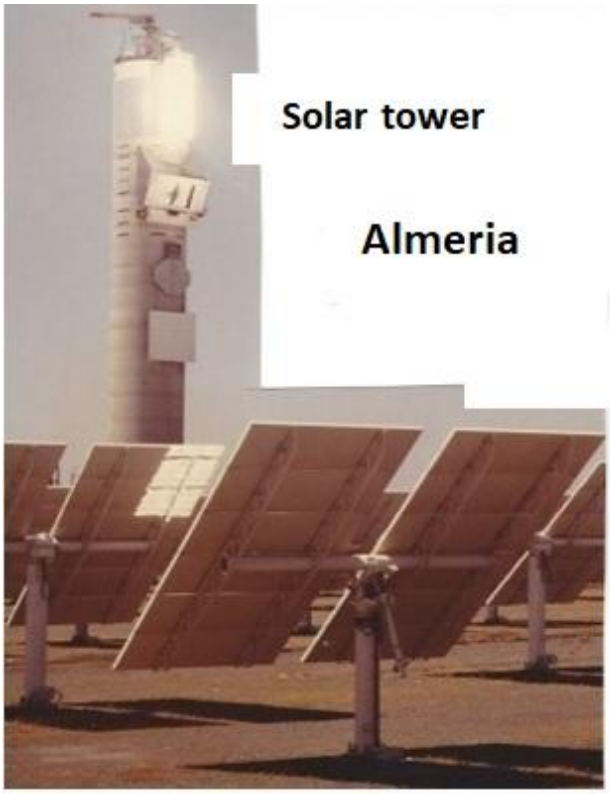


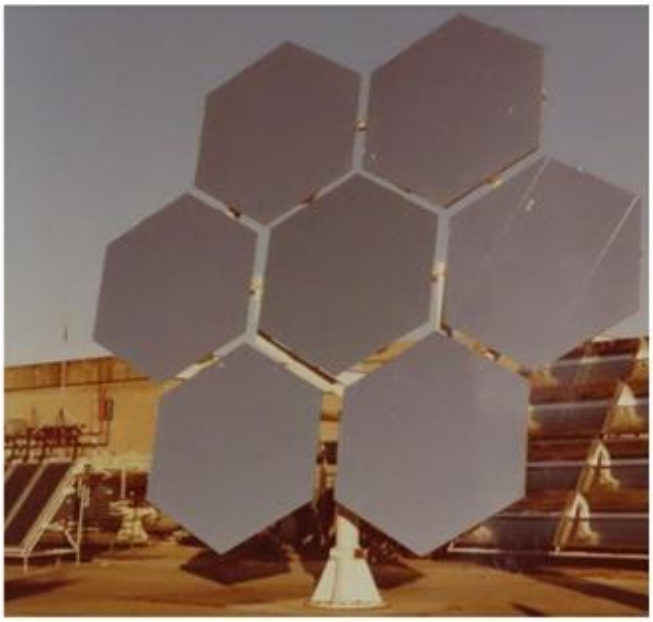


NIESYTO design, S. Guisard,









Solar field





Ariane Launcher Family 1 -5 [Courtesy ARIANESPACE]





Toroidal Water Tank for cooling hot gases



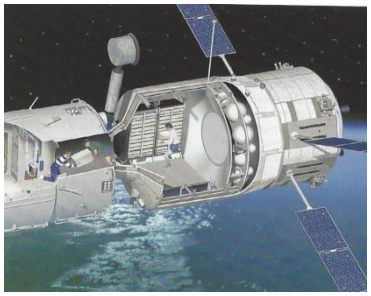
Structural Watertank Ariane 4 during mounting







Thrust frame of the first stage,
load-carrying structure to transfer the loadings of the four engines



Automated Transfer Vehicle (2008) for supply of the ISS space station

CARBON COMPOSITES

Thementag der AG Engineering
"Ermittlung strukturmechanischer Kennwerte und Modellparameter *unter Beachtung von Auslegung, Nachweis und Zulassung*"

- *Betrachtung von Schicht, Laminat, Festigkeitsmodell etc.* –

Zielgruppe: Berechnungsingenieure in Anwendung und Forschung

Donnerstag, 6. November. Beginn: 9:00 Uhr, Ende: ca. 16 Uhr
Atrium-Saal der HWK Schwaben, Siebentischstraße 52-58, 86161 Augsburg
(Unkostenbeitrag Thementag: 95 € + MwSt für Nicht-Vortragende und Nicht-CCeV-Mitglieder)
Am 7.11. ist eine Veranstaltung der 3 AGs Engineering, NDI und Kleben. IHK-Schwaben, Stettenstr., 9 Uhr
Münchner Leichtbauseminar: "Werkstoff- und Bauteildaten für Simulationsmodelle im Leichtbau" 29.10., 12.11., 26.11.

Begrüßung *R. Cuntze (CCeV) , H. Bansemir (vormals Eurocopter)*

Vorträge (5 min Diskussion), Folien, englisch oder deutsch

1. (9.05) **SURVEY: Material Properties and Model Parameters, necessary for the Analysis of Static & Cyclic Stress States.** *R. Cuntze, CCeV-AGs Engineering Maschinenbau* und *Faserverstärkung im Bauwesen*
2. (9.45) **Beitrag zur korrekten Bestimmung der Quer-Längsschubsteifigkeit und Festigkeit und von Pucks Modellparametern zur Erfassung interner Werkstoffreibung.** *A. Bleier, Karl Mayer Textilmaschinenfabrik, Obertshausen; vormals KLuB TU-Darmstadt*
3. (10.15) **Normen und Standards, Normungsportal der Composites Germany**. *F. Fendt, CCeV-AG Normung und Standardisierung*

Kaffee-Pause: (10.45)

4. (11.15) **Prüfmethoden und Werkstoff-Probekörpergestaltung.** *H. Bansemir, vormals Eurocopter)*
5. (11.45) **„Bessere Methoden für bessere Werte", Verbesserungsvorschläge u.a. am Beispiel der Modul-Degradationsmethode.** *T. Haberle, RUAG*

Mittagsbuffet: (12.15)

6. (13.00) **Ermittlung von UD-Kennwerten und Cuntzes Reibungsparametern beim DLR-Braunschweig.** *E. Petersen, DLR-Braunschweig*
7. (13.30) **Welche Baustoffkennwerte benötigen die Textilbetonbauer?** *F. Schladitz, IfM TU-Dresden*
8. (14.00) **Establishing an in-house Process for Composite Testing – an overview**. *J. Bold, Johnson Controls, Burscheid*

Kaffee-Pause: (14.30)

9. (15.00) **Digimat Multi-Scale Modeling Platform. A Paradigm Shift in the Optimal Engineering of Composite Materials & Structures**. *R. Assaker, X-stream, Munich*
10. (15.30) **Neue Prüfmethoden zur Ermittlung temperatur- und dehnratenabhängiger Kennwertfelder für die Luftfahrt- und Automobilindustrie.** *R. Bochynek, Leichtbau-Zentrum Sachsen, Dresden*
11. (16.00) **Diskussion:** Wo drückt der Schuh am meisten? **mit Ausklang im Foyer, Abendbuffet**

Es freuen sich auf eine rege Beteiligung und inhaltsreiche interessante Vorträge

Ihre Ralf Cuntze und Horst Bansemir

CARBON COMPOSITES	*MINUTES OF MEETING (MOM)* THEMENTAG ERMÜDUNG	Februar 14, 2013

Gemeinsame Sitzung mit „Deutsche Arbeitsgruppe BeNa (Betriebsfestigkeits-Nachweis) Ermüdung von Bauteilen aus Faserverbundwerkstoff (FVW)
- Vertiefte Betrachtung von UD-Laminaten mit Ausblick Textile Composites –

Ort: IHK Schwaben, Stettenstrasse 1+3, 86150 Augsburg, Hans-Liebherr-Raum. Zeit: 8.00 bis 17.00.
Vorträge: 20 min + 5min Diskussion
Begrüßung: *(P. Horst, TU-Braunschweig, Leiter AG BeNa)*; einführende 'Folien' *(R. Cuntze, CCeV*
Vorstellung und Ziele der AG BeNa. *P. Horst, TU-Braunschweig*

1. Vom Ermüdungsverhalten von Metallen zu dem von FVW. *G. Kress, ETH Zürich*
2. Ein Lebensdauervorhersagemodell für langfaserverstärkte Laminate. *R. Cuntze, CCeV*
3. ZfP und Festigkeit/Ermüdung. *V. Trappe (BeNa), BAM Berlin*
4. Ein neues physikalisch basiertes Ermüdungs-Schädigungsmodell für Faser-Kunststoff-Verbunde. *R. Rolfes (BeNa), ISD, TU-Hannover*
5. FE-Analyse der Ermüdungsschädigung von FKV. *M. Magin (BeNa), IVW Kaiserslautern*
6. Anforderungen und Herausforderungen an die Betriebsfestigkeiten für Faserverbund strukturen bei der A350XWB. *D. Hartung, Premium Aerotec Augsburg*
7. Composite Fatigue Approach in Airbus. *W. Göbel / L. Ratier, Airbus*
8. Ermüdet Textilbeton? *F. Jesse, BTU-Cottbus*
9. Fatigue Life Simulat. and Verification of Wind Turbine Rotorblades. *E. Eyb, Re-Power*
10. Betriebsfestigkeitsbewertung von Faserverbundwerkstoffen – Übersicht und Ausblick. *M. Hack, LMS Kaiserslautern*
11. Methods for life predict. of comp. materials and adhesively-bonded composite joints. S. *Vassilopoulos, EPFL Lausanne, CH*, editor *"Fatigue life prediction of composites and comp. structures"*, 2010
12. Lebensdauervorhersage bei BMW. *P. Wagner, BMW München*
13. Zur Festigkeitsbewertung von CFK-Strukturen unter PKW-Betriebslasten. *C. Hahne/ U. Knaust, Audi Ingolstadt*
14. Praxiseffekte bei der Schwingfestigkeitsanalyse orthotroper Faserkunststoffverbunde. *Ch. Enke / J. Eulitz / R. Grothaus, EAST-4D Carbon Technology Dresden*
15. (I) Geschichte der Fatigue-Nachweisführung bei Eurocopter (seit 1965). *H. Banvenir.* (II) Vorgehensweise bei dem Fatigue-Nachweis mit der Bestimmung der Wöhlerkurven und Arbeitskurven. *E. Ahci, Eurocopter Donauwörth .* (III) Die dynamische Festigkeit von Kohlefaser-Verbundstrukturen. *A. Weinert, Eurocopter*

Aufnahme von interessierten Industrie- und Behördenmitgliedern in die AG BeNa. :
Laut Teilnehmern (>120) ein erfolgreicher Thementag mit der richtigen Mischung.

1. Workshop "Composite Fatigue",6.2.2014: Bitte um Vortrags-Vorschläge bis zum 1. 9. 2013 an mich.
2. Thementag "Industrielle Anwendbarkeit der Schädigungsmechanik – Schwerpunkt FVW", 24.10.2013, ganztägig in Augsburg vor der Herbstsitzung der AG "Engineering ", Fr.25.10.13
3. Fazit : Die Abschätzung der Lebensdauer von FKV-Bauteilen unter Betriebsbeanspruchung ist eine wichtige Aufgabe, weil man sich nur begrenzten Testaufwand erlauben kann. Generell kann man sagen: Es ist keine allgemein anwendbare Lebensdauervorhersagemethode für Laminate vorhanden und das erst recht für textile Laminate. Ermüdungsgefahr besteht auch seitens der Textilbetonindustrie.

Meinen allerbesten Dank an alle Vortragenden für die gelungenen Vorträge.

Ihr Ralf Cuntze

PS: Nur Mitarbeiter von CCeV-Mitgliedern haben vollen Zugriff auf alle PDFs auf der CCeV-Website.

CARBON COMPOSITES

Experience Composites 2016 – Symposium/Congress, Sept. 21-23

Augsburg Messezentrum **Thementag**

1. (10.00) **Introduction Design and Design Verification.** *R. Cuntze, CCeV, Augsburg*
2. (10.30) **Novel Material models and multi-scale simulation methods for composite materials.** *R. Boehm, ILK Dresden*
3. (11.00) **Simulation of Manufacturing Processes.** *C. Huehne, DLR-Braunschweig*
4. (11.30) **MAI-Cluster, Impacts from Section Design Results.** *R. Hinterhoelzl, LLC, TU-München*

Lunch Break (12.00)

5. (13.30) **Load Introduction in Monolithic and Hybrid Leightweight Structures.** *H. Rapp, UniBw München*
6. (14.00) **Fatigue, BeNa's View State–of-the-Art**: *I. Koch, ILK TU-Dresden (member of German fatigue working group BeNa, Betriebsfestigkeits-Nachweis)*
7. (14.30) **Strength and Curing Simulation of Thick-walled Composites with ANSYS WB 17.0.** *R. Roos, ANSYS Switzerland*
8. (15.00) **Impacts from the NAFEMS Composites Group.** *C. Huehne, DLR-Braunschweig, NAFEMS Steering Committee*

Coffee Break (15.30)

9. (16.00) **The German Aeronautical Handbook HSB: Current contributions and research activities on fundamentals and methods for structural design and analyses.** *M. Schagerl, JKU-Linz, Austria*
10. (16.30) **First-Ply Failure and what then? – Solutions for a detailed simulation of failure.** *Matthias Hörmann, CADFEM GmbH, Grafing*
11. (17.00) **Certification Aspects.** *H. Bansemir, formerly Eurocopter Germany, München.*

CARBON COMPOSITES

Thementag "Industrielle Anwendbarkeit der Schädigungsmechanik"

- *Betrachtung von UD Laminaten bis zu textilen Composites – Grundlagen und Anwendung*

Zielgruppe: Berechnungsingenieure in Anwendung und Forschung

Donnerstag, 24. Oktober. Beginn: 8:15 Uhr, Ende: 16.00 Uhr

A1-01-A1.02-Saal der HWK Schwaben, Siebentischstraße 52-58, 86161 Augsburg

(Am 25. 10. ist die gemeinsame Veranstaltung der 3 AGs Engineering, NDI, Kleben. Hierzu sind alle Teilnehmer ebenfalls eingeladen. Zwei Schädigungsmechanik-Vorträge werden dann nachgeholt. Unkostenbeitrag: 95€ für Nicht-Vortragende und Nicht-CCeV-Mitglieder)

Begrüßung *R. Cuntze (CCeV), R. Böhm (ILK Dresden)*

Vorträge (25 min + 5 min Diskussion): *Betonung: Was geht? Wo drückt der Schuh?*

1. (8.30) **Einführung in die Schädigungsmechanik von Werkstoffen.** *Dr. U. Weber, Prof. S. Schmauder (IWMF Uni Stuttgart), in English or German*
2. (9.00) **Schädigungsmechanik für Faser-Kunststoff-Verbunde: Phänomenologische Ansätze.** *Dr. R. Böhm (ILK Dresden)*
3. (9 .30) **Virtuelle Werkstoffentwicklung mit Multi-Skalen-Simulationen am Beispiel von Leichtbau-Flugzeugturbinen.** *A. Freund (LZS Dresden).*

Kaffee-Pause: (10.00)

4. (10.30) **Modellierung der Schädigungsmechanismen bei keramischen Faserverbundwerkstoffen.** *Dr. S. Hofmann, (DLR Stuttgart)*
5. (11.00) **3D-XFEM-Modellierung des Schädigungsverhaltens von Faser-Kunststoff-Verbunden.** *Dr. M. Kästner, S. Müller, Prof. V. Ulbricht (IFKM Dresden)*
6. (11.30) **A link between damage initiation thresholds in static loading and fatigue strength of textile composites.** *Prof. S. Lomov, MTM Leuven*

Mittagsbuffet: (12.00)

7. (13.00) **Entwicklung der Schädigungsmechanik für Faser-Kunststoff-Verbunde (FKV) von 1970-2013.** *Prof. A. Matzenmiller (Uni Kassel)*
8. (13.30) **Anforderungen an die Schädigungsmechanik von FVK-Laminaten für die virtuelle Fahrzeug Crash-Auslegung.** *Dr. M. Nossek (BMW AG)*
9. (14.00) **Failure Analysis at Airbus.** *Dr. Anja Wetzel (Airbus, Hamburg)*

Kaffee-Pause: (14.30)

10. (15.00) **Mechanism-based Three-dimensional Constitutive Model for Anisotropic Damage in Fiber-reinforced Composites.** *M. Chatiri (CADFEM)*
11. (15.30) **Diskussion zur erreichten Anwendbarkeit der schädigungsmechanischen Ansätze**

Ausklang im Foyer, Abendbuffet, Zeit für Gespräche

Freitag, 25.10. Nachläufer (Vortragende vorlesungsmäßig am 24. belegt) im Rahmen der AG *Engineering*:

1. **Modellierung von Material- und Strukturschädigung des Verbundwerkstoffs Stahlbeton.** *Prof. V. Penyna (TU-Berlin)*
2. **Schädigungsmechanik für Faser-Kunststoff-Verbunde – Mikromechanisch basierte Ansätze.** *Prof. R. Rolfes (ISD Uni Hannover),*

Bitte Herrn Jahn (CCeV) mitteilen: (1) Wegen Catering, Teilnahme an welchen Buffets; (2) Übersendung des Vortrag-PDFs

Es freuen sich auf eine rege Beteiligung und inhaltsreiche interessante Vorträge

Ihre Ralf Cuntze und Robert Böhm

CARBON COMPOSITES

Gemeinsame Sitzung der 3er-CCeV-AG

Engineering, Zerstörungsfreie Werkstoff- u. Bauteilprüfung, Kleb- und Verbindungstechnik,

am **9. 3. 2018 beim CCeV, Am Technologiezentrum 5, D 86159 Augsburg**
CCeV-Kontakt Bernhard Jahn (Bernhard.Jahn@carbon-composites.eu).

Agenda (Folien deutsch oder englisch, 25 + 5 min)

9:00	**Begrüßung**
9:15	Vortragstitel. *NN, LCC, München (Kümmerer Dr. Hartmann)*
9:30	**Betrachtungen zur Betriebsfestigkeit von CFK-Triaxialgeflechten.** *F.Herrla, Institut für Leichtbau, UniBw, Neubiberg*
10:00	**Novel Lifetime Prediction for UD-materials**. *R. Cuntze, CCeV Augsburg*
10:30	*Kaffeepause*
11:00	**Schwingfestigkeit von Klebverbindungen unter multiaxialer Schwellbelastung**. *C. Nagel, IFAM Bremen*
11:30	**Festigkeitssimulation in Klebverbindungen**. *R. Sachse, DLR Stuttgart*
12:00	**Einbeziehung geklebter Fensterbänder und Glasfronten in die Festigkeit von Schiffen**. *O. Klapp, IFAM Bremen*
12:30	*Mittagspause*
13:30	**Carbon Fiber Armored Polymer – a novel economic process?** *R. Müller, Kube GmbH Ingenieurbüro, Plochingen*
14:00	**Konzentrierte Lasteinleitung in CFK-Strukturen unter Anwendung der lokalen Metall-hybridisierung**. *E.Petersen, DLR Braunschweig*
14:30	**Faseroptische Prüfmethoden zur Inspektion von CFK-Komponenten.** *D. Samiek, Polytec GmbH*
15:00	*Kaffeepause*
15:30	**Koppelmittelfreie Prüfung von CFK und CFK-Metall-Klebeverbindungen mit Hilfe von Luftultraschall.** *R. Steinhausen, Forschungszentrum Ultraschall*
16:00	**Einsatz des Nichtlinearen Ultraschalls für die Untersuchung geklebter CFK-Strukturen.** *M. Kreutzbruck, Institut für Kunststofftechnik, Uni Stuttgart*
16:15	**Resumee, Abschlussdiskussion**
	Get Together

Wir freuen uns auf eine rege Beteiligung und interessante Vorträge

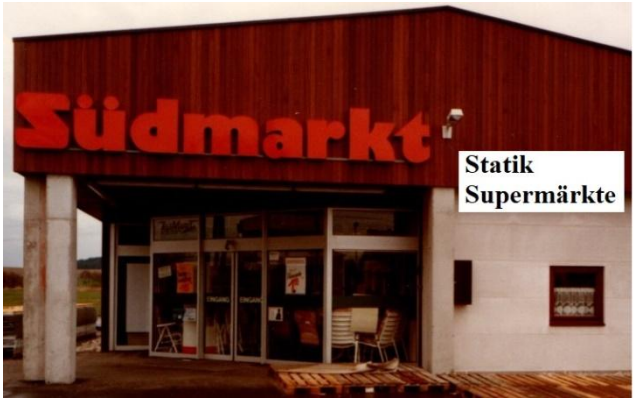
Ihre Ralf Cuntze (08136-7754), Marc Kreutzbruck und Markus Brede

Hinweise: **Sitzungstermine: 16. 11. 2018, gemeinsam mit CC Austria, FH OÖ Campus Wels (Österreich), Dr. R. Hinterhölzl (Leiter Studiengang Leichtbau und Composite-Werkstoffe); 8. 3. 19 UniBw, Neubiberg (Institut für Luft- und Raumfahrt, Prof. H. Rapp)**

Working in Civil Engineer Applications







Structural engineering, armouring plans, pile foundation

Carbonbeton – die Zukunft des Bauens hat begonnen



Foto: Silvia Statt-mayer

Prof. Dr.-Ing. Ralf Cuntze

Als sich 1970 zum ersten Mal Carbonfasern (CF) in meine Fingerspitzen bohrten, wusste ich noch nicht, wie schmerzhaft erst der weitere Weg in Richtung Anwendung sein würde. Die damals gegenüber heute hundertfach teurere Carbonfaser fand praktisch nur Einsatz in Raumfahrt, Luftfahrt oder ultraschnellen Zentrifugen, also im Maschinenbau, und sie war eingebettet in eine Kunststoffmatrix. So waren Ende der 1970er Jahre Diskussionen mit Prof. Rupert Springenschmid, damaliger Institutsleiter „Zentrum Baustoffe und Materialprüfung" der TU München, über den Einsatz von Carbonfasern im Bauwesen schlicht visionär. Erst als ich etwas später bei Prof. Urs Meier, eidgenössische Materialprüfanstalt EMPA, einen sechs Meter langen Biegeträger aus Glasfaserkunststoff bei einem erfolgreichen Langzeit-Ermüdungstest bewundern konnte, bekamen Gedanken bzgl. der Verwendung von Faserkunststoff und Faserbeton im Bauwesen wieder einen Nährboden. An einen Einsatz der immer noch sehr teuren Carbonfasern im Bauwesen war aber noch nicht zu denken.

Der Einsatz z. B. von Kurz-Glasfasern in Faserbeton zur Erhöhung der Zugfestigkeit war ein erster Schritt in Richtung Fasereinsatz, allerdings darf dieser derzeit nicht als anrechenbarer Anteil von tragender Bewehrung gesehen werden, sondern als eine signifikante räumliche Erhöhung lokaler Festigkeit, die sonst zusätzlich durch „händisch" zu armierende Lasteinleitungsstellen abgedeckt wird. Für solche Fälle könnten mm-lange Carbonfasern, hergestellt aus „gemahlenem" rezykliertem Carbonfaser-Gewölle, räumlich verteilt in trockenen Zement, sicherlich ihren Einsatz finden. Erst als es gelang, Stahlstäbe in Stahlbewehrungsmatten durch textile Gelege aus polymermatrixbeschichteten alkaliresistenten Glasfaserrovings und später auch Carbonfaserrovings zu ersetzen (entspricht einem Faser-Kunststoff-Verbund), war der Startschuss für professionelle Anwendungen gegeben und der sogenannte Textilbeton geschaffen. Natürlich ist die Betonmatrix an die jeweilige Faserverstärkung anzupassen. Zulassungen für Bewehrungsstäbe gibt es für Glas.

Durch die im Vergleich zum Stahlbeton kleinere Maschenweite der Carbon-Bewehrungsmatte und die feinere Betonmatrix werden die lokale Rissbildung und somit das Eindringen von Feuchtigkeit stark verringert. Damit wird das gefürchtete Beton-Abplatzen (stahlkorrosionsbedingtes Abplatzen gibt es nicht mehr) nach einigen Jahren als Folge der sogenannten Alkali-Aggregat-Reaktion behindert und die Dauerhaftigkeit des Bauteils erhöht. Bauwerke mit der immer noch relativ teuren Carbonfaser „rechnen sich", wenn man die minimale Wartung, die geringere Betonmasse sowie den niedrigeren Montageaufwand lebenszyklusbezogen kostenkalkuliert. Dies gilt speziell für den anstehenden riesigen Aufwand zur Bauwerkserhaltung und -verstärkung!

Energieverbrauch und CO_2-Erzeugung sind wesentlich geringer als bei Betonstahl, wobei die Einsparpotenziale noch nicht ausgeschöpft sind. Carbonbeton, diese neue Art des Bauens, wird somit sicherlich einen wesentlichen Innovationsschub im Bauwesen auslösen. Leichtere und filigranere Konstruktionen bis hin zu einem neuen Möbeldesign werden Wirklichkeit. Bauen wird ressourcenschonender, nachhaltiger und effizienter werden. Wünschenswert wäre es, wenn die langwierige Zulassungsprozedur weniger Hürden hätte, aber auch die Planung von Bauten mehr auf der Basis von Nachhaltigkeit durchgeführt würde.

Lassen Sie sich durch die Beiträge in diesem Heft begeistern. Besonders möchte ich Ihnen dabei die Vorstellung der sogenannte Planermappe ans Herz legen, mit der die notwendige Überzeugungsarbeit bei Architekten, Baufirmen und Zulassungsstellen einfacher wird.

Ihr *Ralf Cuntze*
(R C = Reinforced Concrete)

CC BAU

CARBON COMPOSITES

Bemessung und Nachweis

- *vom Werkstoff bis zur Zulassung von Bauteilen aus Polymermatrix und Betonmatrix* -

Veranstaltung von allen CC Bau-AGs

Zielgruppen: Bauwirtschaft, Architekten, Planer, Handwerker, Auftraggeber, Zulassungsstellen

22. Oktober 2019 in Weimar, beim Institut für Angewandte Bauforschung Weimar gGmbH

Örtlicher Kontakt: Frau Schalling, 03643 8684 148, k.schalling@iab-weimar.de>

CCeV-Kontakt Bernhard Jahn (Bernhard.Jahn@carbon-composites.eu).

Thementag: 95 € für Nicht-Mitglieder, frei für Vortragende, Presse.

Folien: englisch, deutsch. Vorträge: 25 + 5 min Diskussion.

8:30	Registrierung der Teilnehmer, Kaffee und Brezeln o.ä.
8:45	**Einführende Worte mit Ausrichtung CC Bau.** *R. Cuntze / J. Ridzewski*
9:00	**Vorstellung Institut:** *Dr.-Ing. Barbara Leydolph, IAB Weimar*
9:15	**Verwendete Baustoffe mit Schwerpunkt Carbonbeton:**. *M. Butler, Institut für Baustoffe, TU Dresden*
9:30	**Fertigungsverfahren: Bauteile mit Polymermatrix.** *J. Ridzewski, IMA Dresden*
10:00	**Fertigungsverfahren: Bauteile mit Betonmatrix**. *G. Eisewicht, BCS Natur- und Spezialbaustoffe GmbH Dresden*
10:30	*Kaffeepause*
11:00	**Festigkeitsmodellierung der Baustoffe Beton und Lamelle**. *R. Cuntze, CC Bau Augsburg*
11:30	**Lasten, Sicherheitskonzept und Zulassungsaspekte.** *S. Rempel, Solidian Albstadt*
12:00	**Dimensionierungsbeispiel, GFK-Behälter** (nach BüV 2010). *M. Oppe, Büro Knippers-Helbig Stuttgart*
12:30	*Mittagspause*
13:30	**Dimensionierungsbeispiel, Faserbetonbauteil.** *B. Wietek, Sistrans, Tirol*
14:00	**Dimensionierungsbeispiel, CF-Textilbeton-Bauteile**: *S. May, Carbocon-GmbH. Dresden*
14:30	**Dimensionierungsbeispiel, CLT-Modellierung und Bemessung einer Textilbeton-Schale.** *D. Franitza, FE-Union GbR, Chemnitz*
15:00	*Kaffeepause*
15:30	**Abteilungsversammlung**
16:00	**Get Together**

Wir freuen uns auf Ihre Beiträge Ihr Ralf Cuntze und weiterer CC Bau-Vostand

Hinweise: CC Bau, ehemals CC TUDALIT, Fachabteilung des CCeV, besteht ab 1.1. 2018 aus den 4 AGs: Bemessung und Nachweis (Prof. Ralf Cuntze), Faserverbundarmierte Betone (Dr. Ingelore Gaitzsch), Faserverstärkte Kunststoffe (Prof. Jens Ridzewski), Automatisierte Fertigung im Bauwesen (kommissarisch: Ralf Cuntze)

Termine 2019: 22. Februar, AG „Faserarmierter Beton", Uni Dresden, 13. Juni, AG „Automatisierte Fertigung im Bauwesen", Uni Innsbruck

Termine 2020: Workshop am 19. Februar, Ulmer Betontage bzgl. „Wie bekomme ich Carbonbeton-Anwendungen auf die Bausstelle"?; CC Bau-AGs-Sitzung, 24. Februar, Siegen (weitere Sitzungsplanung mit Möglichkeiten Aachen, Dresden,

CC BAU CC AUSTRIA CC SCHWEIZ CARBON COMPOSITES

DACH-Veranstaltung aller Arbeitsgruppen der CCeV-Fachabteilung „CC Bau“

am 21.06.2018, Raum MY 01.09, bei der
ZHAW Architektur, Gestaltung und Bauingenieurwesen,Gebäude MY, Lagerplatz 21, 8400 Winterthur,
Frau Sydow, 0041 58 934 69 82, CCeV-Kontakt: Bernhard Jahn (Bernhard.Jahn@carbon-composites.eu).

Das Bauwesen ist eine Branche, bei der das Thema Hochleistungsfaserverbund einerseits noch nicht etabliert ist, andererseits jedoch ein enormes Anwendungspotential besteht. Vor diesem Hintergrund hat sich der Carbon Composites e.V. (CCeV) entschieden, das Thema für seine Mitglieder weiter aufzubereiten, zu vertiefen und gemeinsam voranzutreiben. Am 28. September 2017 wurde daher „CC Bau“ als CCeV-eigene Fachabteilung gegründet. CC Bau knüpft direkt an die bisherige Gemeinschaftsabteilung CC Tudalit von CCeV und Tudalit e.V. an. Auch in Zukunft wird die Fachabteilung CC Bau zum Mehrwert der Mitglieder eng mit anderen Netzwerken wie Tudalit e.V. und C^3 – Carbon Concrete Composite e.V. kooperieren. Die Fachabteilung CC Bau bietet mit ihren Arbeitsgruppen eine Plattform für Kontakte, Wissenstransfer und Erfahrungsaustausch auf dem Gebiet leichter faser- und textilverstärkter Verbundstrukturen für Anwendungen im Bauwesen. Eingeladen sind Vertreter aus Wissenschaft, Forschung und Lehre, Unternehmer aus der gesamten Wertschöpfungskette von textilverstärkten Verbundstrukturen sowie Planer, Vertreter von Behörden und interessierte Bauherren. Die Arbeitsgruppen unterstützen mit Vortrags- und Gesprächsangeboten die Entwicklung neuer Projekte und innovative Zusammenarbeit.

CCeV-Thementag: CCeV-Mitglieder und Vortragende frei, Nicht-CCeVler 95€ (zzgl. 19%MwSt)

Programm (Folien deutsch oder englisch, 25 + 5 min),

9:15	**Begrüßung** - *Prof. Cuntze, Prof. Kurath*
9:30	**Mit Carbon stark vorgespannte, sehr dünne Betonplatten CPC** - *Prof. J. Kurath, ZHAW Winterthur, Architektur, Gestaltung und Bauingenieurwesen*
10:00	**3D Carb.** - *Prof. P. Ermanni/ 3D Carb-Beteiligter, ETH Zürich*
10:30	*Kaffeepause*
11:00	**22 Jahre Forschung über mit Karbonfasern vorgespannten Beton an der EMPA.** - *Prof. G. Terrasi, EMPA, Dübendorf*
11:30	**Faserverbundwerkstoff-Visionen der 1970er und 80er Jahre: Update 2018.** - *Prof.. U. Meier, EMPA, Dübendorf*
12:00	**Eigenschaften und Anwendungsfelder gestickter textiler Bewehrungen.** - *Prof. J. Feix / M. Egger, Institut Massivbau und Brückenbau, Uni Innsbruck*
12:30	*Mittagspause*
13:30	**Stickerei als Fertigungstechnologie für die Bautechnik.** - *Prof. T. Bechtold, Textilchemie, Uibk Vorarlberg*
14:00	**Zur Bemessung von Brücken und Dächern aus Faserverbundwerkstoffen.** - *Prof. T. Keller, EPFL-ENAC-CCLAB, Lausanne*
14:30	**CFK- Verstärkungen in Deutschland.** - *Dr. H. Peters, Büro HPS (Carbon for Civil Engineering Stuttgart / T. Lepinski, Entecsol, Wittstock,*
15:00	*Kaffeepause*
15:30	**Die TUDALIT-Planermappe.** *(Autoren: U. Assmann /. P. Offermann, TUDALIT e.V. - Dresden)* - *Prof. Cuntze*
16:00	**ZHAW-Besichtigung**
	Get Together

Ihr Ralf Cuntze (08136-7754) mit Ingelore Gaitzsch, Jens Ridzewski, Otto Kellenberger

Hinweise: Nächste Veranstaltungen aller Arbeitsgruppen der CCeV-Fachabteilung CC Bau ist am 09.11.2018 in Stuttgart (DLR Stuttgart, Pfaffenwaldring 38-40, Hörsaal, 70569 Stuttgart, Campus Vaihingen).
10. Carbon- und Textilbetontage, 25.-26.9. 2018 in Dresden.

4. Thementag der AG 'Automatisierte Fertigung im Bauwesen inklusiv Serielles Bauen'

Dienstag, 30.03.2021
Zoom-Videokonferenz

CUeV-Kontakt: Bernhard Jahn (Bernhard.Jahn@carbon-composites.eu).
Teilnehmergebühr: 55 € für Nicht-Mitglieder, frei für CU-Mitglieder, Vortragende und Presse.
Folien englisch, deutsch. Vorträge: 25 + 5 min Diskussion, in Deutsch, falls möglich .

08:30	**Registrierung der Teilnehmer**
09:00	**Begrüßung**. *CU BAU* (Cuntze und Dr. Thomas Heber für Roy Thyroff)
09:10	**Kurzvorstellung Composites United mit CU Bau + Einführung.** *Prof. Dr.-Ing. habil. Ralf Cuntze*
09:30	**Industrieller 3D-Druck im Bauwesen – Anwendung des Powder-Binder-Jettings.** *Dipl.-Ing. Tobias Grün; Voxeljet AG, Friedberg*
10:00	**'3D-Druck' in der Baupraxis – Erfahrungen der ersten zugelassenen Gebäude in Deutschland.** *Dr. Fabian Meyer-Brötz, Leitung 3D Construction Printing, Peri GmbH, Weissenhorn*
10:30	**Additive Fertigung im Bauwesen: Neue Herausforderungen für numerische Simulations-methoden.** *M.Sc. Alexander Paolini, Lehrstuhl für Computergestützte Modellierung und Simulation, TU München*
11:00	*Kaffeepause*
11:30	**Klassifizierung digitaler Fertigungsverfahren im Betonbau.** *Prof. Dr.-Ing. Viktor Mechtcherine, Institut für Baustoffe, TU Dresden*
12:00	**Connecting Value Chains – Status Quo der Robotik im Bauwesen .** *Dipl.-Ing. Thomas Adams, Individualized Production in Architecture/RWTH Aachen University*
12:30	*Mittagspause*
13:30	**Automatisierung im Bauwesen – Robotereinsatz auf der Baustelle (Mauerwerksrobotik).** *M.Sc. Adrian Fehrle, Lehrstuhl für Fertigungsautomatisierung und Produktionssystematik, FA-Uni Erlangen-Nürnbg*
14:00	**Additive Fertigung im Bauwesen durch selektive Zementaktivierung.** *M.Sc. Daniel Talke, Lehrstuhl für Holzbau und Baukonstruktion, TU München*
14:30	*Kaffeepause*
15:00	**Produktion individueller Teile für Decken und Träger bei ersten Praxisprojekten.** *Dipl. Ing. Eduard Artner, BauMinator / '3D Druck', Baumit GmbH, Wopfing, Österreich*
15:30	**3D-Welding - WAAM im Bauwesen.** (Auftragsschweißen) *Dipl.-Ing. Christoph Holzinger, Assoc.-Prof. DI. Dr.nat.techn. Andreas Trummer, Technische Universität Graz*
16:00	**Virtuelle Besichtigung der 3D-Druck-Einrichtungen des IGCV-Neubaus in Augsburg.** *Dipl.-Ing. M. Binder, IGCV Fraunhofer Augsburg, Additive Fertigung – Werkstoffe und Prozessentwicklung*
16:45	**Schlusswort / Get Together**

Programmgestaltung: Ralf Cuntze

Letzte und kommende Termine der Fachabteilung CU BAU:
20.10. 2020: CU-Bau AG Faserverbundarmierter Beton. Zoom-Videokonferenz
19.11. 2020: CU Bau-Thementag „Richtlinien, bauaufsichtliche Zulassungen und Bauartgenehmigungen für die potenziellen Anwender Architekten, Tragwerksplaner und Bauherrn"
25. 02. 2021: CU Bau-Forum „Carbonbeton-Anwendungen in der Praxis – auf der Baustelle und im Fertigteilwerk". Ulmer Betontage.

Definition: ISO/ASTM 52900 defines (digitized) Automatic Fabrication (Fertigung, nicht 'Manufaktur') as "Process of joining materials to make parts from 3D model data, usually layer upon layer". 3D-Druck ist ein Verfahren innerhalb AF, nicht korrekt oft noch immer *Manufacturing* genannt, obwohl automatisiert
'3D-Druck' bedeutet laut VDI-Ri 3405 „Kaltes Extrusionsverfahren, wobei der Baustoff über eine Düse strangweise abgelegt wird" oder baubezogen "Extrudierte Ablage von Betonsträngen". 3D-Druck ist im Wesentlichen ein "Pulverbett-basiertes Verfahren", wie es z.B. Voxeljet für die Herstellung von Schalung benutzt.

CC Bau-Forum

"Carbonbeton-Anwendungen in der Praxis - auf der Baustelle und im Fertigteilwerk"

Transformation von praktischem Anwendungswissen.

Zielgruppe: Hersteller, Sanierer, Vertreter der Betonbranche

am 25. Februar, Donnerstag, als Podium integriert bei den Ulmer Betontagen vom 23. - 26.02.2021

25 min Vortrag + 5 min Diskussion. Folien: deutsch oder englisch. Vortrag: falls möglich möglich deutsch

08:30	*Kaffeepause – Networking*
09:00	**Einführende Worte** *Prof. Dr.-Ing. habil. Ralf Cuntze, CU Bau, Augsburg. Composites United e.V. CUeV (formerly CCeV)*
09:15	**Digitale Entwicklung – von der Faser zum textilen Gelege.** *Roy Thyroff, rothycon – Roy Thyroff Consulting, Naila*
09:30	**Carbonbeton: Zwischen Theorie & Praxis.** *Dipl.-Ing. Oliver Heppes, GOLDBECK Bauelemente Bielefeld SE*
12:10	**Größer, stärker, wirtschaftlicher - Carbonbewehrungen in neuen Dimensionen.** *Dipl.-Ing. Stephan Gießer, Solidian, Albstadt*
12:40	***Mittagspause und Besuch der Ausstellung***
14:00	**Tragwerksplanung des C^3–Ergebnishauses „CUBE" – Bemessung, Nachweisführung und Zulassung im Einzelfall.** *Dipl.-Ing. Hendrik Ritter, Assmann Beraten und Bauen, Dresden*
14:30	**Modulare Brückenbauwerke aus Carbonbeton** *M.Sc. Sven Bosbach, Lehrstuhl und Institut für Massivbau, RWTH Aachen*
15:00	**Bauen mit CPC-Carbonbetonplatten, einer komplett neuen Bauweise in Beton – Verfahren, Konstruieren, Bemessen.** *Prof. Joseph Kurath, ZHAW Winterthur, Schweiz*
15:30	**Stadtbahnbrücke Stuttgart: CFK-Zugglieder finden Akzeptanz.** *Prof. Dr. Urs Meier, EMPA, Dübendorf, Schweiz*
16:00	**Ausgewählte Ingenieurbauwerke - nachträgliche Bauteilverstärkung mit Carbon-Faser-Kunststoffen „CFK" (geklebte Lamellen).** *Dr.-Ing. Horst Peters, HPTL Carbon GmbH, Ditzingen*

Ihr Ralf Cuntze und der weitere Vorstand des Netzwerks CU Bau

Weitere Termine 2020 / 2021 des Netzweks CU Bau:

- 19.11. 2020: CU Thementag „Richtlinien, bauaufsichtliche Zulassungen und Bauartgenehmigungen für die potenziellen Anwender Architekten, Tragwerksplaner und Bauherrn". Zoom-Konferenz
- 17.03.2021: Thementag aller Arbeitsgruppen des Netzwerks CU BAU mit TU Chemnitz. Zoom-Konferenz?
- 30.03.2021: 4. Thementag der AG „Automatisierte Fertigung im Bauwesen inkl. Serielles Bauen". Zoom-Konferenz?

Das Netzwerk CU Bau, besteht aus 4 Arbeitsgruppen: Bemessung und Nachweis (Prof. Ralf Cuntze), Faserverbundarmierter Beton (Dr. Ingelore Gaitzsch), Faserverstärkte Kunststoffe (Prof. Jens Ridzewski), Automatisierte Fertigung im Bauwesen inkl. Serielles Bauern (Cuntze)

Project Idea "Nano2Beton" (2014-2015)

High Performance Concrete, optimized with CNTs and nano-structured cement, with and without fiber reinforcement from basalt and carbon fibers. A Carbon Nano Tube CNT is a nanometer-sized tube.

The aim was to develop a dense, ultra-high-strength concrete in order to produce by the use of short fiber reincorcement mass, strength, fracture toughness and wear-optimized components with a long service life. In addition to the use of specially activated CNTs, the use of nanostructured cement helps to achieve this, which means CO2 savings by avoiding energy-intensive clinker burning due to the use of blast furnace sand. Therefore, the dispersion of multi-k roving snippets is required, so that a stochastic spatial distribution of the individual fibers homogeneously reinforces the concrete matrix. The fiber volume fraction will be about 1%. This helps to avoid the introduction of locally necessary, time-consuming reinforcement at local stress concentration points, such as edges, load introductions, boreholes of structural parts. It was planned to produce a dry mixture for direct processing.
The author who gave the project idea took care of the compilation of the future consortium partners and the preparation of the project documents since spring 2014. These were project partners from medium-size industry and universitities. At the final request of the NanoCarbon project management to submit the completed application, three partners unfortunately rejected the application.

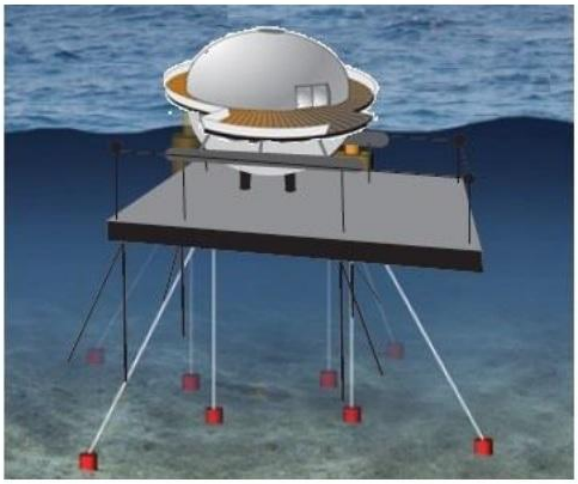
Projekt Idea „ArcOval", Schwimmendes Gebäude (2014-2015, 2017)

Development of an energy-self-sufficient floating building made of carbon concrete (no corrosion) with fixation on the seabed by means of a tension leg platform TLP. The building can be used both as a permanent residence and as a holiday home. The habitable area should be between 120-160 square meters. Vision and idea: Ingenieur-Büro purist Heck und Daum, Karlsruhe. Project document: Architect Martin Maria Daum

The following consortium is involved in the development of this project:
- Dr.-Ing. habil. Sandra Gelbrich, Technische Universität Chemnitz, Fachbereich Strukturleichtbau
- Prof. Dr.-Ing. Frank Dahlhaus, Technische Universität Bergakademie Freiberg,- Fachbereich Baukonstruktion und Massivbau
- Prof. Dr.-Ing. Frank Hülsmeier, Hochschule für Technik, Wirtschaft und Kultur Leipzig, Fachbereich Bauwesen
- Dr.-Ing. Peter Strangfeld, Brandenburgische Technische Universität Cottbus, Institut für schwimmende Bauten
- Organization of the consortium: Prof. Dr.-Ing. habil. Ralf Cuntze.

Requirements for the floating building:
- CE seawater suitability category B. The floating building must withstand extreme weather conditions at sea. The effects of wind, waves, temperature differences and solar radiation must be taken into account. It must be statically taken into account that the building is firmly anchored to the seabed by the TLP
- It should be able to drive independently to its destination, even outside the 12-mile zone
- It must be designed in such a way that it is unsinkable and produces a maximum draught of 5 metres. Absolute watertightness must be achieved for building bodies and openings

- The type of propulsion must meet EU standards for motor boats up to 24 m in length
- The electrical energy supply, air conditioning, as well as the heating of drinking and process water must be permanently self-sufficient through the energy supply. The 75 m^2 photovoltaic-system is used for self-sufficient energy supply, light, hot water heating, air conditioning and power supply. The solar-generated electricity is stored by means of lithium-ion batteries. While driving to the desired docking station, excess energy is supplied to the electric motor of the hybrid drive
- Absolute immobilization thanks to fixation with a specially developed ArcOval-Tension Leg Platform TLP. In addition to fixing the building, this should meet other conditions. These include anchoring methods for dinghies as well as a spatial demarcation to the seabed. The principle of TLP was developed for anchoring large oil rigs and offshore wind turbines. At sea depths of over 30 meters, this anchoring method offers significant cost advantages over conventional steel structures. The lower right picture shows the design principle of a TLP for offshore wind turbines, developed by the Bergakademie Freiberg
- The enormous buoyancy of the 400 m^3 ArcOval buoyancy body is compensated by the color-coded ballast bodies placed on the seabed as part of the TLP principle. A stiffening rope construction combines ballast and buoyancy. The ArcOval platform, which floats below the water surface, is almost immune to wave movements and ocean currents due to this construction and provides a solid surface for fixation.



ArcOval round version



Dimensions



Unfortunately the possible investordid not accept the project idea.

15 Continuum Mechanics, Continuum (micro-)Damage Mechanics and Multiscale Modeling

15.1 Continuum Mechanics (CM) Design Features

Design Verification is the pre-condition of serial production of a structural component. It is usually to be performed on macro-mechanical level but with capturing micro-mechanical failure behavior. For an originally intact material under increasing static or cyclic loading micro-damage occurs. This is usually treated by Continuum Mechanics (CM) methods and is nowadays partly performed by Continuum (micro-)Damage Mechanics (CDM) methods. If micro-damage is localized and if finally a macro-damage crack has developed, then fracture mechanics with its Damage Tolerance tools is to use to complete Design Verification DV. However, ideas exist to extend the CDM into the regime of macro-crack growth.

In order to achieve Design Verification for the critical location of the 'intact' but not flawless material one needs Strength Failure Conditions (SFCs, *failure criteria*) and accurately computed 3D-stress states which are to be inserted into the SFCs. These accurate 3D stress states are often effortful to determine in the nonlinear analysis cases involving ductile and brittle materials. Here, one has to distinguish the inelastic plastic behavior of ductile materials from inelastic behavior of brittle materials. In the first case a flow potential is to employ and in the brittle case an *inelastic* potential in order to set up the necessary interrelations of the complicated 3D stress-strain relations in structural analysis.

Engineers prefer macro-mechanical models to be able to design on the macro-scopic design level. Referring to Cuntze's Failure-Mode-Concept (FMC) – primarily based on *material symmetry* – the typical features of the FMC-based failure criteria on macro-mechanical level are:

- ***Each failure mode represents 1 independent failure mechanism,***
  and thereby represents 1 piece of the complete (global) failure surface
- ***Each failure mechanism is governed by 1 basic strength*** *(this is witnessed)*
- ***Each failure mode can be represented by 1strength criterion.*** Therefore, equivalent stresses can be computed for each mode.
- Consequently, the FMC-approach requires the interaction of all macro-scopic failure modes: isotropic (generic number 2) and transversely-isotropic UD (5) by the equation

$$Eff = \sqrt[m]{(Eff^{\text{mode }1})^m + (Eff^{\text{mode }2})^m + ...} = 1 = 100\% , \; if \;\; \text{Onset of Failure .}$$

From engineering reasons, Cuntze takes the same interaction exponent *m* for each transition domain between two failure mode domains. The interaction of the adjacent failure modes is modelled by a 'series failure system". That permits to formulate the total material stressing effort from all activated failure modes as 'accumulation' of *Effs* or as the sum *Eff* of all the failure danger proportions, marking the Onset-of-Failure.

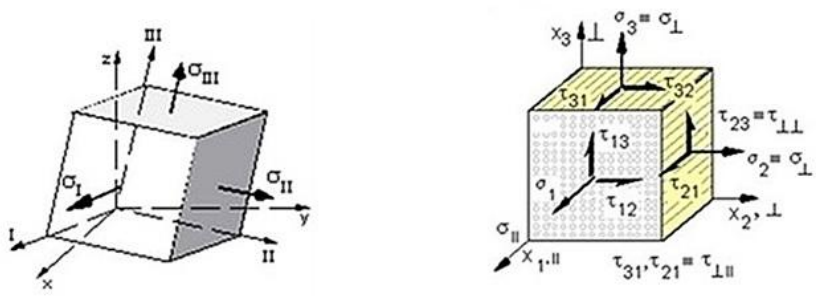
Eff = 1 represents the mathematical description of the surface of a failure body.

Intentionally here now, deeper investigated shall be the situation of brittle UD materials experiencing 5 failure modes. For the Design Verification process thus follows: The provision of all 5 material properties and 5 stress-strain curves, hopefully with the provision of the softening curve

part in the case of the 3 Inter Fiber Failure modes IFF considering embedded layers of a laminate. For the 2 FF modes it is most often sufficient to model linear-elastically. For isotropic materials the generic number is 2 and for orthotropic materials 9 (6 if F = W). Transferring the non-linear treatment of a fully ductile case ('Mises') with one failure mode 'yielding' to a brittle material with 2 fracture failure modes in the isotropic case and 5 in the UD case is a challenge. For non-linear analyses required is: (ductile) Yield-driven ***Plastic Potential (flow or yield potential)*** ↔ ***(***brittle) flaw-driven ***(micro-)Damage Inelastic Potential.***

Before investigating CDM some basic relationships shall be repeated: The stress-strain relationships are given for isotropic and for UD material. The associated compliance matrices principally involve the elasticity quantities-linked CDM parameters. See *Fig.15-1* and *Table 15-1*.

Design parameters



isotropic

transversely-isotropic

$$\{\sigma\} = (\sigma_x, \sigma_y, \sigma_z, \tau_{yz}, \tau_{xz}, \tau_{xy})^T \qquad \{\sigma\} = (\sigma_1, \sigma_2, \sigma_3, \tau_{23}, \tau_{13}, \tau_{21})^T$$

$$\{R\} = (R^t, R^c)^T \text{ with } \mu \qquad \{R\} = (R^t_{||}, R^c_{||}, R^t_{\perp}, R^c_{\perp}, R_{\perp||})^T \text{ with } \mu_{\perp||}, \mu_{\perp\perp}$$

Fig.15-1: Stresses and strength of isotropic and transversely-isotropic UD material

Table 15-1: Elasticity matrices of isotropic and transversely-isotropic UD materials

$$\begin{Bmatrix} \sigma_x \\ \sigma_y \\ \sigma_z \\ \tau_{yz} \\ \tau_{zy} \\ \tau_{xy} \end{Bmatrix} = \frac{E}{(1+\nu)\cdot(1-\nu)} \begin{bmatrix} 1\text{-}\nu & \nu & \nu & 0 & 0 & 0 \\ \nu & 1\text{-}\nu & \nu & 0 & 0 & 0 \\ \nu & \nu & 1\text{-}\nu & 0 & 0 & 0 \\ 0 & 0 & 0 & 0.5\cdot(1\text{-}2\nu) & 0 & 0 \\ 0 & symm. & 0 & 0 & 0.5\cdot(1\text{-}2\nu) & 0 \\ 0 & 0 & 0 & 0 & 0 & 0.5\cdot(1\text{-}2\nu) \end{bmatrix} \cdot \begin{Bmatrix} \varepsilon_x \\ \varepsilon_y \\ \varepsilon_y \\ \gamma_{yz} \\ \gamma_{zy} \\ \gamma_{xy} \end{Bmatrix} = [C]\cdot\{\varepsilon\}$$

$$\begin{Bmatrix} \varepsilon_x \\ \varepsilon_y \\ \varepsilon_z \\ \gamma_{yz} \\ \gamma_{xz} \\ \gamma_{xy} \end{Bmatrix} = \begin{bmatrix} \frac{1}{E} & \frac{-\nu}{E} & \frac{-\nu}{E} & 0 & 0 & 0 \\ \frac{-\nu}{E} & \frac{1}{E} & \frac{-\nu}{E} & 0 & 0 & 0 \\ \frac{-\nu}{E} & \frac{-\nu}{E} & \frac{1}{E} & 0 & 0 & 0 \\ & & & \frac{1}{G} & 0 & 0 \\ & (symm.) & & & \frac{1}{G} & 0 \\ & & & & & \frac{1}{G} \end{bmatrix} \cdot \begin{Bmatrix} \sigma_x \\ \sigma_y \\ \sigma_z \\ \tau_{yz} \\ \tau_{xz} \\ \tau_{xy} \end{Bmatrix} = [S]\cdot\{\sigma\}$$

Maxwell-Betti $\frac{-\nu_{\perp||}}{E_{||}} = \frac{-\nu_{||\perp}}{E_{\perp}}$

Applicable after microdamage, too

$$\begin{Bmatrix}\varepsilon_1\\ \varepsilon_2\\ \varepsilon_3\\ \gamma_{23}\\ \gamma_{13}\\ \gamma_{12}\end{Bmatrix} = \begin{bmatrix} \frac{1}{E_\parallel} & \frac{-\nu_{\perp\parallel}}{E_\parallel} & \frac{-\nu_{\perp\parallel}}{E_\parallel} & 0 & 0 & 0 \\ \frac{-\nu_{\parallel\perp}}{E_\perp} & \frac{1}{E_\perp} & \frac{-\nu_{\perp\perp}}{E_\perp} & 0 & 0 & 0 \\ \frac{-\nu_{\parallel\perp}}{E_\perp} & \frac{-\nu_{\perp\perp}}{E_\perp} & \frac{1}{E_\perp} & 0 & 0 & 0 \\ & & & \frac{1}{G_{\perp\perp}} & 0 & 0 \\ & (symm.) & & & \frac{1}{G_{\parallel\perp}} & 0 \\ & & & & & \frac{1}{G_{\parallel\perp}} \end{bmatrix} \cdot \begin{Bmatrix}\sigma_1\\ \sigma_2\\ \sigma_3\\ \tau_{23}\\ \tau_{13}\\ \tau_{12}\end{Bmatrix}, \quad \text{Maxwell-Betti } \frac{-\nu_{\perp\parallel}}{E_\parallel} = \frac{-\nu_{\parallel\perp}}{E_\perp}$$

$$\begin{Bmatrix}\varepsilon_W\\ \varepsilon_F\\ \varepsilon_3\\ \gamma_{F3}\\ \gamma_{W3}\\ \gamma_{WF}\end{Bmatrix} = \begin{bmatrix} \frac{1}{E_W} & \frac{-\nu_{FW}}{E_W} & \frac{-\nu_{W3}}{E_W} & 0 & 0 & 0 \\ \frac{-\nu_{WF}}{E_F} & \frac{1}{E_F} & \frac{-\nu_{F3}}{E_F} & 0 & 0 & 0 \\ \frac{-\nu_{3\,W}}{E_3} & \frac{-\nu_{3\,F}}{E_3} & \frac{1}{E_3} & 0 & 0 & 0 \\ & & & \frac{1}{G_{F3}} & 0 & 0 \\ & (symm.) & & & \frac{1}{G_{W3}} & 0 \\ & & & & & \frac{1}{G_{WF}} \end{bmatrix} \cdot \begin{Bmatrix}\sigma_W\\ \sigma_F\\ \sigma_3\\ \tau_{F3}\\ \tau_{W3}\\ \tau_{WF}\end{Bmatrix}, \quad \text{Maxwell-Betti } \frac{-\nu_{WF}}{E_W} = \frac{-\nu_{FW}}{E_F}$$

In the isotropic case the stiffness matrix [C] is still more complicate than the compliance matrix [S]. This is the more valid for UD and orthotropic materials. Therefore for them the [S] are provided, only. $\{\varepsilon\} = [S] \cdot \{\sigma\}$ with $[S]$ *c*ompliance matrix, $\{\sigma\} = [C] \cdot \{\varepsilon\}$ with $[C]$ *S*tiffness matrix.

UD Strength criteria

FF1: $Eff^{\parallel\sigma} = \breve{\sigma}_1 / \bar{R}_\parallel^t = \sigma_{eq}^{\parallel\sigma} / \bar{R}_\parallel^t$ with $\breve{\sigma}_1 \cong \varepsilon_1^t \cdot E_\parallel$ (matrix neglected)

FF2: $Eff^{\parallel\tau} = -\breve{\sigma}_1 / \bar{R}_\parallel^c = +\sigma_{eq}^{\parallel\tau} / \bar{R}_\parallel^c$ with $\breve{\sigma}_1 \cong \varepsilon_1^c \cdot E_\parallel$

IFF1: $Eff^{\perp\sigma} = [(\sigma_2 + \sigma_3) + \sqrt{\sigma_2^2 - 2\sigma_2 \cdot \sigma_3 + \sigma_3^2 + 4\tau_{23}^2}] / 2\bar{R}_\perp^t = \sigma_{eq}^{\perp\sigma} / \bar{R}_\perp^t$

IFF2: $Eff^{\perp\tau} = [a_{\perp\perp} \cdot (\sigma_2 + \sigma_3) + b_{\perp\perp}\sqrt{\sigma_2^2 - 2\sigma_2\sigma_3 + \sigma_3^2 + 4\tau_{23}^2}] / \bar{R}_\perp^c = \sigma_{eq}^{\perp\tau} / \bar{R}_\perp^c$

IFF3: $Eff^{\perp\parallel} = \{[b_{\perp\parallel} \cdot I_{23-5} + (\sqrt{b_{\perp\parallel}^2 \cdot I_{23-5}^2 + 4 \cdot \bar{R}_{\perp\parallel}^2 \cdot (\tau_{31}^2 + \tau_{21}^2)^2}] / (2 \cdot \bar{R}_{\perp\parallel}^3)\}^{0.5} = \sigma_{eq}^{\perp\parallel} / \bar{R}_{\perp\parallel}$

$\{\sigma_{eq}^{\text{mode}}\} = (\sigma_{eq}^{\parallel\sigma}, \sigma_{eq}^{\parallel\tau}, \sigma_{eq}^{\perp\sigma}, \sigma_{eq}^{\perp\tau}, \sigma_{eq}^{\parallel\perp})^T$, $I_{23-5} = 2\sigma_2 \cdot \tau_{21}^2 + 2\sigma_3 \cdot \tau_{31}^2 + 4\tau_{23}\tau_{31}\tau_{21}$.

$a_{\perp\perp} \cong \mu_{\perp\perp} / (1 - \mu_{\perp\perp})$, $b_{\perp\parallel} \cong 2 \cdot \mu_{\perp\parallel}$. $0 < \mu_{\perp\parallel} < 0.3$, $0 < \mu_{\perp\perp} < 0.2$, $2.5 < m < 2.9$.

$Eff^m = (Eff^{\parallel\tau})^m + (Eff^{\parallel\sigma})^m + (Eff^{\perp\sigma})^m + (Eff^{\perp\tau})^m + (Eff^{\perp\parallel})^m = 100\%$ *if failure.*

$\{R\} = (R_\parallel^t, R_\parallel^c, R_\perp^t, R_\perp^c, R_{\perp\parallel}, \mu_{\perp\perp}, \mu_{\perp\parallel})^T$ with $1 \equiv \parallel$, $2, 3 \equiv \perp$.

Design Verification DV

Design Verification is performed as follows: Assuming a known stress state the non-initiation of failure is demonstrated by inserting the stresses into a SFC obtaining a Reserve Factor *RF* > 1.

What is to be considered thereby is the interaction of all stresses in the 3D stress state. This is performed in the FMC by interaction of the *Eff* -portions from all activated modes and is captured by *Eff* < 1 =100%. In the linear case it is directly valid *RF = 1/ Eff*.

In multi-layered laminates the deformation-controlled laminas experience softening and still thereby contribute to laminate strength and stiffness. Softening is to capture in the stress–strain relations if a realistic non-linear final failure calculation inclusively a realistic 3D stress state as SFC input is required. For brittle UD materials there is not so much matrix yielding in the case of thermosets that contributes to the nonlinear deformation. For thermoplastic matrices the effect is higher.

Before coming to CDM details again one should discriminate micro-damage (Schädigung) from macro-damage (Schaden). Macro-damage like cracks are to investigate by fracture mechanics tools.

15.2 Modelling Stress-strain curves including strain-hardening and strain-softening

Essential for CM and CDM is the full uniaxial stress-strain curve, see *Fig.15-2*.

Thereby it is to discriminate:

*In the experiment the test specimen either is load-controlled or deformation-controlled tested.

*The strain-hardening part of the stress-strain curve is load-controlled measured and terminates at the maximum load peak which is the fracture failure load which corresponds to the strength point of the uniaxial test specimen. This is principally valid for brittle and ductile materials.

*The strain-softening part is deformation-controlled tested and the critical location strain–controlled by the 'hot spot' material vicinity. This is given for ductile metals and embedded brittle layers (laminas, thermoset matrix) and is the more of interest for less brittle laminas with for instance a thermoplastic matrix in the vicinity of the other laminas of the laminate. Strain-controlled embedded layers still contribute to the laminate's stiffness and load-carrying capacity after passing the strength point and this as long as the vicinity can manage the resulting load transfer. Final fracture occurs if the *'structure laminate'* fails. A softening part is strain-controlled by the vicinity and is usually to assume because its measurement is difficult. Assumptions have to be made regarding the decaying properties of the actually degrading layer.

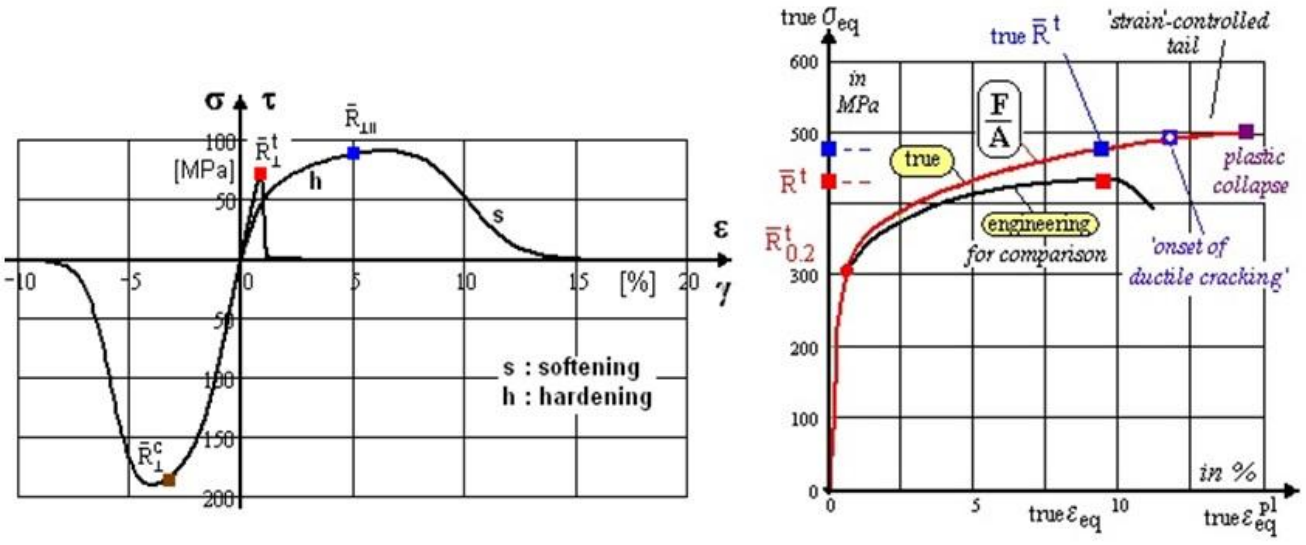


Fig.15-2 Full stress-strain curve with load-controlled hardening and deformation-controlled softening: (left) semi-brittle embedded UD material layer; (right) vicinity strain-controlled ductile aluminum metal modelled by Ramberg-Osgood considering engineering and true quantities, uniaxial stress state marks the hardening part and a multi-axial stress state the softening part with $\sigma \rightarrow \sigma_{eq}$

In the case of testing very stiff test rigs are required and a specific model is to create in order to evaluate (map) the strain measurements of the laminate broken down to the envisaged embedded lamina as *'composite material'* for which the softening curve part is to determine. In an earlier section a test procedure of the author was mentioned. It is a distinct fracture mechanics test, because the laminate test specimen includes the cracked UD layer embedded within the stack. Such a crack is inserted into the laminate test specimen.

A softening situation is further given for a ductile material tension rod in the necking cross-section, where the outer regions strain-control the 3D tensile stress state in the rod center.

Model for Strain-hardening: (*short repetition*)

For strain-hardening materials the Ramberg-Osgood (R-O) equation can be used for mapping ('fitting'), because the well-known MIL-Handbook 5 (now MMPDS) applies it as an engineering mapping tool, and it is well recognized in industry. This equation must be used for each single failure mode, as it is known, that each strength is linked to a distinct failure mode and a distinct stress-strain curve as well. The R-O-equation (metal suffixes m, p in *R* are skipped) reads

$$\varepsilon_{hard} = \sigma / E_0 + 0.002 \cdot (\sigma / \bar{R}_{0.2})^n, \text{ example } \gamma_{21} = \tau_{21} / G_{||\perp} + 0.002 \cdot (\tau_{21} / \bar{R}_{\perp||0.2})^n .$$

The R-O exponent) reads $n = \ell n\left(\varepsilon_{pl}(\bar{R})\right) / \ell n\left(\bar{R} / \bar{R}_{0.2}\right)$

and is estimated from the strength point $\left(\bar{R},\ \varepsilon_{pl}(\bar{R})\right)$ and the 'yield' point. The moduli read

$$E_{sec}^{hard} = \frac{\sigma}{\varepsilon} = \frac{\sigma}{\frac{\sigma}{E_0} + 0.002 \cdot (\frac{\sigma}{\bar{R}_{0.2}})^{\bar{n}}} = \frac{E_0}{1 + 0.002 \cdot \frac{E_0}{\bar{R}_{0.2}} \cdot (\frac{\sigma}{\bar{R}_{0.2}})^{\bar{n}-1}},\ E_{tan}^{hard} = \frac{d\sigma}{d\varepsilon} = \frac{E_0}{1 + 0.002 \cdot \bar{n} \cdot \frac{E_0}{\bar{R}_{0.2}} \cdot (\frac{\sigma}{\bar{R}_{0.2}})^{\bar{n}-1}}.$$

Model for Strain-softening:

In general, the full stress-strain curve of a material consists of a hardening part which can be load-controlled measured and a softening part which is strain-controlled by the vicinity. The associate two separate formulas are linked in the strength point. The author's approach is based on the idea that a distinct function is used to factorize the Ramberg-Osgood hardening function. Therefore, a simple function was used to map softening in order to then derive the secant or tangent modulus necessary for a full non-linear analysis. The equations for this 'effective' curve (*smeared over the micro-cracks*) read:

$$\sigma_{soft} = \bar{R} / (1 + exp[(a_{soft} + \varepsilon) / b_{soft}]) = \bar{R} \cdot \eta \qquad \text{using} \quad \exp[z] = e^z ,$$

where η is a degradation function and equals 1 in the hardening domain. The two curve parameters a_{soft}, b_{soft} are determined from two calibration points at least (*applying a point* $(1.0 \cdot \bar{R},\ \varepsilon(\bar{R}))$ *as input is numerically not permitted)*

$$(0.995 \cdot \bar{R},\ \varepsilon(\bar{R})) \qquad \text{and} \qquad (0.1 \cdot \bar{R},\ \varepsilon(0.1 \cdot \bar{R}))$$

or from curve fitting if enough test data is available in the softening domain. Further reads

$$E_{sec}^{soft} = \frac{\sigma}{\varepsilon} = \frac{E_0}{1 + 0.002 \cdot \frac{E_0}{R_{0.2}} \cdot (\frac{\sigma \cdot \eta}{R_{0.2}})^{n-1}} \qquad \text{with} \qquad \eta = \frac{1}{1 + exp(\frac{a_{soft} + \varepsilon}{b_{soft}})} .$$

Fig.15-3 visualizes an application to the shear curve of an embedded UD layer.

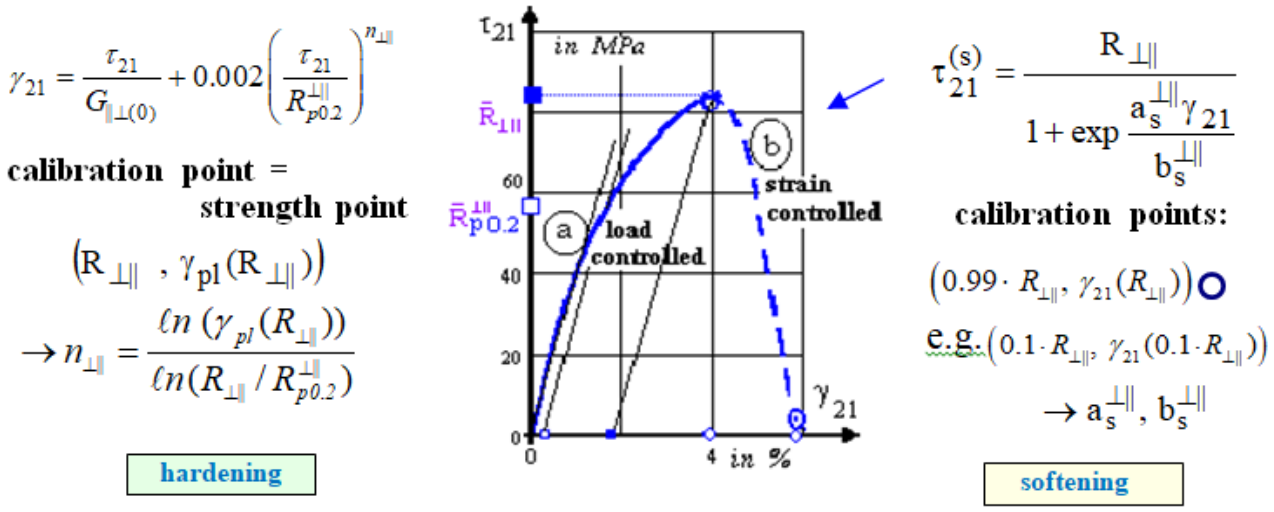


Fig.15-3: Application. Measured hardening shear stress–shear strain curves and asumed softening curve

Fig.15-4 presents an example where for a similar UD shear curve the test data set (crosses) of the hardening part was provided and where by factorization, using the dark red exponential function, the **blue** softening curve was predicted. In other words: The further running hardening part curve (see *Fig.15-2*, too) is reduced by factorization with the exponential function above.

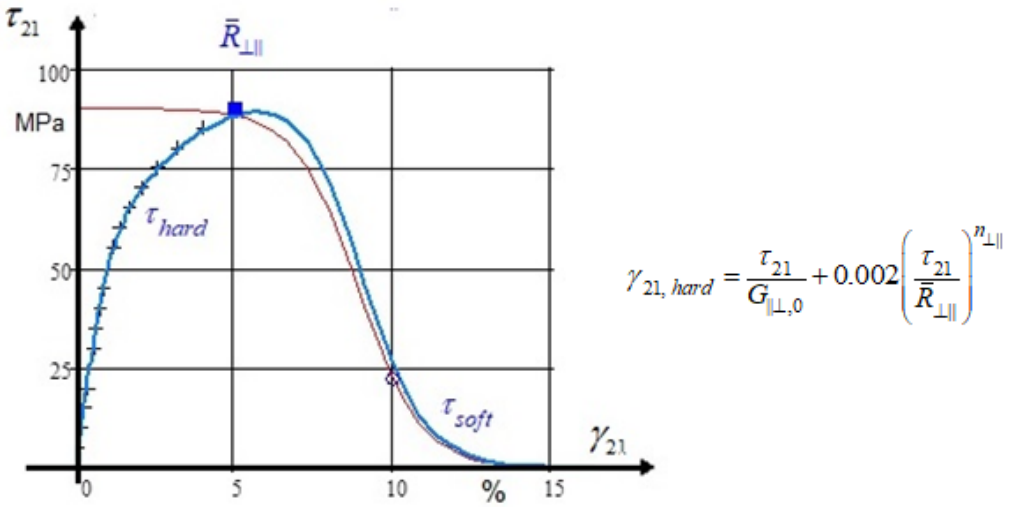


Fig.15-4: In-plane shear stress-shear strain curve of an embedded layer

The degree of UD non-linearity in the ***strain hardening*** regime essentially depends on the degrading matrix material. Beyond IFF strength and stiffness subsequently strain-controlled decay which affects the 3 secant IFF moduli. Again, in this post-IFF regime the embedded lamina experiences no sudden death but still has residual strength and stiffness. This is a *so-called in-situ effect*.

Fig.15-5 shows two cross-sections of the 2D failure body: Originally and after shrinking due to a distinct IFF degradation level. Fibers take over load from matrix as long as the fibers do not reach FF, see the marks 1 and 2. The mapping function models for fracture onset and growing yield surface are given below.

$$\left(\frac{\sigma_2}{\bar{R}_{\perp}^{t}}\right)^m + \left(\frac{|\tau_{21}|}{\bar{R}_{\perp\parallel} - \mu_{\perp\parallel}\cdot\sigma_2}\right)^m + \left(\frac{-\sigma_2}{\bar{R}_{\perp}^{c}}\right)^m = 1 \text{ (fracture onset)}, \quad \frac{I_3}{(\bar{R}_{\perp\parallel 0.2})^2} + \frac{I_4}{(\bar{R}_{\perp 0.2}^{c})^2} = c_y{}^2 \text{ (growing yield surface)}$$

Note: Above UD yield condition has to be verified, of course, by experiment of a number of stress states with corresponding multi-axial strain measurements.

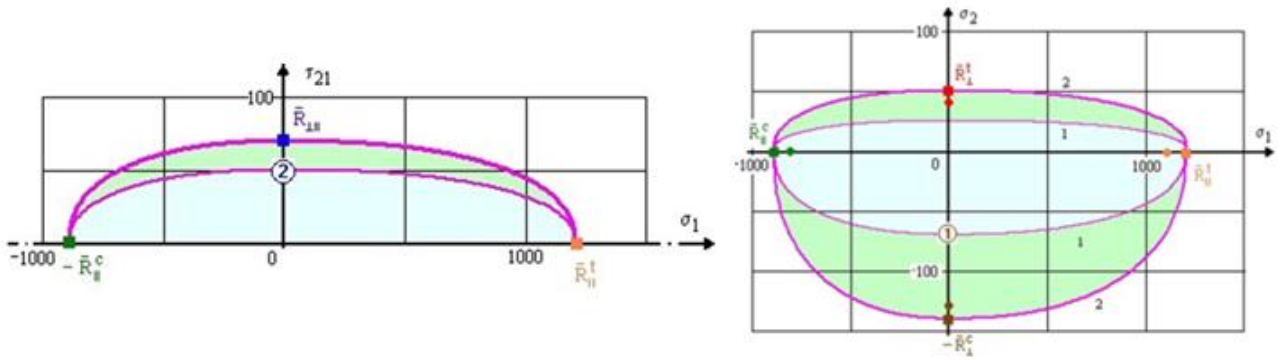


Fig.15-5: Micro-damage shrunk Inter Fiber Failure surface.
(1) IFF fracture failure surface, (2) onset of yield

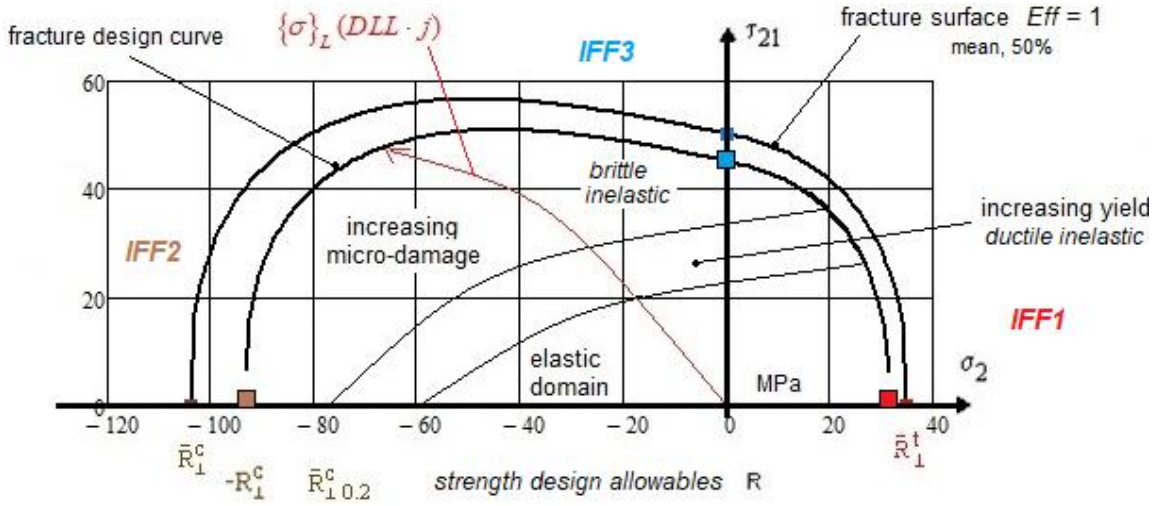


Fig.15-6: Scheme of the different material behavior domains of semi-brittle UD material.
DLL is Design Limit Load, j is design factor of safety. $\bar{R}$ is mean strength, R is statistically reduced strength

In the same context, above *Fig.15-6* depicts the interesting micro-damage domains of a lamina. It further outlines the development of a stress-state under load increase and shows the design curve to be considered in Design Verification regarding the 3 IFF modes.

15.3 Continuum (micro-)Damage Mechanics (CDM) of brittle and ductile materials

15.3.1 General

CDM is a tool in solid mechanics that takes concern of growth and distribution of flaws in a material.

CDM expresses the micro-scopic failure processes by (micro-)damage parameters or state variables, respectively. These state variables may be measurable e.g. by monitoring the micro-crack density development, or inferred from the effect they have on a macro-scopic property, such as modulus of elasticity (stiffness), coefficient of thermal expansion, on remaining life etc.

CDM is applied for ductile and brittle materials. The loading may be static and cyclic, requiring fatigue investigations. Regarding stress-strain curves, CDM captures the load-controlled hardening part and the deformation-controlled softening part. Softening part examples is the still mentioned embedded UD layer and the ductile metal tensile rod. Results of analyses employing the softening

art can be used for instance to better design notches, openings in pressure vessels (fuel tank task in Ariane 5 upper stage). CDM is basically used to capture the evolution of the micro-damage state from micro-damage $D = 0$ up to Onset-of-Failure at maximum, denoted here *maxD*, which is for brittle materials at the end of hardening or at achieving the strength *R*. (*The letter D is used for decades*).

In CDM, the formulation of the constitutive equations is based on one of the following two approaches (*a constitutive equation is an equation that describes the relationship between two physical quantities, for example between the stress put on a solid material and the strain produced there. Here the stress-strain curve is meant*):

(1) The strain equivalence principle approach or

(2) The stress equivalence principle approach. F*rom engineering side, the latter is preferred because 3D stress states and residual stresses have to be considered in design dimensioning.* The constitutive relationships are formulated in the effective undamaged configuration $\sigma_{eff} = \sigma / (1-D)$ with a stress-strain relation linked by the stiffness elasticity matrix [C], that reduces due to micro-damage

$$\{\sigma\} = [C] \cdot \{\varepsilon\} \quad \text{(not } [D] \cdot \{\varepsilon\} \text{ as found in the Ansys manual)} \ .$$

Mind: Micro-Damage-free and crack (= macro-damage)-free does not mean free of flaws.

D is the accumulation of the micro-damage process portions and it is theoretically terminated by max*D* at the strength point in the case of brittle materials and at the rupture point for very ductile materials. These portions may occur during a monotonically increasing static loading. For brittle materials micro-damage starts at 'elastic' limit a level where *Eff* has still reached a value, see <u>*Fig.15-7*</u>.

For the very ductile metallic materials the tension rod test shows that a significant onset-of-micro-damage is at the necking point (strength $\bar{R}^t$) or also termed at 'end of uniform elongation' or further of load-controlled loading, respectively.

The growing *D* of very ductile materials, driven from increasing porosity, is predicted by the 'Gurson-model' and its modifications.

Micro-damage may similar occur under cyclic loading. In fatigue, $D_{fatigue}$ is the accumulation of the cyclic micro-damage portions $D_{fatigue,k}$ induced by degradation within the $k \rightarrow n$ cycles. For the quantification of a portion *k* it is permitted to employ a static SFC. Although using the letter *D* for this accumulated micro-damage there is a difference $D_{fatigue}$ to *D:* $D_{fatigue}$ can be seen as a logical continuation of *Eff* = 100% (at n =1), because it remains 100% (n >1) for the constant amplitude SN curves (Woehler curves), see *Fig.10-7*..

For a load-spectrum, which cannot map a real loading history physically, $D_{fatigue}$ = 100% is not accurate and applicable. This is considered by applying the so-called 'Relative Miner' instead of the classical 'Palmgren-Miner Rule'.

Maximum *D* in static CDM also cannot become 100% due to its modelling basis, see *Fig.15-7*. The <u>center figure</u> outlines how a stress-man views the onset of micro-damage of a slightly brittle material. In the elastic domain there is no contribution. The blue 'flow curve' then will contribute. The <u>right figure</u> from Abaqus outlines that micro-damage first begins with void nucleation and void

coagulation. Question: Does really not any micro-damage happens before? → At least, confusion is given for a stress-man, when examining the right picture.

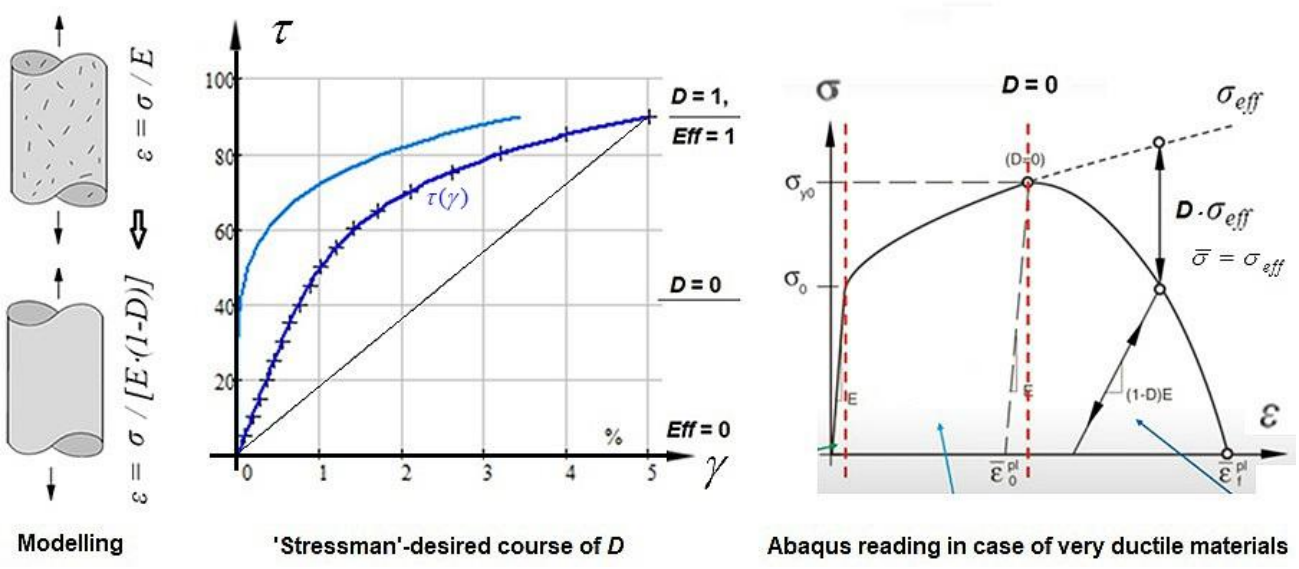


Fig.15-7: The various 'Onset- of- Failure' envelopes: (left) smearing of the micro-damaged material, (center) slightly brittle material, (right) ductile material

15.3.2 Modelling of uniaxial Micro-Damage Evolution

Following the 'Principle of strain equivalence' [*Lemaitre*] it is described for uniaxial states (σ = nominal stress, D = micro-damage parameter, E = elasticity modulus) by

$$\varepsilon = \frac{\sigma}{E} \rightarrow \varepsilon = \frac{\sigma_{eff}}{E \cdot (1-D)} \quad \text{employing } E_{sec}^{hard} = \frac{\sigma}{\varepsilon} = E_0 \cdot (1-D_{sec}),\ E_{tan}^{hard} = \frac{d\sigma}{d\varepsilon} = E_0 \cdot (1-D_{tan}).$$

For a uniaxial stress-strain curve the degradation of the elasticity modulus can be mapped via the secant modulus, the course of the tangent modulus is of interest for non-linear analyses.

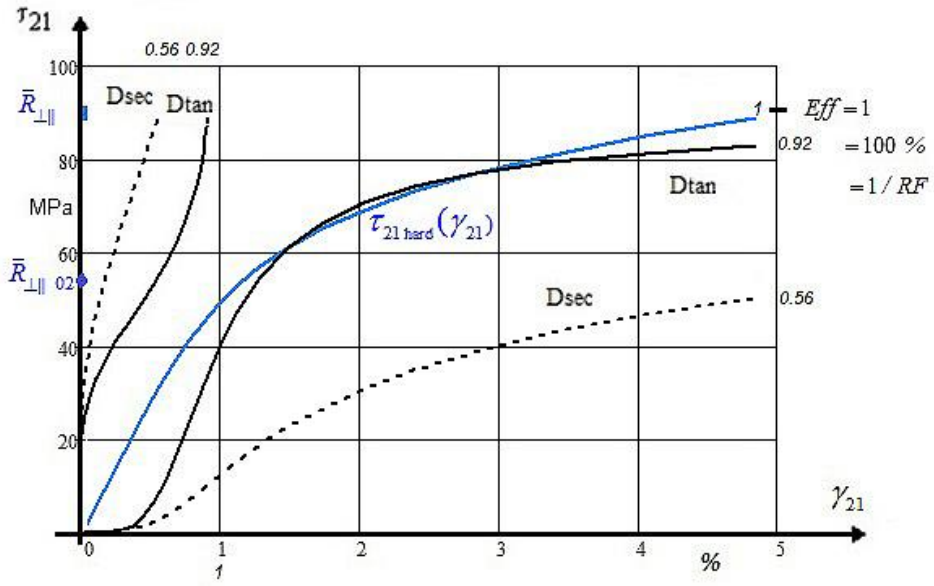


Fig.15-8: Course of Dsec(τ), Dsec(γ), Dtan(τ), Dtan(γ) with measured $\tau_{21}(\gamma_{12})$ on hardening curve part Eff during hardening of a shear stress loaded UD layer Discrepancy in Abaqus CDM modelling

Fig. 15-8 shows for an in-plane shear stress-shear strain curve the evolution of the micro-damage as a decrease of the elasticity stiffness [C] here used to quantify the micro-damage. Both moduli are employed in the figure. From the practical engineering side, it is desired that D should be 1 at fracture, *Fig.15-7.* This is not possible if a stiffness degradation model is applied to determine the damage variables, i.e. using the secant modulus gives $D = 1 - (E_{sec} / E_0)$. It would work better if the tangent modulus were employed $D = 1 - (E_{tan} / E_0)$. Then 1 would be approximately better obtained.

Conclusions of this example:

- The tangent modulus better approaches $D \rightarrow 1$, however is more sensitive during the final approach and the secant modulus is with 0.56 far from a desired value $D = 1$, *Fig.15-8*
- The 'stress-man' will not understand that at maximum load, which is at the *strength point*, the sum of micro-damage does not approach 100%.

15.3.3 Material Modelling of multi-axial Micro-Damage Evolution, example UD material

In the multi-axial anisotropic case the strain stress-relations of the degraded material read:

$$\varepsilon = \frac{\sigma_{eff}}{E \cdot (1-D)} = S_{eff} \cdot \sigma_{eff} \quad \rightarrow \quad \varepsilon_i = S_{eff,ij} \cdot \sigma_{eff,j} \quad \text{for} \quad i, j = 1 \ldots 6$$

with D_{ij} the micro-damage tensor, containing all micro-damage variables. Matrix diagonal means i = j. *Fig.15-9* presents a survey of the damage variables in the full compliance matrix [*S*].

$$S_{ij} = \begin{bmatrix} \frac{1}{E_1 \cdot (1-D_{11})} & \frac{-\nu_{21}}{E_1} & \frac{-\nu_{31}}{E_1} & 0 & 0 & 0 \\ \frac{-\nu_{12}}{E_2} & \frac{1}{E_2 \cdot (1-D_{22})} & \frac{-\nu_{32}}{E_2} & 0 & 0 & 0 \\ \frac{-\nu_{13}}{E_3} & \frac{-\nu_{23}}{E_3} & \frac{1}{E_3 \cdot (1-D_{33})} & 0 & 0 & 0 \\ 0 & 0 & 0 & \frac{1}{G_{23} \cdot (1-D_{44})} & 0 & 0 \\ 0 & (sym) & 0 & 0 & \frac{1}{G_{31} \cdot (1-D_{55})} & 0 \\ 0 & 0 & 0 & 0 & 0 & \frac{1}{G_{21} \cdot (1-D_{66})} \end{bmatrix},$$

$$D_{ij} = \begin{bmatrix} D_{11} & D_{21} & D_{31} & 0 & 0 & 0 \\ D_{12} & D_{22} & D_{32} & 0 & 0 & 0 \\ D_{13} & D_{23} & D_{33} & 0 & 0 & 0 \\ 0 & 0 & 0 & D_{44} & 0 & 0 \\ 0 & (sym) & 0 & 0 & D_{55} & 0 \\ 0 & 0 & 0 & 0 & 0 & D_{66} \end{bmatrix} \quad \text{matrix-collected } D \text{ portions}$$

$$\{E\} = (E_{||}, E_{\perp}, G_{\perp\square}, G_{\perp\perp}, \nu_{\perp||})^T \quad \text{with } \nu_{\perp\perp}, \nu_{\perp||} \text{ off-diagonal, and } G_{\perp\perp} = E_{\perp} / (2 + 2 \cdot \nu_{\perp\perp})$$

Fig.15-9: Compliance matrix [S] (here D_{ik} set 1) and micro-damage matrix [D].
By inversion of S_{eff} the decaying stiffness matrix C_{eff} is obtained.

With respect to the Poisson's ratios and the not diagonal (off-axis) quantities: *Thermo-mechanics requires that Maxwell-Betti is also valid for the degraded material.*

Usually in CDM just the diagonal micro-damage variables D_{ii} are considered. From them D_{11} can be set zero for practical applications of CFRP, GFRP. D_{22}, D_{33}, D_{44} and $D_{66} = D_{55}$ are to determine. The influence of the off-diagonal acting Poisson's ratio $\nu_{\perp\square}$ or of the D_{ik} is to assess.

15.3.4 Interaction in CD and CDM

General CM:

In the case of 3D modal SFCs (*FMC for instance*) the common microdamage-caused degradation is considered by an interaction equation that reflects the micro-damage influence of all acting stress states and associated modes. The single mode efforts are interact via the interaction exponent *m* of about *m* = 2.6.

'Ansys' CDM as FE code example: UD material

Ansys uses the 4 failure modes of Zvi Hashin (*shear mode IFF3 is missing!*) and multiplies the single micro-damage portions according to *Fig.15-10*. $0 < \mathbf{d} < 1$ with 1 at the complete loss of stiffness in a mode. As example the simple 2D CDM use case is found in the Ansys manual. For this stress state it follows from 3D $\{\sigma\} = [C] \cdot \{\varepsilon\} \;\rightarrow\; \{\sigma\} = [Q] \cdot \{\varepsilon\}$, due to $\sigma_3 = 0$ reformulation using [C].

$$\begin{Bmatrix} \sigma_1 \\ \sigma_2 \\ \tau_{21} \end{Bmatrix} = \frac{1}{1-\nu_{12}\cdot\nu_{21}} \begin{bmatrix} E_1 & E_1\cdot\nu_{12} & 0 \\ E_2\cdot\nu_{21} & E_2 & 0 \\ 0 & 0 & G_{12}\cdot(1-\nu_{12}\cdot\nu_{21}) \end{bmatrix} \cdot \begin{Bmatrix} \varepsilon_1 \\ \varepsilon_2 \\ \gamma_{21} \end{Bmatrix} = [Q]\cdot\{\varepsilon\} \quad \text{Standard}$$

$$\Rightarrow \quad \mathrm{Q_{ij,\,eff}}^{2D} = \frac{1}{A} \cdot \begin{bmatrix} (1\text{-}d_f)\cdot E_f & E_f\cdot\nu_{fm} & 0 \\ E_m\cdot\nu_{mf} & (1\text{-}d_m)\cdot E_m & 0 \\ 0 & 0 & A\cdot(1\text{-}d_s)\cdot G_{fm} \end{bmatrix} \qquad \text{in Ansys}$$

$A = 1-\nu_{12}\cdot\nu_{21}\cdot(1\text{-}d_f)\cdot(1\text{-}d_m)$. These sufixes mark fiber and matrix and do not mark a composite.

Therefore it should correctly read in standard composite terms $d_f \rightarrow d_{\square}$, $d_m \rightarrow d_{\perp}$, $d_s \rightarrow d_{\perp\square}$

and $E_f \rightarrow E_{\square}$, $E_m \rightarrow E_{\perp}$, $G_{fm} \rightarrow G_{\perp\square}$.

In Ansys reads $d_{\perp\square} = 1-(1\text{-}d_f^t)\cdot(1\text{-}d_f^t)\cdot(1\text{-}d_m^t)\cdot(d_m^t)\cdot$ No correspondance $d_{ik} \leftrightarrow D_{ik}$.

Fig.15-10, 2D: $\{\sigma\} = [Q]\cdot\{\varepsilon\}$ Ansys formulations of the micro-damage portions

Unfortunately no standard formulations are applied, some confusion due to use *d* instead of *D*.

The micro-damage variables increase gradually based on the energy amounts dissipated in the modes. In order to obtain an objective response, the energy dissipated in each single mode is to regularize from numerical reasons. It is to fulfill that the energy dissipated per volume finite element:

g_{vol} = energy g_c dissipated by unit area / characteristic length of the element $L_{element}$

with $L_{element} = 1.12 \cdot \sqrt{area}$ (square element) or $1.52 \cdot \sqrt{area}$ (triangular element)

With the characteristic length the stress-strain relation is converted to a stress-displacement relation. For each mode, for *onset-of-damage* an equivalent displacement is to apply and for *fracture* when the material reaches its strength R^t using strength failure criteria and especially viewing the Ansys approach: The micro-damage evolution functions are derived from Hashin's failure criteria and are therefore the only criteria one can apply in this code for detecting essential onset-of–damage. In the manual the equivalent stresses and the equivalent deformations are given for the four micro-damage modes..

LL:
** The author could not sort out a consistent procedure that might be used in design verification. A clear derivation of the maximum micro-damage values seems to be missing.*
** From an engineering design point of view, C-fiber types must not be attributed a micro-damage variable.*
** Just for failure the damage mode becomes a failure mode.*

,

15.3.5 Aspects of Design Verification in CM and CDM (examples: brittle UD, ductile metal)

In engineering, several structural mechanics tasks are faced. Main task is the design verification: This requires a reliable stress-strain analysis using proven stress-strain relationships like Ramberg-Osgood and a stress state evaluation by strength criteria (strain criteria are not standard).
Exemplarily for the 3 micro-damage–prone Inter-Fiber-Failure IFF modes of UD materials the required full design verification procedure shall be presented for traditional CM. This may serve as a guideline for the CDM that captures the hardening and the softening part.

In order to be able to perform the Design Verification work in the critical material location it is to provide:

CM: *An Analysis with a fixed input data set is to execute, 'only'*

1) 3 moduli and 3 strengths *(the stiff FF modes are not regarded here)*
2) 2 Poisson ratios $\mu_{\perp\square}$, $\mu_{\perp\perp}$ acting off the matrix [*S*]-diagonal, are considered due to practical experience
3) 3 IFF stress-strain curves for the stress-strain analysis
4) 3 3D-IFF strength criteria to determine the material stressing effort *Eff* (Werkstoff-anstrengung) $0 < Eff < 100\%$
5) Interaction equation of the associated 3 IFF *Effs* because commonly acting modes trigger micro-damage (*interaction IFF-FF here is not addressed*)
6) Strength values are statistically-based
7) Safety Concept and Design FoS are given
8) → Determination of the Reserve Factor $RF > 1$ for $Eff \leq 100\%$.

CDM: *A Simulation with its test data-based input data adaption is to perform*

1) Points 1-3, see CM
2) 3D-microdamage criteria to assess the micro-damage state in the critical location
3) Interaction equation of all D^{modes} because commonly acting modes trigger the joint degradation

4) Influence of Poisson's ratios is to consider
5) At onset of non-linearity is $D = 0 \rightarrow$ however mind, then the *Eff* value is still > 0
6) Design verification requires a statistical base. Question: How can one obtain statistically-based micro-damage parameters *D*?
7) From standards Safety Concept and Design FoS are practically prescribed for stress-strength problems, based on long term experience. Question: How can CDM manage this, considering exemplarily admissible micro-damage values below?
8) → Determination of the necessary, load-level defined *RF*

   $D < D_{admissible}$ (should be statistically based) = *? < 1* at failure.

Table 15-2 lists the basic features CM ↔ CDM

⇒ CM: all model properties and uniaxial UD stress-strain curves i.e. are measured
⇒ CDM: not all model properties can be directly measured.

* In the context above it is to remind: In CM one must stick in Design Dimensioning and Design Verification to a statistically based approach with a distinct minimum number of measurable design parameters. Usually, a structural analysis is performed and no test data driven simulation with a change of the design input parameters to better simulate or fit the test results
* Since about 100 years in CM the letter C is used for the stiffness matrix [*C*] and [S] for the compliance matrix. In CDM since some decades [D] is used for the damage matrix. Why does ANSYS use [*D*] instead of [C] and [D_d] instead of [D]? This is confusing and probably is one of the acceptability reasons why CDM is not used in a way it might be applied
* In Abaqus, compare *Fig.15-7* with *Fig.15-8,* can be found that $D = 0$ at onset-of-failure = end of load-controlled loading or begin of necking! This practically means: Plastic deformation does not harm the ductile material. Really, or? In the case of a strain-controlled brittle material this is physically not accurate because micro-damage has still begun when becoming inelastic in the hardening domain. This is another confusion that may block CDM acceptance. For the author: CDM applicability seems to be 'usually' linked to the level of material ductility, but it should be always clearly discriminated depicted in a FE manual 'brittle and 'ductile CDM'
* For more physical information on the micro-damage behavior CDM is employed: Exemplarily in the case of a crash analysis task, where usually crash test results are available, highly non-linear material models like "Gurson" are applied in the performed simulation with many material model parameters that cannot become statistically based. Such a procedure does then not represent a traditional Design Verification (the simulation of crash situations is just a small application domain of structural design)
* Beyond the strength point R^t, R^c (isotropic) softening of a more brittle material is marked by a constant *Eff*. The material is 'ruined' - although not broken - because the vicinity around the critical location can still take over some additional loading → *D* grows but *Eff* remains 100%
* Beyond the strength point R^t softening of a very ductile material nucleation and coalescence of micro-voids are generated and a porosity-driven micro-damage increases with increasing necking → *D* grows but *Eff* remains 100% (effective *Eff*)
* Softening can be not used if the stress situation in a critical material location is load-controlled like a a so-called 'single failure path' membrane wall
* Micro-crack-based CDM can support FM-based macro-crack growth.

Table 15-2: Basic features of CM and CDM

CM	statistically-based design parameters (strengths, ..)		
static	*at fracture , n=1*	:	*Eff* = 1
cyclic (fatigue)	*1< n < N*	: *on S-N curve*	D_{fat} = 1
CDM	statistically-based design parameters (*D*admissible, ..)		
static	*at fracture , n=1*	:	*static Ddam < static Dadmissible < 1*
cyclic (fatigue)	*1< n < N*	:	*cyclic Ddam < cyclic Dadmissible < 1*

There is some confusion with the letter D regarding CM and CDM,

Note on Stress effort versus micro-damage development:

For the designer of interest is how the material's stiffness decreases with increasing stress effort or load, respectively. Design allowable *R* and average strength $\overline{R}$ lead to different stress efforts in *design verification* and in *modelling of material damaging* (50% value = highest expectance probability), see *Fig.15-11.* The enlarging effect of the design factor of safety j on the stress effort to be considered is still included in the depicted design verification curve (dashed line) when reaching failure. The more reserve is, indicated by a positive Margin of Safety *MoS*, the lower the stress effort is. This has an effect on the actual strain in the non-linear analysis case. It is smaller.

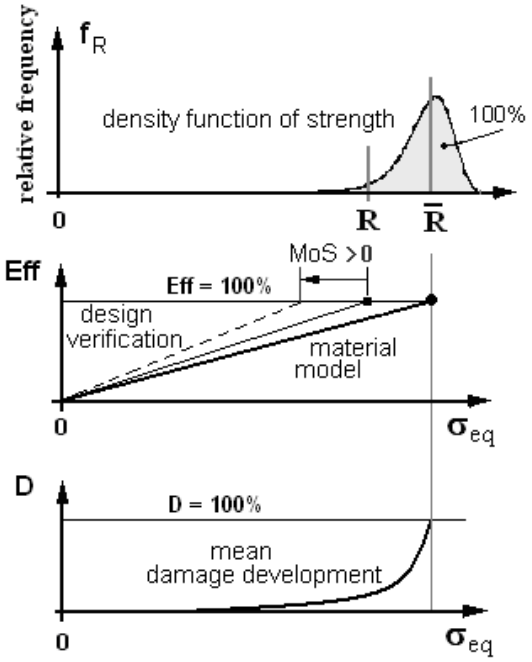


Fig.15-11:
Visualization of the development of stress effort, strength value, equivalent strength, and
damage understanding
of a stress-man.

MoS = RF - 1

LL:

- *It is desirable to incorporate CDM knowledge into the component development process. But then of course, all the prerequisites above must be met to obtain a reliable structural design. Micro-cracks develop within a local process zone around the flaws*
- *When reaching the strength point Eff becomes 1 and this continues on the SN curve by $D_{fatigue} = 1$. On the softening curve σ and R strain-controlled decay similarly → hence it remains $Eff = \sigma_{ef}/R_{ef} = 1$, due to the actually effective values of σ, R. An 'Over Eff' does not exist*
- *In fatigue the switch for failure loading works: From 1 cycle (static case) to n > 1 means Eff = 100% is followed by a micro-damage sum D =100% along the SN curve*
- *The fixation of critical values, as accepted to be reliable in design development, is the challenge*
- *For the 'stress-man' a not–redundant load-controlled structural element built from a ductile material is at its end at the tensile strength point, CDM however says D = 0 (Abaqus figure). This is a conflict. The practical engineer cannot understand this*
- *The 'onset-of micro-damage' is dependent on the ductility level of the envisaged material*
- *The reaction of an embedded material 'point' is different to that one which is located at the structure's surface. Flaws in the material at a surface are more critical than embedded ones*
- *Commonly acting failure modes further degrade all affected failure modes. This causes a joint stiffness loss that is to consider in a further analysis step*
- *After a certain state of micro-damage the initially isotropic material can become anisotropic such as concrete under tension and compression*
- *The author, who had to perform Design Verifications in the past, desires a clear maxD definition and a clear depiction of the practical design importance of the accumulated micro-damage portions discriminating ductile inelastic and brittle inelastic behavior and regarding load carrying capacity.*

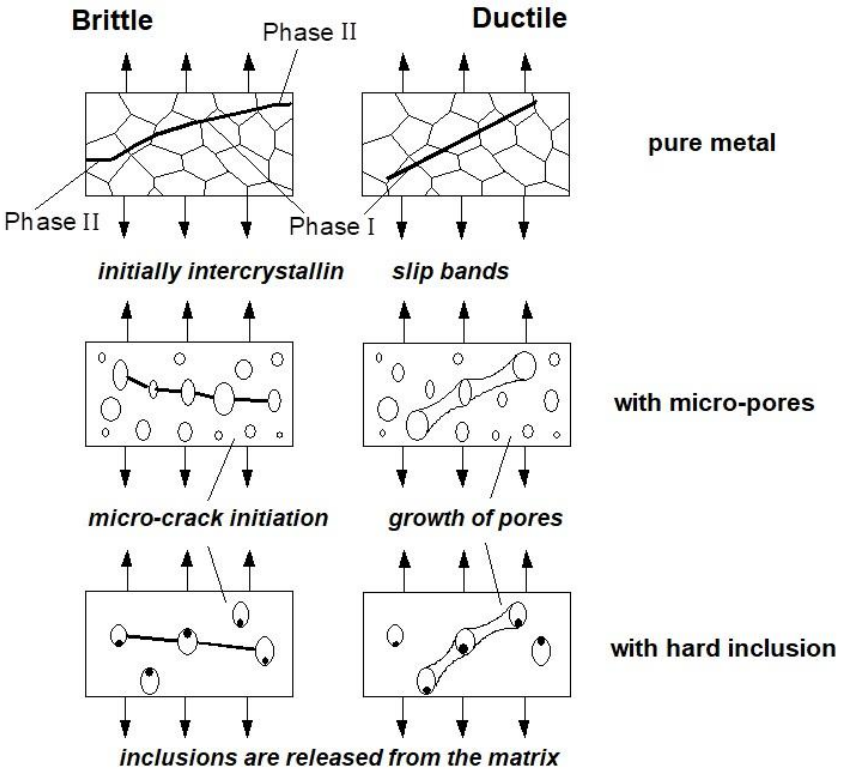


Fig.15-11: Initiation of micro-cracks and micro-voids (phase I means micro-ductility)

Fracture Origins:

Fracture is understood here as a separation of material, which is free of damage such as cracks but not free of flaws prior to loading. In this context *crushing* of a porous material has to be seen a separate *fracture mechanism* respectively *(fracture) failure mode* and *type*. In the next illustration, the initiation of a micro-crack, a pore under tension and the influence of them and their orientation are presented using the example of metal. Influence of defect type and orientation are presented using the example metal in *Fig.15-11 above*.

See further *Fig.2-8 on effect of flaws, micro-cracks, notches and inclusions and flaw orientation as originators of fracture due to tension [Pli95]*.

15.4 CDM of Ductile Materials described by a 'Gurson Model'

A couple of micro-damage models are used to date such as the Rousselier model, the Rice-Tracey model, the Gurson model, or the Gurson-Tvergaard-Needleman model (GTN model [*Nee84*]). Referring to the latter the different micromechanical mechanisms of ductile fracture consist of:

* void nucleation at second phase particles by debonding or micro-cracking
* void growth controlled by stress Triaxiality Factor *TrF* and equivalent plastic strain ε_{eq}^{pl}, and
* coalescence of voids by shear stress-driven internal necking with later rupture.

A Gurson model comes to act when the Mises cylinder begins elliptically to deform (*Fig.15-12c*) due to the effect of the growing voids (*increasing micro-damage*) and their final coalescence. This shrinking of the CDM failure surface is the bigger the more void volume is generated. It stops when reaching the final load-carrying capacity of the 'thinned' tensioned bar, termed rupture, which depends on the Triaxiality Factor *TrF* and the grade of strain control of the load-sharing cross-section vicinity. In other words: By the increasing porosity the hardening effect is surpassed by the related micro-damage causing softening.

Originally, Gurson proposed for a metal, containing well distributed voids, a yield condition based solution for a single spherical void. Tvergaard introduced q_1 and q_2 as coefficients of the void volume fraction and the hydrostatic 'pressure' $\sigma_{hyd} = I_1/3$ to improve the predictions. Hence, the relatively simple Gurson model ([*Gur77*]

$$F_{Gurson} = \frac{3 \cdot J_2}{\sigma_F^{\,2}} + 2 \cdot f \cdot \cosh\left(\frac{I_1 \cdot q_2}{2 \cdot \sigma_F}\right) - f^2 = 1,$$

modified later by Tvergaard and Needleman, includes the porosity f and the increasing Flow stress σ_F of the 'matrix' material. The porous body, called bulk material (*smeared material*), consists of the matrix material and the voids or pores. The voids are nucleated in tension, only.

This model is based on a representative volume element with an initial void. The dense matrix phase follows the HMH ('Mises') model, and f represents the mean void volume fraction or porosity (*average value of a porous matrix*) as the so-called internal damage variable. For $f = 0$, the fully dense material, the model reduces to that of HMH, whereas a maximum value f_{ult} implies that the material is ultimately voided that it looses its stress carrying capacity due to local ductile rupture.

The model parameters cannot be measured directly, but are usually determined by FE analyses which best model the deformation of the test specimen. The FE mesh must be very fine in order to

sufficiently well resolve the critical locations. Therefore, the optimal model parameters depend on the mesh fineness.

The conventional visualization – as a parameter investigation - of the Gurson model is presented in *Fig.15-12a* with *f* being the parameter of the curves. Another visualization, usually practised in structural mechanics, is given by using the Westergaard-Lode parameters. This leads to a change in the shape, *Fig.15-12b*. For $f = 0$ the Mises cylinder is obtained.

Fig.15-12c displays the development of the subsequent failure surfaces because an increasing true stress is considered. This is relevant for the critical material location. After achieving the tensile strength a small further radial increase of the surface is obvious together with the initiation of an elliptic failure surface. With increasing degradation the F_τ^t failure surface becomes more and more elliptical. This reminds of Beltrami: According to the reduction of the volume change of the solid material element from $\nu_0\,(\text{ellipse}) \rightarrow \nu_{pl} = 0.5\,(\text{cylinder})$ it turns here to the opposite, according to the volume increase reducing $\nu_{pl} = 0.5\,(\text{cylinder}) \rightarrow$ ellipse with < 0.5. A growing *f* means higher true stress but less cross-section or load-carrying material in the strain-controlled 'hot spot'. This is displayed in the figure by the change of the cylinder shape versus an egg shape.

The more refined the 'Gurson'-model becomes, the more micro-mechanical curve parameters are to determine. An example for such a parameter set, the values of which were determined for the metal aluminum alloy AA2219, is given in *Table 15-3* (*from a collaboration of MAN with IWM Freiburg*).

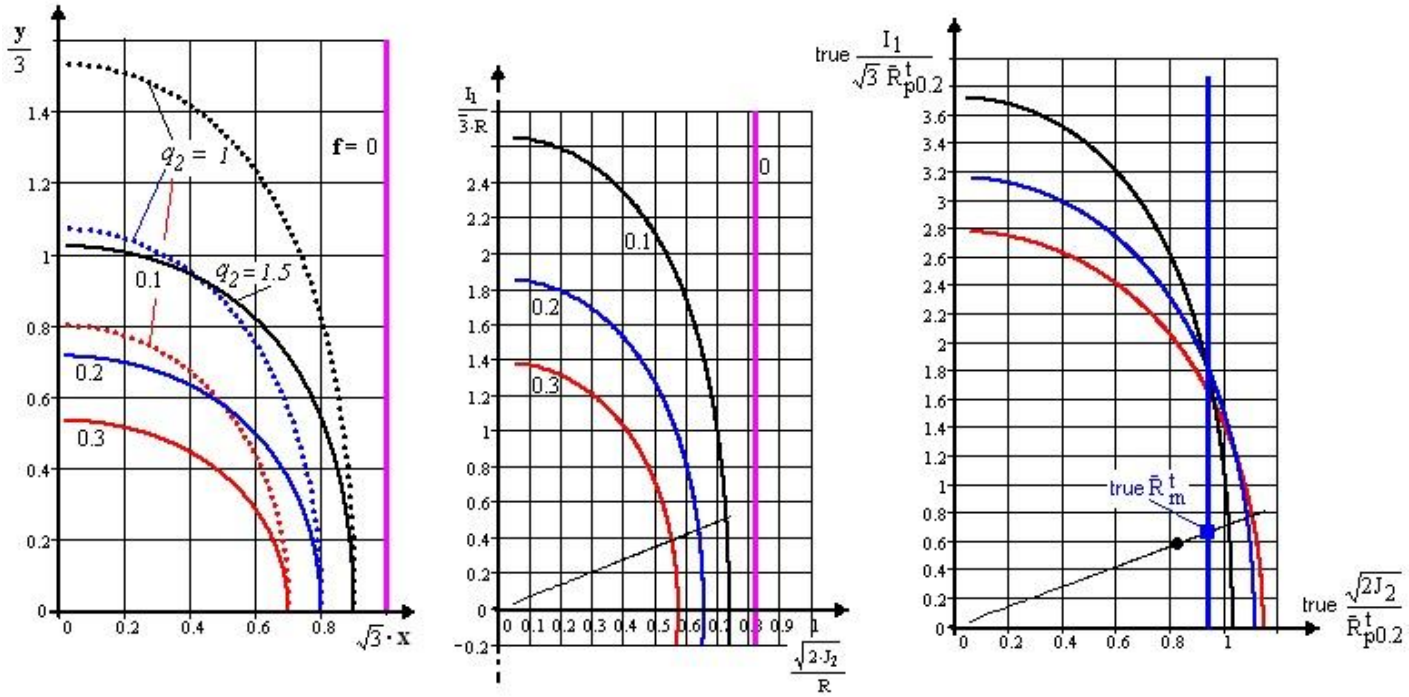


Fig. 15-12: (left) Usual 3D-display of curve parameter porosity f influence, using the 'Gurson' coordinates x = $(\sqrt{J_2}/\sigma_F)$, *y=*(I_1/σ_F), $\sigma_F = \bar{R}^t_{p0.2}$; *(center) 3D-visualisation of the Gurson yield model in Westergaard-Lode parameters* $\bar{R}^t_{p0.2}$ *= normalisation strength); (right) Schematic: now as 3D-Gurson failure criterion with* σ_F *as increasing true Flow stress*

Table 15-3:
Parameters of a refined ' Gurson' model f_0 f_n f_c f_F q_1 q_2 ε_n s_n

Practically, all these parameters have to be *inversely* determined by a excellent simulation of the test specimen's behavior. Therefore, the design engineer *must* ask. What about the scatter of the parameters? Without knowledge of the scatter there is no design verification permitted. Might it be not better to apply a simpler model with 2 or 3 parameters at dispense of the little gain of the last load carrying portion? Only a reduced procedure with less model parameters has the chance to capture the statistical design verifications requirements. The author will later present a proposal.

LL: Increasing porosity also means decreasing Poisson's value v and a more elliptic shape..

CDM is pretty linked to multi-scale modelling with its tool 'Representative Volume Element' RVE. This shall be shortly outlined.

15.5 Multi-scale Materials Modelling MMC

"***Approach, that employs models on different levels to investigate an engineering problem, supporting the design development of the envisaged structural component***".

Before going into details the designer reminds:

Simulation in CD and CDM: Performance of many analyses in order to simulate the component behavior to finally achieve a reliable design parameter set. This work is performed before any Design Verification of the final design is executed.

Design Verification (*Nachweis*) in CD: Demonstration not to meet any failure state (strength, fatigue life, crack growth or a permeability limit etc.) by one distinct analysis *(Berechnung*) of the *Final* Design. Design parameters are principally statistically–based given. Design Verification applies a validated material model and the final design as outcome of the simulation process.

On the envisaged levels, models are generated for the description of the level-associated phenomenon. Hence, in structural engineering multi-scale material modelling spans from micro-scale level to macro-scale level and thereby models are set up on these different levels in order to transfer properties from the lower to the higher level and vice versa. The bridge is built by the so-called meso-models, see *Fig.15-13*, using representative volume elements RVE.

The different models are linked together either analytically or numerically. In this context the author believes to distinguish the treatment of multi-scale modelling of ductile and brittle materials as follows:

- Ductile: Yield failure criterion 'Mises' is applicable, $E^t = E^c$, friction μ not relevant.
  Modelling: Nano → micro → macro, probably with meso-models on different levels
- Brittle: Strength *fracture* failure criteria are to apply, Mohr-Coulomb friction is relevant.
  Modelling: Micro → macro, probably with a meso-model between micro and macro.

What is meso?

Meso is no scale, per definitionem! See below

* Micro-scale > μ *m*, macro-scale > *mm*.
* The author experienced in a BMFT R&D discussion round on three MaTech Competence centers (1999) - after one day - that the term meso-scale is used in polymer mechanics by the research colleagues at the nano-level which is a level of one thousand smaller than the solid mechanics people use it.

* Classification of porous materials according to pore size: 'microporous' pores < 2 nm, 'mesoporous' pores between 2 nm and 50 nm, 'macro-porous' pores > 50 nm. [*International Union of Pure and Applied Chemistry*].

LL: The term meso is a task-linked chosen size level. Conclusion: Apply the term meso-model, not scale, and define it. In structural engineering meso is defined at about 0.1 mm.

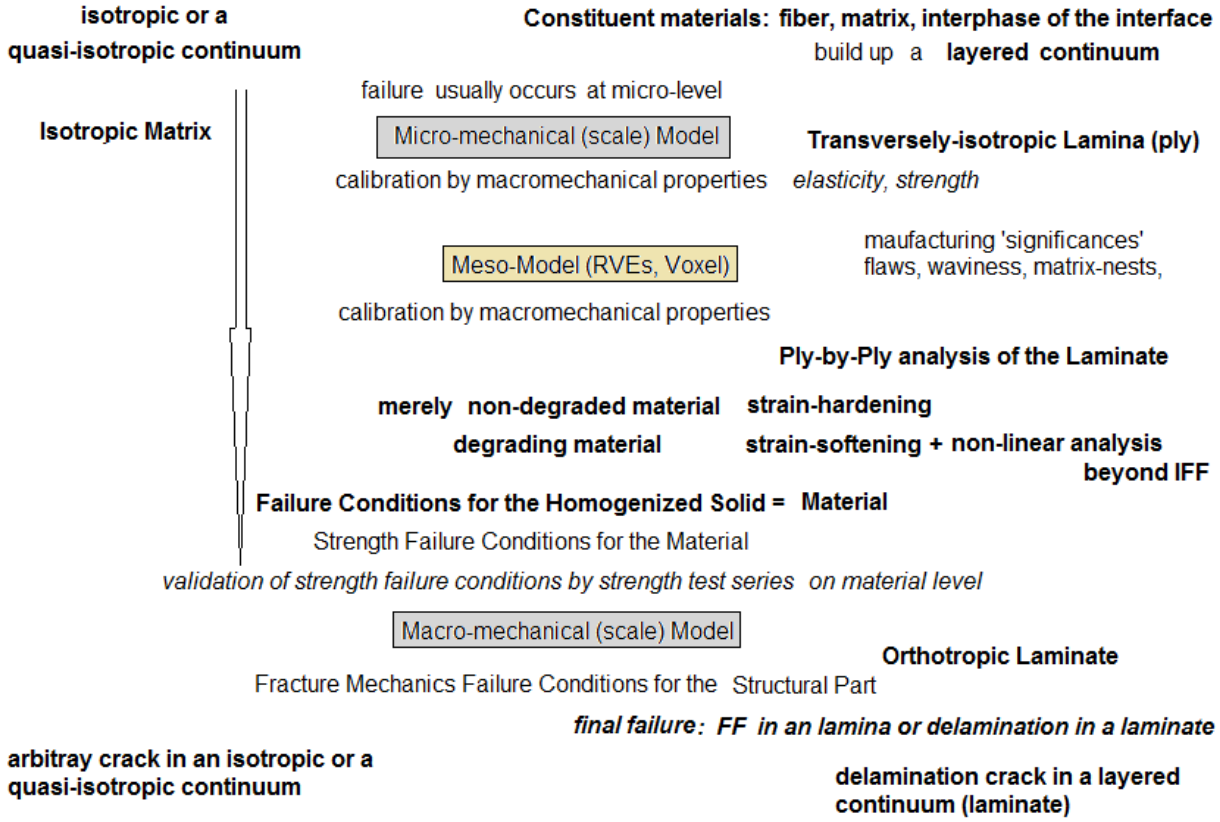


Fig.15-13:Multi-scale modelling, example FRP, brittle.
2 scales. RVE: Representative Volume Element, Voxel: volumetric pixel

Flaws still act at the nano scale *nm.* Then, the caused micro-damage grows passing the *µm* scale and the *mm* scale until fracture of the macro-damaged structural component is caused. Over the scales the affected micro-and macro-damages may also die out according to topology, strength and stress state. Experienced extreme crack at the end of the length scale: In offshore industry the insurance-driven question arises *"How much time does it (hopefully) still take that a 10 meter long crack becomes of a critical size, assuming stable crack growth".*

It is worthwhile – also in the context of the micro-damage mechanics above - to investigate the behavior of ductile materials (metals) in the micro-scale regime in order to achieve more information about the behavior of Short Cracks, which do not follow the Long Crack rules.

15.6 Metallic example for a Multi-scale Material modelling (MMM), Mlikota model

15.6.1 Introduction

In future, for homogeneous isotropic materials, computer power will probably allow 'Computational material mechanics' from nano-scale models (*Molecular Dynamics-treated and test results-supported from statically and cyclically loaded 10 µm thick pillars for instance)* via micro-scale to bridge with the necessary properties (*hopefully statistically based*) to the proven macro-scale models

in structural design. Multiscale materials modelling (MMM) will grow and become a significant tool for understanding complex material micro-damage processes for many materials. In this context shall be cited *[Schmauder Siegfried and Schaefer I, Multiscale materials modeling, Volume 19, Issue 3, Page 130–131] "An extensive simulation-based description of the mechanics of materials can be achieved. For this purpose more than two simulation methods have to be connected for the integral description of materials behavior from the nanoscale to the microscale and finally to the macroscale*".

Here, intentionally prepared for a wider engineering understanding to sort out similarities on the length scale levels, a successful 3-scale application to a cyclic problem of a ductile material will be shortly displayed with the permission of Dr.-Ing. Marijo Mlikota, whose dissertation on "Multiscale Modelling and Simulation of Metal Fatigue and its Applications" is the basis of the following body text and figures. The present advantage for the stress engineer is that he can better understand micro-mechanical failure processes, at least those of ductile metals.

The intention in the dissertation is the numerical determination of the complete fatigue lifetime of an austenitic stainless steel (*poor of flaws*) by taking into account the influence of the material's microstructure at micro-crack initiation. A micro-model containing the microstructure of the material is positioned at the highly stressed location where the micro-crack initiation is expected. The number of cycles needed for micro-crack initiation is estimated on the basis of the physically-based Tanaka-Mura model (*see later*). Micro-crack coalescence then leads to a short crack SC that may grow to a long crack LC or macro-crack, respectively.

Fatigue is characterized by a series of upward and downward loadings. During cycling, flaws in the form of dislocations multiply and accumulate within the material (from [*Mli19*]). This behavior results in an increase in the dislocation density. Consequently, in many materials, strain is localized in the form of slip bands. The slip bands or lines appear fine and sharp in several favorably oriented crystals (grains) within the microstructure and as more cycles accumulate, more crystals display signs of slip bands, the existing bands widen, and ultimately some of them develop into short cracks.

The number of slip systems in metals is usually high, and those that are active possess an orientation near to the planes with maximum shear stress. Under uniaxial loading the planes of micro-cracks are always inclined approximately 45° to the direction of the applied loading (*Fig.15-14*).

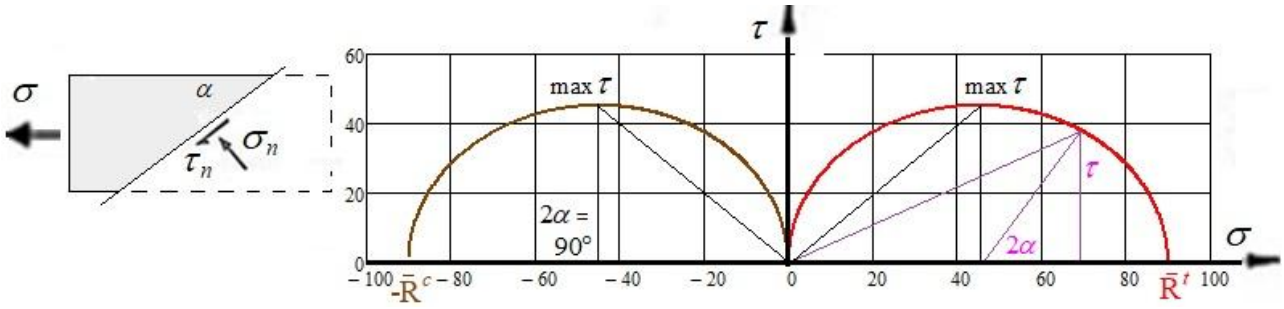


Fig. 15-14: Mohr stress circle for a compressive and a tensile uniaxial stress of a ductile material

$\tau_n = \sigma \cdot \cos(\alpha) \cdot \sin(\alpha)$ with α the angle to σ direction, $2 \cdot \max\tau = \sigma$ for $\alpha = 45°$

In single crystals, the lattice structure is spatially oriented in such a way that a sliding plane is obtained at an angle of 45°. In poly-crystalline metals with randomly distributed lattice sub-

structures this might change a little. For information in the case of brittle materials under compression: The computation of the failure angles with the Mohr-Coulomb model (*presented in chapter ?9.1*) delivers exemplarily for a material friction value $\mu = 0 \rightarrow 45°$ and for $\mu = 0.2 \rightarrow 50°$.

Once micro-cracks have nucleated due to strain accumulation from cyclic slip, they grow in the early stage typically in the order of the material's grain size. In the course of further cyclic loading, micro-cracks (*here termed Microstructurally Short Cracks MSC*) - formed along these slip bands - will grow and link together, *Fig.15a*. In metals and alloys they grow predominantly along the crystallographic planes because they are highly affected by microstructural barriers such as grain boundaries or other micro-structural features.

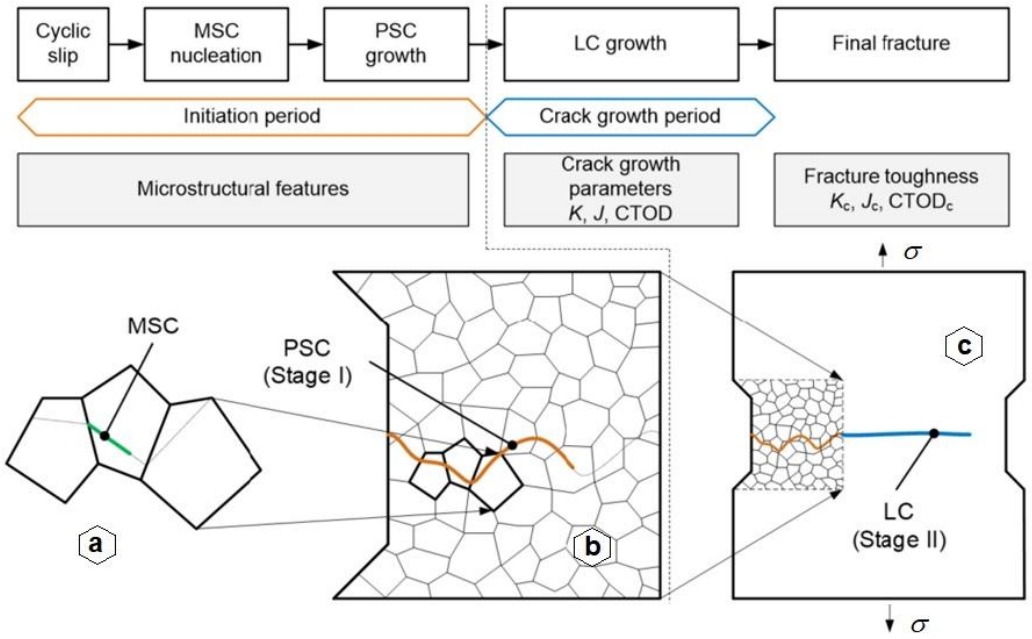


Fig. 15-15: Stages of a metal fatigue crack during its growth:(left) Microstructurally Short Crack (MSC) on the grain size scale, (center) Physically Short Crack (PSC) on the microstructure size scale (Stage I), and (right) Long crack (LC) on the specimen size scale (Stage II).[M. Mlikota, S. Schmauder* *) Institute for Materials Testing, Materials Science and Strength of Materials (IMWF), University of Stuttgart]. K stress intensity factor and Kc critical stress intensity factor or fracture toughness in MPa/ $\sqrt{m}$, J the crack initiation energy in N/mm, CTOD crack tip opening displacement in mm*

Thank you Siegfried and Dr. Mlikota for allowing me to use your work results for an example.

If MSCs have grown through several grains they are considered to be a Physically Short Crack (*PSC, in structural engineering termed 'short crack', only*) whereby the length of PSCs is usually in the range from several grains up to 1-2 mm, *Fig.15-15b*. Upon reaching the end of the PSC regime the microstructural influences become negligible and such micro-cracks start propagating in a continuous manner perpendicularly to the outer tensile loading direction. Thereby they become a crack termed long crack LC, *Fig.15-15c*. The change from the PSC to the LC regime is called the transition from Stage I (*crystallographic growth*) to Stage II (*non-crystallographic growth*) or transition from crack initiation to crack growth. In engineering applications, the first two stages are usually termed the crack initiation period while LC growth is the macro-crack growth period. The dominant short crack becomes a long crack LC. The crack initiation period generally accounts for most of the service life, especially in the high-cycle fatigue (HCF) regime.

15.6.2 On Short Cracks (SC) and Long Cracks (LC)

The coalescence of trans-granular micro-cracks in the numerical simulation of crack initiation is performed on the basis of the modified Tanaka-Mura equation (*see next paragraph*). Namely, if two micro-cracks meet each other at the same grain boundary (red solid line in *Fig.15-16*) and if the average stress in between their tips surpasses the elastic limit Re of the material's new micro-crack is created on this grain boundary line, uniting the two trans-granular micro-cracks into a single one. In the example case of pure iron Re is 260 MPa, $R_e \equiv R_{\text{p (proportional)}} \approx R_{0.01}$ structurally practical. Indicator is a temperature increase during tensile testing.

Already nucleated crack segments tend to extend along the whole grain, causing local stress relaxation as well as concentrations at their tips and by that amplifying the likelihood for new crack formation in the vicinity. In the course of further sequences of simulating, micro-cracks form along these slip bands grow and link together.

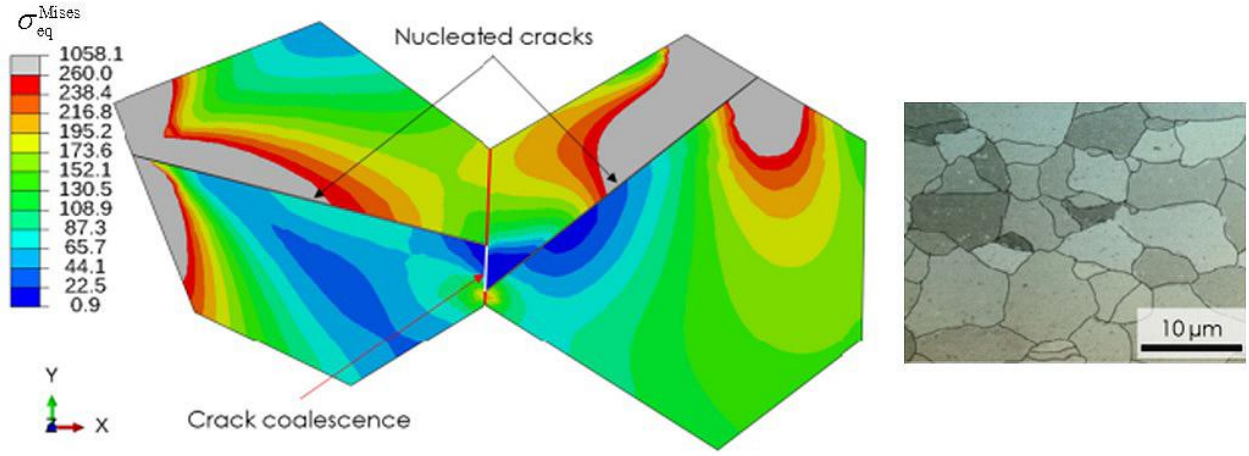


Fig.15-16: Simulation of AA micro-crack coalescence (Lorenzino, P.; Navarro, A. & Krupp, U. (2013), 'Naked eye observations of microstructurally short fatigue cracks', Int. J. of Fatigue 56(0), 8-16.

The change of the crack plane from active crystallographic plane to a non-crystallographic plane perpendicular to the external stress axis is called the transition from Stage I (*crystallographic growth*) to Stage II (*non-crystallographic growth*) or transition from the micro-crack initiation to micro-crack growth stage resulting in a short crack, as depicted in *Fig.15-17*.

However, the dominant short crack does not always continue propagating similar to a long crack. Namely, in the case of a lower stress level, the short crack may stop growing, i.e. it retards. Such situations are typically known as run-outs, see again *Fig.15-17*, which indicates that at very low stress levels an infinite life may be obtained. Run-out below the endurance limit means crack-retardation.

In the long-crack regime the fatigue crack growth rate da/dn can be characterized by the stress intensity factor range ΔK as a dominant driving parameter. A typical fatigue crack growth rate curve da/dn(ΔK) for the long crack is illustrated in *Fig.15-17*, too. If in a double logarithmic scale the LC propagation rate follows a straight line in region II, in sufficient distance from the threshold ΔK_{th} .

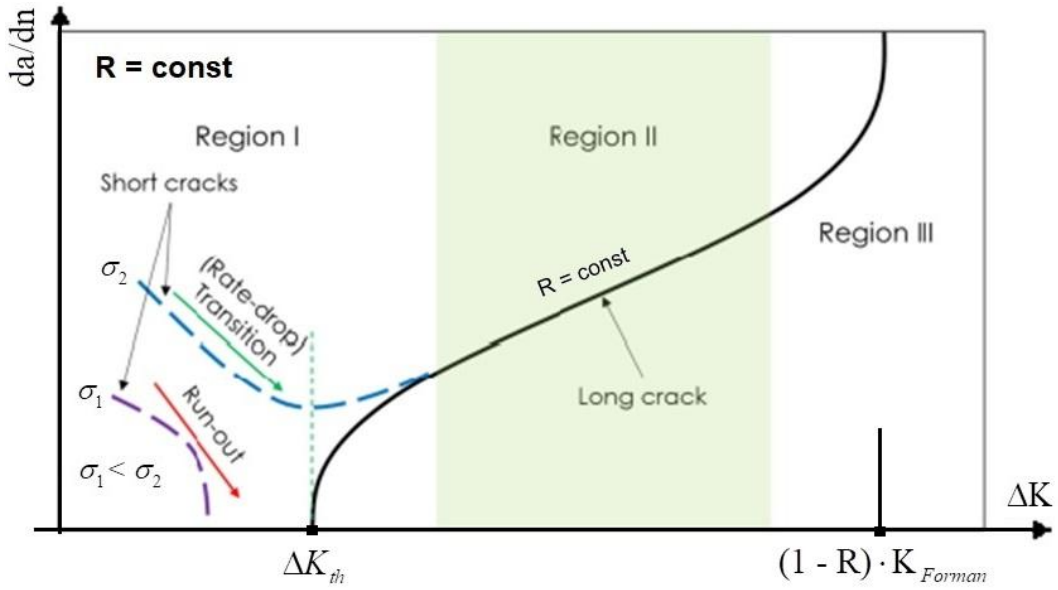


Fig.15-17: Fatigue growth rates of micro-cracks (short) and long cracksin dependence of Δ stress intensity factor. Schematic reperesentation of the loading level- dependent transition from region I into region II. (Newman, J.; Phillips, E. & Swain, M. (1999), 'Fatigue-life prediction methodology using small-crack theory', Int. Journal of Fatigue 21(2), 109-119)

In the LC fatigue crack growth rate domain in Region II most engineering alloys under a certain stress level can be well described by the so-called Paris law:

$$\text{Paris:} \quad da/dn = C_{Paris} \cdot \Delta K^{n_{Paris}} \quad , \quad \text{Forman:} \quad da/dn = \frac{C_{Forman} \cdot \Delta K^{n_{Forman}}}{(1\text{-R}) \cdot K_{Forman} - \Delta K} \quad [HSB\ 63205\text{-}01]$$

In the formula above da/dn is the crack growth increment per cycle, ΔK is the range of stress intensity factor (ΔK = maxK – minK), and C (intercept with the y-axis) and n (slope) are material curve parameters that are deducted by fitting the course of experimental data. K_{Ic} is the so-called fracture toughness.

In order to map all 3 regimes by one function Forman's formula above is to mention. As former contributor to the HSB I like to mention the mathematically excellent procedure of the IASB colleague J. Broede in [*HSB 62211-05*].
For above two 'laws', the curve parameters for many metallic materials are provided in the respective HSB sheets, too, (*however just HSB sheets-contributing IASB members have access*).

By combining the modelling approaches on the different scales, the final numerical result of lifetime is obtained. Eventually, Damage Tolerance demonstrate in the Regions II and III by fracture-mechanical methods using deterministic methods for crack growth and for residual strength or more refined, probabilistic-based methods where risk analysis is required.

LL, viewing structural metals
Metals with different crystallographic structures, namely body-centered cubic (ferrous metals) and face-centered cubic ones show different behavior [Mli19]. Ferrous materials (including steels) generally show a sharp "knee" in the SN curve at about 10^6 cycles, after which the curve increasingly flattens and an endurance limit seems to be obtained. Most of the materials – like the non-ferrous ones - exhibit a gradual flattening between 10^7 and 10^8 cycles. The so-called Haibach approach by 'halving the angle' is then often applied.

15.6.3 Numerical Modelling in Multiscale Materials Modelling, Mlikota model

The polycrystalline, microstructural FE-model of an aluminum alloy AA is given in *Fig.15-18*. Its microstructure mesh contains around 250 grains in total, with the average grain size of 60 μm. The size approximately corresponds to a grain size of high purity AA.

Upon nucleation of a first segmental crack in the model, the cycles required to nucleate a new crack are again calculated for all grains and all slip line segments in the microstructure on the basis of the new stress field that is locally influenced by the newly nucleated crack. The new stress field can also change the likelihood of some grains for the crack formation, in both directions. In the same manner as in the case of the undamaged microstructure, the next segment that is stressed beyond the level of 2·CRSS (C*ritical Resolved Shear Stress*) and that needs a minimal number of cycles for crack nucleation is identified and a micro-crack is introduced in the RVE.
Slip in a single crystal on slip plane begins only after the applied stress has reached above certain minimum value, called CRSS. It is the stress to move a large number of dislocations to produce a macroscopically measurable strain.

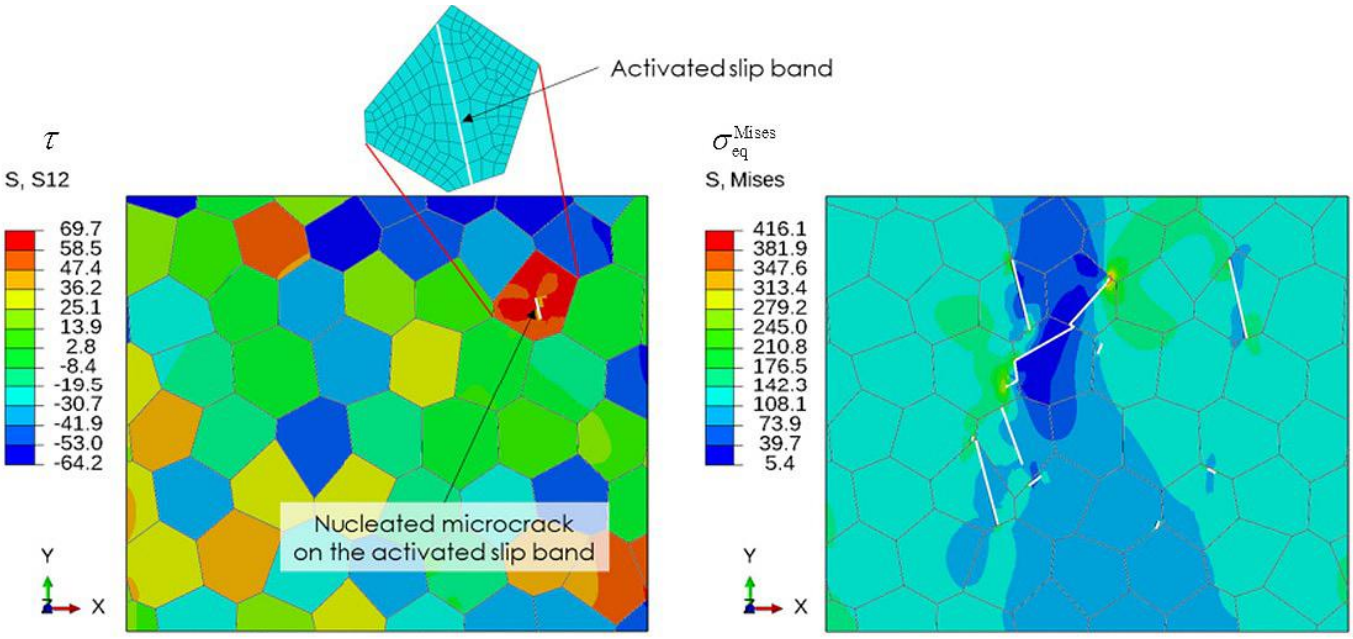


Fig.15-18: (left) First micro-crack in a micro-model, (right) Coalescence of existing micro-cracks in the micro-model. [Mli19]. Under tension→ S12 = τ < 2·CRSS, CRSS =14 MPa for high purity AA

Each micro-crack is formed in the model in a separate simulation sequence. After the micro-crack condition has been satisfied in one simulation sequence, the model gets updated with the latest crack and re-meshed for the following sequence where the condition is applied again and a new weakest slip line segment is traced. The remaining parallel slip planes of the grain are not further considered for cracking after the activation of the weakest slip plane.
The dislocations generated in a most favorably oriented grain under a tensile stress are piled up against the grain boundary. If the dislocations piled up on a plane would move in the opposite direction under reverse loading, there would be no accumulation of dislocations, so no fatigue fracture would take place.

15.6.4 Tanaka-Mura fatigue micro-crack nucleation Model

In the Region I the prediction of lifetime for the ductile metals is performed employing the theory of Tanaka and Mura which takes its final form to determine the fracture cycle number according to

$$N_g = 8 \cdot G \cdot W_c / [\pi \cdot d \cdot (1-\nu) \cdot (\Delta\tau - 2 \cdot CRSS)^2)]$$

with the curve parameters: G the shear modulus, υ Poisson's ratio, grain size d = 2a = dislocation pile-up length, $\Delta\tau = \max\tau - \min\tau = \tau 1 - \tau 2$ is the applied shear stress range (*input comes from FEA*) and W_c the specific fracture energy per a unit area along the slip band, or in other words the crack initiation energy [*Mli19*]. The CRSS is - according to *critical stress ≡ strength* - a micro-shear strength. There is a hope for some ductile materials in future to estimate the endurance limits of various metallic materials in the Ultra HCF regime just by knowing their CRSS values ! The CRSS is the resistance for the dislocations to move through the crystal. It is governed by the present strengthening mechanisms in the crystal.

Tanaka-Mura's fatigue micro-crack nucleation model was reworked based on the true strain definition and by replacing the grain-breaking cycle number Ng by segment-breaking cycles Ns, and the slip line length d by the slip line segment length ds and finally by including the stress ratio via (1 – R). It reads $N_S = 8 \cdot G \cdot W_c / [(1-\nu) \cdot d_S \cdot [\Delta\bar{\tau}_S \cdot (1-R) - 2 \cdot CRSS]^2]$.

Fig.15-19 displays the CRSS- determination by µm-pillar testing.

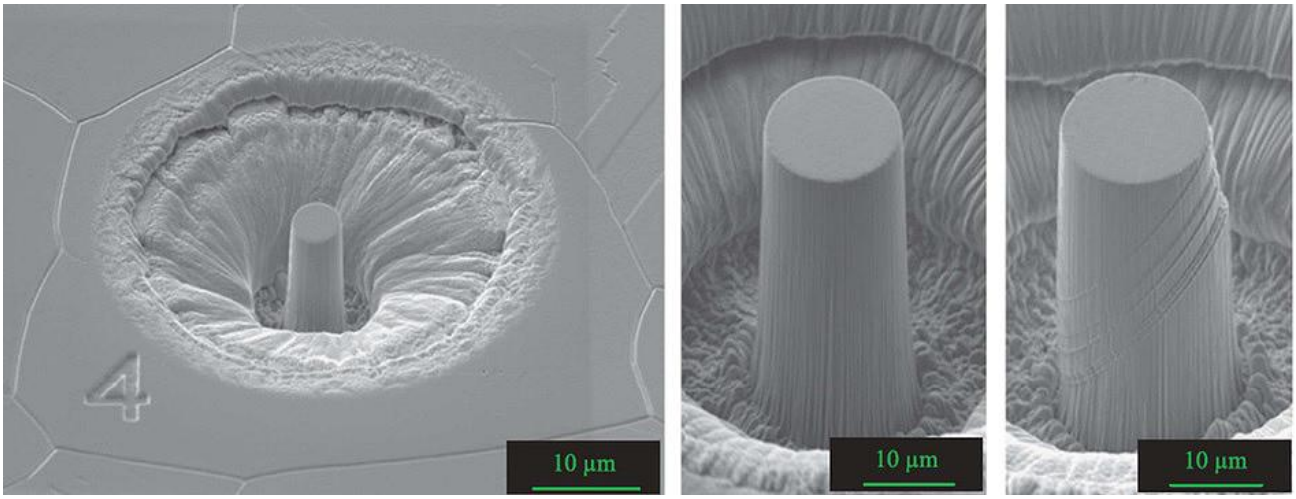


Fig.15-19: Example of a 10µm pillar, cut within a large grain. (left) Pillar shown with respect to the grain boundaries, (middle) Zoomed view, (right) Deformed pillar after compression testing.(Monnet, G. & Pouchon, M. A. (2013), 'Determination of the critical resolved shear stress and the friction stress in austenitic stainless steels by compression of pillars extracted from single grains', Mater. Letters 98, 128-130. As the yield mechanism in fully ductile metals is the same instead of a tension loading a compression loading can be applied in the test.

The method of pillar compression testing provides the investigation of specific areas on the surface of a polycrystalline material, and thereby gives deeper insight into the underlying dislocation mechanisms that eventually contribute to the plastic flow resistance, Fig.15-20. This also enables to determine the CRSS value from the measured $\Delta\tau_{cr}/2$. The deformation markings are visible as slip traces on the surface (*Fig.15-19,* Fig.15-21) of the investigated cylindrical single-crystalline pillars. Presumption for the application of method: *No micro-instability occurs at loading of the pillar.* Since the envisaged material is ductile the compressive test results can be

transferred to the tensile domain. A pillar size effect is physically given. With smaller pillars higher failure values are obtained together with a higher scatter because the number of flaws scatters. Hence, larger pillars experience lower failure values and lower scatter expressed by the coefficient of variation, *Fig.15-21*. This is a flaw volume-linked Weibull effect, even though the number of surface flaws comes in.

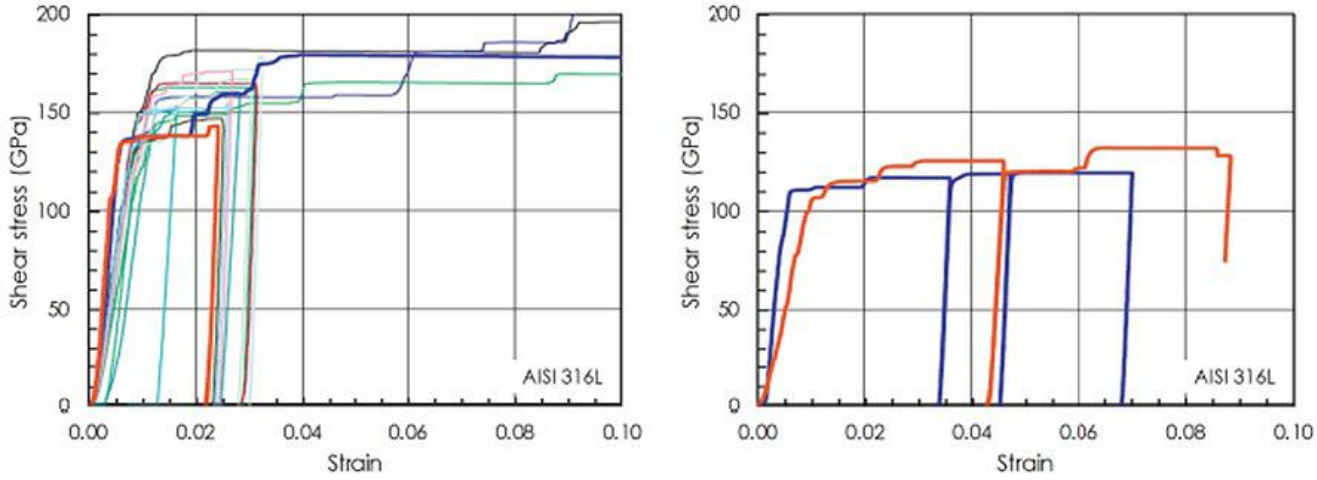


Fig.15-20: Resolved shear stress-shear strain curves of differently sized pillars made of AISI 316L austenitic stainless steel. (left) 5µm pillar, (right) 15µm pillar. [Monnet, G. & Pouchon, M. A. (2013), 'Determination of the critical resolved shear stress and the friction stress in austenitic stainless steels by compression of pillars extracted from single grains', Materials Letters 98, 128-130]

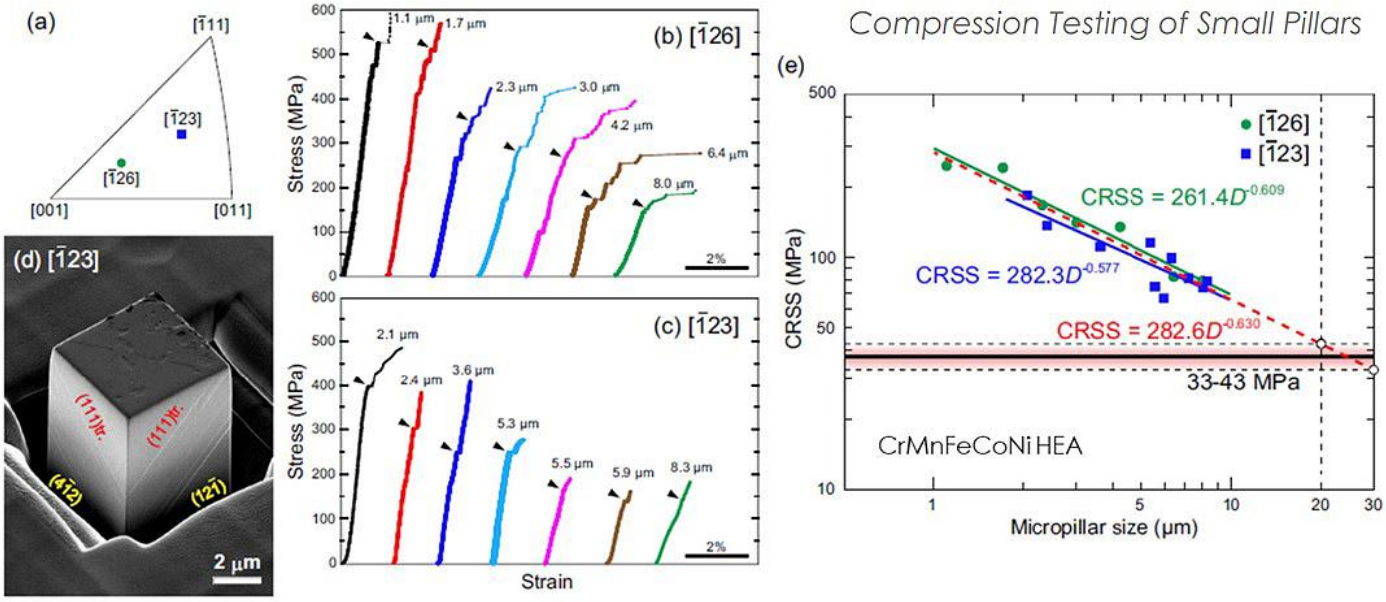


*Fig.15-21: Compressiom tests of single-crystalline micropillars of the equi-atomic CrMnFeCoNiHEA;(b,c) Selected **stress-strain** curves of single-crystalline micropillars with loading axis orientations of (b)* [$\bar{1}$26] *and (c)* [$\bar{1}$23]*; (d) Secondary-electron image taken in a scanning electron microscope showing* [111] *slip traces on the side surfaces of the deformed test specimen*

Understanding strain-hardening of ductile metals [*basically from Wikipedia*]:

Atoms in a metal move at atomic distances along the slip plane to result in producing a step. Each step appears as a line called slip line. Slip does not occur on just one plane but over small regions of parallel planes to result in a number of slip lines, together called slip band. Slip lines are lines of

maximum shear stress following 45° to the stress direction. The slip lines under plastic flow conditions intersect with each other at 90°. In plastic deformation, those dislocations are moved in whose sliding system a certain limit value of the shear stress is reached or exceeded. Where the operated sliding plane intersects the free crystal surface, a sliding track is created. A dislocation movement creates further dislocations, which as obstacles complicate the dislocation movements. As a result, strain-hardening is observed in most metallic materials. As deformation progresses, the crystal lattice twists until the maximum shear stress acts in another sliding system and this takes over the further deformation of the crystal. The stress required for this will generally be higher than in the first active sliding system, which is a further contribution to strain-hardening. Clear slip steps at the angle of 45° are only present in specially oriented single crystals. However, single crystals can only be produced with great technical effort (*turbine blade, silicon chip*). In general, metals do not have a uniform lattice orientation. Many small microscopic grains are found in a metal, each with a different lattice orientation. Such crystals are also referred to as poly-crystals. Thus, in such poly-crystals several slip systems with different slip plane orientation are always simultaneously activated which leads to multiple gliding.

15.6.5 Results addressing Multiscale Materials Modelling MMM, Mlikota model

Multi-scale modelling is executed for static and cyclic problems. In the cyclic case, there are three key 'points' that separate these regions in *Fig.15-22*:

- Ultimate strength ($R_m^{\,t}$): Is the stress level required to fail with one cycle, n = 1
- Onset of Yield stress (Re): Stress at onset of plastic behavior with $R_e < R_{0.2}$
- Endurance limit (Se): Stress corresponding to the horizontal asymptote (*if applicable*).

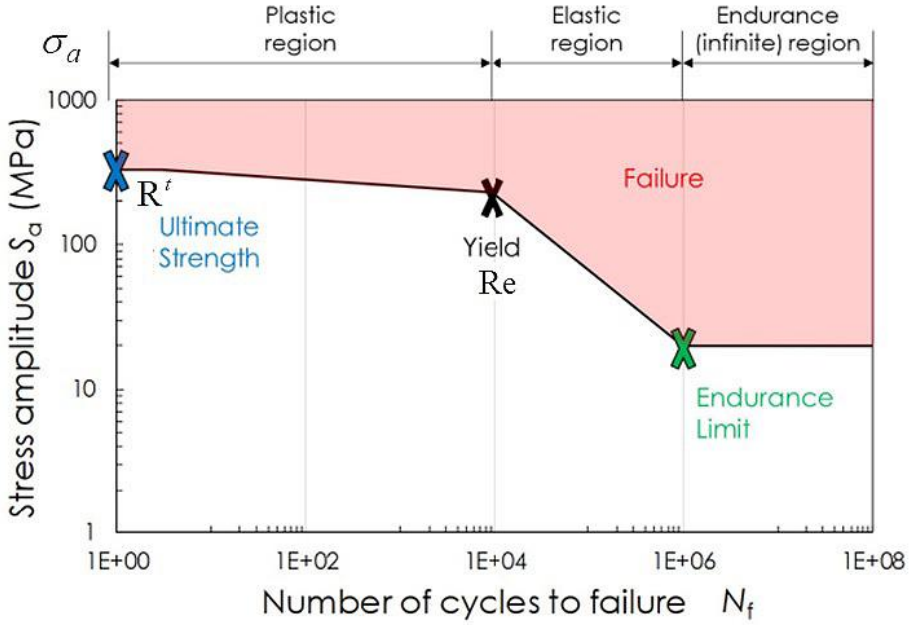


Fig.15-22: Relevance of ultimate strength R^t, yield onset stress Re and endurance limit stress amplitude. [Hiatt, J. (2016), 'What is a SN-Curve?', Technical report, Siemens PLM Community). $N_f = N_{initial} + N_{crackgrowth}$. *Run-out below the endurance limit means crack-retardation]*

Finally *Fig.15-23* displays the full multi-scale modelling approach.

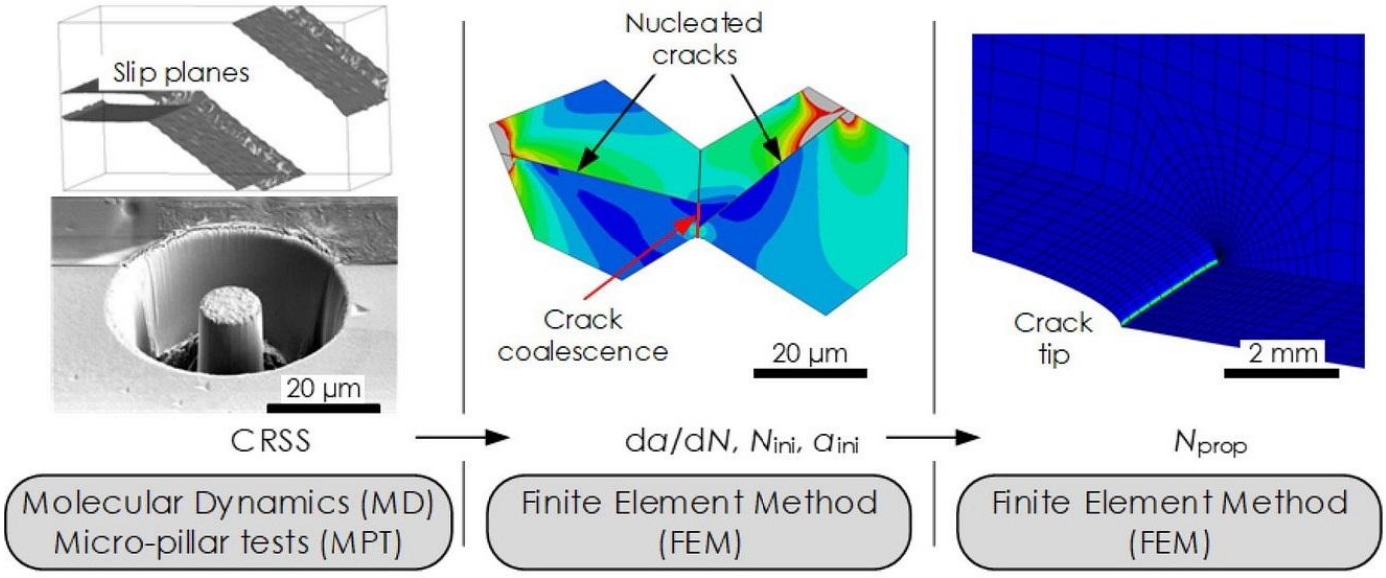


Fig.15-23 Full modelling approach. CRSS critical resolved shear stress, da/dn crack growth rate, N_{in} number of stress cycles until short-crack initiation, a_{ini} initiation short-crack length, N_{pro} number of stress cycles until short-crack propagation. [Mlikota M. & Schmauder S. (2018), 'On the critical resolved shear stress and its importance in the fatigue performance of steels and other metals with different crystallographic structures', Metals 8(11), 883]

Final remarks in [*Mli19*]:

- The fatigue crack growth modeling procedure in the HCF regime should include the following steps: - Micro-crack nucleation within a grain; - Coalescence of already existing micro-cracks and/or arrest at grain boundaries; - Short crack or Stage I growth; - Transition from Stage I to Stage II growth; and - Long crack (Stage II) growth
- The discovered relation between endurance limit and the CRSS provides a facet of fatigue theory that is numerically predictive and which allows the virtual selection of those types of materials, which are more fatigue resistant! The physically-based MMM approach represents a breakthrough in the field of fatigue research. The higher the CRSS magnitude of the metal of interest, the higher the loading stress level needed to accomplish the transition from infinite to finite life
- The multiscale fatigue simulation approach is capable of properly taking into account the mean stress $\sigma_m = max\,\sigma \cdot (1+R)/2$ with the stress concentration factor K_t, which are highly relevant influencing factors when designing structural components.
- Experimental tests demonstrate that there is a drop in resistance to fatigue fracture with the increase of the grain size.

LL:

**A grain is usually polycrystalline with crystal planes in various spatial orientations. Hence, a metallic material can be only termed homogeneous and isotropic if these orientations are randomly distributed in order to become quasi-homogeneous. By the way, this is the same for an isotropic short fiber-reinforced polymeric material. Otherwise, the so-called orientation tensor has to take care of the non-isotropy.*

** Kinking in Fiber Reinforce Plastics may occur analogous to a crystal which decreases its length under compressive stress due to a new slip system that becomes operative if an associated UD limit stress CRSS would be met.*

15.6.6 UD-material example for Multi-scale Material Modelling

Mixture Rules or micro-mechanical formulas, example UD lamina (ply):

Creep investigations and pressure-related effects on the matrix and in consequence on the UD material of composite materials usually require a micro-mechanical input. For the example creeping the non-creeping constituent fiber is to separate from the creeping/relaxing constituent matrix. In order to capture these features the use of 'micro-mechanical mixture rules' in structural engineering is common practice. It requires properties of the constituents and a so-called mixture rule, how these constituent properties are linked, to be able to predict properties of the envisaged ('smeared') material on the macro-scale. A problem thereby is: Not all micro-mechanical properties applied can be measured.

Solution is obtained by setting up the micro-mechanical formulas (mixture rules), and calibrate them via macro-mechanical test results on the lamina macro-level. This represents an inverse parameter identification.
The application of a micro-mechanical formula underlies a constraint: Micro-mechanical properties can be used only together with the formulas they have been determined with, like in *Table 15-4.*

Table 15-4: Non-creeping anisotropic fiber [Schuermann, Puck]. Modelling material macro properties on basis of micro-mechanical constituent properties [VDI 2014, p.29]. V_f *is fiber volume* fraction.
The superscripts ^{f} and ^{m} stand for filament or fiber and matrix.

$$E_{\parallel} = E_{\parallel f} \cdot V_f + E_m \cdot (1 - V_f) \cong E_f \cdot V_f, \quad \text{within regime } 0.3 \le V_f \le 0.65;$$

$$\nu_{\perp\parallel} = \nu_{\perp\parallel f} \cdot V_f + \nu_m \cdot (1 - V_f), \quad G_m = E_m / (2 + 2 \cdot \nu_m).$$

$$E_{\perp} = \frac{E_m}{1 - \nu_m^{\,2}} \cdot \frac{1 + 0.85 \cdot V_f^{\,2}}{(1 - V_f)^{1.25} + V_f \cdot E_m / (E_{\perp f} \cdot (1 - \nu_m^{\,2}))}; \quad G_{\perp\parallel} = \frac{G_m \cdot (1 + 0.4 \cdot V_f^{\,0.5})}{(1 - V_f)^{1.5} + V_f \cdot G_m / G_{\perp\parallel f}}.$$

Above equations may be used for the regime $0.3 \le \nu_f \le 0.65$ if they have been verified by a top-down-bottom-up approach or in other words a two scale simulation on the upper scale which is the lamina in the actual micro-mechanical case. Such an approach links two scales or structural levels and the micro-mechanical model utilized in this approach is to be validated on the upper level. Hence, the non-measurable properties can be clearly computed backward from the macro-mechanical lamina test data employing 5 unknowns and 5 equations. For instance just the constituent properties ν_m and E_m remain to be measured and $E_{\perp f}$ is then to be resolved by inserting the measured $E_{\perp}$. Laser diffractography provides average values of about $\nu_{\perp\parallel f}$ = 0.27 [*Kru9*1

Micro-mechanical formulas are applied in the:
* Elasticity domain: Often helpful tools (see above), an adjustment to the composite is necessary
* Strength domain: Attempted, but not yet successful for engineering (*safety concept is a problem*).

LL*: considering CM and CDM*

- *Above mixture rules can be used in mechanical & civil engineering (i.e. carbon concrete)*
- *For modelling the so-called 2nd-Tg shift effect* (polymer changes its stiffness beyond 200 bar as with the glass transition temperature *Tg) in the WWFE-II micro-mechanical properties were provided but not the associated micro-mechanical mixture rule. The author sorted out a difference by a factor of two for the desired UD-material property, when using his own micro-mechanical formulas (above)as substitute of the not provided ones. Such a discrepancy should be not encountered in a world-wide exercises*
- *Material Properties shall be measurable*
- *Model parameters should be physically explainable*
- *Micro-mechanical modelling only with known formula*.

[Boe08] Boehm R: *Bruchmodebezogene Beschreibung des Degradationsverhaltens textilverstärkter Verbundwerkstoffe*. Dissertation, TU Dresden 2008

[Cun01] Cuntze R: *Assessment of Load- and Strain-controlled States of Stress in 'Hot Spots'.-On the way to an Industrial Approach for Gurson Materials*-. Europ. Conf. on Spacecraft Structures, Materials and Mechanical Testing. CNES, DLR, ESA, ISU; Strasbourg, Dec. 2001.

[Cun03] Cuntze R and Memhard D*: Evaluation of the Tension Rod Test for Ductile Material Behavior*. European Conference on Spacecraft Structures, Materials & Mechanical Testing CNES, DLR; ESA, ISU: Toulouse, 11-13 December, 2002. Conference Proceedings

[Gur77] Gurson A L*: Continuum Theory of Ductile Rupture by Void Nucleation and Growth*. Part 1: Yield Criteria and Flow Rules for Porous Ductile Media. J. Eng. Mater. Technol. 99 (1977), 2-15

[Kop88] Koplik J and Needleman A*: Void Coalescence in Porous Plastic Solids*. Int. J. Solids Structures 24 (1988), 835-853

[Kru91] Krucinska I and Stypka T: *Direct measurement of the axial Poisson's ratio of single carbon fibers*. Composites Science and Technology 41(1991) 1-12

[Nee84] Needleman A and Tvergaard V*: Analysis of Ductile Rupture in Notched Bars*. J. Mech. Physics Solids 32 (1984), 461-490

[Ram43] Ramberg W and Osgood W R : *Description of stress-strain curves by three parameters.* NACA TN No. 902 , July 1943

[Tve81] *Tvergaard V.: Influence of Voids on Shear Band Instabilities under Plane Strain Conditions*. Int. J. Fracture 17 (1981) 389-407

The author recommends the book [Bus06. Busse G, Kröplin B and Wittel F K: Damage and its Evolution in Fiber-Composite Materials: Simulation and Non-Destructive Evaluation. SFB 381, Stuttgart, ISBN 3-930681-90-3]. It is a comprehensive collection of the SFB 381 'Characterization of Damage Evolution in Fiber-Reinforced Composites by Non-Destructive Testing Methods'. The contributions from all engineering disciplines in this book also address civil engineers.

Production of optimal structural components firstly requires an optimum design including all connections / joints and possible materials.
Then the locally best materials are to determine and to sort out - regarding production - to ensure the required optimum component properties considering sustainability.

16 Structural Tests, Material Tests of Isotropic, UD, and Fabric Materials

The next figure displays the development logic of a structural product with respect to test and design. The activities affiliated to the various phases in the product's development are allocated to the engineering fields. This logic or philosophy should be applied to the development of complex, high-tech constructions with high reliability requirements and also of simple products in an appropriate, reduced procedure. From application to application of course, there may be a different number of loops, and a phase may be dropped on the basis of previous results.

Fig.16-1 shows the famous "test strategy pyramid" with its stepwise growth of the test specimens. It was originally presented in the MIL-Handbook 17 (*Fig.16-2)* and gives a first good survey and hints - not only for aerospace engineers and composite parts designers - regarding structural and material testing.

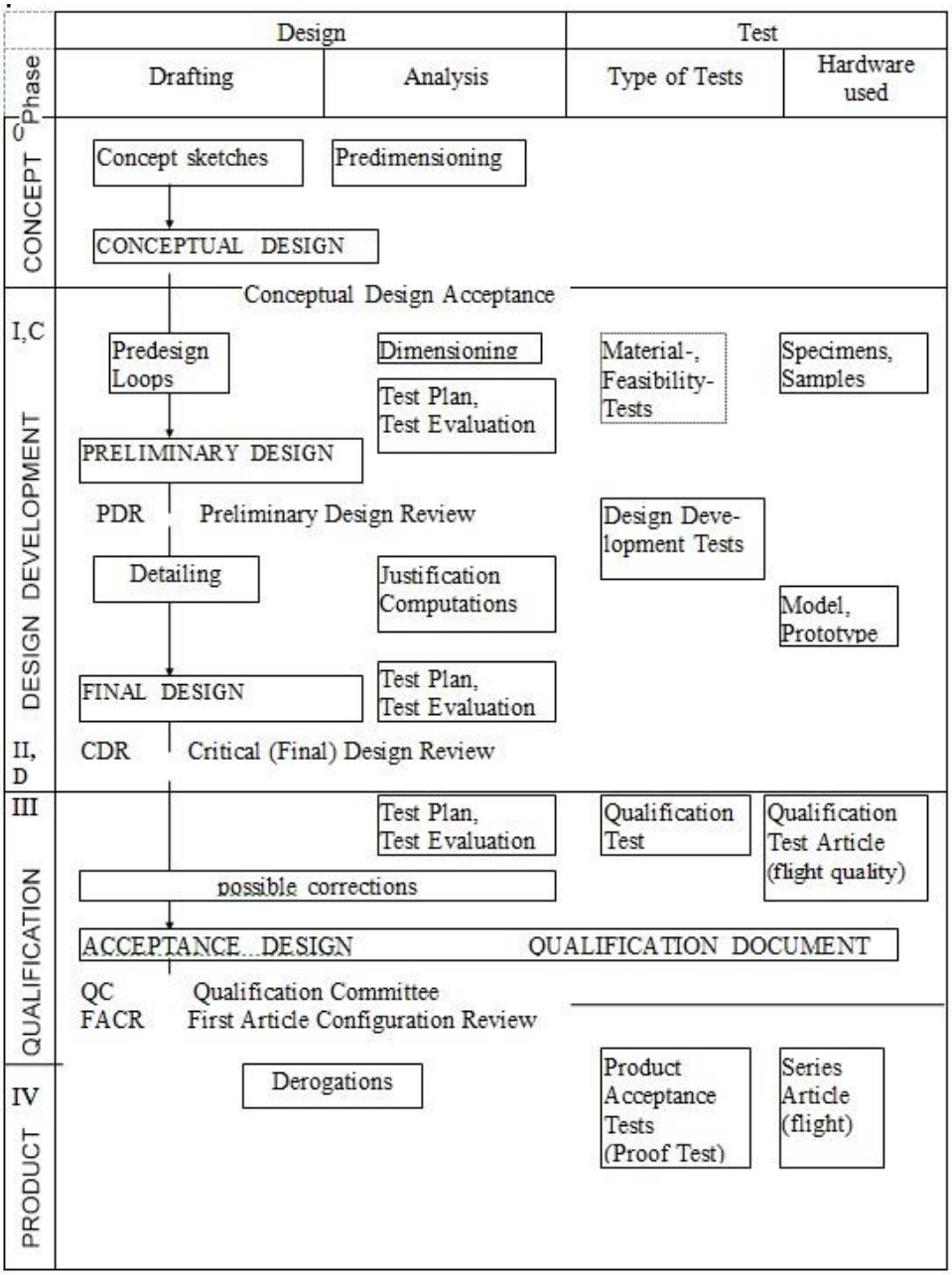


Fig.16-1: Development Procedure and Phase Activities (example flight hardware)

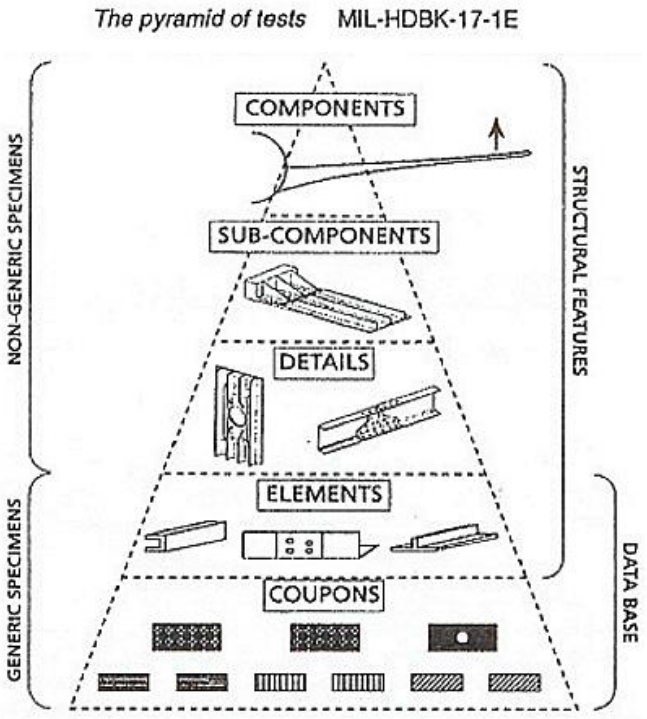


Fig16-.2: Test strategy of MIL-HDBK 17 (original edition about 1970). MIL-HDBK-17/1F (VOL. 1 OF 5), DEPARTMENT OF DEFENSE HANDBOOK: COMPOSITE MATERIALS HANDBOOK - POLYMER MATRIX COMPOSITES GUIDELINES FOR CHARACTERIZATION

The design-development tests are the first of three kinds of tests conducted in a typical hardware development program. Qualification tests are conducted to demonstrate that structural design requirements have been achieved. Acceptance tests verify that the materials, manufacturing processes, and workmanship used to produce the flight hardware have met the design specifications. With the satisfactory completion of these tests, the flight hardware is considered to be structurally and operationally adequate for flight /NASA/.

Detailed theory and test activities are undertaken to obtain at the end of the development process the certification of the product by an aerospace authority. To achieve this, the product developer has to provide a complete set of a so-called Qualification Document which consists of the Qualification-Test report and the theoretical Design Verification report. In the Q-Doc the product has to be shown to be qualified "*in order to verify capability and compliance with the design requirements of the product's Technical Specification to ensure certification*".

In structural design one basically faces 3 types of testing**:**

- Structural Testing (destructive, non-destructive)
- Materials Testing (destructive, non-destructive)
- Non-Destructive Testing of structure and material (NDT, NDI, NDE).
  Other tasks here are: Failure detection, localization, size + shape, Failure assessment (risk-based).

All tests to be performed aim to uncover a deficiency: Workmanship, design mistake, oversight of a failure mode, tightness, shock resistance etc.

If a structure is not redundant, a fail safe design not applicable, then the performance of a static qualification test avoids the otherwise necessary application of higher FoS with its mass penalty. Before the delivery of a structure and before qualification testing a proof test is executed as an acceptance test checking the quality of workmanship and the fulfilment of some functional requirements. Generally, analytical proof, only, is not permitted.

Of interest for testing is the different failure behavior of the various materials: From ductile shear failure with final rupture to cleavage fracture failure in the case of brittle metals and to time-dependent viscoelastic-viscoplastic creep failure. The loadings may be static, cyclic and dynamic (impact) and are all influenced by the environment. Under above loadings a generated crack may remain stable or become unstable.

Avula stated in 1987 "Experimental observations and measurements are generally accepted to constitute the backbone of physical sciences and engineering because of the physical insight they offer to the scientist for formulating the theory. Concepts, which are developed from observation, are used as guides for the design of new experiments, which in turn are used for validation of the theory. Thus, experiments and theory have a hand-in-hand relationship".

Hence we should keep in mind:

- **Test results can be far away from the reality like an inaccurate theoretical model.**
- **Theory creates a model of the reality, one experiment shows one realization of the reality.**

16.1 Structural Testing

For a large structure as a launcher, the Analytical Work (detailed finite element modelling etc.) can be too large to be easy to use, to such an extent that the application of the sub-structuring technique is necessary. For instance, it is not (in future regarding CPU power: it was not) possible to perform a detailed calculation at the level of the total launcher. In addition, various contractors design specific sections of the launcher and provide finite element substructures for the complete mathematical model. This model is dedicated to a dynamic analysis. For these reasons, a large structure like a launcher is split (sectioned) into sub structures and all the analyses are carried out at the level of these sub-structures. *Fig.16.1-1* visualizes how the launcher ARIANE 5 has been sub-structured and how the loadings are applied for a structure like the front skirt at the interface between the main cryogenic tank and the upper stage.

In such a large cooperation project the Test Work is to distribute, too. The test task is to split into several parts for the international project partners and therefore to define interface conditions. In this context often experienced is, that a too high interface stiffness has been fixed. From the author's painful experience: Unfortunately, due to the rigid mechanically-unsound splitting rule, even in cases where the adjacent structure was with the same partner, the partner-known interface stiffness could be not applied.

Modern fast FEA codes allow taking into account realistic boundary conditions by including the finite element models of the adjacent structures. Of course it increases the size of the computational model. In fact, the way to include the adjacent structure is always a compromise between the size of the adjacent finite element models and the will to simulate some realistic boundary conditions in

stiffness

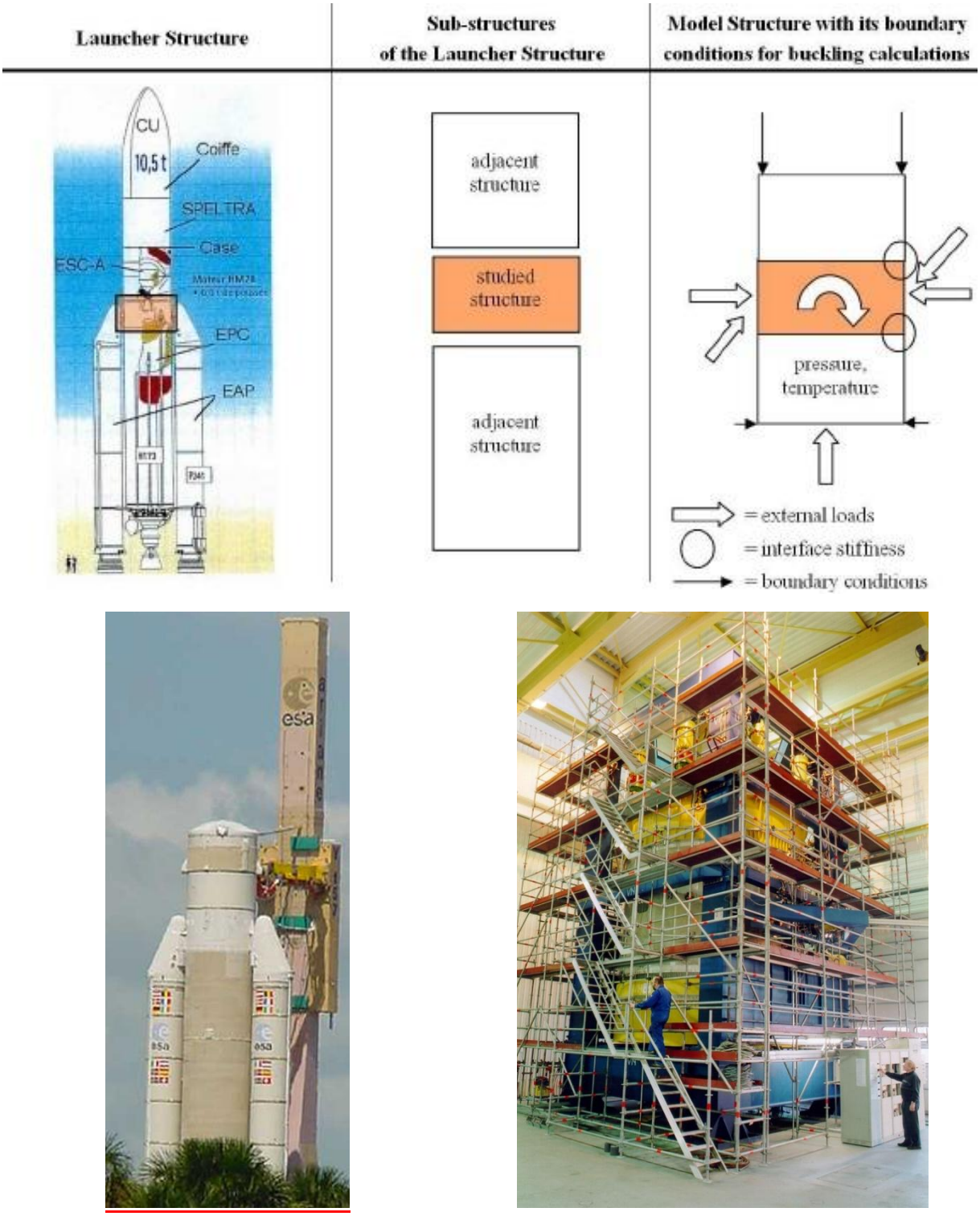


Fig.16.1-1: (top) Sub-structuring of the Ariane 5 launcher; (down) assembly of Ariane 517, Front Skirt test

The measurement of the test article is always accompanied by analyzing the test article by an analytical model. On this basis the evaluation of the test results may cause a re-analysis to better simulate the test results and to finally improve the Design Verification.

Another not desired result of this splitting of a large structure is: The first buckling mode can appear on an adjacent structure and not on the studied one. In this case the designer can locally

modify the structural stiffness of the adjacent parts in order to make the buckling mode appear first in the studied structure. In any case, the load path should not be changed by these modifications. This kind of process is based on much engineering experience. To improve the precision of the results in the critical areas where buckling is supposed to appear, some detailed models can be directly introduced into the global model. For the linear buckling analysis, the nominal thickness should be used to ensure the correct elastic behavior of the structure. For the nonlinear collapse analysis, the minimal thickness is used to take thickness variations as imperfections into account.

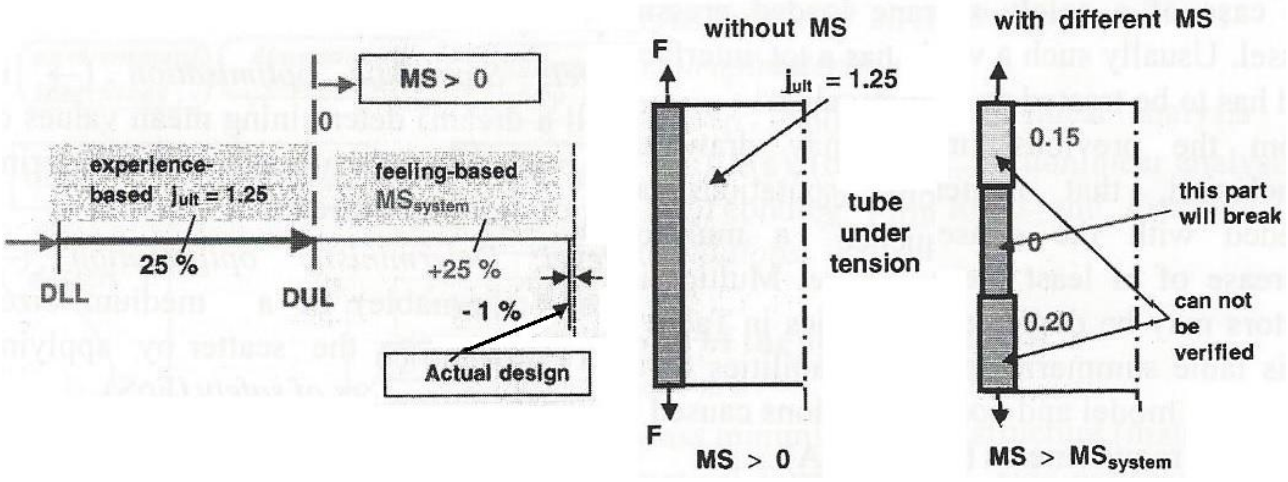


Fig.16.1-2 Non-testability effect when using different System Margins [Cun00], MS = MoS

In some spacecraft projects on top of the FoS so-called system-margins (*MoSsys* ≠ *MoS*= *RF* -1) are required to be met in the structural tests. The left part figure of *Fig.16.1-2* depicts one example in which on a distinct structural component composed of several sub-structures, according to an associated uncertainty 'feeling', an additional margin of MoS_{sys} = 25% is put on top. Unfortunately, for adjacent sub-structures the required values had been different. This leads to non-testability of sub-components as the right part figure for the simple example tube proves. Why does one apply a 'feeling-based' *MoSsys* on top of the *FoS j*, however then feel threatened by a *MoS* = - 1% (being theoretically 25% -1% = +24%)? This should not cause a redesign.

LL:

(1) We know: Only well-understood experiments can verify the design assumptions made!

(2) Mandatory for a realistic qualification of a sub-structure is a realistic set of cross-section loadings and pressure loading with an accurate structural designing of the interface stiffness of the adjacent structural parts. If the interface is too stiff in the test assembly this will attract loading and lead to a non- realistic failure site (experience from Ariane 5 tests)

(3) Put strain gauges there where a clear stress situation is in order to avoid useless discussions about the interpretation. Check locally by strain measurements and then rely globally on FEA-test result comparison

(4) Using different MoS_{sys} (nonsense in aTechnical Specification), then not all critical locations can be tested without overloading other integrated parts. Components of such a structural assembly cannot be verified by a qualification test, because so-called system margins cannot be used locally like a 'fitting factor'. They should have been considered directly in the Ariane 5 as a usual design FoS, applying $j_S = (MS_{sys} +1)\cdot j$. Otherwise, the design process is obscured and is prevented from applying the most economic measure in order to take risk out of the structure.

(5) So-called test correction factors are applied to adjust the design verifications by accurately evaluated structural test results.

Eventually, *Table 16.1-1*, gives a survey on the structural tests considering purpose, load level and the kind of hardware used. This scheme can be transformed into other technical disciplines.

Table 16.1-1: Structural Tests during Development of engineering an airplane

Tests	Load levels	Purpose	Type of hardware used
Design-development	Variable, often to destruction.	To determine ultimate strength and design feasibility	decided by engineering.
Qualification	To design to DUL (not necessarily to failure)	To verify structural adequacy.	flight quality.
Acceptance	Usually not exceeding flight-limit loads (except for pressure-proof tests)	To ensure hardware meets specifications.	flight

In the design of components and systems as well as for the development of suitable structural materials, the evaluation and avoidance of fracture and micro-damage processes play the essential role in order to ensure technical safety, service life and CoSt-effectiveness.
For a specific structural test evaluation a qualification pressure tank is taken. It will be evaluated deterministically and probabilistically in order to get a feeling about the evaluation goodness.

Test Data Evaluation of a Qualification Pressure Tank (deterministic and probabilistic)

1 Task Internal pressure vessel of a motor housing; Qualification test series (old examples)

- Design requirements:
  Action *S*: MaximumExpectedOperatingPressure MEOP ≡ DesignLimitLoad DLL, DUL = $j_{ult} \cdot$ DLL

  Given : μ_S = 17.0 MPa (N/mm^2), σ_S = 1.70 N/mm^2

  Resistance *R*:

  Given : μ_R = 17.0 N/mm^2, σ_R = 1.70 N/mm^2
- Safety Concept:

  UT = UpperTolerance limit = $\mu_S + 2.3 \cdot \sigma_S$ and LT = LowerTolerance limit = $\mu_R - 2.3\ \sigma_R$

  Deterministic: j_{ult} = 1.5, proof test j_{proof} = 1.3 , extra a $MoS_{nominal}$ = 0.2

  Probabilistic: Reliability value = survival probability $\Re = 0.99999$ or failure probability $p_f = 1 - \Re$
- Searched for achievement of test design verification by meeting in the:
  Deterministic evaluation: $MoS_{nom} > 0.2$, Probabilistic evaluation: $\Re > 0.99999$.

2 Test Data

The qualification tests lead to the following results for mean, standard deviation and density distribution: μ_R = 33.7 N/mm^2, σ_R = 3.3 N/mm^2, Normal Distribution.

3 Statistical Evaluation of the Test Results

The test verification was carried out for above main design parameter, the internal pressure p_{int}. The distribution of its action $f_S(x)$ is the density distribution of the maximum motor pressures measured in operation and the distribution of the resistance, the load capacity $f_R(x)$, is the density distribution of all burst pressures measured in the qualification series.

The probabilistic calculation can be carried out in this simple case with the help of the Gaussian integrals employing the Hasofer-Lind Z-transformation:

$\mu_Z = \mu_R - \mu_S = 16.7$ N/mm^2, $\sigma_Z = (\sigma_R^2 + \sigma_S^2)^{0.5} = 3.48$ N/mm^2,

$\beta = \mu_Z / \sigma_Z = 4.8.$ → from a statistical handbook $\Phi(\beta) = 0.99999922 = \Re = 1 - p_f > 0.99999$

or $p_f = 7.8 \cdot 10^{-7} < 1 \cdot 10^{-5}$.

Margins for nominal safety are obtained from

$UT_S = 17.0 + 2.3 \cdot 1.70 = 20.9$ N/mm^2, $LT_R = 33.7 - 2.3 \cdot 3.03 = 26.7$ N/mm^2

$MoS_{nom} = LT_R / UT_S - 1 = 0.27 > 0.2$ and for information $MoS_{central} = \mu_R / \mu_S - 1 = 0.98$.

4 Assessment of Reliability $\Re$ ('safety')

The distance from the required level of reliability is sufficiently, > one potency. The nominal safety margin is very small. The result shows that with a probabilistic evaluation a more realistic evaluation is possible. Of course, due to the limited amount of information, the reliability parameters $\Re$ and β can generally only be regarded as operational and not absolute variables.

As a result of the usual performance of acceptance tests the resistance distribution at MEOP·j_{proof}, can be truncated. This realistic consequence of an acceptance test cannot be quantified deterministically but probabilistically!

Note: Test verification is basically performed on the primary action level design parameter force, moment or pressure. In the case of loading-combinations the determination of a *MoS* on the load level becomes difficult because just one loading can be increased up to fracture or another limit. Then, the relationship analysis-test is forced to act: A numerical model must break the test results down to stress level and enables to calculate a *MoS* for the stress state under the loading-combination.

***LL**:*
Behavior of designed structure: The best prediction of the typical behavior of the structure is performed with typical values = average values, such as the average strength $\bar{R}$.
Design verification: Dependent on the requirements the average, the upper or a lower value of the property is used for the various properties. In the case of strength a statistically reduced value R. To achieve a reliable design the so-called Design Allowable has to be applied. It is a value, beyond which at least 99% ("A" value) or 90% ("B" value) of the population of values is expected to fall, with a 95% confidence (on test data achievement) level, see MIL-Hdbk 17. The B-value can be used for the multi-layered, redundant laminates.

16.2 General on Material Testing and some Material Testing Methods

16.2.1 Introductory Remarks considering Material Testing

- Measurement data is the result of a Test Agreement (norm or standard), that serve the desire to make a comparability of different test procedure results possible
- The Test Agreement consists of test rig, test specification, test specimen and test data evaluation method and the Test Procedure. Therefore, one can only speak about 'exact test results in the frame of the obtained test quality'
- Hence, there are no exact property values. Generally, properties are the result of the material model applied. Material properties inclusively mapping process
- Further, stresses, strength, strains, elasticity properties cannot be directly measured
- Check of assumptions is necessary before designing *(example: WWFE on UD-material).* Pore-free material, specimen surfaces polished, well sealed, fiber volume is constant, tube specimens show no warping and do not bulge, perfect bonding, no layer waviness, edge effects do not exist, etc .
- Sometimes one must live with a substitute test situation in order to get some approximate properties (Example, later: a Tension/Compression-Torsion test device was issing then an Arcan test device was taken)

- Before thinking about test data evaluation the associated underlying micro-damage processes must be sorted out in order to get a better understanding of failure
- Comparisons between theoretical predictions and test data help to identify the major discrepancies, limitations, and areas which require further theoretical and experimental work. There is always a lot to be done, and, following Moslik Saadi ***"All is difficult prior to becoming simple"!*** This begins with the provision of appropriate test specimens for the various material families being extreme ductile or brittle and ends with appropriate test procedures and an appropriate test data evaluation
- Test specimens shall be manufactured like the structure ('as-built')
- Considering FE-results: We must more and more 3D-design! However the situation of properties, especially for composites is: „3D-property data test sets are seldom sufficiently available".

Table 16.2-1 presents a survey for which mechanical fields properties have to be provided.

Table 16.2-1: Survey on the various mechanical fields where properties must be determined

Initial Situation	**crack-free not flawless**	**crack-free not flawless**	**notched**	**cracked, delaminated**
Theory	Classical continuum Mechanics CM	Continuum Damage Mechanics CDM	Notch Fracture Mechanics	Fracture Mechanics FM
Static situation	strength failure conditions SFC	damage mechanics failure conditions	'Neuber-like' failure conditions	fracture mechanics failure conditions
	stresses, equivalent stresses	effective stresses	stress concentrations	Stress intensity factors (intensities)

Experience forces to add: The use of novel materials - partly requires - the development of novel test methods, test set-up and of test specimens. This then causes the development of novel evaluation procedures. The field of fracture mechanics to assess macro-damage like cracks and delaminations by damage tolerance tools is one domain.

The properties to be known in design were still depicted in the *Tables 1-2a* through *1-2c* but shall be united in one table, Table 16.2-2.

The shadowed boxes in the tables indicate how many mutually independent - termed here 'basic' - properties a material possesses due to its material symmetry conditions. The input on a *material* card should not require more basic properties unless a specific *material model* needs further ones, e.g. in strength conditions for brittle behaving materials so-called internal friction coefficients μ of the distinct material are physically necessary to design dimension in compression.

The given elasticity values belong to the elastic domain.

If the analysis takes place in the in-elastic domain reduced values have to be respected, and the designer has to discriminate the tensile $E = E^t$ from the compressive E^c.

Table 16.2-2: Summary table of properties

9	**general orthotropic**	R_1^t	R_2^t	R_3^t	R_1^c	R_2^c	R_3^c	R_{12}	R_{23}	R_{13}
5	**UD, ≅ non-crimp fabrics**	$R_{\|}^t$ NF	$R_{\perp}^t$ NF	$R_{\perp}^t$ NF	$R_{\|}^c$ SF	$R_{\perp}^c$ SF	$R_{\perp}^c$ SF	$R_{\|\perp}$ SF	$R_{\perp\perp}$ NF	$R_{\|\perp}$ SF
6	**fabrics**	R_W^t	R_F^t	R_3^t	R_W^c	R_F^c	R_3^c	R_{WF}	R_{F3}	R_{W3}
9	**fabrics general**	R_W^t	R_F^t	R_3^t	R_W^c	R_F^c	R_3^c	R_{WF}	R_{F3}	R_{W3}
5	**mat**	R_{1M}^t	R_{1M}^t	R_{3M}^t	R_M^c	R_{1M}^c	R_{3M}^c	R_M^τ	R_M^τ	R_M^τ
2	*ductile* **isotropic** *brittle*	R_m SF	R_m SF	R_m SF	*deformation-limited*			R_m^τ	R_m^τ	R_m^τ
		R_m NF	R_m NF	R_m NF	R_m^c SF	R_m^c SF	R_m^c SF	R_m^σ NF	R_m^σ NF	R_m^σ NF

9	*general. orthotr.*	E_1	E_2	E_3	G_{12}	G_{23}	G_{13}	ν_{12}	ν_{23}	ν_{13}	**comments**
5	***UD, ≅ non-crimp fabrics***	$E_{\|}$	$E_{\perp}$	$E_{\perp}$	$G_{\|\perp}$	$G_{\perp\perp}$	$G_{\|\perp}$	$\nu_{\|\perp}$	$\nu_{\perp\perp}$	$\nu_{\|\perp}$	$G_{\perp\perp} = E_\perp/(2+2\nu_{\perp\perp})$ $\nu_{\perp|} = \nu_{|\perp} E_\perp / E_| $ *is perpendicular to quasi-isotropic 2-3-plane*
6	*fabrics*	E_W	E_F	E_3	G_{WF}	G_{W3}	G_{W3}	ν_{WF}	ν_{W3}	ν_{W3}	*Warp = Fill*
9	*fabrics general*	E_W	E_F	E_3	G_{WF}	G_{W3}	G_{F3}	ν_{WF}	ν_{F3}	ν_{W3}	*Warp ≠ Fill*
5	*mat*	E_M	E_M	E_3	G_M	G_{M3}	G_{M3}	ν_M	ν_{M3}	ν_{M3}	$G_M = E_M/(2+2\nu_M)$ *1 is perpendicular to quasi-isotropic mat plane*
2	*isotropic*	E	E	E	G	G	G	ν	ν	ν	$G=E/(2+2\nu)$

9	general orthotropic	α_{T1}	α_{T2}	α_{T3}	α_{M1}	α_{M2}	α_{M3}
5	UD ≅ non-crimp fabrics	$\alpha_{T\|}$	$\alpha_{T\perp}$	$\alpha_{T\perp}$	$\alpha_{M\|}$	$\alpha_{M\perp}$	$\alpha_{M\perp}$
6	fabrics	α_{TW}	α_{TW}	α_{T3}	α_{MW}	α_{MW}	α_{M3}
9	fabrics general	α_W	α_F	α_F	α_{MW}	α_{MF}	α_{M3}
5	mat	α_{TM}	α_{TM}	α_{TM3}	α_{MM}	α_{MM}	α_{MM3}
2	isotropic for comparison	α_T	α_T	α_T	α_M	α_M	α_M

Table of structural properties

Strength properties: *NF:= Normal Fracture, SF:= Shear Fracture, R:= strength, σ,τ := indicate the fracture responsible normal or shear stress acting on the fracture 'plane'.*

Hygro-thermal properties*: T:= Thermal, M:= Moisture and Mat. λ , c : not listed.*

Elasticity properties: *E:=Young's modulus, v:=Poisson's ratio, G:=shear modulus. ||:= parallel to the fiber, ⊥ := transversal to the fiber direction; W:= Weft, F:= Fill, M:= Mat . $\nu_{\|\perp}$:= (here!) larger Poisson's ratio. 1:= lamina fiber direction, 2:= lamina transverse fiber direction across the width or the plane, 3:= through-thickness direction; x ,y := principal in-plane laminate directions, z:= thickness direction (interlaminar)*

In the further text it will be clearly stated whether an average (*also termed typical or characteristic)* value for modelling of the material (*mapping of test data*) or a statistically-based value for design verification is addressed. This means for instance for strength: $\overline{R}$ is the average value (*in statistics a bar over the R denotes the mean value of the n specimen results of a test sample, and this bar is taken over to indicate the average value, too*) and *R* as the usual designation of a so-called strength design allowable. Of course, if the property is generally addressed then no bar is utilized as well.

Specific design aspects of the utilized materials that affect testing methods:

Isotropic metallic lightweight materials usually applied in aerospace are behaving ductile. They exhibit no much sensitivity to stress concentration but to fatigue. The residual stresses caused by manufacturing are to be considered.

-Very ductile materials require the use of true stress-true strain curves. This is of highest interest for 'metal forming engineers' and for the structural designer of interest if a final structural design can be saved by demonstrating an additional load capacity reserve.

Transversely-isotropic composite materials are built up from laminas (ply, layer), which are either flat tapes, or layers of woven fabrics. The stack of the laminas at various angles determines the stiffness properties of the laminate wall.

Therefore, an accurate application of UD properties needs some comments:

- The effect of micro-crack growth alters not just elasticity properties but CTE and CME as well. The 'virgin' values change with micro-damage. It further influences the residual stresses from curing in isolated laminas (micro-mechanical stresses of 2nd kind or on filament-matrix level) and in embedded laminas of a laminate.
- It is generally assumed that the effect of the *micro*-mechanical residual stresses from curing on the strength is the same in the lamina material test specimen as in the (embedded) lamina of the real structural laminate wall. Therefore, it is regarded to be incorporated in the *macro*-mechanical material test data applied.
- The CTE and CME serve to determine *macro*-mechanical stresses and macro-hygrothermal-mechanical residual stresses (of 1st kind) in the laminate.
- The behavior of an embedded lamina is different (due to redundancy within the stack) to that of an isolated (non-embedded = non redundant)) lamina where one gets the property data from UD test specimen. This most often benign difference is usually not considered.

Building block of the laminate is the lamina which is relatively brittle in case of usually applied fiber reinforced plastics (FRP). Nevertheless, the laminate may behave quasi-ductile according to the redundancy built in by the stacking sequence. In contrast, layered materials such as GLARE, which is applied in the Airbus 380 are behaving ductile and are modelled and designed as a ductile metal with hybrid properties. UD-composed laminates exhibit high sensitivity to stress concentration but low sensitivity to fatigue.

Orthotropic fabrics: Future load-carrying structural components will be built from woven fabrics, too. Such laminas consisting of FRP or FRC behave brittle due to the fiber crossing effect. They experience still at low stresses inter fiber failure (IFF) and thereby degradation. This is to be considered in stability analysis w.r.t. stiffness reduction. Fabrics exhibit high sensitivity to stress concentration but low to medium sensitivity to fatigue which depends on the material chosen.

Strengths are normally Weibull-distributed (WD) or LogN-distributed (logND), the physical properties are modelled as Normal-distributed (ND; Gauss).

If data from different test series exist it has to be checked by the statistical acceptance rules whether they might be combined in one lot (see e.g. HSB, chapter 10000).

Material test specimens are of the types flat coupons, round bars, tubes, cruciforms et al.

16.2.2 Note on the Determination of Material Model Parameters

- Material Model (constitutive equation): establishes a relation between thermo-mechanical actions (heat, stresses) and deformation measures (strains). Examples: non-linear Ramberg-Osgood power law or a bi-linear approximation of the σ-ε curve or cohesive stress with critical separation in the cohesive model
- Material Behavior: behavior which may be elastic, visco-elastic, inelastic brittle and inelastic ductile, hygro-thermal, strain-rate and time-dependent (creep, relaxation), isotropic or anisotropic
- Material Properties: material intrinsic (inherent, seldom a constant) quantities, being not dependent on geometry, stress state, constraints. A material parameter shall depend on the material only and possibly on additional variables like temperature, moisture, strain rate etc., but not on a particular stress state in a test specimen in order to facilitate the transfer from the material to the structural component
- Material Model Parameters c: e.g. parameters in a failure function like $F = c_1 \cdot J_2 + c_2 \cdot I_1 = 1$ or in the Ramberg-Osgood stress-strain mapping equation. They should be a function of measurable properties, only. ***This is the case in the author's FMC-based strength criteria***!
- Measurement and Modelling level: Properties of structural materials are determined on macro-scopic level and seldom on micro-scopic level. Modelling may be also performed on a so-called meso-level (*artificially chosen, in structural design between micro and macro length scale*).

Material properties are always defined in the context of a certain material model: Young's modulus E and Poisson's ratio *v* are defined on the background of a generalized 'Hooke's law' for isotropic, linear elastic materials. Yield strength implies 'von Mises plasticity', the creep exponent 'Norton's law', and finally fracture toughness implies 'Irwin's stress intensity factor' approach. In the case of more sophisticated material models like 'Gurson-Tvergaar-Needleman model' for non-linear, high-straining metals the applied parameters must be obtained numerically by an inverse identification process using hybrid methods. Test together with a numerical model commonly takes over the task to deliver model parameter values. Such hybrid methods bridge between experimental and numerical methods for material characterization.

There are always questions on the uniqueness of a material parameter set obtained from tests, on the sensitivity of the mechanical response to variations of these parameters and on the design of adequate tests capable of identifying certain model parameters.

In material testing, Uniaxial tests serve for the delivery of properties and Multi-axial tests for the validation of strength criteria required to assess multi-axial stress states. Here, it is the aim to look in detail at the evaluation of ductile test results.

It is not the aim here to present Standard Tests, just specific ones will be depicted, especially, the measurement and evaluation of strengths *R* and the associated friction value μ.

Table 16.2-1 comprises how the preliminary strength design values for the pre-dimensioning and its associated very preliminary design verification are generated, and finally the strength design allowables for the final verification, the A- and B-values. The various values applied are defined as follows:

- ***S-value:*** *Procurement value.*
- ***A-, B-value****: Strength Design Allowables= statistically defined according to MIL-Hdbk 5. Number of different batches is required.*
- ***T99/T90-value****: Material strength values. The determination follows the same statistical procedure as with the Strength Design Allowables. However, the data volume and batch requirements are less stringent. A > S, only allowed if premium selection of material is applied. Normally A > S,* ***A*** *≤ T99/T90-value to remain on the safe side.*

Table 16.2-1: Establishment of pre-dimensioning values and of strength design allowables (after HSB).

Material Supplier	**Customer**			
Manufacture 1 raw data, T99 / T90 data **Manufacture 2** raw data, T99 / T90 data **Manufacture n** raw data, T99 / T90 data	**in-house tests** raw data, T99 / T90 data	Pooling of T data, S-value adjustment: **Material Procurement** **Fixation of** ***Strength Design Values***	full data set applicable: **Determination of *Strength Design Allowables*** *(A-, B-values)* based on statistical rules in MMPDS Hdbk (formerly MIL Hdbk 5)	**approval** of design allowables by handbook committee , agency etc.
		for **design + analysis** ***pre-dimensioning***	for **final** **design verification**	

In the context of the table above an example for the determination of a Lower Resistance Tolerance limit LT_R shall be given for different pre-knowledge levels. The numbers clearly depict how pre-knowledge supports the goodness.

- Under consideration of the confidence interval in the case of a middle-size sample of ($15 < n < 40$):

  $\mu_R \Leftarrow \bar{x} - t_{1-\alpha}\, s / n^{0,5}$ (s.a. § 14); $\bar{x}$ = 99.6 MPa; s = 9.8 MPa

  $\sigma_R \Leftarrow \chi_0 \cdot s = 1.27 \cdot 9.8 = 12.4$ MPa

  with $t_{1-\alpha} = 1.699$ for f = n - 1 = 30 - 1 = 29 ; $1 - \alpha = 95$ % (one-sided)

  and c0 = 1.27 for n = 30 ; $u_P = 2.326$ (P = 99 %)

  from [*Graf, Henning, Stange*]

  $LT_R = \bar{x} \,.\, [1 - (t_{1-\alpha} / n^{0,5} + u_P \cdot \chi_0) \cdot s / \bar{x}\,]$

  $= 99.6 \cdot [1 - (1.699/\sqrt{30} + 2.326 \cdot 1.7) \cdot 9.8 / 99.6] = 99.6 \cdot [1 - 0.32] = \underline{67.6}$ MPa .

- Under consideration of the confidence interval in the case of a small sample size of ($6 \leq n$) however

  with an always desirable knowledge about pre-information of the basic population

  f : = ND; cov = 9 % (pre-information from significance tests, from similar tests)

LT_R = "A"- value (p = 99 %; confidence 1 - α = 95 %, one-sided)

= $\bar{x}$. (1 - $u_P \cdot cov$) / (1 + $u_c \cdot cov / n^{0,5}$)

= 99.6·(1 – 2.326 · 0.09) / (1 + 1.29 · 0.09/$\sqrt{30}$)

= 99.6·(1 – 0.209) / 1.02 = <u>77.2</u> MPa

with u_P = 2.326 (F-integral table, § 14); u_c = 1.29 .

- Without taking into account confidence intervals. In the case of experimental re-calculations with current data and probabilistic calculations, it is the best "estimation" type:

μ_R $\Leftarrow$ $\bar{x}$ = 99.6 MPa, σ_R $\Leftarrow$ s = 9.8 MPa (s/$\bar{x}$ = 9.9 %), meaning $n \to \infty$

LT_R = μ_R – 2.326 ·σ = <u>76.8</u> MPa .

16.2.3 Engineering and True Stresses and Strains of Ductile Isotropic Metals

Two measures are to use to describe the behavior of the solid: These are the percent elongation and the percent area reduction under a force *F*, defined as $(\ell - \ell_0) / \ell_0$, $(A_0 - A) / A_0$. Presuming constant volume (full yielding) and uniform elongation it is valid $\ell / \ell_0 \equiv A_0 / A$. Hence, after end of uniform elongation or 'onset-of-diffuse necking' no relationship exists anymore between the two formulations. The elongation in the minimum neck cross-section becomes too small for an axial measurement, since the length of the gage section accounts now. To measure an axial strain requires another measurement technique. This is possible if moving from $(\ell - \ell_0) / \ell_0$ to the measurement of the plastic strain defined by diameter reduction $(A_0 - A) / A_0$. This means, once necking starts to use, to replace $\varepsilon_{ax}^{true} = \ell n(1 + eng\varepsilon_{ax}) = \ell n(\ell / \ell_0)$ by $\varepsilon_{ax}^{true} = 2\ell n(A_0 / A)$.

In contrary to the technical stress-strain curve, in the case of a true stress-true strain curve, stresses and strains are based on the actually smallest cross-section

* up to the strain level of $\bar{A}_{gl}$ (plastic strain at $\bar{R}^t$, more accurate $true\bar{R}^t$): <u>*Table16.2-2:*</u>

$$true\sigma_{ax} \equiv \sigma_{ax}^{true} = eng\sigma_{ax} \cdot (1 + eng\varepsilon_{ax}) \,,\; true\varepsilon_{ax} \equiv \varepsilon_{ax}^{true} = \ell n(1 + eng\varepsilon_{ax}) \,,$$

* beyond the level $\bar{A}_{gl}$: $\sigma_{ax}^{true} \Rightarrow \sigma_{eq}^{true}$, $\varepsilon_{ax}^{true} \Rightarrow \varepsilon_{eq}^{true} = 2 \cdot \ell n(A / A_0)$.

If $eng\sigma_{ax} = F/A_0 = eng\bar{R}^t$ then 'Onset-of- (diffuse) Necking' takes place = 'End of uniform elongation'

Strength design input is usually $engR^t$, the engineering stress-strain curve ends at the strength point

or $true\sigma_{ax} = F/A = true\bar{R}^t$ then 'Onset-of- (diffuse) Necking' takes place.

If $true\sigma_{ax} = F/A > true\bar{R}^t$ then $true\sigma_{ax}$ becomes $true\sigma_{eq}(true\sigma_{ax} + \sigma_{hyd}, \sigma_{hyd}, \sigma_{hyd})$

considering tension bar (rod) test specimen.

The larger the strains the more the engineering stresses lose their applicability in structural dimensioning. Therefore then, above true stresses and logarithmic (*usually termed true*) strains have to be used in the dimensioning process. <u>*Fig.16.2-1*</u> contains the true and the engineering stress-strain curve. The behavior of the material here, described by these curves, show no yield limit features such as different upper and lower onset-of-yield limits (*Lüder elongation*). The figure presents a general view and uses a classical Ramberg-Osgood mapping. Mapping of the course of stress-strain data in the non-linear domain is much better performed by the Ramberg-Osgood

Table 16.2-2: Derivation of true stresses and strains with true-engineering relationships

True Strains (logarithmic strains):

The application of engineering strain cannot be correct for larger strains, since it is based on the original gage length ℓ_0, whereas the length is continuously growing. Ludwik $[Lud09]$ therefore introduced the true strain $(\text{logarithmic strain})$, the increment of which for a given length is defined as

$d(true\varepsilon) = d\ell / \ell$ and the total true strain, integrated from ℓ_0 to current length ℓ, is

$$true\varepsilon_{ax} = \int_{\ell_0}^{\ell} d\ell / \ell = ln(\ell / \ell_0) = ln(1 + eng\varepsilon_{ax}) .$$

Above equation delivers an accurate value up to 'onset-of-necking' or $\bar{R}^t$.

The replacement of the logarithmic function by a Taylor series

$$true\varepsilon_{ax} = eng\varepsilon_{ax} - eng\varepsilon_{ax}{}^2 / 2 + eng\varepsilon_{ax}{}^3 / 3 - .. +$$

clearly shows that identity is given for small strains, only. Applying the true strain has a physical and a numerical advantage: The incompressibility equation really becomes zero

$$\sum true\varepsilon_i = true\varepsilon_I + true\varepsilon_{II} + true\varepsilon_{III} = 0,$$

whereas in terms of engineering strains the correct equation from solid geometry reads

$$(1 + eng\varepsilon_I) \cdot (1 + eng\varepsilon_{II}) \cdot (1 + eng\varepsilon_{III}) - 1 = 0,$$

which reduces to 0 for negligible strains, only.

Once necking starts most of the deformation occurs in the smallest cross section. The longer the gage length used the smaller the percent elongation will be. Therefore, a better procedure is the measurement of the reduction of the cross-section. $\rightarrow$ Beyond $\bar{R}^t$, the true σ-ε curve can be more accurately obtained by measuring the radial strain

$$eng\varepsilon_{radial} = (r - r_0) / r_0 = r / r_0 - 1 \quad \text{and} \quad true\varepsilon_{radial} = -ln(1 + eng\varepsilon_{radial}) = -ln(r / r_0),$$

provided, the tensile test specimen has a circular cross-section, a rod. In this case $\varepsilon_{radial} = \varepsilon_{hoop}$

$$true\varepsilon_{ax} + true\varepsilon_{radial} + true\varepsilon_{hoop} = 0 \quad \text{and it holds} \quad true\varepsilon_{ax} = -2true\varepsilon_{radial} = 2\,ln(r / r_0),$$

which delivers an accurate value above 'onset-of-necking'. The equivalent strain in the center reads

$$true\varepsilon_{eq} = \frac{\sqrt{2}}{3} \cdot \sqrt{(true\ \varepsilon_{ax} - true\ \varepsilon_{hoop})^2 + 0 + (true\ \varepsilon_{hoop} - true\ \varepsilon_{ax})^2}$$

$$= \frac{\sqrt{2}}{3} \cdot \sqrt{2(2 - (-1))^2} \cdot true\varepsilon_{radial} = \frac{2}{3} \cdot \sqrt{3^2} \cdot true\varepsilon_{radial} = 2\,ln(r / r_0)$$

$\Rightarrow$ Transferring strain data: $true\varepsilon = ln(1 + eng\varepsilon),\ eng\varepsilon = e^{true\ \varepsilon} - 1.$

True Stresses

Trueσ can be obtained from engσ, if the small changes in volume at the end of the transition domain are neglected. Then, incompressibility $\sum \varepsilon_i^{pl} = 0$ can be assumed and it follows:

engσ = F/ A_0, trueσ = F/A with $A \cdot \ell = A_0 \cdot \ell_0$, F: = load F_{ax}

wherein ℓ_0 : = original gage length, and A, ℓ current values of the necking cross-section.

Introducing the equation $\varepsilon_{ax} = (\ell - \ell_0) / \ell_0$ derived above, the true stress is linked by

$$true\sigma_{ax} = F / A = (F / A_0) \cdot (\ell / \ell_0) = eng\sigma \cdot (1 + eng\varepsilon_{ax}) = \sigma_{ax} \cdot (1 + \varepsilon_{ax})$$ usually written

$\Rightarrow$ Transferring stress data: $true\sigma = eng\sigma \cdot (1 + eng\varepsilon)$ and $eng\sigma = true\sigma / exp(true\varepsilon)$.

equation for the true stress-true strain curve than for the engineering curve.. In *Fig.16.2-1* the difference between the strength values $\text{eng}\bar{R}^t \rightarrow \text{true}\bar{R}^t$ is 8%.

Concerning sheet test specimens the measurement problem increases because *localized necking* will occur *('onset-of-ductile cracking*) which depends on the thickness of the specimen.

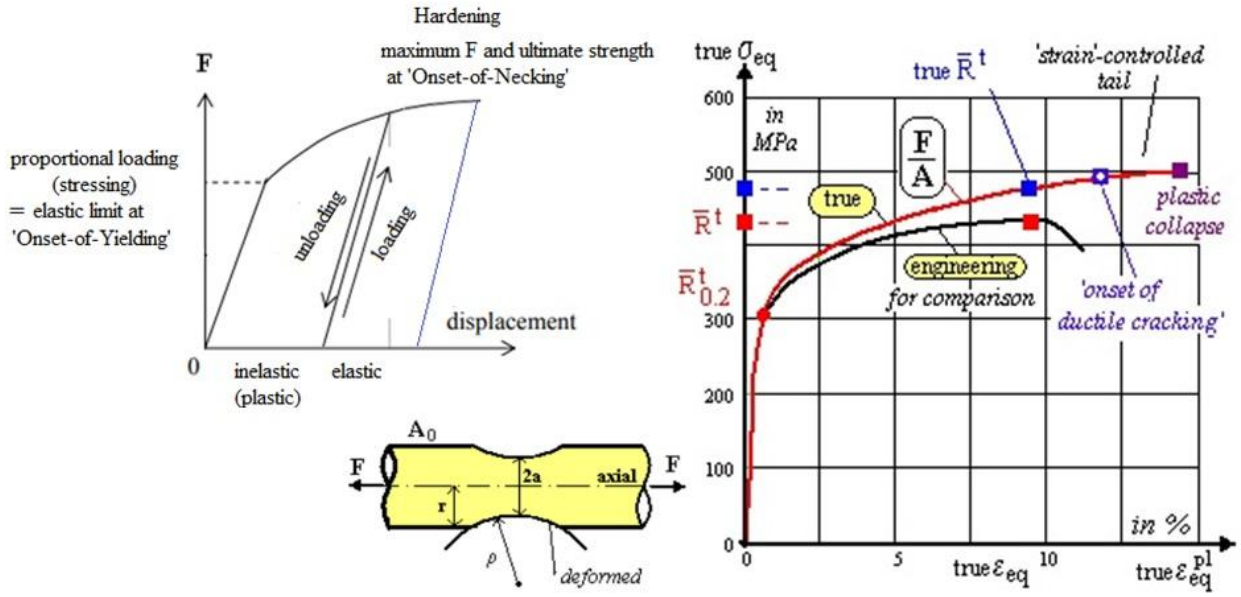


Fig. 16.2-1: Ramberg-Osgood-mapped true and engineering stress-strain curves of AA2219. F:=Force F_{ax}, A_0 := original cross-section, A:= actual cross section of the necked rod. $\bar{R}^t = \max F / A_0$, $\varepsilon \le \bar{A}_{gl}$ (permanent strain linked to load-controlled fracture at $\bar{R}^t$). Necking radius is ρ. A bar over R indicates a mean value, no bar over R indicates a 'design allowable'.

***LL**:*

** The determination of the properties of a solid material requires a force-elongation curve which is then accurately to transfer into a stress-strain curve that is independent from the specimen type.*

** Before any performance of a non-linear analysis is executed it is to check whether true or engineering quantities are to provide for input and which is the then given in the FEA output (True-in requires True-out and an assessment by* $\text{true}\bar{R}^t$

** Beyond R^t necking occurs generating a hydrostatic stress σ_{hyd} which lowers the stress-strain curve (see a later sub-chapter).*

16.2.4 Estimation of the volume strains of a material element under a uniaxial stress $\sigma_I = \sigma^t$

In the tri-axial stress state, Hooke's law reads

$$E_o \cdot \varepsilon_I = \sigma_I - \nu_o(\sigma_{II} + \sigma_{III}),\ E_o \cdot \varepsilon_{II} = \sigma_{II} - \nu_o(\sigma_{III} + \sigma_I),\ E_o \cdot \varepsilon_{III} = \sigma_{III} - \nu_o(\sigma_I + \sigma_{II})$$

with Young's modulus E_o and Poisson's ratio ν_o being macro-mechanical constants in the elastic regime of an isotropic material (micro flaws and second phase particles are of subscale level).

In the case of uniaxial stress $E_o \cdot \varepsilon_I = \sigma_I$, $E_o \cdot \varepsilon_{II} = -\nu_o \cdot \sigma_I = E_o \cdot \varepsilon_{III}$

introduced into the geometrical formulation of the volume change

$$\Delta V = V - [(\ell + \Delta\ell_I)(\ell + \Delta\ell_{II})(\ell + \Delta\ell_{III})]$$

follows $\Delta V/V \approx [\Delta\ell_I + \Delta\ell_{II} + \Delta\ell_{III}]/\ell$ or $\varepsilon_{Vol} = \varepsilon_I + \varepsilon_{II} + \varepsilon_{III}$.

An example for tensioned AA 2219 with $\sigma^t = 340$ MPa $< R^t_{0.2}$, $E_o = 70.000$ MPa, $\nu_o = 0.28$ delivers a volume strain $\varepsilon_{Vol} = \sigma^t \cdot (1-2\nu_o)/E_o = 340\cdot(1-2\cdot 0.28)/70000 = 0.002 \cong 0.2\%$.

16.3 Isotropic Material Testing

The evaluation of fracture tests of ductile materials is more challenging than for brittle materials, which do not neck and where the load-controlled engineering fracture strength $\bar{R}^t$ usually marks the design limit. In case of tension loading, depending on the analysis to be performed and on the applied code, both engineering and true quantities are applied whereas in case of compression loading just engineering stresses are utilized. In compression, in case of ductile isotropic materials, strains higher than the technical yield limit, the -0.2% offset value, are often not permitted from the design requirements, in practice, according to a de-stiffening effect. The application of true compressive stresses makes no sense due to the effect of the barreling specimens, see *Fig.16.3-2*.

16.3.1 General on uniaxial and plane test specimens

There are very different stress-strain curves in the elastic-plastic transition domain, see *Fig.16.3-1*. Some show an 'Onset-of-yield' at an upper yield stress level R_e^{upper} and others at a lower yield strength R_e^{upper}. In this case usually the lower yield point is taken as the yield strength of the steel.

By the way, the actual 'Onset-of-yielding can be determined by a temperature measurement. If a metallic material is subjected to tensile stress, it first cools down in the area of elastic elongation analogous to an ideal gas (thermo-elastic effect). With onset of plastification heat is released, which leads to an increase in temperature. This temperature is measurable with glued thermocouples.
Low-alloy iron usually has an upper yield limit R_e^{upper} (R_{eH}, *Streckgrenze*). If it is stretched during the tensile test, a spontaneous yielding in the crystalline compound takes place under loading. This so-called Lüder's effect disappears until all crystals are finally commonly stretched. Austenitic steels do not have a protermced yield strength. For these materials, the graphically defined '0.2% off-set strain associated stress' is used, usually termed yield strength $R_{p0.2}$ in design.
Lüder's elongation effect is a part of plastic stretching. It describes the range until the onset of hardening in the stress-strain diagram.

Regarding other materials - for a conflict-free understanding – it will be denoted $R_{p0.2}$ ($\rightarrow R_{0.2}^t$) and $R_{c0.2}$ ($\rightarrow R_{0.2}^c$). At the maximum of the curve, characterized by necking in the ductile material case, the tensile strength R_m ($\rightarrow R^t$) is given. For very ductile materials is valid $R_{0.2}^c \cong R_{0.2}^t$.
Above the tensile strength level $\bar{R}^t$ a multiaxial state of stress follows in the tensioned ductile behaving test specimen. Therefore, the index ax holds up to the end–of–uniform elongation (Gleichmaßdehnung) at $\bar{R}^t$ (*index pl for plastic strain and for onset-of-ductile necking, index oon*). In this respect, any formulations in this domain afford equivalent quantities in order to achieve an accurate non-linear analysis with a correct σ(ε)-input.

Properties, to be provided in case of ductile materials, vectorial displayed:

$$\{R\} = (R^t, R^t_{0.2}, R^c_{0.2})^T,\ \mu\ ;\quad \{E\} = (E,\ \nu)^T,\ \text{whereby}\quad G = E/(2+2\cdot\nu)\ .$$

There are two different stress-strain curves existing: the ***monotonic*** and the ***cyclic stress-strain curve***. The first curve is derived by the static test above, whereas the second one is generated by fatigue tests. Strain-controlled hysteresis loops are performed on different strain levels with several test specimens. Dependent on hardening and softening behavior of the actual material these two curves may discriminate significantly.

Monotonic stress-strain curves have long been used to obtain design parameters for limiting stresses on engineering structures and components subjected to static loading. Similarly, cyclic stress-strain curves are useful for assessing the durability of structures and components subjected to repeated loading.

Essential for an accurate analysis is a stress-strain curve which is derived from a set of test curves. delivering distributions for the *design parameters* $R_{p0.2}$, R_m, ε_{on}^{pl} *and* ε_{fr}^{pl} .

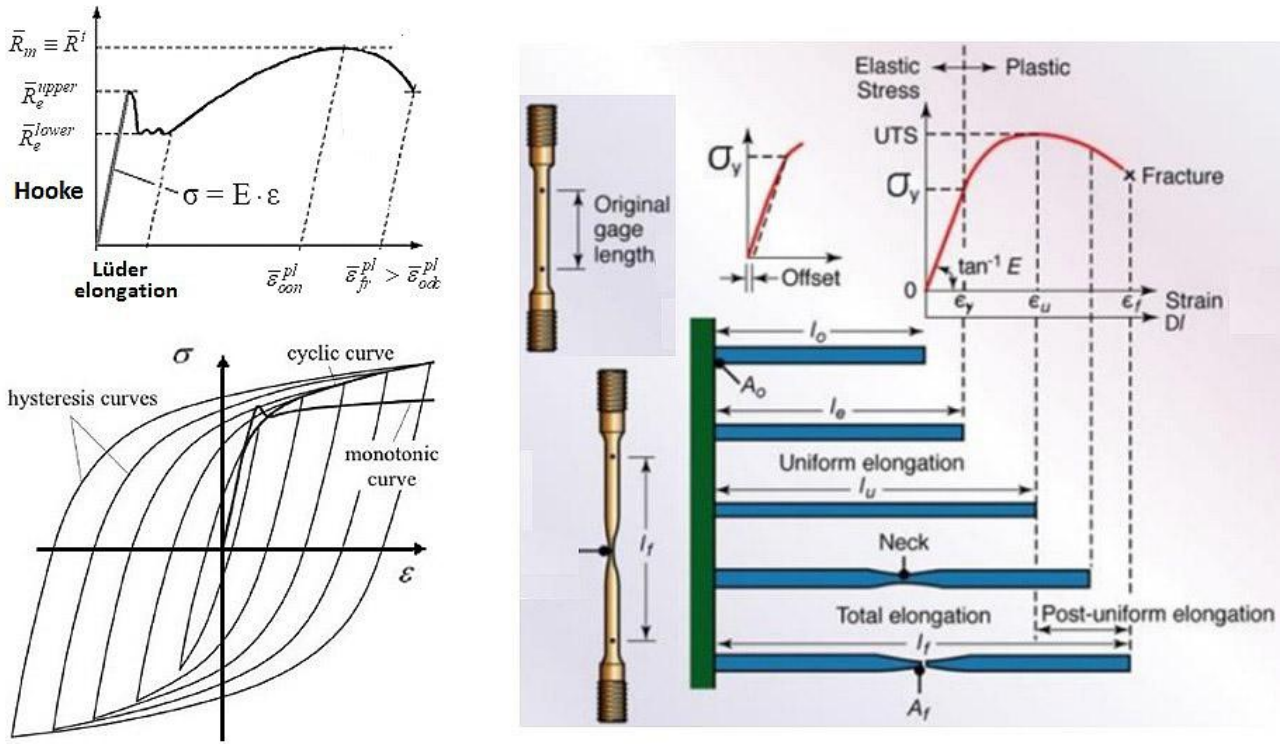


Fig.16.3-1: (left,up) Typical curve for mild steel showing the yield point phenomenon, termed Lüder's elongation effect. (left,down) Cyclic curves. (right) Tensile-test specimen with gage length, elongation before and after testing and finally after rupture [Kal15]

Fig.16.3-2 left shows the scatter and distributions of some strength and strain quantities.

Fig.16.3-2 right up demonstrates that a compression test can – due to barreling - just give a value for the yield strength $R_{0.2}^{c}$. The figure also informs that for a static test specimen of a product the directions are marked by the subscripts L, LT and ST and that these are used for the description of sheet-type test specimens. These specimens are machined in the rolling direction (letter L), transversal direction (T) and thickness direction (S). In the case of thick structural parts smooth tension bar test specimens are cut out, in the case of thin plates flat test specimens are investigated, which better represent 2D-structural shapes. (Above convention mentally leads over from the not fully isotropic materials to the transversely-isotropic ones).

This is similarly performed for the radial and axial direction of a cylindrical test specimen.

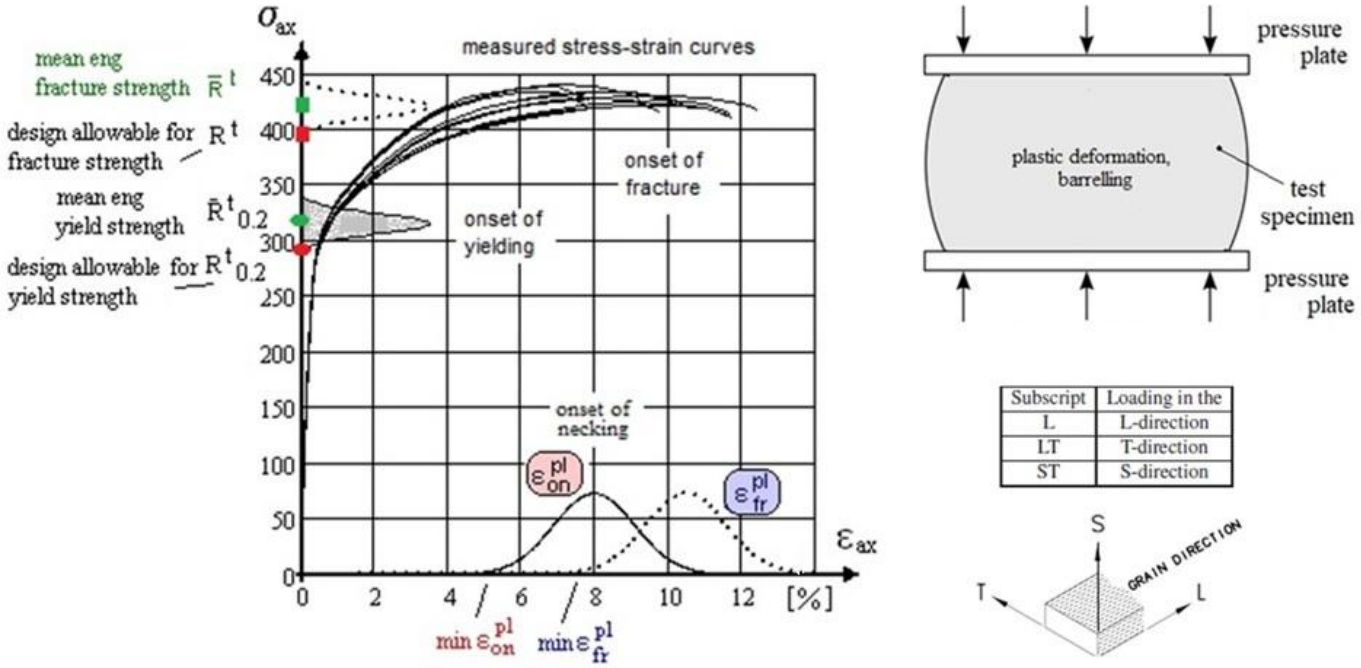


Fig.16.3-2: (left) Set of measured engineering curves, (right upright) Deformation of a compressed ductile test specimen. (right down) Marking of sheet-type test specimens

For notched axisymmetric tensile specimen, the stress tri-axiality *TrF* is a function of notch geometry with values larger than 1/3 (smooth bar). Higher stress tri-axiality results in a smaller failure strain.

16.3.2 Test specimens

Uniaxial Testing:

Mechanical properties are basically obtained from tensile tests, namely $R_{p0.2}$, R_m, ε_{oon}^{pl}, ε_{fr}^{pl}, E_0, ν_0 applying Standard (ASTM, ISO etc.) Herein ε_{oon}^{pl} is the strain value at the 'End of uniform elongation' (*German: Gleichmaßdehnung, index gl*) of a ductile material and it also represents the 'Onset-of–(diffuse) necking' (index oon). Unfortunately, Onset-of-(diffuse)necking is often termed post-necking. However, post-necking describes the increasing necking elongation regime, namely after hardening.

DIN EN ISO 6892-1: Short bar (rod) tensile test specimens show higher elongations at fracture than long ones. For this reason, an index is given for the plastic or permanent fracture strain, i.e. in Germany, A5 for short and A10 for long test specimens. The index refers to the ratio of original length L_0 and initial diameter d_0 (A5: $L_0 = 5 \bullet d_0$). Hence, the aspect ratio A5 delivers the permanent strain of a rod test specimen with the aspect ratio 5 at rupture. The actual change in length is measured on the broken test specimen.

The ductile fracture strain is composed of the uniform elongation and the necking elongation part (*Einschnürdehnung*). The uniform elongation is independent of the specimen length. Its end is at 'onset-of-necking' at the load-controlled fracture point. *true* $A_{gl}(\bar{R}_m^t)$, being the plastic strain at end of uniform elongation, specifies up to what percentage a material can be formed, *Fig.16.3-3.* As an

additional ductility characteristic, the necking value **Z** (*Brucheinschnürung*) is calculated on the basis of the plastic cross-sectional reduction at fracture of the test specimen compared to the initial cross-section and is expressed in %.

Mechanical properties have to be assigned as part of the procurement specification requirements. These values shall adequately represent the effects coming from:

- Form: bar, sheet, plate, laminate stack;
- Size, thickness range:
- Manufacturing : metals (extrusion, rolling, forging),
  fiber reinforced plastics etc. FRP (curing),
  textiles (weaving, braiding, stitching etc.), fiber crossings
- Direction: metal grain (longitudinal, long. transverse, short transverse),
  fibers (parallel, transverse, thickness);
- Tempering: heat treatment for metals and fibers parts (*TP matrix*),
  cold working, (*remaining residual stresses*) *and*
- Test direction.

Susceptibility to environmental effects such as temperature, humidity radiation and cyclic loading has to be taken into account. For a specific project the required data may be tailored to match the particular profile and circumstances of the project in agreement with the customer.

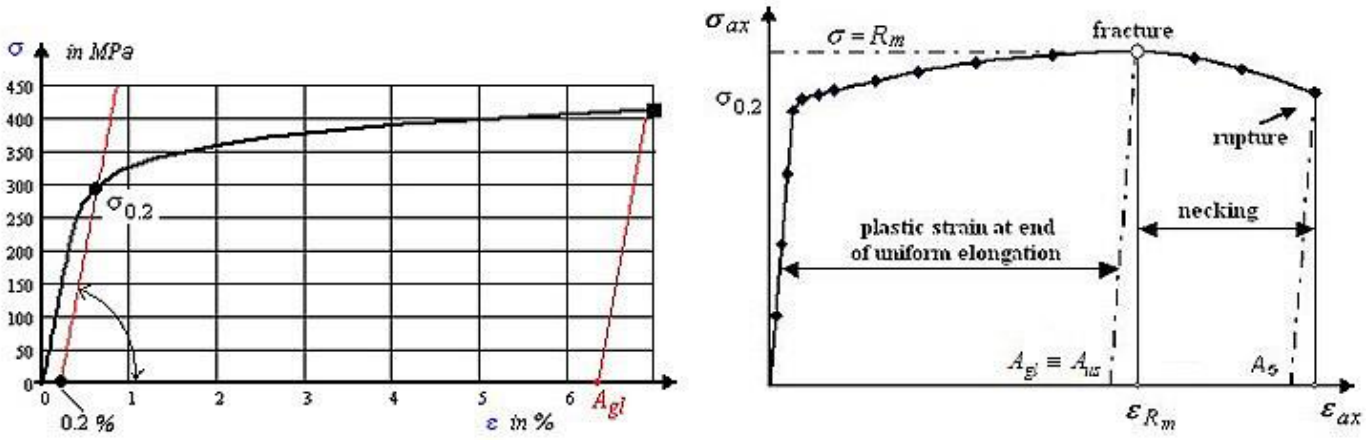


Fig.16.3-3: R-O mapping of a single engineering measurement test results. $A_{gl} = \min \varepsilon_{oon}^{pl}$

Typical engineering stress-strain curve of a ductile metal material. End of uniform elongation (Gleichmassdehnung ε_{gl} *)*

LL:

** Before executing any analysis with a distinct code the designer has to check whether the actual stress-strain curve fits to the shape of the implemented curve.*

** For the best possible estimation of the component behavior, the average stress-strain curve* $\overline{\sigma\varepsilon}$ *must be taken.*

** The average stress-strain curve* $\overline{\sigma\varepsilon}$ *does not necessarily run through the means of yield (* $\bar{\sigma} - \bar{\varepsilon}$ *)*$_{yield}$ *and of fracture (* $\bar{\sigma} - \bar{\varepsilon}$ *)*$_{fr.}$

Tensile Test Example on a specific aluminum alloy AA2219:

These tensile tests were performed at the IWM Freiburg (*contract with MAN*) on smooth tension rods with a cross section diameter of 4 mm and a gauge length of 20 mm (*Table 16.3-1*). All tensile tests were conducted quasi-statically at room temperature. For the determination of true stress-true

strain curves the reduction of specimen diameter was measured continuously using a CCD camera; the change in gauge length was measured using a clip-gage.

The failure occurred by fast shear fracture as it appears on the fracture surface image in *Fig.16.3-4*. A low deformation ductile fracture appearance is revealed with internal necking from larger inclusions and secondary necking from smaller second phase particles, between the large inclusions, which is a possible mechanism for the fast shear fracture.

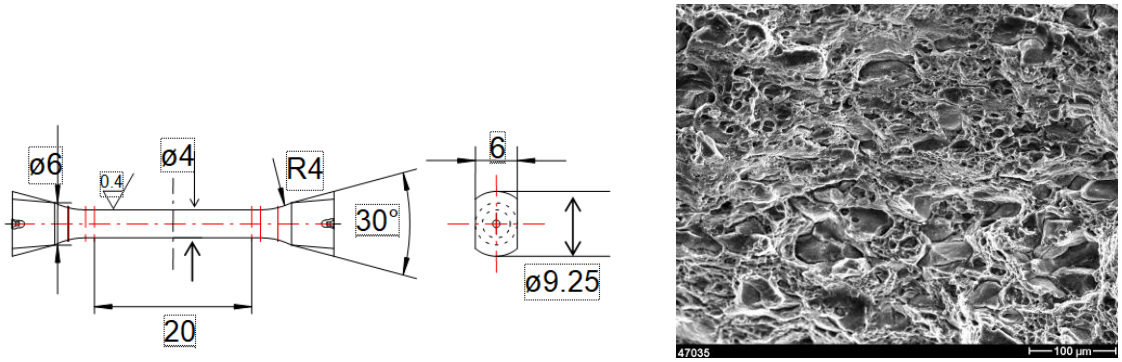


Fig.16.3-4: (left) Geometry of the tensile rod; (right) Voids on the fracture surface [IWM]

Mean technical and mean true strengths together with the associated design allowables as well as the interesting strain values are listed in *Table 17.3-1*.

Table 16.3-1, Properties example from tension test: [IWM]
(stresses in MPa, strains in %). Material AA2219, A_{gl} = Aus = εoon .

$\overline{R}_{p0.2}$	$true\overline{R}_{p0.2}$	$\overline{R}_m$	$true\overline{R}_m$	$\overline{R}_{odc}$		A_{gl}	A_5	Z	$R_{p0.2}$	R_m	R_{odc}
352	354	453	478	535		4.06	7.7	20	297	417	492
averages (mean, typical, characteristic)						minima					

The effect of probably initially not pore-free material is captured in the initial property values.

Bi-axial testing:

Biaxial testing of ductile materials is a big issue for achieving design information under plane stress states and when forming metals. Whereas the stress-man as designing engineer looks at the strengths (strength criteria) the production engineer must look in the forming process at the strains (strain limit criteria) in order to evaluate the formability of metal sheets.
A standard test specimen is missing, different cruciforms (below), tubes and hemi-spheres (*domes of Ariane tanks*) are applied.

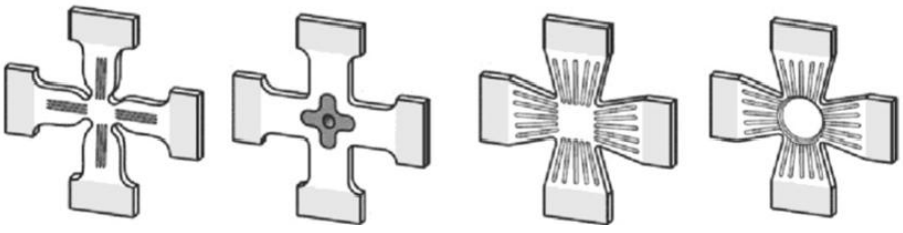


Fig.17.3-5: Geometries of cruciform test specimens used in bi-axial tensioning [Zid10]

For the often used cruciform it is challenging to distribute the loading evenly to the gauge reducing stress concentrations due to the stiffness situation of the specimen's geometry.
This type of test specimen is basically used for the establishment of the Forming Limit Diagram (FLD) in manufacturing design.

Forming Limit Diagram FLD

Dealing with large strains makes to look over the fence at forming sheets. FLDs are useful for the evaluation of the strain-defined workability of formed metal sheets. They provide in the principal strain space the strain limit of 'Onset-of-necking'. At MAN these were the application cases Ariane Booster cylinders and the bottoms of the tanks.

Although cracking is the ultimate limit in forming processes, Onset-of-necking is usually considered as not desired and seen as limit. In this context, so-called Forming limit diagrams are prepared to depict the limits of forming. FLDs are generated by mapping the failure points on a plot with the major and minor strains as coordinates. The major strain is the maximum strain and the minor strain is the strain perpendicular. The major strain is always positive whereas the minor strain can be positive or negative (see *Fig.16.3-6*). Major and minor strains can be measured using a sheet with a grid pattern, which deforms under straining up to failure. Most often, failure data is derived from forming tests with a hemispherical punch. Different stress conditions are simulated by changing the width of the circular shaped strips used for testing
The forming limit diagram can be determined for strain paths ranging from biaxial tension (as given in stretch forming) to equal tension and compression (*as in deep drawing, Ariane Booster cylinders*). See *[DenUijl12]* for more general details.

The formability is influenced by the strain rate. Forming of thin sheets (t <≅ 100 µm) is more effected by flaws than forming of thick ones.

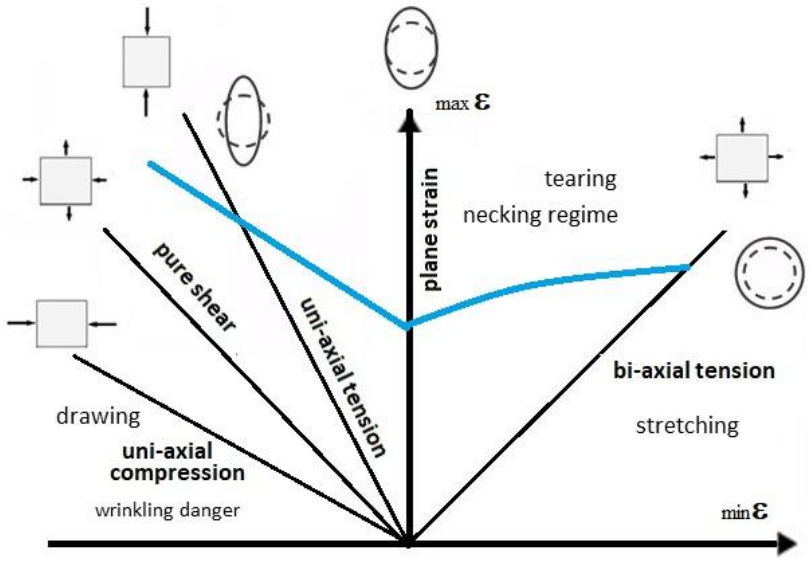


Fig.16.3-6: Schematic Forming Limit Diagram FLD = limit regarding 'Onset-of diffuse necking', at R^t

16.3.3 Ramberg-Osgood-mapped Stress-strain curves of Ductile Isotropic Materials

The R-O-relationship is an often used mapping function and mathematical representation of the stress-strain curve. It represents (*if applicable to the actual material)* a possibility of well mapping the course of test data. A representation of the stress-strain curve is possible using engineering or true stresses and strains. The R-O-function is a monotonously increasing function and was originally developed for stresses up to the yield strength only. Using it, the elastic strain and additional plastic strain are determined separately. It reads, see Fig.16.3-7,

$$\varepsilon = \frac{\sigma}{E} + 0.002\left(\frac{\sigma}{R_{0.2}}\right)^{n} \qquad \text{with} \quad n = \frac{ln\left(A_{us}/0{,}2\%\right)}{ln\left(R_m / R_{p0.2}\right)} \quad \text{with } A_{us} = A_{gl},$$

where the plastic strain portion follows a power relationship. The stress-strain curve is determined by the mechanical properties E and $R_{0.2}$ and by the material dependent hardening exponent *n*. Typical R-O curves are based on an average *E* and an average $\bar{R}_{0.2}$. Values of *n* are derived from test data. Remind the average stress-strain curve $\overline{\sigma\varepsilon}$ of a bundle.

For tension and compression the same equation is used, with different values of E, $R_{0.2}$ and *n* for tension and compression. Both, for tension and compression, positive values of ε, σ and E shall be inserted. For compression, the obtained values of ε and σ can be made negative after adaption of the function.

Applying engineering stresses and strains, the R-O-relationship often yields an adequate approximation of the test data for stresses up to the yield strength. When true stresses and strains are used, the region where a good approximation is obtained can be extended from onset-of-diffuse necking up to the strain where local necking starts and further (see some pages later).

The value of *n* depends on material, condition, product form and loading direction (in L, LT or ST-direction). Usually, only typical values of *E* and *n* are presented in literature and in material data sheets. For the yield strengths and for the ultimate strengths usually only strength design allowables are given (statistically determined minimum values). For A_5 generally only specification values are presented as $\min A_5$ values. Consequently, if no test data is available, only these values can be used to obtain an average R-O-function. Typical values of *n* are presented in the MMPDS-2 (*the former Mil-Hdbk 5*) and in the HSB. It should be noted that a value of *n* is always related to specific values of E and $R_{p0.2}$. For a typical stress-strain curve the value of *n* is different from the value for a minimum curve, see *Fig.16.3-7.* The applied value of *n* must therefore match with the other applicable mechanical properties! Given minimum strength values have to be transformed to average values to achieve a stress-strain average curve. The typical values of *n*, given in MiL-Handbook and HSB, are valid for $\varepsilon \le 1.2 \cdot \left(R_{0.2} / E_0 + 0.002\right)$. Using the R-O stress-strain relationship, the often applied tangent and secant modulus can be expressed as a function of the stress in the hardening domain:

$$E_{sec}^{hard} = \frac{\sigma}{\varepsilon} = \frac{\sigma}{\frac{\sigma}{E_0} + 0.002 \cdot (\frac{\sigma}{\bar{R}_{0.2}})^{\bar{n}}} = \frac{E_0}{1 + 0.002 \cdot \frac{E_0}{\bar{R}_{0.2}} \cdot (\frac{\sigma}{\bar{R}_{0.2}})^{\bar{n}-1}}, \quad E_{tan}^{hard} = \frac{d\sigma}{d\varepsilon} = \frac{E_0}{1 + 0.002 \cdot \bar{n} \cdot \frac{E_0}{\bar{R}_{0.2}} \cdot (\frac{\sigma}{\bar{R}_{0.2}})^{\bar{n}-1}} \cdot$$

Also the value of Poisson's ratio ν, which increases when stresses become plastic, can be determined as a function of the stress. And vice versa it decreases with increasing porosity in the

case of ductile metals. This is analogous to brittle porous material, which was still mentioned in the distinct sub-chapter. The change of ν with the changing density will be elaborated in a later sub-chapter.

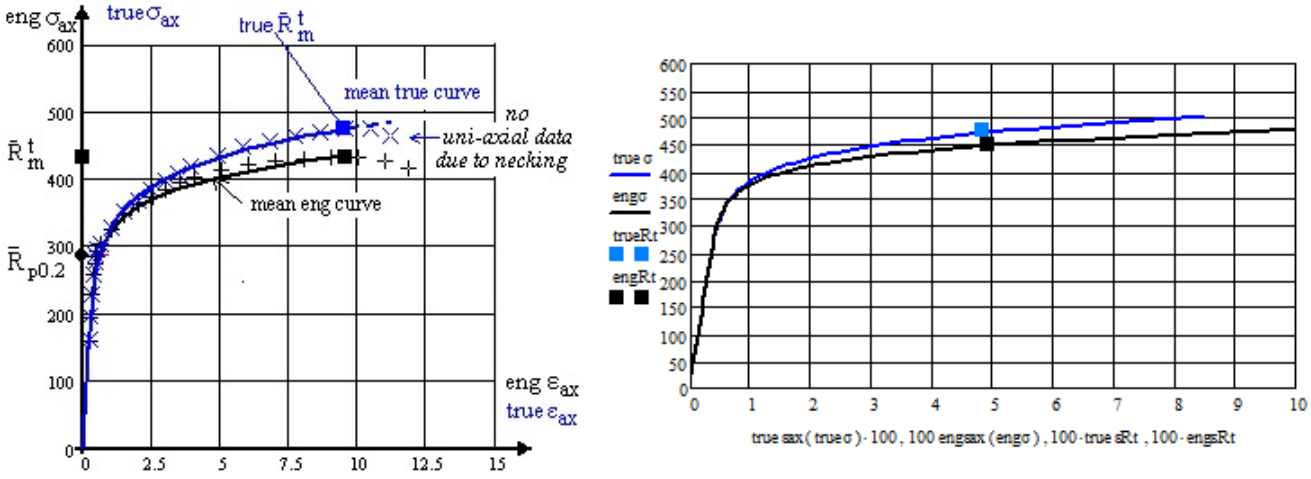


Fig.16.3-7: (left) Differences in R-O-mapping of engineering and true stress-strain curve, single measurement. (right) Extrapolation of R-O-mapped curve, bar over R indicates a mean value.

'End of uniform elongation' = 'Onset-of-(diffuse) Necking'

16.3.4 Bridgman's tri-axiality approach: Mises-based Correction of true $\sigma - \varepsilon$ Curve

Equivalent stress: $\text{true}\sigma_{ax} \rightarrow \text{true}\sigma_{eq}$

The validity of the uniaxial stress-strain curve measured in a smooth tension bar (rod) test is terminated at the load-controlled strength point $\max\sigma_{true} = \bar{R}^t = max\, F / A$, which corresponds to the maximum load F achieved and to the actual minimum cross section of the neck. However, FEA requires in this 'post-Onset-of-diffuse necking' regime an equivalent stress σ_{eq}^{Mises} in order to capture the multi-axial stress task if the task is strain-controlled. The extrapolation of the curve beyond $\bar{R}^t$ does not provide a physically accurate curve, because the necking-generated 3D-residual stress state (Eigenspannungszustand) σ_{hyd} is to consider in the evaluation of tension bar (tensile rod) test results in order to obtain the $\text{true}\sigma_{eq}$. The three stresses within σ_{hyd} reach their maximum values at the center of the tension bar specimen, with approximately equal values $\sigma_{radial} = \sigma_{hoop}$, except close to the surface, as depicted in *Fig.16.3-8* below.

Fig.16.3-8 shows the external axial stress and the superimposed σ_{hyd} together with the geometry in the neck regime. Under tensioning, the lateral contraction of the material at the center of the neck is impeded by neighboring material leading to a 3D-stress state. The generation of σ_{radial}, σ_{hoop} raises also σ_{ax}. The necking radius ρ changes with increasing further tensioning. The former F/A-quantified yield capacity becomes continuously reduced with increasing necking. The true stress-strain F/A curve must be corrected. Meanwhile, there are several methods to correct the uniaxial

curve to obtain a corrected equivalent stress. These methods are differently far valid, because they treat the same problem employing a different number of simplifying assumptions.

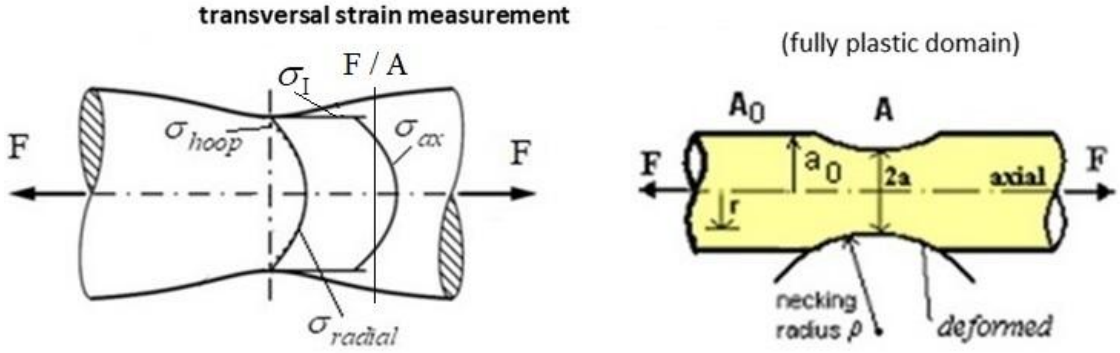


Fig.16.3-8: Transversal (radial) strain measurement.
F:=force, := original cross-section, A0:= minimum actual cross section.

P.W. Bridgman's correction formula is widely used, although it is not the most accurate one for very high straining among the analytical methods that are valid for the round bar test specimens. As it is a practical model the author based his investigations on Bridgman. Each material exhibits a specific hardening rule and may be differently to map, like with R-O. Task for design is the necessary transfer from the uniaxial trueσ_{ax}(trueε_{ax}) → tri-axial trueσ_{eq} (trueε_{eq}) in the necking regime. Bridgman provided a correction means how to lower trueσ_{ax} (trueε_{ax}) *by* accounting for the 3D-hydrostatic stress state.

His method to adjust trueσ_{ax} makes some essential assumptions: *The cross section of the necked region remains circular; *the inner axial contour of the neck can be approximated by the arc of a circle with the radius ρ; *The 'Mises yield criterion' applies; the effect of growing voids is not considered. As result Bridgman proposed an analytical solution for the 3D-stress distribution of σ_{hyd} in the minimum cross section of the necked bar test specimen.

'At end of uniform elongation' or at the associated 'Onset-of-(diffuse) Necking' in the minimum cross-section of the round tension bar the 3D-state of stress is developing due to a superimposing internal hydrostatic *tensile* stress state σ_{hyd}. This stress state is a deformation-dependent residual stress state. Its radial distribution can be Mises-based estimated after Bridgman [*Bri52*] (*see* Fig.16.3-8) subjected to axial loading $\{\sigma\} = (\sigma_I, \sigma_{II}, \sigma_{III})^T = (F/A, 0, 0)^T$ by

$$\sigma_{hyd}(a,\rho,r,\text{true}\sigma_{ax}) \approx \sigma_I \cdot ln\left(1+\frac{a^2-r^2}{2\cdot a\rho}\right) \quad \text{with } \sigma_I < \frac{F}{A}=\frac{F}{\pi\cdot a^2} \quad \rightarrow \frac{F}{\pi\cdot 4^2\cdot \text{mm}^2}$$

and F:= load, a:= 4 mm radius of actual cross section of neck, ρ:= radius of curvature at neck, and F/A an integral quantity capturing the external loading F (Pay attention: *unfortunately, the letter A is also used for plastic strain quantities*).

Hence, the distribution of the tensile axial and radial stresses over the true cross-section – due to *Fig.16.3-8* – can be described as

$\sigma_{ax}^{t}(r) = \sigma_I + \sigma_{hyd}(r)$ and $\sigma_{radial}(r) \approx \sigma_{hoop}(r) = \sigma_{hyd}(r)$ and the equivalent stress

For a single stress follows $\rightarrow \sigma_{eq}^{Mises} = \sqrt{3 \cdot J_2} = \sqrt{\frac{1}{2}} \cdot \sqrt{\left[(\sigma_I)^2 + (0)^2 + (-\sigma_I)^2 \right]} = \sigma_I$ and also

for a superimposed $\sigma_{hyd} \rightarrow \sigma_{eq}^{Mises} = \sqrt{3 \cdot J_2} = \sqrt{\frac{1}{2}} \cdot \sqrt{\left[(\sigma_I - \sigma_{hyd})^2 + (\sigma_{hyd} - \sigma_{hyd})^2 + (\sigma_{hyd} - \sigma_I)^2 \right]} = \sigma_I$.

In the adjusting process of the F/A-curve in the necking regime the first step is to integrate the varying axial stress. From load balance is then yielded

$$F/A = 2 \cdot \int_o^a \sigma_{ax}^{t} \cdot \pi \cdot r \cdot dr / (\pi \cdot a^2) = 2 \cdot \int_o^a (\sigma_I + \sigma_{hyd}(r)) \cdot \pi \cdot r \cdot dr / (\pi \cdot a^2)$$

$$= \frac{F}{A} = 2 \cdot \int_o^a (\sigma_I + \sigma_I \cdot ln\left(1 + \frac{a^2 - r^2}{2 \cdot a \cdot \rho}\right)) \cdot \pi \cdot r \cdot dr / (\pi \cdot a^2).$$

After integration the following equation is derived

$F / A = \sigma_I \cdot (1 + 2 \cdot \rho/a) \cdot \ln(1 + a/2 \cdot \rho)$ and with $\sigma_{eq}^{Mises} = \sqrt{3 \cdot J_2} = \sigma_I$ follows

cross-section integrally $\sigma_{eq}^{Mises} = \frac{F}{A} / (1 + 2 \cdot \rho/a) \cdot \ln(1 + a/2 \cdot \rho)$, valid $> \bar{R}^t$ or $A < Aoon$,

an equation in which the ratio a/ρ is not known. This equivalent Mises stress, smeared over the cross-section, represents the yield capacity. Following Lorrek-Hill's approach [*Lor*72]

$\frac{a}{\rho} = \sqrt{\ln(A_0 / A) - ln(A_0 / A_{oon})}$ with $\min A_{fr}(Z)$ at maximum necking, ductile rupture

with A_0 as original cross section, A_{fr} the cross section at fracture, and A_{oon} the cross- section at 'onset of diffuse necking' available from material data sheets, i.e. A_5.

Hence, in the micro-damage critical cup/cone center ('hot spot') the 3D-state of stress reads

$$max\sigma_{hyd}\ (r = 0) = \sigma_I \cdot ln\ (1 + \frac{a}{2 \cdot \rho}),\ max\sigma_{ax}^{t}(r = 0) = \sigma_I + max\sigma_{hyd}$$

with the TrF-essential 3D-stress state in the rod's center $(\max\sigma_{ax}^{t}, \max\sigma_{hyd}, \max\sigma_{hyd})^T$.

The neck radius ρ can be computed during testing by measuring the shape change of the neck via a real-time Digital Image Correlation (DIC) 3D full-field measurement optical technique of the surface strains and an associated surface geometry model. Materials that do not fail when the tensile strength is reached show necking. This is accompanied by the fact that *maxF* does not essentially change over a certain range of the axial strain because hardening still works until a slight kink will occur due to void coalescence and destruction of piled–up dislocations. Degradation wins over hardening at the **odc**-point.

Equivalent strains: $\text{true}\varepsilon_{ax} \rightarrow \varepsilon_{eq}$

For the strain is valid in the plastic domain:

$$\varepsilon_{eq}^{Mises} = \frac{\sqrt{2}}{3}\cdot\sqrt{(\varepsilon_I-\varepsilon_{II})^2+(\varepsilon_{II}-\varepsilon_{III})^2+(\varepsilon_{III}-\varepsilon_I)^2} = \frac{\sqrt{2}}{3}\cdot\sqrt{(\varepsilon_I^{\,pl}-\varepsilon_{II}^{\,pl})^2+(\varepsilon_{II}^{\,pl}-\varepsilon_{III}^{\,pl})^2+(\varepsilon_{III}^{\,pl}-\varepsilon_I^{\,pl})^2}$$ with

consideration of plastic volume constancy (incompressibility) $\Sigma\varepsilon_i^{pl} = 0$ during plastic deformation it becomes

$$\varepsilon_I^{\,pl}/2 = -\varepsilon_{rad}^{\,pl} = -\varepsilon_{tan}^{\,pl} \text{ and } \varepsilon_{rad}^{\,pl} = ln(r/a) = \varepsilon_{tan}^{\,pl},\ \varepsilon_I^{\,pl} = -2\cdot ln(r/a)$$

$$\varepsilon_{eq}^{Mises} = \frac{\sqrt{2}}{3}\cdot\sqrt{((\varepsilon_I^{\,pl}+\varepsilon_{rad}^{\,pl})-\varepsilon_{rad}^{\,pl})^2+0+(\varepsilon_{rad}^{\,pl}-(\varepsilon_I^{\,pl}+\varepsilon_{rad}^{\,pl}))^2} == \frac{\sqrt{2}}{3}\cdot\sqrt{2\varepsilon_I^{\,pl2}} = \frac{2}{3}\cdot\varepsilon_I^{\,pl}\ .$$

16.3.4 Bridgman's tri-axiality approach: Cuntze's Gurson-based Correction of true $\sigma-\varepsilon$ Curve

For visualization firstly an input data set shall be given that includes mapping and estimation of $\sigma-\varepsilon,\ \bar{R}_{odc}\ ,\ \bar{R}_{rup}\ .$

***** In a MAN-contract with the institute IWF at Freiburg at first by axial strain test the properties have been determined: AA2219, T2, t = 6mm plate, test specimen tensile rod d = 4.0 mm = 2a.

$$\text{eng}\bar{R}^t = 477\text{ MPa},\ \text{eng}\bar{R}_{0.2} = 395\text{ MPa},\ E_0 = 70000\text{ MPa},\ \ell_0 = 20\text{ mm (gage)}.$$

Single test: Measurement points n = 179, A5 = 5.4 % plastic strain, reduction of cross-section-related necking value Z = 20.1 %.

Given plastic strain A5 and given final necking value Z are usually minimum and not average values. This makes the derivation of the Bridgman-corrected curve a little more an estimation.

Listing of analysis-relevant quantities: in MPA and %

$$\text{eng}\varepsilon R_{02} = 0.76,\ \text{eng}\varepsilon R^t = 5.6,\ \text{true}R_{02} = 396,\ \text{true}R^t = 504,\ \text{true}\varepsilon R^t = 5.4$$

R/O-mapping delivers: $\text{eng}n = 17,\ \text{true}n = 13.1.$

As second step for the envisaged domain beyond onset of diffuse necking, R^t, the method radius-decrease measurement is used to investigate in this full plastic domain the influence of the hydrostatic stress.

This means a reduction of the yield capacity is experienced through σ_{hyd} and an increase is faced of TrF > 1/3 (smooth).

***** Of practical advantage is to map the test curve by the above given R-O-model (bar over skipped)

$$\varepsilon_{rad}^{\,pl} = \ln(r/a) = \ln(\sqrt{A/A_0}) = \ln(D_{00n}/2a) = \ln(3.93/2\cdot 2) \rightarrow \varepsilon_{ax,\,00n}^{\,pl} = -2\cdot\varepsilon_{rad}^{\,pl} \text{ at } R^t$$

$$\varepsilon = \varepsilon^{el} + \varepsilon^{pl} = \frac{\sigma}{E} + 0.002\left(\frac{\sigma}{R_{0.2}}\right)^n \text{ with } n = \frac{\ln\left(\varepsilon_{ax,\,00n}^{\,pl}/0{,}2\%\right)^n}{\ln\left(R^t/R_{p0.2}\right)}\ .$$

Because the R/O-model excellently maps the true strength course of test data, its plastic part can be employed to estimate the *plastic points* 'Onset-of-ductile-cracking' (*of interest for plastic structural design*) and 'Ductile rupture'. This can be executed by using the measured reduction of the initial radius a of the test specimen and employing the plastic volume constancy, shown above

$$\varepsilon^{pl} = 0.002\left(\frac{\sigma}{R_{0.2}}\right)^n,\ \varepsilon_{rad}^{\,pl} = \ln\left(\frac{r}{a}\right),\ Z = \frac{\Delta A}{A_0} = \frac{A_0-A}{A_0} = 1-\frac{A}{A_0} \rightarrow \frac{A}{A_0} = 1-Z,\ \frac{A}{A_0} = \frac{r^2}{a^2}$$

with A5 (type: $L_0 = 5 \bullet d_0$, original length L_0 and initial diameter $d_0 = 2a$) as plastic or permanent change in length, measured on the load-controlled broken test specimen and Z the necking value (plastic), calculated on the basis of the cross-sectional reduction at strain-controlled rupture of the test specimen compared to the initial cross-section.

* Estimation of F/A-defined $\bar{R}_{odc}$, $\bar{R}_{rup}$ as good guess

From the measured plastic cross-section reduction the plastic portion ε_{odc}^{pl} can be estimated and R_{odc} computed. The course of the area reduction shows a slight kink at 'Onset-of-localized necking' which is here taken as 'Onset-of-ductile cracking (**odc**)' according to the void coalescence.
(Uniaxial) strength points on the true F/A curve can be computed if the associated plastic strain is known. This value is fixed by the diameter reduction.
From cross-section reduction given is:

Reduced diameter at 'Onset-of-diffuse necking' $d_{oon} = 3.89$ mm,
at 'Onset-of-ductile cracking' $d_{odc} = 3.78$ mm.

R-O-estimation of the two strength points at 'odc' and final ductile rupture:

$$\varepsilon_I^{pl}/2 = -\varepsilon_{rad}^{pl} = -\varepsilon_{tan}^{pl} \text{ and } \varepsilon_{rad}^{pl} = ln(r/a) = \varepsilon_{tan}^{pl},\ \varepsilon_I^{pl} = -2 \cdot ln(r/a)$$

$$\varepsilon_{eq}^{Mises} = \frac{\sqrt{2}}{3} \cdot \sqrt{((\varepsilon_I^{pl} + \varepsilon_{rad}^{pl}) - \varepsilon_{rad}^{pl})^2 + 0 + (\varepsilon_{rad}^{pl} - (\varepsilon_I^{pl} + \varepsilon_{rad}^{pl}))^2} == \frac{\sqrt{2}}{3} \cdot \sqrt{2\varepsilon_I^{pl\,2}} = \frac{2}{3} \cdot \varepsilon_I^{pl}$$

'Onset-of-ductile cracking' $\bar{R}_{odc}$, true $\varepsilon_{odc} = 14\%$

$$\varepsilon_{rad}^{pl} = ln(r/a) = ln(\sqrt{A/A_0}) = \text{?? \%},\ \varepsilon_{ax}^{pl} = -2 \cdot \varepsilon_{rad}^{pl}$$

$$\varepsilon = \varepsilon^{el} + \varepsilon^{pl} = \frac{\bar{R}_{odc}}{E} + 0.002\left(\frac{\bar{R}_{odc}}{R_{0.2}}\right)^n \rightarrow \cong \bar{R}_{odc} = R_{0.2} \cdot \sqrt[n]{\varepsilon_{ax}^{pl}} / 0.002 = 542 \text{ MPa.}$$

'Ductile rupture' $\bar{R}_{rup}$, true $\varepsilon_{rup} = 23\%$

$$\varepsilon_{rad}^{pl} = ln(r/a) = ln(\sqrt{1 - Z_0}) = 20.1\ \%,\ \varepsilon_{ax}^{pl} = -2 \cdot \varepsilon_{rad}^{pl}$$

$$\varepsilon = \varepsilon^{el} + \varepsilon^{pl} = \frac{\bar{R}_{rup}}{E} + 0.002\left(\frac{\bar{R}_{rup}}{R_{0.2}}\right)^n \rightarrow \cong \bar{R}_{rup} = R_{0.2} \cdot \sqrt[n]{\varepsilon_{ax}^{pl}} / 0.002 = 564 \text{ MPa.}$$

LL:

**The established test curve beyond R^t inherently involves the effects of σ_{hyd} and increasing void growth.*

**The application of the Bridgman-correction is not sufficient for the prediction of a very large forming process. However, for design it is sufficient because the allowable design strains are just of a few percent.*

**The Bridgman-correction is applied by using the 'Mises' yield condition and not a 'Gurson-type' void growth-capturing yield condition. This led the author 20 years ago to propose his so-called 'Extended Mises' yield condition, presented in the following chapter.*

** Measurements prove that for the same strain value of the growing tensile yield surface it holds that equi-biaxial stress ('strength') $\bar{\sigma}^{tt}(2D) > \bar{\sigma}^{t}(1D)$. This equi-biaxial ductile tensile behavior is sign-oppositely similar to brittle concrete in the compressive domain, where $\bar{R}^{cc} > \bar{R}^{c}$ and demonstrates the validity of the 120°-axial symmetry in the ductile case too! This means, the Lode angle is to consider and – again - the invariant J_3 helps to map*

** The applicability of axial measurement ends with 'End-of-uniform elongation' at !.*

Fig.16.3-9 up (AA2219) shows the test data crosses. The R-O function maps the true F_{ax}/A test data set curve very well.
The *middle* graph proves that the application of a cross-section reduction measurement makes sense at 'onset-of diffuse necking', first.
The *bottom* graph visualizes with the decaying magenta-colored equivalent Mises stress curve the reduction of ductility compared to F_{ax}/A.

The application of the Bridgman model is limited to about 30% cross-section reduction, due to not considering the void growth when moving from

$$\text{true } F_{ax}/A \equiv \text{true}\,\sigma_{eq}^{Mises}\ (\sigma_I = \sigma_{ax}) \rightarrow \text{ corrected true}\,\sigma_{eq}^{Mises}(\sigma_I, \sigma_{hyd}).$$

In order to consider the void growth, the author proposes to replace the Bridgman-corrected Mises-model, presented some pages before and down again, by the simple ***'Gurson model-linked Extended Mises-model'***:

$$\frac{3J_2}{\bar{R}_{0.2}^{t\ 2}} = c_\tau^{\text{Mises}} \quad \Rightarrow \quad \frac{3J_2}{\bar{R}_{0.2}^{t\ 2}} + c12\frac{I_1^{\ 2}}{\bar{R}_{0.2}^{t\ 2}} = c_\tau^{\text{ExtMises}}$$

$$\text{corrected true}\,\sigma_{eq}^{\text{Mises}} \quad \Rightarrow \quad \text{corrected true}\,\sigma_{eq}^{\text{ExtMises}}.$$

$$\sqrt{3\cdot J_2} = \sigma_{eq}^{\text{Mises}} = \frac{F}{A} / (1+2\cdot\rho/a)\cdot\ln(1+a/2\cdot\rho)\text{ , valid} > \bar{R}^t \text{ or } A < Aoon,$$

$$\sqrt{3\cdot J_2 + c12\cdot I_1^2} = \sigma_{eq}^{\text{ExtMises}} = \frac{F}{A} / (1+2\cdot\rho/a)\cdot\ln(1+a/2\cdot\rho)\text{ , valid } \bar{R}^t < \bar{R}_{odc}\ .$$

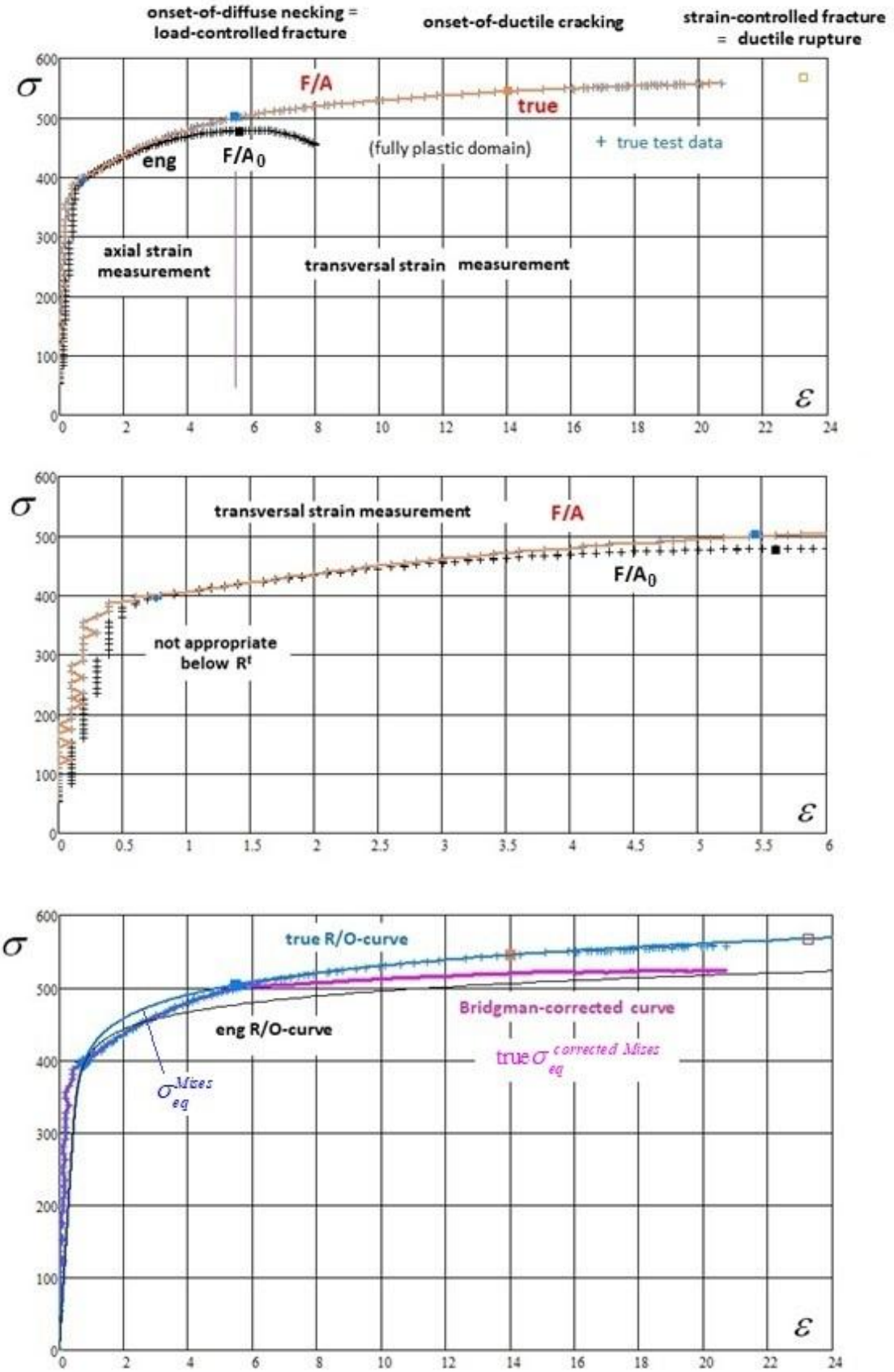


Fig.16.3-9: True and engineering test data courses, R/O-mapped test data courses and Bridgman-corrected curve beyond load-controlled fracture strength R^t. $\sigma_{ax}^{true} = \sigma_{ax} \cdot (1 + eng\varepsilon_{ax})$, $\varepsilon_{ax}^{true} = \ell n(1 + eng\varepsilon_{ax})$. F = uniaxial F_{ax} , σ_{eq} = multiaxial

Tri-axiality Factor TrF:

Since, for example in notches, tri-axialities in the range of 1 occur, a fracture failure surface must of course also be provided in this area of application. This applies to both the load-controlled and the strain-controlled failure surfaces. Therefore, test specimens with higher degrees of tri-axiality must also be examined. It should be noted that *TrF* usually increases further with increasing necking from an initial value. Achievable initial values for the different specimens are in the following table:

Table 16.3-1: Possible tri-axialities realized in test specimens

Specimen type	notch factor K^t	TrF		Triaxiality $TrF = \sigma_{mean} / \sigma_{eq}^{Mises}$	possible TrF domain
torsion bar	1	0		Flat tesile test specimen, unnotched	1/3
round bar	1	1/3		Cruciform	1/3 → 2/3
pressure tube	1	0.577		Notched round tension bars	2/3 → 5/3
crucimen	1	2/3		Tubes	0 → 2/3
round bar	> 1	0.49 → 0.95			

<u>*Fig.16.3-10*</u> gives an overview of how the lines of constant *TrF* run in the cross-section of the rotationally symmetrical failure body.

For a mechanically accurate evaluation of the rod test data the determination of the triaxiality *TrF* is a concern. The center axis r = 0 contains the 'hot spot' and is marked by *max*TrF

$$TrF(r) = \sigma_{mean} \,/\, true\sigma_{eq}^{Mises} = (I_1 / 3) / \sqrt{3J_2} = \left[\sqrt{2} / 3\right] \cdot (I_1 / \sqrt{3}) / \sqrt{2J_2} \quad .$$

From the results above the invariants can be deduced

$$\sqrt{3J_2} = \frac{F}{A} \cdot [\,(1+2\rho / a) \cdot \ln(1+a / 2\rho)] \quad \text{with} \quad \text{F, A, } \rho\text{, a} \quad \text{linked to another} \quad \text{and}$$

$$I_1 = max\,\sigma_{ax}^{t} + max\,\sigma_{radial} + max\,\sigma_{hoop} = \sqrt{3 \cdot J_2} + 3 \cdot \sigma_{hyd} = \sqrt{3J_2} \cdot [1 + 3 \cdot \ell n(1 + \frac{a}{2\rho})] \,.$$

This leads in the center, after insertion of the two invariants, to the highest TrF-value, reading

$$TrF(r = 0) = \sigma_{mean} \,/\, \sigma_{eq}^{Mises} = (I_1 / 3) / \sqrt{3J_2} = \frac{1}{3} \cdot [1 + 3 \cdot \ell n(1 + \frac{a}{2\rho})] \;>\; \frac{1}{3} \quad \text{(if smooth)} \quad .$$

<u>*Mind:*</u> Assuming equally distributed flaws in a specimen a tension <u>strip</u> specimen possesses a higher ratio of surface area/volume than the smooth tensile <u>rod</u>. It includes therefore more flaws at the surface in relationship to the volume. This results in a higher risk of fracture than for the rod.

<u>*LL:*</u>

** Tensile tests deliver information on the integral (global or average) response and if DIC is used they provide additional surface strain results as evaluation input*

**All the used equivalent stress-strain curves ($\overline{\sigma\varepsilon}$) are smeared cross-section quantities of the test specimen*

**Bridgman converts the true uniaxial stress as a function of the true uniaxial plastic strain in the neck into an equivalent smeared stress-strain curve applicable in multi-axial FEA. The approach does not consider voids generated beyond 'Onset-of-necking'. The Bridgman correction deals with a dense material, called matrix*

*'Gurson models' separate the dense 'Mises described, void free so-called matrix from a model part that considers the void growth after 'Onset-of-necking' via co-agglomeration of the voids before final rupture starts.

* Tensile strength is not used in the construction of ductile static elements, since the design practices prescribe the use of the yield strength.

*For 'Mises-describable' ductile material behavior σ_{hyd} has no influence on yielding or σ_{eq}^{Mises}. In the negative case $p_{hyd}=\sigma_{hyd}$ this behavior is called 'pressure insensitive'.

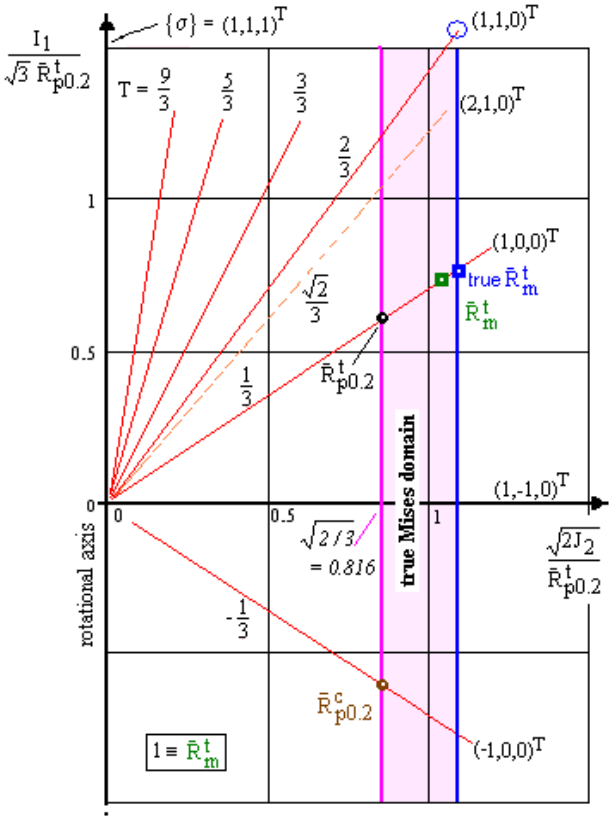


Fig.16.3-10:

Schematic graph visualizing tri-axiality values.

Assumption average curves,

Onset-of-ductile cracking and ductile rupture

Fig.16.3-11 intentionally will inform about the very different stress-strain curves used and further *Fig.16.3-12* on the porosity distribution in the neck cross-section. Both these features play a role when replacing the Mises approach in the Bridgman correction by a Gurson approach.

IWF-Freiburg performed computations (*contract with MAN*) on finding a distribution of the porosity in the neck center and found: If there is a significant decay of strength in one FE element of the envisaged structure *tensile rod* averaging over the whole cross section is no longer meaningful, a stress-strain relation could be calculated for this respective element. However, here is no means to compare it with the experiment since the latter only delivers the global response, i.e. an average value.

Material source: AA2219 variant, T2, t = 6mm plate. Sample size n = 179, test specimen tensile rod d = 4.0mm, A5 = 7.4 %, Z = 20.1 %,

$R^t = 479$ MPa , $R_{0.2} = 395$ MPa , $E_0 = 70000$ MPa , $\ell_0 = 20$ mm (gage)

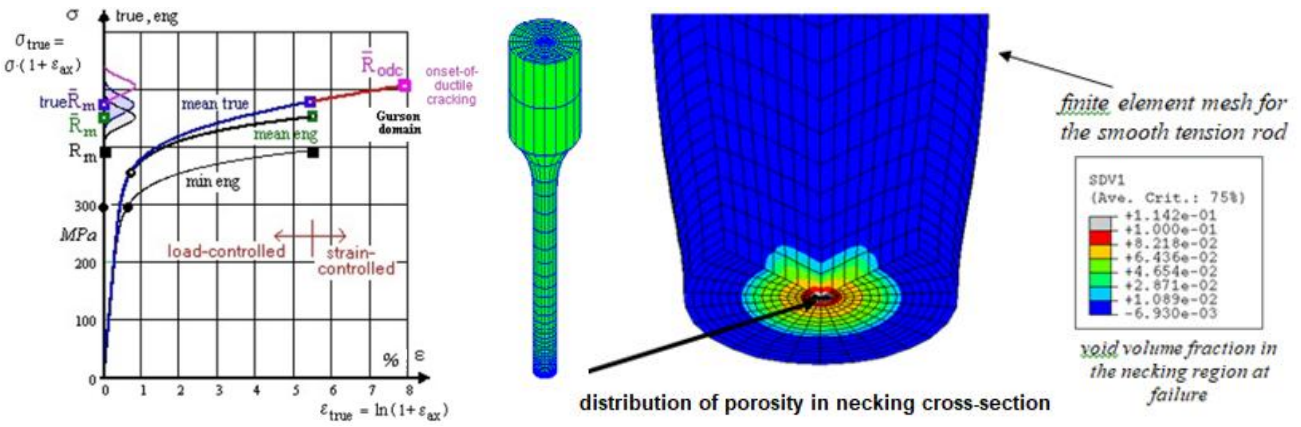


Fig.16.3-11: Presentation of the different stress-strain curves
Fig.16.3-12: Porosity distribution in the 'Hot spot' center of the tensioned rod. AA2219, Elasticity properties are E =70000MPa, ν =0.3)

Data sets achieved from R. Schiffmann [*Sch01*] were evaluated and the rersults displayed in the following table. In addition given are the associated original *TrF*-values generated in the elastic range.

The test campaign contained a set of typical un-notched (smooth) and pre-notched test specimen. All values move into the direction of the hydrostatic stress axis, $TrF = \infty$ or $\{\sigma\}=(1,1,1)^T$, according to the stress re-distribution caused by increasing plasticity.

Table 16.3-2: Evaluation of test results of differently necked round tensile bars, from [Sch01]

$\{\sigma\}/R_m^t$	$\sigma_{eq}^{Mises} / \bar{R}_m^t$	ε_{eq}^{Mises}	ε_I	ε_{II}	ε_{III}	TrF
$\bar{R}_{p0.2}^{\,t} = 352$ MPa, $\bar{R}_m^t = 453$ MPa, $\bar{A}_{gl} = \bar{\varepsilon}_{oon}^{\,pl} = 5.7\%$, $\bar{n} = 12.7$, $\bar{E}_0 = 70000$ MPa AA2219 type						
(1, - 0.5, 0)	1.32					0.13
(1, 0, 0)	1	5.05	5.70	-2.72	-2.72	1/3
(1, + 0.5, 0)	0.83	1.15	1.54	0.13	-1.29	0.58
(1, 1, 0)	1	5.02	2.97	2.97	-5.41	2/3
(1.15, 1.15, 0.5)	0.65	0	0.43	0.43	-0.12	1.44
(1, 1, 1)	0	0	0.26	0.26	0.26	∞

In [*LaRosa00*] for instance an investigation is executed to improve the Bridgman correction for notched and un-notched round test specimens.

LL:

- *'Onset-of-necking' (index oon) is, when the decrease of the cross-sectional area is greater than the increase in load carrying capacity of the test specimen due to work (strain) hardening. Further elongation occurs under decreasing external tensile loading of the bar*
- *Pre-conditions of a successful analysis of ductile materials are: (modeling requires bar over!)*

**Stress-strain curve $\bar{\sigma}_{eq}(\varepsilon_{eq})$ that considers $\bar{\sigma}_{hyd}$ (Bridgman approach) and porosity (Gurson approach, described by a so-called dense matrix part (Mises) and a porous part*

**Yield (flow) condition: 'Mises' below $\bar{R}^t$ for the dense material and beyond $\bar{R}^t$ a 'Gurson' type one to map the increasingly porous becoming material*

**Failure criteria: Mises for 'Onset-of -yielding' at $\bar{R}_{02}$ and load-controlled for 'Onset-of-fracture' at ($\bar{R}^t$, ε^{pl}_{oon}) and further, strain-controlled a Gurson type for 'Onset-of-ductile cracking' at ($\bar{R}^t_{odc}$, ε^{pl}_{odc}) before the final or ultimate ductile rupture occurs $\bar{R}^t_{rup}$*

- *The deformation-controlled testing in the softening domain requires a very high frame stiffness.*

16.3.3 Properties of a very Brittle Material (example: concrete)

Properties: $\{R\} = (R^t, R^c)^T$ with μ ; $\{E\} = (E,\ \nu)^T$ including ν, whereby $G = E/(2+2\cdot\nu)$

R^t, R^c are measured according to the Standards. In construction, the very low and not used tensile strength R^t of concrete is usually estimated by the so-called Brazilian Disk method. The compressive strength is measured in a test rig as shown below. According to the height of the friction value μ and the flaw distribution the test specimen fractures as depicted left. The friction value μ is determined like $\mu_{\perp\perp}$ for the transversely-isotropic material. The determination of the p*hysical properties* α_T, λ , c is not subject here.

Fig.16.3-12 presents test rig and specimens for compression as the basic loading situation.



Fig.16.3-12: Brittle materials. Test rig and test specimens of concrete

As already discussed in the associated previous chapter multi-axial compression testing is performed under axial loading with hydrostatic pressure. This requires tests on distinct stress states involving the three meridians: Tensile Meridian TM (ϑ = +30°) inside located meridian with respect to the 120°-symmetric fracture body, Neutral Meridian NM (0°) and Compressive Meridian CM (ϑ = -30°), outside. Test points lie on the respective meridian, determined by ϑ, which means on

different distances from the axis for a specific value of $I_1 / \sqrt{3 \cdot \bar{R}^t}$. The tensile strength is used for normalization in the case of brittle materials. In construction usually 'Design by analysis' is only possible on top of a reliable material property basis.

Evaluation of experiments with interpretation by numerical analyses of the test results:
The verification of a '*design by test'* has to be performed in the Qualification-test on load level for a load-quantity as the main design parameter such as for a force, a moment or a pressure. In case of load combinations such as "moment with axial force" a CoStly interaction test program has to be run. Or the theory has to be employed to relate the loadings to a stress state being then able to deliver margins of safety or reliability for the combinations. These combinations usually represent worst case conditions.

Finally, an evaluation of a tensile test series of a semi-brittle matrix material is presented.

Example: Statistical evaluation of a bending fracture test of an epoxy resin test specimen

1 Task Determination of the basic distribution parameters μ_R , σ_R, f_R and the lower tolerance limit.
Assumption: Bending fracture stress practically represents the tensile strength.

2 Test data set and statistical evaluation (performed in the nineties)
The table below lists the measurement results of a sample of n = 30 measurements together with the associated statistical evaluation. Checks regarding the type of the distribution have been carried out.
Load F acts at center of the hinged beam. Strength evaluation follows $\bar{R}_j^t$ = (F·L / 4) / w·h^2 / 6).
Test conditions: Room temperature, short-term loading, bending fracture strength

w_j width	h_j height	$F_{b\,j}$	$\bar{R}_j^t$
mm	mm	N	N/mm^2
4.050	10.08	395.7	115.2
3.904	10.53	346.7	96.0
4.968	10.72	296.7	77.9
3.943	10.19	365.3	106.9
4.124	10.43	388.0	103.6
4.095	10.22	346.4	97.1
4.074	10.63	337.9	87.9
4.239	10.45	393.5	102.0
4.173	10.07	359.3	101.8
3.686	10.10	332.0	105.8
3.718	10.08	358.4	113.8
3.941	10.23	337.2	97.9
3.686	10.62	308.3	82.6
4.026	10.32	396.2	110.7
4.226	10.38	374.3	98.5
3.963	10.56	361.0	98.0
4.142	10.41	388.7	103.7
4.174	10.30	303.3	82.1
3.940	10.65	352.0	94.3
3.908	10.19	323.8	95.7
3.972	10.23	407.1	117.3
4.175	10.79	416.4	102.6
3.863	10.48	382.6	108.2
3.896	10.85	334.5	87.4
4.070	10.62	341.0	89.0
4.141	10.35	364.3	98.3
4.110	10.36	361.1	98.1
4.089	10.74	380.1	96.5
3.830	10.37	380.2	110.6
4.088	10.65	409.7	105.9

4.02	10.43	361.0	99.6	$\bar{x}_{30}$
0.14	0.23	31.7	9.8	s_{30}
NV	NV	NV	=NV	f(x)
3.5%	2.2%	8.8%	9.9%	cov_{30}

3 Estimation of the statistical parameters of the basic distribution

Simple estimation:

For the purpose of demonstrating the calculation method in view of the sample size n, as "estimator" for the mean of the basic population μ the value $\bar{x}$ is used and s as "estimator" for the basic standard deviation σ without taking into account confidence intervals. This procedure is the right one for test recalculation. This procedure results in $\mu_R = \bar{x}_{30}$; $\sigma_R = s_{30}$; cov = σ/μ . For the Lower Tolerance limit - chosen as 3σ-value - follows $LT_R = \mu_R - 3\sigma_R = 99.6 - 3 \cdot 9.8 = 70.2$ N/mm^2.

Application of a statistics code:
The statistical evaluation was carried out with the program STATREL [*RCP collaboration with MAN*] for the tensile strength R^t. For this purpose, the Normal Distribution (ND), the lognormal distribution (LogND) and the Weibull distribution (WD) have been considered as distribution functions. For each of these distributions, a maximum likelihood estimate is performed and then a χ^2- test for the assumed distribution function. This will result in the following significance probabilities: ND: 0.079, LogND: 0.055, WD (τ=0): 0.572. So the Weibull distribution is preferable to the other models.
The parameters of the Weibull distribution, estimated according to the maximum likelihood method, are for known lower limit τ = 0, w = 103.3 N/mm^2 and k = 11.8 (without dimension). Then, the lower 10% quantile is determined as 85.8 N/mm^2 and the MIL-B value determined by an asymptotic method becomes 78.9 N/mm^2.

LL: Not the average strength is only decisive, but also its scatter, because the scatter essentially affects the strength design allowables to be determined.

Example: It is design relevant to sort out the most affecting variable and reduce its *scatter!*

Probabilistic Evaluation of the Bending Tests of a simple Epoxy Beam

1 Task How worthwhile is it to reduce the scatter of that variable that impacts a reliability target, the survival reliability $\Re = 1 - p_f = 1 - 3 \cdot 10^{-6}$ or a required nominal MoS = 0.30 most.

DLL (Sichere Last) = Upper Tolerance limit value $UT_S = \mu_S + 2 \cdot \sigma_S$;

Strength: $LT_R = \mu_R - 3 \cdot \sigma_R = \mu_R (1 - 3 \cdot cov_R)$.

2 Design Verification calculation

- Mechanical model: Line loading; Bending beam system:
  Failure model with definition of failure modes:
  - Critical location: beam center at L/2
  - **Material is brittle (due to shock hardening), homogeneous, isotropic. Linear elasticity is valid**
  - Fracture failure from bending

  according to $\sigma = (q \cdot L^2/8) / (w \cdot h^2/6)$ = moment / area moment of resistance.

  - Limit state function: $g = g(\underline{X}) = g(q, w, h, R^t) = R^t - \sigma^t = 0$ (*with σ being a stress here*)
- Stochastic Model of the 5 design variables X_j

fixed	L			
scatter	q	w	h	geometry
scatter	R^t			strength

X_j	μ_j	cov_j	f_j
L	80.0 mm	0	-
q	4.0 N/mm	0.05	Gumbel D
w	4.02 mm	0.03	ND
h	10.43 mm	0.02	ND
R^t	99.6 N/mm^2	0.099	WD

- Logical model of the failure system:
  Series system,
  - No redundancy and correlation.

- Solution:

$p_f = P\ (R \le S) = P\ (R-S \le 0) = P(g(\underline{X}) \le 0 = \int_V f_{\underline{X}}(x)\ dx$

Integration of 4-dimensional density function $f_{\underline{X}}$ in the failure domain V, meaning $g_1 < 0$, with the code COMREL (COMposite RELiability) of [*RCP Munich with MAN*]. X_1 is fixed, X_2 through X_5 are scattering quantities or uncertain basic variables.

3 Solution and Evaluation *[RCP]*

The calculation with COMREL of the **reliability ℜ** or of p_f results in a value for the reliability index β. From COMREL (First Order Reliability Method) FORM an approximate β–result β_{FORM} = 3.98 is obtained. Another way is executed by exactly formulating the stress as a random variable dependent on the uncertain basic variables. 'Design point' with the coordinates x^*_j (*most probable failure point*) and sensitivities α^*_j are tabled below. Probability of failure $p_f\ (\beta = 3.94) = 4.07 \cdot 10^{-5} > 3 \cdot 10^{-6}$ → specified ℜ was not met.

MoS: For $\sigma^t = 0.75 \cdot q \cdot L^2/(w \cdot h^2)$ approximately is achieved a LogND with $\mu_\sigma = 44.2$ N/mm², $\sigma_\sigma = 3.32$ N/mm²; and further $\mu_R{}^t = 99.6$ N/mm² and $\sigma_R{}^t = cov_R{}^t \cdot \mu_R{}^t = 0.099 \cdot 99.6 = 9.86$ N/mm² (*with σ standard deviation*) and $MoS_{nominal} = LT_R/UT_S - 1 = (\mu_R - 3 \cdot \sigma_R)/(\mu_S + 2 \cdot \sigma_S) - 1 \approx [99.6 \cdot (1 - 3 \cdot 9.86) / (44.2 + 2 \cdot 3{,}32)] - 1 \approx 0.38$ → nominal MoS is met.

(*For comparison the not allowed* $MoS_{central} = \mu_R / \mu_S - 1 = (99{,}6 / 44{,}2) - 1 = 1.26$)).

β_{FORM}	3.98
β	3.94

X_j	$X°_j$	α_j
q	4.10	-0.161
w	3.96	0.104
h	10.3	0.129
R^t	96.7	0.973

LL:

** Not only the increase of a strength property is important, but as it is depicted above, the scatter has a high impact*

** Above the strength variable R is of highest influence (α = 0.973). A reduction of its scatter essentially increases the survival probability. It is worthwhile for design to execute as much tests as possible on the strength variable in order to increase the strength design allowable*

** Sensitivities give a hint to sort out, where design-improving production tolerance limits one could get narrower there, where it is more economic. The sensitivity measures outline their influence on the target reliabilty. This procedure helps to achieve the desired Robust Design.*

[DenUIij12] Den Uijl N J and Carless L J*: Advanced metal-forming technologies for automotive applications.* In Advanced Materials in Automotive Engineering, 2012

[Far16] Fariba F, Ahmadpour M and Bahrami H: *A new method for correcting the stress strain curves after bulging in metals.* J. of Stress Analysis, Vol.1, no2, winter 2016-17

[Fon14] Fonseca Iván Darío Romero: *Correction of the post-necking true stress-strain date using instrumented nano-indentation*. Diss.2014

[LaRosa03] La Rosa G, Risitano A, Mirone G: *Post-necking elastoplastic characterization: Degree of approximation in the Bridgman method and properties of the flow-stress/true-stress ratio*. Metall MaterTrans A. 2003;34 (3):615-624.47

[LeR81] Le Roy G, Embury JD, Edwards G, Ashby MF. *A model of ductile fracture based on the nucleation and growth of voids.* ActaMetall. 1981;29 (8):1509-1522

[Kal15] Kalpakjian S and Schmid S: *Evaluation of the Possibility of Estimating Cyclic Stress-strain Parameters and Curves from Monotonic Properties of Steels*. Manufacturing Engineering & Technology. 2013: Pearson Education.

[Zid10] Zidane I, Guines D, Leoting L and Ragneau E: *Development of an in-plane bi-axial tensile test specimen for limit strain analysis by FEM.* Meas. Sci. Technol. 21, 055701 (2010)

[Zha20] Shengwen Tu,| Xiaobo Ren,| Jianying He,| Zhiliang Zhang: *Stress–strain curves of metallic materials and post-necking strain hardening characterization: A review*. Fatigue Fract Eng Mater Struct. 2020;43:3–19.

16.4 Transversely-isotropic UD-materials Testing

Table 16.4-1 reminds about the properties to be provided in case of fiber-reinforced materials.

Table 16.4-1: Properties of various homogenized fiber-reinforced materials

• **UD-lamina** (transversally-isotropic, isotropic ⊥ to fiber direction or lamina plane)

2D: $(\sigma_1, \sigma_2, \tau_{12})$ $(R_{\parallel}^t, R_{\parallel}^c, R_{\perp}^t, R_{\perp}^c, R_{\perp\parallel})$
$(E_{\parallel}, E_{\perp}\ G_{\perp\parallel}, \nu_{\perp\parallel})$ → 2D-shell elements

3D: $(\sigma_1, \sigma_2, \tau_{12}, \tau_{23}, \tau_{13}, \sigma_3)$ $(R_{\parallel}^t, R_{\parallel}^c, R_{\perp}^t, R_{\perp}^c, R_{\perp\parallel})$
$(E_{\parallel}, E_{\perp}, G_{\perp\parallel}, \nu_{\perp\parallel}, \nu_{\perp\perp})$ or $G_{\perp\perp} = E_{\perp}/(2+2\nu_{\perp\perp})$ → 3D-volume elements

"2,5"D (Extended shear deformation theory): Holds for $\ell > 5 \cdot t$ slenderness
$(\sigma_1, \sigma_2, \tau_{12}, \tau_{23}, \tau_{13})$
$(E_{\parallel}, E_{\perp}, G_{\perp\parallel}, \nu_{\perp\parallel}, \nu_{\perp\perp})$ → "2,5D"-shell elements

• **Mat lamina** (transversally-isotropic, quasi-isotropic in lamina plane)

2D: $(\sigma_x, \sigma_y, \tau_{yx})$ (R_m^t, R_m^c)
E, ν

3D: $(\sigma_x, \sigma_y, \tau_{yx}, \tau_{y3}, \tau_{x3}, \sigma_{3)}$ $(R_m^t, R_m^c, R_3^t, R_3^c, R_{3m})$
$(E_m, \nu_m, E_3, G_{3m}, \nu_{3m})$

• **Fabric lamina** (rhombically-anisotropic, Warp ≠ Fill)

2D: $(\sigma_W, \sigma_F, \tau_{WF})$ $(R_W^t, R_W^c, R_F^t, R_F^c, R_{WF})$
$(E_W, E_F, \nu_{FW}, G_{WF})$

3D: $(\sigma_W, \sigma_F, \tau_{WF}, \tau_{W3}, \tau_{F3}, \sigma_3)$ $(R_W^t, R_W^c, R_F^t, R_F^c, R_3^t, R_3^c, R_{WF}, R_{W3}, R_{F3})$
$(E_W, E_F, \nu_{FW}, G_{WF}, E_3, \nu_{3W}, \nu_{3F}, G_{W3}, G_{W3})$

"2,5D":

Table 16.4-2 depicts the requirements of the distinct lamina modelization.

Table 16.4-2: Modelisation of Laminas

Lamina	=	basic element of computation = homogenized Material
	=	plane, heterogeneous "structure"
UD-lamina	=	matrix + UD-fiber-reinforcement transversely-isotropic
Fabric lamina	=	matrix + fabric-reinforcement (orthotropic in the plane)
Mat-lamina	=	matrix + mat-reinforcement (isotropic in the plane)

with Material Properties applied such as

- macro-mechanical values from tests
- micro-mechanical values, only, if it is mandatory and if the micro-mechanical formula and determination of the constituents data are linked

16.4.1 Strengths, Elasticity Properties, Stress-Strain Curves

Dependent on the modelling very different input data sets are to provide for the structural analysis, because the modelling may be lamina-based, sublaminate-based or laminate-based.

Used test specimens shall be maximally correspond to the cured material of the plane or curved structural component. UD analysis requires:

$$\{R\} = (R_{\parallel}^{t}, R_{\parallel}^{c}, R_{\perp}^{t}, R_{\perp}^{c}, R_{\perp\parallel})^{T} \quad \text{plus} \quad \mu_{\perp\square}, \mu_{\perp\perp} \qquad \text{with} \quad 1 \equiv \square, \quad 2,3 \equiv \perp$$

$$\{E\} = (E_{\parallel}, E_{\perp}, G_{\perp\square}, G_{\perp\perp}, \nu_{\perp\parallel})^{T} \quad \text{including} \ \nu_{\perp\perp}, \nu_{\perp\parallel} \quad \text{whereby} \quad G_{\perp\perp} = E_{\perp} / (2 + 2 \cdot \nu_{\perp\perp})$$

The next figure presents a survey on possible test specimens collected by Tarnopolski as early as 1982.

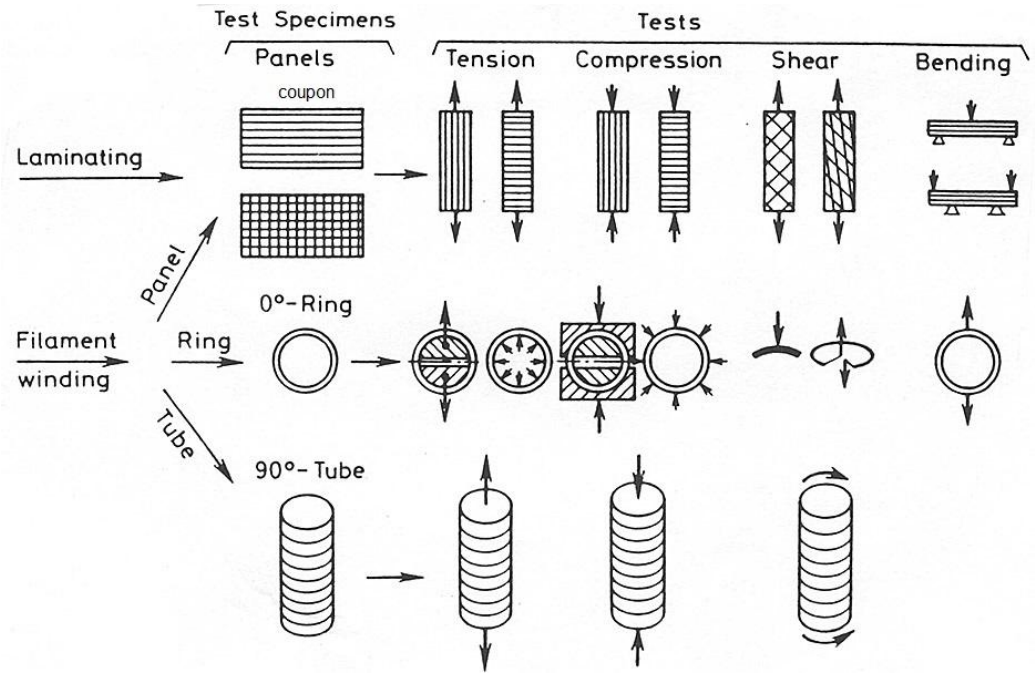


Fig.16.4-1: Test techniques for several test specimens [Tarnopolski 1981]

For Fiber-Reinforced Polymer (FRP) composites a variety of test standards are not yet available or qualified, appropriate test specimen procedures are partly missing. The figure above gives a

survey on the variety of possible test specimens used to determine strengths, fracture strains, stress-strain curves and elasticity properties.

Fig.16.4-2 displays the tension-compression-torsion test and the parts and points of the UD fracture body where uniaxial and multi-axial test results can be provided. Included is a picture of the tube test specimens applied at MAN where a tension/compression-torsion test rig was run.

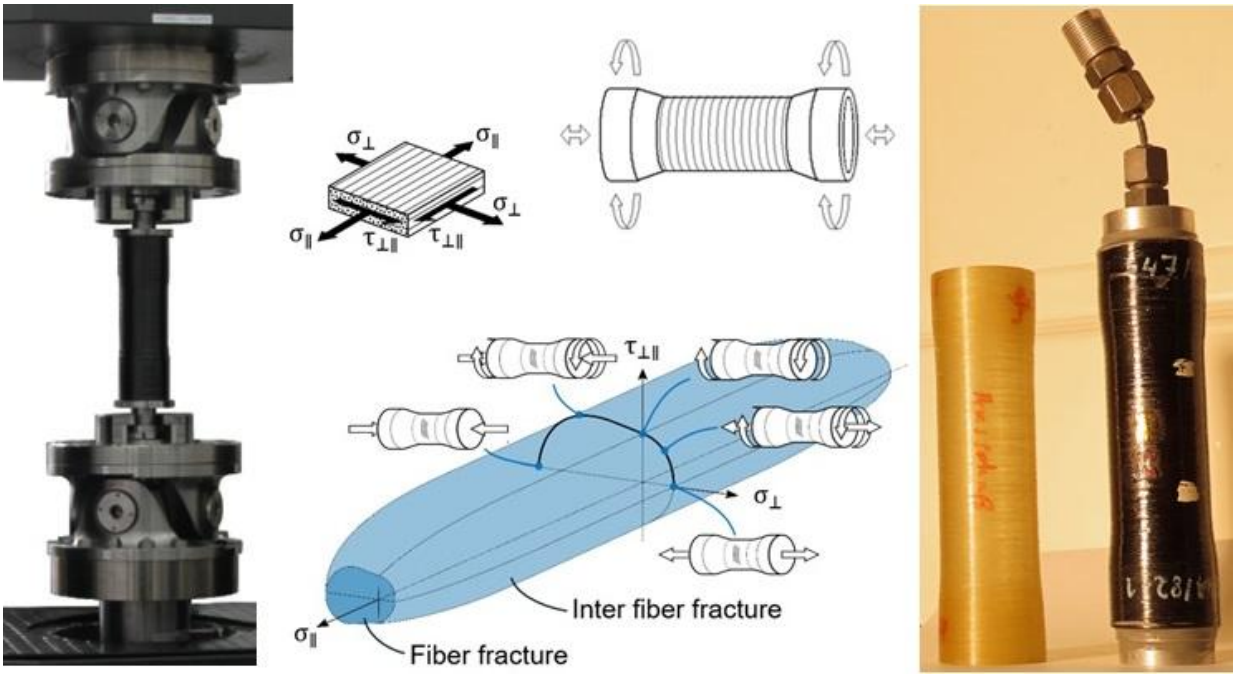


Fig.16.4-2: The tension-compression-torsion test: Test set-up Leibniz-Institut für Verbundwerkstoffe GmbH Kaiserslautern and (right) GFRP and CFRP test specimens of MAN Technologie

Fig.16.4-3 displays FMC-mapped bi-axial IFF curves. *In this context it shall noted again: Both, 0°-tubes and 90°-wound tubes are tested but the bi-axial test results cannot be simply put into the same graph as has been unfortunately done in* WWFE-I, TC2, *(see the presented distinct WWFE example).*

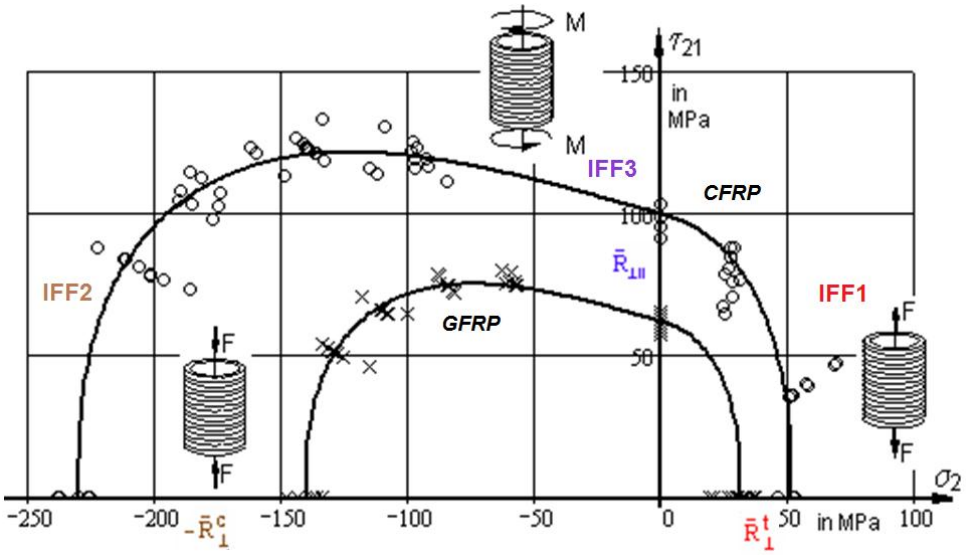


Fig.16.4-3: (σ_2, τ_{21})- fracture curves derived by a tension/compression-torsion test

Fig.16.4-4 gives a survey of measured uniaxial UD stress-strain curves provided in WWFE-I.

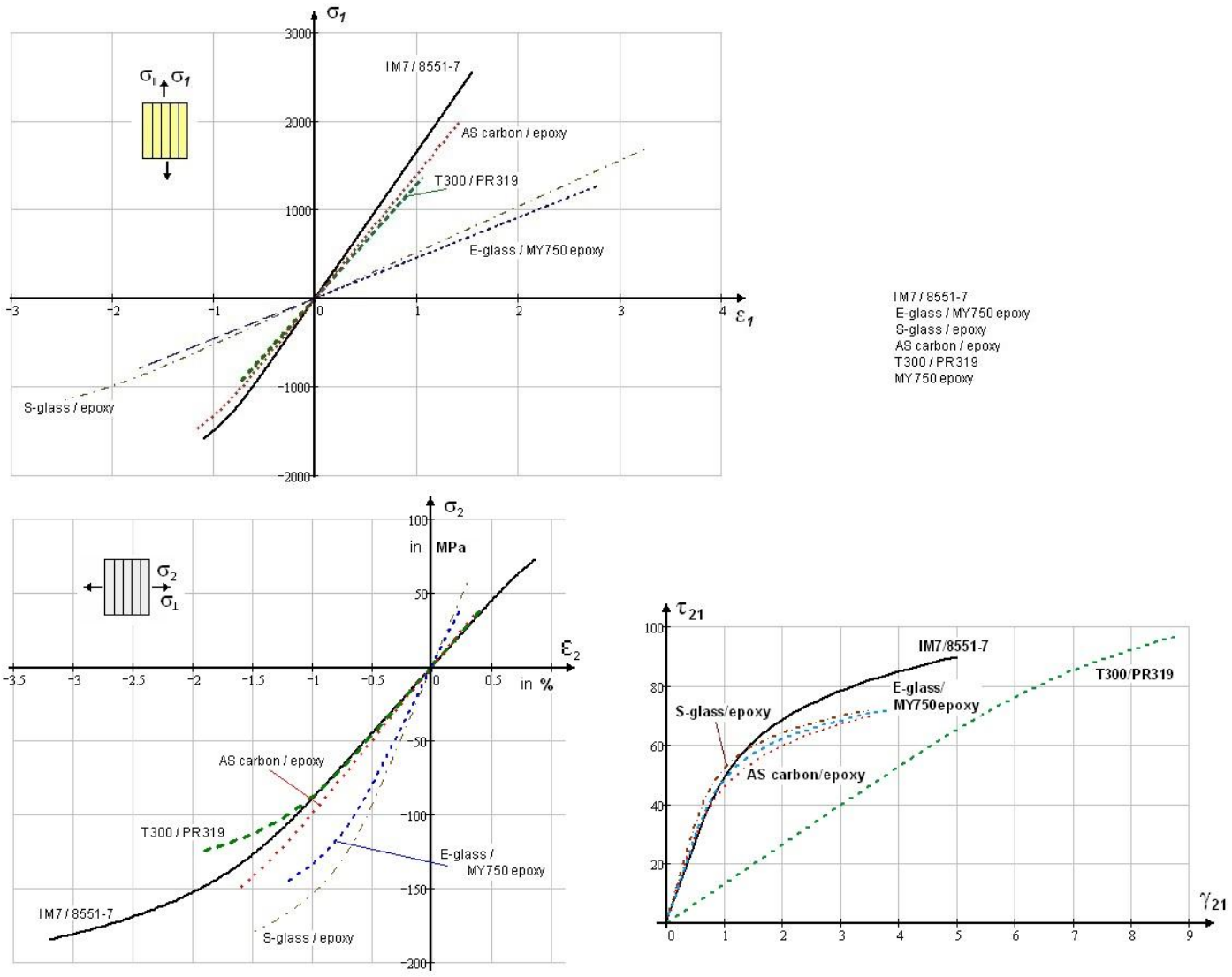


Fig. 16.4-4: Uniaxial UD stress-strain curves provided in the WWFE

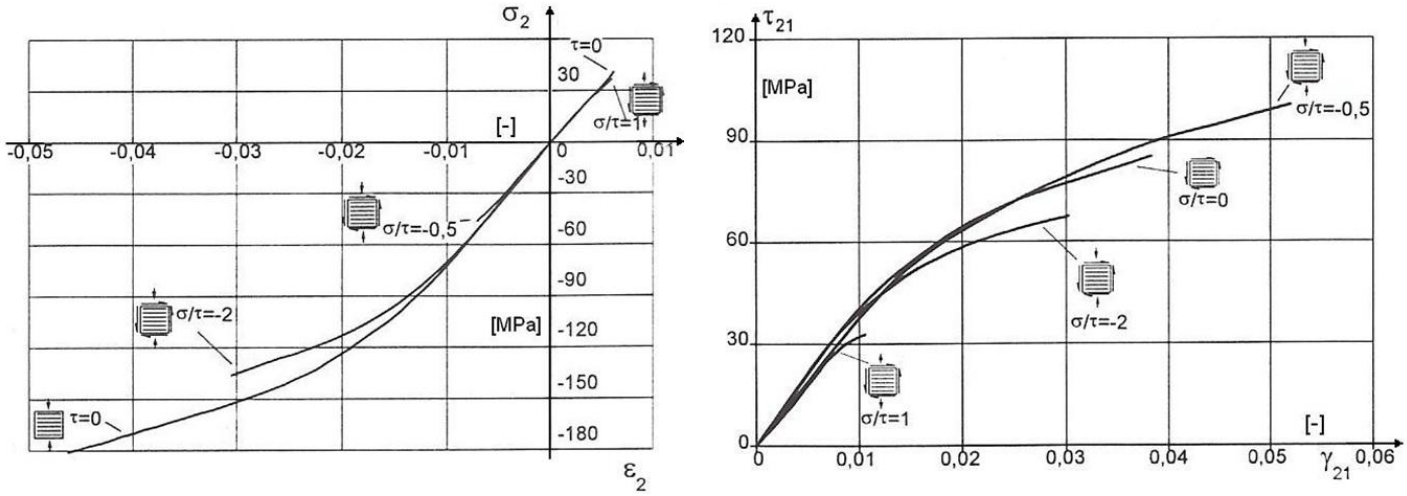


Fig16.4-5 Bi-axial UD stress-strain curves [courtesy IKVAachen]

Fig.16.4-5 presents different the transversal strain and the shear strain curves for several combinations of bi-axial stress states (σ_2, τ_{21}) . It would be helpful for future non-linear analyses to prove by the inelastic potential procedure that the chosen approach captures bi-axial stress and associated strain relations.

Note:
Above plots give a look how normal strain and shear strain change due to an acting bi-axial stress state. Continuum theory has to tackle this. The chosen potential must capture matrix yielding and micro-damage caused by the flaws. The plots represent bi-axial stress-strain curves that should be the output of the inelastic modelling.

16.4.2 Trial to estimate the level of Inter Fiber Fracture under bi-axial compression $\sigma_2^c = \sigma_3^c$

Considering Poisson's ratio a test specimen bi-axially compressed should Fiber Fracture (FF) without any external loading σ_1^t . Then filament fracture due to σ_f^t is the fracture stress [VDI97]. A bi-axial compression test is very difficult to perform: The test specimen is fitted into the groove by shims and loaded by the very stiff, practically non-deformable stamp. The crushing path is recorded as a function of the stamp force. An approximate detection of frontal surface deformation and longitudinal elongation ε_1 was carried out with sensors. The modelling with associated assumptions depends on how the test specimen behaves in the groove. It is first squeezed into the width under the "rigid" compression plate and thus contacts the "rigid" side walls. However, the broad squeeze is very low because of the shims and is neglected. After the contact with the side wall, a sidewall reaction σ_3^c is awakened with a further increase of $\Delta\sigma_2^c$ as a result of the obstructed transverse contraction. The test specimen rubs against the pressure plate and longitudinal surfaces during expansion, so that the stress state in the test specimen is not as uniform as desirable due to this friction effect.

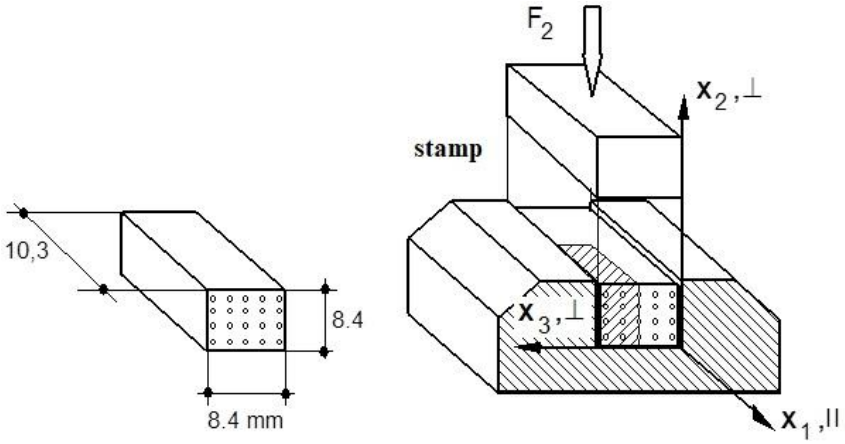


Fig.16.4-6: Loads and dimensions of test specimens and groove [VDI 97]

Due to the brittle behavior of FRP, it can be assumed that during the test essentially Hooke's general law of elasticity provides 3 equations for an estimation

$$\begin{Bmatrix}\varepsilon_1\\ \varepsilon_2\\ \varepsilon_3\end{Bmatrix} = \begin{bmatrix} 1/E_{\parallel} & -\nu_{\perp\parallel}/E_{\parallel} & -\nu_{\perp\parallel}/E_{\parallel} \\ & 1/E_{\perp} & -\nu_{\perp\perp}/E_{\perp} \\ \text{symm.} & & 1/E_{\perp} \end{bmatrix} \begin{Bmatrix}\sigma_1\\ \sigma_2\\ \sigma_3\end{Bmatrix}.$$

Due to the rigid walls, $\varepsilon_3 = 0$, so that with $\sigma_1 = 0$ at a given squeeze or compressive stress σ_2^c , the quantities σ_3 and ε_1 can be estimated from

$$\nu_{\perp\perp} \cdot \sigma_2^{\,c} / E_\perp = \sigma_3 / E_\perp \quad \text{or} \quad \sigma_3 = \nu_{\perp\perp} \cdot \sigma_2^{\,c} \rightarrow \varepsilon_1 = \frac{-\nu_{\perp\parallel}}{E_\parallel} \cdot (\sigma_2^{\,c} + \sigma_3) = \frac{-\nu_{\perp\parallel}}{E_\parallel^{\,t}} \cdot (\nu_{\perp\perp} + 1) \cdot \sigma_2^{\,c} .$$

For GFRP failure strains of about $e_{1f} = 2\%$ are obtained. Thus, in turn, an associated compressive stress under the stamp can be inferred, assuming $\nu_{\perp\parallel} = 0.3$ and $\nu_{\perp\perp} = 0.4$, of about

$$\sigma_2^{\,d} \approx -\varepsilon_1 . E_\parallel^{\,z} / (\nu_{\perp\parallel} \cdot (1+\nu_{\perp\perp})) = -0{,}02 \cdot 44500/(0{,}3(1+0{,}4)) \approx -2000 \text{ MPa}$$

which determines the maximum required test force of 200 kN.

For the comparison with the measurement results, the compression is essential For the comparison with the measurement results, the compression is essential

$$\varepsilon_2^{\,c} \cdot E_\perp = \sigma_2^{\,c} - \nu_{\perp\perp} \cdot \sigma_3 = \sigma_2^{\,c} \cdot (1-\nu_{\perp\perp}^{\,2}) .$$

Thus, a numerical estimation leads regarding the assumed values

$\varepsilon_1 = 1.9\ \%$; $\nu_{\perp\parallel} = 0.35$; $\nu_{\perp\perp} = 0.45$ (behavior approaches volume constancy, $\nu = 0.5$),

$E_\perp^{\,c} \approx 10000$ MPa (due to the not so high quality of this specimen and for linearization reasons not taken the usually typical 12500 MPa) to the following compressive stress and strain

$$\sigma_2^{\,c} \approx -1665 \text{ MPa} \quad \text{und} \quad \varepsilon_2^{\,c} \approx \sigma_2^{\,c} / (E_\perp (1-\nu_{\perp\perp}^{\,2})) = -21\ \% .$$

Note:
From above example one can learn: The fulfillment of a fracture condition is a necessary but not yet sufficient condition for the actual occurrence of a fracture. A potential shear fracture, for example, must also be able to form, which for instance is prevented by above rigid walls.

16.4. 3 Designing test specimens

The minimum number of necessary material parameters is given by the homogenized material symmetry demands.
Choosing and designing the associated test specimen follows some demands, example tube below:

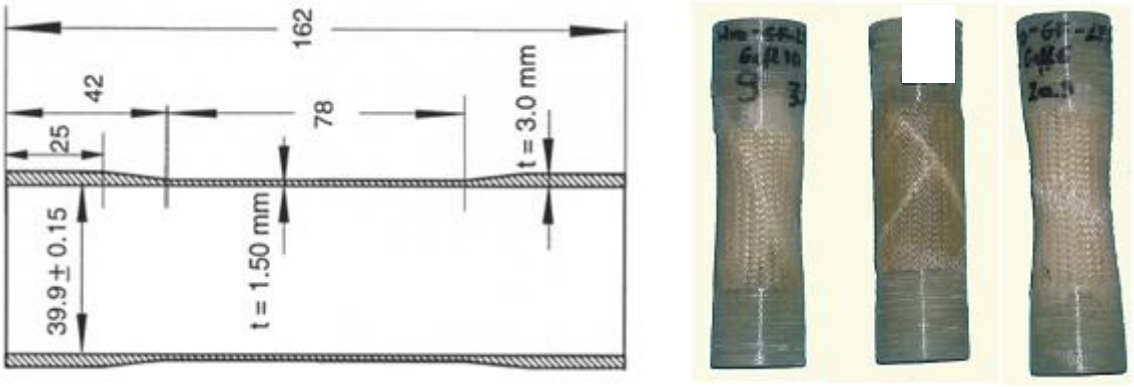


Fig.16.4-6: Tension/compression-torsion-tube test specimen, 90°-winding (UD) and tube failures

1. In the critical locations of the test specimen a distinct size of a homogeneous stress state domain should be given in order to clearly transfer the failure stress state into a uniaxial or a multi-axial strength.

2. Mechanical properties and stress-strain curves of metallic materials are determined using standard test specimens and procedures. According to these procedures, a uniaxial load is applied with a specified rate of displacement, elongation, shortening. Usually, engineering stresses and strains are determined. The engineering stress is the stress based on the initial cross-sectional area of the test specimen. It is the ratio of the applied load to the originally un-deformed cross-sectional area. The engineering strain is the total strain measured along the applied gage length.
3. The data set, obtained from the tests, is valid for the applied geometry of the test specimen, the rate of displacement and the temperature.
4. Similarity of the manufactured specimen's material and the material in the structural part is to be achieved as far as possible. This is the more valid for composite materials from isotropic concrete to orthotropic ceramic fabrics

In the *[VDI 97]* Weibull volume and Surface effects have been investigated. This could be only performed for geometries scaled by about 2. An effect could not be found which can be explained regarding the usual scatter.

The next figure gives some hints how to achieve different stress states by changing a distinct parameter. *Fig. 16.4-7* informs about possibilities to obtain different stress ratios with the same test arrangement by changing load ratios and when including a differently placed proof test layer.

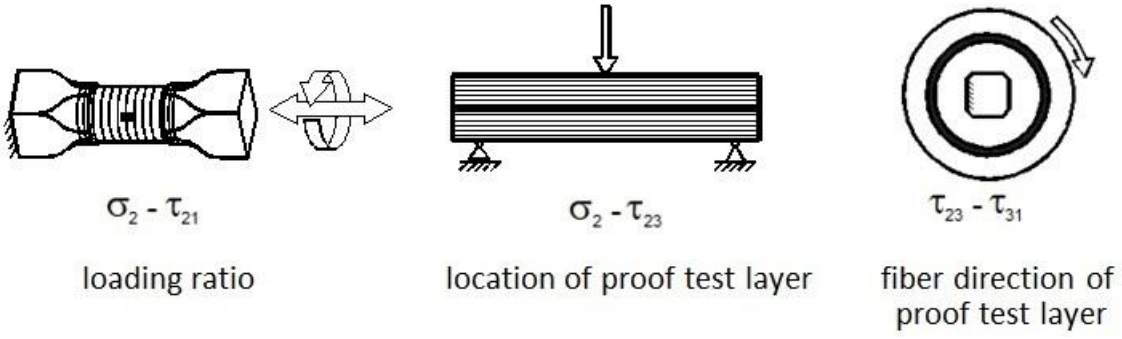


Fig.16.4-7: Test specimens for the generation of different stress states [VDI 97]

Example: Evaluation of 'Thin'-walled and 'Thick'-walled Test , Tubes

'Thin' walled tube : thin $t / d_{mean} < 1 / 10$; p_{int}, p_{out}

Torsion *:* $\tau_{mean} = M_t$ / true cross section area

Pressure *:* $\sigma_{ax}^{p\,int} = 0.25 \cdot p_{int} \cdot d_{mean} / t$ closed bottom

$$\sigma_{hoop}^{inner\ surface} = 0.5 \cdot p_{int} \cdot d_{mean} / t \cong \sigma_{hoop}^{outer\ surface}$$

$$\sigma_{radial}^{nner\ surface} = - p_{int} \quad \text{and} \quad \sigma_{radial}^{outer\ surface} = - p_{ext}.$$

'Thick' walled tube (p_{int}, p_{out})

$$\sigma_{ax}^{p\,int} = (p_{int} \cdot r_{int}^{\,2} - p_{out} \cdot r_{out}^{\,2}) / (r_{out}^{\,2} - r_{int}^{\,2}) \text{ if closed ends}$$

$$\sigma_{hoop} = [(p_{int} \cdot r_{int}^{\,2}) / (r_{out}^{\,2} - r_{int}^{\,2})] / (1 + r_{out}^{\,2} / r^2)$$

$$\sigma_{radial} = [(p_{int} \cdot r_{int}^{\,2}) / (r_{out}^{\,2} - r_{int}^{\,2})] / (1 - r_{out}^{\,2} / r^2)$$

(solid cylinder: $\sigma_{hoop}^{outer\ surface} = - p_{hyd} = \sigma_{radial}^{outerr\ surface}$)

Example of a test data table for CFRP, T300-epoxy, wound with rovings [*courtesy HSB***]**

procurement		**specification from manufacturer**					
fiber		Toray T300-6K-50B, Ø 7µm		ρ_f = 1.76 g/cm^3		V_f = 61%	
matrix		Araldite: LY556 / HT976		ρ_m = 1.30 g/cm^3			
curing specification		110° (8h) + 160° (12h)					
test temperature		23°C					
moisture of test specimen		normal moisture conditions (DIN 50005)					
Quantities		$\bar{x}$	$s/\bar{x}$ in %	n	„B-value“	„A-value“	reference
strengths							
Weibull-distributed (WD)	$R_{\|\|}^t$ in MPa	1650	4	15			
	$R_{\|\|}^c$ in MPa	900	7	6			
	$R_{\perp}^t$ in MPa	60	10	15			
	$R_{\perp}^c$ in MPa	180	9	6			
	$R_{\perp\|\|}$ in MPa	120	5	6			
	ILSS in MPa	90	5	6			
elasticity properties							
initial values (tangent moduli). Normal distributed (ND)	$E_{\|\|}$ in GPa	140	3	15		-	
	$E_{\perp}$ in GPa	8	4	6		-	
	$G_{\perp\|\|}$ in GPa	5.5	4	6		-	
	$\nu_{\perp\|\|}$	0.3	5	6	-	-	
	$\nu_{\perp\perp}$	0.4	5	6	-	-	
fracture strains							
Weibull-distributed (WD)	$e_{\|\|}^t$ in %	1.08		6			
	$e_{\|\|}^c$ in %	0.85		6			
	$e_{\perp}^t$ in %	0.68		6			
	$e_{\perp}^c$ in %	3.0		6			
	$e_{\perp\|\|}$ in %	4.0		6			
hygro-thermal properties							
assumed (ND)	$\alpha_{T\|\|}$	-1·10^{-6}/K			-	-	
	$\alpha_{T\perp}$	30·10^{-6}/K			-	-	
	$\alpha_{M\|\|}$	0			-	-	
	$\alpha_{M\perp}$	0.40			-	-	
glass point	T_g in °C						

Example: Statistical evaluation of compression tests of CFRP-HT test specimens

$E_{\|\|}^c$	$R_{\|\|}^c$	
/mm²	N/mm²	
197800	2304	
173400	1920	
148800	1558	
182700	2038	
194000	2072	
173200	1942	
168900	1758	
166800	2040	
179600	2038	
160000	2116	
179200	2276	
168600	1958	
154200	1652	
198100	2214	
187200	1970	
180500	1960	
194300	2074	
151700	1642	
176000	1886	
161900	1914	
203500	2346	
208200	2052	
191300	2164	
167200	1748	
170500	1780	
182200	1966	
180500	1962	
190000	1930	
190100	2212	
204900	2118	
179710	1987	$\bar{x}_{30}$
15708	195	s_{30}
0.087	0.098	cov_{30}

Test data evaluation and findings

$E_{\|\|}^c$ and $R_{\|\|}^c$ are positively correlated with a correlation coefficient of $\rho_{30} = 0{,}77$.

The Kolmogorov-Smirnov test, applied here despite the relatively small sample, shows a normal distribution for $E_{\|\|}^c$ and a Weibull distribution for $R_{\|\|}^c$ as the best assumptions.

Confidence limits for the mean of $E_{\|\|}^c$ are calculated at 173844 ↔185576.

A t-test for an actual value of $E_{\|\|}^c$ = 180000 N/mm² gives high significance.

The MIL-B strength design allowable $R_{\|\|}^c$ is calculated as 1572 N/mm² with an expected 10%-quantile of 1710 N/mm². [*RCP, MAN*]

16.4.3 Note on in-plane UD Poisson's ratio

The alteration of the major Poisson's ratio (here termed $\nu_{\perp\|}$) is linked to the failure behavior if it is brittle or to the yield state if ductile. In the brittle case successive micro-cracking reduces $\nu_{\perp\|}$ according to the generation of micro-spaces. Hence, in the case of shear failure under compressive lateral stresses the value of $\nu_{\perp\|}$ will be higher than that for tensile lateral stresses. Hydrostatic compression impedes the generation of micro-spaces until a finally pretty brittle fracture will occur. Therefore it is to be discriminated between tensile loading and hydrostatic compression loading.
Respecting the low effect Poisson's ratio often has in tensile loading - if using FRP with stiff fibers - the following estimation will be a good approach before failure occurs:

$F_{\perp}^{\sigma}$: $\nu_{\perp\|} = \nu_{\perp\|,0} \cdot E_{\perp,\sec} / E_{\perp,0}$. Also in the case of $F_{\perp\|}$ the value for $\nu_{\perp\|}$ is reduced similarly. In the case of multi-axial pressure Poisson's ratio might increase due to condensation. Possessing no input

for Poisson's ratio and with respect to the quality of the other affecting properties, for the compressive stress states the value is kept constant in the analyses.
For a lamina which is orthotropically to be treated, Poisson's ratio in the thickness direction is different $\nu_{31} \neq \nu_{\perp\parallel}$. The value depends on density and failure state.

16.5 Measurement of Friction Values $\mu_{\perp\square}$, $\mu_{\perp\perp}$

Also in compression and shear design of composite materials the use of material internal friction values is mandatory, but for their determination a standard does not exist. Tube test specimens are the best test specimens to measure the friction values.

16.5.1 Tension/compression-shear tube and test set-up

I In-plane friction $\mu_{\perp\parallel}$

The use of tube test specimens under torsion provides a good method to obtain a pure and homogeneous shear stress state if edge effects can be avoided. In the FMC approach the 'pure' failure mode conditions are just represented by straight lines! For fitting usually the least-mean-square fit is employed. In practice, the available average strength values are taken and a good estimation for the internal friction delivers the straight line $\mu_{\perp\parallel} = (R_{\perp\parallel} - \tau_{21}^e) / \sigma_2^e$.

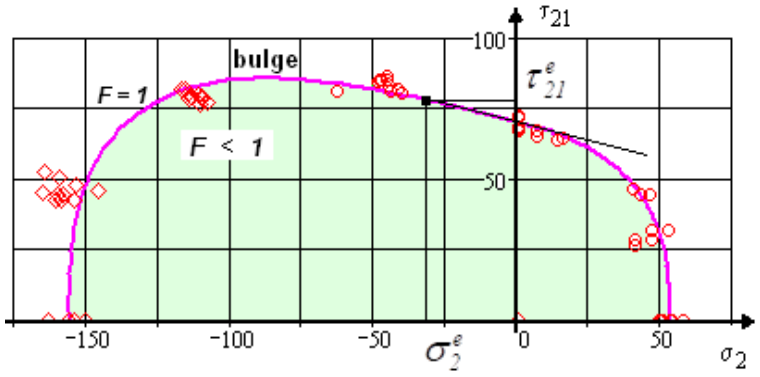


Fig.17.5-1: (σ_2, τ_{21})-IFF curve. Hoop wound GFRP tube, E-glass/LY556/HT976

II Out-of-plane friction $\mu_{\perp\perp}$

- Measurement of the friction angle (see below)
  One approach is to measure the occurring fracture plane angle Θ_{fp}. In a research project, compiled in [*VDI97*], test have been performed to determine $\mu_{\perp\perp}(\rho)$ as function of the friction angle ρ

$$C_{fp}^c = \cos(2 \cdot \Theta_{fp}^c{}^\circ \cdot \pi / 180°): \ \mu = -\tan\rho \cong - \ C_{fp}^c.$$

- Measurement of a bi-axial compressive fracture stress state
  The better way would be to bi-axially compress a test specimen and determine the fracture stress set in order to compute the friction value from $\mu_{\perp\perp} = (R_\perp^c + \sigma_3^e) / \sigma_2^e$. However, the danger to buckle is to face.

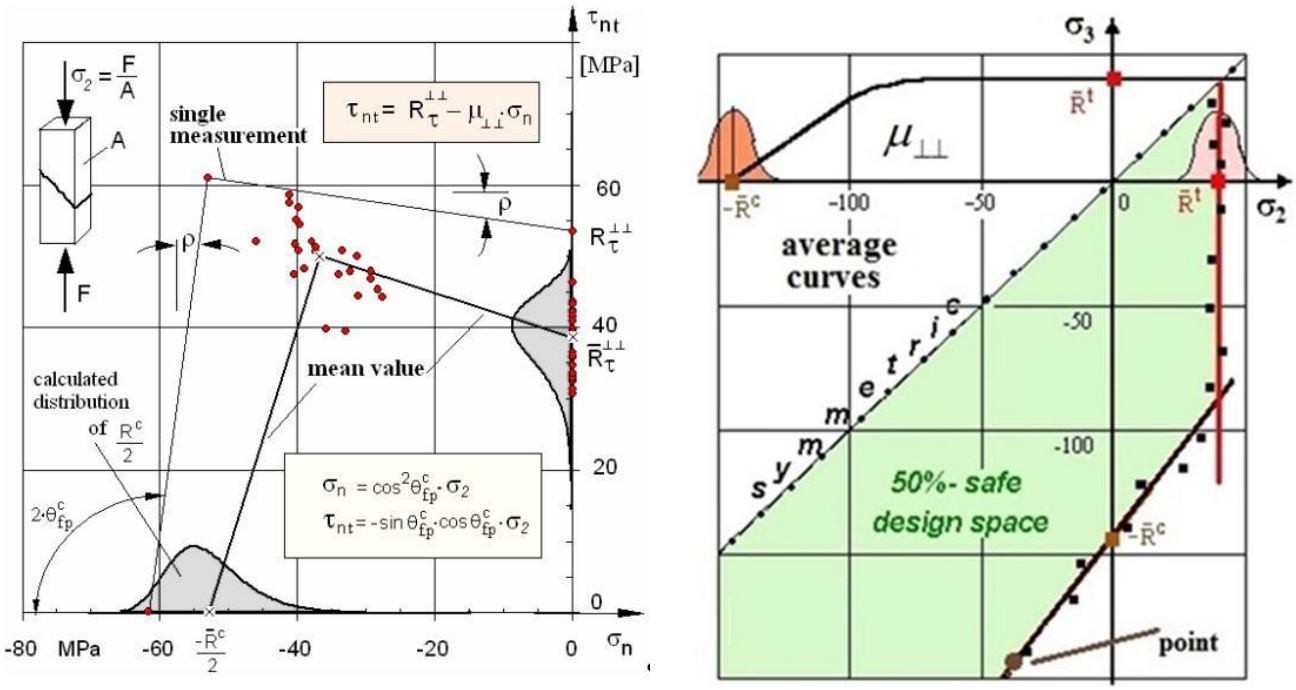


Fig.16.5-2: (left) Evaluation of prismatic transverse pressure samples with a "linear" friction approach. (right) Evaluation when obtaining a bi-axial compression test point (σ_3^e, σ_2^e)

16.5.2 Measurement with ARCAN test set-up [Pet15], an approximate estimation

Often, a tension-compression/torsion test rig is not at hand, but sometimes an ARCAN test rig may be available. This means, a compromise is to accept in order to estimate an approximate value at least. Nevertheless, employing an ARCAN test procedure also causes a high effort for the preparation of the test specimen. About 30 mm thick plates must be fabricated to cut out the required test specimens, see [*Pet15*]. Therein, UD prepreg material HexPly M21 / 34% / UD194 g/m^2/ T700GC CFRP material produced by Hexcel is considered. The plies were 0.13 mm thick. Milling is used to produce the specimen geometry inclusively the notches. Loading rate of 1 mm/min is used. Chosen is a layup of 16 unidirectional plies leading to a specimen thickness of about 2.1 mm. The ARCAN test setup introduces the load with discs in a certain loading angle φ as depicted in the following figure. Different angles in the range 0° < 90° are possible. The placement of the test specimen in the ARCAN apparatus causes load-stress relationships according to: $\sigma = F \cdot \mathrm{CoS}(\varphi)/\mathrm{A}$, $\tau = F \cdot \sin(\varphi)/\mathrm{A}$.

The compression-shear specimen is considered to produce an IFF3 stress state composed of τ_{31} and σ_3. For this stress state the ARCAN test fixture is prepared with an angle φ = 75°, leading to a stress ratio of τ/σ = 3.7. <u>*Fig.16.5-3*</u> depicts the test rig, the test specimens and the stress path with associated angle φ of the force where the measurements have been performed at. The ARCAN test specimen can be tested in a standard servo-hydraulic test machine to determine the material behavior under combined compression and shear stresses. The loads are introduced with disks mounted at a certain loading angle φ.

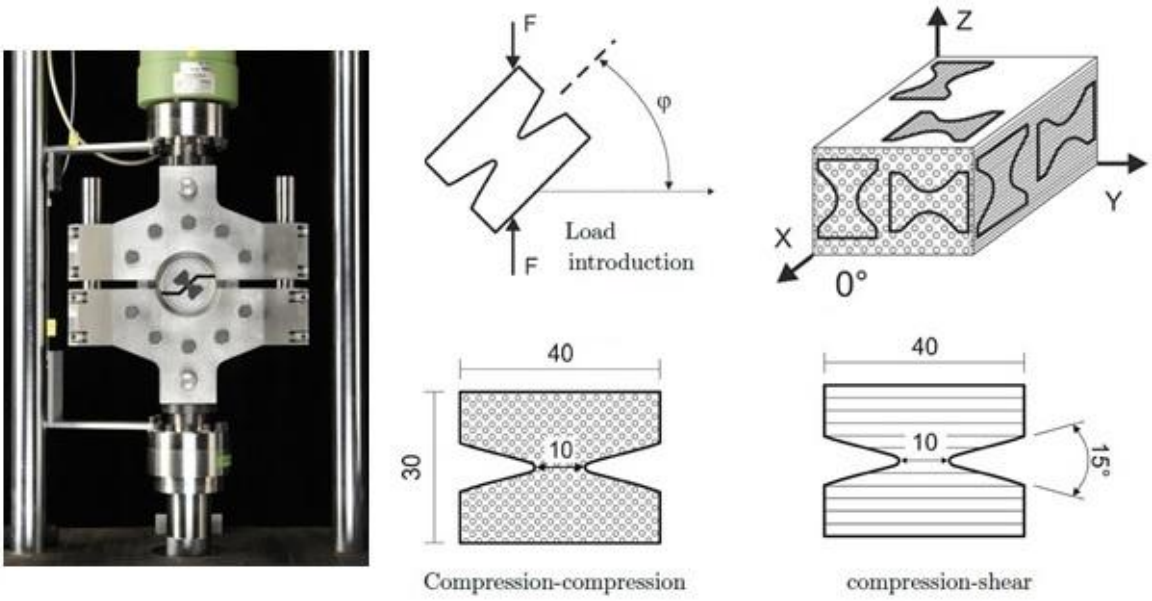


Fig.16.5-3: ARCAN test rig with test specimens cut out of a thick UD panel. [Pet15] Petersen E, Cuntze R and Huehne C: Experimental Determination of Material Parameters in Cuntze's Failure-Mode-Concept-based UD Strength Failure Conditions. Composite Science and Technology 134, (2016), 12-25

The initiation of IFF is identified through sudden strain changes, recorded with strain gauges and digital image correlation. Further, the strength values for the specific material M21/T700GC are determined. Both friction values are determined by bi-axial compression-shear tests employing the ARCAN test set-up. For $\mu_{\perp\parallel}$ IFF3 is to take and for $\mu_{\perp\perp}$ IFF1 with IFF2, because in the ARCAN test no pure bi-axial compression stress states can be generated, just compression combined with shear, composed of a tension IFF1 and a compression component IFF2. It is to note that IFF2 is the significant mode. The influence of the affected IFF1 mode can be considered by employing the interaction formula to resolve for the only unknown $\mu_{\perp\perp}$. *Fig.16.5-4 right* presents the loading path plus results in the mode transition zone. In addition $\mu_{\perp\parallel}$ was determined, *Fig.16.5-4 left*.

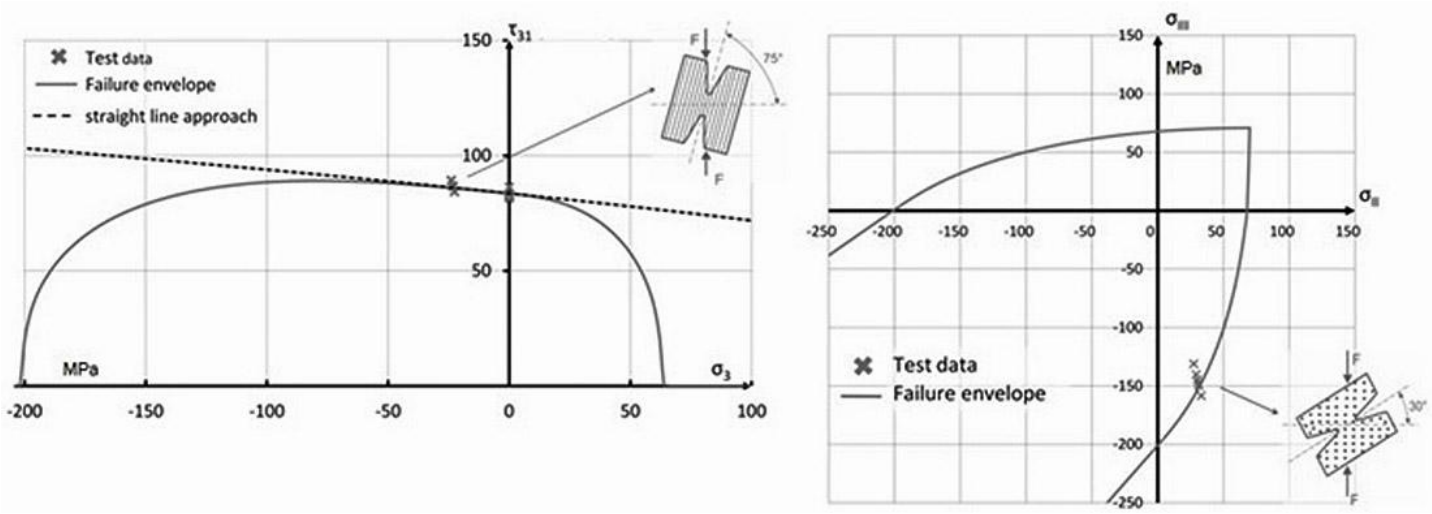


Fig.16.5-4: ARCAN tests performed on distinct stress paths. UD prepreg **** TEXT***

The test rig only allows running a $\mu_{\perp\perp}$ -test in the transition zone. Therefore, for the evaluation the interaction equation had to be employed, shown by the following procedure:

* Estimation of $\mu_{\perp\perp}$: from ($-\bar{R}^c_\perp$,0) + bi-axial test ($\sigma^t_{2,fr}$,$\sigma^c_{3,fr}$), φ=30°.

Test data of the test in the *transition zone* of the two modes: $\tau_{23} = 0$

$\bar{R}^c_\perp$ = 202 MPa, $\bar{R}^t_\perp$ = 71 MPa, m = 2.6; $\sigma^t_{2,fr}$ = 31 MPa , $\sigma^c_{3,fr}$ = –145 MPa.

Application of the interaction formula:

$$Eff^{\perp\sigma} = [(\sigma_2 + \sigma_3) + \sqrt{(\sigma_2 - \sigma_3)^2 + 4\tau_{23}{}^2}\,] / 2\bar{R}^t_\perp$$

$$Eff^{\perp\tau} = [(\frac{\mu_{\perp\perp}}{1-\mu_{\perp\perp}})\cdot(\sigma_2 + \sigma_3) + \frac{1}{1-\mu_{\perp\perp}}\sqrt{(\sigma_2 - \sigma_3)^2 + 4\tau_{23}{}^2}\,] / \bar{R}^c_\perp$$

Mathcad implicite calculation: *Vorgabe* $\mu_{\perp\perp}$:= 0.1 (estimation)

$$([(\sigma_2 + \sigma_3) + \sqrt{(\sigma_2 - \sigma_3)^2 + 0}\,] / 2\bar{R}^t_\perp)^m + ([(\frac{\mu_{\perp\perp}}{1-\mu_{\perp\perp}})\cdot(\sigma_2 + \sigma_3) + \frac{1}{1-\mu_{\perp\perp}}\sqrt{(\sigma_2 - \sigma_3)^2 + 4\tau_{23}{}^2}\,] / \bar{R}^c_\perp)^m = 1 = Eff = 100\% .$$

Search *Suchen* ($\mu_{\perp\perp}$) $\Rightarrow$ $\mu_{\perp\perp} = 0.21$.

In [*Pet15*] also in-plane friction values have been determined. Two points on the failure curve IFF3 are used to estimate the friction parameter $\mu_{\perp\parallel}$ from average values of the strength point and a reasonable bi-axial failure stress state point (τ_{21}, σ_{2c}). For achieving a good guess the use of a straight line is sufficient. It represents a linear Mohr-Coulomb formulation.

* Estimation of $\mu_{\perp\square}$: from strength point (0, $\bar{R}_{\perp\square}$) + bi-axial test point ($\sigma^c_{2,fr}$, $\tau_{21,fr}$) , φ = 75°:

$\bar{R}_{\perp\square}$ = 71 MPa, $\sigma^c_{2,fr}$ = -24 MPa , $\tau_{21,fr}$ = 76 MPa $\rightarrow$ $\mu_{\perp\parallel} = (\bar{R}_{\perp\parallel} - \tau^e_{21,fr}) / \sigma^e_{2,fr} \approx 0.2$, $cov = 5\ \%$. .

16.6 Coefficients of Thermal Expansion and of Moisture Expansion of a UD material

Of highest interest for composite structural components in the specified operational temperature range is the thermal mismatch of neighboring components. The difference in thermal or moisture expansion between members of a construction or between the constituents of a composite or a coated material can induce large stresses and strains and may lead to failure. Therefore, the relative humidity and temperature during production and the storage environment have to be controlled and monitored. This is also mandatory when conditioning the test specimens.

As the properties of composite materials are susceptible to changes induced by the absorption of moisture during production of these components built-in stresses are received. For instance moisture uptake before the launch of the spacecraft, and then desorption of polymer-based materials occurring in the space vacuum induces hygro-thermal stresses.

Mind: CTE as well as CME may essentially vary with the temperature.

Some specific literature for CME :

[Nie 84] Niederstadt G. und Nitsch P.: *Diffusion, Wärmeausdehnung und Quellung von CFK*. Braunschweig, 1984, DFVLR-IB 131-84/06

Gitschner, H.-W.: *Diffusionsbedingte Verformungs- und Spannungszustände in glasfaserverstärkten Verbundwerkstoffen*. Dissertation RWTH-Aachen, DS 8011 (1980)

Ishai O. et al.: *Hygrothermal effects on the mechanical behavior of CFRP*. Composites, 17, (Jan 1986) 1, pp 23-32
Schacht A.: *Untersuchungen zu Feuchtedehnungskoeffizienten von Faserverbundwerkstoffen*. MAN-Technologie. Diplomarbeit 1988, FH Hamburg
Schulz: *Bestimmung des Schwellverhaltens und der Feuchtigkeitsaufnahme von verstärktem und unverstärktem Epoxidharz*. MBB, TN-LHE 244-11/86
Pritzer , Frisch und Helwig: *Vermessung der Feuchtedehnung*. Dornier System, PN-2002-5100 DS 7006 (ROSAT), 1988

Thermal expansion causes a change of shape, volume and area of the structural part.

It is a function of molecular movement. Usually materials contract with decreasing temperature, Carbon fibers however may a little elongate in its direction. The size of the induced thermal stresses is influenced by the boundary conditions and constraints within the part.

Thermal strains in materials are described by the material-dependent coefficient of thermal expansion CTE and the temperature difference ΔT. Normally, the thermal strain is not proportional to the temperature difference but the relationship is nonlinear. To take this into account, the CTE is formulated as a function of the temperature. This formulation additionally requires the definition of a reference point (T_0, $\varepsilon_{th,0}$). Temperature and thermal strain are measured as differences relative to this reference.

The classical definition of the coefficient of thermal expansion (*secant method*) is given by $\alpha_T(T) = (\varepsilon_{th} - \varepsilon_{th,0}) / (T - T_0)$. Commonly, the reference strain is tacitly assumed as $\varepsilon_{th,0} = 0$. The reference temperature T_0 is shown in data sheets or diagrams for the CTEs. Frequently, ambient temperature is chosen as T_0.

The unit is usually α_T in 10^{-6} mm / (mm·K) = 10^{-6} / K, linearized in the operational regime.

In the case of constraints under ΔT the part will experience thermal stresses. Thereby, different situations are to consider: *Different temperatures within the part, limited displacement due to mechanical boundary conditions and i.e. constrained displacement in a composite of materials with different CTEs in the various layers or constituents.*

The following table gives some data for a FRP-composite and constituents.

Table 16.6-1: Properties [courtesy HSB 37157).

Example: T300/914C *CFRP*: $\alpha_{T\parallel} = -0.23 \cdot 10^{-6}$ / *K*, $\alpha_{T\perp} = 29 \cdot 10^{-6}$ / *K*

fiber: E-Glass	matrix: resin CY209
$E_f = 73000$ MPa	$E_m = 3500$ MPa
$\nu_f = 0.25$	$\nu_m = 0.35$
$\alpha_{Tf} = 4.8 \cdot 10^{-6}$ 1/K	$\alpha_{Tm} = 60 \cdot 10^{-6}$ 1/K

fiber: T300	matrix: resin 914C	UD-Laminate, $\varphi_f = 60$ %
$E_{f\parallel} = 218800$ MPa	$E_m = 3500$ MPa	$E_\parallel = 132700$ MPa
$E_{f\perp} = 28000$ MPa		$E_\perp = 9300$ MPa
$G_{f\parallel\perp} = 50000$ MPa	$G_m = 1300$ MPa	$G_{\parallel\perp} = 4600$ MPa
$\nu_{f\parallel\perp} = 0.23$	$\nu_m = 0.35$	$\nu_{\parallel\perp} = 0.28$

Moisture Expansion causes a similar change of the structural part
, however is not always present in materials. The classical definition of the coefficient of moisture expansion is given by $\alpha_M(M) = (\varepsilon_{th} - \varepsilon_{th,0}) / (M - M_0)$.

The unit of the coefficient of moisture CME is practically chosen as α_M in 10^{-4} / % , linearized in the operational regime. Up to a distinct moisture content M_p no swelling occurs; the moisture is stored in open matrix pores and later additionally in cavities generated under operation, *Fig.16.6-1up-left.*

In the case of constraints the part will experience under ΔM moisture stresses. Different situations are to consider: *different moisture within the part, limited displacement due to mechanical boundary conditions and i.e. constrained displacement in a composite of materials with different CMEs in the various layers.*

Table 16.6-2 displays data sets for some FRP materials. The values are average ones because average physical properties should be such used in design dimensioning, at first.

Table 16.6-2: Average properties measured at room temperature (the dash means not available (HSB))

Matrix type	M_p [%]	α_{Mm}	Source
LY556/HT976 (160°)	0.4	27.3	[5]
LY556/HT976 (180°)	0.35	26.5	[5]
M10 (prepreg)	0	22.8	[6]
MY750/HY917/DY070	0.10	14.6	[5]

UD composite	M_p [%]	$\alpha_{M\|\|}$	$\alpha_{M\perp}$	φ [%]	Source
T300-LY556/HT976 (160°)	0.07	–	40.1	54.4	[5]
T800-LY556/HT976 (180°)	0.05	–	37.2	59.4	[5]
M10-33-1055	0.03	–	23.5	56.0	[5]
M10-M40A	–	1.3	34.8	60.0	[6]
M40-MY750/HY917/DY070	0.02	–	29.8	56.3	[5]
T300-913C	0.17	–	50.1	–	[5]
T400-6376-5-35/40	0.03	–	38.5	–	[5]
M40-LY556/HY906/DY062	–	2.3	24.6	–	[7]

Prepared:	Checked:	Date:	
Dr. Cuntze / Schülein	Dr. Geier	08.06.1989	MAN / DLR

Table 16.6-3 completes the information CMEs.

Table 16.6-3: Average properties for Fig.16.6-4. α_{Mm} was obtained by recalculation.($V_f \equiv \varphi$)

available constituent properties							measurement composite			
fiber	E_f	$\nu_{\|\|\perp f}$	matrix	E_m	ν_m	α_{Mm}	$\alpha_{M\|\|}$	$\alpha_{M\perp}$	φ	ψ
T300	218800	0.23	914C	3500	0.35	24.2	0.81	42.0	60	69
E-glass	74500	0.25	CY209	3500	0.35	25.5	0.3	55.2	60	76

The internal strain state in a laminate test specimen is rather dependent on a qualified conditioning, and this determines the level of residual stresses. Saturation conditioning leads to a more or less uniform moisture distribution and thereby to the lowest residual stresses. Therefore, for the lesser known features of FRPs some remarks on conditioning, measurement and assessment of test results shall be additionally made:

1. The moisture content is defined as the ratio of the ‘moisture mass taken up by the laminate’ to the ‘dry mass of the laminate’. The CMEs are defined in a similar way as the CTEs.

They describe the alteration of strain as a function of the alteration of the moisture content. Within the operational regime the CMEs are usually averaged.

2. The moisture content depends on the relative humidity of the surrounding medium, air or another medium. The maximum moisture content that can be reached under a given condition is termed saturation moisture M∞.
3. Diffusion requires time. Its speed increases with increasing temperature. Therefore, in case of a higher temperature, M∞ is reached in a shorter time. Due to the long lasting diffusion time, the moisture in the laminates may be not uniformly distributed over the thickness, see *Fig.16.6-1up-right* and Refs. [2, 3].

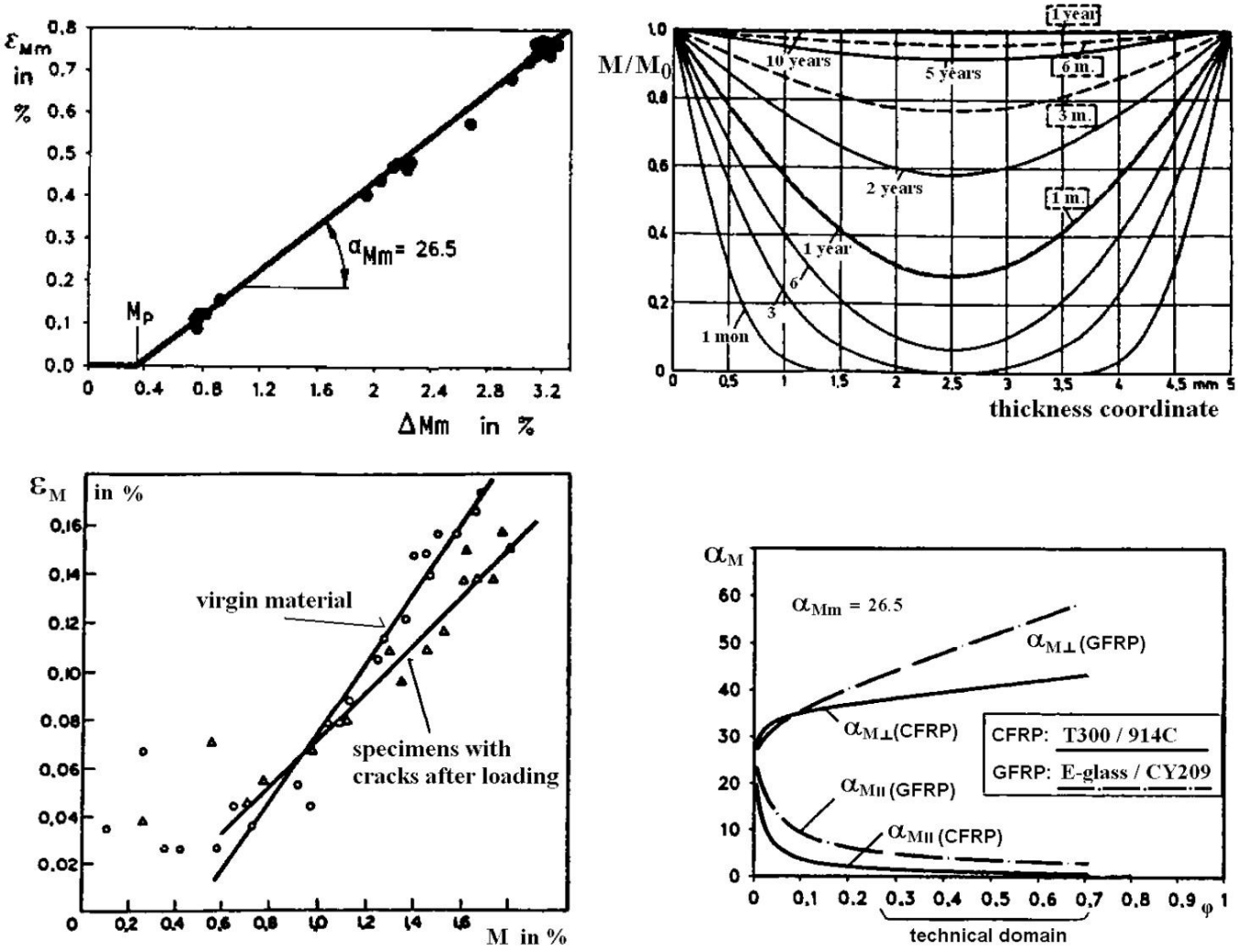


Fig.16.6-1 up-left: Matrix elongation ε_{Mm} versus moisture difference

Fig.16.6-1 up-right: Conditioning. Moisture profile across thickness (measurement data T300/fiberdux 914C, [Nie84]. Laminate thickness 5mm from both sides at ambient temperature. Matrix (dashed line), CFRP (solid line)

Fig.16.6-1down-left: Difference of virgin material and IFF-micro-cracked material

Fig.16.6-1down-right: Computed CME courses (Table 16.6-2 data) as function of the fiber volume content

Task: Moisture content calculations

An initially dry laminate of T300/Ep5208, 1.5 mm thick, is moisture-conditioned : will be finished

40°C , on both surfaces a moisture of Φ = 70 % beaufschlagt (siehe /FVL/ u. Blatt 4.):

How high is the saturation humidity?

$M_\infty = M_{100}\,(\Phi/100)\,b = 1.05$

mit $M_{100} = 1.5$; $b = 1$ nach Tab. 2; $\Phi = 70$ %.

Wie hoch ist der Feuchtegehalt nach 120 Tagen?

$t = 120 \cdot 24 \cdot 3600 = 0.1037 \cdot 10^8$ s

$D = D_0\, e^{-C/T} = 3.984 \cdot 10^{-8}$ mm^2/s

mit $D_0 = 0.58$; $C = 5165$ nach Tab. 2; $T = 273.15 + 40 = 313.15$ K

$s = 1 \cdot 1.5 = 1.5$ mm, $\bar{t} = t \cdot D/s^2 = 0.184$

$G(\bar{t}) = 0.868$ (linear interpoliert in Tab. 2)

$M = G\,(M_m - M_0) + M_0 = 0.91$ ($M_0 = 0$, $M_p = 0$ porenfrei).

How long does it take to saturize the laminate?

The laminate will saturized at $\bar{t}$ = 0,67 with 99.9 % (Tab. 2). This means a time span

$t = \bar{t} \cdot s^2/D = 3.784 \cdot 10^7$ s = 14 months !

How much time is necessary to obtain M = 1.025 moisture in the laminate?

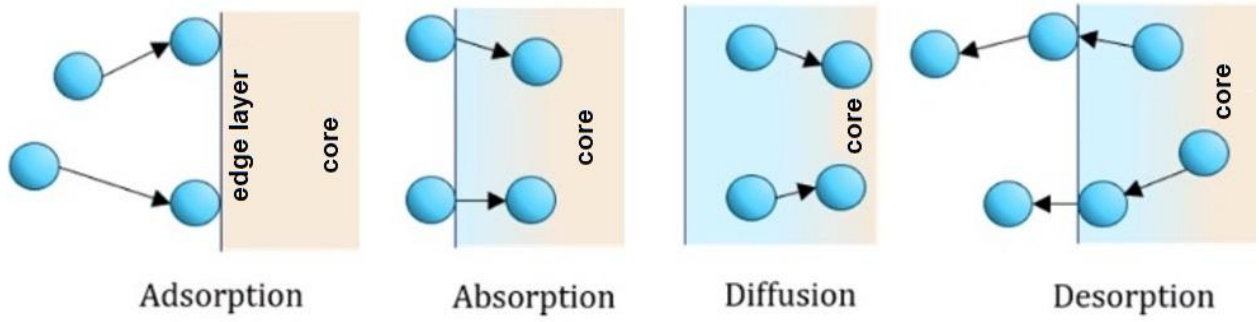
$G = \dfrac{M - M_0}{M_\infty - M_0} = 0.976 = 97.6$ % with $M = 1.025$; $M_\infty = 1{,}05$; $M_0 = 0$

$\bar{t}\,(G) = 0{,}369$ (linear interpoliert in Tab. 2)

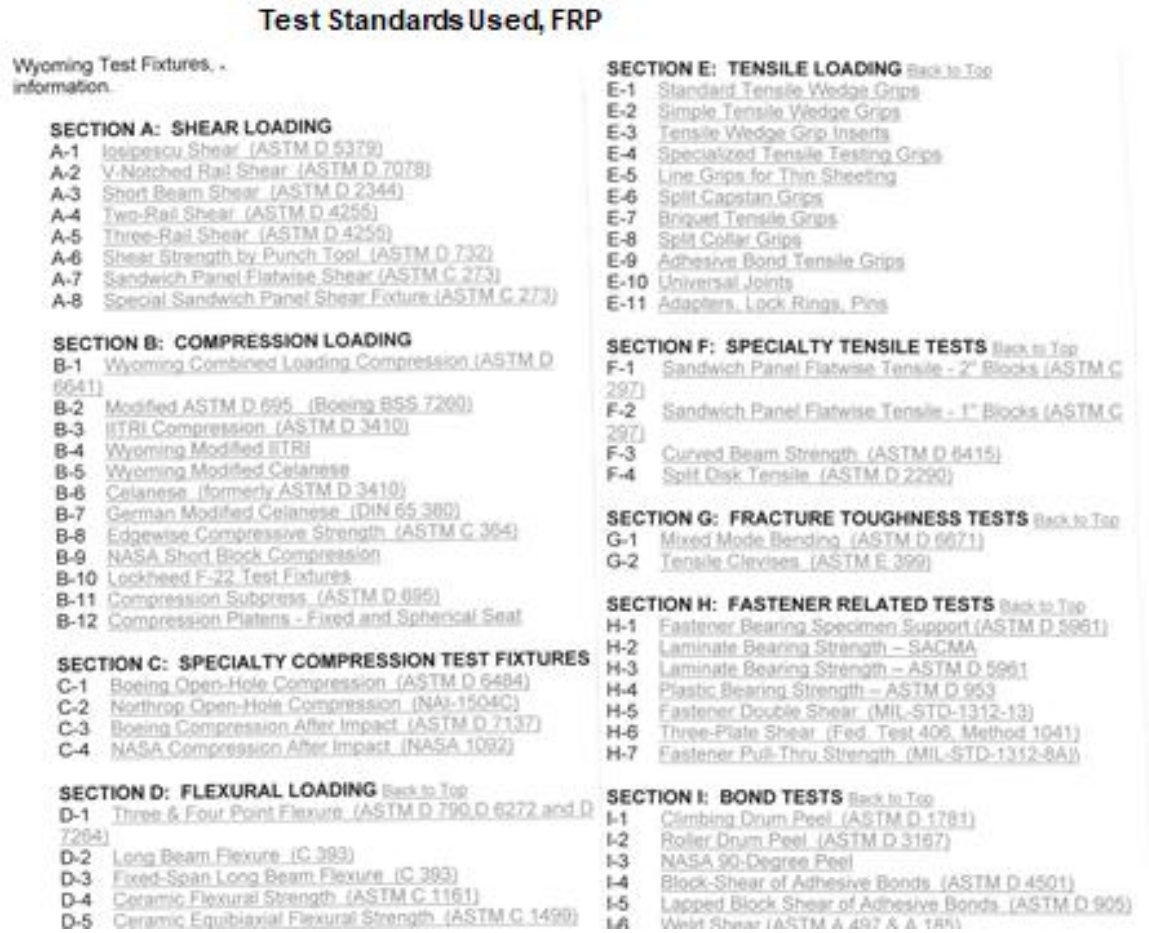
$\rightarrow \quad t = \bar{t}\ s^2 / D = 2.084 \cdot 10^7$ s = 8 months.

Table 2

Concluding, the next figure shall depict the basic processes regarding moisture uptake and moisture release [*courtesy: Presentation Oct.2022, M.Sc. Anna Katharina Sambale (Leibniz-Institut für Polymerforschung IPF, Dresden*].



In this document just for FRP-materials a collection of Test Standards shall be presented →



[ASM] ASM International: *Tensile Testing*. 1992

[Bor99] Bormann P*: Analyse elastisch-plastischer Eigenschaften*. Dissertation, TU Chemnitz (1999)

[Bri52] Bridgman P W*: Studies in Large Flow and Fracture*. McGraw-Hill, London - New York 1952

[CMDH] *Cryogenic Materials Data Handbook* AFML-TDR-64-280 Volume I (1970)

[Cun04a] Cuntze Rand Freund A: *The Predictive Capability of Failure Mode Concept-based Strength Criteria for Multidirectional Laminates, Part A*. Composites Science and Technology 64 (2004), 343-377

[Cun04b] Cuntze R: The Predictive Capability of Failure Mode Concept-based Strength Criteria for Multidirectional Laminates, Part B. Composites Science and Technology 64 (2004, 487-516

[Cun06] Cuntze R: *Efficient 3D and 2D Failure Conditions for UD Laminas and their Application within the Verification of the Laminate Designs*. Composites Science and Technology 66 (2006), 1081-1096

[Cun07] *Prediction of Static and In-plane Fracture Failure of UD Laminas composed of Fiber-reinforced Plastics*. 4th NAFEMS Nordic Seminar on Material's Modelling. Sandvika, March 2007. Conference CD

[Hin04] Hinton M J, Soden P D and Kaddour A S: *Failure Criteria in Fiber Reinforced Polymer Composites: The World-Wide Failure Exercise*. Elsevier Science & Technology Bookstore, 2004

[HSB] Deutsches luftfahrttechnisches Handbuch für Struktur-Berechnung *'Fundamentals and Methods for the Design and Evaluation of Aeronautical Structures' (*in English 2007)

[MIL17] MIL-HDBK 17 "Polymer Matrix Composites": *Vol I "Guidelines for Characterization of Structural Materials"; Vol II "Material Properties"; Vol. III "Utilization of Data*". Dep. of Defence (DOD), Technomic Publishing USA

[MMPDS-02]: *Metallic Materials Properties Development and Standardization* (MMPDS). Battelle. Formerly MIL-HDBK-5 "Metallic Materials and Elements for Aerospace Vehicle Structures"

[Puc96] Puck A: *Festigkeitsanalyse von Faser-Matrix-Laminaten*. Modelle für die Praxis. Hanser Verlag, 1996

[SMH07] ESA *Structural Materials Handbook*

[Tar81] Tarnopolskii Y M and Kincis T : *Static Test Methods for Composites*. Van Nostrand, New York

[VDI 2014] German Guideline, sheet 3 " *Development of FRP Components, Analysis*". 2006, Beuth Verlag (in German and English) 1982.

17 Material Models from the ‘Elastic State’ and ‘Onset-of-Yielding’ via load-controlled ‘Onset-of-fracture’ until deformation-controlled ‘Full Plastic Fracture’ (rupture) substantiated by hints on the performance of Linear and Non-linear Stress Analyses

Accurate 3D stress states are effortful to determine in non-linear analysis cases. Also one has to distinguish (inelastic) plastic behavior of ductile materials from inelastic behavior of brittle materials. In the first case a flow (yield) potential F is searched and in the brittle material case an inelastic potential to set up the interrelations within the complicated 3D stress-strain situation. In the following chapter several models will be investigated which might serve as such inelastic potentials.

At first some general facts on the behavior of ‘dense’ materials shall be presented for a better understanding and as a reminder of fracture failure mechanisms. Fracture appearance of a certain type depends on whether the stress state $\{\sigma\}$ causes ductile or brittle behavior of the distinct material. The occurrence of SF instead of NF under tension also means that the resistance in the shear fracture plane against sliding is lower than against normal fracture, dimple fracture occurs. For the material thus considered, the model assumption of homogeneity applies, and that imperfections (flaws) such as inclusions, cavities and dislocations are small and statistically evenly distributed. In the case of porous, brittle materials, a "crumble break" termed here crushing fracture of the microstructure volume occurs under compression instead of the SF.
Fracture is understood here as a separation of material, which is free of micro-cracks but not free of flaws prior to loading. In this context the above *crushing* of a porous material has to be seen a separate *fracture mechanism* and *failure mode*.

Essential mechanism in brittle micro-damage behavior is the formation and growth of the micro-cracks and later their merging to form a crack at a distinct macro-mechanical level. The term brittle behavior is used here for low-deformation macroscopic behavior.
In the case of ductile micro-damage behavior, it is the nucleation of voids (micro-pores), the growth of voids and finally the coalescence of the grown voids. Inclusions in the matrix that have different properties (*rigid versus soft*) are nuclei for micro-pores.
In microscopic areas - such as in front of a crack tip - a material can have high ductility, which hardly has to be noticeable at macroscopic fracture mechanics level.

It can be seen that a crack-shaped imperfection is differently failure-triggering according to its orientation, but a round micro-pore or a brittle inclusion remain equivalent, see ***Fig.17-1*** (intentionally repeated here). 1D-, 2D- and 3D-states of stresses obviously have also different effects. Of interest for fracture failure is the distribution of the large pores and micro-cracks together with their orientation in the field of tension. Flat crack-shaped imperfections cause growth and possibly NF-failure under normal stresses perpendicular to their orientation; pores and brittle inclusions have a SF- or NF-causing effect in every direction of stress.

The phases until ductile rupture begin at the ‘Onset-of-necking’ with micro-void nucleation. Brittle and soft particles build the locations where the micro-voids are nucleated. Then micro-void coalescence occurs and micro-cracking starts inducing separation within the solid. Finally, ductile micro-crack growth is faced until rupture, thereby experiencing a localization of the deformation in the solid into a shear deformation slip band.
Plastic deformation of metals is the result of dislocation movements along the slip planes (see § 16.6) of the lattice of the distinct crystal caused by shear stresses. The pile-up of dislocations in poly-crystalline metals leads to a negligible elastic dilatation. Increasing dislocation density

generates the strain-hardening. Slip lines are lines of maximum shear stress. The slip lines under plastic flow conditions intersect with a free surface at 45° and with each other at 90°.

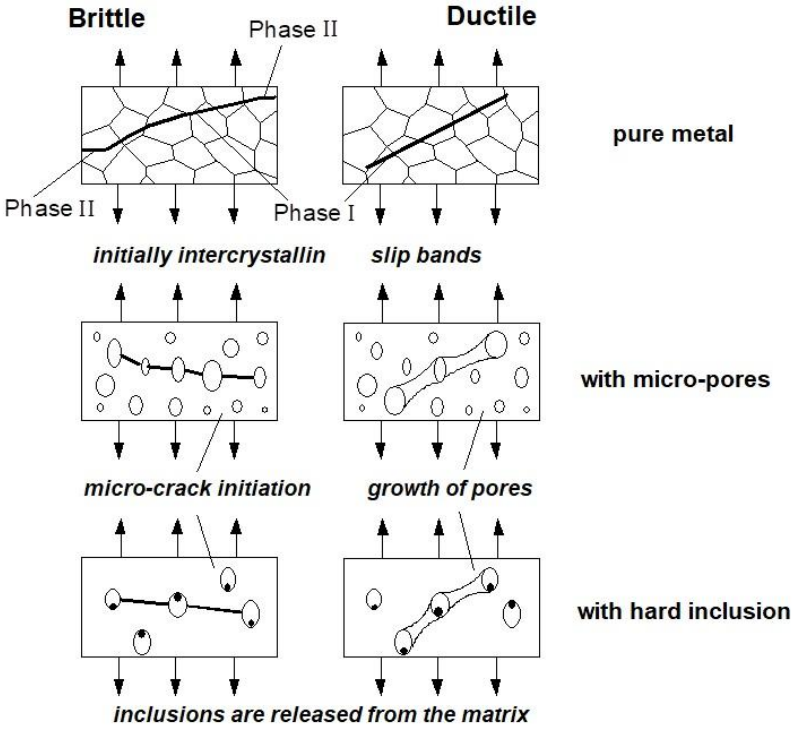


Fig 17-1: Metals. Orientation-driven initiation of micro-cracks and micro-voids (phase I means micro-ductility)

The stress $\sigma(\varepsilon_{pl})$ considering only the plastic deformation or plastic flow of the material is called flow stress σ_F. Yield strength is a material property defined as the stress at which a material begins to deform plastically whereas yield point is the point where nonlinear (elastic + plastic) deformation begins. If it is not well-defined (*remind the Lüder elongation effect of mild metals*) on the stress-strain curve. The yield stress is defined by determining the point of intersection of the stress-strain curve and a line offset 0.2 percent to the right and parallel to the straight portion of the stress-strain curve.

Task is to provide flow potentials *F* that capture for ductile materials the 'Mises domain' (no voids) and the high-strain 'Gurson domain' (voids). Further, for performing the yield analyses a flow rule is required to define the stress-strain relationships, whereby a so-called *associated flow rule* is desired. This means that the principal axes of the plastic strain increment coincide with the principal axes of the applied stress. Unfortunately, these often differ from the principal axes of the stress increment. The plastic strain increment fixes the size of $d\varepsilon_i^{pl} = d\lambda \cdot \partial F / \partial \sigma_i$. Herein, the scalar proportionality factor $d\lambda$ depends on the strain history of the increasing plastic flow.

In the high strain domain several researchers presented models for the yield potential *F*. Rice-Tracey depart with their model from the zero dilatation plastic flow visualized by the Mises-cylinder. Gurson, followed by Tvergaard, Needleman and further investigators, followed to model the shrinking failure body towards the vertex at $\max I_1$ as the limiting tensile point on the failure body, where $TrF = \infty$.

As surprisingly there is some similarity between the elastic Beltrami domain and the maximum yield 'Gurson domain' the representative models shall be presented now.

17.1 Elasto-plastic Transition Domain ($\bar{R}_p < \bar{R}_{p0.2} \equiv \bar{R}^t_{0.2}$, $\nu_0 < \nu < 0.5$)

17.1.1 Beltrami, Schleicher et al, dense material, potential surface

Beltrami, Schleicher et al. assumed that at initiation of yielding the strain energy rate $\dot{W}$ in a material element consists of two portions which read after inserting Hooke's law for isotropic materials

$$\dot{W} = \dot{W}_{volume} + \dot{W}_{shape} = [\frac{2+2\nu}{3} \cdot 3J_2 + \frac{1-2\nu}{3} \cdot I_1^{\,2}] / 2E, \quad \text{in tensor notation} \quad \dot{W} = \sigma_{ij}\varepsilon_{ij}.$$

Both portions in the bracket above are used to formulate failure functions F, as was still shown, whereby $I_1^{\,2}$ represents the volume change and J_2 the shape change. The reason for mentioning Beltrami again is the idea to transfer logic and formulation from the elastic-plastic transition 'Beltrami domain' with decreasing volume strain to the 'Gurson domain' with increasing volume strain, namely to the 'porosity increasing domain' of very ductile isotropic materials where voids are generated at 3D-high stressing of the material. Beltrami's formulation shall be also later the basis for the author's porosity-capturing simple 'Extended Mises model'.

Beltrami bridges the elastic domain with the plastic domain. His formulation for the potential surface is not a failure function but a descriptive function to predict subsequent Beltrami surfaces $\nu(\bar{R})$, see *Fig.17.2*. This means: a pair (ν, R) must be given for each desired ν-curve in the axial cross-section of the rotational symmetric Beltrami surface. His usual formulation ($3 \cdot J_2$ is Mises part) reads:

$$F^{Bel} = 3 \cdot J_2 + \kappa \cdot I_1^{\,2} = c^{Bel} \cdot \bar{R}^{t\,2}_{0.2} \quad \text{with} \quad \kappa = (1\text{-}2\nu)/(2\text{+}2\nu)$$

Inserting $(\bar{R}^t_{0.2}, 0, 0)^T$ with $I_1 = \bar{R}^t_{0.2}$, $J_2 = 2\bar{R}^t_{0.2} / 6$ one obtains as size factor $c^{Bel} = 1 + \kappa$.
For the subsequent ellipsoidal Beltrami surfaces (ν-dependent Beltrami eggs) follows
that pairs $(\bar{R}(\nu), \nu) \rightarrow I_1 = \bar{R}$, $J_2 = 2\bar{R} / 6$ are to insert into $3 \cdot J_2 + \kappa \cdot I_1^{\,2} = (1+\kappa) \cdot \bar{R}^2$
in order to obtain the different 4 failure body shapes in *Fig*.17 – 2 and in the principal stress plane section A-A (there is no physical relation between ν and $\bar{R}$*!*)
*R*elevant for the elliptical shape is Poisson's ratio ν.

17.1.2 Ismar and Mahrenholtz, porous material, $\sigma < \bar{R}^t_{0.2}$, fracture failure surface

Brittle 'porous' materials may still fracture in the elasto-plastic transition domain**.** Ismar and Mahrenholtz [*Ism82*] developed a Beltrami-based SFC model which describes the behavior of a material between the proportional limit and the 'onset of yielding'. The failure function for this transition domain (suffix $_{tr}$) reads

$$F_{tr} = a_{tr} \cdot 3 \cdot J_2 / \bar{R}^{t2} + b_{tr} \cdot I_1^{\,2} / \bar{R}^{t2} = c_{tr}^{\,2} \quad \text{with} \quad a_{tr} = (2\text{+}2\nu)/3\,, \; b_{tr} = (1\text{-}2\nu)/3$$

with $\bar{R}$ an appropriate strength value for reasons of normalization and c_{tr} the size parameter of the failure body. Each value c_{tr} marks a surface of equal potential. The two shape-responsible

parameters become for a foam with $\nu = 0 \rightarrow a_{tr} = 2/3 = 2 \cdot b_{tr}$. This represents a sphere described by $F_{tr} \cdot \bar{R}^{t2} = 2 \cdot J_2 + I_1^2 / 3$. The maximum ν value is achieved for $b_{tr} = 0 \rightarrow \nu = 0.5$, $a_{tr} = 1$ and the function represents the 'Mises cylinder'.
Ellipsoids are obtained by parameter sets lying in between.

$$F^{NF} = c^{NF} \cdot \Theta^{NF} \cdot \frac{\sqrt{4J_2 \cdot \Theta^{NF} - I_1^2/3} + I_1}{2 \cdot \bar{R}^t} = 1 \leftrightarrow F^{CrF} = c^{CrF} \cdot \Theta^{CrF} \cdot \frac{\sqrt{4J_2 \cdot \Theta^{CrF} - I_1^2/3} + I_1}{2 \cdot \bar{R}^c} 1$$

$$Eff^{NF} = c^{NF} \cdot \frac{\sqrt{4J_2 \cdot \Theta^{NF} - I_1^2/3} + I_1}{2 \cdot \bar{R}^t} = \frac{\sigma_{eq}^{NF}}{\bar{R}^t} \quad \leftrightarrow \quad Eff^{CrF} = c^{CrF} \cdot \frac{\sqrt{4J_2 \cdot \Theta^{CrF} - I_1^2/3} + I_1}{2 \cdot \bar{R}^c} = \frac{\sigma_{eq}^{CrF}}{\bar{R}^c}.$$

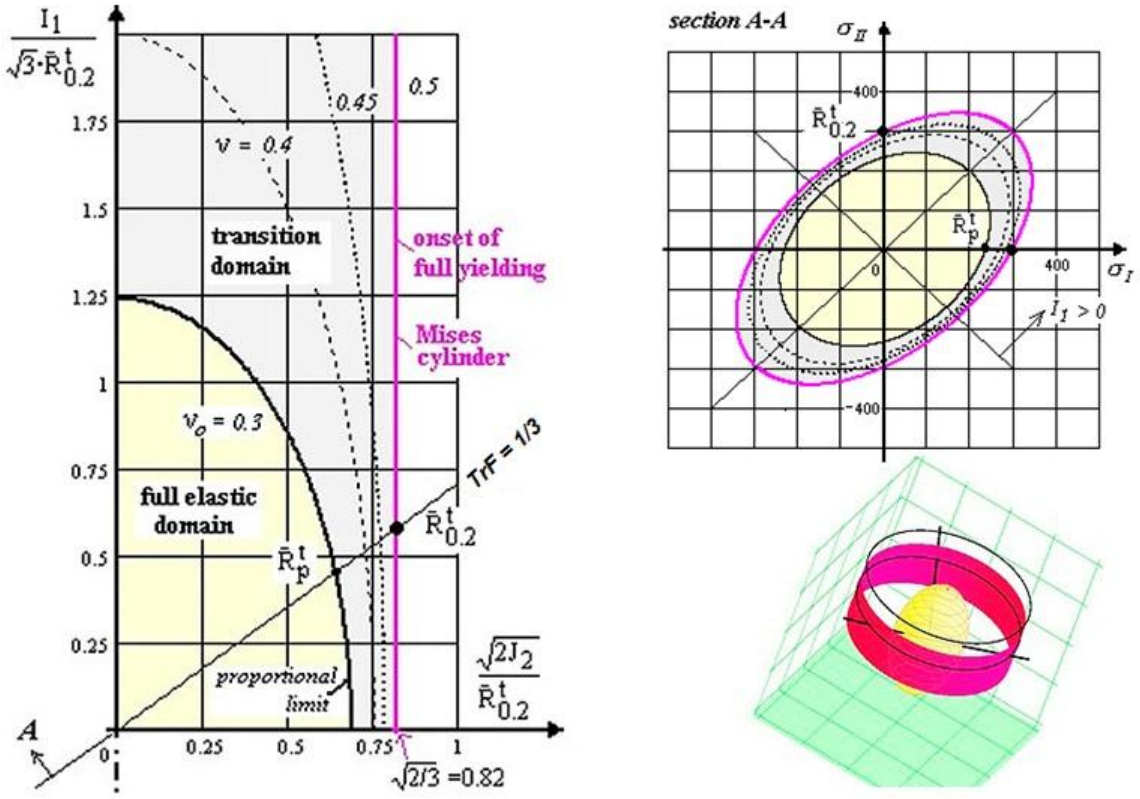


Fig.17-2: Elasto-plastic transition domain, development of the Beltrami surfaces from egg shape ($\nu > \nu_0 = 0.3$ for metals) to 'Mises cylinder ($\nu = 0.5$) depicted in Lode-Westergaard coordinates and (right) in principal stresses the cross-section A-A

$\bar{R}^t_{p0.2}$ is a practical engineering fixation of the yield limit. In case of ductile materials it is used as normalization strength instead of $\bar{R}^t_m$. In the case of very brittle materials $\bar{R}^t_{p0.2}$ might be not given and foam is such a material.

17.2 Hencky-v.Mises-Huber (yield condition: $\bar{R}^t_{0.2} < \sigma < \bar{R}^t$, $\nu = 0.5$; $1 < c_\tau < \bar{R}^t / \bar{R}^t_{0.2}$)

At first exemplarily for the 'Mises' yield condition some essential facts shall be outlined:

* Subsequent yield surface: $F_\tau^{Mises} = 3J_2 / \bar{R}^{t\,2}_{0.2} = c_\tau^{\,2}$, $\sigma_{eq}^{Mises} = \sqrt{3J_2} \rightarrow$ nonlinear analysis,
  with $c_\tau = \bar{R}^t / \bar{R}^t_{0.2}$, 'better' $c_\tau = \text{true}\bar{R}^t / \text{true}\bar{R}^t_{0.2}$.

* 'Onset-of-Yield' failure surface: $F_\tau^{Mises} = 3J_2 / \bar{R}^{t\,2}_{0.2} = 1$, $\sigma_{eq}^{Mises} = \bar{R}^t_{0.2} \rightarrow$ criterion, SFC.

Onset-of-yield is defined engineering failure limit, the design has to be verified to. It is not fracture.

- Onset-of-fracture $F_\tau^{Mises} = 3J_2 / \bar{R}^{t2} = 1$, $\sigma_{eq}^{Mises} = \bar{R}^t$ → failure criterion, SFC

Mises equivalent stress

Plastic flow is induced by shear stresses, causing e.g. in metals, a dislocation movement. It is usually formulated by the Hencky-Mises-Huber (HMH) or shortly 'Mises'-hypothesis applying

$$F_\tau^{Mises} = 3J_2 / \bar{R}_{0.2}^{t\,2} = c_\tau^{\,2} \quad \text{with} \quad \sigma_{eq}^{Mises} = \sqrt{3J_2},$$

$$6 \cdot J_2 = (\sigma_I - \sigma_{II})^2 + (\sigma_{II} - \sigma_{III})^2 + (\sigma_{III} - \sigma_I)^2 = (\sigma_x - \sigma_y)^2 + (\sigma_y - \sigma_z)^2 + (\sigma_z - \sigma_x)^2 + 6 \cdot (\tau_{xy}^2 + \tau_{zx}^2 + \tau_{yz}^2)$$

$$\sigma_{eq}^{Mises} = \sqrt{\frac{1}{2}} \cdot \sqrt{\left[(\sigma_I - \sigma_{II})^2 + (\sigma_{II} - \sigma_{III})^2 + (\sigma_{III} - \sigma_I)^2 \right]} = \sqrt{2} \cdot \sqrt{\tau_{III}^2 + \tau_I^2 + \tau_{II}^2}$$

Examples: Shear $\tau_{xy} = \sigma_I = -\sigma_{II} \rightarrow I_1 = 0,\ J_2 = \tau_{xy}^2 = \sigma_I^2 \Rightarrow \sigma_{eq}^{Mises} = \sigma_I \cdot \sqrt{3}$

Tension σ_I $\rightarrow I_1 = \sigma_I$, $J_2 = \sigma_I^2/3 \Rightarrow \sigma_{eq}^{Mises} = \sigma_I$

which means: The equivalent stress is depending on the principal shear stresses. The curve parameter c_τ determines the actual size of the subsequent Mises cylinders as yield surfaces. It changes between 1 at 'onset of yielding' and $c_\tau = \text{true}\bar{R}^t / \text{true}\bar{R}_{0.2}^t > eng\bar{R}^t / eng\bar{R}_{0.2}^t = \bar{R}^t / \bar{R}_{0.2}^t$ as may be seen from the *Fig.18-3 right* . The shape re-mains cylindrical up to $\bar{R}_m^t$.

With $\nu = 0.5$, $\kappa = 0$ follows $F^{Beltrami} \rightarrow F^{Mises}$.

In <u>*Fig.17*-3</u> included are the points of some stress states. The single stresses are given in multiples of the *design allowable.* It turns out from the figure that the stress states are placed: 6., 5. and 3. in

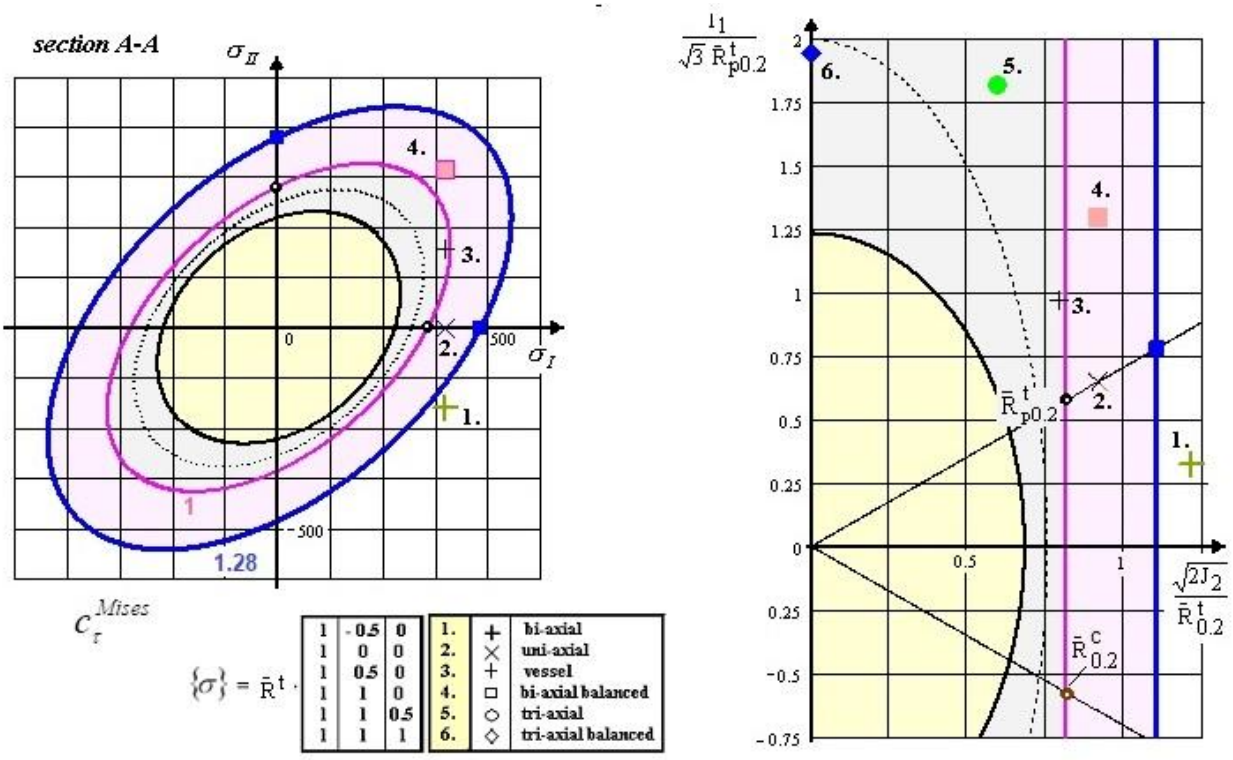


Fig.17-3: 2D-potential surfaces with points indicating distinct stress–states as inclined cross-section of the rotationally-symmetric body

the elastic-plastic domain; 4. and 2. in the full plastic domain; and 1. outside the ellipse. Further, 1. through 4. are depicted in the 2D-cross-section A-A running through the uniaxial strength points..

Mises equivalent strain

Nonlinear analysis of general stress states requires the determination of the equivalent strain. In order to perform this the principal strains have to be determined and inserted into the equation for the total equivalent strain

$$\varepsilon_{eq}^{Mises} = \frac{\sqrt{2}}{3} \cdot \sqrt{(\varepsilon_I - \varepsilon_{II})^2 + (\varepsilon_{II} - \varepsilon_{III})^2 + (\varepsilon_{III} - \varepsilon_I)^2} \cdot$$

The previous equation reduces for $\varepsilon_{II} = \varepsilon_{III}$ (*round bar as tensile test specimen*) to $\varepsilon_{eq} = 2 \cdot (\varepsilon_I - \varepsilon_{II})/3$.

In the case of large plastic strains the extent of plastic flow (yield) can be expressed by the equivalent plastic strain *increment*, which depends on the principal strain increments, as

$$d\varepsilon_{eq}^{pl} = \sqrt{\frac{2}{9}} \cdot \sqrt{[(d\varepsilon_I^{pl} - d\varepsilon_{II}^{pl})^2 + (d\varepsilon_{II}^{pl} - d\varepsilon_{III}^{pl})^2 + (d\varepsilon_{III}^{pl} - d\varepsilon_I^{pl})^2} \ .$$

Equivalent stress and equivalent plastic strain are linked by the 'plastic' part (= 'flow curve') in the *stress-plastic strain relation* as, e.g. if described by Ramberg-Osgood

by $\varepsilon_{eq}^{pl} = 0.002(\sigma / \bar{R})^{\bar{n}}$, which maps the course of true test data better than those of the engineering test data, *Fig.17-4*.

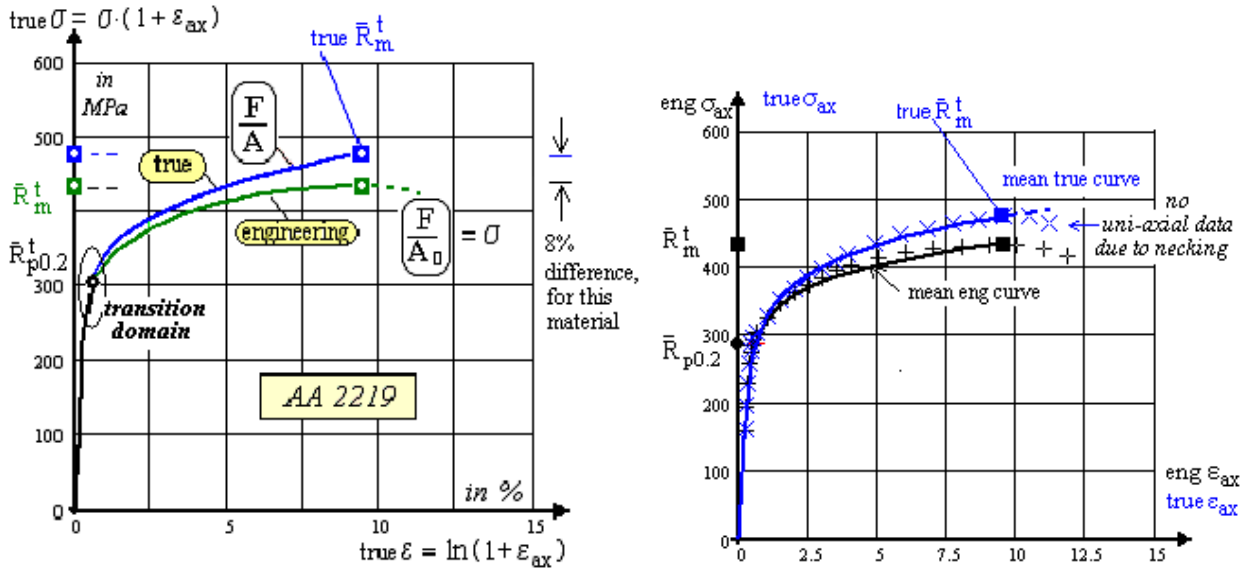


Fig.17-4: (left) R/O mapping (solid lines) of the course of engineering and of true test data points. (right) Improved R/O-mapping of true curve

The flow curve reads $\sigma_F(\varepsilon_{eq}^{pl})$ and might be given in engineering or in true quantities.

Equivalent plastic strain increment and Flow Rule of the Mises model

A yield condition describes the plastification of the material and delivers the Flow Potential whereas the so-called Flow Rule model connects between stress and strain state. Or, the Flow Rule establishes the incremental stress-strain relations for plastic material. It describes the differential

changes in the plastic strain as a function of the current stress state. Plastic flow is induced by shear stresses. *Table 17-1* shows the derivation.

For the nonlinear analysis a yield surface is needed which is dedicated to the material. Mandatory for the accurate choice of the yield surface formulation is whether the material is dense (non-porous) or porous from voids in the virgin material or voids nucleated and grown under a tri-axial tensile stress state, or near crack tips under uniaxial far stress.

Plasticity models most often use a so-called incremental theory in which the mechanical strain is decomposed into an elastic and an inelastic part (if a plastic part then volume is incompressible, invariant), respectively. A flow rule defines the inelastic deformation that occurs if the material is no longer elastically behaving, and an evolution law that defines the hardening.

Table 17-1: Derivation of the plastic strain increment, HMH potential

HMH (shortly termed Mises yield function) $F^{Mises} = f(J_2) = \sqrt{3 \cdot J_2} \;/\; \bar{R}^t_{0.2}$

and for the subsequently growing failure surface ($c_\tau \rightarrow c_\tau^{Mises}$ for discrimination)

$F^{Mises}_{grow} = f(J_2, c_\tau^{Mises}) = \sqrt{3 \cdot J_2} \;/\; \bar{R}^t_{0.2} = c_\tau^{Mises}$ with $1 < c_\tau^{Mises} < \bar{R}^t \;/\; \bar{R}^t_{0.2}$.

with the size parameter c_τ^{Mises}. One can assume that the elastic strain increment is negligible to the plastic strain increment and - following Prandtl-Reuss - then holds

$$d\varepsilon_{ij} = d\varepsilon^{el}_{ij} + d\varepsilon^{pl}_{ij} \rightarrow \; d\varepsilon_{ij} \cong d\varepsilon^{pl}_{ij} .$$

Introducing $F^{Mises} = \sqrt{3 \cdot J_2} \;/\; \bar{R}^t_{0.2}$ as flow potential into the Flow Rule (associated) above

yields $d\varepsilon^{pl}_{ij} = d\lambda \cdot \partial F / \partial \sigma_{ij}$, $\partial F / \partial \sigma_{ij} = \partial J_2 / \partial \sigma_{ij} = s_{ij}$ (stress deviator) $\rightarrow \; d\lambda \cdot s_{ij} = d\varepsilon^{pl}_{ij}$

$$\sigma_{ij} = s_{ij} + I_1 / 3 \cdot \delta_{ij} \quad \text{with special case } \sigma_{hyd} = I_1 / 3$$

after decomposition of the stress tensor into a volumetric stress tensor and a stress deviator tensor part.

Finally, the increment of the proportionality factor becomes $d\lambda = \sqrt{(d\varepsilon^{pl}_{ij} \cdot d\varepsilon^{pl}_{ij}) / (2 \cdot J_2)} \geq 0$

with actual incremental strains and invariant J_2 from the stress analysis.

The previous model reports volume constancy according to $d\lambda \cdot s_{ii} = d\lambda \cdot 0 = d\varepsilon^{pl}_{ii} = 0$.

For further information :

Bulk modulus K = *ratio between pressure increase and resultant decrease in volume.*

K = -V · dp/dV and $\nu = (3 \cdot K - 2 \cdot G)/(6 \cdot K + 2 \cdot G)$ with G shear modulus

[*G. E. Dieter, McGraw Hill, SI Metric Edition*]

⇒ Design Dimensioning of ductile materials requires analyzing plastic yielding which means a deviatoric stress namely a shear stress must be employed.
This requires the deviatoric invariant J_2.

In order to understand specific terms some remarks considering Hencky, Drucker, Prandtl-Reuss, and Levi-Mises:

Table 17-2: Terms related to Hencky, Drucker, Prandtl-Reuss and Levi-Mises

Hencky proved in 1924 that the Von Mises model $F^{Mises} = \sqrt{3 \cdot J_2} \;/\; \bar{R}^t_{0.2} = \sigma^{Mises}_{eq} \;/\; \bar{R}^t_{0.2} = 1$

is equivalent to assuming "Yielding occurs when the distortional energy W reaches a critical value"

$$2 \cdot E \cdot W = (\sigma_x^{\,2} + \sigma_y^{\,2} + \sigma_z^{\,2}) - 2\nu \cdot (\sigma_x \cdot \sigma_y + \sigma_y \cdot \sigma_z + \sigma_x \cdot \sigma_z) + (\tau_{xy}^2 + \tau_{zx}^2 + \tau_{yz}^2) \cdot E / G =$$

$$= (\sigma_I^{\,2} + \sigma_{II}^{\,2} + \sigma_{III}^{\,2}) - 2\nu \cdot (\sigma_I \cdot \sigma_{II} + \sigma_{II} \cdot \sigma_{III} + \sigma_I \cdot \sigma_{III}).$$

Following Drucker (1951) " The total plastic strain vector, must be normal to the yield surface".

The yield body expands during uploading which requires a non-negative energy dissipation $\sigma_{ij} \cdot d\varepsilon_{ij}^{pl} \geq 0$ with an incremental strain vector $d\varepsilon_{ij}^{pl}$ normal to the yield surface. This so-called Normality Rule makes the yield body to be convex. As depicted: Convexity is not given for PMMA in the tensile domain ! ?

The flow rule describes the differential changes of the plastic strains as a function of the current stress state. The Incremental Theory "elastic-perfectly plastic" shall be applied. In this case the strain increment is seen to be composed of an elastic part and a plastic part $d\varepsilon_{ij} = d\varepsilon_{ij}^{\,el} + d\varepsilon_{ij}^{\,pl}$.

Regarding the Flow Rule for "elastic-perfectly plastic" the plastic strain increment will be linked.

The Prandtl-Reuss general representation of the flow rule is $d\varepsilon^{pl} = d\varepsilon^{pl}_{eq} \cdot \partial\sigma_{eq} / \partial\sigma$,

where $d\varepsilon^{pl}_{eq}$ and $\partial\sigma_{eq}$ are equivalent plastic strain increment and equivalent stress increment.

The equation expresses the condition that the direction of in-elastic straining is normal to the yield surface. This condition is called the normality condition.

The **Levi–Mises** equations (also called flow rules) describe the general relationships between stress and strain for an ideal plastic solid where the elastic strains are negligible. They can be written as

$$d\varepsilon_1 / s_1 = d\varepsilon_2 / s_{12} = d\varepsilon_3 / s_3 = \mathrm{d}\lambda \qquad \text{with deviatoric stresses} \quad s_i = \sigma_i - I_1 / 3.$$

LL:

- *The course of true test data can be better mapped by R/O than that of the engineering data*
- *Mapping is to be performed for the mean failure body*
- *Large strain non-linear analyses require the true stress-true strain curve*
- *Above $\bar{R}^t_m$ -level: true $\sigma_{ax} \rightarrow$ trueσ_{eq} due to 3D-stress state*
- *Course of strain-controlled tail of the stress-strain curve in the porous domain is not fully known.*
- *Shell elements in FEA, which reflect volume constancy, will provide true stresses in non-linear analysis. Therefore: Why should in such cases the higher true stresses notto be compared with the higher true strength values, in future?*
- *Stress-controlled: The material stressing effort Eff is $\leq$ 100%. There is no overstressing possible.*
- *Strain-controlled: Due to the less stressed vicinity of a 'hot spot' an overstraining is possible.*

For transferring theory into practical application an example shall be presented in *Fig.17-5* . *Table 17-3* presents the associate computation.

Example *Plain Strain Compression of a Ductile Metal Material Block*

Onset-of-Yielding' , 1-sided constrained. *from [Kelly, Solid Mechanics, Part II]*

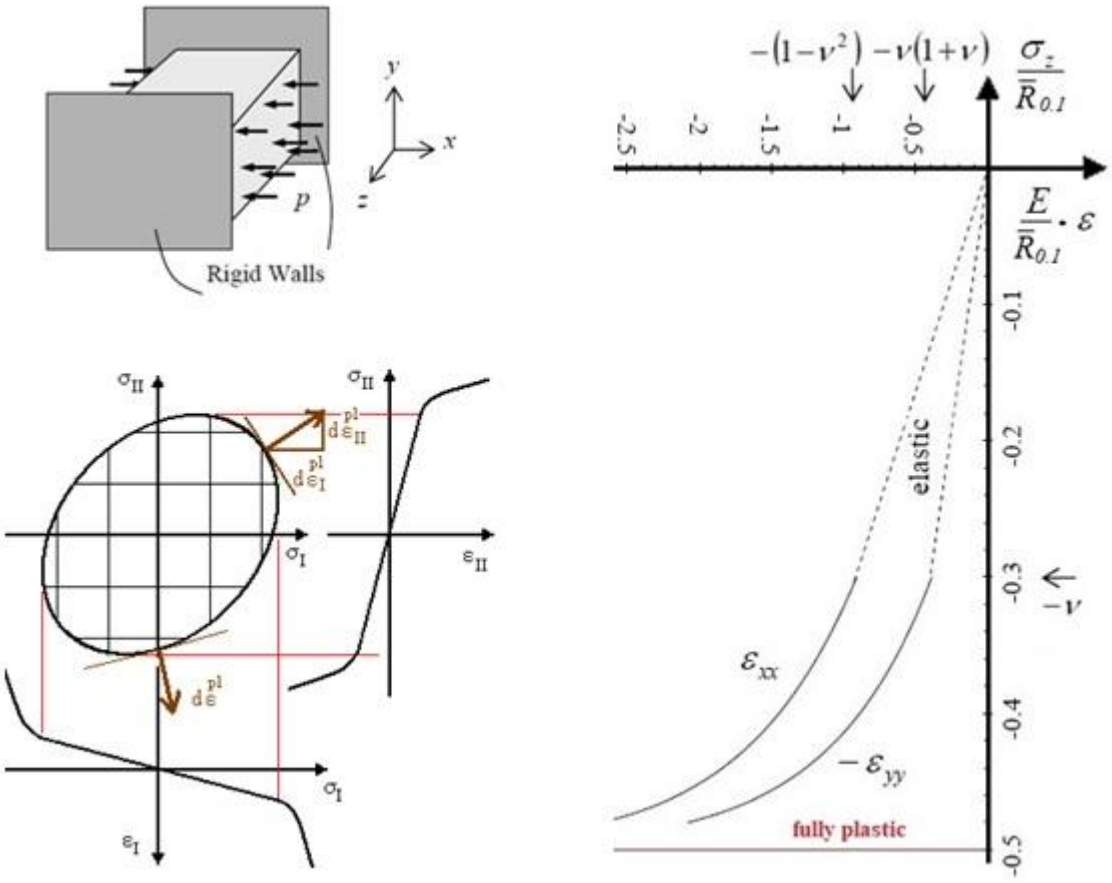


Fig.17-5: Stress situation under the pressure p in x-direction and normality illustration. Normalized stress-strain curve under the uniaxial stressing

Table 17-3: Derivation of the pressure-dependent stress-strain curve

Solution of elastic problem: Mohr stresses $\sigma_I > \sigma_{II} > \sigma_{III}$

$\{\sigma\} = (\sigma_I, \sigma_{II}, \sigma_{III})^T = (\sigma_y = 0,\ \sigma_z = -\nu \cdot p,\ \sigma_x = -p)^T$ and

$\{\varepsilon\} = (\varepsilon_x,\ \varepsilon_y,\ \varepsilon_z)^T = (-p \cdot (1-\nu^2)/E,\ p \cdot (\nu+\nu^2)/E,\ 0)^T$

Solution of elastic-perfect plastic problem via Prandtl-Reuss equations, in engineering terms,

$$d\varepsilon_x = [d\sigma_x - \nu \cdot (d\sigma_y + d\sigma_z)]/E + \frac{2}{3} d\lambda \cdot [\sigma_x - 0.5 \cdot (\sigma_y + \sigma_z)], \quad \mathrm{d}\gamma_{xy} = \frac{1+\nu}{E} \cdot \mathrm{d}\tau_{xy} + d\lambda \cdot \tau_{xy}$$

$$d\varepsilon_y = [d\sigma_y - \nu \cdot (d\sigma_x + d\sigma_z)]/E + \frac{2}{3} d\lambda \cdot [\sigma_y - 0.5 \cdot (\sigma_z + \sigma_x)], \quad \mathrm{d}\gamma_{yz} = \frac{1+\nu}{E} \cdot \mathrm{d}\tau_{yz} + d\lambda \cdot \tau_{yz}$$

$$d\varepsilon_z = [d\sigma_z - \nu \cdot (d\sigma_x + d\sigma_y)]/E + \frac{2}{3} d\lambda \cdot [\sigma_z - 0.5 \cdot (\sigma_x + \sigma_y)], \quad \mathrm{d}\gamma_{zx} = \frac{1+\nu}{E} \cdot \mathrm{d}\tau_{zx} + d\lambda \cdot \tau_{zx}$$

shortly tensorially expressed as $\mathrm{d}\varepsilon_{ij} = \frac{1+\nu}{E} \cdot d\sigma_{ij} - \frac{\nu}{E} \cdot \delta_{ij} \cdot d\sigma_{kk} + d\lambda \cdot s_{ij}$.

The magnitude of the plastic straining is determined by the so-called 'plastic multiplier' $\mathrm{d}\lambda$ or (proportionality factor).

For simplification Tresca (and not Mises) is employed, which states σ_x = -Y which is set here = - $\bar{\mathrm{R}}_{0.1}$ at onset of yield .

*A*pplying above equations considering no shear stress, $\sigma_y = 0$, σ_x = - $\bar{\mathrm{R}}_{0.1} \rightarrow d\sigma_x = 0$, $d\varepsilon_z = 0$ delivers

$$d\varepsilon_x = [d\sigma_x - \nu \cdot d\sigma_z]/E + \frac{2}{3} d\lambda \cdot [\sigma_x - 0.5 \cdot \sigma_z],\ d\varepsilon_y = [0 - \nu \cdot (d\sigma_x + d\sigma_z)]/E + \frac{2}{3} d\lambda \cdot [-0.5 \cdot (\sigma_z + \sigma_x)],$$

$$0 = [d\sigma_z - \nu \cdot d\sigma_x]/E + \frac{2}{3} d\lambda \cdot [\sigma_z - 0.5 \cdot \sigma_x)] \ \rightarrow\ d\lambda = \frac{-3}{E} \cdot \frac{d\sigma_z}{2 \cdot \sigma_z - \sigma_x} \equiv \frac{-3}{E} \cdot \frac{d\sigma_z}{2 \cdot \sigma_z + \bar{\mathrm{R}}_{0.1}}$$

Inserting λ into the first two Prandtl-Reuss equations these equations read:

$$\mathrm{E} \cdot\ d\varepsilon_x = [-\nu + \frac{\bar{\mathrm{R}}_{0.1} \cdot}{\sigma_z + 0.5 \cdot \bar{\mathrm{R}}_{0.1}} + \frac{0.5 \cdot \sigma_z}{\sigma_z + 0.5 \cdot \bar{\mathrm{R}}_{0.1}}] \cdot d\sigma_z, \quad \mathrm{E} \cdot\ d\varepsilon_y = [-\nu - \frac{0.5 \cdot \bar{\mathrm{R}}_{0.1}}{\sigma_z + 0.5 \cdot \bar{\mathrm{R}}_{0.1}} + \frac{0.5 \cdot \sigma_z}{\sigma_z + 0.5 \cdot \bar{\mathrm{R}}_{0.1}}] \cdot d\sigma_z$$

These equations have to be integrated by using the relation $\int \frac{x}{x+a} \cdot dx = x - a \cdot ln(x+a)$

$$\frac{E \cdot \varepsilon_x}{\bar{\mathrm{R}}_{0.1}} = -\frac{3}{4} \cdot ln\left(\frac{1-2\cdot\nu}{1+2\cdot\sigma_z/\bar{\mathrm{R}}_{0.1}}\right) + \frac{(1-2\cdot\nu)\cdot\sigma_z}{2\cdot\bar{\mathrm{R}}_{0.1}} - \frac{2-\nu}{2},\ \frac{E \cdot \varepsilon_y}{\bar{\mathrm{R}}_{0.1}} = \frac{3}{4} \cdot ln\left(\frac{1-2\cdot\nu}{1+2\cdot\sigma_z/\bar{\mathrm{R}}_{0.1}}\right) + \frac{(1-2\cdot\nu)\cdot\sigma_z}{2\cdot\bar{\mathrm{R}}_{0.1}} - \frac{3\cdot\nu}{2}.$$

In the *Fig*. 17 - 5 the plane strain compression of the solid block is presented for a metal with $\nu_0 = 0.3$.

With increasing $\sigma_z/\bar{\mathrm{R}}_{0.1}$, limit at 0.5, the effect of imcompressibility comes to act.

For info: 2 *sides constrained*, elastic case:

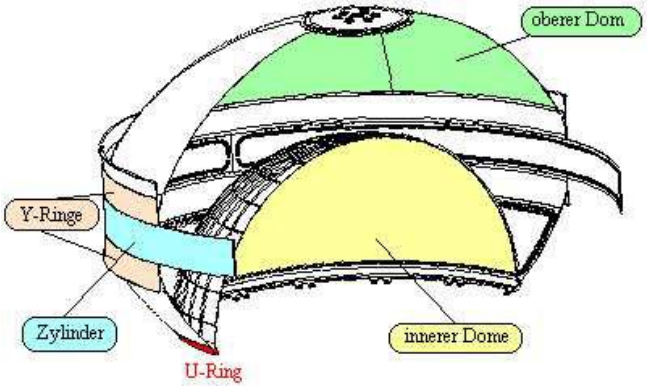
$$\varepsilon_x = \frac{-p}{E} \cdot \frac{(1+\nu)\cdot(1-2\nu)}{1-\nu}\ , \quad \sigma_y = -p \cdot \frac{\nu}{1-\nu} = \sigma_z, \quad \{\sigma\} = (-p,\ \sigma_y, \sigma_z)^T\ .$$

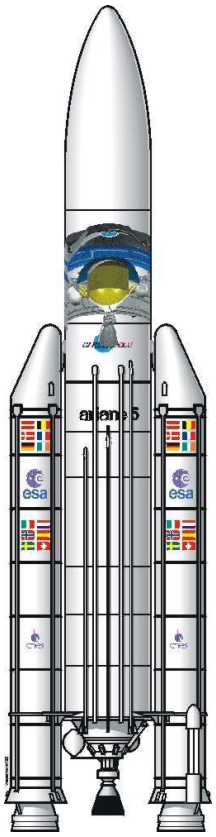
17.3 'Extended Mises' Yield Condition ($\bar{R}^{t}_{m} < \sigma_{eq} < \bar{R}_{ODC} < \bar{R}_{rupture}$; 0.5 ≥ actual ν)

LH2-tank of Ariane 5 upper stage

About 20 years ago for tank applications of the Ariane 5 a seven parameter 'Gurson type model' has been employed in a cooperation MAN-IWM-Freiburg.

Subject has been a more realistic assessment of the strain-controlled failure of the tank openings, to be based on a highly non-linear analysis.





The 'Gurson parameters' have been evaluated by performing and modelling a test with a round smooth tension rod and then optimally fitting the numerical results with the corresponding experimental results at rupture, as described in [*Nee84, Sun85*]. A successful simulation of the tensile rod test specimen determines the values for these parameters.
The measured and calculated load versus diameter reduction curves for the aluminum alloy AA2219 are given in *Fig.17-6* with the result: The global deformation behavior and the displacement at failure are well predicted by the model with the selected micromechanical Gurson parameters, determined for this metal and summarized in the table associated.

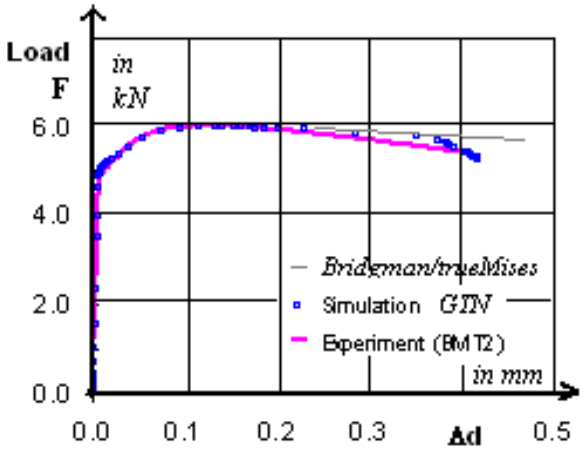
Thinking about statistically-based parameters required in design verification, for the author the question arose:

> "*Is it possible to perform non-linear analysis and design verification in a simpler way reducing the necessary multi-parameter fitting as much as reasonable? All parameters should be measurable and thereby can be statistically described."*

His idea: It is known that for the subsequent growing 'Mises-cylinder' one parameter is necessary, namely the size factor c^{Mises} for fixing the cylinder diameter. Since Beltrami it is further known that with changing volume (*here the increasing porosity of the highly plastified metal material*) the cylinder forms elliptically. This just requires one more parameter, a shape factor termed c_{12}.

17.3.1 Proposal of a Two Parameter Yield condition in the porosity domain ('Gurson domain')

Failure conditions enable the designer to assess multi-axial states of stress $\{\sigma\}$ by an equivalent stress σ_{eq} and to map multi-axial stress-strain behavior $\sigma_{eq}(\varepsilon_{eq})$ by a measured uniaxial stress-



f_0	f_n	f_c	f_F	q_1	q_2	ε_n	s_n
0.00	0.05	0.04	0.15	1.5	1.0	0.20	0.01

Fig.17-6:

Dependency of diameter reduction on load F.

Comparison of global simulation and test.

f are damage variables

Tensile rod diameter 4 mm = 2·a

strain curve $\sigma_{ax}(\varepsilon_{ax})$ if $\sigma < R_m$. When the stress state in a 'hot spot has to be assessed', e.g. in a structural tank, two cases have to be distinguished: The load- and the strain-controlled case. If it is load controlled, then, if the load reaches its maximum the structural part will fail like a tensioned membrane? This is not the case for strain-controlled 'hot spots' in unnotched structures built from ductile behaving materials. Here, stress redistribution is given due to redundancy effects of the material in the 'hot spot' vicinity. The envisaged 'hot spot' is unloaded due to the stiffness reduction caused by the increasing plasticity effects from non-linear stress-strain curve, from necking and further, from void growth with coalescence. Mass saving forces the designer to give not away any real strength reserve. Therefore, the difference of load- and strain-controlled strength assessment necessarily has to be tackled in order to use the benefit at least when a built structure is to save due to later load changes. The topic here is not a fatigue-linked one.

When searching the failure function it is to consider: Increasing porosity is linked to volumetric (dilatational) strains which are one part of the true plastic strains ε^{pl} involving now both, dilatational and distortional plastic strains. Cuntzes Failure Mode Concept (FMC) requires for a shear stress–based shape deformation of a material element the application of J_2 (*characterizes the shape change of the material element*), and for a *volume* change I_1^2. This change of volume or of density, respectivly, is *macro*-mechanically *described* by the principal stresses, however on the lower scale, the volume change of the voids or pores is *activated* by *meso*-level shear stresses (*therefore the index* $_\tau$) around the pores. In consequence of this, as yield condition for the subsequent failure surfaces is to formulate

$$F^{ExtMis} = c_1^{FMC} \cdot \frac{3J_2}{\bar{R}_{0.2}^{t\ 2}} + c_2^{FMC} \cdot \frac{I_1^2}{\bar{R}_{0.2}^{t\ 2}} = 1 \quad \Rightarrow \quad \frac{3J_2}{\bar{R}_{0.2}^{t\ 2}} + c12\frac{I_1^2}{\bar{R}_{0.2}^{t\ 2}} = c_\tau^t$$

with the equivalent stress and the Triaxiality Factor

$$\sigma_{eq}^t = \sqrt{3 \cdot J_2 + c12 \cdot I_1^2} = c_\tau^t \cdot \bar{R}_{p0.2}^t \quad \text{and} \quad TrF = \frac{1}{3} = \frac{\sigma_{mean}}{\sigma_{eq}^{Mises}} = \frac{I_1 / 3}{\sqrt{3 \cdot J_2}} = \frac{2 \cdot \text{true}\bar{R}^{tt} / 3}{\sqrt{3 \cdot J_2}} = \frac{2}{3} \cdot \frac{\text{true}\bar{R}^{tt}}{\sqrt{3}}.$$

The chosen yield surface condition describes an Extended Mises model, indexed ^{ExtMis}, which considers subsequent void growth for $I_1 > 0$, captured by the porosity-reigned shape parameter c_{12}.

17.3.2 Transformation 'Gurson' Yield Condition $(\bar{R}_m^t < \sigma_{eq} < \bar{R}_{rupture}; 0.5 \geq \nu)$, $F^{GTN} \rightarrow F^{ExtMis}$

Reminder, see again §16.3: The continuum mechanical description of ductile, micro-porous materials is carried out with micro-damage-mechanical models. To quantify these micro-damages,

damage variables are used, the development of which is described under the local stress state. The pore volume fraction f is used as a measure of the present material micro-damage and of the associated basic micro-damage variable. If the critical value f_{cr} is reached (*coalescence of the pores, defined as failure occurrence, which marks the threshold value for rapid void growth and decay of true strength*), then fracture is also achieved analogous to the tensile strength in the load-controlled case. With subsequent accelerated increase in porosity, maximum porosity with f_{rup} is achieved when ductile rupture (fracture) occurs.
The imperfection nuclei density determines the formation of new pores. With micro-damage mechanical models, local micro-material internal failure can be detected against the macro-material strength hypotheses. Known are the models of Rice and Tracey which at first depart with their model from the zero dilatation plastic flow visualized by the Mises-cylinder. They were followed by Rousseliier, Gurson and Tvergaard/Needleman, which are for simplification addressed here under the term 'Gurson model'.

The yield function for the relatively simple Gurson model ([*Gur77]*, parameter q_2=1) reads

$$F^{\text{GTN}} = \frac{3 \cdot J_2}{\sigma_F{}^2} + 2 \cdot \tilde{f} \cdot \cosh\left(\frac{I_1 \cdot q_2}{2\sigma_F}\right) - \tilde{f}^2 = 1 \quad \text{with} \quad \tilde{f} = q_1 \cdot f \qquad [Gur77, Nee84]$$

with the porosity micro-damage variable $f(I_1^2)$ and σ_F the increasing *F*low stress of the dense 'matrix' material. The porous body (smeared material) consists of the base material (so-called matrix) and the pores. The (dense) matrix phase follows the Mises model, and f is the mean void volume fraction or porosity (*average value of a porous matrix*) as the so-called internal damage variable. Rupture by shear band interaction between neighboring voids is marked by f_{rup} when the material loses completely its load bearing capacity due to local strength instability.

A Gurson model comes to act when the Mises cylinder begins elliptically to deform due to the effect of the growing voids and their final coalescence. This deformation of the potential surface is the more, the more void volume is generated and this runs oppositely (indicated by $0.5 > \nu$) to the presented Beltrami potential surfaces ($\nu_0 < 0.5$). An equivalent stress cannot be simply explicitly determined for F^{GTN} but may be roughly approximated by $\sigma_{eq}^{'Gurson'} \cong \sigma_{eq}^{'Mises'} \cdot (1-f)$.

Above function F^{GTN} caused the author to generate a simpler so-called Extended Mises model

$$\text{F}^{\text{ExtMis}} = \text{c}_1^{FMC} \cdot \frac{3J_2}{\bar{R}_{0.2}^{t\ 2}}(\textit{incompressible dense matrix}) + \text{c}_2^{FMC} \cdot \frac{I_1^{\ 2}}{\bar{R}_{0.2}^{t\ 2}}(\textit{porosity}) = 1.$$

This procedure is fully in context with the FMC because two features of the material solid are to describe, namely by J_2, I_1^2. A 'Comparison-of-coefficients' will be applied in order to link the 'Gurson parameter *f*' with the 'Extended Mises parameter'. The next lines show the transformation of above subsequent 'Gurson' type yield model into the Extended Mises model.

If the cosh-function is replaced by the first two terms of the associated Taylor series *[Cun98,Cun01]*

$$\rightarrow \quad \cosh(I_1 \cdot q_2 / 2 \cdot \bar{R}_{02}^{t}) = 1 + (I_1^{\ 2} / 8 \cdot \bar{R}_{02}^{t\ 2})\, q_2^{\ 2} + .. + .$$

and if the increasing true flow stress σ_F is set constant $\sigma_F = c_{GTN} \cdot \bar{R}_{0.2}^{t}$ fixed for a following comparison of coefficients, then the following micro-damage failure function will be achieved

$$F^{GTN} = \frac{3J_2}{\bar{R}^{t\ 2}_{0.2}} + 2\cdot\tilde{f}\cdot(1+\frac{I_1^2\cdot q_2^2}{8\cdot\bar{R}^{t\ 2}_{0.2}}) - \tilde{f}^2 = 1 \quad \Rightarrow \quad \frac{3J_2}{\bar{R}^{t\ 2}_{0.2}} + \frac{\tilde{f}}{4}\cdot\frac{I_1^2\cdot q_2^2}{\bar{R}^{t\ 2}_{0.2}} = (1-\tilde{f})^2,$$

which allows for the 'comparison of coefficients' between 'Gurson' and 'Extended Mises model'

$$\frac{3J_2}{\bar{R}^{t\ 2}_{0.2}} + [\frac{q_2^2\cdot\tilde{f}}{4}]\cdot\frac{I_1^2}{\bar{R}^{t\ 2}_{0.2}} = (1-\tilde{f})^2 \quad \Rightarrow \quad c_1^{FMC}\cdot\frac{3J_2}{\bar{R}^{t\ 2}_{0.2}} + c_2^{FMC}\cdot\frac{I_1^2}{\bar{R}^{t\ 2}_{0.2}} = 1$$

$$\frac{3J_2}{\bar{R}^{t\ 2}_{0.2}} + \frac{c_2^{FMC}}{c_1^{FMC}}\cdot\frac{I_1^2}{\bar{R}^{t\ 2}_{0.2}} = \frac{1}{c_1^{FMC}} \quad \leftarrow \text{ re-worked 'Extended Mises'}$$

This delivers two equations $\frac{1}{c_1^{FMC}} = (1-\tilde{f})^2$ and $\frac{c_2^{FMC}}{c_1^{FMC}} = \frac{q_2^2\cdot\tilde{f}}{4}$ and after solving

$$c_1^{FMC} = 1/(1-\tilde{f})^2, \quad c_2^{FMC} = \frac{1}{(1-\tilde{f})^2}\cdot\frac{q_2^2\cdot\tilde{f}}{4} \text{ and } \rightarrow c_{12} = c_1^{FMC}/c_2^{FMC} = \frac{q_2^2\cdot\tilde{f}}{4}.$$

Values for the increasing porosity f are strain-controlled detectable and therefore, the ratio is fixed. However, a further equation is needed to determine the size parameter, such as with the Mises cylinder.

Fig.17-7 left depicts the various strength values applied in mapping and design verification. The average strengths $true\bar{R}^t, \bar{R}_{odc}$ are then inserted into the right figure which presents for four porosity

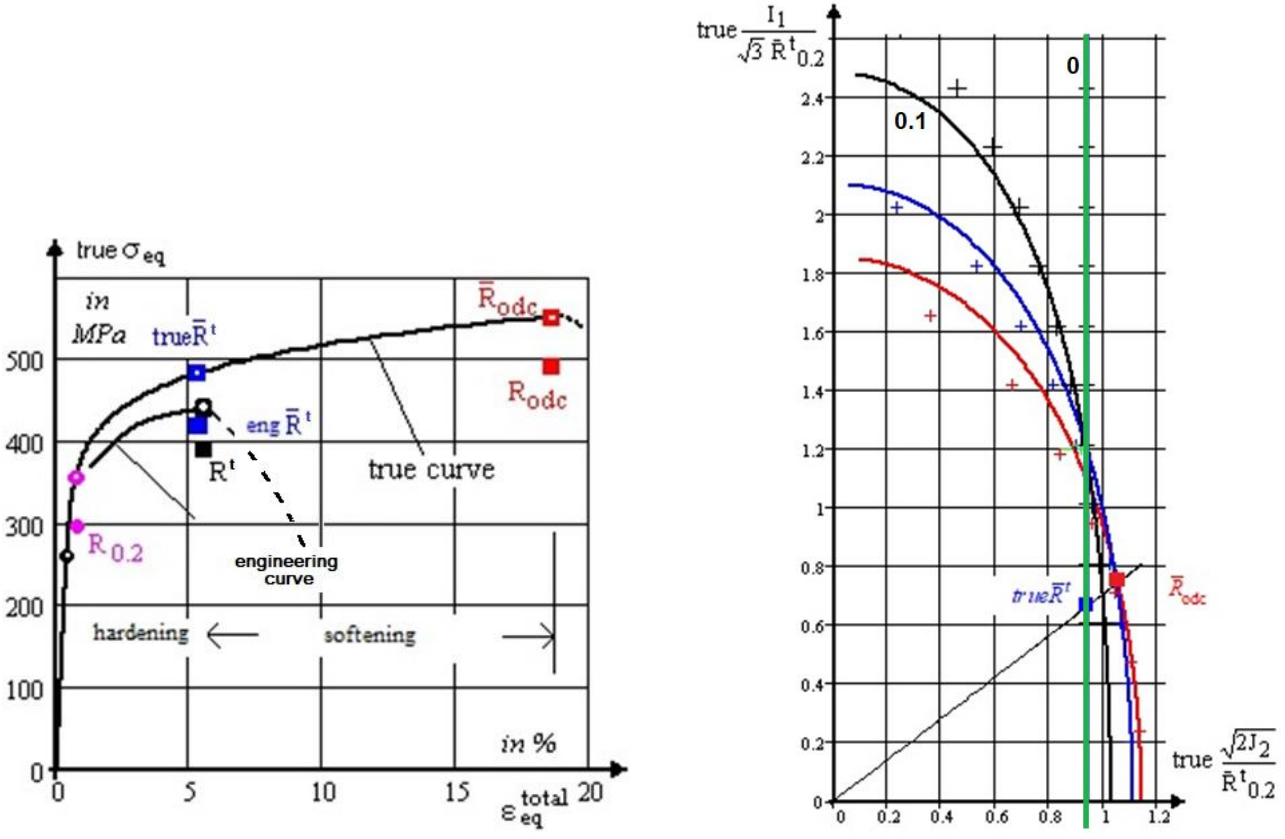


Fig.17-7 left: Equivalent true stress-equivalent true plastic strain curve. Proposed local strain-controlled extended stress-strain curve incl. mean fracture points and strength design allowables.
right: Schematic, AA2219: 3D- Gurson modelling (dots) compared with ExtMises modelling (q2=1.5, $q2_{ExrM}$=1.13) $true\bar{R}^t, \bar{R}_{odc}$ *. Using Lode-Haigh-Westergaard coordinates leads to a change in the shape in comparison to the conventional 'Gurson' plots*

volume fractions *f* (0, 0.1, 0.2, 0.3) a fictitious comparison of Gurson model and Extended Mises model. There was no adjustment made by a simulation process in order to get a better fit. Adjustment only makes sense if test curve points are available.

Fig.17-7 right presents the subsequent rotationally symmetric yield surfaces and finale rupture surface. Parameter of the failure surface is the porosity *f*. The figure displays the development of the subsequent failure surfaces. After achieving the tensile strength a further small radial increase of the surface is obvious together with the initiation of an elliptic surface. With increasing degradation the yield failure surface turns more and more elliptically. In the compression domain, existing voids are becoming closed and therefore, the curves are straight remaining a cylinder. Also the strain-controlled fracture surface ends porosity-dependent at a vertex point

$(\text{true}\bar{R}^{ttt}, \text{true}\bar{R}^{ttt}, \text{true}\bar{R}^{ttt})$, TrF = ∞ on the ordinate axis.

The deformation of the surface is the larger, the more void volume *f* is generated. It stops when reaching the load-carrying capacity which depends on the triaxiality *TrF* and the grade of strain control. By the increasing porosity the damage causing softening surpasses the in-situ time-parallel hardening of the matrix.

To calibrate the two curve parameters means to carry out fracture tests on smooth and notched test specimens at distinct triaxiality levels. Then, the evaluation of the strain-controlled test results has to be Bridgman-evaluated (or by FEA) which leads to the finally achieved value of *TrF* and to the size of the ellipsoidal surfaces.

In the FEA-based establishment of a (σ, ε)-curve beyond $\bar{R}_m^t$ a problem comes up:

* The test specimen tensile rod becomes a *structure* and is not any more a smooth material properties delivering *material test specimen*.
* The real (σ, ε)-curve as final output would have been still needed as input in the test data analysis.

17.3.3 Equivalent Plastic Strain and Flow Rule of Extended Mises model, Non-linear Analysis

Increasing porosity was to capture. That is linked to volumetric (dilatational) strains which are part of the true plastic strains ε^{pl} involving now both, dilatational and distortional plastic strains. As *yield function* or *yield potential (flow potential),* that considers dilatation, it is taken for the subsequent void growth considering yield surface

$$F^{\text{ExtMis}} = c_1^{FMC} \cdot \frac{3J_2}{\bar{R}_{0.2}^{t\ 2}} + c_2^{FMC} \cdot \frac{I_1^{\ 2}}{\bar{R}_{0.2}^{t\ 2}} = 1 \ \Rightarrow \ \frac{3J_2}{\bar{R}_{0.2}^{t\ 2}} + c12\frac{I_1^{\ 2}}{\bar{R}_{0.2}^{t\ 2}} = c_\tau^t$$

$$= \frac{3J_2}{\bar{R}_{0.2}^{t\ 2}} + c12 \cdot \frac{I_1^{\ 2}}{\bar{R}_{0.2}^{t\ 2}} = \frac{3 \cdot 0.5 \cdot s_{ij} \cdot s_{ij})}{\bar{R}_{0.2}^{t\ 2}} + c12 \cdot \frac{\sigma_{kk}^{\ 2}}{\bar{R}_{0.2}^{t\ 2}},$$

Flow Potential: $\hat{F} = 3 \cdot 0.5 \cdot (\sigma_{ij} - \delta_{ij} \cdot \sigma_{kk} / 3)^2 + c12 \cdot \sigma_{kk}^{\ 2}.$

If the ε^{pl} are large compared to the elastic ones ε^{el}, one can assume that the elastic strain ε^{el} is negligible. Then, the model $\varepsilon_{ij} = \varepsilon_{ij}^{pl}$ holds as before for 'Mises' with the total strain tensor [*Lip97*]. This is assumed to be valid for strain rates, too. According to an assumed so-called *associated flow rule* the strain rate becomes

$$\dot{\varepsilon}_{ij} = \dot{\lambda} \cdot \frac{\partial F}{\partial \sigma_{ij}} = \dot{\lambda} \cdot \frac{\partial\ (3 \cdot 0.5 \cdot (\sigma_{ij} - \delta_{ij} \cdot \sigma_{kk} / 3)^2 + c12 \cdot \sigma_{kk}{}^2)}{\partial \sigma_{ij}} = \dot{\lambda} \cdot [3 \cdot 0.5 \cdot 2 \cdot s_{ij} + c12 \cdot 2 \cdot \sigma_{kk} \cdot \delta_{ij}]$$

with the volumetric strain rate part

$$\dot{\varepsilon}_{vol} = \dot{\varepsilon}_{kk} = \varepsilon_{11} + \varepsilon_{22} + \varepsilon_{33} = \dot{\lambda} \cdot 2 \cdot c12 \cdot 3 \cdot \sigma_{kk} = \dot{\hat{\rho}} / \hat{\rho}$$

with the shape parameter $c12_{\tau}^{t}$ depending on the relative porosity *f** or on its counterpart the relative density $\hat{\rho}$. It further follows $\sigma_{kk} = \dot{\varepsilon}_{vol} / (6 \cdot \dot{\lambda} \cdot c12) = I_1$.

The rate of plastic energy dissipation is given for porous material by the expression $\dot{W}^{pl} = \sigma_{ij} \cdot \dot{\varepsilon}_{ij}$.

Substituting $\dot{\varepsilon}_{ij}$ into $\dot{W}^{pl}$ yields $c12$

$$\dot{W}^{pl} = \sigma_{ij} \cdot \dot{\lambda} \cdot [3 \cdot s_{ij} + 2 \cdot c12 \cdot \sigma_{kk} \cdot \delta_{ij}] = \dot{\lambda} \cdot [3 \cdot s_{ij} \cdot \sigma_{ij} + 2 \cdot c12 \cdot \sigma_{kk} \cdot \delta_{ij} \cdot \sigma_{ij}]$$

$$= \dot{\lambda} \cdot [3 \cdot s_{ij} \cdot s_{ij} + 2 \cdot c12 \cdot \sigma_{kk}{}^2 \cdot \delta_{ij}] = \dot{\lambda} \cdot (3 \cdot J_2 + c12 \cdot I_1^2)$$

There is an equivalence of general stress state and equivalent stress state in the tensile rod test specimen. According to the equivalent strain energy principle equivalent formulations are

$$\dot{W}^{pl} = \sigma_{eq} \cdot \dot{\varepsilon}_{eq}^{pl} \qquad \textit{multi-axial}$$

and $\dot{W}^{pl} = c_{\tau}^{t} \cdot \bar{R}_{0.2}^{t} \cdot \dot{\varepsilon}_{eq}^{pl}$ *uniaxial,* given by $\varepsilon_{eq}^{pl} = 0.002\ (true\sigma_{eq} / \bar{R}_{0.2})^{\bar{n}}$.

Considering a true uniaxial stress state $(\tilde{\sigma}_{eq}, 0, 0)$ the two invariants read

$$I_1 = \tilde{\sigma}_{eq}, \quad J_2 = \tilde{\sigma}_{eq}^2 / 3.$$

Then, for the associated uniaxial strain holds

$$\dot{\varepsilon}_{11} = \dot{\tilde{\varepsilon}}_{eq} = \dot{\lambda} \cdot [3 \cdot \tilde{\sigma}_{eq} - \tilde{\sigma}_{eq} + 2 \cdot c12 \cdot \tilde{\sigma}_{eq}] = 2 \cdot \dot{\lambda} \cdot [1 + c12] \cdot \tilde{\sigma}_{eq}$$

which leads after resolving to an expression for the *Lagrange multiplication (proportionality) factor*

$$\dot{\lambda} = \dot{\tilde{\varepsilon}}_{eq} / 2 \times (1 + c12) \cdot \tilde{\sigma}_{eq}.$$

Herewith, the yield condition for the considered uniaxial stress state takes the form

$$(1 + c12) \cdot \tilde{\sigma}_{eq}^2 = c_{\tau}^{t\,2} \cdot \bar{R}_{0.2}^2 \text{ or respectively } \tilde{\sigma}_{eq} = \sqrt{c_{\tau}^{t\,2} \cdot \bar{R}_{0.2}^2 / (1 + c12)}$$

which is to be compared to $\sigma_{eq}{}^{t} = \sqrt{3 \cdot J_2 + c12 \cdot I_1^2}$.

Now, the Cauchy stress tensor σ_{ij} is derivable from the equation

$$\dot{\varepsilon}_{ij} = \dot{\lambda} \cdot [3 \cdot \sigma_{ij} - \sigma_{kk} \cdot \delta_{ij} \cdot (1 - 2 \cdot c12)] \text{ after resolving } \sigma_{ij} = \frac{-1}{18 \cdot \dot{\lambda}} \cdot [-6 \cdot \dot{\varepsilon}_{ij} \cdot c12_{\tau}^{t} - \dot{\varepsilon}_{vol} (1 - 2 \cdot c12)].$$

Eventually, the equivalent plastic strain rate $\dot{\varepsilon}_{eq}^{pl} = (\sigma_{ij} \cdot \dot{\varepsilon}_{ij}) / (c_{\tau}^{t\,2} \cdot \bar{R}_{0.2}^{t})$ is obtained from

$$\dot{\varepsilon}_{eq}^{pl} = \left(\frac{-1}{18 \cdot \dot{\lambda}} \cdot [-6 \cdot \dot{\varepsilon}_{ij} \cdot c12 - \dot{\varepsilon}_{vol} \cdot (1 - 2 \cdot c12)]\right) \cdot \dot{\lambda} \cdot [3 \cdot \sigma_{ij} - \sigma_{kk} \cdot \delta_{ij} \cdot (1 - 2 \cdot c12)] / (c_{\tau}^{t\,2} \cdot \bar{R}_{0.2}^{t}).$$

→ Non-linear analysis can be started.

17.3.4 Proposal for a Bullet-shaped Ductile Fracture Failure Surface for design dimensioning

Main objective of the author is an 'industrial approach' for an improved assessment of strain-controlled 'hot spots' in a structural part, in order to outline the benefit of the remaining load

carrying capacity. The approach will be backed up by one validation, the metallic 'round tension bar specimen or tensile rod'.

Preliminary analyses of test results let assume a kink in the true(σ,ε)-curve due to void coalescence because degradation from micro-damage wins over hardening, see *Fig.17-8*. This let the author to put there a limit for his model. The limit point $\bar{R}_{odc}$ at 'Onset-of-ductile cracking = Onset of void coagulation' is indicated in the figure by the decrease of the curve. The analysis results, carried out at about 2001 and visualized by the plot, depict that due to the relation $I_1^2 \square f$ an essential porosity increase will occur. The SFCs read

$$\frac{3J_2}{\bar{R}_{0.2}^{t\ 2}} + c12\frac{I_1^{\ 2}}{\bar{R}_{0.2}^{t\ 2}} = c_\tau^t \qquad \rightarrow \quad \sigma_{eq}^{ExtMises} = \sqrt{3\cdot J_2 + c12\cdot I_1^2} = c_\tau^t \cdot \bar{R}_{0.2}^t ,$$

Bridgman void-corrected test, §16.3: $\sigma_{eq}^{ExtMises} = \frac{F}{A} / (1+2\cdot\rho/a)\cdot\ln(1+a/2\cdot\rho)$, valid $\bar{R}^t < \bar{R}_{odc}$.

Capturing '120°-rotational symmetry' requires to replace J_2 by $J_2 \cdot \Theta$.

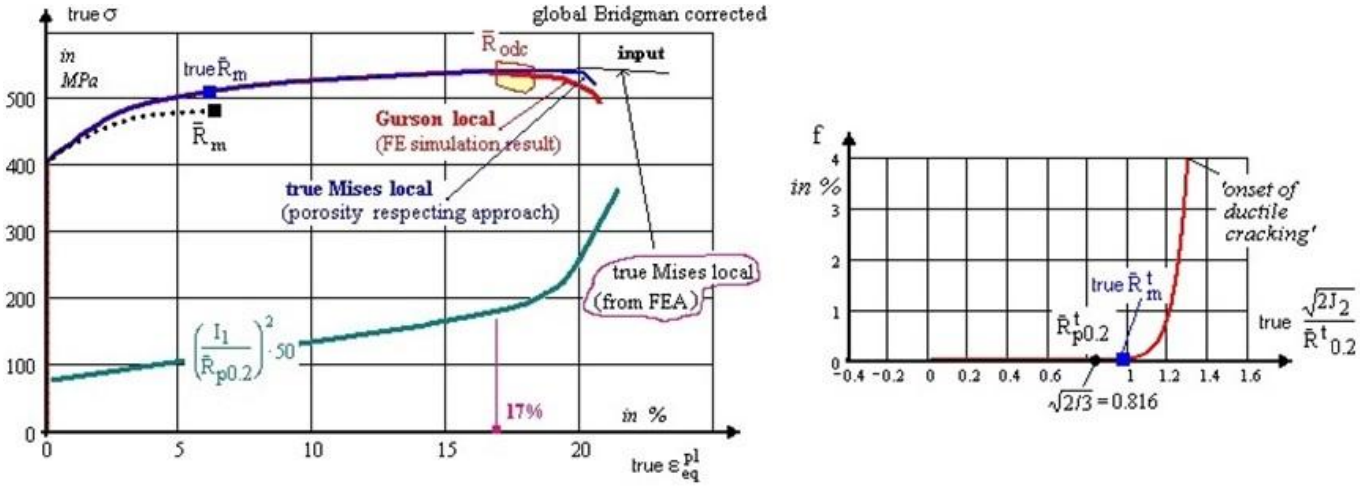


Fig. 17-8: (left) AA2219, visualization of the author's design verification idea (about 2000). (right) Modelling of the development of porosity f

Here, $f_{cr} < f_{rup}$ is employed as that porosity which is connected to 'onset of ductile cracking', in order to 'remain on the safe side'. The evolution function of f is assumed to be

$$f = c_1 \cdot \exp\left(\frac{J_2}{J_{2cr}} - 1\right)^{c_2} \quad \text{with} \quad J_{2cr}(\sigma_{eq}^{ExtMises}(\bar{R}_{odc})) .$$

Question is: "*How much Gurson material modelling is necessary to achieve a reliable prediction of the local design-driving ductile fracture level of the structure?"* This failure mode 'ductile fracture' is defined here to be met at 'onset-of-ductile cracking' and it shall correspond to DUL. Application is there, where the deformation-controlled strength value $R_{odc} > R^t$ can or must (*safe the final design or deliver a design rescue*) be used instead of the load-controlled strength value R^t.

Fig. 17-9 shows the void volume fraction in the necking region at failure. The highest values are reached in the center of the specimen (Element 20) as expected. From the central region micro-damage spreads out over the whole cross section and ends with unstable tensile failure

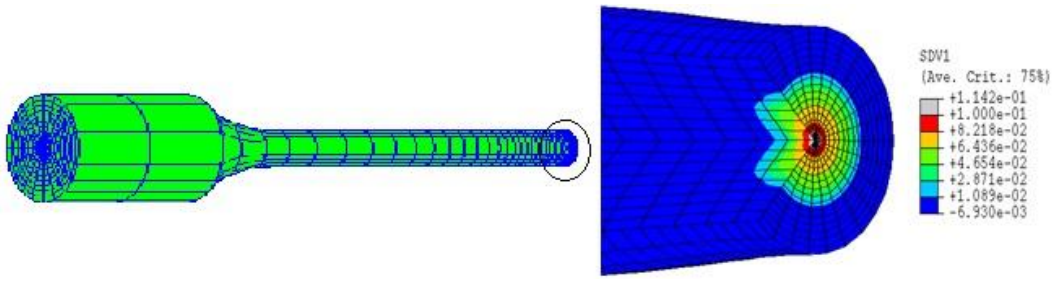


Fig. 17-9: Finite element mesh of the smooth tension rod. (right) Void volume fraction in the necking region at failure [Sun97] $\rho_{initial} = \propto \equiv smooth$, *2 a = 4mm*

The searched failure body looks bullet-shaped.

Gurson, Tvergaard, Needleman and further investigators followed to model the failure body which ends at a vertex as the limiting point, defined by the 3D ductile fracture stress state $(\bar{R}^{ttt}, \bar{R}^{ttt}, \bar{R}^{ttt})$. Such a bullet-shaped ductile failure body can be also described by the 'ExtMises' model which maps the shape change from the cylinder to the vertex as end of an ellipse. The location of the vertex and thereby the determination of the non-measurable average equi-triaxial strength value $\bar{R}^{ttt}$ is the challenging task the stress man is interested to get it efficiently estimated by minimum test effort and statistically-based model parameters. The determination of a closing cap of the fracture failure surface in the tensile range up to about TrF ≈ 2 is to perform.

In this tensile test specimen (*Fig.17-9*) micro-damage starts in the center of the tensile rod (*being smooth or containing differently sharp notches*), where highest equivalent stress and stress triaxiality are located, *Fig.17-10*. The plot outlines the applicability of the ExtMises model. Its range is outside of the Mises cylinder model. Also the decay is protermced which indicates some Gurson model quality.

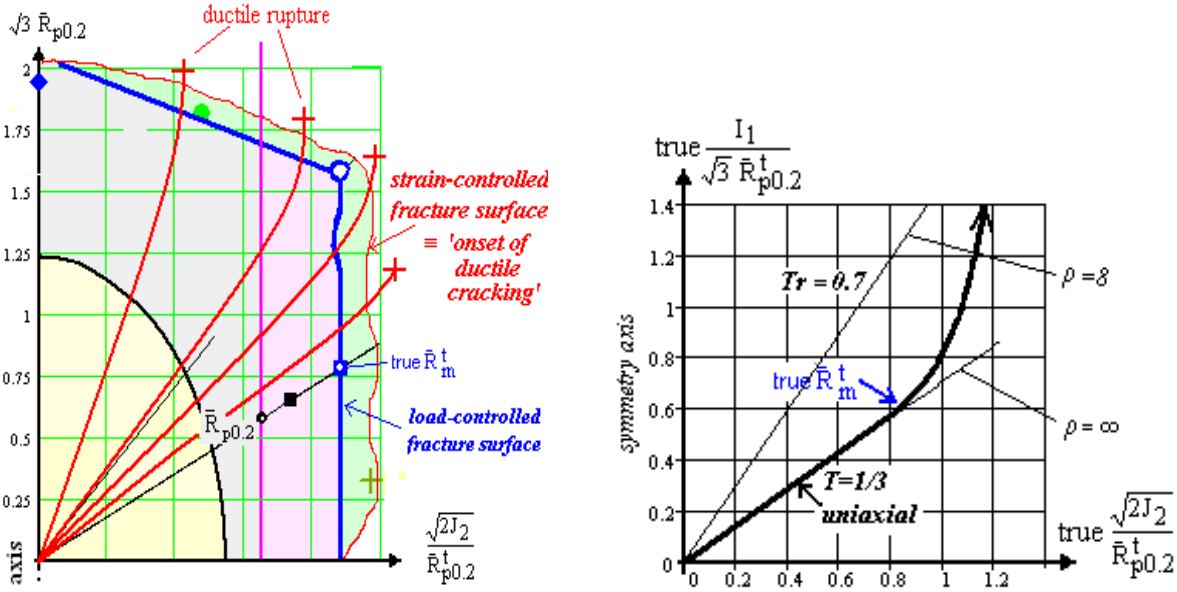


Fig. 17-10: (left) Subsequent strain-controlled 2D and 3D yield failure surfaces beyond the load-controlled limiting curve and after degradation). (right) *Scheme: change of true equivalent stresses with necking curvature ρ to higher triaxiality in the center of the tension rod.,* $\rho_{initial} = \propto \equiv smooth$, *2 a = 4mm. Above figures further show how the initial tri-axiality changes in the neck center with increasing diameter reduction of a round tensile specimen (un-notched/notched round tensile specimens TrF ≈ 2/3 to 5/3).*

From this result the conclusion may be drawn: The Extended Mises model delivers a satisfying engineering approach for the prediction of 'onset of ductile cracking' which is defined here as the ductile fracture limit corresponding to DUL.

In order to completely perform this Extended *'Proof of Design'* one has to define a new failure limit. As such a limit will be proposed the triaxiality dependent 'onset of cracking' The idea is to replace above simple failure function by a formulation of the used form. The modifications of Needleman and Tvergaard and other scientist have too many model parameters that cannot be measured. This concept builds on an extension of the applicability domain of the HMH, which means an extension of the stress-strain curve up to that level, where the designing engineer captures most of the softening-linked remaining load-carrying capability. This is only possible if the vicinity of the hot spot can take over overloading at the hot spot and is also only applied if a design is to save.

The next figure presents stress-strain curves of ductile and brittle materials (*applied in the design verification*) with average and statistically reduced strength values. The graphs base on measurements with the rod test specimen. Mind, again: The author questions the use of the minimum curve in design dimensioning.

Fig. 17-11 presents a final survey about the different non-linear stress-strain situations.

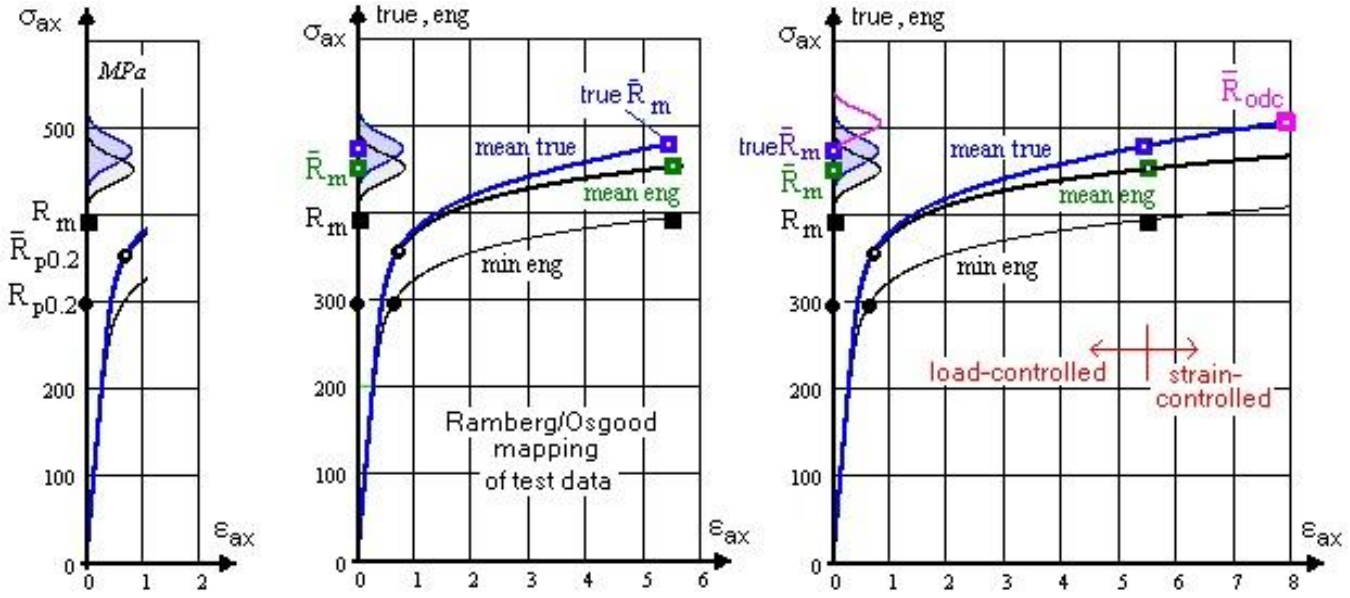


Fig.17-11: Visualization of the different nonlinear stress-strain curves with some strength distributions. (left) practically elastic, (center) medium plastic, (right) fully plastic

17.4 Development of Poisson's Ratio in the "Beltrami" and in the "Gurson" Domain

17.4.1 "Beltrami", transition zone to fully plastic, growth $v_0 < v < 0.5$

Beltrami bridges the elastic domain with the plastic domain. His formulation is not a failure function but a descriptive function to predict subsequent Beltrami surfaces $v(\bar{R})$, which are surfaces of equal potential. This means: A pair (v, R) must be given for each desired v-curve.

The usual formulation reads:

$$F^{Bel} = 3 \cdot J_2 + \kappa \cdot I_1^{\,2} = c^{Bel} \cdot \bar{R}_{0.2}^{t\;2} \quad \text{with} \quad \kappa = (1\text{-}2\nu)/(2\text{+}2\nu)$$

after inserting the point $(\bar{R}_{0.2}^{t}, 0, 0)^T$ with $I_1 = \bar{R}_{0.2}^{t}$, $J_2 = 2\bar{R}_{0.2}^{t} / 6 \rightarrow c^{Bel} = 1 + \kappa$.

Under the condition of uniaxial loading, Poisson's ratio is the absolute ratio value of lateral strain to axial strain.

In the Beltrami regime Poisson's ratio $\nu = \nu_{el} = \nu_0$ is approximately 0.3 for metals. Entering into the plastic range, the value of ν increases with increasing axial stress, finally up to 0.5.

In literature and FEA codes two proposals are presented:

$$\nu = 0.5 - (E_{sec} / E_0) \cdot (0.5 - \nu_0) \rightarrow \nu_{\text{engsec}} ,$$

in stability analyses (compression, shear) it is usual habit to apply in the plastic region

$$\nu = 0.5 - (E_{tan} / E_0) \cdot (0.5 - \nu_0) \rightarrow \nu_{\text{tansec}} .$$

A derivation of ν basically follows [*Bor99*] and uses the relationships:

$$true\varepsilon = true\varepsilon^{el} + true\varepsilon^{pl} \quad \text{general}$$

$$\rightarrow true\varepsilon_{ax} = \varepsilon_{ax}^{ela} + true\varepsilon_{ax}^{pl} \quad \text{and} \quad true\varepsilon_{lat} = true\varepsilon_{lat}^{el} + true\varepsilon_{lat}^{pl}$$

$$true\varepsilon_{lat}^{el} = -\nu_0 \cdot \varepsilon_{ax}^{ela} \quad \text{with} \quad \varepsilon_{ax}^{ela} = 0.01 \text{ as practical proportional strain limit}$$

$$\varepsilon = \varepsilon^{el} + \varepsilon^{pl} = \frac{\sigma}{E} + 0.002\left(\frac{\sigma}{R_{0.2}}\right)^n \quad \text{with} \quad n = \frac{ln\left(A_{us} / 0{,}2\%\right)}{ln\left(R_m / R_{p0.2}\right)} .$$

Measurements are usually performed on round bars which results for the envisaged incompressibility in $true\varepsilon_{lat}^{pl} = -0.5\, true\varepsilon_{ax}^{pl}$ (see Bridgeman-derivation before) into the formulas.

For the following data set, containing all possible true and engineering mapping curve parameters and further the statistically reduced design parameters, the various ν -functions are compared

$$AA2219, E_0 = 70000 \text{ MPa}$$

$$eng\,\bar{R}_{p0.2}^{t} = 352;\; eng\,\bar{R}_m^{t} = 453;\; eng\,\bar{n} = 12.7 \quad / \quad eng\,R_{p0.2}^{t} = 297;\; eng\,R_m^{t} = 395;\; eng\,n = 10.6 ,$$

$$true\bar{R}_{p0.2}^{t} = 354;\; true\,\bar{R}_m^{t} = 478;\; true\,\bar{n} = 10.6 \quad / \quad trueR_{p0.2}^{t} = 298;\; true\,R_m^{t} = 417;\; true\,n = 8.97 ,$$

$$A_g = 4.06\%,\; A_{fra} = 7.7\%, \quad eng\bar{A}_g = 4.9\%,\; true\,\bar{A}_g = 4.8\%, \quad true\,\bar{A}_{fra} = 7.5\% .$$

$$\text{true}\varepsilon = \frac{\text{true}\sigma}{E_0} + 0.002\left(\frac{\text{true}\sigma}{\text{true}R_{0.2}}\right)^{truen} , \quad \text{eng}\varepsilon = \frac{\text{eng}\sigma}{E_0} + 0.002\left(\frac{\text{eng}\sigma}{\text{reng}R_{0.2}}\right)^{engn} .$$

There are several formulations how *v* is changing in the elastic-plastic transition domain. comprises them.

$$E_{sec} = \sigma / \varepsilon = E_{(0)} / [1 + 0.002 \cdot E_{(0)} / \bar{R}_{p0.2} \cdot (\sigma / \bar{R}_{p0.2})^{\bar{n}-1}]$$

$$E_{tan} = d\sigma / d\varepsilon = E_{(0)} / [1 + 0.002 \cdot \bar{n} \cdot E_{(0)} / \bar{R}_{p0.2} \cdot (\sigma / \bar{R}_{p0.2})^{\bar{n}-1}]$$

$$\text{Etruetan} := \frac{E0}{1 + 0.002 \cdot \frac{truen \cdot E0}{trueR02} \cdot \left(\frac{true\sigma}{trueR02}\right)^{truen-1}}$$

$$\text{Eengtan} := \frac{E0}{1 + 0.002 \cdot \frac{engn \cdot E0}{engR02} \cdot \left(\frac{eng\sigma}{engR02}\right)^{engn-1}}$$

$$\nu truetan := 0.5 - (0.5 - \nu 0) \cdot \frac{Etruetan}{E0}$$

$$\nu engtan := 0.5 - (0.5 - \nu 0) \cdot \frac{Eengtan}{E0}$$

$$\text{Etruesec} := \frac{E0}{1 + 0.002 \cdot \frac{1 \cdot E0}{trueR02} \cdot \left(\frac{true\sigma}{trueR02}\right)^{truen-1}}$$

$$\text{Eengsec} := \frac{E0}{1 + 0.002 \cdot \frac{1 \cdot E0}{engR02} \cdot \left(\frac{eng\sigma}{engR02}\right)^{engn-1}}$$

$$\nu truesec := 0.5 - (0.5 - \nu 0) \cdot \frac{Etruesec}{E0}$$

$$\nu engsec := 0.5 - (0.5 - \nu 0) \cdot \frac{Eengsec}{E0}$$

$$true\varepsilon plax_j := 0.002 \cdot \left(\frac{true\sigma_j}{trueR02}\right)^{truen}$$

$$eng\varepsilon plax_j := 0.002 \cdot \left(\frac{eng\sigma_j}{engR02}\right)^{engn}$$

$$true\nu_j := \frac{-\left(-\nu 0 \cdot \varepsilon elaax - 0.5\, true\varepsilon plax_j\right)}{\left(\varepsilon elaax + true\varepsilon plax_j\right)}$$

$$eng\nu_j := \frac{-\left[-\nu 0 \cdot \varepsilon elaax - 0.5\left(eng\varepsilon plax_j\right)\right]}{\left(\varepsilon elaax + eng\varepsilon plax_j\right)}$$

Fig. 17-12 demonstrates the variation of ν with the various stresses, engineering and true ones. The graph helps to build up to understand the failure surface shape considering what the transition yielding domain has taught regarding ν.

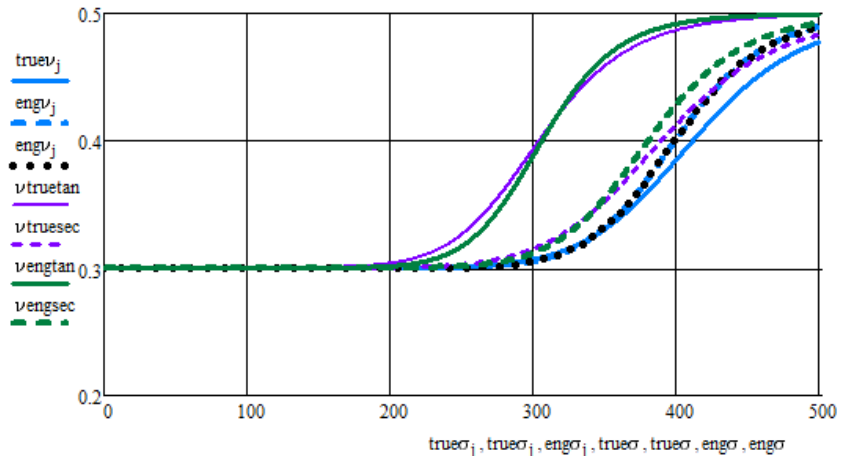


Fig.17-12: Dependency of ν on true and engineering stresses. Material example AA2219

According to missing test data an accurate formula is presently not to define, as a practical approach it is recommended

$$\nu\text{engsec} = 0.5 - (0.5 - \nu_0) \cdot (E_{sec} / E_0).$$

17.4.2 Void Porosity-linked reduction of Poisson's ratio $0.5 > \nu$

Porosity means volume change due to void coalescence and volume change may be transferred to a decaying Poisson's ratio (remind Beltrami). From the ExtM-model can be deduced geometrically taking $f^* = f \cdot q_2^2$,

$$c_{12} \cdot \frac{f^*}{4} = \frac{1-2\cdot\nu}{2+2\cdot\nu} \qquad \text{and} \qquad \nu = (4 - f^*)/ (8 + 2\cdot f^*).$$

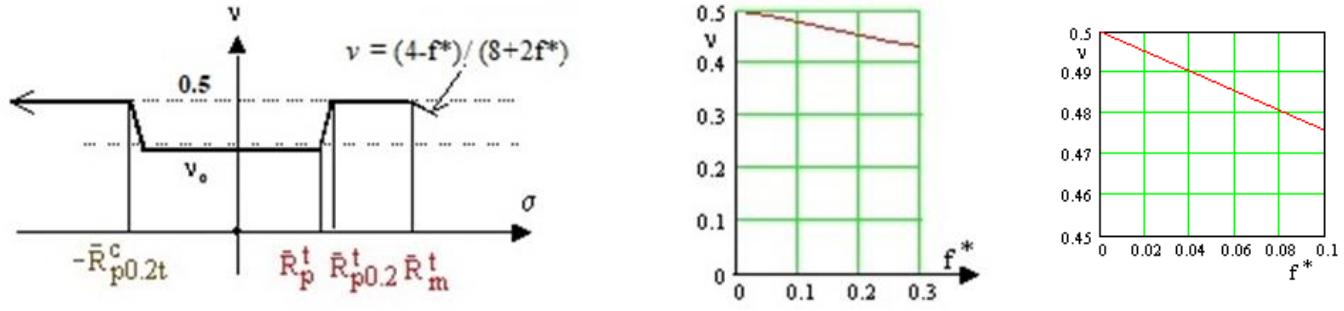


Fig. 17-13: Schematic dependence of ν in the elastic –plastic domain and the porosity-increasing domain

LL:

- ✓ *Whereas with the elasticity formulation of Beltrami the Poisson ratio v is growing this is opposite with the formulation of the Gurson-based models due to the increasing porosity*
- ✓ *The hypotheses from Beltrami via Mises until the refined Gurson ones describe an increase or decrease of a constant potential surface. The shape of the surface theoretically begins with $\nu = 0$ (sphere with foams) growing up from $0 < \nu$ to $\nu = 0.5$ via the growing Mises cylinder ($\nu = 0.5$) and ending with an ellipsoid, shrinking into a spherical direction represented by $0.5 > \nu$. This is essential for the stress analysis*
- ✓ *For two domain limits a clear value for the varying Poisson ratio is given:*

  $$\textit{proportional limit } \sigma \le \bar{R}_p^t \Rightarrow \nu = \nu_0 \quad \textit{and} \quad \textit{yield limit } \sigma = \bar{R}_{p0.2}^t \Rightarrow \nu = 0.5$$

- ✓ *Designing requires to use limit state formulations, termed failure criteria (SFCs). These are fracture failure criteria for brittle materials namely for 'Onset-of-fracture' and yield failure criteria for ductile materials. In practice, for ductile materials these failures are 'Onset-of-yielding' and - for the author - 'Onset-of-void coagulation = Onset of ductile Cracking ' in the case where strain-softening applies.*

17.4.3 Some conclusions considering Design Dimensioning and Design Verification

Highest challenge of the design engineer is a good prediction of a reliable MoS value.
In the design verification of structures with a strong mass requirement and built from ductile metals specifically the assessment of strain-controlled 'hot spots' lacks of a practical procedure.
There, failure may be called either 'onset-of-yielding' or 'onset-of-ductile cracking' that practically means fracture failure. A fracture failure surface confines the 'yield surface domain'. Such a fracture surface might be a strength (material is not cracked) failure surface or a (macro-)damage tolerance (*material is cracked*) one. In the case of ductile behavior it is to discriminate load- and deformation-controlled stressing. Fracture is practically reached in the load-controlled case at 'onset-of-diffuse necking' (here *the reduction of cross section overrules hardening*). Load-carrying capacity is then reached for a non-redundant, statically determined system in the brittle case as well as in the ductile case.

* Present Design Philosophy features

- Non-linear analyses, needed for the determination of an accurate (ductile) MoS_{ult} - in spite of the much higher numerical effort - become more and more 'popular', whether it is absolutely necessary from Standard requirements or not
- Some ESA-specifications and new ISO vessel codes seem to rule out for ductile material the 'cheap' and permitted development way of 'designing structures to MoS_{yield} (*linear analyses only*) instead to MoS_{ult}
- In order to simplify the design development by parallelly performing stress analysis and strength Design Verification or Proof-of-Design (*here to apply are minimum values = strength design allowables*) minimum curves are sometimes requested to apply. This is physically not accurate and design-risky
- 'Strength analysis' for Design Verification can be only combined with 'stress analysis' in one computation if the structure is not redundant such as a membrane shell, if a priori the critical material locations are known (*statically determined systems like above membrane shell*)
- Considering the true stress-strain curve, which is applicable if the non-linear analysis regards the thinning of the wall, then true stresses are the FEA output and in design verification the engineering tensile strength R^t is to replace by the true strength $R^t \cdot (1+_{eng}\varepsilon)$

* Findings

- Usually applied stress-strain curve is the engineering stress-strain curve. Its applicability ends with reaching onset-of-diffuse necking at R^t. This is the limit when the material at the local hot spot is load-controlled
- Beyond R^t a void-caused micro-damage makes the equivalent true stress-equivalent true plastic strain hardening curve flatter. A high hardening rate of a material implies considerable strength reserves after surpassing R^t
- Beyond R^t the Bridgman-evaluation of the tensile rod test delivers the basement for an improved effective equivalent stress-strain curve, which can be used for an appropriate subsequent yield condition and a final fracture condition
- If around a ductile 'hot spot' stress redistribution is possible then the real structure fracture will be observed at loading levels higher than for locally achieving the tensile strength R^t, because the failure system of the structure is deformation-controlled and redundant. Despite of the fact, that the material has reached *Eff* = 100% in the 'Hot spot' volume the decaying strength and stiffness capacity still contribute to the structure
- In general it is observed that 'onset of ductile cracking' is indicated before the plastic limit load is reached. Thus, in strength analysis attention should focus on true stresses and true strains at this load level marked by the effective strength R_{odc}. For load-carrying structures the tail is only relevant in case of deformation-controlled 'hot spots' within redundant structures. This final curve part up to the rupture point is of marginal design value
- The Extended Mises model delivers a satisfying engineering approach for the prediction of 'onset of ductile cracking' which is defined here as the ductile fracture limit that corresponds to Design Ultimate Load.
- A procedure must be mechanically consistent. This leads to CoSt saving and helps to avoid redesign.

* Proposed Procedure

- Out-sorting, whether the simpler linear analysis may be applied due to the ratio $j_{0.2} / j_{ult} = R_{0.2} / R^t$. If yielding is design-driving one can quickly linearly perform a design trade-off
- Application of the always mandatory (macro)Damage Tolerance Design Verification, which usually captures MoS_{ult}
- Non-linear analysis of the structural part, applying the Bridgman-corrected, voids-considering Extended Mises equivalent stress curve. Determination of the effective $\bar{R}_{\text{odc}}$ and crit $\varepsilon_{eq}^{pl} = \varepsilon_{\text{odc}}^{\text{pl}}$. Recommended design constraint $\varepsilon_{\text{odc}}^{\text{pl}} < 4\%$ for the example AA2219. FoS j_{ult} is to apply
- Each structural tank is redundant and has to be analyzed by the application of the *mean thickness* and a *mean (σ,ε)-curve* in order to find both, the most probable best design and the real 'hot spots' as a result of stress and deformation analysis. Of course, eventually a 'post strength analysis' regarding local *'min.* thickness' is obligatory.
- That $\bar{R}_{\text{odc}} (\approx F_{\text{odc}} / A_{\text{odc}}) > \bar{R}^t$ depends on the reducing effective cross-section. In an accurate non-linear analysis the wall thinning is considered.
- Application of the porosity considering Bridgman correction: $\bar{R}_{0.2}^t$ is normalizing strength

$$\frac{3J_2}{\bar{R}_{0.2}^{t\ 2}} = c_\tau^{\text{Mises}} \quad \Rightarrow \quad \frac{3J_2}{\bar{R}_{0.2}^{t\ 2}} + c12\frac{I_1^{\ 2}}{\bar{R}_{0.2}^{t\ 2}} = c_\tau^{\text{ExtMises}}$$

$$\sqrt{3 \cdot J_2} = \text{corrected true}\,\sigma_{\text{eq}}^{\text{Mises}} = \frac{F}{A} / (1 + 2 \cdot \rho/a) \cdot \ln(1 + a/2 \cdot \rho)\text{ , valid} > \bar{R}^t$$

$$\sqrt{3 \cdot J_2 + c12 \cdot I_1^2} = \text{corrected true}\,\sigma_{\text{eq}}^{\text{ExtMises}} = \frac{F}{A} / (1 + 2 \cdot \rho/a) \cdot \ln(1 + a/2 \cdot \rho)\text{ , valid } \bar{R}^t < \bar{R}_{\text{odc}}\ .$$

* Compilation of the various formulas applied in isotropic analysis

Table 17-2 shall provide a collection of failure limit state functions (*strength criteria*) of isotropic materials in the complete strain domain. Criteria, using I_1 are termed 'pressure–sensitive'.

The following table visualizes for various stress states the capacity to yield indicated by the associated tri-axiality factor as a measure which is responsible for some 'embrittleness' (Versprödung). In addition principle strains are provided.

$\{\sigma\} / R_m^t$	$\sigma_{eq}^{Mises} / \bar{R}_m^t$	ε_{eq}^{Mises}	ε_I	ε_{II}	ε_{III}	TrF
$\bar{R}_{p0.2}^{\ t} = 352,\ \bar{R}_m^t = 453.\ \bar{A}_g = 7.7\%, \bar{n} = 12.74, \bar{E}_0 = 70000$ MPa						
(1, - 0.5, 0)	1.32					1.26
(1, 0, 0)	1	5.05	5.70	-2.72	-2.72	1/3
(1, + 0.5, 0)	0.83	1.15	1.54	0.13	-1.29	0.58
(1, 1, 0)	1	5.02	2.97	2.97	-5.41	2/3
(1.15, 1.15, 0.5)	0.65	0	0.43	0.43	-0.12	1.44
(1, 1, 1)	0	0	0.26	0.26	0.26	∞

Table 17-2: Collection of failure limit states of isotropic materials

Failure Limit States for static **Design Verification** of *'Dense'* Materials (*design allowables)

* Onset-of-Yielding (set $\Theta = 1$) $\quad F_\tau^{Mises} = \dfrac{3 \cdot J_2 \cdot \Theta}{R_{0.2}^{t\ 2}} = 1$ ductile , $Eff^{Mises} = \sqrt{3J_2 / R_{0.2}^t}$, $I_1 >=< 0$

* Onset-of-load-controlled Fracture $\dfrac{3 \cdot J_2 \cdot \Theta}{R_{0.2}^{t\ 2}} = \dfrac{R^{t2}}{R_{0.2}^{t\ 2}}$ $\Theta \geq 1$, d >1 mild steels; $\Theta \cong 1$ high strength steels, $I_1 > 0$

* Onset-of-Ductile Cracking' before rupture ($_{odc}$) $\quad c_{1\tau}^t \cdot \dfrac{3 \cdot J_2 \cdot \Theta}{R_{0.2}^{t\ 2}} + c_{2\tau}^t (porosity\ f) \cdot \dfrac{I_1^{\ 2}}{R_{0.2}^{t\ 2}} = 1$ ductile , $I_1 > 0$

* Normal Fracture: $F_\sigma^t = F^{NF} = c^{NF} \cdot \Theta^{NF} \cdot \dfrac{\sqrt{4 \cdot J_2 \cdot \Theta - I_1^{\ 2}/3} + I_1}{2 \cdot R^t} = 1$, $\Theta \leq 1$, d < 1, brittle, $R^t < R^{tt}$, $I_1 > 0$

* Shear Fracture: $F_\tau^c = F^{SF} = c_1^{SF} \cdot \dfrac{3 \cdot J_2 \cdot \Theta}{R^{c\ 2}} + c_2^{SF} (friction\ \mu) \cdot \dfrac{I_1}{R^c} = 1$, $\Theta \geq 1$, d >1, brittle, $-R^c > -R^{cc}$, $I_1 < 0$

Mode domain description (subsequent potential surfaces, *mapping values 50%)

* Potential surfaces in elastic Beltrami domain $\nu_0 \leq \nu \leq 0.5$: $F^{Bel} = 3 \cdot J_2 + \kappa \cdot I_1^{\ 2} = c^{Bel} \cdot \bar{R}_{0.2}^{t\ 2}$ with $\kappa = \dfrac{1\text{-}2\nu}{2+2\nu}$

* Yielding in Mises domain $\nu = 0.5$, $\sigma^t < \sigma^{tt}$: $\dfrac{3 \cdot J_2 \cdot \Theta}{\bar{R}_{0.2}^{t\ 2}} = c_\tau$, $Eff^{Mises} = \sqrt{3J_2 / \bar{R}_{0.2}^t}$

$\max c_\tau = \bar{R}_m^t / \bar{R}_{0.2}^t$, $\sigma_{eq}^{Mises} = \sqrt{3J_2} = \sqrt{0.5} \cdot \sqrt{\left[(\sigma_I - \sigma_{II})^2 + (\sigma_{II} - \sigma_{III})^2 + (\sigma_{III} - \sigma_I)^2 \right]} = \sqrt{2} \cdot \sqrt{\tau_{III}^2 + \tau_I^2 + \tau_{II}^2}$

$c_\tau = \bar{R}^t / \bar{R}_{0.2}^t$ better $\rightarrow$ $c_\tau = \text{true}\bar{R}^t / \text{true}\bar{R}_{0.2}^t$.

* Large Yielding in Gurson domain $0.5 \geq \nu$, $F_\tau^{ExtMises} \rightarrow \dfrac{3J_2}{\bar{R}_{0.2}^{t\ 2}} + c_{12} \cdot \dfrac{I_1^{\ 2}}{\bar{R}_{0.2}^{t\ 2}} = c_\tau^{ExtMises} (porosity\ f)$.

$\max c_\tau^{ExtMises} < \bar{R}_m^t / \bar{R}_{0.2}^t > \bar{R}_{odc} / \bar{R}_{0.2}^t$

120°-rotationally symmetry: Effective with all isotropic materials, brittle and ductile ones (size different)

c^{NF} ,Θ^{NF} from the two points $(\bar{R}^t,\ 0,\ 0)$ and $(\bar{R}^{tt}, \bar{R}^{tt},\ 0)$ or by a minimum error fit, if data available,

c^{SF} ,Θ^{SF} from the two points $(-\bar{R}^c,\ 0, 0)$ and $(-\bar{R}^{cc}, -\bar{R}^{cc}, 0)$ or by minimum error fit .

$I_1 = (\sigma_I + \sigma_{II} + \sigma_{III}) = f(\sigma)$, $\quad 6J_2 = (\sigma_I - \sigma_{II})^2 + (\sigma_{II} - \sigma_{III})^2 + (\sigma_{III} - \sigma_I)^2 = f(\tau)$

$27J_3 = (2\sigma_I - \sigma_{II} - \sigma_{III}) \cdot (2\sigma_{II} - \sigma_I - \sigma_{III}) \cdot (2\sigma_{III} - \sigma_I - \sigma_{II})$,

$\sigma_I, \sigma_{II}, \sigma_{III}$ are principal stresses, $\sigma_I > \sigma_{II} > \sigma_{III}$ are mathematical stresses (> means more positive)

A 2-fold acting mode or an orthogonal stress state makes the rotationally symmetric fracture body 120°-symmetric and is modelled by using the invariant J_3 and Θ as non-circularity function with d as non-circularity parameter $\Theta = \sqrt[3]{1 + d \cdot \sin(3\vartheta)} = \sqrt[3]{1 + d \cdot 1.5 \cdot \sqrt{3} \cdot J_3 \cdot J_2^{-1.5}}$, with the Lode angle ϑ , here set as $\sin(3 \cdot \vartheta)$ taking the 'neutral' shear meridian angle $\vartheta = 0°$

If a failure body is rotationally symmetric, then $\Theta = 1$ as set for the neutral shear meridian.

$$\varepsilon_{eq}^{Mises} = \sqrt{2} \cdot \sqrt{(\varepsilon_I - \varepsilon_{II})^2 + (\varepsilon_{II} - \varepsilon_{III})^2 + (\varepsilon_{III} - \varepsilon_I)^2} / 3, \qquad \sigma_{eq}^{Mises} = \sqrt{3 \cdot J_2}.$$

$true\varepsilon = \ln(1 + eng\varepsilon)$, $eng\varepsilon = e^{true\ \varepsilon}$ - 1, $true\sigma = eng\sigma \cdot (1 + eng\varepsilon)$ and

$eng\sigma = true\sigma / \exp(true\varepsilon)$, $true\varepsilon_{ax} = \ln(\ell / \ell_0) = \ln(1 + eng\varepsilon_{ax})$.

** Finally mind the Bridgman-based evaluation of the tensile rod test with considering the material porosity.

Fig.17-13 depicts stress-strain curves and essential strength points.

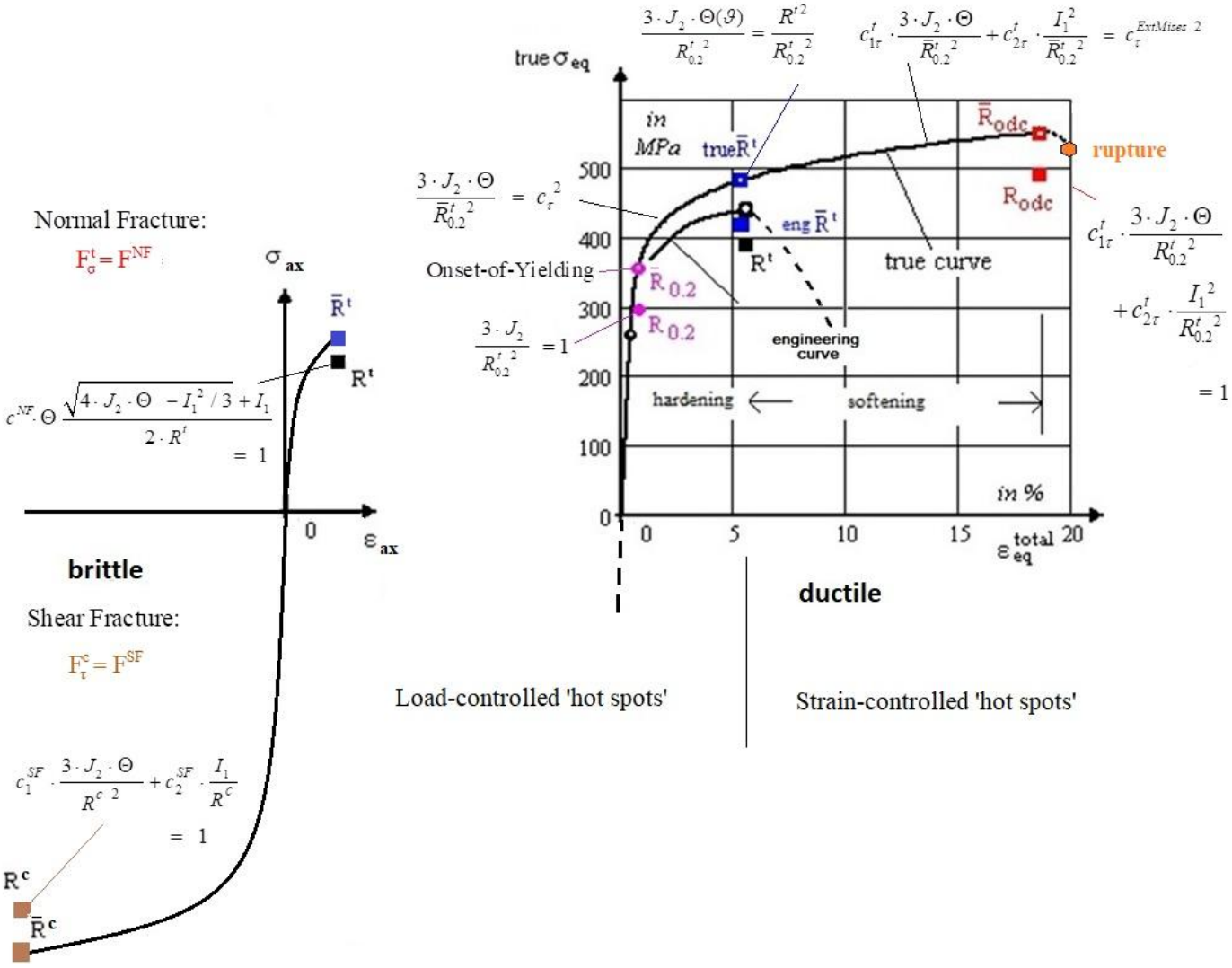


Fig.17-13: Evaluation of the stress-strain curve of a ductile and a brittle rod test specimen. Failure criteria at the failure points and domain descriptions are depicted. (Θ represents the 120°-material symmetry)

* Proposed Design Verification

In the design of ductile metals design dimensioning and design verification is to perform for load-controlled and strain-controlled design cases.

- Load-controlled: The subsequent growing Mises-Cylinder is terminated by a ductile fracture cap, where the

$$\nu_0 \le \nu \le 0.5) \;\Rightarrow\; \text{true}\bar{R}_{0.2}^t \le \text{true}\sigma_{eq} \le \text{true}\bar{R}^t \;\; (= \text{fracture})$$

- Strain-controlled: post-failure regime regarding the load determined case

$$0.5 \ge \nu \;\Rightarrow\; \text{true}\bar{R}^t \le \text{true}\sigma_{eq} \le \text{true}\bar{R}_{rupture}^t \;)$$

The MoS are computed using the following ($R_m = R^t$ or R^c) formulas:

a) Small strains:
$$MoS = \frac{design\ allowable\ engR_m}{j_{ult} \cdot eng\sigma(DLL)} - 1$$

b) Small strains, large deformations: $MoS = \dfrac{design\ allowable\ engR_m}{j_{ult} \cdot eng\sigma(DLL)} - 1$

c) Large strains, large deformations: $MoS = \dfrac{design\ allowable\ trueR_m}{true\sigma(\ j_{ult}\ \cdot DLL)} - 1$

d) Strain-controlled design allowable: $MoS = \dfrac{design\ allowable\ trueR_{\mathrm{odc}}}{true\sigma_{\mathrm{eq}}(\ j_{\mathrm{ult}}\ \cdot DLL)} - 1$.

The behavior of a *strain*-controlled 'hot spot' is similar to that of a 'fail-safe' construction. The load resistance is determined by a stress limit, associated to load- (trueRm) or a strain-controlled (R_{odc}) 'Onset-of-ductile cracking' fracture conditions applying

$$trueR_m = R_m \cdot (1 + A_{gl}),\ \text{with}\ R_m, A_{gl}\ \text{and}\ R_{\mathrm{odc}}\ \text{to be determined}.$$

Some of the information used had been provided by colleagues Dr. T. J. Reinke, Dr. J. Albinger, Dr. R. Beck, and Dr. H. Haller. R. Schiffmann from the RWTH Aachen handed over his PhD test results for a preliminary validation of the author's approach. I gratefully acknowledge these contributions and especially the valuable discussions with all of these persons about 2000.

LL: After stringent design alterations as with loadings makes such an effortful rescue operation for an already manufactured component or of a final design in the high plasticity domain necessary.

17.5 Mises (HMH) Yield Hypothesis or Tresca Yield Hypothesis? What counts?

The following belongs to a tough Ariane Design discussion ending with a compromise to use Misca (not given here) as a nonphysically-based mathematical mixture of Mises and Tresca.

Both the hypotheses are yield hypotheses.
In the past right, Tresca was preferred from numerical hand calculation reasons. Now, its corners make numerical problems in 3D-FE-analysis and there would be no need any more for applying Tresca, but this is not the case.

For the design of pressure vessels (*here, Ariane 5 Booster steel tank*) with their typical stress state of 2:1 the design against Onset-of-Yielding is penalized by 15% less if one uses Tresca and not Mises. This effect, sometimes termed 'flattening effect' (*Fig.17-14*) means that the Mises ellipse becomes dented, and this marks a strong design drawback. This flattening of the Mises ellipse occurs in the positive quadrant and depends on specimen quality, grain size, grade of ductility and testing and the specific stress state as will be shown.
Not to fully lose above 15% the author investigated literature and own experiments with the result that theory, test results, fracture morphology and non-linear analyses outline:

'Onset of yield failure' in case of ductile behaving materials:

* Test results show differences to Mises between 0 and about 7 % in the positive stress domain as the domain of highest principal stresses. Test results confirm that 'Onset-of-Fracture' begins at the outer surface of the traditional tube test specimen loaded by internal pressure
* The Mises ellipse outlines for a stress state (2:1) the highest principal tube stress. Before plastic collapse this principle stress, a hoop stress, wanders under increasing loading from the inner to the outer surface. This complies with the fact that bad polished tubes generate a

distance to Mises. There, considering Tresca, one would give away for (2:1) all 15 % compared to Mises. This is about double the measured value the author could ever find.

* As well-known, the highest principal stress determines fracture mechanics failure. Physically there is a smooth transition from flaws via micro-cracks to technical cracks or from continuum-mechanics to fracture mechanics, respectively. *Fig.17-15* proofs that the NF-hyperboloid has its shortest distance to the axis for (2:1). Regarding, that the principal stress has its maximum at 2:1 means, that a micro-crack driven tensile failure might occur. This exactly fits to the straight NF-line of the principal stress plot and in the *Fig.17-15 right* that the F_σ^t-hyperbola narrows the axis most and let assume to have a fracture mechanical task

$$\sigma_1 = \frac{\sigma_x + \sigma_y}{2} \pm \sqrt{\left(\frac{\sigma_x - \sigma_y}{2}\right)^2 + {\tau_{xy}}^2} \;\rightarrow\; \sigma_1 = \sigma\left[\frac{2+1}{2} + \sqrt{\left(\frac{2-1}{2}\right)^2}\right] = 2\sigma \leftrightarrow\; \sigma_1 = \sigma \text{ (uniaxial)}$$

The 3D-'pop in' corresponds to the 2D-'flattening'.

Some further thoughts about the flattening effect: From mini-vessel tests on D6AC steel can be learned [*Tay90*]: Possible flattening of the Mises fracture ellipse may be not caused by a ductile *strength failure mode* but by a principal stress-driven *fracture mechanics failure mode. For a* 'vessel stress ratio' (2:1) or the stress vector $(2,1,0)^T$ the principal stress value is the largest and the so-called flattening effect may play a role considering the following: Assuming that a higher triaxiality usually causes a higher failure risk, it is understandable that *TrF* (= Tr) = 1/3 (uniaxial stress state 1:0) is less critical than *TrF* = √2 / 3 (stress state 2:1). The minor straining at the outer wall surface changes with increasing ductile behavior up to the level at the inner surface. This means, that the flaws at the outer surface may grow (*2D stress state*) and drive ductile rupture. On the inner surface, the internal normal compressive stress from pressure (*3D stress state)* reduces *Eff* and thereby the rupture danger.

Fig.17-15 left shows that also TrF is larger for the 2:1 stress case than for the uniaxial stress case.

Dawicke and Pollock cite in NASA CR 4782: "*The von Mises yield criterion was shown to accurately describe the (ductile) behavior of 2219-T87 aluminum alloy*". All this speaks for the application of Mises as the more correct condition for shear stress-driven failures. Therefore, Mises is recommended as basic yield condition and as yield potential. The applicability of a *yield* failure condition as a SF failure condition depends on how far the final shear failure is still shear stress-governed and not yet fracture mechanics-governed. Because Tresca is a yield hypothesis it shall be not used for final failure despite of the fact that the line is straight like the NF-curve.

→ A practical approach is to reduce the Mises ultimate strength by 7% in the case of load-controlled 'hot spots' on structural surfaces of good quality. Damage tolerance always must check the design.

LL: The theory of plasticity requires a: (1) Yield SFC (for indicating onset of yielding + consideration of multiaxial stressing), and (2) Strain hardening rule for the progression of plastic deformation (isotropic or kinematic strain hardening + Ramberg-Osgood or a power-law); and (3)Flow rule which relates the plastic increments (not the elastic ones) to the stresses.

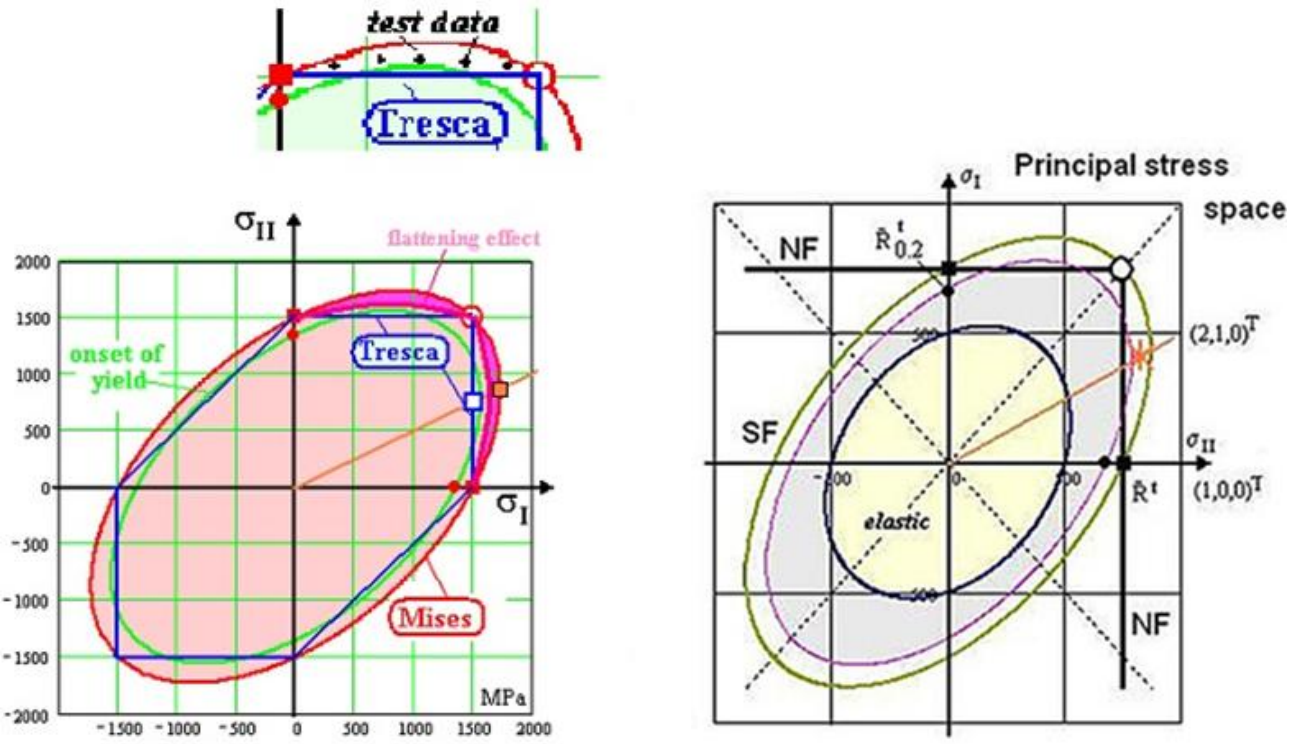


Fig. 17-14: Mises, Tresca and flattening of AA2219 regarding the ratio 2/1.
Tresca corners in the figure are smooth in reality.

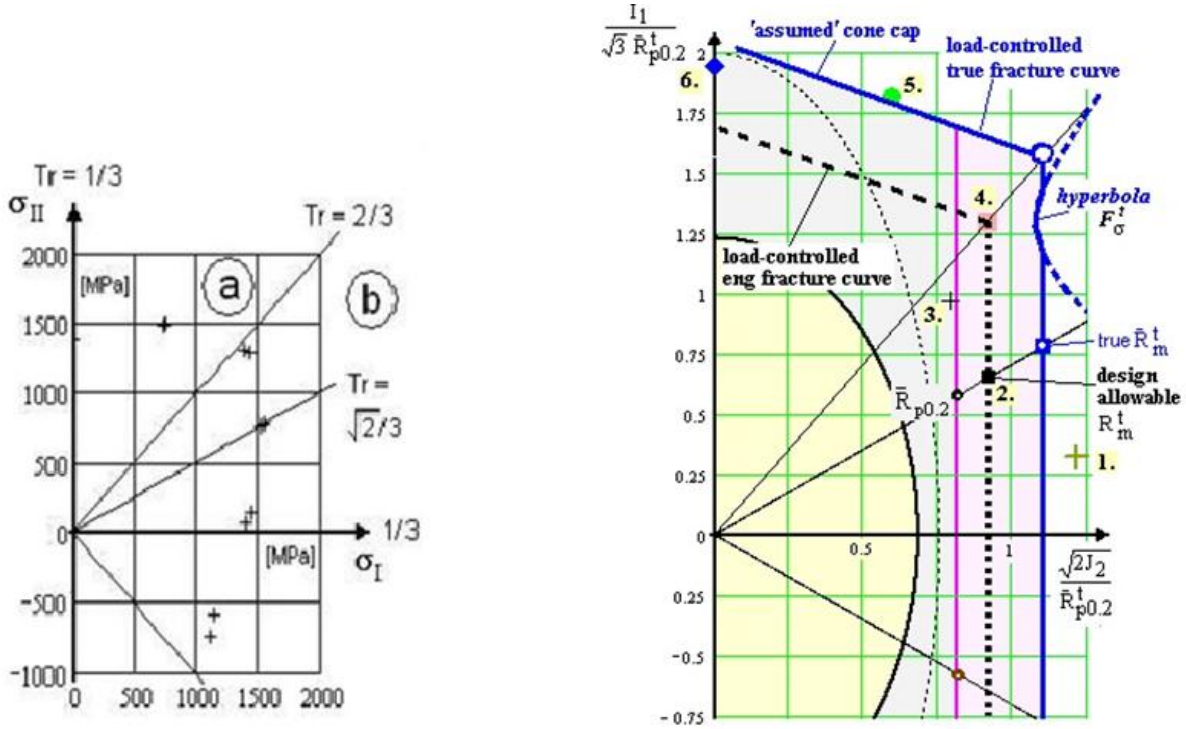


Fig. 17-15: (left) TrF lines. (right) Meridinal cross-section of the failure body

Fig. 17-15 2D- and 3D-Visualisation : (left) Ttriaxialities. (right) $-\infty < I_1 < maxI_1$, hyperbola shows load-controlled, damage tolerance based fracture

17.6 Average Properties and Average Stress-strain Curve in Mapping and Design

Very essential for an accurate analysis is the stress-strain curve which has to be derived from a set of test curves. The evaluation of such a set of (σ,ε)-curves delivers distributions and a statistical basis for the more or less correlated engineering design parameters.

Remind at first, please: *Strengths and strains are derived quantities, which cannot be directly measured. They are 'Standard-defined, commonly agreed definitions'.*

17.6.1 Average stress strain curves (hardening branch)

Non-linear stress-strain analysis should use the average strengths $\{\bar{R}\}$ and the average stress-strain curves and thereby the average stiffness, especially if the structure is statically indeterminate.

For the solution of specific tasks the average stress-strain curve is required, *Fig.17-16*. Otherwise the test cases examples TC2→TC4, presented in the chapter WWFE-II, could not have been solved, for instance!

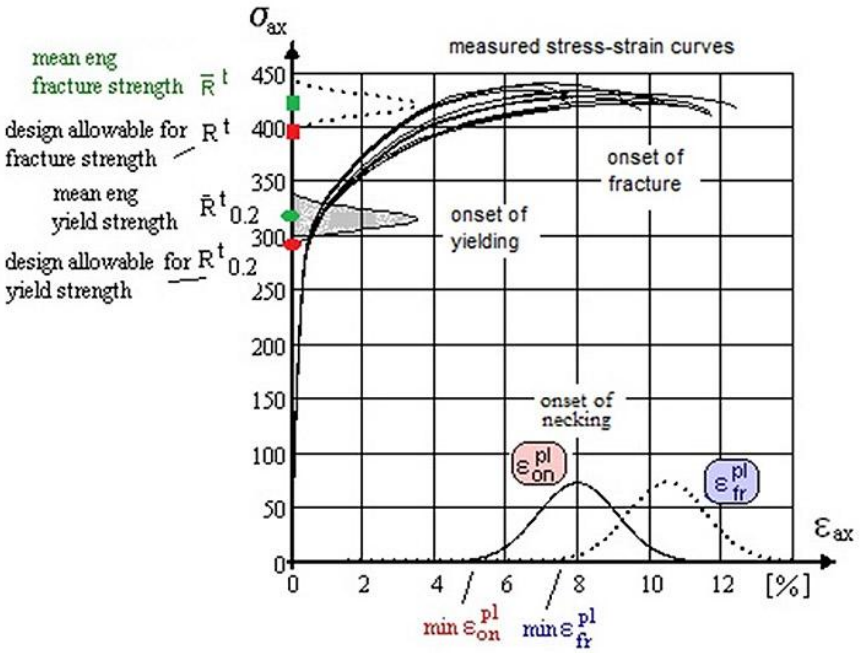


Fig.17-16: Average stress–strain curve versus average fracture strain and average strength. Example: a bundle of aluminum alloy AA2219test curves

At the onset-of-necking, see *Fig.17-16*, the stress must be linked to the reduced area, and then engineering stress should be replaced by true stresses and strains in analysis, see below and *§ 12*.

Furthermore the figure displays various strength quantities and the distribution of the plastic strain at onset-of-necking and at fracture (ductile rupture).

The total strain-stress curve, mapped by Ramberg-Osgood (§3.10) reads

$$\varepsilon(\sigma) = \varepsilon^{el} + \varepsilon^{pl} = \sigma / E_0 + 0.002\,(\sigma / \bar{R}^t_{0.2})^{\bar{n}} \quad \text{with} \quad \bar{n} = \ell n\left(\varepsilon^{pl}(\bar{R}^t)\right) / \ell n\left(\bar{R}^t / \bar{R}^t_{0.2}\right).$$

The R-O exponent *n* can be estimated from the design data $R^t_{0.2}$, R^t and ε_{gl} (= A_{gl} *Gleichmaßdehnung. suffix* $_{gl}$). It is a measure for the transfer from linear elastic to nonlinear. This looks similar to the interaction exponent *m* in case of the author's strength criteria.

The R-O-based flow strain curve reads $\varepsilon_{hard} = \sigma / E_0^{mode} + 0.002\,(\sigma / \bar{R}_{0.2}^{mode})^n$.

Flow strain curve, defined as plastic part, only: $\varepsilon^{pl} = 0.002\,(\sigma / \bar{R}_{0.2}^{t})^{\bar{n}}$. plastic $^{pl} \equiv$ inelastic ^{ie}

$\bar{R}^t$ = ultimate tensile strength (stress at necking), $\bar{R}_{0.2}^t$ = off-set yield strength (engin. strength)

$\bar{R}_p^t$ = proportional strength $\rightarrow \bar{R}_{0.1}^t$ (engineering value), $\bar{n}$ = R-O interaction linear-nonlinear

(One model for a flow stress curve is the Power law hardening formulation $\sigma = K \cdot \varepsilon^{se}$

with se = average strain-hardening exponent, K = strengthening coefficient.)

UD material experiences slight yielding (*thermoplastics more than thermosets*) from the matrix and quasi-yielding from micro-damage. Also here, of course, the application of average curves in test data mapping of a test specimen bundle is stringent.

17.6.2 Derivation of a suitable average strain-stress curve including updating, example UD

The measured stress-strain curves are approximated by a mapping function. That makes it possible to extract, store and update the complete nonlinear behavior of above metals or of composite materials in form of a distinct number of real parameters.

Three different evaluation methods are presented for the statistical analysis of a sample (bunch) of test curves. (The derivation is found in [*Evaluation of Stress-strain Test Results for effective use in Computational Analysis and Adequate Statistical Quantities curves*. Ralf Cuntze, M.A.N.-Advanced Technology Division München, and Gustav Löbel (Institute of Technical Mechanics, Erlangen. Germany). ICOSSAR 85 4th Int Conference on Structural Safety and Reliability, III-664→668].)

Introduction: At least in the vicinity of the fracture point, the physical nonlinearity in the behavior of composite materials has to be taken into account. Since stress-strain curves of composite materials may show a vast scatter, a practical method of handling, analyzing and averaging theses curves has to be found. The aim is the development of a simple yet sound mathematical way of a general description for the nonlinear and statistically scattering stress-strain behavior of materials.

Test data recording: The material properties, usually extracted from recorded stress-strain curves are E_0, R and ε_{fr}. However, the amount of information contained in a nonlinear stress-strain curve is much larger. A complete storage of all curves is quite an effort. For numerical analyses, it would therefore be very advantageous to be able to work with only a few parameter values describing a substitute curve. So, for effective storing and processing of a large number of complete curves on a digital computer it is inevitable to substitute the test curves by analytical functions. In addition this leads to a representation, which is very suitable for computational analysis. The industry most often applies the well-known 3-parameter R-O function (*see Mil Hdbk 5, now MMPDS*), still used for aluminum before, that proved to be very suitable for composites (*the envisaged example*), too. The R-O function can be applied as mapping function (*Mind: In material data sheets like in the HSB R-O-parameters for strain-hardening are provided for metals*). For shear inter fiber failure IFF3 (torsion tests) it reads

$$\varepsilon_{hard} = \sigma / E_0^{mode} + 0.002\,(\sigma / \bar{R}_{0.2}^{mode})^n \rightarrow \text{example} \quad \gamma_{21} = \tau_{21} / G_{\|\perp} + 0.002 \cdot (\tau_{21} / \bar{R}_{0.2\,\perp\|})^n,$$

and one can accept the excellent mapping quality of the R-Ofunction in the inelastic regime (hardening curve part . The four values E_0, R, ε_{fr} and n represent in compacted form the complete

nonlinear behavior of the test specimen. The curve, or at least a good approximation, can easily be retrieved from them by the R-O formulas. By the way, the values E_0, R, ε_{fr} and R_{02} are also acceptance test values needed for quality assurance.

Statistical evaluation of a bundle of test curves: In *Fig.17-7* nine single stress-strain curves from identical tube torsional experiments made of the same CFRP-material are reproduced. For design analyses this vastly scattering bundle of curves has to be averaged. For the visualization: If we imagine all the curves being written by purling sand onto a surface, the result would be a hill shape, *Fig.17-7 right*. The height of the sand hill at each point is a measure of the probability with which a single curve passes through exactly this place. And the ridge of the resulting hill defines a meaningful average curve $\overline{\varepsilon\sigma}$ not to be mixed up with a mapping through the mean points, indicated by $\overline{\varepsilon}(\overline{\sigma})$ and described in Method I.

Method I: As a first naive trial it looks plausible simply to take the arithmetic averages of the curve parameters $\overline{E}_0$, $\overline{R}$, $\overline{\varepsilon}_{fr}$, $\overline{R}_{02}$ or $\overline{n}$, respectively. This method, described by $\overline{\varepsilon}(\overline{\sigma})$, fails due to the strong non-linearity.

Method II: not detailed here, because to being extremely complicate. *See ICOSSAR 85*.

Method III: To avoid the horrendous calculations necessary, within method II, a third procedure was developed with the following steps:

- harmonic averages for $\overline{E}_0$ from values $E_{0,i}$,
- harmonic averages for $\overline{R}_{02}$ from values $R_{02,i}$,
- arithmetic averages for R_i, $\varepsilon_{fr,i}$ with computing *n* using the averages above.

(*The harmonic average is a numerical average. It is calculated by dividing the number of observations by the reciprocal of each number in the series. Thus, the harmonic mean is the reciprocal of the arithmetic mean of the reciprocals. Steps to calculate the arithmetic average: Count the number of values in the set. Add all the values together. Divide the sum by the number of values in the set to obtain the arithmetic average.)*

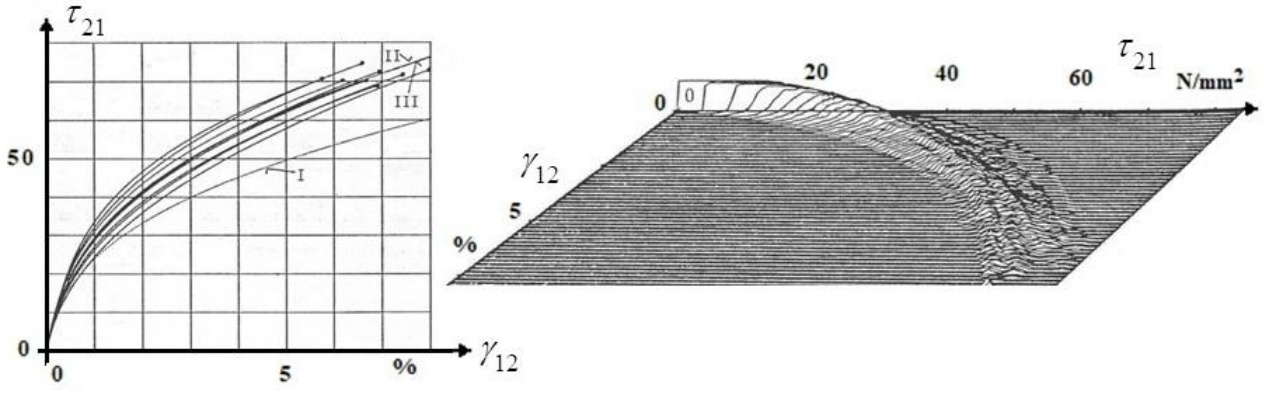


Fig.17-17: (left) R-O- 'reconstructed' curves from a torsion tube test specimen sample test. (right) Probability 'density hill' (fiber T300/ matrix EP)

Fig.17-7 left shows the results graphically. As can be seen, method I leads to a curve, which is not acceptable. The curve defined by the parameters according to method II gives accurately what is wanted but this is not engineering-like. Method III renders the same, but with less effort and is therefore recommended for usual practice.

17.6.3 Updating of statistical quantities in the design phase

The mathematical abstraction of the sand mountain mentioned above is probability density function $\Phi(\sigma,\varepsilon)$ defining the chance of a test curve running through a point (σ,ε). The parameters of this function have to be estimated from finite samples. If we assume any horizontal cut of i.e. $\Phi(\sigma = const,\varepsilon)$ to be a normal distribution, all the standard formulas for estimation of the parameters hold true. The updating of the parameters, necessary through obtaining further test results, respective the "addition" of these later test results to the former ones, works applying the following equations

Mean value $\bar{x}_{update} = \dfrac{n_0 \cdot \bar{x}_0 + n_1 \cdot \bar{x}_1 + ...}{n_0 + n_1 + ...}$, Standard deviation $s_{update} = \sqrt{\dfrac{(n_0\text{-}1)\cdot s_0^{\,2} + (n_1\text{-}1)\cdot s_1^{\,2} + ...}{(n_0\text{-}1)+(n_1\text{-}1)+(..)}}$

Coeff. of var. $cov_{update} = \sqrt{\dfrac{(n_0\text{-}1)\cdot cov_0^{\,2} + (n_1\text{-}1)\cdot cov_1^{\,2} + ...}{(n_0\text{-}1) + (n_1\text{-}1) + ...}}$ with $cov_0 = s_0 / \bar{x}_0$, $cov_1 = s_1 / \bar{x}_1$, .. .

The following two procedures enable to compute lower and upper design tolerance limit values:

(1) Sample size n > 30: This precondition leads to a reasonable mean value $\bar{x}$ and a standard deviation s of the sample. So for example a lower A-value can be calculated from /3/ as "A_{lower}" = $\bar{x} - k_A \cdot s$ with the tolerance limit factor k_A (*99 reliability P, 95 confidence level C, one or two sided tolerance interval*). cov ≡ $cov_{\bar{x}}$

(1) Sample size n > 6: If from equivalent tests on similar materials the cov_μ of the parent distribution is known. Then in the design phase only a small number of specimens is needed (n > 6) to get a reasonable estimation for the A-value (*see also statistical chapters 12, 13*)

$$UT, LT = \bar{x} \cdot (1 +\!\!- u_p \cdot cov_\mu) / (1 -\!\!+ t \cdot cov_\mu / \sqrt{n}) \quad \textit{(Student t distribution)}$$

where in the case of one sided tolerance limits u_p = 2.326 and t = 1.645 is to take.

LL: *The average stress-strain curve $\overline{\sigma\varepsilon}$ does not run through the mean points of yield $(\bar{\sigma},\bar{\varepsilon})_{yield}$ and of fracture $(\bar{\sigma},\bar{\varepsilon})_{fr}$.*

17.6.4 Estimation of average values from statistically-based design values

At first not to forget, structural test evaluation on the different test levels also require average stress-strain curves and average design values. This is not a problem if on the low 'coupon' level material tests are run and one uses the updating method above. However, it becomes difficult if on sub-component and on component level different material batches are applied, possibly even from different suppliers. This leads to a complicate test data evaluation and design verification analysis.

Another difficulty is: Often just lower bound strength design values are provided. In order to perform the best prediction of the average structural behavior or to perform a distinct fatigue life and damage tolerance analysis mean (average) values are required. So the task is given to estimate from these values the average design values.

Mechanical engineering, Aerospace: As a rough estimation may serve (*a better proposal is going to be published in the HSB*):

Average of basic population $\mu \approx$ B-value / (1 - $2 \cdot cov_\mu$) and

$\mu \approx$ A-value / (1 - 3·cov_μ) with the coefficient of basic population cov_μ.

Construction: Average values are required in construction, too. Here, the basic design value is the so-called characteristic value (*in contrast to other disciplines the term characteristic does not mean typical or average and the value is a still statistically slightly reduced value*), the 5% fractile or quantile, respectively. A proposal is presently prepared in the German construction community!

17.6.5 On using adequate statistical quantities in mechanical engineering and civil engineering

In engineering design adequate statistical quantities have to be taken: ***Proposal of the author***

Structural behavior and Determination of cross-section forces and moments for design dimensioning

The optimally achievable estimate is a 50 % expectance value.

- If the average physical behavior of the material has to be simulated an average stress-strain curve a $\overline{\varepsilon\sigma}$ -curve and not a $\overline{\varepsilon}(\overline{\sigma})$ - curve has to be taken in a calculation.

Design verification

- If a deformation constraint is given, the lower A-value (for example) of the elasticity property, E_0 etc. must be used.
- A strength problem needs the lower strength tolerance limit value.
- If a frequency window has to be met, both the upper and the lower A-value of the elasticity property are necessary.
- In design of civil aircrafts the so called B-value (95 survival reliability P, 95 confidence level C) is required because the design philosophy behind is the Damage Tolerance Concept *(redundancy to load transfer).* In military aircraft design the philosophy follows the Safe Life Concept one which asks for an A-value with 99% P.

Remark on one and two sided tolerance factors

- A one-sided factor is used to establish a limit, above or below which it is predicted that at least a distinct percentage of the values lie. A two-sided factor is used to establish an interval or range within which it is predicted. that at least a distinct percentage of the values lie
- Plate thickness and elasticity modulus are normally of the two-sided tolerance factor type, the fatigue life is of the one sided type.

Literature (1985)

[1] Ramberg W and Osgood W R: *Description of Stress-Strain Curves by Three Parameters*. NACA-TN 902, July 1942.

[2] Military Standardization Handbook (MIL HDBK 5c), *Metallic Materials and Elements or Aerospace Vehicle structures*. Vol. I and 11. Chapter 9. Dep. of Defense, Washington D.C. (1978)

[3] German Aircraft Handbook for Structural calculations HSB. *Sheets 04200-01, -02,- 03*. Head of Board: Dr. E. Schreiner, MBB-UF, Ottobrunn, Germany.

17.7 Linear and Non-linear Analyses of Ductile and Brittle Materials including UD Materials

17.7.1 Classification of nonlinear analyses

There are many sources of nonlinearity as depicted in *Table 17-3*. This table tries to give a short survey on topics met when performing non-linear analyses: Large deformations (*deep drawing of metals, draping of semi-finished composite products*) and small deformations. Large strains or large strains combined with large demonstration faced with ductile materials in the plastic range and the hyper-elastic range viewing rubber. Of high challenge are abrupt stiffness changes and kinematic-driven situations at contact loci where gapping and friction may take place.

Linear analyses are convenient approximations which are often adequate when designing. They have the advantage that the principle of superposition of load cases can be applied provided the boundary conditions are the same. A linear analysis is inadequate when the structure's stiffness changes as it deforms. This causes nonlinearity because a part of deformation will remain after removing the load.

Table 17-3: Topics in nonlinear analysis

Non-linear Analysis			
Weak Nonlinearity (*monotonic hardening*) ⇔ Strong Nonlinearity (*material softening, instability*)			
Geometry	Material	Boundary conditions	Loading
structural instability with bifurcation	Ductile materials hardening Brittle materials hardening (micro-damage-caused inelasticity) Material softening	constraints, contact, gap, friction between parts, supports hinged, clamped, elastic foundation	follower forces, nonlinear action
large deformation (buckling after small initial displacement)	large strains		load step increments
FEA issues, 1D→ 2D→ 3D			
Solver	FE mesh	FE elements	Time
implicit, explicit	coarse, fine , h-adaptive	linear, higher, p-adaptive	short (creep, relaxation) and long integration time steps (crash, strong nonlinear problem)

[*Basically Wikipedia*] In h-adaptive meshing the size of the distinct mesh domain is physically adjusted where a refined mesh is needed, while p-adaptive meshing adjusts the polynomial element order to improve accuracy. This is performed by the software, however, based on the desired accuracy. Explicit methods calculate the state of a system at a later time from the state of the system at the current time, while implicit methods find a solution by solving an equation involving both the current state of the system and the later one. Implicit methods, considering all loads $\Sigma F = 0$, should be used when the effect of strain rates $\dot{\varepsilon}$ is minimal. Explicit analysis, considering F = m·acceleration, offers a faster solution in cases of a dynamic equilibrium, such as a crash, ballistic impact.

FEA software is widely used to simulate the behavior of isotropic metallic engineering structures with pretty good results. For the more complicated *orthotropic* fiber-reinforced composites the required accuracy is not yet given. However also, when simulating *isotropic* metal applications involving highly non-linear features such as extensive plasticity, or when simulating very high temperature effects and material damage, the designing engineer should keep in mind that there are limitations to the capabilities of the FEA software in representing these problems. In such cases, the accuracy of the FE-solutions must be questioned and, whenever possible, verified against accurate experimental test data.

17.7.2 Influence of Execution of Finite Element Analysis (FEA) on Reserve Factor values

Usual concern is combining stress analysis and strength analysis in one single computation step - in order to save time and money - by using minimum input values. However, strength analysis can be only combined if the structure is not redundant (*hyperstatic or statically un-determined, such as*

it is the case with a membrane) or - in other words - if the location of the 'hot spots' would be known a priori. As structures are most often redundant in order to find both, the most probable best design and the locations of the 'hot spots', average thickness and average true stress-strain curve are to apply. A single 'Design Verification run', still regarding the local minimum thickness, just then makes sense if a simple membrane stress state is faced: $\sigma(t_{\min}) = (t_{mean} / t_{\min}) \cdot \sigma(t_{mean})$.

3D stress states: execution of a local FEA of the envisaged 'hot spot' domain with boundary conditions from global FEA. Usually a linear approach results in a conservative approach and wasting mass.

A further concern is the determination of the stress state in the 'hot spot' by a reliable post-processing. Most often the 'hot spots are located at the surface. The accuracy to get there reliable stresses depends on:

** Mesh density of the FE model, in general*
** Grid point spacing in regions of large stress gradients*
** Finite element shape (initially, and distortion after loading)*
** Type of loading*
** Boundary conditions and on*
** Output : corner, center*

Quality checks have to be performed such as:

**Asymptotic behavior proven by at minimum two different meshes*
**Stress discontinuity of grid point stresses and of element stresses*
**Distortion of created finite elements (bottle-neck of the automatic mesh tool).*
**High mesh density around regions of high stress, the 'hot spots':*
Nevertheless, even for a good mechanical model the error size of the stress values might be several percent .

17.7.3 FoS-driven facts met in a material-driven nonlinear design safety concept

Some specifications and standards (such as the ISO 14623) even for ductile behaving materials require the determination of MoS_{ult}, only, as the design driving limit (*without rationale*). However, a realistic, nonlinearly computed MoS_{ult} is effortful to obtain in the case of ductile materials. In consequence of this requirement there are two demands: An efficient non-linear analysis and a reworked procedure of how the Ultimate Strength Proof of Design has to be performed regarding MoS_{ult}.

Non-linear stress analysis and the design verification at a 'hot spot' requires a yield condition, which is usually the Mises yield condition. The limit of the validity of Mises may be exceeded in the so-called 'hot spots', however, the material is still capable of carrying load. Due to the fact that a non-linear design verification is very time consuming, the designer asks for a clear engineering design procedure. This includes the non-linear analyses in order to predict the stress and deformation behavior and the Strength Design Verification which focuses on the assessment of the normally multi-axial state of stresses in the 'hot spots'.

In order to fully exploit the potential of a ductile material one has to distinguish two different types of such 'hot spots', the first is load-controlled and the second is strain-controlled. The load-carrying limit of the latter is determined by the given redundancy or -in other words- by the remaining load carrying capacity of the lower stressed vicinity of the 'hot spot'. Here, redundancy means that the

load locally changes its load path and generates a stress redistribution. This stands for a load reserve. As most of the 'hot spots' are strain-controlled the engineer should only give away from the full reserve existing as much as is necessary to formulate a less effortful 'engineering approach'. This is to be verified by the company and accepted by the authority, of course.

Also the ESA-specifications (ECCS) seem to rule out for ductile material the 'cheap' development way 'Pre-dimensioning structures to MoS_{yield}' (linear analyses only) instead to $MoS_{ult.}$. The reason for taking MS_{ult} probably comes from a typical linear analysis thinking: MoS_{ult} is the design driver if $f_{RF,ult} = R_m^t / j_{ult} < R_{p0.2}^t / j_{p0.2}$ with $MoS = f_{RF} - 1$.

This delivers for the example 'aluminum alloy AA2219':

(R_m^t = 390 MPa, $R_{p0.2}^t$ =290 MPa; $j_{p0.2}$=1.1, j_{ult}=1.25), R_m^t /1.25=312 MPa > $R_{p0.2}^t$ /1.1 = 264 MPa

and proves, that MoS_{yield} is here the design driver but not MoS_{ult}! And above that, this check is based on a linear analysis, only, which does not outline that the non-linear experience provides an additional reserve. As still mentioned for brittle (behaving) materials MoS_{ult} is the essential *proof, whereas for ductile materials* (AA2219 for tanks or D6AC steel for the booster of the Ariane5) $MS_{po.2}$ is the more critical one.

On top it is to remind: f_{RF} is a material stress-linked, linearly derived value and RF a load-defined nonlinearly derived value, $f_{RF} < RF = MoS + 1$.

17.7.4 Inelasticity topics of ductile and brittle materials

Some topics in stress assessment read:

* Viewing for instance the FE codes NASTRAN MARC and Abaqus considering their nonlinear modules one has to require from them to deliver results that consistently remain on engineering (σ,ε)-level or on true level. Design verification with the resulting higher true stresses compared to the engineering design allowable R_m^t is principally not accurate. In this context: Shell elements, which reflect *volume constancy* will provide *true stresses* in non-linear analysis. Why should in such cases *true stresses* not to be compared with *true strength values*?

* Residual stresses have to be respected on $\bar{R}_{p0.2}$-level for $MoS_{0.2}$. In the case of ductile behaving materials they are of vanishing influence on MoS_{ult} ($\bar{R}_m$-level) due to the stress redistribution in the non-linear domain. The higher the fracture strain the smaller the influence

* A nonlinear computation ends at that *final load* level where numeric stops due to the fact that the load equilibrium is violated. This leads, at reaching *Eff* = 100%, to a margin

$$MoS_{ult} = \textit{final load} / (j_{ult}\,DLL) - 1.$$

* Engineering FEA stresses have to be assessed by engineering strengths

* Beyond $\bar{R}_m^t$: true $\sigma_{ax} \rightarrow$ trueσ_{eq} due to a 3D-stress state applying Bridgman modelling

* True stresses, computed by non-linear FEA, are higher than engineering stresses and therefore afford true strength assessment.

* Large strain non-linear analyses require the *true stress-true strain curve*.

17.7.5 Some thoughts concerning Linear Analysis versus Non-linear analysis

- Often only linear FE analyses are carried out. With the average curve and nominal wall thickness, an average stiffness is calculated in the component analysis and typical stresses are determined. The stresses calculated in this way are compared with minimum values (*design allowables*) in static or cyclic strength design verification. Considering the design limit strains when using structural materials: There is seldom a larger design limit strain than 1.5 %.
- Linear analysis is a convenient approximation which is sometimes still fully adequate for design. It has the advantage that the principle of superposition of load cases can be applied provided the boundary conditions are the same. A linear analysis is inadequate when the structure's stiffness changes as it deforms or in other words if a part of deformation will remain after removing the load. Structures are very often inherently non-linear.
- Non-linearity can take many forms such as geometric (*large deformation, instability*), material (*yielding & fracture*), and boundary/joint (*contact, joint non-linearity*). These different forms interact and increase the risk of failure! The principle of superposition is not valid anymore, results cannot be scaled, because the stress behavior is not anymore proportional to the loading applied. This makes realistic results expensive
- If a yield SFC is needed then an accurate choice is mandatory regarding whether the material is dense ('non-porous'), porous in the virgin material (*i.e. a foam*), or voids nucleated and grown under the tensile stress state
- Hence, the dimensioning engineer is faced to decide „How much nonlinear analysis is required to solve a distinct task" or „Can the response of a load-carrying structure be assessed by using the simpler linear analysis, only". A decision on CoSt versus accuracy is required
- In the non-linear case three effects have to be considered: * non-linear stress-strain behavior of hardening (*metal below and beyond necking or a lamina material below IFF*), *degradation caused softening (*smeared embedded lamina beyond IFF*), and *non-linear geometrical behavior concerning large strains and large deformations of the structural part
- Average σ-ε-curve is to be utilized in stress and deformation analysis and for the computation of section forces and moments for dimensioning. This is a topic in construction!
- Proportional loading causes sub-proportional stressing in non-linear case
- For initial IFF a linear analysis is sufficient in practice
- In case of well-designed, fiber-dominated laminates, very often, linear analysis is sufficient even for final failure because the embedded laminas are strain-controlled and experience no large operational strain (< 1% strain domain in the case of high-performance UD material)
- One must think in a practical case "Can the situation become critical if non-linearity is not enough respected"? A bolt for instance, bending in a connection, leads to a loss in structural part stiffness and probably to a change of the load distribution path. Then a question arises: Does the part still carry DUL if the bolt will only bend and not break? May then buckling be generated in any element of the structural part?
- Remind: It is better to finish a linear analysis in time - after well-considering the physics behind the model - than perform a non-linear analysis that comes too late.

17.7.6 General on the stress-strain curves to be used

The next figure presents the tensile stress-strain curves for a variety of materials considering engineering and true stresses and strains.

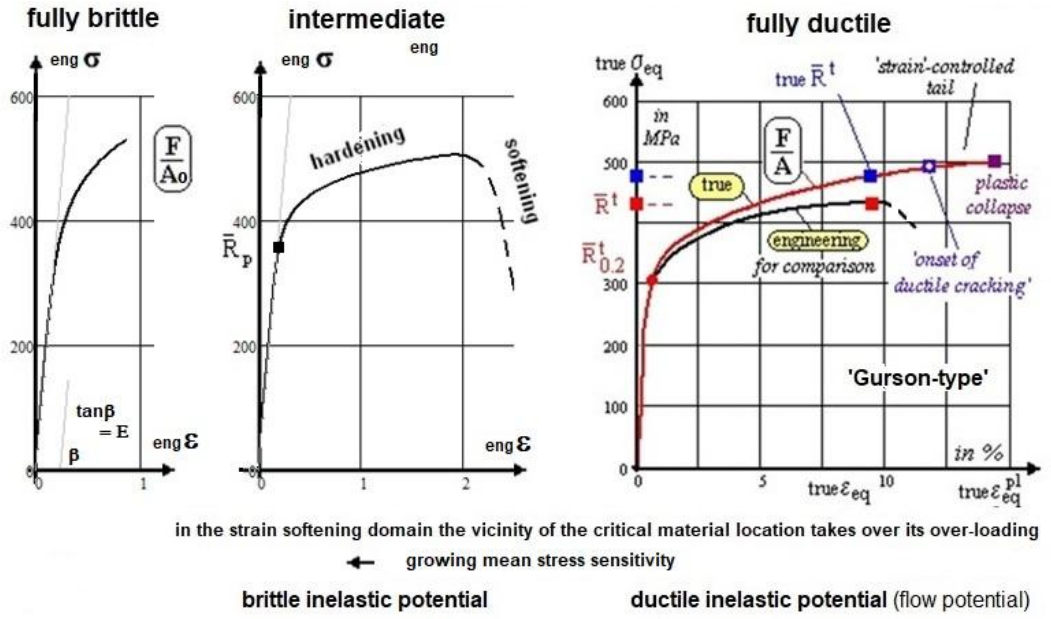


Fig.17-18: Tensile stress-strain curves addressing hardening and softening of brittle and ductile materials

This figure offers some background for the following statements:

*If one wants to obtain the most reliable description of the physical structural behavior, the R/O equation of the real average stress-strain curve $\overline{\varepsilon}\overline{\sigma}$ is to apply. Depending on nonlinearity and FEA code, average engineering or average true stresses are to use. In the case that a finite element analysis with large strains is to use, then – consistently – a true stress-strain curve must also be applied.

*In a FE calculation with the $\min\sigma(\varepsilon)$-curve, the component proves to be less rigid. This usually leads to the prediction of smaller stresses and greater strains than when calculating with the mean curve. Higher stresses can be predicted in some areas of the component and lower stresses in others. Depending on whether a strength criterion or a deformation criterion is used, this leads to either a non-conservative or a conservative assessment. A procedure, in which one wants to achieve a conservative design verification with a $\min\sigma(\varepsilon)$-curve is therefore extremely problematic.

*For certain stiffness cases, the application of a $\max\sigma(\varepsilon)$-curve for the FE calculation is also mandatory

*From above follows for a statically indeterminate structure, that the location of the critical point and of the associated stress state depends on the choice of the $\sigma(\varepsilon)$-curve

* One can conclude: Just for a 'one load path case' i.e. for the membrane area of a pressure vessel *(no redistribution possible, statically determined problem*), here, $\min\sigma(\varepsilon)$-curve can be used both, for design dimensioning and design verification

* For a nonlinear deformation analysis of a rotor at overspeed (*statically determined*), the minimum value curve can be used. The proof of deformation is conservative because the 'softest' material was considered. The rotor does not bump into the housing. The use of the average curve would predict a typical and thus smaller deformation. Beside the ULS also the SLS (*serviceability limit state*) is fulfilled

* For a reliable stress-strain analysis as a test result prediction the average curve is to apply

Depending on the evidence to be provided (strength, stiffness, deformation), it would be necessary

to check which calculation curve is to be used. Proof of deformation and proof of strength may have conflicting requirements. It is generally therefore recommended to calculate with average curves and to take into account required conservatisms by the assessment criteria (*design allowables, predetermined deformation limits, etc.*) during the design verification analyses.

The statements before are more addressing ductile and brittle isotropic materials. Therefore, a paragraph is added regarding the challenge of non-linear analysis of transversely-isotropic UD-materials, namely the progressive failure analysis of laminates (*this was an essential subject in WWFE-I and -II*).
An accurate failure prediction firstly consists of a physically non-linear stress analysis if the corresponding lamina stresses are high and of a geometrically non-linear analysis if the laminate will extremely deform. If the computed lamina stresses do not respect this, strength and deformation analyses and thereby design verification are not acceptable. The prediction of laminate behavior up to fracture is ab effortful challenge. As procedure the so-called 'ply-by-ply' analysis method - based on CLT - is applied with the concern on the so-called First-Ply-Failure which is usual an IFF.
To perform a non-linear stress analysis the relevant non-linear stress-strain curve is to be provided, which involves the so-called hardening and the softening part. There are all 3 IFF–linked curves to consider. The 2 FFs always mean fracture for the high-performance UD materials. Strain hardening is the domain at the end of which the stress reaches a strength limit $\bar{R}_{\perp}^{t}, \bar{R}_{\perp}^{c}, \bar{R}_{\perp\square}$, which is addressed here as an initial failure level of IFF type. From that level on, that means for the further progressive failure or damage regime, the term softening is used. Of course, some micro-damage already begins with increased material hardening. Softening works for a lamina (ply), if it is embedded in a laminate and still contributes to the strength capacity and the stiffness capacity of the laminate. After the onset of micro-damage only so-called 'effective stresses' can be calculated for the micro-cracked lamina. The effective stresses are smeared stresses, namely 'smeared' over a number of micro-cracks.

For model validation, properties are not only needed for the pure failure mode domains but for the several 'mode-interaction domains' or Mixed Failure Domains (MiFD) too, where the actual stress state affects more than one mode. The influence of the stress state in a MiFD on the secant modulus of each affected mode was considered by the author in his simple "E_{sec}-approach" in the WWFEs by 'triggering'. This approach increases the *Eff* of the affected mode (*the secant modulus becomes smaller*) in the case of hardening and softening. After the onset of IFF 'smeared stresses' can be inserted into the SFCs only.

Some further aspects and tasks:

- The lamina is the general building brick or basic computational element for the prediction of laminate behavior
- To perform a reliable nonlinear analysis the clear identification of the design driving IFF mode is mandatory
- *Eff* = 100% remains valid throughout the analysis in the softening domain
- The high internal redundancy of a multi-layered laminate is better modelled by a probabilistic code. Probabilistic tools should be applied in order to gain some experience to practically improve the deterministic procedures and to smooth (*due to joint failure probability*) the relatively sharp corners of a laminate's failure envelope. Deterministic failure path and probabilistic failure path may be not the same w.r.t. the different scatter of the design parameters effected, see [*Rac86*]

- The determination of effective mode softening curves for embedded laminas is future work. Appropriate test specimens and test evaluation have to be discussed.
- In order to implement the multi-fold non-linearity approach into a commercial FEA code and taking advantage of a code's effective solution architecture an analogue procedure to 'yield failure conditions + associated flow potential' of ductile materials has to be provided for the 3 IFF conditions 'fracture failure condition (presented) + associated inelastic potential' for brittle UD materials, exemplarily.

REFERENCES

[Bor99] Bormann P: *Analyse elastisch-plastischer Eigenschaften*. Dissertation, TU Chemnitz (1999)

[Bri52] Bridgman P W: *Studies in Large Flow and Fracture*. McGraw-Hill, London - New York 1952

[Cha85] Chan K S, Lindholm U S and Wise J: *Biaxial Strength of HY80 Steel*. Trans. of the ASME 107 (1985), pp. 132-137

[Chr97a] Christensen R M: *Yield Functions/Failure Criteria for Isotropic Materials*. Proc. R. Soc. Lond. A (1997) 453, 1473-1491. *Yield Functions/Failure Criteria for Isotropic Materials*. Proc. R. Soc. Lond. A (1997) 453.

[Chr98] Christensen R M: *The Numbers of Elastic Properties and Failure Parameters for Fiber Composites.* Transactions of the ASME, Vol. 120 (1998), 110-113

[Cun99] Cuntze R: *The Failure Mode Concept - A new comprehensive 3D-strength Analysis Concept for Any Brittle and Ductile behaving Material*. Europ. Conf. on Spacecraft Structures, Materials and Mechanical Testing. ESA-CNES-DGLR-DLR; Braunschweig, Nov. 1998, ESA SP-428, 269-287

[Cun96] Cuntze R: *"Fracture-type Strength Criteria" formulated by Invariants which consider the Materials Symmetries of the Isotropic/Anisotropic Material used*. Conf. on Spacecraft Structures, Materials and Mechanical Testing. ESA-CNES-DARA: Noordwijk, March 1996 (Conf. Hdbk)

[Cun99] Cuntze R: *Progressive Failure of 3D-stressed Laminates: Multiple Nonlinearity treated by the Failure Mode Concept (FMC*). DURACOSYS 99, Brussels, July 1999

[Cun00] Cuntze R: *Proofs of Design of Crack-free Structures built from Brittle and Ductile Isotropic Materials viewing Damage Mechanics and Fracture Mechanics*. 33.DVM AK "Bruchvorgänge". Paderborn, Febr 20-21, 2001. Plenary session talk, handout

[ECSS E-30-bs] ESA-ESTEC: draft standard on '*Structural design and verification of pressurised hardware'*. March 2001

[Daw97] Dawicke, D.S. and Pollock, W.D.: *Biaxial Testing of 2219-T87, Alluminium Alloy using Cruciform Specimens*. Aug. 1997, NASA CR-4782

[Dru52] Drucker D C and Prager W: *Soil Mechanics and Plasticity Analysis of Limit Design*. Quaterly Appl. Math. 10,(1952), 157-165

[Eft01] Eftis J and Nemes J A: *Constitutive microdamage Description of Ductile Dynamic Fracture.* In 'Non-linear Fracture and Damage Mechanics' chapter 5, WIT Press Southampton.

[ESIS P6-98] *Procedure to Measure and Calculate Material Parameters for the Local Approach to Fracture using Notched Tensile Specimens*. Subcommittee TC1.1 on 'Local Approach' of the European Structural Integrity Society (ESIS), March 1998

[Gie96] Gierlinski, Smith, Thoft-Christensen, Santos, Cuntze, Gollwitzer: *Reliability-based Design of Structural Components*. Proceeding of the int. Symp. on Advanced Materials for Light weight structures, ESTEC, Noordwijk, March 1994 (ESA-WPP-070), 121-125

[Gur77] Gurson A L: *Continuum Theory of Ductile Rupture by Void Nucleation and Growth*. Part 1: Yield Criteria and Flow Rules for Porous Ductile Media. J. Eng. Mater. Technol. 99 (1977), 2-15

[Han75] Hancock J W and Mackenzie A C: *On the Mechanisms of Ductile Failure in High-strength Steels subjected to Multi-axial Stress States.* J. Mech. Phys. Solids 24 (1976), pp.147-169

[Hes00] Hesebeck O: *Zur Modellierung von Schädigungsprozessen in elasto-plastischen Materialien.* Diss., University of Karlsruhe, Germany, Jan. 2000

[Hol45) Hollomon J H: *Tensile Deformation*. Trans. AIME162 (1945), p. 268-290

[Ism82] Ismar H and Mahrenholtz O: *Über Beanspruchungshypothesen für metallische Werkstoffe*. Konstruktion 34 (1982), 5, 305-310

[Lem92] Lemaitre J: *A Course on Damage Mechanics*. Springer, 1992

[Lip97] Lippmann H and Iankov R: *Mathematical Modeling of Sintering During Powder Forming Processes*. Int. J. Mech. Sci. 39 (no.5), 1997, pp585-596

[Lip97] Lippmann H, Mannl V, Bontcheva N, Iankov R and Beer O: *Numerical Simulation of Density Distribution During Compaction of Iron Powders.* Archive of Applied Mechanics 67 (1997), Springer 1997

[Lor72] Lorrek W: Dissertation, TU Clausthal 1972

[Lud09] Ludwik P: *Elemente der technischen Mechanik*. Springer, Berlin (1909)

[Kop88] Koplik J and Needleman A: *Void Coalescence in Porous Plastic Solids*. Int. J. Solids Structures 24 (1988), 835-853
[Men83] Mendelson A: *Plasticity: Theory and Application*. Robert E. Krieger Publ. Comp. Reprint, 1983
[Mis13] v. Mises R: *Mechanik der festen Körper im plastisch deformablen Zustand*. Göttinger Nachrichten, Math.-Phys. Kl., 1913, pp. 582-592
[Nee84] Needleman A and Tvergaard V: *Analysis of Ductile Rupture in Notched Bars.* J. Mech. Physics Solids 32 (1984), 461-490
[Ric69] Rice J R and Tracey D M: *On the Ductile Enlargements of Voids in Triaxial Stress Fields*. J. Mech. Phys. Solids (17), 1969, pp. 201-217
[Sch01] Schiffmann R: *Experimentelle Bestimmung und modellmäßige Beschreibung der Schädigung beim Gleitbruch von metallischen Werkstoffen*. Dissertation, RWTH Aachen, 2001
[Ser97] Serafin T P: *Spacecraft Structures and Mechanics -from concept to Launch-*. Kluwer Academic Pub-lishers, 2nd printing (1997)
[Ste97] Steglich D and Brocks W: *Micromechanical Modelling of the Behavior of Ductile Materials including Particles*. Comp. Mat. Science 9 (1997), 7-17
[Sun97] Sun D Z, Sester M and Schmitt W: *Development and Application of Micromechanical Material Models for Ductile Fracture and Creep Damage*. Int. J. of Fracture 86, 75-90, 1997
[Str83] Strut M G, Hecker S S and Bourcier R: *An Evaluation of Anisotropic Effective Stress-Strain Criteria for the Biaxial Yield and Flow of 2024 Aluminum Tubes*. Trans. of the ASME 105 (1983), pp. 242-249
[Tay90] Taylor N: *Biaxial Tests on D6AC Steel Tubes* (Ariane 5 Booster Case). MAN Technologie, A5-RE-1121000-A-016-MAN
[Tre1864] Tresca H: *Sur l'ecoulement des corps solids soumis à des fortes pression*. Compte. Rend. 59, 1864, p. 754
[Tsc71] Tschoegl N W: *Failure Surfaces in Principal Stress Space*. In proceedings of the chemical society symposium (1971), John Wiley & Sons, 239-269
[VDI97] Cuntze R et.al.: *New Fracture Criteria and Strength Verification for FRP subjected to a Multi-axial State of Stress -Modelling and Experiments-*. VDI-Fortschrittbericht, Reihe 5, Nr. 506. BMBF-Vorhaben 03N8002 (book, 250 pages, in German)
[Voc48] Voce E: *The Relationship between Stress and Strain for Homogeneous Deformation*. J. Inst. Metals 74 (1948), p. 537-562
[Zha01] Zhang Z L: *A Complete Gurson Model*. In 'Non-linear Fracture and Damage Mechanics' chapter 8, WIT

18 Structural Vibration and Work Cases

Vibration [*Wikipedia*]: *Mechanical phenomenon. The word comes from the Latin nominative 'vibration' which means shaking. Oscillations may be periodic, such as the motion of a pendulum or random, such as the movement of a tire on a gravel road*.

Vibration versus oscillation:

- Vibration: broadly any motion which might not repeat or have any specific frequencies or amplitudes. A motion linked to some average position.
  Movement of a body about its average (mean) position which can be linear, circular, periodic or non-periodic. Can be in all directions. Vibration is seen as a mechanical oscillation.
- Oscillation: Movement of a body from its equilibrium position (resting place) to the maximum distance on one side and then to the maximum distance on the other side. Is a repeated variation about a central value. Oscillation has a definite time period which means the body takes a definite time to complete one oscillation and will remain same for all oscillations if there is no outer force working on the system. Has a definite time period which means the body takes a definite time to complete one oscillation and will remain same for all oscillations if there is no outer excitation force or damping working on the system,

In this chapter some works shall be added to the document out of the author's remaining fields.

Caused by a longer MAN-Technologie cooperation with Prof. K. Magnus in the seventies on multi-body dynamics his book [*Mag69*] "Schwingungen. Teubnerverlag, 1969" is applied. Inwith some basic information on the later used terms (*letters shall fit to the 'not vibration text'*) and vibration equations

18.1 General on Oscillation/Vibration

18.1.1 Introduction to linear differential equations

A mechanical oscillation is a temporal-periodic movement of a physical quantity (*state variable*), of a body around an equilibrium position, a resting position. The prerequisite for this is a reversing force in the direction of equilibrium. The natural frequencies of such an oscillating system are those frequencies ω_0 with which the system can oscillate without the influence of external forces after a single excitation. The natural frequencies can be determined by solving the vibration equation of the system. The general form of oscillation is a linear combination of all natural vibrations of the system. Any vibration of a system can be expressed by superimposing the natural vibrations. (A wave is defined as the propagation of a vibration in space in which energy is transmitted but no substance is transported). If a body oscillates in one of its natural frequencies under external excitation, which then results in a vibration with a large amplitude, this natural frequency is a resonance frequency. The natural frequencies of a vibrating system depend on its geometry, its structure and its material properties.

Modes are special movements of a vibrating system. These are the movements that the system performs when left to its own devices. This includes the uniform movements as well as all natural vibrations. The latter are free and undamped vibrations and are approximately considered harmonic. The overall movement of the system can be represented as a superposition of different modes. The number of modes of such a system is related to its degrees of freedom: The system can have a

maximum of as many natural frequencies as degrees of freedom and has just as many eigenmodes as degrees of freedom (*This is the same as with the strength failure modes and the associated strengths!).* The eigenmodes result from the equations of motion of the system (= eigenvectors of this system). The frequencies of the eigenmodes are the associate eigenvalues of the system. A uniform motion is represented as a mode with the frequency zero (present later in § GUZ).

Vibration analysis captures:

- Free vibration without damping
- Free vibration with damping
- Forced vibration with damping.

The analyses further must capture single and multiple Degrees of Freedom DoF.

Before going into details some basic terms shall be introduced below:

state variable: $x(t) = x(t+T)$ with t = time coordinate, T = time period, period of oscillation,

frequency of oscillation: $f = 1/T$, circular frequency: $\omega = 2 \cdot \pi \cdot f$,

amplitude of oscillation: $x_a = 0.5 \cdot (x_{max} - x_{min})$, $x_m = 0.5 \cdot (x_{max} + x_{min}) \leftrightarrow$ examples σ_a, σ_m

- Free oscillation of a not damped oscillator *homogeneous solution*

According to *Fig.1*, the force equation of the linear oscillator results in the differential equation

$$m \cdot \ddot{x} + c \cdot x = 0 \quad \rightarrow \quad \ddot{x} + \frac{c}{m} \cdot x = 0 \quad \text{with abbreviation} \quad \omega = \sqrt{c/m} \quad \Rightarrow \quad \ddot{x} + \omega^2 \cdot x = 0$$

with m is mass, c is spring stiffness, $\dot{x} = dx/dt$ is velocity and $\ddot{x}$ is acceleration.

→ Inserting the approach $x_{hom} = x_0 \cdot e^{-i \cdot \lambda \cdot t}$ results in the so-called characteristic equation and in the searched eigenvalues

$$(-\lambda^2 + \omega^2) \cdot x_0 \cdot e^{-i \cdot \lambda \cdot t} = 0 \quad \rightarrow \text{eigenvalue} \quad \lambda = \omega = \omega_0 \text{ a natural frequency, eigenfrequency}$$

.

→ Inserting the approach $x_{hom} = c_1 \cdot \cos \omega t + c_2 \cdot \sin \omega t$ which contains both the solution parts it follows after trigonometric combination

$$x_{hom} = c_{12} \cdot \cos(\omega \cdot t - \varphi) \text{ with } c_{12} = \sqrt{c_1^2 + c_2^2}, \ \tan \varphi = c_2 / c_1.$$

To determine the two constants c and φ, the initial values of the oscillation x namely $x = x_0$, $\dot{x} = v_0$ are inserted into above equations delivering directly $c_1 = x_0$, $c_2 = v_0 / \omega$.

For the free vibration system the energy relationship reads $\frac{1}{2} \cdot m \cdot \dot{x}^2 + \frac{1}{2} \cdot c \cdot \dot{x}^2 = E_{kin} + E_{pot} = const$

.

- Free oscillation of a viscous-damped oscillator *homogeneous solution*

Now, the force equation of the linear oscillator results in the differential equation

$$m \cdot \ddot{x} + d \cdot \dot{x} + c \cdot x = 0 \qquad \Rightarrow \qquad \ddot{x} + \frac{d}{m} \cdot \dot{x} + \omega \cdot x = 0$$

with d the damping resistance (*loss factor*). Case constant coefficients d and c.

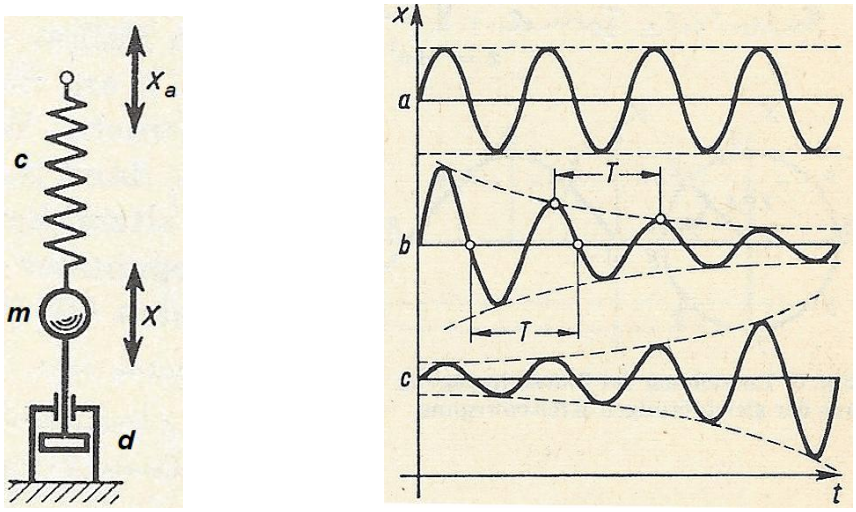


Fig.1: (left) Equilibrium at the mass element. (right) (a) Harmonic oscillation, (b) damped oscillation, (c) fanning oscillation

For simplifying the solution process above equation shall be made dimensionless by introducing the dimensionless time $\tau = \omega_0 \cdot t$. This requires the derivations

velocity v: $\dot{x} = (dx/d\tau) \cdot (d\tau/dt) = (dx/d\tau) \cdot \omega_0 = x^* \cdot \omega_0$ and acceleration: $\ddot{x} = x^{**} \cdot \omega_0^2$.

These terms are inserted into $\ddot{x} + \frac{d}{m} \cdot \dot{x} + \omega_0^2 \cdot x = 0$, which leads to the form

$$x^{**} \cdot \omega_0^2 + \frac{d}{m} \cdot x^* \cdot \omega_0 + \omega_0^2 \cdot x = 0 \quad \text{or} \quad x^{**} + \frac{d}{m} \cdot x^* / \omega_0 + x = 0 \text{ and finally}$$

$$\Rightarrow \quad x^{**} + 2D \cdot x^* + x = 0 \qquad \text{with} \qquad D = d/2 \cdot m \cdot \omega_0 \text{ Lehr's damping measure}$$

and ω_0 as the circular natural frequency (eigenfrequency).

Only with weak damping (i.e. $D < 1$) the system does emit periodic oscillations; with strong damping ($D > 1$) it returns to equilibrium position in an aperiodic creep movement. Performing measurements the so-called logarithmic decrement ϑ can be easily determined from two measurements due to

$$\vartheta = \ln\left(x_n / x_{n+1}\right) \text{ and after some reformulations } \rightarrow D = \frac{\vartheta}{\sqrt{4 \cdot \pi^2 + \vartheta^2}} \text{ ([}Mag69\text{], p.71)}.$$

In order to achieve a more practical way of solution, Magnus takes a specific exponential approach ([*Mag69*], p. 66) $x = y \cdot e^{-D \cdot \tau}$ which after insertion gives

$$y^{**} + (1 - D^2) \cdot y = 0.$$

→ Inserting the approach $x = y \cdot e^{-D \cdot \tau}$ into above equation of motion results in

$$y_{hom} = c_{hom} \cdot \cos(\upsilon \cdot \tau - \varphi) \quad \text{with} \quad \upsilon = 1 - D^2.$$

Inserting $x = y \cdot e^{-D \cdot \tau}$ leads after differentiation to the further needed velocity

$$dx/d\tau = x^* = -c_{hom} \cdot e^{-D \cdot \tau} \left[D \cdot \cos(\upsilon \cdot \tau - \varphi) + \upsilon \cdot \sin(\upsilon \cdot \tau - \varphi) \right].$$

To determine the constants, the initial values of the oscillation x, namely

$x = x_0$, $x^* = x^*_0$ for $\tau = 0$ are inserted into above equations delivering

$$c_{\text{hom}} = \sqrt{x_0^2 + \left(\frac{x^*_0 + D \cdot x_0}{\upsilon} \right)^2}, \quad \tan\varphi = \frac{x^*_0 + D \cdot x_0}{\upsilon \cdot x_0} \quad .$$

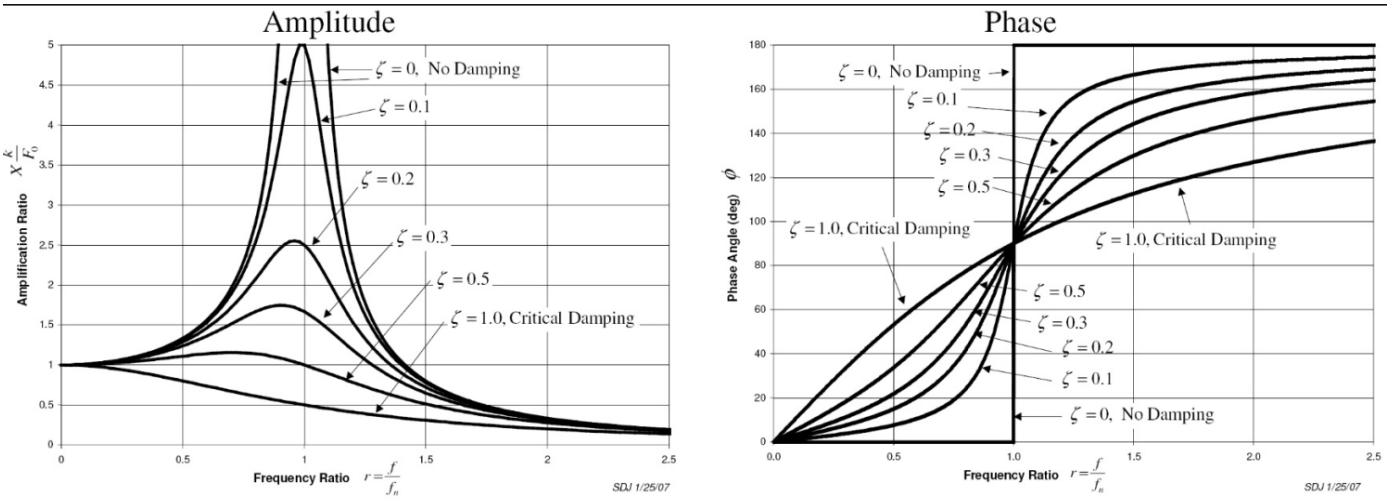


Fig.2: Influence of damping on the amplitude and Phase [Wikipedia ,.....].

Damping ratio ς = damping coefficient / $2 \cdot \sqrt{m \cdot c}$

- Harmonic excitation of a viscous-damped oscillator *particular solution*

The equation in dimensionless format reads after inserting the excitation function [*Mag69*, p.161]

$x_a = x_0 \cdot \cos(\eta \cdot \tau)$ follows $x^{**} + 2D \cdot x^* + x = x_0 \cdot \cos(\eta \cdot \tau)$ (*Fig*.1)

with the *frequency ratio* $\eta = \Omega / \omega_0$ and Ω the *excitation circular frequency* .

building the particular solution of the equation of motion.
Magnification function and phase curve can be determined from

$$\text{Magnification Factor} \quad MF = \frac{1}{\left(1 - \eta^2\right) \cdot \cos\psi + 2 \cdot D \cdot \eta \cdot \sin\psi} \quad \text{and} \quad \text{phase angle} \quad \tan\psi = \frac{2 \cdot D \cdot \eta}{1 - \eta^2}$$

- In the case of transient vibrations, both the solutions must be superimposed, the homogeneous and particular one.

18.1.2 Numerical treatment and future modeling possibilities

A look at the actual numerical treatment is given by NAFEMS (*author was member of the NAFEMS composite work group*). Higher operating loads, rotational speeds, lightweight structures, extreme application requirements (*natural disasters, accidents, and terrorist attacks*) and comfort properties (*acoustics and vibrations*) require a safe and economical design of machines, transport systems, components, plants and buildings with the help of structural dynamic simulations. In addition to functional and comfort aspects, safety aspects require structural dynamic analyses of constructions. Hence, structural dynamic simulations at all stages of product development and research are part of the standard procedures in almost all areas of industry (*Mind: An analysis is a calculation for instance for the design verification of the final design whereas a simulation always captures a corrective due to test information i.e.*).

The numerical methods that are used to simulate dynamic events are relatively mature but new capabilities are constantly appearing that allows more complex behavior to be represented. The use of model reduction techniques allows larger models to be analyzed in a time efficient manner, helping dynamic analysis to be more easily integrated into the design process. Model updating technologies and validation with measurements allows high qualified modelling for the simulation methods. Theory, software, and hardware (*HighPerformanceComputers and measurement systems*) developments have opened up many possibilities for a more realistic modelling and simulations in structural dynamics. In particular, the combination of FEM with Multi Body Dynamics (see § GUZ) and acoustic as well Computational Fluid Dynamic programs, that could incorporate a wide variety of physical and nonphysical inputs, has considerably expanded the possibilities of mapping real relationships of entire systems and complex structures. The range of applications that can be tackled by the different toolkits increased. It provides the opportunity to chain different methods together, to go beyond component and part simulation and start to analyse the whole dynamic system.

18.1.3 Note on Natural Frequencies and Modes

Necessary equations are to provide for bending, longitudinal and torsional vibration.
This includes the effects of rigid and elastic supports as well as additional single masses and shear-rigid beams and plates.
The influence of shear flexibility and of rotatory inertia increases with the mode number.

Natural frequencies and vibration modes of beams with uniformly distributed mass are to address.

Additional axial force loading Tensile axial force loading of the beam has a stiffening effect in bending vibration and increases the eigenvalues, whereas compressive axial force loading acts de-stiffening and includes the risk of buckling. Therefore - and due to practically unavoidable imperfections – higher modes than the first one have no useful meaning in case of compressive axial, at least.

LL: For predesign, the estimation of the usually only requested lowest mode is often sufficient.

18.2 Damping and Damped Vibrations

18.2.1 General

Damping requires a deeper insight.

In every real vibration system mechanical energy is converted into other forms of energy, i.e. heat. The causes of this phenomenon, known as damping, are manifold: molecular friction and friction at grain boundaries, changes in dislocations (*material damping*), friction due to sliding motion at the junctions of components, air inlet and outlet in porous materials, friction in bearings, guides, brackets, interaction with surrounding fluids (*air, water, etc*.), special damping devices. The damping therefore depends on many influences. As a result, the transmission of damping characteristics is very limited and even the reproducibility of experimental results is only guaranteed in certain areas (*text from the preparation of my draft HSB 73100, 1983]*

In the vibration calculation, an exact recording of the damping forces is hardly possible. Therefore, one usually expects small dampings, as long as no special damping elements are used. If the damping forces are very low, natural frequencies can be calculated by neglecting the damping. In the case of forced vibration, on the other hand, the vibration amplitudes are significantly reduced by relatively low damping values; this is especially true in the resonance range. The consideration of the damping is therefore primarily used to estimate resonance amplitudes, while outside the resonance usually damping-free can be calculated.

In the mathematical description of the damping problem, a distinction is made between different types of damping: * viscous damping, * Coulomb-based friction damping and * material damping respectively hysteretic damping. As damping models one can consider the Kelvin body in the viscous case and the Coulomb body in the case of friction damping.

Mechanical replacement system and its characteristic values (see /VDI 2062/): Since vibration calculations on the real system are only possible with great effort, they are carried out on substitute surrogate systems; these are simplified, idealized representations that contain only the vibrationally important properties of the real structures, including their environment. Such a replacement system also determines the excitation forces, movements, ignition mechanisms, friction effects or the desired interactions. The real structure is modelled in the substitute system with rigid masses and massless bonds which presupposes that the natural frequencies of these individual parts are far enough above the frequency range of the entire system to be investigated (*This caused a sectioning that was a problem of the large structure Ariane launcher*). Simplifications and specific assumptions are made in order to describe and identify the phenomena of interest.

Simplifications or assumptions made to represent one or one of the phenomena of interest by a replacement system are characterized by terms such as ~ linear system: system with linear binding elements and linear deformation geometry (linear differential equations) as opposed to a nonlinear system - degree of freedom: number of coordinates necessary to clearly describe the movements of a oscillator - simple oscillator: rigid body with a 1DoF vibration system: several masses with several degrees of freedom - continuum: system continuously occupied with mass and stiffness. The results obtained for the replacement system are only partially transferable in accordance with the simplifications made. When describing a system, a distinction must be made between material characteristics, component characteristics and system characteristics.

Material characteristics:

The inertial characteristics or properties of the substances are completely determined by the density. The deformation properties of a material element are clearly shown in the stress-

deformation diagram. The modulus of elasticity E and the shear modulus G characterize the elastic behavior of the material, while the loss factor *d* describes its damping properties.

Component characteristics:

The characteristics of the components (*component quantities, which always occur as dimension-based parameters in the calculations*) depend on the material properties (material characteristics) and the geometric shape (*shape characteristics*) of the elements such as springs, and dampers is independent of the overall structure of the system.

System characteristics:

System characteristics characterize the combined action of the components (*masses, springs, joints, bonds*) or the relationship between an excitation effect (input) and the system response (output). System characteristics always refer only to the structure or the selected replacement system in each individual case. The system characteristics are usually described by one or more differential equations built up with the help of the component characteristics which depend on the number of DoFs of the complete system). From this, system characteristics such as natural frequencies, eigenmodes (*forms of movement*), damping quantities, dynamic magnification function (*ratio of the maximum dynamic deflection to the maximum static deflection*) and phase angle ψ can be obtained.

18.2.2 Modeling

The computational consideration of the damping influence is difficult due to the manifold causes and manifestations, some of which are not exactly known; it also often leads to difficult-to-handle mathematical expressions. It therefore makes sense to use simple approaches to describe the damping. In this context the three types of damping shall be shortly described.

Viscous damping: With this type of damping, a vibrational velocity proportional (*i.e. frequency and amplitude dependent*) damping force is defined, as it arises mainly by liquid or air friction. bV refers to the damping resistance or the damping constant, respectively. This convenient approach is most commonly used, although it only describes the damping behavior more or less correctly..

Coulomb surface friction damping: This Coulomb 'external' damping results from energy dissipation-causing sliding friction between dry surfaces and occurs at clamping and connecting points such as rivet and screw connections of elastic structures. The frictional force is almost constant.

Material damping: This Coulomb 'internal' damping results from energy dissipation-causing effects inside the material and is recognizable by the fact that the force-deformation diagram does not match that under loading with that under unloading. Both curves form a hysteresis loop in stationary motion, the area of which represents a measure of the loss energy of a volume element during a full oscillation and provides the so-called specific damping work. Based on the elastic deformation energy W of the volume element at maximum deflection, this defines the element damping or the so-called proportional material damping. There is a dependenc on temperature, history of the material, state of stress, frequency and vibration form.

The difference between material parameters and component parameters is due to the fact that the stress distribution in the component is generally not uniform and therefore not all elements contribute to the overall damping at the same time. In addition to a number of other influences, the element damping essentially depends on the shear amplitude of the stress-causing alternating load.

Overall damping of a structure or construction is very complex. It generally consists of more than one of the three types of damping mentioned above. The interaction of the individual types of damping is so complicated that it is not possible to calculate a summary damping constant. With regard to the analytical treatment of vibration problems, it is therefore necessary to draw on empirical values. Results of vibration measurements on similar structures serve as a basis. If the "natural" damping of a system is not sufficient to sufficiently suppress interference vibrations, additional damping systems must be fitted. The task of such additional systems is to reduce the maximum amplitudes of special eigenforms without negatively affecting other eigenforms. Possibilities for this are offered by artificial viscous dampers or Coulomb's friction dampers.

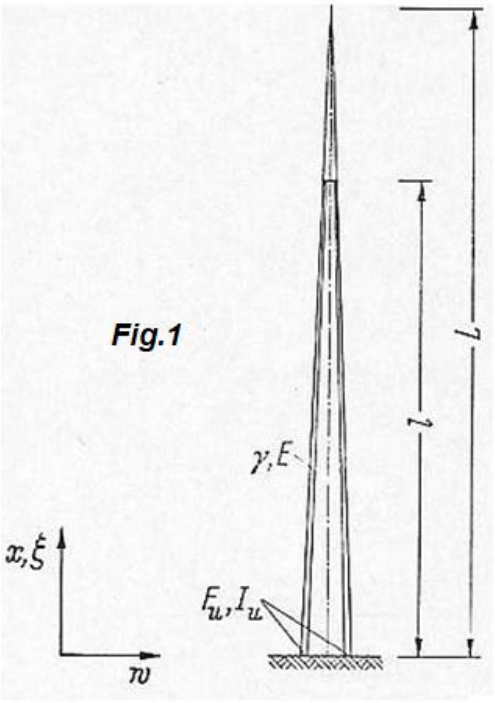
18.3 The Influence of Dead Mass and Elastic Clamping on the Bending frequency of a slender Tower with linearly reducing Thickness (1969)

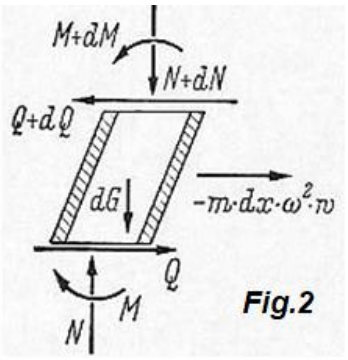
In the course of the years, on the basis of the latest technological findings, ever higher and slender tower structures could be created. Due to the high slenderness, such a tower oscillates (see *Fig.1*) with a very low fundamental frequency, so that there can be a risk of resonance with slowly changing excitation forces. In order to determine a more precise natural frequency value, the influence of the dead weight and the elastic clamping in the soil must therefore no longer be neglected in general.
At that time: Moscow TV Tower 530m, now Burj Kalifa 828m). Below scientific work followed a justification supporting work for a bell tower of a church at Hannover.

Lohse dealt with the dynamic behavior of elastic bars (beams) of constant thickness in [*Loh55*]. Natural vibrations of conical bars were investigated in [*Mon21, Con64*]. Nikitin took into account in [*Nik64*] the influence of the dead weight in the calculation of the Moscow TV Tower.

1 Task

* Derivation and solution of the frequency differential equation
* Computation of a schematic example.





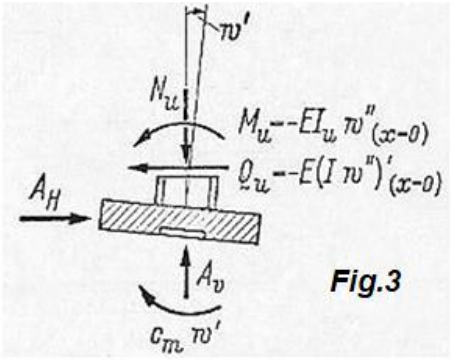


Fig.1: System sketch. Fig.2: Forces on the rod element. Fig.3: Forces and moments on the foundation

2 Analysis

From the three equilibrium conditions on the rod element (see *Fig.2*) follows the well-known differential equation

$$E\left[I(x)\cdot w''(x)\right]'' + \left[N(x)\cdot w'(x)\right]' - m(x)\cdot\omega^2\cdot w(x) = 0. \qquad (1)$$

This equation is rewritten to the dimensionless variable ξ . With the relationships

$$x = l\cdot\xi, \quad w = l\cdot\eta, \quad w' = \frac{d(l\cdot\eta)}{dx} = l\cdot\frac{d\eta}{d\xi}\cdot\frac{d\xi}{d\eta} = l\cdot\dot{\eta}\cdot\frac{1}{l}, \quad w'' = l\,\ddot{\eta} \qquad (2)$$

and the functions

$$I(\xi) = I_u(1-\alpha\cdot\xi)^4, \qquad (3.1)$$

$$N(\xi) = \gamma\cdot F_u\cdot\frac{L}{3}\left[(1-\alpha)^3-(1-\alpha\cdot\xi)^3\right] \qquad (3.2)$$

$$m(\xi) = \varrho\cdot F_u\cdot(1-\alpha\cdot\xi)^2, \qquad (3.3)$$

employing the abbreviation $\alpha = \ell / L$ it finally reads

$$\left[(1-\alpha\,\xi)^4\,\ddot{\eta}\right]^{\cdot\cdot} + \frac{\beta_N}{3}\left[(1-\alpha)^3-(1-\alpha\,\xi)^3\right)\dot{\eta}\Big]^{\cdot} - \lambda^4\left[(1-\alpha\,\xi)^2\eta\right] = 0. \qquad (4)$$

As abbreviations are included in (4)

$$\beta_N = \frac{\gamma\cdot F_u\cdot l^3}{E\cdot I_u}\cdot\frac{L}{l} = \beta_{N0}/\alpha, \quad \lambda^4 = \beta_{N0}\cdot\frac{l\,\omega^2}{g}. \qquad (5)$$

To solve the differential equation, the power series approach

$$\eta(\xi) = \sum_1^\infty a_n\cdot\xi^{n-1} \qquad (6)$$

is used, whose series members will be known after fulfillment of boundary conditions and differential equation. From the boundary conditions at the bottom (see *Fig.1* and *3*) follows

$$\eta\,(\xi=0): \quad a_1 = 0 \qquad (7.1)$$

$$c_m\,\dot{\eta}\,(\xi=0) = +E\,I_u\,l\,\ddot{\eta}\,(\xi=0) : a_2 = \frac{2\,E\,I_u}{l\,c_m}\,a_3 = \varepsilon\cdot a_3. \qquad (7.2)$$

The boundary conditions at the top $E\,I_u\,l\,\ddot{\eta}(\xi=1) = 0 \quad \text{und} \quad E\,(I\,l\,\ddot{\eta})^{\cdot}\,(\xi=1) = 0$

provide two homogeneous equations in series form

$$\sum_3^\infty a_n\,(n-1)\,(n-2) = 0 \qquad (7.3) \qquad \sum_4^\infty a_n\,(n-1)\,(n-2)\,(n-3) = 0, \qquad (7.4)$$

in which only two unknowns a_3, a_4 are incorporated, since the higher row members depend on them according to the linear combination $a_n = F_n\cdot a_3 + G_n\cdot a_4$ (8)

The entities Fn and Gn are obtained for n > 4 after insertion of (6) into (4) and a subsequent 'comparison of coefficients'. As initial values are available

$$\left.\begin{aligned} &F_1 = 0, \quad F_2 = 0, \quad F_3 = 1, \quad F_4 = 0, \\ &F_5 = -\frac{1}{24}\left(24\,\alpha^2 + 2\,\frac{\beta_N}{3}\left[-3\,\alpha + 3\,\alpha^2 - \alpha^3\right] + \varepsilon\beta_N\,\alpha\right) \\ &F_6 = \frac{1}{120}\left(288\,\alpha F_5 + 48\,\alpha^3 + 4\,\beta_N\,\alpha - 2\,\varepsilon\,(\beta_N\,\alpha^2) + \varepsilon\lambda^4\right). \end{aligned}\right\} \qquad (9.1)$$

.

The recursion formula for n > 6 results in

$$\begin{aligned} F_n = \frac{1}{(n-1)\,(n-2)\,(n-3)\,(n-4)}\Big(&\lambda^4\,\alpha^2\,F_{n-6} + \\ &+\left[-2\,\lambda^4\,\alpha - (n-4)\,(n-6)\,\beta_N\,\frac{\alpha^3}{3}\right]F_{n-5} + \left[\lambda^4 - (n-4)(n-5)\cdot\right. \\ &\left.\cdot\left((n-3)(n-6)\,\alpha^4 - \beta_N\,\alpha^2\right)\right]F_{n-4} - (n-4)^2\left[-(n-3)(n-5)\,4\,\alpha^3 + \right. \\ &\left.+\beta_N\,\alpha\right]F_{n-3} - (n-3)\cdot(n-4)\cdot\left((n-3)\cdot(n-4)\,6\,\alpha^2 + \right. \\ &\left.+\frac{\beta_N}{3}\left(-3\,\alpha + 3\,\alpha^2 - \alpha^3\right)\right)F_{n-2} + (n-2)(n-3)^2(n-4)\,F_{n-1}\Big). \end{aligned} \qquad (9.2)$$

For the G_n the following expressions are obtained

$$G_1 = 0, \quad G_2 = 0, \quad G_3 = 0, \quad G_4 = 1, \quad G_5 = \frac{1}{24} \cdot 48\,\alpha$$

$$G_6 = \frac{1}{120} \cdot \left(288\,\alpha\,G_5 - 36\,(6\,\alpha^2) - 6\,\frac{\beta_N}{3}[-3\,\alpha + 3\,\alpha^2 - \alpha^3]\right) \tag{9.3}$$

$$G_n = \text{analog}\,F_n. \tag{9.4}$$

Introducing the former expressions into (7.3) and (7.4), provides us with the frequency determinant |D|

$$D = \begin{vmatrix} \sum_3^\infty F_n\,(n-1)(n-2)\,a_3 & \sum_3^\infty G_n\,(n-1)(n-2)\,a_4 \\ \sum_4^\infty F_n\,(n-1)(n-2)(n-3)\,a_3 & \sum_4^\infty G_n\,(n-1)\,(n-2)\,(n-3)\,a_4 \end{vmatrix} \tag{10}$$

as function of the parameter $\lambda^4(F_n, G_n)$ and finally |D| = 0 the eigenvalues $\lambda_1^4, \lambda_2^4 \to \lambda_n^4$.

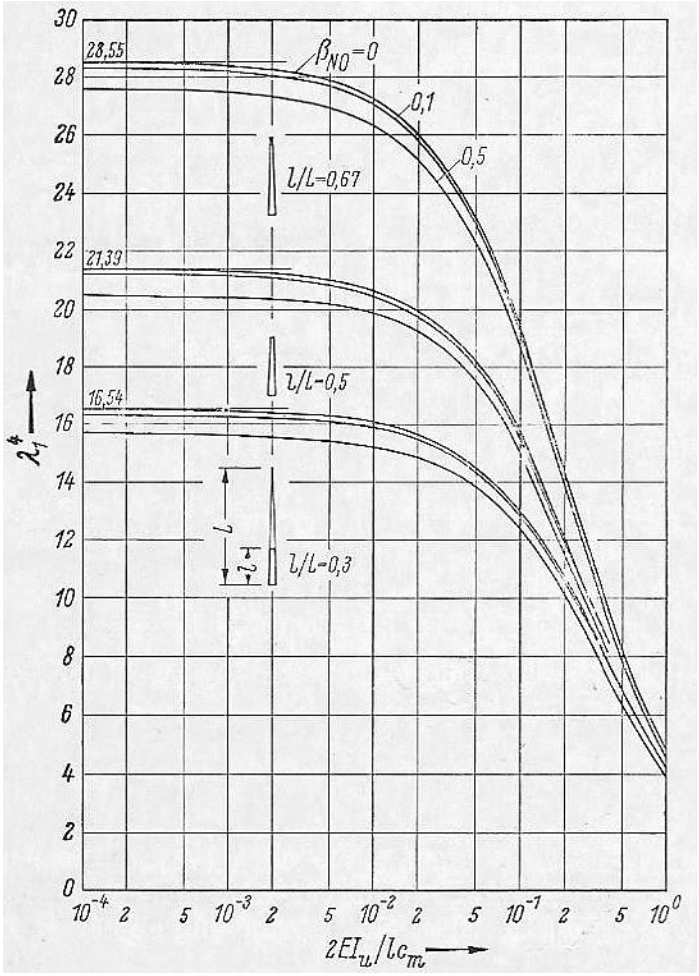


Fig.4: Solution curves for the first eigenvalue

3. Results and Discussion

Fig. 4 shows a recording of the first eigenvalue as a function of the parameters clamping and dead weight. It turns out that low clamping in the ground significantly reduces the natural frequencies of the structure. If one follows the curves outside the area recorded here, but no longer of interest, the curves for large abscissa values, as expected, strive against the following limit cases:

1. Vibration of the one-sided hinged rod $\beta_{N0} = 0,\ c_m = 0.$ The associated curves aim towards zero.

2. Buckling problem of the elastically clamped rod $\beta_{N0} > 0,\ \omega_1 = 0.$ The curves have a zero crossing at $\varepsilon = \varepsilon(\beta_{N0})$.

Furthermore, it can be seen that the influence of the dead weight on the natural frequency (not the eigenvalue) increases with slenderness λ / ℓ. In addition, the influence of the dead weight increases with decreasing clamping.

In the case of fixed clamping $c_m \to \infty$, the values already found in [3] are obtained.

4. Example

$$l = 170\ \text{m},\ \alpha = 0{,}5,\ I_u = 160\ \text{m}^4,\ \gamma = 2{,}6\ \text{Mp/m}^3,\ F_u = 11\ \text{m}^2,\ \Delta F_u = 9\ \text{m}^2,$$
$$E_{dyn}\,(\text{B } 450) \approx 4 \cdot 10^6\ \text{Mp/m}^2 \quad (\text{vgl. [5], S. 43}),$$
$$f = 0{,}45,\ F_F = 270\ \text{m}^2,\ I_F = 3{,}2 \cdot 10^4\ \text{m}^4,$$
$$E_{dyn}\,(\text{Boden}) \approx 3 \cdot 10^4\ \text{Mp/m}^2 \quad (\text{vgl. [5], S. 48}).$$

Addition for expanding of the tower ΔF_u. For the modulus of elasticity, the scattering range was not taken into account for simplicity. With the quantities above the parameters

$$c_m = \frac{E_{dyn\,(\text{Boden})}}{f\sqrt{F_F}} I_F \ (\text{vgl. [5], S. 49}) = 1{,}3 \cdot 10^3\ \text{Mp/m}^3,\quad \varepsilon = 0{,}06,\quad \beta_{N0} = 0{,}4$$

are yielded and with these in application of the diagram on *Fig.4* the vibration duration

$$T_1 = \frac{2\pi}{\omega_1} = 2\pi \sqrt{\frac{l}{g}} \cdot \frac{\lambda_1^*}{\sqrt{\beta_{N0}}} = \begin{pmatrix} 4{,}2 \\ 3{,}8 \end{pmatrix} \text{ s für } \beta_{N0} = \begin{matrix} 0{,}4 \\ 0{,}0 \end{matrix}\Bigg).$$

Annex:

- *The parameters of the ground (soil) have to be adapted to the actual building standard.*
- *With an increase in water saturation, the E_{dyn} values increase in cohesive soils*
- *In higher frequency ranges, the importance of the soil spring system decreases, beyond 40Hz meaningless*
- *Former units: 1 Mp/m^2=100kp·100 $^{-2}$/cm^2 = 0.1 kp/cm^2=0.98 N/cm^2. 1MPa = 1 N/mm^2*
- *Some data for the soil type of the building ground: in kp / cm^2 = 9.8N / cm^2*

Type	E_{static}	$E_{dynamic}$
Sand, dense	*400 → 1000*	*2000 → 5000*
Gravel sand, dense	*800 → 1500*	*3000 → 8000*
Clay, pretty stiff	*80 → 300*	*1200 → 2500*
Soils, mixed	*50 → 200*	*700 → 1500*

Literatur

1. Lohse G: *Das dyn. Verhalten von elastisch eingespannten Bauwerken*. VDI-Berichte 4 (1955), S. 57-60.
2. Mononobe N: *Die Eigenschwingungen eingespannter Stäbe von veränderlichem Querschnitt*. Zamm 1 (1921), S. 444-451
3. Conway H D,. Becker E C H and Dubil J F : *Vibrations Frequencies of Tapered Bars and Circular Plates*. [ourn. Appl. Mech. 31, (1964), S. 329--351
4. Nikitin N V: *Dynamische Berechnung eines hohen Turmes*. Stroitelnaja mechanica i rascet sooruzenij 6 (1964) No. 3, S. 37-42
5. Kanya J: *Glockentürme*. Wiesbaden: Bauverlag 1968
6. Drechsel W: *Turmbauwerke*. Wiesbaden: Bauverlag 1966.

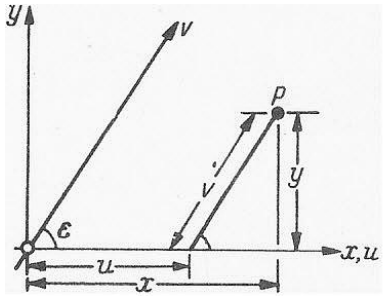
18.4 Natural Frequencies of Thin Inclined Isotropic Plates (*Cuntze,1969*)

Natural frequencies of inclined plates have already been approximated. Argyris used in [*Arg67*] a displacement method to calculate the natural frequencies of a cantilever plate, clamped at all sides. Barton in [*Bar55*] also examined the cantilever plate using Rrrz's method. He confirmed the theoretical values by measurement results.

In this work, in contrast to the aforementioned methods, a closed solution is specified.

1 Task

* Derivation of the vibration differential equation of motion
* Derivation of an analytical solution to determine the eigenvalues $\lambda \rightarrow \omega(\lambda)$. Intention was to just show the complicate procedure. Implementation including numerical analysis was not foreseen.



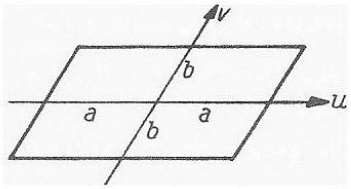


Fig.1: Coordinates and CoS of the skew plate. Fig.2:Geometry of the skew plate

2 Differential equation with solutions

After transforming the differential equation of the oscillating plate from right-angled coordinates (x, y) to skewed coordinates (u, v), we obtain the oscillation differential equation by means of the transformation equations $x = u + CoS(\varepsilon)\cdot v$ and $y = \sin(\varepsilon)\cdot v$

$$(1)\quad w_{uuuu} - 4\,c\,(w_{uuuv} + w_{uvvv}) + 2\,(1 + 2\,c^2)\,w_{uuvv} + w_{vvvv} + s^4 \frac{-\omega^2\,\varrho\,h}{N}\,w = 0$$

(see also[3], p. 207). Here ρ is the plate density and (exceptional letter) $N = E\,h^2/12\,(1 - \nu^2)$ mean the plate stiffness if h is the plate thickness, E is the modulus of elasticity and ν is the transverse contraction number of the material. ω is the angular frequency of the natural oscillations.

A suitable approach for solving the differential equation is

$$(2)\quad w(u, v) = \sum_{(m)} e^{i\,\lambda_m (u + c\,v)} \sum_{r} A_{rm}\; e^{i\,\lambda_m \overset{*}{k}_{rm}\, s\, v} + \sum_{(n)} e^{i\,\lambda_n (c\,u + v)} \sum_{s} A_{sn}\, e^{i\,\lambda_n \overset{*}{k}_{sn}\, s\, u}\,.$$

If we insert the approach above into (1), we get a characteristic equation for the wave numbers k^*

$$(3)\quad \begin{cases} 1 - 4\,c\,[(c + \overset{*}{k}_{rm}\,s) + (c + \overset{*}{k}_{rm}\,s)^3] - \\ \quad - 2\,(1 + 2\,c^2)\,(c + \overset{*}{k}_{rm}\,s)^2 + \\ \quad + (c + \overset{*}{k}_{rm}\,s)^4 - e_m = 0 \\ \text{und} \\ (c + \overset{*}{k}_{sn}\,s)^4 - 4\,c\,[(c + \overset{*}{k}_{sn}\,s)^3 + (c + \overset{*}{k}_{sn}\,s)] + \\ \quad + 2\,(1 + 2\,c^2)\,(c + \overset{*}{k}_{sn}\,s)^2 + 1 - e_n = 0 \end{cases}$$

$$(4.1)\quad e_m = s^4 \frac{\omega^2\,\varrho\,h}{N} \frac{1}{\lambda_m^4}$$

$$(4.2)\quad e_n = e_m \left(\frac{\lambda_m}{\lambda_n}\right)^4.$$

with the eigenvalue (4.1) and an entity (4.2) that depends on it. After rearranging (3), , considering the abbreviations (6), the equations (5) result

$$(5)\quad \begin{cases} k_{r\,m}^4 - 4\,c\,k_{r\,m}^3 + 2\,(1+2\,c^2)\,k_{r\,m}^2 - \\ \qquad - 4\,c\,k_{r\,m} + 1 - e_m = 0 \\ \text{und} \\ k_{s\,n}^4 - 4\,c\,k_{s\,n}^3 + 2\,(1+2\,c^2)\,k_{s\,n}^2 - \\ \qquad - 4\,c\,k_{s\,n} + 1 - e_n = 0\,. \end{cases} \qquad (6)\quad \begin{aligned} k_{r\,m} &= c + \overset{*}{k}_{r\,m}\,s \\ k_{s\,n} &= c + \overset{*}{k}_{s\,n}\,s\,. \end{aligned}$$

We must now go to the roots of the above equations (5). In doing so, we will fully assume that these equations of the 4th order are expressed in the form of

$$(7)\qquad (k+\alpha+\beta_1)\,(k+\alpha-\beta_1)\times(k+\alpha+\beta_2)\,(k+\alpha-\beta_2) = 0\,.$$

After performing the multiplication the result is

$$k^4 + k^3\,(4\,\alpha) + k^2\,(6\,\alpha^2 - \beta_1^2 - \beta_2^2) + k\,2\,\alpha\,(2\,\alpha^2 - \beta_1^2 - \beta_2^2) + (\alpha^2 - \beta_1^2)\,(\alpha^2 - \beta_2^2) = 0\,.$$

The coefficient comparison with (5) provides the relationships

$$\begin{aligned} &(8.1) && -4\,c = 4\,\alpha\,, \\ &(8.2) && 2\,(1+2\,c^2) = 6\,\alpha^2 - \beta_1^2 - \beta_2^2\,, \\ &(8.2) && -4\,c = 2\,\alpha\,(2\,\alpha^2 - \beta_1^2 - \beta_2^2)\,, \\ &(8.4) && 1 - e = (\alpha^2 - \beta_1^2)\,(\alpha^2 - \beta_2^2)\,. \end{aligned}$$

This means 4 equations are given for 3 unknowns. A unique solution can therefore only be found if two equations are identical. By inserting (8.1) in (8.2) and (8.3) we get the two equations

$$2 + 4\,c^2 = 6\,c^2 - \beta_1^2 - \beta_2^2\,, \qquad 4 = 2\,(2\,c^2 - \beta_1^2 - \beta_2^2)\,.$$

Hence, we get the same equation of determination in both cases

$$(9)\qquad 2 - 2\,c^2 = -\,(\beta_1^2 + \beta_2^2)\,,$$

so that the approach (7) is justified. From (8.1), (8.4) and (9) the roots result in:

$$(10)\quad \begin{cases} \alpha = -\,c\,, \\ i\,\beta_{\substack{11\\12}} = \sqrt{1 - c^2 \mp \sqrt{e}} = \bar{\beta}_{\substack{11\\12}}\,, \\ i\,\beta_{\substack{21\\22}} = \sqrt{1 - c^2 \pm \sqrt{e}} = \bar{\beta}_{\substack{21\\22}}\,. \end{cases}$$

As we can conclude from identities we can set for simplification

$$\beta_{11} = \beta_1\,, \qquad \beta_{12} = \beta_2\,.$$

As a solution of the differential equation we find definitive and transitioning to the angular functions

$$\begin{aligned} w(u,v) = &\sum_{(m)} e^{i\,\lambda_m(u+c\,v)}\,[A_{1\,m}\,e^{i\,\lambda_m(\alpha+\beta_{1\,m})\,s\,u} + \\ &+ A_{2\,m}\,e^{i\,\lambda_m(\alpha-\beta_{1\,m})\,s\,v} + A_{3\,m}\,e^{i\,\lambda_m(\alpha+\beta_{2\,m})\,s\,v} + \\ &+ A_{4\,m}\,e^{i\,\lambda_m(\alpha-\beta_{2\,m})\,s\,v}] + \\ &\sum_{(n)} e^{i\,\lambda_n(c\,u+v)}\,[B_{1\,n}\,e^{i\,\lambda_n(\alpha+\beta_{1\,n})\,s\,u} + \\ &+ B_{2\,n}\,e^{i\,\lambda_n(\alpha-\beta_{1\,n})\,s\,u} + B_{3\,n}\,e^{i\,\lambda_n(\alpha+\beta_{2\,n})\,s\,u} + \\ &+ B_{4\,n}\,e^{i\,\lambda_n(\alpha-\beta_{2\,n})\,s\,u}] \end{aligned} \qquad (11)$$

$$
\begin{aligned}
w(u,v) = \sum_{(m)} & [\cos\lambda_m (u + c\,v) + i \sin\lambda_m (u + c\,v)] \times \\
& \times [\cos\lambda_m c - i \sin\lambda_m c] \times \\
& \times [D_{1m} \cos\lambda_m \beta_{1m} s\,v + i\,D_{2m} \sin\lambda_m \beta_{1m} s\,v + \\
& + D_{3m} \cos\lambda_m \beta_{2m} s\,v + i\,D_{4m} \sin\lambda_m \beta_{2m} s\,v] + \\
& + \sum_{(n)} [\cos\lambda_n (c\,u + v) + i \sin\lambda_m (c\,u + v)] \times \\
& \times [\cos\lambda_n c - i \sin\lambda_n c] \times \\
& \times [E_{1m} \cos\lambda_n \beta_{1n} s\,u + i\,E_{2m} \sin\lambda_n \beta_{1n} s\,u + \\
& + E_{3n} \cos\lambda_n \beta_{2n} s\,u + i\,E_{4n} \sin\lambda_n \beta_{2n} s\,u] .
\end{aligned} \tag{12}
$$

In it, both the real and the imaginary parts are solutions in themselves. After multiplying, four groups *(I through IV)* of solutions are obtained by combining real and imaginary elements

$$
\begin{aligned}
w(u,v) = \sum_{(m)} & \{\cos\lambda_m (u + c\,v) \cos\lambda_m c\,(D_{1m} \cos\lambda_m \beta_{1m} s\,v + D_{3m} \cos\lambda_m \beta_{2m} s\,v) - \\
& - \sin\lambda_m (u + c\,v) \cos\lambda_m c\,(D_{2m} \sin\lambda_m \beta_{1m} s\,v + D_{4m} \sin\lambda_m \beta_{2m} s\,v)\} + \\
& + \sum_{(n)} \{\cos\lambda_n (c\,u + v) \cos\lambda_n c\,(E_{1n} \cos\lambda_n \beta_{1n} s\,u + E_{3n} \cos\lambda_n \beta_{2n} s\,u) - \\
& - \sin\lambda_n (c\,u + v) \cos\lambda_n c\,(E_{2n} \sin\lambda_n \beta_{1n} s\,u + E_{4n} \sin\lambda_n \beta_{2n} s\,u)\} + \\
& + \sum_{(m)} \{\sin\lambda_m (u + c\,v) \sin\lambda_m c\,(D_{1m} \cos\lambda_m \beta_{1m} s\,v + D_{2m} \cos\lambda_m \beta_{2m} s\,v) + \\
& + \cos\lambda_m (u + c\,v) \sin\lambda_m c\,(D_{2m} \sin\lambda_m \beta_{1m} s\,v + D_{4m} \sin\lambda_m \beta_{2m} s\,v)\} + \\
& + \sum_{(n)} \{\sin\lambda_n (c\,u + v) \sin\lambda_n c\,(E_{1n} \cos\lambda_n \beta_{1n} s\,u + E_{3n} \cos\lambda_n \beta_{2n} s\,u) + \\
& + \cos\lambda_n (c\,u + v) \sin\lambda_n c\,(E_{2n} \sin\lambda_n \beta_{1n} s\,u + E_{4n} \sin\lambda_n \beta_{2n} s\,u)\} + \\
& + \sum_{(m)} \{i \cos\lambda_m (u + c\,v) \cos\lambda_m c\,(D_{2m} \sin\lambda_m \beta_{1m} s\,v + D_{4m} \sin\lambda_m \beta_{2m} s\,v) \times \\
& \times i \sin\lambda_m (u + c\,v) \cos\lambda_m c\,(D_{1m} \cos\lambda_m \beta_{1m} s\,u + D_{3m} \cos\lambda_m \beta_{2m} s\,v)\} + \\
& + \sum_{(n)} \{i \cos\lambda_n (c\,u + v) \cos\lambda_n c\,(E_{2n} \sin\lambda_n \beta_{1n} s\,u + E_{4m} \sin\lambda_n \beta_{2n} s\,u) \times \\
& \times i \sin\lambda_n (c\,u + v) \cos\lambda_n c\,(E_{1n} \cos\lambda_n \beta_{1n} s\,u + E_{3n} \cos\lambda_n \beta_{2n} s\,u)\} - \\
& - \sum_{(m)} \{i \sin\lambda_m (u + c\,v) \sin\lambda_m c\,(D_{2m} \sin\lambda_m \beta_{1m} s\,v + D_{4m} \sin\lambda_m \beta_{2m} s\,v) + \\
& + i \cos\lambda_m (u + c\,v) \sin\lambda_m c\,(D_{1m} \cos\lambda_m \beta_{1m} s\,v + D_{3m} \cos\lambda_m \beta_{2m} s\,v)\} - \\
& - \sum_{(n)} \{i \sin\lambda_n (c\,u + v) \sin\lambda_n c\,(E_{2n} \sin\lambda_n \beta_{1n} s\,u + E_{1n} \sin\lambda_n \beta_{2n} s\,u) + \\
& + i \cos\lambda_n (c\,u + v) \sin\lambda_n c\,(E_{1n} \cos\lambda_n \beta_{1n} s\,u + E_{3n} \cos\lambda_n \beta_{2n} s\,u)\}
\end{aligned} \tag{13}
$$

I, II, III, IV

with eight free constants each. These groups and their constants are to be considered independently of each other, because each of these groups corresponds to a class of oscillations (see also [4] and [2]). The constants are to be determined from the boundary conditions. This will be explained for a special case in the third chapter. For this purpose, however, the trigonometric sum expressions in (13) must be split by means of the addition theorems.

3 Determination of the free constants from the boundary conditionsof the plate

For the special example - the plate mounted at all sides - the free constants are now determined. In this case the following boundary conditions are present: (see [3], p. 207).

$$
\begin{cases}
\text{a) Ränder} \quad u = \pm a : w = 0 , \\
\qquad\qquad \Delta w = \dfrac{1}{s^2} (w_{uu} - 2\,c\,w_{uv} + w_{vv}) = 0 , \\
\text{b) Ränder} \quad v = \pm b : w = 0 , \qquad \Delta w = 0
\end{cases} \tag{15}
$$

Within the scope of the present work, we only want to show the solution of the first (I) of the four vibration groups in (13). Here the equations w of the bending surface and its derivation are

$$
\begin{aligned}
w = & \sum_{(m)} \cos \lambda_m c \times \\
& \times \{(\cos \lambda_m u \cos \lambda_m c v - \sin \lambda_m u \sin \lambda_m c v) \times \\
& \times (D_{1m} \cos \lambda_m \beta_{1m} s v + D_{3m} \cos \lambda_m \beta_{2m} s v) - \\
& - (\sin \lambda_m u \cos \lambda_m c v + \cos \lambda_m u \sin \lambda_m c v) \times \\
& \times (D_{2m} \sin \lambda_m \beta_{1m} s v + D_{4m} \sin \lambda_m \beta_{2m} s v)\} + \\
& + \sum_{(n)} \cos \lambda_n c \times \\
& \times \{(\cos \lambda_n c u \cos \lambda_n v - \sin \lambda_n c u \sin \lambda_n v) \times \\
& \times (E_{1n} \cos \lambda_n \beta_{1n} s u + E_{3n} \cos \lambda_n \beta_{2n} s u) - \\
& - (\sin \lambda_n c u \cos \lambda_n v + \cos \lambda_n c u \sin \lambda_n v) \times \\
& \times (E_{2n} \sin \lambda_n \beta_{1n} s u + E_{4n} \sin \lambda_n \beta_{2n} s u)\}
\end{aligned} \tag{16}
$$

$$
\begin{aligned}
\Delta w = & \sum_{(m)} \lambda_m^2 \cos \lambda_m c \times \\
& \times \{(\cos \lambda_m u \cos \lambda_m c v - \sin \lambda_m u \sin \lambda_m c v) \times \\
& \times (\overset{*}{D}_{1m} \cos \lambda_m \beta_{1m} s v + \overset{*}{D}_{3m} \cos \lambda_m \beta_{2m} s v) - \\
& - (\sin \lambda_m u \cos \lambda_m c v + \cos \lambda_m u \sin \lambda_m c v) \times \\
& \times (\overset{*}{D}_{2m} \sin \lambda_m \beta_{1m} s v + \overset{*}{D}_{4m} \sin \lambda_m \beta_{2m} s v)\} + \\
& + \sum_{(n)} \lambda_n^2 \cos \lambda_n c \times \\
& \times \{(\cos \lambda_n c u \cos \lambda_n v - \sin \lambda_n c u \sin \lambda_n v) \times \\
& \times (\overset{*}{E}_{1n} \cos \lambda_n \beta_{1n} s u + \overset{*}{E}_{3n} \cos \lambda_n \beta_{2n} s u) - \\
& - (\sin \lambda_n c u \cos \lambda_n v + \cos \lambda_n c u \sin \lambda_n v) \times
\end{aligned} \tag{17}
$$

with the abbreviations

$$
\begin{aligned}
\overset{*}{D}_{1m} &= D_{1m} (1 - c^2 + \beta_{1m}^2 s^2), & \overset{*}{E}_{1n} &= E_{1n} (1 - c^2 + \beta_{1n}^2 s^2), \\
\overset{*}{D}_{2m} &= D_{2m} (1 - c^2 + \beta_{1m}^2 s^2), & \overset{*}{E}_{2n} &= E_{2n} (1 - c^2 + \beta_{1n}^2 s^2), \\
\overset{*}{D}_{3m} &= D_3 (1 - c^2 + \beta_{2m}^2 s^2), & \overset{*}{E}_{3n} &= E_{3n} (1 - c^2 + \beta_{2n}^2 s^2), \\
\overset{*}{D}_{4m} &= D_{4m} (1 - c^2 + \beta_{2m}^2 s^2), & \overset{*}{E}_{4n} &= E_{4n} (1 - c^2 + \beta_{2n}^2 s^2).
\end{aligned} \tag{18}
$$

- We now insert the boundary conditions at the Boundaries u = +- a:

As we can see when inserting, the boundary conditions contain functions of v whose coefficients do not disappear identically. They can be split into a portion of even functions of v on the one hand, and odd functions of v on the other. Each such proportion must disappear identically, which in some cases is only possible after a series development. After the separation into even and odd functions, follow for <u>w = 0</u> , taking into account

$$
\cos \lambda_m(\pm a) = 0 \qquad \left(\lambda_m = \frac{\pi}{a} \frac{2m - 1}{2}\right), \tag{19.1}
$$

the even (19.2) and odd (19.3) portions

$$
\begin{aligned}
& \sum_{(n)} \cos \lambda_n c \cos \lambda_n v \times \\
& \times [\cos \lambda_n c a (E_{1n} \cos \lambda_n \beta_{1n} s a + E_{3n} \cos \lambda_n \beta_{2n} s a) - \\
& - \sin \lambda_n c a (E_{2n} sin \lambda_n \beta_{1n} s a + E_{4n} \sin \lambda_n \beta_{2n} s a)] = 0
\end{aligned} \tag{19.2}
$$

$$
\begin{aligned}
& \sum_{(m)} \cos \lambda_m c \cdot \sin \lambda_m a \times \\
& \times [\sin \lambda_m c v (D_{1m} \cos \lambda_m \beta_{1m} s v + D_{3m} \cos \lambda_m \beta_{2m} s v) + \\
& + \cos \lambda_m c v (D_{2m} \sin \lambda_m \beta_{1m} s v + D_{4m} \sin \lambda_m \beta_{2m} s v)] + \\
& + \sum_{(n)} \cos \lambda_n c \cdot \sin \lambda_n v \times \\
& \times [\sin \lambda_n c a (E_{1n} \cos \lambda_n \beta_{1n} s a + E_{3n} \cos \lambda_n \beta_{2n} s a) + \\
& + \cos \lambda_n c a (E_{2n} \sin \lambda_n \beta_{1n} s a + E_{4n} \sin \lambda_n \beta_{2n} s a)] = 0.
\end{aligned} \tag{19.3}
$$

And for <u>Δw = 0</u> , even (19.4) and odd (19.5 portions

$$
\begin{aligned}
& \sum_{(n)} \lambda_n^2 \cos \lambda_n c \cos \lambda_n v \times \\
& \times [\cos \lambda_n c a (\overset{*}{E}_{1n} \cos \lambda_n \beta_{1n} s a + \overset{*}{E}_{3n} \cos \lambda_n \beta_{2n} s a) - \\
& - \sin \lambda_n c a (\overset{*}{E}_{2n} \sin \lambda_n \beta_{1n} s a + \overset{*}{E}_{4n} \sin \lambda_n \beta_{2n} s a)] = 0
\end{aligned} \tag{19.4}
$$

und der ungerade Anteil

$$
\begin{aligned}
& \sum_{(m)} \lambda_m^2 \cos \lambda_m c \cdot \sin \lambda_m \alpha \times \\
& \times [\sin \lambda_m c v (\overset{*}{D}_{1m} \cos \lambda_m \beta_{1m} s v + \overset{*}{D}_{3m} \cos \lambda_m \beta_{2m} s v) + \\
& + \cos \lambda_m c v (\overset{*}{D}_{2m} \sin \lambda_m \beta_{1m} s v + \overset{*}{D}_{4m} \sin \lambda_m \beta_{2m} s v)] + \\
& + \sum_{(n)} \lambda_n^2 \cos \lambda_n c \cdot \sin \lambda_n v \times \\
& \times [\sin \lambda_n c a (\overset{*}{E}_{1n} \cos \lambda_n \beta_{1n} s a + \overset{*}{E}_{3n} \cos \lambda_n \beta_{1n} s a) + \\
& + \cos \lambda_n c a (\overset{*}{E}_{2n} \sin \lambda_n \beta_{1n} s a + \overset{*}{E}_{4n} \sin \lambda_n \beta_{2n} s a)] = 0.
\end{aligned} \tag{19.5}
$$

- We now insert the boundary conditions at the Boundaries v = +- b:

The calculation at these edges is done in the same way. Taking into account

$$(20.1) \qquad \cos \lambda_n (\pm b) = 0 \rightarrow \left(\lambda_n = \frac{\pi}{b} \frac{2n-1}{2}\right)$$

results in analogy in the following even and odd proportions to

$$(20.2) \qquad \sum_{(m)} \cos \lambda_m c \cos \lambda_m u \times$$
$$\times [\cos \lambda_m c b (D_{1m} \cos \lambda_m \beta_{1m} s b + D_{3m} \cos \lambda_m \beta_{2m} s b) -$$
$$- \sin \lambda_m c b (D_{2m} \sin \lambda_m \beta_{1m} s b + D_{4m} \sin \lambda_m \beta_{2m} s b) = 0$$

und der ungerade Anteil zu

$$(20.3) \qquad \sum_{(m)} \cos \lambda_m c \sin \lambda_m u \times$$
$$\times [\sin \lambda_m c b (D_{1m} \cos \lambda_m \beta_{1m} s b + D_{3m} \cos \lambda_m \beta_{2m} s b) +$$
$$+ \cos \lambda_m c b (D_{2m} \sin \lambda_m \beta_{1m} s b + D_{4m} \sin \lambda_m \beta_{2m} s b)] +$$
$$+ \sum_{(n)} \cos \lambda_n c \sin \lambda_n b \times$$
$$\times [\sin \lambda_n c u (E_{1n} \cos \lambda_n \beta_{1n} s u + E_{3n} \cos \lambda_n \beta_{2n} s u) \times$$
$$\times \cos \lambda_n c u (E_{2n} \sin \lambda_n \beta_{1n} s u + E_{4n} \sin \lambda_n \beta_{2n} s u)] = 0.$$

$$(20.4) \qquad \sum_{(m)} \lambda_m^2 \cos \lambda_m c \cos \lambda_m u \times$$
$$\times [\cos \lambda_m c b (\overset{*}{D}_{1m} \cos \lambda_m \beta_{1m} s b + \overset{*}{D}_{3m} \cos \lambda_m \beta_{2m} s b) -$$
$$- \sin \lambda_m c b (\overset{*}{D}_{2m} \sin \lambda_m \beta_{1m} s b + \overset{*}{D}_{4m} \sin \lambda_m \beta_{2m} s b) = 0$$

und den ungeraden Anteil

$$(20.5) \qquad \sum_{(m)} \lambda_m^2 \cos \lambda_m c \sin \lambda_m u \times$$
$$\times [\sin \lambda_m c b (\overset{*}{D}_{1m} \cos \lambda_m \beta_{1m} s b + \overset{*}{D}_{3m} \cos \lambda_m \beta_{2m} s b) +$$
$$\times \cos \lambda_m c b (\overset{*}{D}_{2m} \sin \lambda_m \beta_{1m} s b + \overset{*}{D}_{4m} \sin \lambda_m \beta_{2m} s b)] +$$
$$+ \sum_{(n)} \lambda_n^2 \cos \lambda_n c \sin \lambda_n b \times$$
$$\times [\sin \lambda_n c u (\overset{*}{E}_{1n} \cos \lambda_n \beta_{1n} s u + \overset{*}{E}_{3n} \cos \lambda_n \beta_{2n} s u) \times$$
$$\times \cos \lambda_n c u (\overset{*}{E}_{2n} \sin \lambda_n \beta_{1n} s u + \overset{*}{E}_{4n} \sin \lambda_n \beta_{2n} s u)] = 0.$$

And for $\Delta w = 0$, the even portions (20.2, 20.4) and the odd portions (20.3, 20.5).

The number of unknown constants matches that of the equations. From the equations (19.2) and (19.4) the constants D_{3m} and D_{4m} can be calculated as a function of D_{1m} , D_{2m} , and from (20.2) and (20.4) the E_{3n} and E_{4n} accordingly as a function of E_{1n} and E_{2n}. The remaining unknowns D_{1m}, D_{2m}, E_{1n} and E_{2n} are determined from the equations not yet used. This must be done in such a way that the odd functions (19.3) and (19.5) are developed in Fourier-series according to $\sin(\lambda_n v)$ and (20.3) and (20.5) according to $\sin(\lambda_m u)$ (see [5] p.61 and [6] p.125). After inserting the Fourier coefficients, two homogeneous systems of equations result, in which once (Σ over m) and infinite number of unknowns D_{1m} and D_{2m} occur compared to the two unknowns E_{1n} and E_{2n}. On the other hand for each m (Σ over n) infinitely many unknown E_{1n} and E_{2n} compared to the two D_{1m} and D_{2m}. Care must be taken to ensure that for imaginary ß-values the trigonometric functions are converted into hyperbolic ones.

We get a homogeneous system of equations with $2 \cdot (m + n)$ equations, the coefficient determinant of which must disappear. From similar problems we know that in the diagonals there are considerably larger values than in the other places, so that these systems of equations are quite well suited for numerical calculation. As the calculation for a cantilever deep beam in ([5] p. 64) showed, it was sufficient to take $(m + n) = 10$ constants, since then the natural frequency practically did not change. In the present case, one could still eliminate two unknowns in order to achieve a smaller system of equations, but one accepts a full matrix, and the occupation of the field in numerical analysis becomes much more complicated.

Literatur

1 Argyris J H : *Matrix Displacement Analysis of Plates and Shells*. Ing. Arch. 35 (1967)

2 Barton M V: Journal of Applied Mechanics 1951, 129

3 Lardy P: *Die strenge Lösung des Problems der schiefen Platte*. Schweizerische Bauzeitung, Nr. 15, (1949), 207

4 Iguchi S: *Die Eigenschwingungen nnd Klangfiguren der vierseitig freien rechteckigen Platte.* Ing. Archiv 22, S. 808 (1953).

5 Cuntze R: *Beitrag zur Berechnung von Eigenfrequenzen dünner Rechteckscheiben unter Berücksichtigung von randparalleler Orthotropie*. Dissertation, TU-Hannover (1968).

6 Gröbner W and Hofreiter N: *Integraltafeln*, 1. Teil. Wien und Innsbruck 1957, Springer-Verlag.

18.5 Natural Frequencies (eigenfrequencies) of Orthotropic Deep Beams (Diss.1968,to add)

18.6 The influence of Cross-sectional Shear Flexibility and Rotatory Inertia on the Natural Frequencies of Beams with Uniformly Distributed Mass

Based on the differential equation for the "Timoshenko beam", diagrams are presented that record above influences for five technically important beam boundary conditions. From these diagrams one can read the corresponding influence numerically with the help of the curves of the normalized correction coefficient K_{SD} capturing shear rigidity $_S$ and rotatory inertia.

In the case of thin-walled beams, beams made of multi-layer fiber composite material and sandwich beams, the influences of low shear rigidity and rotatory inertia are often of great importance. As a rule, such beams are not particularly shear-stiff. This means that the influences that reduce the bending natural frequency are already noticeable in relatively long beams even in the basic mode or tone (*lowest bending vibration shape,* n = 1). It would be of great help to the user if he could find the magnitude of these influences in diagrams for his calculations, in such a way that they are based on the bending natural frequencies of the shear-rigid beam of classical beam theory

The curve for the correction coefficient K_{SD} would then directly represent the percentage influencing factor (f_o the bending natural frequency of the shear-rigid beam with = = 0, λ eigenvalue when using the classical beam theory, E modulus of elasticity, I geometrical moment of inertia of the cross-section, density, A surface of the beam cross-section, l length).

18.6.2 Theoretical Relations

According to [1] and Fig.1, the equilibrium conditions at the oscillating beam element are

, w deflection (displacement), angular frequency, inclination (rotation) of the beam section, M bending moment, w' = dw/dx inclination of the beam line against the horizontal, w'- shear distortion angle, Q lateral force, G shear modulus, As effective shear area. The elimination of the angle leads to the differential equation

As parameter represent shear flexibility influence (shear rigid =0) and the influence of rotatory inertia; κ = A/As shear correction factor.

$$f_{SD} = K_{SD} \cdot f_0 = K_{SD} \cdot \alpha_0^2 \, [(E \cdot I / \rho \cdot A) / l^4]^{0.5} / 2\pi$$

Fig.1: Distortions and equilibrium conditions at the oscillating element of the Tirnoshenko beam

The approach provides a characteristic equation whose four roots are derived from the equation

In the case of classical beam theory, .

Finally, the solution function is in the areas I and II

A natural frequency curve can thus pass through two areas. To determine the free values over the four boundary conditions of the single-spar beam one needs the relations for w, M and Q. However, the consideration of the boundary conditions is much easier if one does not choose w but starts from Q. This is allowed because the four basic solutions are available in Q as well as in w. Thus, the consideration of the boundary conditions is now approached from the outset

As is well known, there are four homogeneous equations for the **ck,** which provide the frequency determinant and finally the frequency equation. A compilation of the frequency equations for the technically important bar boundary conditions considered later in Fig.4 to 8 is contained in [7]. There is also a discussion of solution area II using the example of the beam mounted on both sides.

After determination of the zero points of the frequency equation as function of , and α_{SD} the corresponding correction coefficient (index n of a tone omitted) can be determined.

It turns out that for each mode instead of a solution or eigenvalue curve as in classical beam theory, there are now two. So it is better no longer to speak of a mode (sound), but of a mode family that - from a physical point of view - has a higher and a low frequency vibration shape. With the continuum theory, this means e. g. in the case of deep beams the application of the plate theory, resulting in an infinite number of eigenvalue curves within one family.

The higher frequency vibration form (*upper eigenvalue curve*) is not considered, since a limitation to the two lowest and usually also technically most important natural frequency values of the respective "lower" spectrum branch ($(\omega_{11}, \omega_{21}, \omega_{31}, \ldots \omega_{\infty 1})$. However, the lowest eigenvalues $\omega_{12}, \omega_{22}, \omega_{32}$ of the "upper" spectrum are usually already above ω_{21} as confirmed in *Fig.3* as a function of the shear influence for the parameter $\delta = 0.0208$. In Fig. 2 (a length of the beam; $\psi =$ h/a) this is also shown in the related natural angular frequency curves determined on deep beams with the plate theory.

The Timoshenko beam gives two solution curves. Physically, this means that because of the degree of shear freedom, there are two degrees of freedom for the vibration shape of the cross-section; in plate theory, there are then infinitely many.

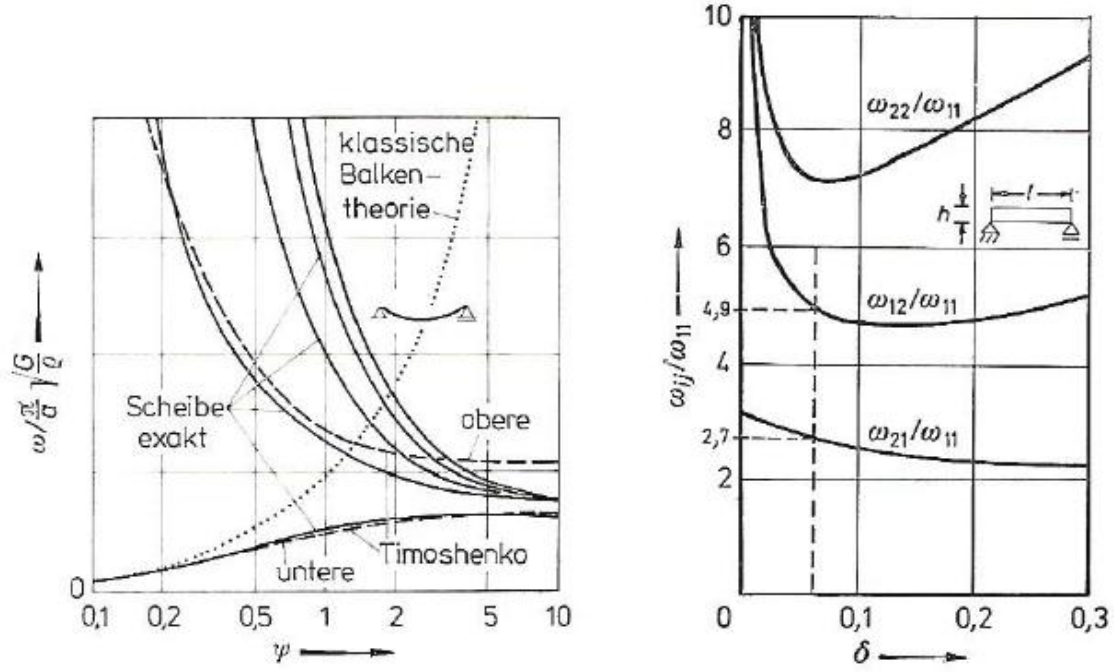


Fig.2: (left) Hinged beam; Representation of the natural frequency curves of the deepest

transverse tone family for ν = 0,16. (right) natural frequency ratios for n = 0.0208 (ν= 0.30; ~ = 1,18; h / l = 0,5; ; = 0.064)

18.6.3 General physical conclusions

Fig. 4 to *8* show the natural vibrational shapes of the shear rigid beam, its eigenvalues and the curves of the correction coefficient K_{SD} for different boundary conditions. The parameters were n = 0; 0,01; 0,05; 0.1 and as abscissa the shear influence δ.

How the various influences affect the order of magnitude is illustrated in an approximation by Timoshenko in the case of the double-sided hinge supported beam, which can be traced back to a correction coefficient curve

$$K_{SD}(n) = 1 - n^2 \frac{\pi}{2} (\delta + \vartheta)$$

(n ordering number of vibration). Above equation depicts, that the influence essentially increases with the square of the order of the vibration. It also shows how quickly the natural frequencies determined according to classical beam theory become inaccurate with increasing influencing parameters δ and ϑ.

The validity of the differential equation of the Timoshenko beam - and thus also that of K_{SD} - depends, analogous to classical beam theory, on the ratio of the vibration nodes distance to the cross-section height, but also on the type of boundary conditions. It becomes - as seen in the approximation - smaller with increasing order of the vibrational form. However, an exact upper limit cannot be given, since a comparative calculation must be carried out, e.B. for deep beams with the plate theory, i.e. a continuum must be calculated. For the tones ω_{l1}, ω_{l2}, The improved beam theory of Timoshenko also provides acceptable results for the ratio vibration node distance / beam height = 1, whereby the quality of the values of the hinge-supported (articulated) beam is even very good.

The effect of the influences on the support (boundary) conditions can be summarized as follows: The natural frequency decreases more and more via cantilever, hinge-supported beam, free-free beam, single-sided-one-sided-hinged beam up to the beam clamped on both sides. This indicates a connection with the increase in beam curvature, as can be seen from the images of the natural oscillation shape. It is also noteworthy that the natural frequency of the free-free beam, which in the shear-rigid case is equal to that of the clamped beam, falls with larger ϑ and δ values to considerably lower values than with the associated clamped beam.

From the curves and other considerations it can be deduced:

* In the case of isotropic, shear rigid beams, the classical beam theory becomes unusable when the ratio beam height to vibration node distance comes to the range of 0.30, This statement also indicates how early the classical beam theory will fail with harmonics (upper modes) with its ever smaller vibration node spacing even with slender beams.

*With less shear-rigid layered beams, the classical beam theory loses its validity even earlier. One can see from the curves that with short beams (ϑ large) even with high shear stiffness (δ small) a large frequency drop occurs.

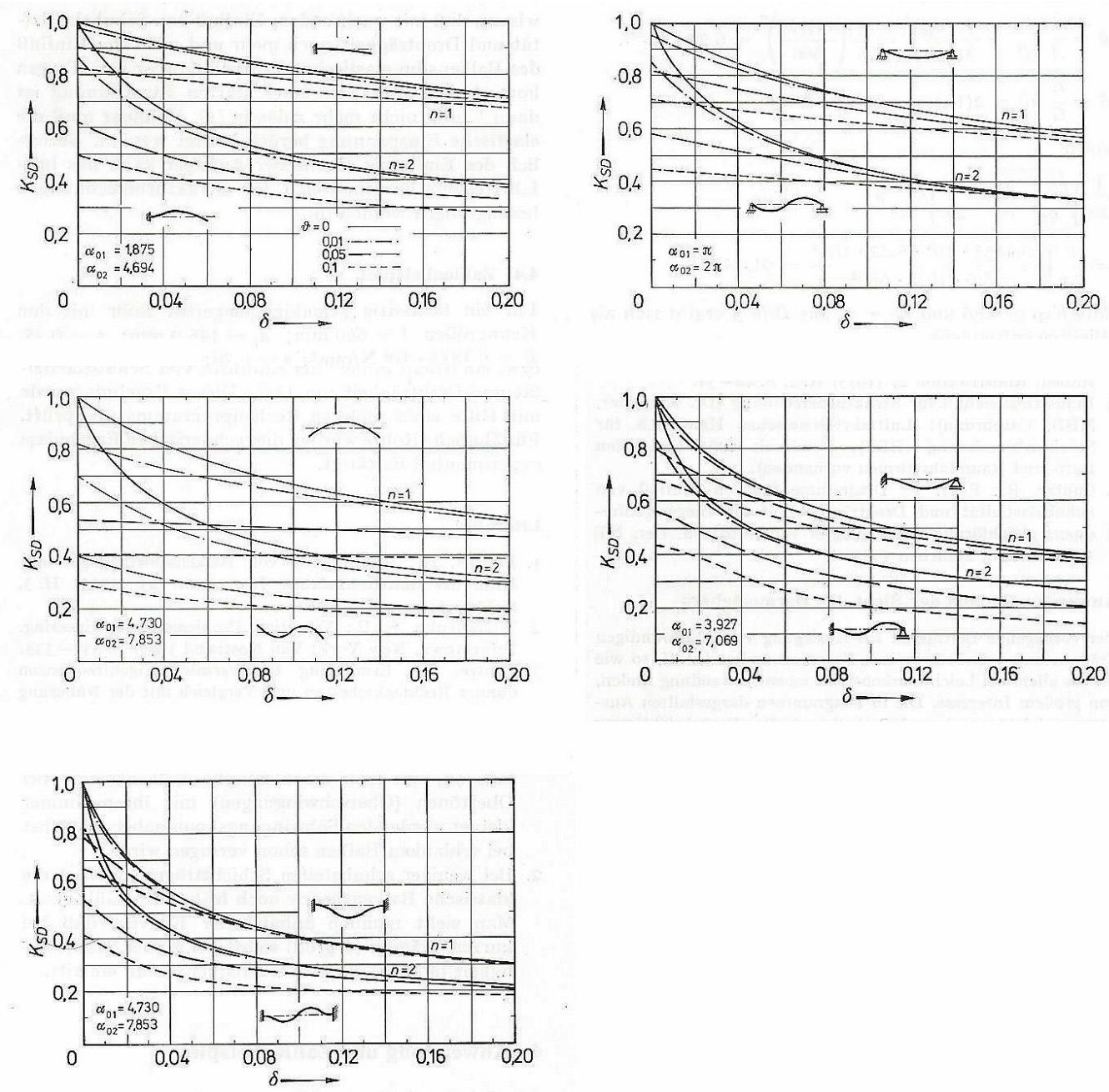


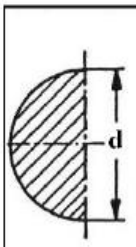
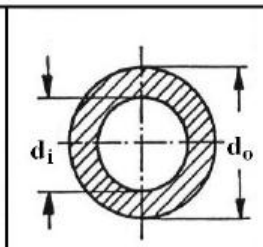
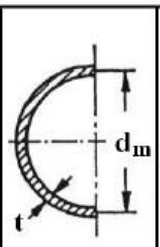
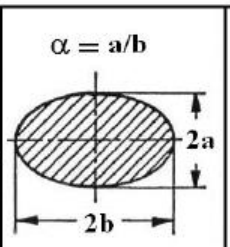
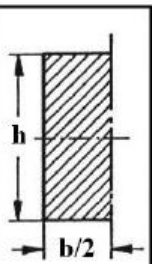
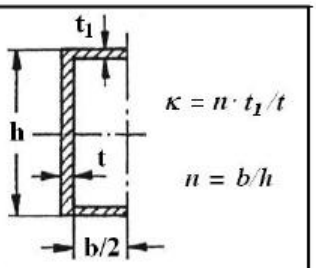
Fig.4: Cantilever beam; *Fig.5: Double hinge supported beam; Fig.6: Free-free beam; Fig.7: Beam, one side hinged, one side clamped; Fig.8: Beam, clamped at both ends*

18.6.4 Application and isotropic numerical example

Shear correction factors and cross-section quantities

A quick calculation of κ is made possible by applying *Table 1*, which indicates the value of some cross-sections. When using them, however, it should be borne in mind that κ depends on ν and here only applies exactly to the frequently used transverse contraction number $\nu = 0.30$. However, the values determined according to *Table 1* can be used as an approximation.

Table 1: Shear correction factors κ of some isotropic beam cross sections for ν = 0.30 [4]

					
1.13	$\frac{1}{39}\left(44+\frac{118\ d_i^2/d_o^2}{(1+d_i^2/d_o^2)^2}\right)$	1.89 *for* $t/d_m \le 0.1$	$\frac{511\alpha^4+190\alpha^2+3}{156\cdot(3\alpha^4+\alpha^2)}$	1.18	$\frac{15.3+91.8\kappa+190.5\kappa^2}{13\cdot(1+3\kappa)^2}+\frac{108\kappa^3+n^2(33\kappa+30n^2)}{13\cdot(1+3\kappa)^2}$ *for a thin quadrant of constant thickness* $= 2.30$

This no longer applies to beams that are made up of different layers, such as the sandwich plate or a wound layered tube. In this case, the effective values of the parameters of the total cross-section from the individual cross-sectional parts must be determined and inserted into the calculation:

$$(E \cdot I)_{\text{eff}},\ (G \cdot A_S)_{\text{eff}},\ (\rho \cdot A)_{\text{eff}},\ (\rho \cdot I)_{\text{eff}} / (\rho \cdot A)_{\text{eff}} \quad .$$

Note on boundary conditions:

Both, in the interpretation of measured natural frequencies and in the more precise computational calculation, it is important for the user to know that with the increasing influence of shear flexibility and rotatory inertia, the influence of the elastic clamping also comes into play more and more. The assumption of a rigid clamping is then often no longer permissible, rather the elastic spring clamping must be taken into account. With regard to the influence of elastic supports, the aeronautical manual HSB can be used for structural calculations [6].

Numerical example

Task: Natural bending frequency of a tube hinge-supported at both ends

Given: 1 = 660 mm; d, = 147 mm; ν = 0,35; E = 185500 N/mm^2, v = 0,30; G=713500 N/ /mm^2

= 8,0' 10-9 Ns2jmm4 und" κ= 1,89 from Table

Parameter values:

$$A = \pi \cdot d_m \cdot t;\ \text{I} = \pi \cdot d_m{}^3 \cdot t / 8 \ \rightarrow\ I / A,\quad G = E / (2+2\nu) = 71350\ \text{N/mm}^2$$

$$\vartheta = \frac{I}{A} \cdot \frac{1}{l^2} = \frac{1}{8}\left(\frac{d_m}{l}\right)^2 = \frac{1}{8}\left(\frac{147{,}25}{660}\right)^2 = 6{,}22 \cdot 10^{-3},$$

$$\delta = \frac{E}{G}\,\varkappa\vartheta = 2(1+\nu)\,\varkappa\vartheta = 3{,}06 \cdot 10^{-2}$$

$$\frac{1}{2\pi}\sqrt{\frac{EI}{\varrho A} \cdot \frac{1}{l^4}} = \frac{1}{2\pi}\sqrt{\frac{E}{\varrho l^2}\,\vartheta} = \frac{1}{2\pi}\sqrt{\frac{0{,}1855 \cdot 10^6 \cdot 6{,}22 \cdot 10^{-3}}{8{,}0 \cdot 10^{-9} \cdot 660^2}} = 91{,}58\ \text{s}^{-1}.$$

With $K_{SD} = 0{,}86$ and $\alpha_{01}^2 = \pi^2$ from *Fig.5* a bending natural frequency $f_{SD} = 0{,}86 \cdot \pi^2 \bullet 91{,}58 / s$ = 777 Hz is calculated. This is a decrease of 14 Hz as the result of the influences of shear effect and rotational inertia. This result was verified with the help of another calculation program. For similar tubes, the computational results were confirmed experimentally.

Literature:

1. Buckens F: *The importance of shear deformation in the calculation of critical speeds of rotating shafts*. In: P. Y. Willems (ed.): Gyrodynamics. Berlin, Heidelberg, New York: Springer 1974, S. 71-78
2. Cowper G R: *The Shear Coefficent in Timoshenko's Beam Theory*. J. Appl. Mech. 33 (1966) H. 2, S. 335-340
3. Cuntze R: Ermittlung transversaler Eigenfrequenzen dünner Rechteckscheiben und Vergleich mit der Näherung von Timoshenko. Acta Mechanica 7 (1969) H.4, S.233-247
4. Cuntze R : *Der Einfluß der Schubelastizität und Drehträgheit auf die kritischen Drehfrequenzen gleichförmig massebelegter, einfeldriger Wellen*. Ingenieur-Archiv 54 (1984), 368-377
5. Cuntze R und Eder J: *Einfluß von Schubelastizität und Drehträgheit auf die Biegeeigenfrequenz gleichförmig massebelegter Einfeldbalken*. Konstruktion 35 (1983) , H.5, 183-186
6. Dimentberg F M: *Flexural vibrations of rotating shafts*. London: Butterworths. 1961
7. Fuhrke H: Bestimmung von Balkenschwingungen mit Hilfe des Matrizenkalküls. Ing. Arch. 23 (1955) H.3, S.329-348
8. HSB , Luftfahrttechnisches Handbuch für Strukturberechnung
9. Pederson P T: *On forward and backward precession of rotors*. Ing. Arch. 42 (1972), 26-41
10. Pederson P T: *On seIfexcited whirl of rotors*. Ing.-Arch. 4 (1973), 267 -284
11. Timoshenko S P: *Vibration Problems in Engineering. Princetown*, New York: Van Nostrand 1947, S.337-338

LL:

As in other disciplines like buckling or like strength, also in vibration it is similarly experienced:

Two narrow-located neighboring modes (natural frequency, eigenfrequency) interact which leads to a lower combined frequency!

18.7 Analysis of the Natural Frequencies of Laminated Beams of low 'Shear-rigidity'

1 Task Estimation of Lowest Natural Frequency for Beam examples cantilever, hollow shaft

Laminate lay-up and material:

a) Lay-up of 8 prepreg layers $[90/0_2/90]_S$, $[45/0_2/-45]_S$
Tension test specimen with b = 16 mm, t_k = 0.125 mm.

b) Laminate stack $[90/0_2/90]_S$.

CFRP: Fiber T300-3000 x 40 B, Matrix LY556/HT976

$E_{\|\|}^z$	160000 N/mm^2
$E_{\perp}^z$	9300 N/mm^2
$G_{\|\|\perp}$	5400 N/mm^2
$\nu_{\perp\|\|}$	0.32
$\nu_{\perp\perp}$	0.40

ρ	$\approx$ 1.6 g/cm^3
$\varphi \equiv V_f$	0.62 b)
φ	0.60 a)

2 Solution

Analogous to before the general relationship, taking into account shear stiffness and rotational inertia influence, is

$$f_{SD} = K_{SD} \cdot f_0 = K_{SD} \cdot \alpha_0^2 \, [(E \cdot I / \rho \cdot A) / l^4]^{0.5} / 2\pi$$

with the reference frequency f_0 as the bending natural frequency of the shear rigid, torsional inertia-free beam according to the classical beam theory and EI := bending stiffness, A := cross-sectional area of the cantilever beam or the tube, as well as α_0 := bending eigenvalue, K_{SD} := correction coefficient, both to be read from the HSB diagrams in chapter 19.6. For reading, the influencing factors

Shear $\delta = [(EI)/(GA_S)]/ l^2 = [(E \cdot I)/(G \cdot A/\kappa)] / l^2$

Rotatory inertia $\theta = [(\rho \cdot I)/(\rho \cdot A)]/ l^2$,

Gyroscopic effect $\bar{\theta} = \theta \, (1 - 2\,\Omega/\omega)$,

are required, whereby $\omega = 2\pi \cdot f_{SD}$ and κ the shear correction factor.

In the non-isotropic or in the inhomogeneous case, effective values are to be used in the aforementioned formulas. These depend on the lay-up and the stack, as well as on stiffness and density distribution.

2.1 Cantilever, determination of influence quantities

- Bending stiffness:
  For the vibrating cantilever the static cross-section relations of the wall read

$$\begin{Bmatrix} n \\ m^0 \end{Bmatrix} = \begin{Bmatrix} 0 \\ m^0 \end{Bmatrix} = \begin{bmatrix} A & B \\ B & D \end{bmatrix} \begin{Bmatrix} \varepsilon^0 \\ \chi \end{Bmatrix}$$

  where under uniaxial bending {n} = 0, a symmetric stack (B_{ik} = 0) remains

$$m_x^0 = (D_{11} - D_{12}^2/D_{22}) \cdot \chi_x \qquad \text{(beam: } \chi_y \neq 0,\ \chi_{xy} = 0)$$

$$m_x^0 = D_{11} \cdot \chi_x \qquad \text{(strip: } \chi_y \equiv 0,\ \chi_{yx} = 0)$$

  (analogous is fact in the case of uniaxial straining: $\{ m^0 \} = 0$, $\gamma_{xy} = 0$ and beam $\varepsilon_y \neq 0$; strip $\varepsilon_y \equiv 0$).

  The calculation and also the measurement are carried out for a "cantilever strip". Thus, it must be determined

$$(EI)_{eff} = b \cdot D_{11} = b \sum_{k=1}^{n} Q'_{11,k} (z_k^3 - z_{k-1}^3)/3 .$$

- The shear correction factor $\kappa > 1$ depends on the interlaminar shear stress distribution (parabola in the isotropic rectangular cross-section under shear Q_x, whereby the interlaminar shear stress distribution is not constant for wide cross-sections, (see also Rohwer, HSB). An approximation for κ - otherwise a complex calculation according to a distinct HSB sheet has to be carried out - which corrects integrally over the cross-section, so that with the geometry data and the average shear stresses τ_{xz} the mean shear strains γ_{xz} over the cross-section height can be calculated. For isotropic beams the value $\kappa = 1.2$. For a strip is valid

  $(GA)_{eff} = (G_{xz} \cdot A)_{eff} = b\,(A_{55} - A_{45}^2/A_{44})$, with $A_{ij} = \sum_{k=1}^{n} C'_{ij,k}\, t_k$ (i,j = 4,5)

  $C'_{44} = c^2 \cdot G_{\perp\perp} + s^2 \cdot G_{\perp\parallel}$, $C'_{45} = s \cdot c \cdot (G_{\perp\perp} - G_{\perp\parallel})$, $C'_{55} = s^2 \cdot G_{\perp\perp} + c^2 \cdot G_{\perp\parallel}$. s = sinα, c = CoSα.

- Effective inertias:
  In the present case, the same material is used in all layers, so that using the equation in (2) follows

  $(\rho I)_{eff} \rightarrow \rho I$, $(\rho A)_{eff} = b \cdot \Sigma\,(\rho_k \cdot \tau_k) \rightarrow \rho A$, $(\rho I)_{eff}/(\rho A)_{eff} = \rho I/\rho A = t^2/12$, $\theta = t^2/(12 \cdot l^2)$.

2.2 Hollow shaft, determination of influence quantities

For the vibrating hollow shaft, the same total cross-section conditions apply as before, whereby the effective stiffness must be determined via the laminate wall quantities

- Effective bending stiffness for the thin-walled tube experiencing cross-section bending:

  $(EI)_{eff} = E_x I \approx (A_{11}/t) \cdot t\, \pi d_m^3 = A_{11}\, \pi d_m^3$

- Effective shear stiffness, shear correction factor is $\kappa \approx 1{,}9$

  $(GA)_{eff} = G_{x\varphi} \cdot A \approx (A_{66}/t) \cdot t\, \pi d_m = A_{66}\, \pi d_m$

- Effective inertia quantities:

  $(\rho I)_{eff} = \rho I \approx \rho A\, d_m^2/8 = \rho t\, \pi d_m^3/8$, $(\rho A)_{eff} = \rho A \approx \rho t\, \pi d_m$, $\theta = (\rho I)/(\rho A l^2) \approx d_m^2/8l^2$

3 Results with discussion

3.1 *Cantilever*

	$[90/0_2/90]_S$	$[45/0_2/45]_S$	
A_{11} in N/mm	85160	105200	$A_{16} = 0$
A_{12} in N/mm	2994	20830	$A_{26} = 0$
A_{22} in N/mm	85160	24420	
D_{11} in N/mm/mm	5912	7997	
D_{12} in N/mm/mm	250	2015	
D_{22} in N/mm/mm	8281	2765	
$(EI)_{eff}$ in N/mm^2	95000	126000	
$(G_{xz} \cdot A)_{eff}$ in N	70000	78000	
$(\rho A)_{eff}$ in Ns^2/mm^2	$2.46 \cdot 10^{-8}$	$2.46 \cdot 10^{-8}$	
δ	$1.1 \cdot 10^{-4}$	$1.3 \cdot 10^{-4}$	
$\theta = t^2/12 \cdot l^2$	$6 \cdot 10^{-6}$	$6 \cdot 10^{-6}$	

f_0 in Hz (α_0 = 1.875)	409	471	sei
K_{SD} see §19.6	≈ 1.0	≈1.0	
ω_{SD} in s^{-1}	408 ± 2.5 % 1)	470 ± 2.5 %	Theory
f_{SD} in Hz	654	75	
ω_{SD} in s^{-1}	385 ± 3.4 %	387 ± 7.2 %	Test

- Discussion:
  The test result is considerably - as usually - lower than the calculation result, which is partly due to the fact that the test specimens were already somewhat aged, which had an influence on the outer 90° layers and thus on D_{11}. Another more protermced fact is that the clamping constraint in reality is not fully stiff.

3.2 Hollow shaft quantities

-

		$[90/0_2/90]_S$		
	A_{11} in N/mm	85160		
	A_{66} in N/mm	5400		
	$(E_x \cdot I)_{eff}$ in N/mm^2	$9.03 \cdot 10^{11}$		
	$(G_{x\varphi} \cdot A)_{eff}$ in N	$2.54 \cdot 10^6$		
	$(\rho \cdot A)_{eff}$ in Ns^2/mm	$7.54 \cdot 10^{-9}$		
	$\delta = A_{11} (d_m/l)^2 / 8$	0.43		
	$\theta = d_m/l)^2/8$	$6.5 \cdot 10^{-3}$		
	f_0 in Hz ($\alpha_0 = \pi$)	3945		
	K_{SD} from 1)	0.31		
$\frac{\Omega}{\omega} = 0$	ω_{SD} in $s^{-1} = 2\pi f_{SD}$	7792	1240	f_{SD} in Hz (bending frequency)
	with gyro influence: K_{SD} 2)	≈ 0.4		f_{SD} in Hz (synchronization critical rotational frequency)
Bild 4.2	ω_{SD} in s^{-1} (eigenfrequency)	9900	1600	

1) K_{SD} = 1 - π/2 (δ + Θ) · n^2 für Ω/ω = 0 = 1 - π/2 (0.43 + 0.0065)·1^2 = 0.31 (*Ing. Archiv 54 (1984), S. 373*)[1]

2) K_{SD} from curve extrapolated for Ω/ω = 1.

18.8 Influence of low Cross-sectional Shear Rigidity and Rotatory Inertia on the Critical Speeds of Shafts with Uniformly Distributed Mass *(1984)*

1 Introduction

The influence of low shear rigidity and rotational inertia of the cross-section is usually only to be taken into account in the case of shafts at higher vibration modes. However, if the shafts are made of fiber composite material (*G/E and A/I become small*) or, for example, if the shafts are built of thin steel tubes the influences are often important even with the low vibration modes. Timoshenko's theory must then be used in order to be able to calculate the critical speeds accordingly.

A detailed derivation of the influence of shear elasticity and rotational inertia on the bending natural frequencies of the beam with a hinge at the ends can be found in [1], where a frequency ratio over the degree of the slenderness grade of the beam is depicted. Based on this, bending natural frequencies for the remaining bearing cases are calculated in [2].

The beam rotating around a transverse axis has been investigated in [3] taking into account rotational inertia and shear elasticity. Timoshenko's theory has also been used for the rotating shaft in various publications [4-6], although a comparison with results from classical theory is missing. Only in [7] such a comparison appears to some extent. For the main support (*boundary*) cases, a compiling calculation with comparison of the bending-critical speeds of the classic model and the Timoshenko model is therefore missing.

As a result of the investigations, the physical background is presented in a concise form and the influences are further plotted in the form of diagrams. This enables the user to carry out a rapid estimation of the natural frequency f_{SD} of the shaft via the bending natural frequency f_0 of the shear-rigid and rotation-free beam of the classical beam theory as a reference frequency. As a critical rotational frequency of the shaft under shear and rotational inertia influence can then be determined very easily after insertion of the corresponding bending eigenvalues α_o

$$f_{SD} = K_{SD} \cdot f_0 = K_{SD} \cdot \alpha_0^2 \, [(E \cdot I / \rho \cdot A) / l^4]^{0.5} / 2\pi \, .$$

The parameters for the shaft are: E = modulus of elasticity, I = moment of inertia, A = cross-sectional area, l = length of the shaft, ρ = density.

The curve for the correction coefficient K_{SD} will directly represent the percentage influencing factor. The dependence of the correction coefficient on the excitation frequency f is taken into account by the fact that it is specified for the absolutely necessary frequency ratios $f / f_{SD} = \Omega/\omega = 1/2$ indirectly and +1 of the (*Gleichlaufkritische*) synchronization angular frequency where excitation angular frequency Ω and natural angular frequency ω are the same. The specification of the calculation results for the synchronous frequency ratio Ω/ω = -1 was omitted due to the low practical importance for the design of a shaft.

2 Theoretical relations

The equilibrium conditions already known from [8] on the oscillating, rotating shaft element are for the plane x-z

$$-\frac{\partial M_y}{\partial x} + Q_z = \varrho I \frac{\partial^2 \theta_y}{\partial t^2} + 2\varrho I \Omega \frac{\partial \theta_z}{\partial t}; \qquad \frac{\partial \theta_z}{\partial x} = \varrho A \frac{\partial^2 w_z}{\partial t^2}; \qquad M_y = -EI\theta_y'; \quad Q_z = GA_S(w_z' - \theta_y)$$

and for the plane x-y with $\partial(\partial t) = \dot{}$, $\partial(\partial x) = '$

$$-M_z' + Q_y = \varrho I\ddot{\theta}_z - 2\varrho I\Omega\dot{\theta}_y; \qquad Q_y' = \varrho A\ddot{w}_y; \quad M_z = -EI\dot{\theta}_z; \qquad Q_y = GA_S(w_y' - \theta_z);$$

M_z, M_y, Q_z, Q_z bending moments and shear forces in the planes xz and xy

w_z, w_z, w_z, w_z deflections and bending angle referred to the elastic line of these planes

$2\rho \cdot I \cdot \Omega \cdot \dot{\Theta}_z$, $2\rho \cdot I \cdot \Omega \cdot \dot{\Theta}_y$ gyroscopic moments

G shear modulus, A_S effective shear area .

After appropriate summary with elimination of the bending angles θ_y and θ_z of the equations above to a single equation each, the two remaining equations can be represented by a single equation via the approach $w_0 = w_z + i \cdot w_y$ with $i = \sqrt{-1}$. Applying the natural oscillation approach $w_0 = w \cdot e^{i \cdot \varpi \cdot t}$ this oscillation differential equation is finally called

$$w^{IV} + \frac{\alpha_{SD}^4}{l^2}(\delta + \bar{\vartheta})\, w^{II} - \frac{\alpha_{SD}^4}{l^4}(1 - \alpha_{SD}^4 \delta\bar{\vartheta})\, w = 0;$$

$$\delta = \frac{EI}{GA_S}\frac{1}{l^2} = \frac{(EI)}{(GA)}\frac{\varkappa}{l^2}; \quad \vartheta = \frac{(\varrho I)}{(\varrho A)}\frac{1}{l^2};$$

with $x = A/A_S$ as the so-called shear distribution number, and the further abbreviations

$$\bar{\vartheta} = \vartheta \cdot (1\text{-}2\frac{\Omega}{\varpi}), \quad \alpha_{SD}^2 = \varpi_{SD} / \sqrt{\frac{E \cdot I}{\rho \cdot A} \cdot \frac{1}{l^4}}, \quad \varpi_{SD} = 2\pi \cdot f_{SD} \ .$$

As parameters, δ stands for the shear influence, ϑ for the influence of the rotational inertia and Ω/ω for the influence of the gyroscopic effect.

The approach $w = \tilde{C} \cdot exp(\lambda \cdot x / l)$ provides the characteristic equation and provides 4 solutions

$$\lambda^4 + \alpha_{SD}^4(\delta + \bar{\vartheta})\,\lambda^2 - \alpha_{SD}^4(1 - \alpha_{SD}^4\delta\bar{\vartheta}) = 0, \quad \begin{pmatrix}\Lambda_1\\ \Lambda_2\end{pmatrix} = \alpha_{SD}\sqrt{\pm\frac{\alpha_{SD}^2}{2}(\delta + \bar{\vartheta}) + \sqrt{1 + \frac{\alpha_{SD}^4}{4}(\delta - \bar{\vartheta})^2}}\ .$$

In the case of classical beam theory $\Lambda_1 = \Lambda_2 = \alpha_{SD} = \alpha_0$ holds.

As a solution function, after conversion of the e-functions using the Euler formulas, is obtained

$$w_I = \bar{C}_1 \cosh \Lambda_1 \frac{x}{l} + \bar{C}_2 \sinh \Lambda_1 \frac{x}{l} + \bar{C}_3 \cos \Lambda_2 \frac{x}{l} + \bar{C}_4 \sin \Lambda_2 \frac{x}{l}$$

While Λ_2 is always positive, Λ_1 changes the sign if $\alpha_{SD}^4 \cdot \delta \cdot \vartheta > 1$. In this solution area, the solution part with the hyperbolic functions will change to a form with trigonometric functions.

For five support cases, the free constants $\bar{C}_i$ for the beam were determined and compiled in [10]. They also remain valid for the shaft if one replaces ϑ by $\bar{\vartheta}$.

After determining the zeros of the frequency equation as a function of δ, ϑ, Ω/ω and of the frequency parameter α_{SD}, the corresponding correction coefficient can be computed

$$K_{SD} = \frac{\alpha_{SD}^2}{\alpha_0^2} = \frac{\varpi}{\varpi_0} = \frac{f_{SD}}{f_0} \ .$$

3 Range and limit value considerations

Each eigenvalue curve can pass through two solution areas. However, if one sets only one of the two influences δ or ϑ equal to zero in the characteristic equation, one does not get into the second solution range. The same applies if $\bar{\vartheta} = 0$ or $\Omega/\omega = +1 / 2$.

In *Fig.1* natural frequency curves f_{SD} are represented as a function of the rotational frequency Ω of the shaft. Parameter is the ordinal number n of the tone. It can be seen here, analogous to the bending eigenvalues, that two are now obtained for each tone instead of an eigenvalue curve, as in classical beam theory. So it is better to no longer speak of a mode, but of a mode (tone) family that physically has a higher ω_{n2} and a lower frequency ω_{n1} vibration shape.

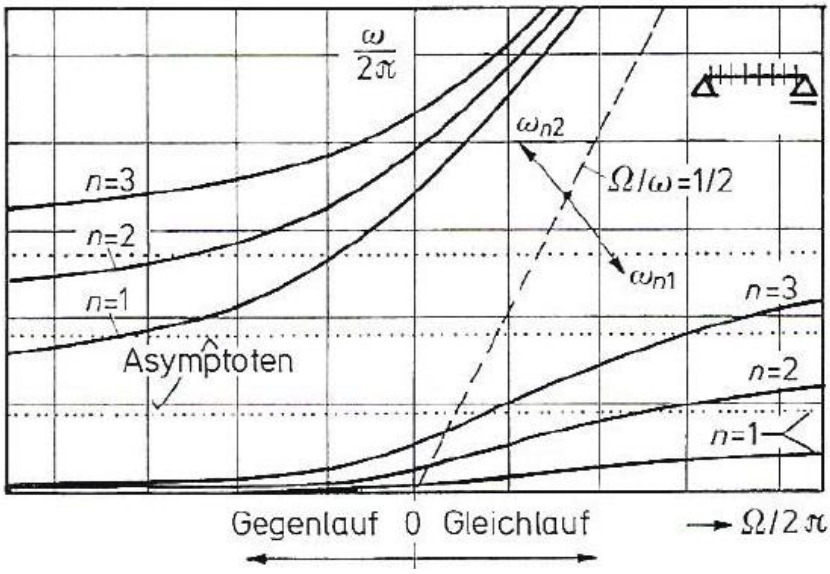


Fig.1. Natural frequency value curves for the double hinge-supported rotating shaft (Special example according to [8])

The right side of *Fig.1* belongs to a synchronous critical frequency (*forward precession, Gleichlaufkritische*) and the left side to the so-called counter-critical rotation ones (*backward precession, Gegenlaufkritische*)

We do not want to consider the higher frequency oscillation form (*upper eigenvalue curve*), as we limit ourselves here to the two lowest and usually technically most important natural frequencies ω_{11} and ω_{21} of the whole spectrum. The eigenvalues ω_{12}, ω_{22}, ω_{32} are already higher than ω_{21}.

4 Results

4.1 General information on the evaluation of results

According to *Fig.1* and *Fig.2* prominent points of each natural frequency curve are synchronous critical rotation frequency $f = f_{SD}$ ($\Omega/\omega = 1$), the bending natural frequency f_{SD} ($\Omega/\omega = 0$), SD(O) and the counter-critical rotation frequency f_{SD} ($\Omega/\omega = -1$.

Rotational frequencies of the shaft of the synchronous critical frequency are dangerous, since then the always existing residual imbalances lead to resonance. Counter-critical rotational frequencies are less important, as they can only lead to resonance in the ideal case of perfect rotor symmetry, which is hardly ever available. The counter-rotation area is therefore no longer listed in *Fig. 2*.

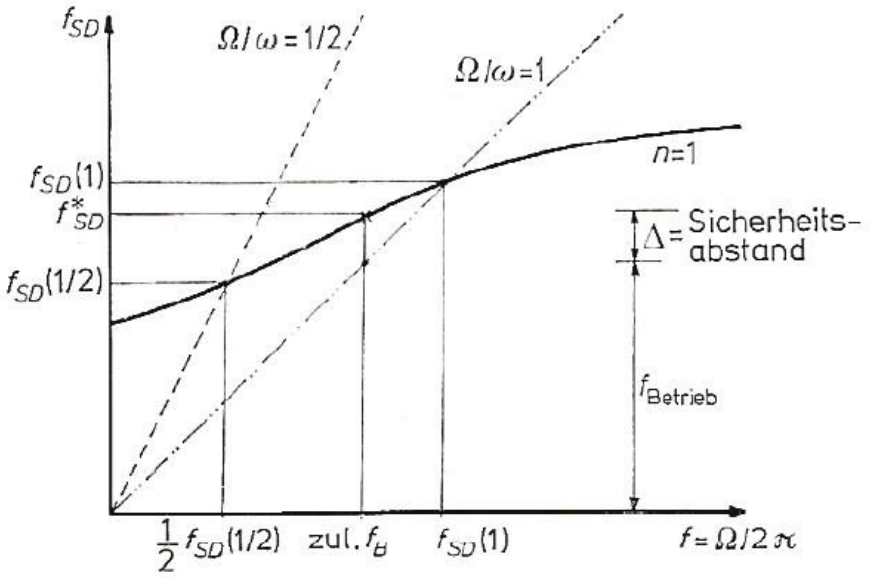


Fig.2. Definition of the different frequency values, Λ is safety distance

Fig.2 also shows that for a certain operating (*Index $_B$ for Betrieb*) frequency f_B an associated natural frequency value belongs, e.g f^*_{SD} in the synchronous range, which is below the synchronous critical rotation frequency. A safety distance of 15 to 25 % is to be strived for against f^*_{SD} and not towards $f_{SD}(1)$, depending on the balancing quality. In the important application that in operation - as shown above - subcritical, namely below the lowest synchronous critical rotation frequency the shaft is run, the associated natural frequency value can be estimated quite accurately by straight interpolation between the support points Ω/ω = 1/2 and Ω/ω = 1. The determination equation for the permissible operating frequency is then at Δ percent safety distance, taking into account permissible $f_B = f^*_{SD} \cdot (100\text{-}\Delta) / 100$,

$$\text{zul } f_B = \frac{100 - \Delta}{100} \frac{(2 - \bar{K})\, f_{SD}\left(\frac{1}{2}\right)}{2\left(1 - \frac{100 - \Delta}{100}\bar{K}\right)} \quad \text{mit} \quad \bar{K} = \frac{f_{SD}(1) - f_{SD}\left(\frac{1}{2}\right)}{f_{SD}(1) - \frac{1}{2} f_{SD}\left(\frac{1}{2}\right)}.$$

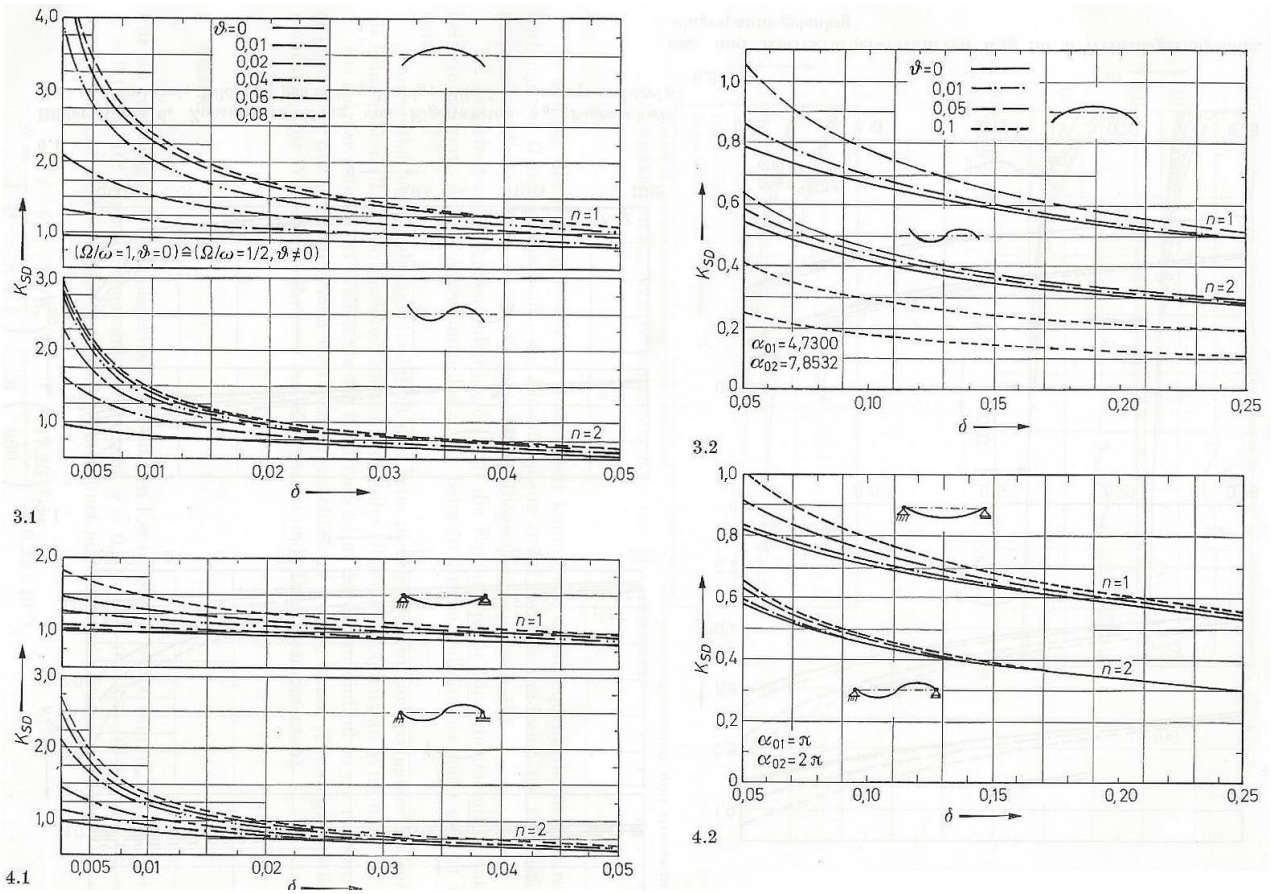
The quantity *K* characterizes the influence of the gyroscopic effect. For $f_{SD}(1) = f_{SD}(1/2)$ the gyroscopic effect is zero.

4.2 Presentation of the correction coefficient curves

In the *Figs. 3* to *7*, the correction coefficient K_{SD} for $\Omega/\omega = 1$ is plotted as a function of the shear influence number δ and the rotational inertia influence value θ as a parameter.

For large values of δ θ = 0; 0.01; 0.05 and 0.1 was chosen, for small values δ the row θ = 0; 0.01; 0.02; 0.04; 0.06; 0.08.

For the five most important boundary cases, the results are displayed graphically. To each case belong two pictures, since the application for small and large shear influence values had to be done separately. It is a compilation of eigenvalues α_0, of vibration modes and of correction coefficient curves K_{SD} for 5 support cases of a single span beam (Ω/ω = 0).



Single span beam: Eigenvalues α_0, natural vibration modes and correction value K_{SD} curves
Fig.3-1: Free-free beam; Fig.3-2: Detail of Fig.3-1
Fig.4-1: Double hinge supported beam; Fig.4-2: Detail of Fig.4-1

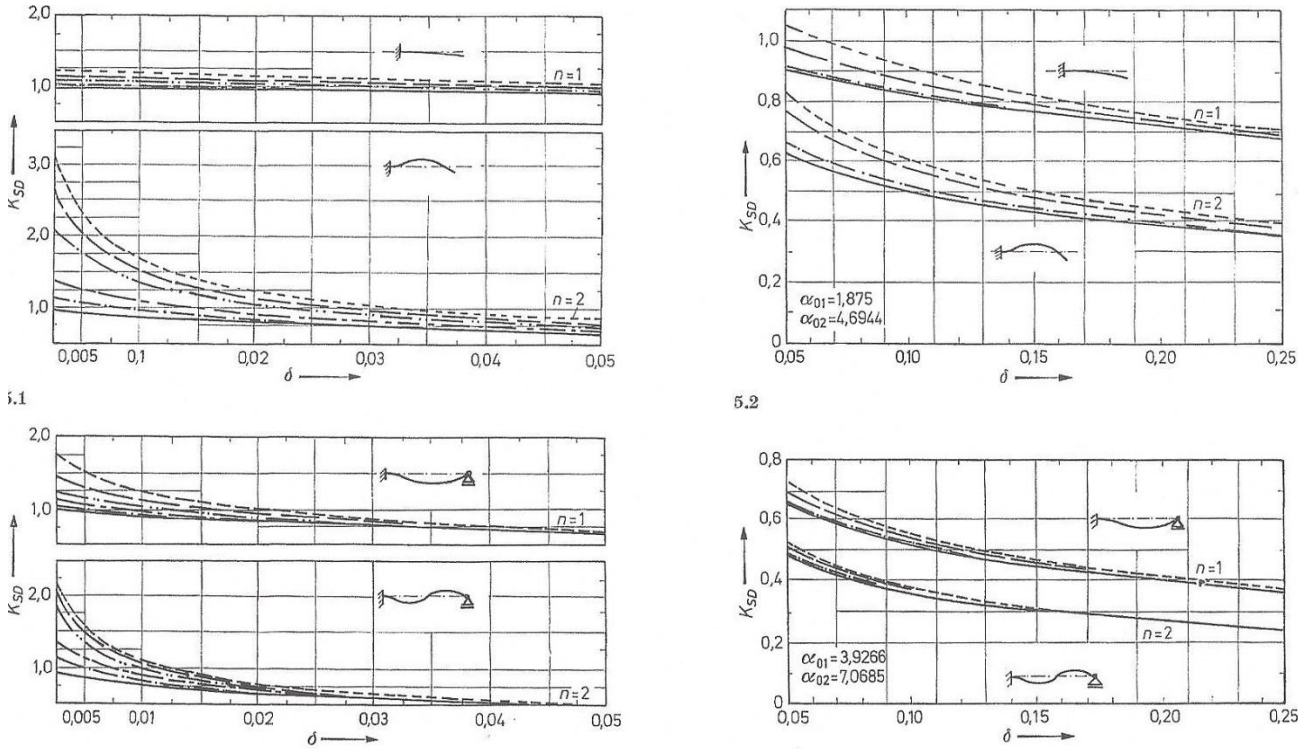


Fig.5-1: Cantilever beam; Fig.5-2: Detail of Fig.5-1
Fig.6-1: Beam, one side hinged, one side clamped; Fig.6-2: Detail of Fig.6-1

Comments on the individual figures in the order of numbering:

*The free-free beam has the lowest degree of fixation and thus represents a limit value with which other boundary cases can be compared. Striking here is a strong increase in K_{SD} against small values of δ; the influence of the gyroscopic effect increases sharply below δ = 0.01. At a large δ, on the other hand, this influence disappears.

*As can be seen in the other figures, an increase in the influence of rotational inertia ϑ causes K_{SD} to grow, i.e. the K_{SD} curve with the largest parameter value ϑ is the top curve of bundle. In *Fig.3.2,* however, the curves for ϑ = 0.1 for the 1st and 2nd tone are well below the rest of the curves. A physical explanation could not be found at that time, not even the confirmation that the cause of the unexpected curve lies in the numeric. So be careful when using these two curves.

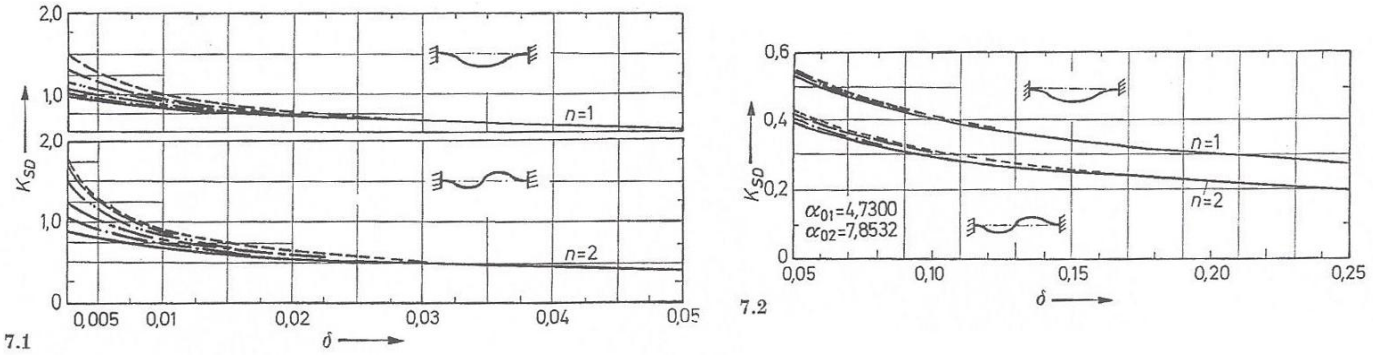
*The next boundary case in the *Figs.4.1* and *4.2* is the double *hinge-supported* and the *one side hinged, one side clamped* shaft. Less than in the previously discussed case, K_{SD} increases at low ϑ values; the less influence of ϑ makes the group of curves to get more densely together.

*Finally, in the case of clamped-free *Fig.5*, the ϑ influence almost disappears at least in the 1st mode (tone), only the second tone still shows the natural frequency-increasing gyroscopic influence in the range of smaller δ.

*There remain 2 boundary cases *Fig.6* with strong constraints (clamped), in which the influence of ϑ largely no longer plays a role.

Findings:

The following statements can be made in summary for all five types of boundaries. With decreasing shear stiffness δ, the K_{SD} value decreases or the synchronous critical rotation frequency decreases. For small shear stiffness values δ, the rotatory inertia influence disappears compared to the shear influence. All ϑ-curves approach ϑ = 0.



Eigenvalues α_0, natural mode shapes and correction value K_{SD} curves
Fig.7-1: Beam, clamped at both ends; Fig.7-2: Detail of Fig.7-1

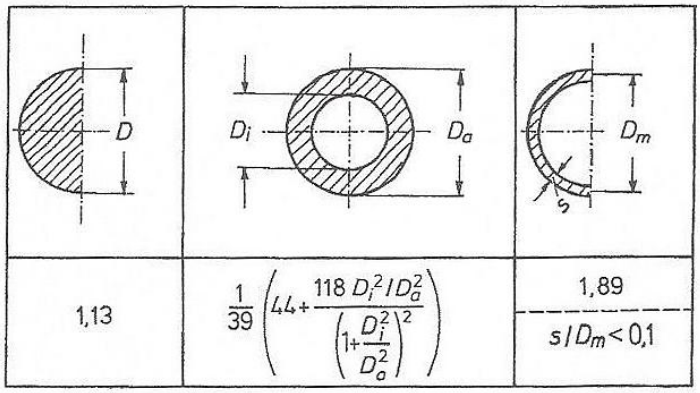
The less the shaft is bound, the more the natural frequency-increasing gyroscopic effect comes into its own, i.e. the natural frequency decreases from the free-free to the firmly clamped shaft relative to the respective bending natural frequency $f_{SD}(0)$. With fixed shear influence variable δ, the natural frequency increases for increasing inertial influence values ϑ. *(The exception case ϑ = 0.1 in the free-free case could not be clarified*).

LL:
The influences of shear and inertia are less important for the lower tone than for the higher

tone. They gain in effect with increasing synchronization frequency. In the case of more strongly bound tube shafts than the free-free ones, the gyro influence can be so small that it can be neglected compared to the other two influences. Of course, this no longer applies to shafts or rotors with final masses and moments of inertia.

5 Example

For a tube shaft - mounted on both sides - with the parameters l = 660 mm ; d_m = 147,25 rnm ; E = 185.5·10^3 N/mm^2; Poisson ratio ν = 0.30; G = 71.3·10^3 N/mm^2; ρ = 8.0 · 10^{-9} Ns^2/mm^4 und κ = 1,89 (see *Table 1*) at first the parameter values are determined:



1,13	$\frac{1}{39}\left(44+\frac{118\,D_i^2/D_a^2}{\left(1+\frac{D_i^2}{D_a^2}\right)^2}\right)$	$\frac{1,89}{s/D_m<0,1}$

Table 1. Schubverteilungszahlen κ (from [11])

$$\frac{1}{2\pi}\sqrt{\frac{EI}{\varrho A}\frac{1}{l^4}}=\frac{1}{2\pi}\sqrt{\frac{E}{\varrho l^2}\vartheta}=\frac{1}{2\pi}\sqrt{\frac{0{,}1855\cdot 10^6\cdot 6{,}22\cdot 10^{-3}}{8{,}0\cdot 10^{-9}\cdot 660^2}}=91{,}58\ \mathrm{s}^{-1}.$$

For the first tone, one obtains as the bending natural frequency according to the classical beam theory $\alpha_{01}=\pi \qquad f_0=f_0(0)=\pi^2\cdot 91{,}58=904\ \mathrm{Hz}.$

A list of the essential natural frequency values for $\Omega/\omega=0$ and 1 in different combinations of influences is given in Table 2.

Tabelle 2. Einige wesentliche Eigenfrequenzwerte des Zahlenbeispiels

Ω/w	δ	ϑ	K	
0	0	0	1	f_0 = 904 Hz
0	0	0,00622	0,97 aus	f_D = 876 Hz
0	0,0306	0,00622	0,86 [3]	f_{SD} = 777 Hz
1	0	0	1	f_0 = 904 Hz
1	0	0,00622	1,03 aus	f_D = 932 Hz
1	0,0306	0,00622	0,96 Bild 3	f_{SD} = 806 Hz

Fig.8 shows the variability of the two lowest natural frequencies as a function of the rotational frequency f in the case of rotatory inertia influence alone(f_D dashed line) and for the case of shear and rotatory inertia influence together (f_{SD} solid line).

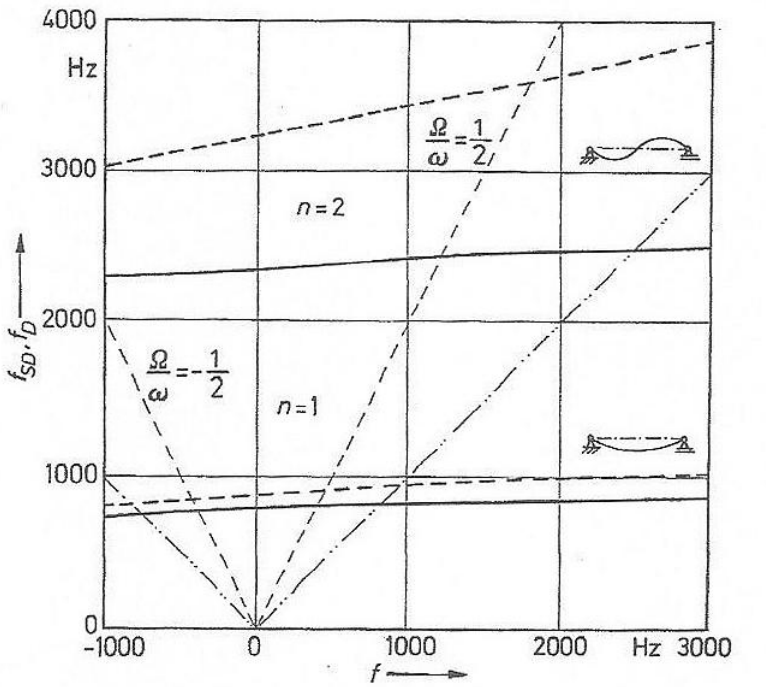


Fig.8: Display of natural frequency curves for the parameters ϑ =0.00622, δ =0.0306. (solid) f_{SD} shear rigidity and rotatory inertia, (- - - dashed) f_D Rotatory inertia, f_0 (.....) without

Finally, ***Fig.9*** uses the chosen example to illustrate the numerical significance of shear, rotational and gyroscopic influence.

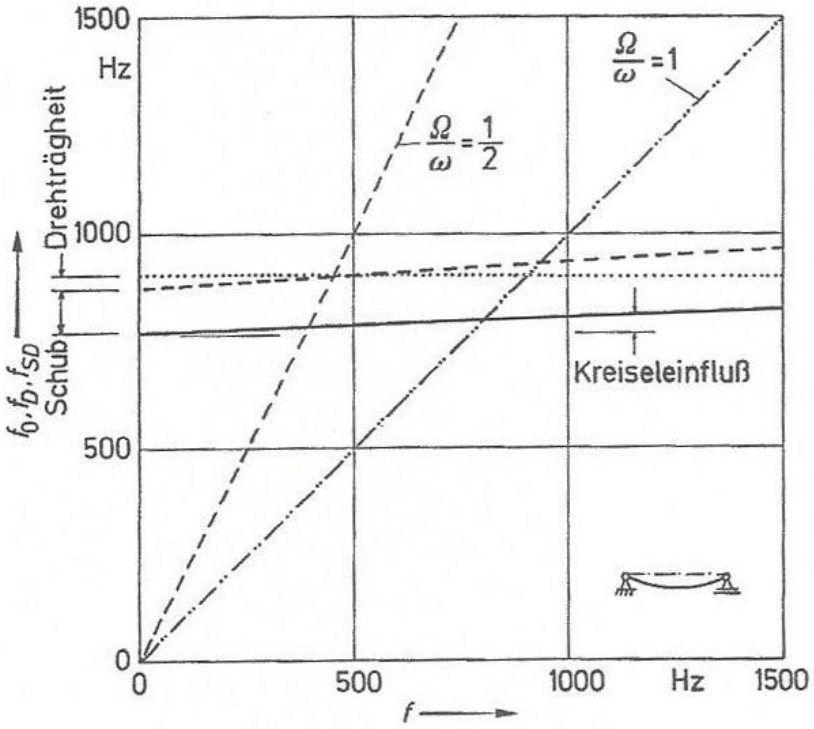


Fig.9: Splitting of the lowest natural frequency value curve of the number example into the individual influences((- - - without shear rigidity and rotatory inertia influences)

18.9 Natural Frequencies of a Cracked Beam for Production Quality-testing of Rotor blades

18.9.1 Introduction

From cracked steam turbine blades, including our small windmill AeroMAN, to material samples on the resonance test bench it is known, that cracks reduce the bending natural frequencies. Of user interest is an estimation of the associate decay. Here, as a relatively simple example and as a substitute for a component, a cantilever beam of constant thickness with a rectangular cross-section with the help of fracture mechanical results shall be considered. The compliance caused by a crack at the clamping cross-section and the resulting natural frequency reduction is simulated by a clamping torsion spring. Fracture mechanics then provides a means for the estimation of the magnitude of the spring's stiffness. The aim of this study further is to show that fracture mechanics - if solutions are available - can not only be applied to strength problems.

The problem of cracked components has often been dealt with in the literature. Especially in the case of rotor shafts, transverse cracks [1-3] and circumferential cracks [4] have been mathematically recorded with regard to their effects on vibration behavior. Initially, the focus was on the problem of incorporating the increased compliance in the crack area into the equations of motion. Numerical values for torsion spring constants c, which were used to model the crack problem, mostly came from experiments [5]. However now, the linear elastic fracture mechanism allows the determination of a relationship for the torsion spring constant c_φ, which captures the compliance of the cracked cross-section [6,7]. This relationship, together with the differential equation of motion of the elastically clamped beam, then provides a relationship between the crack depth at the clamping point and the natural frequency of the beam. Although studies in this direction are already available in [5], the coupling of fracture mechanics and structural dynamics has so far (1985) been missing.

18.9.2 Theoretical Relations

*** Surrogate Model**

As use case for the natural frequency calculation, an elastically clamped cantilever according to *Fig.1* with a height to length ratio of 0.1 is to investigate. Thus, the influence shear compliance can be neglected. In the fracture mechanical substitute model in *Fig.2* it is assumed that the crack occurs symmetrically on both sides and has the same depth there. This assumption enforces a "gaping" crack model with equal natural frequencies for the upward and downward movement. Linear elastic fracture mechanics can be applied.

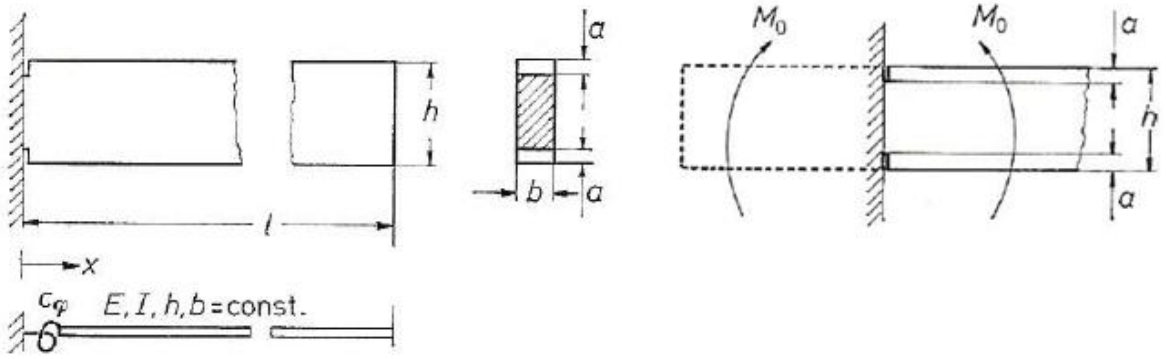


Fig.1: Substitute model of a cracked cantilever

The differential equation of motion for the here used Euler-Bernoulli beam is well known ([8]) and reads after separation of the variables by means of the Bernoulli approach

$$w^{\mathrm{IV}} - \frac{\lambda^4}{l^4} w = 0 \qquad \text{mit} \qquad \frac{\lambda^4}{l^4} = \frac{\omega^2 \varrho A}{EI}$$

and the relations w = deflection of the beam, 1 = length of the beam, λ = eigenvalue, A = Area, ρ = density, Ω = natural angular frequency, I = geometrical moment of inertia, E = Young's modulus.
The solution of this differential equation is (x = length coordinate) is

$$w(x) = C_1 \sin \lambda \frac{x}{l} + C_2 \cos \lambda \frac{x}{l} + C_3 \sinh \lambda \frac{x}{l} + C_4 \cosh \lambda \frac{x}{l}.$$

By insertion of the boundary conditions

$$w(x = 0) = w^{\mathrm{I}}(x = 0) = w^{\mathrm{III}}(x = l) = 0, \quad EIw^{\mathrm{II}}(x = 0) = c_\varphi w^{\mathrm{I}}(x = 0),$$

and with c_φ as torsion spring stiffness the four open constants C_i can be eliminated and the frequency equation

$$\frac{c_\varphi l}{EI\lambda}\left[1 + \frac{1}{\cosh \lambda \cos \lambda}\right] = \operatorname{tg} \lambda - \tanh \lambda,$$

is obtained, which reflects the relationship between the desired natural angular frequency ω and the torsion spring stiffness c_φ. This spring stiffness must be determined now.

*** Determination of the torsion spring stiffness c_φ**

For the crack fracture mechanical problem (*Fig.1*) one finds several relationships in the literature for the so-called stress intensity factor K [9, 6, 7]. Of the various equations, cited for K, the following relationship [9]

$$K = f\left(\frac{a}{h}\right) \frac{6M_0}{bh^2} \sqrt{\pi a}$$

captures the full domain 0 < a < h / 2 employing the parameters shown in *Fig.1* and with f the so-called geometry correction function

$$f\left(\frac{a}{h}\right) = 1{,}130 - 1{,}374\left(\frac{a}{h}\right) + 5{,}749\left(\frac{a}{h}\right)^2 - 4{,}464\left(\frac{a}{h}\right)^3 + 15{,}25\left(\frac{a}{h}\right)^6 - 9{,}315\left(\frac{a}{h}\right)^7$$

From energy consideration follows a relationship, known to everyone in fracture mechanics (see i.e. [6]),

$$\frac{K^2}{E'} = -\frac{\partial \tilde{U}}{b\,\partial a} \qquad \text{mit} \qquad E' = \begin{cases} E(1 - \nu^2) & \text{für ebenen Verzerrungszustand} \\ E & \text{für ebenen Spannungszustand} \end{cases}$$

and $\tilde{U}$ as the energy W- A_a released for the crack progress, i.e. the difference between the elastic energy W present in the cracked cantilever minus the initiated external work A_a. With

$$W = \frac{1}{2} \cdot \frac{\varphi^2}{s_\varphi(a)} \quad , \quad A_a = M_0 \cdot \varphi$$

whereby $s_\varphi = 1 / c_\varphi$ and φ the twisting angle of the rigid beam, follows

$$\frac{\partial \tilde{U}}{\partial a} = \frac{\partial W}{\partial a} - \frac{\partial A_a}{\partial a} = \frac{\partial}{\partial a}\left(\frac{1}{2}\frac{\varphi^2(a)}{s_\varphi(a)}\right) - M_0 \frac{\partial \varphi}{\partial a} = \frac{\varphi}{s_\varphi}\frac{\partial \varphi}{\partial a} - \frac{1}{2}\frac{\varphi^2}{s_\varphi^2}\frac{\partial s_\varphi}{\partial a} - M_0 \frac{\partial \varphi}{\partial a} = -\frac{1}{2} M_0^2 \frac{\partial s_\varphi}{\partial a}.$$

Then the derivation of $\tilde{U}$ becomes

$$-\frac{\partial \tilde{U}}{b\,\partial a} = \frac{1}{2b} M_0^2 \frac{\partial s_\varphi}{\partial a} = \frac{K^2}{E'} \quad \Rightarrow \int_0^a \frac{K^2}{E'}\,\mathrm{d}a = \int_{s_{\varphi_0}}^{s_{\varphi_a}} \frac{M_0^2}{2b}\,\mathrm{d}s_\varphi,$$

which, after integration over the crack depth a, results in the searched compliances *s* with the associated constants

$$s_{\varphi_a} - s_{\varphi_0} = \frac{72\pi}{Ebh^2}\left(\frac{a}{h}\right)^2 \sum_{\nu=0}^{14} \tilde{a}_\nu \left(\frac{a}{h}\right)^\nu$$

$\tilde{a}_0 = 0{,}6385$,	$\tilde{a}_5 = -7{,}3324$,	$\tilde{a}_{10} = 6{,}9304$
$\tilde{a}_1 = -1{,}0351$,	$\tilde{a}_6 = 6{,}7990$,	$\tilde{a}_{11} = 0{,}0000$
$\tilde{a}_2 = 3{,}7202$,	$\tilde{a}_7 = -6{,}9954$,	$\tilde{a}_{12} = 16{,}611$
$\tilde{a}_3 = -1{,}5774$,	$\tilde{a}_8 = 20{,}0942$,	$\tilde{a}_{13} = -18{,}9$
$\tilde{a}_4 = 7{,}5530$,	$\tilde{a}_9 = -22{,}1142$,	$\tilde{a}_{14} = 5{,}4231$

The spring stiffness c_φ can be obtained by inserting $s_{\varphi 0} = \infty$ and $E' = E$ from

$$c_\varphi = \frac{1}{s_\varphi} = \frac{EI}{h}\left(\frac{1}{6\pi}\right)\left[\left(\frac{a}{h}\right)^2 \sum_{\nu=0}^{14} \tilde{a}_\nu \left(\frac{a}{h}\right)^\nu\right]^{-1}.$$

Now, c_φ is inserted into the frequency equation

$$\frac{c_\varphi l}{EI\lambda}\left[1 + \frac{1}{\cosh\lambda\,\cos\lambda}\right] = \mathrm{tg}\,\lambda - \tanh\lambda \quad \Rightarrow \quad \frac{\lambda^4}{l^4} = \frac{\omega^2 \varrho A}{EI}$$

and then the task is numerically solved. The result is plotted in the *Figs.2a* and 2*b*.

18.9.3 Conclusions

At the beginning of cracking for $a / h < 10$ there is just a little influence on the natural frequency; in both examples (h / l = 0.10 and 0.15). This would require very high accuracies in frequency measurement during a product qualification procedure.

The decrease in the natural frequency is strongly dependent on the degree of slenderness: For a height to length ratio of 0.15, the first two natural frequencies decrease faster than at h / l = 0.10.

A comparison of the influence of the crack depth *a* on the different natural frequencies shows that above all the first natural frequency is lowered by a compliance in the clamping. Responsible for this is the bending angle at x = 0, which is always greater for the lowest natural vibration mode shape than for the higher mode shapes.

LL:

* *For measurements to detect, observe and monitor cracks, the 1st natural frequency will therefore preferably be used.*
* *Nevertheless, one has to keep in mind that the assumption 'full clamping' cannot be fully met in reality with the result that the first natural frequency becomes a little smaller.*

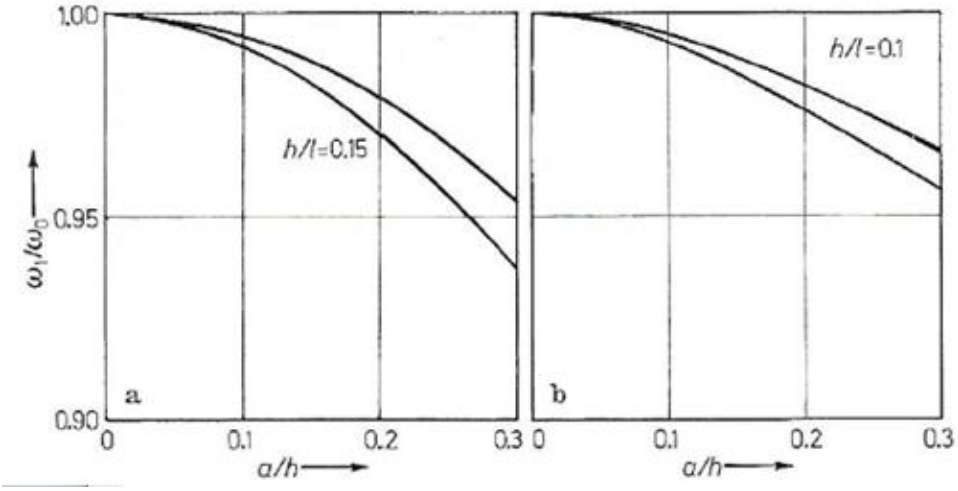


Fig.2a: First natural frequency ratio in dependence of a/h
Fig.2b: Second natural frequency ratio in dependence of a/h

Literatur

Contents from the publication Cuntze R and Hajek M: *Eigenfrequenzen eines angerissenen Kragträgers*. Ingenieurarchiv 55 (1985), 237-241

1. Ziebarth H, Schwerdtfeger H and Mühle E-E: *Auswirkung von Querrissen auf das Schwingungs verhalten von Rotoren*. VDI-Berichte NI'. 320 (1978)
2. Grabowsky B and Pöppel, R.: *Das Schwingungsverhalten eines Rotors mit Querriß*. VDI-Berichte Nr. 456 (1982)
3. Gasch R: *Dynamisches Verhalten des Lavalläufers mit angerissenem Wellenquerschnitt*. VDI-Berichte NI'. 269 (1976)
4. Dimarogonas A and Massourus G: *Torsional vibrations of a shaft with a circumferential crack*. Engng. Fracture Mech. 15 (1981) 439-444
5. Chondros T G and Dimarogonas A: *Identification of cracke in welded joints of complex structures*. J. Sound and Vibration 69 (1980) 531-538
6. Schwalbe K-H: *Bruchmechanik metallischer Werkstoffe*. München, Wien: Carl Hanser 1980
7. Wilson VV K: *Stress intensity factors for deep cracks in bending and compact tension specimen*. Engng. Fracture Mech. 2 (1970) 169-174
8. Laura P A A, Maurizi M J and Pombo J. L.: *A note on the dynamic analysis of an elastically restrained-Iree bar with a mass at the free end.* J. Sound and Vibration 41 (1975) 397 -405

18.10 Equivalent Sinusoidal Acceleration corresponding to an Excitation by Random Vibration

From HSB 76100-01, based on Öry H.: Satellitenstrukturen, Entwurf, Berechnung und Versuch. WGLR / DGRR- Jahrestagung, Karlsruhe, 1967

1 General

Failures may be caused by static fracture and by fatigue.
The latter makes the simulation of the spectrum necessary. This requires for performing analysis and test the determination of an *equivalent* sinusoidal acceleration.

For larger structural components and also structural elements like equipment random loading and sinusoidal impulses have to be considered for the design. Since usually only spectral densities (*depending on the frequencies*) are specified, it is necessary to transform the random impulses to equivalent accelerations. This sheet contains the determination of the sinusoidal acceleration due to random vibrations. W = Power Spectral Density PSD indicated as g2/Hz or m^2/s^3.

Symbol	Unit	Description
a_{eq}	m/s^2	equivalent sinusoidal acceleration static: consideration of brittle fracture fatigue: simulation of spectrum loading
f_i	Hz	natural frequency of the structure
g	m/s^2	gravity acceleration
Q	-	magnification factor, normally $5 \leq Q \leq 20$
T	s	operating time for fatigue loading
$W[f_i]$	g^2/Hz	spectral density
δ	-	damping ratio
Δn_i	-	load cycles to be expected (fatigue)

- $g = 9.81\ m/s^2$
- If the value $Q = \frac{1}{2\delta}$ is not known, then take $Q = 10$.

The signals measured are composed of sinusoids, so that there is a simple connection (t time) between the measured vibrational acceleration $\ddot{y}$, vibrational rate (speed) $\dot{y}$, vibration path *y*, amplitude *yo* and the frequency *f*. $y = y_0 \cdot sin(\omega \cdot t) = y_0 \cdot sin(2 \cdot \pi \cdot t) \rightarrow \ddot{y} = y_0 \cdot (2 \cdot \pi \cdot f)^2 \Rightarrow a_{eq}$.

2 Analysis (input always referenced to g = 9.81 m/s^2)

Static case:
Assuming a normal distribution for the static failure condition and considering further its statistic 3σ-value it follows the equivalent acceleration:

$$a_{eq,\,static} = 36.9 \cdot \sqrt{Q \cdot W[f_i] \cdot f_i}$$

Fatigue case:
Assuming that the positive random response shows a Rayleigh-distribution, it follows:

$$a_{eq,\,fatigue} = 26.7 \cdot \sqrt{Q \cdot W[f_i] \cdot f_i}$$

3 Application

For the usage of the random shaker test the following is to be considered:

(1) $\Delta n_i = f_i \cdot T$. (2) The analytical evaluation can be done using MINER's-Rule.

Öry, H.: Satellitenstrukturen, Entwurf, Berechnung und Versuch. WGLR / DGRR- Jahrestagung, Karlsruhe, 1967

For larger structural components (e.g. complete satellites) and smaller structural equipment random loading and sinusoidal impulses have to be considered for the design. Since only spectral densities (*depending on the frequencies*) are usually specified, it is necessary to transform the random impulses to equivalent accelerations. This sheet contains the determination of the sinusoidal acceleration being equivalent to the envisaged random vibration.

Procedure:

Symbol	Unit	Description
a_{eq}	$\mathrm{m/s^2}$	equivalent sinusoidal acceleration static: consideration of brittle fracture fatigue: simulation of spectrum loading
f_i	Hz	natural frequency of the structure
g	$\mathrm{m/s^2}$	gravity acceleration
Q	-	magnification factor, normally $5 \leq Q \leq 20$
T	s	operating time for fatigue loading
$W[f_i]$	g^2/Hz	spectral density
δ	-	damping ratio
Δn_i	-	load cycles to be expected (fatigue)

$g = 9.81\ \mathrm{m/s^2}$

If the value $Q = \frac{1}{2\delta}$ is not known, then take $Q = 10$.

Prepared:	Checked:	Date:	
Prof. Cuntze	Dr. Broede	18.12.2006	IASB

The equivalent sinusoidal acceleration is to be assessed for the static and fatigue case.

Assuming a normal distribution for the static brittle failure condition and considering further its statistic 3σ-value it follows: $$a_{eq,\,static} = 36.9 \cdot \sqrt{Q \cdot W[f_i] \cdot f_i}$$.

Assuming that the positive random response shows a RAYLEIGH-distribution, it follows:

$$a_{eq,\,fatigue} = 26.7 \cdot \sqrt{Q \cdot W[f_i] \cdot f_i}$$.

For the usage of the random shaker test the following is to be considered:

- $\Delta n_i = f_i \cdot T$
- The analytical evaluation can be done using MINER's-Rule.

19 Some Flywheels and Rotors

Energy can be stored in a flywheel. Since mechanical energy is needed directly in many cases, the need for a loss-rich energy conversion is too eliminate. Properly designed and dimensioned, such a flywheel is very robust.

19.1 Metallic Energy storage Flywheel for the floating crane ship Swartow (1982)

Task: Outline of the basic procedure, only

The energy required to lift and lower the load arm of a floating crane is to be reduced by an energy storage wheel. For this purpose, a steel flywheel was to design and its operability had to be proven statically, cyclically and crack fracture mechanically. Foreseen is a disc-shaped flywheel with an internal bore, mounted on both sides.

When lifting, the energy-supplying wheel is braked When lowering the gripper, the speed of the constantly running energy storage wheel is increased by the present freewheel circuit.

A wheel shape optimum for operational 'strength' had to be determined by the author. Shrink seat is required. A protection of the flywheel is not possible. Therefore highest safety requirement and optimum inspectability NDI is mandatory.

19.1.1 Design input

Data Input: *Fig.1*

Mass < 4850 kg, design space. Mass inertia moment $\Theta = 3250\ kg \cdot m^2$

Storage wheel: Raw material 250 mm thick sheet of ST 52.3 steel material ($R_{p0.2}$ =520 MPa) and not a forged material, shaft 42CrMo4 ($R_{p0.2}$ = 900 MPa) . In the case of press fitting, the shaft must be adapted in order to keep the hard shrinkage as small as possible Heating of the energy storage wheel for shrinkage to 200°C

Fatigue and fracture mechanics design verifications shall show in the relevant load case of hard shrinkage that a service life of 20 years is achieved under the assumptions made

Sea climate, ambient temperature > 5°C (operating instructions)

Unbalance sizes according to VDI 2060 (bending moment of the shaft).

Targeted 'synchronous critical speed' > maxn·1.2= 1680 rpm. Any 'bearing critical speed' should be an order of magnitude lower in order to be able to drive through this frequency quickly

Design criteria

The determining operating speed range in rpm is 900 < n < 1200

Good inspectability, no material delivery problem

Design safety factors: hard shrink fit j = 3, fatigue life j = 2, j_D = 1.2 (endurance limit)

Operation: 60 load cycles per hour, one shutdown/week (*increased by a FoS j= 1.5 for the calculation*), 5000 operational hours per year

Course of operating within 1 load cycle, in rpm: 900→1200→1000→1200

Controlled maximum speed: 1400 rpm

Maximum torque of the shaft (bolt fracture level): 4000Nm

Rotational movement around longitudinal axis (*important for gyroscopic moment*): $\pm 1.85° / 7s$.

Analyses

From the 12 load cases the following design-driving Dimensioning Load Cases were sorted out: (I) n =1200 rpm, smooth shrink fit, (II) n = 0, hard shrink fit, (III) n =1400 rpm, smooth shrink.

Torsion moment $M_t = N/\Omega$: maximum 40000 N·m (*due to bolt fracture*), in service 19000 N·m.

Energy uptake $dE = \frac{\Theta}{2} \cdot (\frac{\pi}{30})^2 \cdot (\max n^2 - \min n^2) = 3.1$ kWh . As service power is available $\Rightarrow N = \frac{dE}{dt} = \Theta \cdot (\frac{\pi}{30})^2 \cdot (n \cdot \frac{dn}{dt})$ (same letter N as fracture cycle number).

and it can be transmitted at n= 1000 rpm a power N = 1980 kW.

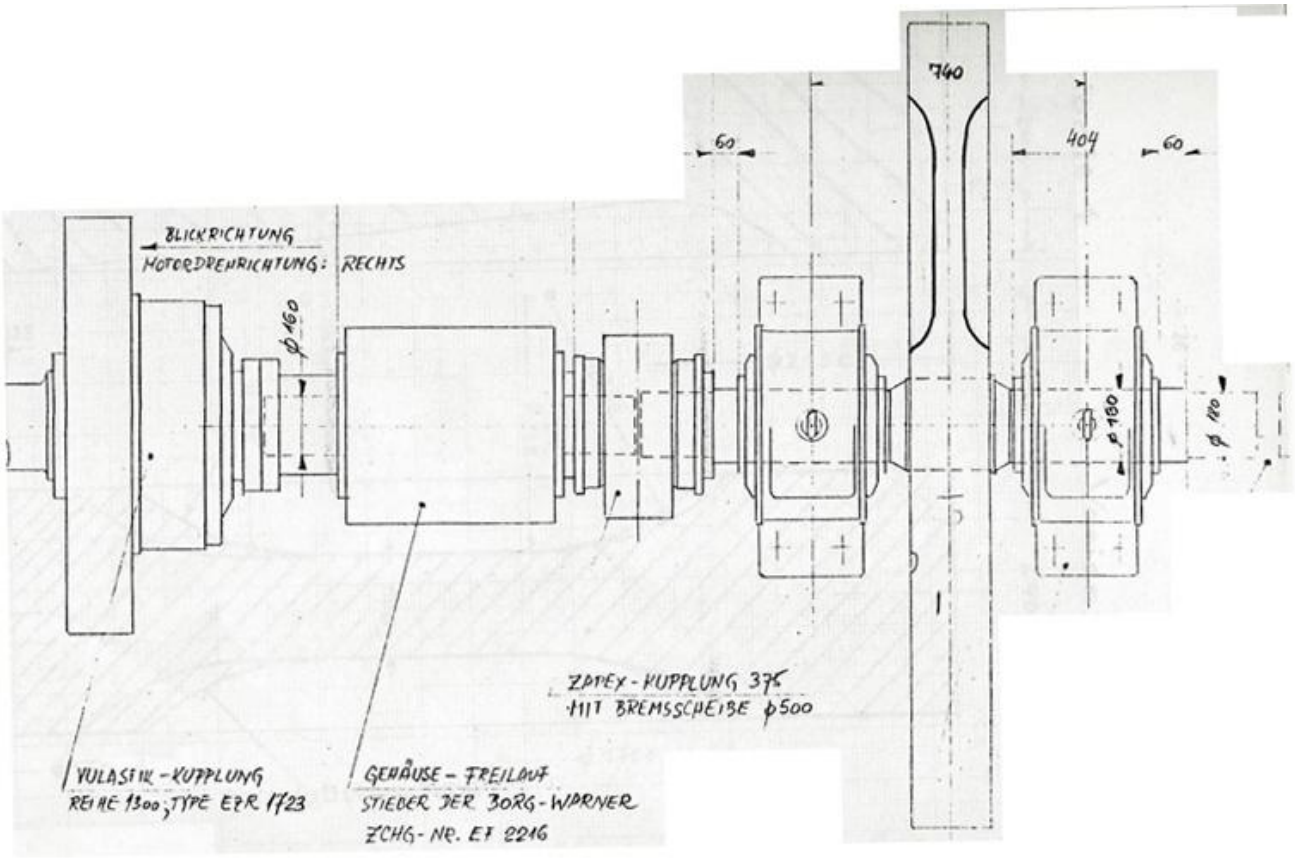


Fig.1: Arrangement of wheel and shaft

Shrink fit: (DIN 7157), Ø 250 mm, H7 / r6: interference values in mm

Maximum interference in service: 0.113 - 0.000 = 0.113, minimum interference 0.084 - 0.046 = 0.038. In order to cover the catastrophic load case, the FoS j = 3 must be achieved.

Life, 20 years: $20 \cdot 5000 \cdot 60 = 6 \cdot 10^6$ load cycles

Stress ratios: $R1 = 900^2/1200^2 = 0.56$ with $6 \cdot 10^6$, $R2 = 1000^2/1200^2 = 0.69$ with $n = 6 \cdot 10^6$ cycles

Maximum acceleration: j = 1.5 from Dutch Standard

In service (without j): $\ddot{x} = 0.292$ m/s², $\ddot{y} = 0.292$ m/s², $\ddot{z} = 0.292$ m/s²

On sea without operation (without j): $\ddot{x} = 0.929$ m/s², $\ddot{y} = 1.480$ m/s², $\ddot{z} = 4.817$ m/s²

Maximum pitch (rotational motion, Stampfen): max $\Omega y = 0.5 \cdot 0.0273$ s$^{-1} \cdot 1.5 = 0.041$ s^{-1}

Maximum yaw (Gieren): max Ωz, negligible.

Choice of material: The stress ratio R allows to take the economic steel St 52.3 (W0, B6).

The crane construction standard DIN 15018 allowed for $2 \cdot 6 \cdot 10^6$ load cycles - for information – an *allowable stress* (not a design allowable) of 220 N/mm^2 for yielding.

Gyroscopic moments and forces:

With rotational movements around the y-axis gyroscopic moments occur that are less important for the wheel (*means only a certain change in the stress distribution above the hub height*) than for the shaft and bearing. Only the gyroscopic moment M_{ky} is important, for which reads for n = 1300 rpm

$$M_{ky} = \Theta \cdot max\Omega \cdot \Omega_{y\,max} = 3275\ \mathrm{kg \cdot m^2} \cdot 135\ \mathrm{s^{-1}} \cdot 0.042\ \mathrm{s^{-1}} = 18100\ \mathrm{N \cdot m},\ (\mathrm{kg = N \cdot s^2/m})\,.$$

Friction coefficient μ:

According to DIN 7190, Table 7, μ = 0.14 applies to a steel-steel cross-press fit in the case of "shrinkage, normal after heating of the outer part up to 300°C in the furnace". If the press surface is degreased, μ still grows.

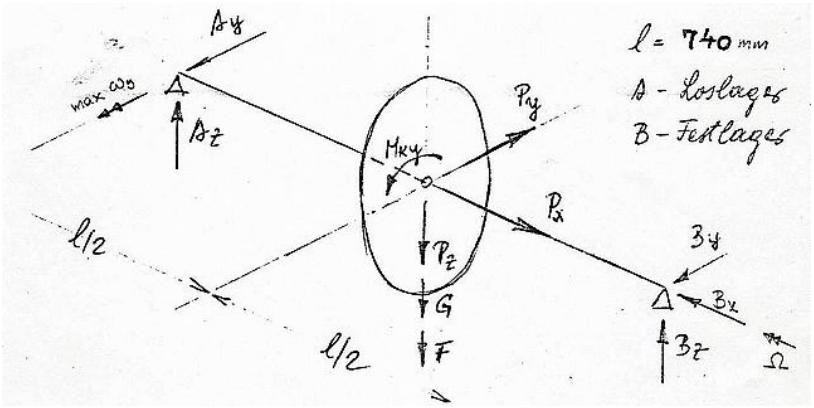


Fig.2: Gyroscopic moment and forces

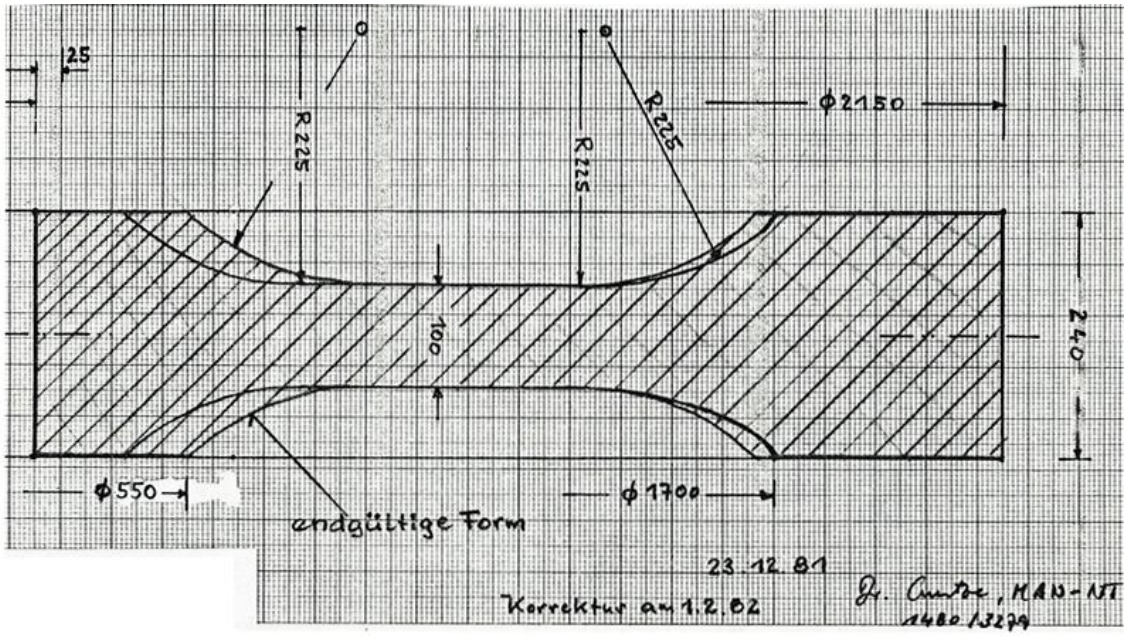


Fig.3: Disc of the full fly wheel (final hub height 240 mm)

19.1.2 Design Dimensioning (Auslegung, Bemessung)

In Design Dimensioning at first data sheets were used and then the analyses were refined by FEA.

- **Disc** with hub

For the proof of fatigue strength according to the crane construction standard DIN 15018, the fatigue strength values for St 52.3 were taken from this using the Smith diagram there in order to capture the mean-stress effect. For this pretty ductile material the Mises yield condition can be applied in order to capture multi-axial stress states. Residual stresses were considered.

Statically:
Pre-stressing should be as high as possible for a safe shrink seat and as low as possible for the service life. In order to avoid wobbling, which leads to transverse impacts and thus to gyroscopic moments, the press fit should be as long as possible.
The iteration led to a change in the design with thickening of the hub from 250 to 240 mm in *Fig.3* and reduction of the headband.

Lifetime (cyclic fatigue**):**

With the shaft, the stress level is lower than with the disk including the hub. In addition, fracture strength and yield strength are higher. Therefore, only the disk is considered.

The performed analyses do not follow the modern safety concept where the old concept of allowable design stresses has been changed to a strength design allowable concept. Therefore it makes no sense to show the old procedure. Just, the old standard had been fulfilled.

Fracture mechanically:
Both, sudden fracture of the disk with a presumed crack and a possible too large crack growth have been parallelly checked during the design optimization process.

Check of the transferable torsional moment:

$$M_t = \tau \cdot A \cdot r = \mu \cdot min\,\sigma_{radial} \cdot 2\pi r \cdot h \cdot r = 0.14 \cdot |-40| \cdot 2\pi \cdot 240 \cdot 125^2 = 132000\ \mathrm{N \cdot m}$$

$$RF = \text{feasible (transferable) } \mathrm{M_t} \text{ / maximum } \mathrm{M}_t = 132000/40000 = 3.3 > \text{required } 3.$$

- **Shaft**

The stresses in the shaft from the bearing loads, drive torque, gyroscopic torques and centrifugal force are not decisive under the pessimistic assumption that the shaft can bend freely. The corresponding analyses are therefore not listed here for reasons of space.

Check of the assumption ”The shrink fit works in the elastic domain”: At the hub edge the Mises equivalent stress from radial and tangential stress delivers the confirming value $\sigma_{eq}^{Mises} = 240\ \mathrm{N/mm^2}$.

19.1.3 Design Verifications (Nachweis) of the chosen disk design

Statically: Fulfilled by the design change above.

Lifetime (cyclic fatigue):

In parallel to above also a linear “Palmgren-Miner micro-damage accumulation” procedure was applied. The result of the load case contributions gave a damage value $D = 0.28$.

This leads in the "normal Miner" case to a Reserve Factor $RF = 1/0.28 = 3.5 >> 1$.

Applying "Relative Miner" a feasibleD has to be determined in order to capture the load history aspects and model uncertainties. From experience, estimating feasibleD as 0.35 follows and this is more realistic RF = feasibleD / 0.28 = 0.35/0.28 = 1.25 > 1.

Fracture-mechanically:

For steels with a yield strength of 1000 N/mm2, the pre-requisites for the application of simpler linear fracture mechanics are only given for thick-walled structural components (*flat deformation state, small plastic zone at the crack tip).* This is true here, since

$$t_{min} \approx 2.5 \cdot (K_{Ic}/R_{p0.2})^2 = 2.5 \cdot (3500/510)^2 = 118 \text{ mm} < 240 \text{ mm}.$$

Crack Growth under service conditions

For safety maintenance reasons one has to know whether a fictitious initial crack might continue to grow. Its size is determined by what else the measuring device can measure. As a crack shape and position one assumes the most unfavorable, which results in the wheel (hub). Quality assurance delivered a minimum measurable equivalent flaw size that forms the maximum area 25 mm^2. The most unfourable shape is an elliptical one with a/2c = 0.1, *Fig.3*.

This delivers, applying $25 = a \cdot c \cdot \pi \rightarrow a \approx 2$ mm.

Employing the crack-growth equation, inserting the stress intensity factor range ΔK and regarding the crack geometry factor leads - simplified for the major load case with $n = 2 \square 2 \cdot 10^6$ - to the estimation a = 38 mm >> possible a. Nevertheless it is recommended to perform after two years a US-inspection.

Sudden fracture under extreme loading

Given: Fracture toughness at 5°C, $K_{Ic} = 3500$ N·mm$^{-3/2}$, $\max\sigma = 180$ N/mm^2, $Q(\max\sigma / R_{p0.2} = 0.7) \approx 1.0$,

Calculation: $a_{cr} = K_{IC}^2 \cdot Q / (1.21 \cdot \pi \cdot \max\sigma^2) = 90$ mm >> possible a .(*Fig.4*)

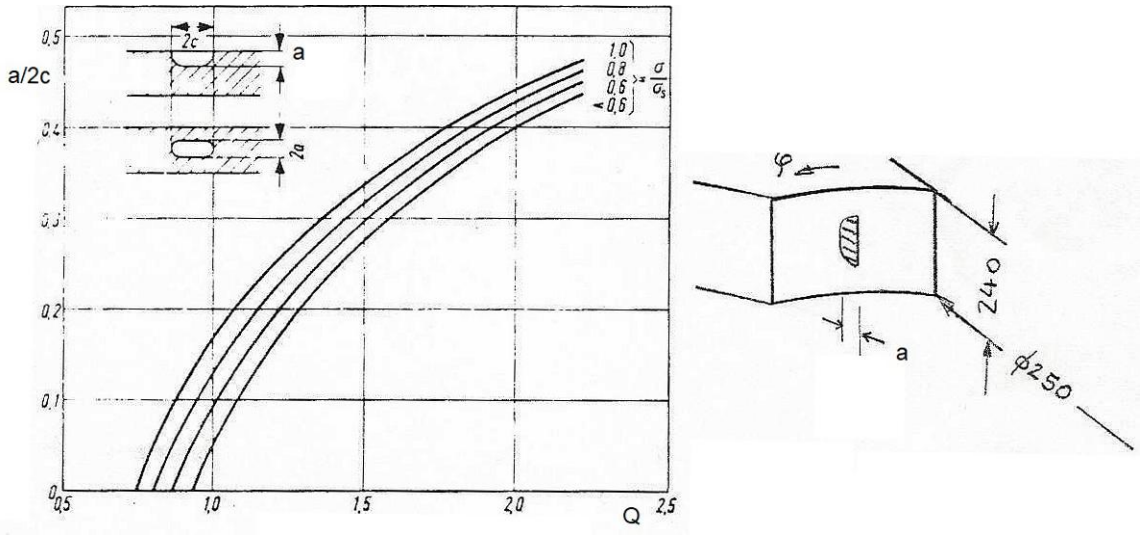


Fig.4: Crack entities

Comments for the German TÜV:

Practical measures

- Factory inspection certificate of the material ($R_{p0.2}$, R_m^t, δ_5) ,
- Ultrasonic testing of the wheel with normal and angle probes in all directions
- Fine balancing of the shrunken wheel
- Short-term operation with overload (1500 rpm))
- Measurement and display of lubricating oil and bearing temperature SOWle lubricating oil quantity
- Contact protection housing
- Safe limitation of the maximum speed by appropriate control
- Braking from nominal speed to 200 rpm by ballast resistance, then down to 0 rpm with brake
- Stress relief heat treatment
- Testing of the crack-free surface (magnetic particle process or similar).

Maintenance:

- Testing for flaws (with ultrasound) after proof run
- First inspection after about one tenth of the expected service life.

Theoretical (computational) measures:

- Calculation of the stress curve for centrifugal force, shrinkage and gyroscopic forces
- Proof of safe press fit
- Proof of the service life of wheel and shaft
- Control of critical speeds
- Proof of bearing life for the specified bearing loads by the bearing manufacturer.

19.2 A New concept of a Composite Flywheel due to novel fiber-reinforced materials (1988)

19.2.1 Introduction

Flywheels are applied for storage and release of a certain amount of energy in a certain speed range in order to save drive energy. Due to novel available (1988) different fiber plastic composite materials it is possible to significantly reduce the risk of delamination due to excessive radial straining. *Fig.1 right* depicts this problem for a highly spun GFRP ring. For this purpose, low-modulus fibers must be installed on the inside and higher-modulus fibers outside.

Idea of the author: The inner layers expand and pressure the stiffer outer layers of T800 for instance. Since an intermediate curing is provided, one could choose 2 inner sub-laminate shells 'low stiff'. The effect can be easily proven with two FE calculations, one with the same higher stiff 'circumferential fibers' in all layers and once with T300 fibers in the 2 inner shells. *Fig.1 (left)* presents such a flywheel composed of different fiber-reinforced polymers.

19.2.2 Design input of an energy-storing novel FRP-hybrid rim

1 loose bearing, 1 fixed bearing, aluminum hubs, epoxy resin matrix, $\Omega = 100$ Hz (reference frequency), 104 - 105 load clearances.

Task: Just the load case Centrifugal Loading is to consider. Confirmation of the idea as basis for further applications

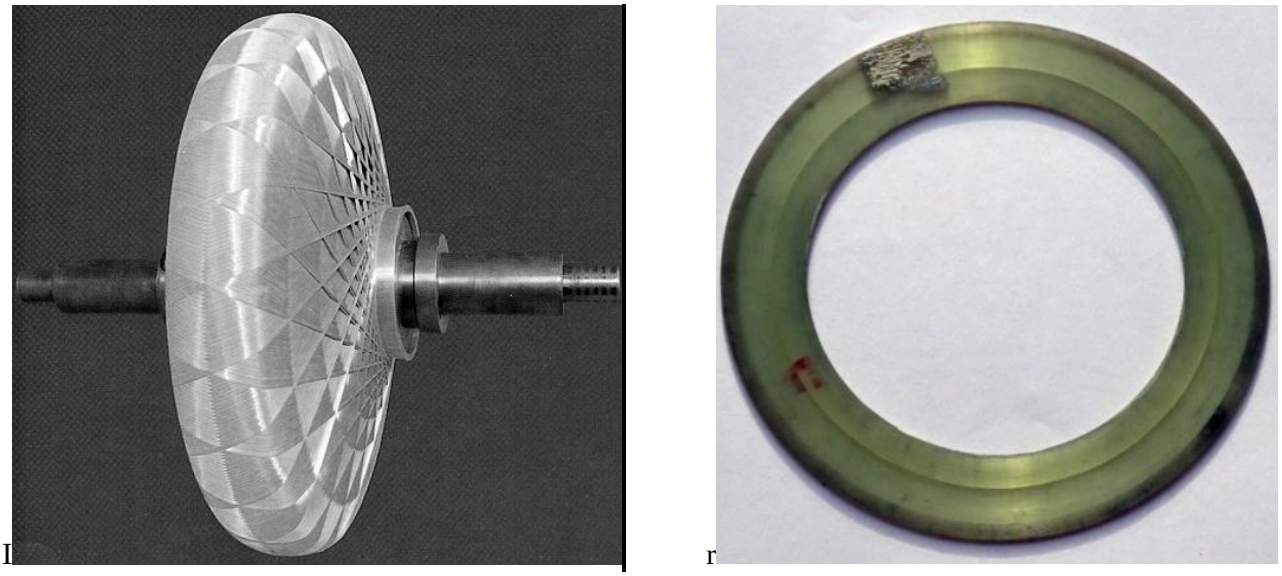


Fig.1: (left).Brake energy storage flywheel in composite design for a city bus.
(right) Cracks in a hoop wound thick ring from centrifugal loading (the rotor drive plate is not shown) .
[Cuntze R and Zaun J: Delamination Optimization of Hoop-Wound Composite Fly-wheels. ICCM 7, Beijing, August 1 - 4, 1989]

Design requirements:
* Increase in specific power/energy by 50% compared to metallic storage wheels –
* Reduction of delamination between the layers of the flywheel (balancing avoidance)
* Radial stress distribution in the rim, stresses and deformations in the housing.

Design Dimensioning

* Model: Thick-walled massive rim ring (continuum theory), thin-walled outer shell (shell bending theory)
* Limit state function: IFF1 tensile inter-fiber failure
* FEA: NASTRAN, PATRAN
* Material properties

		GFRP E-Glas	CFRP T300	CFRP T800	Alum.
$E_{\parallel}^{t}$	N/mm^2	50000	130000	185000	71000
$E_{\perp}^{t}$	N/mm^2	9000	8500	6500	-
$G_{\#}$	N/mm^2	5000	5500	5000	-
$\nu_{\perp\parallel}$	-	0,32	0,30	0,22	0,30
$\nu_{\perp\perp}$	-	0,38	0,40	0,40	-
$R_{\parallel}^{t}$	N/mm^2	600	1200	1700	-
$R_{\parallel}^{c}$	N/mm^2	500	1000	1300	-
$R_{\perp}^{t}$	N/mm^2	30	40	35	-
$R_{\perp}^{c}$	N/mm^2	100	140	135	-
$R_{\#}$	N/mm^2	50	65	60	-
ρ	g/cm^3	2,01	1,59	1,56	2,80
V_f	%	60	60	60	-

19.2.3 Design verification

Design Idea Verification, *Fig.2*

FEA proves that there are no radial tensile stresses that would create delamination around the hoop. The results also show that IFF1 only occurs beyond 600 m/s. Static fracture of the flywheel should be around 800 m/s.

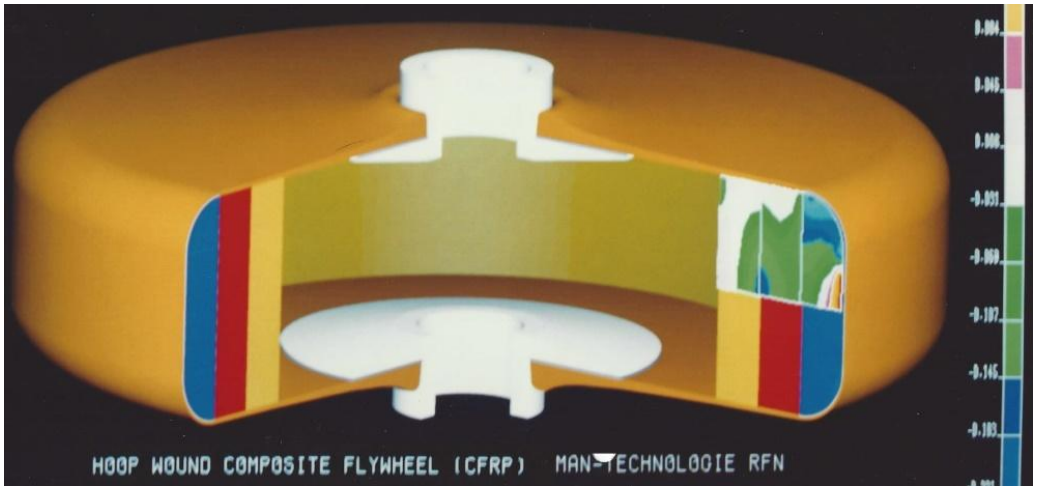


Fig.2: Demo Hybrid Flywheel

Fig.3 shows the structure of the entire storage wheel with the 3 different fiber composites of the energy-storing massive rim ring.

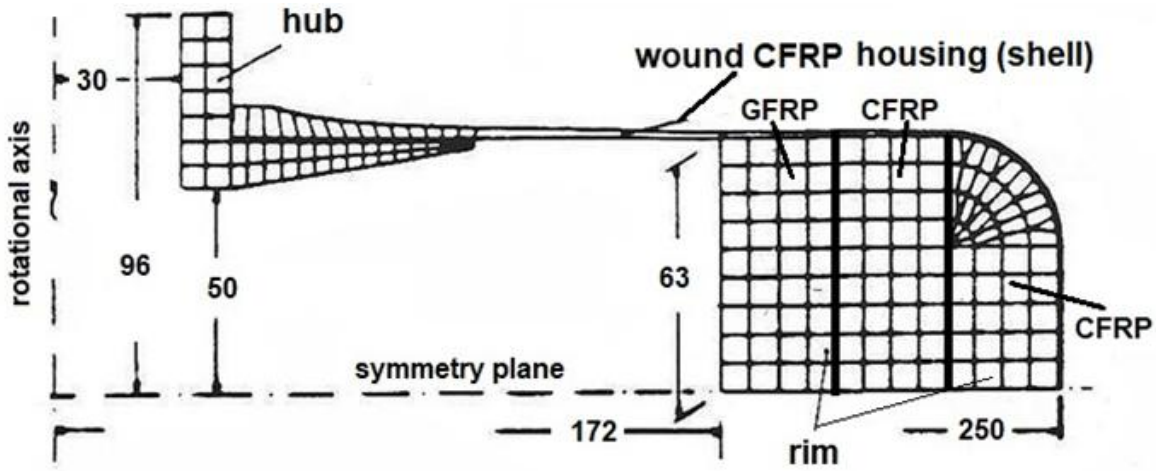


Fig.4: FE mesh

Fig.5 proves that no tensile radial strain is faced. Static fracture should be beyond 800 m/s.

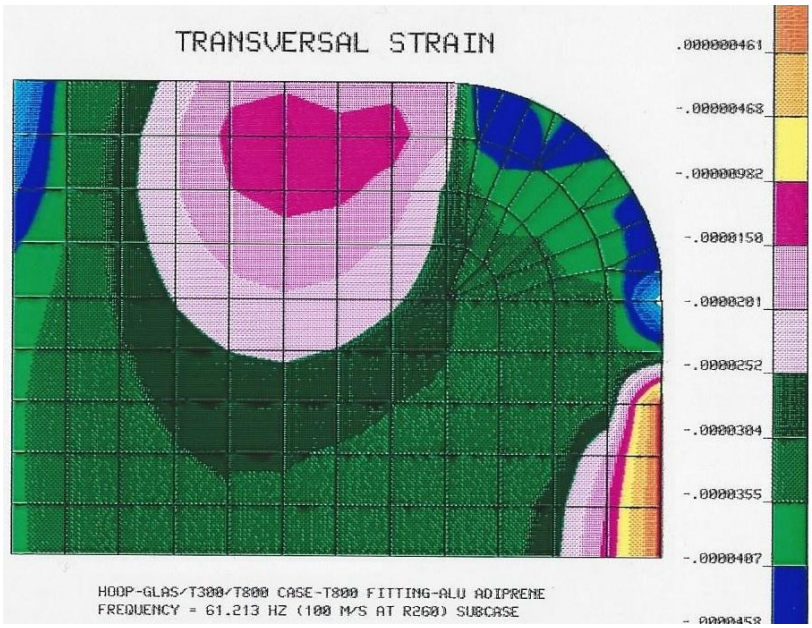


Fig.5: Details of the model showing the design-driving radial strain (1979)

Fig.6 gives a full look at the FE Model.

Result

The new availability of differently stiff fibers enabled to design a flywheel that does not experience radial tensile stresses. Such aflywheel impedes imbalances, which is a pre-condition for a safe running.

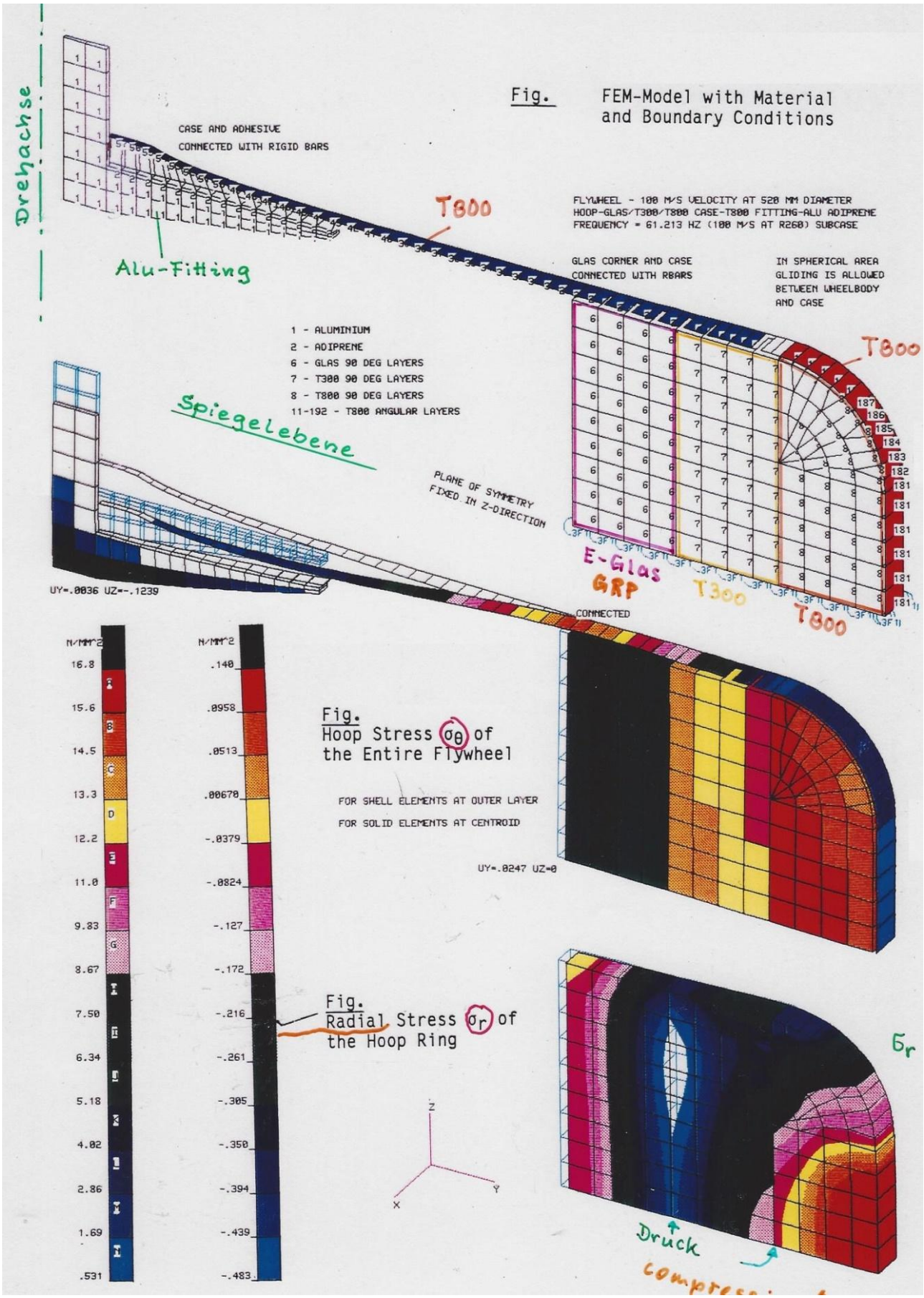


Fig.6: FE results

19.3 An Axial Energy Storage Rotor, the 'EnWheel' (2015)

19.3.1 Introduction with structural perspective

The author thinks that this concept can serve to store locally abundant wind energy or solar energy.

For a short time storage and the release of significant power with high power gradients fly-wheels are used. The EnWheel®, as developed by Stornetic GmbH, charges and discharges within seconds/minutes, is virtually wear-free with a maintenance-free technology and shows long-lasting capacity irrespective of the charging cycles or power load". The energy is stored kinetically by a rotor which speeds up to to n = 45000 revolutions per minute. Needing more energy or power, then, with DuraStor® multiple EnWheel® machines are combined to provide a range of system power up to 1000 kW. The containerized fast power storage system is a modular solution to meet a variety of application needs such as dynamic load flow management, load peak shaving, smart grid stabilization or power supply protection.

Fig.1 presents the solutions of the Stornetic GmbH. The left part shows a sketch of the EnWheel® and the rotor with its components. The right part shows the DuraStor® system including multiple flywheels to deliver local power where necessary. The system is capable to adapt to store and release the amount of electrical power and energy required by the given local task. Since the kinetic storage structure is not a disk (usually denoted wheel), the present tube structure is termed rotor. Regarding confidentiality the following may be considered as an exemplary essay.



Fig.1: EnWheel rotor components and modular DuraStor® fast power storage system.
Final design choice: FRP rotor tube, metal closure

Rotors are designed to be used for the intended service life between a maximum and a minimum rotor circuit frequency $\Omega = 2\pi \cdot f$ with *f* as rotor frequency and *t* as time. For its design 2 basic equations are to consider: The associated mechanical stresses increase proportionally to Ω^2. This means that the stress ratio R - being important for the lifetime estimation - is $R\,(\mathrm{minf}^2/\mathrm{maxf}^2)$. *(Unfortunately, the letter* R *is not only common for strength R (according to Resistance, skew letter) but also for the stress ratio* R *(according to* R*atio, straight letter.* $R \equiv R_\sigma$*, because in the case of ductile materials also a strain ratio* R_ε *is used).*

The basic relationships of energy storage rotors are:

Rotational energy: $RotEn = 0.5 \cdot \Theta \cdot \Omega^2$ and electrical power $N = \Theta \cdot \Omega \cdot d\Omega / dt$,
Design requirement: Usable share of energy $RotEn_{\text{usable}} = 0.5 \cdot \Theta \cdot (max\,\Omega^2 - min\,\Omega^2)$.

The task is therefore to raise max$f$ as far as possible regarding strength and service life. In order not to get too large speed fluctuations $n = f \cdot 60$ in the energy output, which would be bad in terms of service life, the so-called polar moment of inertia Θ is increased as much as possible by means of wall thickness magnification. However, this may lead to a radial tensile strength problem for the matrix. Namely, a thick-walled tube experiences significant radial tensile stresses during rotation, and these the higher the thicker the tube is (*see example before*). This is associated with the formation of micromechanical matrix cracks, which are not desirable for reasons of imbalance and must therefore be prevented, both constructively and materially. In order to obtain an optimal rotor (*bearing is to consider*), the rotor tube wall must first be structurally optimized. Further, an optimized matrix formulation is desired for the chosen FRP tube material allowing a distinct radial tensile strain. Experience proves that the matrix tensile fracture strain should be < 6% in order to balance the stress concentration around a single filament.
The necessary closures of the rotor tube are a 'cap' and a 'bottom'. These may be built from steel or fiber-reinforced materials. The bottom may be integrally generated by filament winding or by braiding. The use of a lightweight braided CFRP closure is positive, because the crash protective recipient, that is always to be transported, can then be thinner and thus lighter. In addition, the forces from a FRP closure fracture would be significantly smaller → benign crash. However, in design dimensioning it must be checked that the composite closure does not experience too large and non-rotationally symmetrically distributed micro-crack formation, which would mean unbalanced and not sustainable.
Essential for the development of the rotor is an optimal connection of the rotor closures to the bearings in terms of the cyclic operational strength, i.e. of the rotor cap (= loose bearing, top) and the rotor bottom or 'hub' (= fixed bearing) with seat of the motor.

19.3.2 Design Dimensioning of Rotor Tube

1 Input

- Fabrication possibilities:
  - Several part walls (shells), individually cured or separately cured
  - Separate closures versus integrated closures.
- Operation: The rotor has several critical frequencies. So-called bearing critical frequencies are passed through quickly and the lowest bending critical of the tube must then be at a suitable distance above the maximum rotation frequency max$f$. When determining this bending-critical natural frequency, the influence of shear rigidity and rotational inertia must be taken into account (see example before).
  Lifetime: 10 years
- Loadings: *proportional stress states*
  - maximum frequency max$f$ (DUL = ULS)
  - operational load spectrum ('variable amplitude') with an amount of un-loadings (R = 0)
  - R = minf^2 / maxf^2 = 0.3. Max$f$ is controlled by a safety system
- Safety concept: *assumed values for display of the procedure*
  - j_{ult} = 1.5, considering ULS
  - j = 1, considering residual strength after operation (*if maintenance-driven operation*)

- $j_{Life} = 3$, applying the Palmgren-Miner rule
- $D_{feasible} = 0.5 <$ D =1= 100% as maximum of the Palmgren-Miner rule.

- Optimization with side restrictions:
  Maximize $RotEn_{usable}$ of the tube, regarding the following restrictions
  - Bending frequency $f_{bending}$
  - Choice of different fiber volume fractions V_f, that influence the density parameter ρ_{FRP}
  - No delamination under radial stresses
  - Check of IFF in the helix layers
  - Check of lifetime.
- Material properties of UD tube: below
  Assumption: transversely-isotropic $\rightarrow E_3 = E_2 = E_\perp$, $G_{\perp\perp} = E_\perp / (2 + 2\nu_{\perp\perp})$, $R_3 = R_2 = R_\perp$
- The rotor is to drive as 'elastically' as possible otherwise the fatigue-caused micro-damage may become too high.

Fibers, foreseen for the helix layers which give the rotor tube the necessary bending stiffness and for the strength-delivering circumferential layers are found in a manufacturer data sheet and the resin systems (*matrix = cured resin system*) as well. Composite property values are given there usually for V_f = 60% (*as below performed*). This means, that for lower or higher fiber volume fractions the 60% data sets are micromechanically to adjust.

Of course, no product-specific, confidential information can be made here. But it's more about the procedure for such a development anyway. Just one information shall be given: The less stiff T300 is used for the inner 90°-layers. For the outer layers fibers of higher stiffness are applied.

The design of the rotor usually envisages driving the rotor above the two so-called bearing-critical level and below the bending-critical speeds. Hence, the bending stiffness of the tube is decisive for the distance to the bending-critical speed. It is practically provided by the helix layers and the value of its angle ω.

2 Design Proposals for the tube walls

Determination of Helix angle

The classical winding process always leads to a pair of + - ω-layers. The helix angle ω is a function of the required minimum angular frequency that is fixed by the bending stiffness which is a function of the lay-up. The optimum angle ω is to search.

Laminate design lay-up possibilities: basic layer directions are $90°$ and $\pm\omega°$

Critical for the formation of micro-cracks are the interface stress states between 90°-hoop layer and ω°-helix layer. Variations are to investigate under the precondition that the depicted restrictions especially the bending stiffness are met. Some of these are:

* Reduction of the fiber volume fraction V_f from a usually > 60% to < 50% considering the inner partial shell. More matrix content inside does not matter
* Helix (angular) layers also wound with T700 fibers stiffer than the T300 fibers
* Inner hoop shells with T300. This reduces the modulus of elasticity $E_\perp = V_f \cdot E_f$ and increases the desired radial compression of the outer shells $\rightarrow \sigma_\perp < 0$

* Separately pre-cured, slightly conical partial shells, which are pushed into each other. This reduces radial tolerance problems.

Tube life estimation model (*just for the tube part foreseen here*), 'proportional stressing' given

Given is a load spectrum. This means a loss of the sequence of the loading is to face and this causes some uncertainty which influences the block-wise computed micro-damage accumulation *D* after Palmgren-Miner.

The estimation of the service life of the tube can be carried out easily because the thick-walled rotor tube is designed to be fiber-dominant. The stress ratio $R_\sigma = \min\sigma_{\|} / \max\sigma_{\|}$ can thus be practically estimated for the critical hoop layer from a SN curve $R_\sigma = 0.1$.

3 Analytical Static Verification of the chosen tube design (after design dimensioning loops)

For certification an analytical verification and a test verification are required.
In the design loops, varying the fiber volume fraction V_f of a layer (inner), the associate micromechanical formulas must be indicated. Otherwise, the estimation can become nonsensical, because the determined fiber values are linked to the formula, the full link micro-macro is to consider in both the directions.

$$E_{\|} = E_{\|f} \cdot V_f + E_m \cdot (1 - V_f) \cong E_f \cdot V_f, \quad \text{within regime } 0.3 \le V_f \le 0.65;$$

$$\nu_{\perp\|} = \nu_{\perp\|f} \cdot V_f + \nu_m \cdot (1 - V_f), \quad G_m = E_m / (2 + 2 \cdot \nu_m).$$

$$E_\perp = \frac{E_m}{1 - \nu_m^{\,2}} \cdot \frac{1 + 0.85 \cdot V_f^{\,2}}{(1 - V_f)^{1.25} + V_f \cdot E_m / (E_{\perp f} \cdot (1 - \nu_m^{\,2}))}; \quad G_{\perp\|} = \frac{G_m \cdot (1 + 0.4 \cdot V_f^{\,0.5})}{(1 - V_f)^{1.5} + V_f \cdot G_m / G_{\perp\|f}}.$$

The required 3D-SFCs for 'Onset of fracture failure' prediction of a 3D-stressed lamina are shown below. The input of the necessary stresses and strains are delivered by a 3D-FEA.

FF 1: $Eff^{\|\sigma} = \breve{\sigma}_1 / \bar{R}_{\|}^{\,t} = \sigma_{eq}^{\|\sigma} / \bar{R}_{\|}^{\,t}$ with $\breve{\sigma}_1^{\,*} \cong \varepsilon_1^t \cdot E_{\|}$ (matrix negligible),

FF 2: $Eff^{\|\tau} = -\breve{\sigma}_1 / \bar{R}_{\|}^{\,c} = +\sigma_{eq}^{\|\tau} / \bar{R}_{\|}^{\,c}$ with $\breve{\sigma}_1^{\,*} \cong \varepsilon_1^c \cdot E_{\|}$,

IFF 1: $Eff^{\perp\sigma} = [(\sigma_2 + \sigma_3) + \sqrt{(\sigma_2 - \sigma_3)^2 + 4\tau_{23}^{\,2}}] / 2\bar{R}_\perp^{\,t} = \sigma_{eq}^{\perp\sigma} / \bar{R}_\perp^{\,t}$,

IFF 2: $Eff^{\perp\tau} = [(b_{\perp\perp} - 1) \cdot (\sigma_2 + \sigma_3) + b_{\perp\perp} \sqrt{(\sigma_2 - \sigma_3)^2 + 4\tau_{23}^{\,2}}] / \bar{R}_\perp^{\,c} = +\sigma_{eq}^{\perp\tau} / \bar{R}_\perp^{\,c}$

IFF 3: $Eff^{\perp\|} = \{[b_{\perp\|} \cdot I_{23-5} + (\sqrt{b_{\perp\|}^{\,2} \cdot I_{23-5}^{\,2} + 4 \cdot \bar{R}_{\perp\|}^{\,2} \cdot (\tau_{31}^2 + \tau_{21}^2)^2}] / (2 \cdot \bar{R}_{\perp\|}^{\,3})\}^{0.5} = \sigma_{eq}^{\perp\|} / \bar{R}_{\perp\|}$

with $I_{23-5} = 2\sigma_2 \cdot \tau_{21}^2 + 2\sigma_3 \cdot \tau_{31}^2 + 4\tau_{23}\tau_{31}\tau_{21}$, ^{t} = tension, ^{c} = compression

The friction parameters *b* can be computed from available friction values of the UD material due to the relationships derived in chapter 8.2 : $b_{\perp\|} \cong 2 \cdot \mu_{\perp\|}$, $b_{\perp\perp} \cong 1 / (1 - \mu_{\perp\perp})$.

Total effort: $Eff = [(Eff^{\|\sigma})^m + (Eff^{\|\tau})^m + (Eff^{\perp\sigma})^m + (Eff^{\perp\|})^m + (Eff^{\perp\tau})^m]^{m^{-1}}$.

For the laminate internal delamination (*not including the laminate edge effect*) is valid:

Tension/shear stressing: $(Eff^{\perp\sigma})^m + (Eff^{\perp\|})^m = 1$, $\{\sigma\}_{\text{lamina}} = (0, \sigma_2^t, \sigma_3^t, \tau_{23}, \tau_{31}, \tau_{21})^T$

Compression-shear stressing: $(Eff^{\perp\tau})^m + (Eff^{\perp\|})^m = 1$, $\{\sigma\}_{\text{lamina}} = (0, \sigma_2^c, \sigma_3^t, \tau_{23}, \tau_{31}, \tau_{21})^T$.

As lamina guiding case a general 3D-stress state is investigated as numerical example: CFRP/EP.

The material UD data set reads:

$(E_{||}, E_{\perp}, G_{||\perp}, \nu_{\perp||}, \nu_{\perp\perp}) = (13000,\ 8500,\ 5500,\ 0.32,\ 0.39),\quad \rho = 1{,}55 \cdot 10^{-3} \cdot \mathrm{g/mm^3}$

$\mu_{\perp\square} = \mu_{\perp\perp} = 0.2,\ \alpha_{T||} = -1 \cdot 10^{-6} \cdot \mathrm{mm/(mm \cdot K)},\ \alpha_{T\perp} = 26 \cdot 10^{-6} \cdot \mathrm{mm/(mm \cdot K)}.$

$\{\sigma\} = (\sigma_1, \sigma_2, \sigma_3, \tau_{23}, \tau_{31}, \tau_{21})^T = (1200,\ -15,\ -5,\ 10,\ 10,\ 0)^T,$ times FoS $j_{\mathrm{ult}} = 1.25$

$\{\bar{R}\} = (\bar{R}_{||}^t,\ \bar{R}_{||}^c,\ \bar{R}_{\perp}^t,\ \bar{R}_{\perp}^c,\ \bar{R}_{\perp||})^T = (1980,\ 1500,\ 51,\ 172,\ 71)^T$ MPa, average value

$\{R\} = (R_{||}^t,\ R_{||}^c,\ R_{\perp}^t,\ R_{\perp}^c,\ R_{\perp||})^{\mathrm{T}} = (1700,\ 1350,\ 40,\ 140,\ 60)^{\mathrm{T}}$ MPa, statistically reduced

$\left\{Eff_{\mathrm{eq}}^{\mathrm{mode}}\right\} = \left(Eff_{eq}^{||\sigma},\ Eff_{eq}^{||\tau},\ Eff_{eq}^{\perp\sigma},\ Eff_{eq}^{\perp\tau},\ Eff_{eq}^{||\perp}\right)^T = \left(0.88,\ 0,\ 0,\ 0.21,\ 0.20\right)^T,$

$\left\{\sigma_{\mathrm{eq}}^{\mathrm{mode}}\right\} = \left(\sigma_{eq}^{||\sigma},\ \sigma_{eq}^{||\tau},\ \sigma_{eq}^{\perp\sigma},\ \sigma_{eq}^{\perp\tau},\ \sigma_{eq}^{||\perp}\right)^T = \left(1500,\ 0,\ 0,\ 28.7,\ 12.2\right)^T.$

The results above deliver the following material reserve factors $RF \equiv f_{RF}$ (linear)

$Eff = 0.90 \rightarrow RF = 1.11;\ Eff_{FF} = 0.88 \rightarrow RF_{FF} = 1.14;\ Eff_{IFF} = 0.27 \rightarrow RF_{IFF} = 3.7.$

Above static design verification computations consider mode interaction and Design Ultimate Level.

→ Static design is accepted.

Mind, please in laminate modeling:

- A lamina is the computational model and a layer or a ply is a physical model. A lamina may represent more than one layer but also less than one layer.

4 Analytical Cyclic Verification of the chosen tube design

Mapping of available SN-test data with determination of the Ψ-parameters and function

Available SN-curves are R =0.5, 0.1. Further SN curves are needed, which can be successfully performed by application of Kawai's 'Modified fatigue strength ratio' and by the (see chapter 10) mapping function of the SN-curve $\sigma_{max}^{Master}(N, \mathrm{R}) = \sigma_{R=0.1} = c_1 + (\bar{R}^t - c_1) / \exp\left(\frac{\log(N)}{c_1}\right)^{c_2}$

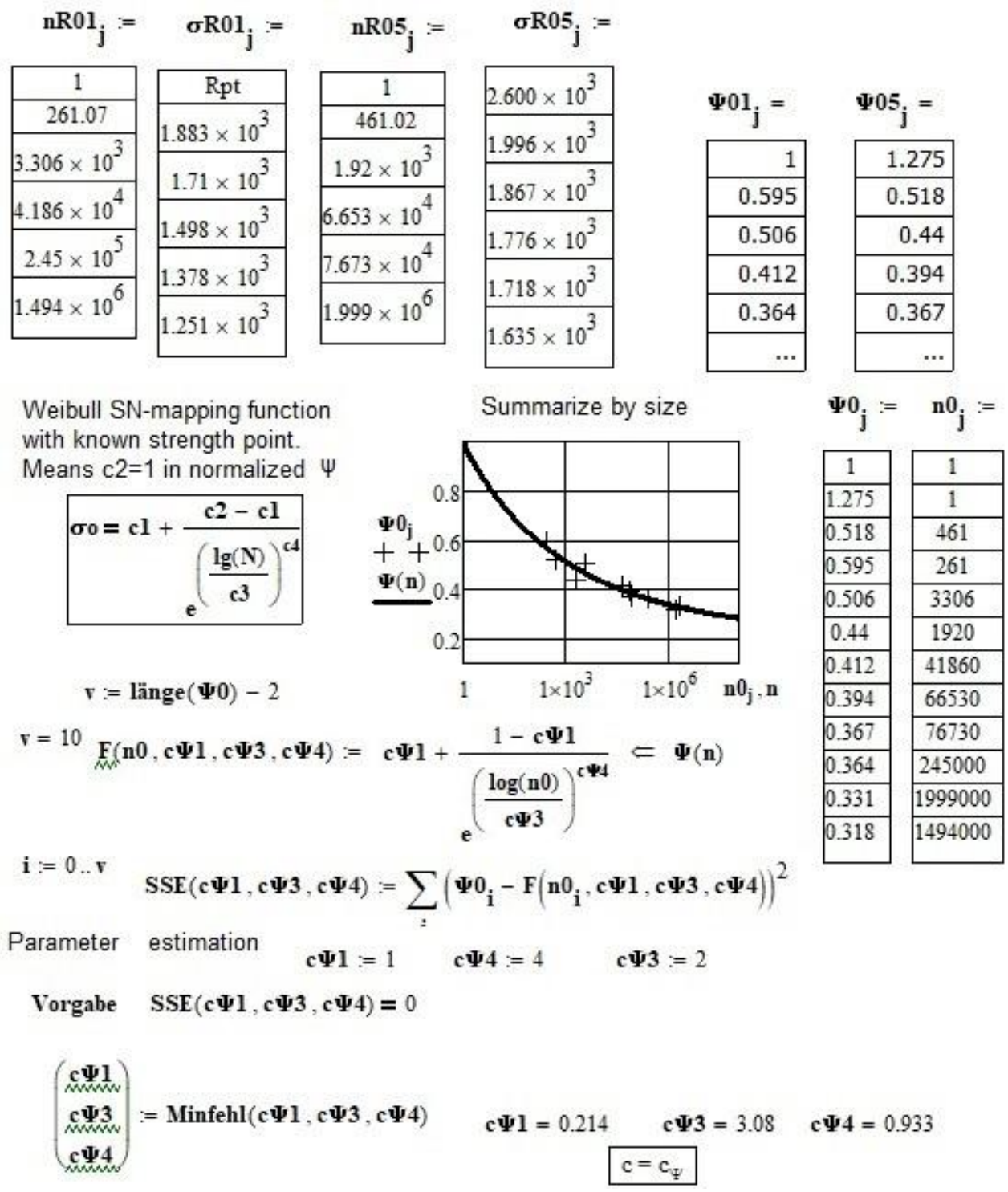
How Kawai's 'Modified fatigue strength ratio' Ψ (normalized, defined positive)

$$\Psi_{Master}^t = \frac{0.5 \cdot (1 - \mathrm{R}) \cdot \sigma_{\max}^{\mathrm{Master}}}{\bar{R}^t - 0.5 \cdot (1 + \mathrm{R}) \cdot \sigma_{\max}^{\mathrm{Master}}}\ .$$

is obtained and how the parameters therein can be determined show the procedure in *Fig.2*.

Depiction of available SN-test curves and SN-predicted curves R= 01, 0.3, 0

Mapping of the available test data sets R = 0.1 and 0.5 of Kawai-Suda is performed by using Kawai's 'Modified fatigue strength ratio' Ψ. This delivers an average Ψ-curve which has to be 'reduced' to a Ψ-'design curve' by statistical means. According to the low test basis this task is performed by reducing the static strength - origin of the SN-curve - by 5% .



1
261.07
3.306×10^3
4.186×10^4
2.45×10^5
1.494×10^6

Rpt
1.883×10^3
1.71×10^3
1.498×10^3
1.378×10^3
1.251×10^3

1
461.02
1.92×10^3
6.653×10^4
7.673×10^4
1.999×10^6

2.600×10^3
1.996×10^3
1.867×10^3
1.776×10^3
1.718×10^3
1.635×10^3

1
0.595
0.506
0.412
0.364
...

1.275
0.518
0.44
0.394
0.367
...

1	1
1.275	1
0.518	461
0.595	261
0.506	3306
0.44	1920
0.412	41860
0.394	66530
0.367	76730
0.364	245000
0.331	1999000
0.318	1494000

Fig.2: Determination of the parameters of Kawai's 'Modified fatigue strength ratio'

In the following Table the formulations for the interesting five SN curves are collected.

Fig.3 then visualizes the associated 5 tensile strength normalized curves, obtained by applying Kawai's model, mode-associated by the author. The upper border line R =1 (*static strength*) is accurately obtained as asymptote. Further, the graph represents the mapping quality of the two test curves R = 0.1, 0.5.

Table 1:Formulations of the 5 searched SN-curves

$$\sigma_{R=0.}(\mathrm{N}=0,\mathrm{R}) \;=\; 2\cdot c_1 + (\bar{R}^t_{\square} - c_1)\,/\,\exp\left(\frac{log(N)}{c_1}\right)^{c_2} / (\Psi^t_{Master} - \mathrm{R} + \mathrm{R}\cdot\Psi^t_{Master} + 1)\,,\quad \mathrm{R}=0 \text{ (border)}$$

$$\sigma_{R=0.1}(\mathrm{N}=0,\mathrm{R}) \;=\; 2\cdot c_1 + (\bar{R}^t_{\square} - c_1)\,/\,\exp\left(\frac{log(N)}{c_1}\right)^{c_2} / (\Psi^t_{Master} - \mathrm{R} + \mathrm{R}\cdot\Psi^t_{Master} + 1)\,,\ \mathrm{R}=0.1$$

$$\sigma_{R=0.3}(\mathrm{N}=0,\mathrm{R}) \;=\; 2\cdot c_1 + (\bar{R}^t_{\square} - c_1)\,/\,\exp\left(\frac{log(N)}{c_1}\right)^{c_2} / (\Psi^t_{Master} - \mathrm{R} + \mathrm{R}\cdot\Psi^t_{Master} + 1)\,,\ \mathrm{R}=0.3$$

$$\sigma_{R=0.5}(\mathrm{N}=0,\mathrm{R}) \;=\; 2\cdot c_1 + (\bar{R}^t_{\square} - c_1)\,/\,\exp\left(\frac{log(N)}{c_1}\right)^{c_2} / (\Psi^t_{Master} - \mathrm{R} + \mathrm{R}\cdot\Psi^t_{Master} + 1)\,,\ \mathrm{R}=0.5$$

$$\sigma_{R=1}(\mathrm{N}=0,\mathrm{R}) \;=\; 2\cdot c_1 + (\bar{R}^t_{\square} - c_1)\,/\,\exp\left(\frac{log(N)}{c_1}\right)^{c_2} / (\Psi^t_{Master} - \mathrm{R} + \mathrm{R}\cdot\Psi^t_{Master} + 1)\,,\quad \mathrm{R}=1 \text{ (border).}$$

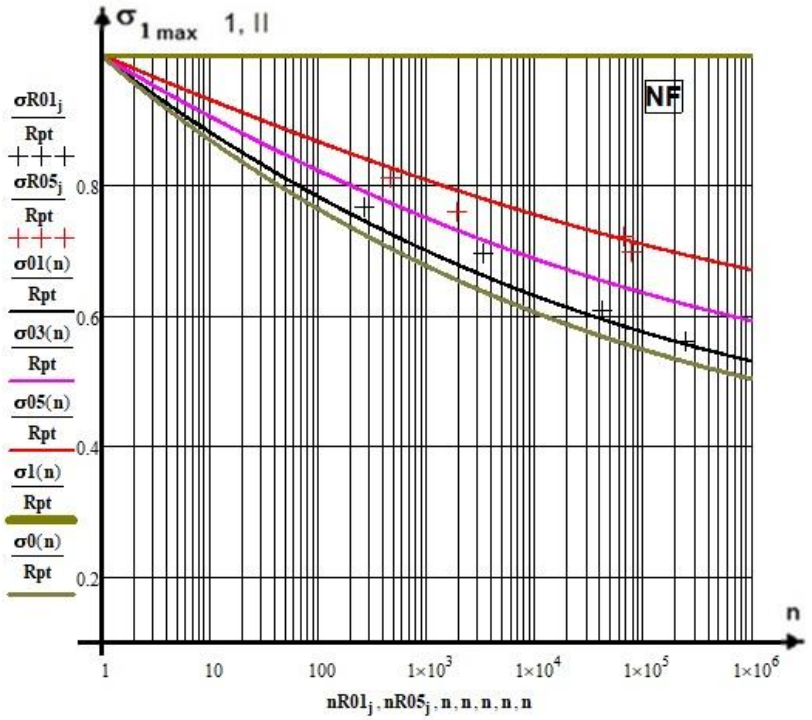


Fig.3: Display of the 5 SN-curves above, normalized by the fiber tensile strength

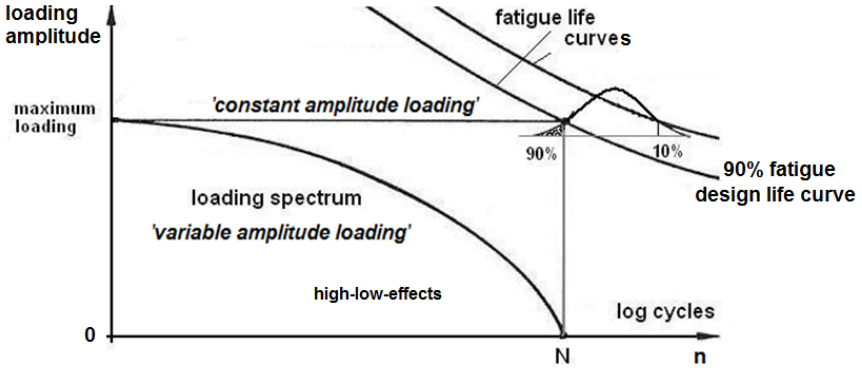


Fig.4: Loading spectrum, variable and 'constant amplitude loading'

The present loading type of the rotor and thereby of the rotor tube is a loading spectrum which represents variable amplitude loading. Such a given loading spectrum can be split into constant amplitude loading blocks to compute the micro-damage portions of each block.

A loading spectrum is of less damaging character than a constant amplitude loading as *Fig.4* proves.

Essential for the the EnWheel is that electrical shutdown fixes the value of $_{max}\Omega$.

For simplification reasons, the swelling load-carrying 90°-layers are fatigue-dimensioned by just using the stress-ratio $R_{0.1}$-curve instead of employing the service spectrum divided into several blocks. Further, a Relative Palmgren-Miner micro-damage accumulation rule is employed. Residual stresses are neglected here in the dimensioning of the fiber-oriented 90°layers. Hence for simplification, in a trade-off study during the design dimensioning phase the harsher constant amplitude loading is often applied employing in the case of tension swelling just the standard SN curve R = 0.1. R = 0 is a little bit harsher than R = 0.1 but not measured from test execution reasons (*buckling danger*) . The more benign acting loading spectrum with mixed R-values will balance this.

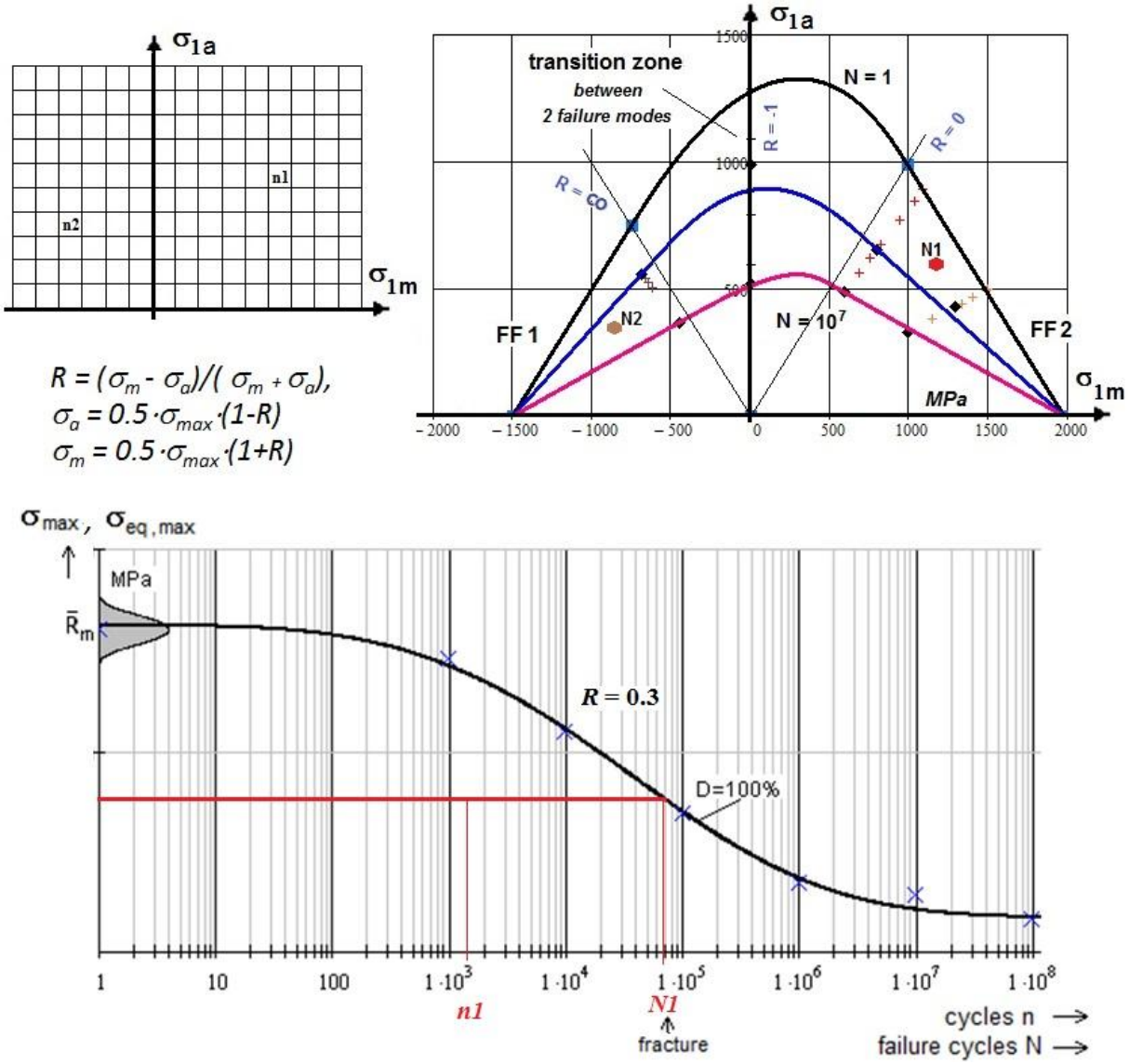


Fig.5: T300, FF-linked scheme for the determination of a damaging portion, FF1, $R_\sigma = 0.3$.

Test data set Kawai-Suda in § 10

According to the wide scatter of measured fatigue lives the accumulated maximum allowable micro-damage portion of D =100% is reduced to a smaller value termed D_{feasible}. It is chosen here to be 0.5. Employing an appropriate D_{feasible} permits not to change a given FoS j_{life} but to react to the specific fatigue scatter of a distinct material.

Eventually, in ***Fig.5*** an assumed schematic example was presented for the most stressed hoop layer. The shown simplified presentation shall repeat the procedure.

If applicable, according to a planned maintenance concept, at the foreseen time point sufficient residual strength after the fatigue-caused micro-crack damage (*not to be confused with the residual strength of a macro-cracked structural component, §10)* has to be demonstrated for the maximum speed, however without magnifying the stresses by j_{ult}.

Cyclic design verification computations

The following procedure captures 'Mode interaction' and 'Variable amplitudes'. It is performed at 'Design Limit Load' level or the maximum operational load level, respectively.

The multi-axial static failure body shrinks with the number of the micro-damage generating cycles n. As experienced, for brittle FRP materials the static failure criteria can be applied and this involves the interaction of failure modes (*In the ductile metal case the Mises criterion with the Mises equivalent stress does this, there is just one single mode, namely 'Onset-of-yielding'*). Hence, in the case of multi-axial stress states with $\sigma \rightarrow \sigma_{eq}$ and *Eff follows*

$$\{\sigma\} = (\sigma_1, \sigma_2, \sigma_3, \tau_{23}, \tau_{31}, \tau_{21})^T = (1000,\ -15,\ -5,\ 10,\ 10,\ 0)^T, \quad \text{FoS } j = 1$$

$$\{\bar{R}\} = (\bar{R}^t_{\parallel},\ \bar{R}^c_{\parallel},\ \bar{R}^t_{\perp},\ \bar{R}^c_{\perp},\ \bar{R}_{\perp\parallel})^T = (1980 \cdot 0.95,\ 1500,\ 51,\ 172,\ 71)^T \text{ MPa}$$

Reduction is now to perform for the SN-curve, which here means for the Kawai model, via Ψ.

Due to lack of test data this is simply performed here by setting a reduction factor on $\bar{R}^t_{\parallel}$,

$$\left\{Eff^{\text{mode}}_{\text{eq}}\right\} = \left(Eff^{\parallel\sigma}_{eq},\ Eff^{\parallel\tau}_{eq},\ Eff^{\perp\sigma}_{eq},\ Eff^{\perp\tau}_{eq},\ Eff^{\parallel\perp}_{eq}\right)^T = (0.53,\ 0,\ 0,\ 0.13,\ 0.14)^T,$$

$$\left\{\sigma^{\text{mode}}_{\text{eq}}\right\} = \left(\sigma^{\parallel\sigma}_{eq},\ \sigma^{\parallel\tau}_{eq},\ \sigma^{\perp\sigma}_{eq},\ \sigma^{\perp\tau}_{eq},\ \sigma^{\parallel\perp}_{eq}\right)^T = (1000,\ 0,\ 0,\ 23,\ 9.9)^T.$$

The stress state above delivers the following material stressing efforts (linear)

$$Eff = 0.54;\ Eff_{FF} = 0.53;\ Eff_{IFF} = 0.18.$$

Eff_{FF} indicates that a simplified worst case scenario can be applied: The maximum stress $\sigma_1 = \sigma^{\parallel\sigma}_{eq} = \sigma_{\parallel}(\max\Omega) = 1000$ MPa is representative! A realistic cyclic life would lead to a smaller accumulation of micro-damage portions and possess a higher lifetime. This is the clear come-out of the following result table.

Concerning the reduction on the resistance side: Instead of reducing the static strength R and applying a FoS j_{ult}, now a reduction of the cyclic curve is employed together with a high FoS j_{Life} and a material-typical reduction of the accumulated maximum sum of micro-damages from D = 1 to D_{feasible} = 0.5. Facing a variable amplitude loading and Kawai's 'Modified fatigue strength ratio' Ψ is to apply (§10) to save test CoSts the normalized master curve Ψ has to be transferred to a master design curve. In the actual case, due to the few test results,

Cyclic interaction $D(D_{\square}, D_{\perp}, D_{\perp||})$ *is generally not well investigated, see C.Hahne [Hah14].*

Result table: stresses in MPa, N and n in cycles, N means D = 100 %.

$D_{f\,easible} = 0.5$, $j_{Life} = 3$, worst case scenario

(1) Assumed, two full blocks: R = 0, n0 = 3000 with R = 0.3, n3 = 150000

R = 0: $\sigma_{1a} = \sigma_{1m} = 500$ MPa, N = 262600 with R = 0.3: $N = 3 \cdot 10^9$

$D = \Sigma D_i = \Sigma n_i / N_i = 3000 / 262600 + 150000 / 3 \cdot 10^9 = 0.011$

$\rightarrow \quad RF_{0103Life} = D_{f\,easible} / (D \cdot j_{Life}) = 14.5.$ variable amplitude

(2) Assumed, just one constant amplitude block: R = 0.1, n1 = 153000

R = 0.1: N = 1416200 $\Rightarrow D(R=0.1) = 15300 / 1416200 = 0.073.$

$\rightarrow \quad RF_{01Life} = D_{f\,easible} / (D \cdot j_{Life}) = 1.5.$ constant amplitude

5 Thoughts about the difficult Test design verification of material and structure

Material characterization: Elasticity and strength properties

These properties are available from the standard test procedure. As winding is the fabrication process the tension/compression-torsion test specimen is to prefer because it meets 'as built' best. To be tested are also combinations of stresses.

To consider is embedding of a layer (ply), thin-layer effect, fiber volume fraction, stacking sequence and loading types.

1 : Flat coupon material test specimens (relatively cheap compared to tubes) however winding is the fabrication process and this should be considered

2 : Tension/compression-torsion tube test specimens $(\sigma_1, \sigma_2, \tau_{21})$

3 : Sub-laminate test specimens (with internal proof ply and outer supporting plies)

4 : Flat off-axis coupons (*shortcomings 'free edge effect' + bi-axial stiffness loss not accurately considered*) with $\{\sigma\} = (\sigma_1, \sigma_2, \sigma_3, \tau_{23}, \tau_{31}, \tau_{21})^T \rightarrow \sigma_{||}^t,\ \sigma_{||}^c,\ \sigma_{\perp}^t,\ \sigma_{\perp}^c,\ \tau_{\perp||}$

Loading types, applied for the operational lifetime estimation, are:

- Constant-amplitude loading : delivers SN curves (Wöhler curve)
- Block-loading: is a more realistic Fatigue Life testing
- Random spectrum loading : Fatigue Life (Gaßner) curve.

Centrifugal test on a demonstrator as a representative rotor tube surrogate test specimen:

Proof of service life can be only achieved by effortful expensive spin tests, because the radial strain distribution is practically impossible to generate otherwise, i.e. hydraulically via internal pressure. A smaller centrifugal stand could be used. The static up-scaling to the intended nominal diameter can be done by FEA. Creep is negligible in the rotor tube regarding the fiber-controlled load-carrying 90° hoop layers.

Gyroscopic rotor dynamics requires a distinct ratio of the inertias, which reduces the length of a demonstrator to be less than the diameter in order to run the demonstrator stable! For testing, a surrogate test specimen (*a demonstrator*) is required, with which – *'run time-conditioned' by increasing speed* $n > {}_{max}n$ *- energy-efficient and fast* enough service life experience could be gained.

This test specimen should be manufactured by the same production process in order to meet 'as-built'.
Unfortunately, however, there is no practical test series in sight that enables an *economic* design verification of such a rotor by experiment. Confidence in the construction of the rotor tubes can be only achieved through reliable FE calculations paired with measured reliable material data and surrogate spin test results with varying speed.

Some general remarks especially linked to this application:

* *Theory creates a model of the reality 'only', and an experiment is 'just' one realization of the reality. Find a compromise to CoSt-optimally achieve a satisfying joint verification procedure 'analysis-test' for a robust design of the flywheel as precondition of a flywheel certification.*
* *The composite tube requires metallic connections. This means: When developing composite parts, holistic concurrent engineering is more essential than with metals, alone.*
* *Experience has shown so far that as long as laminates are statically designed for a design limit of about 0.3%, they have suffered virtually no fatigue damage if layers with four fiber direction are present. Lightweight construction, however, requires a higher material utilization.*
* *Which model accuracy is enough for trade-off studies and which for a verification?*
* *All the laminas of the "failure system laminate" act together and cause in-situ effects as well as a so-called joint failure behavior. For instance, an IFF in one embedded lamina will follow a load redistribution with increasing micro-damage which might make another lamina critical. For a better understanding, the associated degradation behavior could be investigated by employing structural reliability. A laminate is a random but not a deterministic failure system of its building blocks, the laminas!*

Acknowledgement

Many thanks to Dr.-Ing. Christoph Schäfer, info@stornetic.com, for his general check.

19.4 Increasing the Limit of Usability of CFRP Tubes by Built-in-Stresses (1993)

From R. Cuntze MAN Technologie AG, Bauschingerstrasse 20, D 8000 München 50 & R. Heibel URENCO Ltd, Oxford Road, Marlow, Bucks., UK, SL72NL, Composite Structures 24 (1993) 251-264

The limit of usability of a CFRP structure is often determined by Inter-Fiber-Failure (IFF) indicated by interfiber/rnatrix cracking. It will be shown how for certain types of CFRP structures this crack initiation threshold can be delayed. The process used here is prestraining in analogy to that of prestressed concrete. It is a so-called thermo-mechanical post- treatment, inducing advantageous compression built-in stresses, i.e. negative strains transverse to the fibers.
Cylindrical tube specimens were wound, prestrained and submitted to hydraulic pressurisation or spin load testing. Acoustic emission monitoring and crack counting following sectioning confirmed an increase in crack threshold level for this specimen type from $\varepsilon_{hoop} = 0.8\%$ to 1.3%, which is higher than the operational strain, normally defined as tensile failure strain $\varepsilon^t_{\perp}$ of the fiber divided by the usual design factor j_{ult} = 1.5. Theoretical investigations were done in support of the design of the prestraining device and of the tube specimen, as weil as an evaluation of experimental data.

Avoiding tensile stresses-caused micro-cracking especially provides advantages in the operation of cyclically stressed rotors. Better. It is usually a requirement.

INTRODUCTION AND FORMULATION OF THE PROBLEM

Carbon fibre reinforced plastics (CFRP) find an increasing number of applications where materials are required which have high specific strength and modulus, e.g. pressure vessels, rotating printing rollers, torsion shafts and rotors of centrifuges (see Refs 3 and 2).

However, the performance of multilayer CFRP is often limited by the occurrence of interfibre/matrix cracking at first ply failure (FPF) in the sense of interfibre failure (IFF). In other words, with respect to the tube the transverse stress $\sigma^t_{\perp}$ in the crack sensitive helix layers of a multilayered tube reaches its (low) strength value $R^t_{\perp}$ and its microcrack initiation level at pressures far below burst pressure. Hence, this cracking often prevents utilisation of the full potential in fibre parallel strength $R^t_{\parallel}$ offered by fibre reinforced plastics (FRP) — determining last ply failure (see Fig. 1) — especially when employing the recently developed high strength and high modulus fibres. When examining such IFF cracks by scanning electron microscopy (SEM) it becomes obvious that they are occurring in between the fibres and could either be entirely within the matrix or at the interface between fibre and matrix. These cracks

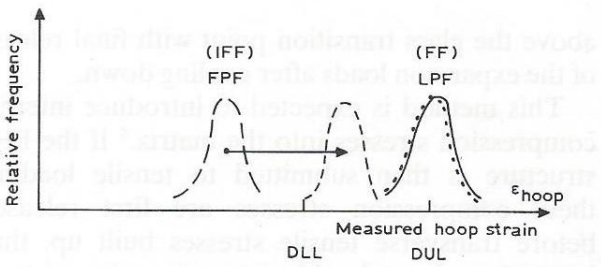


Fig. 1. First ply failure and last ply failure limits. FPF ≈ interfibre failure (IFF). DLL, Design limit load; DUL, design ultimate load; FF = fibre failure; j_u, DUL/DLL (i.e. 1·5).

are caused by transverse tensile stresses $\sigma^t_{\perp}$ in interaction with intralaminar shear stresses $\tau_{\#}$. The cracks first occur in those layers of a multilayer FRP where the fibre direction is transverse, or almost transverse to the prime load direction.

In order to utilise the intrinsic fibre strength in multilayer FRP, the onset of interfibre/matrix cracking has to be delayed and it was the aim of an EURAM project (MA1E/0049/C) to achieve this by applying design/manufacturing means (Fig. 2), which are in analogy to the concept of prestressed concrete. The following method was pursued: controlled expansion of a FRP structure by using an expandable mandrel. Expansion is done on a finished standard wound tube at a temperature

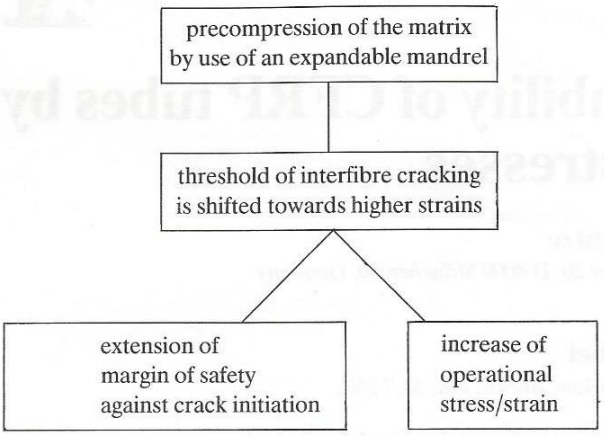


Fig. 2. Method to increase the onset of interfibre/matrix cracking.

Table 1. Overall objectives of the project

— Increase of the limit of usability (weeping level) of pressure vessels without liner
— Increase of operational frequency of fast rotating tubes (cracks cause out-of-balance loadings)
— Improvement of damage tolerance behaviour (impact resistance) of structures
— Improvement of resistance against environmental loadings (aggressive fluids, etc.)

above the glass transition point with final release of the expansion loads after cooling down.

This method is expected to introduce internal compression stresses into the matrix.[4] If the FRP structure is then submitted to tensile loading, these compression stresses are first released before transverse tensile stresses built up, thus increasing the tolerable operating stress/strain range before interfibre/matrix cracking does occur. Standard wound tubes (no prestrain) were tested to gain reference data.

The project was aimed at an improvement of structural behaviour under operational loads due to the effects from a compressed matrix and the lack of microcracks (see Table 1). This is achieved by transferring biaxial stressing from operational loading to simple $\sigma_{\parallel}$-stresses. An advantage here is the fact that $R^{c}_{\perp}$, is several times higher than $R^{t}_{\perp}$ and in addition that the interactively working pair of stress components $(\sigma^{c}_{\perp}, \tau_{\#})$ is less crack critical than the combination $(\sigma^{t}_{\perp}, \tau_{\#})$.

As a means to achieve the project's objectives first a single reproducible economic fabrication method has to be selected and then applied to the tube chosen. Table 2 summarises the manufacturing steps for the 'precompressed tube' and Table 3 the verification plan for the project.

Table 2. Manufacturing steps for a 'precompressed tube'

— Winding of a tube on standard mandrel
— Completion of gelling and curing
— Transfer to expandable mandrel
— Heating to glass transition temperature
— Diametral expansion
— Cooling down with expansion load applied
— Release of expansion load

The partners collaborating in the project are URENCO (UK), MAN (Germany) and RISØ (Denmark); their distribution of tasks is shown in Table 4.

2 MATERIALS AND FABRICATION OF TUBE

As constituent materials of the FRP duroplastic or thermosetting matrices and fibres like carbon (C), glass and kevlar might be used.

For this project, carbon fibres and a thermoset matrix were chosen as well as a thin-walled tube (Fig. 3 and Table 5) with a lay-up pattern of [90/ ±25/90] wound from T800 and M40 carbon fibres using a hot curing epoxy resin as matrix. A detailed list of the composite's thermo-mechanical properties is given in Table 6. Figure 4 shows the dependency of the stress–strain curve of the matrix on temperature.

It is known from literature that the thickness of a 'transversely loaded, embedded layer' has an influence on its interfibre/matrix cracking: the thicker the layer the more sensitive it is to cracking. As in this study a low threshold level for the onset of interfibre/matrix cracking is desirable, this lay-up pattern with a relatively thick helix layer was chosen; thick, with respect to what can be achieved in production winding. The thickness ratio of hoop wound layers to helix layer is 0·67. When submitted to either hydraulic pressurisation or to rotational spin load testing the prime stress direction is the circumference of the tube, but tensile stresses are also generated in axial direction. A stress/strain analysis revealed that at a strain $\varepsilon_{\parallel}$ of 1·2% in the hoop layers a transverse fibre strain $\varepsilon_{\perp}$ of approximately 0·96% (factor 0·8) in the helix layers occurs; this is much higher than the transverse failure strain $e^{t}_{\perp}$ of a unidirectional M40 layer. Therefore, extensive interfibre/matrix cracking had to be expected for this specimen.

Table 3. Verification plan for the 'precompression tube' project. Goal: shift FPF threshold level from $\varepsilon_{hoop} = 0{\cdot}8\%$ to $1{\cdot}3\%$

Requirements/constraints	Verification approach
The choice of an optimal precompression process	Theoretical comparison of several processes
A simple, reproducible precompression process inclusively mandrel	Design, analysis, manufacturing and application of the mandrel
Reliable material data for the investigation	Material test programme
Creep will be of no significant influence on precompression effect	Creep tests on matrix, 90°, ±45° specimen
The creation of a theoretical basis for the analysis	Compilation of (linear elastic) classical laminate theory with creep theory
A creep analysis	Numerical, by FEM code MARC
Mechanical load induced cracks will really arise later	Proof by acoustic emission measurement and crack counting
Uncontrolled moderate temperature rise will hardly affect precompression state	Stress relief tests
The ultimate tube strain (LPF) will almost remain in the new process	Burst tests
The level of prestrain on FPF shift is of importance and to be investigated	Comparison of basis test specimens (0%) with the 0·4% and 0·8% precompressed, comparison with analytical results
The precompressed tubes keep shape over time	Geometrical measurements on specimens
The formulation of design recommendation	Evaluation of theory and test results

Table 4. Distribution of tasks

URENCO	Project management Design expandable mandrel Procurement/testing carbon fibres Theory
MAN	Design/manufacture expandable mandrel Development winding/expansion route Manufacture test specimens Short term mechanical testing of matrix, unidirectional laminae Spin load testing Microstructural examinations Theory
RISØ	Short/long term mechanical testing Hydraulic pressurisation tests with acoustic emission Microstructural examinations Theory

Table 5. Material used

Carbon fibres by Toray	
M40–6K–50B, ø ≈ 7 μm, helix T800H–12K–40B, ø ≈ 6 μm, hoop	
Matrix material by Ciba-Geigy	
Epoxy resin:	MY750
Hardener:	HY917
Accelerator:	DY070
Mixing ratio:	MY750/HY917/DY070(100/87/0·5)
Gelling:	4 h at 105°C
Curing:	4 h at 160°C

For the compression process the knowledge of the glass transition temperature T_G is essential. As changes of the mechanical properties in the glass transition domain are of interest, dynamical mechanical analysis (DMA) was selected as the method for measuring the damping curve which allows determination of T_G(DMA). Unidirectional test specimens were made using both fibre types and the epoxy system selected.

3 DEVELOPMENT OF PRECOMPRESSION PROCESS AND PRESTRAINING DEVICE

It has long been attempted to overcome the before-mentioned deficiencies of FRP by employing more suitable plastics respectively matrix materials, especially with increased elongation at failure (e_m^t). In this sense some trials have been undertaken with a more flexible matrix to increase crack initiation; however, a bad effect on fibre–matrix bonding was observed. There was also a lower environmental resistance of this more flexible matrix and this was another reason to abandon these investigations.

Table 6. Thermo-mechanical properties

	'Hard' matrix (RT)		'Soft' matrix (T_G)		
	T800	M40	T800	M40	Remarks
$E_{\parallel}$ (N/mm²)	170 000	230 000	167 000	225 000	
$E_{\perp}$ (N/mm²)	9 000	6 500	900	650	*a*
$G_{\#}$ (N/mm²)	7 500	6 000	750	600	*a*
$G_{\perp}$ (N/mm²)	3 200	2 320	—	—	*b*
$\nu_{\perp\parallel}$	0·28	0·26	0·43	0·43	*c*
$\nu_{\perp\perp}$	0·40	0·40	—	—	*b*
$R^t_{\parallel}$ (N/mm²)	2 700	1 500	—	—	
$R^t_{\perp}$ (N/mm²)	50	55	—	—	
$R^c_{\parallel}$ (N/mm²)	1 400	1 000	—	—	
$R^c_{\perp}$ (N/mm²)	140	140	—	—	
$R_{\#}$ (N/mm²)	80	70	—	—	
ILSS (N/mm²)	89	76			*b*
$\alpha_{T\parallel} \times 10^6$	−3	−2	−3	−2	
$\alpha_{T\perp} \times 10^6$	+40	+50	(+40	+50)	*b*
$\alpha_{M\parallel}$	0	0	—	—	
$\alpha_{M\perp}$	0·37	0·30	—	—	*b*
$e^t_{\parallel}$ (%)	1·68	0·51	—	—	
$e^t_{\perp}$ (%)	0·70	0·58	—	—	
$e^c_{\parallel}$ (%)	0·60	—	—	—	
$e^c_{\perp}$ (%)	3·36	2·67	—	—	
$e_{\#}$ (%)	>1·7	—	—	—	

Matrix: MY750 (100)/HY917 (87)/DY070 (0·5). Curing: 4 h, 105°C + 4 h, 160°C.
a, Respecting temperature and relaxation time; *b*, not relevant; *c*, estimated by formula, via $\nu_m(t, T)$.
ILSS = Interlaminar shear strength.

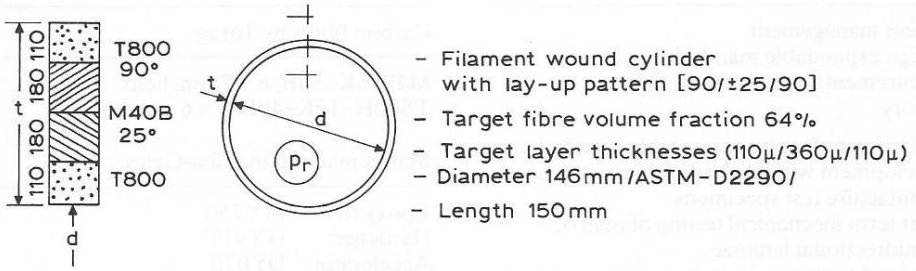


Fig. 3. Geometrical description of the tube specimen.

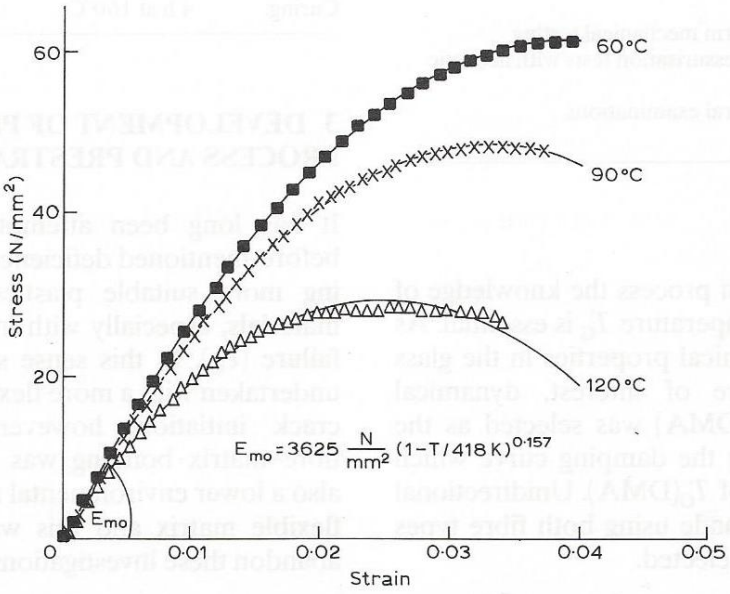


Fig. 4. Stress–strain curve of matrix at different temperatures.

A much higher improvement can be obtained by using very thin layers in the laminate, using the beneficial effect of layers embedding the crack sensitive layer. This effect can be explained by fracture mechanics.

In the past, several approaches for increasing the threshold for crack initiation were investigated. Table 7 summarises the typical approaches.

Within the scope of this research work it was intended to introduce built-in stresses into a CFRP composite by a so-called thermo-mechanical treatment with the use of an expandable mandrel. Three process variants were initially considered. In the first process variant the CFRP structure is wound on the expandable mandrel, and immediately following winding and prior to any gelling and curing the mandrel is expanded. Gelling and curing is done on the expandable mandrel with the wind being in the expanded state. Following cooling down to ambient temperature the expansion is released.

The second process variant considered is a variant of the previous one. The CFRP structure is wound on a standard mandrel and is part-gelled on this mandrel, i.e. it is heated to the gelling temperature of 105°C and kept there for 2 h, which is half of the standard gelling duration. This makes the wind strong enough to be transferred to the expandable mandrel. On the expandable mandrel the wind is then heated up again to the gelling temperature and the mandrel is expanded to a predefined strain. Gelling and curing is completed in the expanded state; the wind is then cooled down to ambient temperature and the expansion is released. The third variant was regarded to be the most promising approach. It follows a patent by Puck[3] for the fabrication of improved hollow bodies. The multilayer CFRP structure is wound on a standard mandrel and gelling and curing is completed as normal. The wind is then transferred to the expandable mandrel and the hard or glass elastic tube is then heated up to an optimal process temperature T_{GO}, and then radial-pressure loaded, i.e. expanded to predefined radial strain. The expansion is kept at this temperature for a short time. In the expanded state the tube is then cooled down to the hard-elastic state, locking internal stresses in the layers when the expansion is released. The resulting structure is internally stressed or prestressed and therefore particularly well suited to alternating directions of loading or, according to the orientation of the fibres produced, to resisting variable loads in a given direction.

Table 7. Ideas to 'lift' the level of crack initiation

Use of a more flexible matrix
Use of several thin layers instead of one thick layer
Mutual thermo-mechanical constraining of parts of a structure (like an autofrettage)
Thermo-mechanical treatment of
• an uncured structure
• a partly gelled structure
• a cured structure (see Ref. 3)

Based on previous work the first variant was not followed up in this research. Such a process would have required a complicated mandrel design and the earlier experiments had shown that applying expansion to a CFRP structure prior to any gelling presses the epoxy out of the wind, resulting in a non-uniform fibre volume fraction distribution.

For better understanding, a comparison with the well known prestressed concrete process will be made. This is a process which in a single *layer* stresses the fibres against the matrix (concrete). In the authors' process this effect is implicit (microscopic stresses ≡ built-in stresses of the second type) in each layer but the main effect is the mutual constraining of all layers in a *laminate* (macroscopic stresses ≡ built-in stresses of the first type). The microscopic stresses above are in equilibrium across the thickness of each layer, whereas the macroscopic stresses are in equilibrium across the laminate. From the laminate strains the microscopic stresses and strains may be derived.

An expandable mandrel suitable for the two remaining expansion processes has been designed, manufactured and commissioned. The principal lay-out of the mandrel and the design requirements were as given in Fig. 5. The mandrel is a mechanically expanding one made up of eight wedge-shaped segments, which are hydraulically driven in the axial direction over internal wedge-bearing surfaces, thus producing a radial expansion. The angle of inclination of the bearing surfaces is 2°. The mandrel shaft is supported at both ends. The mandrel can be rotated by a drive unit, which is connected to one end of the mandrel. It is heated internally by an oil heating system. A cross-section through the mandrel is also shown in Fig. 5: one can see the inner massive shaft and the eight wedge segments. The longitudinal gaps which will occur between the segments during expansion are bridged by a thin sleeve made from high strength maraging steel.

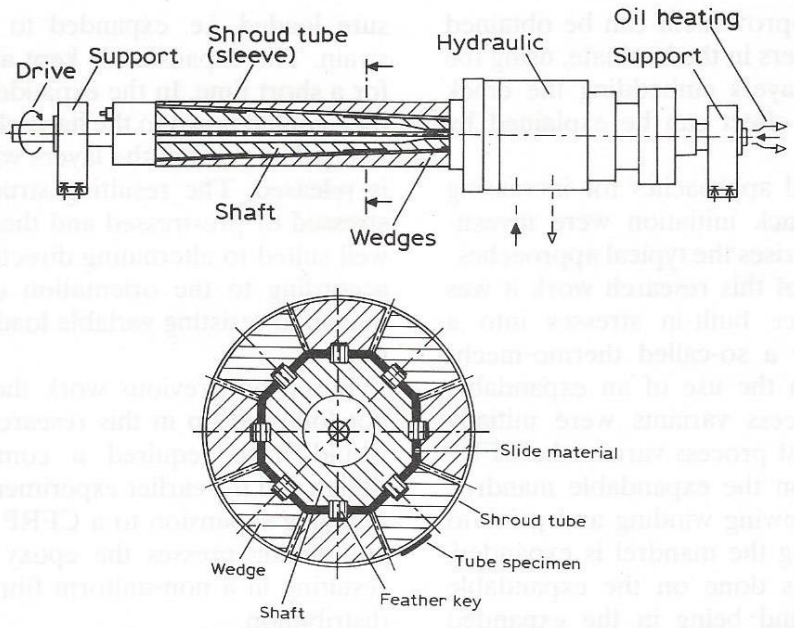


Fig. 5. Description of expandable mandrel. Design requirements: capability for diametral expansion to 1·2%, operating temperature range up to 160°C, expansion of wind section of 600 mm length, easy handling and operation.

This sleeve represents the outer surface of the mandrel. For the surfaces of the internal wedge bearing a material was chosen whose coefficient of friction reduces with temperature; this prevents self-locking of the wedges at elevated temperature. The hydraulic pressure is applied by a manual pumping system. During operation the mandrel is surrounded by a heat insulation box to minimise heat losses to the environment.

Project design development tests (commissioning trials) were carried out to establish an operating process for the expandable mandrel. It was found that (see Ref. 3):

- an oil temperature of 180°C was required for heating a CFRP wind being on the mandrel to a maximum temperature of 160°C; cooling down was done by pumping cold oil through the heating system;
- at 160°C process temperature a gradient of less than 3°C was measured over the total length of the mandrel;
- the uniformity of the diametral expansion of the mandrel was found to be less than 0·02 mm in axial and hoop direction; and
- there was a linear correlation between the axial movement of the mandrel during expansion and the diametral expansion; this allowed the diametral expansion to be monitored by the axial mandrel movement.

The choice of optimum temperature and hold time is of great importance for the process. The process has to guarantee a good relaxation of the matrix by viscous flow and non-visco-elastic redeformation. Relaxation depends on temperature and time. To avoid squeezing, the optimum temperature should be some degrees above T_G(DMA) (see Fig. 6). Measurements were made at a frequency of 1 Hz covering the temperature range 25–210°C. The maximum of the damping curve is about 145°C and it was therefore decided to carry out the expansion 5° above the glass transition temperature at $T_{GO} = 150$°C. To support the decision on taking 5°C above T_G the much more rapid decay of the G-modulus in the case of pure resin has to be considered. Such a DMA curve for the matrix chosen, but gelled and cured using slightly modified parameters, is depicted in Fig. 7.

Thus, the optimum (shortest) duration of the expansion process can be defined. Based on earlier work, a hold time at the optimum temperature T_{GO} was estimated to be 10–15 min and is determined by the creep behaviour of the matrix as the only constituent of the FRP exhibiting creep. Figure 8 outlines the essential process data of the precompression process.

The different prestrain levels do not make a difference in hold time because higher prestrain obviously needs more relaxation but the higher stress due to the higher prestrain equilibrates this. Stress is the third parameter that influences relaxation.

In the following, specimens expanded according to Puck's process (third process variant) are

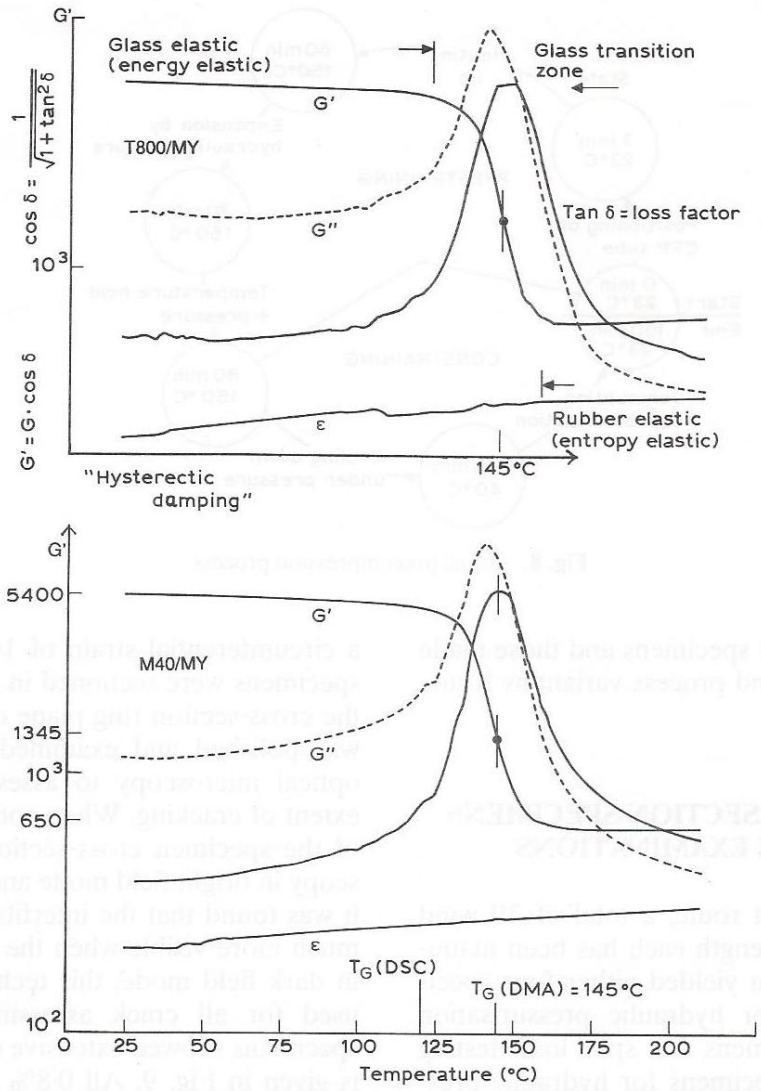


Fig. 6. DMA-curves of the tube materials, torsion pendulum test. G = shear modulus.

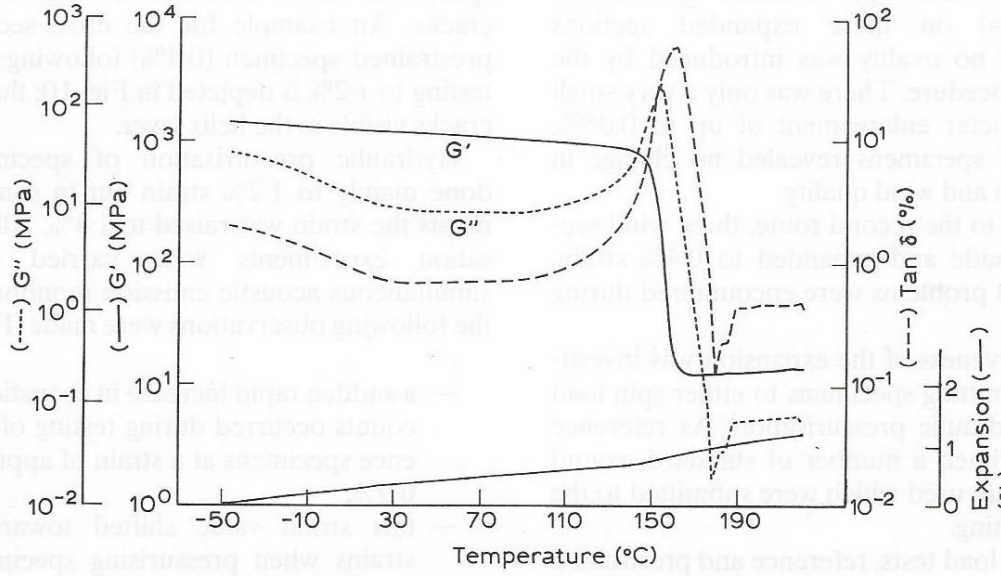


Fig. 7. DMA curve of matrix, MY750-HY917-DY070. DN 53445.

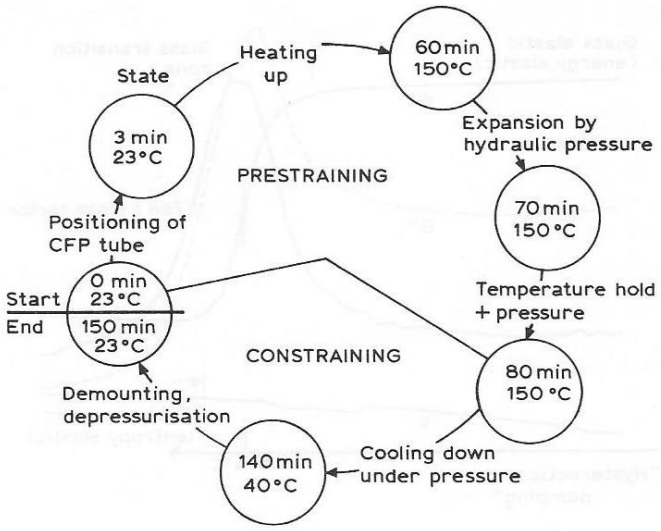


Fig. 8. Final precompression process.

referred to as Route 1 specimens and those made according to the second process variant as Route 2 specimens.

4 TESTS ON TUBE SECTION SPECIMENS INCLUDING CRACK EXAMINATIONS

According to the first route, a total of 39 wind sections of 600 mm length each has been manufactured. Each section yielded either four specimens of 150 mm for hydraulic pressurisation testing or two specimens for spin load testing together with two specimens for hydraulic pressurisation testing. Of these 39 wind sections 10 have been expanded to 0·4% strain and nine to 0·8% strain. Metrology (detailed geometrical measurements) on these expanded sections revealed that no ovality was introduced by the expansion procedure. There was only a very small residual diameter enlargement of up to 0·05%. Sectioning of specimens revealed no change in lay-up pattern and wind quality.

According to the second route, three wind sections were made and expanded to 0·4% strain. Also here, no problems were encountered during expansion.

The effectiveness of the expansion was investigated by submitting specimens to either spin load testing or hydraulic pressurisation. As reference or basis specimen a number of standard wound specimens were used which were submitted to the same load testing.

In the spin load tests, reference and prestrained specimens were spun to a speed corresponding to a circumferential strain of 1·2%. Afterwards the specimens were sectioned in the centre plane and the cross-section ring plane of one specimen half was polished and examined by high resolution optical microscopy to assess quantitatively the extent of cracking. When comparing examination of the specimen cross-section by optical microscopy in bright field mode and in dark field mode, it was found that the interfibre/matrix cracks are much more visible when the examination is done in dark field mode; this technique was therefore used for all crack assessments. All reference specimens showed extensive cracking; an example is given in Fig. 9. All 0·8% and almost all 0·4% prestrained Route 1 specimens were free of cracks; in the latter case, one out of a total of nine specimens tested exhibited a small number of cracks. An example for the cross-section of a prestrained specimen (0·4%) following spin load testing to 1·2% is depicted in Fig. 10; there are no cracks visible in the helix layer.

Hydraulic pressurisation of specimens was done mainly to 1·2% strain but in some experiments the strain was raised to 1·4%. All pressurisation experiments were carried out with simultaneous acoustic emission monitoring. Here the following observations were made (Fig. 11):

- a sudden rapid increase in acoustic emission counts occurred during testing of the reference specimens at a strain of approximately 0·9%;
- this strain value shifted towards higher strains when pressurising specimens were prestrained to 0·4%;

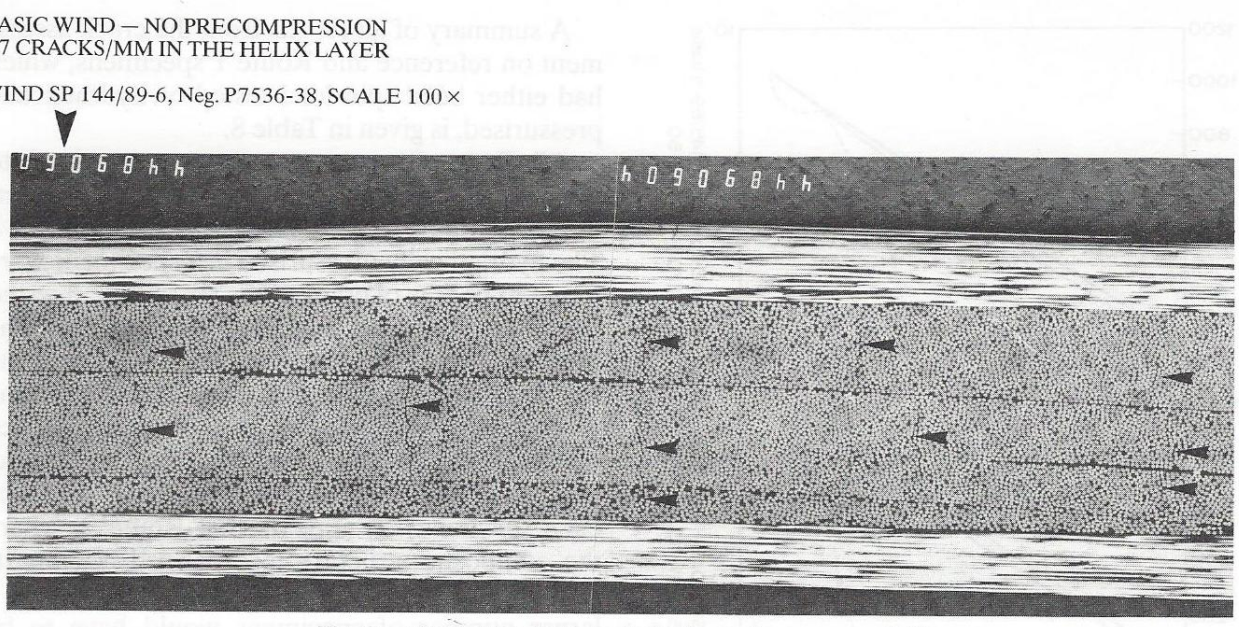


Fig. 9. Crack examination of a basis specimen: $\varepsilon_{hoop} = 1{\cdot}2\%$.

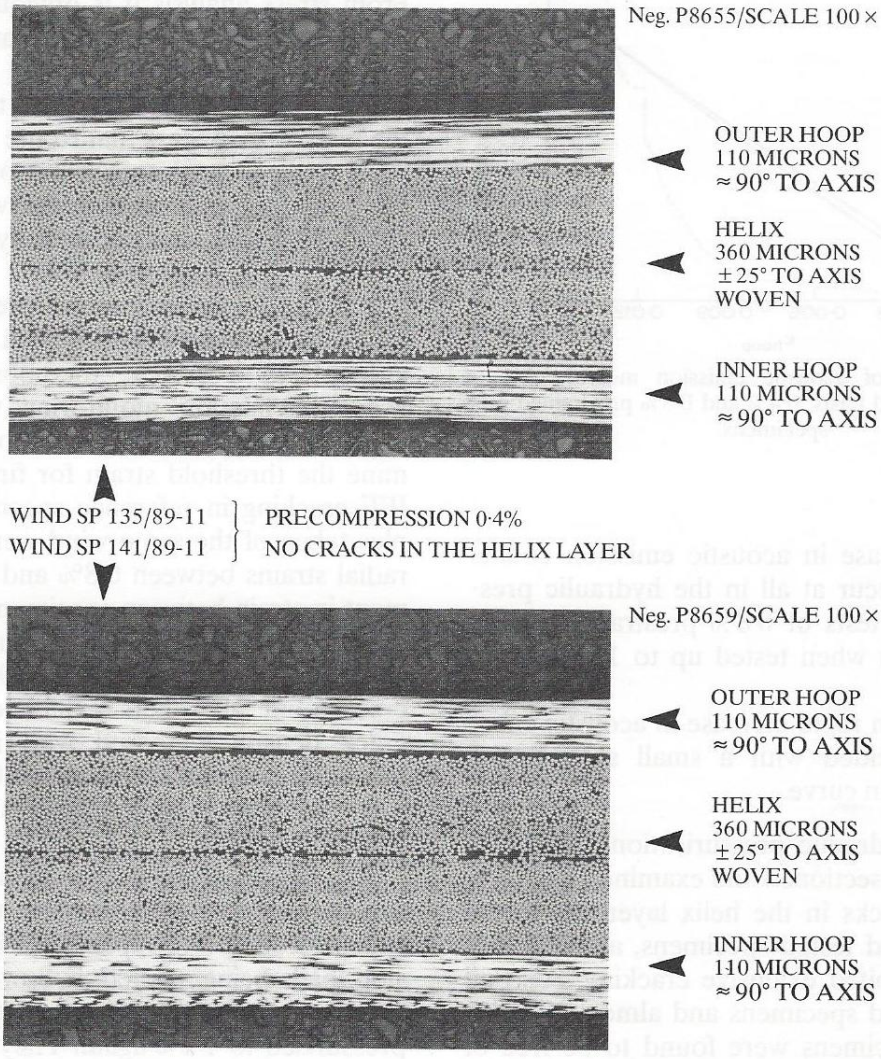


Fig. 10. Crack examination of a 0·4% precompressed specimen by optical microscopy in bright field. Mechanical loading: $\varepsilon_{hoop} = 1{\cdot}2\%$.

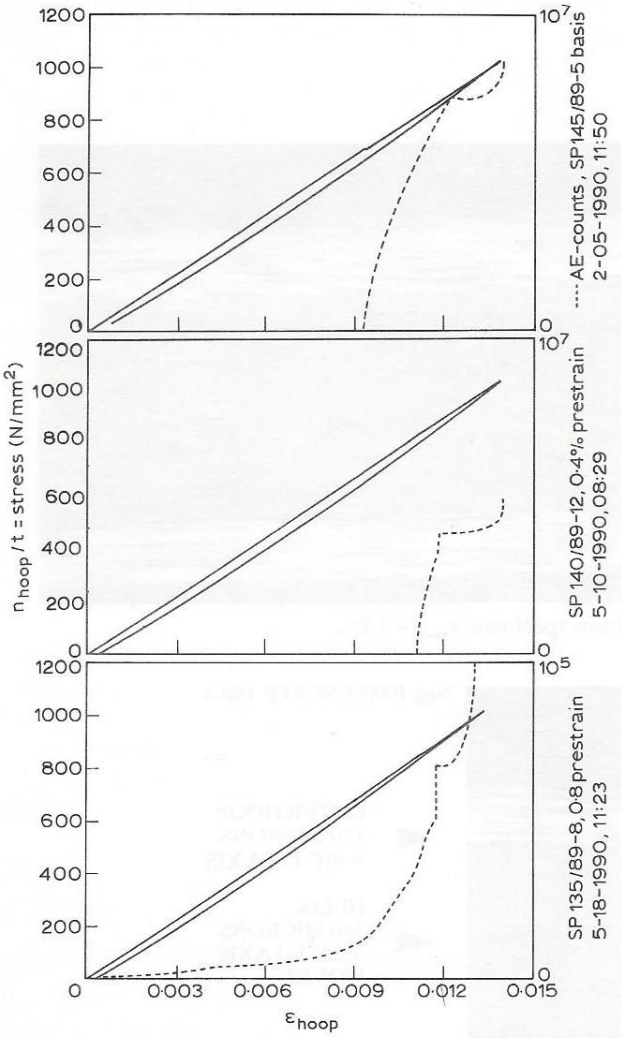


Fig. 11. Results of acoustic emission measurement of hydraulically loaded basis, 0·4% and 0·8% prestrained tube specimens.

- such increase in acoustic emission counts did not occur at all in the hydraulic pressurisation tests of 0·8% prestrained specimens even when tested up to 1·4% strain; and
- this sudden rapid increase in acoustic emission coincided with a small step in the stress/strain curve.

Following hydraulic pressurisation testing, all specimens were sectioned and examined for interfibre/matrix cracks in the helix layer. As in the case of spin load tested specimens, all reference specimens exhibited extensive cracking. Also all 0·8% prestrained specimens and almost all 0·4% prestrained specimens were found to be free of cracks; in the latter case one out of 10 specimens had a moderate number of cracks.

A summary of all results from the crack assessment on reference and Route 1 specimens, which had either been spin load tested or hydraulically pressurised, is given in Table 8.

All Route 2 specimens were prestrained to 0·4% and then submitted to either spin load testing or hydraulic pressurisation to a strain of 1·2%. The hydraulically pressurised test specimens were found to be free of cracks. The six spin load tested specimens revealed a different behaviour; one specimen was completely free of cracks and the remainder exhibited little or moderate cracking with crack densities between 0·05 and 1·84 per millimetre. In all these cases the number of cracks was considerably smaller than observed on reference specimens. It appears that Route 2, where the composite structure is expanded after part-gelling, is less effective than Route 1. However, a larger number of specimens would have to be tested before any final conclusions can be drawn. From stress analysis it is obvious that spin load testing and hydraulic pressurisation lead to different through-thickness stress states with spin load testing, creating transverse tensile stresses in the matrix. It appears that Route 2 leads to somewhat reduced precompression of the matrix and this could explain why cracks were found after spin load testing, but not after hydraulic pressurisation.

Finally, further hydraulic pressurisation tests on Route 1 specimens have been carried out in an attempt to correlate the observations from acoustic emission monitoring with the results from microstructural examinations and to determine the threshold strain for first occurrence of IFF cracking in reference specimens. Five samples taken of the same wind were pressurised to radial strains between 0·8% and 1·2%; the increment in strain between specimens was 0·1%. The results are shown in Fig. 12 (see also Fig. 13). The specimen pressurised to only 0·8% was free of cracks, but all others exhibited cracking. The crack density increased with increasing strain indicating a crack threshold of 0·88%. Also, the total acoustic emission counts increased with increasing strain.

In a last experiment, specimens were submitted to only the thermal treatment they would have experienced during expansion without any expansion loads being applied. Following this temperature cycle, the specimens were hydraulically pressurised to 1·2% again. They exhibited extensive IFF cracking; thus, temperature on its own does not lead to the desired effect.

Table 8. Summary of crack counting results of spin loaded and hydraulically loaded specimens

Specimen type	Spin load test		Hydraulic pressurisation	
	No.	Crack density (1/mm)	No.	Crack density (1/mm)
Reference/basis:				
tested to 1·2%	6	3·30 ± 0·73	8	2·33 ± 2·25
tested to 1·4%	—		2	4·88 ± 0·76
0·4% Prestrained:				
tested to 1·2%	9	< 0·01	4	< 0·26
tested to 1·4%	—		6	0
0·8% Prestrained:				
tested to 1·2%	8	0	5	0
tested to 1·4%	—		5	0

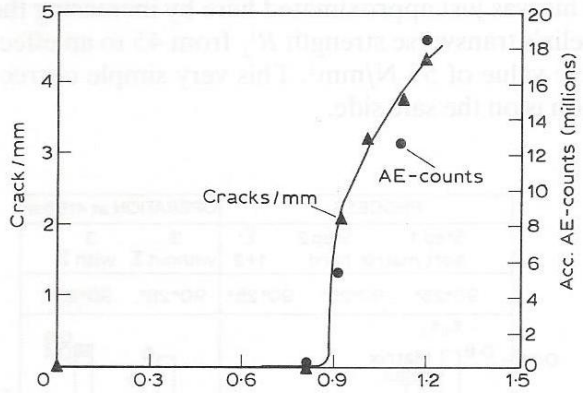


Fig. 12. Crack density and acoustic emission (AE) counts versus hoop strain (RISØ).

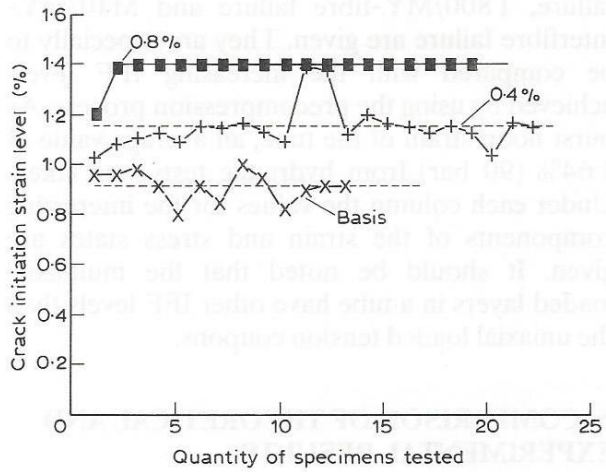


Fig. 13. Summary of RISØ's acoustic emission results of the tube.

During this research, some information was also obtained on the effect of storage on matrix precompression as the time between specimen manufacture/expansion and testing was varied and periods up to 14 months were covered. It was found that storage had no influence on the occurrence of IFF cracking and thus on the effectiveness of the matrix precompression.

5 SUPPORTING THEORETICAL INVESTIGATIONS

For calculations in support of the process one assumption has to be made concerning the structure. It should be working almost like a stable fibre network; that means a portion of endless fibres should lie in the main load directions, e.g. in hoop direction for a centrifugally loaded tube or axially for a hollow tension-compression strut. Another assumption is that the burst strain at fibre failure (FF) should be much higher than the strain at interfibre failure (IFF) in interpretation of Fig. 1.

To carry out the theoretical investigations, the data for thermal and mechanical properties of the two carbon fibre types, the matrix material, and unidirectional laminae have been established. The experiments for determining the long term creep parameters for matrix and unidirectional specimens have not yet been completed. The evaluation of the data is still ongoing and will be reported elsewhere. Judging from the test results there seems to be no significant creep effect.

Table 9 summarises the theoretical investigations made in the framework of this project and Fig. 14 highlights the steps for the computation of the process and signals the superposition of the operational loading.

Finally, the bars in Fig. 15 indicate the states of strain in the T800-hoop ($\varepsilon_{\parallel}$) and the M40-helix layer ($\varepsilon_{\perp}$) during the two process steps, at comple-

tion of the expansion process end as built-in strains, and during operation at IFF level with and without precompressioning.

For the sake of a little increase of the stress in the load carrying T800-hoop layers, the crack critical M40-helix layer is shifted after the process into an advantageous compression state. The last bar indicates, due to the low values of $\varepsilon^t_\perp$, that the precompression process will lift the IFF level significantly.

The IFF level is computed by using the IFF failure criterion of the VDI 2014 guideline.[5]

Figure 16 draws attention to the strain limits achievable in tests by the various tensile test coupons as a measure for the comparison with the tube specimens. As strain limits, values for matrix failure, T800/MY.-fibre failure and M40/MY.-interfibre failure are given. They are especially to be compared with the increasing IFF levels achieved by using the precompression process. As burst hoop strain of the tube, an average value of 1·64% (90 bar) from hydraulic tests was taken. Under each column the values for the interesting components of the strain and stress states are given. It should be noted that the multiaxial loaded layers in a tube have other IFF levels than the uniaxial loaded tension coupons.

6 COMPARISON OF THEORETICAL AND EXPERIMENTAL RESULTS

In Fig. 17 a comparison of the theoretical strains for two prestrain levels (0·4% and 0·8%) with the equivalent test results supported by acoustic emission and crack counting results is done. The 'theory' columns give strain values $\varepsilon_\parallel$ and $\varepsilon_\perp$ at the IFF levels with $\varepsilon_\parallel$ corresponding to ε_{hoop} of the tube. The test results are plotted against increasing ε_{hoop} up to the tube's average burst strain of 1·64% at 90 bar (one single tube reached the extreme values $e_{hoop} = 1{\cdot}84\%$, $e_{ax} = -0{\cdot}31\%$ at 100 bar).

The two test techniques show a good agreement with the IFF levels predicted assuming that the designer has to take minimum strength values and the tests here should represent average values. To obtain better agreement between test results and predictions the thin layer effect in the helix layer has to be considered more accurately. This was just approximated here by increasing the helix's transverse strength $R^t_\perp$ from 45 to an effective value of 55 N/mm^2. This very simple correction is on the safe side.

Table 9. Supporting theoretical investigations

Calculations for mandrel design
Mechanical modelling of the tube
Analysis of the precompression process of the tube
Analysis of creep parameters
Development of a layer creep-model
Creep computations with FEM-code MARC
Test-theory comparison aiming at design recommendations

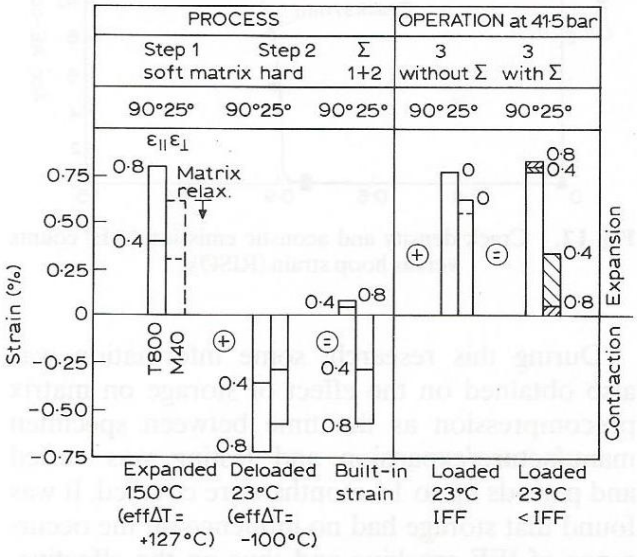


Fig. 15. Hoop strain ε_{hoop} and IFF indicator strain $\varepsilon_\perp(25°)$ of the tube at the two process steps and during operation. IFF failure criterion from VDI 2014. Dotted, without thin layer strength correction on $R^t_\perp$ of helix layers; $\varepsilon_{hoop} = \varepsilon_\parallel$ (T800).

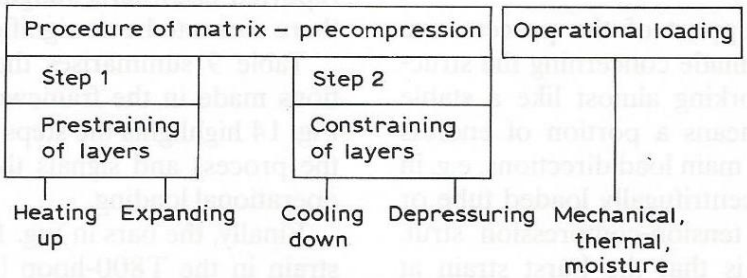


Fig. 14. Determination of the built-in stresses — computational steps.

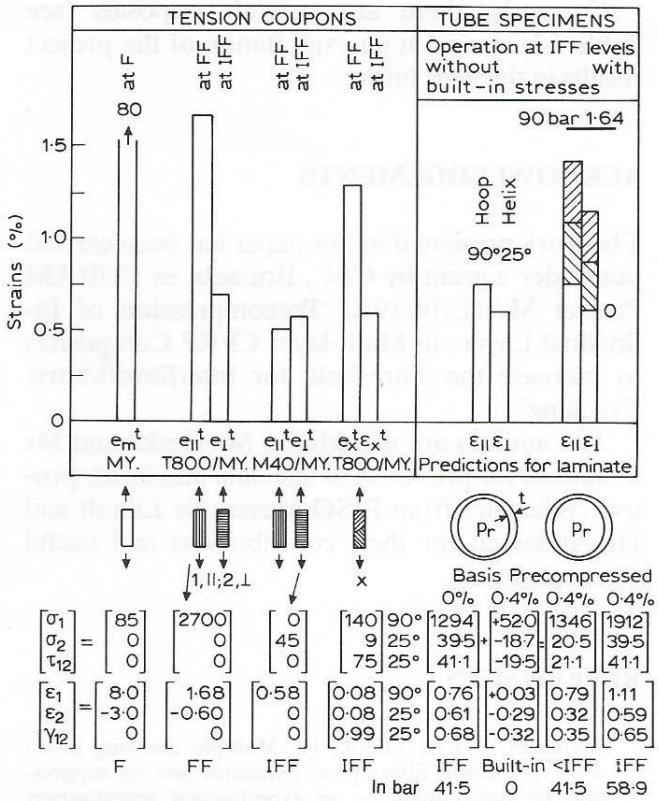


Fig. 16. States of strain and stress (in N/mm²) in test specimens; short term, ambient temperature. Matrix, MY750/HY917/DY070; 1, ∥; 2, ⊥.

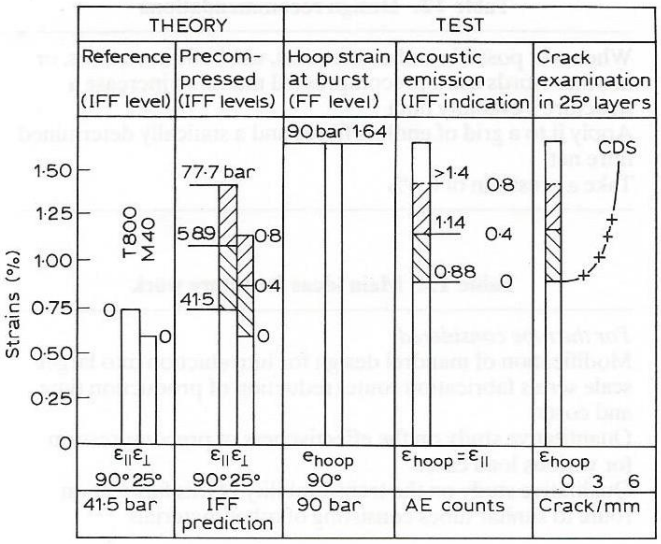


Fig. 17. Comparison of IFF predictions and test results of the tube. Loaded at 23°C; $\varepsilon_{hoop} = \varepsilon_{\parallel}$ (T800 layer); IFF levels: 41·5 bar (0%), 58·9 bar (0·4%), 77·7 bar (0·8%).

Table 10. Check of tube wall stiffness

	Measured in tube test	Predicted from coupon data
$\nu_{ax,hoop}$	0·205	0·206
E_{hoop}	68(70) GPa	69 GPa
Fibre volume fraction	Thickness (mm)	
$\varphi = 64\% \pm 2\%$	0·105	0·360 average values 0·110

Table 11. Compliance with project goals

Goals to be proved	Proof of achievement
A reliable reproducible precompression process	The equipment worked reliably and the application turned out a small scatter
Temperature rises have no influence	Stress relief tests at 100°C
The ultimate tube load will almost remain at the same level	Burst pressure in the case of precompression decayed just slightly
Precompressed tubes keep shape over time (no creep effect)	Geometrical measurements showed no significant changes with 0·4% and 0·8% specimens
A tube to be crack-free until $\varepsilon_{hoop} = 1{\cdot}3\%$	Crack counting was supported by acoustic emission tests

An evaluation of the crack counting results (sign +) from reference tubes outlined a good correlation for the crack initiation levels obtained from acoustic emission, load drop in stress–strain curve and subsequent crack examination. It also suggested asymptotic behaviour in the direction of a critical damage state (CDS). Matrix cracks in the 25°-layer were initiated at 0·9% hoop strain, and the crack density was 4–5 cracks/mm obtained after loading to 1·4% strain. The crack initiation level for the prestrained tubes was raised to 1·1–1·2% strain for the samples initially prestrained to 0·4% strain, and for the 0·8% initial prestrain the crack initiation level is in excess of 1·4% strain.

The comparison of measured and predicted stiffness data (Table 10) confirmed the validity of the elasticity properties, thus giving confidence in the elasticity computations to be carried out.

7 CONCLUSIONS AND DESIGN RECOMMENDATIONS

Being in the final phase of the project the compliance with the project aims can be said to be very good (Table 11) and the various steps of the verification plan have been successfully accomplished by the partners.

The results obtained so far clearly indicate that within a CFRP structure precompression of the

Table 12. Design recommendations

Whenever possible and economical, use built-in stresses, or in other words use a precompressed matrix to increase a structure's usability limit
Apply it to a grid of endless fibres and a statically determined fibre net
Take a prestrain of 0·4%

Table 13. Main ideas for future work

For the tube considered
Modification of mandrel design for introduction into larger scale series fabrication route (reduction of production time and costs)
Quantitative study on the effectiveness of precompression for various load cases
Qualitative study on the transferability of this fabrication route to similar tubes consisting of other materials
For other structures
Application to spacecraft pressure vessels having precompressed liners
Application to torsion shafts

matrix can be achieved using an expandable mandrel and that this leads to an increase in the tolerable stress/strain range as the threshold for interfibre/matrix cracking is shifted towards higher strain values. This increase can either be used for extending the margin of safety against cracking or for increasing the operational stress/strain with the margin being unchanged compared with non-expanded structures.

As main recommendation of this research work the designer should try to apply a 'built-in stress process' wherever possible and economical (Table 12).

Currently, there are several proposals (see Table 13) aiming at an exploitation of the project results in the near future.

ACKNOWLEDGEMENTS

The work presented in this paper has been carried out under a grant by CEC, Brussels, as EURAM Project MA1E/0049/C 'Precompression of Individual Layers in Multi-layer CFRP Composites to Increase the Threshold for Interfibre/Matrix Cracking'.

The authors are thankful to Mr Deska and Mr Schuelein for provision of test data and to the project colleagues from RISØ Messrs Dr Lilholt and Dr Andersen for their contributions and useful discussions.

REFERENCES

1. Andersen, S. I. & Lilholt, H., Multiple cracking in 0°/±65°/0° carbon fibre/epoxy laminates and its suppression by prestraining — an experimental investigation. EUROMECH Coll. 277, SICOMP Technical Report 91-014, June 1991.
2. Heibel, R., Precompression of individual layers in multi-layer composites to increase the threshold for interfibre/matrix cracking. BRITE-EURAM and EUREKA Workshop on Polymer Technologies and Industrial Applications, Ferrara, Italy, 13–15 May 1991.
3. Puck, A., Method of fabricating a hollow body. European Patent EP 0174296 B1, 13 June 1990.
4. Schürmann, H., Gezielt eingebrachte Eigenspannungen erhöhen die Belastbarkeit von Bauteilen aus Fraser-Kunststoff-Verbunden. *Kunststoffe*, **74** (9) (1984) S. 520–6.
5. VDI 2014: German Guideline on 'Development of FRP Structures'. Beuth Verlag, Cologne.

Similar Concepts: Remind the mentioned Pre-tensioning in civil engineering.

19.5 The large Windmill GroWiAn GROWIAN (1977-1982), development and build

19.5.1 Introduction Wind Energy

Wind turbines extract energy from the wind and convert it into electricity.

Wind energy rotors are built with the tower before (leeward) or tower behind (windward rotor position). Windward (Luv) and leeward generally refer to the location of a place relative to the prevailing wind direction, see *Figs.1, 2, 3*. Blade tip speed ratio (*two-blade rotors are faster*), angle of air attack, mass of the wind turbine blade and the blade material involve the essential characteristics.

Classification of wind turbines

Even classical windmills can be allocated to the two basic systems present with the modern wind turbines, too. These can be classified into the categories horizontal orientation of the shaft axis termed Horizontal Axis Wind Turbine HAWT *(meaning rotating axis is normal to the ground*) such as the GROWIAN *(Grosse WindEnergieAnlage),* and vertical orientation VAWT (*axis of rotation is perpendicular to the air stream, Darrieux, Savonius).* These can be characterized:

HAWT characterization: Yaw control mechanism is required to adjust the rotor around a vertical axis to keep it facing the wind. The heavy nacelle containing the gearbox, generator, etc. is mounted at the top of the tower, thus the design and installation is complex. Power coefficient and tip speed ratio are high. (from *wttps://alldifferences.net/difference-between-horizontal-and-vertical-axis-wind-turbine/).* Main components are: Turbine blades, Hub, Nacelle, Power transmission system, Generator, Yaw control, Brakes, Tower. The yaw drive around the vertical HAWT tower takes the rotor to face the wind. The pitch drive rotates the blades in order to reduce the amount of lift when the wind speed becomes too great

VAWT characterization: No orientation of rotor is required; these turbines can generate power with the wind coming from any direction. The nacelle is not required because the gearbox, generator, etc. are located at the ground, thus the design and installation is simpler. Power coefficient and tip speed ratio are relatively low. Main components are: Rotor shaft or Tower, Blades, Support structure, no yaw mechanism is required.

Betz law applied for blade number decision

Albert Betz (*Göttingen*) formulated in 1919 that an ideal rotor can extract a maximum of 59% of the energy from the wind. This is the so-called Betz limit, associated to the kinetic energy extracted from the air flow. It reads

$$P = 0.5 \cdot \rho \cdot A \cdot v^3 \quad \text{with} \quad \rho \text{ air density, A swept area, v air velocity.}$$

If one tries to get more energy out of the wind, the wind slows down further. This reduces the supply of wind to the turbine. Further, there are also losses in the system such as tip losses, wake effects, drive train efficiency losses in the mechanical assembly within the nacelle and blade shape design-based simplification losses.

Number of Blades

In 2007, Siemens found that modern three-bladed wind turbines may achieve 80% of the Betz limit thanks to an improved blade design and an optimally chosen rotation speed. With a two-blade turbine the obtained efficiency is about 5% less. Three-bladed rotors appear to look more aesthetically and orderly. Therefore, the vast majority of wind turbines currently being installed has

three blades. Nowadays two-blade rotors can be designed almost similarly efficient as the three-blade rotors *[Robert Delgado]*

*([Schu12]Peter J. Schubel * and Richard J. Crossley. "Review Wind Turbine Blade Design". Energies 2012, 5, 3425-3449; doi:10.3390/en5093425) and " How many blades are best for wind energy production?" May 29, 2019/0 Comments/by WES - Wind Energy Solutions, Sjoerd Overpelt).*
https://commons.wikimedia.org/wiki/File:Wing_profile_nomenclature.svg#/media/File:Wing_profile_nomenclature.svg).

In the joint German GROWIAN research project (*MAN Neue Technologie was the industrial leader*) - following a contract with the *DLR Göttingen* - the decision in 1978 was for a two-bladed rotor due to less mass, material and maintenance CoSts. The intended first goal of the project was the preparation of documents ready for construction for a plant.

During the project time a fruitful knowledge exchange with the Danish colleagues was realized.

Blade materials, Airfoil profile and Design of the blade

Wood, metals, glass fiber-reinforced composite GFRP, carbon fiber reinforced polymers CFRP, natural fiber reinforced polymer and even armored concrete were the various materials used. These materials have different properties.

Tip speed ratio λ is that essential parameter which influences the rotor performance (*energy output*) most:

$$\lambda = v_{tip} / v = \Omega \cdot r / v \quad \text{with} \quad \Omega \text{ angular (rotational) velocity, } r \text{ radius, } v \text{ air velocity}$$

A higher tip speed λ (*Schnelllaufzahl*) leads to a narrower blade profile and an increase in centrifugal and aerodynamic forces. Aerodynamics of the blade design becomes more critical and noise is increased. The lower torque at lower speeds results in a difficult self-starting.
Fig.1 presents the main features of the airfoil profile of the blade.

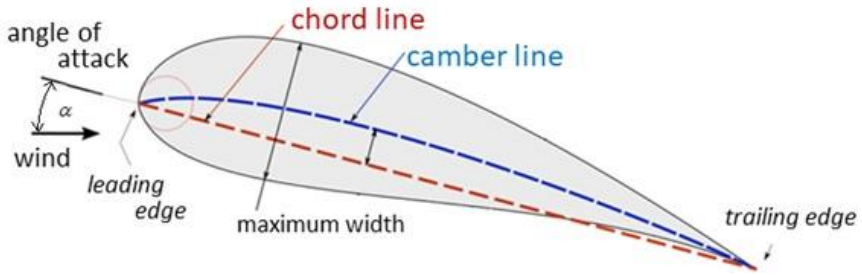


Fig.1: Airfoil profile (Tragflächenprofil) of the rigid rotor blade. Angle of attack. Chord (Sehne), camber (Wölbung). The chord line is a straight line going from the leading edge to the trailing edge; the mean camber line is constituted by the midpoints of all airfoil cross-section segments. Airfoil thickness definitions are different

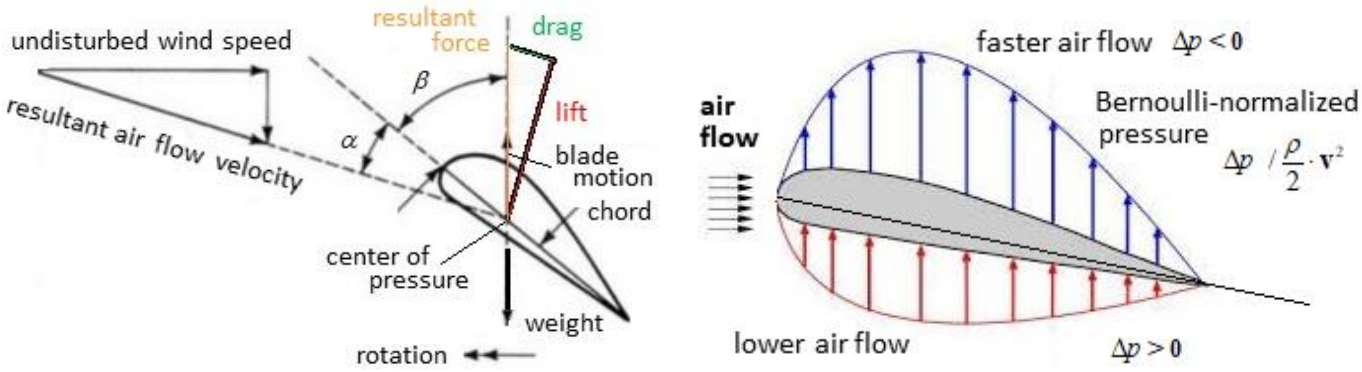


Fig.2 Rigid blade in motion: (left)Aerodynamic forces, center of pressure, pitch angle β and angle of attack α

.

(right) Pressure distribution around the airfoil

The resultant wind velocity in *Fig.2 left* is the vectorial sum of the undisturbed wind velocity and the instantaneous velocity of the blade in motion. The lift (*Auftrieb*) force is normal to the resultant wind velocity, whereas the drag (*Widerstand*) is in direction of the resultant wind velocity.

The aerodynamic moment according to the distance axis of aerodynamic center of pressure to the elastic axis of the blade is to equilibrate by an elastic moment around the elastic axis. In general, the centers of pressure, gravity and stiffness are different.

The ideal blade is defined by above Betz limit, considering the air velocities at the foreseen site and the lift dependent on the shape of the airfoil. Wind turbine blade airfoils are shaped so that the air moving around the blade travels faster on the downwind side of the blade than that moving across the upwind side of the blade, see *Fig.2 right*.

Along the blade length usually the blade consists of several airfoil profiles, twisted by an angle to another, in order to optimize the performance. However, production desires a reduction of too many different profiles and twist angle sizes.

Tower and Foundation

GROWIAN was projected as a leeward (downwind) runner, namely behind the tower. *Fig.3* outlines the diferences of the two rotors types. The cone angle generates bending stress under centrifugal loadings which partly balance the wind bending loadings. The angle ° must be so high to not meet the tower or a guy rope.

The foundation fully depends on the soil situation at the exact site.

Design Load Cases (DLCs) from Standards at present

A worst case loading scenario is presently applied dependent on blade size and method of control. In practice several load cases are considered with published methods detailing mathematical analysis for each of the IEC DLCs. *(OPEN ACCESS. The Load Level of Modern Wind Turbines according to IEC 61400-1. Partial safety factor for fatigue (see IEC 61400-3, 7.6.3).*

Taken into account are: Wind condition, wind with wave (*if offshore*) direction, fatigue life limit state with ultimate strength limit state, partial safety factor concept discriminating three IEC-DLC classes. Input for the start-up, normal shutdown, and emergency shutdown events of DLCs are given.

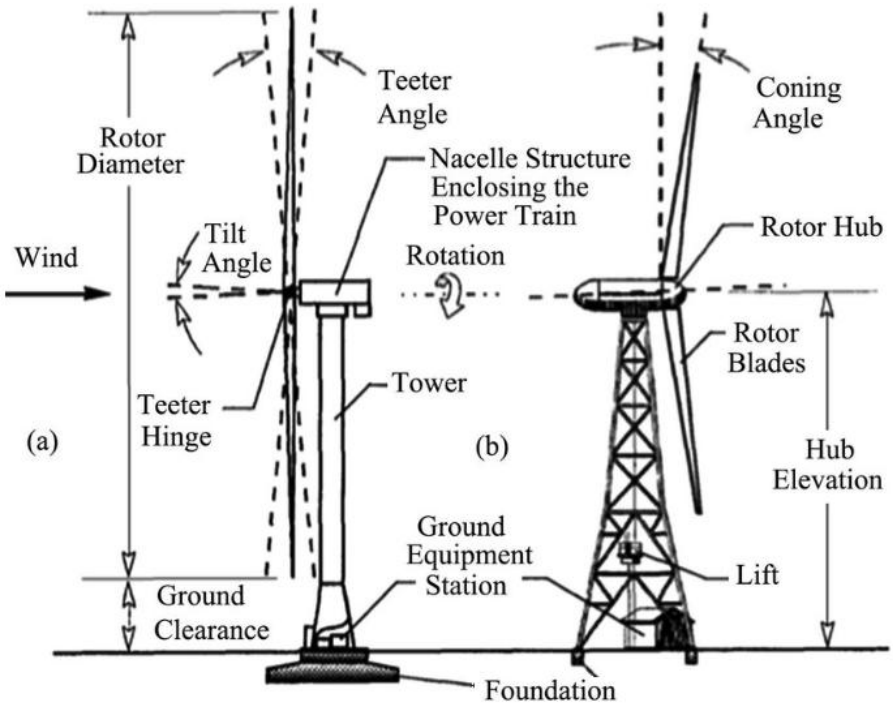


Fig.3: (a) Two-bladed teetered-hub (schwankende Nabe) upwind rotor, (b) Two-bladed rigid-hub leeward rotor. From "CoSt Optimization Modeling of Renewable Energy Sources in Smart-Grid Using SCADA"

19.5.2 Introduction GROWIAN with Task

Back to the root in Germany (reality in the past)

With the exception of the generator, the earlier plants had almost everything that modern wind energy rotors have, but oil, gas and nuclear power have repeatedly overtaken wind energy despite all the research and development efforts. Only energy bottlenecks such as in the first oil crisis in 1973 and global warming changed the situation.

The blade model for GROWIAN comes from the pioneer Ulrich W.Hütter (*1959 university lecturer in aircraft construction at the then Technical University of Stuttgart*) with his prototype for wind turbines, the two-bladed StGW-34. The rotor blades, each 17 meters long, which stood on a 22-meter-high tower, were firstly manufactured using glass-fiber-reinforced plastic (GFRP) and generated an output of 100 kW, which were fed into the grid. Hütter was the first to apply the principles of aircraft aerodynamics to the profiles of wind turbine blades and introduced their rotation mechanism, the "pitching", *Fig.4*.

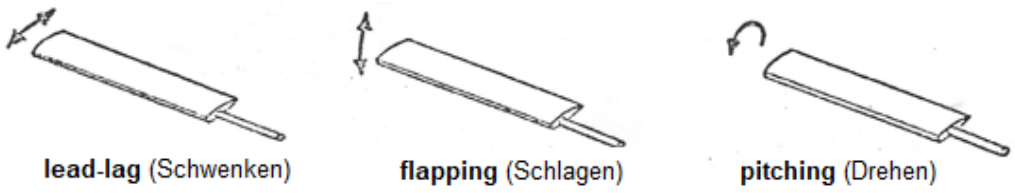


Fig. 4: Motions of the rigid rotor blade

The profile for the GROWIAN blade came from Franz Xaver Wortmann (*from 1974 head of the Institute for Aerodynamics and Gas Dynamics at the University of Stuttgart. He mainly investigated*

questions of turbulence influence in order to achieve a laminar flow). His excellent laminar profiles (*indexed FX*) have been used on many GFRP gliders.

By the early 1980s, almost all successful gliders had them.

The GROWIAN wind energy plant, a challenging civil engineering task

A large scale wind energy converter with a generator of the electrical output 3 MW had to be developed and built. Further design documents for future large plants from the experiences should be created.

GROWIAN was specified to be a horizontal wind turbine HAWT with a two blade rotor with teetered hub in so-called downwind position (*means wind stable position but creates perturbations from the tower*). The rotor diameter should be 100 m and the hub height also. GROWIAN shall produce electricity for direct feed into the grid at wind speeds beyond 6 m/s. Cut-out wind is designed at 24 m/s, nominal wind speed at 12 m/s. Rotor speed is set to 18.5 *rpm* $\pm$15% so that the lowest nominal excitation frequency at operation is f_{op} = 0.44 Hz, $\Omega = 2 \cdot \pi \cdot f$. A planetary gear transfers rotation to a special variable speed generator with a frequency controlled output to the grid. Power regulation is to provide by an electromechanically activated variable pitch, that turns the blades off-wind.

Originally CFRP composite blades were foreseen by the government.

The aerodynamic blade design had to find a geometry that takes sufficient account of strength and stiffness with good aerodynamic performance. In other words: A 'robust design' was to search regarding the variabilities. This required a relatively large blade thickness (chord width) which was fulfilled by the aerodynamic optimal airfoil profiles of F. X. Wortmann. On top, this profile is pretty stable against flutter which is a feared self-excited oscillation.

The Structural parts of GROWIAN were:

Rotor blade, hub (Nabe), nacelle (Gondel, Maschinenhaus), drive train, tower with guys, foundation.

Table 1 collects the design verifications to be executed before certification (Germanische Lloyd).

Table 1: Theoretical design verifications (Sicherheitsnachweise) and some related calculations (Civil Engineering)

1. Stress
2. Static Stability
3. Tip over (Standsicherheit)
4. Deformation (Formänderung)
5. Load-carrying capacity (Tragsicherheit)
6. Usability of materials which are 'not normative' (→ CFRP needs a Single Case Approvement ZiE)
7. Operational Lifetime
8. Fracture Brittleness of Material
9. Operational frequency-compatible Natural frequencies of the Structural Parts
10. Dynamic Behavior (periodic, stochastic and gust impact excitations)
11. Dynamic Stability Behavior of the Full System.

In trade-off studies preliminary design dimensions had to be calculated. This included the type of tower including foundation and possible guy system, number and material of blades, natural frequencies of the full plant following a preliminary design.

19.5.3 Trade-offs, necessary enablers of a good Design Dimensioning

1 Tower Design

With regard to the vibration properties of the system, a parameter analysis showed that a single supercritically operated tower provides construction CoSt advantages over the somewhat more safety-offering subcritically operated towers (*top load mass was taken into account in each case*). Passing with the second excitation frequency through the first tower natural frequency does not allow any inadmissible oscillation deflections to be expected. Therefore, the medium-rigid tower solution was chosen for the to be assumed ground conditions, namely a guyed (stayed*, abgespannt*) tower simply supercritically operating. (*Similarity: the centrifuge in the next chapter is doubl-supercritically run).*

The 100 m hub height emerged as a compromise between higher energy yield, construction CoSts, tower bending natural frequency and unknown assembly/maintenance CoSts (no cranes at that time). Further, vortex vibrations require an outer diameter of the tower of almost 4 m.

For the steel solution, pipe shots of about 9 m length with approximately 20 mm wall thickness and stiffeners at each end of the shot are foreseen. In addition, due to the Reynolds value $R_e \approx 4.5 \cdot 10^6$, as design space limits $D < 3.7$ m and $h < 105$ m were determined.

2 Excitation of the Tower due to turbulent wind

An elastic tower acts like a mechanical filter in the turbulent wind, which only addresses those load components in the wind load frequency spectrum that are in the immediate vicinity of its own frequencies. The tower can therefore perform oscillations in its natural frequency in the stochastic wind. Statements can be made about the expected amplitude in such a random process, since such random processes obey statistical laws. The stochastic random process wind must be determined and can then be described for analytical investigations.

3 Vortex excited transverse oscillation in constant wind flow (vortex resonance excitation)

The so-called 'Karmann vortex road' generates oscillatory transverse driving forces. Significant for the vortex detachment on the flowing circular profile of the tower is the so-called Strouhal number

$$S = f_W \cdot D \cdot / v_W$$ with characteristical diameter D perpendicular to wind,

v_W constant wind velocity, f_W wind release frequency .

The Strouhal number is a function of the Reynolds number

$$Re = v \cdot D \cdot \rho / \mu$$ with ρ air density and μ the kinematic toughness of the air

at 15°C, 1018 hPa $\rho = 1.23\ \mathrm{kg/m^3}$, $\mu = 15 \cdot 10^{-6}\ \mathrm{m^2/s}$

As can be seen from *Fig.3*, S for the operating speed range 6→12 m/s lies in the so-called supercritical range of the Reynolds numbers $1.5 \cdot 10^6$ to $3 \cdot 10^6$.

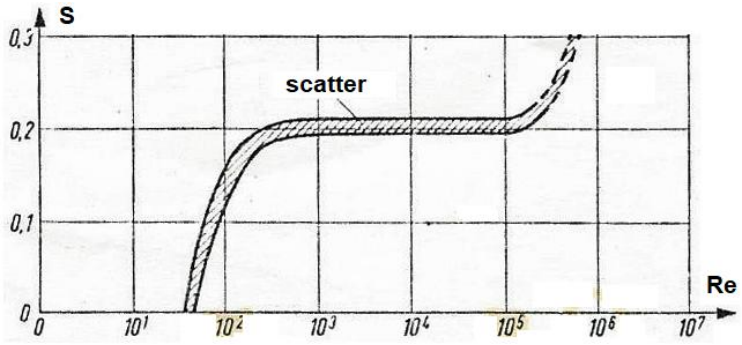


Fig. 4: Dependence of Strouhal number S on Reynolds number Re during the flow around a rigid cylinder

→ So there is practically no periodic excitation for the steel tower.

4 Ovalling of the steel tower

Cross-sectional vibrations of thin circular cylindrical shell constructions can also be resonantly excited by periodic vortex detachments. These are usually done with 2 waves per circumference. The ratio of the hoop natural frequency of the shell to the vortex shedding frequency, can be a critical integer multiple of 1, so that the critical velocity reads:

$$v_{crit} = f_{shell} \cdot D_{shell} / (S \cdot n) \quad \text{with } n = 1, 2, 3, 4, ..$$

→ However, the calculation for the foreseen steel tower wall proves to have no ovalling problem.

5 Guy ring, guy rope and guy foundation

The design of the three guy ropes (*parallel wire bundle each*) is carried out from the point of view: Little scatter of the first tower natural frequency with a preload force that the rope does not become limp (slack, *schlaff*) in any load case. Higher preload force increases the CoSt of guying ring and guy foundation. The guy ring is detachable. Depending on the soil conditions and groundwater level at the installation site, a heavyweight foundation or a ground anchorage (*high groundwater level*) can be useful as a guying foundation.

For a reinforced concrete solution (*concrete Bn 450*) the wall thickness would be about 25 cm (*production using slip formwork*).

6 Blade Design

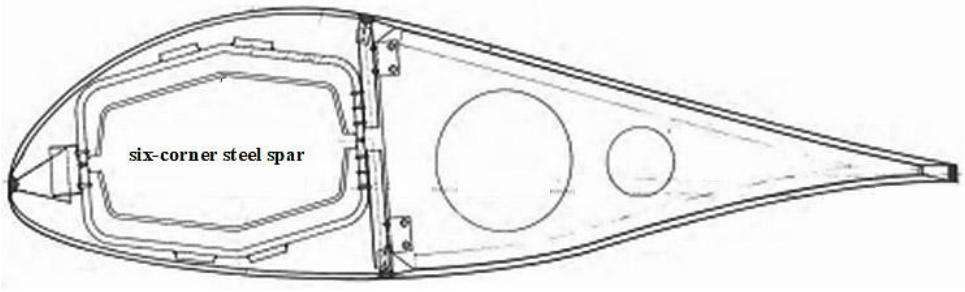


Fig.5: Sketch of a blade cross section depicting the six-corner steel spar

The construction concept was a mixed method with a steel box spar as the load-bearing element. The blade outer skin, connected to the spar via fittings, were made of GFRP. Thus, the rotor blade structure reads: The spar box is designed as a welded construction, the fittings - as connections to

the skin - are welded and have a tolerance-compensating effect, transverse ribs and blade skin are made of GFRP as standard. This design, which originates from glider construction, makes it possible to meet the required low surface roughness and waviness of the selected laminar profile.

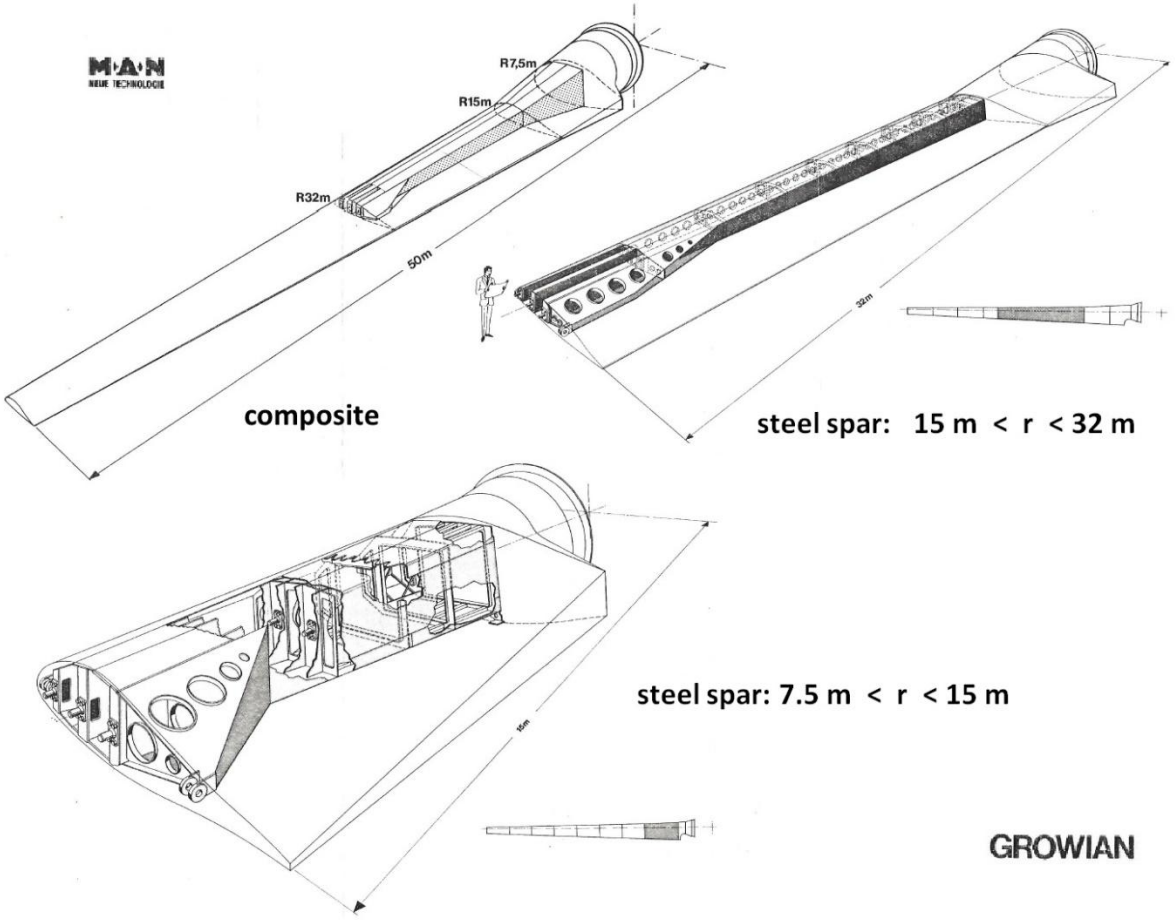


Fig. 6: Segments of the steel spar (Holm)

7 Natural Frequencies

Main task is the fitting of the natural frequencies into the free areas, often termed design 'frequency windows', which are determined by the first and second operating frequencies including an associated scattering range, the so-called tuning. Tuning is performed by separating the natural frequencies from each other and from the excitation frequencies, a very unfavorable system-dynamic coupling is counteracted.

Fig.7 presents the so-called Campbell-Diagram as the means to visualize, how the separation of natural frequencies and excitation frequency is to perform. It is to note that the straight horizontal natural frequency lines are curved in practice due to non-linear effects.

Specification target value is set by the basic operational frequency f_{op} = n / 60 s = 18.5 rpm / 60 s = 0.44 Hz as the essential exciting operational frequency. The first requirement is not to get a coupling of the natural frequencies of the tower with the excitation frequencies of the rotor. Two excitation frequencies must be observed: The first 'exciting' provides the relevant unbalance loads circulating around the rotor axis. The second 'exciting' results from the number of blades times the operating frequency, which gives $2 \cdot f_1$. When over-speeding, 35% higher speeds could be achieved in a short time (*blade becomes adjusted).*

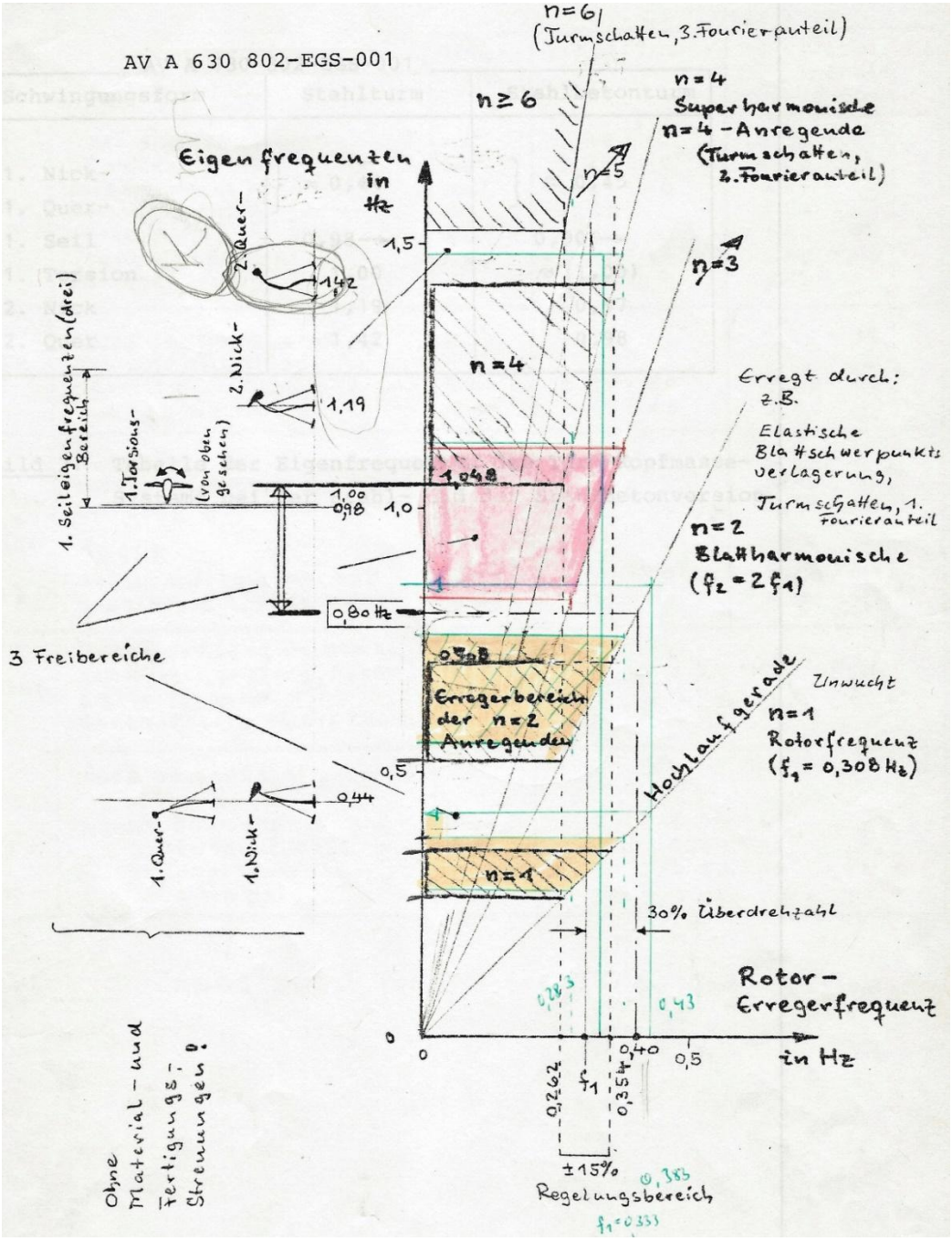


Fig.7: Tuning of the GROWIAN system using the Campbell Diagram [author's sketch 1979]

Subcritically operated towers are stiff, so that the lowest natural frequency is already above the lowest 'exciting'. Single supercritically operated towers are medium rigid, so that the lowest natural frequency of the tower is above the first 'exciting'. For control reasons, a scattering frequency range of ± % is to consider.

To compare are free towers and simply guyed towers. The 'frequency windows' are to regard as depicted in *Fig.3*.

Blade: Determination of the associated natural frequencies. An adjustment of the flapping (*stroke, beating*) natural frequency in the second free area shall be carried out.
Tower: Assumption *Rotor with nacelle are modelled by an excentrical dead head mass at the tower tip*. The data set of the head mass can be subdivided into a firm and a rotating portion. No natural frequency shall be at the blade stroke natural frequency. For clamping in the ground, a joint (*soft ground*) must be considered in addition to the bending spring of a solid ground c_{bend}.

The main data input is put here with the *preliminary data set of the* assembly modules:

module tower:

Height 96.6 m, outer diameter 3.50 m; tower mass without head and ropes 200 t; torsional and bending stiffness at the foot $c_{\text{torsion}} = 1 \cdot 10^{13}\,\text{N} \cdot \text{mm}$, $c_{\text{bending}} = 4 \cdot 10^{13}\,\text{N} \cdot \text{mm}$; wall thickness above 10 m height of t = 18 mm possessing the necessary cross-section area, shear area, area moment of inertia and torsional moment of inertia

double ropes:

Guying height 83 m; guy angle 19°; guy rope mass 35 t; guying ring mass 10 t; cross-sectional area per double rope 11.9 cm^2; Pre-tension force: with unloaded tower 4300 kN, minimum if loaded tower 2860 kN (*one rope in wind direction*), maximum if loaded tower 4900 kN

head:

* Head without rotor and absorber (*Tilger*) 157 t; centre of gravity height 100 m; centre of gravity distance to tower axis -0.70 m; moments of inertia with respect to centre of gravity $J_y = 5.5 \cdot 10^8\,\text{N} \cdot \text{mm} \cdot \text{s}^2$, $J_z = 7.6 \cdot 10^8\,\text{N} \cdot \text{mm} \cdot \text{s}^2$

* Rotor: 118 t, hub point height 102 m, hub point distance to tower axis 8.17 m.

In order to fulill the specified value 0.44 Hz, the obtained natural frequency 0.43 Hz had to be lifted. The practical solution is lifting the height of the guy anchor ring, where the ropes are fastened at the tower.

8 Some short notes on Vibration of the Multi-body System

"The rotor hub is the link between the nacelle and the two rotor blades. It is designed as a pendulum hub. The purpose of the pendulum hub is to compensate for unequal wind forces within the rotor and thereby relieve the rest of the structure of the turbine.

The rotatable rotor blades are connected to each other by the pendulum frame. The pendulum frame is connected to the traverse via the two spherical bearings. The traverse is welded to the rotor shaft mounted in the rotor bearing. The rotor bearing absorbs the weight and forces of the rotating rotor. The pendulum frame absorbs the centrifugal forces of the two rotor blades, the blade bending moments in the wind direction and the circumferential forces from the rotor torque

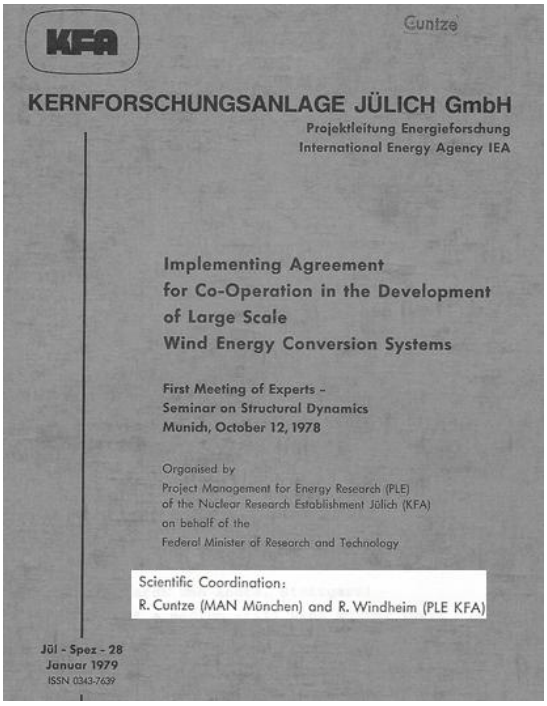
Studies on the rotor component show that of the 3 elastic degrees of freedom of the blade flapping is the lowest frequency. In addition to securing the flutter stability, one then has to check to what extent an elastic modeling of the flapping is necessary. The test showed that the stochastic wind excitation yields virtually no dynamic elevations, so that the overall system can be modeled in a simplified way.

The analysis of the influence of individual disturbances (*monthly gust at operating speed, annual gust at transverse rotor)* shows that with increasing steepness of the wind rise, the dynamic elevation coefficients increase, especially at the wing tips. This fact is understandable, since a maximum dynamic increase is to be expected for an impulsive load of half the duration of the period of blade impact movement (*approx. 0.35 s*). Of the various load cases, the case 'blade passage behind tower' comes closest to this condition, so that the strongest dynamic elevations occur there.

The development of a comprehensive calculation model for the entire system of GROWIAN with all its essential parameters for the dynamic behavior was an extraordinarily extensive task. Initially, therefore, a simplified calculation model for the stability investigation was used. It has a rigid rotor whose impact motion is defined by the position of the blade tip plane in space. The movements of the tower are characterized by two mutually perpendicular bending movements and a torsion. The use of co-rotating rotor coordinates amounts to an investigation with time-averaged parameters of the intrinsically periodic system of a two-blade rotor with asymmetrical bearings. The stability investigation becomes therefore particularly simple, but is not complete with regard to parameter-excited vibrations [*MT-department EGD*].

Targeted local arrangement of a frequency vibration absorber (Tilger) > 10 t in order not only to influence the fundamental frequency f_{op}.

The first phase documents to be drawn up were intended to obtain building and operating permits for a final certification. *Fig.8 left* and *right* document in two conferences the results achieved.


Cuntze

KFA

KERNFORSCHUNGSANLAGE JÜLICH GmbH

Projektleitung Energieforschung
International Energy Agency IEA

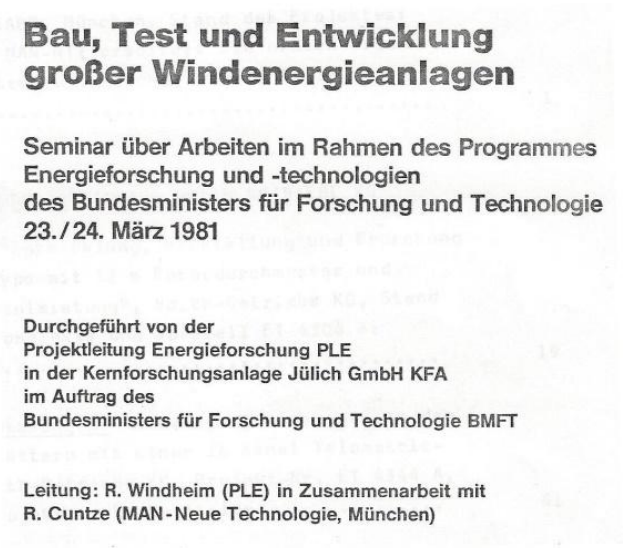
Implementing Agreement
for Co-Operation in the Development
of Large Scale
Wind Energy Conversion Systems

First Meeting of Experts –
Seminar on Structural Dynamics
Munich, October 12, 1978

Organised by
Project Management for Energy Research (PLE)
of the Nuclear Research Establishment Jülich (KFA)
on behalf of the
Federal Minister of Research and Technology

Scientific Coordination:
R. Cuntze (MAN München) and R. Windheim (PLE KFA)

Jül - Spez - 28
Januar 1979
ISSN 0343-7639


Bau, Test und Entwicklung
großer Windenergieanlagen

Seminar über Arbeiten im Rahmen des Programmes
Energieforschung und -technologien
des Bundesministers für Forschung und Technologie
23./24. März 1981

Durchgeführt von der
Projektleitung Energieforschung PLE
in der Kernforschungsanlage Jülich GmbH KFA
im Auftrag des
Bundesministers für Forschung und Technologie BMFT

Leitung: R. Windheim (PLE) in Zusammenarbeit mit
R. Cuntze (MAN-Neue Technologie, München)

Fig.8 (left) International wind energy conference at MAN (1978),
(right) Seminar Research project from KFA Jülich GmbH (1981)

19.5.4 Design Dimensioning, Table 1

Design Load Cases: (1) Nominal operation, (2) Alternating operational loading, (3) Extreme gust.

When determining the safety factors of wind energy rotor plants, it must be taken into account whether an interchangeable component is considered or a practically irreparable component.

Statics: The result of blade *(*see *Fig.9*) pre-dimensiong was:

L = 50 m, blade depth at the root 4.25 m, blade depth at the tip 1.3 m. The load transfer at the root of the blade followed mathematically over hole-bearing but practically it was the bonding.

Fatigue Life: FoS j = 1.2 on top of the windload of all cases. (1) N = 10^8 cycles at nominal operation Ω; (2) N = 10^3 cycles at extreme gust; (3) N = 10^4 cycles at positive with negative swelling loading.

Vibration:

The vibrational forms of impact bending, edge bending and torsion unfortunately occur coupled. Specified as lowest natural frequency was f_1 =0.44 Hz.

An essential change in the design had to be performed because for the originally foreseen CFRP blade a curing procedure for the required root thickness of about 35 mm was not yet available. Therefore, the blade got a 'standard' German Railway St 52.3 steel blade and a GFRP skin.

Structural dynamics of the tower:

The rope-guyed tower was statically and dynamically developed by the bureau of Prof. Jörg Schlaich, Leonhard & Andrä, Stuttgart. The determination of the rope pretensioning forces on the loaded tower was carried out according to (*Abgespannte Maste und Schornsteine. Bauingenieur Praxis, Heft 76, Wilhelm Ernst & Sohn, p.18*). For this purpose, the horizontal force at guying height is required for the dimensioning of the tower. With NASTRAN and ANSYS the eigenshapes, natural frequencies, generalized masses and eigenvectors of the hub point shift were determined as the basis for the overall system-dynamic calculations.

For the tower foundation is planned with an outer diameter of 6.5 m. For a more precise design, the local dynamic soil characteristics at the intended location must be determined (BAM). $E_{dyn} \approx 3000$ kp/cm^2 was used as assumption to estimate the spring stiffnesses $c_{torsion}$ and $c_{bending}$ in the soil.

Table 1: Final technical data of GROWIAN

Performance characteristics: Nominal electrical power 3000 kW, specific area power 380 W/m^2, wind speeds at hub height: switch-5.4 m/s, nominal 12.0 m/s, shut-off 24 m/s, max. survival 60.0 m/s. Annual energy output at 9.3 m/s nominal wind speed approx. 12 GWh.

Rotor: Number of rotor blades 2, diameter 100.4 meters, speed 18.5 rpm. Arrangement to the tower leeward, λ= 8 at nominal wind speed, profile depth at blade tip 1.3 meters, profile depth at the root 4.93 meters, twisting by 18 degrees nonlinear, area 105 square meters, aggravation 0.26, aspect ratio 15.4. Profile at R=0.3 FX-77-W343, at R=0.6 FX-77-W-258, at R=1.0 FX-79-W-151. Leaf mass 23 tons. Material of the rotor blades: steel spar with GRP shell, blade adjustment mechanical-electrical, hub type pendulum hub.

Gearbox: 2 planetary, 1 spur gear stage, total ratio 1:81. Engine house: Steel shell design, wind direction tracking automatically via electric motor, nacelle mass incl. rotor 375 tons

Tower: steel cylindrical, 1-fold guyed, height 100 meters, tower mass 350 tons

Control principle: combined speed-power control via blade setting angle and direct converter.

Generator: asynchronous type, double powered, rated power 3443 kVA at nominal speed, nominal voltage 6.3 kV, speed 1500 rpm, nominal frequency 50 Hz.

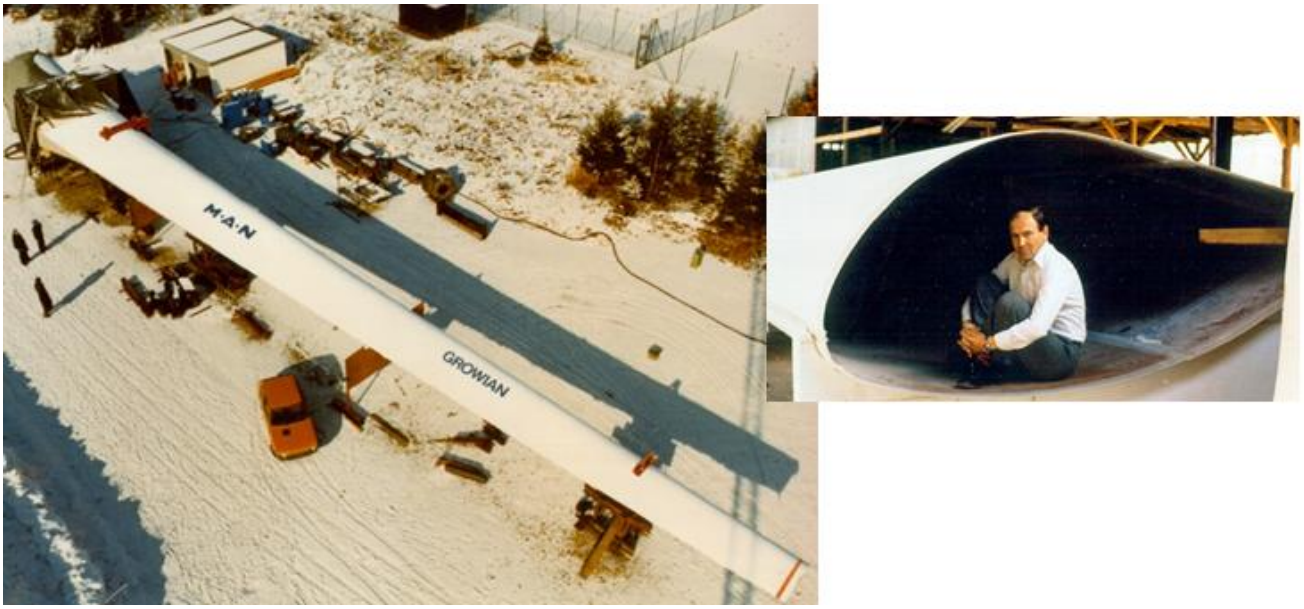


Fig.9: (left) Testrotorblade at IABG 1980, 50 m;
(right) GFRP airfoil at R=15.7 m, colleague Deter Muser presents 'his skin'

Fig.11shows the full plant with the measurement masts in the background.

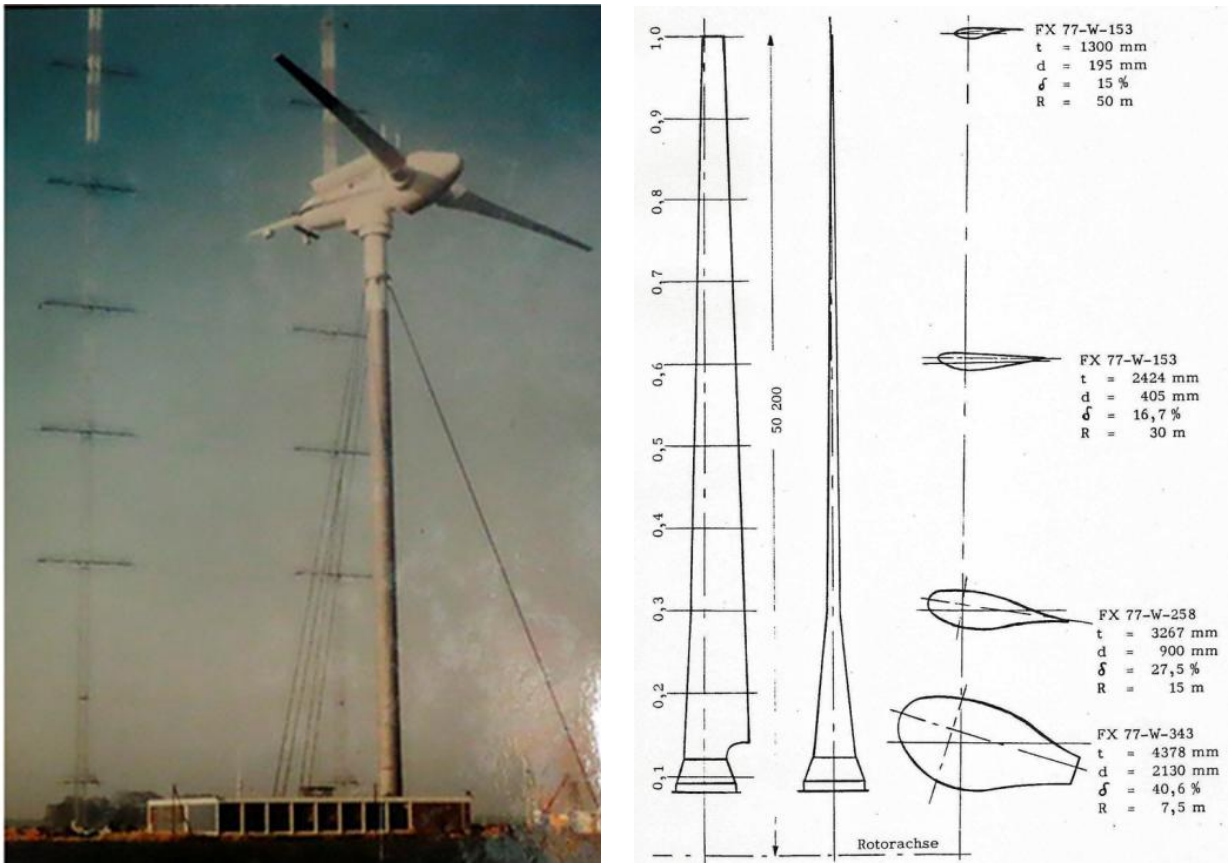


Fig.10: (left, 1982-1987, Kaiser-Wilhelm Koog) GROWIAN with wind speed measurement facility in the background. (right) Cross-section data

Fig.11 depicts the location of the cracked pentulum frame.

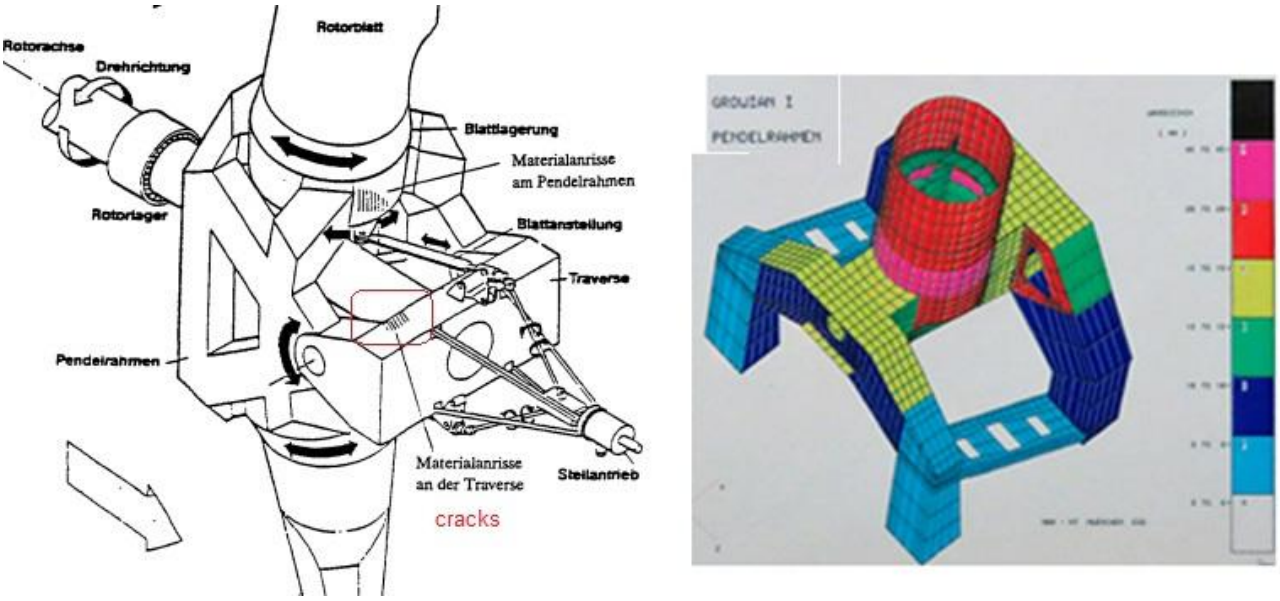


Fig.11: (left) Cracks in the pendulum frame, (right) Necessary FEA to clear design questions of the nacelle cracks, [MAN; Körber (Baureife Unterlagen 1980), S. 79]

Some problems faced during development and operation:

- Deformation compatibility of GFRP skin with steel spar (Holm): *Solved by a smart laminate design of the GFRP skin tuned to steel.* The connection proved to be fatigue-resistant
- There were no large cranes at that time: Hence, a special expensive mounting system for pulling up the rotor with nacelle (hub) had to be developed, *Fig.12*
- Cracks in the door edges of the hub pendulum frame: Too sharply notched by the supplier as the FE-calculations later proved *(many days for 1 CPU run at that time), Fig.11 right)*
- Wind loads showed to be to low: An extra measurement project had to be planned (mast to be seen in *Fig.7, left*).to further provide reliable wind design load cases

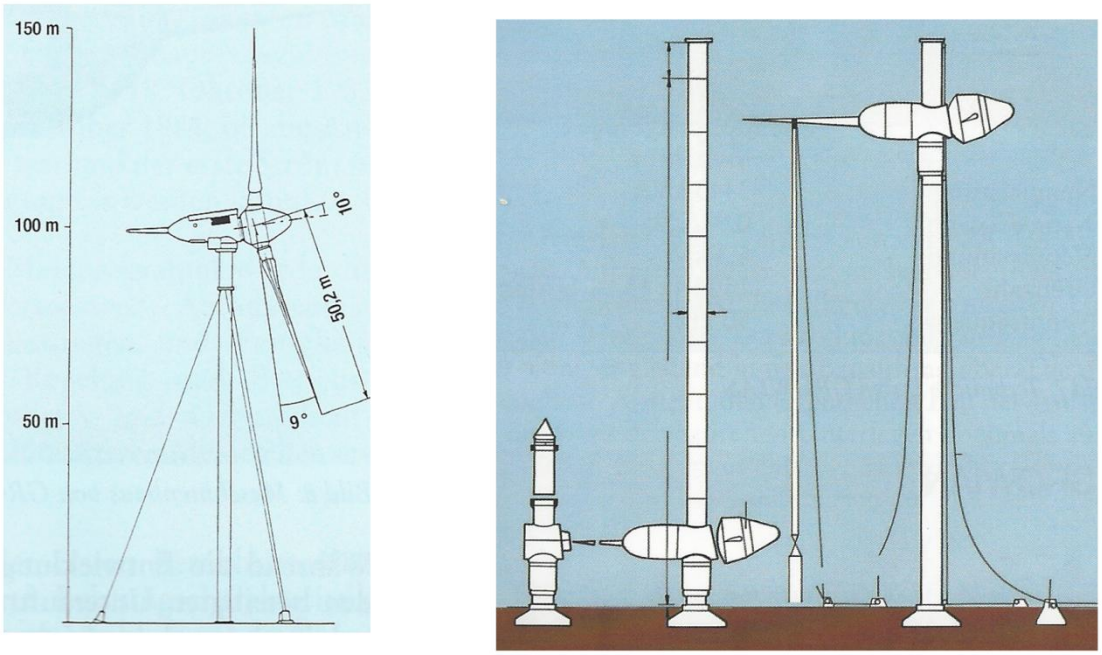


Fig.12: Mounting system

For further information Fig.13 shows the GROWIAN nacelle and the set-up of the AEROMAN which was built in series.

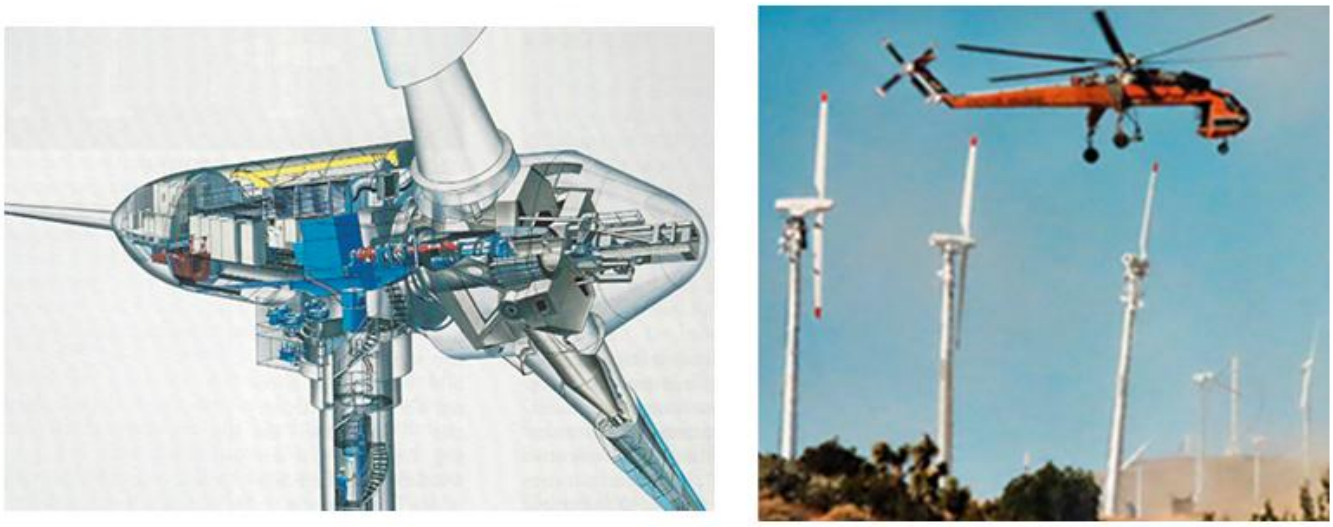


Fig.13:(left) Nacelle (Maschinenhaus) of GROWIAN, (right) Two-blade AEROMAN wind mills in California

Following the 3-blade trend, *Fig.14* presents the two types built at MAN Technologie.

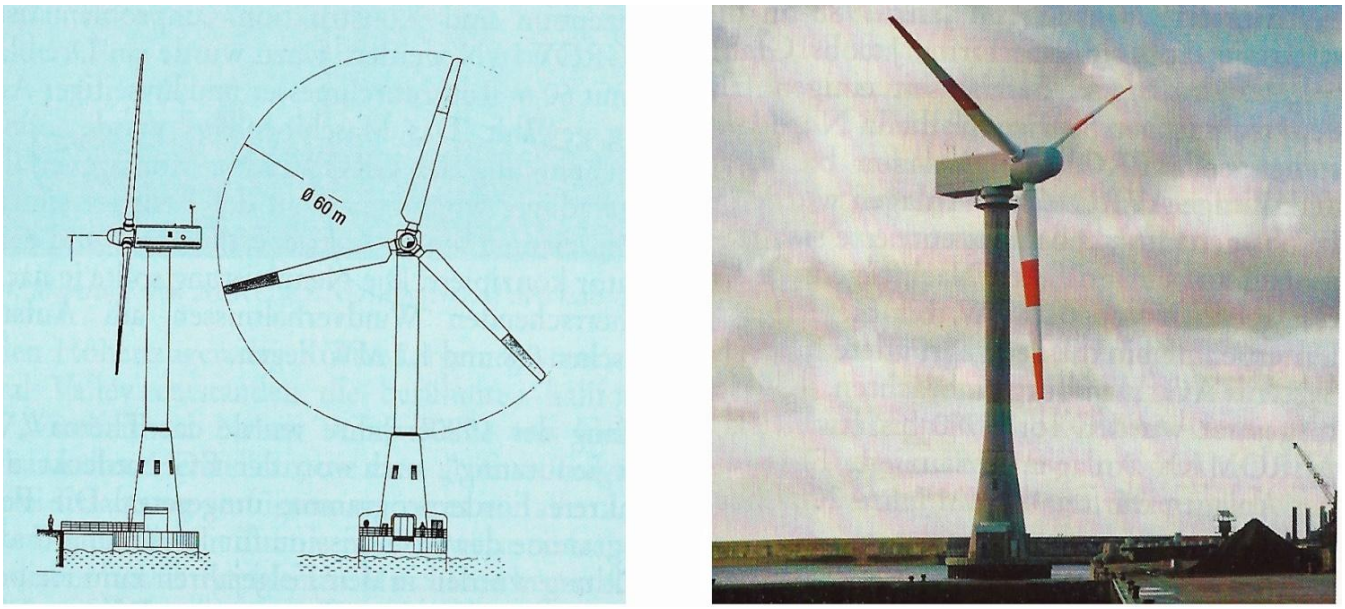


Fig.14: (1989) MAN's WKA 60m 3-blade wind turbine in Helgoland.

19.5.5 GROWIAN-associated Measurement Campaign

Basic focus in the program were the action of the wind and the reaction of the plant in order to capture dynamics, loadings sepecially its level and the control process.

Fig.15 presents the modes one had to take care of thereby.

For the wind measurement, a measuring grid in front of the turbine was used, see *Fig.16*. The tendency of leeward runners behind a cylindrical tower to noise emission had to be investigated. The figure depicts the locations of interest.

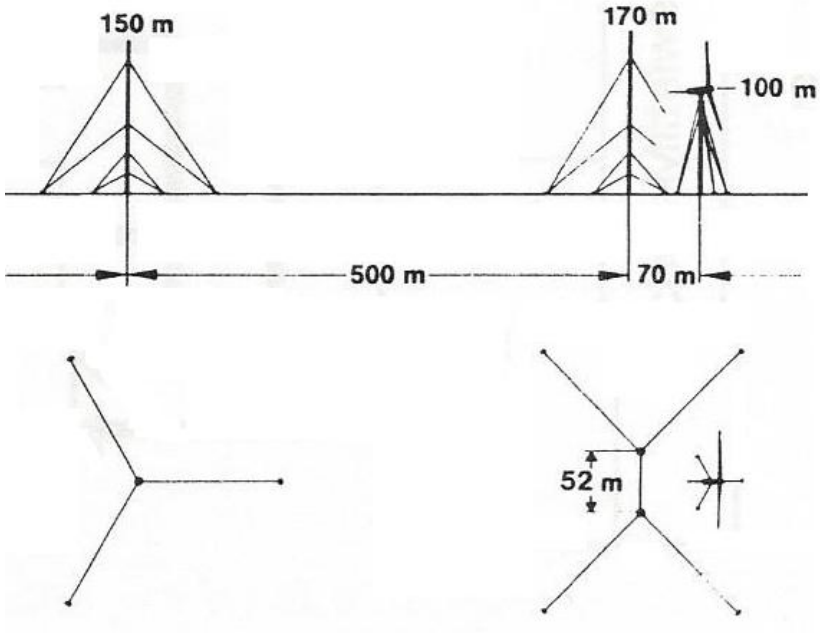


Fig.15: Arrangement on test site

The document includes own notes, departmental documents and MAN Neue Technologie Documents, as well as text from the book "Von Ideen und Erfolgen – 40 Jahre MAN Technologie" [H-G Hansen, H. Rauck editor]

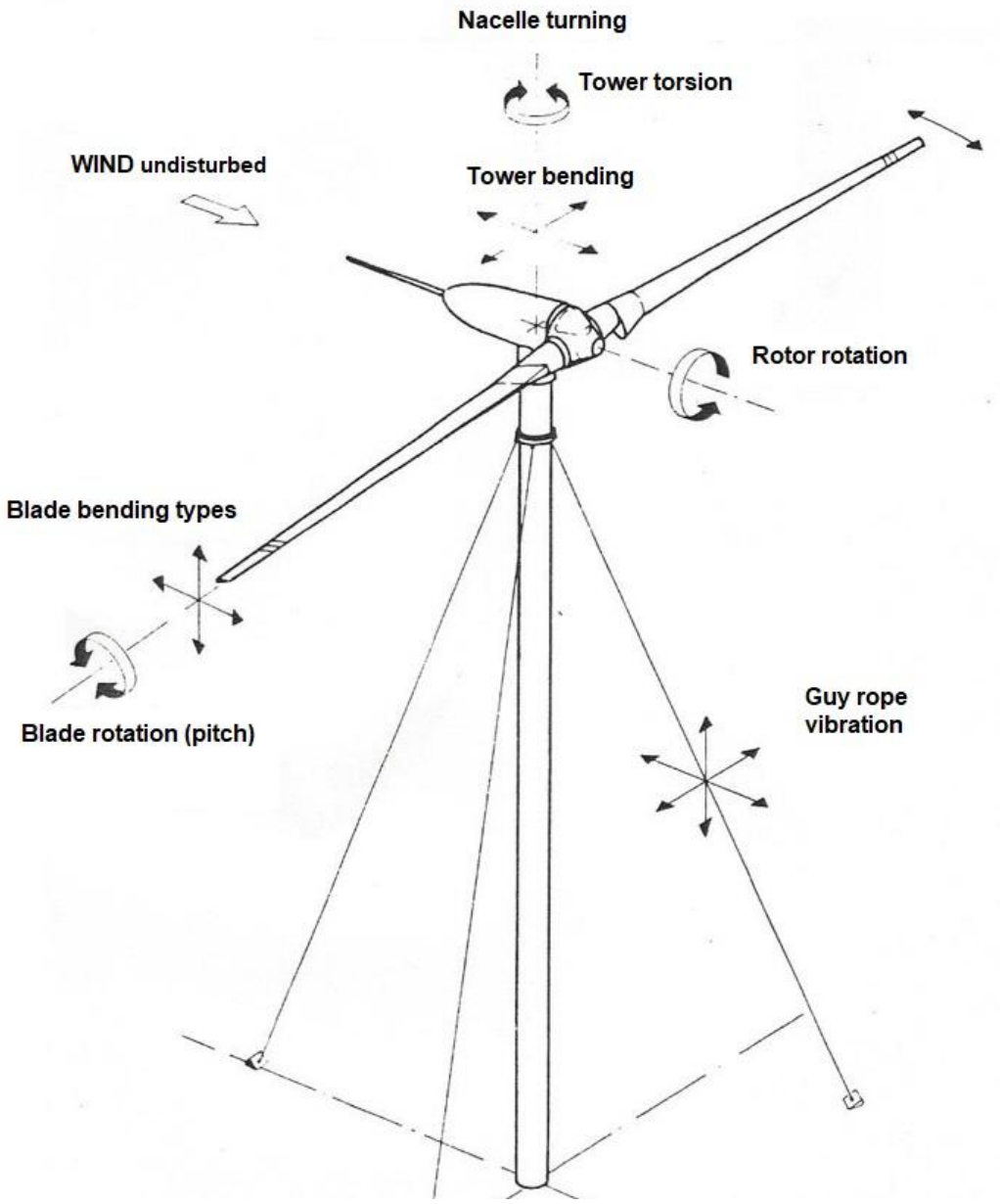


Fig.16: Measurement campaign - Vibrational degrees of freedom and associated Modes of the wind energy rotor plant

Remark of the author on citations found in the Web about GROWIAN

"*GROWIAN was the largest wind turbine in the world at the time, but due to design flaws it could not run at full power and stood idle for most of its lifetime from 1983 to 1987. The design as a leeward rotor resulted in uncontrollable loads and material problems, which is why the plant is still considered the greatest failure in wind energy history*."

And *"The fact that this happened was largely due to the rotor. Its two huge wings had put particular strain on the mechanics. She acknowledged this with cracks and failures; 1988 was the end*".

This quote is *superficial* and does not address the real problems, so the reader cannot derive any real benefit from the text. From the author's memory, the main problems were as follows:

- Initially no drilling at the end of the blade, so that penetrated water could not get out and created imbalance due to unequal amount in both blades

- The applied design wind loads were much too low, as the measurement - later carried out - showed. These results were introduced into the novel load standard and improved the novel wind energy rotor design!
- The openings in the pedulum frame were relatively cut sharp-edged at the supplier MAN–crane construction and soon led to inadmissible cracks at the corners (*this was proven by FEA, which then had to be carried out in the author's department at MAN-Technologie*. *A crane faces a fully different fatigue behavior. However we could not convince the MAN–crane colleagues to smooth the corners out).* The problem part was not the blade or the fittings, as feared!
- Yes, well running a rotor is the consequence of the goodness of the control concept. Leeward running faces air flow perturbations from the tower wind shade. However, this for instance has nothing to do with material problems as it is cited in the internet
- The alu tape lightning protection had to be replaced after a lightning strike.

Special comment on citation "the plant is still considered the *greatest failure* in wind energy history": Is this really the case or is the contributor just not really informed about GROWIAN?

- GROWIAN was a joint German technology research project to establish a basis for the development of upcoming large wind energy converters
- It delivered data for novel static load standards
- It enabled the responsible authority 'Germanische Lloyd' to establish novel procedures regarding fatigue life (*Phase 2 of fatigue life: Miner, summation of micro-mechanical damage*) and to think about crack growth macro-damage tolerance (*Phase 3, crack growth life*)
- There was no large crane existing!
- The necessary multi-body system dynamic program had to be self-made
- A computation program 'Blade design' was established [*Bureau W.Weber, D.Muser]* and used in future large rotor designs!
- For the skin material GFRP no reliable fatigue data were available
- And the more for a CFRP-spar, originally intended by the government: Here we could convince the Project Management at Jülich that taking CFRP was too risky viewing the cure process capabilities known at that time.
- In this context it is further to mention: About 1978 even for the widely used German railway standard steel St 52.3 (*then applied for the six corner steel spar*) no SN-curves were available!! (*However, the author was allowed to use preliminary test results from the LBF-Darmstadt in the blade design. Thank you, still now again*)
- No application of a Computational Fluid Dynamics CFD method was possible, only relatively simple static FE and fatigue calculations could be performed.
- Structural dynamics of the guyed wind turbine considering damping could be executed
- Cast nacelle beams and rotor hubs made of spheroid ductile iron were developed and became standard and applied in the later MAN WKA 60 and AWEC 90.

A restructuring at MAN-Technologie led to an end
of transferring the development experience gained into a marketable product.

19.6 Design of a Fiber-reinforced Gas-Ultra-Centrifuge Cylinder, GUZ (1971-1986)

19.6.1 Introduction

Uranium enrichment refers to the various processes used to increase the proportion of the isotope U235 in the natural uranium. Natural uranium consists of about 99% of U238 and unfortunately only 0.7% of the desired U235 [*Wikipedia*]. In order to be able to use it for civilian purposes in light-water reactors, it must be enriched to 3 to 4%. From an enrichment level of 85% one speaks of weapon-compatible material.

The process medium used is uranium hexafluoride UF6 (a medium, aggressive to materials), the only chemical compound of uranium that has sufficient volatility for the separation process at room temperature. This is obtained from the uranium ore by leaching. In a uranium enrichment plant, natural uranium ("feed") is separated into two fractions, one of which has a higher proportion of U235 compared to the starting material, the other a lower proportion of U235. The work performed by a separation device is quantified in kilograms of uranium separation work.

There are mainly two enrichment methods: Gas-Ultracentrifuge method and Diffusion method. In terms of energy consumption, enrichment by centrifuges is superior to the diffusion method by a factor of about 10. For information: Humans always absorb some natural uranium through food, air and water, as uranium is found everywhere in small concentrations. Natural uranium is not harmful as long as natural concentrations are not exceeded.

MAN Neue Technologie (New Technology at that time) cooperated with Dr. Gernot Zippe, father of the German GUZ. The original development took place during his Russian confinement after the 2nd World War. For information: He transported natural uranium in his suit pocket.

The separation effect is enhanced in modern centrifuges by creating an axial heat circulation flow by heating the lower part and cooling the upper part of the centrifuge. The biggest mass difference between the mass flow that is accumulated and depleted with U235 is no longer density-driven between the axis and the rotor wall, but between the ends of the centrifuge (see *Fig.1*). High vacuum technology is required.

The UF6 is directed into the interior of the vertical, rotating cylinder. Under the influence of centrifugal acceleration and negative pressure, the heavier 238-UF6 molecules concentrate on the outer wall of the cylinder and the slightly lighter 235-UF6 molecules near the rotor axis. The separation of the isotopes is enhanced by creating an axial circulating flow by heating the lower part and cooling the upper part of the centrifuge. The biggest difference in concentration is then between the ends of the centrifuge. The enriched fraction ("product") is removed by an extraction tube at the lower end, the depleted fraction at the upper end of the cylinder. Therefore, such a centrifuge is also called a counter-current centrifuge. A parallel connection of centrifuges increases the enrichment output, series connection in the cascade plant increases the enrichment volume further, see *Fig.1, right*.

The separation performance of a centrifuge can be increased with the power of the hoop speed v_{hoop} and proportionally to the length of the cylinder. In order to be able to build and drive longer centrifuges, elastic elements (*so-called bellows*) are used between the tube parts arranged one above the other. This means a further number of critical rotational frequencies have to be run through during start-up.

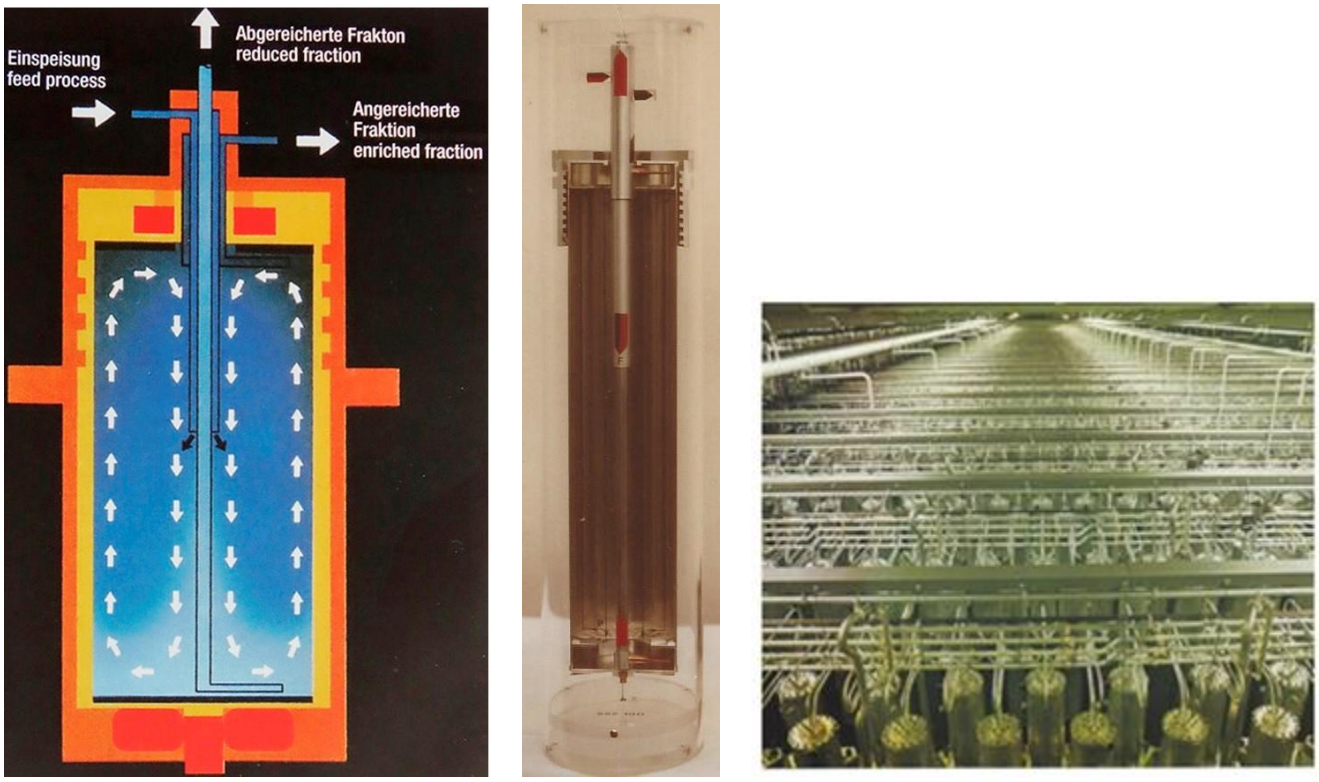


Fig.1: (left) Scheme of separation proces, (center) demonstrator metal variant, (right) Urenco cascade plant of centrifuges

19.6.2 Design Dimensioning of the Cylindrical Tube

1 Task:

Optimization of the cylindrical tube considering bending stiffness, strength and product output using a high performance CFRP laminate to achieve high speeds.

2 Input

- Operational time > 20 →30 years
- Assumed Failure rate of the GUZ: 1% / year. This is based on the joint failure probability of the *failure rate* of all mechanical and electrical devices and the *failure state* of the highest loaded part, the tube. In order to get no risk from the tube it must be very safely designed with failure probabilities < $p_f = 10^{-6}$ (theoretical desire)
- Choice of several composite material candidates and lay-ups
- Layer thickness 0.125 mm, V_f > 60%. Varaint: 90° layers (T300), helix layers (M40) $T300 : E_{\square} = 140000\ \text{N/mm}^2$; $M40 : E_{\square} = 140000\ \text{N/mm}^2$
- Static centrifugal loading $_{max}v = {}_{max}\Omega \cdot r \cdot (1+\varepsilon) \rightarrow p_r = t \,/\, r \cdot \rho_{FRP} \cdot {}_{max}v^2$ and operational perturbations are to consider
- Consideration of:
  - shear correction factor for the tube shear stiffness by $\kappa = 1.89$ (*Table in § 18.3.4)*
  - radial deformation $r \cdot (1+\varepsilon)$, that causes a nonlinear analysis
  - symmetric lay-up from winding
  - long time strength values, no creeping
  - evacuation, in ordrer to keep the energy demand very low.

3 Determination of the lay-up and winding angles of the cylindrical tube

The separation performance can be increased by increasing the tube length and in particular the rotational speed Ω, which is due to the material properties of the high speed rotor as well as natural frequency-related restrictions. Basic knowledge at that time: $v = \Omega \cdot r = 400$ m/s has been achieved with aluminum alloys, 500 m/s with high-strength steels and over 700 m/s with fiber-reinforced materials. Task was to sort out fibers, available at that time, for instance CFRP with the fibers T300/Ep (*strength*), M40/Ep (*stiffness*). Originally further developed maraging high-strength steels have been seen as candidate materials, too. *To give more information and results is not permitted).*

Dicscussion of hoop winding width in production

As the number of individual filaments in the winding roving increases, its width grows. This increasing width prevents a 90°-circumferential position from being placed at 90°. For example, instead of a theoretical lay-up [90/+ω/-ω/90], [+87/+ω/-ω/+87] results.

The principle of the lathe winding technique used here leads to an angle of the same direction, so that the effect of an asymmetrically built stiffness matrix [K] for the laminate of the GUZ wall gets some influence. Changing the feed direction would make $\pm 87°$ possible, but it is too CoStly. In addition, tube shortening and expansion have a certain influence on the bearing and the desired smallest possible distance to the recipient.

In the helix-layer planes, the greatest risk of micro-cracking is due to inter-fiber failure IFF, triggered by relatively high transverse tensile stresses with shear stresses. Their exact values are determined in a nonlinear analysis with the $\tau_{12}(\gamma_{12})$ shear stress-shear strain curve. From rotor imbalance reasons micro-cracking should be avoided because it does not happen symmetrically. However, there is a benign effect: The helix layers are embedded, so that the cracking of the present very thin layers is hindered. In this context remember: The strength values used are the result of tests with isolated test specimens.

Determination of an optimum helix winding angle ω

An optimization Trade-off was started in the author's department, initiated by Dr. Zippe (father of the GUZ), that focussed:.

- Objective: CoSt-Production-optimal U 235-separation as function of lay-up (stack), helix angle regarding the ratio of helix to hoop layers
- Optimization space, parameter width: tube length, tube diameter, laminate wall thickness, CFRP combinations, helix angle ($25° < \omega < 30°$), fiber volume fraction V_f for the strength responsible hoop layers t_{90} and the bending stiffness (*natural frequencies and critical speeds*) responsible helix layers
- Side constraints: tube widening, distance of rotor angular speed $\Omega = 2\pi \cdot f_{op}$ to the (*higher located*) lowest natural angular bending speed $\omega = 2\pi \cdot f_{bending}$ of the cylindrical tube (also here the letter ω is most often used)
- Assumptions in the seld-made program RotOpt: Separation length of the rotor $L_{sep} = L_{cylinder}$ – height of the upper and lower rotor cover.
- Speed-driven separation is proportional to $v^?$.

To give more information and results is not permitted).

The internally created RotOpt then served as program to capture above optimization task.

19.6.3 Dynamic Analysis of the Rotor System GUZ

System modeling and equations of motion

The following text is basically from the contribution of Dr. Peter Meinke† in the Chapter Rotordynamik von Zentrifugen in the book „Von Ideen und Erfolgen", 40 Jahre MAN Technologie. Paartal Verlag. (2008). Editor: Hans-Georg Hansen und Horst Rauck. And is further from "Rotor System Dynamic Analysis (1971) natural freqencies, eigen modes and critical speeds". Thanks Peter.

The GUZ model shown in *Fig.2* is a two-story, rigidly modelled rotor with the rotor mass m_R and with *I* as the moment of mass inertia around the vertical axis. It is isotropically elastic in its upper and lower bearings, whereby the bearing masses are elastically and damping is coupled to the housing. The rotor has an eccentric center of gravity due to static imbalance (*statische Unwucht*) as well as it experiences deviation moments due to dynamic imbalance.

By applying the theorems of impulse and momentum, the equations of motion of the rotor system can be obtained relatively clearly. The momentum theorem forms the equilibrium with the attacking forces from the scalar product of the participating masses m_o, m_R and M_u with their speeds, whereas the momentum theorem stands for the equilibrium with the attacking moments. Applying the momentum theorem causes the equations of motion of the individual coordinate directions to couple. But one can make the assumption that the transverse movements of the rotor will be small of the first order compared to the dimensions of the rotor and that the imbalances are also small of the first order so that they can be neglected. In order to fulfil this the rotor needs to be well balanced!

What remains are the nonlinear terms, in which the moment of mass inertia *I* is multiplied by the rotor speed Ω and one of the radial rotational velocities. This allows the 'vertical dynamics' to be decoupled from the 'lateral dynamics', such that for the vertical dynamics a (desired) separate differential equation system is obtained. And further, the simplified lateral dynamics can be described in a classical way as a system of differential equations (scalar multiplication ·, vectorial multiplication x):

$$\mathbf{M}\cdot\ddot{\underline{x}}+\mathbf{P}\cdot\dot{\underline{x}}+\mathbf{Q}\cdot\underline{x}=\underline{\mathbf{U}}(t) \quad \textbf{with} \quad \mathbf{P} = \mathbf{D}+\mathbf{G}\,.$$

In this equation, the mass matrix **M** (*capital letter*) contains all masses m_i of the multi-body vibrator. The matrix P is composed of two parts: The damping matrix **D**, in which the damping constants can be found of the upper d_a and d_u of the lower bearing and further the gyroscopic matrix **G** (*Kreiselterme),* in which the vector product *I* x Ω appears skew-symmetrically and contains the angular rotational speed Ω. The unbalanced terms in **U** remain as time-dependent quantities on the right side of the differential equation system. It is therefore mandatory in rotor dynamics to solve the equation of motion considering damping.

A one-story (part) rotor has its optimal length under the given side constraints. Enlarging the separation length is dynamically only possible if the single tube parts are connected by an elastic bellow joint. This causes an additional, intermediate level of critical speeds which are also to pass after start and this is managed by the up-speed operating control system.

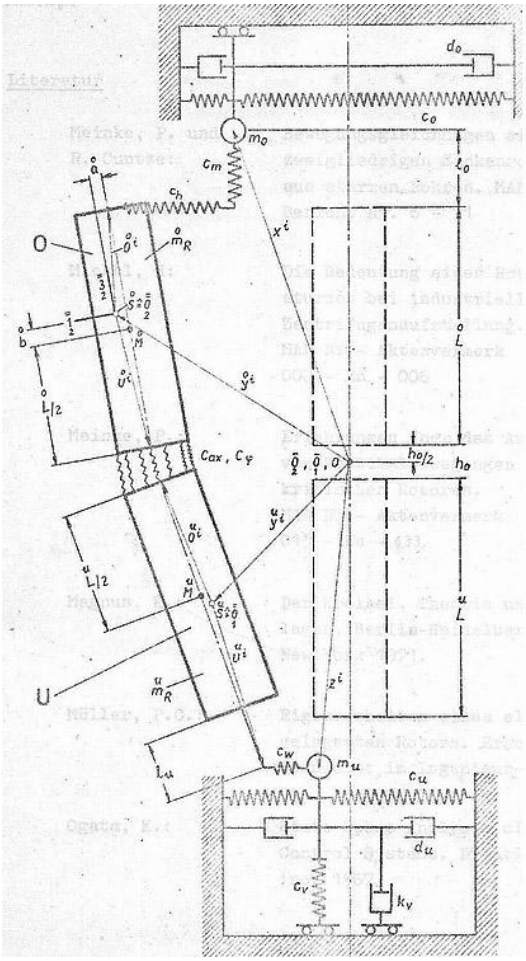
There were single and multi-part rotors to analyze. *Fig.2* exemplarily presents the system of a two-story rotor with a bellow as elastic joint. Task in the dynamic analysis was to investigate the inherent behavior and the unbalanced influences of this two-part rotor with the elastic joint

between. The idealization of the boundary conditions by springs and dampers is clearly indicated. This challenging task at that time we do now call: 'Multibody Simulation Analysis of systems and mechanisms'. Software is now available but was not 50 years ago. The program had to be generated and this was successfully performed. Some rotors are running since about 50 years.

Operation of the rotor, excitation and damping

If the rotor slowly ramps up to operating speed, it will always occur that the operationing rotor's rotational frequency matches one of the natural frequencies Since there are no imbalance-free technical rotors, resonances occur. The imbalances stands on the right side of the differential equation system. However, the occurrence of imbalance resonance phenomena is linked to certain conditions: •Rotational frequency and natural frequency coincide. •Rotational sense of the rotor and that of the intrinsic natural mode shape *(Eigenform*) match and are therefore concurrent. This condition is immediately understandable, because how could a rotating imbalance excitation stimulate a so-called opposite motion (*"Gegenlaufkritische*"). An excitation is only possible for so-called concurrent motions ("*Gleichlaufkritische*").

The vibrational system involves two deep natural frequencies of the rigid assumed two-story GUZ (*sufficiently good model at low frequencies*) parts according to the springs of the bearings and a decade higher a natural frequency due to the bellow spring. These three natural frequencies have to be passed after starting the GUZ on the way to the operational frequency. The Campbell Digram in the previous chapter displayed the relationships natural frequencies versus excitation fequencies of the GROWIAN. This is analogously to apply to the GUZ which runs 3-fold-supercritical.



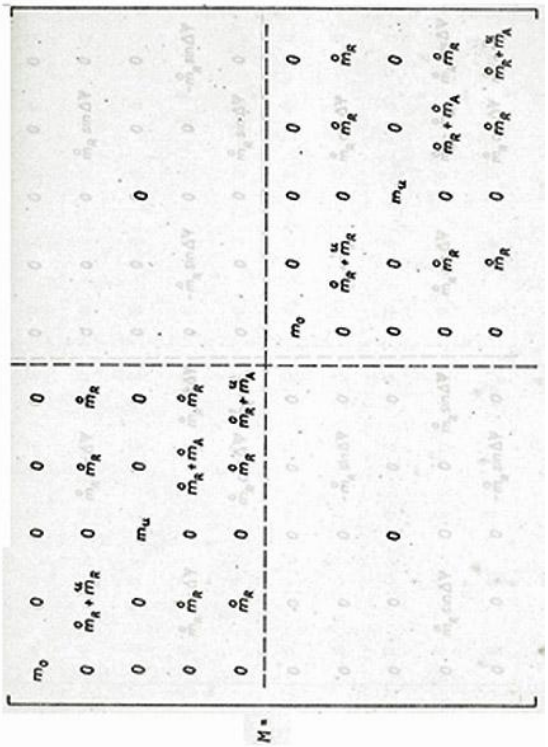


Fig.2: (left) Rotor dynamic system of a two-story GUZ, (right) Mass matrix of the dynamic system. (1971), [Meinke, Cuntze, Celep]. Top and bottom bearings, elastic joint, tubes

In the context above the term "critical speed" is used: It is the resonance excitation of a concurrent natural motion due to imbalance. Of course, in principle all natural modes could be stimulated by a rotor housing excitation. However again, the imbalance distribution on the rotor then must be such that it can stimulate the mode vibration.

A damping of the rotor system is necessary at least when driving through the critical speeds. In the case of the GUZ damping can only be introduced via bearing damping. A vibration excitation of the rotor cylinder leads to a damping-necessary foot point excitation of the bearing mass. Their spring-damping setting must be adjusted in such a way that sufficient energy is taken from the rotor system by sufficient bearing movement.

Hence, when starting a rotor it should quickly pass the low boundary (*support, bearing*)-natural critical speeds and then operate at a distance below the bending critical speeds. This distance is to specify.

Outlook: In order to increase the U235-output multi-story GUZ have been investigated, system dynamic programs developed and then built and operated.

19.7 Some Winding Theory on Filament Wound Pressure Vessels going to be included

19.7.1 Basic Introduction, formulations

Contents from the tensorial-based Habilitation work, 1978, "Grundlagen für die Berechnung von Rotationsschalen aus Faserverbundwerkstoff (Fundamentals for the calculation of rotational shells made of fiber composites)" and from the Buchmanuskript "Auslegung von Bauteilen aus Faserverbundwerkstoff", 1975, duplication of the private document at M.A.N. - Neue Technologie, 600 pages. This Manucript has not been published because the first edition of 'Mechanics of Composite Materials' by Robert Jones became published. For this first work for the designing engineers many thanks to Bob.

Above private investigations were partly executed for a better design understanding of the tanks wound at MAN Technology.

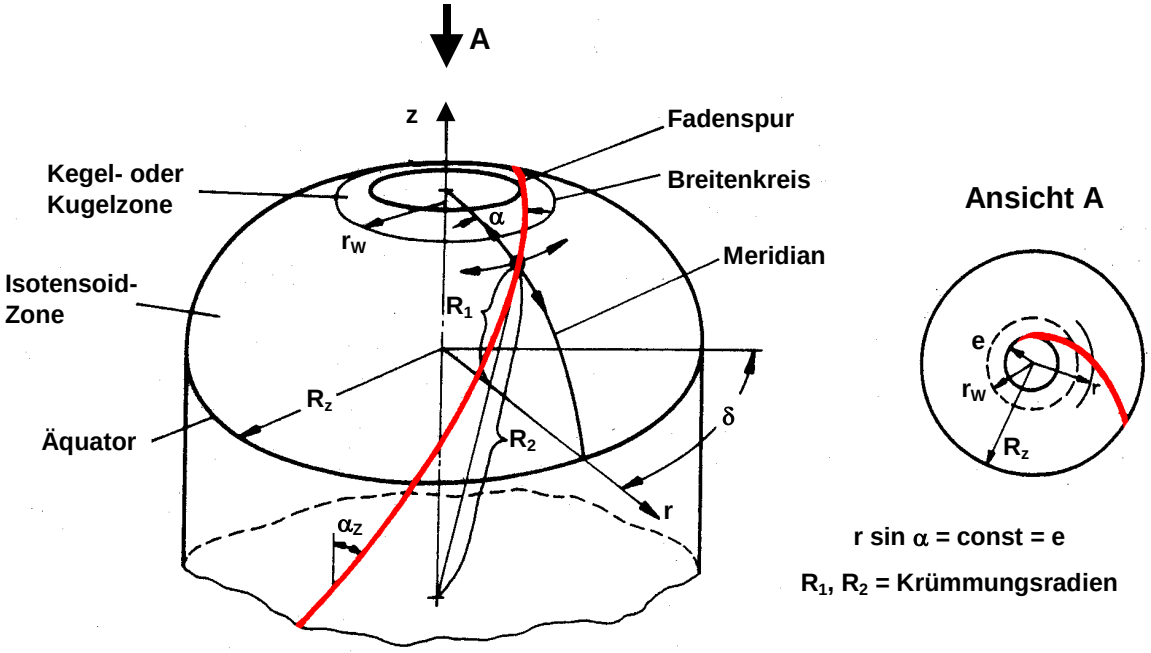


Fig.1:

19.7.2 Some Winding Theory on Filament Wound Pressure Vessels going to be included

Some Winding Theory on Filament Wound Pressure Vessels going to be included

Planar, geodesic and isotensoidal winding, Winding patterns meine Ausarbeitung

Design of Low and High pressure vessels Fotos auf Kamera

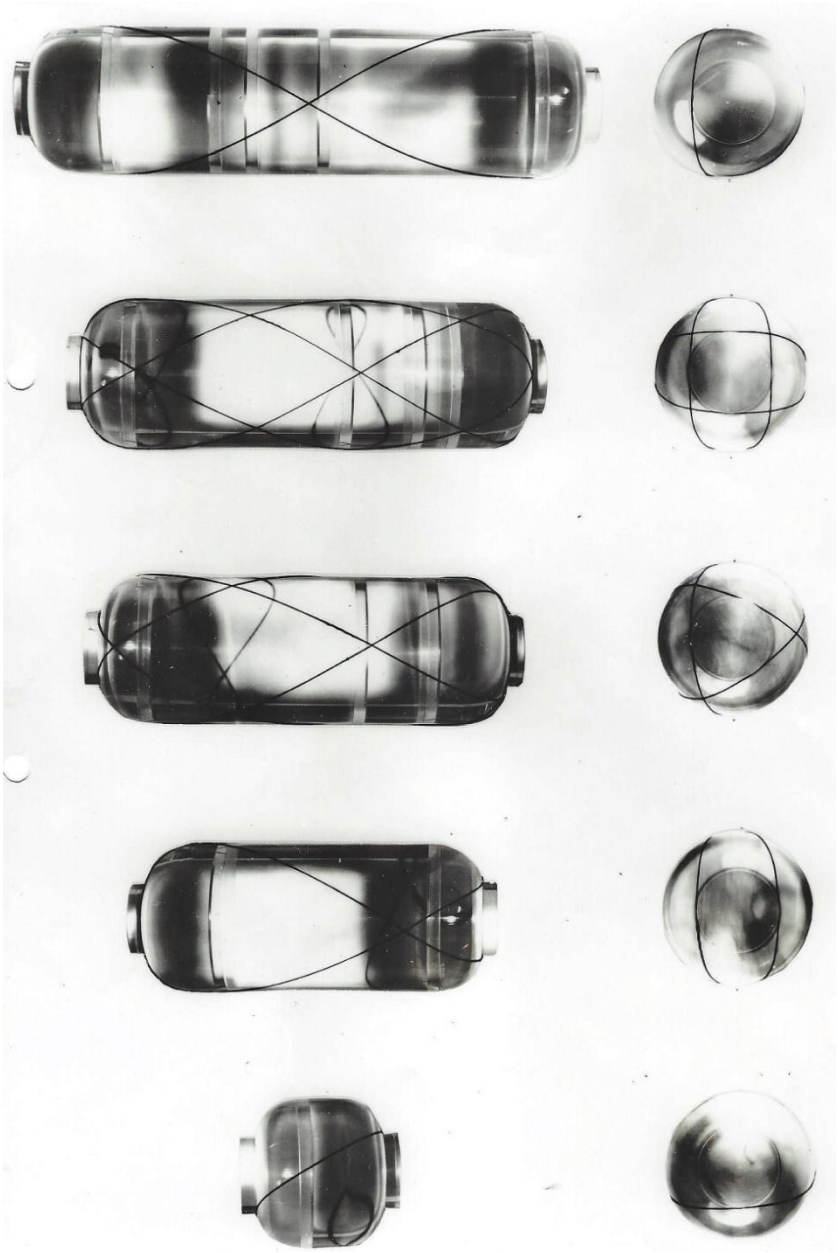


Fig.2: Winding patterns for different ratioslength/diameter

Residual stresses

Important for the determination of residual stresses is the knowledge of the variable thread tension during winding, the winding core, the winding pattern with its not so favorable crossing points in terms of strength.

There are residual stresses at the micro-mechanical and the macro-mechanical level. Those at the micro-mechanical level (*filament matrix*) are regarded as considered in the measured macro-mechanical material characteristics. In the case of non-tightly crosslinked matrix systems such as thermoplastics, the undesirable residual stresses can be reduced by annealing (*Tempern*). Chemical shrinkage (*Schwindung*) and thermal shrinkage (*Schrumpfung*).

In the case of EP matrices, it is well known that no reduction of the residual stresses caused by production (*addressed here are the equilibrium system of circumferential residual stresses over the pipe thickness)* can be achieved by annealing. This frozen residual stress state is released by cutting open a ring test specimen. The cut ring deforms both in the virgin state and in the already damaged

by corresponding load cycles. The micro-cracks occurring in the latter case reduce the residual stress state because it can partially relax (*in the final state, grid theory would be applicable instead of continuum theory and the residual stress state would have disappeared*). In our pipe rings, the deformations occurring during cutting become smaller with increasing thickness.
During the hardening of the partial shell, a first residual stress state is generated. As a result of the intermediate hardening of the partial shells, the respective associated residual stress state in the partial shell is not so large with optimal, decreasing variable winding pretension thread. By joining the partial shells in the further winding process, a second residual stress state is then superimposed. Both states are then responsible for the deformation behavior. For the estimation of the occurring residual stress state, previously unloaded, virgin rings are to provide

.

Load stresses

Critical for the formation of micro-cracks are the stress states between the 90° layer and the ω layer (*the more internal 90° layer remains 'behind'*). The load stress state includes the shear and tensile stresses in the ω-layer

19.7.3 Applications of Winding Theory at MAN Technologie

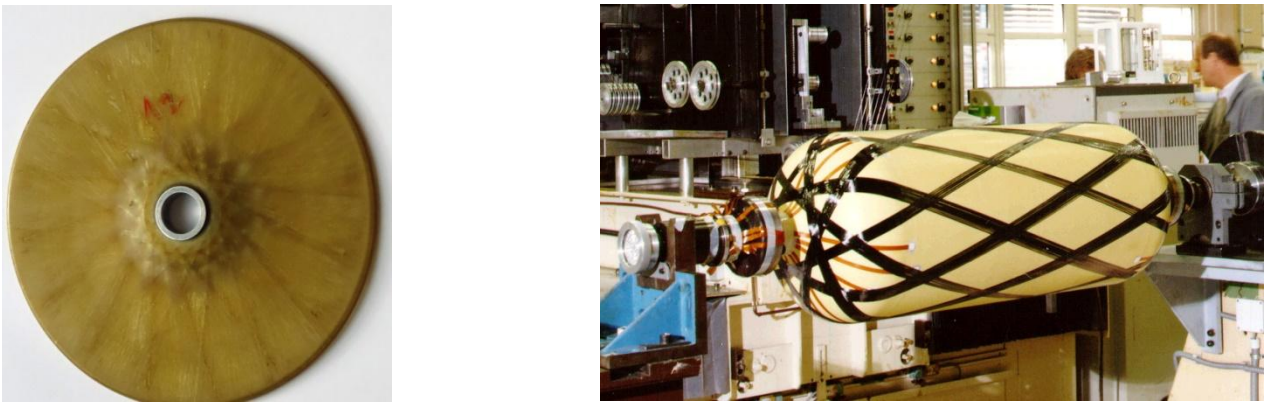


Fig.3: Pattern of a GFRP Disc and a CFRP pressure tankwound on a lathe

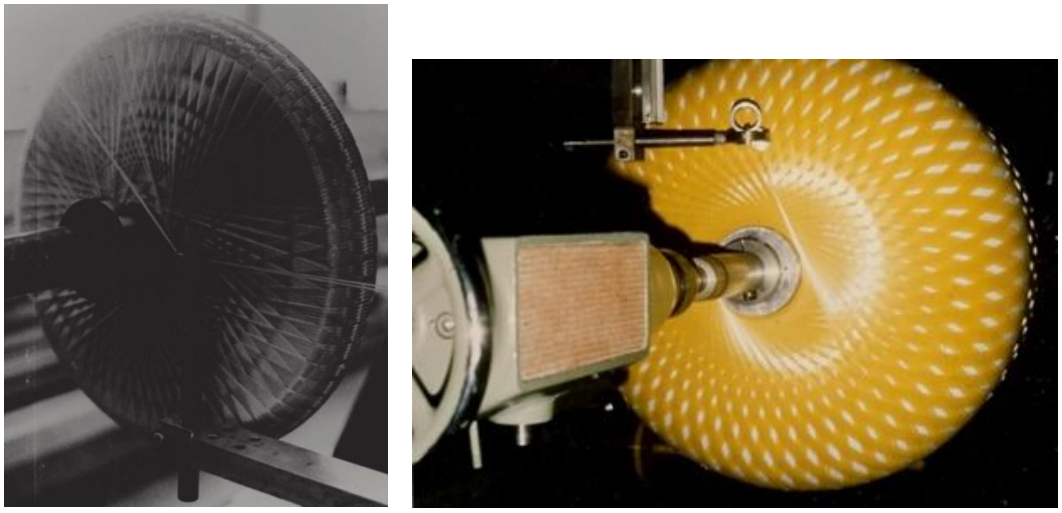


Fig.4: Pattern of a CFRP and a AFRP fly wheel

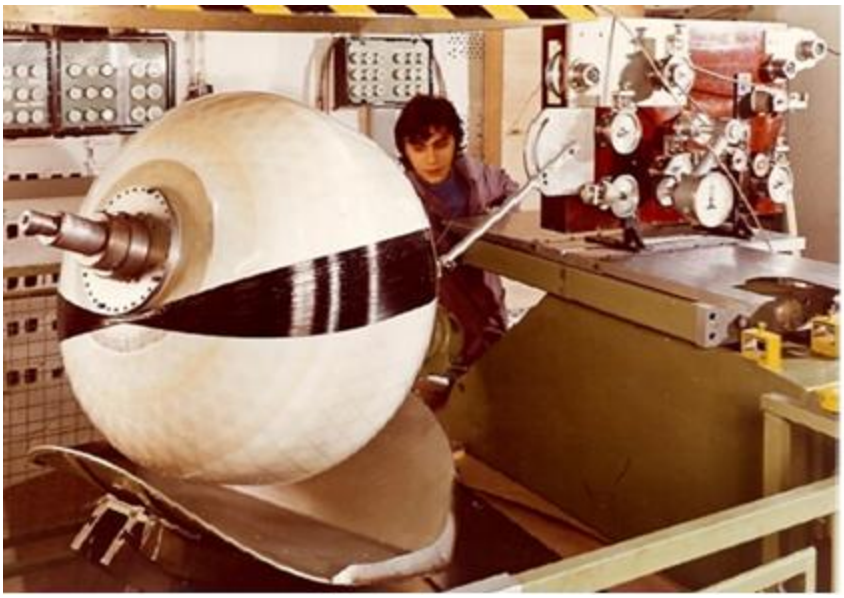




Fig.5: (left) Carbon roving filament winding on a mandrel.(right) Pattern of an AFRP HighPressureTank





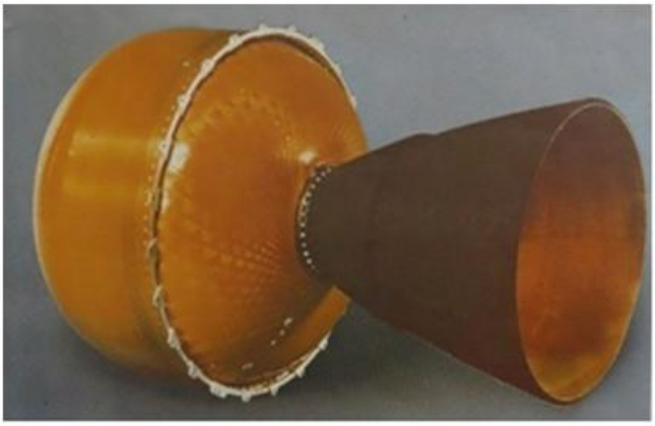


Fig. 6: MAGE/IRIS solid rocket motor AFRP (Kevlar) casings



Fig. 7: Mounting of the Airbus A330/340 drinking water tanks





Tanktyp	GAM-Hochdruck-tank (Bild 1)	GAT-Hochdruck-tank (Bild 2)
Volumen	183 l	520 l
Operationsdruck	230 bar	450 bar
Mindest-Berstdruck	460 bar	900 bar
Durchmesser	400 mm	400 mm
Länge	1700 mm	4400 mm
Masse	59 kg	200 kg

Fig. 8 for ARIANE 5: GAT-HighPressureTank with PROSIAL heat protection coating, (below) GAM-HighPressureTank

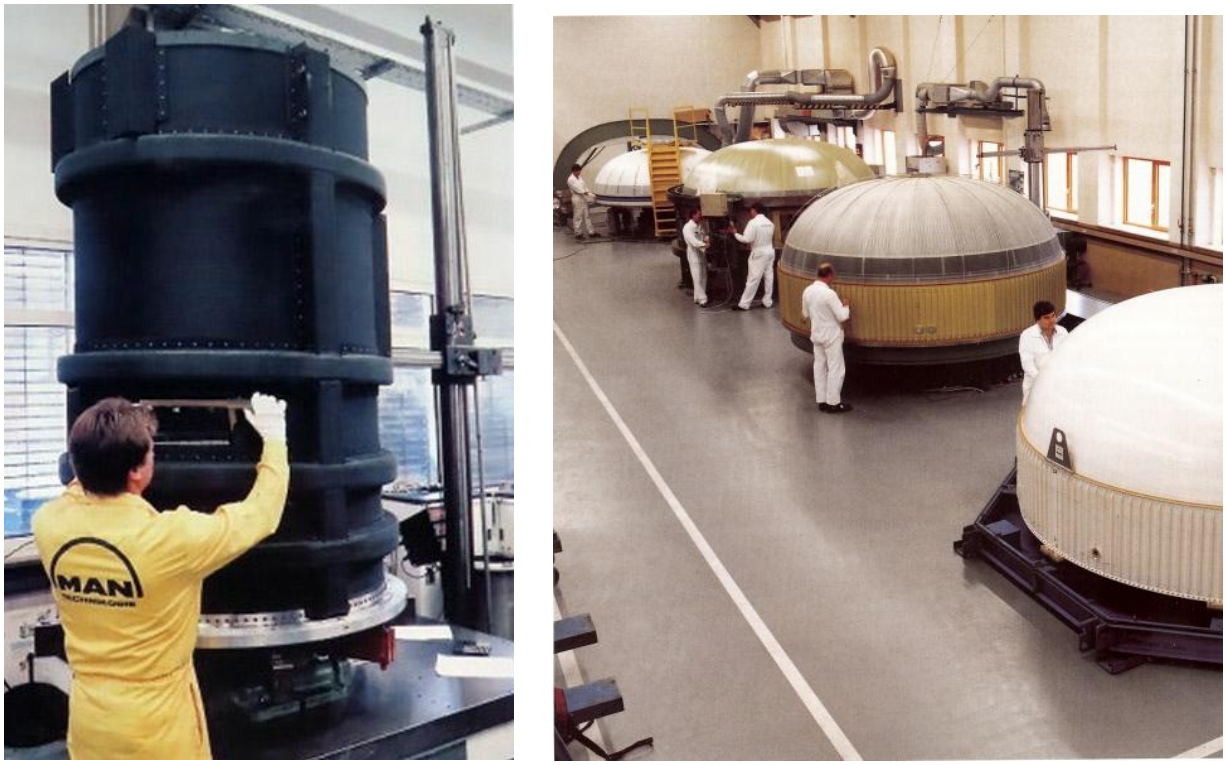


Fig. 9: (left) CFRP ORPHEUS telecope structure. (right) Domes, tape-layed

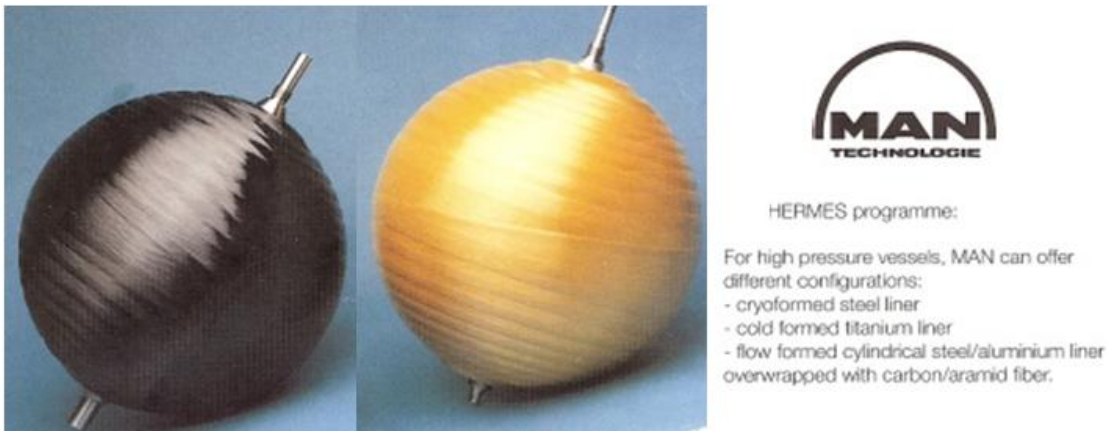


Fig. 10: Spherical HighPressureTank, CFRP and AFRP
CFRP-HighPressureTanks for METEOSAT (1977), AFRP for ITALSAT

<u>Novel idea</u> <u>Fraunhofer-Zentrum für Hochtemperatur-Leichtbau HTL</u> (2022) on Sphere CFRP vessels or 'balls' for future hydrogen transport application

Hydrogen storage in ultra-light high-pressure spherical tanks without complex cooling as with liquid hydrogen. The patented PS-HySphere ball tank will be available in different sizes and for different operating pressures (350 or 700 bar).Development of an isotensoidic winding or tape-laying *algorithm. Construction of a robot system for isotensoidic winding. Development of a novel diffusion barrier with ORMOCEREN.® Production of an ultra-light polyamide/polyimide liner.*

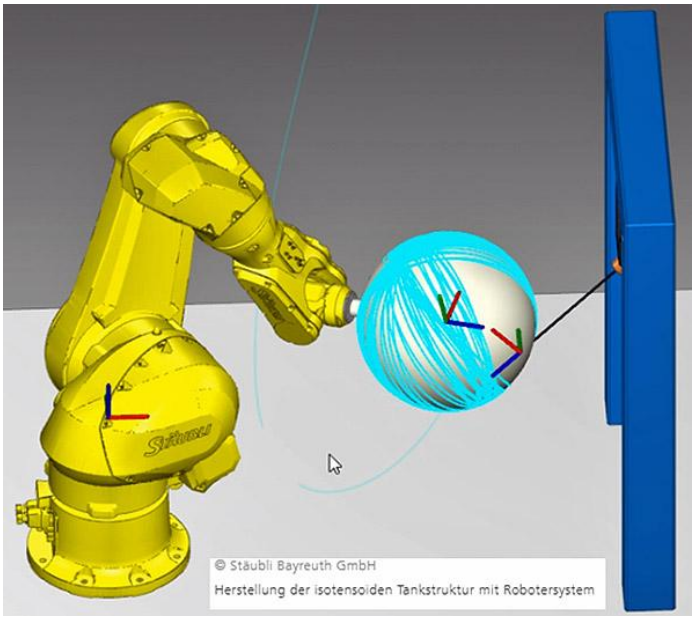


Fig. 11: Roboter-fabricated ball tank (jan-marcel.hausherr@isc.fraunhofer.de), 2022

19.8 Application of winding technology, re-calculation of above AFRP tank

1 Task

For a wound internal pressure vessel made of Kevlar fibers (Meteosat) and epoxy resin, the dimensioning according to the mesh theory and the calculation according to the continuum theory is to demonstrate.

2 Input

- Loading: MEOP = maximum operational pressure (DLL level) p_{int} = 51 bar (*short time stressing*)
- Design safety factor: j_{ult} = 1,5 → $p_{DUL} = j_{ult} \cdot$ MEOP
- Internal radius at equator r_{in} = 377 mm; pole-openings e = 124 mm; volume 260 dm^3
- Properties:
  Strength Kevlar-Fiber: R_f > 1950 N/mm^2, Elasticity moduli: E_f = 1.4·105 N/mm^2 , $E_m = 3 \cdot 10^3$ N/mm^2
  UD properties for $\varphi_{ax} = \varphi_{90} = \varphi = V_f$ = 0.60 and resin 0502/hardener (HT 972) in mix 100/34:
  $E_{||} = 85 \cdot 10^3$ N/mm^2; $E_\perp = 5.6 \cdot 10^3$ N/mm^2; $G_{\perp||} = 2.1 \cdot 10^3$ N/mm^2; $\nu_{\perp||} = 0.34$; $\rho_{||} = 1.39$ g/cm^3
  Strength design allowables short time for loading:
  $$\{R\} = (R_{||}^t,\ R_{||}^c,\ R_\perp^t,\ R_\perp^c,\ R_{\perp||})^T = (1250,\ -,\ 10,\ -,\ 50)^T \text{ MPa}\ .$$
- Production:
  Use of a winding tape consisting of two rovings with each 4·768 filaments
  with the filament cross-section of the aramide filament of 12 µm
  $A_2 = 2 \cdot 0.35 = 0.70$ mm^2 → $A = A_2/\varphi = 1.17$ mm^2.
  As bandwidths were measured for two rovings W_{90} = 6.0 mm (wider placed) und W_α = 3.75 mm .
  Pull-off speed of the winding tape 0.2 m/s. Winding tension per tape: F^t = 30 N
  Processing temperature of the resin: 50°C. Curing: 19 h at 60°C, 5h at 80°C and 10 h at 110°C.
  Layers: Hoop (90°) and helix (α).

2 Design dimensioning using net theory

- Winding angle, winding pattern and contour:
  For most tank designs, the volume is fixed. Since the pole openings are generally fixed for design requirements, e (*Fig.1*) is still known. If the tank shape is still roughly prescribed, the pattern can be found with known e and r_{cyl}. For the geodetic winding type, the winding angle can then be calculated from

  $r_{cyl} = r_{in} + \approx 1 = 378$ mm of mid plane, $\mathbf{r_{cyl}} \cdot \sin \alpha_{cyl} = e = 122 + 3.75/2 = 124$ mm $\rightarrow a_{cyl} = 19.2°$.

  For a possible 'winding pitch number' T = 1 causing the pattern, a cylindrical length results after integration of the contour differential equation CDE and the volume content of the bottom of $L_{cyl} = 250$ mm. For the production of the construction drawing, the inner and outer liner contour of the bottom must now be determined and the coordinates of these contours must be recorded for production. For this purpose, the contour in the validity area of the CDE ($\alpha < 54.75°$) is applied to the extent that a meaningful final contour can be designed up to the pole.

  In the present case, the liner's outer contour including fitting area from $\alpha = 45°$ is continued with the meridian curvature radius $R_2 = R(45°)$ present at $\alpha = 45°$. The difference to a conical end is very small. The liner contour including fitting area is found by simple geometric relationships with the help of the outer contour.

- Wall thickness:
  The following equations are used to determine the total composite thickness

$$erf\, t_{\alpha\, cyl} = p_{DUL} \frac{1/2\, R_{cyl}}{R_{\parallel}^{t} \cdot cos^2\, \alpha_{cyl}} = 7.65\,\text{mm} \qquad \frac{378}{2 \cdot 1250 \cdot cos^2\, 19{,}2^{\circ}} = 1.30\,\text{mm} \quad \text{and}$$

$$erf\, t_{90} = p_{DUL} \cdot \frac{R_{cyl} \cdot \left(1 - 0.5 tan^2\, \alpha_{cyl}\right)}{R_{\parallel}^{t}} = 7.5 \cdot \frac{378 \cdot \left(1 - 0{,}5\, tan^2\, 19.2^{\circ}\right)}{2 \cdot 1250 \cdot cos^2\, 19.2^{\circ}} = 2{,}17\,\text{mm} \rightarrow \text{Chosen: 2.35 mm.}$$

  For $V_f = \varphi = 0.60$, these composite thicknesses correspond to pure fiber thicknesses of $t_{\alpha f} = 0.60 \cdot 1.30 = 0.78$ mm and $t_{90f} = 1.41$ mm.

  As wall thicknesses are thus present in the cylinder area $t = 1.30 + 2.35 = 3.65$ mm.

  The wall thicknesses of the individual layers are thus calculated from ($\alpha = +\omega, -\omega$)

$$t_{90}^{(1)} = \frac{A}{W_{90}} = \frac{1.17}{6.0} = 0.195 \quad \text{and} \quad \frac{A}{W_{\alpha}} = \frac{1.17}{3.75} = 0.312\,,$$

  where A is the cross-section of the winding tape. W_{90} and W_{α} are the laying widths of the winding tape during hoop and helix winding.

  The winding provides an orthotropic, asymmetrically constructed laminate [$\pm\omega$/ $\pm\omega$/ 90/ 90/ 90/ 90/ 90/90], which means 2 cross layers $\alpha = \pm\omega$, plus the hoop layers in the cylindrical area.

3 Design Verification using continuum theory

The determination of the stresses and deformations of the present orthotropic composite in the operating state is carried out according to the continuum theory. Therefore it is assumed, that the laminate of the cylinder is non-cracked. The calculation takes into account shell bending and non-symmetrical laminate lay-up.

Provided is the vector of laminate mean stresses $\{\hat{\sigma}\} = j_{ult} \cdot (1/2\, p_{DLL} \cdot R_{cyl},\, p_{DLL} \cdot R_{cyl},\, 0)^T$

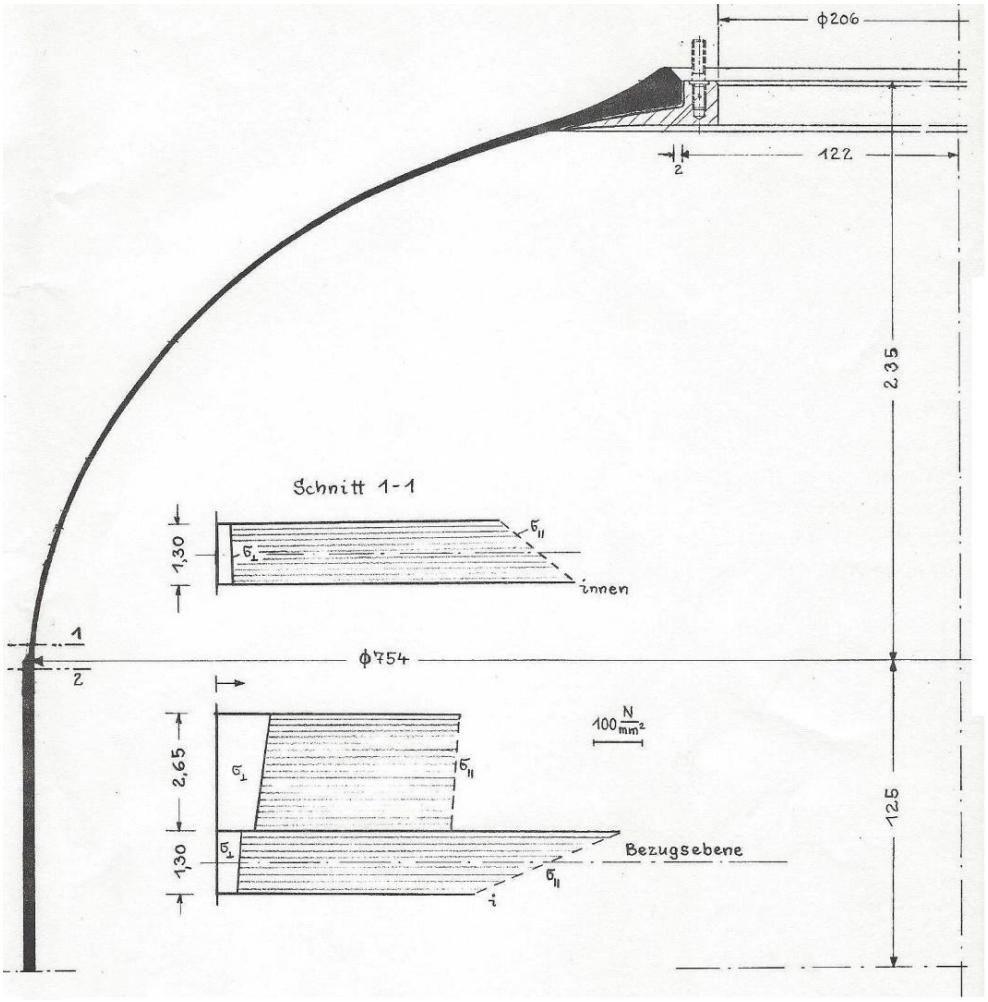
and the elasticity matrix of the layer $[Q] = \begin{bmatrix} 85650 & 1919 & 0 \\ 1919 & 5643 & 0 \\ 0 & 0 & 2100 \end{bmatrix}$ in N/mm^2 .

From the elasticity matrix of the single layer we come to the sizes of the laminate, which has a layer structure in the cylinder area - from the inside to the outside - of [19.2/-19.2//19.2/-19.2/90/90/90/90/90/90]. The reference plane (*Bezugsebene*) lies between the helix layers, (*Fig.12*).. This results in the stiffness matrices (N and mm are used as units)

$$[D] = \begin{bmatrix} 764300 & 18840 & 0 \\ 18840 & 62980 & 0 \\ 0 & 0 & 20480 \end{bmatrix}, \quad [B] = \begin{bmatrix} 367300 & 8228 & 584 \\ 8228 & 24200 & 4652 \\ 589 & 4652 & 9006 \end{bmatrix}$$

For the preceding matrices, [B] and [D] show how asymmetrical the present stratification is. Due to this asymmetrical stack, bending stresses are present during operation (42 bar). They are based on the in reality greater widening (according to the net theory is the same widening) of the cylinder compared to the bottom side at the equator. Here they amount to up to 15 % of the membrane calculation value In order to reduce the bending stresses, reinforcements can be applied in the cylinder area and the equatorial points, if possible and can be produced, compared to the net theory design.

When compared with test results, although only a very similar tank design was tested, a linear increase in strain was observed in the fiber direction at all measuring points up to $\varepsilon = 1$ %. Furthermore, with proper production, the burst pressure calculated according to the net theory was in the tolerance range +5% of the actually achieved, average burst value.



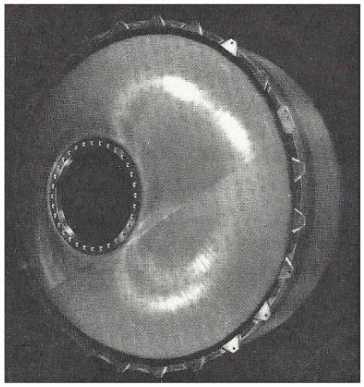


Fig.12: Vessel (tank) dimensions and some layer (ply) stresses. Wound with Kevlar fibers

20 Introduction to Beams with Thin-walled Cross-sections **going to be included**

The following contents was formerly planned as contribution to the HSB by Prof. Dr. Helmut Rapp and the author.

21 Notch Mechanics **going to be included**

Fracture and Notch mechanics Ultimate Ductile Design: Neuber, Extended Mises ('Gurson domain')

22 FMC-Conclusions and FMC-linked Literature

22.1 Failure-Mode-Concept, considering the investigated 3 Material Families

- Formulation basis: Does the material element experience a volume change, a shape change and friction. Then, following Beltrami's statement, a successful demonstration of the advantageous use of the 'physics-based' invariants I_1 and J_2 is given when mapping the very different isotropic materials Normal Concrete, Ultra-High-Performance-Concrete, PMMA [*Cun20b*] and foam [*Cun16*] could be presented. For UD material the same success could be achieved but for orthotropic materials – due to the missing 3D test results – still lack of a sufficiently well mapping and validation
- The FMC does not build on a material but on the material's solid deformation behavior!
- FMC-based SFCs (strength criteria) are simple but describe physics of each single failure mechanism pretty well. Delivers a combined formulation of independent modal failure modes, without the well-known shortcomings of global SFC formulations, which mathematically combine in-dependent failure modes
- The determination of model parameters is to perform by mapping in each pure failure domain and of the interaction exponent *m* by determination in the transition zone between the modes
- Direct use of the friction value μ in the SFC - *instead of using a friction model parameter* - better matches with the engineer's thinking
- The use of the entity material stressing effort $Eff = \sigma_{eq} / R$ brings clarity. It excellently supports 'understanding the multi-axial strength capacity of materials' and tells in which critical failure mode the design screw has to be turned
- Clear equivalent stresses can be calculated for the presented Modal SFCs. Unfortunately, equivalent stresses are differently defined. For instance V. Kolupaev in his Springer book 'Equivalent Stress Concept for Limit State Analysis' [*Kol 17*] and other authors define equivalent stress for Global SFCs. One question comes up then: *Which strength does one refer to the determined equivalent stress*?
- Fracture stresses are acting stresses divided by the stress effort *Eff* in order to fulfil the failure condition $F = 1$
- A SFC can be validated, principally, by 3D test data sets, only. If just 2D test data is available, then the 2D-reduced 3D-SFC is applied. Then, the required High-Fidelity is not fully achieved. This means that the necessary 3D mapping quality is not fully proven
- A test series of an isotropic material along a tensile meridian (it delivers R^t, R^{cc}) or along a compressive meridian (delivers R^c, R^{tt}) alone is not sufficient, on both the meridians tests must be performed. For a general 3D-mapping at least multi-axial failure stress states (R^{tt}, R^{cc}) are required which generate two-fold failure modes. Then the significant inherent 120°-symmetry of brittle isotropic materials can be mapped using the invariant J_3
- When creating an SFC, Eff^{mode} must become zero if the driving stress τ in the case of SF and σ^t in the case of NF becomes zero
- Rounding-off, by employing an interaction equation in the transition zone of adjacent modal failure curves (2D) or of partial failure surfaces is leading to a pseudo-global failure curve or surface. In other words, again a 'single surface failure description' is achieved, however, without the mentioned shortcomings of Global SFCs.

- The FMC is an efficient concept, that improves prediction + simplifies design verification, applicable to brittle and ductile, dense and porous, isotropic, transversely-isotropic and orthotropic materials if clear failure modes can be identified and the material element can be well homogenized.

LL:

- *A usual SFC just describes a 1-fold occurring failure mode (mechanism)*
- *A multi-fold occurrence of a failure with its joint probabilistic effects must be additionally considered in the formulas*

22.2 Structural Mechanics Building, presumption 'homogeneous material'

The author believes that the investigations prove a generic number of 2 for isotropic and of 5 for transversely-isotropic materials. Orthotropic 'materials' are practically still of structural nature and require a 'material'-dedicated special treatment.

Intension of this investigation was to demonstrate, as far as test data was available, that material symmetry might be a sound basis for obtaining a more 'closed' building in mechanics desired by the author since about 30 years.

The following results can be now provided supporting the existence of a generic number 2 for isotropic materials:

- *Assessment of critical multi-axial stress states*: The formulations of invariant-based isotropic SFCs just need 2 invariants. Due to the fact that a stress state may activate a multi-fold fracture failure type NF or SF the original rotational symmetric fracture body becomes 120°-symmetric. This is tackled by employing the invariant J_3.
- *Failure type Normal Yielding NY*: It could be test data-based shown that this 2nd yield type exists in parallel to Shear Yielding SY. Considering the concave failure surface Drucker's stability postulate is to discuss
- *Existence of SIF* $K_{IIcr}^{\ c}$: The author also tried to pave the way for a 2nd 'basic' SIF $K_{IIcr}^{\ c}$ in parallel to $K_{Icr}^{\ t} \equiv K_{Ic}$, where the self-explaining suffix $_{cr}$ must replace the classical $_c$ (because ^{t} denotes tensile and ^{c} compression) in order to generally not confuse readers with two c as indices. The term 'basic' is given to $K_{Icr}^{\ t}$ and $K_{IIcr}^{\ c}$ because the original fracture stress state-induced flaw inclination angle remains 'stable' under further loading and no turning crack under tension or a wing as secondary crack under compression is activated. The SIF K_{IIcr} and K_{IIIcr} are necessary (friction-free crack surface) for crack-turning Mixed Mode Fracture investigations. The basic SIFs $K_{Icr}^{\ t}$ (see *Table 4-2*) and $K_{IIcr}^{\ c}$ show equilibrium!

LL:

- *In the case of isotropic materials – capturing ductile and brittle - for the material's entities a generic (basic) number of 2 is inherent. This is valid for modes, invariants, yield strengths, fracture strengths, fracture mechanical SIFs, fatigue modes and more. In the transversely-isotropic case this number is 5.*
- *Material macro-mechanics seems to possess a mathematical order. Does this not simplify the engineer's situation and lead to a 'closed macro-mechanical building'?*
- *Validated isotropic 3D SFCs enable to predict the 120°-symmetric fracture failure body and further they enable to 'judge' the provided 3D fracture stress states for physical plausibility.*

A further aspect regarding above building was the generation of the Mohr-Coulomb failure curve.

1. Proof, that the structural stresses-formulated fracture curve $\sigma_{II}(\sigma_{III})$ isotropic and $\sigma_{2\,(}\sigma_{3})$ transversely-isotropic can be transferred into a Mohr-Coulomb one $\tau_{nt}\,(\sigma_n)$
2. Demonstration that a dependence of the shear fracture plane angle $\Theta_{fp}°$ with growing hydrostatic compressive stress p_{hyd} is given, as far as shear fracture SF is the primary failure mode. The angle decreases which looks like becoming more ductile. Failure occurs in that plane where the driving shear stress τ or equivalently where Eff^{SF} is maximum
3. The interaction formula maps the course of test data in the mode transition zone. For very brittle materials the mapping quality of shear fracture SFCs F^{τ} and IFF2 is sufficient for design verification as it is conservative. For an accurate determination of the altering fracture plane angle $\Theta fp°$ both the SFCs had to made more 'physically correct' by a degradation function f_d
4. The huge effort spent for the generation of $\Theta_{fp}°$ and the Mohr-Coulomb failure curve paid off for the isotropic and for the UD material as well. For the isotropic material the effort was even higher because $\Theta_{fp}°$ also alters with the meridian-marking Lode angle ϑ caused by the intrinsic 120°-rotational symmetry which impacts $\tau_{nt}\,(\sigma_n)$
5. The interesting failure angle relations between brittle FSF and ductile FMises could be bridged
6. The determination of the cohesive strength $\bar{R}^{\tau}$, by considering the SF-mode only from touch point information ($\tau_{nt}^{c}, \sigma_n^{c}$), is just an *extrapolation,* because in the case of brittle materials $\bar{R}^{\tau}$ is usually located in the transition domain NF-SF. Hence, a realistic cohesive strength can be not predicted by properties just belonging to the SF mode if the NF mode is activated, too. An interaction of the modes is mandatory! At least for Normal Concrete test data sets were available and shall outline this by the following predictions, regarding $\bar{R}^{c} = 40$ MPa, $\bar{R}^{t} = 4$ MPa, $\mu = 0.19$:
   - Linear Mohr-Coulomb, single mode SF: $\bar{R}^{\tau} = \tau_{nt}^{c} + \mu \cdot \sigma_n^{c} = \tau_{nt}^{c} + \mu \cdot \sigma_n^{c} = 17$ MPa
   - FMC-extrapolation, single mode SF, rot-symm: $\Theta^{MC} = \Theta^{c} = \text{constant} \rightarrow \bar{R}^{\tau} = 13.5$ MPa
   - FMC-extrapolation, single mode SF, 120°-model: $\bar{R}^{\tau} = 12.5$ MPa
   - FMC, interaction SF-NF, 120°-model, considering f_d: $\bar{R}^{\tau} = 11$ MPa .

   LL:
   The cohesive strength τ_{nt} (σ_n = 0) of isotropic and transversely-isotropic materials cannot be estimated by an extrapolation of the 'touch point' since the value is a result of a joint micro-damage of SF + NF .

22.3 Fatigue and Some specific material conclusions

Fatigue

Chapter 8 provided a novel life time prediction way indicating:

- A continuous determination of *constant fatigue life* curves CFL $\sigma_a(\sigma_m, N = const.)$ *in the Haigh diagram* $\sigma_a(\sigma_m)$ on basis of the FMC-based static SFCs with interaction equation to capture the transition zone between the modes and on basis of available SN test curves depicted as fatigue (reserve) strength σ_{res}(R, *N).* The chosen fitting function practically is the 4 parameter Weibull curve model (*strength point with three curve parameters*).

- Mapping in the transition zone became possible because the author used a decay function which terminates the influence of the SF (compression) part in the Haigh diagram when the NF part begins at R=0 and vice versa for NF. Essential is that the FMC-based static SFCs are equivalent stress curves $\sigma_{min,eq}$(R, N) and $\sigma_{max,eq}$(R, N) of a mode like the Mises equivalent stress in the case of ductile materials to capture multi-axial stress states
- The author's mode-dedication of Kawai's Modified Fatigue Strength Ratio Ψ optimizes Kawai's idea to firstly determine a strength-normalized master SN curve for each mode. Other necessary SN curves, necessary for the verification of the usually faced variable amplitude operational loading, can then be derived from this Master curve. Also the boundary mode SN curves R=0 and R= $+\infty$ ($\cong$ 100) may then be determined and could be used as basic SN curves.

LL:

- *A continuous constant fatigue life curve as a closed formulation can be derived on basis of one master SN-curve and a model (Kawai) that involves a relationship between the SN-curves.*
- *Here one may add: "Theory (a model) is the Quintessence of all Practical Experience" [August Föppl], engineering scientist for mechanics and head of the materials testing office for mechanical engineering at the TU Munich.*

Isotropic material

- Shear fracture emerges orthogonally to that plane, where the maximum effort Eff^{SF} stresses the solid. Mechanically, this is as well given in the uniaxial compression case in the axial cross-section of the fracture body as in the bi-axial compression stress case
- With the 'isotropic' invariant J_3 the bi-axial strength capacity of isotropic brittle materials is captured. This bi-axial strength capacity (σ_{fr}, σ_{fr}) is $\neq$ the uniaxial strength R in the compressive domain and in the tensile stress domain, too. For dense materials is valid $R^{cc} \equiv \sigma_{fr}^{cc} > R^c$, and for porous materials $\sigma_{fr}^{cc} < R^c$. Under bi-axial tension for brittle and porous materials holds $\sigma_{fr}^{tt} < R^t$. J_3 can be employed in each case
- Due to the Poisson effect, bi-axial compression leads to an axial tensile straining $\varepsilon_3 = -2\,\nu \cdot \sigma^{cc}/E$
- Porous Concrete Stone: the fracture body is 120° rotational symmetric, fully non-circular and the dents - in contrast to Normal Concrete - are oppositely located in the $I_1<0$ domain to those in the $I_1>0$ domain. Any high 3D-compression state is possible for compression-condensed porous materials, however, the material cannot be used further due to crushing
- Concrete: The Poisson effect, generated by a Poisson ratio ν (estimation, for $\nu > 0.2$), may cause tensile failure under 2D compression, because concrete fractures under an internal axial tensile straining
- UHPC: Due to redundancy effects ('healing' of the fracture inducing flaws) the non-circularity of the failure body will reduce with increasing $p_{hyd.}$. For the pretty flawless UHPC - in comparison to Normal Concrete – this effect still holds. Under much higher hydrostatic loading stresses a volume reduction effect occurs.

LL: The 120°-located dents of the isotropic fracture failure body, are the joint probabilistic result of a 2-fold acting of the same failure mode and can be mapped by J_3.

Transversely-isotropic UD material

- For UD materials the failure curve denting bi-axial strength capacity $R^t > R^{tt} = (\sigma_{fr}^{tt}, \sigma_{fr}^{tt})$ could be captured (analogous to J_3) by an additional part in IFF1, if required by the given special task

- Due to the Poisson effect, bi-axial compression leads to a tensile straining $\varepsilon_3 = \varepsilon_{\parallel}$ captured by a tensile stress of the axially placed fibers. Hence, under hydrostatic pressure p_{hyd} 'dense' UD materials will fiber-fracture due to $\varepsilon_{\square} \cdot E_{\square} = R^t_{\square}$ at about thousands of MPa.
- Ply, Lamella, Sheet in construction: The fracture body is the well-known flattened 'cigar' of UD materials
- Successful evaluation of the not very appropriate ARCAN test data to quantify $\mu_{\perp\perp}$
- Creation of a relatively simple novel model IFF2$^{\text{porosity}}$ for a porous UD material in the quasi-isotropic domain

LL: UD lamina may even fracture under a 3D compression stress state by FF1!

Ceramic materials group: isotropic, transversely-isotropic, orthotropic

- For ceramic materials test data sets are practically merely available in literature. The author could only provide some 2D graphs.

22.4 Some remarks considering fidelity in Engineering Design, Analysis, Simulation and Test

For a successful, faster and low-risk design development, a meaningful interaction of the above design topics: design, analysis, simulation and test is mandatory. This will help industry to reduce CoSts, time to market and by-passes the re-design process in case of small design changes. At any stage of the design development, product decisions must rely more and more on virtual tests based on reliable and robust structural analysis processes attached to realistic simulations. Time-consuming and CoStly physical tests can be commonly better run due to cross-fertilization of both the disciplines. A simulation-driven design development reduces later - due to the virtual test possibilities by investigating multiple design options - very CoStly bad design decisions in the early design phase. Further, a minimum number of material and structural tests can be focused. Response is given to "Which physical tests are stringent necessary?" Uncertainty in design is turned into a more robust design. *(Basically from NAFEMS information sheets: The author was a long-time member of the NAFEMS composite WG).*

In the case of critical structural tasks the engineer must have system knowledge about the product, its physics behind and the right tools to solve the task. Therefore, the author cannot see – considering the engineer's responsibility to design reliable structures – a general change for the often proclaimed 'Democratization of design, analysis and manufacture'. For him this might lead to the use of black boxes for not enough well experienced designing engineers. I think Ian Symington, NAFEMS, makes the democratization idea, basically for less critical applications - more realistic by saying: "*The users have to be educated so that they understand the limitations of the method they are using and also educated so that they are aware of their own limitations!"*

Virtual testing creates new responsibility for the engineer to guarantee the required confidence level by building confidence for taking decisions in design verification and product certification. Therefore SFCs are mandatory to reduce failure risk. Physical testing on material level becomes more important to obtain really 3D-validated SFC models that can demonstrate their predictive capability. Further confidence will be given if a clearly structured and reliable 'Macro-mechanics building' is given indicating which verifications must be performed.

Above procedure requires High Fidelity. In this context shall be reminded:

- Design driving Load Cases have to be selected

- Concerning the material models used: Usual assumption for the models is an ideally homogeneous material.
- Input in Structural Analysis: The best prediction of the typical behavior of the structure is performed with typical values = average values. In the later design verification, *dependent on the project requirements*, the average, the upper or the lower value of the respective property is to use
- Be similarly good in the design considering models, properties, calculation etc.!

22.5 Lessons Learned LL from the application of the SFCs

- It is advantageous from physical and from modelling reasons not to employ 'global' SFCs
- The challenge is not so much the establishment of a SFC but the convincing test data–based visualization of its associated fracture failure body and in this context for isotropic materials the display of the failure curve in the principal stress plane as a bias cross-section of the failure body. In the case of brittle isotropic materials, heavy test effort causes the depiction of the different meridian curves as the axial cross-sections of the failure body with inward and outward dents along the axis of the 120°-symmetric isotropic failure body
- The use of the entity *Eff* excellently supports to understand a multi-axial strength capacity of a material, visualized on some displayed failure body Figures and Tables
- It is too discriminate bi-axial fracture stress state and (uniaxial) strength, defined as technical strength in engineering. Just for practical reasons the term bi-axial strength (R^{tt}, R^{cc}) is used for marking the bi-axial fracture stress state. In this context mind: Under multi-axial compression states the (material) strength is not increased but the risk of shear fracture failure is decreased, indicated by an $Eff^{SF} < 1$. $Eff = 1$ represents also the inward or outward dent of the failure surface. Visualization of the influence of 2D- and 3D-compression stress states on the strength capacity by the material stressing effort Eff and proving that all the failure stress states are located on the failure surface Eff = 100%. The technical strength is not increased. Probably one might only call this 'increase of strength
- 'Touch point': It's coordinates (τ_{nt}^{c}, σ_n^{c}) in Mohr stresses correspond to the compressive strength point (R^{c}, 0) in structural stresses. Of-course, friction quantities, which are determined in the Mohr-Coulomb touch point, remain the same for the rotationally-symmetric model and for the 120°-rotationally-symmetric mode, $c_{2\Theta}^{SF} = c_2^{SF}$, μ, C^c of the isotropic material. They must not be dependent
- Multi-axial compression works as quasi-plasticizer
- Due to the redundancy effect ('healing', which causes an increase of the load carrying ability) found with 'dense' concrete and grey-cast iron under bi-axial compression (in contrast to porous foam and concrete stone) the dent in the negative I_1-domain is oriented outward, opposite to the tensile domain
- Flaw distribution effect: Activation of the critical fracture plane depends on the spatial distribution and orientation of the flaws
- Hoop Planes = deviatoric planes = π–planes are convex. Meridian planes are **not convex** at max I_1 (tension) and for UHPC in the high hydrostatic compression domain. Question arises: Is the convexity condition linked to uniaxial stressing?
- The applicability of a SFC ends (example UD) when the driving mode stress σ^t (IFF1) or τ (IFF2) becomes zero and the associate *Eff* becomes negative. Therefore, the traditional use to just apply the so-called 'Proportional Loading (stressing)' concept in order to derive *Eff* from *F* must be checked whether the condition above is fulfilled or not (see *§ 8.3.3*). For mathematically homogeneous and non-homogeneous SFCs the difference of Failure Index |F| and material stressing effort Eff can be outlined. In this context the concept of

'proportional loading' and the concept idea of 'driving stress' were presented. This invites for discussion regarding linear and non-linear stress analyses

- Limits of the applicability of the (material-linked) SFCs: Structural failure may occur which cannot be described by a SFC because it is not a material failure anymore (UD examples: instability of a tube test specimen under compression; filament-upon-filament compression within an ultra-highly compressed stack, as in Test Case 12 of WWFE-II, *§ 6.2*)
- A physically based strength model possesses a minimum number of model parameters. After proven demonstrations of a good mapping of the courses of accurate test data ('goodness of fit') such a model is able to even sort out false test data results of a successful qualification of a material model.

It's one thing to have an idea, the FMC theory, but it's another to make it fly.
Theory must not be an *end in itself*!
A big task is to make a theory understandable.

22.6 Notes on Analyses

Stress and strain analysis

Considers the external boundary conditions and internal restraints and converts the environmental loadings into internal forces, fluxes, stresses and strains for all the load cases by the :

- Use of adequate models to map the structural behavior
- Consideration of all relevant load cases
- Use of adequate physical properties such as
  - average (typical) values of the stochastic design variables in order to end up with a structural behavior which meets real behavior best (which means with a 50% expectance value)
  - average stress-strain relationship (is to be seen as a physical quantity) in the applied models
- Consideration of environmental influences such as temperature, humidity, radiation. They may have a substantial impact on the coefficient of thermal expansion, Young's modulus and strength design allowables.
- Data input from a material handbook is to be carefully selected in order to match the real hardware (e.g. with respect to plate, sheet, extrusion, heat treatment).
- Utilized are average elasticity properties and nominal geometry (thickness, length) to represent average structural behavior.
- Physical properties to be used in analysis shall be adequate: Required are mean (typical, average) values of the stochastic design variables in order to end up with a structural behavior, which meets the real behavior best (*50% expectance value*). The stress-strain relationship is a feature of the applied physical models, and is to be seen as a physical quantity !
- Strength Demonstration (*design verification*): One-sided tolerance bands (*for static and fatigue strength*) and two-sided tolerance bands (*for thickness, Young's modulus*) are considered.
- Stiffness Demonstration: Due to stiffness requirements upper and lower tolerance limits
- Application of a statistically based A-value and B-value Design Allowables:
  - A-values: Application of the Safe Life Concept (single load path, where failure of a single element leads to the loss of structural integrity)
  - B-values: Application of the Damage Tolerance Concept (multiple load paths, redundancy).

Note: In structures with multiple load paths, loads are distributed according to the stiffness properties of the individual load paths. Therefore, it is essential to use average stiffness values (material and geometrical properties) to end up with typical load distributions. Otherwise it might happen that predicted load distributions are 'un-typical' with the result that stresses may be predicted too low and incorrect locations of critical points are assessed.

LL:

- *UD lamina may even fracture under a 3D compression stress state by FF1!*
- *Failure probability pf does not dramatically increase if MoS turns slightly negative. A local safety measure MoS = -1 % is no problem in design development. The MoS value does not outline the risk or the failure probability! Do not overreact by a costly re-design. Apply a ' Think (about) Uncertainties' attitude by recognizing the main driving design parameters and reducing the scatter (uncertainty) of them.*
- *Increasing property mean value and decreasing standard deviation lower the failure probability*

Strength analysis

- Strength of a design is demonstrated, if 'No relevant strength failure condition (*to be understood as the limit state of a failure mode*) is met or exceeded for all dimensioning load cases', resulting in a non-negative (positive) Margin of Safety MoS.
- Generally, strength analysis can be not performed in one shot together with stress-strain analysis (*in fact, it is an iterative process*). Has to be performed separately as a 'post-processing work' to account for: Scatter of the design variables (e.g. upper or lower E-modulus), the strength design allowable (*statistical minimum values, and etc.).*
- Strength analysis can be separately performed as a 'post-processing work' to account for:
  - scatter of the design variables (*e.g. upper or lower Young's modulus in stiffness requirement cases, minimum local thickness values*),
  - strength design allowables (*statistical minimum values*).
- Essential in the strength analysis is the used Strength Failure Condition F = 1. Its aim is to assess multi-axial stress states by just utilizing the basic uniaxial strength values, which are mandatory in design, anyway. Types of SFCs are the global and the modal ones (*see representative chapter*), namely

$$F\left(\{\sigma\},\{R\}\right)=1 \quad \text{and} \quad F\left(\{\sigma\},\{R_{\text{mode}}\}\right)=1 \rightarrow F\left(\{\sigma\},\{R_{\text{mode}},\mu_{\text{mode}}\}\right)=1 \quad \text{with the FMC}$$

If the structural analysis requires a non-linear treatment then some features are to keep in mind:

- Stressing is re-distributed to stiffer regimes (*in case of composites to the fibers*)
- In contrast to the linear model, an altered load path (*according to local weakening*) may be predicted by the non-linear model
- Large strains and large displacements may occur (*which in principle includes yielding of metals and micro-cracking caused quasi-yielding*)
- Change of shape of the loaded structure is possible
- Release of residual stresses according to degradation growth in case of monotonic and cyclic loading and in hygro-thermal environment
- The assessment of the critical stress state is performed with the obtained Eff and the strength design allowable. Global yielding is never permitted. If a critical strain state has to be assessed then a limit design strain needs to be defined.

Stability analysis

Even for 'simple' stability-endangered structural elements seldom a test series is available to compute statistically-based stability design allowables. Aircraft certification standards usually do not require statistics to be performed on stability tests. For example, in EASA CS 25.307 (b) is cited: "When static or dynamic tests are used to show compliance with the requirements of CS 25.305 (b) for flight structures, appropriate material correction factors must be applied to the test results, unless the structure or part thereof, being tested has features such that a number of elements contribute to the total strength of the structure and the failure of one element results in the

redistribution of the load through alternate load paths." Thus, for all multiple load path structures a statistics-aimed testing is not required by CS 25.

In spacecraft, an improvement of the predictions of the traditional stability analysis result is aimed at by applying a statistically based estimation procedure for the failure load. This requires knowledge about the design variables such as geometrical tolerances, imperfections and scatter of properties. This knowledge is the input of - for instance a Monte-Carlo method - which predicts sensitivities and delivers a statistically based failure load, an improved value compared to the traditional analysis one.

LL on modelling:

- *Physics have to be modelled accurately! The choice of the task-corresponding stress-strain curve has to be carefully performed (min or mean or max values).*
- *Robust (tolerant) design or robustness to later changes of the design parameters with identification of the most sensitive design parameters is a NEED*
- *Basis of a good design is the modelling work of an experienced engineer. This requires an understanding of the full system supported by a basic technical knowledge such as mechanics. Then tools like artificial intelligence can be successfully applied, because the user can interprete the results.*
- *To proceed, we must improve the interdisciplinary work. System Engineering is mandatory.*

22.7 General FMC-linked Literature

[Arg73] Argo A S: *Physical basis of distortional and dilatational plastic flow in glassy polymers.* J. Macromol. Sci. Phys B8 (1973), 573-596

[Awa78] Awaji H and Sato S: *A Statistical Theory for the Fracture of Brittle Solids under Multiaxial Stresses*. Int. J. of Fracture 14 (1978), R 13-16

[Bec94] Becker W. and Kress G: *Stiffness Reduction in Laminate Coupons due to the Free-edge Effect*. Comp.Science and Technology 52 (1994), 109-115

[Bil11] Bilisik K: *Advances in Modern Woven Fabrics Technology*. Edited by Savvas Vassiliadis, ISBN 978-953-307-337-8, 252 pages

[Bir38] Birch R.: *The Effect of Pressure Upon the Elastic Parameters of Isotropic Solids, according to Murnaaghan's Theory of Finite Strains*. Journal of Applied Physics 9 (4), 279-288.

[Boe08] Böhm R: *Bruchmodebezogene Beschreibung des Degradationsverhaltens textilverstärkter Verbundwerkstoffe*. Dissertation, TU Dresden, 2008

[Boer89] de Boer, R. and Dresenkamp, H.T.: *Constitutive Equations for concrete in failure state*. J. Eng. 115 (8), 1989, 1591-1608

[Boe85] Boehler, J.P.: *Failure criteria for glass-fiber reinforced composites under confining pressure*. J. Struct. Mechanics 13, 371-393

[Boe87] Boehler J P : *Introduction to the invariant formulation of anisotropic constitutive equations*. 1987. In: Boehler J.P. (Ed.) *Applications of Tensor Functions in Solid Mechanics*. CISM Course no.292. Springer-Verlag. In addition a personal note from J. Boehler on UD invariants which were later applied by the author in his FMC

[Bre79] Breuer H und Stabenow J: *Schädigungskriterien glasiger Polymere im Hinblick auf deren Schlagzähmodifizierung*. Die Angewandte Makromolekulare Chemie 78 (1979), 45-65. SF-shape is SY-shape

[Bri52] Bridgeman P.W.: *Studies in Large Plastic Flow and Fracture*. McGraw-Hill, New York, 1952

[Bro18] Brocks W: *Plasticity and Fracture.* Springer, Series Solid Mechanics, Applications.

[Bus06] Busse G , Kröplin B-. and Wittel F K: *Damage and its Evolution in Fiber-Composite Materials: Simulation and Non-Destructive Evaluation.* SFB 381, Stuttgart, ISBN 3-930681-90-3

[Car93] Carpinteri A, Valente S, Ferrara G and Melchiorri G: *Is mode II Fracture Energy a real Material Property*? Computers & Structures 48 (1993), No3, 397-413

[Che11] Cherif Ch: *Textile Werkstoffe für den Leichtbau*. Springer-Verlag, 2011

[Che13] Cherif, editor: *Leichtbau mit Textilverstärkung für Serienanwendungen: Bindermaterialien – Textile Preforms – Verbundbauteile; Buch zum DFG-AiF-Clustervorhaben – Leichtbau und Textilien.* Verlag Wissenschaftliche Skripten, 2013, ISBN 978-3-942267-81-6

[Chr98] Christensen R M: *The Numbers of Elastic Properties and Failure Parameters for Fiber Composites*. Transactions of the ASME, Vol. 120 (1998), 110-113

[Cun87] Cuntze R: *Failure Path Analysis of Multi-layered Fiber Reinforced Plastic Components with the Reliability Calculation Programme FRPREL*. ESA/ESTEC conference Noordwijk, Oct. 1987

[Cun93] Cuntze R: *Deterministic and Probabilistic Prediction of the Distribution of Inter-Fiber Failure Test Data of Pre-strained CFRP Tubes composed of Thin Layers and loaded by radial pressure*. Wollongong. *Advanced Composites ,93, 579-585. The Minerals, Metals & Materials Society, 1993*

[Cun96a] *Bruchtypbezogene Auswertung mehrachsiger Bruchtestdaten und Anwendung im Festigkeits-nachweis sowie daraus ableitbare Schwingfestigkeits- und Bruchmechanik-Aspekte*. DGLR-Kongreß 1996, Dresden. Band 3

[Cun96b] Fracture-type strength criteria , formulated by invariants which consider the material symmetries of the isotropic, anisotropic material. Conference on Spacecraft Structures, Materials & Mechanical Testing. 27-29 March 1996, ESA SP-386 pp 399-409

[Cun97] Cuntze R: Evaluation of Multi-axial Test Data of UD laminas by so-called "Fracture-type Strength criteria" and by supporting probabilistic means, ICCM 1997, 14 pages*

[Cun98a] Cuntze R: *Strength Prediction for Multi-axially Loaded CMC-Materials*. 3rd European Workshop on thermal Protection Systems. ESA-ESTEC: Noordwijk, March 1998, WP P141

[Cun98b] Cuntze R: *Application of 3D-strength criteria, based on the so-called "Failure Mode Concept", to multi-axial test data of sandwich foam, concrete, epoxy, CFRP-UD lamina, CMC-Fabric Lamina*. ICCE/5, Las Vegas, July 1998 (presentation)

[Cun98c] Cuntze R and Sukarie G.: *Effective Dimensioning of 3D-stressed UD-laminas on Basis of Fracture-type Strength Criteria. Int. conf. on Mechanics of Composite Materials*. Riga, April 20-23, 1998. *Conference handbook*, presentation

[Cun98d] Cuntze R: *The Failure Mode Concept- a new comprehensive 3D-sterength Analysis Concept for any Brittle and Ductile behaving Material*. European Conference on Spacecraft and Structures, Materials and Mechanical Testing. ESA-CNES-DGLR-DLR, Braunschweig, Nov.4-6 1998

[Cun99] Progressive Failure of 3D-stressed Laminates: Multiple Non-linearity treated by the Failure Mode Concept (FMC). DURACOSYS99, Brussels, July 1999. Balkema, Rotterdam, 2000

[Cun00a] *Static Design and Strength 'Proof of Design' of Pressure Vessels, built from Ductile or Brittle Materials*. Problems of the North; Yakutsk 2000

[Cun00b] *Are there CoSt Drivers in the Structural Analysis of the ARIANE 5-Development*? Noordwijk, 29. Nov./1. Dec. 2000.

[Cun01] *Assessment of Load- and Strain-controlled States of Stress in 'hot Spots' – On the way to an Industrial Approach for Gurson Materials*. 3rd European Conference on Launcher Technology. CNES, DLR, ESA-ESTEC, ISU: Strasbourg, Dec. 11-14, 2001.

[Cun02] Cuntze R. and Memhard D.: *Evaluation of the Tension Rod Test for Ductile Material Behavior - Key item for the establishment of a procedure to assess strain-controlled 'hot spots'*. European Conf. On Spacecraft Structures, Materials and Mechanical Testing; ESA-CNES-DGLR-DLR, Toulouse 2002, Conference handbook

[Cun04] Cuntze R.: *Should we consider Matrix Yielding when investigating the Deformation Behavior?* 9th European-Japanese Symposium on Composite Materials.. Technical University of Hamburg –Harburg, May 2014

[Cun04a] Cuntze R and Freund A: *The predictive capability of failure-mode-concept-based strength criteria for multidirectional laminates*. WWFE-I, Part A. Comp. Science Technology 2004 , pp 343-377

[Cun04b] Cuntze R: *The Predictive Capability of Failure Mode Concept-based Strength Criteria for Multidirectional Laminates*. WWFE-I, Part B. Comp. Science and Technology 64 (2004), 487-516

[Cun05] Cuntze R: *Is a CoStly Re-design really justified if slightly negative margins are encountered? Konstruktion*, März 2005, 77-82 and April 2005, 93-98 (*reliability treatment of the problem*)*

[Cun05] Cuntze R: *Efficient 3D and 2D failure conditions for UD laminas and their applications within the verification of the laminate design*. Comp. Sci and Technology 66 (2006), 1081-1096

[Cun06] Cuntze R: *Failure Conditions for Isotropic Materials, Unidirectional Composites, Woven Fabrics - their Visualization and Links*. https://www.ndt.net › cdcm2006 › papers › cuntze, PDF

[Cun07] Cuntze R: FDM

[Cun08] Cuntze R.: *Strength Failure Conditions of the Various Structural Materials: Is there some Common Basis existing*?. SDHM, vol.074, no.1, pp.1-19, 2008

[Cun12] Cuntze R: *The predictive capability of Failure Mode Concept-based Strength Conditions for Laminates composed of UD Laminas under Static Tri-axial Stress States*. WWFE-II, Part A . Journal of Composite Materials 46 (2012), 2563-2594

[Cun13] Cuntze R: *Comparison between Experimental and Theoretical Results using Cuntze's Failure Mode Concept model for Composites under Tri-axial Loadings* – Part B of the WWFE-II. Journal of Composite Materials, Vol.47 (2013), 893-924

[Cun13b] Cuntze R.: *Tackling Uncertainties in Design – uncertain design parameters, safety concept, modelling and analysis*. Verbundwerkstoffe, GDM, 18. Symposium, Chemnitz 30.3. – 1.4. 2011

[Cun14] Cuntze R: *The Fracture Failure Surface of Foams, derived on basis of the author's Failure Mode Concept*. PPT presentation, Carbon Composites e.V. (CceV), meeting of the working group 'Engineering', July 11, 2014*

[Cun14b] Cuntze R: *The WWFEs I and II for UD Materials – valuable attempts to validate failure theories on basis of more or less applicable test data*. In Conference Handbook SSMET 2014:= Europ. Conf. on Spacecraft Structures, Materials and Environmental Testing. Braunschweig, 1- 4 April 2014, 8 pages

[Cun14c] HSB 01501-01: *Essential Topics in the Determination of a Reliable Reserve Factor*. IASB, Issue A, 2014 (Cuntze author) TIB Hannover, 20 pages,

[Cun15a] Cuntze R: *Static & Fatigue Failure of UD-Ply-laminated Parts – a personal view and more*. ESI Group, Composites Expert Seminar, Uni-Stuttgart, January 2015, 27-28, keynote presentation*

[Cun15b] Cuntze, R: *Reliable Strength Design Veriftcation – fundamentals, requirements and some hints*. 3rd. Int. Conf. on Buckling and Postbuckling Behavior of Composite Laminated Shell Structures, DESICOS 2015, Braunschweig, March 26 ~27, Extended Abstract, Conf. Handbook, 8 pages

[Cun15c] Cuntze R: *Basis Document, Update ComPoLyX Manual chapter Cuntze and Relationship of Cuntze's UD friction parameters b with Mohr's friction coefficients.* CCeV website, May 4, 2015 *

[Cun16a] Cuntze R: *Fracture failure surface of the foam Rohacell 71G*. 3. NAFEMS Regionalkonferenz, 25.-27. April, 2016. Berechnung und Simulation, 35 slides *

[Cun16b] Cuntze R: *Introduction to the Workshop – from Design Dimensioning via Design Verification to Product Certification*. Experience Composites 16 (EC16), September 21 – 23, 2016, Augsburg. Extended Abstract in the Symposium Abstracts. 10 pages*

[Cun16c] Cuntze R: *Progress reached, in Static Design and Lifetime Estimation*? Mechanik-Kolloquium, TU-Darmstadt, December 21, 2016 (UD and isotropic materials, Extended Presentation, 150 slides) *

[Cun17] Cuntze R: *Fracture Failure Bodies of Porous Concrete Stone (isotropic foam-like), Normal Concrete, Ultra-High-Performance-Concrete and of the Lamella (sheet) – generated on basis of Cuntze's Failure-Mode-Concept (FMC).* NWC 2017, June 11-14 Stockholm. Extended Abstract, Symposium Handbook, 13 pages *

[Cun19a] Cuntze R: presentation in the author's working group CU AG "Engineering" on *3D-Festigkeitsbedingungen für spröde Werkstoffe isotrop, transversal–isotrope UD-Schicht und orthotropes Gewebe – ermittelt auf Basis des Failure-Mode-Concepts (FMC) von Cuntze*. June 25, 2019 Basel (English slides) *

[Cun19c] Cuntze R: *Technical terms for composite components in civil engineering and mechanical engineering*. Fachbegriffe mit Erklärung und Definition. In: *Fachbegriffe für Kompositbauteile – Technical terms for composite parts.* Springer Vieweg, Wiesbaden, 2019, 171 pages *

[Cun20a] Cuntze R: Einführungsvortrag des Autors als Leiter der AG „Bemessung und Nachweis" zum CU-Thementag „*Richtlinien, bauaufsichtliche Zulassungen und Bauartgenehmigungen für die potentiellen Anwender Architekten, Tragwerksplaner und Bauherrn"*. Zoom conference, 19. Nov. 2020. 40 slides (English and German) *

[Cun20b] Cuntze R: *Normal Yielding NY and Compression-induced Critical Stress Intensity Factor $K_{IIcr}{}^{c}$-Missing Links in an Isotropic 'Closed' Macro-Mechanics Building*. 30 pages *

[Cun21] Cuntze R: *Strength capacity of bi-axially compressed UD strands at turning points of rotor blade loops and of hangers of network arch bridges.* CU-AG "Engineering", May 20. *

[Cun21b] Cuntze R: *The Mohr Coulomb Fracture Failure Curve $\tau_{nt}(\sigma_n)$ and Associated Topics*. Jun 21, pp 59*

[DeTer99] De Teresa S.J.: *Failure of a composite lamina under three-dimensional stresses*. UCRL-JC-135664

[DeTer04] DeTeresa S J, Dennis C, Freeman O C, and Groves S E: *The Effects of Through-thickness Compression on the Interlaminar Shear Response of Laminated Fiber Composites*. J. Compos Mater, V 38, No. 8, pp681-697, 2004

[Dru52] Drucker D C and Prager W: *Soil mechanics and plastic analysis for limit design*. Quarterly of Applied Mathematics, 1952, vol. 10, no. 2, pp. 157–165

[Ern07] Ernst G., Vogler M, Hühne C. and Rolfes R.: *Multi-scale Simulation for Stiffnesses and Strengths of Textile Composites*. NAFEMS Seminar, Simulating Composite Materials and Structures. Bad Kissingen, Nov. 2007

[Fla82] Flaggs D L and Kural, MH: *Experimental Determination of the In Situ Transverse Lamina Strength in Graphite Epoxy Laminates*. J. Comp. Mat. Vol 16 (1982), 103-116

[Gai19] Gaier C and Dannbauer H: *Eine Software-basierte Methode zur Betriebsfestigkeitsanalyse von Strukturbauteilen aus CFK*. Engineering Center Steyr, Magna, J. Maier, G. Pinter, Montanuniversität Leoben

[Gei97] Geiwitz W, Theuer A and Ahrends F J: *Experimentelle Bestimmung eines Versagenskriteriums für faserverstärkte Keramik*. Tagungband "Verbundwerkstoffe und Werkstoffverbunde", Kaiserslautern september 1997

[Ger94] Germanovich JN, Dyskin AV. *A model of brittle failure for material with cracks in uniaxial loading*. Mechanics of Solids 1988;23(2):111-123

[Gie94] Gierlinski j t & Smith M (WS Atkins, UK); Thoft-Cristensen P (CSR Denmark); Santos J L T (IST Portugal); Cuntze R (MAN) & Gollwitzer S (RCP), Germany: *Reliability–based Design of structural components.* Proc. Symp. On Advanced Materials for Lightweight Structures at ESTEC Noordwijk, March 1994, ESA –WPP-070, pp 121 -125

[Gol66] Goldenblat, I.I., Kopnov, V.A.*: Strength of Glass-Reinforced Plastics in the complex stress state*. Polymer Mechanics of Mechanical Polimerov, Vol. 1 1966, 54-59

[Gur77] Gurson A L: *Continuum Theory of Ductile Rupture by Void Nucleation and Growth. Part 1:Yield criteria and flow rules for porous ductile media*. J.Eng. Mater. Techn.99 (1977), 2-15

[Fla82] Flaggs D L and Kural M H*: Experimental Determination of the In Situ Transverse Lamina Strength in Graphite Epoxy Laminates*. J. Comp. Mat. Vol 16 (1982), S. 103-116

[Gri21] Griffith, A.A.: *The phenomena of rupture and flow in solids*. Philosophical Transactions of the Royal Society of London, 1921, A 221: 163–198

[Gur77] Gurson A L: *Continuum Theory of Ductile Rupture by Void Nucleation and Growth. Part 1:Yield criteria and flow rules for porous ductile media*. J. Eng. Mater. Techn.99 (1977), 2-15

[Hah15] Hahne C: *Zur Festigkeitsbewertung von Strukturbauteilen aus Kohlenstofffaser-Kunststoff-Verbunden unter PKW-Betriebslasten*. Shaker Verlag, Dissertation 2015, TU-Darmstadt, Schriftenreihe Konstruktiver Leichtbau mit Faser-Kunststoff-Verbunden, Herausgeber Prof. Dr.-Ing Helmut Schürmann

[Har93b] Hart-Smith L J: *An Inherent Fallacy in Composite Interaction Failure Curves*. Designers Corner, Composites 24 (1993), 523-524 [Has80] Hashin Z: *Failure Criteria for Unidirectional Fiber Composites*. J. of Appl. Mech. 47 (1980), 329-334

[Has80] Hashin Z: *Failure Criteria for Unidirectional Fiber Composites*. J. of Appl. Mech. 47 (1980), 329-334

[Hin04] Hinton M J, Soden, P D and Kaddour A S: *Failure criteria of fiber reinforced polymer composites*. The World-Wide Failure Exercise. Elsevier, 2004, ISBN 0-08-044475-X, 700 pages

[Hop95] Hoppel C.R.R., Bogetti T.A. and Gillespie J.W.jr.: *Literature review – Effects of hydrostatic pressure on the Mechanical Behavior of Composite Materials*. J. of Thermoplastic Composite Materials 8 (1995), 375-409

[Hoek14] Hoek E and Martin C D: *Fracture initiation and propagation in intact rock – A review*. Journal of Rock Mechanics and Geotechnical Engineering 6 (2014) 287-300

[Hol19] Holschemacherk (editor) et al.:*Entwurfs-und Berechnungstafeln für Bauingenieure*. 8.Auflage, Beuth Verlag GmbH

[HSB] German Aeronautical Technical Handbook '*Handbuch für Strukturberechnung*', issued by Industrie-Ausschuss-Struktur-Berechnungsunterlagen. TIB Hannover

[Irw57] Irwin, G: *Analysis of stresses and strains near the end of a crack traversing a plate.* Journal of Applied Mechanics 24 (1957), 361–364.

[Kad13] Kaddour A and Hinton M: *Maturity of 3D failure criteria for fiber-reinforced composites: Comparison between theories and experiments*. Part B of WWFE-II, J. Compos. Mater. 47 (6-7) (2013) 925–966.

[Kaw04] Kawai M: *A phenomenological model for off-axis fatigue behavior of uni-directional polymer matrix composites under different stress ratios*. Composites Part A 35 (2004), 955-963

[Kaw88] Kawagoe M and Kitagawa M: *On criteria for craze initiation in glassy polymers*. J. of Materials Science 23 (1988), 3927-3932

[Kno03] Knops M.: *Sukzessives Bruchgeschehen in Faserverbundlaminaten*. Diss. 2003. Aachen, Institut für Kunststoffverarbeitung

[Kol12] Kolupaev V A, Bolchoun A and Altenbach H: *Unified Representation and Evaluation of the Strength Hypotheses.* 2012

[Kol17] Kolupaev V A: Equivalent stress concept for limit state analysis. Springer, Vol 86 in Advanced Structured Materials

[Kow83] Kowaltschuk B.I. and Giginjak F.F.: ..in Russian, Kiew, Naikowa Dumka 1983

[Kup73] Kupfer H: *Das Verhalten des Betons unter mehrachsiger Kurzzeitbelastung unter besonderer Berücksichtigung der zweiachsigen Beanspruchung*. In Deutscher Ausschuss für Stahlbeton, Band 229, 1973

[Laf 12] Laffan M.J., Pinho S.T., Robinson P., McMillan A.J., *Translaminar fracture toughness testing of composites: A review*, Polymer Testing (31) 2012, 481-489.

[Laf 12] Laffan M. J., Pinho S. T., Robinson P., Iannucci L., McMillan A. J., *Measurement of the fracture toughness associated with the longitudinal fiber compressive failure mode of laminated composites*, Composites Part A: Applied science and manufacturing (43) 2012, 1930-1938.

[Lan19] Hengxing Lan, Junhui Chen & Renato Macciotta: *Universal confined tensile strength of intact rock.* Scientific Reports | (2019) 9:6170 | https://doi.org/10.1038/s41598-019-42698-6

[Leg02] Leguillon D: *Strength or Toughness? –A criterion for crack onset at a notch.* Europ. J. of Mechanics A/Solids 21 (2002), 61 – 72 end. Ist. D. sci. Lett., Cl. Mat. Nat.18, 705-714 (1885

[Lem08] Lemnitzer L, Eckfeld L, Lindorf A and Curbach M (IfM TU Dresden): *Bi-axial tensile strength of concrete – Answers from statistics*. In: Walraven, J. C.; Stoelhorst, D. (Hrsg.): Tailor made concrete structures. New solutions for our society. Amsterdam, The Netherlands: CRC Press / Balkema, 2008, S. 1101-1102

[Liu14] Liu J, Zhu Z and Wang B: *The fracture characteristic of three collinear cracks under true tri-axial compression.* The scientific World Journal, V 2014, article ID459025, 5 pages

[Lod26] Lode Walter.: *Versuche über den Einfluß der mittleren Hauptspannung auf das Fließen der Metalle Eisen, Kupfer und Nickel*. Z Phys 36:913–939 66.1926

[Mas94] Masters J.: *Fractography of Modern Engineering Materials*. Composites and Metals. 2nd volume. ASTM STP1203,1994

[Mat75] Matsushige K, Radcliffe S V and Baer E: *The mechanical behavior of polystyrene under pressure*. J. of Material Science 10 (1975), 833-845

[Mathcad 13 and 15]: *PTC mathematical program*, used by the author

[Mat95] Matzenmiller A, Lubliner J and Taylor R L .: *A constitutive model for anisotropic damage in fiber-composites*. Mechanics of Materials 20 (1995), 125-152

[Mat07] Matzenmiller A and Koester B.: *Consistently Linearized Constitutive Equations of Micro-mechanical Models for Fiber Composites with Evolving Damage*. Int. Solids and Structures 44 (2007), 2244-2268

[Mec21] Mechtcherine V: *Klassifizierverfahren digitalerFertigungsvefafahren im Betonbau*. March 2012. Cu Bau AG. 4. Thementag (lead by the author) ‚Automatisierte Fertigung im Bauwesen inklusive Serielles Bauen'.

[Mel77] Melville PH: *Fracture mechanics of brittle materials in compression*. Int. J. Frac.13, 532-534 (cited in Liu 14)

[MIL17] MIL-HDBK 17 "*Polymer Matrix Composites*": Vol I "Guidelines for Characterization of Structural Materials"; Vol II "Material Properties"; Vol. III "Utilization of Data". Dep. Of Defence (DOD), Technomic Publishing USA

[Moh00] Mohr O.: *Welche Umstände bedingen die Elastizitätsgrenze und den Bruch eines Materials*? Civilingenieur XXXXIV (1900), 1524-1530, 1572-1577

[Mul67] Mulhern J F, Rogers T G and Spencer A J M: *A Continuum Model for Fiber-Reinforced Plastic Materials*. Proceedings of the Royal So ciety, Series A, Vol. 301,1967, p. 473

Mur09] Murthy A R, Ch, Palani G S and Iyer N: *State-of-the-art review on fracture analysis of concrete structural components*. Sadhana Vol.34, Part 2, April 2004, 345-367

[Nem90] Nemeth, N.N., Manderscheid, J.M. and Gyekenyesi, J.P.: *CARES (Ceramic Analysis and Reliability Evaluation of Structures) users and Programmers Manual*. NASA Technical Paper 2916, August 1990

[Ott77] Ottosen N S: *A failure criterion for concrete*. Journal of the Engineering Mechanics. ASCE, 103(EM4):527–535, August 1977

[Oro68] Orowan E: *Fracture and strength of solids*. Reports on Progress in Physics XII, 1948, 185–232

[Pae96] Pae K D: *Influence of Hydrostatic Pressure on the Mechanical Behavior and Properties of Uni-directional, Laminated, Graphitefiber/Epoxy matrix Thick Composites*. Composites Part B 27B (1996), 599-611

[Pag81) Page A W : *The biaxial compressive strength of brick masonry*. Proc. Inst.Civil Engrs.; 71(2) (1981)., pp. 893–906.

[Pag83] Page A W: *The strength of brick masonry under biaxial tension–compression.* International Journal of masonry constructions; 3 (1), (1983),pp. 26-31.

[Pap96] Papa E : *A unilateral damage model for masonry based on a homogenization procedure*. Wiley online library, Volume1, Issue4, October 1996. Pages 349-366

[Pau61] Paul, B.: *A Modification of the Coulomb Mohr Theory of Fracture*. J. of Appl. Mech. (1961), 259-268

[Pet15] Petersen E, Cuntze R and Huehne C: *Experimental Determination of Material Parameters in Cuntze's Failure-Mode-Concept-based UD Strength Failure Conditions.* Composite Science and Technology 134, (2016), 12-25 *

[Pin06] Pinho S T, Robinson P, Iannucci L, *Fracture toughness of the tensile and compressive fiber failure modes in laminated composites*, Composites Science and Technology 66 (2006), 2069–2079.

[Pha03] Phan A V, Napier J A L , Gray L J and Kaplan T: *Stress intensity factor analysis of friction sliding at discontinuity interfaces and junctions*. Computational Mechanics 32 (2003), 392 -400

[Puc96]Puck A: *Festigkeitsanalyse von Faser-Matrix-Laminaten – Modelle für die Praxis*. Carl Hanser Verlag München

[Puc02] Puck A and Schürmann H: *Failure Analysis of FRP Laminates by Means of Physically-based Phenomenological Models*. Composites Science and Technology 62 (2002), 1633-1662

[Puc02b] Puck A, Knops M and Kopp J: Guidelines for the determination of the parameters in Puck's action plane strength criterion. Comp. Science and Technology 62 (3) (2002) 371–378

[Rac87] Rackwitz R and Cuntze R: *System Reliability Aspects in Composite Structures*. Eng. Opt. 11 (1987), 69-76

[Ric68] Rice, J.R.: *A path independent integral and the approximate analysis of strain concentration by notches and cracks*. Journal of Applied Mechanics 35 (1968), 379–386

[Ric13] Richard H., Eberlein A. and Schirmeisen N-H.: *Experiments on Cracks under Spatial Loading*. 13th Int. Conf. On Fracture, Beijing June 16-21 2013

[Ren38] Rendulic, L.: Eine *Betrachtung zur Frage der plastischen Grenzzustände.* Der Bauingenieur, 19 (1938), 159-164

[Rou87] Rousselier, G.:, *Ductile fracture models and their potential in local approach of fracture*. Nucl. Eng. Design. 105: 97-111, 1987.

[Ric69] Rice, J.R. and Tracey, D.M.: *On the Ductile Enlargements of Voids in Triaxial Stress Fields*. J. Mech. Phys. Solids (17), 1969, pp. 201-217

[Roh14] Rohwer K.: *Predicting Fiber Composite Damage and Failure*. Journal of Composite Materials, published online 26 Sept. 2014 (online version of this article can be found at: http://jcm.sagepub.com/content/early/2014/09/26/0021998314553885) (on Carbon Connected, CceV)

[Sch06] Schürmann H.: *Konstruieren mit Faser-Kunststoff-Verbunden*. Springer-Verlag 2005

[Ste97] Steglich, D. and Brocks, W.: *Micromechanical Modelling of the Behavior of Ductile Materials including Particles.* Comp. Mat. Science 9 (1997), 7-17

[Ste73] Sternstein S S and Myers F A: *Yielding of glassy polymers in the second quadrant of principal stress space*. J. Macromol. Sci, Phys. B 8 (1973), 539-571

[Tal94] Talreja, R. (Hrsg.): *Damage Mechanics of Composite Materials*. Elsevier, Amsterdam/ London/New York/Tokyo 1994

[Tay02] Taylor D.: *The Theory of Critical Distances – a new perspective in fracture mechanics.* Elsevier, Oxford, UK, 2000

[The96] Theuer, A.: *Experimentelle Untersuchungen zum thermomechanischen Verhalten von Faserkeramik. Dissertation*. Univ. Stuttgart, 1996

[Thi07] Thielicke B: *Die Ermittlung der interlaminaren Scherfestigkeit von kohlenstoff-faserverstärkten Kohlenstoffen mit dem Druckscherversuch im Temperaturbereich zwischen Raumtemperatur und 2000°C*. Dissertation, Uni Karlsruhe, 1997

[Tsa71] Tsai S W and Wu E M: *A General Theory of Strength for An-isotropic Materials*. Journal Comp. Materials 5 (1971), 58-80

[Tsa15] Tsai S W and Melo J D : *Composite Materials design and Testing* (*unlocking mystery with invariants). ISBN 978-0-9860845-1-5*

[Tve81] Tvergaard, V.: *Influence of Voids on Shear Band Instabilities under Plane Strain Conditions.* Int. J. Fracture 17 (1981) 389-407

[Vas10] Vassilopoulos A P: *Methods for fatigue life prediction of composite materials and bonded composite joints*. Composite Construction Laboratory Lausanne

[VDI97] Cuntze R, Deska R, Szelinski B, Jeltsch-Fricker R, Meckbach S, Huybrechts D, Kopp J, Kroll L, Gollwitzer S, and Rackwitz R: *Neue Bruchkriterien und Festigkeitsnachweise für unidirektionalen Faserkunststoffverbund unter mehrachsiger Beanspruchung –Modellbildung und Experimente –*.VDI-Fortschrittbericht, Reihe 5, Nr. 506 (1997), 250 pages. (*New fracture criteria (Puck's criteria) and Strength 'Proof of Design' for Uni-directional FRPs subjected to Multi-axial States of Stress –model development and experiments*-. In German) * BMBF-Vorhaben 03N8002 (A. Puck, adviser 1995)

[VDI2014] VDI 2014: German Guideline, Sheet 3 *Development of Fiber-Reinforced Plastic Components, Analysis*. Beuth Verlag, 2006. (in German and English, author was convenor)

[Wei15] Weißgräber P, Leguillon D and Becker W: *A review of Finite Fracture Mechanics: crack initiation at singular and non-singular stress raisers*. Arch. Appl. Mech. DOI 10.1007/s00419-015-1091-7, Springer-Verlag Berlin Heidelberg 2015

[You15] Strength criterion for rocks under compressive-tensile stresses and its application.. J. of Rock Mechanics and Geotechnical Engineering 7 (2015) , 434-439

[Yu02] Yu M: *Advances in Strength Theories for Materials under Complex Stress States in the 20th Century*. Appl. Mech. Rev, vol 55, no3, May 2002

[ZTL80] Dornier, Fokker, MBB, DLR: *Investigations of Fracture Criteria for Laminas* (in German). 1975-1980, Grant from Ministry of Defence, BMVg, Koblenz

Some guidelines considering fiber-reinforcement in mechanical and civil engineering (construction):

[VDI 2014] VDI 2014: German Guideline, Sheet 3 "*Development of Fiber-Reinforced Plastic Components, Analysis*". Beuth-Verlag, 2006 (in German and English. Cuntze was convenor and contributor. This guideline was initiated, driven and edited primarily by construction engineers!)

[BÜV10] "*Tragende Kunststoffbauteile im Bauwesen [TKB] – Entwurf, Bemessung und Konstruktion*" . Upcoming update of the Bau-Überwachungsverein: BÜV-Arbeitskreis „Tragende Kunststoff-bauteile im Bauwesen" aufgestellte Entwurf. Formelzeichen sind der DIN EN 1990BÜV-Empfehlung Stand 08 / 2010 (re-worked presently)

[D36] DafStb UA: *Nichtmetallische nm Bewehrung: (Entwurf, in Bearbeitung). DafStb-Richtlinie "Betonbauteile mit nichtmetallischer Bewehrung*". Anwendungsbereich dieser DafStb-Richtlinie. Dieses Dokument gilt für den Entwurf, die Berechnung und die Bemessung von Hoch- und Ingenieurbauten aus Beton, die mit nichtmetallischen Bewehrungselementen bewehrt sind. Bewehrungselemente sind dabei in der Regel Stäbe und bi-axiale Gitter.

[FKM] Richtlinie „*Rechnerischer Festigkeitsnachweis für Maschinenbauteile*"., Standard für einen statischen und zyklischen Festigkeitsnachweis vom Forschungskuratorium Maschinenbau (FKM) entwickelt

Some further works of the author: *MAN-Technisches Infozentrum Augsburg NT, MT etc.*

1. Dissertation, TH Hannover 1968, ***Ermittlung von Eigenfrequenzen dünner, schiefwinkliger isotroper Platten***. ZAMM 49 (1969)
2. *Ermittlung transversaler Eigenfrequenzen dünner Rechteckscheiben und Vergleich mit der Näherung von Timoshenko*. Acta Mechanica (1969)

3. *Theoretische Ermittlung der dreidimensionalen Spannungsverteilung in Radialverdichterrädern*. DLR-FB-70-16 (1970), 73Seiten
4. *Der Einfluß von Eigengewicht und elastischer Einspannung auf die Biegeeigenfrequenzen eines schlanken Stabes von linear veränderlicher Dicke*. Der Bauingenieur (1971)
5. Meinke, Celep, Cuntze: *Eigenverhalten und Umwuchteinflüsse eines zweigliedrigen Rotors mit elastischem Gelenk*. MAN-NT 71 (1971)
6. Meinke P und Cuntze R: ***Bewegungsgleichungen eines starren zweigliedrigen Sickenrotors***. NT 6/71
7. *Reduktion der Randstörungen von Rotationsschalen durch gezielte Formgebung des Randauflagerung*. NT 25/71, 19 Seiten
8. ***Vergleich faserverstärkter und fasergewickelter Behälter mit Metallbehältern***. MAN-FB-72002 (1972)
9. Cuntze R und Celep Z: *Freie Bewegungen 2- und 3-stöckiger Rotoren*. NT 39/71
10. Kreft, Wolf, Cuntze: *Investigation of Fibers and Composites Applicable to the Design of High Pressure Vessels for Satellites*. ESTEC Contract No. 1485/7111, ESRO-Bericht (1972)
11. *Festigkeitsqualifikation der G2-Zentrifuge zur Urananreicherung*. NT 20/72
12. *Eine Bemerkung zur Anwendung des Finite-Element-Verfahrens in der Strukturmechanik*. Die Konstruktion (1973)
13. ***Gehäuse-Auslegungsstudie zur Definition eines Standard-Feststoff-Apogäumsmotors***. NT 11/74
14. MAN-Beitrag zur Entwicklungsstudie „CFK-Bauteile für Spacelab". NT 30/74
15. ***Compendium über Auslegung von Bauteilen aus Faserverbundwerkstoff (design of structures built from FRP).*** M.A.N.-Neue Technologie (1975), 600 Seiten. Eigendruck MAN
16. Cuntze R und Thiele H-M: *Vorstudie über Möglichkeiten einer experimentellen und rechnerischen Lebensdauerbestimmung eines Nutzfahrzeugs und seiner Strukturteile. NT 9/77*
17. *Schwierigkeiten bei der Ermittlung von genauen Spannungen und Verformungen an Rotationsschalen aus Faserverbundwerkstoffen*. Strukturmechaniktagung 1.6./2.6.1977 in Ottobrunn über Probleme der Festigkeitsforschung im Flugzeugbau und Bauingenieurwesen. Sonderheft der DFVLR (1977).
18. Cuntze R and Zaun J: ***Calculation of the Natural Frequencies of the braced GROWIAN tower with dead head mass*** (1978). KFA-Jül. Spez-28, Jan.79. ISSN 0343-7639
19. ***Entwurf und Festigkeitsanalysen fließgedrückter Rohre***. NT 29/78
20. Habilitationsschrift, TU München, 1978: ***Grundlagen für die Berechnung von Rotationsschalen aus Faserverbundwerkstoff***
21. ROTTSCHWIMM 32- *Einsatz eines 5 t schweren* ***Energiespeicherrades*** *bei einem Schwinmmkran – Auslegung und bruchmechanischer Nachweis*. NT 4/82 (*viele Jahre in Betrieb*)
22. Cuntze R. und Eder J: *Einfluß von Schubelastizität auf Drehträgheit und Biegeeigenfrequenz gleichförmig massebelegter Einfeldbalken*. Die Konstruktion 35 (1983), H.5, S 183-186
23. *Der* ***Einfluß von Schubelastizität und Drehträgheit auf die kritischen Drehzahlen gleichförmig massebelegter, einfeldriger Wellen.*** Ing.-Archiv (1984)
24. Cuntze R und Wein J: *Strukturauslegung und –nachweis in Einbindung leistungsfähiger Pre- und Postprozessorsysteme*. DGLR-Fachausschuß „Festigkeit und Bauweisen". Neubiberg, 5.7.1984. Tagungshandbuch
25. *Probleme bei der Übertragung eines Zwischenfaserbruchkriteriums von einem UD-Probekörper auf einen Mehrschichtenverbund*. DGLR-Symposium „Entwicklung und Anwendung von CFK-Strukturen". TU, Berlin. 8./9.11.1984
26. *CAE-Einsatz beim Projekt ARIANE. Ein Anwenderbericht.* CAE-Journal, Heft 6 (1984), 24-31
27. Cuntze R and Löbel G.: *Evaluation of Stress Strain Test Results for Effective Use in Computational Analysis and Adequate Statistical Quantities*. ICOSSAR 85, 4th Intern. Conf. on Structural Safety and Reliability. Kobe, Japan
28. *Bruchverhalten von kohlenstoffaserverstärkten Kunststofflaminaten. – Theor. Untersuchungen –* Bericht: MAN-NT 44/83 (20.12.84). BMFT-Forschungsvorhaben 01ZA 029-/K/NT/NTS 1022
29. *Strukturberechnung. Teil der Bauteilentwicklung – ein Überblick*. Konferenzbericht der Tagung Mechanik und Industrie. IGLS, Österreich. 26./27. Februar 1985. Herausgeber: Institut für Mechanik, Universität Innsbruck. Springer, Wien 1986

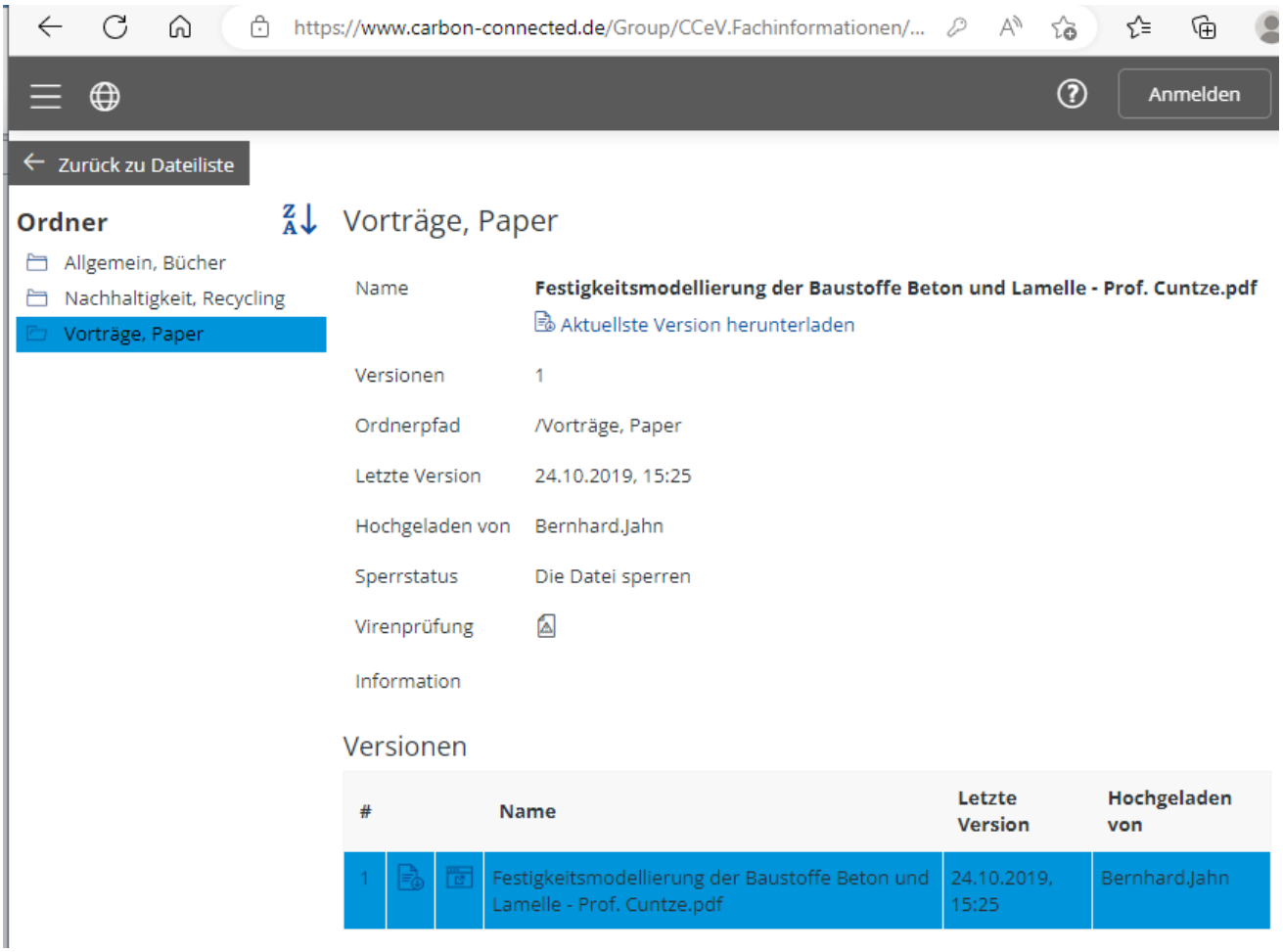
30. Cuntze R und Hajek M.: ***Eigenfrequenz eines angerissenen Kragträgers***. Ing. Arch. 55 (1985), S. 237-241
31. Crostack H.A., Nolte F., Zeilinger H. und Cuntze R.: *Untersuchung des Schädigungsablaufes in kohlenstoff-faserverstärkten Kunststoffen.* Zeitschrift für Werkstofftechnik 16 (1985) 366-372
32. Rackwitz, R. and Cuntze, R.: *Formulations of Reliability-oriented Optimization with Application*. NATO Advanced Study Institute. Conference on Computer Aided Optimal Design, Troia, Portugal. June 29-July 11, 1986. Springer
33. Cuntze R and Grimmelt M: *Influence of the Variation of Structural Properties on the Probability of a Composite Plate to meet a Target Eigenfrequency*. EUROMECH Coll. 219, Sept. 23-25, 1986, Kassel
34. Cuntze R und Schuelein R.: *Einsatz der Bruchmechanik bei der Entwicklung von Struktur-Bauteilen aus Faserkunststoffverbund (FKV).* Vortragsveranstaltung „Bruchmechanik bei Verbund-werkstoffen" bei der Dechema. Frankfurt, 19.02.1987
35. Rackwitz R and Cuntze R: *System Reliability Aspects in Composite Structures*. Eng.' Opt., 1987, Vol. 11, pp. 69-76
36. Cuntze R: ***Failure Path Analysis of Multilayered Fiber Reinforced Plastic Components with the Reliability Calculation Programme FRPREL***. Noordwijk, Oct. 1987
37. Cuntze R: *Influence of the Stochastic Behavior of Design Parameters on the First Ply Failure (FPF) in Pressurized CFRP-Tubes*. ESA/ESTEC, Noordwijk, March 1988
38. Scharringhausen J. and Cuntze,R: *FEM-Calculations on the Domes of Fiber Reinforced Plastic Cases for Solid Propellant Motors.* ESA/ESTEC Workshop, Noordwijk, March 23-25, 1988
39. Cuntze R and Zaun J: ***Delamination Optimization of Hoop-Wound Composite Fly-wheels***. ICCM 7, Beijing, August 1 – 4, 1989
40. Cuntze R and Schuelein R: ***Werkstoffdatenbanken*** *im industriellen Einsatz (material data banks in industrial use) – aus der Sicht eines Anwenders*. MAN Technologie GmbH, München. Bericht und Vortrag MAN-intern (Febr. 23, 1989). Fachgespräch bzgl. MAN Werkstoff-Informations-System
41. Grimmelt M and Cuntze R: ***Probabilistic Prediction of Structural Test Results as a Tool for the Performance Estimation in Composite Structures Design***
42. . VDI-Bericht 771 (1989), 191-200
43. Dr. med. Stock W und Dr.-Ing. Cuntze R: ***Computergestützte biomechanische Untersuchungen zur Knochen-transplantation.*** Vortrag, BMFT Seminar. Hamburg, 1988
44. Cuntze R und Schuelein R: *Werkstoffdatenbank: Qualitätswerkzeug für die Entwicklung zuverlässiger Bauteile. VMPA-Tagung „Qualität und Zuverlässigkeit durch Materialprüfung*", München, April 1990
45. *Auslegung, Nachweis und Zuverlässigkeitsoptimierung von Faserkunststoffverbund-Bauteilen. Fachtagung „Rechnereinsatz beim Konstruieren von Kunststoff-Formteilen".* Süddeutsches Kunststoffzentrum, Mannheim, Mai 1990
46. Cuntze R: *Influence of the Stochastic Behavior of Design Parameters on the First Ply Failure (FPF) in Pressurized CFRP-Tubes*. ESA/ESTEC, Noordwijk, March 1988
47. *Structural Design, Optimization and Reliability Justification – a comparative survey related to the example: Axially compressed strut*. GAMM/IFIP-Workshop "Stochastic Optimization", Neubiberg, May 1990 (not published)
48. Cuntze R. and Heibel R: *Increasing the Limit of Usability of CFRP Tubes by Built-in Stresses*. X. Int. Herman F. Mark-Symposium. Wien, 1991
49. *Prediction of the Distribution of Inter-Fiber-Failure Test Data of Radial Loaded, Pre-strained CFRP Tubes composed of Thin Layers*. 5th Workshop "Composite-Forschung in der Mechanik", Paderborn, October 1992
50. Gollwitzer S, Cuntze R, Grimmelt M and Zwerev A.: *Structural Reliability Applications in Aerospace Engineering.* ICOSSAR 93, Innsbruck, 1993
51. *Deterministic and Probabilistic Prediction of the Distribution of Inter-Fiber-Failure Test Data of Pre-strained CFRP Tubes composed of Thin layers and loaded by radial pressure*. Wollongong, Advanced Composites '93. The Minerals, Metals & Materials Society, 1993
52. *Evaluation and Application of a New Physically Based 2D/3D-Inter-Fiber-Fracture (IFF) Strength Criterion*. Proceedings of International Symposium on Advanced Materials for Lightweight Structures, Noordwijk, März 1994, ESTEC, 133-139

53. Gierlinski, Smith, Thoft-Christensen, Santos, Cuntze, Gollwitzer: ***Reliability-based Design of Structural Components***. Proceeding of the int. Symp. On Advanced Materials for Light weight structures, ESTEC, Noordwijk, March 1994 (ESA-WPP-070), 121-125
54. „*Quick Design", Entwurfsregeln und Normen zur Strukturberechnung.* Kolloquium „Ausgewählte Probleme der Strukturmechanik", 11.5.95, zu Ehren von Dr.-Ing. B. Geier. IB 131-95-13, DLR-Braunschweig
55. *Festigkeitskriterien für Werkstoffe aus Faserkunststoffverbund (FKV).* Symposium „Berechnungen von Faserverbundstrukturen unter Anwendung numerischer Verfahren". München, Techn. Uni, 13/14. März 1996
56. *"Fracture-type Strength Criteria" formulated by Invariants which consider the Material Symmetries of the Isotropic/Anisotropic Material used*. Conf. on Spacecraft Structures, Materials and Mechanical Testing. ESA-CNES-DARA: Noordwijk, 27-29 March 1996, pp. 399-409
57. *Zum verbesserten Festigkeitsnachweis von FKV-Bauteilen*. Werkstoffwoche 96, Stuttgart 28.- 31. Mai 1996. Projektberichterstattung
58. *Bruchtypbezogene Auswertung mehrachsiger Bruchtestdaten und Anwendung im Festigkeitsnachweis sowie daraus ableitbare Schwingfestigkeits- und Bruchmechanikaspekte*. DGLR-Kongreß 1996 Dresden. Kongreß-Band
59. *Evaluation of Multiaxial Test Data of UD-laminas by so-called "Fracture-type Strength Criteria" and by supporting Probabilistic Means*. ICCM-11, Gold Coast, 1997
60. Cuntze R et.al.: ***Neue Bruchkriterien und Festigkeitsnachweise für unidirektionalen Faserkunststoffverbund unter mehrachsiger Beanspruchung – Modellbildung und Experimente***. VDI-Fortschrittbericht, Reihe 5, Nr. 506 (1997), 250 pages. [New fracture criteria (Puck's criteria) and Strength 'proof of Design' for Unidirectional FRPs subjected to Multi-axial States –model development and experiments-, in German]
61. *Stand von Auslegung und Nachweis von Bauteilen aus Faserkunststoffverbund nebst einigen Ausblicken*. Plenarvortrag, DGM-Tagung "Verbundwerkstoffe und Werkstoffverbunde", Kaiserslautern, Sept. 1997
62. *Strength Prediction for **Multi-axially Loaded CMC-Materials***. 3rd European Workshop on Thermal Protection Systems. Conf. on Spacecraft Structures, Materials and Mech. Testing. ESA-ESTEC: Noordwijk, March 1998, WP P141
63. *Application of 3D-strength criteria, based on the so-called "Failure Mode Concept", to multi-axial test data of sandwich foam, concrete, epoxy, CFRP-UD lamina, CMC-Fabric Lamina*. ICCE/5, Las Vegas, July 1998 (presentation)
64. *The Failure Mode Concept - a new comprehensive 3D-strength Analysis Concept for Any Brittle and Ductile behaving Material*. Europ. Conf. on Spacecraft Structures, Materials and Mechanical Testing. ESA-CNES-DGLR-DLR; Braunschweig, Nov. 1998, ESA SP-428, 269-287
65. *Progressive Failure of 3D-stressed Laminates: Multiple Non-linearity treated by the Failure Mode Concept (FMC).* DURACOSYS99, Brussels, July 1999. Balkema, Rotterdam, 2000
66. *Static Design and Strength 'Proof of Design' of Pressure Vessels, built from Ductile or Brittle Materials*. Problems of the North; Yakutsk 2000
67. *Are there CoSt Drivers in the Structural Analysis of the ARIANE 5-Development?* Noordwijk, 29. Nov./1. Dec. 2000
68. *Assessment of Load- and Strain-controlled States of Stress in 'hot Spots' – on the way to an Industrial Approach for Gurson Materials*. 3rd European Conference on Launcher Technology. CNES, DLR, ESA-ESTEC, ISU: Strasbourg, Dec. 11-14, 2001
69. Huybrechts D, Cuntze R., Druwen S, and Lutz G.: ***VDI-Richtlinie 2014, Blatt3, Berechnungen***. SAMPE 2002.
70. Cuntze R: ***Non-linear Failure Analysis of FRP Laminates composed of UD Laminas – a comparison of the author's predictions with test results within the Failure Exercise in the UK***. 3rd Int. Conf. on Fracture and Damage Materials; Paderborn, September 2-4, 2003

Downloading of literature marked by *

* https://www.carbon-connected.de/Group/CCeV.Fachinformationen/Wiki/Start/Overview.





23 Basic Terms and Definitions

Borders between engineering disciplines are disappearing, more and more. However, it can also be noticed that especially in the various application fields of the fiber-using industry different "languages" are used and that technical terms are sometimes applied very differently. Several groups of engineers would therefore have to be connected conceptually so that they understand each other correctly when making the necessary common project decisions.

This chapter, that may be termed a Glossary, is a compilation of terms and partly their definitions stemming from the author's as well as from numerous other Glossaries/origins/publications. It is provided by the author 'as is' and without any warranty hoping to make the addressed engineers fit for their specific purposes.

23.1 Introduction

23.1.1 General

The construction industry is an industry in which the topic of high-performance fiber composites is not yet established on the one hand, but where there is enormous application potential on the other. Against this backdrop, Carbon Composites e.V. (CCeV) in Augsburg in 2011 asked the author to found a specialist working group in this field department which developed last year to the Cluster "CC Construction"(CC Bau). This repositioning meant that both fiber polymer composite FPC - also known as fiber-reinforced plastic FRP - and the various fiber-reinforced concrete matrices had to be covered, i.e. 'fiber-reinforced concrete'. The latter involves '(roving)-reinforced concrete' RC, i.e. GRC, CRC, as well as '(short) fiber reinforced concrete' FRC, i.e. CFRC, PPFRC.

The following applications, for example, must therefore be captured:

(1) Polymer matrix-related:

Glass fiber plastic pipes and GFRP containers, wind rotor blades and pedestrian bridges in GFRP and CFRP, the huge architectural building around the Kaaba, the 80 t heavy 'Apple Campus 2 roof supporting structure' or bridge profiles.

(2) Concrete matrix-related:

Textile concrete bridges and textile concrete machine foundations, overhead line masts, industrial floors, multi-story car parks, silos, prefabricated garages, transformer houses, offshore applications, tubbings, sandwich façade panels, untensioned (slack armoring) and tensioned bending panels, bridge ceiling panels, textile concrete shells and bridges. Besides concrete constructions (thickness dependent) hardly permeable for water additively manufactured building constructions will come up.

Various application possibilities offer themselves with the retrofitting, like with load-bearing structure reinforcements, cover plates, floor plates, parking garage decks (reorganization in the compression zone and tension zone range), bridge caps, monument protected buildings, silos, balcony reorganizations, construction units with high chloride effects, and free form constructions for architects, that make new shell load-bearing structures possible. Further examples can be found, such as CFRP lamella reinforcement of steel-reinforced concrete slabs, ribbed slabs, edges of slab openings (replacement reinforcement) floor slab under groundwater overpressure. But also a carbon concrete-timber frame composite construction is part of the large variety of applications.

As can be seen from the previous texts, the main focus is carbon concrete CRC, in German abbreviated by CB, analogously to the (steel) reinforced concrete StB (Stahl-Beton). Special advantages of the non-corrosive CRC compared to steel-reinforced concrete are lower maintenance CoSts and thus also life cycle CoSts, weather resistance, high durability of the reinforcing layer of textile concrete compared to de-icing salts. The elimination of additional protective mechanisms such as surface protection systems significantly saves CoSts for corrosion damage removal. Further advantages are high water impermeability due to the finer microcrack structure of the CRC, light and filigree construction methods allow modern shell constructions that were previously unthinkable in StRC. Some building constructions will already pay for

themselves now, if one would and should pay for oneself sustainably, because the use of CRC promises savings in life cycle CoSts.

Several groups of engineers are to be combined conceptually in order to understand each other correctly:

* For this purpose, the necessary contents should lead to a clear use of the terms - such as non-crimp fabrics, lamella and grid - in the aforementioned different but related technologies. It should also show the essential terms to be used for reinforcement material.
*Furthermore, an order scheme for fiber-reinforced components should help to ensure that in future the 'same language' is spoken in these areas and that the material used or the semi-finished product is correctly designated.

Writing a Glossary is made more difficult by the fact that some terms have evolved away from the original definition and further by the fact that, for example, the letter C has long been used for composite, carbon, concrete, ceramics and compressive as well. Such a problem is not new, as the quotations below show:

"Unfortunately, we have used these words in so different ways that we no longer clearly understand each other when we say them" [A. Donabedian, 1982]. Or, "A general system of signs and symbols is of high importance for a logically consistent universal language for scientific use!" (attributed to Gottfried Wilhelm Leibniz, 1700).

It should be remembered here that the 'timber engineers' created the first documents and terms for the construction material wood as the first theoretically treated fiber-reinforced material.

Of special importance is the choice of the symbols for the strength:

Mechanical Engineering

*Fracture strength, compression: R_{mc} (*R* from resistance maximale), yield strength $R_{c0.2}$

*Fracture strength, tension: R_m . In the case of tension, the index t (tensile) is not used, because tension is the mostly faced stress case for the mostly metallic material. However, with fiber reinforced materials both the indices c and t are written.

One strives to '*index as simple as possible'.* No additional material-dedicated index for metals, ceramics, composites is attached. In clear tables no material index is necessary with the exception of equations that combine materials.

Civil Engineering

*Fracture strength, compression: $f_{cd} \equiv R_{mc}$ (*f* from Festigkeit) .Vice versa to mechanical engineering in the case of compression, the Index c (compressive) is not used, because compression is the mostly faced stress case for the mostly used material (concrete). However, for concrete material the index c for concrete is attached. This firstly leads to an optical confusion of concrete with the compressive sign. Secondly it leads to an accumulation of indices, if one exemplarily likes to index the tensile strength of a short carbon fiber reinforced concrete FRC analogously, namely as f_{FRCt} .

*Fracture strength, tension: f_{ctd} ($\equiv R_{m,\,d}$ means design)

Unfortunately, in mechanical engineering the index *m* is taken for 'maximale' and in civil engineering for marking the mean value. In mechanical engineering the mean value is traditionally marked by the statistics-based sign 'upper bar', such as $\overline{R}$.

Conclusion drawn:

In general one needs just to speak about compression, tension or shear strength. If one uses formulas, evaluates test results or applies property data sheets, then always the dedication of the property to a material will be present. Hence, an index c for concrete is not necessary.

Highly loadable FRPs are essentially closed textile reinforcement structures with a relatively high fiber volume content V_f in the FRP. However, a high loadable reinforced concrete matrix, i.e. 'fiber-reinforced

concrete', is an 'open grid-like' reinforcement structure (*textile grid or rod grid*) with a small fiber volume content in the concrete composite.

A further distinction must be made here between the (short)fiber concrete FRC, in which the properties of the concrete matrix are improved with short fibers or possibly long fibers, and the aforementioned ' fiber-reinforced concrete' RC, in which endless (continuous) fibers are usually used.

The design engineers are particularly addressed with regard to the terms important to them and their contents for the correct understanding of the task, and this before any modelling and subsequent calculation.

It is important for the concrete-related modeler that the concrete is considered 'cracked in the tensile area' according to its low tensile strength of about one tenth of the compressive strength: The reinforcement must therefore absorb the tensile force. For (short)fiber concrete FRC, where the concrete matrix properties are improved, the credit of the strength improvement on the tensile side has to be proven by tests.

23.1.2 Fixation of some important Terms in order to minimize confusion

Fiber-Composite-Material (FCM): FCM is the generic term for all composite materials that contain fibers in order to obtain certain properties in order to fulfil certain functions. The later defined notions 'composite material' and 'material composite' shall be captured by FCM for reasons of simplification.
The load-carrying or reinforcing function is usually the most important of these functions. With the fiber-reinforced polymer (plastic) composite FRP – such as GFRP, CFRP, AFRP - the terms 'reinforced' and 'composite' are not illustrated in German by a letter! The same applies to (short)fiber concrete which has been written just FRC, but should read sFRC as a proposal. Unfortunately, in English FRC is written instead of FC, and thus the word "reinforced" is used despite of the fact whether reinforcement is the main function or not! If one would drop the R in F~~R~~C, then one achieves a pretty common logical system. (short)Fiber-Reinforced Concrete FRC, for instance, confuses with the endless fiber terms. FRP, und F(R)C form subgroups of Fiber-Composite-Material FCM. See *Fig.23-1*.

Composite Material versus 'Material-Composite': It is important to clarify terms within FCM. The above terms *composite material* and *material composite* exist for decades, but unfortunately the different contents are not applied correctly: *Composite material* = composite of different materials, *material composite* = homogenized composite of different components, which are at least mathematically homogenizable and thus 'smearable'. Both (steel)reinforced concrete and carbon concrete are therefore a 'material composite' in the sense of current calculation methods, as it is with a sandwich load-bearing structure. However, if it is possible to model a reinforced concrete slab layer-by-layer, then one has concrete layers and - possibly justifiable according to the model - smearable layers = composite material layers, namely roving-reinforced layers of concrete. One can then apply the well-known so-called classical laminate theory CLT. Hybrid materials are usually a material composite and require the more effortful 'multi-material design' that has been tried and tested for several years.

Fiber-Matrix(-Composite) and Carbon- Concrete (-Composite): A definition always poses a great challenge, because much of the word is supposedly firmly established: According to VDI 2014, the traditional fiber composite business of mechanical engineering is called 'fiber-polymer composite' (FKV in German). CF-EP or GF-UP, for example, are supplied as FKV products. The letter C for composite is therefore not shown. If one wants to emphasize that reinforcement is the main function of the fiber, then one writes fiber-reinforced polymer (plastic) FRP.

In the traditional building industry it has always been called 'steel-reinforced concrete', a word that was chosen in the tradition of the original term 'ferro-concrete', knowing that the quality of steel is much higher then for the former iron material. Hence, why shouldn't the development of the term CB continue like this when carbon is used? As you can see, the word composite is not mentioned at StB either. The

abbreviated product description CF-EP-CEM III could be applied, for example, when an EP-impregnated roving CF-EP is used.

It is recommended not to use the word fiber-reinforced with the German terms, already for simplification reasons and also for logical consequence - as already mentioned - with the concrete matrix, as well as with the polymer matrix. Except the load-bearing function also other functions are often very important, such as electrical heating or battery storage. Probably the English technical literature has gone one step too far with its general inclusion of R as Reinforced in all of their abbreviations.

Ordering Scheme:

An ordering scheme for all fiber matrix combinations is proposed: It includes in particular the reinforcement variants *long* and *continuous (endless)* fibers. Of particular interest here in Germany is that Fiber-reinforced polymer matrix FVK (Faser-Verstärkter-Kunststoff) is a subset of FK(V) (Faser-Kunststoff-Verbund) and fiber-reinforced concrete F(V)B (Faser-Verstärkter-Beton) is a subset of fiber-concrete-composite FB(V). Geotextiles are not included. Hybrid combinations such as wood with polymer matrix or with concrete have to be 'thought of' by the reader in the already very extensive scheme.

The structural engineer's view as a structural modeler is chosen as a helpful point of view for the definition of the terms. This results, for example, in UDB:= uni-directionally beam- or UD-lamella-reinforced concrete and CC:= carbon concrete, as a proposal analogous to the letter-reduced StB name definition.

In the DIN EN 206-1/ DIN 1045-2 the term *fine concrete* is not defined, so that occasionally the not so catchy long term 'concrete with small grain size' is used (*see [1)] in the order scheme*). The smallest permissible grading curve (grain particle size distribution curve) is that for 8 mm maximum grain size. For practical reasons, however, the 4 mm maximum grain size was selected for an approximate range separation.

The letter F (fiber) is traditionally written for fiber concrete (*usually short fibers, as the longer steel fibers are not addressed here*), see StFB (short fiber reinforced) compared to StB (endless reinforced) and analogously CFB (Carbon-*kurz*Faser-Beton) compared to CB (Carbon-Beton) for the started use of carbon fibers in concrete.

For simplification, F and V are not written for continuous fiber reinforcement of concrete (StBV, analog CFBV). In the case of continuous fiber reinforcement of a polymer matrix, on the other hand, the letter F is traditionally written (CFK, CFRP), unfortunately as in the case of short-fiber reinforced fiber concrete. The above confusing differences are due to earlier determinations, see green color in *Fig.25-1*.Short fiber reinforced components such as FRC (also possibly used as shotcrete) and fiber plastic (injection molding SMC) can be 2D or 3D materials depending on the manufacturing process. For natural fibers, the long term ‘Natural fiber RP’ is intentionally used.

The so-called ‘3D print’ as sub-group of ‘Additive Manufacturing’ only provides 2D reinforcements due to the accumulation of thin layers of the respective x-y component cross section in the z-direction, while the usual additive manufacturing can certainly provide spatial 3D reinforcements. Injection molding and shotcrete with short fibers are related, can be selected as additive manufacturing and were included in the scheme. In the ordering scheme, 3D is a spatial material and not a semi-finished product transformed into a 3D spatial structure such as a reinforcement cage.

*The order scheme is conceptually not complete, neither on the English nor on the German side. A really logically built scheme would afford some adjustments

*The main difference between English and German is that the letter R (reinforced) is used everywhere

*The correction proposals received, very much welcomed by the author, showed that - as expected - contradictions exist which must be cleared up over time.



Fig.23-1a: Ordnungsschema für Faser-Verbund-Werkstoffe FVW

wie Faser-Kunststoff-Verbund FKV, Faser-Beton-Verbund FBV, Faser-Verstärkter-Beton FVB, Carbon-Beton CB, BasaltBeton BsB, bi-direktional stabverstärkter Beton BDB, UHP-Carbon(kurz)Faser-Beton UHP-CFB. In grün, bereits früher festgelegte Begriffe. [Cuntze, Kimm, Heppes, Diestel, Butler, Bielak]

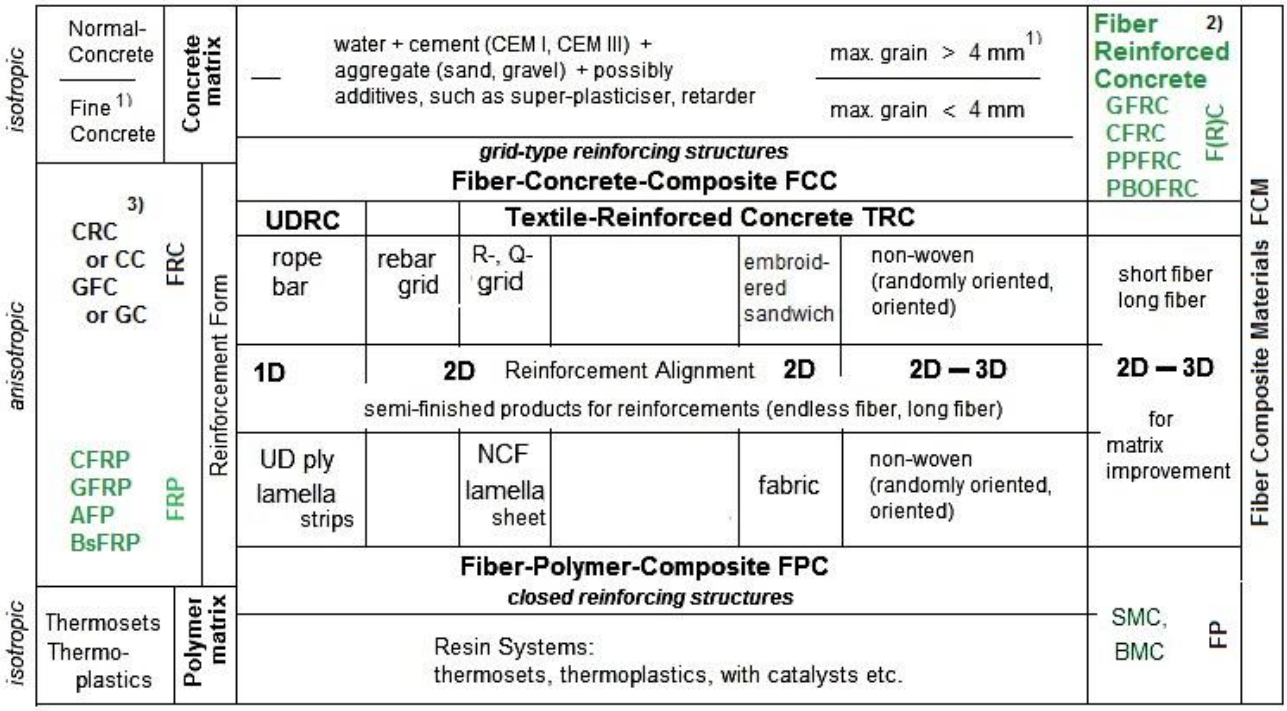


Fig.23-1b: Ordering scheme proposal for Fiber-Composite Materials FCM, construction-linked

such as Fiber-Reinforced Polymer FRP, Fiber-Reinforced Concrete FRC, CFRC:= CarbonFiber–Reinforced Concrete, Bi-Directionally Reinforced Concrete BDRC, UHP-(short)Fiber-Reinforced Concrete, UHPFRC. Green couloured are still fixed notions.

Matrix types of the Reinforcements FRPm = Fiber-Reinforced Polymer matrix, Fiber-Reinforced-Mineral matrix FRMm. International subscipts f = filament, m = matrix; superscripts t = tension, c = compression

23.2 English Technical Terms with Definitions

→ As the body text should be applicable for engineers in mechanical, civil, fiber and geotechnical engineering basic terms shall be provided for common understanding:

A-Basis Design Allowable (or "A"-Value): statistically-based material property, above which at least 99% of the population of values is expected to fall, with a confidence level of C = 95%

Action (S): externally applied loading in design. Examples are loads, fluxes, forced deformation, or a pressure as well as hygro-thermal loading, external differential pressure, line load, stress states, suction, thermal constraint, patch/local load, friction load)

Additive manufacturing in construction, polymer and concrete matrices: process of composing materials layerwise to make objects from 3D-model data sets, as opposed to subtractive manufacturing methodologies. (3D-print is a subset, where the full cross-section area is produced thin layer upon thin layer)

Adhesion: state, in which two surfaces are held together at an interface by forces or interlocking action or both

Aging: effect of exposure to an environment for a period of time

Algorithm: a set of instructions for solving logical and mathematical problems, or for accomplishing some other task (is the completed dish defined sequence of operations to solve a problem). A recipe is a good example of an algorithm because it says what must be done, step by step. It takes inputs (ingredients) and produces an output

(design) Allowable: design quantity (usually a statistically reduced resistance or strength), being allowable with respect to the actual design requirements

Allowable stress: notion that belongs to a former safety concept. (should not be used anymore since 1926. It is confusing and causes errors when applying modern safety concepts

Ambient: state of the surrounding environmental conditions

Analysis: refers to the whole process of representing a product, to modelling, calculation and interpreting results in terms of product performance. Is the execution of a calculation with fixed model parameters

Anisotropic: not isotropic, due to having different mechanical and/or physical properties in different directions

Angle-ply: balanced laminate, consisting of plies at arbitrary angles of plus and minus, where α is the angle of the fibers with the principal laminate axis

ARAMIS: optical measuring system (GOM)

As-built status: status, that must be respected in dimensioning

Augmented reality: (angereicherte, erweiterte Realität) interactive experience of a real world environment, alters one's ongoing perception (Auffassung) of a real world

Autoclave: closed vessel for producing a distinct environment while curing

Automatic mesh generation: process of generating a mesh of elements over the volume that is being analyzed. (There are two forms of automatic mesh generation: Free Meshing – where the mesh has no structure to it. Free meshing generally uses triangular and tetrahedral elements. Free meshing can be used to fill any shape. Mapped Meshing – where large regions, if not all, of the volume is covered with regular meshes. This can use any form of element. Mapped meshing can only be used on some shapes without elements being excessively distorted [NAFEMS])

Availability : Aptitude of a product to be –at a certain time or during a certain time- in a position to provide the functions, expressed in terms of probability (probability that an item will be operable when needed)

Average strength: typical strength, utilized in test data mapping. (*Is the statistical mean strength in the case enough test data are available*)

Axisymmetry: geometrical situation when a shape can be defined by rotating a cross-section about a line then it is said to be an axisymmetric model, e.g. a cone. (*Such a model can be used to simplify the numerical modelling of the system)*

Balanced laminate: composite laminate in which all laminas at angles other than 0° and 90° occur only in ± pairs, and not necessarily adjacent. (*necessarily not symmetric*)

Bandwidth: half bandwidth of a matrix is the maximum distance of any non-zero term in the matrix from the leading diagonal of the matrix. (*The bandwidth for a symmetric matrix is then twice this*)

Bar, rod: pultruded fiber reinforced polymer rods used as rebars for strengthening concrete, timber and masonry structures. (Challenge is to produce an efficient load-transferring surface profile)

Basic population (Grundgesamtheit):

Basic variables X, X_i: a basic or 'input' variable is one of a set of independent variables governing 'loading' or resistance which may influence the reliability of a structure. The definition of these by a code committee (or preferably a group of code committees) is an essential preliminary to the determination of partial factors to provide consistent structural reliability. Examples of typical basic variables are given in use cases

Batch(lot, staple, charge): technical term in several disciplines to address togetherness. (Examples are (1) Generally, a distinct quantity of material (same raw material) formed during the same process or in one continuous process and having identical characteristics throughout. (2) Fabrics woven from one warp loom setup. (3) Batch may be a large or small amount of resin or adhesive, or woven fabric. See ASTM D 907. (4) Production run of prepreg material that is preimpregnated using one batch of resin and fabric, all in one continuous operation. A batch of prepreg may consist of one or more rolls of material) [SAE]

Bauschinger Effect: effect, observed in plasticity when, after initial tensile loading into the plastic region, the yield stress in compression is less than the equivalent value in tension

B-Basis Design Allowable (or "B"-Value): statistically-based material property, above which at least 90% of the population of values is expected to fall, with a confidence level of 95%

Bifurcation point: in stability theory, point on a non-linear load-displacement curve where the load path forks into two or more solution paths that satisfy equilibrium. (o*nly one path is stable, the others are unstable*)

Binder, polymers: bonding resin, used to hold strands together mechanically, chemically, by adhesion or cohesion in a mat or a preform during manufacture of a molded object

Binder, concrete: organic (see above) and inorganic substance that holds or draws other materials together.
(reactive mineralic fine particles, such as from Portlandcement, Puzzolane, that harden when adding water)

Bleeder cloth: nonstructural layer of material used in the manufacture of composite parts. (*allows the escape of excess gas and resin during cure. The bleeder cloth is removed after the curing process and is not part of the final composite*)

Bobbin: spindle or cylinder on which a yarn is wound

Bond: adhesion of one surface to another, with or without the use of an adhesive as a bonding agent

Braiding: textile process where two or more strands, yarns or tapes are intertwined in the bias direction to form an integrated structure

Brittle material behavior: materials, subjected to especially tensile stress, will break without significant plastic deformation. *(Brittle materials absorb relatively little energy prior to fracture, even those of high strength. Breaking is often accompanied by a snapping sound. Brittle materials include concrete, most ceramics and glasses which practically do not deform plastically and some polymers, such as PMMA and polystyrene. Many steels become brittle at low temperatures (remind: ductile-brittle transition temperature) and according to corrosive environment, depending on their composition and processing [Wikipedia]*. Brittle: about $R^c / R^t > 3$, *concrete still exhibits* $f_c / f_t > 10$*! Brittle behaving materials are unforgiving to overloading)*

Buckling: geometric instability, generally caused by compressive forces in thin-sectioned bodies. (can be analyzed as a special case of geometric non-linearity using eigenvalue analysis)

Buckling resistance: resistance of the structure equal to the smallest load under which the structure can respond in more than one system equilibrium state. *(1) characteristic buckling resistance: buckling resistance determined under the prerequisite of possible inelastic material response, geometrical and structural imperfections, follower load effects and residual stresses. (2) critical buckling resistance: buckling resistance determined with a model under the prerequisite of idealized conditions. (3) design buckling resistance: design value of the buckling resistance taking into account the uncertainties of model-based predictions*

Bundle: collection of parallel filaments or rovings, tows, strands

Buckling factor: factor to obtain the critical buckling resistance of the investigated structural system from a generic problem characterizing quantity. (*the term buckling factor includes the effects of different support conditions, different cross section properties and non-uniformly distributed applied stresses. It is also applicable for prediction of the critical buckling stress*)

Buckling load: load level at which buckling occurs. (*buckling load is not a load (action) but a resistance property of the structure or the structural item*)

Buckling stress: key value of a stress field associated with the buckling resistance in the non-buckled equilibrium state.

Buckling resistance: resistance of the structure equal to the smallest load under which the structure can respond in more than one equilibrium state

Bulk data**:** all of the data are put into a file

buy-to-fly: ≡ buy-to-use in civil engineering. quotient of material input (buy) and product output (fly, use). (*improved characterization of material waste*)

Carbon fiber CF: man-made fiber produced by the pyrolysis of organic precursor fibers such as rayon, polyacrylonitrile (PAN), and pitch in an inert atmosphere. (*term is often used interchangeably with "graphite"; however, carbon fibers and graphite fibers differ in the temperature at which the filaments are made and heat-treated, and the amount of carbon produced. Carbon filaments (= structural materials) typically are carbonized at about 1300°C and contain 93 to 95 % carbon, while graphite filaments are graphitized at 1900 to 3000 C and contain more than 99 % elemental carbon. Pitch-based filaments have a higher E-modulus than PAN-based ones and are thereby stiffer*)

Category of importance of analysis (analogous hardware): the analysis refers not only to the importance of the product regarding risk to human life or CoSt of malfunction, but also to the significance of the finite element analysis in the demonstration of integrity /NAFEMS/

Vital: To fall into this category, two major conditions must be satisfied. The product itself must be such that its malfunction or failure is certain to place human life in danger or to endanger property or the environment on the scale of a public disaster. The analysis must be an integral part of the integrity demonstration such that, in its absence, there would be no reasonable case for the contractor to claim the full discharge of his legal safety obligations.

Important: the product itself must be such that its failure would at least pose a serious danger to human life or cause direct or consequential damage beyond the contractor's normal limits of liability. The product failure itself may be vital in the sense of category 1, but the analysis is not an exclusive part of the integrity demonstration.

Advisory: This category is applied to all situations not covered by the previous definitions, but were the analysis contributes significantly to product integrity and product failure would cause financial embarrassment to the contractor or disruption of services

Cauchy stress: see true stress

Cement: fine-grained compound that turns into a solid when mixed with water. (*cement is used to bind mixtures of materials into a composite solid. Grain size distribution 1 < 20 < 100 µm*)

Certification: written declaration stating that the structural product complies with requirements

Characteristic buckling resistance: resistance determined under the pre-requisite of possible inelastic material response, geometrical and structural imperfections, follower load effects and residual stresses

Characteristic (compressive) strength $\mathbf{f_{ck}}$, concrete cube (index $_c$), characteristic (index $_k$): strength of the concrete below which not more than p = 5 % of test results are expected to fall *(under the assumption 'Normal distribution of the data of the test series is applicable' the strength value of concrete specimens casted and tested as per given code of practice and cured for a period of 28 days; 95 % of tested specimens should not have a value less than this value or less than 5% of the test specimens are expected to fail, respectively. For a confidence level of C=95 %, k = 1.64 (varies on chosen or fixed C), from transferring sample test data into a basic distribution. Cube Ø = 150 mm, tested at 28 days.* The specified characteristic strength is a value p of the lowest acceptable level of quality and corresponds to a situation where the production process is statistically in control. In practice, statistical methods of quality control and acceptance testing can be used to assess whether this minimum level of quality is being achieved.

Characteristic value x_k: see example calculations in chapter 13

Chopped strand mat: random fiber mat that provides equal strength in all directions. (*chopped strand mat is produced by chopping a continuous strand or roving into short lengths of usually < ≈ 7 mm*)

Classical Laminate Theory CLT: 2D continuum theory used in laminate composites analysis. (*CLT bases on Kirchhoff's classical plate theory where the normal hypothesis is applied and transverse shear deformation is neglected*)

Coating: impregnation of the surface, only. (*does not go into the depth of the roving; example CF rovings in construction coated with aqueous film-forming dispersion Styrene Butadiene SB*)

Co-bonding: curing-together of two or more elements, of which at least one has already been fully cured and at least one is uncured. (*requires film adhesive between any precured and uncured interface, BDS 1330*)

Co-curing: simultaneous curing together of two or more uncured elements, BDS 1330). (*bonding while curing a laminate*)

Coefficient-of-variation cov: non-dimensional measure of the dispersion (variability) of a random variable, defined for a sample as $cov_x = s / \overline{x}$ where s is the sample standard deviation and $\overline{x}$ is sample mean

Cohesive model: traction-separation law describing distinct non-linear separation process of the material (is neither an elasticity-dedicated nor a plasticity–dedicated model)

Cohesive strength: maximum tensile stress σ^t (≡ separation strength R^t) of bonding between surfaces or of tensile stressed particles building a material. However, in rock and soil mechanics cohesive strength is 'differently' defined as the inherent shear strength $R^\tau = \tau_{nt}$ of a plane, where the normal compressive Mohr stress $\sigma_n{}^c = 0$ on the about $\Theta_{fp}° \approx 70°$ bias shear fracture plane and whereby the cohesive strength value R^τ is extrapolated from compression point-associated quantities. This seems to be not accurate because R^τ is an brittle-dependent entity of the transition zone between shear fracture mode SF and Normal Fracture mode NF → *Difference* between the terms in the technical disciplines

Cohesive zone model: fracture mechanics model for analyzing the separation of the surfaces across an extended crack tip, termed cohesive zone. (*describes the cohesive forces which occur when material elements are being pulled apart*)

Commingled yarns: blends where two types of filaments were put together

Compaction: densification of the solid material compacting its elements, such as loose, granular ones, which results in reduced porosity and causes a volumetric reduction

Composite: material, composed of distinct elements, parts

Composition: way, in which distinct elements are put together

Composite material (Verbundwerkstoff): combination of constituent materials, different in composition. *((1) The constituents retain their identities in the composite; that is, they do not dissolve or otherwise merge completely into each other although they act in concert. Composite materials provide improved characteristics not obtainable by any of the original constituents acting alone. (2) Normally the constituents can be physically identified, and there is an interface between them. (3) Composites include*

fibrous materials, fabrics, laminated (layers of materials), and combinations of any of the above. (4) Composite materials can be metallic, non-metallic or a hybrid combination thereof, and carbon concrete is a further example. (5) probably homogenizable to a smeared material such as FRC, SMC, UD-ply and lamella. The lamella is smearable and not a 'material composite' or 'material composition' (Werkstoffverbund). Therefore it can be modelled as a 'composite material'(Verbundwerkstoff). (6) Layered materials and foam materials are also forms of composite materials)

Composite design challenges FRP: faced with thick composite sections with large number of plies, regions of significant ply-drop-offs, T-joints, highly loaded locations, structural shapes causing changes in draping angle and thickness, edge effects, failure criteria choice

Component: combination of parts, devices and structure, usually self-contained, which performs a distinct function (acts on one or more inputs to produce an appropriate output) in the operation of an equipment; for example, a converter, gas generator, amplifier.

Compound: mixture of polymers

Compressibility: property of a material, showing volume reduction under compressive forces. (low means high Poisson's ratios ν and vice versa)

Computational modelling, FEA: common application of the disciplines mathematics, physics and computer science to study the behavior of complex systems by computer analyses

Concrete cover: adequate thickness as protection. (*used to tackle the insufficient corrosion resistance of steel. Many cm for the corroding steel reinforcement are needed and much less for a CF textile reinforcement*)

Concrete matrix: material composed of cement, fine aggregates (sand) and coarse aggregates mixed with water which hardens with time. (*Portland cement is the most often used cement for concrete production. Different types of binding material are also used such as lime for lime concrete and bitumen for asphalt concrete in road construction*)

Concrete splitting: longitudinal cracks, which form under compression. (*larger internal flaws may cause concrete splitting due to effects describable by a fracture mechanical condition. It is a failure beside the so-called cone failure due to shear fracture failure that is predictable by a strength failure condition*)

Concurrent engineering: parallel technical working of all involved technical disciplines

confidence - a measure of assurance that a statement based on statistical data is correct. The probability that an unknown parameter lies within a stated interval.

Conditioning: process of exposure of a material to a property-altering environment prior to subsequent testing, applying equilibrium conditioning and fixed-time conditioning

Confidence level (C): interval estimate of a population parameter (design variable) used to indicate the reliability of an estimate. (*describes, how frequently the observed interval contains the parameter is determined by the confidence level or confidence coefficient*)

Confining pressure p_{conf}: maximum level of compression applied in a tri-axial compression test of a concrete or a neat resin test specimen defined by $(\sigma_{ax}, \sigma_{conf}, \sigma_{conf}) = (\sigma_{ax,p} - p_{hyd}, -p_{hyd}, -p_{hyd})$ with σ_{ax} (from test brushes) $= \sigma_{ax,p} - p_{hyd}$

Confining lithostatic pressure: p_{hyd} + overlying weight

Concrete: composite material, primarily consisting of mortar and aggregates or of a mixture of cement, sand and gravel

Consistence of a material: dense or porous or mixed. (*consistence is essential for the choice of the right strength failure condition*)

Confidence interval: one-sided or two sided region within which an unknown parameter is said to lie with a stated probability.

Confidence limit : bound of a confidence interval

Constant amplitude loading: fatigue loading of a test specimen when the amplitude remains constant

Constituent: element of a higher level material. (*examples are fiber and matrix of a UD ply*)

Constitutive equation: description of any linear or non-linear material behavior law, usually relating strain, stress and temperature

Constraint: fixed relationships between the basic degrees of freedom in a finite element model

Contact elements / gap elements: elements, as lines or areas, used to model states of contact between surfaces

Contamination: action or state of making or being made impure by polluting or poisoning

Convergence: situation, achieved for any non-linear solution procedure, when sufficient iterations within a given increment of time or loading have produced an equilibrium state regarding a given convergence criterion

Convolution integral: mathematical expression representing the operational probability of failure

Correlation: measure of the linear dependence between tow random variables expressed in terms of the correlation coefficient ρ which varies in the range $-1 < \rho < +1$. Variables which are perfectly positively (negatively) correlated have a correlation coefficient of + 1 (-1). Variables which are stochastically independent have a correlation coefficient of zero.

Composite material versus material composite (2 structural composite types): Composite Material (*Verbundwerkstoff*) combination of constituent materials, different in composition. Material Composite (*Werkstoffverbund*) structural-mechanically a composite 'construction of different materials (a not smearable 'conglomerate' such as i.e. carbon mat-reinforced concrete which is not a 'composite material' despite it is usually termed so)

Connection versus joints: connection is (uncountable) the act of connecting while joint is the structural point where two components of a structure join.

Condition versus criterion: $F = 1$ versus $F <= > 1$

Confining pressure: lithostatic pressure in geo-mechanics, the pressure forced on a layer of soil or rock by the heaviness of the overlying substance. Corresponds to a hydrostatic pressure p_{hyd}

Confining stress: usually stress σ_z caused by p_{hyd} at level z

Crack a: large flaw of the size a (*a_0 is the initial crack size, distinguish micro-crack and macro-crack*)

Crack propagation , fracture mechanics: process by which a crack can propagate through a structure. (*it is assumed that a crack occurs if a critical value of stress or strain is reached and that the crack propagates if it can release more than a critical amount of energy by the crack opening*)

Crack width verification: concrete proof, grouped by the exposure class in EN 1992-1-1, chapter 7.3

Crazing, organic matrix like PMMA: result of a fine network of apparent micro-cracks at or under the surface of the matrix (*then a so-called whitening may happen to be*)

Creep: time-dependent deformation $\varepsilon(t,T)$ of a material under loading and temperature (*creep terminates by stress rupture if straining is not brought to a halt*)

Cross-ply: layers with rovings running cross-wise

Cross-section: intersection of a physical body or a virtual failure body with a plane

Cross section of a fracture failure body (surface)**:** (1) convex π-plane ≡ plane I_1 = constant ≡ hoop plane; (2) deviatoric plane = meridian planes (tensile, compressive, shear), may be not convex at $I_1 \rightarrow$ max I_1 because this will depend on the ratio R^{tt}/R^{t}, or f_{ctt}/f_{ct} (index $_c$ for concrete)

Critical buckling resistance: buckling resistance determined with a model under the pre-requisite of idealized conditions. Design buckling resistance: design value of the buckling resistance taking into account the uncertainties of model-based prediction. (*associated knock-down factors may be obtained from statistical evaluation of test results*)

Criticality: 1. Catastrophic: failure mode causes damage to other systems or equipment. 2. Critical: failure mode causes loss of the function of the system or equipment. 3. Major: failure mode causes major degradation of the system or equipment. 4. Minor: all other failure modes.

Cross sections of the fracture failure body (surface): (1) convex π-plane ≡ plane I_1 = constant ≡ hoop plane, deviatoric plane.(2) meridian planes (tensile, compressive, shear), may be not convex at $I_1 \rightarrow$ max I_1

Critical material location ('point', 'hot spot'): grainsize-dependent critical material volume

Crushing: failure mode of brittle behaving materials under compression

C-stage: usually fully cured state

Curing (Vernetzung): process where a chemical reaction takes place. (*change of properties of a thermosetting resin irreversibly by chemical reaction. Example: condensation, ring closure, or addition. Cure may be accomplished by addition of curing (cross linking) agents, with or without catalyst, and with or without heat. Cure may occur also by addition, such as it occurs with an-hydride cures for epoxy resin systems)*

Cyclic loading: loads that repeatedly oscillate between maximum and minimum values over time, alternating loading

Damage (*Beschädigung*): physical harm, which captures in English as well *micro-damage D* (*Schädigung*) as the *macro-damage* (*Schaden*) crack, delamination.((1) Unfortunately in English literature the term damage is used for a damaging process wherein the results, the micro-damages finally accumulate to a critical technical macro-damage size such as a macroscopic delamination. Damaging of brittle materials begins when the elasticity domain ends. (2) It is to be noted that also a local cloud of macro-damages such as technical cracks might exist and grow together)

(macro-)Damage (*Schaden*): sum of the accumulated micro-damages or a macro-damage such as an impact failure that is judged to be critical. (*then, Damage Tolerance Analysis is used to predict the growth of the damage under further cyclic loading or static failure under Design Ultimate Load*)

(micro-)Damage accumulation**:** accumulation of micro-damages. *(1) Unfortunately in English literature the term damage is used for the damaging process wherein the results, the damaging portions, finally accumulate to a critical damage size such as a macroscopic delamination. Damaging begins when the elasticity domain ends. (2) It is to be noted that also a local cloud of damages such as technical cracks might exist and grow together*

Damage tolerance: capability of a structure to resist failure due to the presence of large flaws or other damage for a specified period of usage without inspection or repair.

(Note: Continued operation with the damage will not produce an imminent failure)

Damage Tolerance Assessment DTA**:** assessment, whether the structure's damage tolerance capability can withstand the envisaged damage state.

(Note: With threat assessment of e.g. a tool drop, with no-growth requirement of non-detectable flaws during inspection time, with proofing enough strength against Design Ultimate Load after fatigue and impact loading (BVID < 0.3 mm) and against Design Limit Load (VID > 1 mm in aerospace design)

Damage variable (Schädigungsvariable): variable that is used to describe and quantify the damaging process

Defect (take flaw)*:* manufacturing anomaly created by processing, fabrication or assembly procedures. flaw, manufacturing imperfection. (*defect should not be used for legal reasons regarding product warranty. Instead for laminates, it should be taken flaw or manufacturing imperfection such as for a pore, ply waviness, matrix nests, debonding of fiber from matrix, fiber misalignment*)

Deflection**:** term to describe the magnitude to which a structural element deforms laterally or bends under loading

Deformation**:** change in shape of a structural part caused by the application of a load or force or hygrothermal loading

Deformation-controlled testing**:** stress, in for instance an embedded lamina (ply) in a laminate depends on the adjacent layers. *(strain-controlled testing is practically not possible)*

Degradation**:** process of deterioration in the material or in a structural element. *(deleterious change in chemical structure, physical properties or appearance)*

Degrees of Freedom DoF**:** number of equations of equilibrium for the system.

(Note: In dynamics, the number of displacement quantities which must be considered in order to represent the effects of all of the significant inertia forces)

Delamination: separation of material layers within a laminate or also in a textile reinforced concrete. *(may be*

local or may cover a large area of the laminate. It may occur at any time in the cure or subsequent life of the laminate and may arise from a wide variety of causes)

Democratization**:** novel FEA-provider idea enabling the use of software by not well educated users (*danger of "black box use")*

Density ρ: mass per unit volume

(structural) Design: common work of a team of engineers to develop conceptual and detailed designs.

(design that meets the design specifications, to finally achieve a sustainable construction especially for large load-carrying damage-tolerant infrastructure structures such as bridges, buildings, wind tribune blades, offshore structures. Sustainability, however, needs some presumptions:

- *designed by qualified and experienced personnel [see EUROCOMP Design Code]*
- *adequate supervision and quality control in plants and on site*
- *construction executed by experienced personnel*
- *construction materials and products are used as specified*
- *structure will be adequately maintained*
- *structure will be used in accordance with the design requirements.*

This means, the design procedures are good only when the requirements for construction and workmanship are met and they are good further, when the life-span CoSts are reduced)

Design allowables**:** values for the design parameters such as load, strength, Youngs Modulus, fracture strain, structural detail properties that have been determined from test data and chosen to assure a high degree of confidence in the integrity of the complete structure

Design allowable **(**for resistances!**):** statistically-based minimum value of the strength capacity w.r.t. a failure mode. *(in terms of resistance to a loading, a strength, or a strain limit with respect to a failure mode where some examples are fracture, rupture, collapse, detrimental deformation or an unacceptable flaw growth. Examples: strength design allowable, limit strain design allowable)*

Design dimensioning , Auslegung): static and cyclic sizing

Design of Experiments (DoE**):** concept to optimally plan tests and to sort out the significant number of design variables focussing a reduced number of test specimens. *(a DoE approach is implemented by using a statistical ANalysis Of VAriance (ANOVA) to investigate the influence of the design variables)*

Design (working) life: project-defined lifetime of a product

Design Limit Load DLL: maximum load, or combination of loads, which a structure is expected to experience with a given probability during the performance of specified missions in specified environments

Design Load**:** maximum amount (of loading) a (load-carrying) system is to be designed to.(*(1) Examples are design limit load DLL or design yield load DYL or design ultimate load DUL (≡ ULS) or design buckling load. (2) analogous for the case of pressure loading)*

Design load cases: relevant load cases, to be extracted from the numerous load cases given by single loads, load combinations, stiffness requirements etc. Subset Dimensioning load case: physically possible, driving design load case which is of a certain probability of occurrence

Design parameters: complete set of design variables (initially unknown) and design constants (initially fixed). The design parameters can be stochastic (X) or deterministic (x)

Design point , β point : combination of values of the basic variables most likely to cause failure, used as a basis for design. (*point in structural reliability hyperspace which represents or includes all nominal values of the significant design variables calculated in the analysis. For a particular structure, the design point is the point on the failure boundary where the probability of failure density is a maximum*)

Design principle: design of a structure is the result of the design principle chosen. Such design principles are 'fail safe', 'safe life', damage tolerant

Design sensitivity analysis DSA: DSA is to study how the uncertainty in the output of a mathematical model or system, an analysis, which provides the derivatives of output variables with respect to specified design

parameters. These derivatives are commonly referred to as sensitivities, because they provide a first-order measure of how sensitive the output variable is to a change in the design parameter, see examples in Chapter 13

Design space: multidimensional combination and interaction of input variables (e.g. material attributes) and process variables

Design value: value of a property used in design that is assumed to consider its uncertainty

Design variable (parameter)**:** physical feature which influences the design performance. *(according to the nature of the design variables, linked to loading, geometry, tolerances, and material properties, different design problems can be identified such as structural sizing for the dimensioning of beams, shells, plates; further shape optimization; material selection and finally structural topology tasks)*

Design principle: design of a structure is the result of the design principle chosen. Such design principles are 'fail safe', 'safe life', damage tolerant

Design verification: see definition of verification

demonstration that the design fulfils the requirement's data defined in the final customer-tender 'performance requirements specification'.

(Note: Process, whereby a structural design is comprehensively examined and qualification-tested to ensure that it will perform in the required way, before and during operational use. Proof by determination of the Reserve Factor RF on basis of a statistically reduced strength failure body with its strengths spanning the fracture body)

Desorption: process in which an absorbed or adsorbed material is released from another material. *(desorption is the reverse of absorption, adsorption or both)*

Deviatoric stress and strain: shear components of stress and strain tensor. *(components in the remaining tensor after deducting the hydrostatic stress σ_{hyd} or strain. The deviatoric components govern plastic and creep flows, when there is a change in shape but not of the volume. Deviatoric stress: $\sigma_{dev} = \sigma' = \sigma - \sigma_{hyd}$ with $\sigma_{hyd} = I_1/3$)*

Deviatoric stress plane: σ_{hyd} = constant plane, π-plane

Diffuse damaging: micro-damage occurring from onset of micro-cracking on until the onset of discrete local macro-cracks, indicated by whitening in the case of polymers. *(essential for ductile thermoplastics connected to void initiation and void growth, linked to the termination of the linear elastic stress-strain curve)*

Digital (virtual) twin, see also BIM: counterpart to the physical twin in product development

Dilatation **(**dilation US**):** amount of shear stress-generated increase of the solid's volume accompanied by degradation. *(due to $\nu < 0.5$ the material solid under compression elastically reduces its volume until dilatation is superimposed, initiated shortly before fracture of the test specimen occurs. Dilatation decreases under growing high confining stresses, e.g. hydrostatic stress states, and is suppressed finally*)

Dimensioning load case**:** physically possible, driving design load case which is of a certain probability of occurrence

Discrete crack model: model that attempts to follow individual crack in non-linear concrete analysis

Discrete (micro)damage**:** localization of micro-damage after the diffuse state

Drucker's postulate: for so-called 'stable' materials the postulate is fulfilled if the 'normality condition' holds (hardening domain !)

Drucker-Prager yield criterion: elasto-plastic material model using both hydrostatic and deviatoric stresses in compressive stress cases. *(its failure surface is a cone in the principal stress space. Used for instance in soil mechanics)*

Ductile fracture: type of fracture occurring in a material the behavior of which is ductile. *(such fracturing occurs, after some general plastic deformation as the load builds up, in metals at temperatures above the range of the brittle-ductile transition temperature)*

Dwell time: amount of time, e.g. between test cycles

Durability verification (*Dauerhaftigkeitsnachweis)*: ability to withstand wear, pressure, or damage. In construction to have considered the design rules, execution of construction work, concrete cover etc

Effective stress:

effective, wirksam: here, real out-come or real performance

Effective stress: stress that considers a reduced load-carrying cross-section $\sigma_{eff} = \sigma / (1 - D)$ or degraded material-related stress that considers a reduced load-carrying cross-section. *(scalar quantity, with degradation sum D and nominal stress σ of the intact material. It is defined in the case of ductile behaving materials usually as the Von Mises stress. For brittle behaving materials like concrete other failure conditions must be applied, namely, fracture failure conditions)*

Eigenvalues: roots of the characteristic equation of the structural system. *(1) If a system has n equations of motion then it has n eigenvalues. The square root of the eigenvalues are the resonant frequencies. These are the frequencies that the structure will vibrate at. (2) There are other problems that require the solution of the eigenvalue problem, the buckling loads of a structure are eigenvalues, too)*

Element: generic element of a more complex structural member (e.g. skin, stringers, shear panels, sandwich panels, joints or splices).

(strain) energy release rate SERR, fracture mechanics quantity: energy dissipated during fracture per unit of newly created crack surface area

End, thread: a single bundle of fibers

End-of-life: end of usable time of a product

Endurance limit, fatigue limit: cyclic strength without causing failure

Engineering stress: ratio of acting load and initial area or non-deformed area. *(difference to true stress)*

Equilibrium: state of a loaded body when the internal stresses are in equilibrium with the externally applied loads

Equivalent stress σ_{eq}: author's view on ductile and brittle materials

(1) Equivalent (in German, gleichwertig dem Spannungszustand) to a multi-axial stress state combining the effects of those stresses that are active in a distinct failure mode. Examples: Von Mises Equivalent Stress in the case of the associated 'shear yielding' failure mode; or Maximum Principal Stress in the case of Rankine's brittle 'tensile fracture' failure mode NF. (2) The uniaxial scalar σ_{eq}-value (in German termed 'Vergleichsspannung' = vergleichbar mit Festigkeit) can be compared to the mode-'reigning' associated uniaxial 'basic' strength R or f of the activated failure mode

Environment: external, non-accidental conditions (excluding mechanical loading) separately or in combination, that can be expected in service life

(mode !) Equivalent stress σ_{eq}^{mode}: mode–dedicated equivalent stress. The highest mode equi-valent stress gives the designer a possibility where to turn the design screw. (a) equivalent (gleichwertig) to the stress state, as performed in σ_{eq}^{Mises}, and (b) comparable (vergleichbar) to the value of the strength *R* which dominates one single failure mode or failure type, respectively

Eulerian formulation: geometrically non-linear formulation where the equilibrium conditions are evaluated in the deformed configuration

Eurocode, major concepts: Fulfillment of the fundamental requirements safety, serviceability, fire and robustness. *(structure and structural members should be designed, executed and maintained in such a way that they meet the following: (1) Serviceability requirement – the structure during its intended life, with appropriate degrees of reliability and in an economic way, will remain fit for the use for which it is required.(2) Safety requirement – the structure will sustain all actions and influences likely to occur during execution and use. (3) Fire requirement – the structural resistance shall be adequate for the required period of time. (4) Robustness requirement – the structure will not be damaged by events such as explosion, impact or consequences of human errors, to an extent disproportionate to the original cause*

Expectation: average of a random variable or function is called the expectation of the variable and is written E(x). The analogous quantity in a statistical sample is the sample mean $\bar{x}$

Explicit method**:** method for integrating equations of motion. *(explicit methods can deal with highly non-linear systems but need small steps. Implicit methods can deal with mildly non-linear problems but with large steps*

Fabrics (Stoffe): 2D-woven textile semi-finished products (interlocking of fibers) and 2D-non-woven ones. *(from a practically zero fiber amount in the transversal direction up to multi-axially woven fabrics. Non-crimp fabrics NCF have the best fiber alignment and – when stacked - can be modelled as a composition of UD-laminas. Hybrid fabrics composed of different fibers in the various directions are further available)*

Face sheet: cover sheet of a sandwich

(design) Factor of Safety (FoS): Safety Factor, mechanical engineering. Deterministic factor - based on long experience - which increases or factors the level of the given loading. *(in civil engineering the design improving Partial Safety Factor concept is applied)*

Fail-Safe: design philosophy in which products are designed in such a way that failure, prior to the required operational life, is not catastrophic

Failure: performance below a specified minimum level or outside a specified tolerance interval. Malfunction on a specified level in a specified time (burst, deformation too large or stiffness too low, missing of a safety or an availability requirement). Or, state of inability of an item to perform a required function in its limit state, also loss of a function under stated component part conditions → A situation when a structural part does not fulfil its functional requirements such as the failure modes Onset-of-Yielding, brittle fracture (NF, SF, Crushing Fracture CrF), Fiber-Failure FF, Inter-Fiber-Failure IFF (matrix failure), leakage, abrasive wear, deformation limit (tube widening), fretting corrosion, delamination size limit, frequency bound, or heat flow etc. *A failure is a project-defined 'defect' or limit state.* For each failure mode a Limit State with F = Limit State Function or Failure Function is to formulate. A specific mark for failure exemplarily is: A second loading, under a distinct failure mode (here SF), cannot be sustained anymore, like a slightly porous UltraHighPerformanceConcrete UHPC compression test specimen after a crushing test under p_{hyd} = 1000 MPa where the first loading of the crumbles might have been still further increased, densification enables it)

(Strength) Failure Condition (SFC): mathematical formulation of the failure surface that takes the form F = 1 = 100 % . *(1)Most often meant is a strength failure condition SFC. Aim of a Failure Condition is to assess multi-axial states of stresses by just utilizing the uniaxial strength values, which are always mandatory in design. Usual SFC describe just a 1-fold occurring failure mode or mechanism! (2) A multi-fold occurrence of a compressive concrete failure (i.e. $f_{c,cc}$) with its joint probabilistic effects must be additionally considered in the formulas. In other words, the accumulation of two damaging portions works and must be considered)*

Failure Mode Concept FMC**:** invariant, failure mode-based general concept to generate strength failure conditions for single failure modes. It is a 'modal' formulation in contrast to 'global' concepts where all failure modes are mathematically linked. Is ac oncept for materials that can be homogenized (smeared). The applicability of a SFC ends if homogenization as pre-requisite of modeling is violated and no longer valid

Failure criterion: formulation that takes the form F > 1, F = 1, F < 1

Failure function F : mathematical description of the failure $F = 1$ → (limit state function (Grenzzustand) $\mathcal{G} = F - 1$

Failure index FI**:** value of the failure function used with polymer composites. *(corresponds to the material stressing effort Eff (Puck uses the term exposure) Eff only in cases where the considered stress terms are linear (homogeneous) in the strength failure condition)*

Failure initiation (onset) : event that initiates a certain defined failure

Failure limit state**:** termination of the ability of an item to perform a required function (limit state, such as stability, ductile tearing, (brittle) cleavage fracture, onset of yielding, deformation limit, leaking. *(material failure, e.g. a strength failure mode or a structural failure, such as stability failure)*

Failure mechanism: underlying phenomenon that determines the mode of failure

Failure mode: observable effect of the mechanism through which the failure occurs. (*(1) Examples are rupture, collapse, global and local buckling, leakage, degradation, excessive wear, corrosion, fiber-fracture FF, inter-fiber-fracture IFF, delamination, initiation of yielding, deformation limit, or any other phenomenon resulting in an inability to sustain design loads, design pressures with associated environments. (2) There are different levels of failure types: (a) Material failure type: designation of failure for a ductile or brittle failure material (ductile means a gradually occurring and brittle a rapidly occurring sudden failure);(b) Structural failure type like buckling*). Failure mode is a commonly used generic term for all types of failures, is a name for a potential way a system may fail (*in design verification usually a project- associated failure*)

Failure-Mode-Concept-based failure criteria **(**Cuntze idea**):** failure mode-wise formulated strength failure conditions SFC ('criteria') for the three brittle material families and isotropic ductile ones.*((1) Stress-invariant-based concept, like Mises with the invariant J_2, obtaining equivalent stresses σ_{eq}. (2) Applicable for isotropic materials [Cun17 for concretes], transversely-isotropic materials [Cun17 for UD-laminas and the lamella] and orthotropic materials. (3) The number of independent strength failure modes is fixed by the material symmetry requirements which demand 2 for isotropic, 5 for transversely-isotropic and 9 for generally isotropic (9 reduces to 6, if weft ≡ fill and identical to warp, a situation given with plain weave fabric materials). For the lamella, a UD layer, there are 3 Inter Fiber Failure IFF conditions and 2 Fiber Failure FF ones. These are based on averaged lamina stresses [Cun04, Cun13, Cun16]. (4) The combined effect of commonly acting failure modes is considered by an interaction equation. (5) SFC capture one failure mode just once. Multi-fold acting failure modes must be considered additionally, because the danger to fail multiplies. For concrete this is usually modelled by the invariant J^3, see examples in [Cun17])*

Failure surface ($F = 1$): formulation of a mathematical condition under which materials or structures fail. *(an example shall be the load-driven growing yield failure surface (yield failure body), analogous to Von Mises cylinder $F = \sqrt{3 \cdot J_2} \,/\, R_{p0.2}$,and s as growing radius of the yield loci located on the 'Mises cylinder'. This yield failure surface, growing under further loading, is terminated by a fracture failure body*

Failure Mode Concept FMC **:** invariant, failure mode-based general concept to generate strength failure conditions for single failure modes, a 'modal' formulation. In contrast to 'global' concepts where all failure modes are mathematically linked. Concepts for materials that can be homogenized (smeared). The applicability of a SFC ends if homogenization as pre-requisite of modeling is violated and no longer valid

Failure modes, effects and critically analysis (FMECA): systematic investigation of actual or potential single origin fault conditions form observed cause to performance deviation from nominal conditions and the classification of this deviation in terms of the resulting degree of loss of mission objectives.

Failure ***rate***: number of failures of an item per unit measure of life (cycles, time, events etc. as applicable for the item). For devices described by the exponential model, the positive constant l. It is the reciprocal of mean-time-between failures. Bath tub course of failures (See also Failure state!)

Failure ***state***: here, failure of a structural component or of a material

Failure system: Both, failure state and failure rate contribute to the failure of a system, see the given schematic example in Chapter 12

Failure surface: graphical representation of a failure condition or surface of the strength failure body, with the shape defined by $F = 1$ or $Eff = 1 = 100\%$. (The $F = 1$ envelope contains the non-failed domain F < 1 or the non-failure body, respectively)

Failure initiation (onset) : event that initiates a certain defined failure

Failure mechanism : underlying phenomenon that determines the mode of failure

Failure system versus System failure: Failure system is a joint failure action of failure modes which finally might result in a system failure. System failure is a problem that causes a system to end its intended function (malfunction)

(strength) Failure type: strength failure mode Normal Fracture NF, Shear Fracture SF under compression, Crushing Fracture CrF, Normal Yielding NY, Shear Yielding SY, Fiber Failure FF, Inter-Fiber-Failure IFF etc

Far-field stress**:** stress far away from a notch or a crack

Fatigue**:** deterioration of a material under dynamic/cyclic loading. *(micro-damage process in which repeated cycles of increasing and decreasing stress finally may lead to the development of a fatigue damage. Principally, fatigue life captures the phases crack initiation and crack propagation)*

Fatigue limit**:** endurance limit, fatigue strength: limiting cyclic stress. *(cyclic loadings can be applied to the material (structure) without causing failure)*

Felt**:** non-woven fabric

Fiber: term used to refer to filament materials. *((1) Unfortunately, fiber is sometimes synonymously used for the filament but also in textile production for a bundle of filaments (thread, strand, roving, tow) consisting of thousands of filaments. (2) Length: short (chopped) fiber < 5 mm (is differently fixed), long fiber < 50mm, and endless (continuous) fiber. Hooked steel fibers used in FRC are > 50 mm). (3) In most cases the fiber is prepared by drawing from a molten bath, spinning. Fibers can be continuous or of specific short lengths (discontinuous). (4) From load transfer reasons the finite length should be at least 100 times its diameter)*

Fiber architecture**:** fibrous preform or part in which the fibers are arranged in a particular way to achieve a desired result. *(braided, stitched and woven fabrics are common forms of fiber architecture)*

Fiber bridging: fiber material bridging layers in a laminate and thereby strengthening in z-direction. *(increases ILSS)*

Fiber classes (carbon fibers):

Designation		**Tensile Modulus GPa**	**Tensile Strength MPa**
HT	(high tensile)	225 - 265	4000 - 5000
IM	(intermediate modulus)	270 - 320	5400 - 6500
HM	(high modulus)	330 - 400	3200 - 4700
UHM	(ultra high modulus)	430 - 590	3800 - 4700
Typical properties of carbon fibers			

Pultruded CF-profiles are lighter than aluminum, stronger than steel. HM–fibers ($V_f = 60\%$) are stiffer than steel

Type	Density [kg/dm3]	Tensile strength [Gpa]	Tensile modulus [Gpa]
HS1	1.75	3.31	228
HS2	1.80	5.0	248
IM	1.74	4.50	296
HM1	1.81	2.41	393
HM2	1.96	1.52	483
UHM	2.15	2.24	724

Typical properties of carbon fibres

http://www.exelcomposites.com/en-us/english/composites/rawmaterials/reinforcements.aspx

Fiber efficiency: Faserausnutzbarkeit: exploitability of the reinforcing fibers

(short, discrete) Fiber-Reinforced Concrete FRC, Faserbeton: concrete with usually stochastically distributed short fibers. *((1) Primary intention is to isotropically improve the concrete matrix properties such as tensile strength. Reinforcement in order to withstand high local stress states. In future, the 'load carrying participation effect' should be considered in civil engineering. (2) Technical Groups FIB (TG 8.3 "Fiber reinforced concrete" and fib TG 8.6 "Ultra high performance FRC". (3) Short fibers used are steel, polymer, AR glass or CF of the length 6 mm up to 20 mm. An example for such a concrete with short fibers added is Carbocrete, SGL)*

(endless) Fiber Reinforced Concrete FC**:** concrete, reinforced by a bar grid or a R-mat or a Q-mat. *(the abbreviation FRC confuses as it does not fit to the old term FRP for the polymer matrix)*

Fiber-Reinforced Polymer (plastic) FRP: composite material made of a polymer matrix reinforced with (long) fibers.

(Note: The fibers are usually glass, carbon, aramid, basalt. . The polymer is usually an epoxy, vinyl ester or polyester thermoset, and further thermoplastic resin systems are applied in construction industry)

Fiber grid: structure, which consists of grid-type fiber semi-finished reinforcement products

Fiber volume content V_f in %: amount of fiber present in a composite. *(usually expressed as a percentage of fiber volume fraction V_f or less often as a fiber weight fraction of the composite W_f)*

Filament: endless single fiber, thinly spun single fiber. *(Carbon fiber CF, alkali-resistant glass fiber AR-GF, polymer, aramid, basalt). CF types 7 mm ϕ ; (1) PAN precursor-based, derived from the controlled pyrolysis of poly(acrylonitrile) fiber after oxidation and carbonization, (2) Pitch precursor-based, derived from petroleum or coal tar pitch - for generation of high stiffness fibers - after oxidation and graphitization. (3) In civil engineering, a CF of the type High Tensile is exemplarily used with $E \approx 200$ GPa, $\rho \approx 1.75$ g/cm^3, f_t ($= R_{||}^t$) ≈ 2700 MPa (N/mm^2), and Coefficient of Thermal Elongation CTE $\equiv \alpha_T \approx 0 \cdot 10^{-6} \cdot K^{-1}$)*

Filament winding: manufacturing technique of winding rovings under some pre-tension over a rotating mandrel

Fill (weft): filling yarn in a woven fabric running at right angles to the warp. *(replaces the normally used term weft in order to avoid the index-letter conflict with warp)*

Fine-grained concrete ('Feinbeton'): mortar due to the fine grain definition (< 4 mm ∅), however termed concrete due to application as matrix

Finish: material, with which filaments are treated, which contains a coupling agent to improve the bond between the filament surface and the resin matrix in a composite material

First order: first order method of reliability analysis is so-called because it requires a 'first order'
(linear) approximation of the limit state function.

First ply failure: initial failure of a laminated or similar multi-layer composite material which can be predicted by an established failure criterion (The structure may be capable of carrying additional loads after this initial failure but this must be substantiated by consideration of the appropriate failure mode(s) to establish 'the last ply failure').

Flaw (Ungänze): local discontinuity in a structural material. Example: Scratch, notch, crack, void or pores in case of metallic and homogeneous non-metallic material; delamination or porosity in case of composite material. (due to legal reasons one should avoid the term defect)

Flaw versus micro-crack: a micro-crack is a sharp flaw, grade of singularity is decisive

Flow curve: $\sigma(\varepsilon^{pl})$

Flow rule: rule, used in plasticity to define a relationship between the plastic strain increment $d\varepsilon^{pl}$ and the stress increment, also called a plastic potential. (*hence, both the normal to the yield surface and the plastic strain tensor are perpendicular to the stress tensor and have the same direction if associated.*

Above quantity is equal to zero for purely elastic behavior. Flow rule is associated to a failure condition. The assumption of co-directionality is called the normality condition)

Associated Flow rule: considering a flow potential $d\varepsilon^{pl}$ of ductile materials or an inelastic potential $d\varepsilon^{inel}$ with and the normal to the failure surface have the same direction. Flow rule is associated to a failure condition. The assumption of co-directionality is called the normality condition

Folding (draping) of semi-finished products: process, performed for organic sheets and green textile concrete elements

Non-associated Flow rule: flow rule where the vector of $d\varepsilon^{pl}$ is not normal to the failure surface of the SFC

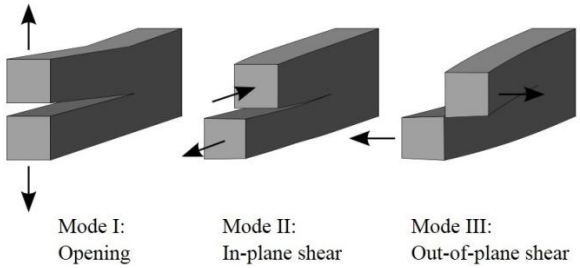
Fracture: separation of a whole into parts

Fracture 'plane' angle Θ_{fp}°: average value of the scattering fracture plane that is seldom a plane. A tensile stress causes an angle perpendicular to the stress direction of 90°. This definition matches with the 90°-wound UD tensile-compression-torsion test specimen

Fracture (failure) body: surface of all the vector tips of 3D- and 2D-fracture stress states, mathematically described by a strength failure condition SFC, representing $F = 1 \equiv 100$ % material stressing effort *Eff*

Fracture mechanics: solid mechanics theory, concerning the propagation of cracks in structural materials

Fracture mechanics modes: (tension-driven classical) modes, defined by the three ways of crack propagation used in Irwin's model (mode I opening, mode II sliding, mode III tearing), loaded by far-field stresses)



Fracture mechanics test specimens: test specimens for the 3 fracture mechanics modes and combinations thereof. *(brittleness-depending geometry presumptions for the test specimen-dimensions must be met!)*

Fracture toughness K_{cr}: ability of a material to withstand a loading in the presence of a sharp crack ≡ critical stress intensity factor K. (us*ually just indexed c, but this is still the much older index for compression*)

Free edge effect, laminate: stress singularity and stress 'intensities' (intensity factors) situation at the edges of outer plies. *((1) Singularity, caused by mismatch of the plies in a laminate. At the edge, all stresses are zero and must be build up to the size of the 'internal' ply stresses. This causes an outer 3D-stress state. (2) Further, due to flaws, micro-mechanically based stress 'intensities' (intensity factors) occur)*

Freeform (contoured) surface:

complex shapes, desired in architecture design

Friction: material attribute addressing the Mohr-Coulomb-linked internal material friction behavior. (t*he friction value μ is a strength property to be applied to capture compressive stressing in the respective strength failure function F. Often, indirectly described by the term 'Pressure-dependent material' behavior)*

Friction (material internal): slope of the Mohr-Coulomb failure curve (Mohr failure envelope) defined after the ratio of the derivation shear stress $d\tau_{nt}$ to normal stress $d\sigma_n$ at failure in the so-called touch point. The ratio $d\tau_{nt} / d\sigma_n$ is termed material internal friction value μ. *(Isotropic: μ as (internal) strength property to be applied when capturing compressive stressing of dense brittle materials. Range $0.05 < \mu < 0.3$, whereby the use of a lower value is more conservative. transversely-isotropic UD lamina, lamella strength property. (Note: $\mu_{\parallel\perp}$, $\mu_{\perp\perp}$ with $0.05 < \mu_{\parallel\perp} < 0.3$ and $0.05 < \mu_{\perp\perp} < 0.2$)*

Fused Deposition Modeling FDM**:** additive manufacturing process. *(Stratasys, 3D-Druck-*

Schmelzschichtungsverfahren mit PP, PA6, PEEK), see SLS)

Gap**:** missing contact

Gauss point: strategic location within finite elements where numerical integration and stress evaluations are made. *(depends on element types and can differ depending on usage for both numerical integration and stress evaluation)*

Gel-coat: resin, applied to the mold after the mold-release agent to provide a good surface

Glass fibers: fiber, spun from an inorganic product of fusion which has cooled to a rigid condition without crystallizing. *((1) E-glass: alumina-calcium-borosilicate glass where strength and high electrical resistivity are required. R-glass: calcium-alumino-silicate glass where strength temperature resistance is required. S-glass: magnesium-alumino-silicate glass where high strength, modulus and durability under high temperature and in corrosive media are required. AR-glass: alcaliresistant. (2) Static 'fatigue' under long time static loading of the GF is worse than that of CF)*

Glass transition temperature T_g**:** approximate midpoint of the temperature range over which the glass transition takes place

Grain curve**:** curve, where the grains (after DIN EN 933-1) must lie between the limiting grain curves in order to meet the filling requirements

Grid (textile reinforcement): reinforcing structure as a flat, open-grid fabric 2D grid of a plane or of a curved shape with 2 or 3 roving directions and probably different grid spacing

Grid (rebar): reinforcing structure, automatically composed at a plant or hand-made at the construction site

Grid '3D'**:** usually parallel grids of a plane or a curved shape which build a stitch-fiber joined upper layer with a lower layer. *(sandwich faces–like, better termed 2.5D-grid)*

Grid spacing**:** distance of strands, yarns, tows in the grid

Haigh-Westergaard coordinates**:** coordinates of the stress space $\rho = I_1 / 3$, $q = \sqrt{3} \cdot \sqrt{J_2}$

Haigh-Westergaard-Lode coordinates $I_1 / (\sqrt{3} \cdot R)$ as y-coordinate (*axial*) and $\sqrt{2 \cdot J_2} / R$ as x-coordinate (coordinates of the stress space where the stress combinations are equally measured in all directions)

Hardening, work or strain (Verfestigung): strengthening of a material during increasing deformation. *((1)With metals, it occurs because of dislocation movements and dislocation generation within the crystal structure of the material. (2) With composite materials, after a straight elastic part the following hardening branch is basically linked to a diffuse damaging (especially in the case of woven textiles) whereas in the softening branch preferably discrete damaging is experienced. The hardening branch of the stress-strain curve corresponds with the test on so-called 'isolated' test specimens finally delivering the 'isolated' (basic) strengths of the material. The softening branch of the stress-strain curve (discrete, localized damaging and cracks) may be determined by novel fracture mechanics test specimens on sub-laminate level. (3) Under tension, fabrics may behave over-linear due to lengthening effects of the usually not fully straight tows)*

Hardening curve: part below Onset-of-Fracture of the 'full' stress-strain curve

Hazard function: existing or potential condition that can result in an accident

Heavy tow: tow, consisting of 50 k or 100 k filaments. *((1) 100 k-CF-tow = 6667 tex ≈ 6.7 kg / km. (2) 105 filaments = 2 x 3300 tex ≡ 1 kN)*

heterogeneous: descriptive term for a material consisting of dissimilar constituents, separately identifiable. *(medium, consisting of regions of unlike properties separated by internal boundaries. Non-homogeneous materials are not necessarily heterogeneous)*

homogeneous**:** descriptive term for a material of uniform composition throughout. *(medium which has no internal physical boundaries; a material whose properties are constant at every point or - in other words - constant with respect to spatial coordinates)*

Hybrid laminate, mixed 'composite material': composite laminate composed of laminas (plies) of two or

more materials. *(examples are CFRP with metal, Glare, Arall, organo-sheets)*

hybrid**:** combination of different materials

Hydrogen embrittlement**:** process by which metals become brittle and break due to the introduction and subsequent diffusion of hydrogen into the metal (steel reinforcement)

Hydrostatic axis**:** σ_{hyd}–axis. *(equally measuring Lode-coordinates should be used in visualization of an isotropic fracture body)*

Hydrostatic failure point: vertex **(**top cap) or bottom closure of an isotropic strength failure body, [Cun17]. *(statistically estimated tri-axial failure point (failure behavior acts three-fold). Such a three-fold failure point cannot be predicted by a 'one-fold' SFC!)*

Hydrostatic pressure p_{hyd} **:** absolute value of hydrostatic compression. *(hydrostatic stresses σ_{hyd} have signs, of course)*

Hydrostatic stress**:** stress arising from a uniform pressure load on - for instance - a cube of material. *(used term, when generating principal stresses, defined as average value of the 3 stresses at any point in the body. These 3 stresses are equal in the hydrostatic pressure case. Seldom, a positive 3D-stress state can be subdivided into a positive σ_{hyd} plus further parts)*

Hypothesis: hypothesis is a proposed explanation for a phenomenon. (*For a hypothesis to be a scientific hypothesis, the scientific method requires that one can test it. Scientists generally base scientific hypotheses on previous observations that cannot satisfactorily be explained with the available scientific theories [Wikipedia])*

Hypothesis testing: use of test data to assess the weight of evidence for or against a hypothesis and to accept or reject the hypothesis based on a statistical decision rule

Hydrostatic failure point (top cap or bottom closure of failure body): statistically estimated tri-axial failure point (failure behavior acts three-fold). Note of the author: "Such a point cannot be calculated from a 'one-fold failure condition" as it is unfortunately sometimes executed

Hydrostatic pressure: absolute value of hydrostatic compression test (hydrostatic stresses have signs!)

IFF modes: the 3 different Inter Fiber Failure (fracture) modes of UD materials, known from fractography. *(each of these modes is governed by an associated strength.*

Impact: force or action of one object hitting another one

Imperfection: state or instance of being imperfect or a shortcoming, such as flaws being generated manufacturing imperfections. *(a traditional imperfection is of geometrical type*)

Implicit method: method for integrating equations of motion. *(implicit methods can deal with mildly non-linear problems but with large steps)*

Impregnation: saturation of the voids and interstices of a reinforcement with a resin inclusion. *((1) Impregnation of the roving (EP-, TP-compatible) as component of the tow (48 k heavy tow with a fiber grid of e.g. warp 3300 tex, fill > 800 tex. Only a good filament impregnation guaranties an equal straining and thereby a high mechanical stressing ('stressability') of the roving-internal filaments. (2) Impregnation captures infiltration, infusion, injection)*

Impulse: integral over a force acting in a time interval $t_2 - t_1$, formulated by $I = \int F(t) \cdot dt$, in [N·s], with F = force

Inclusion: part, trapped inside a material. *(inclusions are often capable of transmitting some structural stresses, but in a noticeably different manner from the parent material. They are often the source of stress concentrations)*

Incompressibility: straining with zero volumetric strain or with no change in volume, like soft materials

Inclusion: part, trapped inside a material. *(inclusions are often capable of transmitting some structural stresses, but in a noticeably different manner from the parent material. They are often the source of stress concentrations)*

Incompressibility**:** straining with zero volumetric strain or with no change in volume, like soft materials

Inelastic behavior**:** behavior, that captures yield flow of ductile materials and micro-damage of brittle

materials. (*non-linearity, caused by ductile behavior of materials such as with yield flow, creep and further nonlinearity caused by micro-damaging of brittle behaving materials and time-dependent visco-plastic behavior. De-loading runs a different path than up-loading)*

Inelastic potential versus yield potential (plastic): *inelastic* → micro-damage, brittle, fracture mod***es***, friction occurs and is indicated by the paraboloid-shaped SFCs (*an inelastic potential shall be not termed yield potential); plastic* → metal plasticity, ductile, yield mod***e***, frictionless sliding indicated by the cylinder shape of 'Mises', yield potential

Infiltration, polymer composite: deep impregnation of the fiber bundle by resin

Infusion, polymer composite: impregnation under a pressure less than 1 bar

Injection, polymer composite: impregnation under a pressure higher than 1 bar

Injection molding: manufacturing process for producing parts by injecting molten material into a mold. (a *thermoplastic or a thermoset polymer is injected under some pressure into the cavity of the injection mold, probably adding short fibers for improving the polymer matrix generating a Sheet Molding Compound, SMC. Such a SMC is most often composed of Polyester- or Vinylester-resins and glass fibers)*

Initial failure, laminate: 'practical' onset of degradation (initial failure is usually indicated by the occurrence of a distinct knee in the stress-strain curves of a laminate, and this is determined by the first IFF mode of failure

In-situ measurement: measurement under loading and environment

In-situ strength**:** strength capacity of the built-in material. *((1) Exemplarily, the strength of a UD layer, embedded within a laminate, is different (redundant due to embedding, therefore obeying to a 'parallel failure system') to the strength values from the usual 'isolated' material test specimens (weakest link behavior, obeying to a 'series failure system'). (2) The in-situ strength might be termed an 'effective' strength)*

Integrity demonstration: means any procedure, endorsed by the contractor and acceptable to Approval and Safety Authorities, whereby the product is demonstrated as safe and functionally reliable. It is implied that such a demonstration is deemed sufficient to satisfy the contractor's legal obligations to assure product integrity

Interaction: process of a combined action of stresses, or loadings, or failure modes. (*Interaction occurs between strength failure modes FF and IFF, NF and SF, between different stability modes, however also between stability failure modes and strength failure modes. It is a common triggering*)

Interface**:** boundary or surface between the individual, physically distinguishable constituents of a composite. *(surface between filament and matrix and also used for the surface (2D) that separates two parts or two laminate layers)*

Interfacial shear strength, fiber-matrix: maximum stress when sliding fracture begins. *(determined by the single fiber push-out method)*

inter-laminar: descriptive term pertaining to an event (e.g. fracture), or a stress field (e.g. shear stress) referenced as existing or occurring between two or more adjacent laminas

Inter-laminar shear stresses (ILS): shear stresses τ_{23}, τ_{13} in a 3D-stressed UD ply. *(the normal stress σ_3 completes the 3D stress state)*

Inter-laminar shear strength (ILSS): max. shear stress reached in the respective ILSS laminate specimen test

intra-laminar: descriptive term pertaining to a single lamina existing entirely, 2D, in the plane

Interphase material**:** material at the interface between fiber and embedding matrix. (*often micro-mechanically modelled as gradual from fiber stiffness down to matrix stiffness because its properties are practically not determinable)*

Invariant: combination of stresses or strains. Its value does not change when altering the coordinate system. The stresses in the invariants may be powered (exponents may be 2 or 3 or 4) or not powered (1). Invariants are advantageous when formulating the usually desired scalar failure conditions. Such

material-associated invariants are utilized for isotropic, transversely-isotropic and orthotropic materials. $I_1/3$ is often termed hydrostatic stress σ_{hyd}

Isotropic material: material with identical properties in all directions

Isotropic hardening: behavior, when plastic strains increase after initial yielding. *(in this case, the yield surface in principal stress coordinates expands uniformly about the origin while still maintaining its shape and orientation)*

Justification: verification of safety/reliability

Knitting: method of constructing a fabric by interlocking (inter-looping or inter-meshing) series of loops of one or more yarns

Kissing bond, NDI: zero-volume disbond. *(there are two types of kissing bonds (1) adherend and adhesive are in dry solid-solid contact, and (2) a surface contamination caused by a thin liquid layer)*

Lace: open space fabric

Lagrangian formulation: geometrically non-linear formulation where the equilibrium conditions are satisfied in the fixed reference configuration

Lamella, plural is lamellae (latin) or lamellas (US): small plate or fine sheet and designation used in civil engineering for tapes to reinforce a concrete construction. See also lamina. *((1) A lamella may be a line strengthening element being a UD lamina or a multi-axial NCF. There are applications such as bonded tapes, concrete inserted strips, 45°-reinforcement cages for shear-strengthening. (2) CFRP lamellas are used for strengthening of concrete slabs, timber beams, masonry and steel structures. (3) Lamellas are glued to the structure as external strengthening by an epoxy resin adhesive (e.g. Sikadur, minimal tensile strength of the old concrete should be 1.5 MPa)*

Lamina**,** plural laminas (latin) or laminas (US): thin plate or layer, used as designation of a single ply. *(Notes: (1) A lamina may be a uniaxial UD lamina or a multi-axial NCF. Lamina is the designation of the single ply as computational element of the laminate, respectively used as laminate subset or building block for modeling. (2) The term lamina does not necessarily mean the physical single layer as it is realized in the laminate. (3) The single layer of a non-crimped fabric NCF layer, e.g. $[0/90/45]_s$, is usually modelled using 3 distinct laminas with orientation angles 0°, 90° and 45°)*

Lamina, ply: computational element of the laminate. (*lamina in mechanical engineering becomes a lamella in the construction industry and then serves as a semi-finished product for the so-called upgrading of bridges, ceilings and silos*!)

Lamina properties **(**isolated**):** properties obtained from traditional 'isolated' test specimens for UD lamina material. *((1) The values used in analysis despite of the fact that they cannot consider the effect of embedding in the laminate which may improve the property values. (2) Embedded lamina properties are obtained from special sub-laminate test specimens, where the test ply is embedded between other plies which break at higher load levels than the test ply. (3) UD lamina properties are applicable for different laminate stacks*

Laminate: designation of a complete lay-up or stack of several laminas (laminas) which are bonded together

Laminate properties: properties obtained from laminate test specimens. *(data principally applicable for the tested stack, only)*

Layer (ply): physical element from winding, tape-laying process, etc. *(subset of a laminate)*

Lay-up, stack: process of fabrication involving the assembly of successive layers of fiber-reinforced material, dry or prepreg. *((1) The reinforcing material placed in position in the mold. (2) The process of placing the reinforcing material in position in the mold. (3) The resin-impregnated reinforcement. (4) A description of the component materials, geometry, etc., of a laminate. (5) A stack-up of composite materials that forms either a cured or uncured part, (BDS 1330). (6) A process of fabrication involving the assembly of successive layers of resin impregnated material)*

Lay-out: pre-dimensioning

Length scales: official

macroscopic: 1 mm - 1000 mm ≡ 1m

microscopic: 1 μm - 1000 μm ≡ 1 mm (scale where practically damaging occurs is < 0.1mm)

nanoscopic: 1 nm - 1000 nm ≡ 10^{-3} mm.

Micro: length scale where usually damaging and fracture occurs (> 1μm). Micro: length scale where usually damaging and fracture occurs (> 1μm). *Macro*: desired engineering length scale for composites modeling. However, (> 1mm) strength criteria formulations must consider that fracture occurs at micro-scale. Meso: per definitionem no length scale. Is used and defined on very different length scales – as an intermediate scale – in order to mark a specific meso-model level (one should use the term meso-model and not meso-scale)

(design) Limit Loads**:** maximum external loads expected in service. *(Examples: Design Limit Load DLL, Design Ultimate Load DUL as a DLL·j_{ult}-factored load)*

Life Cycle Assessment LCA**:** method that estimates the environmental footprint of a product from chosen materials via manufacturing until end-of-life

Lifetime**:** span of time during a material or a structural component must work. *(definition is specified in any actual project)*

Limit point: point along the equilibrium path where the instantaneous stiffness is zero

Limit state: state in which a structure or a material comes to a distinct limit

Limit state design: design that the structure satisfies two principal criteria: the ultimate limit state (ULS = GZT) and the serviceability limit state (SLS)

Limit state function *G* or *g* (Grenzzustandsfunktion): limiting condition $g = F - 1$ beyond which a structure or element is to be assumed to become unfit for its purpose. Any number of limit states may be specified by a code committee for a particular class of structure. They may be broadly classified as either ultimate (collapse) limit states or serviceability limit states (which require definition for each code). Many of these limiting design requirements are implicit in early design Codes, but there is now a tendency for them to be started explicitly. The adoption of such a limit state format is in no way dependent on whether a code has a probabilistic or deterministic reliability basis, but in the last few years both probabilistic methods and limit state formats have been developing concurrently.

Linear Elastic Fracture Mechanics LEFM**:** method that linearly deals with cracks. *(a given crack inside a loaded structure behaves in conditions of LEFM, if the crack field in the vicinity of the crack tip is assumed to be elastic, and any significant plastic behavior can be neglected)*

Load collective**:** 'shape' of the load spectrum. *(marked by the number of cycles n, and the number of cycles to failure N)*

Load combination: sum or envelope of certain load cases. (a combination of load occurs when different types of loadings act simultaneously or together in a structure. Load combination is derived from extreme environmental, operational, serviceability, transportation, lift, dead or launch loads

Load-controlled and strain-controlled 'hot spots': *Load-controlled 'hot spots'* may stressed up to the level of ultimate tensile strength which is linked to a reduction of cross-section due to necking. *Strain-controlled 'hot spots'* have reserves due to stress redistribution in their vicinity

Load-controlled testing: procedure where the load controls testing. *(stress max σ in the tested structure is determined by the associated failure load and the cross section area, the load has to be transferred through. This stress does not depend on the deformation. Strength R or f ≡ max σ)*

Load cycle: closed alteration of load change

Load history**:** loadings, experienced during life

Loading: loads (including normal and shear forces, moments, torques), pressures, temperature and moisture applied to the structural system

Load path **(**Lastpfad): path, the force runs in the structural body and (2) strength test condition 'proportional loading'. *(there are structures of non-redundant (single load paths) and redundant type (multiple load paths): If non-redundant, the applied loads are distributed through a single member within an assembly,*

the failure of which would result in the loss of structural integrity of the component involved ('series failure system'). If redundant, the applied loads are safely distributed to other load-carrying members in case of failure which means a multiple load path ('parallel failure system'))

Load(ing) scenario: defined result of the evaluation of all loadings relevant for the design

Load spectrum**:** spectrum of loads used in fatigue analysis

Logarithmic strains**: see** true strain

Log-book: book in which product information is recorded

Loom: machine, used for weaving fabrics

Lot, batch, charge: specific amount of material produced at one time using the same process and the same conditions of manufacture, and offered for sale as a unit quantity. (o*ne batch of prepreg material or a portion of one batch that is shipped to a purchaser for acceptance at one time. A lot may be one or more rolls of material but cannot exceed the amount of material produced in the batch the rolls are taken from [SAE])*

Macroscopic length scale**:** physical scale, having a characteristic dimension above 1 mm. *(desired engineering length scale, originally used when modeling and analyzing composite laminas and laminates denoting the ply characteristics. In the early days the thicker fibers (boron) caused ply thicknesses larger than one mm. Therefore the homogenized ply or lamina was addressed as macroscopic. (2) This is not always kept any more in the literature and the FE codes. (3) Macroscopically formulated strength failure condition should consider in its formulations that fracture occurs at micro-scale)*

Maintainability : probability that the product can be kept in or returned to a state in which it can provide its functions, when maintenance is applied. (*Maintenance comprises adequate storage, controls, preventive actions, e.g. repair of surface protection*)

Mapping of a course of test data: average test data fit (mean curve)

Margin of safety MoS or Safety Margin: decimal fraction by which the failure load exceeds the design load, defined by the relationship to the reserve Factor as MoS = RF -1

Mat**:** originally fibrous material consisting of randomly oriented chopped or swirled filaments loosely held together with a binder. *(term is also used in construction for open reinforcement grids)*

Material: 'homogenized' structural (macro-)model of the envisaged complex solid or heterogeneous material combination which principally may be a metal, a lamina or further a laminate stack analyzed with effective properties. *(on the considered scale (level) the homogenized model of the envisaged complex solid is modelled as a smeared solid. On engineering level a macro-model is preferred and normally used. Homogenizing (smearing) simplifies modelling*

Material behavior: *brittle* behavior can be characterized with the complete loss of tensile strength capacity at first fracture, R^t. Quasi-brittle behavior shows – after reaching R^t – a slight strain hardening followed by a gradual decay of tensile strength capacity during a strain softening domain. Thereby *Eff* remains 100%. *Ductile* behavior is accompanied by a gradual increase of tensile stress (strain hardening), and after reaching R^t a strain softening domain follows

Material composite **(**Werkstoffverbund): structural-mechanically a composite 'construction of different materials. *(a not smearable 'conglomerate' such as TRC is not a 'composite material')*

Material design allowable: statistically derived value used for design verification

Material properties: physical properties, required to define the material behavior for analysis purposes. (*(1) For stress analysis some typically required material properties are Young's modulus, Poisson's ratio, density and coefficient of linear expansion. (2) Material properties should be obtained by experiment)*

Material Stressing Effort (*Werkstoffanstrengung, nicht Werkstoffausnutzung*) *Eff*: exertion, a material experiences under a stress state generated by external loading and residual stresses. ((1) Percentage (portion) of the 'load' carrying capacity of the envisaged material such as metal, lamina, concrete. *Eff* is caused by a stress state in a distinct failure mode and is the mode-dedicated ratio $Eff^{mode} = \sigma eq^{mode} / R^{mode}$, which means equivalent stress divided by strength. (2) Artificial technical term, as compromise

created about 2001 together with QinetiQ, UK, during the World-Wide-Failure-Exercises (*since 1991*) in order to obtain an English expression for the German term Werkstoffanstrengung. (3) If non-linear analysis is required, then the computation must run up to a theoretical fracture loading at *Eff* = 100% in the final 'Hot spot' in order to determine the required load-defined deterministic reserve factor *RF*. RF is not of the same value as the material reserve factor f_{RF} obtained if linear analysis is permitted. The total Material stressing effort *Eff = f (Eff* modes) represents as interaction equation – capturing the damaging portions of all activated modes - the mathematical equation of the surface of the fracture (failure) body. Just for 100%: *F = Eff*

Mathematical stresses: structural stresses, used mathematically, means $\sigma_I > \sigma_{II} > \sigma_{III}$

Matrix**:** resin system or mortar system, cured or non-cured. *(essentially a homogeneous material (polymer, concrete) in which the fiber reinforcement system of a composite is embedded)*

Matrix (contracted) notation**,** example UD material: form of notation for writing sets of equations in a compact manner. *($\{\sigma\} = (\sigma_1, \sigma_2, \sigma_3, \sigma_4, \sigma_5, \sigma_6)^T$ instead of the engineering formulation $\{\sigma\} = (\sigma_1, \sigma_2, \sigma_3, \tau_{23}, \tau_{31}, \tau_{21})^T$*

Maxwell-Betti theorem: reciprocal work theorem (Gegenseitigkeit der Verschiebungsarbeiten). *(reads for the example UD material $\nu_{\perp\parallel} \cdot E_\perp = \nu_{\parallel\perp} \cdot E_\parallel$, and is applicable for the degraded elasticity matrix, too. Thereby, it is showing symmetry to the diagonal of the elasticity matrix)*

Mean: arithmetic mean of a statistical sample of size n of a uncertain basic variable X is defined as $x = \Sigma x_i/n$. The first moment of a probability distribution about its origin; the expected value of a random variable. The mean is the most commonly used measure of central tendency

Mechanical properties **(**see also material properties): properties of the material such as elastic, physical, or strength properties. *(1) When analyzing the structural behavior, usually average (≡ typical) elastic and average physical properties (e.g. hygro-thermal ones) are used. (2) Generally, a stress-strain curve is also such a physical property of the material. (3) In strength analysis, statistically-based ('reduced') strength properties are used to capture the scatter of the material strength*

Mechanical stress: stress caused by an action such as loading, temperature

Median: defined as the mid value in an ordered list of the sample values (*such that the set of values less than the median, and the set greater than the median, each have probabilities no greater than one-half*)

Meridian, isotropic materials: axial cross-section of the isotropic yield and fracture failure body (*of special interest for concrete. The meridians, mathematically defined, are those paths where tests are usually performed along. Here, the shear meridian is the neutral meridian*)

(1) Tensile meridian (extension, $\sigma_I > \sigma_{II} = \sigma_{III}$) involves tensile strength point, means axial tension + p_{hyd};

(2) Compressive meridian ($\sigma_I = \sigma_{II} > \sigma_{III}$): inv. compr. strength point, means axial compression + p_{hyd};

(3) Shear meridian involves the strength state $\sigma_I = -\sigma_{II}$ or $\sigma_2 = -\sigma_3$ and is origin of hoop (Lode) angle ϑ

Mesh, web: fabric, that has a large number of narrow spaced holes

Mesh adaptivity**:** automatic alteration of meshes to provide refinement where the calculated variables vary rapidly and coarsening where they vary slowly

Mesh design: creation of a suitable mesh model, to represent the given structure with suitable refinement in regions of high field variation with a good representation of boundaries, and incorporating all other required features

Meso-model: model that is used at an intermediate length scale being an artificially chosen scale

Meso-'scale': artificially chosen intermediate scale for so-called multi-scale analyses.

((1) Not a traditional scale or level, but often used as a model-characterizing term at different length levels such as the micro-scale defined below. It has to be clearly defined in each application case and is used also by polymer researchers in the nano-region. (2) with composites, the term meso is referred to the fiber architecture within a textile lamina. Unfortunately, since some time it is also sometimes applied when citing lamina characteristics. Due to thicker fibers in the past, the lamina was originally termed to be macro, which is not accurate anymore in the case of the thin CF-plies)

Micro-mechanical formulas and properties: formulations determined by micro-mechanical properties. Micro-mechanical properties can be used on the macro-mechanical engineering level only together with the equations they have been determined with!! (i*n the WWFE i.e. not accurately performed*)

Micro-scale: physical scale, having a characteristic dimension typically ranging from 1 μm to 999 μm, which means below 1 mm. *(above term is not always used the same. In case of composites it addresses the constituents matrix, fiber, inter-phase and small flaws such as pores, inclusions etc.)*

Mixed (fracture) failure domain MiFD**:** strength failure conditions

a stress state may jointly activate different but commonly acting strength failure modes.

(Note: Example is Normal Fracture NF with Shear Fracture SF. The interaction of fracture modes increases the danger to fail. Failure test data under multi-axial stress states are 'joint-probabilistic' results, see 3D-UHPC fracture test data sets, modelled in [Cun17])

Mixed Strength (fracture) Failure: several different failure modes may be activated by the acting stress state. The *interaction* of both the activated fracture mode types Normal Fracture NF with Shear Fracture SF under compression increases the danger to fail! Hence, the associated fracture test data are so-called joint-probabilistic results of several acting modes (2, if isotropic)

Mixed (fracture) Failure: Different failure modes are activated by the acting stress state (example: isotropic Normal Fracture NF + Shear Fracture SF under compression). Interaction of fracture modes increases the danger to fail! Associated test data are 'joint-probabilistic' results

Mixing water: water, necessary to achieve the optimal amount of hydration water, which is essential to obtain an ideal mortar for pumping and paving as well as an optimal interphase material between filament and cementitious matrix [EN 1008]

Mock-up: full-size structural model showing how the structure will look or might work. *(mock-up is some sort of a dummy and should not be confused with a still functionally working prototype)*

Model: representation of a physical, conceptual, or mathematical representation of a real phenomenon

Modeling: process of idealizing a system and its loading to produce a numerical (finite element) model or an analytical model. *(modeling structural parts, the modeling of joints and connections is the most numerically challenging item because these usually are pretty flexible locations within the full FEA-model (weak conditions))*

Mode equivalent stress σ_{eq}^{mode}: mode–dedicated equivalent stress. *(highest mode equivalent stress gives the designer a hint where to 'turn the design key')*

'Modal' versus 'Global' SFCs: Modal means that only a test data set of one failure mode domain is mapped whereas global (*examples: Drucker-Prager isotropic, Tsai UD) means that mapping is performed over several mode domains*)

(failure) Mode-interaction: several failure modes are in common action. *(interaction must be considered in order to capture the difficult consideration and measurement of the mode-coupled degradation. For instance, two commonly acting failure modes mutually lower both the associated elastic properties)*

Mohr-Coulomb 'yield' condition: generalization of the Coulomb friction failure law. *(condition,used for brittle materials like concrete, rock and soils, showing a non-linear stress-strain curve in the compression domain. The displayed condition is an inverted hexagonal pyramid using the principal stress space (see and compare Cuntzes FMC-based conditions for brittle behaving materials [Cun17])*

Mold-release agent: lubricant, applied to mold surfaces to facilitate release of the part

Molding**:** forming of a composite part into a solid of prescribed size and shape

Monomer**:** compound, consisting of molecules each of which can provide one or more constitutional units

Monte Carlo simulation method: reliability simulation method, where a huge number of random tests with combinations of the uncertain design parameters lead to a random distribution that can be probabilistically evaluated (response surface)

Mortar: fresh or hardened mixture of inorganic binders (cement) + additives + water + aggregates (size 0 mm - 4 mm)

Multi-fold (fracture) Failure Mode: The acting stress state with maximally equal orthogonal stresses activates the same mode multi-fold. Hence, the associated fracture test data are so-called joint-probabilistic results of a multi-fold acting mode! Usually, SFCs consider just one single failure mode (mechanism) and do not capture the bi-axial effect of $\sigma_I = \sigma_{II}$ or hydrostatic tensile or compressive failure stress states. This must be considered by an additional term in the SFC!

Multi-fold (fracture) failure mode domain MfFD, $f \equiv R$: the acting stress state with pretty equal orthogonal stresses activates the same mode multi-fold.

((1) Example isotropic says $\sigma I = \sigma II$ is 2-fold, $\sigma I = \sigma II = \sigma III$ is 3-fold). Example transversely-isotropic UD.material says $\sigma 2 = \sigma 3$ is 2-fold).

(2) A multi-fold fracture mode

- *increases the danger to fail ! $R^t > R^{tt}$ (weakest-link effect), $I_1 > 0$*
- *increases the danger to fail ! $R^c > R^{cc}$ (weakest-link effect), $I_1 < 0$, porous*
- *decreases the danger to fail ! $R^{cc} > R^c$ (redundancy effect), $I_1 < 0$, dense*

(3) Multi-fold failure must be considered capturing the joint damaging effect demonstrated by $R^{tt} < R^t$, $R^{cc} > R^c$ (porous foam $R^{tt} < R^t$, $R^{cc} < R^c$). A multi-fold occurrence of a failure with its joint probabilistic effects must be additionally considered in the strength conditions, e.g. if $\{\sigma_{fr}\} = (R^{cc}, R^{cc}, 0)^T$

Multi-material composite, Werkstoffverbund: see material composite. *(composite of different materials that are structure-mechanically still a structure, such as a semi-finished sandwich fiber grid product or a rebar grid in the concrete)*

Multiple-site 'damage' MSD: wide local damage process. Arrangement of small, visually non-detectable small cracks ('micro-cracks')

Multi-scale analysis: analysis that is executed on several levels. *(micro-scale and macro-scale using meso-modeling of the fiber architecture. In the associated analyses a bottom-up approach - micro to macro - combined with a top-down approach is mandatory because a closed system is necessary: micro-mechanical data in the HSB or other data sheets can be only used together with the micro-mechanical formulas they have been based on!)*

Natural frequency, eigenfrequency: frequency at which resonance occurs

Natural mode: shape of a vibration at a distinct natural frequency

(near) Net shape: fabrication to final dimensions that do not require final machining or cutting

Netting theory analysis: analysis where the fibers are assumed to take all the load. (cannot be used for inelastic analyses which need the real stiffness)

NOL ring: parallel filament- or tape-wound hoop test specimen developed by the Naval Ordnance Laboratory (NOL). (*for approximately measure various mechanical strength properties of the material, such as tension and compression, by testing the entire ring or segments of it*)

Nominal life: life span from release via transport to the termination of use. *(project-specific differently formulated*)

Nominal specimen thickness: summation over the thickness of nominal plies multiplied by the associated number of plies

Nominal value: value assigned for the purpose of a convenient designation. (*a nominal value exists in its name preferably*)

Non-crimp fabrics: laid webs. Type of fabric that consists of plies of unidirectional material laid up at any required angles and held together by a bonding agent or cross stitching (z-threads). (*avoids the crimping involved with woven materials and results in higher laminate properties when impregnated with a suitable resin and fully cured*)

Non-linear analysis: analysis, to be applied when at least one of the design parameters, such as stiffness, mass or damping vary with displacement or time where superposition cannot be used anymore

Non-redundant and redundant structures: types of different structural failure behavior. There are non-redundant (or single load path) and redundant (or multiple load path) structures. (*((1) Non-redundant: applied loads are distributed through a single member within an assembly, the failure of which would result in the loss of structural integrity of the component involved. Has to sustain for instance DUL until exchange of the critical part or until end of service life. For multiple load path structural parts B-values may be used. (2) Redundant: applied loads are safely distributed to other load-carrying members in case of failure. A new load path can be generated that has to sustain in case of failure of one path just design limit load DLL A redundant cross-section carries bending loads until cross-section will fully yield*)

Non-woven fabric**:** neither woven nor knit fabric. Planar textile structure produced by loosely compressing together fibers, yarns, rovings, tows

Normal probability distribution ND: most prominent distribution in statistics, frequently referred to as the Gaussian or bell-shaped distribution

Normality rule: direction of the plastic strain increment, measning that the direction is normal to a surface defined by the plastic potential F

Notion (Vorstellung): conception of something or belief about something

Term: process or set of rules to be followed in calculations or other problem-solving operations, especially by a computer [Wikipedia]

Onset-of-Delamination: separation failure in a laminate. *(laminate, composed of several UD-plies, may experience inter-laminar fracture failure caused by inter-laminar stresses, preferably σ_3, or by 3D-states of stresses that notch the surface of the next ply. The prediction of the progress of delamination is a damage tolerance task)*

Onset-of-Fracture: max. load with/without necking) versus

Onset-of-Rupture: load at maximum straining of very ductile materials, after onset of void agglomeration

Onset-of-Yielding: stress ($\bar{R}_{0.2}$ for modeling, $R_{0.2}$ for design-verification (proof)) as an engineering agreement at 0.2% permanent strain offset of a ductile material or with micro-cracking of a not fully brittle material

Opening width: distance within textile reinforcement grids.*((1) Minimum reinforcement distances of $> \approx 4 \cdot$ maximum grain Ø. (2) Grain curve distribution ≈ 0.5 mm - 2 mm, see grid width)*

Optimization structural: tool, to find the best solution from all feasible structures. *(optimization can be grouped into topology, shape and sizing optimization)*

Organic sheet: semifinished sheet product involving organic reinforcements. *(hybrid technology can be extended even further if, instead of a steel sheet or an aluminum sheet, fiber-reinforced plastic sheets are used. These are flat, semi-finished plastic sheets, reinforced with a woven or non-woven fabric of glass, carbon, aramid or blended fibers, which give the component particularly high mechanical performance and draping capacity)*

orthotropic**:** having three mutually perpendicular planes of elastic symmetry

Over-lap length: length of two reinforcement (bars or grid) to transfer loads. *((1) Not fully the same for tension and compression. (2) Equals about the end-anchorage length)*

Panel: flat or curved thin-walled structural element. *(it may be also a stiffener-reinforced part as the barrel of a fuselage section. Therefore, it is not fully compatible to the term flat plate)*

PAN fiber**:** fiber derived from the pyrolysis of a polyacrylonitrile fiber as precursor

Parametric modelling: parameters in solid modeling to define its dimensions in the given design space.

(initial parametric studies may be conducted on simplified models to determine the important parameters for the solution of the full problem. These studies are often used to determine the basic FE-mesh density)

Parametric design: automatic design process in which the functional, manufacturing and constructive requirements for the design space are provided. *(in future, an AI-driven learning computer will propose design variants that fulfill the requirements best*

Parent distribution: characterization of the occurrence of a test data basic population as *the largest possible set of measurements.(Samples represent portions of the basic population. The parent population might consist of an infinite number of values. The variability for the parent distribution is a fixed value σ, while for a sampling distribution it's related to σ but also depends on the sample size n*)

Part consolidation: design-and-fabrication process in which a number of previously discrete parts are combined in a single component to reduce or eliminate assembly operations and associated CoSts

Partial Safety Factor Concept**:** safety concept, applied in civil engineering. *(replaces the old, global safety concept in civil engineering by putting partial safety factors γ according to the necessity to capture the different uncertainties of the design parameters on the action side (loadings) and on the resistance side (material, geometry, modelling). See Safety concepts)*

Peel ply Abreißgewebe: layer of material applied to a prepreg lay-up surface. *(layer of open-weave material, usually polyester, fiberglass or heat-set nylon, applied directly to the surface of an uncured lay-up. It protects the to be bonded surface from contamination during manufacturing or repair operations. The peel ply is removed from the cured laminate immediately before the bonding operations, leaving a clean, resin-rich surface that needs no further preparation for bonding, other than application of a primer where one is required. Peel ply is available wet (pre-preg), dry and with or without release agent. It is important to evaluate which type of peel ply is appropriate for a specific application)*

Percentile: if p percent of the values taken by a variable x are less than or equal to X, then X is defined as the path percentile of x

Perfect plasticity**:** plastic behavior where the yield stress remains constant for all values of plastic strain

Performance: characteristic, how well a product fulfils given requirements

Performance requirements**:** final specification between customer and tender

Pitch fibers: reinforcement fiber manufactured from petroleum or coal tar pitch possessing a higher modulus

Phase angle**:** ratio of the in-phase component of a signal to its out-of-phase component (fatigue significant)

Plasticizer: material of lower molecular weight added to a polymer to separate the molecular chains. *(application results in a depression of the glass transition temperature, reduced stiffness and brittleness, and improved processability. Many polymeric materials do not need a plasticizer)*

Plastic deformation: permanent deformation of a solid body without micro- cracking

Ply (synonym for lamina or layer): a single layer of a laminated stack

Ply-by-ply analysis**:** term used in laminate analysis if each ply (lamina) is analyzed

Ply-discounting approach**:** degradation model of the ply

Poisson's ratio, UD ply: ratio of transverse strain and longitudinal strain of a uniaxially tensioned test specimen. *(of course, there is no objective reason to write ν_{21} or ν_{12} but in the early days indexing of Poisson's ratio followed 'location before cause'. This makes more sense and - in addition - follows the convention for the load quantities. This is the reason why - after many discussions and extensive literature work of the working group – the VDI 2014 guideline still sticks to the 'old' sequencing ν_{21} for the larger Poisson's ratio. However, for the larger Poisson's ratio in the last two decades - more and more - ν_{12} has been used, especially in the FE codes. This might have been the reason for the change. Meanwhile, Stephen Tsai turned back in his newest book 'Strength and Life of Composites', 2011, to the old sequencing ν_{21})*

Polymer (plastic): organic material composed of molecules characterized by the repetition of one or more types of monomeric units

Polymerization**:** chemical reaction in which the molecules of monomers are linked together to form polymers

via two principal reaction mechanisms. *(addition polymerization proceeds by chain growth and most condensation polymerizations through step growth)*

Porosity: aggregation of micro-voids. *(condition of trapped pockets of air, gas, or vacuum within a solid material, usually expressed as a percentage of the total non-solid volume to the total volume or solid plus non-solid of a unit quantity of material. Porosity may decrease stiffness and strength.). Classification of porous materials according to pore size: 'microporous' pores < 2 nm, 'meso-porous' pores between 2 nm and 50 nm, 'macroporous' pores > 50 nm. [International Union of Pure and Applied Chemistry]*

Post-buckling**:** designation, if the structural element operates in a region where the applied load has exceeded the buckling resistance

Post-processing: interrogation of the results after the analysis phase, usually done graphically

Pot life**:** period of time during which a reacting thermosetting composition remains suitable for its intended processing after mixing with a reaction initiating agent

Precursor for carbon fibers: PAN or pitch fibers from which carbon fibers are produced. *(future: oil-independent, bio-mass-derived acrylonitrile precursors are presently investigated)*

Prediction: judgement of the characteristics of an item by means of engineering analysis, using generic data and/or historical data obtained from antecedent items.

Preform: uncompleted part after preliminary shaping (semi-finished product). *(assembly of dry fabric, which has been prepared for one of several different wet resin injection processes. The preform may be stitched or stabilized in some other way to hold its shape. A commingled preform may contain thermoplastic fibers and may be consolidated by elevated temperature and pressure without resin injection, example is an organic sheet)*

Premature failure: failure occurring or existing before the normal or expected time

Prepreg: ready to mold or cure material in sheet form which may be tow, tape, cloth, or mat

Pressure: maximum differential pressure that can be expected to occur in service under the expected operating environments. This pressure is also known as maximum expected operating pressure (MEOP)

Pressure independent material: elastic-plastic material in which plasticity exhibits only in the deviatoric stress-strain response, whereas the volumetric stress-strain response is linear-elastic and is independent of the deviatoric response

Prestressed concrete: concrete in which the reinforcement is stretched via tensioned tendons and anchored to compress it in order to increase its resistance to tensile stresses

Principal axis**:** transversely-isotropic UD lamina material coordinate axis that coincides with the fiber direction

Principal plane**,** isotropic material: planes on which the shear stresses are zero. *(3 such planes exist at every point in a stressed isotropic body)*

Principal stress**,** isotropic material: remaining components of the stress tensor after the original basis is transformed in such a way that the shear stresses of isotropic materials become zero

'Principal stresses hypothesis' of Rankine**:** normal stress-based hypothesis. *(possesses a tension-cut-off, is a three-corner SFC)*

Probability: likelihood that failure occurs

Profile: here a load-carrying structural element (pultruded, rolled from organo sheets)

Probability: measure of the chance (risk) that an event will occur, generally expressed on the scale 0 to 1. 0 signifies that an event is certain not to occur and 1 that it is certainto occur.

Probability density function: for a continuous random variable X, the probability density function $f_x(x)$ is defined such that, for an ifinitesimal increment dx of X, the product $f_x(x) \cdot dx$ is the probability that X lies in the interval x to $x + dx$. The function may be considered as representing the relative frequencies of occurrence of different values of X laying in certain intervals (as a histogramme), the area under the probability density curve between two values, x1 and x2, defining the relative frequency of occurrence of the range of values between those limits.

Probability of failure: inverse of reliability ($p_f = 1-\Re$)

Probability theory and fuzzy set theory: two common mathematical tools to model indeterminacy phenomena in engineering

Process-induced distortions PID**:** effect when the production of composite structures ends with warpages and curvatures. (l*eads to internally balanced residual stresses in laminated plates. Compensation is undertaken by adjusting the tools)*

Progressive failure**,** ply, amina, lamella: behavior after onset of degradation of an internal ply of the loaded laminate. *((1) Failure often starts as a tiny crack between the fibers and matrix. Continuous loading leads to the formation of multiple micro-cracks in the lamina. (2) The increase of loading is accompanied by progressing damaging, up to the FF loading level. In the critical ply a material stressing effort of Eff = 100% (Werkstoff-Anstrengung) will be reached in the hardening domain. However in this ply strength and stiffness are not exhausted. Along the softening domain, Eff remains 100% ='lowering effective stress' / 'lowering strength', when further progressing damaging occurs. (3) The behavior is not deterministically but probabilistically determined. Hence, progressing failure events are dependent on the typical size of the coefficient of variation of each ply strength)*

Progressive failure, FRP laminate: progressive series of failure events in the components, plies of the composite part. *(microcracks decrease the stiffness of the matrix causing the fibers or surrounding plies to carry a higher stress than they normally would carry. Stress redistribution is activated. The laminate experiences a kink in the laminate stress-strain curve. Consequently, capturing stress redistribution is the key to a realistic simulation of the progressive failure of laminate structures.)*

Proof load: load applied during a proof test

Proof test: test of a hardware under proof load or proof pressure loading to give evidence of satisfactory workmanship and material quality or to establish the initial crack sizes in the hardware

Properties: 'agreed to values' in order to achieve a common and comparable design basis by using a standard. *(material properties should be test-provided with average value and coefficient of variation)*

Proportional loading, test and analysis: loading situation, when all the external loads are applied simultaneously and when these increase in proportion to one another throughout the loading history. (*this clearly does not occur when one component of load is applied and another late,r reading 'out-of-phase')*

Proportional stressing**,** analysis: simultaneously increased multi-axial stress state loading procedure

Pultrusion**:** continuous process for manufacturing composites in rods, tubes, and structural shapes having a constant cross section. (a*fter the reinforcement is passed through the resin-impregnation bath, it is drawn through a shaping die to form the desired cross section; curing takes place before the pultruded part can depart from that cross section)*

Qualification test: test or series of tests conducted on actual typical production items such as pressure vessels which establish that the general design and fabrication are acceptable for the intended use

Quasi-isotropic laminate: laminate approximating isotropy by orientation of plies in several directions like [0/60/-60]

Quasi-laminar composite**:** designation for a textile composite which basically behaves 2D-like

Rainflow counting**:** counting method, used in the analysis of fatigue data in order to reduce a spectrum of the varying stress into a set of simple stress reversalsR-curve (crack extension resistance curve):

curve of strain-energy release rate *G* versus crack length a. *(a positive slope indicates unstable crack propagation and a negative that the crack growth is stable)*

Ramberg-Osgood 'law': stress-strain relationship where strain is proportional to a power of stress

Random process: process is defined as random if the sequence of events (or occurrence of different values of the variables) is entirely unpredictable. A stochastic process is a particular form of random process in which the frequency of occurrence of different events (or different values) follows a statistical pattern

Random variable: measurable function defined on a sample space. A random variable may take any of a specified set with a specified relative frequency of probability

RAMS: part of the Product Assurance activities that captures the points reliability, availability, maintainability and safety

Raw material fiber CoSt **:** carbonfiber roving**,** production CoSt of CF on a bobbin is currently 16 €/kg. *(Example: CF CoSt per m^3 for V_f = 0.2% → mass · ρ · price ·V_f =(1·m)³ ·1700 kg/m³ · 16 €/kg ·0.002 ⇒ ≈ 50 € for FRC. For comparison: Normal Concrete: 60 -80 €/m^3, Fine Concrete: still ten times Normal Concrete)*

Reaction force**:** force, generated at support points when a structure is loaded

Realisation: possible combination of basic variables

Rebar**,** steel, fibers: reinforcing bar, used as a tension device in reinforced concrete and reinforced masonry structures to strengthen and hold the concrete in tension. *(rebar surface should be patterned to get a geometrical contact and a better 'bond' with the concrete. Helix pultrusion saves waste compared to grinding a pattern. Rebars are also used for generating bar-grids, e.g. Solidian GFRP REBAR Ø 4, 6, 8, 10, 12–A)*

recycled: if a product is produced that can be sold (index r)

Recycling**,** CF: pyrolysis process. (*(1) The recycled fiber amount rCF is about 50 % of presently (2018) ca. 25000 t / year (from production waste material, prepreg cooling interruptions, bad parts due to manufacturing error, wind mill blades etc). They are going to CoSt about 50 % of the new price. Due to the experienced degradation process – they show 75 % of the short time properties of new material. (2) Information: A yearly CF output of 50000 t equals 4 min steel production (2018). The yearly concrete production equals oil production.. (3) Generated by treatment in a furnace, which vaporizes the resin that holds the carbon fiber layers together and leaves behind a material, which is cleaned and sold to companies in the electronics and ground transportation industries for making laptop cases, car parts and other products)*

Redundant structure**:** structure where all of the unknowns cannot be found from equilibrium considerations alone. *(in the case the structure is said to be redundant then compatibility equations must also be used)*

Reinforced concrete RC (my initials!): concrete, armored by an arbitrary endless fiber product with polymer impregnation (P) or mineral impregnation (M) hopefully in future for better fire resistance. (t*his will lead to some discrimination between FRP-reinforced concrete and FRM-reinforced concrete. Index R)*

Reinforcement, Bewehrungsstruktur: reinforcing semi-finished product. *(in construction industry performed by bars, bar-grids, and textile grids also termed mat, mesh)*

Release agent**:** see mold release agent

Reliability ℜ: aptitude of a product to perform the required functions at certain performance levels under specific conditions and for a given period of time, expressed in terms of probability. *((1)Structural reliability considers the probability of combinations of the recognized significant scattering design variables (stochastic, random). (2) Currently in mechanical engineering, the two essential design variables load and strength are separately treated, but not really stochastically combined as in real structural reliability applications where a probabilistic concept is applied. (3) Reliability is a probability measure to guarantee during lifetime the limit states ultimate, serviceability, fatigue. (4) in the most general sense, structure reliability is the probability that the structure will not attain any specified limit state, or a number of limit states during its intended life span. In a full probabilistic analysis, it may be possible to express the probability level in terms of a relative frequency. Often the probability is only of relative significance, in which case it is termed an operational or notional probability*)

Reliability index ß (safety index): coefficient, used as a measure of relative structural reliability with regard to any limit state. The index may be referred to as 'Safety Index' when applied to the ultimate limit state

Rendulic plane coordinates**:** ξ-ρ-plane coordinates of the strength failure body

Reserve factor, mechanical engineering: ratio of a 'resistance value' and a so-called 'action value'. *RF* > 1 permits a further increase of loading. *((1) Resistance value means here Predicted or Measured 'failure*

load / (design factor of safety x Design Limit Load)'. (2) If linear analysis is permitted RF will correspond to the material reserve factor, derived from 'f_{RF} = strength / design stress'. A value higher than one would allow an increase of loading. (3) For brittle behaving materials, the decisive static limit state is the Design Ultimate Load case. The Design's strength is demonstrated if (a) no relevant strength failure, respectively limit state of any failure mode, is met and (b) all dimensioning load cases are respected by the following formulas, reaching values > 1 = 100%

linear model permitted (f_{RF} = 1)

$$f_{RF} = \frac{design\ allowable\ \text{"strength"}}{j \cdot \sigma(DLL)}$$

non-linear model required (Eff = 100%)

$$RF_{ULT} = \frac{Final\ Failure\ Load}{Design\ Ultimate\ Load} = MoS + 1 = \frac{design\ allowable\ \text{"load resistance"}}{Design\ Ultimate\ Load}$$

(4) The Final Failure Load in the non-linear case is reached when Eff becomes 100% 'material stressing effort' (Werkstoffanstrengung) in the last critical Hot Spot, when no more stress redistribution in the structural component is possible. (5) Assumption in usual deterministic procedure is most often: 'Worst case scenario with respect to loading, temperature and moisture, and to undetected damage')

Residual strength**:** fracture stress after pre-damage and re-loading

Residual stress: stress, generated by external and internal loadings according to constraining. (*stress that remains in a structure after processing, fabrication, assembly, testing or operation. An internal equilibrium system is given)*

Resin**:** organic polymer or pre-polymer used as a matrix or gluing material. *(application as a matrix to contain the fibrous reinforcement in a composite material or as an adhesive. It may be a thermoset EP or a thermoplastic TP. Neat resin is the purest resin containing just the main polymers)*

Resin system**:** mixture of resin, with ingredients such as catalyst, initiator, diluents or additives to influence handling, processing behavior and ultimate properties of the final product.

Resin-Transfer molding (RTM): molding process in which catalyzed resin is transferred into an enclosed mold into which the fiber reinforcement has been placed. *(cure normally is accomplished without external heat. RTM combines relatively low tooling and equipment CoSts with the ability to mold large structural parts)*

Resistance R: material property or a structural property counteracting the applied loadings.

(Example load resistance and buckling resistance, which are structural resistance properties at load level. Example strength, which is a material resistance property R at stress level or sometimes given as a limiting strain level ε_{design}. (3) The letter R (italics written here) is unfortunately the same as for the stress ratio R*)*

Risk: probability of loss of personnel capability, loss of system, or damage to or loss of equipment or property. Risk = severity of the failure x probability of occurrence

Robust design: design that performs optimally under the variable operating conditions during lifetime or optimally captures the scatter of the design parameters.

Robustness**:** robustness = 1/ (uncertainty · complexity) = 1/ fragility [definition of Ontonix]. *(robustness and reliability are cross-linked to some extent)*

Robust Design Optimization**:** tool to evaluate the combined action of the scattering design variables such as fiber waviness, layer orientation and undulation as manufacturing significances, material properties

Rod: here, reinforcing semi-finished product. *(pultruded carbon fiber reinforced polymer (CFRP) rods designed for strengthening concrete, timber and masonry structures)*

Room temperature, ambient (RTA)**:** usual reference temperature for material properties. *((1) Environmental condition of 23 ± 3° C at ambient laboratory relative humidity; (2) Material condition where, immediately following consolidation or cure, the material is stored at (23 ± 3° C and at a maximum*

relative humidity of 60 %)

Roving**,** tow, strand: number of yarns or ends collected in a parallel bundle with approximately no twist. *(term is applied most commonly to glass, carbon and aramide (Kevlar), see ISO 472. The cross-section of a roving is an oval, round cross-sections are caused by protection twist of about 10 rotations. The roving must be through-impregnated not only surface-coated in order to equally load each single filament. It is marked in thousands (k) of filaments. Instead of roving the term tow is often used in construction industry.*

R-ratio, fatigue: ratio of minimum stress and maximum stress or load

Rupture**:** break of the final cross section area of a ductile behaving tensile test specimen. *(rupture comes after necking, and therefore should be not confused with fracture, which is associated with the maximum load of the test specimen at onset of necking. See stress rupture)*

Safe life**:** design philosophy in which products are designed to survive a specific operational life with a chosen reserve or period, during which the structure is predicted not to fail in the expected service life environment. *(newly also used as 'fracture control design policy', for which the largest undetected flaw - that might exist in the part - does not grow to failure when subjected to the cyclic and sustained loads and environments encountered in the service life)*

Safety **(**security**):** defined as 'absence of circumstances liable to cause death, or degradation or loss of equipment within limits of probability of occurrence' of these events. *(Safety is - in contrast to structural design safety - related to human beings if they might be excessively endangered)*

Safety concepts**:** deterministic, semi-probabilistic or even probabilistic concepts (formats) to capture uncertainties in order to implement structural reliability into the design. *(above concepts are working as follows: (1) The deterministic concept accounts for design uncertainties in a global (lumped) manner by enlarging the design limit loads by a multiplication with FoS j (usual way in mechanical engineering). (2) The semi-probabilistic concept puts partial FoS γ_i on the i design-relevant uncertain design variables (civil engineering). (3) The probabilistic concept maps each single design parameter's uncertainty into a probability density function. Thereby, the 'joint probability of failure' caused by a combination of all the design variables (scattering design parameters) is considered)*

Safety Factor concept , mechanical engineering**:** deterministic safety concept using one factor by which the level of the given loading is increased. The applied so-called Factors of Safety *FoS* are load-increasing factors, see [Cun12]. *((1) Present Safety Concept: by a distinct FoS j the design limit loads (DLL) are multiplied in order to account for uncertainties of the loadings (or stresses in the case of linear behavior), of the verification methods, the uncertainties in manufacturing process and material properties, the failure criteria for purposes of analytical assessment or also the test verification of design accuracy in strength, stiffness and stability). This deterministic concept enlarges the deterministic loads (stresses) and causes thereby a distance to the load resistance (strengths). This difference is represented by the required positive Margin of Safety MoS. (2) Former 'Allowable (permissible) Safety Factor concept': this old deterministic concept reduces the load resistances (strengths) with the consequence that it cannot deliver accurate MoS in the case of non-linear analyses according to the fact 'load is not proportional to the stress any more'. Therefore: The citation of the term 'allowable stress' is restricted to the old concept and shall be not applied within the present concept anymore. Why? The use of the abbreviating term 'allowable' instead of 'design allowable' may not confuse, 'allowable stress' however does, because $j \cdot$ allowable stress = strength design allowable ! The 'allowable stress safety concept' shall be not employed if non-linear analysis is required*

(partial) Safety Factor concept, civil engineering: see Partial Safety Factor Concept. *(the'Allowable (permissible) Safety Factor concept', which uses a global safety factor to reduce the strength was replaced in DIN 1054 by the Partial Safety Factor concept. This applies safety factors and combination factors for general service loads, live loads, snow, ice loads, and wind loads as. Temperature effects are specified in DIN 1055-100)*

Sample (Probe)**:** small portion of a material or product intended to be representative of the whole. *(statistically, a sample is the collection of measurements taken from a specified population or of a set of measurements on a test specimen)*

Sample variance**:** see variance, applied for a sample

Satin weave fabric: fabric where the woven edges of a fabric lie parallel to the warp

Saturation **(**Sättigung): equilibrium condition in which the rate of absorption under prescribed conditions practically falls to zero. *(essential for conditioning of polymer matrix composite test specimens prior to testing. The MIL-HDBK 17, paragraph 2.2.7.2 formulation is: saturation content is the largest value of moisture equilibrium content for a given material under humid conditions at 100% relative humidity RH)*

Scatter factor: factor which indicates the variation of a fatigue property. *(in fatigue analysis it is practically a knock-down factor by which the number of cycles or the life time is multiplied in order to account for uncertainties in the statistical distribution of loads and cycles as well as uncertainties in fatigue analysis, manufacturing processes and material properties are considered. The term is explicitly reserved for the lifetime ratio T50% / T90% survival data which stem from SN curves)*

Secant modulus**:** ratio of stress to strain at any point of a stress-strain curve (tension, compression, torsion, shear). *(elasticity modulus (stiffness) defined by the slope of the line from the origin to the current point of interest on a load/deflection curve)*

Secondary bonding**:** joining by the process of adhesive bonding, of two or more already cured composite parts, during which the only chemical or thermal reaction occurring is the curing of the adhesive itself

Secondary components **(**structures, parts, elements**):** components of a structure, that are not of direct interest but may have some influence on the behavior of the part of the structure which is of interest, namely the primary component, and have to be included in the analysis in some approximate form

Secondary stresses**:** stresses induced by needs of internal compatibility or compatibility with the boundary conditions. *(secondary stresses are associated with imposed loading or imposed displacements such as temperature, pre-stressing, settlement, shrinkage. These stresses are not required to achieve equilibrium between an internal stress state and the external loading. They build up residual stress states*)

Section: station at a distinct length coordinate x of the structure. *(in practical applications, the term section is unfortunately used as well as for an extruded beam, e.g. a product form such as a fabricated composite angle section or a channel section, as well as the cross section forces and moments at a section cut at the coordinate x and dedicated to a distinct cross section)*

Section force **(**Schnittkraft): force acting at a distinct cross section

(cross) Section quantities**:** forces and moments acting at a cross section or node (beams: forces N, Q , moments M; shells and plates: n, q, m being width-related)

Semi-finished product **(**Halbzeug, Halbfabrikat): intermediate product which is further processed to become a final finished product. *(in [Che11] different textile semi-finished products are discriminated due to (1) geometry (1D, 2D, 3D), (2) structure of the reinforcement alignment UD, bi-axial, tri-axial), and (3) z-reinforcement dependent structure i. e. cross-breeding yarns or interlacing yarns). (4) SFPs with continuous z-reinforcement may be treated as 'smeared 3D-materials')*

Semi-probabilistic Safety Concept**,** see Euro Codes: concept where the uncertainties on action and resistance side are accounted for, separately. They are reflected by the load (action) factor γ_S and the resistance factor γ_R. *((1) For comparison the deterministic approach uses an experience-based global safety factor that is meant to incorporate all uncertainties $R / \gamma > S$. (2) The partial safety factor version is more refined and represented by $R / \gamma_R > S / \gamma_S$. The computation remains purely deterministic but since the partial safety factors are calibrated to match a predefined probability of failure level (= acceptable probability of failure), the approach is classified as semi-probabilistic)*

Serviceability: condition in which a structure is considered to perform its design function. A serviceability limit represents a condition beyond which the structure will not continue to perform satisfactorily,

requiring remedial work or restrictions on use (e.g. excessive deflection of a beam causing damage to partitions)

Serviceability (Gebrauchstauglichkeit, SLS limit state): conditions under which a building is still considered useful. Should these limit states be exceeded, a structure that may still be structurally strength sound would nevertheless be considered unfit. Serviceability limit state design of structures includes factors such as durability, overall stability, fire resistance, deflection, cracking, excessive vibration. After [*Wikipedia*]

Service life: interval of time beginning with an inspection after manufacturing of an item and ending with completion of its specified life

Severity: consequence of a failure

Shrinkage, polymer or concrete matrix: chemical shrinkage and physical shrinkage due to deformation mismatch, moisture, temperature

Side constraints **(**optimization**):** based on e.g. past product experience and manufacture. *(objective function f(x needs to be satisfied considering equality constraints (hard constraints)* $g_i(\boldsymbol{x}) = c_i$ *and* $h_j(\boldsymbol{x}) \geq d_j$ *(soft constraints)*

Simulation**:** from latin verb simulare = make it similar (this takes time): Modelling of real-world processes and systems in order to arrive at insights that can be transferred to reality. *(The simulation model represents a system or a process, whereas the simulation itself represents the operation of the system. Simulation consists of several analysis loops or many analyses (Berechnungen), respectively, and lasts until the system is imitated. One application example, multi-parameter material model: Adaption due to test information in order to determine the non-measurable model parameters by an appropriate fitting process of a representative real world example such as the necking ductile tensile test specimen. Design verification, after the simulation process, requires just one analysis of the found design)*

Site construction**:** construction, performed at the construction site

Sizing, compare finishing: coating of filaments to protect the surface during textile processes such as weaving. *((1) Starch, gelatin, oil, wax, and man-made polymers such as polyvinyl alcohol, polystyrene, polyacrylic acid, and polyacetates are employed. (2) Generic term for compounds which are applied to yarns to bind the fiber together and stiffen the yarn to provide abrasion-resistance during weaving.). (3) The treatment contains ingredients that provide surface lubricity and binding action but, unlike a finish, contains no coupling agent. Before final fabrication into a composite, the size is usually removed by heat cleaning, and a finish is applied. Sometimes, size is incorrectly used to mean "finish".*

Specimen (test)**:** piece or portion of a sample or other material taken to be tested. *(test specimens normally must be conditioned and are prepared to conform with the applicable test method)*

Slenderness ratio λ **:** ratio of the effective length of a column to the least radius of gyration of its cross section is called the slenderness ratio (stability analysis)

Slit tape**:** prepreg-tape of width 3 mm through 50 mm, cut out from standard-tapes.

Smeared crack models**:** models used in non-linear analysis of concrete and other brittle structures

Smearing (homogenization): ability of a 'multi-material' that it can be replaced by a simpler treatable material model

SN curve (Woehlerkurve**):** stress-life curve of a material, in terms of cycles N, for a determined applied stress ($\sigma(N)$, advantageous when brittle) or an applied stress amplitude $\Delta\sigma(N)$. *(renders the weakening of a repeatedly loaded material)*

(strain) Softening (Entfestigung): degradation of strength with increasing strain (phenomenon observed in damaged quasi-brittle materials, including fiber-reinforced composites and concrete. Resistance capacity, that can be only used if the vicinity has reserve, redundancy)

Softening curve: degradation branch of the full stress-strain curve

Spalling concrete: process of surface failure in which spall is shed where spall are flakes broken from a larger solid body

Specific mass: weight per unit volume of a material. *(e.g. concrete, ρ = 2400 kg/m^3 with 1 kg ≡ ≈ 10 N)*

Specific strength**:** material strength divided by its density

Stacking sequence**,** stack, lay-up: arrangement of ply orientations and material components in a laminate specified with respect to some reference direction

Splitting (longitudinal): failure mechanism, resulting from compression loading that creates cracks parallel to the compression load axis generated by perpendicular tensile stresses acting at internal flaw tips which are usually combined with so-called wing cracks

Standard deviation of a random variable: measure in statistics, used to quantify the amount of variation of a set of data values. *(represented by the lower case Greek letter sigma σ (basic distribution) and the Latin letter s (sample)*

Staple fiber**:** fibers cut to a distinct length (staple length). *(either short natural fibers or of lengths cut from fibers)*

State I , construction**:** state, where the cross-section has a not yet 'cracked' concrete matrix. *(micro-cracking is always presumed)*

State IIa**:** state, when macro-cracks occur after multi-fold (micro-)crack generation

State IIb**:** state, when the final crack state is reached

State-of-the-Art**:** highest level of development, as of a device, technique, or scientific field, achieved at a particular time

State variable**:** (design constraint) a 'state' variable, Y, is a random quantity which is functionally dependent on a number of basic random variables, X_i, through an appropriate mechanical model $Y = g_y (X_1, X_2, ..., X_n)$, but is a quantity which is not directly measurable in a physical sense (e.g. the flexural capacity of a beam, a nodal displacement c.f. output variable)

Statically-determinate structure**:** structure where all of the unknowns can be found from equilibrium considerations alone

Statically indeterminate structure: structure where not all of the unknowns can be found from equilibrium considerations alone, compatibility equations must be used also. (a *structure is said to be redundant if it provides more load paths than are necessary to satisfy equilibrium)*

Statistical distribution**:** arrangement of values of a variable showing their frequency of occurrence. *(a function describing the probability that a given value will occur is called the probability density function PDF, and the function describing the cumulative probability that a given value or any value smaller than it will occur is called the distribution function or cumulative distribution function, abbreviated CDF. Applicable for strength are the Weibull distribution and the logarithmic normal distribution. For loads, extreme value distributions are used)*

Steel fibers**:** reinforcing fibers such as Ni/Ti, 22MnB5

Stiffness**:** rigidity of a structure, and elasticity of a material

Stitch**:** single turn or loop of the thread or yarn in sewing, knitting [GlossWi]

Stitch parameters**:** parameters which define stitching such as stitch pattern, stitch length, stitch gage

Stochastic design parameter**:** uncertain basic variable, scattering design parameter which is uncertain before realization and random after realization

Stochastic design parameter (uncertain basis variable) x_j: design parameter which is uncertain before realization and random after realization

Storage life**:** amount of time a material can be stored and remain suitable for use

Strain: length change per unit length due to force, temperature, moisture. *(strain is frequently expressed in meters per meter or percent %. It describes the change in the metric properties of a continuous body in the final displacement from an initial placement)*

Strain verification approach: approach, if limiting strains are used in design. Not advantageous in case of brittle materials where on top residual stresses have to be considered

Strain Energy Release Rate (SERR) $\mathcal{G}$**:** change in strain energy dU due to the creation of a new crack surface

dA. *(is related to the change in crack area, so if one uses U for strain energy, the strain energy release rate is numerically dU/dA. The elastic energy released = surface energy + plastic deformation energy)*

Strain (work) hardening**:** strengthening of a material during increasing plastic deformation

Strain rate effect**:** influence of the speed of straining dε/dt on the measured property. (*(1)material properties may change due to a fast strain change, in $\dot{\varepsilon}$ = % / s. (2) If there is a strength increasing effect of the material under impact, then the material is a strain-rate dependent one)*

Strand (Strang): normally an untwisted bundle or assembly of continuous filaments used as a unit. *(includes the terms rovings, tow, ends, yarn, etc. Unfortunately, sometimes a single fiber or filament is called a strand)*

Strength *R* (resistance): in engineering linked to a uniaxial fracture stress. Fracture tensile stress $\sigma^+ \equiv$ ultimate tensile strength R^t, ultimate compressive strength R^c. In test data mapping, in order to validate a strength criterion model the average failure curve or average failure body, respectively surface, is searched. Therefore, the task 'avearge test data fit' is tackled by applying average strength values *R*. In design verification, when determining an *RF* a statistically reduced surface (shrunken failure body) is used applying a strength value marked *R* (1) Characteristic strength: in mechanical engineering the typical average strength, in civil engineering a reduced (5% fractile) average strength value! (2) Design strength: a statistically reduced average strength. *R* = general strength and also the statistically reduced 'strength design allowable. $\bar{R}$ (bar over the *R)* means *average* strength and is to apply when mapping, like here

Strength *R*, uniaxial**:** generally a *R*esistance capacity of a structure or of a material to withstand loading actions:

(1) Uniaxial strength of a material referred to a level of stress) at which there is a significant change in the state of the material, e.g. stress at onset of yielding, fracture stress;

(2) Strength of a structure refers to a level of loading which produces a significant change in the state of the structure, e.g. inelastic deformations, collapse;

(3) In structural design should be demonstrated both material strength (applying strength failure conditions SFC as well as structural strength (applying buckling resistance conditions). The strength of construction materials is linked to strength failure modes such as NF, SF, SY, FF, IFF;

(4) In engineering, the uniaxial strength (≡ failure stress) R may be termed ('basic') strength and is a fixed value in design obtained from a standard test series under a uniaxial load, capturing one strength failure mode. Fracture tensile stress $\sigma_t \equiv$ ultimate tensile strength R_m;

(5) Multi-axial failure stress states are better termed multi-axial strength capacities, because damaging according to more than one failure mode may happen and increase the danger to fail;

(6) In test data mapping - in order to validate a SFC model - the average 2D failure curve or the multi-axial average failure surface (body) is searched. Therefore, the task 'average test data fit' must be tackled by applying average strength values $\bar{R}$. In design verification, when determining a RF a statistically reduced surface (shrunken failure body) is used applying a strength value marked R or fd)

Strength analysis: assessment of stresses or strain of a structure in a given mechanical environment that demonstrates the structure is able to sustain the applied loads without unacceptable behavior (e.g. rupture, detrimental deformation, buckling). The strength analysis leads to the design justification, on the basis of computed MoS.

Strength designations: *R* is strength, in general, and also the statistically-reduced value. $\bar{R}$ denotes the average strength which is used when mapping a course of test data points. In construction, still most often used letter $R \rightarrow f$. *A change to take R is presently coming*

Strength, equi-biaxial**:** isotropic materials: tensile R^{tt}, compressive R^{cc} and for UD materials $R_\perp{}^{tt}$, $R_\perp{}^{cc}$

Strength, tri-axial isotropic materials: recommended tensile R^{ttt}, compressive R^{ccc} (porous materials)

(design**)** Strengths of a lamella**,** UD ply, civil engineering: property values in the partial safety factor-based design. *((1) A 5% fractile is applied to the test data which is less than for the A-values). (2) Partial safety factors are put on the main scattering, uncertain design parameters.*

(design**) S**trengths of a lamina,UD ply, mechanical engineering: A-values or B-values (= statistically reduced, see definitions of these terms) values, deterministic-based values for design verification.

(*Notes: (1) A single action or loading increasing safety factor is put on. (2) Under compression, following Mohr-Coulomb the respective friction value* $\mu_{||\perp}$ *or* $\mu_{\perp\perp}$ *must be considered (in the isotropic case, just one friction value* μ *acts). (3) In test data mapping, average values (mean) are determined usually marked by a bar over. (4) Obtaining tension and compression strength of a UD-lamina parallel to fiber direction careful experiments, carried out by Bansemir and Schürmann, on test specimens with really straight fibers proved* $R_{||}^{\,c} \approx R_{||}^{\,t}$. *Measured values* $R_{||}^{\,c} < R_{||}^{\,t}$ *is the result of micro-buckling and therefore not a strength value but a structural instability value, which better represents the local structural situation and not the material.* $\{\overline{R}\} = (\overline{R}_{||}^{\,t}, \overline{R}_{||}^{\,c}, \overline{R}_{\perp}^{\,t}, \overline{R}_{\perp}^{\,c}, \overline{R}_{\perp||})^T$

(6) In design verification to apply are the statistically reduced values are taken, no bar over

$$\{R\} = (R_{||}^{\,t}, R_{||}^{\,c}, R_{\perp}^{\,t}, R_{\perp}^{\,c}, R_{\perp||})^T$$

Strengths of fabrics**,** smeared material, A- or B-values: $R_W^{\,t}$, $R_F^{\,t}$, $R_W^{\,c}$, $R_F^{\,c}$, R_{WF}, $R_3^{\,t}$, $R_3^{\,c}$, R_{W3}, R_{F3} for general fabric (6 instead of 9 if warp = fill)

Strength of impregnated rovings in textile grids**:** design values $R_{||}^{\,t} \approx R_f \cdot V_f \equiv f_{||td}$ with a further index $_W$ and $_F$ if warp ╪ fill (weft) in case of hybrid and different reinforcement in grids)

Strength of textile grid reinforced concrete**:** design value $f_{td,tex}$ (index $_W$ and $_F$ if warp ╪ fill (weft)

Strength capacity **(**multi-axial**):** see strength versus strength capacity

Strength ratio**:** ratio of compressive strength to tensile strength. (*gives an idea about how brittle a material is. Separates in the Haigh diagram compression from tension domain* $\rightarrow$ $R^{transition} = -R^{\,c}/R^{t}$. *Advantageous, compared to run* $R = -1$!

(uniaxial) Strength versus (multi-axial) strength capacity**:** terms capturing different contents in strength domain. *((1) One should not mix up an increase of the measured uniaxial 'basic' strength with a calculatory increase of strength resistance under multi-axial stressing, described by the material stressing effort Eff and derived from SFC application. (2) In the multi-axial stress state case the resistance Eff may be reduced which can take place under an external loading superimposed by hydrostatic stressing. This physical effect can be demonstrated by UHPC measurements at the TU Dresden: fracture test results (Eff = 100%) with uniaxial strength* $\{\sigma_{fr}\} = (-160, 0, 0)^T$ *MPa* $\Rightarrow$ *multi-axial strength capacity* $\{\sigma_{fr}\} = (-224, -6, -6, -6)^T$ *MPa. This proves that the external axial compressive loading capacity increases from -160 MPa to -224 MPa. It has nothing to do with an increased 'basic' uniaxial strength)*

Strength design allowables: statistically reduced average values such as A- and B-values or 5% fractiles in civil engineering

Strength Failure Condition SFC ("criterion") $F = 1$**:** mathematical formulation of the strength failure surface , the limit state, here the strength limit state to assess a 'multi-axial failure stress state in a critical location of the structural component).

((1) A physically based strength model possesses a minimum number of model parameters. After proven demonstrations of a good mapping of the courses of accurate test data ('goodness of fit') such a model is able to even sort out false test data. (2) Principally, a SFC can describe one failure mode, only! (3)There are so-called Global or Lumped SFCs (describe the full failure surface by one single equation capturing all existing failure modes such as Normal Fracture NF, occurring under tension and shear or Shear Fracture SF, under compression and shear, which means mapping all failure modes in one failure condition) and Modal SFCs (describing each failure mode-associated part of the full failure surface by one equation, respectively mapping each single failure mode separately). (4) Failure at micro-scopic level must be considered in a macro-scopic SFC. Hence, the usually macro-mechanical SFC should

consider, that failure usually occurs at a lower than the macro-mechanic level, micromechanically, such as the matrix in a macro-mechanically described UD SFC)

Strength failure surface**:** visualization of the failure function $F = 1$. *(a strength failure surface is a fracture failure surface in case of brittle materials, such as concrete)*

(mechanical**)** Stress**:** quantity σ = *Force/Area* = F/A in MPa = N/mm^2 where F is the force acting on an area A. *(A can be the undeformed area or the deformed area, depending on whether an engineering stress or a true stress is of interest)*

Stress analysis**:** computation of stresses (or strain) in a structure, due to loads carried by the structure in a given mechanical environment.

Stress component**:** component of a shear stress composed of a compressive and a tensile part *(Example:* $\sigma_x = \tau_{xy} / \sqrt{2},\ \sigma_y = -\tau_{xy} / \sqrt{2}$. *The often used term 'stress component' instead of stresses is not accurate. It must read stress tensor or matrix components)*

Stress concentration: local stress area of the structure where the stresses are significantly higher than the general stress level. *(a fine mesh of elements is required in such regions if accurate estimates of the stress concentration values are required)*

Stress corrosion cracking SCC**:** type of corrosion that leads under static tensile stress and a harmful medium to fracture. *(may lead under tensile stress below $R_{p0.2}$ incl. residual stresses and an corrosive environment (sulphide, chloride) to unexpected sudden failure of usually ductile behaving materials due to microscopic cracking, transcrystalline and intercrystalline)*

Stress intensity factor**:** measure for the intensity of the stress state in the vicinity of the crack tip

Stress state, bi-axial (σ_x, σ_y): effect on strength capacity. Stress state where different stresses act together and where the signs determine the effect. *((1) σ_x^c with σ_y^t leads to a load-carrying reduction in the compressive x-direction due to the fact that two failure effects occur: shear damaging under compression σ_x^c and tensile damaging under σ_y^t. For concrete, the reduction effect increases with increasing concrete quality. However, it might be not harmful (mind GZG) if a minimum reinforcement is provided. It is valid for plain and for short fiber reinforced concrete, too. (2) In contrast (σ_x^c, σ_y^c) leads to a load-carrying increase due to internal stabilization [Cun17])*

Stresses, isotropic 3D**:** $\{\sigma\} = (\sigma_x, \sigma_y, \sigma_z, \tau_{yz}, \tau_{zx}, \tau_{xy})^T = (\sigma_I, \sigma_{II}, \sigma_{III})^T$

Stresses, general fabric 3D**:** $\{\sigma\}_{fabric} = (\sigma_W, \sigma_F, \sigma_3, \tau_{3F}, \tau_{3W}, \tau_{FW})^T$

Stresses, transversely-isotropic 3D UD-material**:** $\{\sigma\}_{UD} = (\sigma_1, \sigma_2, \sigma_3, \tau_{23}, \tau_{31}, \tau_{21})^T$

Stress-free temperature**:** temperature at which a material is free of residual stresses

Stress ratio R: ratio of minimum stress (mathematically, less positive) to maximum stress, $R = R_\sigma = \min\sigma / \max\sigma$, under load-controlled (σ-based) cyclic (*dynamic*) fatigue loading. The other ratio used is the strain-based ratio $R_\varepsilon = \min\varepsilon / \max\varepsilon$. For brittle materials, the alternating test loading $R_\sigma^{trans} = -R^c / R^t$ is to prefer to the traditional R = - 1

Stress rupture **(**static fatigue**):** time-dependent behavior of a material, here w.r.t. strength)

Stress vector**:** vector which incorporates mechanical stresses from external and internal loads + hygro-thermal stresses due to environment + residual stresses from manufacture

Structural analysis**:** procedure to find and measure the effect of external forces on physical objects like built structure. *(used to predict the behavior of structures upon loads acting on them. On the basis of structural analysis the material choice is performed and structural elements are designed)*

Structural component**:** major section of the structure (e.g. wing, body, fin, horizontal stabiliser) which can be tested as a complete unit to qualify the structure.

Structural stability (Standsicherheit): condition of safely transferring static and cyclic loads as impact loadings on the building like self weight of the building and live load on the building (the resistance

offered by a structure to undesirable movement like sliding, collapsing and over turning is called stability. Stability depends upon the support conditions and arrangements of structural members*)*

Structural integrity**:** characteristic of a structural part enabling it to withstand the loadings within the environment and the imposed service conditions

Strip for rehabilitation: usually a narrow UD laminate tape

Structural element**:** generic element such as a stringer, a sandwich panel, or a girder of a structure

Structural reliability**:** ability of a structure to fulfill the functional requirements during a distinct lifetime with a distinct reliability. (*(1) Considers the probability of combinations of the significant scattering (stochastic, random) design parameters (better: design variables). (2) Currently, in aerospace the 2 essential design variables load and strength are separately treated, but not really stochastically combined as in structural reliability applications using a probabilistic concept to determine the survival probability* $\mathcal{R} = 1 - p_f$ *with* p_f *as failure probability)*

Structural optimization **(**FEA**):** structural analysis tool consisting of the objective function and constraints. *(tool to approach the design objective 'Right first time' including all functional requirements such as mass, life time, operating CoSts, maintenance CoSts, manufacturing constraints, stiffness performance, thermal deformation, electrical and thermal conductivity, end-of-life requirements (recycling, sustainability* CO^2*-reduction) and consideration of the scattering parameters in order to be robust. Manufacturing effort most often sets the limit for design freedom*)

Superplasticizer: chemical admixtures to reduce water amount and the ratio of water/cement

Ssuperposition principle**:** principle how stress states may be combined. *(for a linear system the response is the same by adding together two or more separate forcing functions and then solving the equations or by solving for the separate forcing functions and then adding the responses together. The method of solving for each forcing function and adding the response is superposition)*

(rigid) Support**:** fixed point of the structural model. *(Degree of freedom where the variable is known before the solution is found. Typically, the zero displacements at fixed points in a structural analysis or the points of known temperature in a heat conduction analysis. Generally there must be some points of known value, i.e the structure must be supported before the equations can be solved)*

Sustainability, sustinere, to hold up: aim of a development that meets the needs of the present without compromising the ability of the future [*UN March 1987*]

Symmetric lay-up (stack**):** stack in order to reduce unfavorable distortions. *(can practically not be realized when winding)*

Tack: stickiness of the prepreg

Tailored blanks **(**maßgeschneiderte Blech-Halbzeuge): designed and then tailored semi-finished sheets to reduce waste and CoSts

Tailored Fiber Placement TFP**:** textile manufacturing technique based on the principle of sewing for a continuous placement of fibrous material for composite components. *(the fibrous material is fixed with an upper and lower stitching thread on a base material. Compared to other textile manufacturing processes fiber material can be placed near net-shape in curvilinear patterns upon a base material in order to create stress adapted composite parts. It is a fiber-steering process that lays tows upon the load-optimal path direction in order to save mass and increas stiffness*)

Tangent stiffness: slope of the load/deflection curve for the current solution position

Tape**:** see UD fabric: usually narrow UD-prepreg strip (lamellas), however further, NCF tapes (to increase beside the axial strength capacity also the shear strength capacity of for instance girders by NCF lamellas).*(fabricated in widths up to 1200 mm wide for carbon (UD tapes, NCF tapes, CF/PA6 tapes etc.)*

Tension cut-off: vertex of failure body, mathematically defined by

$$\{\sigma\} \quad < \quad (\sigma_I = \bar{R}^{ttt},\ \sigma_{II} = \bar{R}^{ttt},\ \sigma_{III} = \bar{R}^{ttt})^{\mathrm{T}}$$

Tendon: prestressing element, comprising tensioned elements like bars, strands that apply compression to the surrounding concrete

Term (Begriff): expression with a specific meaning

Test: experiment, performed physically or virtually by realistic digital simulations

Test specimen **(**Prüfling, Probekörper): here, structural item to obtain structural properties, material properties.

((1) Concrete test specimens that must be dimensioned due to a thickness > 3·Ø maximum grain). (2) single layer test specimens, such as the brittle behaving UD material coupons, are so-called isolated test specimens (≡ lamella strips) which experience a so called Sudden Death failure. (3) Embedded layers, however, experience a deformation-controlled benign failure behavior, which should be considered as it delivers the usually desired post-failure deformation capacity. (4)'Embedded' test specimen = sub-laminate test specimen can be tested deformation-controlled in a very stiff testing machine. This delivers an output for the laminate, however can be evaluated by a non-linear lamina-composed laminate model working as inverse parameter identification

Test procedures regarding loading: Load-controlled → The stress in a structure is determined by the load and the cross section area, the load has to be transferred through. This stress does not depend on the deformation. Strain (deformation)-controlled → The stress in embedded lamina (ply) depends on the adjacent layers

Tex: fineness of a roving measured in g/1000 m

Textiles **(**technical, structural**):** 'terminus technicus' for textiles utilized in structural engineering for high performance applications involving 2D planar pre-forms such as woven, knitted, non-woven, 3D one–step processed pre-forms or reinforcing structural elements

Textile failure**:** complex failure of a textile structure. *(Unfortunately for most of the structural textiles, fractography will not exhibit clear strength failure modes. In these materials, always multiple cracking is caused under tension, compression, bending, or shear. No clear mode-related strengths are observed. Therefore, homogenizing to a material is permitted, strengths can be defined according to the number orthotropic material symmetry requires)*

Textile-reinforced concrete TRC**:** textile reinforced fine grained high strength mortar, usually reinforced by high-performance fibers composed in a fiber grid. *((1) The obtained 'fine grain concrete' such as with Pagel TF 10 involves: grains Ø 1-7 µm, f_c > 65 MPa, $E_0 \approx 25$ GPa. CF filament Ø 7 µm, cured roving $f_{||t} \approx 3000$ MPa. (2) The generated filigree reinforcement with relatively small grid sizes compared to a steel 'mat' is causing more but smaller cracks, which is advantageous for crack width limitation. (3) Similar to StB, the TRC is a composite of materials, that practically cannot be homogenized*)

Thermoplastic TP: polymer (plastic) that repeatedly can be softened by heating and hardened by cooling through a temperature range characteristic of the plastic, and when in the softened stage, can be shaped by flow into articles by molding or extrusion. *((1) TP is partly crystalline in contrast to the strongly linked thermosets and thereby residual stresses may be reduced by a thermal treatment. (2) Characteristic of the plastic in the softened stage, it can be shaped by flow into parts by molding or extrusion.)*

Thermoset EP: polymer (plastic) that is substantially infusible and insoluble after having been cured by heat or other mean

Thread count**,** carpet characterization: Number of warp threads per length plus number of weft (fill) threads per length

Time domain**:** physical data sets, such as a structural forcing function and its response, are usually given or defined in terms of time histories. *(the Fourier transform of the time domain gives the corresponding quantity in the frequency domain)*

Toughness**:** measure of a material's ability to absorb work, or the actual work per unit volume or unit mass of a material that is required to rupture it. *(toughness is proportional to the area under the load-elongation*

curve from the origin to the breaking point).

Tow **(**tow rope = Abschleppseil): untwisted bundle of continuous filaments. Commonly used in referring to man-made fibers, particularly carbon and graphite fibers, in the composites industry *((1) When filaments are grouped together in a loose, continuous rope without twist, man-made filaments are called tow. In composites industry commonly used for carbon and graphite fibers but also glass and aramid. Heavy tow such as 48k, 96k (= thousand) filaments, with a 96k-CF-roving= 6400 tex ≈ 6.4 kg/km. Commonly used in referring to man-made fibers, particularly carbon. (3) Equivalent meaning to "roving" in glass[SAE])*

Traceability: ability to follow a specific item at input of a phase of the software life cycle to a specific item at the output of that phase. The item may be software or documentation

Trade-off: comparison of alternative options

Transient analysis**:** analysis performed when at least one of the parameters involved in the boundary conditions, material properties or loading conditions is time dependent

Transition zone **(**mode**s):** zone between mode domains in static and cyclic (Haigh diagram) cases linking compression and tension

Transverse (lateral) tensile strength**:**

(1) strength of a textile reinforced concrete transversal to its 'plane' (inter-laminar) R_{3t} .

(2) Lateral in-plane strength of the transversely-isotropic UD –lamina $R_{\perp t}$ (intra-laminar) or lamella $f_{\perp t}$

Transversely-isotropic: descriptive term for a material exhibiting the special case of orthotropicit y in which properties are identical in two orthotropic dimensions, but not the third; having identical properties in both transverse directions but not the longitudinal direction

Tri-axial stress state 3D**:** most general stress state (spatial)

Tri-axial textiles = 2D**:** textile, marked by the 3 in-plane directions of the fibers (is not a 3D textile material)

Tri-axiality factor: defined as $TrF = \sigma_{hyd}/\sigma_{eq}^{Mises} = (I_1/3)/\sqrt{3J_2}$

True strain**:** particular strain measure, used in large strain elasto-plasticity being the log of 1 plus engineering strain ε, or the integral of the incremental change of length over the current length

True stress (Cauchy stress)**:** force divided by the current (instantaneous) area. See also

Twill weave**:** fabric woven with a pattern of diagonal parallel ribs, made by passing the weft threads over one warp thread and then under two or more warp threads

UD-fabric**:** fabric (such as a woven or a NCF) with a high amount of parallel tows, hold together by a small amount of weft respectively stitching fibers. *(this textile can be used for the manufacturing of composites dry or as a prepreg)*

UD-lamina**,** lamella: lamina (ply) with a unidirectional reinforcement, being the building block of a laminate. *(definition of the positive fiber orientation angle is $x \Rightarrow x_1$ (clockwise) of the embedded lamina, often the mid-plane is used as reference plane [CLT])*

Ultimate design load: Maximum expected load = Design Ultimate Load DUL

Ultimate Limit State: (Grenzzustand der Tragfähigkeit) ULS,

Ultimate strength**:** maximum stress (tensile, compressive or shear) a material experiences at fracture. *(maximum load the material test specimen can withstand without incurring fracture divided by the associated original cross section area (rupture or collapse are differently used limits!). The stress represents uniaxial tension, uniaxial compression (essential, just in case of brittle behavior, as given with concrete) or pure shear)*

Uncertain basic variable: defined by distributions given by an expert and related to random variables and fuzzy numbers

Uncertain quantities: physical (loads, material properties, dimensions); statistical (distribution parameters); model (mechanical/mathematical)

Uncertainty (fuzzyness, Ungewißheit, Unsicherheit): unclearniness in loadings, strengths, and other design parameters such as geometrical parameters, applied engineering models etc. *(it must be discriminated (1)*

Epistemic uncertainty within technical measurements of geometry, material properties etc., which is improvable by better and more measurements, test data evaluation and additional information. (2) Aleatoric uncertainty due to usual measurement tolerances where 'nothing' can be improved concerning the given test situation)

Uncertainty quantification**:** formulation of a statistical model to characterize imperfect and/or unknown information in engineering simulation and physical testing for predictions and for decision making

Uncertainty types: (1) Epistemic (lack of knowledge). (2) Aleatory (measurements not precise, sample size too small, test data evaluation). (3) Ontologically (unclearness of the same term with different meanings, interpretation is uncertain)

Undulation**:** waviness of yarns, tows

Validation**:** validus = strong, kräftig, wirksam. Control whether the design requirements in the performance specification are met

Validation of model (validus = strong, kräftig, wirksam): 'qualification' of a created model by well mapping physical test results with the model

Variable : characteristic or property that is appraised in terms of scalar values.

Variance: measure of the dispersion of a random variable about its mean value. In testing, variance is a measure of random errors in a series of measurements.

(design) Verification (from Latin, veritas facere): fulfillment of a set of design requirement data. (*Proof, that the product fulfils the product requirements data, defined in the performance requirements specification (= Pflichtenheft). Performed by a computation and/or a physical experiment such as a structural test like with a girder being below a given deformation limit under loading)*

Verification versus validation**:** When is what fulfilled? Example 'maximal girder deformation'.

(Customer's validation objective was "to maximally obtain a bending deformation δ of the Girder". Material tests validated the material model, the structural model was proven by a pre-test. Then, 3 structural loading tests are performed according to a specified test plan with a product verification load P and measurement of the deformation δ_i. This means for the official achievement of verification and validation that:

$P_1 = P$, $\delta_! < \delta$: *verification (+), validation (+),* structure is stiffer than assumed, usability not restrictred

$P_2 = P$, $\delta_2 = \delta$: *verification (+), validation (+),*

$P_3 = P$, $\delta_3 > \delta$: *verification (+), validation (-),* structure is less stiff than assumed

$P_4 < P$, $\delta_3 > \delta$: *verification (-), validation (-),* structure exceeds δ still under a not achieved P

(design) Verification procedure (Nachweisverfahren): provision of required evidence = verification

Vibration corrosion cracking**:** high strength steels, cracking caused by vibration fatigue. *(vibration corrosion cracking or corrosion fatigue may lead under all stress ratios and a corrosive medium finally to sudden failure)*

Virtual prototype**:** a tool to validate a preliminary design before producing a physical prototype by testing different functions

Virtual testing**:** novel approach to accelerate designing from screening of materials via material characterization to design verification. *(approach from test specimen level to structural component level by reducing the physical testing effort and by for instance estimating B-values from standard coupon tests)*

Virtual reality**:** replacement of the real world environment by a simulated one

VisCoSity**:** resistance to flow of a material

Void**:** here pocket of entrapped gas or fluid that has been cured into a laminate. *((1) A physical and mechanical discontinuity occurring within a material or a part which may be 2D such as thin flat disbonds, delaminations or 3D-pockets such as vacuum-, air-, or gas-filled pockets. (2) Voids are essentially incapable of transmitting structural stresses or non-radiative energy fields. (3) Porosity is an aggregation of micro-voids and may decrease stiffness and strength)*

Von Mises stress**:** stress determined by the second invariant of the deviatoric stress tensor $\sigma_{eq,Mises} = \sqrt{2} \cdot J_2$.

(scalar value, used to relate a multiaxial stress state to a 1D tensile test strength value. It is classically called equivalent stress)

Von Mises yield criterion**:** criterion, used to describe the yield of ductile materials. *(assumes that yielding commences when the Von Mises equivalent stress reaches a critical value)*

Warp**:** longitudinally oriented yarn in a woven fabric

Warpage**:** out-of-plane deformation of a cross section

Warp knitted fabrics**:** fabric types with more or less straight reinforcing fibers

Water-cement ratio**:** water-cement w/c-ratio or water-binder w/b ratio

Weaves or Woven fabrics**,** types: plain (Leinwandgewebe), twill (Köpergewebe), harness satin (Atlasgewebe). *((1) The weave may be UD, tri-axial plain, near-net shape, polar, a spacer weave (Abstandsgewebe) or also 3D. (2)Uusually semi-finished 2D structure products, constructed by interlacing yarns, fibers, to form above fabric patterns. (3) Warp and weft tracer fibers of another material may be incorporated into the fabric)*

Weft or fill**,** in German Schuss: 'filling' material of the fabric or the transversely oriented yarn, respectively. *(for a weft property the index $_F$ is used to separate weft from warp)*

Winding pattern**:** regularly recurring pattern of the filament path in a filament winding after a certain number of mandrel revolutions

Woven fabric**:** fabric formed by weaving. *(stretches bias, between the warp and fill directions)*

Yarn: assembly of twisted or practically un-twisted (rovings) filaments (in yarns) suitable in textile fabrication (from fiber via yarn to fabric)

Yarn **(**Garn): group, bundle or assembly of twisted or practically un-twisted filaments suitable in textile fabrication. *(assembly from either natural or manufactured fibers to form a continuous length that is suitable for use in weaving or interweaving into textile materials. Staple fiber yarns, such as cotton, only a few inches long, must be tightly twisted together to produce a satisfactory yarn length. Filament yarns are usually thinner and smoother than staple yarns)*

Yarn count**:** fineness, measured in tex = g / 1000m

Yield stress**:** stress in a uniaxial or multi-axial stress-strain state of a yielding material, $\sigma_{yield} \geq R_{p0.2}$

Yield strength (technical): $R_{p0.2} \equiv f_y$, corresponds to the stress $\sigma_{p0.2}$ at 0.2% remaining strain in a uniaxial stress state. *(Note: Stress level at onset of yielding, proportionality then practically away)*

Yield strength: distinct stress linked to yielding. As it is difficult to determine a precise onset-of-yield point, in general, one should discriminate from practical engineering reasons the proportional (tensile) limit R_p ($\equiv f_y$) and $R_{p0.2}$ ($\equiv R_{0.2}^t$), where the offset yield point is taken as the stress at which 0.2% plastic deformation remains (*in English literature $R_{p0.2}$ is termed proof stress).* Onset-of-Yielding: stress $\bar{R}_{0.2}$ for modeling), $R_{0.2}$ for design-verification (proof) are an engineering agreement at 0.2% permanent strain

Young's modulus**:** material property, defined by the ratio 'uniaxial stress' / 'corresponding strain'

Zone of safety: nominal or central distance between action distribution and resistance distribution

Z-reinforcement**:** reinforcement in third direction by so-called Z-pinning, necessary to introduce a mechanical link by e.g. a stiff carbon fiber between the different plies of the composite

x-y-plane, 2D: in composite laminates, the reference plane coinciding often with the mid-plane of the laminate

z-axis**:** in composite laminates, the reference axis normal to the plane of the laminate

3D composite structures**:** three-dimensional fiber preforms arranged into complex three-dimensional reinforcement structures.

3D composite material**:** three-dimensional composite materials created from a 3D-weaving process, a 3D-braiding process, or a 3D-lay-up or of distributed short fibers

3D printing: additive manufacturing of pretty thin cross section wide layers. *(subset of additive manufacturing. In civil engineering practically not applied, but could be used to manufacture free-shape formwork (Schalung))*

120°-symmetry of the isotropic brittle and ductile failure body: wording according to the equality of the 3 principal stresses each ‘perturbation’ of the rotational failure body exists 3 times.

Technique versus Technology:

* The term technique is derived from the ancient Greek word "technikós", which can be referred to "expert". Technique has two meanings. On the one hand, the word describes procedures that make findings of the natural sciences practically usable and on the other hand, fixed procedures.
* The term "technology" is composed of the two Greek words "téchne" for technique and "lógos" for logic. Technology is therefore the teaching of techniques.

Wording in Additive Fabrication, 3D-print:

For the ‘printing’ of a product a filament is used. which exemplarily consists of a polymer or a metal.

Unfortunately, instead of the longtime used filament it is also used endless fiber. This is per definition right but fully confuses if the product is reinforced by endless fibers of glass or carbon. One should stick to filament and use the still older term endless fiber if the reinforcement is addressed.

23.3 Deutsche Fachbegriffe in Englisch

Deutsch	**Englisch**
Abbinden	cure
Abplatzung	spalling
Abreißgewebe	peel ply
Abstandsgewebe	spacer fabric
Abwitterung	scaling
allgemeine bauaufsichtliche Zulassung abZ	general construction approval
Alterung	aging
Anrißlebensdauer	number of cycles until initiation of a technical crack
Arbeitsablauf	workflow
Arbeitsvermögen	deformation capacity
Atlasgewebe	satin-woven fabric
Ausdehnung	dilatation
Auslegung, Bemessung	design dimensioning
Ausnutzbarkeit	exploitability (e.g. of a material)
Aussparung	opening
Bahn (breiteres Band)	tape
Balken	beam
Balken, gedrungen	deep beam
Band (hier: Gelegeband ≡ breite Lamelle)	tape
Bauen im Bestand	building in the stock
Bauindustrie	building and construction industry
Baumaterialien	conctruction (building) materials
Baukastenprinzip	building-block-approach:
Bauphasen	Planung, Bau, Nutzung, Abbruch, Recycling
Baustahlmatte, Baustahlgewebematte,	steel reinforcement grid (mat, mesh)
Beanspruchungsfall	stress case
Betonstahlmatte (s. Baustahlmatte)	
Baustelle	building site
Bauteil	structural component, part of a building
Bauweise	method of construction
Bauwesen	civil engineering
Beanspruchung	mechanical stress
Bedingungen	constraints (in optimization, programming)
Begriff	Term, notion,
Belastung	loading
Belastungsarten	loading types
Bemessung, Auslegung	(design) dimensioning
Bemessungsfestigkeit	reduced characteristical strength, design strength f_d
Beschichtung	coating
Beschlichtung	sizing
beständig	resistant, enduring, durable
Bestandserfassung	stock-taking
Beton	concrete
Betonfertigteile	precast concrete elements
Betonfestigkeit	concrete strength
Betongüte	concrete quality
Betonmatrix	concrete matrix
Betonspaltung	concrete splitting

Deutsch	Englisch
Betonstahl	rebar
Betonstahlmatte	steel reinforcement grid (mat, mesh)
Betonüberdeckung	concrete cover
Betonzusatzmittel	concrete admixtures
Betonzusatzstoffe	concrete additives
Betonzuschlag	concrete aggregate
Beurteilung	assessment
Bewehrung	reinforcement or armoring
Bewehrung, schlaffe	reinforcement, non-tensioned or un-prestressed
Bewehrungsgitter	reinforcement grid
Bewehrungsgrad	percentage (degree) of reinforcement
Bewehrungskorb	reinforcement cage
Bewehrungsstab	rebar
Bezeichnung	designation
Bindemittel	binder
Bindemittelsystem	binder system
Bruchzähigkeit	fracture toughness K_{Ic}
Bügel (Schub-Bewehrung)	stirrup (shear reinforcement)
CarbonBeton CB	carbon concrete
Carbonfaser	carbon fiber CF
charakteristische (Nenn)Festigkeit	statistically reduced compressive strength value f_{ck} of a series of cured concrete /mortar test specimens, determined after 28 days
Datenmigration	data migration
Dauerfestigkeit	endurance strength, fatigue limit, fatigue strength
Dauerhaftigkeit	durability
Dauerstandfestigkeit	long-term static strength incl. creep resistance
Decke	ceiling slab
Deckenplatte	slab
Dehnkörper	tensile test specimen
Dehnrateneffekt	strain rate effect
Delamination	delamination
Dichte	density ρ
Drehergewebe	leno-woven fabric
Drehung	twist
Duromer	thermoset material
Eigengewicht	dead load; net weight
Einspannung (Zurückhaltung)	restraint
Einschränkungen	constraints
Einwirkung S (Belastung)	action
Einzelstab	single bar
Endlosfaser	continuous or endless fiber
Endverankerung	end anchorage
Entfestigung	softening
Ermüdung	fatigue
Ermüdungsfestigkeit	fatigue strength
Ertüchtigung, Nachverstärkung	upgrading, retrofitting
Expositionsklasse	exposure class
Faden	thread
Fadenspreizung (Tow)	thread spreading
Faser	fiber (US), fiber (UK)
Faserauszug	fiber pull-out

Deutsch	Englisch
(Kurz)Faserbeton FB	fiber reinforced concrete FRC
Faser-Kunststoff-Verbund FKV	Fiber Polymer Composite
Faser-Rezyklat	recycled fiber material
Faserschlichte (s. Beschlichtung)	sizing
Faserarten	fiber types
Faserspule	bobbin
faserverbund-armierter Beton	concrete, armored by an endless fiber product
Faser-Verstärkter Kunststoff FVK	Fiber-Reinforced Polymer FRP
Faservolumenanteil	fiber volume fraction V_f in %
Feinbeton	fine-grained concrete
feinkörnig	fine-grained
Festigkeit (effektiv)	effective strength
Filament	filament
Fließmittel	super-plasticiser
früher Zwang (Eigenspannungen, Zwängung)	residual stresses causing early cracking
Garn (Filamentbündel)	yarn
Garn-Feinheit	yarn count or fineness
Gebrauchstauglichkeit	serviceability
Gebrauchszustand	use state
gedrungener Balken	deep beam
Geflecht	braided fabric
Gelege	non-crimp fabrics or laid webs
Geo-Textilien	geo-textiles
gerissene Zugzone	cracked concrete tensile zone
geschnitten	chopped (fibers, strands, rovings)
Gesteinskörnung (Zuschlag)	aggregate
gestickt	embroidered
Gestrick	weft-knitted fabric
Gewebe	woven fabric
Gewirke	warp-knitted fabric
Gitter (Stab-Gitter)	rebar grid
Gitter (textiles)	flat, open fabric grid structure
Gitterweite	s. Maschenweite
Grenzfläche	failure surface (strength criteria), also interface (composites)
Grenzflächenscherfestigkeit	interfacial shear strength
Grenzzustand	limit state
Grenzzustand der Gebrauchstauglichkeit	limit state of serviceabilty
Grenzzustand der Tragfähigkeit	ultimate limit state ULS
Grundgesamtheit	basic population
Haftung	bond (e.g. filament-matrix)
Haftvermittler	adhesion promoter
Halbzeuge	semi-finished product
Harz	resin
Harzsystem	resin system
Hochbau	building construction
Hohlkastenträger	box girder
Hydratation	hydratation
hydrostatische Achse	hydrostatic axis
Imprägnierung	impregnation
Infiltrierung	infiltration

Deutsch	Englisch
Infusion	infusion
Injektion	Injection (with pressure)
Instandsetzung	repair or retrofitting
inter-laminar	interlaminar
Interphase	interphase
intra-laminar	intralaminar
Intrusion	intrusion
Kardierverfahren	carding procedure
Kaschierung (Schichtbildung)	lamination
Kette	warp
Kettfaden	warp yarn
Konditionierung	conditioning
konstruktive Bewehrung	secondary (structural) reinforcement
Koordinatensystem	coordinate system
Köpergewebe	twill-woven fabric
Korb (Bügel-Korb)	cage
Lage	layer, ply
Lagermatte	stock ‘mat’
Lamelle (UD Schicht-Gelegestreifen)	lamella
Lamelle (schmale Lamelle)	strip
Lamina	lamina
Laminat	laminate
Last, sichere	(Design) Limit Load DLL
Lastannahmen für Bauten	design loads for buildings [EC1]
Lasten (Bauwesen), ständige	static (constant) loads
Lastenheft (Anforderungsliste des Kunden)	tender specification of customer
Leichtbeton	lightweight concrete
Leistungsverhalten	performance
Leinwandgewebe	plain weave fabric, canvas weave or linen fabric
Listenmatte	indiviual grid due to length, width, ∅
Maschenweite	mesh width
Massivbau	solid construction
Matrix (Matrizes)	matrix (matrices)
Matte	mat
Mattenware	mat ware
Mindestbewehrung	minimum reinforcement
Mischung	compound
Modellierung ausgehärteter Halbzeuge	modelling of semi-finished products
Mörtel	mortar
Multiaxial-Gelege (MAG)	multi-axial non-crimp fabric NCF
Multiaxial-Gitter	multi-axial grid
Nachbruch(beginn)verhalten	post-failure behavior
Nachrechnung	recalculation
Nachrechnungsrichtlinie	recalculation guideline
Nachrüsten	retrofit (of old structures)
Nachweis	design verification (design proof)
Nähen	stitching (referred to grids), sewing (referred to confection technology)
Nähfaden	sewing thread
Neubau	new construction (building)
nicht-gewebt	non-woven
Nutzlast	payload

Deutsch	**Englisch**
Öffnungsweite (Gitterweite)	opening width
orthotrop	orthotropic
passive Schädigung	passive damaging
Pflichtenheft	customer-tender (final) performance requirements specification
Platte	slab (base slab = Bodenplatte)
Polymer	polymer (plastic)
Preform (Vorformling)	preform
Prepreg	pre-impregnated fiber product
Probekörper	test specimen
Profil	profile
Querkraft	shear force, lateral force
Querkontraktionszahl	Poisson's ratio ν
Querzugfestigkeit	transverse (lateral) tensile strength
R-Beton; resourcenschonender Beton	resource-saving concrete (*a small letter r would be correct!)*
Rechnerischer Nachweis	computational proof (justification)
Redundanz	redundancy
Referenzexperiment	reference experiment
rezykliertes Material	recycled material
Riss	crack (micro and macro)
Rissbreitenbeschränkung	crack width limitation
Rissbreitennachweis	crack width verification
Roving	roving
(technischer) Schaden	(technical) damage
Säule	column
Schädigung	damaging process, damaging (is unique compared to damage)
Schädigung(sportion)	damaging portion
Schädigungsakkumulation	accumulation of damaging portions
Schädigungsmass	degree of damaging
Schalentragwerk	shell load-bearing structure
Schalung	formwork
Schicht	lamina, ply (layer = physical ply)
Schichtweise Bruchanalyse	ply-wise fracture analysis (of laminates)
Schlaffe-Bewehrung	non-tensioned (un-prestressed) reinforcement
Schlichte (Avivage, s.a. Beschlichtung)	sizing (water-based formulation)
Schnittfaser	chopped strand
Schnittgrössen	cross section quantities or stress resultants
Schnittkraft	section force
Schrumpfen	physical shrinking
Schubfluss	shear flow
Schuss ('füllen')	weft ≡ fill
Schussverstärkt	weft-inserted
Schwinden	chemical shrinking
Schwingungsrisskorrosion	vibration corrosion cracking or corrosion fatigue
Sichere Last	(Design) Limit Load DLL
Sieblinie	grain curve
Spaltung	splitting
Spannglied ohne Verbund	tendon without bond (for pre-stressed concrete)
Spannkabel (-glied)	tendons (tensioned or non-tensioned)
Spannung	stress (in MPa = N/mm^2)
Spannungsrisskorrosion	stress corrosion cracking SCC
Spannungsverhältnis	stress ratio $R(\sigma)= \sigma_{min} / \sigma_{max}$

Deutsch	Englisch
Spritzguss	injection molding
Spritzbeton	shotcrete
Spule	bobbin
Stab	bar, rod
Stabstahl	rebar
Stahlbeton	(steel) reinforced concrete
Stahlbetonfertigteile	prefabricated reinforced concrete parts
Stahlgitter	steel mesh, mat or grid
Ständige Einwirkungen	permanent actions
Ständige Lasten	static (constant) loads
Standsicherheitsnachweis	proof of safe status (proof of 'stability')
Stapelfasermatte	chopped strand mat
Statische Berechnung	structural analysis
Stehfaden	stand thread, warp yarn
Stichprobe	sample (set of test specimen or of measurements)
Sticken	stitching (embroyding)
Strang	strand (= subset of a yarn)
Strebe	strut
Stricken	weft knitting
tex	tex (measure of fineness of a yarn in g/km)
Textilbeton	textile-reinforced concrete TRC
(technische) textile Halbzeuge	textile semi-finished products
Textilerzeugnis (flächig)	fabric
textiles Gitter	fiber grid
Thermoplast TP	thermoplastic material
Topfzeit	pot life
Tow	tow
Tragwerk	load-bearing structure
Träger, Binder	girder
Tragfähigkeit	load carrying capacity (ultimate limit state)
Tränkung	impregnation
transversal-isotrop	transversely-isotropic
Trennfestigkeit	cohesion
Trennmittel	release agent
tri-axial	triaxial
Übergreifungslänge (Überlappungslänge)	overlap length
UD-Schicht	UD lamina
Umschnürungsbewehrung	confining (hoop) reinforcement
Unschärfe, Unsicherheit	fuzziness, uncertainty
Validierung	validation
veränderliche Einwirkungen	variable actions
Verankerungslänge	anchoring length
Verarbeitung	processing
Verbindungen:	joints, connections
Verbundwerkstoff [2]	composite material
Verfestigung	hardening
Verfügbarkeit	uptime reliability
Verifizierung	verification
Versagen	failure
(Festigkeits-)Versagensoberfläche	(strength) failure surface
Verschnitt	waste

Deutsch	Englisch
Versprödung	embrittlement
Verstärkung	reinforcement
Verzögerer	retarder
Vliesstoffe	non-wovens (principally no fabric)
Voreinstellung	default
Vorform	preform
Vorgespannte Bewehrung	prestressed reinforcement
Vorspannung	pre-stressing load
vorwiegend ruhende Lasten	predominantly static loads
Wasserbindemittel	water binder
Wasserstoffversprödung	hydrogen embrittlement
Welligkeit	waviness of a ply, ondulation of a roving
Werkstoff	material
Werkstoffanstrengung	material stressing effort *Eff*
Werkstoffverbund [1]	composite of different materials
Wickelkörper	filament-wound structure
Widerstand, Beanspruchbarkeit	resistance
Wirken	warp knitting
Wirkfaden	warp knitting thread
wirr angeordnet	randomly oriented
Wöhlerkurve	SN curve
Zeitstandverhalten	stress rupture or static fatigue behavior
Zement	cement
Zementleim	cement paste
Zerstörungsfreie Prüfverfahren ZfP	non-destructive testing NDT
Zeuge (Beweisprobekörper)	testify experiment
Zugabewasser	mixing water
Zugzone, gerissene Zugzone	cracked concrete tensile zone
Zusatzmittel	additives
Zuschlagstoff	aggregate
Zustand I	state I
Zustand IIa	state II
Zustand IIb	final crack state
Zuverlässigkeitsindex β	reliability index β (not safety index)
Z-Verstärkung	Z-reinforcement
Zwang, Einschränkung	constraint
Zwirn	twisted yarn
3D-Komposite-Werkstoff	three-dimensional composite material

23.4 Abbreviations/Abkürzungen

A	AR-Glas mit Vinylester (Solidian, Stabbewehrung)
AAB	alkalisch aktivierte Bindemittel (bei Säureangriff, Industriefußböden)
AAE	AR-Glas mit EP-Tränkung (Solidianproduktabkürzung, AA:= in beiden Richtungen AR-Glas-Bewehrung)
AAS	AR-Glas mit Styrol-Butadien-Tränkung (Solidian)
aaRdB	allgemein anerkannte Regeln der Baukunst (bewährte technische Regeln für den Entwurf und die Ausführung baulicher Anlagen
abZ	allgemeine Bauaufsichtliche Zulassung des DIBt. Beispiel: Z-31.10-182, Verfahren zur Verstärkung von Stahlbeton mit TUDALIT (textilbewehrter Beton)
AF	Aramid Faser, aramid fiber
AFK	Aramid Faserverstärkter Kunststoff
AFP	Automated Fiber Placement (for complex structure manufacture). Verfahren zur Verarbeitung von Halbzeugen mit thermoplastischer Matrix im AFP-Prozess
AFRP	Aramid-Fiber-Reinforced Polymer (or Plastic)
AI	Artificial Intelligence (see machine 'learning')
ALM	• Advanced Laser Materials such as ALM HP 11-30, short CF 3D-reinforced PA 11 material • Application Lifecycle Management (Entwicklung und Betreuung von Applikationen über Lebenszyklus) • Additive Layer Manufacturing
AM	Additive Manufacturing
AR	• Alcali-Resistant • Augmented Reality
ASR	Alcali-Silica-Reaction
ASTM	American Society for Testing and Materials (test standards)
ATL	Automated Tape Laying
ATP	Automated Tape Placing (placing of patches)
AWV	Ausgeglichener WinkelVerbund (balanced angle-ply laminate)
B	Basaltfaser mit Vinylester (*Solidian*, Stabbewehrung. *Mit B wird die Borfaser abgekürzt, daher wäre besser Bs*)
BAP	Balanced Angle-Ply laminate
BAuA	Bundesamt für Arbeitsschutz und Arbeitsmedizin
BauPG	Bauproduktengesetz
BBQ	BetonBauQualität (DAfStb: zukünftige Einführung von Klassen, um unterschiedliche Bau-Randbedingungen betreffend Bauwerk/Bauteil, Beton, Bauausführung besser abbilden zu können)
BBS	Basalt mit SBR (in beiden Richtungen eine Basaltfaser-Bewehrung, Solidian)
BC	Boundary Condition
BD	Bi-Direktional, bi-directional
BDCB	Bi-Direktional verstärkter CarbonBeton
BIM	Building Information Modeling (besser wäre Management)
BMC	Bulk Molding Compound (containing short fibers = 3D-SMC Pressmasse, Spritzguss)
BÜV	Bauüberwachungsverein
BVID	Barely Visible Impact Damage (observation limit at inspection, < 0.3 mm)
bvse	Bundesverband Sekundärrohstoffe und Entsorgung

C	Composite, Carbon, Concrete, Ceramics, Cube, Compression
C/C	Carbon/Carbon (ceramics)
C/SiC	Carbon/Silicium Carbide (ceramics)
C^3	Carbon Concrete Composite (cluster research project at Dresden University)
CAD	Computer-Aided Design
CAE	Computer-Aided Engineering
CAI	Compression-After-Impact
CAM	Computer-Aided Manufacturing
CB	CarbonBeton
CC	Carbon Concrete
CCC	Carbon Concrete Composite
CCE	Carbon Concrete mit EP (Solidian)
CCS	Carbon mit SBR (Solidian)
CDM	Continuum Damage Mechanics
CDS	Characteristic Damage (better damaging) State
CE	Cyanate-Esther
CE-Zeich.	Conformite Europeenne (erfüllen BauPR, Produkte dürfen innerhalb EU frei gehandelt werden)
CEB	Comite Europeen du Beton
CEM	CEMent types classified by DIN EN 197 (examples: CEM I Portland cement, CEM II Portland composite cement)
CEN	Comité Européen de Normalization (Europäisches Komitee für Normung)
CF	Carbon Fiber
CFD	Computational Fluid Dynamics
CF-EP	Carbon Fiber-EPoxy
CFHT	CF Heavy Tows
CF-HT	CF-HighTensile
CF-HT/EP	CF-High Tensile with EP matrix
CFK	Carbon-Faser-Kunststoff (carbon*faserverstärkter* Kunststoff ist zu einschränkend, s.a. [Sch06])
CFM	Continuous Filament Mat
CF-PP	(Kurz)CF verstärktes PP (ist nicht hygroskopisch)
CFRC	Carbon (short)Fiber-Reinforced Concrete to improve matrix properties *((Kurz)faserbeton als Matrix-verstärkung analog zur Polymermatrix beim SMC!)*
CFRP	Carbon Fiber-Reinforced Polymer (different CF materials available, usually endless fibers!)
CFRP-TP	Carbon Fiber-Reinforced Polymer-ThermoPlastic
CFRTP	Carbon(long)Fiber-Reinforced ThermoPlastic (Covestro)
CFS	Carbon Fiber-based Sensor
CGS	Centimeter Gram Second unit system
CL	Component Level
CLT	• Classical Laminate Theory (klassische Laminattheorie) • Cross-Laminated Timber (Brettschichtholz)
CMC	Ceramic Matrix Composite
CME	Coefficient of Moisture Expansion (Feuchteausdehnungskoeffizient)

CNF	Cellulose NanoFiber ($R_{\parallel}^{t} \approx 1500$ MPa; durch spezielles Verfahren am DESY erzeugte orientierte und enggepackte Nanofasern-Rovings)
COD	Crack-Opening Displacement (applied in fracture mechanics verification, for polymer and concrete parts)
CoS	Coordinate System
Cov	Coefficient of Variation
CPC	Carbon-Prestressed Composite
CPPS	Continuous Profile Preforming System
CPT	Cured Ply Thickness (ausgehäretete Lagendicke)
CPU	Core Processing Unit
CpU	CoSt per Unit
C-RTM	Compression-Resin Transfer Molding
CSH	Calcium Silicate Hydrate
CSM	Chopped Strand Mat
CT	Compact Tension (fracture mechanics test specimen in)
CTE	Coefficient of Thermal Expansion
CVD	Chemical Vapor Deposition
CVI	Chemival Vapor Infiltration
D	accumulated damaging sum (Palmgren-Miner $D = \sum \frac{ni}{Ni} < 1 \geq D_{admissible}$
DAfStb	Deutscher Ausschuss für Stahlbeton (Richtlinie für Schutz- und Instandsetzung von Betonbauteilen)
DBV	Deutscher Beton- und BautechnikVerein e.V.
DCB	Double Cantilever Beam (fracture mechanics test specimen)
DEM	Discrete Element Method
DFP	Dry Fiber Placement (preforming procedure)
DfSS	Design for 6σ (stochastic design optimization concept using the standard deviation σ of an assumed Normal Distribution for the envisaged uncertain scattering design parameter)
DIBt	Deutsches Institut für Bautechnik
DIC	Digital Image Correlation
DIN EN	Deutsches Institut für Normung
DLL	Design Limit Load
DMA	Dynamic-Mechanical Analysis (in Thermoanalysis)
DoE	Design of Experiments
DoF	Degree of Freedom
DP	DuroPlast
DSC	Differential Scanning Calorimetry
DTA	Damage Tolerance Assessment
DUL	Design Ultimate Load = ULS Ultimate Limit State
EAD	European Assessment Documents (Europäische Bewertungs-Dokumente)
EC	EuroCode
Eff	material stressing EFFort (Werkstoffanstrengung)
ELM	ErmüdungsLastModelle (Schwervekehrseinwirkungen, Einwirkungskombinationen, Festlegung von Grenzschwingbreiten Δσ
ENF	End Notched Flexure (fracture mechanics test specimen)

EoL	End-of-Life
EP	EPoxy (thermoset)
EPS	Expanded PolyStyrene
ERB	External Reinforced Bonding
ERC	Exposure Resistance Class
ES	Einzelschicht (Parallelfaser, P-ES; Gewebe, G-ES; Wirrfaser, W-ES)
ETA	European Technical Approval (Zulassung ohne Bemessung)
EU-BauPVO	Europäische BauProduktenVerOrdnung (Bauwerke müssen Grundanforderungen bei normaler Instandhaltung über einen wirtschaftlich angemessenen Zeitraum erfüllen)
F	failure function (F = 1 is failure condition. F > = < 1 is failure criterion), Flow potential function
FAW	Fiber Aerial Weight (Faserflächengewicht)
FB	FaserBruch
FCC	Fleece Concrete Composite
FCM	Fiber Composite Materials
FDM	• Fatigue Damage Model, • Fused Deposition Modeling
FEA	Finite Element Analysis
FEM	Finite Element Method
FF	Fiber Failure
FFF	Fused-Filament-Fabrication (≡ FDM)
FGM	Functionally Graded Material
FI	Failure Index (deterministic measure for failure criticality)
FIB	Féderation Internationale du Béton (internationales Pendant für DIBt)
FKV	Faser-Kunststoff-Verbund (zu bevorzugen, da allgemeiner als FVK)
FLM	Fused Layer Modeling FLM
FM	Facility Management
FMC	Failure Mode Concept
FMEA	Failure Mode Effect Analysis
FMECA	Failure Mode Effect Critical Analysis
FML	Fiber Metal Laminate
FoS	(design) Factor of Safety (prescribed values j or γ)
FPF	First-Ply-Failure (generally, not dedicated to a FF or an IFF)
FPP	Fiber-Patch Placement
FPUR	Flat Pre-stressed Un-bonded Retrofit system
FRC	Fiber-Reinforced Composite (should not be used in case of short fibers!)
FRC	(Short)Fiber-Reinforced Concrete (matrix improvement)
FRCM	(short) Fiber-Reinforced-Cementitious Matrix (composites) ≡ FRC ≡ smart concrete
FRP	Fiber-Reinforced Polymer (plastic)
FSDT	First-order Shear Deformation Theory
FVC	Fiber Volume Content (= fiber volume fraction V_f in %)
FVG	Faser-Volumen-Gehalt

FVK	FaserVerstärkter Kunststoff
FVW	Faser-Verbund-Werkstoff (Oberbegriff) = fiber composite material
GB	Glasbeton
G-ES	Gewebeverstärkte ES
GF	Glasfaser, glass fiber
GFK	Glas-Faser-Kunststoff (Begriff Glasfaserverstärkter Kunststoff ist einschränkend)
GFRP	Glass-Fiber-Reinforced Plastic
GF-TP	Glas-Faser-ThermoPlast-Verbund
GLARE	Glass Laminate Aluminum Reinforced Epoxy (= FML, glasfaser-verstärktes Aluminum)
GMT	GlasMattenverstärkter Thermoplast
GRP	Glass(fiber)-Reinforced Polymer
GTRC	GlassTextile-reinforced Concrete
GZG	Grenzzustand der Gebrauchsfähigkeit
GZT	Grenzzustand der Tragfähigkeit
hEN	harmonisierte Europäische ProduktNormen
HOAI	Honorarordnung für Architekten und Ingenieure (edition 2013)
HM	High Modulus
HMH	Hencky-Mises-Huber (‘Von Mises’) strength condition for initiation of yielding and further yielding
HP	High Performance
HM	High Pressure (i.e. RTM process)
HPAC	Hochleistungsaerogelbeton
HPC	High-Performance Concrete
HSB	(luftfahrttechnisches) Handbuch für Strukturberechnung (German aerospace handbook)
HST	High Strength Tensile
HT	High Tensile
HTA	High Tenacy carbon fiber (< 6k, HTS > 6k)
IFF	Inter-Fiber Failure (cohesive matrix failure and hesive interface failure)
ILC	Infra-Light Concrete
ILEK	Institut für Leichtbau, Entwerfen und Konstruieren
ILS	Inter Laminar Stresses (τ_{31}, τ_{32}, σ_3)
ILSS	Inter Laminar Shear Strength τ_{ILSS}
IoT	Internet of Things
ISO	International Organisation for Standardization (for test standards)
IT	Information Technology, Informationstechnik
ITKE	Institut für Tragkonstruktionen und konstruktives Entwerfen
KI	Künstliche Intelligenz
KKS	Kathodischer Korrosions-Schutz (von chloridkontaminiertem/karbonatisiertem Beton)
KOS	Koordinatensystem
LBO	LandesBauOrdnung
LCA	Life Cycle Assessment (Treiber für Carbon Beton)
LCM	Liquid Composite Molding

LEFM	Linear Elastic Fracture Mechanics
LFT	Langfaser-verstärkter Thermoplast (example: LFT GF50/PA6)
LNV	Logarithmische Normal-Verteilung
LOM	Laminated Object Modeling (of bondable materials)
MAG	Multiaxial-Gelege ≡ NCF
LSS	Laminate Stacking Sequence
MAK	Maximal zulässige Arbeitsplatz-Konzentration für Styrolverdunstung
MBE	Model-Based Engineering
MBSE	Model-Based System Engineering
MD	Molecular Dynamics (novel multiscale simulation tool in design to enhance the performance of composites and parts thereof
MDAO	Multi-Disciplinary-Design-Analysis & Optimization
MDO	Multi-Disciplinary Optimization
MDOF	Multi Degree of Freedom (vibrating systems)
MfFD	Multifold (strength mode) Failure Domain
MiFD	Mixed (strength modes) Failure Domain
MKF	Multi-axially reinforced weft Knitted Fabrics
MKS	m, kg, s - system of units (succeeded the cm, g, s = CGS system)
ML	Machine Learning
MLG	Mehrlagengestrick
MM	Mixed Mode (more than one fracture mechanics mode I, II, III is acting)
MMB	Mixed-Mode Bending (fracture mechanics test)
MMC	Metal Matrix Composites
MN	MegaNewton
MoR	Management of Risk
MoU	Minutes of Understanding
MoS	Margin of Safety (= RF-1)
MRO	Maintenance, Repair, Overhaul
MS	Margin of Safety (= RF-1)
MTTF	Mean Time To Failure (mittlere Zeit bis zum gefahrbringenden Ausfall)
MVF	Metal Volume Fraction
NABau	NormenAusschuss Bauwesen
NAFEMS	National Agency for Finite Element Methods and Standards (independent, Not-for-Profit **I**nternational Association for the Engineering Modelling, Analysis and Simulation Community
NCF	Non-Crimped Fabric (≡ MAG)
NDI	Non-Destructive Inspection
NDT	Non-Destructive Testing
NF	Normal Fracture (failure mode with normal stress σ-activated damaging)
NFK	NaturFaser-Komposite
NH	Normal stress-based ‘principal stresses Hypothesis’
NOL	Naval Ordnance Laboratory
NRC	Non-Recurring CoSts

NSM	Near Surface Mounted (lamella in slits)
NV	Normal-Verteilung von Gauss
NVH	Noise Vibration Harshness (unerwünschte Geräusche)
OEM	Original Equipment Manufacturer
PA6	Polyamid 6 (resin)
PAN	Polyacrylnitril (precurser)
PAW	Prepreg Areal Weight (Prepreg-Flächengewicht)
PC	• PolyCarbonat • Prestressed Concrete
PCC	PolyCarbonatCement (kunststoffmodifizierter zementgebundener Instandsetzungsmörtel (Feinbetonmatrix) mit Haftbrücke und Korrosionsschutz)
PCE	PerChlorEthen (plasticizer)
PCT	Premier Composites Technilogy (on FRP)
PDF	Power Density Function
PDM	Product (process) Data Management
PEEK	PolyEtherEtherKetone (resin)
PEKK	PolyEtherKetoneKetone (resin)
PEI	PolyEtherImide (resin)
P-ES	Parallelfaser-verstärkte ES
PET	Polyethylenterephthalat (Polyester resin)
PFHC	Pneumatic Forming of Hardened Concrete (process to obtain free-form surfaces, is load path-oriented)
PI	PolyImide (resin)
PiD	Process-induced Distortion
PLM	Product-Lifecycle-Management
PM	Project Management
PMC	Polymer Matrix Composites
PP	Poly-Propylen (resin)
Prepreg	Pre-impregnated endless fiber system (UD-Band, Multiaxialgelege, Gewebe)
PSD	Power Spectral Density
PSE	Professional Simulation Engineer (NAFEMS certification)
PT	PostTensioning
PTFE	PolyTetraFluoroEthylene
PU (PUR)	PolyURethan
PUR	Pre-stressed Un-bonded Retrofit
PÜZ	Prüf-, Überwachungs- und Zertifizierungssystem
PVA	PolyVinylAlcohol
PVC	PolyVinylChloride (polymer)
R, f	Resistance, **f**estigkeit, (strength)
RAMS	Reliability Availability Maintainability Safety
RC	Reinforced Concrete; Recurring CoSts; Resistance Class (concrete); Resin Content
RCC	Reinforced Concrete Column

rCF	recycled Carbon Fiber (*RCF is not correct*! Leads to confusion in construction)
rConcrete	Reycled concrete
RDO	Robust Design Optimization (tool to evaluate the combined action of the scattering design variables such as fiber waviness, layer orientation and undulation as manufacturing significances, material properties)
REACH	Registration, Evaluation, Authorisation and Restriction of Chemicals
REM	RasterElektronenMikroskop
RF	ReserveFaktor
RFEM	3D-FEM for general static dimensioning
RFID	Radio-Frequency Identification (Identifizierung mit Hilfe elektromagnetischer Wellen)
RILEM	Reunion Internationale des Laboratoires et Experts des Materiaux, Systemes de Construction et Ouvrages (International Union of Laboratories and Experts in Construction Materials, Systems, and Structures)
RT	Room Temperature (ambient temperature)
RTA	Room Temperature Ambient
RTM	Resin-Transfer-Molding
RVE	Representative Volume Element (concrete > $(4 \cdot \emptyset \text{ max grain})^3$, [Newman])
SAE	Society of Automotive Engineers (prepares Standards in Mechanical Engineering)
SB	(Styrol) Styrene Butadien co-polymer
SBR	(Styrol) Styrene Butadien Rubber (flexibles Tränkungsmittel, aber nicht so temperaturstabil)
SCC	• Self Compacting Concrete
SCC	• Stress Corrosion Cracking
SCF	Stress Concentration Factor
SDM	Simulation Data Management
SE	Simultaneous Engineering
SEA	Schall-Emissions-Analyse
SEAM	Screw-Extrusion-Additiv-Manufacturing
SERR	Strain Energy Release Rate
SF	Shear Fracture (τ-activated damaging under compressive stress)
SFC	Strength Failure Condition (Festigkeitsbedingung)
SFC	Strength Failure Condition (means here interaction of stresses within one mode)
SFP	Semi-Finished Product (Halbzeug)
SGF	Short Glass Fiber
SHM	Structural Health Monitoring
SI	Système International (international system of units)
SiC	Silicium Carbide
SiC/SiC	Silicium Carbide (fiber)/Silicium Carbide (matrix)
SIMP	Solid Isotropic Material (Microstructure) with Penalization (Topologyansatz)
SIVV	(Beton) Schützen, Instandsetzen, Verbinden und Verstärken
SLA	StereoLithography (“3D-Print”) Apparatus
SLM	Selective Laser Melting (metal “3D-print)
SLS	Serviceability Limit State
SLS	Selective Laser Sintering (powder-based additive manufacturing, PA12)
SMA	Shape Memory Alloy (Formgedächtnislegierung)

SMC	Sheet Molding Compound containing short fibers = flächige Pressmasse (CF-SMC, GF-SMC), Spritzguss
SME	Small Medium Enterprise (≡ KMU)
PCC	Portland Cement Concrete (Spritzbar, keine Haftbrücke aufzutragen)
SPDM	Simulation Process and Data Management
SPMC	Smart Polymer Matrix Composites
SPP	SchwerPunkt Programm
SpRK	SpannungsRissKorrosion
StB, Stb	StahlBeton, Stahlbeton (steel-reinforced concrete)
STL= SL	STereoLithography
SV	SchichtenVerbund
TC	Technical Committee
TF10	abZ (Z-31.10-182)-definierter Feinbeton von PAGEL/TUDALIT
TFP	Tailored Fiber Placement (Sticktechnik)
TNCF	Tailored Non-Crimp Fabrics
TP	Thermo-Plast
TPE	ThermoPlastische Elastomere
TR UHPC	Textile-Reinforced UHPC
TRC	Textile-Reinforced Concrete
TS	Thermo-Set
TUDALIT	Markenname für CF-Textilbeton der TU-Dresden AG
Ü	Bauprodukte 'Übereinstimmungszeichen'
UC	Unit Cell
UD	Uni-Directional
UHFB	Ultra-Hoch-Fester Beton
UDRC	Uni-Directionally Reinforced Concrete (by bars, lamellas)
UHP TRC	Ultra-High-Performance TRC
UHPC	Ultra-High-Performance Concrete (f_c > 150 MPa)
UHPFRC	Ultra-High-Performance-(short)Fiber-Reinforced Concrete (UHPC-Faserbeton ≡ UHPC-FB)
UL	Ultimate Load (fracture failure load in test)
ULS	Ultimate Limit State
UP	Ungesättigtes Polyesterharz (Duromer)
UTS	Ultimate Tensile Strength R_t (general materials), f_{ct} (concrete)
ÜZ	Produktkennzeichnung nach Übereinstimmungszertifikat durch eine anerkannte Zertifizierungsstelle
VARTM	Vacuum-Assisted Resin Transfer Molding
VAP	Vacuum-Assisted Process (as an infusion process)
VARI	Vacuum-Assisted Resin Infusion
VCCT	Virtual Crack Closure Technique
VDMA	Verband Deutscher Maschinen und Anlagenbau
VFIB	Verein zur Förderung der Ausbildung zur Brückenprüfung, Brückeninspektion und Bauwerksprüfung nach DIN 1076
VMAP	Vector Map (interface standard for integrated virtual material modelling in manufacturing industry)

VOB	Vergabe- und Vertragsordnung für Bauleistungen
WEA	WindEnergieAnlage
W-ES	Wirrfaserverstärkte ES
WF-ply	Woven-Fabric- ply
WHO	World Health Organisation
WP	Wet Pressure
wPK	werkseigene ProduktionsKontrolle
WV, WD	Weibullverteilung, -Distribution (geeignet für Festigkeits-Testdaten mit mehreren Abbildungsfunktionen)
WWFE	World-Wide-Failure-Exercise (on UD strength criteria)
XFEM	Extended Finite Element Method (extends the classical FEM approach to model the propagation of discontinuities such as cracks and weak material interfaces)
Zfb,ZFB	Zwischenfaserbruch (inter fiber failure IFF)
ZfP	Zerstörungsfreie Prüfung
ZiE	Zustimmung im Einzelfall (single case approval)
ZIM	Zentrales Innovationsprogramm Mittelstand
ZTV	Zusätzliche Technische Vertragsbedingungen
ZTV-W	Zusätzliche Technische Vertragsbedingungen für Schutz und Instandsetzung der Betonbauteile von Wasserbauwerken
2D	two-dimensional, bi-axial
2K	zwei Komponenten-Harzsystem, two component resin system (building the matrix)
2k	two-thousands of filaments
3D	Räumlicher Verstärkungs-Werkstoff (Material), d.b. 3 Richtungen in der Ebene, verbunden mit sog. z-Fäden in der 3. Raumrichtung ≡ z-Richtung *(3D wird leider bei Kompositthalbzeugen oft für eine Verstärkungs-Struktur verwendet, die räumlich ist*)
3DP	3D-Printing
e.g.	(exempli gratia) for example
i.e.	(id es) that is

23.5 Terms and Symbols *considering the guideline VDI 2014 and DIN 1055-100*

Roman Symbols

A	Fläche, area, permanent strain at failure, cross-section area of beam
A_i	influence factors or knock-down factors for composites in construction *(Note: these reduction factors are similar to those used for FRP in VDI 2014, part 1)*
[A]	laminate in-plane (or stretching) stiffness, sub-matrix of [K]
[K]	laminate stiffness matrix
[B]	laminate bending-stretching coupling, sub-matrix of [K]
BsF	basalt fiber (BF is Bor Fiber!)
C	fracture angle measure $C = 1/3$ with $\Theta_{fp}° = 35°$ (very ductile); $C = 0$, $\mu = 0$ with $\Theta_{fp}° = 45°$ (bound of F^{SF}); C = - 1 with $\Theta_{fp}° = 90°$ (very brittle, tension)
$E_{\parallel}$, $E_{\perp}$	Young's moduli of UD-lamina material, parallel and transverse to fiber direction
E_m, E_f	Young's moduli of the matrix, fiber material
[C]	3D elasticity stiffness matrix of the lamina for 3D-stress state (referring to lamina-COS) (Werkstoff-Steifigkeitsmatrix)
[C']	rotated 3D elasticity stiffness matrix of the lamina for 3D-stress state (referred to laminate-COS)
D	accumulated value of damaging portions or accumulated damaging sum Palmgren-Miner $D = \sum \frac{ni}{Ni} < 1 \geq D_{admissible}$
D	Coefficient of diffusion and non-circularity parameter in the strength condition F of the fracture failure body (failure surface).
[D]	laminate bending stiffness, sub-matrix of [K]
d	non-circularity parameter of the hoop cross-section of the failure body which is here a fracture failure body or also termed π-plane shape parameter
d_s	static height
E	elastic modulus, Young's modulus
E, Ec	Young's modulus in tension, compression
e	Betondeckung (*bei Stahlbewehrung in Betonstahl-Ø-Vielfachen wegen Korrosions-gefahr, bei Carbonbewehrung deswegen viel dünner ausführbar*)
E_{cm}	average E-modulus under compression *(index $_c$ for concrete not for compression!)*
$E_{cm,7d,\parallel}$	average E-modulus, after 7 days, in fiber direction measured
F	force
f	strength (*Festigkeit*) in *civil engineering (*in the context of the development of partial safety factor concept in Germany about 1985 it was going to become replaced by *R* and this the more viewing the future EuroCodes) → one should not wait and replace *f* by *R* to become clearer. The tensile strength of a non-metallic $_{nm}$ reinforcement $f_{nm,k}$ is defined as a characteristic value (index $_k$)
f	index of pure fiber. Could be applied for a non-cured fiber-matrix strand (roving, tow)
f_c	concrete compressive strength, measured by using rigid compression plates
f_c'	concrete compressive strength, measured by using load introduction brushes
$f_{c,cc}$, $f_{c,tt}$	concrete 'equi-bi-axial strength', compression, tension, better compressive and tensile strength capacity if $\sigma_I = \sigma_{II}$ *(technical strength is 'uniaxial'-dedicated)*

$f_{c,ccc}$, $f_{c,ttt}$	concrete tri-axial compressive and tensile strength capacity (tri-axial 'strength') if $\sigma_I = \sigma_{II} = \sigma_{III}$
$f_{c,cube}$	Concrete compressive strength, tested on the cube (100 mm)^3
$f_{c,cyl}$	concrete compressive strength, from cylinder (test specimen) test, Ø = 150 mm or 200 mm. *(slightly inclined textile reinforcement layers in concrete cube test specimens exhibit spalling analogous to kinking with compression-loaded UD-CFRP specimens*)
f_{cd}	Bemessungswert der Betondruckfestigkeit in N/mm^2, design compressive concrete strength statistically reduced strength (index $_d$ for design. ≡ *ultimate compressive strength R_{mc} if compared to A- or B-value in mechanical engineering)*
f_{ci}	einzelnes Prüfergebnis für die Druckfestigkeit von Beton
$f_{c,mpr}$	concrete compressive strength from mortar prisma, 160/40/40 in mm
$f_{c,pr}$	concrete compressive strength, from prisma, 400/100/100 in mm
f_{cm}	concrete mean strength (in mechanical engineering $_m$ for 'maximale'
$f_{cm,j}$	concrete average (statistical distribution-dependent, a mean or a median) compressive strength (≡ $\bar{R}_m^c$) measured after j days [Baunetz Wissen]
$f_{c\mathbf{k}}$	concrete characteristic compressive strength (examples $f_{ck,cube}$, $f_{ck,cyl}$ [DIN EN 206-1/DIN 1045-2]. Index $_c$ for concrete and $_k$ for characteristic)
$f_{ck,cube}$	charakteristische Betondruckfestigkeit, Würfel
$f_{ck,cyl}$	charakteristische Betondruckfestigkeit, Zylinder
$f_{p0.1m}$	mittlere 0.1%-Dehngrenze für hochfeste gerippte Betonstahlstäbe *(z. B. für SIGMA Spannstahl ST 1470/1620 N/mm^2 ≈ 1500 N/mm'. Im Maschinenbau* $\bar{R}_{p0.1}$
f_R	bezogene Rippenfläche der Betonstahlstäbe *(auf eine zur Stabachse rechtwinklig stehende Schnittfläche projizierte Rippenfläche, bezogen auf den Nennumfang und den mittleren Rippenabstand*)
f_{ct}	concrete tensile strength measured by using bars or cylinders (*the maximum grain size determines the test specimen's geometry, f_{ct} triggers f_c due to lateral tensile stresses in the test specimen generated under uniaxial compression*)
$f_{ct,I}$	Betonzugspannung bei Erstrissbildung (Ende Zustand I)
f_{ctk}	concrete characteristic tensile strength
f_{ctm}	concrete average (mean) tensile strength
$f_{\|k}$	charakteristische Kurzzeitzugfestigkeit des Rovings, Faserstrangs, Tows ermittelt am standardisierten Faserstrangversuch
f_{FRCk}	charakteristische Kurzzeitdruckfestigkeit des Faserbetons FB (≡ FRC)
$f_{ct,0}$	concrete in-situ tensile strength
f_{yd}	Bemessungsstreckgrenze Betonstahl
f_{ym}	mittlere Fließgrenze von warmgewalzten Betonstahlstäben *(rebars, z. B. 550 N/mm^2 für BSt 500, Ø 10 mm)*
$G_{\|\perp}$	in plane shear modulus
G	shear elasticity modulus

$\mathcal{G}$	critical strain energy release rate $\mathcal{G}$ = Rate at which energy is transformed as a material undergoes fracture, expressed as the decrease in total potential energy per increase in fracture surface area
$\mathcal{G}$	design limit state (*Grenzzustand*). $\mathcal{G}\ (or\ g) = F - 1 = 0$
j	design factor of safety
g	ständige Lasten
H	height
I_1	first invariant of the stress tensor, isotropic
j	deterministic design factor of safety *(mechanical engineering)*
J_2	second invariant of the deviatoric stress tensor, isotropic
J_3	third invariant of the deviatoric stress tensor, isotropic
I_1,..I_5	invariants, transversely-isotropic UD-material
K	Kelvin, stress intensity factor (SIF)
K_c	critical stress intensity factor = fracture toughness (*Bruchzähigkeit*)
[K]	laminate stiffness matrix *(composed of sub-matrices [A],[B],[D])*
$[K]^{-1}$	inverse laminate stiffness matrix
2K	two resin components
k	Wärmedurchgangswiderstand im Maschinenbau *(in W/(mm^2·K))*
k	one thousand filaments, buckling factor
$k_{cube150/200}$	Umrechnungsfaktor unterschiedlicher Betonwürfelgrößen *(1.05 für Umrechnung von 200 mm Kantenlänge auf 150 mm (schlanker))*
LL	lesson learnt (learned)
M, M_t	bending moment, torque of a beam
M	saturation moisture
m	bending moment per unit width (stress resultant) of a plate or shell
m	index of matrix
N	normal force (beam)
N, M, Q	section loads of a beam
n, m, Q	section loads per unit width of a plane, a shell *(stress resultants)*
n	number of test data; membrane stress resultant per unit length; number of laminas in a laminate or in a fiber-grid assembly; number of cycles of yarns in a thread
nm	non-metallic (reinforcements carbon, glass, basalt, aramide. *nm cannot cover all fiber behaviors. Why does one not finally index the fiber type?*)
p	load from payload per area and pressure loading
p	= $I_1/3$ = hydrostatic stress coordinate *(axis of failure body)*
p_f	failure probability
Q	transverse (lateral) shear force
[Q]	2D elasticity stiffness matrix of the lamina for 2D-stress state *(referred to the lamina-COS)*
q	total load per area, shear force per unit width, veränderliche Lasten,
q	deviatoric stress coordinate = $\sqrt{3 \cdot J2}$
R	index Reinforced, letter for strength and resistance
R	stress ratio (*straight letter*), defined as minσ/maxσ *(mind signs)*
R	resistance, strength design allowable *(skew letter, statistically reduced strength*

	for design verification)
$\bar{R}$	average ('mean') or typical strength *(utilized for test data mapping)*
R^c	(here: compressive ultimate strength of brittle materials
R_m	tensile ultimate strength (can be – *in general* - better captured by R^t)
$R_{p0.2}$	tensile yield strength (can be generally better captured by $R_{02}{}^t$)
$R_{c0.2}$	compressive yield strength *(metals etc., index $_c$ reads compression here)*
R_{bk}	charakteristische Biegezugfestigkeit von Faserbeton mit 5% Quantil, 75% Aussagewahrscheinlichkeit [Wie]. *(Bemessungsbiegezugfestigkeit $R_{bd} = \eta \cdot R_{bk} / \gamma_m$, Faserzement mit Korrekturfaktor η gemäß EN1990 und Werkstoffteilsicherheits-beiwert γ_m)*
R_m	ultimate tensile strength *(resistance maximale (French). Index $_t$ is usually not written in mechanical engineering, because tension is usually dominant, opposite to concrete)*
R_{mc}, f_{cm}	ultimate compressive strength ($_m$ for 'maximale', $_c$ for compression), average compressive strength ($_c$ for concrete, $_m$ for 'mean')
R_{mc}	ultimate compressive strength *(in design verification only significant for brittle materials. For ductile materials a deformation limit is design driving)*
$R_{p0.2}$	tensile yield strength
$R_{\parallel}^t$, $R_{\parallel}^c$	tension and compression strength of a UD-lamina parallel to fiber direction
$R_{\perp}^t$, $R_{\perp}^c$	tension and compression strength of a UD-lamina perpendicular to fiber direction
$R_{\perp\parallel}$	in plane shear strength of a lamina
$\Re$	reliability $\Re = 1 - p_f = \Phi(\beta)$ *(example in Chapter13, assesses the goodness of the calculated deterministic RF by the more realistic, probabilistically determined reliability index β)*
r	recycling (not with capital letter as in Recycled Concrete = RC used in civil engineering. This is in contradiction to the generally used term Reinforced Concrete RC and to recycled Carbon Fiber rCF in EN 206-01)
[S]	3D and 2D elasticity compliance matrix *(Nachgiebigkeitsmatrix*), of the 3D and the 2D-lamina *(referred to lamina-COS = material COS*).
[S']	rotated compliance matrix of the lamina for the 2D-stress state *(referred to laminate-CoS)*
T	temperature
T_D	Streuspanne bei einer Wöhlerlinie
Tg	glass transition temperature in K
$[T]_\sigma$, $[T]_\varepsilon$	transformation matrix for stresses (left) and for strains (right)
t	laminate thickness; time
t_k	thickness of k^{th} lamina (layer) or of the k^{th} layer (laminate or fiber-grid)
tex	mass of the textile semi-finished product divided by 1000 m
w/z	Wasser-Zement-Verhältnis (water/cement ratio *r*)
$\bar{x}, s$	mean value, standard deviation of a sample
X, x	random variable, realization of a variable
x, y	abscissa, ordinate
x, y, z	structural COS (Cartesian), laminate COS

x_1, x_2, x_3	lamina CoS
x_1', x_2', x_3'	turned lamina COS [VDI 2014]
x_I, x_{II}	directions of principal normal stresses 2D
U	Wärmedurchgangswiderstand im Bauwesen *(für Wohngebäude < 0.28* $W/(mm^2 \cdot K)$*)*
V	volume
V_f	fiber volume fraction in %
u,v,w	displacements
w	width.

Greek Symbols

α	fiber orientation angle of the lamina ≡ angle of fiber direction *(right hand COS, positive from* fiber parallel ||-axis *x to x_1 anticlockwise measured)*
β	angle between fiber direction and principal normal-stress direction
$\alpha_{M,(}\alpha)$	linearized coefficients of moisture CME in 10^{-4} / %
$\alpha_{T,(}\beta)$	linearized coefficient of thermal expansion CTE in 10^{-6} / K
$\alpha_T, \alpha_{t\infty}, \alpha_D$	Abminderungsfaktoren im Bauwesen zur Berücksichtigung von Temperatureinfluss, Dauerstandfestigkeit (Index $_{t\infty}$), Dauerhaftigkeit
β	Zuverlässigkeitsindex, reliability index *(distance of the most-likely failure point in the Hasofer-Lind diagram to its origin using the standard normal distribution of Gauß)*
γ	partial design factor of safety in civil engineering, shear angle
$\gamma_{\|t}$	partial safety factor for the tow's tensile strength in the textile grid (≈ 1.2, retrofitting)
γ	shear strain, partial design factor of safety (FoS)
$\boldsymbol{\varepsilon}$	normal strain
$\dot{\varepsilon}$	strain rate
η	visCoSity in Nmm/min *(e.g. CEM mortar)*
Θ	non-circularity function
θ_{fp}°	angle of a strength fracture plane (isotropic, UD)
θ	Lode angle in cross-section or π-plane, circumference of an isotropic strength failure body
κ	curvature, permeability
λ	thermal conductivity, slenderness, parameter of a density distribution function
μ	Mohr-Coulomb material friction value (*practically* $0 < \mu < 0.3$)
μ, σ	mean value, standard deviation of the Basic Normal Distribution derived from the statistical population of the i samples, characterized by (m_i, s_i)
ν	Poisson's ratio, isotropic material *(in civil engineering sometimes the letter μ is used. ν grows). After Onset-of-yielding of ductile materials ν reduces due to void coagulation)*
$\nu_{\perp\|}, \nu_{\perp\perp}$	Poisson's ratios, transversely-isotropic UD-material with $\nu_{\perp\|}$ the major one. *(In the early days, indexing of Poisson's ratio followed the old convention 'location'*

	before 'cause' like VDI 2014 and Tsai now. However, in the FE codes it is most often performed oppositely)
ξ, ρ	Haigh-Westergaard coordinates $\xi = \sqrt{3}\cdot\sigma_{oct}$, $\rho = \sqrt{3}\cdot\tau_{oct}$ or Haigh-Westergaard-Lode coordinates with $I_1 / (\sqrt{3}\cdot R)$ as y-coordinate (*axial*) and $\sqrt{2\cdot J_2} / R$ as abcissa with *R an appropriate normalizing strength*
ρ	density of a material
ρ or ϕ	slope of Mohr-Coulomb curve (Mohr envelope)
σ_{cf0}	(Kurz-)Faserwirksamkeit bzgl. erhöhter Zugfestigkeit des Betons bei Einbringung von Kurzfasern *(index $_c$ für concrete, abhängig von dem Anteil der eingebrachten Kurzfasern, da in der Regel keine stochastische Verteilung)*
σ, τ	stresses in engineering notation, with one index only, similarly with the strains
σ_1, σ_2, τ_{21}	intra-laminar (engineering) stresses of the lamina (ply) in the lamina COS (τ_{12} *is not the failure-driving shear stress*)
σ_3,τ_{32}, τ_{31}	inter-laminar (engineering) stresses of the lamina (ply)
σ_x,σ_y, τ_{xy}	intra-laminar (engineering) stresses of the lamina (ply) in the structural (laminate)
σ_{oct}, τ_{oct}	octahedral stresses. $\sigma_{oct} = I_1/3$, $\tau_{oct} = \sqrt{J2\ /3}$
τ_{fm}	mittlere Verbundspannung zwischen Faser und Betonmatrix
∅	diameter of grains or filaments
Φ, V_f	Faservolumenanteil
ψ	fiber mass fraction in %, Fasermasseanteil
ω	half of the crossing angle of an angle-ply laminate.

23.6 Indexing, Laminate Descriptions and Layer Numbering (ply-book)

Subscripts and Superscripts

$_{A, C, G, F}$	aramid, carbon, glass, fabric
$_{app}$	applied (loading)
$_b$	bending, bond
$_c$	concrete (in f_{cd}) and compression in mechanical engineering *(in civil engineering $_c$ for compression becomes dropped in compressive strength terms $f_{c\ ed}$ whereas in mechanical engineering the index $_t$ for tension usually becomes dropped in tensile strength $R_{m\ t}$)*
$_{cr}$	critical
$_{C,G}$	carbon, glass
$_{CrF}$	crushing fracture (failure mode of compression-loaded brittle material like concrete)
$_d$	marks value of the variable applied in design, kennzeichnet Bemessungswert
$_{eff}$	effective
$_{eq}$	equivalent
$_f$	fiber, Faser
$_{fr}$	fracture
$_i$	marks a fractile-value
$_{in}$	initial
$_{is}$	in-situ

k	running index 1 < k < n of a building block within a laminate or of a fiber-grid within a reinforced concrete plate
k	characteristic value of the concrete tensile strength such as f_{tk}
lim	limit
M	matrix, metal, moisture, mat (cloth)
m	matrix, maximale
n	number of building blocks like UD- layers, Quad NCF layers, Double-Double NCF layers
na	neutral axis
nm	non-metallic
p	pre-tensioned, vorgespannt
pl:	plural
r	recycled,
r	repetition running number of the distinct C-PLY™-layer = sub-laminate = building block *(simpler is to also use the classical suffix k for the C-PLY™-building blocks staying similar to the counting of the UD layers interpreted as building blocks too)*
res	residual, resultant
s	shear, symmetric lay-up, Stabstahl
sec	secant (modulus)
T	temperature
t	tension, torque, twisting, Zug
tan	tangential (modulus)
tex	textile
x, y, z	structural COS (related to the x.y, z-dircetions)
W, F	warp and fill (weft) direction in case of woven fabrics
in	initial value
⊥ , ∥ , ⊥∥	symbolic designations: perpendicular (transverse), parallel, in-plane shear
$( )^T$, $( )^{-1}$	transposed matrix, inverse matrix
0	COS origin, zero, in-situ, reference plane (may be the mid-plane, [CLT])
^	roof (*Roof signs for stress or strain quantities relating to the entire laminate)*
‾	marking of a single center layer in a symmetric laminate

Laminate and Organosheet Coding

Laminate Descriptions

( )	round bracket, applied for laminate families and ply-percentages
[ ]	square bracket, applied for UD-ply-composed fixed lay-ups, such as the 'quad-stacks' used in aeropace
{ }	curly bracket (brace), applied for multi-ply semi-finished products like C-Ply™ - NonCrimpFabrics (NCFs)

For the engineer in production and in design clearness must begiven: A symmetrical 'quad structure' such as $[0/45/-45/90]_S$ – as an example – may consist of 2 x 4 = 8 individually deposited UD-layers (k = 8) or may consist of two NCFs $\{0/45/-45/90\}_S$-layers as a stack of two building blocks (k = 2),

whereby the second NCF must be stored symmetrically. The engineer in production counts layers. Therefore, layer-indexing and counting should be performed as proposed below:

- UD-layer, here intentionally defined too as 'building block' = physical layer = sub-laminate :

(0°, ±45°, 90°)	example of a 4 ply laminate family, termed by Tsai 'Quad'-family
(20%0°, 70%-45°, 10%90°)	definition of a specific laminate showing the thickness fractions of UD lamina orientations (different percentages)
[0/90]s =[0/90/90/0]	definition of a laminate symmetrical $_S$ to the mid-plane (different fiber types)
$[90_2^G /0_3^C /+45_2^A /0^C]_{2s}$	specification of the lay-up of a laminate with respect to the fiber type
[0/45/-45/$\overline{90}$]s	just one center layer = symmetric half , denoted by a bar over
[0/0/45$_F$/90/-45$_F$/0/0]	specification of the lay-up of a laminate with respect to the type of reinforcement (*same UD and fabric material* $_F$)

- So-called 'Quad-NCF' is a *fixed* building block = physical layer = sub-laminate :

$\{0/45/-45/90\}_1$	an example with n = 1 typical balanced 4ply set-up, where [B] ≠ 0. 'Quad-NFCs' could be stacked under angles w.r.t. laminate CoS x,y
$[0/45/-45/90]_n$ or $_{nS}$	n, nS are the total numbers of the stack, whereby in order to indicate symmetry the suffix $_S$ is required. [..] is to be doubled in order to achieve a symmetric laminate, which then maximally can result in 24 permutations for the optimization Using $_{nS}$ captures the case that just one layer is present in the mid-plane
(25/50/25) 	ply percentage of a (0°, +45°, -45°, 90°)

- So-called 'Double-Double-NCF' an *adjustable* building block = physical layer = sub-laminate:

{{φ/-φ/-ψ/ψ} , {φ/-ψ/-φ/ψ}	examples lay-up or stack *(to be designed considering all Dimensioning Load Cases)* are distinct subcases of the quad-NCFs
{19.3/ -67/ -19.3/ 67}$_{10}$	Tsai indexes this laminate {19.3/ -67/ -19.3/ 67}$_{10T}$, where n = 10, with $_T$ the total number of stacked C-PLY™-layers being 'Double-Double-NCFs'. The obtained lay-up is an optimization result and needs not to be stacked under angles w.r.t. laminate CoS x,y. The suffix $_T$ is superfluous because, due to the conventional running index 1 < k < n , the suffix $_T$ fully corresponds to n.

Ply Book: Creation to act as reference during fabrication. It provides details about which building block is placed where on the tooling, at which angle and in which order .'Creating a Ply Book': use Internet example

Product Descriptions

aramid tape	plain weave fabric containing 80% Aramid Twaron (42 tex), 5% Glass yarn (0.3 tex), 15% PES (7.8 tex), 124 g/m^2, width 20 mm, thickness 0.2 mm. Permanent heat resistance 200°C. 124 g/m^2, operational temperature > 200°C, spool ware 250 m
CEM III	In addition to Portland cement clinker, CEM III cements contain only blast furnace slag as another main component. The Heidelberg

	CEM II and CEM III cements are cements according to the European cement standard DIN EN 197-1
CFHT	CF High Tensile
CF-EP	(continuous) Carbon Fiber-EPoxy composite
CF-EP-CEMIII	
CF-EP, Q95/95-CCE-38	Solidian Grid 645 g/m^2, max. 1,2m ·5 m, 95 mm^2/m fiber cross-section, 38 mm roving distance, E=250 GPa, $f_{\|tk}$ = 2300 MPa, $f_{\perp ck}$ = ($f_{lateral,tex}$) = 200 MPa
C-Ply^{TM}	Non Crimp Fabric (NCF) of the company Chomarat (*stitched angle ply, superscript Trade Mark* TM)
GF-PA66	PA66-TPmatrix, compound GF-PA66 with short glass fibers and V_f = 60% compared to the usual 30% (PA66-GF). (*If the polymer is the major component in the compound then the polymer is set first. This is opposite to endless fiber reinforcements!)*
GF-UP	(endless, continuous) Glass Fiber-UP composite
HTA40 12k (not K!)	HTATenax-Faser, 12000 Filamente im Roving
LFT PA6-GF47	PA66-TPmatrix with long glass fibers (*organo sheet)*
PA66-GF	compound with lower GF content
PP-GF 30	30% short glass fiber-reinforced PP
PP-rCF-compounds	SFRP (SMC) using recycled carbon fiber material
Q120-GF-EP-38	Q grid, 120 mm^2/m fiber cross-section, glass fiber (*fiber type missing*), epoxy, grid distance 38 mm
CFHT grids with loops	edge loop CFHT grid (larger anchorage and and overloapping lengths are necessary for heavy tows. Edge loops help to solve this problem)
Tube UD-fabric	Rohr-Schlauch-UD-Gewebe with Leinwandbindung: 48.5% CF (*12k, 800 tex*) + 48.5% AF (*Twaron: 5k, 805 tex*) + 3% Elastic material as coating reinforcement
Grid ware (example Fraas)	SITgrid 025, CF-example (≡ R-Matte, vendor provided data): ρ_{CF} = 1.77 g/cm^3, impregnated, roving with a short term tensile design strength $R_{\|}^{td}$ $f_{\|td}$ =($f_{\mathbf{td},tow}$) = 1700 N/mm^2 and $E_{\|\mathbf{d}}$ = 170000 N/mm^2; warp roving 48k, distance 12.7 mm (length) and reinforcement cross sectional area 141 mm^2/m width, weft (fill) roving 12k, distance 16 mm; deliverables: roll 2.50 m x 25.00 m, sheet 1.25 m x 2.00 m, area weight 309 g/m^2 (with SBR impregnation 346g/m^2), *Fig. 43* (fiber type missing)
Grid ware (Solidian)	Q-Mat or Q-Grid, vendor provided data for Q-95/95-CCE-38: CF-example (≡): ρ_{CF} = 1.77 g/cm^2, EP-impregnated tow with a short term tensile strength $R_{\|tk}$ = $f_{\|tk}$ = ($f_{\mathbf{tk},tow}$)= 2350 N/mm^2 and $E_{f\mathbf{k}}$ ≈ 220000 N/mm^2 (after DIN EN 1990 tensile tests); warp and fill tow 48k, grid distance 38 mm with reinforcement cross sectional area 95 mm^2/m width; *deliverables: roll* 2.50 m x 25.00 m, sheet 1.2 m x 5.00 m, area weight missing g/m^2 with EP impregnation in g/m^2); preformed ware with SBR (fiber type missing !). As stock mat and

	list mat deliverable R-Mat or R-Grid R46/37-AAS-10 x 13 (see abbreviations). As stock mat and list mat deliverable
Fibermod™	PP reinforced with: short GF (3 - 5 mm), long GF (10 - 15 mm), short CF (0.5 - 1 mm)
FIBRACRETE	CF-Kurzfaser-Portlandzement-Mörtel (MRM Augsburg) mit V_f = 1 - 2%, 3 mm Kurzfasern Ø 7µm, > 100 MPa Biegezugfestigkeit).

Layer-numbering:

In the 3 cooperating worlds Manufacturing, CLT–Analysis and Structural FE-Analysis different ways of numbering the plies in the stack are used. This must be checked in each project case in order to reliably orient the fibers in production, see CLT chapter.

Some units in engineering: recommendations for dimensioning

circular natural frequency $\omega = 2 \cdot \pi \cdot f$: Hz (f = eigenfrequency, revolutions per second) = 1/s
circular operational frequency, rotational speed Ω: 1/s
density ρ : $1 g/cm^2 = 1000 kg/m^3 = 1 \cdot 10^{-9} N \cdot s^2/mm^4$; $1000 kg = 1N \cdot s^2/mm$
energy J : $1 W \cdot s = 1 kg \cdot m^2/s^2 = 1 N \cdot m$, 1 kcal = 4.19 kJ; 1 kWh = 3600 kJ (for 30 Cent in 2020) = Actively working on a laptop for about 50 hours.
(*Examples* : (1) *Eating 200 gramm apples ≈ 100 kcal, (2) 1570 kcal ≡ 60 min cycling at 160 Watt → 1570·4.19 kJ = 6578 kJ → 1.8 kWh, only), (3) Specific heat capacity of water is c = 4190 kJ/(kg·K) → 4190 kJ = 1.16 kWh is necessary to heat up 1 kg water by 1 K or °C, (4) heating 1kg water from 15° degree up to 35° degree is equivalent to lift 11.3 t by 1 m ≡ 111 kN·m. Car power: 136 kW, men power: 136 W*
forces and loads : kN, kN/m, kN/m^2, $1 N = 1 kg \cdot m / s^2$
fracture mechanics : the given value of K_{Ic} with the unit $MPa\sqrt{m}$ is to be multiplied by $\sqrt{1000}$ to obtain the value with the unit $MPa\sqrt{mm}$
frequency f: 1/s
impact $m \cdot v^2$: $1 kg \cdot (1000 m/s)^2 = 10^6 kg \cdot m^2/s^2 = 1000 kJ = 1000 / 4.19 kcal$
mass: $1 g/cm^3 = 10^{-9} N \cdot s^2/mm^4$, $1 kg = 1 N \cdot s^2/ m$, $1000 kg = 1 N \cdot s^2 / mm$
momentum, impulse (Impuls): $kg \cdot m/s = N \cdot s$
moments (bending, torsion): $kN \cdot m$
pressure: $10 bar = 1 N/mm^2 = 1 MPa$
revolution: (1 revolution = 360 (old) degrees and 400 new degrees)
revolutions per minute (rpm) : n in 1 per minute
strain: $1000 \mu m/m = 0.1\ ^0/_0 = 1\ ^0/_{00}$
stress, strength: $1 MPa = 1 N/mm^2$,
visCoSity: water at 25°C $0.89 \cdot 10^{-4} Pa \cdot s = 0.89 \cdot mm^2/s$
weight G = mass · acceleration g: $1 kg \cdot 9.82 m/s^2 \approx 10 N$, 1 kg load $\equiv \approx 10 N$
I_p: mm^4 = polar cross section moment of inertia
I_t : mm^4 = torsional cross section moment of inertia.
angle: $\sin(\pi \cdot \alpha°/180°)$.

Much Experience is required in Design! But what is experience?
Experience is not what happens to you; it's what you do with what happens to you.

Aldous Huxley

Final Notes:

Above non-funded work mainly addresses the author's working life in industry with the intension to transfer theory into engineering application. This 'single authored' work includes: *Idea finding, *idea exploitation to generate the FMC-theory, *text writing of this document, *extensive numerical analyses with rendering of results like fracture bodies using the programs Mathcad 13 and 15, *typing of formulas, *difficult visualizations of the calculation results, sketches, diagrams etc. And, facing the program crashes of Word (*three per day, at least*) presumably due to the large document size combined probably due to conflicts with Mathcad 15 that always turns itself on and this together with that Word corrections were indicated to heave been executed but in reality not performed.

All these works have been performed by the author himself.

Many thanks are given to those who believed in my work [*W. Becker*] and had some discussions with me on several topics [*Wolfgang Brocks with Fracture Mechanics, Andreas Freund with Mathcad 13 and UD mapping etc, Martin Grimmelt with Statistics, Probabilistics.*]. This thankyou includes the WWFE organizers within the performance of WWFE-I and –II from 1999 through 2013 especially *Sam (Kaddour)* and those that peered my WWFE-contributions. Not to forget are all those which delivered a basis for some body texts. *B. Szelinski helped not to despair of Mathcad.*

To my wife Maria: *"My heartfelt thanks for allowing me to devote so much time of 'our time together' to my time-consuming hobby"*.

Dedication to all the people who have guided me to the wide variety of technical fields during my 55-years working life. This was challenging but also difficult and at the same time beautiful. Never giving up was the motto.

Desire of the author:

"It were helpful for both the dicsciplines mechanical and civil engineering to act side-by-side such as croco and hippo document it below. Surprising picture, Sambia 2011.

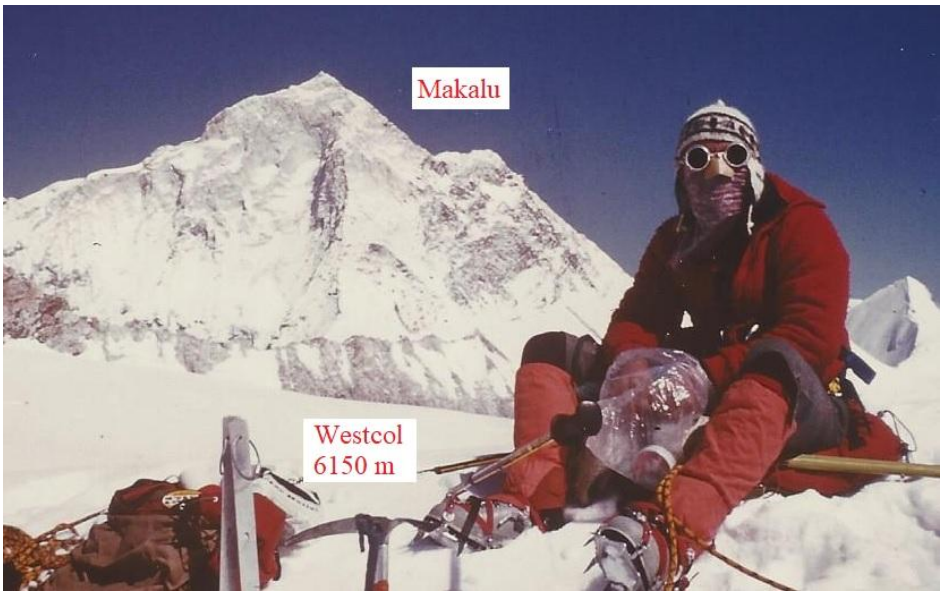


"Quid quid agis, prudenter agas, et respice finem" (*a slogan of my school class*)
Whatever you do, do it wisely and remember where it leads. *(*from *Gesta Romanorum).*
In this context:

If I had known beforehand how much time this work would take, I probably would not have done it.

"Si enim alicui placet mea devotio, gaudebo. Si autem nulli placet, memet ipsam tamen iuvat quod feci"
(A letter from Hrotsvit, nun of Gandersheim, 950 anno domini

If my work pleases anyone, I will be happy,
but if it pleases no one, it will nevertheless be good that I did it.

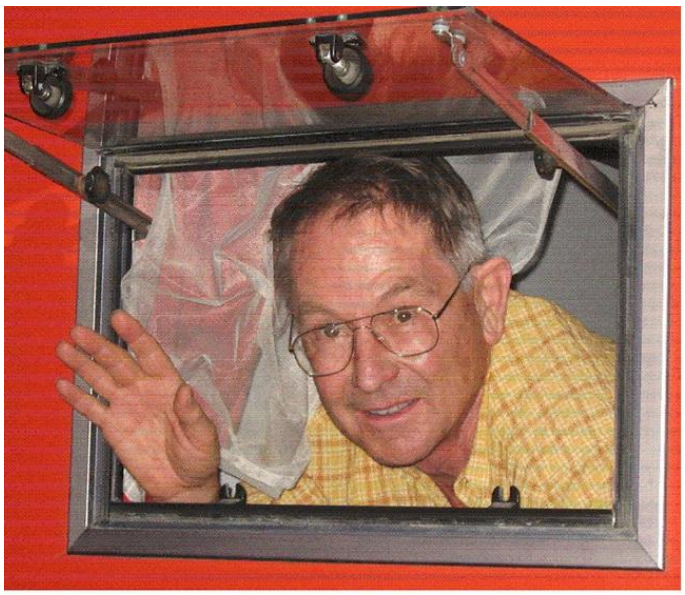


At least one medium high peak has been reached
with a similar effort used for this Life Work Compilation document.

Above:
Since the porters with the equipment were missing, we had to take spare clothes.
Consequence: You have to take what you have!
In this context: In the WWFE, the author also had no FE program available.
But much is possible if a goal is pursued and this was also the case with having some spirited 'idea spare clothes' when successfully investigating some special WWFE-II test cases.

The relative narrowness of a ROTEL sleeping cabin helped the author
to explore the wide world of nature and

his good basic engineering education helped him to widely explore the world of engineering.



Cabin: 80cm x 80cm x 210cm